MEIOSIS: FROM MOLECULAR BASIS TO MEDICINE

EDITED BY: Wei Li, Liangran Zhang, Akira Shinohara and Scott Keeney
PUBLISHED IN: Frontiers in Cell and Developmental Biology

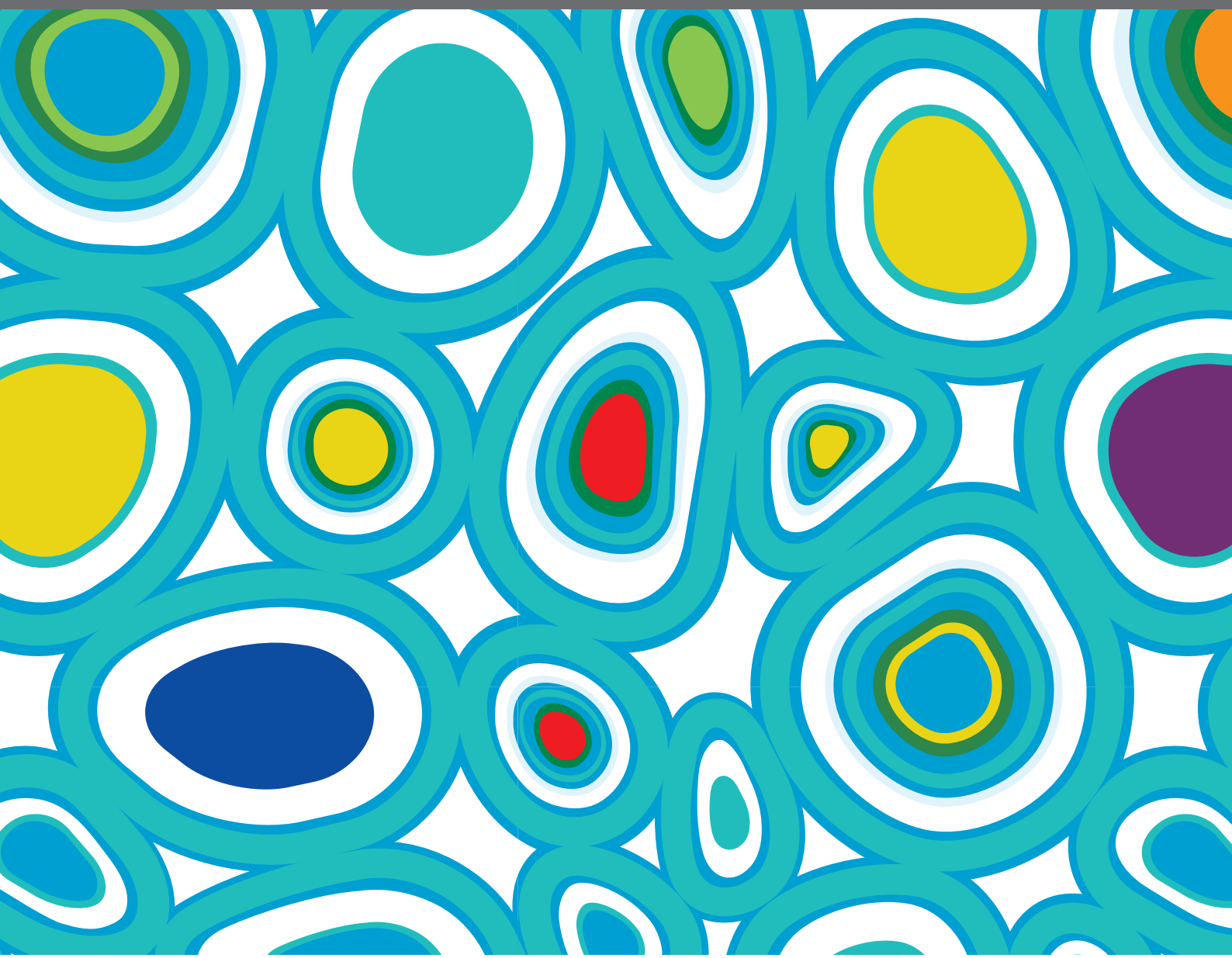

frontiers Research Topics

Frontiers eBook Copyright Statement

The copyright in the text of individual articles in this eBook is the property of their respective authors or their respective institutions or funders. The copyright in graphics and images within each article may be subject to copyright of other parties. In both cases this is subject to a license granted to Frontiers.

The compilation of articles constituting this eBook is the property of Frontiers.

Each article within this eBook, and the eBook itself, are published under the most recent version of the Creative Commons CC-BY licence. The version current at the date of publication of this eBook is CC-BY 4.0. If the CC-BY licence is updated, the licence granted by Frontiers is automatically updated to the new version.

When exercising any right under the CC-BY licence, Frontiers must be attributed as the original publisher of the article or eBook, as applicable.

Authors have the responsibility of ensuring that any graphics or other materials which are the property of others may be included in the CC-BY licence, but this should be checked before relying on the CC-BY licence to reproduce those materials. Any copyright notices relating to those materials must be complied with.

Copyright and source acknowledgement notices may not be removed and must be displayed in any copy, derivative work or partial copy which includes the elements in question.

All copyright, and all rights therein, are protected by national and international copyright laws. The above represents a summary only. For further information please read Frontiers' Conditions for Website Use and Copyright Statement, and the applicable CC-BY licence.

ISSN 1664-8714
ISBN 978-2-88974-102-1
DOI 10.3389/978-2-88974-102-1

About Frontiers

Frontiers is more than just an open-access publisher of scholarly articles: it is a pioneering approach to the world of academia, radically improving the way scholarly research is managed. The grand vision of Frontiers is a world where all people have an equal opportunity to seek, share and generate knowledge. Frontiers provides immediate and permanent online open access to all its publications, but this alone is not enough to realize our grand goals.

Frontiers Journal Series

The Frontiers Journal Series is a multi-tier and interdisciplinary set of open-access, online journals, promising a paradigm shift from the current review, selection and dissemination processes in academic publishing. All Frontiers journals are driven by researchers for researchers; therefore, they constitute a service to the scholarly community. At the same time, the Frontiers Journal Series operates on a revolutionary invention, the tiered publishing system, initially addressing specific communities of scholars, and gradually climbing up to broader public understanding, thus serving the interests of the lay society, too.

Dedication to Quality

Each Frontiers article is a landmark of the highest quality, thanks to genuinely collaborative interactions between authors and review editors, who include some of the world's best academicians. Research must be certified by peers before entering a stream of knowledge that may eventually reach the public - and shape society; therefore, Frontiers only applies the most rigorous and unbiased reviews.
Frontiers revolutionizes research publishing by freely delivering the most outstanding research, evaluated with no bias from both the academic and social point of view. By applying the most advanced information technologies, Frontiers is catapulting scholarly publishing into a new generation.

What are Frontiers Research Topics?

Frontiers Research Topics are very popular trademarks of the Frontiers Journals Series: they are collections of at least ten articles, all centered on a particular subject. With their unique mix of varied contributions from Original Research to Review Articles, Frontiers Research Topics unify the most influential researchers, the latest key findings and historical advances in a hot research area! Find out more on how to host your own Frontiers Research Topic or contribute to one as an author by contacting the Frontiers Editorial Office: frontiersin.org/about/contact

MEIOSIS: FROM MOLECULAR BASIS TO MEDICINE

Topic Editors:
Wei Li, Chinese Academy of Sciences (CAS), China
Liangran Zhang, Shandong University, China
Akira Shinohara, Osaka University, Japan
Scott Keeney, Memorial Sloan Kettering Cancer Center, United States

Citation: Li, W., Zhang, L., Shinohara, A., Keeney, S., eds. (2022). Meiosis: From Molecular Basis to Medicine. Lausanne: Frontiers Media SA.
doi: 10.3389/978-2-88974-102-1

Table of Contents

05 ***Editorial: Meiosis: From Molecular Basis to Medicine***
Wei Li, Liangran Zhang, Akira Shinohara and Scott Keeney

11 ***Tethering of Telomeres to the Nuclear Envelope Is Mediated by SUN1-MAJIN and Possibly Promoted by SPDYA-CDK2 During Meiosis***
Guishuan Wang, Xiaolong Wu, Liwei Zhou, Sheng Gao, Damin Yun, Ajuan Liang and Fei Sun

22 ***SWR1-Independent Association of H2A.Z to the LINC Complex Promotes Meiotic Chromosome Motion***
Sara González-Arranz, Jennifer M. Gardner, Zulin Yu, Neem J. Patel, Jonna Heldrich, Beatriz Santos, Jesús A. Carballo, Sue L. Jaspersen, Andreas Hochwagen and Pedro A. San-Segundo

41 ***Phycocyanin Improves Reproductive Ability in Obese Female Mice by Restoring Ovary and Oocyte Quality***
Xin Wen, Zhe Han, Shu-Jun Liu, Xin Hao, Xiao-Jie Zhang, Xing-Yue Wang, Cheng-Jie Zhou, Yu-Zhen Ma and Cheng-Guang Liang

57 ***Increased Environment-Related Metabolism and Genetic Expression in the* In Vitro *Matured Mouse Oocytes by Transcriptome Analysis***
Hao-Lin Zhang, Yi Xu, Jia-Qian Ju, Zhen-Nan Pan, Jing-Cai Liu and Shao-Chen Sun

67 ***Critical Functions of PP2A-Like Protein Phosphotases in Regulating Meiotic Progression***
Wen-Long Lei, Wei-Ping Qian and Qing-Yuan Sun

73 ***Mechanism and Control of Meiotic DNA Double-Strand Break Formation in* S. cerevisiae**
Vikash Kumar Yadav and Corentin Claeys Bouuaert

93 ***Transcriptomics of Meiosis in the Male Mouse***
Adriana Geisinger, Rosana Rodríguez-Casuriaga and Ricardo Benavente

107 ***Meiotic Recombination Defects and Premature Ovarian Insufficiency***
Chengzi Huang, Ting Guo and Yingying Qin

121 ***Rad9, a 53BP1 Ortholog of Budding Yeast, Is Insensitive to Spo11-Induced Double-Strand Breaks During Meiosis***
Takehiko Usui and Akira Shinohara

136 ***Sycp1 Is Not Required for Subtelomeric DNA Double-Strand Breaks but Is Required for Homologous Alignment in Zebrafish Spermatocytes***
Yukiko Imai, Kenji Saito, Kazumasa Takemoto, Fabien Velilla, Toshihiro Kawasaki, Kei-ichiro Ishiguro and Noriyoshi Sakai

155 ***Dynamic Histone H3 Modifications Regulate Meiosis Initiation via Respiration***
Jian Shi, Yanjie Ma, Hui Hua, Yujiao Liu, Wei Li, Hongxiu Yu and Chao Liu

170 ***Tell the Difference Between Mitosis and Meiosis: Interplay Between Chromosomes, Cytoskeleton, and Cell Cycle Regulation***
Masamitsu Sato, Yasutaka Kakui and Mika Toya

190 ***Phospho-Regulation of Meiotic Prophase***
Funda M. Kar and Andreas Hochwagen

213 ***BRCA1 and BRCA2 Tumor Suppressor Function in Meiosis***
Qianyan Li and JoAnne Engebrecht

227 ***Sexual Dimorphism in Mouse Meiosis***
Rong Hua and Mingxi Liu

236 ***Podophyllotoxin Exposure Affects Organelle Distribution and Functions in Mouse Oocyte Meiosis***
Ping-Shuang Lu, Lan-Ping Xie, Xiao-Han Kong, Yi Xu and Shao-Chen Sun

246 ***PRMT5 Is Involved in Spermatogonial Stem Cells Maintenance by Regulating* Plzf *Expression via Modulation of Lysine Histone Modifications***
Fangfang Dong, Min Chen, Min Chen, Lin Jiang, Zhiming Shen, Longfei Ma, Chunsheng Han, Xudong Guo and Fei Gao

260 ***High Resolution View on the Regulation of Recombinase Accumulation in Mammalian Meiosis***
Aditya N. Mhaskar, Lieke Koornneef, Alex N. Zelensky, Adriaan B. Houtsmuller and Willy M. Baarends

270 ***Echinoderm Microtubule Associated Protein Like 1 Is Indispensable for Oocyte Spindle Assembly and Meiotic Progression in Mice***
Hong Yin, Teng Zhang, Hao Wang, Xin Hu, Xuan Hou, Xianbao Fang, Yaoxue Yin, Hui Li, Lanying Shi and You-Qiang Su,

290 ***Chromosome Organization in Early Meiotic Prophase***
Corinne Grey and Bernard de Massy

310 ***RNAi-Related Dicer and Argonaute Proteins Play Critical Roles for Meiocyte Formation, Chromosome-Axes Lengths and Crossover Patterning in the Fungus* Sordaria macrospora**
Chloe Girard, Karine Budin, Stéphanie Boisnard, Liangran Zhang, Robert Debuchy, Denise Zickler and Eric Espagne

326 ***Knockout Gene-Based Evidence for PIWI-Interacting RNA Pathway in Mammals***
Yinuo Li, Yue Zhang and Mingxi Liu

337 ***Meiotic Crossover Patterning***
Nila M. Pazhayam, Carolyn A. Turcotte and Jeff Sekelsky

357 ***MeiosisOnline: A Manually Curated Database for Tracking and Predicting Genes Associated With Meiosis***
Xiaohua Jiang, Daren Zhao, Asim Ali, Bo Xu, Wei Liu, Jie Wen, Huan Zhang, Qinghua Shi and Yuanwei Zhang

364 ***A Hypothesis: Linking Phase Separation to Meiotic Sex Chromosome Inactivation and Sex-Body Formation***
Yiding Xu and Huanyu Qiao

378 ***The Application of Single-Cell RNA Sequencing in Mammalian Meiosis Studies***
Yiheng Peng and Huanyu Qiao

391 ***Cataloging Human* PRDM9 *Allelic Variation Using Long-Read Sequencing Reveals* PRDM9 *Population Specificity and Two Distinct Groupings of Related Alleles***
Benjamin Alleva, Kevin Brick, Florencia Pratto, Mini Huang and Rafael Daniel Camerini-Otero

411 ***High Temporal Resolution 3D Live-Cell Imaging of Budding Yeast Meiosis Defines Discontinuous Actin/Telomere-Mediated Chromosome Motion, Correlated Nuclear Envelope Deformation and Actin Filament Dynamics***
Tadasu Nozaki, Frederick Chang, Beth Weiner and Nancy Kleckner

frontiers in Cell and Developmental Biology

EDITORIAL
published: 01 December 2021
doi: 10.3389/fcell.2021.812292

Editorial: Meiosis: From Molecular Basis to Medicine

Wei Li[1,2]*, *Liangran Zhang*[3]*, *Akira Shinohara*[4]* and *Scott Keeney*[5]*

[1]Guangzhou Women and Children's Medical Center, Guangzhou Medical University, Guangzhou, China, [2]State Key Laboratory of Stem Cell and Reproductive Biology, Institute of Zoology, Chinese Academy of Sciences (CAS), Beijing, China, [3]Advanced Medical Research Institute, Shandong University, Jinan, China, [4]Institute for Protein Research, Osaka University, Suita, Japan, [5]Molecular Biology Program, Memorial Sloan Kettering Cancer Center, Howard Hughes Medical Institute, New York, NY, United States

Keywords: infertility, chromosome organization, chromosome movement, transcriptional regulation, post-translational modifications

Editorial on the Research Topic

Meiosis: From Molecular Basis to MedicineComments

INTRODUCTION

OPEN ACCESS

Edited and reviewed by:
Philipp Kaldis,
Lund University, Sweden

***Correspondence:**
Wei Li
leways@ioz.ac.cn
Liangran Zhang
zhangliangran@sdu.edu.cn
Akira Shinohara
ashino@protein.osaka-u.ac.jp
Scott Keeney
s-keeney@ski.mskcc.org

Specialty section:
This article was submitted to Cell Growth and Division, a section of the journal Frontiers in Cell and Developmental Biology

Received: *10 November 2021*
Accepted: *11 November 2021*
Published: *01 December 2021*

Citation:
Li W, Zhang L, Shinohara A and Keeney S (2021) Editorial: Meiosis: From Molecular Basis to Medicine. Front. Cell Dev. Biol. 9:812292. doi: 10.3389/fcell.2021.812292

Meiosis is a specialized cell division process in eukaryotes that produces haploid gametes from diploid cells by a single round of DNA replication followed with two successive rounds of chromosome segregation (meiosis I and meiosis II). Different from mitosis, meiosis has a prolonged prophase I characterized by many unique features including the formation of numerous programmed DNA double-strand breaks (DSBs) throughout the genome, most of which are repaired by recombination using the homologous chromosomes as templates. Meiotic recombination promotes the two-by-two pairing of homologous chromosomes and also disrupts the linkage relationships between segments of DNA along individual chromosomes to generate new combinations of alleles in offspring. Meanwhile, drastic chromatin remodeling and chromosome movements are needed to complete these processes, and these events are regulated at both transcriptional and posttranslational levels.

These processes ensure fertility, generate natural variation in populations, and provide the mechanistic basis for the rules of inheritance. Defects in meiosis are responsible for primary sterility, miscarriage, and congenital disorders. Thus, understanding the fundamental mechanisms underlying meiosis is not only very important to diagnosis of infertility and prevention of chromosomal birth defects, but also essential to the development of new strategies for improving animal breeding and crop production.

The 28 articles in this collection address many of the critical aspects of meiosis. They can be divided roughly into five categories: Chromosome Organization, Chromosome Movement, Transcription Regulation, Post-translational Modifications, and Diseases Related to Meiotic Defects.

Overview

Thousands of genes have been reported to be involved in meiosis. A research article by Jiang et al. in this Research Topic developed "MeiosisOnline", a publicly accessible, comprehensive database of known functional genes and potential candidates in meiosis (https://mcg.ustc.edu.cn/bsc/meiosis/index.html). A total of 2,052 genes were manually curated from literature resources and were classified into different categories. This resource provides updated and detailed information about both experimentally verified and predicted genes in meiosis (Jiang et al.).

While most meiotic processes occur similarly during gametogenesis in male and female mammals, significant differences have also been observed, a phenomenon known as sexual dimorphism in mammalian meiosis (Hunt and Hassold, 2002). There are substantial sex-specific differences within species with respect to meiosis-related chromatin reorganization, recombination, and tolerance for meiotic defects. A review by Hua and Liu in this Research Topic provided a comprehensive overview of genetically engineered mice that have been employed to study meiosis, with a particular focus on gene- and gametogenesis-related sexual dimorphism observed in these model animals.

Chromosome Organization

A series of crucial events takes place during meiotic prophase I, including the formation and repair of DSBs, and the pairing, synapsis, and recombination between homologous chromosomes (Zickler and Kleckner, 1999; Handel and Schimenti, 2010). Meiotic DSB formation is catalyzed by the meiosis-specific transesterase SPO11 (Keeney et al., 1997; Milman et al., 2009), which is widely conserved across eukaryotic lineages (Hartung and Puchta, 2000). A review by Yadav and Claeys Bouuaert in this Research Topic described the mechanism of meiotic DSB formation and regulatory pathways in light of recent models. SPO11 has a DNA-binding domain but is not sequence-specific and requires the assistance of several other factors to induce programmed DSB production (Borde and de Massy, 2013). In mammalian cells, PRDM9, a protein with methyltransferase activity, is widely regarded as one of the most important regulators in this process (Baudat et al., 2010; Myers et al., 2010). Using a long-read sequencing approach, Alleva et al. expanded the catalog of known sequence variants within the *PRDM9* gene in human populations, and by mapping meiotic DSBs in testis, they found that small variations in PRDM9 can substantially alter the meiotic recombination landscape. These results demonstrated that minor PRDM9 variants may play an under-appreciated role in shaping patterns of human recombination (Alleva et al.).

After programmed DSB formation, single-stranded DNA near the programmed DSB site is covered by the RPA complex (RPA1/2/3) to protect it from DNA nuclease degradation, and the RPA-bound single strand is recognized by ATR (Harrison and Haber, 2006; Lovejoy and Cortez, 2009). ATM and ATR, as DNA damage-responsive kinases, can phosphorylate downstream effector kinases such as CHK1 and CHK2 (RAD53), thus playing an important role in DSB repair and homologous recombination during the prophase I (Subramanian and Hochwagen, 2014). A research article by Usui and Shinohara in this Research Topic examined how meiotic *Saccharomyces cerevisiae* cells activate Rad53 in response to exogenous DSBs and showed that this activation is dependent on an epigenetic mark, Dot1-dependent histone H3 lysine 79 methylation. This methylation becomes a scaffold for a Rad53 mediator, Rad9, which is an ortholog of mammalian 53BP1 (Usui and Shinohara). Interestingly, Rad9 is specific for exogenous damage, and is insensitive to meiotic DSBs. As an intermediate factor in DSB repair, BRCA1 can also be phosphorylated by ATM and ATR (Caestecker and Van de Walle, 2013), thereby activating the recruitment of BRCA2. BRCA2 and BRCA1 further promote recruitment of RAD51 (Scully et al., 1997; Lord and Ashworth, 2007) and DMC1 (Sharan et al., 2004; Martinez et al., 2016). A review by Li and Engebrecht summarizes work from mice and worms that has shed light on the role of BRCA1 and BRCA2 in meiosis.

Meiotic crossovers are formed via repair of DSBs. The proper number and placement of crossovers are vital to chromosome segregation (Mets and Meyer, 2009). A review by Pazhayam et al. in this Research Topic discussed the history of studies of crossover patterning, developments in the methods used in the field, and the current understanding of the interplay between patterning phenomena.

During meiosis, homologous chromosomes become juxtaposed along their lengths, stabilized by a proteinaceous scaffold known as the synaptonemal complex, consisting of a linear axial element for each homolog bridged by central region proteins (Moses, 1956; Page and Hawley, 2004; Costa et al., 2005; Bolcun-Filas et al., 2009; Schramm et al., 2011). A review by Grey and de Massy in this Research Topic summarized the different actors involved in axial element formation in *Saccharomyces cerevisiae* and mice. They also described the current knowledge of their localization patterns during prophase I, their functional interdependence, their roles in sister chromatid cohesion, formation of higher order loop-axis structure, homolog pairing before meiotic recombination, and recombination (Grey and de Massy). In human and zebrafish spermatocytes, homologous recombination and assembly of the synaptonemal complex initiate predominantly near telomeres (Saito et al., 2013; Pratto et al., 2014). A research article by Imai et al. in this Research Topic demonstrated that *Sycp1* is not required for peri-telomeric DSB formation but is necessary for the complete pairing of homologs during zebrafish meiosis.

In most mammals, chromosomal segments that do not form synaptonemal complex (for example, if there is no homolog present) undergo a transcriptional silencing process called meiotic silencing of unpaired chromatin (MSUC) (Turner, 2015). Meiotic sex chromosome inactivation (MSCI) is the process by which nonhomologous portions of the X and Y chromosomes of male mammals undergo MSUC during meiotic prophase I of spermatogenesis. MSCI is accompanied by formation of a special nuclear territory known as the sex body or XY body. A paper by Xu and Qiao in this Research Topic summarized recent publications on the mechanisms of MSCI and of liquid-liquid phase separation (LLPS), hypothesized a potential link between LLPS and the formation of sex bodies, and discussed the implications for future research.

Chromosome Movement

Dramatic chromosome movements occur during meiotic prophase I in all organisms where this has been evaluated to date (Zickler and Kleckner, 1999; Petronczki et al., 2003; Alleva and Smolikove, 2017). These movements are driven by the attachment of telomeres through the nuclear envelope (NE) to cytoplasmic force-generating cytoskeleton structures via the LINC (linker of nucleoskeleton and cytoskeleton) complex

(Crisp et al., 2006). In mouse, this involves LINC complex components SUN1, SUN2, KASH5, and telomeric adaptor proteins like TERB1, TERB2, MAJIN, SPDYA, and TRF1 (Tapley and Starr, 2013; Wang et al., 2018). Three articles in this Research Topic address this subject. A research article by Wang et al. found that SUN1 not only interacts with TERB1 but also more strongly with MAJIN. They also found that SUN1 interacts with SPDYA, an activator of CDK2. These findings provide the possible mechanism of SUN1, MAJIN, and SPDYA-CDK2 in promoting the telomere-NE attachment during meiosis (Wang et al.). Another research article in this Research Topic by González-Arranz et al. reveals that H2A.Z, a variant of the canonical H2A histone, is an additional LINC-associated factor that contributes to telomere-driven chromosome motion critical for error-free gametogenesis. Nozaki et al. developed a technique combining fluorescent repressor operator system (FROS) labeling with three-dimensional (3D) live-cell imaging at a high temporal resolution to define the detailed kinetics of mid-meiotic prophase I motion for a single telomere-proximal locus in budding yeast.

Accurate chromosome segregation during the two meiotic divisions relies on the attachments between spindle microtubules and kinetochores, multiprotein complexes that assemble on centromeres (McKim and Hawley, 1995). A review by Sato et al. in this Research Topic focuses on lessons from recent advancement in genetic and cytological studies of the fission yeast *Schizosaccharomyces pombe*. They discuss how chromosomes, the cytoskeleton, and cell cycle progression are organized and particularly how these differ in mitosis and meiosis.

In oocytes of many species, the assembly and organization of a specialized acentriolar spindle require the aid of multiple microtubule organizing centers (MTOCs), which contain essential pericentriolar materials (Mullen et al., 2019). A research article by Yin et al. reports that echinoderm microtubule-associated protein (EMAP)-like 1 (EML1), a member of the conserved EMAP family proteins, regulates acentriolar spindle formation and the progression to meiosis II in mammalian oocytes.

Transcriptional Regulation of Meiosis

Unique transcription regulation is involved in the complex and highly organized events during meiosis. Technical advances in recent years, from the improvement of flow cytometry (FCM) to single-cell RNA-seq (scRNA-seq) approaches, allow accurate identification of cell heterogeneities and investigation of meiotic transcriptomes at a higher temporal resolution (Tang et al., 2009; Geisinger and Rodríguez-Casuriaga, 2017; Green et al., 2018).

Two articles in this Research Topic address this subject. A review by Geisinger et al. focuses on murine male meiosis and outlines the diversity of approaches and methodologies, shedding light on the transcriptomic landscape of the complex meiotic process. Particularly, they center on the controversy about gene expression during early meiotic prophase; the widespread existing gap between transcription and translation in meiotic cells; the expression patterns and potential roles of meiotic long noncoding RNAs; and the visualization of meiotic sex chromosome inactivation from the RNA-seq perspective (Geisinger et al.). Another review by Peng and Qiao compared bulk RNA-seq and scRNA-seq to show the advantages of scRNA-seq in meiosis studies. They also summarized scRNA-seq analysis methods and meiotic marker genes from spermatocytes and oocytes. Specifically, they emphasized the different features of two scRNA-seq protocols (Smart-seq2 and Drop-seq) in the context of meiosis studies and discussed their relative strengths and weaknesses.

Meiotic cells have complex transcriptomes, in that they express multiple mRNAs, long non-coding RNAs (lncRNAs), and small non-coding RNAs (sncRNAs) such as microRNAs (miRNAs) and PIWI-interacting RNAs (piRNAs) (Soumillon et al., 2013). These different classes of RNAs play important roles in meiosis and spermiogenesis (Goh et al., 2015; Perez and Lehner, 2019; Dai et al., 2020; Guo et al., 2020). A review by Li et al. in this Research Topic focuses on the current knowledge derived from studies of genetically engineered mouse mutants and summarizes pathways for the biogenesis and function of piRNAs.

RNA interference (RNAi) is an evolutionarily conserved cellular process involving double-stranded RNA (dsRNA) and regulating complementary RNA transcripts (Hannon, 2002). Dicer and Argonaute (Ago) are key proteins involved in this pathway (Carmell et al., 2002; Förstemann et al., 2007). Many studies have demonstrated that RNAi components play essential roles in meiotic processes including DNA repair and chromosome segregation (Burger and Gullerova, 2015; Gutbrod and Martienssen, 2020). A research article in this Research Topic by Girard et al. shows that in the filamentous Ascomycete *Sordaria macrospora*, genes encoding the two Dicer (Dcl1 and Dcl2) and two Argonaute (Sms2 and Qde2) proteins play critical roles for meiocyte formation, chromosome axis lengths, and crossover patterning.

Regulation of Meiosis by Post-Translational Modifications

The acetylation and methylation of histones, as well as the phosphorylation, SUMOylation, and ubiquitination of other protein factors, play important roles during meiosis in the programmed formation and repair of DSBs, the pairing of homologous chromosomes, and the formation of crossovers (Zentner and Henikoff, 2013).

Histone acetylation was the first histone modification discovered to regulate gene transcription by fine-tuning chromatin accessibility (Lee et al., 1993). Histone acetyltransferases (HATs) and histone deacetylases (HDACs) are the main enzymes responsible for lysine acetylation and deacetylation of histones (Legube and Trouche, 2003; Wang et al., 2017). Histone acetylation has an important effect on the meiosis during spermatogenesis and oogenesis (Getun et al., 2017). A research article by Shi et al. in this Research Topic finds that the absence of histone H3 lysine 18 acetylation (H3K18ac) in *S. cerevisiae* impairs respiration, leading to reduced levels of Rim101 protein, which further upregulates Smp1 (a negative

regulator of *IME1* transcription) and blocks the initiation of meiosis.

Histone methylation is perhaps the most well-studied histone modification, and it most frequently occurs on lysine and arginine residues of histones H3 and H4 (Zhang and Reinberg, 2001; Kouzarides, 2002). Methylation of lysine residues is catalyzed by HMTs (histone methyltransferases), including the SET-domain-containing protein family and the non-SET-domain proteins Dot1/DOT1L. Methylation of H3K4, H3K36, and H3K79 is associated with gene activation, whereas methylation of H3K9, H3K27, and H4K20 is generally thought to be involved in gene repression (Martin and Zhang, 2005). A research article by Dong et al. in this Research Topic demonstrates that PRMT5 regulates mouse spermatogonial stem cell development by modulating histone H3 lysine modifications.

Protein phosphorylation, which reversibly occurs mainly on serine, threonine, or tyrosine residues, is another well-studied post-translational modifications. Two articles in this Research Topic address this subject. A review by Kar and Hochwagen discussed common principles and provided detailed examples of how phosphorylation events are employed to ensure faithful passage of chromosomes from one generation to the next. Furthermore, a review by Lei et al. discussed recent discoveries and explored the role of PP2A-like protein, which regulates the dynamic equilibrium of protein phosphorylation and dephosphorylation during meiotic progression.

Diseases Related to Meiotic Defects

Primary ovarian insufficiency (POI) is defined as ovarian follicle depletion or dysfunction before the age of 40. The etiology of POI is heterogeneous. Genetic defects, including monogenic mutations and chromosomal abnormalities (Qin et al., 2015; Jiao et al., 2017), found in approximately 20–25% of POI patients, are considered to be one of the main causes of POI, (Welt, 2008; Nelson, 2009). The review by Huang et al. focused on genes participating in meiotic homologous recombination and categorized the individual gene mutations identified in POI patients and the potential candidate genes for POI pathogenesis.

Xenobiotics, such as medicines and environmental chemicals, have a broad influence on the development of oocytes (Mark-Kappeler et al., 2011; Bhattacharya and Keating, 2012). Podophyllotoxin (POD) is a well characterized lignan, derivatives of which are widely used in clinical treatment due to their strong antitumor and antivirus activities (Ardalani et al., 2017; Zálešák et al., 2019). Exposure to POD can inhibit microtubule dynamics and lead to abnormal meiotic spindle formation, which influences oocyte development and maturation (Hu et al., 2018; Jiang et al., 2020). A research article in this Research Topic by Lu et al. illustrated that exposure to POD might disrupt protein synthesis, transport, degradation, and ATP production through its effects on the distribution and functions of organelles during mouse oocyte meiotic maturation.

Obesity can reduce ovarian and oocyte quality (e.g., spindle defects and chromosome misalignment) and ultimately impinge on female fertility. In addition, maternal obesity increases the level of oxidative stress in the ovarian environment (Silvestris et al., 2018; Igosheva et al., 2010; Jungheim et al., 2010). A research article in this Research Topic by Wen et al. reported that phycocyanin could recover the abnormal morphology of the spindle and reduce the accumulation of oxidative stress in oocytes. They further found that phycocyanin improves fertility by partially increasing ovarian and oocyte quality in obese female mice, providing a new potential strategy for clinically treating obesity-related infertility in women (Wen et al.).

In vitro maturation and other assisted reproductive technologies have been widely applied in the clinic in reproductive medicine centers to address the high rate of infertility worldwide (Cha and Chian, 1998; De Geyter, 2019). A research article in this Research Topic by Zhang et al. compared the global RNA transcription pattern of mouse oocytes from *in vitro* and *in vivo* maturation. They found that *in vitro* maturation resulted in metabolism and gene expression changes by environmental changes compared with *in vivo* matured oocytes.

CONCLUSION

Over the past several years, significant progress has been made in understanding the biological functions and key events of meiosis. Despite these advances described above, many aspects of the biological processes remain poorly understood. Therefore, more comprehensive studies are required to further identify the molecular mechanisms of complex events that occur during meiosis, including regulation of the formation of programmed meiotic DSBs as well as the pairing, synapsis, recombination, and segregation of homologous chromosomes. We need to better understand chromosome interactions and chromosome movements, relying on continuing advancements in novel technologies and methods. Identification of the molecular basis of dynamic transcriptional regulation and protein post-translational modifications in meiosis remains a crucial endeavor. Understanding molecular mechanisms of meiosis could guide future research that is applied for the diagnosis and clinical treatment of infertility related to meiotic defects, and improve the health of our offspring.

AUTHOR CONTRIBUTIONS

All authors listed have made a substantial, direct, and intellectual contribution to the work, and approved it for publication.

FUNDING

This work was supported by the National Science Fund for Distinguished Young Scholars (81925015 to WL). The Keeney lab is supported by funding from the Howard Hughes Medical Institute, US National Institutes of Health grant R35 GM118092, and US National Cancer Institute cancer center support grant P30 CA08748.

REFERENCES

Alleva, B., and Smolikove, S. (2017). Moving and Stopping: Regulation of Chromosome Movement to Promote Meiotic Chromosome Pairing and Synapsis. *Nucleus* 8 (6), 613–624. doi:10.1080/19491034.2017.1358329

Ardalani, H., Avan, A., and Ghayour-Mobarhan, M. (2017). Podophyllotoxin: a Novel Potential Natural Anticancer Agent. *Avicenna J. Phytomed* 7 (4), 285–294.

Baudat, F., Buard, J., Grey, C., Fledel-Alon, A., Ober, C., Przeworski, M., et al. (2010). PRDM9 Is a Major Determinant of Meiotic Recombination Hotspots in Humans and Mice. *Science* 327 (5967), 836–840. doi:10.1126/science.1183439

Bhattacharya, P., and Keating, A. F. (2012). Impact of Environmental Exposures on Ovarian Function and Role of Xenobiotic Metabolism during Ovotoxicity. *Toxicol. Appl. Pharmacol.* 261 (3), 227–235. doi:10.1016/j.taap.2012.04.009

Bolcun-Filas, E., Speed, R., Taggart, M., Grey, C., de Massy, B., Benavente, R., et al. (2009). Mutation of the Mouse Syce1 Gene Disrupts Synapsis and Suggests a Link between Synaptonemal Complex Structural Components and DNA Repair. *Plos Genet.* 5 (2), e1000393. doi:10.1371/journal.pgen.1000393

Borde, V., and de Massy, B. (2013). Programmed Induction of DNA Double Strand Breaks during Meiosis: Setting up Communication between DNA and the Chromosome Structure. *Curr. Opin. Genet. Develop.* 23 (2), 147–155. doi:10.1016/j.gde.2012.12.002

Burger, K., and Gullerova, M. (2015). Swiss Army Knives: Non-canonical Functions of Nuclear Drosha and Dicer. *Nat. Rev. Mol. Cel Biol* 16 (7), 417–430. doi:10.1038/nrm3994

Caestecker, K. W., and Van de Walle, G. R. (2013). The Role of BRCA1 in DNA Double-Strand Repair: Past and Present. *Exp. Cel Res.* 319 (5), 575–587. doi:10.1016/j.yexcr.2012.11.013

Carmell, M. A., Xuan, Z., Zhang, M. Q., and Hannon, G. J. (2002). The Argonaute Family: Tentacles that Reach into RNAi, Developmental Control, Stem Cell Maintenance, and Tumorigenesis. *Genes Dev.* 16 (21), 2733–2742. doi:10.1101/gad.1026102

Cha, K.-Y., and Chian, R. C. (1998). Maturation *In Vitro* of Immature Human Oocytes for Clinical Use. *Hum. Reprod. Update* 4 (2), 103–120. doi:10.1093/humupd/4.2.103

Costa, Y., Speed, R., Öllinger, R., Alsheimer, M., Semple, C. A., Gautier, P., et al. (2005). Two Novel Proteins Recruited by Synaptonemal Complex Protein 1 (SYCP1) Are at the centre of Meiosis. *J. Cel Sci* 118 (Pt 12), 2755–2762. doi:10.1242/jcs.02402

Crisp, M., Liu, Q., Roux, K., Rattner, J. B., Shanahan, C., Burke, B., et al. (2006). Coupling of the Nucleus and Cytoplasm: Role of the LINC Complex. *J. Cel Biol* 172 (1), 41–53. doi:10.1083/jcb.200509124

Dai, P., Wang, X., and Liu, M.-F. (2020). A Dual Role of the PIWI/piRNA Machinery in Regulating mRNAs during Mouse Spermiogenesis. *Sci. China Life Sci.* 63 (3), 447–449. doi:10.1007/s11427-020-1632-5

De Geyter, C. (2019). Assisted Reproductive Technology: Impact on Society and Need for Surveillance. *Best Pract. Res. Clin. Endocrinol. Metab.* 33 (1), 3–8. doi:10.1016/j.beem.2019.01.004

Förstemann, K., Horwich, M. D., Wee, L., Tomari, Y., and Zamore, P. D. (2007). Drosophila microRNAs Are Sorted into Functionally Distinct Argonaute Complexes after Production by Dicer-1. *Cell* 130 (2), 287–297. doi:10.1016/j.cell.2007.05.056

Geisinger, A., and Rodríguez-Casuriaga, R. (2017). Flow Cytometry for the Isolation and Characterization of Rodent Meiocytes. *Methods Mol. Biol.* 1471, 217–230. doi:10.1007/978-1-4939-6340-9_11

Getun, I. V., Wu, Z., Fallahi, M., Ouizem, S., Liu, Q., Li, W., et al. (2017). Functional Roles of Acetylated Histone Marks at Mouse Meiotic Recombination Hot Spots. *Mol. Cel Biol* 37 (3), e00942–e01015. doi:10.1128/mcb.00942-15

Goh, W. S. S., Falciatori, I., Tam, O. H., Burgess, R., Meikar, O., Kotaja, N., et al. (2015). piRNA-Directed Cleavage of Meiotic Transcripts Regulates Spermatogenesis. *Genes Dev.* 29 (10), 1032–1044. doi:10.1101/gad.260455.115

Green, C. D., Ma, Q., Manske, G. L., Shami, A. N., Zheng, X., Marini, S., et al. (2018). A Comprehensive Roadmap of Murine Spermatogenesis Defined by Single-Cell RNA-Seq. *Develop. Cel* 46 (5), 651–667.e610. doi:10.1016/j.devcel.2018.07.025

Guo, J., Nie, X., Giebler, M., Mlcochova, H., Wang, Y., Grow, E. J., et al. (2020). The Dynamic Transcriptional Cell Atlas of Testis Development during Human Puberty. *Cell Stem Cell* 26 (2), 262–276.e264. doi:10.1016/j.stem.2019.12.005

Gutbrod, M. J., and Martienssen, R. A. (2020). Conserved Chromosomal Functions of RNA Interference. *Nat. Rev. Genet.* 21 (5), 311–331. doi:10.1038/s41576-019-0203-6

Handel, M. A., and Schimenti, J. C. (2010). Genetics of Mammalian Meiosis: Regulation, Dynamics and Impact on Fertility. *Nat. Rev. Genet.* 11 (2), 124–136. doi:10.1038/nrg2723

Harrison, J. C., and Haber, J. E. (2006). Surviving the Breakup: the DNA Damage Checkpoint. *Annu. Rev. Genet.* 40, 209–235. doi:10.1146/annurev.genet.40.051206.105231

Hartung, F., and Puchta, H. (2000). Molecular Characterisation of Two Paralogous SPO11 Homologues in *Arabidopsis thaliana*. *Nucleic Acids Res.* 28 (7), 1548–1554. doi:10.1093/nar/28.7.1548

Hu, L.-L., Zhou, X., Zhang, H.-L., Wu, L.-L., Tang, L.-S., Chen, L.-L., et al. (2018). Exposure to Podophyllotoxin Inhibits Oocyte Meiosis by Disturbing Meiotic Spindle Formation. *Sci. Rep.* 8 (1), 10145. doi:10.1038/s41598-018-28544-1

Hunt, P. A., and Hassold, T. J. (2002). Sex Matters in Meiosis. *Science* 296 (5576), 2181–2183. doi:10.1126/science.1071907

Igosheva, N., Abramov, A. Y., Poston, L., Eckert, J. J., Fleming, T. P., Duchen, M. R., et al. (2010). Maternal Diet-Induced Obesity Alters Mitochondrial Activity and Redox Status in Mouse Oocytes and Zygotes. *PLoS One* 5 (4), e10074. doi:10.1371/journal.pone.0010074

Jiang, W.-J., Hu, L.-L., Ren, Y.-P., Lu, X., Luo, X.-Q., Li, Y.-H., et al. (2020). Podophyllotoxin Affects Porcine Oocyte Maturation by Inducing Oxidative Stress-Mediated Early Apoptosis. *Toxicon* 176, 15–20. doi:10.1016/j.toxicon.2020.01.006

Jiao, X., Zhang, H., Ke, H., Zhang, J., Cheng, L., Liu, Y., et al. (2017). Premature Ovarian Insufficiency: Phenotypic Characterization within Different Etiologies. *J. Clin. Endocrinol. Metab.* 102 (7), 2281–2290. doi:10.1210/jc.2016-3960

Jungheim, E. S., Schoeller, E. L., Marquard, K. L., Louden, E. D., Schaffer, J. E., and Moley, K. H. (2010). Diet-induced Obesity Model: Abnormal Oocytes and Persistent Growth Abnormalities in the Offspring. *Endocrinology* 151 (8), 4039–4046. doi:10.1210/en.2010-0098

Keeney, S., Giroux, C. N., and Kleckner, N. (1997). Meiosis-specific DNA Double-Strand Breaks Are Catalyzed by Spo11, a Member of a Widely Conserved Protein Family. *Cell* 88 (3), 375–384. doi:10.1016/s0092-8674(00)81876-0

Kouzarides, T. (2002). Histone Methylation in Transcriptional Control. *Curr. Opin. Genet. Develop.* 12 (2), 198–209. doi:10.1016/s0959-437x(02)00287-3

Lee, D. Y., Hayes, J. J., Pruss, D., and Wolffe, A. P. (1993). A Positive Role for Histone Acetylation in Transcription Factor Access to Nucleosomal DNA. *Cell* 72 (1), 73–84. doi:10.1016/0092-8674(93)90051-q

Legube, G., and Trouche, D. (2003). Regulating Histone Acetyltransferases and Deacetylases. *EMBO Rep.* 4 (10), 944–947. doi:10.1038/sj.embor.embor941

Lord, C. J., and Ashworth, A. (2007). RAD51, BRCA2 and DNA Repair: a Partial Resolution. *Nat. Struct. Mol. Biol.* 14 (6), 461–462. doi:10.1038/nsmb0607-461

Lovejoy, C. A., and Cortez, D. (2009). Common Mechanisms of PIKK Regulation. *DNA Repair* 8 (9), 1004–1008. doi:10.1016/j.dnarep.2009.04.006

Mark-Kappeler, C. J., Hoyer, P. B., and Devine, P. J. (2011). Xenobiotic Effects on Ovarian Preantral Follicles1. *Biol. Reprod.* 85 (5), 871–883. doi:10.1095/biolreprod.111.091173

Martin, C., and Zhang, Y. (2005). The Diverse Functions of Histone Lysine Methylation. *Nat. Rev. Mol. Cel Biol* 6 (11), 838–849. doi:10.1038/nrm1761

Martinez, J. S., von Nicolai, C., Kim, T., Ehlén, Å., Mazin, A. V., Kowalczykowski, S. C., et al. (2016). BRCA2 Regulates DMC1-Mediated Recombination through the BRC Repeats. *Proc. Natl. Acad. Sci. USA* 113 (13), 3515–3520. doi:10.1073/pnas.1601691113

McKim, K. S., and Hawley, R. S. (1995). Chromosomal Control of Meiotic Cell Division. *Science* 270 (5242), 1595–1601. doi:10.1126/science.270.5242.1595

Mets, D. G., and Meyer, B. J. (2009). Condensins Regulate Meiotic DNA Break Distribution, Thus Crossover Frequency, by Controlling Chromosome Structure. *Cell* 139 (1), 73–86. doi:10.1016/j.cell.2009.07.035

Milman, N., Higuchi, E., and Smith, G. R. (2009). Meiotic DNA Double-Strand Break Repair Requires Two Nucleases, MRN and Ctp1, to Produce a Single Size Class of Rec12 (Spo11)-Oligonucleotide Complexes. *Mol. Cel Biol* 29 (22), 5998–6005. doi:10.1128/mcb.01127-09

Moses, M. J. (1956). Chromosomal Structures in Crayfish Spermatocytes. *J. Biophys. Biochem. Cytol.* 2 (2), 215–218. doi:10.1083/jcb.2.2.215

Mullen, T. J., Davis-Roca, A. C., and Wignall, S. M. (2019). Spindle Assembly and Chromosome Dynamics during Oocyte Meiosis. *Curr. Opin. Cel Biol.* 60, 53–59. doi:10.1016/j.ceb.2019.03.014

Myers, S., Bowden, R., Tumian, A., Bontrop, R. E., Freeman, C., MacFie, T. S., et al. (2010). Drive against Hotspot Motifs in Primates Implicates the PRDM9 Gene in Meiotic Recombination. *Science* 327 (5967), 876–879. doi:10.1126/science.1182363

Nelson, L. M. (2009). Primary Ovarian Insufficiency. *N. Engl. J. Med.* 360 (6), 606–614. doi:10.1056/NEJMcp0808697

Page, S. L., and Hawley, R. S. (2004). The Genetics and Molecular Biology of the Synaptonemal Complex. *Annu. Rev. Cel Dev. Biol.* 20, 525–558. doi:10.1146/annurev.cellbio.19.111301.155141

Perez, M. F., and Lehner, B. (2019). Intergenerational and Transgenerational Epigenetic Inheritance in Animals. *Nat. Cel Biol* 21 (2), 143–151. doi:10.1038/s41556-018-0242-9

Petronczki, M., Siomos, M. F., and Nasmyth, K. (2003). Un Ménage à Quatre. *Cell* 112 (4), 423–440. doi:10.1016/s0092-8674(03)00083-7

Pratto, F., Brick, K., Khil, P., Smagulova, F., Petukhova, G. V., and Camerini-Otero, R. D. (2014). Recombination Initiation Maps of Individual Human Genomes. *Science* 346 (6211), 1256442. doi:10.1126/science.1256442

Qin, Y., Jiao, X., Simpson, J. L., and Chen, Z.-J. (2015). Genetics of Primary Ovarian Insufficiency: New Developments and Opportunities. *Hum. Reprod. Update* 21 (6), 787–808. doi:10.1093/humupd/dmv036

Saito, T. T., Lui, D. Y., Kim, H.-M., Meyer, K., and Colaiácovo, M. P. (2013). Interplay between Structure-specific Endonucleases for Crossover Control during *Caenorhabditis elegans* Meiosis. *Plos Genet.* 9 (7), e1003586. doi:10.1371/journal.pgen.1003586

Schramm, S., Fraune, J., Naumann, R., Hernandez-Hernandez, A., Höög, C., Cooke, H. J., et al. (2011). A Novel Mouse Synaptonemal Complex Protein Is Essential for Loading of central Element Proteins, Recombination, and Fertility. *Plos Genet.* 7 (5), e1002088. doi:10.1371/journal.pgen.1002088

Scully, R., Chen, J., Plug, A., Xiao, Y., Weaver, D., Feunteun, J., et al. (1997). Association of BRCA1 with Rad51 in Mitotic and Meiotic Cells. *Cell* 88 (2), 265–275. doi:10.1016/s0092-8674(00)81847-4

Sharan, S. K., Pyle, A., Coppola, V., Babus, J., Swaminathan, S., Benedict, J., et al. (2004). BRCA2 Deficiency in Mice Leads to Meiotic Impairment and Infertility. *Development* 131 (1), 131–142. doi:10.1242/dev.00888

Silvestris, E., de Pergola, G., Rosania, R., and Loverro, G. (2018). Obesity as Disruptor of the Female Fertility. *Reprod. Biol. Endocrinol.* 16 (1), 22. doi:10.1186/s12958-018-0336-z

Soumillon, M., Necsulea, A., Weier, M., Brawand, D., Zhang, X., Gu, H., et al. (2013). Cellular Source and Mechanisms of High Transcriptome Complexity in the Mammalian Testis. *Cel Rep.* 3 (6), 2179–2190. doi:10.1016/j.celrep.2013.05.031

Subramanian, V. V., and Hochwagen, A. (2014). The Meiotic Checkpoint Network: Step-by-step through Meiotic Prophase. *Cold Spring Harbor Perspect. Biol.* 6 (10), a016675. doi:10.1101/cshperspect.a016675

Tang, F., Barbacioru, C., Wang, Y., Nordman, E., Lee, C., Xu, N., et al. (2009). mRNA-Seq Whole-Transcriptome Analysis of a Single Cell. *Nat. Methods* 6 (5), 377–382. doi:10.1038/nmeth.1315

Tapley, E. C., and Starr, D. A. (2013). Connecting the Nucleus to the Cytoskeleton by SUN-KASH Bridges across the Nuclear Envelope. *Curr. Opin. Cel Biol.* 25 (1), 57–62. doi:10.1016/j.ceb.2012.10.014

Turner, J. M. A. (2015). Meiotic Silencing in Mammals. *Annu. Rev. Genet.* 49, 395–412. doi:10.1146/annurev-genet-112414-055145

Wang, L., Tu, Z., Liu, C., Liu, H., Kaldis, P., Chen, Z., et al. (2018). Dual Roles of TRF1 in Tethering Telomeres to the Nuclear Envelope and Protecting Them from Fusion during Meiosis. *Cell Death Differ* 25 (6), 1174–1188. doi:10.1038/s41418-017-0037-8

Wang, L., Xu, Z., Khawar, M. B., Liu, C., and Li, W. (2017). The Histone Codes for Meiosis. *Reproduction* 154 (3), R65–r79. doi:10.1530/rep-17-0153

Welt, C. K. (2008). Primary Ovarian Insufficiency: a More Accurate Term for Premature Ovarian Failure. *Clin. Endocrinol.* 68 (4), 499–509. doi:10.1111/j.1365-2265.2007.03073.x

Zálešák, F., Bon, D. J.-Y. D., and Pospíšil, J. (2019). Lignans and Neolignans: Plant Secondary Metabolites as a Reservoir of Biologically Active Substances. *Pharmacol. Res.* 146, 104284. doi:10.1016/j.phrs.2019.104284

Zentner, G. E., and Henikoff, S. (2013). Regulation of Nucleosome Dynamics by Histone Modifications. *Nat. Struct. Mol. Biol.* 20 (3), 259–266. doi:10.1038/nsmb.2470

Zhang, Y., and Reinberg, D. (2001). Transcription Regulation by Histone Methylation: Interplay between Different Covalent Modifications of the Core Histone Tails. *Genes Dev.* 15 (18), 2343–2360. doi:10.1101/gad.927301

Zickler, D., and Kleckner, N. (1999). Meiotic Chromosomes: Integrating Structure and Function. *Annu. Rev. Genet.* 33, 603–754. doi:10.1146/annurev.genet.33.1.603

Conflict of Interest: The authors declare that the research was conducted in the absence of any commercial or financial relationships that could be construed as a potential conflict of interest.

Publisher's Note: All claims expressed in this article are solely those of the authors and do not necessarily represent those of their affiliated organizations, or those of the publisher, the editors and the reviewers. Any product that may be evaluated in this article, or claim that may be made by its manufacturer, is not guaranteed or endorsed by the publisher.

Copyright © 2021 Li, Zhang, Shinohara and Keeney. This is an open-access article distributed under the terms of the Creative Commons Attribution License (CC BY). The use, distribution or reproduction in other forums is permitted, provided the original author(s) and the copyright owner(s) are credited and that the original publication in this journal is cited, in accordance with accepted academic practice. No use, distribution or reproduction is permitted which does not comply with these terms.

frontiers in Cell and Developmental Biology

ORIGINAL RESEARCH
published: 04 September 2020
doi: 10.3389/fcell.2020.00845

Tethering of Telomeres to the Nuclear Envelope Is Mediated by SUN1-MAJIN and Possibly Promoted by SPDYA-CDK2 During Meiosis

Guishuan Wang[1]†, Xiaolong Wu[1]†, Liwei Zhou[1], Sheng Gao[1], Damin Yun[1], Ajuan Liang[2] and Fei Sun[1]**

[1] Medical School, Institute of Reproductive Medicine, Nantong University, Nantong, China, [2] Reproductive Medical Center, Tongji Hospital, Tongji University School of Medicine, Shanghai, China

OPEN ACCESS

Edited by:
Wei Li,
Chinese Academy of Sciences (CAS), China

Reviewed by:
Philipp Kaldis,
Lund University, Sweden
Hiroki Shibuya,
University of Gothenburg, Sweden

***Correspondence:**
Guishuan Wang
gswang@ntu.edu.cn
Fei Sun
sunfei@ntu.edu.cn

†These authors have contributed equally to this work

Specialty section:
This article was submitted to Cell Growth and Division, a section of the journal Frontiers in Cell and Developmental Biology

Received: 14 June 2020
Accepted: 06 August 2020
Published: 04 September 2020

Citation:
Wang G, Wu X, Zhou L, Gao S, Yun D, Liang A and Sun F (2020) Tethering of Telomeres to the Nuclear Envelope Is Mediated by SUN1-MAJIN and Possibly Promoted by SPDYA-CDK2 During Meiosis. Front. Cell Dev. Biol. 8:845. doi: 10.3389/fcell.2020.00845

During meiosis, telomeres attach to the nuclear envelope (NE) to promote homologous chromosome moving, pairing, synapsis, and recombination. The telomere-NE attachment is mediated by SUN1, TERB1-TERB2-MAJIN (TTM complex), and TRF1. The interaction of the TTM complex with shelterin is mediated by TERB1 and TRF1, but how SUN1 interacts with the TTM complex is not yet fully understood. In this study, we found that SUN1 not only interacted with TERB1 but also interacted with MAJIN, and the interaction of SUN1 with MAJIN is stronger than TERB1. We also found that SUN1 interacted with SPDYA, an activator of CDK2. The binding sites of MAJIN and SPDYA at SUN1 were mapped, and both MAJIN and SPDYA bound to the N-terminal domain of SUN1 and the two binding sites were close to each other. Furthermore, SPDYA bound to SUN1 via the Ringo domain and recruited CDK2 to SUN1. Then, we found that the interaction of SUN1 with MAJIN was decreased by the CDK2 inhibitors. Taken together, our results provide the possible mechanism of SUN1, MAJIN, and SPDYA-CDK2 in promoting the telomere-NE attachment during meiosis.

Keywords: meiosis, telomere, SUN1, MAJIN, TERB1, CDK2, SPDYA

INTRODUCTION

During meiosis, telomeres attach to the nuclear envelope (NE) and cluster to form a bouquet that is conserved and has been found in many organisms (Zickler and Kleckner, 2016). Formation of the bouquet is required for meiosis by tethering telomeres together and facilitating homologous chromosome pairing, synapsis, and recombination (Harper et al., 2004). There are three protein complexes involved in bouquet formation. The LINC (linker of nucleoskeleton and cytoskeleton) complex, which is composed by trans-membrane proteins containing KASH and SUN domains, and localizes at the NE, links the NE to the cytoskeleton where forces are generated to move chromosomes. Moreover, SUN domain proteins provide telomere-anchoring sites at the NE (Hiraoka and Dernburg, 2009; Tapley and Starr, 2013). The shelterin complex localized at the telomeres is required for bouquet formation, especially the core subunit of the shelterin complex, TRF1 (Wang et al., 2018). There is a "linker" bridging LINC and shelterin complexes together. In mouse, this liner consists of TERB1, TERB2, and MAJIN (Conrad et al., 2008; Hiraoka and Dernburg, 2009; Daniel et al., 2014; Shibuya et al., 2015; Wang et al., 2019). Many efforts have been

made to reveal the connection between the linker and shelterin complex, indicating that TERB1 and TRF1 contribute to this connection (Shibuya et al., 2014; Long et al., 2017; Pendlebury et al., 2017; Zhang et al., 2017; Dunce et al., 2018). However, the connection between the linker and LINC complex is not yet fully understood (Shibuya et al., 2014).

CDK2 and its activators, SPDYA and Cyclin E, are required for the bouquet formation (Palmer et al., 2019). In the *Cdk2*, *Spdya,* and *Cyclin E* knockout mice, telomeres dissociate from the NE, indicating that the LINC-linker-shelterin connection is broken down, but where the disconnection occurs is unknown (Viera et al., 2015; Manterola et al., 2016; Tu et al., 2017). CDK2 is a cyclin-dependent kinase, and the typical cyclins, including Cyclin E and A, and atypical cyclin, SPDYA, activate the kinase activity of CDK2 (Link et al., 2014; Tu et al., 2017). The cyclins bind to CDK2 and lead to phosphorylation of T160 on the T-loop to activate CDK2, whereas SPDYA binds to and activates CDK2 regardless of the T loop phosphorylation (Gonzalez and Nebreda, 2020). It has been reported that CDK2 phosphorylates SUN1 (Viera et al., 2015; Mikolcevic et al., 2016), implying that CDK2 may function in the LINC-linker connection.

In this research, we determined how LINC and linker complexes connect together. We found that SUN1 not only interacted with TERB1 but also interacted with MAJIN, and the interaction of SUN1 with MAJIN was stronger than TERB1. We also found that SPDYA interacted with SUN1 via the Ringo domain and recruited CDK2 to SUN1. Moreover, the SUN1-MAJIN interaction was reduced by CDK2 inhibitors.

MATERIALS AND METHODS

Cell Culture and Transfection

HEK293T and Cos7 cells were cultured in Dulbecco's modified Eagle's medium (DMEM, Invitrogen, Carlsbad, CA, United States) supplemented with 10% fetal bovine serum (FBS, Invitrogen) and antibiotics (100 U/mL penicillin and 100 μg/mL streptomycin; Invitrogen). Cells were cultured at 37°C with 5% CO_2 and transfected by the Lipofectamine 2000 reagent (Invitrogen) according to the manufacturer's instructions. To inhibit the kinase activity of CDK2, 24 h after transfection, cells were treated with roscovitine (50 μM, Selleck, Shanghai, China) or milciclib (50 μM, Selleck) for 4 h. Dimethyl sulfoxide (DMSO) was used as a control.

Plasmid Construction

Total RNA of the mouse testis was extracted using TRIzol Reagent (Invitrogen), and cDNA was generated using a PrimeScript 1st Strand cDNA Synthesis Kit (TaKaRa, Dalian, China). Full-length mice Sun1 (NM_024451), Terb1 (NM_180958), Terb2 (NM_028914), Majin (NM_001165919), Spdya (NM_029254), Cdk2 (NM_183417), Cyclin E1 (NM_007633) and E2 (NM_001037134) were amplified by PrimeSTAR Max DNA Polymerase (TaKaRa) from cDNA using primers containing specific restriction sites. The genes were cloned into expression plasmids p3 × FLAG-*myc*-CMV-24 (Sigma, St. Louis, MO, United States), pEGFP-C1 (Clontech, Mountain View, CA, United States), pmCherry-C1 (Clontech), and pCMV-N-Myc (Beyotime Biotechnology, Shanghai, China). Truncated mutants were generated by PCR, and deletion mutants were generated using overlapped primers with mutations. The primers were produced by GENEWIZ (Suzhou, China). All plasmids were verified by Sanger sequencing (GENEWIZ).

Immunoprecipitation Assay

Harvested HEK293T cells were lysed in TNE buffer (10 mM Tris-HCl, pH 7.5, 150 mM NaCl, 1 mM EDTA, and 1% Nonidet P-40) with a protease inhibitor cocktail (Roche, Mannheim, Germany), 1 mM phenylmethylsulfonyl fluoride (PMSF), and 5 mM sodium orthovanadate. The lysates were centrifuged at 18,000 × *g* for 10 min at 4°C, and the supernatants were immunoprecipitated by GFP-Trap (ChromoTek, Munich, Germany) or Anti-FLAG M2 Affinity Gel (Sigma) for 1 h at 4°C on a rotating wheel. The immunoprecipitates were separated by SDS-PAGE and transferred onto nitrocellulose membranes (Sangon Biotech, Shanghai, China).

Western Blotting

Protein samples were separated on SDS-PAGE gels and then electroblotted onto nitrocellulose membranes. The nitrocellulose membranes were blocked for 1 h in 5% non-fat milk in TBST (10 mM Tris, pH 7.5, 200 mM NaCl, and 0.2% Tween 20) followed by incubation with primary antibodies: mouse anti-GFP antibody (Cat. 66002-1-Ig, Proteintech, Rosemont, IL, United States), rabbit anti-GFP antibody (Cat. ab290, abcam, Cambridge, United Kingdom), mouse anti-FLAG antibody (Cat. F3165, Sigma), rabbit anti-FLAG antibody (Cat. 20543-1-AP, Proteintech), rabbit anti-Myc antibody (Cat. 16286-1-AP, Proteintech), mouse anti-β-Actin antibody (Cat. 66009-1-Ig, Proteintech), rabbit anti-CDK2 antibody (Cat. 10122-1-AP, Proteintech), or rabbit anti-pCDK2 antibody (Cat. ab194868, abcam). Two secondary antibodies were used: goat anti-mouse antibody (Cat. ab216776, IRDye 680RD, abcam) and goat anti-rabbit antibody (Cat. ab216773, IRDye 800RD, abcam). Signals were captured by an Amersham Typhoon (GE Healthcare Bio-Sciences AB, Uppsala, Sweden) and analyzed by ImageQuant TL (GE Healthcare).

Immunofluorescence

Cos7 cells were cultured on the glass slides. At 24 h after transfection, the cells were fixed in 4% paraformaldehyde (PFA), permeabilized in 0.1% Triton X-100, blocked in 5% BSA and incubated with rabbit anti-FLAG antibody (Proteintech) 4°C overnight, followed by incubation with a cyanine5-conjugated goat anti-rabbit secondary antibody (Cat. A10523, Invitrogen). Nuclei were stained with Hoechst 33342 (Invitrogen). Images were captured by an Axio Imager under an M2 microscope (Carl Zeiss, Göttingen, Germany).

RESULTS

SUN1 Is Associated With MAJIN

It has been reported that SUN1 interacts with TERB1 (Shibuya et al., 2014), and whether SUN1 interacts with TERB2 or MAJIN is unknown. Immunoprecipitation was performed to

examine interactions between SUN1 and the TERB1-TERB2-MAJIN (TTM) complex. The expression plasmid of GFP-SUN1 was co-transfected with FLAG-TERB1, FLAG-TERB2, and FLAG-MAJIN into HEK293T cells, and immunoprecipitated by GFP antibody (**Figures 1A–C**) and FLAG antibody (**Figure 1D**), respectively. The results showed that SUN1 had a weak interaction with TERB1 but no interaction with TERB2 (**Figure 1**). Surprisingly, a strong interaction was found between SUN1 and MAJIN (**Figures 1C,D**).

NE Localization of TERB1 and TERB2 Is Dependent on MAJIN but Not SUN1

It has been reported that MAJIN localized to the NE and MAJIN mediated the NE localization of TERB1 and TERB2 (Shibuya et al., 2015), we confirmed these data in Cos7 cells. Expression plasmids of mCherry-tagged TERB1, TERB2, and MAJIN were transfected into the cells. Immunofluorescence show that TERB1 was highly expressed in the nucleus (**Supplementary Figure 1Ai**), TERB2 was expressed in the whole cell (**Supplementary Figure 1Aii**), and MAJIN had ring-like localization (**Supplementary Figure 1Aiii**). Then, expression plasmids of mCherry-MAJIN, FLAG-TERB1, and GFP-TERB2 were transfected into Cos7 cells. The results showed that when TERB1 and TERB2 were co-expressed, no NE localization was detected (**Supplementary Figure 1Bi**). When TERB1 or TERB2 were co-expressed with MAJIN, TERB2, but not TERB1, was tethered to NE (**Supplementary Figures 1Bii,iii**). But TERB1 was tethered to NE when co-expressed with MAJIN and TERB2 (**Supplementary Figure 1Biv**) because MAJIN was associated with TERB2, and TERB2 was associated with TERB1 (**Supplementary Figures 1C,D**).

SUN1 interacted with TTM complex, and therefore SUN1 may tether the TTM complex to the NE. To test this hypothesis, mCherry-tagged TERB1, TERB2, and MAJIN were co-transfected with GFP-SUN1. The results showed no NE localization of TERB1 or TERB2 when co-expressed with SUN1 (**Supplementary Figures 1Ei,ii**), but MAJIN showed co-localization with SUN1 (**Supplementary Figure 1Eiii**). These data suggested that the interaction between SUN1 and TERB1 was not enough to support the NE localization of TERB1.

Binding Sites Between SUN1 and MAJIN

We mapped the MAJIN-binding site by a panel of mutants of GFP-tagged SUN1 (**Figures 2A,B**). We found that the N-terminal domain of SUN1 (1–210 amino acid; Aa) interacted with MAJIN. Next, we narrowed down the binding site and found that 1–175 Aa of SUN1 had no interaction with MAJIN, indicating that 175–210 Aa of SUN1 was the binding site of MAJIN (**Figure 2B**). We found that 190–216 Aa of mouse

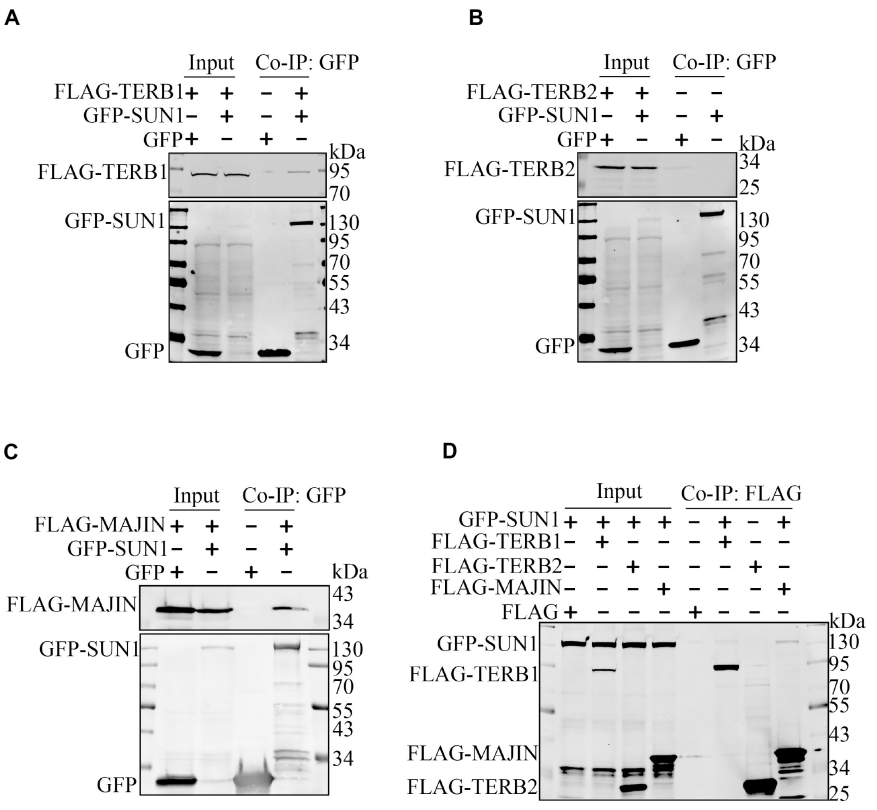

FIGURE 1 | SUN1 is associated with MAJIN. The indicated expression plasmids were transfected into HEK293T cells, and immunoprecipitation was performed to analyze the interactions of SUN1 with TERB1 **(A)**, TERB2 **(B)**, and MAJIN **(C)** by GFP-Trap or Anti-FLAG M2 Affinity Gel **(D)**.

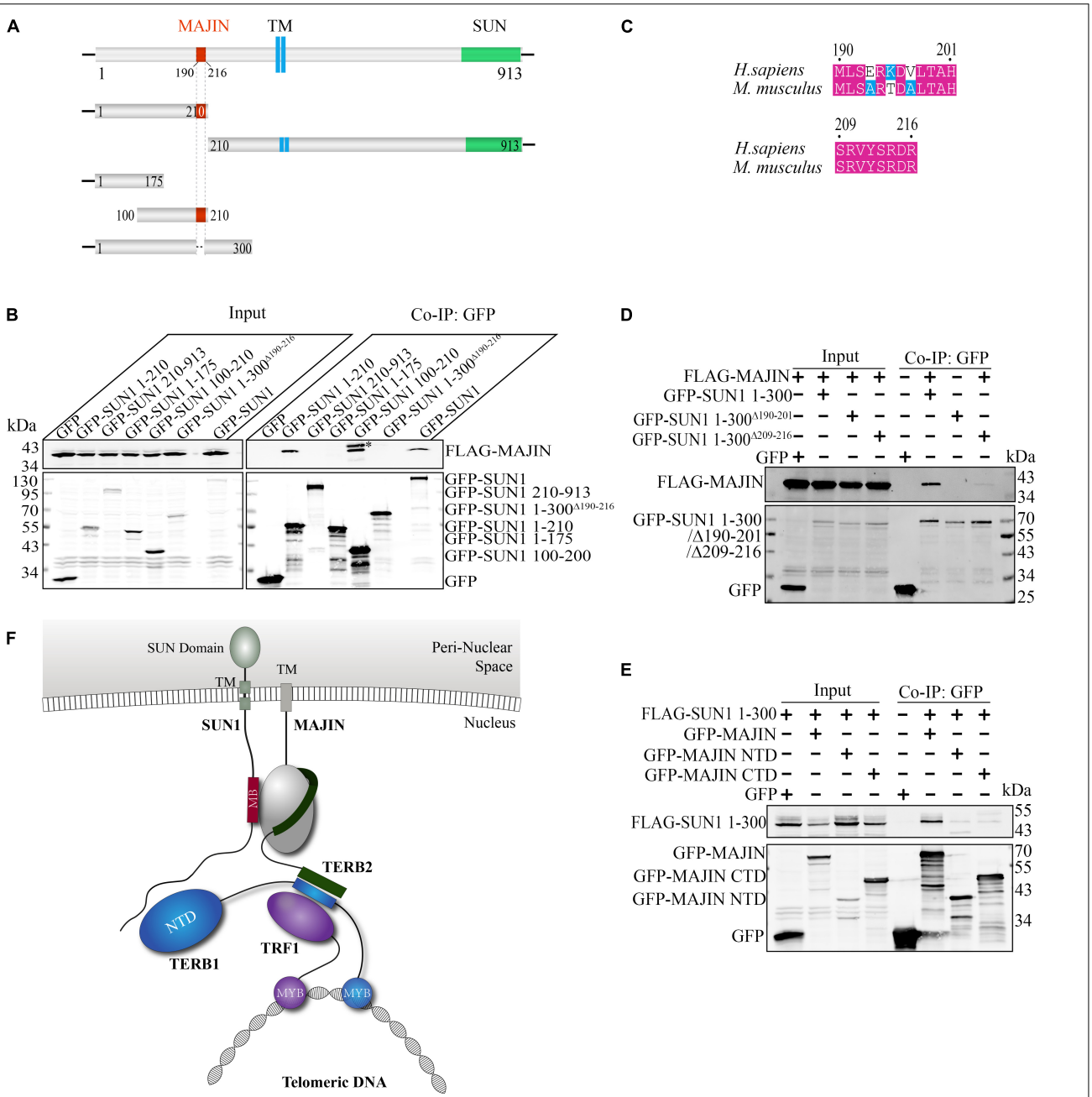

FIGURE 2 | Binding sites between SUN1 and MAJIN. **(A)** Illustration of the MAJIN-binding site at SUN1. The MAJIN-binding site is shown in red, the trans-membrane region is blue, and the SUN domain is green. TM: trans-membrane region. **(B)** The 190–216 Aa of SUN1 is the binding site of MAJIN. *Indicating the band of GFP-SUN1 100–210 Aa. **(C)** Illustration of the two conserved sequences of SUN1 in the MAJIN binding site. **(D)** The SUN1-MAJIN interaction is affected by deletion of 190–201 and 209–216 Aa. **(E)** Both the NTD and CTD of MAJIN interact with SUN1. **(F)** Illustration of the interaction of SUN1 with MAJIN. The MAJIN-binding site is shown in red and named "MB."

SUN1 was conserved with human SUN1 (**Figure 2C** and **Supplementary Figure 2**). GFP-SUN1 1–300 Aa$^{\Delta 190-216}$ with deletion of 190–216 Aa was used to precipitate MAJIN, and we found that this mutant did not interact with MAJIN (**Figure 2B**). In 190–216 Aa of SUN1, there were two conserved sequences, 190–201 and 209–216 Aa (**Figure 2C**). GFP-SUN1 1–300 Aa$^{\Delta 190-201}$ had no interaction with MAJIN, and GFP-SUN1 1–300 Aa$^{\Delta 209-216}$ had very weak interaction (**Figure 2D**), indicating that 190–216 Aa of SUN1 was the MAJIN-binding site.

We also mapped the SUN1-binding site at MAJIN. We found that both the N-terminal domain (1–100 Aa) and C-terminal domain (100–256 Aa) of MAJIN interacted with SUN1 (**Figure 2E**).

These results indicated that 190–216 Aa of SUN1 was the MAJIN-binding site, and MAJIN recruited TERB2 and TERB1 to the NE. The interaction between SUN1 and TTM complex is illustrated in **Figure 2F**.

SUN1 Interacts With SPDYA

It has been reported that some other proteins are also important for the attachment of telomeres to the NE, such as SPDYA, CDK2, and Cyclin E (Mendez, 2003; Viera et al., 2015; Manterola et al., 2016; Tu et al., 2017). Whether SPDYA, CDK2, or Cyclin E have functions in the connection of the TTM complex with SUN1 is unknown.

Therefore, we first examined interactions of SPDYA, CDK2, and Cyclin E with SUN1. Immunoprecipitation showed that SPDYA interacted with SUN1 (**Figure 3A**). CDK2 was associated with SUN1, which was reported in our previous study (**Figure 3B**). Cyclin E had no interaction with SUN1 (**Figures 3C,D**). Next, we investigated the interactions of SPDYA, CDK2, and Cyclin E with the TTM complex. Immunoprecipitation showed that SPDYA, CDK2, or Cyclin E did not interact with the TTM complex (**Figures 4A–D**).

We mapped the SPDYA-binding site as described previously (**Figure 2**). The results showed that SPDYA bound to 125–175 Aa at the N-terminal of SUN1 (**Figures 5A,B** and **Supplementary Figure 3**). We found that 134–171 Aa of mouse SUN1 was conserved with human SUN1 (**Supplementary Figure 2**). GFP-SUN1 1–210 $Aa^{\Delta 134-171}$ with deletion of 134–171 Aa was used to precipitate SPDYA, and the mutant had no interaction with SUN1, indicating that 134–171 Aa of SUN1 was the SPDYA-binding site (**Figure 5B**). Next, the SUN1-binding site of SPDYA was mapped. The results showed that the Ringo domain of SPDYA was the SUN1-binding site (**Figures 5C,D**).

We found that both MAJIN and SPDYA bound to the N-terminal domain of SUN1 and the two binding sites were close to each other (**Figures 2**, **5A,B**). Therefore, we examined the interactions of SUN1 with SPDYA and MAJIN using SUN1 mutants with MAJIN or SPDYA binding site deletion. The results showed that the interaction of SUN1 between SPDYA was not affected by the deletion of MAJIN-binding site (**Figure 5E**), and the interaction of SUN1 between MAJIN was slightly decreased by the deletion of SPDYA-binding site (**Figure 5F**).

SPDYA recruits and activates CDK2 (Tu et al., 2017), indicating that SPDYA may enhance the interaction of SUN1 with CDK2. Immunoprecipitation showed that SPDYA interacted CDK2 (**Figure 5G**), and SPDYA promoted the interaction of SUN1 with CDK2 (**Figures 5H,I**).

These results indicate that 134–171 Aa of SUN1 is associated with the Ringo domain of SPDYA, and SPDYA recruits CDK2 to SUN1. The interaction between SUN1, SPDYA-CDK2, and the TTM complex is illustrated in **Figure 5J**.

The Interaction of SUN1 With MAJIN Is Reduced by CDK2 Inhibitors

SPDYA recruits CDK2 to SUN1, and the MAJIN-binding site is adjacent to the SPDYA-binding site, suggesting that

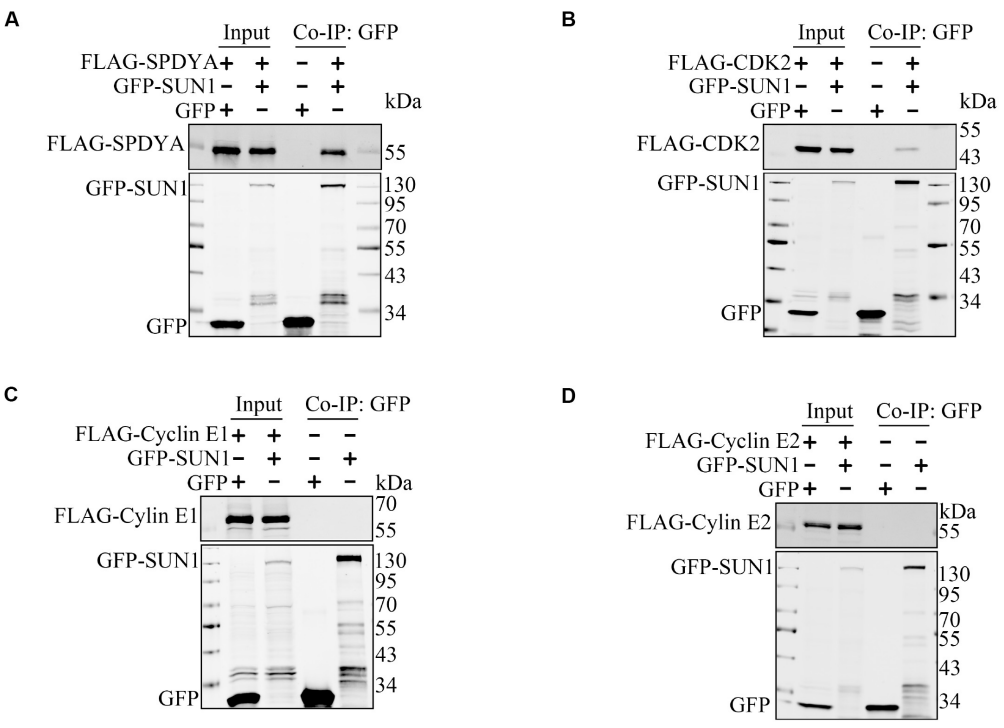

FIGURE 3 | SUN1 interacts with SPDYA. The expression plasmids were transfected into HEK293T cells, and immunoprecipitation was performed to analyze the interaction of SUN1 with SPDYA **(A)**, CDK2 **(B)**, Cyclin E1 **(C)**, and Cyclin E2 **(D)**.

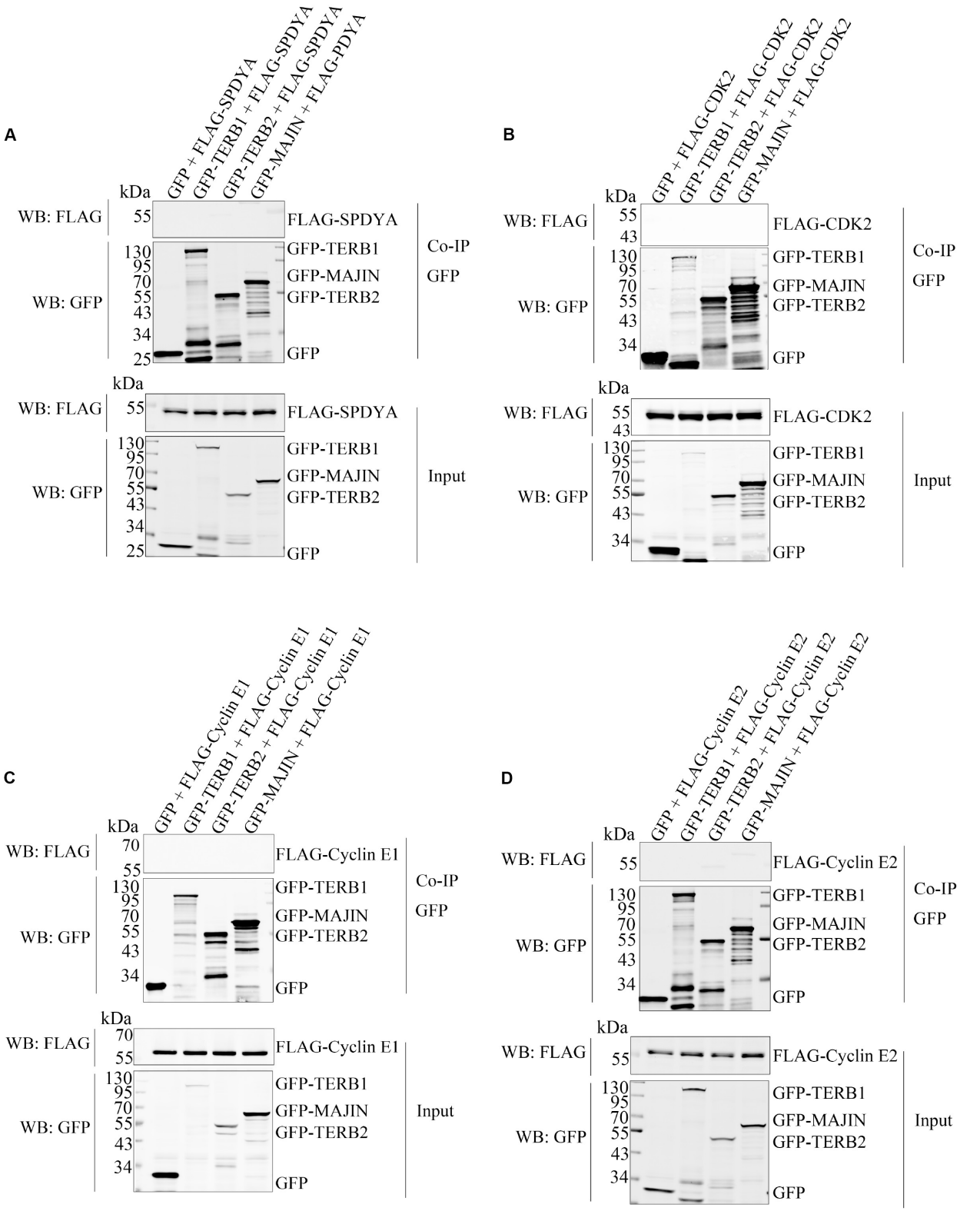

FIGURE 4 | SPDYA, CDK2, and Cyclin E are not associated with TTM complex. The expression plasmids of GFP, GFP-TERB1, GFP-TERB2, and GFP-MAJIN were co-transfected with FLAG-SPDYA **(A)**, FLAG-CDK2 **(B)**, FLAG-Cyclin E1 **(C)**, or FLAG-Cyclin E2 **(D)** into HEK293T cells. Cells were harvested and lysed, 10% cell lysates were used as input, and the remained lysates were incubated with GFP-Trap. After incubation, the GFP-Trap was washed to remove unbound proteins. Then samples of input and Co-IP were subjected to western blotting.

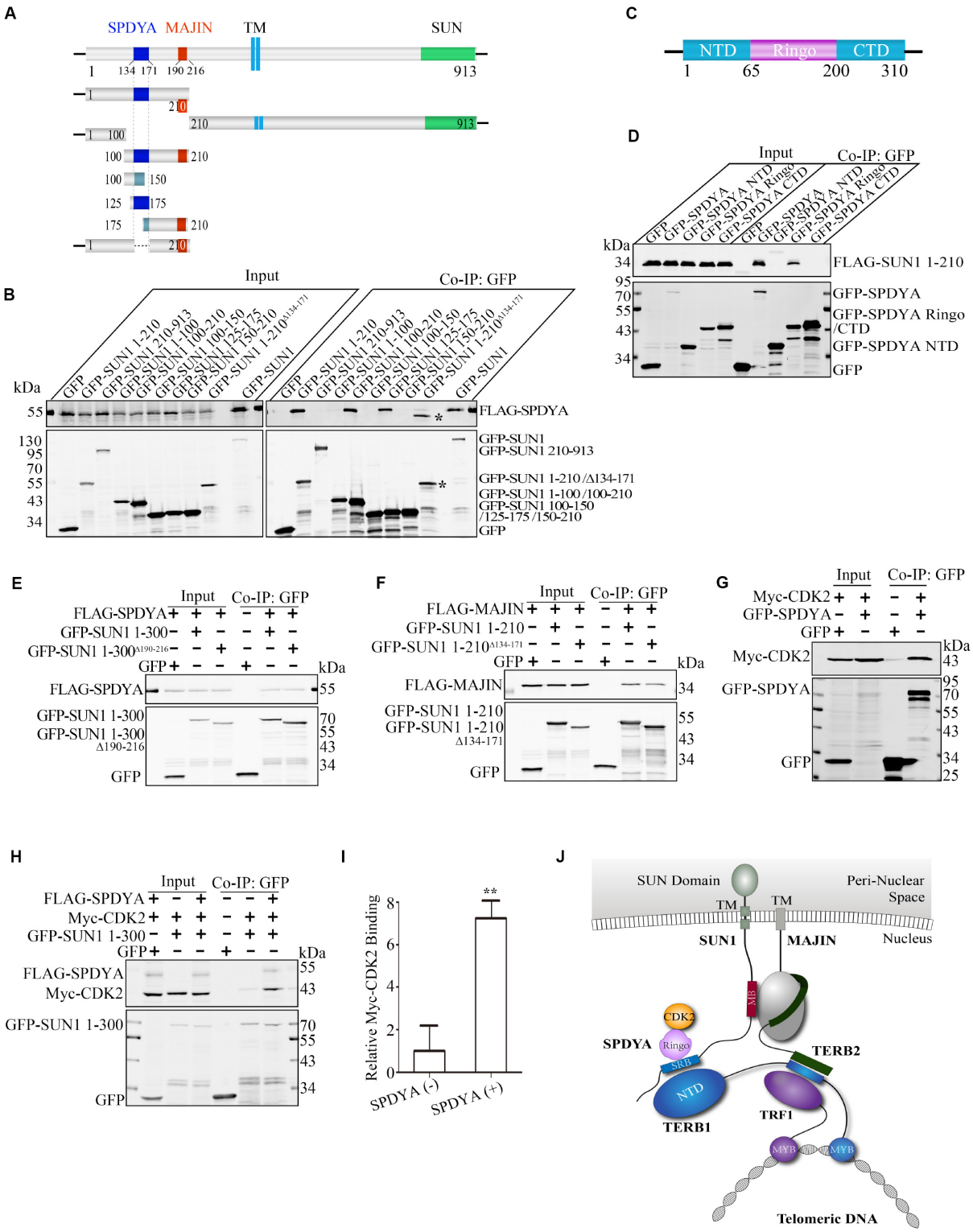

FIGURE 5 | SPDYA recruits CDK2 to SUN1. **(A)** Illustration of the SPDYA-binding site at SUN1. The SPDYA-binding site is shown in dark blue. TM: trans-membrane region. **(B)** The 134–171 Aa of SUN1 in the SPDYA binding site. *Indicating the band of GFP-SUN1 1–210 $Aa^{\Delta 134-171}$. **(C)** Illustration of the SPDYA structure. **(D)** The Ringo domain of SPDYA is the binding site of SUN1. **(E)** The interaction of SUN1 mutant with MAJIN-binding site deletion between SPDYA. **(F)** The interaction of SUN1 mutant with SPDYA-binding site deletion between MAJIN. **(G,H)** SPDYA interacts with CDK2 and recruits CDK2 to SUN1. **(I)** The histogram shows Myc-CDK2 binding in **(H)**, data are presented as mean ± SEM with three repeats. $^{**}P < 0.01$. **(J)** Illustration of the interaction of SUN1 with MAJIN and SPDYA-CDK2. The SPDYA Ringo domain binding site of SUN1 is shown in blue and name "SRB."

the interaction of SUN1 with MAJIN may be regulated by CDK2, especially because the connection of telomeres with the NE is dependent on CDK2 and SPDYA. GFP-SUN1 1–300 and FLAG-MAJIN were co-transfected, followed by treatment with roscovitine and milciclib, two inhibitors of CDK2 and then immunoprecipitation assay was carried out. The results showed that the interaction of SUN1 with MAJIN was decreased by the inhibition of CDK2 activity (**Figures 6A,B**). However, the CDK2 phosphorylation sites of SUN1 and MAJIN are unknown. These results indicate that the interaction of SUN1 with MAJIN is regulated by SPDYA-CDK2 (**Figure 6C**).

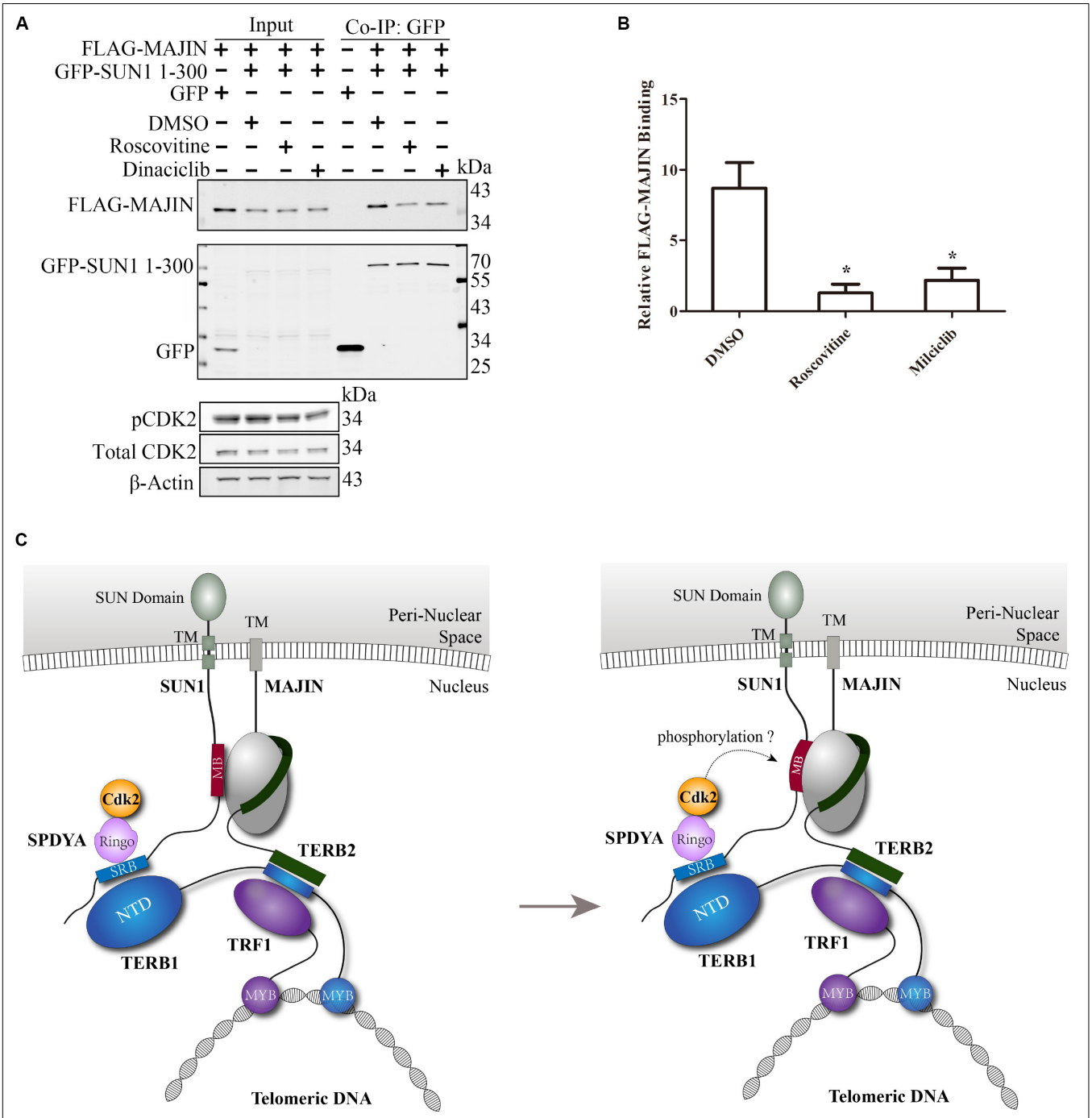

FIGURE 6 | The interaction of SUN1 with MAJIN is reduced by CDK2 inhibitors. **(A)** The SUN1-MAJIN interaction is decreased by CDK2 inhibitors. **(B)** The histogram shows FLAG-MAJIN binding in **(A)**, data are presented as mean ± SEM with three repeats. *$P < 0.05$. **(C)** Illustration of the interaction of SUN1 with MAJIN regulated by SPDYA-CDK2.

DISCUSSION

During meiosis, telomeres are tethered to the NE. This tethering is critical for meiotic chromosome alignment and synaptic pairing of the homologs (Harper et al., 2004; Lee et al., 2015; Zeng et al., 2017). Many proteins are involved in this tethering process, such as the LINC (linker of nucleoskeleton and cytoskeleton) complex, the "adaptor," and the shelterin complex (Shibuya et al., 2015; Burke, 2018; Li and Liu, 2020). The LINC complex consists of Klarsicht, Anc-A, and Syne Homology (KASH) and Sad1 and UNC-84 (SUN) domain proteins. The KASH domain proteins are associated with the outer nuclear membrane, and the SUN domain proteins are in the inner nuclear membrane. The LINC complex provides coupling between the cytoskeleton and nucleoskeleton. During meiosis in the mouse, the LINC complex consists of KASH5 and SUN1 or SUN2, and the SUN domain proteins are the anchoring site of telomeres at the NE (Ding et al., 2007; Wang et al., 2012; Horn et al., 2013; Link et al., 2014). The "adaptor" consists of TERB1, TERB2, and MAJIN (da Cruz et al., 2020). The shelterin complex has six proteins, containing TRF1, TRF2, POT1, RAP1, TIN2, and TPP1. The shelterin complex is localized to the chromosome end and protects telomeric DNA (Palm and de Lange, 2008). The TTM complex acts as a "linker" and bridges the LINC and shelterin complexes together. The connection between TTM and shelterin complexes is well-known, which is mediated by TERB1 and TRF1 (Shibuya et al., 2014; Long et al., 2017; Pendlebury et al., 2017; Zhang et al., 2017; Dunce et al., 2018). However, the connection between the TTM and LINC complex was not fully understood.

In this study, we examined the association between SUN1 and TTM complex by immunoprecipitation assay. We found that SUN1 was associated with TERB1 (**Figures 1A,D**), as reported previously (Shibuya et al., 2014). Moreover, SUN1 was associated with MAJIN, and the SUN1-MAJIN interaction was stronger than SUN1-TERB1 (**Figures 1A,C,D**), but SUN1 was not associated with TERB2 (**Figure 1B**). It has been reported that SUN2 connects a portion of telomeres to the NE in *Sun1* knockout mice (Link et al., 2014), suggesting that SUN2 also mediates the telomere-NE connection. In fact, we found that SUN2 was associated with the TTM complex, and how SUN2 mediates the telomere-NE connection is under study (unpublished data).

The SUN1-MAJIN interaction may be more important than the SUN1-TERB1 interaction in the bridge of LINC and shelterin complexes, because the interaction of SUN1-MAJIN was stronger than TERB1 (**Figure 1**). Moreover, MAJIN has a trans-membrane region and is co-localized with SUN1 to the NE, but TERB1 and TERB2 are not co-localized with SUN1 (**Supplementary Figure 1**), indicating that MAJIN plays a major role in the association of the SUN1-TTM complex. Additionally, in the *Terb1* knockout mouse, overexpressed GFP-MAJIN in spermatocytes is pulled to the centrosome pole and exhibits a crescent-shape distribution but not in the *Sun1* knockout mouse (Shibuya et al., 2015), suggesting that MAJIN interacts directly with SUN1, not mediated by TERB1 as reported previously.

CDK2 is a cyclin-dependent kinase that is required for the telomere-NE connection (Ortega et al., 2003; Viera et al., 2009, 2015; Palmer et al., 2019). SPDYA and Cyclin E are activators of CDK2 and also critical for the telomere-NE connection (Martinerie et al., 2014; Manterola et al., 2016; Mikolcevic et al., 2016; Tu et al., 2017). However, the mechanisms of CDK2 and its activators in promotion of the telomere-NE connection are unclear. We found that SPDYA interacted with SUN1 (**Figure 3A**), and CDK2 was associated with SUN1 (**Figure 3B**), as we reported previously (Liu et al., 2014). However, Cyclin E did not interact with SUN1 (**Figures 3C,D**). SPDYA, CDK2, or Cyclin E did not interact with the TTM complex (**Figures 4A–D**). In *Cyclin E* knockout mice, the telomere localization of CDK2 is reduced (Martinerie et al., 2014), and the shelterin complex protein, TRF2 and RAP1, are decreased (Manterola et al., 2016), suggesting that Cyclin E-CDK2 mainly regulates the connection of TTM with shelterin complexes. Moreover, in the *Spdya* knockout mouse, TERB1 and MAJIN are still localized at the telomere, but not SUN1 (Tu et al., 2017). These results indicate that the connection between SUN1 and TTM complexes may be promoted by SPDYA-CDK2 but not Cyclin E-CDK2.

We mapped the binding site and found that 190–216 and 134–171 Aa of SUN1, which are conserved between mouse and human (**Supplementary Figure 2**), were the binding sites of MAJIN and SPDYA, respectively (**Figures 2**, **5**). Interestingly, the Ringo domain of SPDYA interacted with SUN1 (**Figure 5D**). The Ringo domain is required for telomere localization of SPDYA (Tu et al., 2017). These results indicate that the 134–171 Aa of SUN1 is the anchoring site of SPDYA at the NE and may be responsible for the telomere localization of SPDYA. It has been reported that SPDYA interacts with TRF1 (Wang et al., 2018), suggesting that this interaction is also responsible for telomere localization of SPDYA; however, whether the Ringo domain participates in the interaction of SPDYA-TRF1 is still unknown.

It has been reported that SPDYA recruits CDK2 to telomeres (Tu et al., 2017), implying that SPDYA promotes the interaction of SUN1 with CDK2. To test this hypothesis, the interaction of SPDYA with CDK2 was confirmed by immunoprecipitation (**Figure 5G**). Next, we found that SPDYA increased the interaction of SUN1 with CDK2 (**Figures 5H,I**), suggesting that SPDYA interacts with 134–171 Aa of SUN1 via the Ringo domain, and then SPDYA recruits CDK2 to SUN1 to localize to the telomere.

The kinase activity of CDK2 is important for meiosis and spermatogenesis (Liu et al., 2014; Wang et al., 2014; Chauhan et al., 2016; Palmer et al., 2019). It has been reported that CDK2 phosphorylates SUN1 (Viera et al., 2015; Mikolcevic et al., 2016), but the function of SUN1 phosphorylation by CDK2 is unknown. In this study, we found that the interaction of SUN1 with MAJIN is reduced by the CDK2 inhibitors (**Figures 6A,B**), implying that SPDYA-CDK2 may promote the telomere-NE connection by regulating the SUN1-MAJIN interaction (**Figure 6C**).

In summary, we revealed the mechanism of telomere tethering to the NE during meiosis, which is mediated by the interaction between SUN1 and MAJIN. SPDYA binds to SUN1 via the Ringo domain and recruits CDK2 to the telomere to tether telomeres to the NE.

DATA AVAILABILITY STATEMENT

All datasets generated for this study are included in the article/**Supplementary Material**.

AUTHOR CONTRIBUTIONS

GW and FS conceived and designed the study. GW and XW performed immunoprecipitation and immunofluorescence assay and wrote the manuscript. LZ, SG, DY, and AL performed cell culture and transfection, and plasmid construction. FS revised the manuscript and approved the final version. All authors reviewed the final version of the manuscript.

FUNDING

This work was supported by the National Key Research and Development Program of China (Grant No. 2018YFC1003500 to FS) and the National Natural Science Foundation of China Grants (Grant No. 81671510 to FS).

SUPPLEMENTARY MATERIAL

The Supplementary Material for this article can be found online at: https://www.frontiersin.org/articles/10.3389/fcell.2020.00845/full#supplementary-material

FIGURE S1 | Nuclear envelope localization of TERB1 and TERB2 is dependent on MAJIN but not SUN1. **(A,B,E)** Expression plasmids were transfected into Cos7 cells, and then immunofluorescence assays were carried out. Nuclei were stained with Hoechst 33342. mCh: mCherry. Scale bar = 20 μm. **(A)** Cellular localization of TERB1, TERB2, and MAJIN. **(B)** Nuclear envelope localization of TERB1 and TERB2 is dependent on MAJIN. **(E)** Nuclear envelope localization of TERB1 and TERB2 is independent of SUN1. **(C,D)** Expression plasmids were transfected into HEK293T cells, and immunoprecipitation was performed to analyze the interactions of TERB1-TERB2-MAJIN.

FIGURE S2 | Sequence alignment of human and mouse SUN1.

FIGURE S3 | Uncropped images presented in **Figure 4B**. *Indicating the band of GFP-SUN1 1–210 $Aa^{\Delta 134-171}$.

REFERENCES

Burke, B. (2018). LINC complexes as regulators of meiosis. *Curr. Opin. Cell Biol.* 52, 22–29. doi: 10.1016/j.ceb.2018.01.005

Chauhan, S., Diril, M. K., Lee, J. H., Bisteau, X., Manoharan, V., Adhikari, D., et al. (2016). Cdk2 catalytic activity is essential for meiotic cell division in vivo. *Biochem. J.* 473, 2783–2798. doi: 10.1042/BCJ20160607

Conrad, M. N., Lee, C. Y., Chao, G., Shinohara, M., Kosaka, H., Shinohara, A., et al. (2008). Rapid telomere movement in meiotic prophase is promoted by NDJ1, MPS3, and CSM4 and is modulated by recombination. *Cell* 133, 1175–1187. doi: 10.1016/j.cell.2008.04.047

da Cruz, I., Brochier-Armanet, C., and Benavente, R. (2020). The TERB1-TERB2-MAJIN complex of mouse meiotic telomeres dates back to the common ancestor of metazoans. *BMC Evol. Biol.* 20:55. doi: 10.1186/s12862-020-01612-9

Daniel, K., Trankner, D., Wojtasz, L., Shibuya, H., Watanabe, Y., Alsheimer, M., et al. (2014). Mouse CCDC79 (TERB1) is a meiosis-specific telomere associated protein. *BMC Cell Biol.* 15:17. doi: 10.1186/1471-2121-15-17

Ding, X., Xu, R., Yu, J., Xu, T., Zhuang, Y., and Han, M. (2007). SUN1 is required for telomere attachment to nuclear envelope and gametogenesis in mice. *Dev. Cell* 12, 863–872. doi: 10.1016/j.devcel.2007.03.018

Dunce, J. M., Milburn, A. E., Gurusaran, M., da Cruz, I., Sen, L. T., Benavente, R., et al. (2018). Structural basis of meiotic telomere attachment to the nuclear envelope by MAJIN-TERB2-TERB1. *Nat. Commun.* 9:5355. doi: 10.1038/s41467-018-07794-7

Gonzalez, L., and Nebreda, A. R. (2020). RINGO/Speedy proteins, a family of non-canonical activators of CDK1 and CDK2. *Semin. Cell Dev. Biol.* doi: 10.1016/j.semcdb.2020.03.010 [Epub ahead of print].

Harper, L., Golubovskaya, I., and Cande, W. Z. (2004). A bouquet of chromosomes. *J. Cell Sci.* 117(Pt 18), 4025–4032. doi: 10.1242/jcs.01363

Hiraoka, Y., and Dernburg, A. F. (2009). The SUN rises on meiotic chromosome dynamics. *Dev. Cell* 17, 598–605. doi: 10.1016/j.devcel.2009.10.014

Horn, H. F., Kim, D. I., Wright, G. D., Wong, E. S., Stewart, C. L., Burke, B., et al. (2013). A mammalian KASH domain protein coupling meiotic chromosomes to the cytoskeleton. *J. Cell Biol.* 202, 1023–1039. doi: 10.1083/jcb.201304004

Lee, C. Y., Horn, H. F., Stewart, C. L., Burke, B., Bolcun-Filas, E., Schimenti, J. C., et al. (2015). Mechanism and regulation of rapid telomere prophase movements in mouse meiotic chromosomes. *Cell Rep.* 11, 551–563. doi: 10.1016/j.celrep.2015.03.045

Li, M., and Liu, K. (2020). Protection of the shelterin complex is key for tethering telomeres to the nuclear envelope during meiotic prophase Idagger. *Biol. Reprod.* 102, 771–772. doi: 10.1093/biolre/ioz231

Link, J., Leubner, M., Schmitt, J., Gob, E., Benavente, R., Jeang, K. T., et al. (2014). Analysis of meiosis in SUN1 deficient mice reveals a distinct role of SUN2 in mammalian meiotic LINC complex formation and function. *PLoS Genet* 10:e1004099. doi: 10.1371/journal.pgen.1004099

Liu, W., Wang, L., Zhao, W., Song, G., Xu, R., Wang, G., et al. (2014). Phosphorylation of CDK2 at threonine 160 regulates meiotic pachytene and diplotene progression in mice. *Dev. Biol.* 392, 108–116. doi: 10.1016/j.ydbio.2014.04.018

Long, J., Huang, C., Chen, Y., Zhang, Y., Shi, S., Wu, L., et al. (2017). Telomeric TERB1-TRF1 interaction is crucial for male meiosis. *Nat. Struct. Mol. Biol.* 24, 1073–1080. doi: 10.1038/nsmb.3496

Manterola, M., Sicinski, P., and Wolgemuth, D. J. (2016). E-type cyclins modulate telomere integrity in mammalian male meiosis. *Chromosoma* 125, 253–264. doi: 10.1007/s00412-015-0564-3

Martinerie, L., Manterola, M., Chung, S. S., Panigrahi, S. K., Weisbach, M., Vasileva, A., et al. (2014). Mammalian E-type cyclins control chromosome pairing, telomere stability and CDK2 localization in male meiosis. *PLoS Genet.* 10:e1004165. doi: 10.1371/journal.pgen.1004165

Mendez, J. (2003). Cell proliferation without cyclin E-CDK2. *Cell* 114, 398–399. doi: 10.1016/s0092-8674(03)00649-4

Mikolcevic, P., Isoda, M., Shibuya, H., del Barco Barrantes, I., Igea, A., Suja, J. A., et al. (2016). Essential role of the Cdk2 activator RingoA in meiotic telomere tethering to the nuclear envelope. *Nat. Commun.* 7:11084. doi: 10.1038/ncomms11084

Ortega, S., Prieto, I., Odajima, J., Martin, A., Dubus, P., Sotillo, R., et al. (2003). Cyclin-dependent kinase 2 is essential for meiosis but not for mitotic cell division in mice. *Nat. Genet.* 35, 25–31. doi: 10.1038/ng1232

Palm, W., and de Lange, T. (2008). How shelterin protects mammalian telomeres. *Annu. Rev. Genet.* 42, 301–334. doi: 10.1146/annurev.genet.41.110306.130350

Palmer, N., Talib, S. Z. A., and Kaldis, P. (2019). Diverse roles for CDK-associated activity during spermatogenesis. *FEBS Lett.* 593, 2925–2949. doi: 10.1002/1873-3468.13627

Pendlebury, D. F., Fujiwara, Y., Tesmer, V. M., Smith, E. M., Shibuya, H., Watanabe, Y., et al. (2017). Dissecting the telomere-inner nuclear membrane interface formed in meiosis. *Nat. Struct. Mol. Biol.* 24, 1064–1072. doi: 10.1038/nsmb.3493

Shibuya, H., Hernandez-Hernandez, A., Morimoto, A., Negishi, L., Hoog, C., and Watanabe, Y. (2015). MAJIN links telomeric DNA to the nuclear membrane by exchanging telomere cap. *Cell* 163, 1252–1266. doi: 10.1016/j.cell.2015.10.030

Shibuya, H., Ishiguro, K., and Watanabe, Y. (2014). The TRF1-binding protein TERB1 promotes chromosome movement and telomere rigidity in meiosis. *Nat. Cell Biol.* 16, 145–156. doi: 10.1038/ncb2896

Tapley, E. C., and Starr, D. A. (2013). Connecting the nucleus to the cytoskeleton by SUN-KASH bridges across the nuclear envelope. *Curr. Opin. Cell Biol.* 25, 57–62. doi: 10.1016/j.ceb.2012.10.014

Tu, Z., Bayazit, M. B., Liu, H., Zhang, J., Busayavalasa, K., Risal, S., et al. (2017). Speedy A-Cdk2 binding mediates initial telomere-nuclear envelope attachment during meiotic prophase I independent of Cdk2 activation. *Proc. Natl. Acad. Sci. U.S.A.* 114, 592–597. doi: 10.1073/pnas.1618465114

Viera, A., Alsheimer, M., Gomez, R., Berenguer, I., Ortega, S., Symonds, C. E., et al. (2015). CDK2 regulates nuclear envelope protein dynamics and telomere attachment in mouse meiotic prophase. *J. Cell Sci.* 128, 88–99. doi: 10.1242/jcs.154922

Viera, A., Rufas, J. S., Martinez, I., Barbero, J. L., Ortega, S., and Suja, J. A. (2009). CDK2 is required for proper homologous pairing, recombination and sex-body formation during male mouse meiosis. *J. Cell Sci.* 122(Pt 12), 2149–2159. doi: 10.1242/jcs.046706

Wang, L., Liu, W., Zhao, W., Song, G., Wang, G., Wang, X., et al. (2014). Phosphorylation of CDK2 on threonine 160 influences silencing of sex chromosome during male meiosis. *Biol Reprod.* 90:138. doi: 10.1095/biolreprod.113.116624

Wang, L., Tu, Z., Liu, C., Liu, H., Kaldis, P., Chen, Z., et al. (2018). Dual roles of TRF1 in tethering telomeres to the nuclear envelope and protecting them from fusion during meiosis. *Cell Death Differ.* 25, 1174–1188. doi: 10.1038/s41418-017-0037-8

Wang, W., Shi, Z., Jiao, S., Chen, C., Wang, H., Liu, G., et al. (2012). Structural insights into SUN-KASH complexes across the nuclear envelope. *Cell Res.* 22, 1440–1452. doi: 10.1038/cr.2012.126

Wang, Y., Chen, Y., Chen, J., Wang, L., Nie, L., Long, J., et al. (2019). The meiotic TERB1-TERB2-MAJIN complex tethers telomeres to the nuclear envelope. *Nat. Commun.* 10:564. doi: 10.1038/s41467-019-08437-1

Zeng, X., Li, K., Yuan, R., Gao, H., Luo, J., Liu, F., et al. (2017). Nuclear envelope-associated chromosome dynamics during meiotic prophase I. *Front. Cell Dev. Biol.* 5:121. doi: 10.3389/fcell.2017.00121

Zhang, J., Tu, Z., Watanabe, Y., and Shibuya, H. (2017). Distinct TERB1 domains regulate different protein interactions in meiotic telomere movement. *Cell Rep.* 21, 1715–1726. doi: 10.1016/j.celrep.2017.10.061

Zickler, D., and Kleckner, N. (2016). A few of our favorite things: pairing, the bouquet, crossover interference and evolution of meiosis. *Semin. Cell Dev. Biol.* 54, 135–148. doi: 10.1016/j.semcdb.2016.02.024

Conflict of Interest: The authors declare that the research was conducted in the absence of any commercial or financial relationships that could be construed as a potential conflict of interest.

Copyright © 2020 Wang, Wu, Zhou, Gao, Yun, Liang and Sun. This is an open-access article distributed under the terms of the Creative Commons Attribution License (CC BY). The use, distribution or reproduction in other forums is permitted, provided the original author(s) and the copyright owner(s) are credited and that the original publication in this journal is cited, in accordance with accepted academic practice. No use, distribution or reproduction is permitted which does not comply with these terms.

frontiers in Cell and Developmental Biology

ORIGINAL RESEARCH
published: 22 October 2020
doi: 10.3389/fcell.2020.594092

SWR1-Independent Association of H2A.Z to the LINC Complex Promotes Meiotic Chromosome Motion

Sara González-Arranz[1], Jennifer M. Gardner[2], Zulin Yu[2], Neem J. Patel[3†], Jonna Heldrich[3], Beatriz Santos[1], Jesús A. Carballo[4], Sue L. Jaspersen[2,5], Andreas Hochwagen[3] and Pedro A. San-Segundo[1]*

[1] Instituto de Biología Funcional y Genómica (IBFG), Consejo Superior de Investigaciones Científicas (CSIC) and University of Salamanca, Salamanca, Spain, [2] Stowers Institute for Medical Research, Kansas City, MO, United States, [3] Department of Biology, New York University, New York, NY, United States, [4] Centro de Investigaciones Biológicas Margarita Salas, Consejo Superior de Investigaciones Científicas (CSIC), Madrid, Spain, [5] Department of Molecular and Integrative Physiology, University of Kansas Medical Center, Kansas City, KS, United States

OPEN ACCESS

Edited by:
Akira Shinohara,
Osaka University, Japan

Reviewed by:
Verena Jantsch,
Max F. Perutz Laboratories GmbH, Austria
Sean Burgess,
University of California, Davis, United States

***Correspondence:**
Pedro A. San-Segundo
pedross@usal.es

†Present address:
Neem J. Patel,
Department of Plant and Microbial Biology, University of California, Berkeley, Berkeley, CA, United States

Specialty section:
This article was submitted to Cell Growth and Division, a section of the journal Frontiers in Cell and Developmental Biology

Received: 12 August 2020
Accepted: 11 September 2020
Published: 22 October 2020

Citation:
González-Arranz S, Gardner JM, Yu Z, Patel NJ, Heldrich J, Santos B, Carballo JA, Jaspersen SL, Hochwagen A and San-Segundo PA (2020) SWR1-Independent Association of H2A.Z to the LINC Complex Promotes Meiotic Chromosome Motion. Front. Cell Dev. Biol. 8:594092. doi: 10.3389/fcell.2020.594092

The H2A.Z histone variant is deposited into the chromatin by the SWR1 complex, affecting multiple aspects of meiosis. We describe here a SWR1-independent localization of H2A.Z at meiotic telomeres and the centrosome. We demonstrate that H2A.Z colocalizes and interacts with Mps3, the SUN component of the linker of nucleoskeleton, and cytoskeleton (LINC) complex that spans the nuclear envelope and links meiotic telomeres to the cytoskeleton, promoting meiotic chromosome movement. H2A.Z also interacts with the meiosis-specific Ndj1 protein that anchors telomeres to the nuclear periphery via Mps3. Telomeric localization of H2A.Z depends on Ndj1 and the N-terminal domain of Mps3. Although telomeric attachment to the nuclear envelope is maintained in the absence of H2A.Z, the distribution of Mps3 is altered. The velocity of chromosome movement during the meiotic prophase is reduced in the *htz1*Δ mutant lacking H2A.Z, but it is unaffected in *swr1*Δ cells. We reveal that H2A.Z is an additional LINC-associated factor that contributes to promote telomere-driven chromosome motion critical for error-free gametogenesis.

Keywords: meiosis, chromosome movement, LINC complex, H2A.Z, Mps3, Ndj1, yeast

INTRODUCTION

Meiosis is a special form of cell division that lies at the heart of gametogenesis in most sexually reproducing organisms. During meiosis, a series of complex DNA and chromosome interactions culminate in the accurate segregation of a haploid complement of chromosomes to the gametes (Keeney et al., 2014; Hunter, 2015; Zickler and Kleckner, 2015; San-Segundo and Clemente-Blanco, 2020). Chromatin remodeling events, including histone posttranslational modifications and incorporation of histone variants, play important roles in several processes during meiotic development (Brachet et al., 2012; Yamada and Ohta, 2013; Crichton et al., 2014; Ontoso et al., 2014; Yamada et al., 2018a).

H2A.Z is a variant of the canonical H2A histone that is incorporated into the chromatin by the action of the ATP-dependent SWR1 remodeling complex. SWR1 replaces an H2A–H2B

dimer by H2A.Z–H2B at defined nucleosomes, preferentially in the vicinity of promoter regions (Raisner et al., 2005; Luk et al., 2010). H2A.Z participates in a number of fundamental biological processes in vegetative cells including transcription regulation, chromatin silencing, DNA damage response, and chromosome segregation (Morillo-Huesca et al., 2010; Adkins et al., 2013; Billon and Cote, 2013; Weber and Henikoff, 2014). In addition, although the number of meiotic reports is scarce, the roles of H2A.Z during meiosis are also beginning to be elucidated in some model organisms. In plants and fission yeast, H2A.Z is required for the initiation of meiotic recombination, although the precise event influenced by H2A.Z appears to be different in both organisms. In *Arabidopsis thaliana*, H2A.Z has been proposed to regulate meiotic double-strand break (DSB) formation and repair by its association to hotspots and by controlling the expression pattern of recombination genes, whereas in *Schizosaccharomyces pombe*, H2A.Z impacts meiotic recombination by modulating chromatin architecture and the binding of DSB formation proteins to cohesin-rich domains (Choi et al., 2013; Rosa et al., 2013; Qin et al., 2014; Yamada et al., 2018b). H2A.Z is also required for proper meiotic development in *Saccharomyces cerevisiae*. The budding yeast *htz1*Δ mutant (lacking H2A.Z) displays slower kinetics of meiotic progression, reduced spore viability, and misregulated meiotic gene expression, but meiotic recombination is not, at least drastically, affected. In addition, the meiotic checkpoint response triggered by the absence of the synaptonemal complex (SC) Zip1 protein is altered in the *htz1*Δ mutant (Gonzalez-Arranz et al., 2018). Not surprisingly, many of the meiotic functions mentioned above for H2A.Z rely on its chromatin deposition mediated by the SWR1 complex.

Curiously, the physical interaction of H2A.Z with non-chromatin components has been reported in high-throughput analyses in *S. cerevisiae* (Uetz et al., 2000; Yu et al., 2008; Bommi et al., 2019). In particular, H2A.Z interacts with the SUN domain-containing Mps3 protein (Gardner et al., 2011). SUN proteins are one of the main components of the evolutionarily conserved LINC (linker of the nucleoskeleton and cytoskeleton) complex that physically connects the nuclear contents with the cytoskeletal filaments. The LINC complex is composed of an ensemble of KASH-SUN proteins. The KASH proteins span the outer nuclear membrane to interact with the cytoskeleton and also interact in the perinuclear space with SUN proteins. The SUN proteins, in turn, are embedded in the inner nuclear membrane and protrude toward the nuclear inside (reviewed by Chang et al., 2015). LINC complexes participate in a number of cellular functions, such as nuclear positioning, centrosome dynamics and attachment to the nuclear envelope (NE), and DNA repair (Friederichs et al., 2011; Fernandez-Alvarez et al., 2016; Lawrence et al., 2016; Lee and Burke, 2018). LINC complexes also play a fundamental role in meiotic chromosome movement in all organisms studied (reviewed by Burke, 2018; Link and Jantsch, 2019). In budding yeast, two KASH proteins (Mps2 and Csm4) and one SUN protein (Mps3) have been described. In mitotic cells, Mps2 localizes at the yeast centrosome equivalent called spindle pole body (SPB), forming a non-canonical LINC complex with Mps3 (Chen et al., 2019). In contrast, the meiotically induced Csm4 protein forms LINC complexes with Mps3 along the NE. A recent report has shown that, during the meiotic prophase, Mps2 also interacts with Csm4 at the NE, mediating the coupling with the Myo2 microfilament motor associated to the actin cytoskeleton (Lee et al., 2020). During the meiotic prophase, telomeres are anchored to the nucleoplasmic N-terminal domain of Mps3 by the mediation of the meiosis-specific Ndj1 protein. Forces generated in the cytoplasm by the actin cytoskeleton are transduced through the Myo2/Csm4–Mps3–Ndj1 axis to promote a telomere-led chromosome movement (**Figure 1A**). Besides facilitating homolog interactions that sustain meiotic recombination and chromosome synapsis, these movements have also been proposed to be important in disengaging non-homologous chromosome links (Chua and Roeder, 1997; Conrad et al., 1997, 2007, 2008; Trelles-Sticken et al., 2000; Kosaka et al., 2008; Koszul et al., 2008; Wanat et al., 2008; Rao et al., 2011).

Recent studies have revealed that the telomere-associated Ndj1 protein also localizes to the SPB during the meiotic prophase by interacting with Mps3. Ndj1 protein stability in combination with controlled proteolysis of Mps3 at the SPB half-bridge regulate the separation of duplicated SPBs upon meiosis I entry (Li et al., 2015, 2017). These and other observations in different organisms support a connection between telomere and centrosome functions that coordinate NE dynamics and meiotic progression (Fernandez-Alvarez and Cooper, 2017).

Although most of the roles of the H2A.Z histone variant have been ascribed to its SWR1-dependent chromatin deposition, here, we characterize in detail a SWR1-independent interaction of H2A.Z with LINC-associated components, including Mps3 and Ndj1, during the meiotic prophase. We show that H2A.Z co-localizes with the SUN protein Mps3 at telomeres and demonstrate that the Mps3–H2A.Z interaction does not occur in the context of chromatin, but depends on the stable attachment of telomeres to the NE. We demonstrate that H2A.Z is an additional novel factor connected with LINC complexes during the meiotic prophase that is required for proper meiotic chromosome movement (**Figure 1A**). We propose that at least some of the meiotic defects of the *htz1* mutant may stem from faulty processes impacted by LINC function.

RESULTS

H2A.Z Remains at Chromosome Ends in the Absence of SWR1

Our previous cytological studies have shown that H2A.Z extensively decorates meiotic chromatin in wild-type pachytene chromosomes, except in the ribosomal DNA (rDNA) region where its presence is markedly reduced (Gonzalez-Arranz et al., 2018). In the *swr1*Δ mutant, the bulk of chromatin-associated

Abbreviations: BiFC, Bimolecular fluorescence complementation; DIC, Differential interference contrast; KAc, Potassium acetate; NE, Nuclear envelope; LINC, Linker of the nucleoskeleton and cytoskeleton; rDNA, Ribosomal DNA; SC, Synaptonemal complex; SIM, Structured illumination microscopy; SPB, Spindle pole body; VC, C-terminal moiety of the Venus fluorescent protein; VN, N-terminal moiety of the Venus fluorescent protein; WCE, Whole cell extracts.

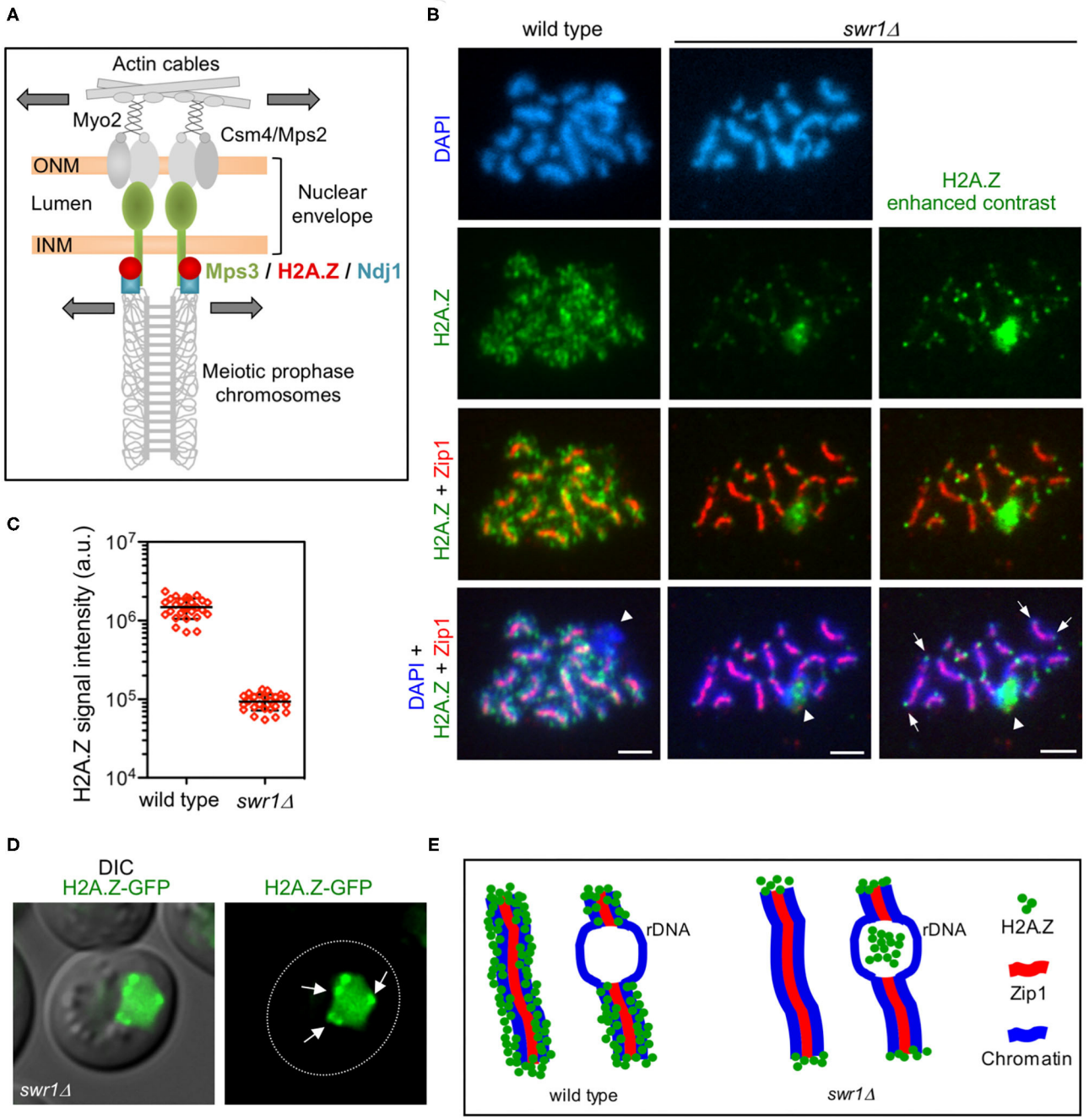

FIGURE 1 | H2A.Z localizes to chromosome ends during meiotic prophase I. **(A)** Model for the linker of the nucleoskeleton and cytoskeleton (LINC)-dependent meiotic chromosome movement. Schematic representation of the main components involved in promoting chromosome motion during meiotic prophase I in *Saccharomyces cerevisiae*, including H2A.Z as described here. *Colored* proteins are the focus of this work. Motion is depicted with *arrows*. See text for details. *ONM*, outer nuclear membrane; *INM*, inner nuclear membrane. **(B)** Immunofluorescence of spread pachytene chromosomes from wild type and *swr1*Δ stained with DAPI to visualize chromatin (*blue*), anti-GFP to detect H2A.Z (*green*), and anti-Zip1 to mark the synaptonemal complex (SC) central region (*red*). The H2A.Z signal in *swr1*Δ was obtained using a four times longer exposure time compared to the wild type. In addition, the contrast of the image shown in the *rightmost column* was computer-enhanced. Representative nuclei are shown. Spreads were prepared 16 h after meiotic induction. *Arrows* point to some telomeric H2A.Z foci. *Arrowheads* mark the nucleolar ribosomal DNA (rDNA) region devoid of Zip1. *Scale bar*, 2 μm. **(C)** Quantification of the total H2A.Z signal in nuclear spreads prepared as in **(B)**. Twenty-seven and 26 nuclei from wild type and *swr1*Δ, respectively, were scored. Mean and standard deviation values are represented. **(D)** Representative images from a *swr1*Δ live cell expressing *HTZ1-GFP* 16 h after meiotic induction. *Arrows* point to H2A.Z foci at the nuclear periphery that stick out over the diffuse pan-nuclear H2A.Z-GFP signal. *Scale bar*, 2 μm. **(E)** Cartoon representing H2A.Z localization in wild-type and *swr1*Δ pachytene chromosome based on our cytological observations. Strains in **(B,C)** are: DP840 (*HTZ1-GFP*) and DP841 (*HTZ1-GFP swr1*Δ). Strain in **(D)** is DP1108 (*HTZ1-GFP swr1*Δ).

H2A.Z is lost (Gonzalez-Arranz et al., 2018), but H2A.Z foci persisted in the absence of the SWR1 complex, as seen in enhanced images (**Figures 1B,C**). Double staining with Zip1 antibodies, as a marker of synapsed chromosomes, showed that these SWR1-independent H2A.Z foci were primarily located at chromosome ends (**Figure 1B**); 65.4% of the *swr1*Δ spread pachytene nuclei scored ($n = 26$) displayed H2A.Z at telomeres. Consistent with this telomeric localization, *swr1*Δ live meiotic cells expressing a functional *HTZ1-GFP* fusion occasionally displayed H2A.Z spots concentrated at the nuclear periphery in addition to a diffused pan-nuclear signal (**Figure 1D**). Curiously, whereas H2A.Z is largely excluded from the rDNA chromatin in wild-type nuclei (88.9%, $n = 27$ nuclei), the *swr1*Δ mutant displayed an accumulation of H2A.Z in the nucleolar area (50.0%, $n = 26$ nuclei) (**Figure 1B**, arrowhead). Nevertheless, this amorphous H2A.Z mass was mainly found inside the loop defined by the unsynapsed rDNA array, characteristic of pachytene chromosomes, but it did not appear to be associated with chromatin. A schematic representation of the H2A.Z chromosomal localization at pachytene based on cytological observations, in both wild type and *swr1*Δ, is depicted in **Figure 1E**.

Genome-Wide Association of H2A.Z to Meiotic Chromatin Requires SWR1

Next, we used chromatin immunoprecipitation sequencing (ChIP-seq) to confirm at higher resolution the SWR1 dependency for H2A.Z binding to chromatin during meiotic prophase I. Samples from cultures of wild-type and *swr1*Δ cells expressing *HTZ1-GFP* were processed at 0 and 15 h after meiotic induction. Samples from an untagged control were also taken at the same time points. The profiles of H2A.Z distribution in all chromosomes showed no strong difference between mitotic ($t = 0$ h) and meiotic prophase cells ($t = 15$ h) and revealed that genome-wide incorporation of H2A.Z is abolished in the absence of SWR1 (**Supplementary Figures 1A–C**). Consistent with previous reports in mitotic cells showing that H2A.Z is enriched at the nucleosomes flanking the transcription start site of genes (Raisner et al., 2005; Luk et al., 2010), our analysis of the H2A.Z position relative to open reading frames (ORFs) revealed that, indeed, H2A.Z was enriched at the beginning of ORFs in vegetative cells, thus validating this ChIP-seq study (**Supplementary Figure 1D**). We also found the same situation in meiotic cells (**Supplementary Figure 1E**). Importantly, the meta-ORF profiles of the *swr1*Δ mutant were similar to those of the untagged control, implying that H2A.Z chromatin binding to gene promoters was completely abolished in the absence of SWR1 (**Supplementary Figures 1D,E**). Thus, like in mitotic cells, the SWR1 complex is absolutely required for genome-wide H2A.Z chromatin deposition also during meiotic prophase I.

H2A.Z Interacts and Colocalizes With Mps3 at Telomeres During Meiotic Prophase

Previous studies in vegetative cells have described a physical interaction between H2A.Z and the Mps3 protein (Gardner et al., 2011; Morillo-Huesca et al., 2019). Moreover, a recent study also reported the co-purification of H2A.Z and Mps3 from meiotic cells using mass spectrometry analysis (Bommi et al., 2019). Consistent with these observations, we found that the H2A.Z-GFP foci detected in some *swr1*Δ live meiotic cells at the nuclear periphery colocalized with Mps3-mCherry (**Figure 2A**, arrows). Note that there was also a peripheral zone with H2A.Z-GFP, but devoid of Mps3-mCherry (**Figure 2A**, arrowhead), that corresponds to the accumulation of H2A.Z observed in the vicinity of the nucleolar area in the *swr1*Δ mutant (**Figures 1B,E**, **Supplementary Figure 2**; see also **Figure 2B**). We next used chromosome spreading for a more detailed analysis of H2A.Z and Mps3 colocalization. It has been shown that, despite being embedded in the inner nuclear membrane, the Mps3 protein remains associated to the telomeres in spread preparations of meiotic prophase nuclei (Conrad et al., 2007; Lee et al., 2012). We detected a significant colocalization of H2A.Z and Mps3 foci at telomeres of meiotic prophase chromosomes (Pearson's correlation coefficient, 0.741; $n = 27$ nuclei) (**Figure 2B**), suggesting that H2A.Z and Mps3 also interact during the meiotic prophase. To confirm the meiotic interaction between H2A.Z and Mps3, we carried out co-immunoprecipitation experiments. We found that Mps3 (tagged with 3HA) was detected in immunoprecipitates of *HTZ1-GFP* strains pulled down with anti-GFP antibodies (**Figure 2C**). Conversely, H2A.Z was present in immunoprecipitates of *MPS3-GFP* meiotic cells pulled down with anti-GFP antibodies (**Figure 2D**). Although the amount of H2A.Z was reduced in whole cell extracts (WCE) from the *swr1*Δ mutant, co-immunoprecipitation of H2A.Z and Mps3 occurred both in wild-type and *swr1*Δ meiotic cells (**Figures 2C,D**). Of note is that the immunoprecipitation of Mps3-GFP specifically brought down H2A.Z, but not the canonical histones (**Figure 2D**). In sum, consistent with previous analyses, these observations indicate that Mps3 and H2A.Z physically interact also during the meiotic prophase in a SWR1-independent manner. The colocalization at the end of chromosomes suggests that the Mps3–H2A.Z interaction occurs, at least, in the proximity of telomeres.

H2A.Z and Ndj1 Interact at the Nuclear Periphery

We used the bimolecular fluorescence complementation technique (BiFC) to further explore the physical interaction between H2A.Z and other LINC-associated components, such as Ndj1. BiFC permits direct visualization of protein interactions in living cells based on the association between two non-fluorescent fragments of a fluorescent protein brought in proximity by the interaction between proteins fused to the fragments (Kerppola, 2008; Miller et al., 2015). We found that H2A.Z and Ndj1 interact at the NE, as manifested by the reconstitution of fluorescence from the Venus variant of the yellow fluorescent protein ($Venus^{YFP}$) at the nuclear periphery in meiotic cells simultaneously expressing both moieties of $Venus^{YFP}$ fused to H2A.Z and Ndj1 (*HTZ1-VN* and *NDJ1-VC*, respectively) (**Figures 3A,D**). Importantly, the H2A.Z–Ndj1 interaction was detected not only in the *swr1*Δ mutant but also in the wild type (**Figures 3B,D**). This result indicates that the telomeric

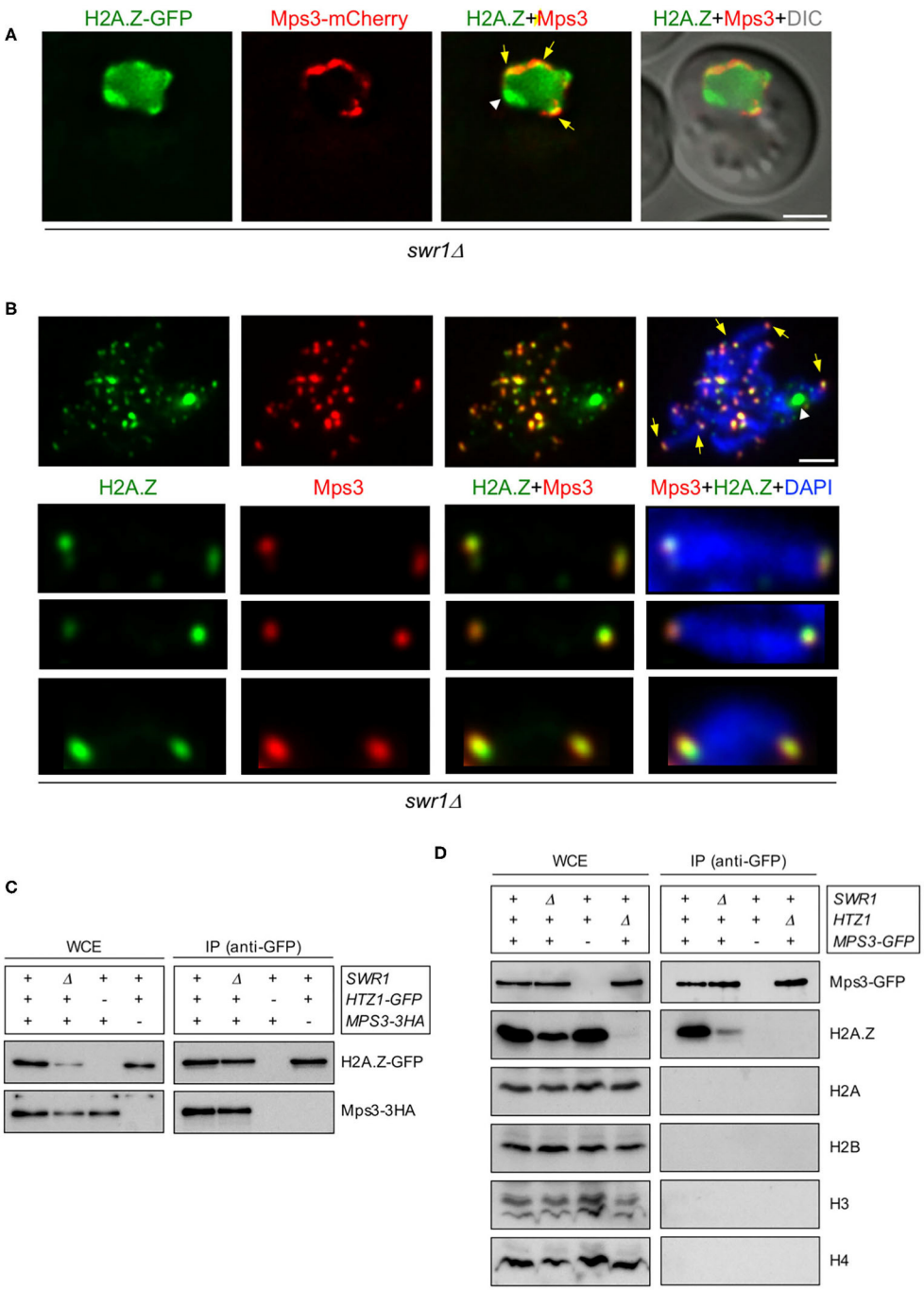

FIGURE 2 | H2A.Z interacts and colocalizes with Mps3 at telomeres. **(A)** Images from a representative *swr1*Δ live cell expressing *HTZ1-GFP* and *MPS3-mCherry* 16 h after meiotic induction. *Yellow arrows* point to areas of the nuclear periphery where H2A.Z and Mps3 display colocalization. The *white arrowhead* points to the presumed accumulation of H2A.Z at the nucleolus. The differential interference contrast (DIC) image is shown as a reference for the cell outline. *Scale bar*, 2 μm. **(B)** Immunofluorescence of spread pachytene chromosomes from the *swr1*Δ mutant stained with DAPI to visualize chromatin (*blue*), anti-GFP to detect H2A.Z (*green*), and anti-mCherry to detect Mps3 (*red*). A representative nucleus is shown. The *bottom panels* display selected individual chromosomes. Spreads were prepared 16 h after meiotic induction. *Yellow arrows* point to some telomeric foci showing H2A.Z and Mps3 colocalization. The *white arrowhead* marks the accumulation of H2A.Z at the nucleolar ribosomal DNA (rDNA) region in *swr1*Δ. *Scale bar*, 2 μm. The strains used in **(A,B)** are DP1108 (*HTZ1-GFP MPS3-mCherry swr1*Δ) and DP1395 (*HTZ1-GFP MPS3-3HA swr1*Δ), respectively. **(C)** Whole cell extracts (WCE) prepared 16 h after meiotic induction were immunoprecipitated using GFP-Trap beads. WCE and immunoprecipitates (IP) were analyzed by Western blot using anti-GFP antibodies (to detect H2A.Z) and anti-HA antibodies (to detect Mps3). The strains used are: DP1394 (*SWR1 HTZ1-GFP MPS3-3HA*), DP1395 (*swr1*Δ *HTZ1-GFP MPS3-3HA*), DP1330 (*SWR1 HTZ1 MPS3-3HA*), and DP840 (*SWR1 HTZ1-GFP MPS3*). **(D)** WCE prepared 16 h after meiotic induction were immunoprecipitated using GFP-Trap beads. WCE and IP were analyzed by Western blot using anti-GFP antibodies (to detect Mps3) and anti-H2A.Z, anti-H2A, anti-H2B, anti-H3, and anti-H4 histone antibodies. The strains used are: DP866 (*SWR1 HTZ1 MPS3-GFP*), DP1102 (*swr1*Δ *HTZ1 MPS3-GFP*), DP421 (*SWR1 HTZ1 MPS3*), and DP867 (*SWR1 htz1*Δ *MPS3-GFP*).

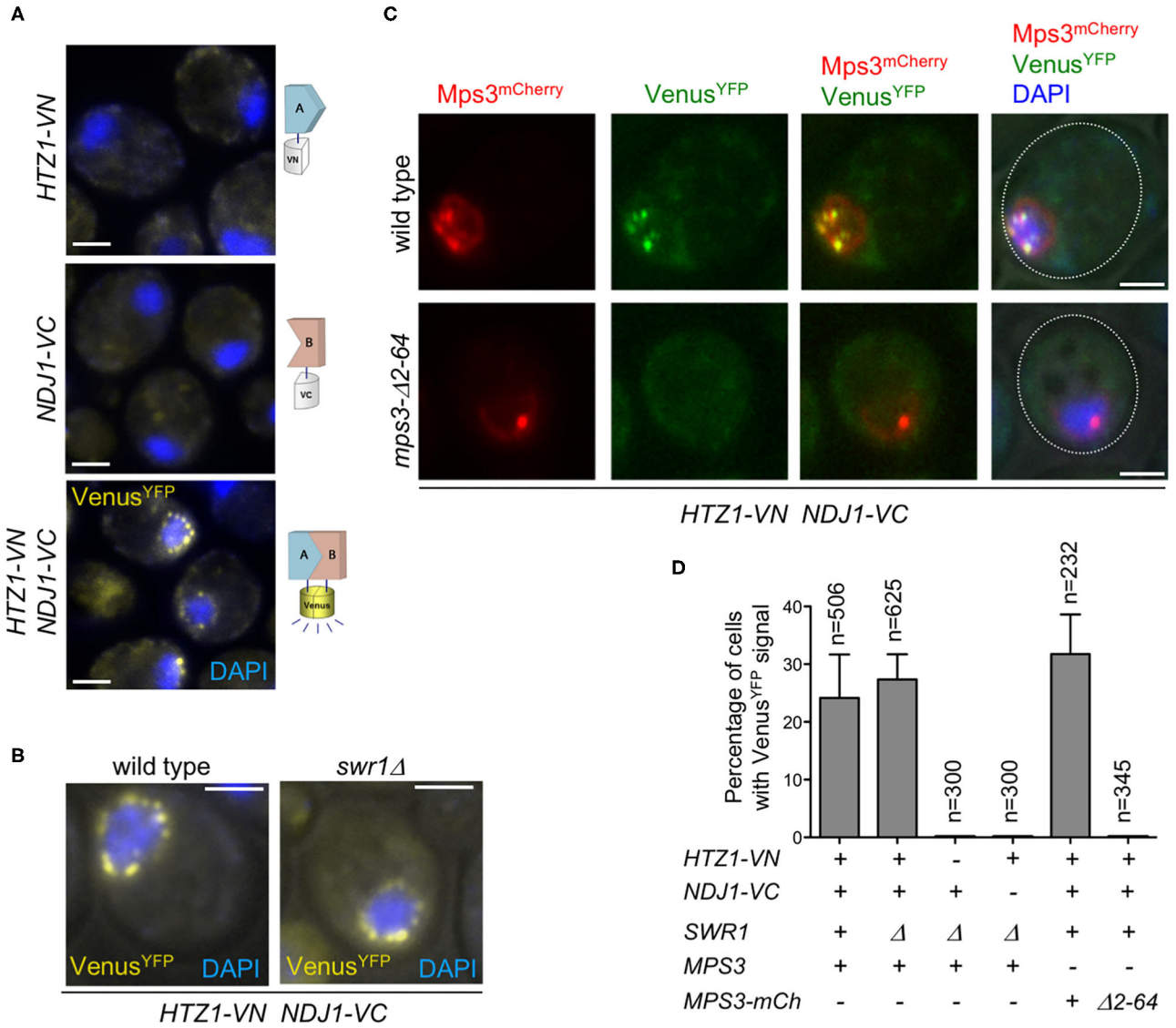

FIGURE 3 | Analysis of H2A.Z and Ndj1 interaction by bimolecular fluorescence complementation (BiFC) assay. **(A,B)** H2A.Z and Ndj1 interact at the nuclear periphery. Microscopy fluorescence images of cells expressing *HTZ1* fused to the N-terminal half of the Venus^{YFP} (*VN*) and/or *NDJ1* fused to the C-terminal half of the Venus^{YFP} (*VC*) as indicated. Nuclei are stained with DAPI (*blue*). The reconstitution of Venus^{YFP} fluorescence resulting from H2A.Z-VN/Ndj1-VC interaction appears in *yellow*. Images were taken 16 h after meiotic induction. The strains in **(A)** are: DP1540 (*HTZ1-VN*), DP1541 (*NDJ1-VC*), and DP1493 (*HTZ1-VN NDJ1-VC swr1*Δ). The strains in **(B)** are: DP1496 (*HTZ1-VN NDJ1-VC*) and DP1493 (*HTZ1-VN NDJ1-VC swr1*Δ). **(C)** H2A.Z and Ndj1 interaction at the nuclear periphery depends on the 2–64 N-terminal domain of Mps3. Mps3-mCherry signal is shown in *red*, Venus^{YFP} in *green*, and DAPI in *blue*. The cells were imaged 16 h after meiotic induction. The strains in **(C)** are: DP1511 (*MPS3-mCherry HTZ1-VN NDJ1-VC*) and DP1512 (*mps3-Δ2-64-mCherry HTZ1-VN NDJ1-VC*). A single medial plane is shown in **(A–C)**. **(D)** Quantification of the percentage of cells displaying Venus^{YFP} fluorescent signal in the experiments shown in **(A–C)**. At least three quantification analyses were performed. The total number of cells scored (*n*) is shown. *Error bars*, SD. *Scale bar*, 2 μm.

localization of H2A.Z is not an exclusive feature of the *swr1*Δ mutant and also occurs in the wild type, where it is masked in our cytological analysis of spread nuclei by the massive deposition of H2A.Z throughout the genome. We detected the reconstituted Venus^{YFP} signal in a fraction of cells in the culture (24.2 and 27.3% for wild type and *swr1*Δ, respectively) that roughly represents the population of prophase cells in the asynchronous BR strain background at the time point analyzed. In fact, a parallel meiotic culture used as a control for staging displayed ≈34% of cells with Zip1-GFP signal at the same time point. Indeed, the use of a *ndt80*Δ mutation that prevents exit from prophase I increased the proportions of cells displaying H2A.Z–Ndj1 interaction to 54 and 55% in *SWR1* and *swr1*Δ, respectively, and the fraction of cells containing the Hop1-GFP prophase I marker to 70% (**Supplementary Figure 3**). That is, the interaction was detected in ≈80% of prophase cells. This is

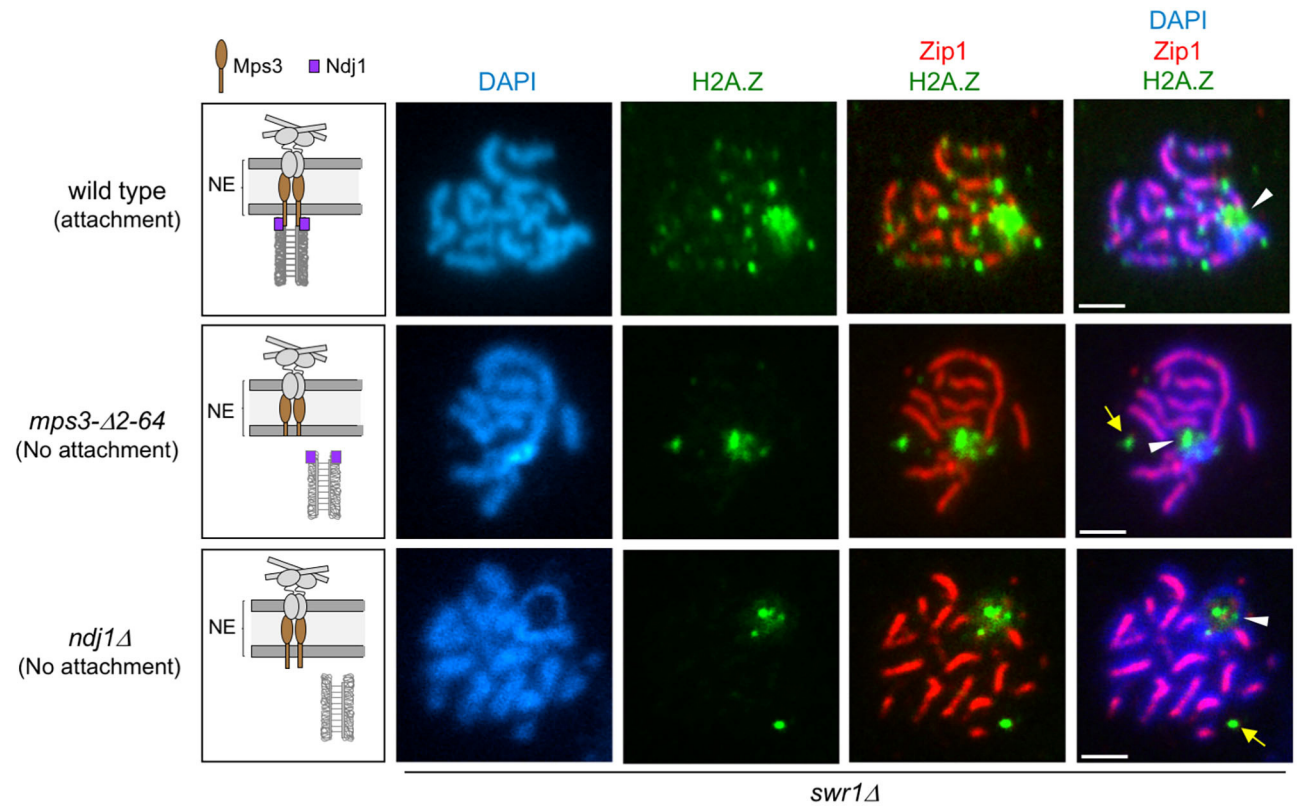

FIGURE 4 | H2A.Z localization at chromosome ends requires telomere attachment to the nuclear envelope (NE). Immunofluorescence of spread pachytene nuclei from the *swr1*Δ mutant stained with DAPI to visualize chromatin (*blue*), anti-GFP to detect H2A.Z (*green*), and anti-Zip1 to mark the synaptonemal complex (SC) central region (*red*). *White arrowheads* mark the ribosomal DNA (rDNA) region lacking Zip1. *Yellow arrows* point to H2A.Z foci likely corresponding to the spindle pole body (SPB; see text). The *cartoons on the left* schematize the linker of the nucleoskeleton and cytoskeleton (LINC) complex and the status of telomeric attachment in the different situations analyzed. *Scale bar*, 2 μm. The strains are DP1182 (wild type), DP1280 (*mps3-Δ2-64*), and DP1305 (*ndj1*Δ). Twenty-six, 28, and 24 nuclei were examined for wild type, *mps3-Δ2-64*, and *ndj1*Δ, respectively.

consistent with the observation that Ndj1-mediated tethering of telomeres to the NE only occurs in meiotic prophase I (Conrad et al., 2007). Of note is that, when the BiFC assay was performed in cells also expressing *MPS3-mCherry*, we observed that the Venus^{YFP} signal resulting from the H2A.Z–Ndj1 interaction largely colocalized with Mps3 foci, thus confirming that it occurs at telomere attachment sites at the NE (**Figure 3C**, upper row).

Telomeric Localization of H2A.Z Depends on Telomere–NE Anchoring

We next examined H2A.Z localization in mutants that compromise LINC-dependent telomere attachment to the NE, such as *mps3-Δ2-64* and *ndj1*Δ. The *mps3-Δ2-64* mutant lacks the 2–64 amino acids of the Mps3 N-terminal domain. In the wild-type Mps3 protein, this region protrudes into the nuclear inside serving as a telomeric docking site via the Ndj1 protein (Conrad et al., 2007); therefore, in both *mps3-Δ2-64* and *ndj1*Δ mutants, telomere anchoring to the NE is impaired (**Figure 4**, left panels). We carried out this analysis in a *swr1*Δ mutant to get rid of the massive deposition of H2A.Z throughout the chromatin, enabling us to detect its telomeric localization. We found that the localization of H2A.Z at telomeres was lost in the *swr1*Δ *mps3-Δ2-64* and *swr1*Δ *ndj1*Δ spread pachytene nuclei (**Figure 4**). Moreover, the H2A.Z–Ndj1 interaction detected by BiFC was abolished in the *mps3Δ2-64* mutant (**Figures 3C,D**), further supporting the notion that H2A.Z is recruited to an intact LINC complex. Of note is that the presence of H2A.Z in the nucleolar vicinity observed in *swr1*Δ was maintained in the *swr1*Δ *mps3-Δ2-64* and *swr1*Δ *ndj1*Δ double mutants (**Figure 4**, arrowheads). Likewise, a strong H2A.Z focus not associated with the chromosomes that likely corresponds to the SPB (see below) was also detected (**Figure 4**, yellow arrows). Thus, these observations suggest that the association of H2A.Z to the telomeric regions specifically requires functional anchoring of the chromosomes to the NE mediated by the inner components of LINC.

H2A.Z Also Colocalizes With Ndj1 and Mps3 at the SPB During Meiosis

Several studies have shown that, in addition to telomeres, Mps3 and Ndj1 are also localized at the SPB in meiotic cells (Rao et al., 2011; Li et al., 2015). Since we have observed the colocalization and interaction between H2A.Z and Mps3/Ndj1 at telomeres, we examined whether H2A.Z is also targeted to the SPB. In

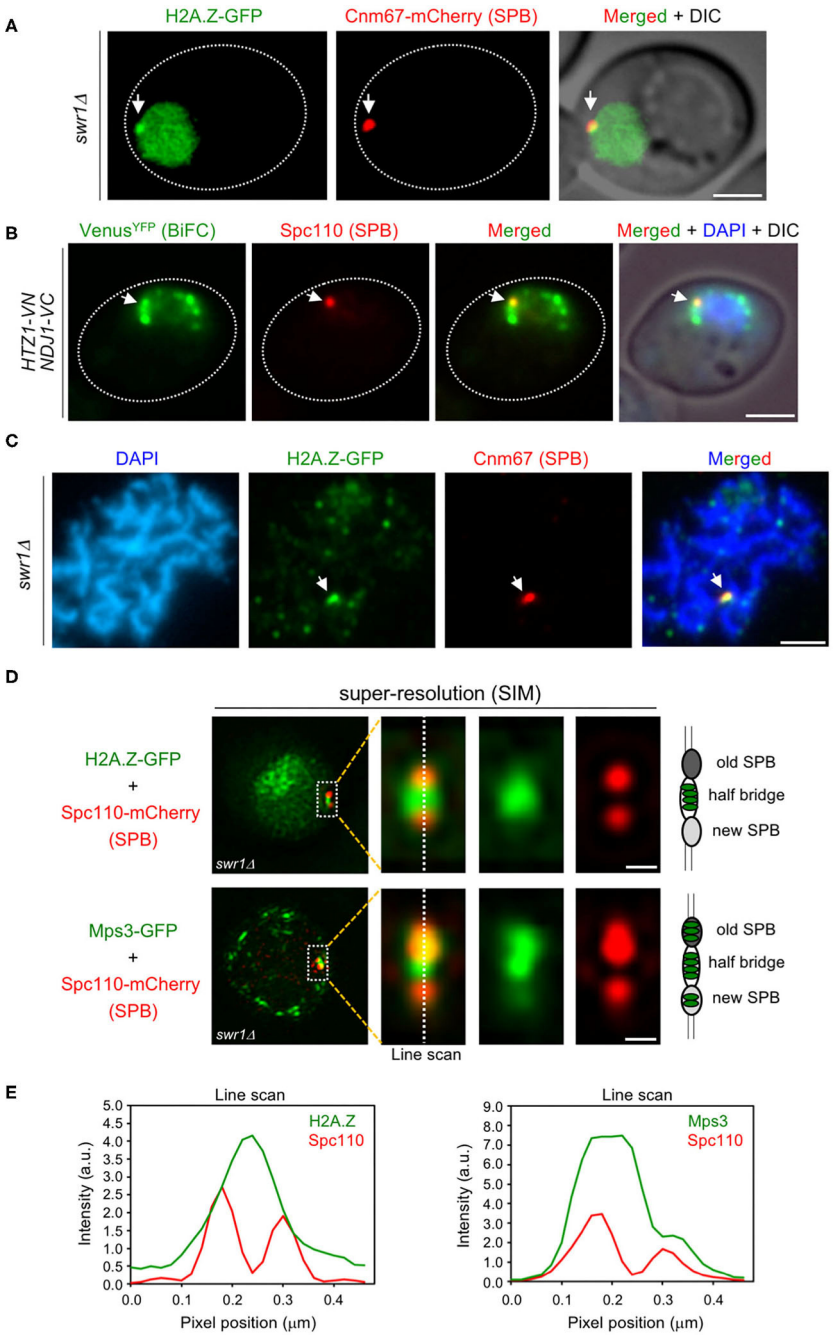

FIGURE 5 | H2A.Z localizes to the spindle pole body (SPB) half-bridge during meiotic prophase I. **(A)** Microscopy fluorescence image of a representative *swr1*Δ cell displaying a peripheral concentrated focus (*arrow*) of H2A.Z-GFP (*green*) colocalizing with the SPB marker Cnm67-mCherry (*red*). Images were taken from 16-h meiotic cultures. *Scale bar*, 2 μm. The strain is DP1172. **(B)** Bimolecular fluorescence complementation (BiFC) analysis of Venus^{YFP} fluorescence (*green*) reconstituted from H2A.Z-VN/Ndj1-VC interaction in cells also expressing the SPB marker Spc110-RedStar2 (*red*). Nuclei were stained with DAPI (*blue*). A representative cell is shown. The *arrow* points to a single BiFC Venus^{YFP} focus colocalizing with the SPB. *Scale bar*, 2 μm. The strain is DP1506. **(C)** Immunofluorescence of a spread pachytene representative nucleus stained with DAPI to visualize chromatin (*blue*), anti-GFP to detect H2A.Z (*green*), and anti-mCherry to mark the SPB (*red*). The *arrow* points to an H2A.Z focus colocalizing with Cnm67 (SPB). *Scale bar*, 2 μm. The strain is DP1172. Twenty-five nuclei were examined. **(D)** Structured illumination microscopy (SIM) fluorescence images of representative *swr1*Δ cells expressing Spc110-mCherry (*red*) and H2A.Z-GFP (*top images*) or Mps3-GFP (*bottom images*), in *green*. *Scale bar*, 0.1 μm. **(E)** Average intensity of the indicated proteins along the depicted line scan in all cells analyzed in **(D)**. The strains are DP1578 (*HTZ1-GFP SPC110-mCherry*) and DP1576 (*MPS3-GFP SPC110-mCherry*); 33 and 26 cells were examined, respectively.

*swr1*Δ live meiotic cells, we observed that one of the peripheral spots of H2A.Z-GFP colocalized with the SPB core component Cnm67-mCherry (**Figure 5A**). Moreover, BiFC analysis revealed that one of the DAPI-surrounding foci where H2A.Z and Ndj1 interact corresponds to the SPB, as shown by the colocalization of the $Venus^{YFP}$ signal with Spc110, another SPB component, tagged with RedStar2 (**Figure 5B**). Immunofluorescence of spread meiotic chromosomes also showed colocalization between Cnm67 and H2A.Z at a defined focus (**Figure 5C**). However, in contrast to the telomeric localization of H2A.Z (**Figure 4**), the presence of H2A.Z at the SPB was maintained in *mps3*Δ*2-64* and *ndj1*Δ mutants during the meiotic prophase, as manifested by the detection of a single H2A.Z focus associated to the characteristic monopolar prophase I spindle stained with tubulin antibodies (**Supplementary Figure 4**). Thus, like in telomeres, our results suggest that Mps3, Ndj1, and H2A.Z also interact at the SPB, but our findings reflect differential requirements for targeting H2A.Z to the various subcellular locations.

H2A.Z Localizes to the SPB Half-Bridge

To determine the precise localization of H2A.Z within the SPB structure during the meiotic prophase, we used structured illumination microscopy (SIM). We examined the colocalization of H2A.Z-GFP, as well as Mps3-GFP for comparison, with the Spc110-mCherry protein, a component of the SPB inner plaque (**Figure 5D**). We focused on prophase cells containing duplicated unseparated SPBs. The old and new SPBs could be distinguished by the stronger and weaker Spc110-mCherry signal, respectively (Burns et al., 2015). Most of the H2A.Z-GFP signal concentrated in the area in between both SPBs that corresponds to the half-bridge, and only a limited overlap with the SPBs was observed (**Figure 5E**, left graph). Like H2A.Z, Mps3-GFP was also detected in the half-bridge, but also displayed a more extensive colocalization with Spc110-mCherry (**Figure 5E**, right graph), consistent with the idea that Mps3 is a dual component of the bridge and the membrane domain that surrounds the SPB core (Chen et al., 2019). Thus, we conclude that the fraction of H2A.Z present in the SPB mainly localizes to the half-bridge structure that tethers duplicated SPBs during meiotic prophase I.

Altered Distribution of Mps3 Along the NE in the Absence of H2A.Z

To further explore the meiotic relationship between Mps3 and H2A.Z, we examined the Mps3 levels and localization in the *htz1*Δ mutant. Western blot analysis of Mps3 production in meiotic cultures showed that the protein was heavily induced during the meiotic prophase and then declined at late time points as meiosis and sporulation progresses (**Figure 6A**). The dynamics of Mps3 production was similar in wild type and *htz1*Δ, but global Mps3 levels were reduced in the *htz1*Δ mutant. To rule out the possibility that the reduction in the amount of Mps3 was exclusively due to an inefficient meiotic progression in *htz1*Δ (Gonzalez-Arranz et al., 2018), we measured the Mps3 levels in the prophase-arrested *ndt80*Δ mutant, monitoring also Mek1 production as a proxy for a meiotic prophase I protein (Ontoso et al., 2013). This analysis revealed that the lack of H2A.Z specifically affects the Mps3, but not Mek1, global levels (**Supplementary Figure 5**). By immunofluorescence of pachytene chromosome spreads, we found that Mps3 remained at telomeres in the absence of H2A.Z. However, Mps3 telomeric localization was lost in the *ndj1*Δ mutant used as a control for comparison (Conrad et al., 2007) (**Figure 6B**). Thus, although H2A.Z telomeric localization depends on the N-terminal domain of Mps3 (see above), the anchoring of Mps3 to telomeres is independent of H2A.Z. We also examined Mps3-GFP localization in live meiotic cells. The presence of a Hop1-mCherry signal was used to stage cells in prophase I (**Figure 6C**). Analysis of the pattern of Mps3-GFP localization in whole meiotic prophase cells revealed foci with a rather uniform distribution along the NE in the wild type. In contrast, Mps3 showed a more irregular distribution, and it appeared to be more concentrated at defined NE regions at a higher frequency in the *htz1*Δ mutant (**Figures 6C,D**, **Supplementary Video 1**). We conclude that H2A.Z is required for the proper distribution of Mps3 along the NE during meiotic prophase I, but not for telomere attachment.

Chromosome Motion Is Reduced in the Absence of H2A.Z

One of the main meiotic functions of the LINC complex is to promote telomere-led chromosome movement during prophase I (Conrad et al., 2008; Koszul et al., 2008). Since we found that H2A.Z interacts with LINC components during meiosis, we hypothesized that H2A.Z could also contribute to meiotic chromosome motion. Initially, we used strains expressing *ZIP1-GFP* to follow chromosome movement, as previously described (Scherthan et al., 2007; Sonntag Brown et al., 2011). In addition to wild-type and *htz1*Δ strains, we also analyzed the *ndj1*Δ mutant as a control for defective chromosome mobility and the *swr1*Δ mutant in which H2A.Z is not deposited into the chromatin (see above). To minimize experimental variation, we mixed wild-type and mutant cells from meiotic cultures (16 h) in the same microscopy culture chamber to analyze chromosome movement in parallel. Wild-type cells could be easily distinguished by the presence of Pma1-mCherry, a plasma membrane protein that was tagged to mark these cells (**Figure 7A**). We tracked the ends of individual synapsed chromosomes and measured the distance traveled during a defined time (**Figure 7B**, **Supplementary Video 2**). We found that the average velocity of chromosome movement was reduced in the *htz1*Δ mutant, although to a lesser extent than in *ndj1*Δ. In contrast, the *swr1*Δ mutant was not affected (**Figure 7C**).

Velocity measurements based on Zip1-GFP rely on the ability to track a single chromosome pair in the maze of all synapsed chromosomes, which is not always possible. Therefore, for a more extensive and accurate analysis of telomere-driven movement, we used a *tetO–tetR* system (Clemente-Blanco et al., 2011) to generate strains harboring the left telomere of chromosome IV (*TEL4L*) labeled with GFP (**Figure 8A**). These strains also expressed *ZIP1-mCherry* as a marker for the prophase I stage and synapsed chromosomes (**Figures 8B,C**). In addition, we also introduced the P_{CUP1}-*IME1* construct to

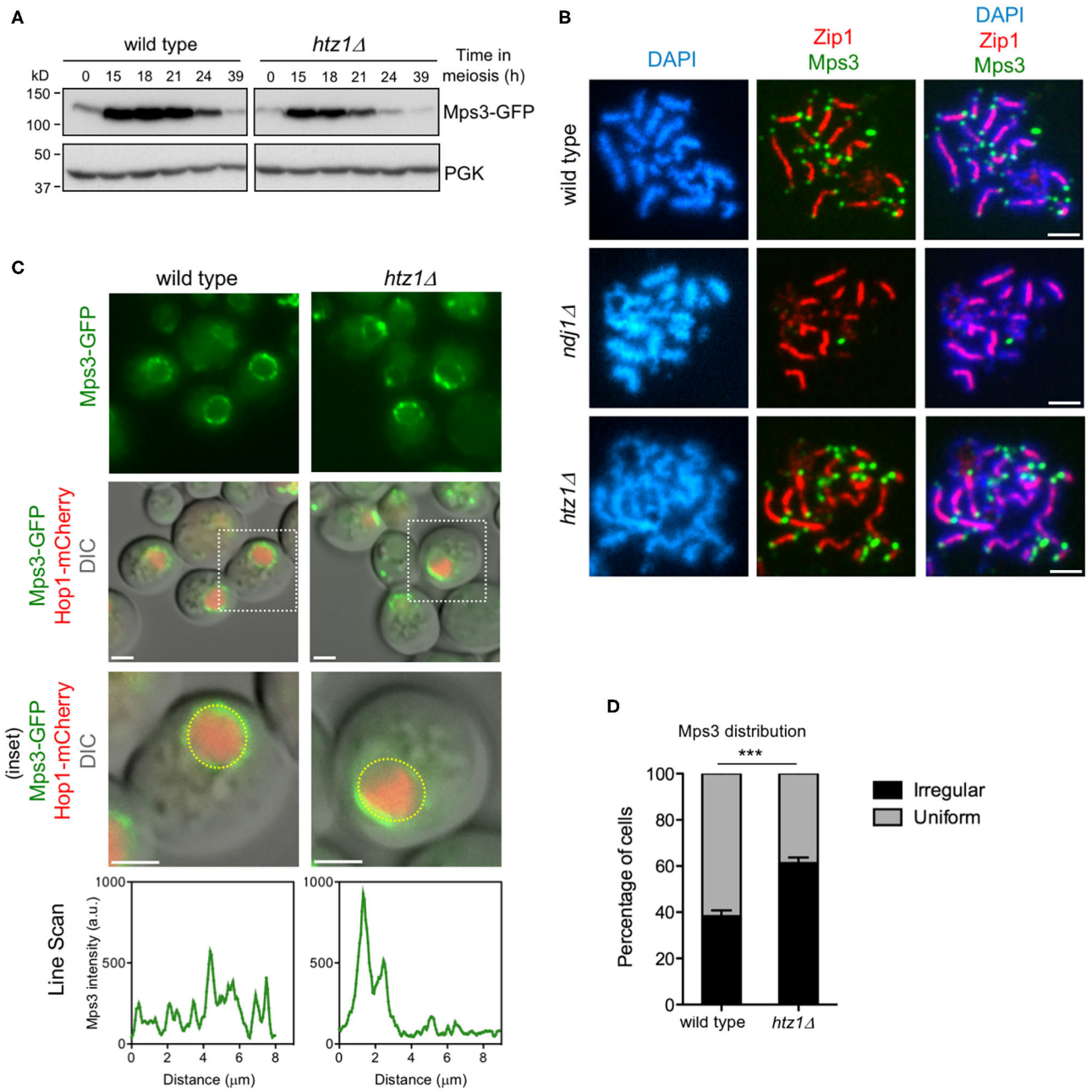

FIGURE 6 | Altered levels and distribution of Mps3 in the absence of H2A.Z. **(A)** Western blot analysis of Mps3 production during meiosis detected with anti-GFP antibodies. PGK was used as a loading control. The strains in **(A)** are: DP866 (wild type) and DP867 (*htz1*Δ). **(B)** Immunofluorescence of spread pachytene nuclei stained with DAPI to visualize chromatin (*blue*), anti-green fluorescent protein (GFP) to detect Mps3 (*green*), and anti-Zip1 to mark the synaptonemal complex (SC) central region (*red*). *Scale bar*, 2 μm. The strains in **(B)** are: DP866 (wild type), DP1103 (*ndj1*Δ), and DP867 (*htz1*Δ). **(C)** Microscopy fluorescence images of cells expressing *MPS3-GFP* and *HOP1-mCherry*. The presence of Hop1-mCherry was used to detect meiotic prophase cells. Stacks of images in the *Z*-axis were taken, but a single central plane from representative cells is shown. The *line scan plots* represent the GFP signal along the depicted *yellow circle line* in the *bottom row cells*. *Scale bar*, 2 μm. **(D)** The distribution of Mps3 was analyzed in maximum-intensity projections from images obtained as in **(C)**. Two categories were established: uniform and irregular. Cells scored as "uniform" display Mps3-GFP signal homogeneously distributed. Cells scored as "irregular" display Mps3-GFP signal concentrated to one area of the nuclear envelope (NE). Only cells displaying the Hop1-mCherry signal were considered in the analysis. This quantification was performed in triplicate. Student's *t*-test: $P = 0.0003$ (***). A total of 383 and 387 cells were scored for wild type and *htz1*Δ, respectively. The strains in **(C,D)** are: DP1032 (wild type) and DP1033 (*htz1*Δ).

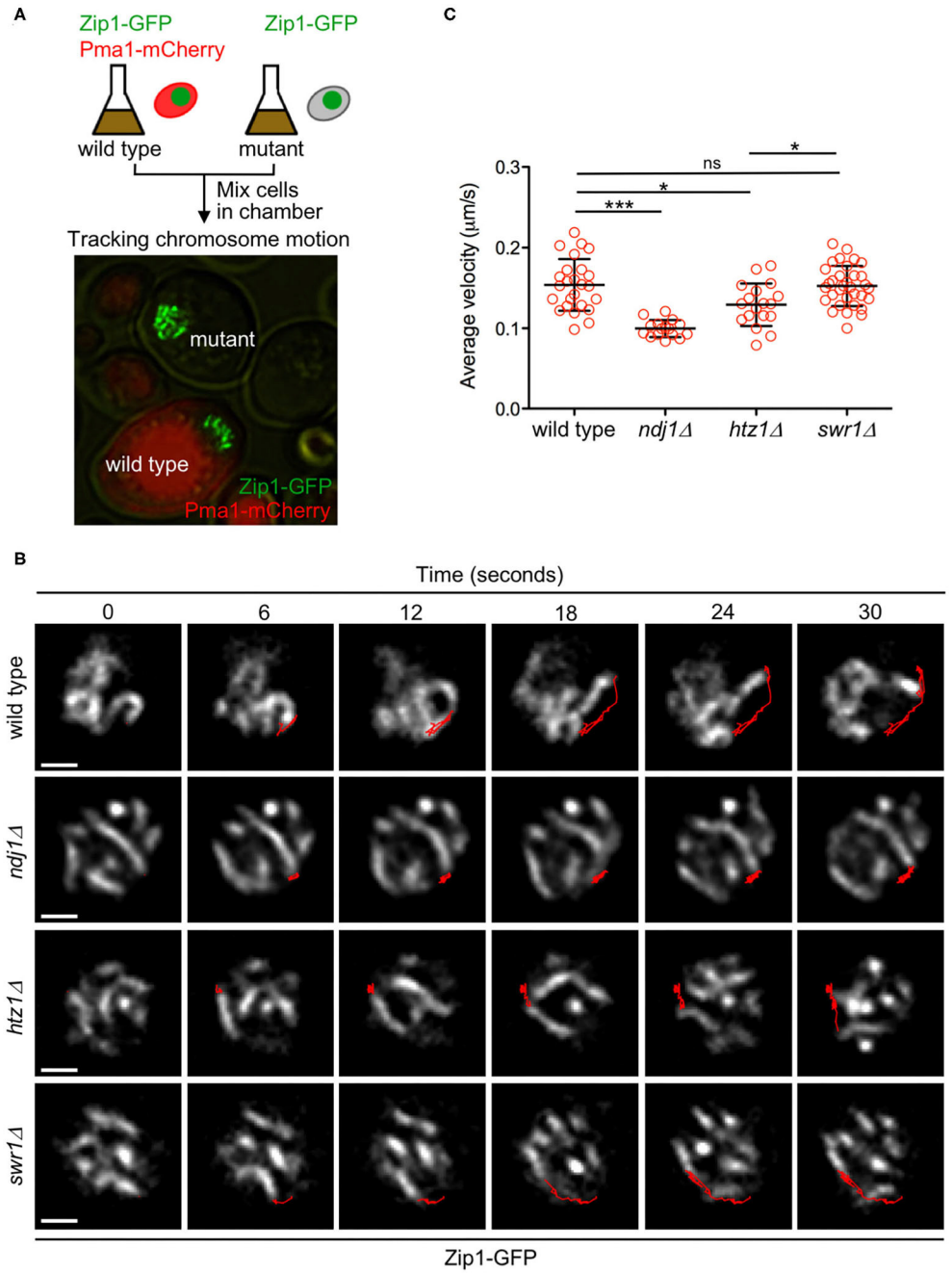

FIGURE 7 | H2A.Z drives prophase chromosome movement. **(A)** Experimental setup to monitor the movement of Zip1-GFP-labeled chromosomes. Aliquots of cells from 16-h meiotic cultures of wild type and *ndj1*Δ, *htz1*Δ, or *swr1*Δ, mutants were mixed in microscopy chambers and followed in parallel by time-lapse fluorescence microscopy. Wild-type cells were distinguished by the presence of Pma1-mCherry. **(B)** Representative images of nuclei from the indicated strains at different time intervals. The Zip1-GFP signal is shown. The *red line* represents the path traveled by an individual chromosome end throughout the time lapse. *Scale bar*, 1 μm. **(C)** Quantification of the average velocity of chromosome movement. The mean and SD are represented. One-way ANOVA was used for statistical comparison (*$P <$ 0.05; ***$P <$ 0.001). The strains are DP1057 (wild type), DP957 (*ndj1*Δ), DP838 (*htz1*Δ), and DP1091 (*swr1*Δ). Twenty-five, 16, 18, and 33 chromosome measurements from different cells of wild type, *ndj1*Δ, *htz1*Δ, and *swr1*Δ, respectively, were performed in several independent time-lapse experiments.

increase the synchrony of the meiotic cultures (Chia and van Werven, 2016). The *TEL4L* trajectory was tracked in time-lapse experiments of the wild-type, *ndj1*Δ, *htz1*Δ, and *swr1*Δ strains (**Figure 8D**, **Supplementary Video 3**). Measurements of both the average and maximum velocity of *TEL4L* movement during prophase I using this system also revealed that

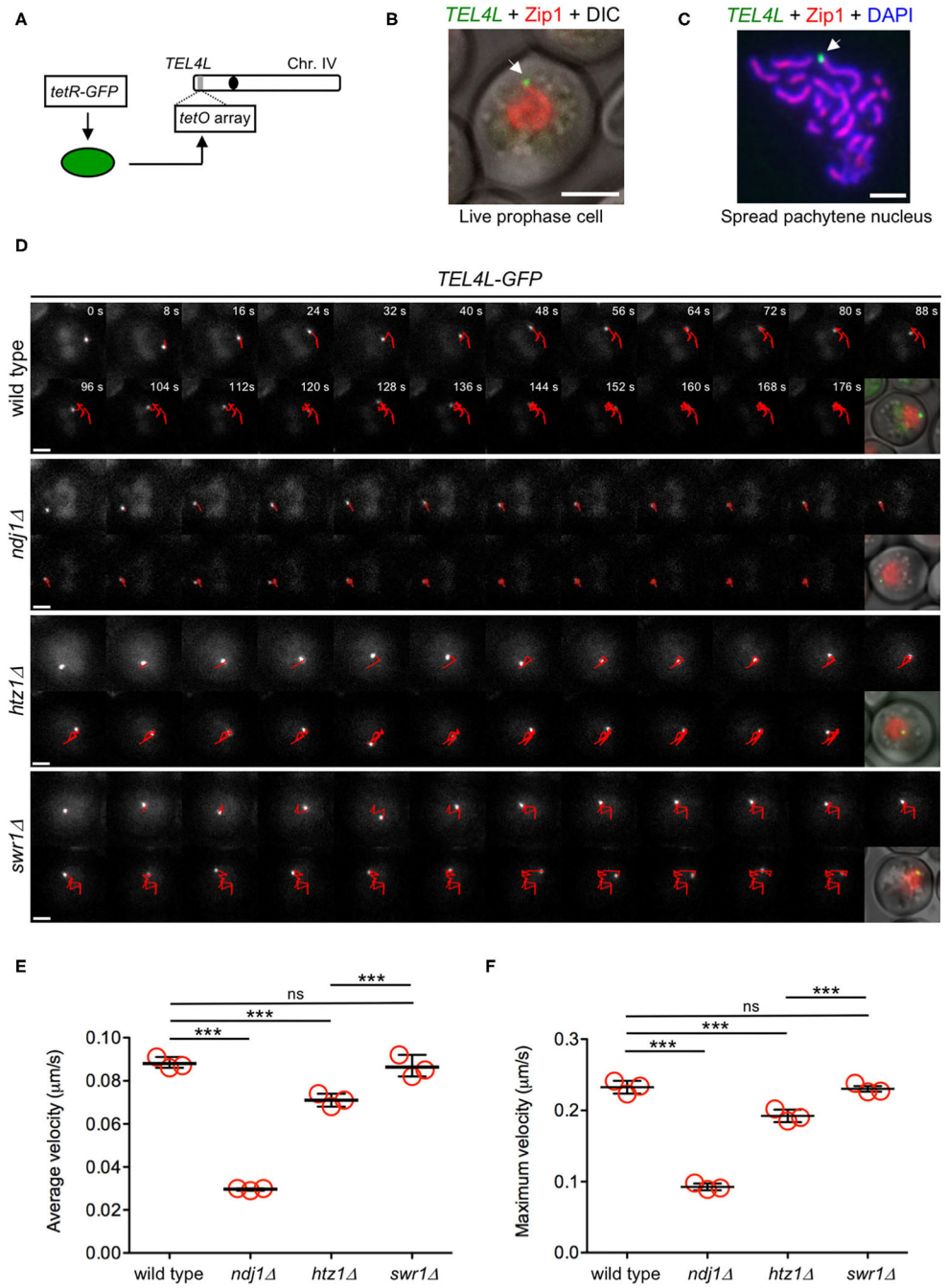

FIGURE 8 | H2A.Z, but not SWR1, is required for proper telomere motion during the meiotic prophase. **(A)** Schematic representation of green fluorescent protein (GFP) tagging of the left telomere of chromosome IV (*TEL4L*). **(B)** Representative image of a live prophase cell expressing *ZIP1-mCherry* (*red*) with *TEL4L* (*arrow*) labeled with GFP (*green*). *Scale bar*, 2 μm. **(C)** Representative image of a spread pachytene nucleus stained with anti-Zip1 (*red*), anti-GFP (*TEL4L*; *green*), and DAPI (*blue*). *Arrow* points to *TEL4L*. *Scale bar*, 2 μm. **(D)** Representative time-lapse fluorescence images of *TEL4L-GFP* at different time intervals (expressed in seconds at the *top panels*). The *red line* depicts the path traveled by *TEL4L-GFP* throughout the time lapse. A merged image of differential interference contrast (DIC), Zip1-mCherry (*red*), and *TEL4L-GFP* (*green*) is shown *after the last frame*. *Scale bar*, 2 μm. **(E)** Quantification of the average velocity of *TEL4L* movement. **(F)** Quantification of the maximum velocity of *TEL4L* movement. In **(E,F)**, the mean values from three independent experiments are plotted in the *graphs*. Data from each individual experiment and all multiple statistical comparisons are presented in **Supplementary Figure 6**. A total of 101, 146, 172, and 139 measurements of *TEL4L* velocity from wild type, *ndj1*Δ, *htz1*Δ, and *swr1*Δ, respectively, were performed in the three independent time-lapse experiments. ***$P < 0.001$; ns, not significant. The strains used in **(D–F)** are: DP1692 (wild type), DP1722 (*ndj1*Δ), DP1693 (*htz1*Δ), and DP1694 (*swr1*Δ).

chromosome motion was significantly reduced in the *htz1*Δ mutant (**Figures 8E,F**, **Supplementary Figure 6**). Interestingly, consistent with the chromatin-independent interaction between H2A.Z and the LINC complex, the *swr1*Δ mutant did not display reduced mobility. As expected, the *ndj1*Δ mutant showed a dramatic reduction in *TEL4L* movement (**Figures 8E,F**, **Supplementary Figure 6**). We conclude that H2A.Z is a novel LINC-associated component required for proper chromosome motion during meiotic prophase I.

DISCUSSION

The H2A.Z histone variant is involved in a myriad of biological processes, both in mitotic and meiotic cells, that rely on its chromatin incorporation at particular genomic positions where the ATP-dependent chromatin remodeler SWR1 is responsible for replacing H2A–H2B dimers to H2A.Z–H2B at nucleosomes (Billon and Cote, 2013). In this work, we characterize in detail an alternative localization of H2A.Z in different sub-compartments of meiotic cells that is independent of SWR1 and, hence, of chromatin. Indeed, our cytological studies of H2A.Z in the *swr1*Δ mutant allowed us to uncover additional locations of H2A.Z (chromosome ends and SPB) that are otherwise masked in wild-type cells due to the widespread incorporation of H2A.Z throughout the chromatin. Like in mitotic cells (Raisner et al., 2005), ChIP-seq analysis of H2A.Z distribution during the meiotic prophase has confirmed the absence of H2A.Z chromatin deposition throughout the genome during meiosis in the *swr1*Δ mutant, in particular at gene promoter regions. Here, we describe chromosome movement as a novel non-canonical meiotic function for this histone variant.

Prompted by our cytological analysis of H2A.Z in the *swr1*Δ mutant during the meiotic prophase revealing a telomeric localization and by an earlier report describing the interaction between H2A.Z and Mps3 in vegetative cells (Gardner et al., 2011), we explored the relationship of H2A.Z with LINC components and LINC-associated components, such as the SUN-domain protein Mps3 and the meiosis-specific telomeric protein Ndj1, respectively. The colocalization of H2A.Z with Mps3 at meiotic telomeres and the physical interaction between H2A.Z and both Mps3 and Ndj1, particularly at the NE, strongly suggest that H2A.Z is an additional LINC-associated factor (**Figure 1A**). It has been proposed that H2A.Z may contribute to the nuclear trafficking of Mps3 in mitotic cells (Gardner et al., 2011); however, we found that Mps3 is still detectable at chromosome ends in the *htz1*Δ mutant, indicating that Mps3 does not require H2A.Z to be delivered to the NE in meiotic cells. Since Mps3 is embedded in the NE, its detection on nuclear spread preparations depends on the attachment of the N-terminal domain to the telomeres via Ndj1 (Conrad et al., 2007). The fact that Mps3 telomeric localization is maintained in the *htz1*Δ mutant also indicates that telomere attachment is not disrupted in the absence of H2A.Z. Nevertheless, we found that the distribution of Mps3 throughout the NE is altered in the *htz1*Δ mutant that often displays an aberrant confinement of Mps3 toward one side of the nucleus. Thus, unlike mitotic cells, Mps3 does not require H2A.Z to reach the NE during meiosis, but H2A.Z is required to sustain the homogeneous distribution of Mps3 along the NE. This accumulation of Mps3 observed in *htz1*Δ is reminiscent of the transient meiotic bouquet (Trelles-Sticken et al., 1999), suggesting that H2A.Z may facilitate the dispersion of telomeres after the bouquet-like stage. The telomeric colocalization and the physical interaction between H2A.Z and Mps3/Ndj1 strongly suggest that H2A.Z directly impinges on LINC dynamics.

We found that disruption of the telomere attachment, either by deleting *NDJ1* or eliminating the 2–64 amino acids of the Mps3 N-terminal domain, prevents the localization of H2A.Z to chromosome ends. This observation suggests that although H2A.Z is not necessary to anchor the telomeres to the NE, it may reinforce the tethering to support robust chromosome movement. A similar scenario has been described in the *mps3-dCC* mutant lacking a fragment of an internal domain of Mps3 located in the lumen of the NE. Like in *htz1*Δ, telomeric attachment is maintained in *mps3-dCC*, but chromosome movement is mildly affected (Lee et al., 2012). Consistent with this notion, the reduction in chromosome velocity detected in *htz1*Δ is not as dramatic as in the *ndj1*Δ mutant where telomere attachment via Mps3 is lost (Conrad et al., 2007). The incorporation of H2A.Z into nucleosomes produces changes in chromatin rigidity (Neumann et al., 2012; Gerhold et al., 2015); thus, it is formally possible that the reduced mobility of *htz1*Δ chromosomes could stem from an altered chromatin compaction preventing proper transmission of the forces generated by the actin cytoskeleton to the chromosomes. However, the *swr1*Δ mutant shows no defect in chromosome movement, indicating that the chromatin deposition of H2A.Z has little impact on this phenomenon. In fact, the interaction between Mps3 and H2A.Z, and between Ndj1 and H2A.Z, persists in the absence of SWR1 both in mitotic (Gardner et al., 2011) and meiotic cells (this work). We hypothesize that the irregular accumulation of Mps3 at certain areas of the NE detected in *htz1*Δ cells may interfere with proper telomere-led movement. Alternatively, it is also possible that the aberrant distribution of Mps3 in the *htz1*Δ mutant could be the consequence, and not the cause, of the reduced chromosome movement. The involvement of H2A.Z in chromatin movement has also been reported in mitotic cells, where H2A.Z promotes the recruitment of unrepairable DSBs to the NE by Mps3 anchoring (Kalocsay et al., 2009; Horigome et al., 2014). However, this nuclear relocalization relies on the SWR1-dependent chromatin deposition of H2A.Z, suggesting that different mechanisms are involved.

In addition to the telomeric localization, we also describe here the presence of H2A.Z in another cellular structure devoid of chromatin, the SPB, in particular, the half-bridge where Mps3 is also located. However, the targeting of H2A.Z to the SPB presents different requirements because, unlike its telomeric localization, it does not require Ndj1 or the 2–64 amino acids of the Mps3 N-terminal domain. Nevertheless, we cannot rule out the possibility that other domains of Mps3, different from the 2–64 N-terminal portion, may be involved in targeting H2A.Z to the SPB. Notably, we detect an interaction between H2A.Z and Ndj1 in the wild type (**Figure 5B**), but not in the *mps3*Δ*2-64* mutant

(**Figure 3C**), consistent with the observation that Ndj1 requires the N-terminal domain of Mps3 for SPB recruitment (Li et al., 2015). What could be the function of H2A.Z at the SPB? During meiotic prophase I, Ndj1, which is recruited to the SPB by Mps3, protects the cohesion between duplicated SPBs (Li et al., 2015). The phosphorylation of Mps3 at S70 promotes the proteolytic cleavage of the protein, enabling irreversible separation of sister SPBs (Li et al., 2017). We speculate that the presence of H2A.Z at the SPB at the same time and location as Mps3 and Ndj1 may be indicative of a role for H2A.Z in SPB dynamics; future experiments will address this question. The fact that Mps3, Ndj1, and, as described here, also H2A.Z colocalize and interact both at telomeres and SPB is consistent with a number of observations indicating that a proper nuclear architecture and LINC-mediated contacts between chromosomes and the NE are important to coordinate interhomolog interactions with subsequent chromosome segregation. In *S. pombe*, multiple lines of evidence support this coordination (Tomita and Cooper, 2007; Fennell et al., 2015; Fernandez-Alvarez et al., 2016; Katsumata et al., 2016).

In sum, we describe here a novel role for H2A.Z in telomere-led meiotic chromosome motion that appears to be independent of its deposition on chromatin by SWR1. The budding yeast *htz1*Δ mutant displays various meiotic phenotypes including a slower meiotic progression and a reduced viability of meiotic products. Interestingly, although the *swr1*Δ mutant also shows meiotic defects, these phenotypes are less severe in *swr1*Δ compared to *htz1*Δ. Indeed, spore viability is 95% in the wild type, 76% in *htz1*Δ and 88% in *swr1*Δ (Gonzalez-Arranz et al., 2018), consistent with the notion that H2A.Z possesses additional meiotic roles unrelated to SWR1. It is tempting to speculate that, at least in budding yeast, H2A.Z may perform both chromatin-dependent and chromatin-independent functions, all of them contributing to sustain accurate gametogenesis. Cytological analyses of H2A.Z localization in mouse spermatocytes have revealed a dynamic spatiotemporal localization of this histone variant on different euchromatin and heterochromatin domains (sex body), suggestive of a functional impact on mammalian meiosis (Greaves et al., 2006; Ontoso et al., 2014). In the future, it will be interesting to determine whether the possible chromatin-independent function of H2A.Z is also evolutionarily conserved.

MATERIALS AND METHODS

Yeast Strains

Yeast strain genotypes are listed in **Supplementary Table 1**. All the strains are isogenic to the BR1919 background (Rockmill and Roeder, 1990). The *swr1::natMX4*, *swr1::hphMX4*, *ndj1::natMX4*, *ndj1::kanMX6*, *htz1::natMX4*, *mps3::natMX4*, and *mps3::hphMX4* gene deletions were made using a PCR-based approach (Longtine et al., 1998; Goldstein and McCusker, 1999). The *htz1::URA3* deletion and the functional *HTZ1-GFP* construct were previously described (Gonzalez-Arranz et al., 2018). The *MPS3-GFP*, *MPS3-3HA*, *NET1-RedStar2*, *SPC110-RedStar2*, *SPC110-mCherry*, *CNM67-mCherry*, *HOP1-mCherry*, and *PMA1-mCherry* gene tagging constructs were also made by PCR (Longtine et al., 1998; Janke et al., 2004; Sheff and Thorn, 2004). To generate P_{CUP1}*-IME1* strains, the 1,760 bp promoter region of *IME1*, including the *IRT1* long noncoding RNA (Chia and van Werven, 2016), was replaced by the *CUP1* promoter amplified from pYM-N1 (Janke et al., 2004). Strains producing a version of Mps3 lacking amino acids 2–64 of the N-terminal domain were created as follows. One allele of the essential *MPS3* gene was deleted in a diploid strain. The heterozygous *MPS3/mps3-hphMX4* diploid was transformed with the *URA3*-based pSS326 centromeric plasmid harboring *mps3*Δ*2-64*. 5-Fluoroorotic acid (FOA)-resistant and hygromycin-resistant spores were selected and further checked for the presence of *mps3*Δ*2-64* expressed from pSS326 as the only source of this protein in the cells. As a control, the same procedure was followed using the pSS269 plasmid expressing wild-type *MPS3*. The *HTZ1-VN* and *NDJ1-VC* strains used in the bimolecular fluorescence complementation (BiFC) assay were constructed using the plasmids pFA6a-VN-TRP1 and pFA6a-VC-kanMX6 containing the N-terminal (VN) or C-terminal fragment (VC) of the Venus variant of yellow fluorescent protein (Sung and Huh, 2007). Strains carrying Tel4L marked with GFP were generated as follows. Firstly, the *tetR-GFP* construct was integrated at *leu2* by transforming with the *Afl*II-digested pSS329 plasmid. Secondly, the *tetO(50)* array was inserted into a region close to the left telomere of chromosome IV (Tel4L) by transforming with the pSS330 plasmid cut with *Afl*II. Strains producing *ZIP1* tagged with mCherry at position 700 were constructed using the *delitto perfetto* approach (Stuckey and Storici, 2013). Basically, a fragment containing *mCherry* flanked by 60-nt *ZIP1* sequences upstream and downstream of the codon for amino acid 700 was obtained by PCR from plasmid pSS266. This fragment was transformed into a strain carrying the CORE cassette (*URA3-kanMX4*) inserted at the position corresponding to amino acid 700 of the *ZIP1* gene. FOA-resistant and G418-sensitive transformants were obtained and correct clones were selected.

All constructs and mutations were verified by PCR analysis and/or DNA sequencing. The sequences of all primers used in strain construction are available upon request. All strains were made by direct transformation of haploid parents or by genetic crosses always in an isogenic background. Diploids were made by mating the corresponding haploid parents and isolation of zygotes by micromanipulation.

Plasmids

The plasmids used in this work are listed in **Supplementary Table 2**. To generate pSS266, a PCR fragment containing 468 nt of the *MPS3* promoter, the *MPS3-mCherry* C-terminal fusion, and the *ADH1* terminator was amplified from the genomic DNA of a strain harboring the *MPS3-mCherry* construct and blunt-cloned into the pJET2.1 vector (ThermoFisher). A *Bgl*II–*Bgl*II fragment from pSS266 containing *MPS3-mCherry* was then cloned into *Bam*HI of pRS424 to generate pSS267. Then, a 3.5-kb *Xho*I–*Not*I fragment from pSS267 containing *MPS3-mCherry* was cloned into the same sites of the centromeric vector pRS316 to generate pSS269. A version of *MPS3-mCherry* lacking the sequences encoding amino acids 2–64 of the N-terminal domain (*mps3*Δ*2-64*) was

made by site-directed mutagenesis of pSS269 using divergent oligonucleotides flanking the region to be deleted to generate plasmid pSS326. The pSS329 plasmid contains the *tet* repressor fused to *NLS-GFP* and expressed from the *URA3* promoter (Michaelis et al., 1997). *Eco*RI or *Afl*II digestion of pSS329 targets TetR-GFP at *leu2*. The pSS330 plasmid harbors an ∼5.4-kb array with 50 tandem repeats of the *tetO* operator inserted between the *HXT15* and *THI13* genes located close to *TEL4L* cloned into *Bam*HI–*Xba*I of pRS406.

Meiotic Cultures and Synchronous Sporulation of BR Strains

To induce meiosis and sporulation, BR strains were grown in 3.5 ml of 2× synthetic complete medium (2% glucose, 0.7% yeast nitrogen base without amino acids, 0.05% adenine, and complete supplement mixture from Formedium at twice the particular concentration indicated by the manufacturer) for 20–24 h, then transferred to 2.5 ml of YPDA (1% yeast extract, 2% peptone, 2% glucose, and 0.02% adenine) and incubated to saturation for an additional 8 h. Cells were harvested, washed with 2% potassium acetate (KAc), resuspended into 2% KAc (10 ml), and incubated at 30°C with vigorous shaking to induce meiosis. Both YPDA and 2% KAc were supplemented with 20 mM adenine and 10 mM uracil. The culture volumes were scaled up when needed.

To increase synchrony in the meiotic cultures for Tel4L-GFP tracking, BR strains containing P_{CUP1}-*IME1* were used. The culture conditions during pre-sporulation were similar to those described above, except that YPDA contained 1% glucose. Cells were transferred to 2% KAc and, after 12 h, $CuSO_4$ was added at a final concentration of 50 μM to induce *IME1* expression and drive meiotic entry. Cells were imaged 6 h after *IME1* induction, when ∼73% of cells in the culture contained linear stretches of Zip1-mCherry.

Western Blotting and Immunoprecipitation

Total cell extracts for Western blot analysis in **Figure 6A** and **Supplementary Figure 5** were prepared by trichloroacetic acid (TCA) precipitation from 5-ml aliquots of sporulation cultures, as previously described (Acosta et al., 2011). The antibodies used are listed in **Supplementary Table 3**. The ECL, ECL2 or SuperSignal West Femto reagents (ThermoFisher Scientific) were used for detection. The signal was captured on films and/or with a ChemiDoc XRS system (Bio-Rad).

For the co-immunoprecipitation experiments, cells from 200 ml of meiotic cultures (16 h after meiotic induction) were harvested and washed with an extraction buffer (20 mM HEPES–NaOH, pH 7.5, 300 mM NaCl, 1 mM EDTA, 5 mM EGTA, 50 mM NaF, 50 mM β-glycerophosphate, 1 mM DTT, 1 mM PMSF) containing one tablet of EDTA-free cOmplete protease inhibitor (Roche). The cell pellet was frozen in liquid nitrogen and ground with a freezer mill (6775 Freezer/Mill). The ground cell powder was allowed to thaw on ice and then resuspended in 9 ml of lysis buffer (extraction buffer plus 0.5% Triton X-100). After homogenization with a homogenizer (ULTRA-TURRAX T10 basic, IKA) for 30 s, the lysates were centrifuged at 3,000 × g for 10 min at 4°C and the resulting supernatant was used for immunoprecipitation, saving 100 μl for input analysis. Then, 50 μl of the GFP-Trap magnetic agarose (Chromotek) were added to the remaining lysate to immunoprecipitate the GFP-tagged proteins. After 3 h incubation with rotation at 4°C, the beads were washed five times with extraction buffer and the bound proteins were eluted by boiling in 2× Laemmli buffer. Samples from both input lysates and immunoprecipitates were analyzed by SDS-PAGE followed by Western blotting.

Chromatin Immunoprecipitation and Illumina Sequencing

At the 0- and 15-h time points, 7 ml of meiotic cultures (OD_{600} = ∼6–7) were harvested and fixed for 30 min with 1% formaldehyde. The cross-linking reaction was quenched by the addition of 125 mM glycine. Chromatin immunoprecipitation was performed as described (Blitzblau et al., 2012). The samples were immunoprecipitated with 3 μl polyclonal rabbit anti-GFP serum per immunoprecipitate (IP). Library quality was confirmed by Qubit HS assay kit and 2200 TapeStation. The 51 bp single-end sequencing was accomplished on an Illumina HiSeq 2500 instrument.

Processing Illumina Data

The sequencing reads were mapped to a high-quality assembly of S288C (Yue et al., 2017) using Bowtie (Langmead et al., 2009). Reads with up to two mismatches across all 51 bp were considered during mapping, and reads with more than one reportable alignment were mapped to the best position. Reads were also mapped to the SK1 genome with similar results. Reads were extended toward 3′-ends to a final length of 200 bp using MACS-2.1.0 (https://github.com/taoliu/MACS) (Zhang et al., 2008) All pileups were SPMR-normalized (signal per million reads) and fold enrichment of the ChIP data over the input data was calculated. The 95% confidence intervals were calculated by bootstrap resampling from the data 1,000 times with replacement. Datasets are available at GEO with accession number GSE153003.

Fluorescence Microscopy

Immunofluorescence of the chromosome spreads was performed essentially as described (Rockmill, 2009). The antibodies used are listed in **Supplementary Table 3**. Images of the spreads and fixed whole cells were captured with a Nikon Eclipse 90i fluorescence microscope controlled with the MetaMorph software and equipped with a Hamamatsu Orca-AG CCD camera and a PlanApo VC ×100 1.4 NA objective. The following exposure times were used: DAPI, 400 ms; Mps3-GFP/Mps3-HA, 500 ms; Cnm67-mCherry, 200 ms; tubulin, 10 ms; and H2A.Z-GFP, 500 ms in wild type and 2,000 ms in *swr1*.

For BiFC analysis, the cells were fixed with 3.7% formaldehyde for 10 min at 30°C with 500 rpm shaking. The cells were washed with 1× phosphate-buffered saline (PBS), permeabilized for 10 min with 70% ethanol, and stained with 1 μg/ml DAPI for 10 min. Images were captured with the Nikon Eclipse 90i fluorescence microscope described above, with the following exposure times: DAPI, 400 ms; $Venus^{YFP}$, 5,000 ms; Mps3-mCherry, 1,000 ms; Spc110-RedStar2, 1,000 ms; and differential interference contrast (DIC), 10 ms.

For the analysis of Mps3-GFP distribution, the cells were fixed with 3.7% formaldehyde and washed with 1 × PBS. Stacks of 30 planes at 0.2-μm intervals were captured for Mps3-GFP (300-ms exposure). Also, a DIC image (25 ms) and a single-plane image of Hop1-mCherry (600-ms exposure), to identify meiotic prophase cells, were captured. Maximum intensity projections were generated using Fiji software (https://imagej.net/Fiji). Images were captured with an Olympus IX71 fluorescence microscope equipped with a personal DeltaVision system, a CoolSnap HQ2 (Photometrics) camera, and a ×100 UPLSAPO 1.4 NA objective. The assignment of nuclei to each of the categories established for Mps3 distribution in **Figure 6D** was performed independently by two different persons in a blinded fashion; that is, without previous knowledge of the genotype (wild type or *htz1*Δ) corresponding to the images scored.

For the colocalization of H2A.Z-GFP (400-ms exposure) and Mps3-MCherry (800 ms), Cnm67-mCherry (1,000 ms), or Net1-RedStar2 (1,000 ms) in live meiotic cells, z-stacks of 25 planes at 0.2-μm intervals were consecutively captured using the DeltaVision microscope described above. Images were deconvolved using the SoftWoRx 5.0 software (Applied Precisions).

For super-resolution analysis (structured illumination microscopy, SIM) of Mps3-GFP, H2A.Z-GFP, and Spc110-mCherry, the cells collected 16 h after meiotic induction were fixed for 15 min in 4% paraformaldehyde (Ted Pella) with 100 mM sucrose and then washed twice in phosphate-buffered saline, pH 7.4. Aliquots of the cells were placed on cleaned slides covered with coverslips (number 1.5). Multicolor 3D-SIM images were acquired using a GE Healthcare DeltaVision OMX Blaze V3 fitted with an Olympus PlanApo N × 100 1.42 NA oil objective. Stacks of 17 planes at 0.125-μm intervals were captured (100-ms exposure for the green and red channels). SIM reconstruction was performed with the Applied Precision SoftWoRx software package (GE Healthcare, Piscataway, NJ) following the Applied Precision protocols. After reconstruction, alignment between the differently colored channels was performed based on calibration from the alignment slide provided by the manufacturer. All analysis was performed using ImageJ and custom plugins written for ImageJ (created in the microscopy center of The Stowers Institute for Medical Research) at http://research.stowers.org/imagejplugins/index.html.

Measurement of Chromosome and Telomere Movement

For the analysis of chromosome movement using Zip1-GFP tracking, cells from 16-h meiotic cultures of the wild type and mutants (*ndj1*Δ, *htz1*Δ, or *swr1*Δ) were mixed in the same microscopy culture chamber (eight-well μ-Slide, Ibidi) previously treated with 0.5 mg/ml of Concanavalin A type IV (Sigma-Aldrich). The chamber was maintained at 30°C during the experiment. Zip1-GFP images were taken during 30 s at 0.6-s intervals with a 100-ms exposure time. To distinguish the wild-type cells (expressing *PMA1-mCherry*) from mutants, red channel images were also taken (800 ms). The images were deconvolved using the SoftWoRx 5.0 software (Applied Precisions). Clearly isolated chromosomes in a nucleus were manually marked at the end and tracked for 50 consecutive frames. Chromosome velocities were calculated using a manual tracking plugin on ImageJ (https://imagej.nih.gov/ij/plugins/track/track.html). A total of 16–25 chromosomes for each genotype in four independent experiments were analyzed.

For the analysis of *TEL4L* movement, meiotic prophase cells from synchronous cultures (6 h after the induction of *IME1* with $CuSO_4$) were placed in Concanavalin A-treated microscopy culture chambers maintained at 30°C. For *TEL4L-GFP* (200-ms exposure) and Zip1-mCherry (800-ms exposure), z-stacks of seven planes (0.6-μm step size) were captured at 8-s intervals during 180 s. A single plane of DIC was also captured in every frame. To correct for possible small displacements of the microscope stage during the time lapse, GFP images were aligned using the DIC images as reference using a script provided by Giovanni Cardone (available upon request). *TEL4L-GFP* dots in the nuclei were manually marked and tracked for 23 consecutive frames. Telomere movement velocities were calculated using the MTrackJ plugin of Fiji (https://imagescience.org/meijering/software/mtrackj/). A total of 101–172 telomere tracks from three different experiments were analyzed for each genotype. The images for both chromosome movement (Zip1-GFP) and telomere movement (*TEL4L-GFP*) were captured with an Olympus IX71 fluorescence microscope equipped with a personal DeltaVision system, a CoolSnap HQ2 (Photometrics) camera, and a ×100 UPLSAPO 1.4 NA objective.

Statistics

To determine the statistical significance of the differences, a two-tailed Student's *t*-test, for pairwise comparisons, or a one-way ANOVA Tukey's test, for multiple comparisons, was used. *P*-values were calculated with the GraphPad Prism 5.0 software. $^{*}P < 0.05$; $^{**}P < 0.01$; and $^{***}P < 0.001$. The nature of the errors bars in the graphical representations and the number of biological replicates are indicated in the corresponding figure legend.

DATA AVAILABILITY STATEMENT

Source data for figures and graphs can be found at **Supplementary Material-Source Data**. Original data underlying **Figures 5D,E** can be accessed from the Stowers Original Data Repository at http://www.stowers.org/research/publications/LIBPB-1519. ChIP-seq datasets are available at GEO with accession number GSE153003.

AUTHOR CONTRIBUTIONS

SG-A contributed to the conceptualization, investigation, formal analysis, and visualization. JG made contributions to the investigation. ZY contributed to formal analysis. NP and JH contributed to the investigation and formal analysis. BS to supervision and project administration. JC and SJ contributed to resources and funding acquisition. AH to resources, formal analysis, and funding acquisition. PS-S to the conceptualization, investigation, supervision, funding acquisition, visualization, and

writing the original draft. All authors revised, commented, and approved the manuscript.

FUNDING

This work was supported by grant BFU2015-65417-R from the Ministry of Economy and Competitiveness (MINECO) of Spain to PS-S, grant RTI2018-099055-B-I00 from the Ministry of Science, Innovation and Universities (MCIU/AEI/FEDER, UE) of Spain to PS-S and JC, the Stowers Institute for Medical Research to SJ, grant R01GM121443 from the National Institute of General Medical Sciences of the National Institutes of Health to SJ, and NIH grants GM111715 and GM123035 to AH. SG-A was partially supported by the Unidad de Excelencia de Biología Funcional y Genómica Ref. 2019/X002/05 from the University of Salamanca. The IBFG was supported in part by an institutional grant from the Junta de Castilla y León, Ref. CLU-2017-03 co-funded by the P.O. FEDER de Castilla y León 14-20. This manuscript has been released as a preprint at bioRxiv (González-Arranz et al., 2020). Open Access publication fee is partially supported by the CSIC.

ACKNOWLEDGMENTS

We thank Andrés Clemente and Félix Prado for useful comments and discussion, Cristina Martín, Andrés Clemente, César Roncero, Raimundo Freire, and Shirleen Roeder for reagents, and Giovanni Cardone for the image alignment script.

SUPPLEMENTARY MATERIAL

The Supplementary Material for this article can be found online at: https://www.frontiersin.org/articles/10.3389/fcell.2020.594092/full#supplementary-material

Supplementary Figure 1 | Genome-wide incorporation of H2A.Z to meiotic chromatin depends on SWR1. (Related to **Figure 1**) Profiles of H2A.Z binding to all chromosomes in wild type **(A)**, *swr1*Δ **(B)**, and the untagged control **(C)**, determined by ChIP-seq. Magenta circles indicate the location of the centromere. **(D,E)** Metagene analysis of H2A.Z binding by ChIP-seq. The ORFs are scaled to the "Start" and "Stop" positions, and up- and downstream flanking regions represent half the size of the ORF. Samples were taken at 0 h and 15 h after meiotic induction. Anti-GFP antibodies were used to immunoprecipitate H2A.Z-GFP. Average profiles from two replicates are shown. Strains are: DP840 (*HTZ1-GFP*), DP841 (*HTZ1-GFP swr1*Δ) and DP421 (*HTZ1* untagged control).

Supplementary Figure 2 | A fraction of H2A.Z accumulates in the vicinity of the nucleolus in *swr1*Δ (Related to **Figure 2**). Microscopy fluorescence images of *swr1*Δ cells expressing *HTZ1-GFP* and *NET1-RedStar2* as a nucleolar marker. A single plane of a representative cell displaying a diffuse peripheral accumulation of H2A.Z is shown. The arrowhead points to the nucleolar area marked by Net1. Images were taken 16 h after meiotic induction. Scale bar, 2 μm. The strain is DP1189 (*swr1*Δ *HTZ1-GFP NET1-RedStar2*).

Supplementary Figure 3 | BiFC analysis of H2A.Z-Ndj1 interaction in *ndt80*Δ cells (Related to **Figure 3**). **(A)** Microscopy fluorescence images of *ndt80*Δ and *ndt80*Δ *swr1*Δ cells expressing *HTZ1* fused to the N-terminal half of the VenusYFP (VN) and *NDJ1* fused to the C-terminal half of the VenusYFP (VC). Nuclei are stained with DAPI (blue). The reconstitution of VenusYFP fluorescence resulting from H2A.Z-VN/Ndj1-VC interaction appears in yellow. A parallel meiotic culture of *ndt80*Δ cells expressing *HOP1-GFP* (green) was used as control for meiotic prophase I staging. Images were taken 24 h after meiotic induction. Representative cells are shown. Scale bar, 2 μm. **(B)** Quantification of the percentage of cells displaying VenusYFP fluorescent signal or Hop1-GFP signal, as indicated. The analysis was performed in triplicate. More than 300 cells were scored in every experiment. Error bars, SD. Strains are: DP1748 (*ndt80*Δ *HTZ1-VN NDJ1-VC*), DP1749 (*ndt80*Δ *swr1*Δ *HTZ1-VN NDJ1-VC*) and DP963 (*ndt80*Δ *HOP1-GFP*).

Supplementary Figure 4 | Localization of H2A.Z to the SPB is independent of Ndj1 and the 2- 64 N-terminal domain of Mps3 (Related to **Figure 5**). Immunofluorescence of representative spread pachytene nuclei stained with DAPI to visualize chromatin (blue), anti-GFP to detect H2A.Z (green), and anti-tubulin to mark the monopolar prophase spindle (red). The arrow points to an H2A.Z focus present at the center of the bushy spindle corresponding to the SPB location. Strains are DP1395 (wild type), DP1280 (mps3-Δ2-64) and DP1305 (*ndj1*Δ). 25, 21 and 23 nuclei were examined for wild type, *mps3-Δ2-64* and *ndj1*Δ, respectively.

Supplementary Figure 5 | Mps3 global levels are reduced in ndt80D-arrested cells lacking H2A.Z (Related to **Figure 6**). **(A)** Western blot analysis of Mps3-GFP and Mek1 production during meiosis detected with anti-GFP and anti-Mek1 antibodies, respectively. PGK was used as a loading control. A representative blot is shown. Quantification of Mps3-GFP **(B)** and Mek1 **(C)** levels normalized to PGK. Average and SEM (error bars) from three independent experiments are shown. Strains are: DP1014 (*ndt80*Δ *MPS3-GFP*) and DP1013 (*ndt80*Δ *htz1*Δ *MPS3-GFP*).

Supplementary Figure 6 | Analysis of *TEL4L* movement (Related to **Figure 8**). **(A)** Measurement of average velocity and maximum velocity in three independent time-lapse experiments tracking *TEL4L* movement marked with GFP as depicted in Figure 8. Error bars, SD. **(B)** ANOVA statistical analysis of the velocity data obtained in every individual experiment as well as combining the data from all three experiments. **(C)** Mean values for average and maximum velocity. Strains are DP1692 (wild type), DP1722 (*ndj1*Δ), DP1693 (*htz1*Δ) and DP1694 (*swr1*Δ).

Supplementary Table 1 | *Saccharomyces cerevisiae* strains.

Supplementary Table 2 | Plasmids.

Supplementary Table 3 | Primary and secondary antibodies.

Supplementary Video 1 | Irregular distribution of Mps3 along the nuclear envelope in the *htz1*Δ mutant (Linked to **Figure 6**). Representative nuclei displaying 3D reconstruction of Mps3-GFP localization in wild type (DP1032) and *htz1*Δ (DP1033). Stacks of 30 planes at 0.2 μm intervals were captured. A 360 degrees rotation over the Y axis is shown at 5 frames per second.

Supplementary Video 2 | Meiotic chromosome movement in Zip1-GFP tagged strains (Linked to **Figure 7**). Time-lapse video of the nuclei displayed in **Figure 7B** shown at 7 frames per second. Zip1-GFP images were captured at 0.6 s intervals during 30 s. Elapsed time is shown in seconds.

Supplementary Video 3 | Meiotic chromosome movement in *TEL4L-GFP* tagged strains (Linked to **Figure 8**). Time-lapse video of the nuclei displayed in **Figure 8D** shown at 5 frames per second. *TEL4L-GFP* images were captured at 8 s intervals during 180 s. Elapsed time is shown in minutes:seconds.

REFERENCES

Acosta, I., Ontoso, D., and San-Segundo, P. A. (2011). The budding yeast polo-like kinase Cdc5 regulates the Ndt80 branch of the meiotic recombination checkpoint pathway. *Mol. Biol. Cell* 22, 3478–3490. doi: 10.1091/mbc.e11-06-0482

Adkins, N. L., Niu, H., Sung, P., and Peterson, C. L. (2013). Nucleosome dynamics regulates DNA processing. *Nat. Struct. Mol. Biol.* 20, 836–842. doi: 10.1038/nsmb.2585

Billon, P., and Cote, J. (2013). Precise deposition of histone H2A.Z in chromatin for genome expression and maintenance. *Biochim. Biophys. Acta* 1819, 290–302. doi: 10.1016/j.bbagrm.2011.10.004

Blitzblau, H. G., Chan, C. S., Hochwagen, A., and Bell, S. P. (2012). Separation of DNA replication from the assembly of break-competent meiotic chromosomes. *PLoS Genet.* 8:e1002643. doi: 10.1371/journal.pgen.1002643

Bommi, J. R., Rao, H., Challa, K., Higashide, M., Shinmyozu, K., Nakayama, J. I., et al. (2019). Meiosis-specific cohesin component, Rec8, promotes the localization of Mps3 SUN domain protein on the nuclear envelope. *Genes Cells* 24, 94–106. doi: 10.1111/gtc.12653

Brachet, E., Sommermeyer, V., and Borde, V. (2012). Interplay between modifications of chromatin and meiotic recombination hotspots. *Biol. Cell* 104, 51–69. doi: 10.1111/boc.201100113

Burke, B. (2018). LINC complexes as regulators of meiosis. *Curr. Opin. Cell Biol.* 52, 22–29. doi: 10.1016/j.ceb.2018.01.005

Burns, S., Avena, J. S., Unruh, J. R., Yu, Z., Smith, S. E., Slaughter, B. D., et al. (2015). Structured illumination with particle averaging reveals novel roles for yeast centrosome components during duplication. *Elife* 4:e08586. doi: 10.7554/eLife.08586

Chang, W., Worman, H. J., and Gundersen, G. G. (2015). Accessorizing and anchoring the LINC complex for multifunctionality. *J. Cell Biol.* 208, 11–22. doi: 10.1083/jcb.201409047

Chen, J., Gardner, J. M., Yu, Z., Smith, S. E., McKinney, S., Slaughter, B. D., et al. (2019). Yeast centrosome components form a noncanonical LINC complex at the nuclear envelope insertion site. *J. Cell Biol.* 218, 1478–1490. doi: 10.1083/jcb.201809045

Chia, M., and van Werven, F. J. (2016). Temporal expression of a master regulator drives synchronous sporulation in budding yeast. *G3* 6, 3553–3560. doi: 10.1534/g3.116.034983

Choi, K., Zhao, X., Kelly, K. A., Venn, O., Higgins, J. D., Yelina, N. E., et al. (2013). Arabidopsis meiotic crossover hot spots overlap with H2A.Z nucleosomes at gene promoters. *Nat. Genet.* 45, 1327–1336. doi: 10.1038/ng.2766

Chua, P. R., and Roeder, G. S. (1997). Tam1, a telomere-associated meiotic protein, functions in chromosome synapsis and crossover interference. *Genes Dev.* 11, 1786–1800. doi: 10.1101/gad.11.14.1786

Clemente-Blanco, A., Sen, N., Mayan-Santos, M., Sacristan, M. P., Graham, B., Jarmuz, A., et al. (2011). Cdc14 phosphatase promotes segregation of telomeres through repression of RNA polymerase II transcription. *Nat. Cell Biol.* 13, 1450–1456. doi: 10.1038/ncb2365

Conrad, M. N., Dominguez, A. M., and Dresser, M. E. (1997). Ndj1p, a meiotic telomere protein required for normal chromosome synapsis and segregation in yeast. *Science* 276, 1252–1255. doi: 10.1126/science.276.5316.1252

Conrad, M. N., Lee, C. Y., Chao, G., Shinohara, M., Kosaka, H., Shinohara, A., et al. (2008). Rapid telomere movement in meiotic prophase is promoted by NDJ1, MPS3, and CSM4 and is modulated by recombination. *Cell* 133, 1175–1187. doi: 10.1016/j.cell.2008.04.047

Conrad, M. N., Lee, C. Y., Wilkerson, J. L., and Dresser, M. E. (2007). MPS3 mediates meiotic bouquet formation in *Saccharomyces cerevisiae*. *Proc. Natl. Acad. Sci. U.S.A.* 104, 8863–8868. doi: 10.1073/pnas.0606165104

Crichton, J. H., Playfoot, C. J., and Adams, I. R. (2014). The role of chromatin modifications in progression through mouse meiotic prophase. *J. Genet. Genomics* 41, 97–106. doi: 10.1016/j.jgg.2014.01.003

Fennell, A., Fernandez-Alvarez, A., Tomita, K., and Cooper, J. P. (2015). Telomeres and centromeres have interchangeable roles in promoting meiotic spindle formation. *J. Cell Biol.* 208, 415–428. doi: 10.1083/jcb.201409058

Fernandez-Alvarez, A., Bez, C., O'Toole, E. T., Morphew, M., and Cooper, J. P. (2016). Mitotic nuclear envelope breakdown and spindle nucleation are controlled by interphase contacts between centromeres and the nuclear envelope. *Dev. Cell* 39, 544–559. doi: 10.1016/j.devcel.2016.10.021

Fernandez-Alvarez, A., and Cooper, J. P. (2017). Chromosomes orchestrate their own liberation: nuclear envelope disassembly. *Trends Cell Biol.* 27, 255–265. doi: 10.1016/j.tcb.2016.11.005

Friederichs, J. M., Ghosh, S., Smoyer, C. J., McCroskey, S., Miller, B. D., Weaver, K. J., et al. (2011). The SUN protein Mps3 is required for spindle pole body insertion into the nuclear membrane and nuclear envelope homeostasis. *PLoS Genet.* 7:e1002365. doi: 10.1371/journal.pgen.1002365

Gardner, J. M., Smoyer, C. J., Stensrud, E. S., Alexander, R., Gogol, M., Wiegraebe, W., et al. (2011). Targeting of the SUN protein Mps3 to the inner nuclear membrane by the histone variant H2A.Z. *J. Cell Biol.* 193, 489–507. doi: 10.1083/jcb.201011017

Gerhold, C. B., Hauer, M. H., and Gasser, S. M. (2015). INO80-C and SWR-C: guardians of the genome. *J. Mol. Biol* 427, 637–651. doi: 10.1016/j.jmb.2014.10.015

Goldstein, A. L., and McCusker, J. H. (1999). Three new dominant drug resistance cassettes for gene disruption in *Saccharomyces cerevisiae*. *Yeast* 15, 1541–553. doi: 10.1002/(SICI)1097-0061(199910)15:14<1541::AID-YEA476>3.0.CO;2-K

Gonzalez-Arranz, S., Cavero, S., Morillo-Huesca, M., Andujar, E., Perez-Alegre, M., Prado, F., et al. (2018). Functional impact of the H2A.Z histone variant during meiosis in *Saccharomyces cerevisiae*. *Genetics* 209, 997–1015. doi: 10.1534/genetics.118.301110

González-Arranz, S., Gardner, J. M., Yu, Z., Patel, N. J., Heldrich, J., Santos, B., et al. (2020). SWR1-independent association of H2A.Z to the LINC complex promotes meiotic chromosome motion. *BioRxiv [Preprint]*. doi: 10.1101/2020.06.30.181016

Greaves, I. K., Rangasamy, D., Devoy, M., Marshall Graves, J. A., and Tremethick, D. J. (2006). The X and Y chromosomes assemble into H2A.Z-containing facultative heterochromatin following meiosis. *Mol. Cell. Biol.* 26, 5394–5405. doi: 10.1128/MCB.00519-06

Horigome, C., Oma, Y., Konishi, T., Schmid, R., Marcomini, I., Hauer, M. H., et al. (2014). SWR1 and INO80 chromatin remodelers contribute to DNA double-strand break perinuclear anchorage site choice. *Mol. Cell.* 55, 626–639. doi: 10.1016/j.molcel.2014.06.027

Hunter, N. (2015). Meiotic recombination: the essence of heredity. *Cold Spring Harb. Perspect. Biol.* 7:a016618. doi: 10.1101/cshperspect.a016618

Janke, C., Magiera, M. M., Rathfelder, N., Taxis, C., Reber, S., Maekawa, H., et al. (2004). A versatile toolbox for PCR-based tagging of yeast genes: new fluorescent proteins, more markers and promoter substitution cassettes. *Yeast* 21, 947–962. doi: 10.1002/yea.1142

Kalocsay, M., Hiller, N. J., and Jentsch, S. (2009). Chromosome-wide Rad51 spreading and SUMO-H2A.Z-dependent chromosome fixation in response to a persistent DNA double-strand break. *Mol. Cell.* 33, 335–343. doi: 10.1016/j.molcel.2009.01.016

Katsumata, K., Hirayasu, A., Miyoshi, J., Nishi, E., Ichikawa, K., Tateho, K., et al. (2016). A Taz1- and microtubule-dependent regulatory relationship between telomere and centromere positions in bouquet formation secures proper meiotic divisions. *PLoS Genet.* 12:e1006304. doi: 10.1371/journal.pgen.1006304

Keeney, S., Lange, J., and Mohibullah, N. (2014). Self-organization of meiotic recombination initiation: general principles and molecular pathways. *Annu. Rev. Genet.* 48, 187–214. doi: 10.1146/annurev-genet-120213-092304

Kerppola, T. K. (2008). Bimolecular fluorescence complementation (BiFC) analysis as a probe of protein interactions in living cells. *Annu. Rev. Biophys.* 37, 465–487. doi: 10.1146/annurev.biophys.37.032807.125842

Kosaka, H., Shinohara, M., and Shinohara, A. (2008). Csm4-dependent telomere movement on nuclear envelope promotes meiotic recombination. *PLoS Genet.* 4:e1000196. doi: 10.1371/journal.pgen.1000196

Koszul, R., Kim, K. P., Prentiss, M., Kleckner, N., and Kameoka, S. (2008). Meiotic chromosomes move by linkage to dynamic actin cables with transduction of force through the nuclear envelope. *Cell* 133, 1188–1201. doi: 10.1016/j.cell.2008.04.050

Langmead, B., Trapnell, C., Pop, M., and Salzberg, S. L. (2009). Ultrafast and memory-efficient alignment of short DNA sequences to the human genome. *Genome Biol.* 10:R25. doi: 10.1186/gb-2009-10-3-r25

Lawrence, K. S., Tapley, E. C., Cruz, V. E., Li, Q., Aung, K., Hart, K. C., et al. (2016). LINC complexes promote homologous recombination in part through inhibition of nonhomologous end joining. *J. Cell. Biol.* 215, 801–821. doi: 10.1083/jcb.201604112

Lee, C. Y., Bisig, C. G., Conrad, M. M., Ditamo, Y., Previato de Almeida, L., Dresser, M. E., et al. (2020). Extranuclear structural components that mediate dynamic chromosome movements in yeast meiosis. *Curr. Biol.* 30, 1207–1216. doi: 10.1016/j.cub.2020.01.054

Lee, C. Y., Conrad, M. N., and Dresser, M. E. (2012). Meiotic chromosome pairing is promoted by telomere-led chromosome movements independent of bouquet formation. *PLoS Genet.* 8:e1002730. doi: 10.1371/journal.pgen.1002730

Lee, Y. L., and Burke, B. (2018). LINC complexes and nuclear positioning. *Semin. Cell Dev. Biol.* 82, 67–76. doi: 10.1016/j.semcdb.2017.11.008

Li, P., Jin, H., Koch, B. A., Abblett, R. L., Han, X., Yates, J. R. III, et al. (2017). Cleavage of the SUN-domain protein Mps3 at its N-terminus regulates

centrosome disjunction in budding yeast meiosis. *PLoS Genet.* 13:e1006830. doi: 10.1371/journal.pgen.1006830

Li, P., Shao, Y., Jin, H., and Yu, H. G. (2015). Ndj1, a telomere-associated protein, regulates centrosome separation in budding yeast meiosis. *J. Cell Biol.* 209, 247–259. doi: 10.1083/jcb.201408118

Link, J., and Jantsch, V. (2019). Meiotic chromosomes in motion: a perspective from *Mus musculus* and *Caenorhabditis elegans*. *Chromosoma* 2019 128:317–30. doi: 10.1007/s00412-019-00698-5

Longtine, M. S., McKenzie, A. 3rd, Demarini, D. J., Shah, N. G., Wach, A., Brachat, A., et al. (1998). Additional modules for versatile and economical PCR-based gene deletion and modification in *Saccharomyces cerevisiae*. *Yeast* 14, 953–61. doi: 10.1002/(SICI)1097-0061(199807)14:10<953::AID-YEA293>3.0.CO;2-U

Luk, E., Ranjan, A., Fitzgerald, P. C., Mizuguchi, G., Huang, Y., Wei, D., et al. (2010). Stepwise histone replacement by SWR1 requires dual activation with histone H2A.Z and canonical nucleosome. *Cell* 143, 725–736. doi: 10.1016/j.cell.2010.10.019

Michaelis, C., Ciosk, R., and Nasmyth, K. (1997). Cohesins: chromosomal proteins that prevent premature separation of sister chromatids. *Cell* 91, 35–45. doi: 10.1016/S0092-8674(01)80007-6

Miller, K. E., Kim, Y., Huh, W. K., and Park, H. O. (2015). Bimolecular fluorescence complementation (BiFC) analysis: advances and recent applications for genome-wide interaction studies. *J. Mol. Biol.* 427, 2039–2055. doi: 10.1016/j.jmb.2015.03.005

Morillo-Huesca, M., Clemente-Ruiz, M., Andujar, E., and Prado, F. (2010). The SWR1 histone replacement complex causes genetic instability and genome-wide transcription misregulation in the absence of H2A.Z. *PLoS ONE* 5:e12143. doi: 10.1371/journal.pone.0012143

Morillo-Huesca, M., Murillo-Pineda, M., Barrientos-Moreno, M., Gomez-Marin, E., Clemente-Ruiz, M., and Prado, F. (2019). Actin and nuclear envelope components influence ectopic recombination in the absence of Swr1. *Genetics* 213, 819–834. doi: 10.1534/genetics.119.302580

Neumann, F. R., Dion, V., Gehlen, L. R., Tsai-Pflugfelder, M., Schmid, R., Taddei, A., et al. (2012). Targeted INO80 enhances subnuclear chromatin movement and ectopic homologous recombination. *Genes Dev.* 26, 369–383. doi: 10.1101/gad.176156.111

Ontoso, D., Acosta, I., van Leeuwen, F., Freire, R., and San-Segundo, P. A. (2013). Dot1-dependent histone H3K79 methylation promotes activation of the Mek1 meiotic checkpoint effector kinase by regulating the Hop1 adaptor. *PLoS Genet.* 9:e1003262. doi: 10.1371/journal.pgen.1003262

Ontoso, D., Kauppi, L., Keeney, S., and San-Segundo, P. A. (2014). Dynamics of DOT1L localization and H3K79 methylation during meiotic prophase I in mouse spermatocytes. *Chromosoma* 123, 147–164. doi: 10.1007/s00412-013-0438-5

Qin, Y., Zhao, L., Skaggs, M. I., Andreuzza, S., Tsukamoto, T., Panoli, A., et al. (2014). ACTIN-RELATED PROTEIN6 Regulates female meiosis by modulating meiotic gene expression in arabidopsis. *Plant Cell* 26, 1612–1628. doi: 10.1105/tpc.113.120576

Raisner, R. M., Hartley, P. D., Meneghini, M. D., Bao, M. Z., Liu, C. L., Schreiber, S. L., et al. (2005). Histone variant H2A.Z marks the 5' ends of both active and inactive genes in euchromatin. *Cell* 123, 233–248. doi: 10.1016/j.cell.2005.10.002

Rao, H. B., Shinohara, M., and Shinohara, A. (2011). Mps3 SUN domain is important for chromosome motion and juxtaposition of homologous chromosomes during meiosis. *Genes Cells* 16, 1081–1096. doi: 10.1111/j.1365-2443.2011.01554.x

Rockmill, B. (2009). Chromosome spreading and immunofluorescence methods in *Saccharomyes cerevisiae*. *Methods Mol. Biol.* 558, 3–13. doi: 10.1007/978-1-60761-103-5_1

Rockmill, B., and Roeder, G. S. (1990). Meiosis in asynaptic yeast. *Genetics* 126, 563–574.

Rosa, M., Von Harder, M., Cigliano, R. A., Schlogelhofer, P., and Mittelsten Scheid, O. (2013). The *Arabidopsis* SWR1 chromatin-remodeling complex is important for DNA repair, somatic recombination, and meiosis. *Plant Cell* 25, 1990–2001. doi: 10.1105/tpc.112.104067

San-Segundo, P. A., and Clemente-Blanco, A. (2020). Resolvases, dissolvases, and helicases in homologous recombination: clearing the road for chromosome segregation. *Genes* 11:71. doi: 10.3390/genes11010071

Scherthan, H., Wang, H., Adelfalk, C., White, E. J., Cowan, C., Cande, W. Z., et al. (2007). Chromosome mobility during meiotic prophase in *Saccharomyces cerevisiae*. *Proc. Natl. Acad. Sci. U.S.A.* 104, 16934–16939. doi: 10.1073/pnas.0704860104

Sheff, M. A., and Thorn, K. S. (2004). Optimized cassettes for fluorescent protein tagging in *Saccharomyces cerevisiae*. *Yeast* 21, 661–670. doi: 10.1002/yea.1130

Sonntag Brown, M., Zanders, S., and Alani, E. (2011). Sustained and rapid chromosome movements are critical for chromosome pairing and meiotic progression in budding yeast. *Genetics* 188, 21–32. doi: 10.1534/genetics.110.125575

Stuckey, S., and Storici, F. (2013). Gene knockouts, *in vivo* site-directed mutagenesis and other modifications using the delitto perfetto system in *Saccharomyces cerevisiae*. *Meth. Enzymol.* 533, 103–131. doi: 10.1016/B978-0-12-420067-8.00008-8

Sung, M. K., and Huh, W. K. (2007). Bimolecular fluorescence complementation analysis system for *in vivo* detection of protein-protein interaction in *Saccharomyces cerevisiae*. *Yeast* 24, 767–775. doi: 10.1002/yea.1504

Tomita, K., and Cooper, J. P. (2007). The telomere bouquet controls the meiotic spindle. *Cell* 130, 113–126. doi: 10.1016/j.cell.2007.05.024

Trelles-Sticken, E., Dresser, M. E., and Scherthan, H. (2000). Meiotic telomere protein Ndj1p is required for meiosis-specific telomere distribution, bouquet formation and efficient homologue pairing. *J. Cell Biol.* 151, 95–106. doi: 10.1083/jcb.151.1.95

Trelles-Sticken, E., Loidl, J., and Scherthan, H. (1999). Bouquet formation in budding yeast: initiation of recombination is not required for meiotic telomere clustering. *J. Cell Sci.* 112, 651–658.

Uetz, P., Giot, L., Cagney, G., Mansfield, T. A., Judson, R. S., Knight, J. R., et al. (2000). A comprehensive analysis of protein-protein interactions in *Saccharomyces cerevisiae*. *Nature* 403, 623–627. doi: 10.1038/35001009

Wanat, J. J., Kim, K. P., Koszul, R., Zanders, S., Weiner, B., Kleckner, N., et al. (2008). Csm4, in collaboration with Ndj1, mediates telomere-led chromosome dynamics and recombination during yeast meiosis. *PLoS Genet.* 4:e1000188. doi: 10.1371/journal.pgen.1000188

Weber, C. M., and Henikoff, S. (2014). Histone variants: dynamic punctuation in transcription. *Genes Dev.* 28, 672–682. doi: 10.1101/gad.238873.114

Yamada, S., Kugou, K., Ding, D. Q., Fujita, Y., Hiraoka, Y., Murakami, H., et al. (2018a). The conserved histone variant H2A.Z illuminates meiotic recombination initiation. *Curr. Genet.* 64, 1015–1019. doi: 10.1007/s00294-018-0825-9

Yamada, S., Kugou, K., Ding, D. Q., Fujita, Y., Hiraoka, Y., Murakami, H., et al. (2018b). The histone variant H2A.Z promotes initiation of meiotic recombination in fission yeast. *Nucleic Acids Res.* 46, 609–620. doi: 10.1093/nar/gkx1110

Yamada, T., and Ohta, K. (2013). Initiation of meiotic recombination in chromatin structure. *J. Biochem.* 154, 107–114. doi: 10.1093/jb/mvt054

Yu, H., Braun, P., Yildirim, M. A., Lemmens, I., Venkatesan, K., Sahalie, J., et al. (2008). High-quality binary protein interaction map of the yeast interactome network. *Science* 322, 104–110. doi: 10.1126/science.1158684

Yue, J. X., Li, J., Aigrain, L., Hallin, J., Persson, K., Oliver, K., et al. (2017). Contrasting evolutionary genome dynamics between domesticated and wild yeasts. *Nat. Genet.* 49, 913–924. doi: 10.1038/ng.3847

Zhang, Y., Liu, T., Meyer, C. A., Eeckhoute, J., Johnson, D. S., Bernstein, B. E., et al. (2008). Model-based analysis of ChIP-Seq (MACS). *Genome Biol.* 9:R137. doi: 10.1186/gb-2008-9-9-r137

Zickler, D., and Kleckner, N. (2015). Recombination, pairing, and synapsis of homologs during meiosis. *Cold Spring Harb. Perspect. Biol.* 7: a016626. doi: 10.1101/cshperspect.a016626

Conflict of Interest: The authors declare that the research was conducted in the absence of any commercial or financial relationships that could be construed as a potential conflict of interest.

Copyright © 2020 González-Arranz, Gardner, Yu, Patel, Heldrich, Santos, Carballo, Jaspersen, Hochwagen and San-Segundo. This is an open-access article distributed under the terms of the Creative Commons Attribution License (CC BY). The use, distribution or reproduction in other forums is permitted, provided the original author(s) and the copyright owner(s) are credited and that the original publication in this journal is cited, in accordance with accepted academic practice. No use, distribution or reproduction is permitted which does not comply with these terms.

frontiers in Cell and Developmental Biology

ORIGINAL RESEARCH
published: 13 November 2020
doi: 10.3389/fcell.2020.595373

Phycocyanin Improves Reproductive Ability in Obese Female Mice by Restoring Ovary and Oocyte Quality

*Xin Wen[1], Zhe Han[1], Shu-Jun Liu[1], Xin Hao[1], Xiao-Jie Zhang[1], Xing-Yue Wang[1], Cheng-Jie Zhou[1], Yu-Zhen Ma[2] and Cheng-Guang Liang[1]**

[1] State Key Laboratory of Reproductive Regulation and Breeding of Grassland Livestock, School of Life Sciences, Inner Mongolia University, Hohhot, China, [2] Inner Mongolia People's Hospital, Hohhot, China

Reproductive dysfunction associated with obesity is increasing among women of childbearing age. Emerging evidence indicates that maternal obesity impairs embryo development and offspring health, and these defects are linked to oxidative stress in the ovary and in oocytes. Phycocyanin (PC) is a biliprotein from *Spirulina platensis* that possesses antioxidant, anti-inflammatory, and radical-scavenging properties. Our previous studies have shown that PC can reduce reactive oxygen species (ROS) accumulation in oocytes in D-gal-induced aging mice. Here, at the Institute of Cancer Research (ICR) mice fed a high-fat diet (HFD) to model obesity were used to test the effect of PC on reversing the fertility decline caused by obesity. We observed a significant increase in litter size and offspring survival rates after PC administration to obese mice. Further, we found that PC not only ameliorated the level of ovarian antioxidant enzymes, but also reduced the occurrence of follicular atresia in obese female mice. In addition, the abnormal morphology of the spindle-chromosome complex (SCC), and the abnormal mitochondrial distribution pattern in oocytes both recovered. The obesity-related accumulation of ROS, increased number of early apoptotic cells, and the abnormal expression of H3K9me3 in oocytes were all partially reversed after PC administration. In summary, this is the first demonstration that PC can improve fertility by partially increasing ovarian and oocyte quality in obese female mice and provides a new strategy for clinically treating obesity-related infertility in females.

Keywords: phycocyanin, obesity, ovary, oocyte, offspring, oxidative stress

OPEN ACCESS

Edited by:
Wei Li,
Institute of Zoology, Chinese Academy of Sciences (CAS), China

Reviewed by:
Qiang Wang,
Nanjing Medical University, China
Wei Shen,
Qingdao Agricultural University, China

***Correspondence:**
Cheng-Guang Liang
liangcg@imu.edu.cn

Specialty section:
This article was submitted to Cell Growth and Division, a section of the journal Frontiers in Cell and Developmental Biology

Received: *16 August 2020*
Accepted: *06 October 2020*
Published: *13 November 2020*

Citation:
Wen X, Han Z, Liu S-J, Hao X, Zhang X-J, Wang X-Y, Zhou C-J, Ma Y-Z and Liang C-G (2020) Phycocyanin Improves Reproductive Ability in Obese Female Mice by Restoring Ovary and Oocyte Quality. Front. Cell Dev. Biol. 8:595373. doi: 10.3389/fcell.2020.595373

INTRODUCTION

The proportion of obese people has increased significantly as the general quality of life has improved (Darbre, 2017), and maternal obesity has been reported to cause a variety of diseases (Rogero and Calder, 2018). For example, obesity can reduce ovarian and oocyte quality, increase the level of oxidative stress in them (Igosheva et al., 2010; Luzzo et al., 2012; Grindler and Moley, 2013), and ultimately damage female fertility (Jungheim and Moley, 2010; Silvestris et al., 2018). Evidence also indicates that obese females have a lower probability for conception and a higher risk for miscarriages, preeclampsia, and congenital defects in their offspring (Machtinger et al., 2012). In addition, maternal obesity has been associated with spindle defects and chromosome misalignment during meiotic oocyte maturation (Jungheim et al., 2010; Luzzo et al., 2012), and

obesity-related maternal metabolic syndrome induced structural, spatial, and metabolic alterations in oocyte mitochondria (Reynolds et al., 2015; Saben et al., 2016). Reactive oxygen species, (ROS), a by-product of oxidative phosphorylation, are simultaneously produced in mitochondria (Balaban et al., 2005), and their levels were dramatically elevated in obese female oocytes (Zhang et al., 2015). Previous reports have demonstrated that ROS accumulation in cells leads to cytoskeleton abnormalities (Yancey et al., 2015), antioxidant system dysfunction (Janda et al., 2016), abnormal distribution of mitochondria (Yu et al., 2016), and cell apoptosis (Liu et al., 2016). Therefore, obesity is harmful to female reproductive capability (Catalano and Ehrenberg, 2006).

A recent prospective study has suggested that specific dietary ingredients may improve obesity-induced reproductive impairment (Han et al., 2017). Phycocyanin (PC) is a major biliprotein extracted from *Spirulina platensis*, and is mostly found in red algae, cyanobacteria, and cryptophaga (Benedetti et al., 2004). As an antioxidant, PC was found to inhibit cell aging and to protect mitochondrial function in many cell types (Fernández-Rojas et al., 2014). Recently, we found that continuous intragastric administration of PC significantly reduced the accumulation of ROS inside oocytes of D-galactose-induced aging mice and improved their oocyte quality, increasing female fertility (Li et al., 2016). Moreover, increasing evidence indicates that PC promotes cell activity, eliminates free radicals, and improves organ function (Li et al., 2013; Hao et al., 2018), and has become widely used as a natural substance with antioxidant, neuro-protective, anti-inflammatory, and oxygen free-radical scavenging properties (Romay et al., 2003; Gupta et al., 2011; Fernández-Rojas et al., 2014).

The negative impact of obesity on oocyte quality is well known (Sohrabi et al., 2015), and the fact that PC improves oocyte quality has also been well-documented (Li et al., 2016), but the effects of PC on ovaries and oocytes damaged by obesity remains unclear. Therefore, the purpose of the present research was to determine whether PC could alleviate the negative impact of obesity on ovary, oocyte quality and fertility. We found that PC did maintain ovary/oocyte quality and fertility in obese mice, and these results may be important for treating obesity-related subfertility in humans.

MATERIALS AND METHODS

Experimental Design, Mouse Feeding, Mating, and Offspring Assessments

All research procedures conformed to the National Research Council Guide for the Care and Use of Laboratory Animals (Garber et al., 2011), and were approved by the Institutional Animal Care and Use Committee at the Inner Mongolia University (Approval number: SYXK 2014-0002). ICR mice were purchased from the Research Centre for Laboratory Animal Science of Inner Mongolia University, and were reared in a special pathogen free animal facility in the Research Centre for Laboratory Animal Science of Inner Mongolia University under the conditions of a 12:12-h light:dark cycle. Throughout the experiments, mice were free to get food and water. At the age of 4 weeks, female mice were randomly divided into three groups and treated as follows. In the control group (CTRL), mice were continuously fed a normal diet (H10010, HFK Bioscience Co., Ltd., Beijing, China) for 14 weeks. During the last 6 weeks, 0.4 ml of normal saline was administered intragastrically each day. In the high-fat diet group (HFD), mice were continuously fed a high-fat diet (D12492, Research Diets Inc., New Brunswick, NJ, United States) for 14 weeks. During the last 6 weeks, 0.4 ml saline was administered intragastrically each day. In the high-fat diet + phycocyanin group (HFD + PC), mice were continuously fed a high-fat diet for 14 weeks. During the last 6 weeks, PC (Zhejiang Binmei Biotechnology Co., Ltd, Taizhou, Zhejiang, China) at a dose of 500 mg/kg/day (dissolved in ultrapure water at a concentration of 50 mg/ml) was administered intragastrically each day. A schematic of the experimental design is shown in **Figure 1A**. Food consumption, and mouse body weights were recorded weekly.

If body weight increased more than 20% compared to controls, mice were defined as obese (Lee et al., 2020). In terms of the PC dosage, its intragastric administration at 500 mg/kg/day improved the reproductive abilities of aging female mice (Li et al., 2016), so we used this dose in the current study.

A single ICR male mouse at 12 weeks of age (with proven fertility) was caged overnight with a single female mouse for mating. Vaginal plugs in the female mice were detected in the morning of the next day. The numbers, weights, and survival rate of the offspring were recorded weekly from delivery to the age of 8 weeks. The sex ratio (male/female) of the pups was determined at 3 weeks of age.

Glucose Tolerance Tests (GTTs) and Insulin-Tolerance Tests (ITTs)

Mice were injected intraperitoneally with glucose (2 g/kg body weight) after 12 h of fasting before GTT analysis. Mice were injected intraperitoneally with insulin (0.75 IU/kg body weight) after 4 h of fasting before ITT analysis. Blood was gathered from the tail vein at the appropriate time point. GTT and ITT levels were measured with the blood glucose meter (Roche, Basel, Switzerland, Germany). GraphPad Prism 7 software was used to calculate area under the curve (AUC) values for both GTT and ITT. *Glucose tolerance* refers to a reduction in the body's ability to regulate blood glucose levels (González-Grajales et al., 2018), and *insulin resistance* refers to a reduction in the response of a peripheral target tissue to a physiological concentration of insulin (Hotamisligil et al., 1993).

Ovary Histology and Follicle Counting

Mouse ovaries were harvested and fixed in 4% paraformaldehyde (Electron Microscopy Sciences, Hatfield, PA, United States) overnight at 4°C, followed by dehydration with ethanol. Paraffin-embedded ovaries were sectioned serially (5 μm thickness) and every fifth section was mounted on slides for hematoxylin and eosin (H&E) staining (Nanjing Jiancheng Bioengineering Institute, Nanjing, Jiangsu, China) and neutral resin fixation,

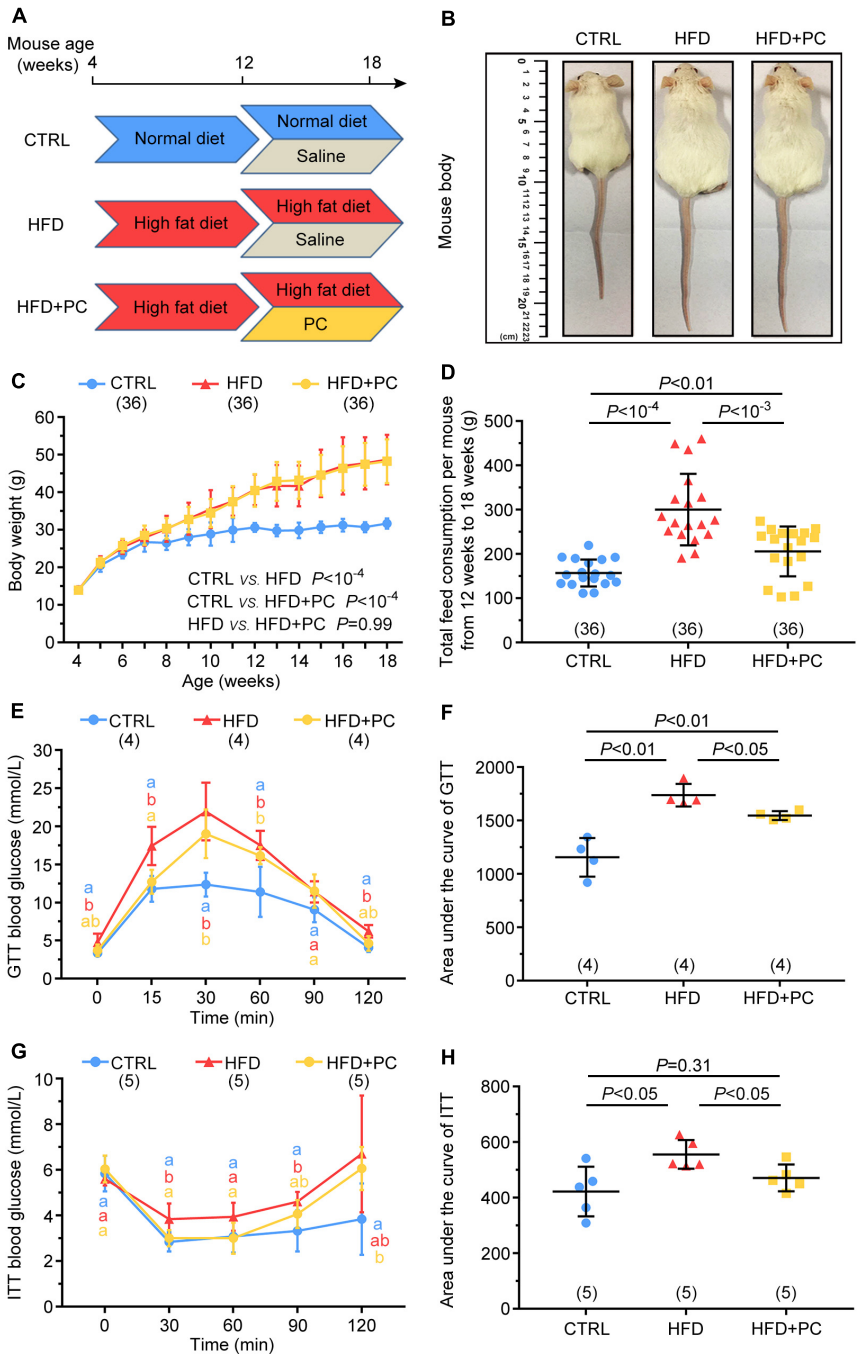

FIGURE 1 | PC improved glucose tolerance and insulin resistance in obese female mice. **(A)** Experimental design. The mice in the CTRL group were fed a normal diet (blue) and had intragastric administrations of saline (gray). Mice in the HFD group were fed a high-fat diet (red) and had intragastric administrations of saline (gray). The mice in the HFD + PC group were fed a high-fat diet (red) and had intragastric administrations of PC (yellow). **(B)** Image of mice at the age of 18 weeks. **(C)** Weight changes in mice (4–18 weeks of age). **(D)** Average food consumption (12–18 weeks of age). **(E)** Blood glucose changes in GTT. **(F)** GTT AUC values. **(G)** Blood glucose changes in ITT. **(H)** ITT AUC values. Data are expressed as mean ± SD and were compared by one-way ANOVA and Newman–Keuls *post hoc* tests. In **(E,G)**, the different letters at the same time point near the error bars indicate statistical significance ($p < 0.05$). The number of mice in each group is shown in parentheses.

then examined by optical microscopy (Nikon ECLIPSE Ci, Tokyo, Japan). For each section, only follicles in which the oocyte nucleus could be clearly visualized were scored. Follicle classifications were made as previously described (Wang et al., 2014), and the numbers of follicles at the different developmental stages were counted.

Quantitative Real-Time Polymerase Chain Reaction (RT-PCR) and Biochemistry Assays

For quantitative RT-PCR, total RNA was extracted from ovaries using the TaKaRa MiniBEST Universal RNA Extraction Kit (TaKaRa, Dalian, Liaoning, China) according to the manufacturer's instructions. cDNA was synthesized using the PrimeScript RT reagent Kit (TaKaRa) following the manufacturer's instructions. The primer sequences were as follows: *BMP4* (Forward: 5′-TCCTGGTAACCGAATGCTGAT-3′; Reverse: 5′-GCTGCTGAGGTTGAAGAGGAA-3′), *GDF9* (Forward: 5′-AATACCGTCCGGCTCTTCAG-3′; Reverse: 5′-GGTTAAACAGCAGGTCCACCAT-3′), *LHX8* (Forward: 5′-CAGTTCGCTCAGGACAACAA-3′; Reverse: 5′-CCTGCAGTTCTGAAACCACA-3′), *GAPDH* (Forward: 5′-CGGCCGCATCTTCTTGTG-3′; Reverse: 5′-CCGACCTTCACCATTTTGTCTAC-3′). RT-PCR was performed with the SYBR Green kit (TaKaRa). The comparative Ct method was used for data analysis, and GAPDH was used as an internal control.

The levels of oestradiol and follicle stimulating hormone (FSH) in serum were measured using an ELISA kit (CUSABIO, Wuhan, Hubei, China). Ovarian catalase (CAT), glutathione peroxidase (GSH-Px), superoxide dismutase (SOD) activities, and malondialdehyde (MDA) content were measured using their corresponding kits (Nanjing Jiancheng Bioengineering Institute). All detection procedures were carried out according to the manufacturers' instructions.

Oocyte Collection, Maturation, Fertilization, and Embryo Culture

The oocytes in GV phase were harvested from female mice 48 h after injection of 5 IU pregnant mare serum gonadotropin (PMSG, Ningbo Sansheng Pharmaceutical Co., Ltd., Ningbo, Zhejiang, China) by puncturing the ovary follicles. Cumulus-oocyte complexes (COCs) were gently transferred into M2 medium to remove cumulus cells. Oocytes were washed and cultured in Chatot-Ziomek-Bavister (CZB) media in a humidified atmosphere of 5% CO_2 at 37°C for maturation. Germinal vesicle breakdown (GVBD) and the first polar body (PB1) were observed 2.5 h and 14 h later, respectively.

For metaphase II (MII) oocytes matured *in vivo*, mice received an intraperitoneal injection of 5 IU PMSG followed by administration of 5 IU human chorionic gonadotropin (hCG, Ningbo Sansheng Pharmaceutical Co., Ltd.) 48 h later. The COCs were released from the oviduct ampullae 14 h after hCG injection. Denuded MII oocytes were obtained by removing the cumulus mass in M2 medium containing 0.3 mg/ml hyaluronidase. PB1 extrusions and oocyte fragmentations were examined.

Oocytes fertilization and early embryonic development were evaluated as previously described (Zhou et al., 2016). Zygotes that developed to 2-cell stage embryos were classified as successfully fertilized oocytes. Embryos were evaluated at 48 h, 72 h, and 96 h after fertilization, and the percentages of embryos at the 4-cell stage, morula stage and blastocyst stage were calculated, respectively.

Immunofluorescence and Confocal Microscopy

Immunofluorescence detecting was performed as previously described (Li et al., 2016). For primary antibodies, we used mouse anti-beta-tubulin (1:1000, Abcam, Cambridge, United Kingdom) and anti-H3K9me3 (1:500, Abcam). For secondary antibodies, we used DyLight 549-conjugated donkey anti-mouse (1:100, Jackson Immuno Research Laboratories, West Grove, PA, United States). DNA was stained with 4′,6-diamidino-2-phenylindole (DAPI, 5 μg/ml, Roche, Mannheim, Germany) for 10 min. After washing, samples were mounted onto glass slides and examined with a confocal laser-scanning microscope (Nikon A1R).

Determining the Distribution of Mitochondria

For determining mitochondrial distribution, MII oocytes were fixed in 4% paraformaldehyde for 30 min in a humidified chamber, and stained with 25 μM MitoTracker Green FM (Molecular Probes, Eugene, OR, United States) for 30 min and 50 ng/ml DAPI for 10 min in the dark. After staining, the samples were mounted onto microscope slides and examined using confocal microscopy as above. The distribution patterns of mitochondria in oocytes were divided into two types: evenly distributed or aggregated. Normally, mitochondria are evenly distributed in MII oocytes (Jia et al., 2018), so *mitochondria-even* denoted this evenly distributed pattern, whereas *mitochondria-aggregation* denoted a distribution pattern where mitochondria were clumped/aggregated.

Mitochondrial Membrane Potential ($\Delta\Psi m$) Measurements

The $\Delta\Psi m$ was assessed using the mitochondrial inner membrane potential dye JC-10 (Beyotime, Hangzhou, Zhejiang, China), according to the manufacturer's instructions. Briefly, oocytes were placed in a working solution with a final concentration of 10 μM JC-10, and cultured in darkness at 37°C, 5% CO_2 for 20 min. Samples were assessed using confocal microscopy as above. The mitochondrial membrane potentials were calculated using the ratio of red to green fluorescence intensities in the oocytes.

ROS Assay

To evaluate ROS production inside oocytes, oocytes were incubated in CZB media containing 10 μM DCFH-DA (Nanjing Jiancheng Bioengineering Institute) for 30 min at 37°C in a 5% CO_2 incubator. Oocytes (10–15) were then transferred to a cell-imaging dish, and the fluorescence intensity of each oocyte was measured using confocal microscopy as above.

Annexin-V Staining

Oocyte apoptosis was evaluated using the Annexin-V-FITC Apoptosis Kit (Vazyme, Nanjing, Jiangsu, China). Oocytes were stained with 195 μl binding buffer containing 5 μl Annexin-V-FITC for 30 min in the dark. After washing three times, fluorescence signals were detected using confocal microscopy as

above, with oocyte-membrane fluorescence as an indicator of early apoptosis.

Statistical Analysis

Results are shown as means ± standard deviations (SD) representing more than three replicate experiments. Statistical comparisons were made using an analysis of variance (ANOVA), and differences among the three groups were assessed using Newman–Keuls multiple-comparison *post hoc* tests. For the female mouse vaginal plug rate, offspring gender rate, and mitochondrial distributions, chi-squared tests in Microsoft Excel software (Microsoft Corporation, Redmond, WA, United States) were used. The offspring survival rate was analyzed using the log-rank test (Mantel-Cox). All other analyses were performed using GraphPad Prism 7.0 statistical software (GraphPad Software Inc., La Jolla, CA, United States). A p value < 0.05 was considered statistically significant.

RESULTS

PC Improved Glucose Tolerance and Insulin Resistance in Obese Female Mice

The weights of mice in each group were measured before feeding to ensure that all mice were comparable. With increasing age and food intake, the weight gains for the HFD and HFD + PC groups were significantly higher compared to the CTRL group ($p < 10^{-4}$). Intragastric administration of PC did not affect the body weights of HFD mice (**Figures 1B,C**). However, it did reduce food consumption in HFD mice between 12 and 18 weeks (**Figure 1D**).

The GTT analysis showed that glucose concentrations in the HFD group were higher than those in the CTRL and HFD + PC groups at 15 and 30 min ($p < 0.05$) (**Figure 1E**). Further AUC analyses confirmed these results (**Figure 1F**). Similarly, the ITT blood test results (**Figure 1G**) and the corresponding AUC values (**Figure 1H**) also showed a significant increase in insulin resistance in the HFD group, indicating intragastric administration of PC improved the glucose metabolism and insulin response in obese female mice.

PC Increased Litter Size and Offspring Viability in Obese Mice

Phycocyanin's improvement effect on obese female mice fertility was also assessed by evaluating the offspring. The mating probabilities of females (indicated by vaginal plugs) in the CTRL, HFD, and HFD + PC groups were comparable ($p > 0.05$), illustrating that a HFD or PC gavage did not affect female mating ability (**Figure 2A**). However, litter size in the HFD group was significantly lower when compared to the CTRL group ($p < 10^{-4}$). The litter size reduction after HFD treatment was partially reversed by PC administration ($p < 0.01$) but was still lower compared to controls ($p < 0.05$) (**Figure 2B**). In terms of the gender ratios, birth weights, and body weights from 1 to 8 weeks after birth, there were no significant differences among the three groups ($p > 0.05$) (**Figures 2C–E**). To our surprise, there was a significant decrease in offspring survival (1–8 weeks after birth) found in the HFD group. Only 58% of the offspring survived after 8 weeks in the HFD group, compared to the CTRL (83%) or the HFD + PC group (75%) (**Figure 2F**). These results indicate that obesity in females has a negative effect on both litter size and offspring survival that can be partially reversed by PC administration.

PC Prevented Ovarian Follicular Atresia, and Improved FSH Levels and Antioxidant Enzyme Activity in Obese Mice

To understand the ability of PC to reverse the HFD effect on female mouse reproductive ability, both ovaries and follicles were assessed. There were no significant gross morphological differences among the three groups of ovary pairs (**Figure 3A**), and ovary-pair wet weights were comparable among the three groups (**Figure 3B**). However, the ovary-ratio coefficient in the HFD group was much lower than that for the CTRL group due to HFD-increased body weights ($p < 10^{-3}$), and PC administration did not reverse these changes in the ovary-ratio coefficient in HFD mice ($p < 0.05$) (**Figure 3C**). The number of ovary follicles at different developmental stages were also assessed using histology (**Figure 3D**). There were no significant differences among the three groups in terms of the number of primordial and primary follicles, secondary follicles, or antral follicles ($p > 0.05$). However, the number of atretic follicles in the HFD group was significantly higher than the number in the CTRL group ($p < 10^{-4}$). Although PC administration reduced the number of atretic follicles in the HFD mice group ($p < 0.05$), this number was still higher compared to that in the CTRL group ($p < 0.05$) (**Figure 3E**). These results indicate that PC had the ability to prevent ovarian follicular atresia in obese mice.

Subsequently, we also examined the mRNA expression levels of *BMP4*, *GDF9*, and *LHX8* related to ovarian follicular development. No significant differences were found among the three groups ($p > 0.05$) (**Figures 3F–H**).

Obesity can disrupt homeostasis and cause hormone disorders. To study the effect of PC on hormones in HFD mice, we assessed the levels of oestradiol and FSH in mice serum. No statistical differences were found in oestradiol levels among the three groups ($p > 0.05$) (**Figure 3I**). However, FSH levels in the HFD group were significantly higher than those in the CTRL group ($p < 0.01$). After intragastric administration of PC to HFD mice, FSH levels were significantly reduced ($p < 0.05$), but still higher than those in the CTRL group ($p < 0.05$) (**Figure 3J**).

Next, we measured ovarian activity and content of antioxidant enzymes. Significantly, CAT activity in the HFD group was higher than that in the CTRL group ($p < 10^{-4}$), and this increase was partially reversed by PC treatment ($p < 0.01$) (**Figure 3K**). In the HFD group, the activities of GSH-Px and SOD were decreased compared with their activities in the CTRL group, and this decrease was not reversed after PC administration (**Figures 3L,M**). Conversely, MDA content in the HFD group was higher compared to the CTRL group ($p < 0.01$), and this abnormality was not reversed by PC treatment (**Figure 3N**).

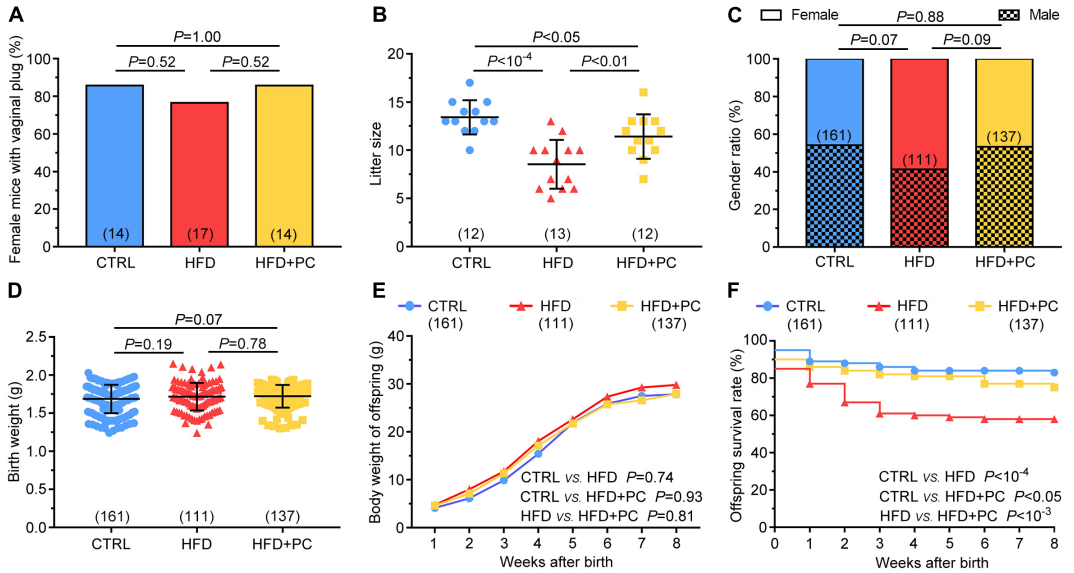

FIGURE 2 | PC increased litter sizes and offspring viability in obese female mice. **(A)** A comparison of mating rates in female mice. **(B)** Offspring litter sizes. **(C)** The gender ratios for offspring. **(D)** Offspring birth weights. **(E)** Body weights for offspring (1–8 weeks of age). **(F)** Offspring survival rates (0–8 weeks of age). Data are expressed as mean ± SD and were compared by one-way ANOVA and Newman–Keuls *post hoc* tests for **(B,C)**, chi-squared tests for **(A,E)**, log-rank tests (Mantel-Cox) for **(D,F)**. The number of mice in each group is shown in parentheses.

PC Improved Oocyte Quality in Obese Mice

As litter size was observed to be increased after PC administration in HFD mice, we wanted to know if this increase was due to an improvement in oocyte quality. Oocytes or 2-cell-stage embryos from both *in vivo* and *in vitro* culture models showed impaired developmental potential in the HFD group, indicated by enlarged perivitelline spaces, and fragmented or dark cytoplasm. In contrast, after PC treatment, the majority of oocytes and embryos exhibited normal morphologies comparable to the CTRL group (**Figure 4A**). After gonadotropin administration, the numbers of GV or MII oocytes superovulated from each mouse were counted. The number of GV oocytes collected from the HFD group was much lower than the CTRL group number ($p < 0.01$). Similarly, the number of MII oocytes from the HFD group was also much lower than the CTRL group number ($p < 10^{-4}$). Although the numbers of both GV and MII oocytes increased after PC administration, there were no statistical differences when compared with the HFD group ($p > 0.05$) (**Figures 4B,C**). For *in vitro* maturation, neither HFD nor PC treatment influenced oocyte meiotic resumption, which was indicated by the comparable occurrence of GVBD (**Figure 4D**). However, PC rescued impaired-oocyte nuclear maturation potential in HFD mice, indicated by the increased percentage of PB1 extrusions ($p > 0.05$) (**Figure 4E**). In addition, a high frequency of fragmentation in *in vivo*-matured oocytes was observed in the HFD group ($p < 10^{-4}$). PC treatment partially reversed this fragmentation rate ($p < 0.01$), but it was still higher than the CTRL group rate ($p < 0.01$) (**Figure 4F**). Moreover, our results show that the early development of embryos generated from IVF was affected both by HFD and PC. The embryo development rates for the 2-cell, 4-cell, morula and blastocyst stages in the HFD group were lower than those in the CTRL group ($p < 0.05$). After PC treatment, the developmental potentials for each stage increased significantly ($p < 0.05$) (**Figure 4G**). Overall, although PC did not increase the number of fully grown oocytes in obese female mice, it significantly improved oocyte quality and embryo development potential.

PC Reversed Spindle-Chromosome Complex (SCC) Malformations in Obese Mice

Staining of beta-tubulin and DNA was carried out to assess the effects of obesity on SCC morphology in MII oocytes. Fusiform-shaped spindles with well-organized chromosomes in metaphase were observed in the majority of oocytes in the CTRL group. In contrast, abnormal chromosome condensation and spindle assembly defects were observed in the HFD groups. These defects included non-spindled poles, multipolar spindles, and dispersed distributions. It is worth noting that these defects were partially reversed in oocytes after PC administration (**Figure 5A**). When the percentages of abnormal SCC formations were analyzed, 49.42% of the oocytes collected from the HFD group had abnormal SCCs, and this percentage was reduced to 33.90% after PC administration ($p < 0.05$), which was comparable to controls ($p > 0.05$) (**Figure 5B**). The ratio of spindle length to oocyte diameter was also measured to evaluate spindle morphology (**Figure 5C**, left panel). Compared with the CTRL group, this ratio decreased in the HFD group ($p < 0.01$) and increased significantly after PC administration ($p < 0.05$) (**Figure 5D**). Similarly, the ratio of chromosome width to oocyte diameter in the HFD group was also significantly higher compared to the

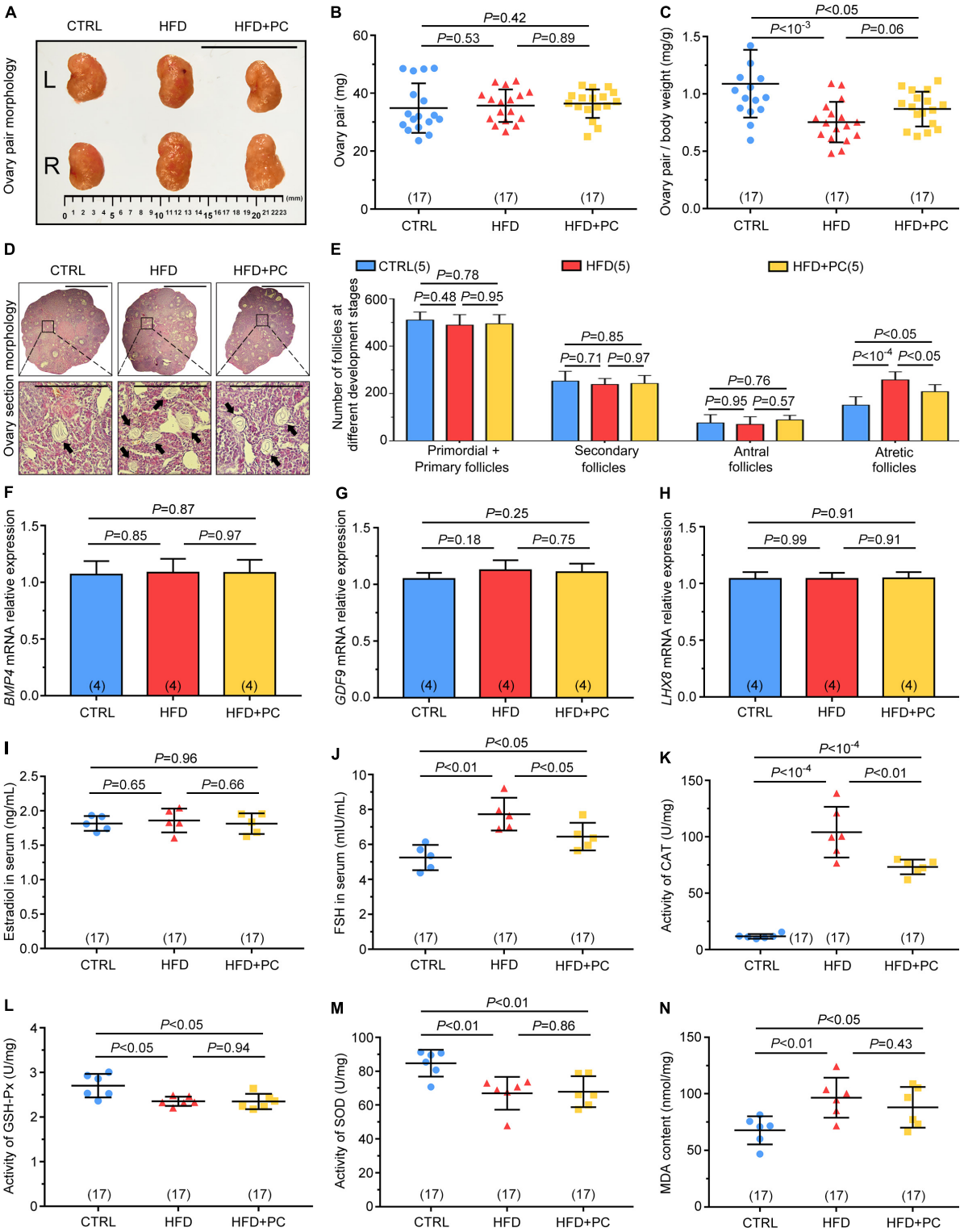

FIGURE 3 | PC promoted follicular development and reduced CAT and FSH levels in obese mice. **(A)** Macroscopic representations of the ovaries, scale bar = 10 μm. **(B)** Ovary-pair weights. **(C)** Ovary-pair ratio coefficients. **(D)** Typical histological image of H&E-stained follicles, scale bar = 50 μm, with black arrows indicating atretic follicles. **(E)** The statistics for follicles at different developmental stages in the ovaries. **(F)** Relative expressions of *BMP4* mRNA. **(G)** Relative expressions of *GDF9* mRNA. **(H)** Relative expressions of *LHX8* mRNA. **(I)** Estradiol levels. **(J)** FSH levels. **(K)** CAT activities. **(L)** GSH-Px activities. **(M)** SOD activities. **(N)** MDA contents. Data are expressed as mean ± SD and were compared by one-way ANOVA and Newman–Keuls *post hoc* tests. The number of ovary pairs in each group is shown in parentheses.

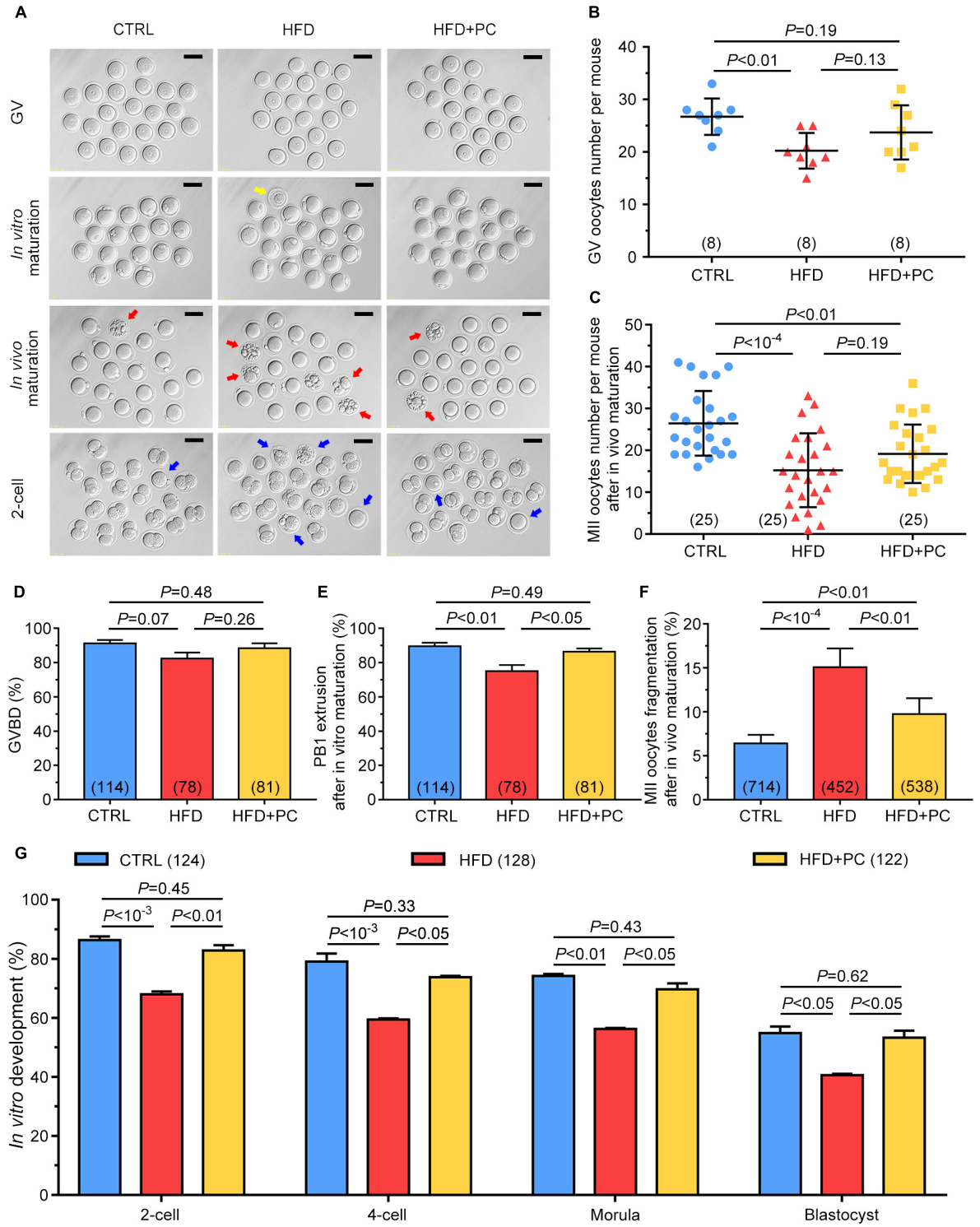

FIGURE 4 | PC rescued oocyte quality in obese mice. **(A)** Representative morphological images of GV, *in vivo* or *in vitro* matured oocytes, and 2-cell stage embryos. The yellow arrow indicates an oocyte with degenerated cytoplasm, red arrows indicate fragmented oocytes, and blue arrows indicate oocytes with failed fertilization or cleavage. Scale bar = 100 μm. **(B)** Number of GV oocytes per mouse. **(C)** Number of MII oocytes per mice after *in vivo* maturation. **(D)** The percentage of oocytes that underwent GVBD. **(E)** The percentage of *in vitro* cultured GV oocytes that underwent PB1 extrusion. **(F)** The percentage of oocytes with fragmentation morphologies. **(G)** The percentage development to 2-cell, 4-cell, morula, and blastocyst embryos. Data are expressed as mean ± SD and were compared by one-way ANOVA and Newman–Keuls *post hoc* tests. The number of mice assessed in each group is indicated in parentheses for **(B,C)**. The number of oocytes or embryos assessed in each group is indicated in parentheses for **(D–G)**.

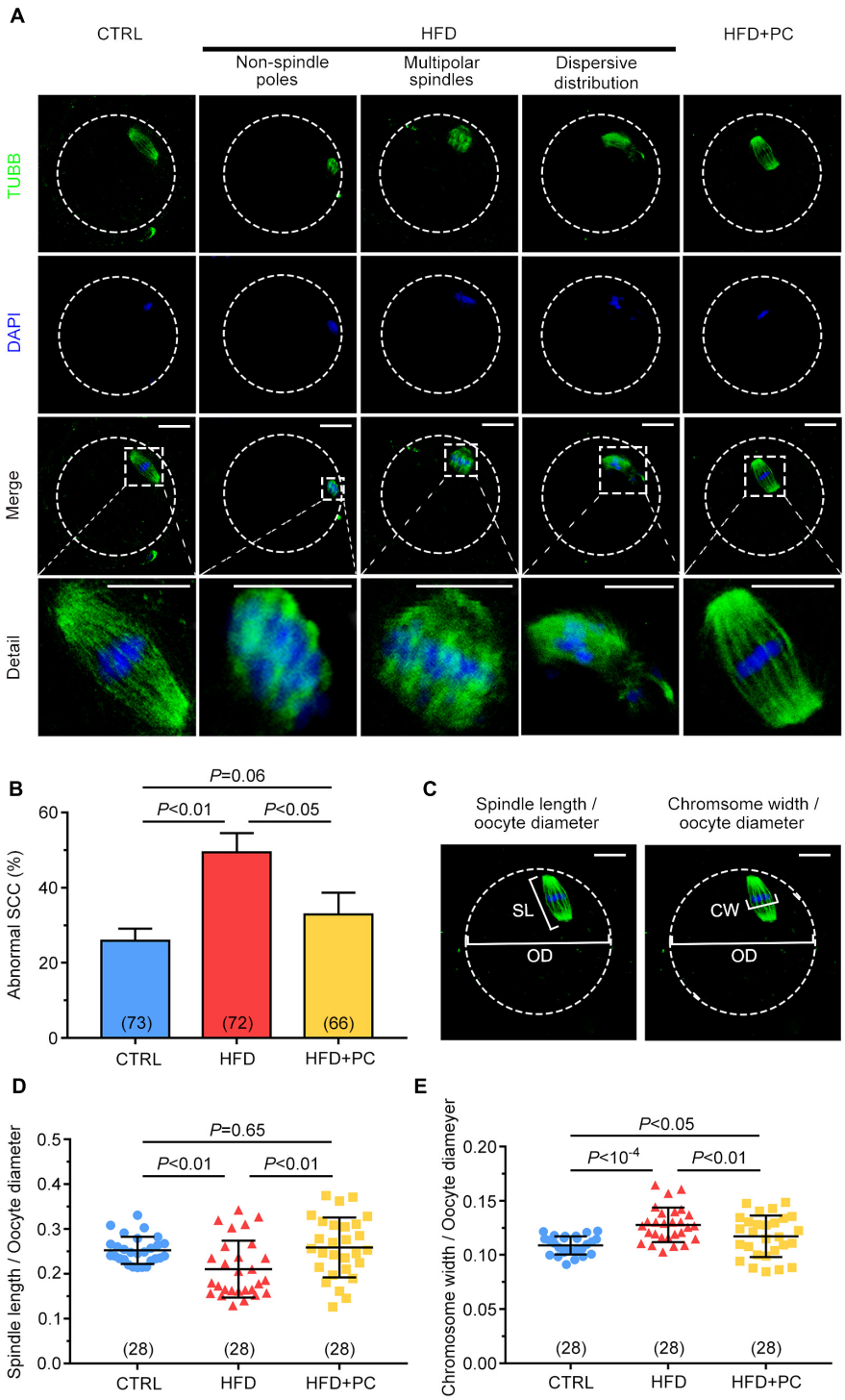

FIGURE 5 | Spindle-chromosome complex (SCC) malformations were reversed after PC administration in obese mice. **(A)** Representative images of SCCs in MII oocytes. Oocytes in the CTRL group exhibited normal spindles and chromosome condensation (left column). Oocytes in the HFD groups displayed abnormal SCCs (three middle columns). Normal oocyte spindle and chromosome condensation in the HFD + PC group (right column). The circular white frame indicates the oocyte edge and the square white square indicates the region shown in detail. Green, tubulin; blue, DNA. Scale bar = 20 μm. **(B)** The ratios of SCC abnormalities in the CTRL, HFD, and HFD + PC groups. **(C)** Schematic representation of spindle length (SL)/oocyte diameter (OD) **(left panel)** and chromosome width (CW)/oocyte diameter (OD) **(right panel)**. Green, tubulin; blue, DNA. The circular white frame indicates the oocyte edge. Scale bar = 20 μm. **(D)** Spindle length/oocyte diameter ratios in MII oocytes. **(E)** Chromosome width/oocyte diameter ratios in MII oocytes. Data are expressed as mean ± SD and were compared by one-way ANOVA and Newman–Keuls *post hoc* tests. The number of oocytes assessed in each group is shown in parentheses.

ratios in the CTRL group ($p < 10^{-4}$), and these morphology defects were partially rescued after PC administration (**Figure 5C**, right panel, and **Figure 5E**). These data indicate that PC administration improved oocytes quality by correcting abnormal SCCs in HFD mice.

PC Restored Mitochondrial Distribution, and Attenuated Both Oxidative Stress, and Early Apoptosis in Obese-Mice Oocytes

As mitochondria play a pivotal role during oocyte maturation, their distributions and membrane potentials were examined in MII oocytes. Mitochondrial distributions were classified as either *Even* or *Aggregated*, indicating either an evenly distributed pattern or an aggregated pattern in MII-stage oocytes (**Figure 6A**). Only 22.2% of MII oocytes in the CTRL group showed an aggregated distribution, but this proportion increased to 70.0% in the HFD group, significantly higher than in the CTRL group ($p < 10^{-4}$). After the administration of PC, the aggregated distribution proportion decreased to 30.2%, comparable to that of the CTRL group ($p > 0.05$) (**Figure 6B**). The JC-10 fluorescent dye, used to detect the mitochondrial membrane potential (**Figure 6C**), showed that there was no statistical difference among the three groups ($p > 0.05$) (**Figure 6D**).

Oocyte oxidative stress can be indicated by ROS levels. In order to detect the effect of obesity and PC on oocyte oxidative stress, DCFH-DA fluorescence intensity was measured to evaluate ROS levels. In MII oocytes from the HFD group, fluorescence intensity was significantly higher than the intensities in both the CTRL and the HFD + PC groups, indicating that obesity led to ROS production (**Figure 6E**). We quantified the relative fluorescence intensities and confirmed that ROS levels were higher in the HFD group ($p < 10^{-4}$). One notable exception was that ROS levels decreased significantly when PC was administered ($p < 0.01$) (**Figure 6F**). These results indicate that the obesity-related production of ROS in oocytes can be partially inhibited by PC administration. Higher intracellular ROS levels can lead to early apoptosis, so we performed Annexin-V staining to determine the proportion of oocytes experiencing early apoptosis. Oocytes experiencing early apoptosis were characterized by an unambiguous green membrane signal (**Figure 6G**). We quantified these fluorescence signals and found that 37.64% of oocytes in the HFD group were apoptotic. After PC administration, the percentage of apoptosis oocytes decreased to 22.64%, significantly lower than the HFD group proportion ($p < 0.05$) (**Figure 6H**).

PC Reversed Oocyte H3K9me3 Expression in Obese Mice

The expression levels of H3K4me2 and H3K9me3 in MII oocytes were examined by immunofluorescence staining to assess the effect of PC on histone methylation in oocytes from HFD mice. For H3K4me2, relatively higher intensities of immunofluorescence were observed in MII oocytes from the CTRL group, and decreased intensities were observed in both the HFD and HFD + PC groups (**Figure 7A**). After signal quantifications, we found that the fluorescence intensities for H3K4me2 were significantly lower in the HFD and HFD + PC groups compared to CTRL group intensities ($p < 10^{-3}$) (**Figure 7B**). Conversely, the expression of H3K9me3 was significantly higher in oocytes from the HFD group ($p < 0.01$), and this abnormal expression was completely inhibited by PC administration (**Figures 7C,D**). Taken together, these results indicate that PC reversed these abnormal epigenetic modifications inside oocytes in obese mice.

DISCUSSION

Obesity induced by a high-fat diet is harmful to the female reproductive system. In this study, we used mice that had been fed a high-fat diet as a model system for obesity, and observed that obesity-induced adverse effects on ovary antioxidant enzymes, follicular development, oocyte maturation, and meiotic spindle morphology were responsible for the reduced litter sizes and decreased survival rates. In addition, we found that the number of births and the survival rate for offspring increased in obese female mice after gavage with PC. These results showed that intragastric administration of PC reduced ovarian antioxidant enzymes, the number of atretic follicles, oocyte meiotic errors, ROS levels, and early apoptosis in obese mice.

Recent research has shown that high-calorie diets can cause hyperphagia and promote obesity. Feeding obese mice with 2-fucosyllactose and anagliptin reduced both body weight and dietary intake (Kohno et al., 2020; Lee et al., 2020). We did observe increased body weights in mice fed a high-calorie diet, and reduced food consumption after PC gavage in obese mice, but PC administration did not reduce mouse body weight, illustrating that weight loss was not an effect of PC administration. The long-term intake of a high-fat diet can lead to an imbalance in energy metabolism and an increased burden associated with the pancreatic insulin secretion, resulting in abnormal glucose metabolism and an abnormal insulin response (Ye et al., 2018). We found that PC gavage reversed this abnormal glucose metabolism and abnormal insulin response in HFD mice. Although a detailed mechanism for this is still unclear, the reduction in food consumption after PC administration may be related to the improvements in glucose metabolism and insulin response.

In our study, reduced litter sizes and offspring survival rates were observed in obese mice. These results are consistent with a recent study that reported decreased litter survival in mice fed a high-fat diet (Smoothy et al., 2019). Our previous study found that PC gavage improved litter sizes and survival rates in D-gal-induced aging mice (Li et al., 2016). Here, similar results were obtained after PC administration in obese mice, indicating that PC can rescue reproductive disorders in HFD mice, shown by increased litter sizes and offspring viability.

Research has also found that obesity can cause a significant increase in the number of atretic follicles by triggering apoptosis in follicular cells (Wang et al., 2014). Our results show that the number of atretic follicles in HFD mice increased significantly,

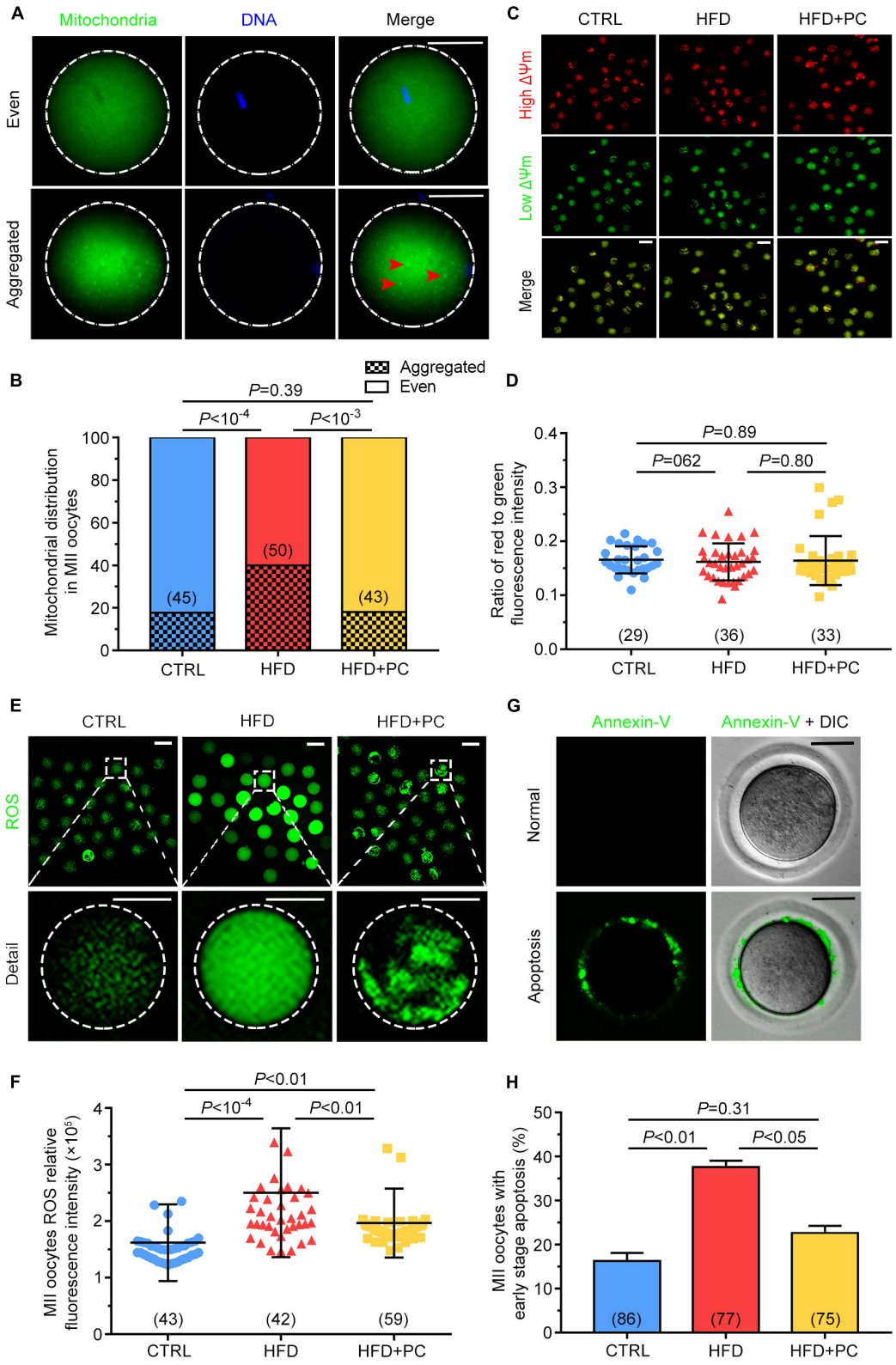

FIGURE 6 | PC restored the mitochondrial distribution in oocytes, and attenuated oxidative stress and early apoptosis in obese mice. **(A)** Representative images of mitochondria with *even* or *aggregated* distributions. Red arrows indicate aggregated mitochondria. Green, mitochondria; blue, DNA. The circular white frame

(Continued)

FIGURE 6 | Continued
indicates the oocyte edge. Scale bar = 20 μm. **(B)** Percentages of MII oocytes with altered mitochondrial distributions. **(C)** Representative images of mitochondrial membrane potentials. Red, high ΔΨm; Green, low ΔΨm. Scale bar = 100 μm. **(D)** Ratio of red to green fluorescence intensities from **(C)**. **(E)** Representative images of ROS generation determined by DCFH-DA fluorescence (green). Scale bar = 100 μm. The square white frame indicates the region shown in detail, and the circular white frame indicates the oocyte edge. **(F)** Quantification of ROS fluorescence intensities. **(G)** Representative images of early stage apoptosis in MII oocytes. No green fluorescence signals were observed in oocyte membranes, indicating no apoptosis **(upper panel)**. Oocytes undergoing early apoptosis were characterized by an unambiguous green membrane signal **(lower panel)**. Scale bar = 100 μm. **(H)** Percentages of oocytes undergoing early stage apoptosis. Data are expressed as mean ± SD and were compared by one-way ANOVA and Newman–Keuls *post hoc* tests. The number of oocytes assessed in each group is shown in parentheses.

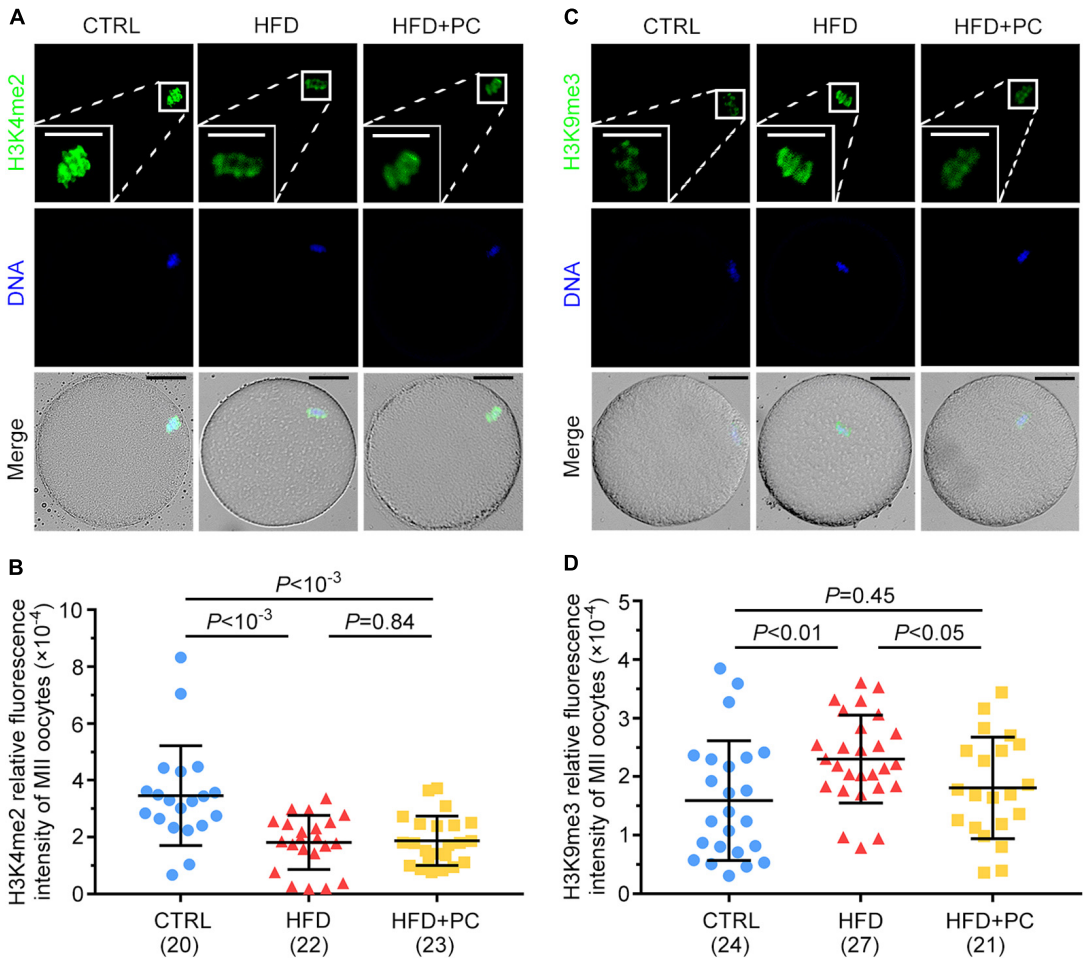

FIGURE 7 | PC reversed the abnormal expression of H3K9me3 in obese mice. **(A)** Representative images of H3K4me2 inside oocytes. Green, H3K4me2; blue, DNA. The square white frame indicates the region shown in detail. Scale bar = 20 μm. **(B)** Quantified fluorescence intensities for H3K4me2. **(C)** Representative images of H3K9me3 inside oocytes. Green, H3K9me3; blue, DNA. The square white frame indicates the region shown in detail. Scale bar = 20 μm. **(D)** Quantified fluorescence intensities for H3K9me3. Data are expressed as mean ± SD and were compared by one-way ANOVA and Newman–Keuls *post hoc* tests. The number of oocytes assessed in each group is shown in parentheses.

and their number was effectively reduced after intragastric administration of PC.

As obesity led to an increase in the number of atretic follicles, we wondered if this increase was induced by the abnormal expressions of the genes *BMP4*, *GDF9*, or *LHX8* that play key roles during ovarian follicular development (Fu et al., 2017; Liu et al., 2017; Stocker et al., 2020). Our results demonstrated that there were no significant differences in their mRNA expression levels among the three mice groups, suggesting that the increased number of atretic follicles was not caused by abnormal *BMP*, *GDF9*, and *LHX8* gene expression.

Follicular development also depends on the regulation and control of the pituitary-gonadal axis. The pituitary glands of female mice fed a HFD have been shown to secrete less endogenous hypothalamic gonadotropin releasing hormone (GnRH) (Sharma et al., 2013). As a GnRH-regulated hormone, serum FSH in the present HFD female mice increased significantly, and this increase was partially blocked after PC

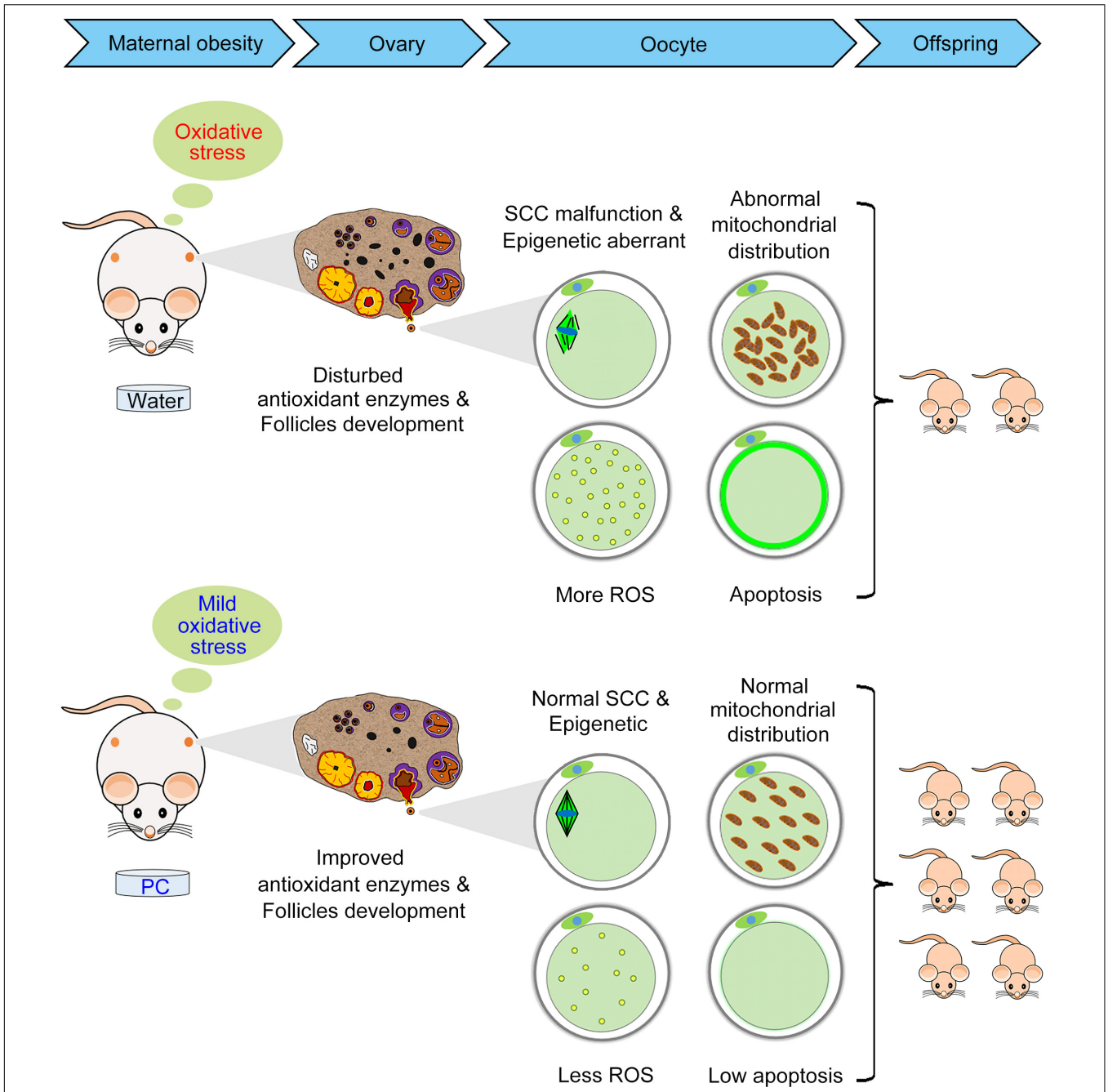

FIGURE 8 | Diagram illustrating the beneficial effects of PC that improved reproductive ability in obese female mice by alleviating oxidative stress-induced ovarian and oocyte damage. The intragastric administration of PC reduced the number of atretic follicles and improved antioxidant enzymes in obese female mice ovaries. The administration of PC also rescued oocyte meiosis defects, including aberrant epigenetic effects, abnormal mitochondrial distribution, ROS accumulation, and early apoptosis. Therefore, ovary/oocyte quality, and the fertility of obese female mice was improved after PC administration.

gavage. However, obesity did not cause any significant changes in serum E2 levels, consistent with the recent study of Li et al. (2020).

Functional ovarian damage in obese females has been associated with abnormal levels of antioxidant enzymes (Lim and Luderer, 2011), and the mammalian ovary possesses antioxidant defenses, including ROS-scavenging enzymes such as CAT, GSH-Px, and SOD (Sato et al., 1992; Hsieh et al., 1997). CAT catalyzes the decomposition of H_2O_2 into H_2O and O_2 to protect cells from H_2O_2 toxicity (Sun et al., 2013). GSH-Px can also reduce toxic peroxides to non-toxic hydroxyl compounds, protecting cells from oxidative damage (Alexa and Jerca, 1996). SOD is the most important free-radical scavenging substance to organisms (Ozata et al., 2002; Belviranli et al., 2018), and

MDA is a marker for lipid peroxidation (Belviranli et al., 2018). Consistent with our experimental results, obesity can significantly reduce the activities of GSH-Px and SOD in mice ovaries, but their activities did not change after intragastric administration of PC, indicating that the effect of PC on fertility was not due to changes in GSH-Px and SOD activities. Similarly, it has been reported that obesity can increase CAT activity in female mice (Kleniewska and Pawliczak, 2019), also consistent with our findings. Interestingly, the administration of PC in obese mice was able to reduce CAT activity, suggesting a possible reason for PC to improve the fertility of female mice by restoring CAT activity in the ovary.

Poor oocyte quality is one of the main reasons for subfertility in obese females. Characterized by cellular fragmentation and degeneration, a high proportion of poor-quality oocytes was observed in HFD mice. As a high level of ROS can induce oocyte apoptosis (Chaube et al., 2005), the ability of PC to minimize fragmentation and degeneration is probably due to its function of inhibiting ROS production. Moreover, the decrease in PB1 extrusions as well as changes in early embryo development in HFD mice could be partially reversed by PC administration, indicating its positive influence on both nuclear and cytoplasmic maturation. These data concur with previous reports (Serke et al., 2012; Nishio and Isobe, 2015; Han et al., 2018), where melatonin-induced inhibition of ROS promoted the developmental potential of early embryos in HFD mice.

Meiotic spindle assembly is essential for accurate chromosome alignment and subsequent oocyte maturation and fertilization (Sun and Schatten, 2006). Abnormalities of the SCC during meiosis can lead to aneuploidy, genetic diseases, and birth defects (Waizenegger et al., 2000; Hassold and Hunt, 2001). The integrity of the SCC in HFD mouse oocytes was disrupted and may have been responsible for the decreased maturation and embryo development potential. However, PC administration in HFD mice stabilized SCC integrity; an improvement in oocyte quality that likely increased offspring number and their survival rate.

Mitochondrial distribution in the cytoplasm plays an important role during oocyte maturation, fertilization, and early embryo development (Van Blerkom, 2011). However, obesity induces an abnormal distribution pattern for mitochondria in oocytes, and increases compensatory responses to oxidative stress, mitochondrial biogenesis, and mtDNA replication, which eventually leads to mitochondrial dysfunction (Grindler and Moley, 2013). Previous studies have reported that the distribution of mitochondria is cytoskeleton-dependent and depends on microtubule organization (Yamochi et al., 2016). Therefore, the disruption in the distribution of mitochondria is likely the result of cytoskeletal disorders in HFD mice (Islam et al., 2016). Although the mitochondrial membrane potential was not altered in HFD mice, PC administration may have improved oocyte mitochondrial distribution via its function of stabilizing SCC integrity in HFD mice.

Our previous study showed that PC improved the distribution of mitochondria by reducing oxidative stress (Li et al., 2016). Abnormal oxidative stress has a variety of detrimental effects on oocyte and embryo development (Agarwal et al., 2005; Snider and Wood, 2019). In particular, the redox state is important for proper assembly of meiotic structures during oocyte meiosis (Wang et al., 2018). Exposure of oocytes to ROS causes mitochondrial damage, prevents embryo development (Komatsu et al., 2014), and induces both oxidative stress and early apoptosis (Yen and Klionsky, 2008). Consistent with these findings, we observed elevated ROS levels in HFD mice, which resulted in oocyte fragmentation and fertilization failure. Therefore, excess ROS production may explain the poor quality of oocytes in obese mice. As an antioxidant, PC inhibited the production of ROS in HFD mice oocytes, and the decline in ROS level played a fundamental role in improving oocyte quality in HFD mice.

Histone methylation modifications play an indispensable role in regulating gene expression during embryo development. H3K9 methylation ensures appropriate gene activation via silencing of gene transcription (Becker et al., 2017). Embryonic development can be greatly improved by reducing the expression of H3K9me3 in mice oocytes (Zhu et al., 2014). Here, the elevated H3K9me3 level in MII oocytes from HFD mice may have disturbed parental genomic reprogramming, which in turn may have led to abnormal embryo development and fetus growth. Significantly, PC restored the elevated H3K9me3 levels in oocytes caused by obesity. H3K4me2 is another key regulator of early embryonic development and a marker for transcriptional activation (Dempsey and Cui, 2019), and obesity can affect the expression level of H3K4me2. However, intragastric administration of PC did not improve the level of H3K4me2 in obese mice.

In summary, we have shown for the first time that PC can maintain reproductive ability in obese mice induced by a HFD via its positive effects on the ovary, oocyte, and offspring births (**Figure 8**). Additional studies are needed to confirm the molecular mechanisms and related pathways by which PC improved ovary/oocyte quality and fertility in these obese female mice. These data have identified the beneficial effects of PC on fertility in obese females and opened a new area of research to treat human infertility.

DATA AVAILABILITY STATEMENT

The raw data supporting the conclusions of this article will be made available by the authors, without undue reservation.

ETHICS STATEMENT

The animal study was reviewed and approved by the National Research Council Guide for the Care and Use of Laboratory Animals and were approved by the Institutional Animal Care and Use Committee at the Inner Mongolia University (Approval number: SYXK 2014-0002).

AUTHOR CONTRIBUTIONS

C-GL and XW: conceived and designed the experiments and analyzed the data. XW, ZH, S-JL, XH, X-JZ, X-YW, and C-JZ: performed the experiments. XW, Y-ZM, and C-GL: wrote

the manuscript. All authors contributed to the article and approved the submitted version.

FUNDING AND ACKNOWLEDGMENTS

This work was supported by the NSF of China (31871508, 31960158, and 31671560 to C-GL; 31900596 to C-JZ); Major Projects of Natural Science Foundation of Inner Mongolia Autonomous Region (No. 2019ZD09 to C-GL); Key technology research plan project of Inner Mongolia Autonomous Region (2019GG103 to C-GL); Science and Technology Major Project of Inner Mongolia Autonomous Region of China to the State Key Laboratory of Reproductive Regulation and Breeding of Grassland Livestock (2020ZD0008 to C-GL). We thank Zhejiang Binmei Biotechnology Co., Ltd for providing phycocyanin.

REFERENCES

Agarwal, A., Gupta, S., and Sharma, R. (2005). Oxidative stress and its implications in female infertility - a clinician's perspective. *Reprod. Biomed. Online* 11, 641–650. doi: 10.1016/s1472-6483(10)61174-1

Alexa, I. D., and Jerca, L. (1996). [The role of oxidative stress in the etiology of pre-eclampsia: changes at the GSH and GSH-Px levels in normal pregnancy and pre-eclampsia]. *Rev. Med. Chir. Soc. Med. Nat. Iasi* 100, 131–135.

Balaban, R. S., Nemoto, S., and Finkel, T. (2005). Mitochondria, oxidants, and aging. *Cell* 120, 483–495. doi: 10.1016/j.cell.2005.02.001

Becker, J. S., Mccarthy, R. L., Sidoli, S., Donahue, G., Kaeding, K. E., He, Z., et al. (2017). Genomic and proteomic resolution of heterochromatin and its restriction of alternate fate genes. *Mol. Cell* 68, 1023.e15–1037.e15.

Belviranli, M., Okudan, N., and Karakuyu, N. (2018). The association between irisin levels, element distribution and oxidative stress markers in adolescent swimmers. *Horm. Mol. Biol. Clin. Investig.* 34:6.

Benedetti, S., Benvenuti, F., Pagliarani, S., Francogli, S., Scoglio, S., and Canestrari, F. (2004). Antioxidant properties of a novel phycocyanin extract from the blue-green alga Aphanizomenon flos-aquae. *Life Sci.* 75, 2353–2362. doi: 10.1016/j.lfs.2004.06.004

Catalano, P. M., and Ehrenberg, H. M. (2006). The short- and long-term implications of maternal obesity on the mother and her offspring. *BJOG* 113, 1126–1133. doi: 10.1111/j.1471-0528.2006.00989.x

Chaube, S. K., Prasad, P. V., Thakur, S. C., and Shrivastav, T. G. (2005). Hydrogen peroxide modulates meiotic cell cycle and induces morphological features characteristic of apoptosis in rat oocytes cultured in vitro. *Apoptosis* 10, 863–874. doi: 10.1007/s10495-005-0367-8

Darbre, P. D. (2017). Endocrine disruptors and obesity. *Curr. Obes. Rep.* 6, 18–27. doi: 10.1007/s13679-017-0240-4

Dempsey, J. L., and Cui, J. Y. (2019). Regulation of hepatic long noncoding RNAs by pregnane X receptor and constitutive androstane receptor agonists in mouse liver. *Drug Metab. Disposition* 47, 329–339. doi: 10.1124/dmd.118.085142

Fernández-Rojas, B., Medina-Campos, O. N., Hernández-Pando, R., Negrette-Guzmán, M., Huerta-Yepez, S., and Pedraza-Chaverri, J. (2014). C-phycocyanin prevents cisplatin-induced nephrotoxicity through inhibition of oxidative stress. *Food Funct.* 5, 480–490. doi: 10.1039/c3fo60501a

Fu, L., Koganti, P. P., Wang, J., Wang, L., Wang, C. L., and Yao, J. (2017). Lhx8 interacts with a novel germ cell-specific nuclear factor containing an Nbl1 domain in rainbow trout (*Oncorhynchus mykiss*). *PLoS One* 12:e0170760. doi: 10.1371/journal.pone.0170760

Garber, J. C., Wayne barbee, R., Bielitzki, J. T., Clayton, L. A., Donovan, J. C., Kohn, D. F., et al. (2011). *Guide for the Care and Use of Laboratory Animals*. Washington, DC: National Academies Press.

González-Grajales, L. A., Pieper, L., Mengel, S., and Staufenbiel, R. (2018). Evaluation of glucose dose on intravenous glucose tolerance test traits in Holstein-Friesian heifers. *J. Dairy Sci.* 101, 774–782. doi: 10.3168/jds.2017-13215

Grindler, N. M., and Moley, K. H. (2013). Maternal obesity, infertility and mitochondrial dysfunction: potential mechanisms emerging from mouse model systems. *Mol. Hum. Reprod.* 19, 486–494. doi: 10.1093/molehr/gat026

Gupta, M., Dwivedi, U. N., and Khandelwal, S. (2011). C-Phycocyanin: an effective protective agent against thymic atrophy by tributyltin. *Toxicol. Lett.* 204, 2–11. doi: 10.1016/j.toxlet.2011.03.029

Han, L., Ren, C., Li, L., Li, X., Ge, J., Wang, H., et al. (2018). Embryonic defects induced by maternal obesity in mice derive from Stella insufficiency in oocytes. *Nat. Genet.* 50, 432–442. doi: 10.1038/s41588-018-0055-6

Han, L., Wang, H., Li, L., Li, X., Ge, J., Reiter, R. J., et al. (2017). Melatonin protects against maternal obesity-associated oxidative stress and meiotic defects in oocytes via the SIRT3-SOD2-dependent pathway. *J. Pineal Res.* 63:e12431. doi: 10.1111/jpi.12431

Hao, S., Yan, Y., Li, S., Zhao, L., Zhang, C., Liu, L., et al. (2018). The in vitro anti-tumor activity of phycocyanin against non-small cell lung cancer cells. *Mar. Drugs* 16:178. doi: 10.3390/md16060178

Hassold, T., and Hunt, P. (2001). To err (meiotically) is human: the genesis of human aneuploidy. *Nat. Rev. Genet.* 2, 280–291. doi: 10.1038/35066065

Hotamisligil, G. S., Shargill, N. S., and Spiegelman, B. M. (1993). Adipose expression of tumor necrosis factor-alpha: direct role in obesity-linked insulin resistance. *Science* 259, 87–91. doi: 10.1126/science.7678183

Hsieh, C. H., Tsai, S. P., Yeh, H. I., Sheu, T. C., and Tam, M. F. (1997). Mass spectrometric analysis of rat ovary and testis cytosolic glutathione S-transferases (GSTs): identification of a novel class-alpha GST, rGSTA6*, in rat testis. *Biochem. J.* 323(Pt 2), 503–510. doi: 10.1042/bj3230503

Igosheva, N., Abramov, A. Y., Poston, L., Eckert, J. J., Fleming, T. P., Duchen, M. R., et al. (2010). Maternal diet-induced obesity alters mitochondrial activity and redox status in mouse oocytes and zygotes. *PLoS One* 5:e10074. doi: 10.1371/journal.pone.0010074

Islam, M. S., Kabir, A. M. R., Inoue, D., Sada, K., and Kakugo, A. (2016). Enhanced dynamic instability of microtubules in a ROS free inert environment. *Biophys. Chem.* 211, 1–8. doi: 10.1016/j.bpc.2015.11.003

Janda, J., Nfonsam, V., Calienes, F., Sligh, J. E., and Jandova, J. (2016). Modulation of ROS levels in fibroblasts by altering mitochondria regulates the process of wound healing. *Arch. Dermatol. Res.* 308, 239–248. doi: 10.1007/s00403-016-1628-9

Jia, Z., Feng, Z., Wang, L., Li, H., Wang, H., Xu, D., et al. (2018). Resveratrol reverses the adverse effects of a diet-induced obese murine model on oocyte quality and zona pellucida softening. *Food Funct.* 9, 2623–2633. doi: 10.1039/c8fo00149a

Jungheim, E. S., and Moley, K. H. (2010). Current knowledge of obesity's effects in the pre- and periconceptional periods and avenues for future research. *Am. J. Obstetr. Gynecol.* 203, 525–530. doi: 10.1016/j.ajog.2010.06.043

Jungheim, E. S., Schoeller, E. L., Marquard, K. L., Louden, E. D., Schaffer, J. E., and Moley, K. H. (2010). Diet-induced obesity model: abnormal oocytes and persistent growth abnormalities in the offspring. *Endocrinology* 151, 4039–4046. doi: 10.1210/en.2010-0098

Kleniewska, P., and Pawliczak, R. (2019). The influence of apocynin, lipoic acid and probiotics on antioxidant enzyme levels in the pulmonary tissues of obese asthmatic mice. *Life Sci.* 234:116780. doi: 10.1016/j.lfs.2019.116780

Kohno, D., Furusawa, K., and Kitamura, T. (2020). Anagliptin suppresses diet-induced obesity through enhancing leptin sensitivity and ameliorating hyperphagia in high-fat high-sucrose diet fed mice. *Endocr. J.* 67, 523–529. doi: 10.1507/endocrj.ej19-0389

Komatsu, K., Iwase, A., Mawatari, M., Wang, J., Yamashita, M., and Kikkawa, F. (2014). Mitochondrial membrane potential in 2-cell stage embryos correlates with the success of preimplantation development. *Reproduction* 147, 627–638. doi: 10.1530/rep-13-0288

Lee, S., Goodson, M., Vang, W., Kalanetra, K., Barile, D., and Raybould, H. (2020). 2'-fucosyllactose supplementation improves gut-brain signaling and diet-induced obese phenotype and changes the gut microbiota in high fat-fed mice. *Nutrients* 12:1003. doi: 10.3390/nu12041003

Li, B., Chu, X.-M., Xu, Y.-J., Yang, F., Lv, C.-Y., and Nie, S.-M. (2013). CD59 underlines the antiatherosclerotic effects of C-phycocyanin on mice. *BioMed. Res. Int.* 2013:729413.

Li, Y.-J., Han, Z., Ge, L., Zhou, C.-J., Zhao, Y.-F., Wang, D.-H., et al. (2016). C-phycocyanin protects against low fertility by inhibiting reactive oxygen species in aging mice. *Oncotarget* 7, 17393–17409. doi: 10.18632/oncotarget.8165

Lim, J., and Luderer, U. (2011). Oxidative damage increases and antioxidant gene expression decreases with aging in the mouse ovary. *Biol. Reprod.* 84, 775–782. doi: 10.1095/biolreprod.110.088583

Liu, G.-Y., Sun, Y.-Z., Zhou, N., Du, X.-M., Yang, J., and Guo, S.-J. (2016). 3,3'-OH curcumin causes apoptosis in HepG2 cells through ROS-mediated pathway. *Eur. J. Med. Chem.* 112, 157–163. doi: 10.1016/j.ejmech.2016.02.019

Liu, X., Li, F., Xie, J., Huang, D., and Xie, M. (2020). Fetal and neonatal genistein exposure aggravates to interfere with ovarian follicle development of obese female mice induced by high-fat diet. *Food Chem. Toxicol.* 135:110982. doi: 10.1016/j.fct.2019.110982

Liu, Y., Du, S. Y., Ding, M., Dou, X., Zhang, F. F., Wu, Z. Y., et al. (2017). The BMP4-Smad signaling pathway regulates hyperandrogenism development in a female mouse model. *J. Biol. Chem.* 292, 11740–11750. doi: 10.1074/jbc.m117.781369

Luzzo, K. M., Wang, Q., Purcell, S. H., Chi, M., Jimenez, P. T., Grindler, N., et al. (2012). High fat diet induced developmental defects in the mouse: oocyte meiotic aneuploidy and fetal growth retardation/brain defects. *PLoS One* 7:e49217. doi: 10.1371/journal.pone.0049217

Machtinger, R., Combelles, C. M. H., Missmer, S. A., Correia, K. F., Fox, J. H., and Racowsky, C. (2012). The association between severe obesity and characteristics of failed fertilized oocytes. *Hum. Reprod.* 27, 3198–3207. doi: 10.1093/humrep/des308

Nishio, N., and Isobe, K.-I. (2015). GADD34-deficient mice develop obesity, nonalcoholic fatty liver disease, hepatic carcinoma and insulin resistance. *Sci. Rep.* 5, 13519–13519.

Ozata, M., Mergen, M., Oktenli, C., Aydin, A., Sanisoglu, S. Y., Bolu, E., et al. (2002). Increased oxidative stress and hypozincemia in male obesity. *Clin. Biochem.* 35, 627–631. doi: 10.1016/s0009-9120(02)00363-6

Reynolds, K. A., Boudoures, A. L., Chi, M. M. Y., Wang, Q., and Moley, K. H. (2015). Adverse effects of obesity and/or high-fat diet on oocyte quality and metabolism are not reversible with resumption of regular diet in mice. *Reprod. Fertil. Dev.* 27, 716–724. doi: 10.1071/rd14251

Rogero, M. M., and Calder, P. C. (2018). Obesity, inflammation, toll-like receptor 4 and fatty acids. *Nutrients* 10:432. doi: 10.3390/nu10040432

Romay, C., González, R., Ledón, N., Remirez, D., and Rimbau, V. (2003). C-phycocyanin: a biliprotein with antioxidant, anti-inflammatory and neuroprotective effects. *Curr. Protein Peptide Sci.* 4, 207–216. doi: 10.2174/1389203033487216

Saben, J. L., Boudoures, A. L., Asghar, Z., Thompson, A., Drury, A., Zhang, W., et al. (2016). Maternal metabolic syndrome programs mitochondrial dysfunction via germline changes across three generations. *Cell Rep.* 16, 1–8. doi: 10.1016/j.celrep.2016.05.065

Sato, E. F., Kobuchi, H., Edashige, K., Takahashi, M., Yoshioka, T., Utsumi, K., et al. (1992). Dynamic aspects of ovarian superoxide dismutase isozymes during the ovulatory process in the rat. *FEBS Lett.* 303, 121–125. doi: 10.1016/0014-5793(92)80502-8

Serke, H., Nowicki, M., Kosacka, J., Schröder, T., Klöting, N., Blüher, M., et al. (2012). Leptin-deficient (ob/ob) mouse ovaries show fatty degeneration, enhanced apoptosis and decreased expression of steroidogenic acute regulatory enzyme. *Int. J. Obes.* 36, 1047–1053. doi: 10.1038/ijo.2011.220

Sharma, S., Morinaga, H., Hwang, V., Fan, W., Fernandez, M. O., Varki, N., et al. (2013). Free fatty acids induce Lhb mRNA but suppress Fshb mRNA in pituitary LβT2 gonadotropes and diet-induced obesity reduces FSH levels in male mice and disrupts the proestrous LH/FSH surge in female mice. *Endocrinology* 154, 2188–2199. doi: 10.1210/en.2012-2218

Silvestris, E., De Pergola, G., Rosania, R., and Loverro, G. (2018). Obesity as disruptor of the female fertility. *Reprod. Biol. Endocrinol.* 16:22.

Smoothy, J., Larcombe, A. N., Chivers, E. K., Matthews, V. B., and Gorman, S. (2019). Maternal high fat diet compromises survival and modulates lung development of offspring, and impairs lung function of dams (female mice). *Respir. Res.* 20:21.

Snider, A. P., and Wood, J. R. (2019). Obesity induces ovarian inflammation and reduces oocyte quality. *Reproduction* 158, R79–R90.

Sohrabi, M., Roushandeh, A. M., Alizadeh, Z., Vahidinia, A., Vahabian, M., and Hosseini, M. (2015). Effect of a high fat diet on ovary morphology, in vitro development, in vitro fertilisation rate and oocyte quality in mice. *Singapore Med. J.* 56, 573–579. doi: 10.11622/smedj.2015085

Stocker, W. A., Walton, K. L., Richani, D., Chan, K. L., Beilby, K. H., Finger, B. J., et al. (2020). A variant of human growth differentiation factor-9 that improves oocyte developmental competence. *J. Biol. Chem.* 295, 7981–7991. doi: 10.1074/jbc.ra120.013050

Sun, G., Wang, Y., Hu, W., and Li, C. (2013). Effects of manganese superoxide dismutase (MnSOD) expression on regulation of esophageal cancer cell growth and apoptosis in vitro and in nude mice. *Tumour Biol.* 34, 1409–1419. doi: 10.1007/s13277-012-0622-x

Sun, Q.-Y., and Schatten, H. (2006). Regulation of dynamic events by microfilaments during oocyte maturation and fertilization. *Reproduction* 131, 193–205. doi: 10.1530/rep.1.00847

Van Blerkom, J. (2011). Mitochondrial function in the human oocyte and embryo and their role in developmental competence. *Mitochondrion* 11, 797–813. doi: 10.1016/j.mito.2010.09.012

Waizenegger, I. C., Hauf, S., Meinke, A., and Peters, J. M. (2000). Two distinct pathways remove mammalian cohesin from chromosome arms in prophase and from centromeres in anaphase. *Cell* 103, 399–410. doi: 10.1016/s0092-8674(00)00132-x

Wang, H., Cheng, Q., Li, X., Hu, F., Han, L., Zhang, H., et al. (2018). Loss of TIGAR induces oxidative stress and meiotic defects in oocytes from obese mice. *Mol. Cell. Proteomics* 17, 1354–1364. doi: 10.1074/mcp.ra118.000620

Wang, N., Luo, L. L., Xu, J. J., Xu, M. Y., Zhang, X. M., Zhou, X. L., et al. (2014). Obesity accelerates ovarian follicle development and follicle loss in rats. *Metabolism* 63, 94–103. doi: 10.1016/j.metabol.2013.09.001

Yamochi, T., Hashimoto, S., Amo, A., Goto, H., Yamanaka, M., Inoue, M., et al. (2016). Mitochondrial dynamics and their intracellular traffic in porcine oocytes. *Zygote* 24, 517–528. doi: 10.1017/s0967199415000489

Yancey, D. M., Guichard, J. L., Ahmed, M. I., Zhou, L., Murphy, M. P., Johnson, M. S., et al. (2015). Cardiomyocyte mitochondrial oxidative stress and cytoskeletal breakdown in the heart with a primary volume overload. American journal of physiology. *Heart Circ. Physiol.* 308, H651–H663.

Ye, T., Chen, Y. H., Gao, J. H., Wang, X. X., Qiang, O., Tang, C. W., et al. (2018). Effect of octreotide on pancreatic fibrosis in rats with high-fat diet-induced obesity. *Int. J. Clin. Exp. Pathol.* 11, 4784–4794.

Yen, W.-L., and Klionsky, D. J. (2008). How to live long and prosper: autophagy, mitochondria, and aging. *Physiology* 23, 248–262. doi: 10.1152/physiol.00013.2008

Yu, W., Zhang, X., Liu, J., Wang, X., Li, S., Liu, R., et al. (2016). Cyclosporine a suppressed glucose oxidase induced P53 mitochondrial translocation and hepatic cell apoptosis through blocking mitochondrial permeability transition. *Int. J. Biol. Sci.* 12, 198–209. doi: 10.7150/ijbs.13716

Zhang, L., Han, L., Ma, R., Hou, X., Yu, Y., Sun, S., et al. (2015). Sirt3 prevents maternal obesity-associated oxidative stress and meiotic defects in mouse oocytes. *Cell Cycle* 14, 2959–2968. doi: 10.1080/15384101.2015.1026517

Zhou, C. J., Wu, S. N., Shen, J. P., Wang, D. H., Kong, X. W., Lu, A., et al. (2016). The beneficial effects of cumulus cells and oocyte-cumulus cell gap junctions depends on oocyte maturation and fertilization methods in mice. *PeerJ* 4:e1761. doi: 10.7717/peerj.1761

Zhu, C.-C., Hou, Y.-J., Han, J., Liu, H.-L., Cui, X.-S., Kim, N.-H., et al. (2014). Effect of mycotoxin-containing diets on epigenetic modifications of mouse oocytes by fluorescence microscopy analysis. *Microsc. Microanal.* 20, 1158–1166. doi: 10.1017/s1431927614000919

Conflict of Interest: The authors declare that the research was conducted in the absence of any commercial or financial relationships that could be construed as a potential conflict of interest.

Copyright © 2020 Wen, Han, Liu, Hao, Zhang, Wang, Zhou, Ma and Liang. This is an open-access article distributed under the terms of the Creative Commons Attribution License (CC BY). The use, distribution or reproduction in other forums is permitted, provided the original author(s) and the copyright owner(s) are credited and that the original publication in this journal is cited, in accordance with accepted academic practice. No use, distribution or reproduction is permitted which does not comply with these terms.

frontiers in Cell and Developmental Biology

ORIGINAL RESEARCH
published: 11 February 2021
doi: 10.3389/fcell.2021.642010

Increased Environment-Related Metabolism and Genetic Expression in the *In Vitro* Matured Mouse Oocytes by Transcriptome Analysis

*Hao-Lin Zhang, Yi Xu, Jia-Qian Ju, Zhen-Nan Pan, Jing-Cai Liu and Shao-Chen Sun**

College of Animal Science and Technology, Nanjing Agricultural University, Nanjing, China

Infertility in humans at their reproductive age is a world-wide problem. Oocyte *in vitro* maturation (IVM) is generally used in such cases to acquire the embryo in assisted reproductive technology (ART). However, the differences between an *in vivo* (IVO) and IVM culture environment in the RNA expression profile in oocytes, remains unclear. In this study, we compared the global RNA transcription pattern of oocytes from *in vitro* and *in vivo* maturation. Our results showed that 1,864 genes differentially expressed between the IVO and IVM oocytes. Among these, 1,638 genes were up-regulated, and 226 genes were down-regulated, and these changes were mainly divided into environmental adaption, metabolism, and genetic expression. Our detailed analysis showed that the expression of genes that belonged to metabolism-related processes such as energy metabolism, nucleotide metabolism, and carbohydrate metabolism was changed; and these genes also belonged to organismal systems including environmental adaptation and the circulatory system; moreover, we also found that the relative gene expression of genetic expression processes, such as protein synthesis, modification, and DNA replication and repair were also altered. In conclusion, our data suggests that *in vitro* maturation of mouse oocyte resulted in metabolism and genetic expression changes due to environmental changes compared with *in vivo* matured oocytes.

Keywords: meiosis, oocyte, *in vitro* maturation, gene expression, transcriptome analysis

OPEN ACCESS

Edited by:
Wei Li,
Chinese Academy of Sciences (CAS), China

Reviewed by:
Xingwei Liang,
Guangxi University, China
Shen Yin,
Qingdao Agricultural University, China

****Correspondence:***
Shao-Chen Sun
sunsc@njau.edu.cn

Specialty section:
This article was submitted to Cell Growth and Division, a section of the journal Frontiers in Cell and Developmental Biology

Received: *15 December 2020*
Accepted: *18 January 2021*
Published: *11 February 2021*

Citation:
Zhang H-L, Xu Y, Ju J-Q, Pan Z-N, Liu J-C and Sun S-C (2021) Increased Environment-Related Metabolism and Genetic Expression in the In Vitro Matured Mouse Oocytes by Transcriptome Analysis. Front. Cell Dev. Biol. 9:642010. doi: 10.3389/fcell.2021.642010

INTRODUCTION

Oocyte meiotic maturation is an important process of oocyte quality control. This process is initiated during the germinal vesicle (GV) stage, and the oocyte undergoes germinal vesicle breakdown (GVBD) and metaphase I, and then is arrested at metaphase II until fertilization (Greenstein, 2005). Most basic research for oocyte maturation is based on the *in vitro* maturation (IVM) approach (Coticchio, 2016). For human reproduction, due to the high infertility rates worldwide, *in vitro* maturation is also widely applied in clinics of reproductive medicine centers (Cha and Chian, 1998). Since the first successful treatment with conventional *in vitro* maturation (IVM), assisted reproductive technology (ART) has become an integral part of modern medicine (De Geyter, 2019), and immature oocytes *in vitro* maturation (IVM) is currently one of the most advanced ART technologies (Zhao et al., 2020). IVM is an effective treatment that has yielded significant results with significant pregnancy and implantation rates (Son et al., 2019). To date,

thousands of babies have been born using the IVM procedure, and a few clinical follow-up studies have shown no significant abnormalities in these babies compared with those conceived using conventional IVM treatment (Chian et al., 2014; Yang and Chian, 2017).

In spite of this, owing to culturing with a nutrient solution, the process of IVM has long been suspected of introducing unexpected modifications that may or may not adversely affect oocytes, which may subsequently manifest in embryonic development (Ye et al., 2020). The commercialized nutrient solution can not completely simulate the internal environment, which means that *in vitro* maturation or development may have a number of differences compared to IVO. It has been shown that the *in vitro* matured oocytes present distinct expression patterns which reflect the oocyte response to its surrounding environment (Katz-Jaffe et al., 2009). In porcine oocytes, *in vitro* maturation influences oocyte morphogenesis, which may also be recognized as significant mediators of cellular maturation capacity in pigs (Budna et al., 2017). A previous study illuminates the compensatory mechanism from a metabolic perspective during human oocyte maturation (Zhao et al., 2019). In addition, there are several differences in the modification of genes between culturing oocytes *in vitro* or *in vivo*. In a small-scale study of human IVM oocytes, one quarter is found to have an altered methylation pattern of the H19 differentially methylated region, which is normally unmethylated in *in vivo* matured oocytes (Borghol et al., 2006). Until now, whether culture conditions induce epigenetic alterations to deregulate gene expression remains contentious (Lu et al., 2018). The difference of the RNA transcriptome expression profile in mouse oocytes during maturation *in vivo* and *in vitro* remains unclear.

In cells, adaptive thermogenesis is a catabolic process that consumes energy-storing molecules and converts the energy into heat in response to environmental changes (Lynes et al., 2019). For example, Atp5e is involved in the biogenesis of ATP synthase, and knockdown of Atp5e produces an insufficient ATP phosphorylating capacity (Havlickova et al., 2010). Numerous supernumerary subunits of mitochondrial respiratory chain complex I (CI), Ndufb11, and Ndufa7, have been found to be targets of phosphorylation by cAMP-dependent protein kinase (mtPKA) and are thus likely to play a part in the regulation of CI activity and biogenesis (Rak and Rustin, 2014). These biological processes are all important for cells to adapt to the environment.

Thermogenesis is regulated by glucose metabolism, while it is has been shown that glucose metabolism is critical for determining oocyte developmental competence (Sutton-McDowall et al., 2010). The performance of the cell culture processes, in terms of both productivity and quality, is significantly influenced by cellular metabolism (Yuan et al., 2013; Rak and Rustin, 2014). Metabolic pathways contain multiple processes, such as glycolysis, fatty acid oxidation, glutamine metabolism (Rohlenova et al., 2018). In these processes, Ndufv3 as an accessory subunit of mitochondrial complex I participates in oxidative phosphorylation (Guerrero-Castillo et al., 2017). In addition, a previous study demonstrated that Cox7b was indispensable for cytochrome C oxidase (COX) assembly, COX activity, and mitochondrial respiration (Indrieri et al., 2012). Umps (uridine monophosphate synthase) was associated with pyrimidine metabolism, while the deficiency of Umps could cause orotic aciduria (OA) (Wortmann et al., 2017). Moreover, Ldhb (Lactate Dehydrogenase B) is involved in pyruvate metabolism by converting lactate to pyruvate (Urbanska and Orzechowski, 2019). These above-mentioned processes are vital components of metabolism.

Metabolism plays an important role in regulating gene expression, protein translation, and protein modification. The genetic expression of a cell, which includes DNA replication and repair, protein synthesis and modification, and other processes, is the kernel of cellular development. Several genes have been shown to be involved in genetic expression processing. 60S ribosomal protein L35 (RPL35) is an important part of the 60S ribosomal subunit, which has a role in protein translation and endoplasmic reticulum (ER) docking (Jiang et al., 2015). A study also found that the loss of zebrafish ns or gnl2 has a major impact on 60S large ribosomal subunit formation and/or function due to cleavage impairments at distinct sites of the pre-rRNA transcript (Essers et al., 2014). The Polymerase delta (POLD1) gene participates in providing the essential catalytic activities of polymerase δ (Polδ), which is essential for replication (Nicolas et al., 2016).

Here we investigated the transcriptome characteristics of mouse oocytes matured *in vitro* to gain a transcriptome-level understanding of the differences between mouse IVM and IVO matured oocytes. We used RNA-seq to screen differentially expressed genes through KEGG, GO, and other analytical methods. We showed that *in vitro* matured oocytes had a different mRNA expression profile from an environmental change response, cellular metabolism, and genetic expression aspect.

MATERIALS AND METHODS

Oocyte Collection and Culture

All procedures with mice were conducted according to the guidelines issued by the Animal Research Institute Committee of Nanjing Agriculture University, China. All the mice used in the experiment were purchased from Qinglongshan Animal Farm in Nanjing. This committee approved the experimental protocols. *In vitro* oocytes were collected from 6- to 8-week-old ICR mice and cultured in M2 medium under paraffin oil at 37°C in an atmosphere containing 5% CO^2. *In vivo* oocytes were collected from the tubal ampulla of 6- to 8-week-old ICR mice. And then each group of oocytes were preserved in lysis buffers provided by Geekgeen in Beijing. Each tube of lysis buffer consists of 350 μL A and 3.5 μL B, abiding by the principle of diluting it when it is used.

Abbreviations: IVM, *In vitro* maturation; IVO, *In vivo* maturation; ART, Assisted reproductive technology; GV, Germinal vesicle; GVBD, Germinal vesicle breakdown; MI, Metaphase I; MII, Metaphase II; DEGs, differentially expressed genes; GO, Gene Ontology; MV, Mitochondria-vesicles; M-SER, Mitochondria-smooth endoplasmic reticulum; DOs, cumulus-denuded oocytes.

RNA-seq Analysis (Transcriptome Sequencing)

Transcriptome sequencing was performed on the IVO group and the IVM group mouse oocytes. We collected 80 oocytes for each group for disposing using Beijing Geek Gene Technology Co. Ltd. The total RNA was first extracted using the RNeasy Micro Kit (QIAGEN, 74004, Quigen, Toronto, Canada) and then quantified by the Qubit RNA Assay Kit T (Invitrogen, Eugene, OR, USA). The protocol was constituted by sequential RNA fragmentation, reverse transcription using random primers, second strand cDNA synthesis, end repair, dA-tailing, adapter ligation, and PCR enrichment. The concentration and quality of libraries were measured by a NanoDrop 2000 spectrophotometer (Thermo Scientific, Wilmington, DE, USA), Q-PCR, and Agilent 2100 Bioanalyzer (Agilent Technologies, Palo Alto, CA, USA). A 150bp anti-terminal sequence was then performed on the library. Filtering out low quality sequences and joint sequences, the Clean Reads were analyzed. Hierarchical clustering was carried out at the gene level, and the data of all sample genes were calculated according to the $\log_2$(FPKM+1). The desired genes were selected and compared to determine the changes in the expression levels of the relevant genes. RNA library sequencing was performed on the Illumina HiseqTM 2500/4000 by Gene Denovo Biotechnology Co., Ltd (Guangzhou, China).

RNA Isolation and Quantitative Real-Time PCR

Mouse oocytes maturated *in vitro* cultured for 12 h, and *in vivo* matured oocytes were obtained from ampullar potion. The oocytes in the IVO group and the IVM group were collected. Total RNA was extracted from exactly 30 oocytes with a Dynabead mRNA DIRECT kit (Invitrogen Dynal, Oslo, Norway). According to the manufacturer's instructions (Invitrogen), the first strand was synthesized with a cDNA synthesis kit (Takara) by Oligo (dT) 12–18 primers. The cDNA was stored at −20°C until analysis. The levels of relevant mRNAs were determined by quantitative RT-PCR using a FastStart Universal SYBR Green Master (Rox; Roche Applied Science, Mannheim, Germany) with One plus Real-Time PCR System (Applied Biosystems, Life Technologies, Carlsbad, CA, USA). Gene expression levels were analyzed using the 2–ΔΔCt method after the melting-curve analysis was completed. The expression levels of the target genes were then normalized to the expression level of GAPDH in each sample. The primers are listed in **Supplementary Table 1**.

Statistical Analysis

For each treatment, at least three valid replicates were tested, and the results are reported as mean ± SEM. Statistical comparisons were made by independent-sample *t*-tests using GraphPad Prism 5 statistical software. Results were considered significant at $P < 0.05$. Bioinformatic analysis was performed using Omicsmart, a real-time interactive online platform for data analysis (http://www.omicsmart.com).

RESULTS

Global Transcriptomes Characteristics Between Mouse IVM and IVO Oocytes

We used a transcriptome analysis to identify the different expression levels of mRNA between IVO and IVM oocytes and the Pearson correlation coefficient between each of the two samples was calculated. As shown in **Figure 1A**, the heatmap indicated that the intraclass samples had a high level of repeatability. We then counted the overlapping genes in the IVO group and IVM group, and we found that there are 7,460 genes detected in both groups (**Figure 1B**). Samples from the IVM and IVO groups were further distinguished by supervised hierarchical clustering (**Figure 1C**). Subsequently, 1,864 differentially expressed genes (DEGs) were screened out by $\log_2$(Fold Change) ≥2.0, among which 1,638 genes were highly expressed in the IVM group and 226 genes were highly expressed in the IVO group (**Figure 1D**) This is also shown by the data analysis of the volcano plot (**Figure 1E**). Therefore, we show that IVM oocytes have significantly differentially expressed genes compared with IVO oocytes.

GO and KEGG Analysis of DEGs for Mouse IVM and IVO Oocytes

We then used Gene Ontology (GO) and KEGG analysis to further sift the significantly DEGs between the IVO and IVM groups. As shown in **Figure 2A**, the top 20 GO terms, classified by –$\log_{10}$(Q value), were significantly enriched in DEGs compared to the genome background Gene Ontology which is an international standardized gene functional classification system. It has three ontologies including the biological process (BP), molecular function (MF), and the cellular component (CC). In terms of the biological process, cellular process, and metabolic process, the biological regulation and regulation of the biological process were shown to be interfered; for the molecular function, binding and catalytic activity showed a significantly close relationship; for the cellular component, cell, cell part, organelle and organelle part were revealed with salient differences (**Figure 2B**). Furthermore, the KEGG enrichment analysis displayed the classification of the top 20 pathways which revealed that these differentially expressed genes were mainly concentrated in four KEGG A classes including metabolism, genetic information processing, organismal systems, and human diseases, which are sorted by pathway type (**Figure 2C**). Among these pathways, five pathways including oxidative phosphorylation, pyrimidine metabolism, pyruvate metabolism, purine metabolism, and the citrate cycle were related to metabolism; seven pathways including ribosome, protein processing in ER, Fanconi anemia pathway, proteasome, homologous recombination, nucleotide excision repair, and ribosome biogenesis in eukaryotes were involved in genetic expression; three pathways including thermogenesis, cardiac muscle contraction, and vasopressin-related water reabsorption were related to organismal systems; and four pathways covering Parkinson disease, Huntington disease, Alzheimer disease and Non-alcoholic fatty liver disease affected human diseases. A detailed graph shows that these genes were related with the first 14 pathways (**Figure 2D**).

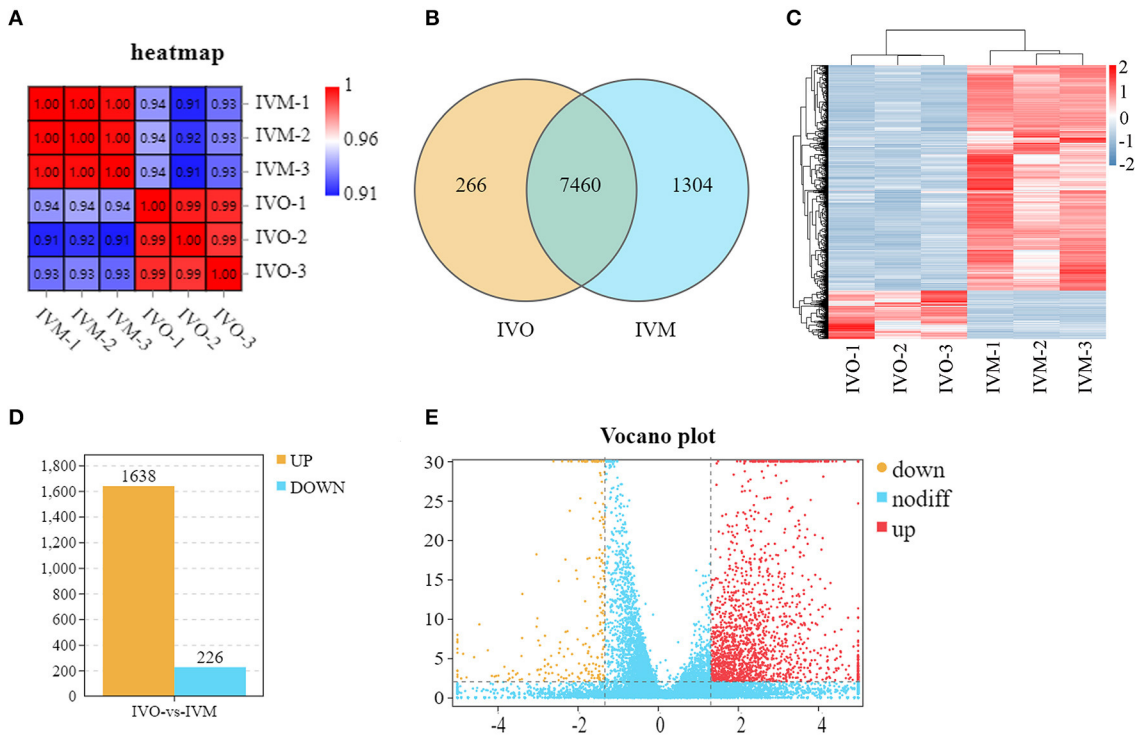

FIGURE 1 | Global transcriptomes characteristics between mouse IVM and IVO oocytes. **(A)** Correlation heatmap showing the repeatability between repetitive samples and the difference between groups. **(B)** Venn diagram showing the number of DEGs in common among the two samples. **(C)** Mouse IVM and IVO oocytes can be clearly distinguished based on their transcriptome characteristics. The color key (from blue to red) of Z-score value (−2–2) indicated low to high expression levels. **(D)** The statistical analysis of differentially expressed genes between IVO and IVM oocytes. **(E)** The volcano analysis of differentially expressed genes with color-coded. The gene with $Q < 0.01$ and FC > 2.5 is marked in red; the gene with $Q < 0.01$ and FC < −2.5 is marked in yellow; the gene with $Q > 0.01$ and −2.5 < FC < 2.5 is marked in blue.

Increased Metabolic Pathways in IVM Oocytes Compared With IVO Oocytes

It has been shown that glucose concentration in the *in vitro* culture environment could affect oocyte metabolic pathways (Sutton-McDowall et al., 2010). In the KEGG column diagram, we also found that the pathways related to metabolism, like energy metabolism, nucleotide metabolism and carbohydrate metabolism fluctuated. We first analyzed the oxidative phosphorylation-related genes, and the results showed that more than 45 genes were up-regulated in the IVM oocytes compared with IVO oocytes (**Figure 3A**). To further verify this, we examined these gene expressions through quantitative real-time PCR, and the results showed that the genes, Ndufv3, Ndufa5, Ndufa12, etc., were all increased compared with IVO oocytes (**Figure 3B**). Moreover, we also found that the pyrimidine-related genes, such as Upp1, Umps, Polr2l, which were related with nucleotide metabolism, also showed different expressions compared with IVO oocytes (**Figure 3C**), and this was also confirmed by the quantitative real-time PCR results (**Figure 3D**). Likewise, the expression of more than 16 carbohydrate metabolism-related genes were altered, and several prominent genes, including Pcx, Ldhb, Ldhc, Aldh2, and Aldh7a1 showed increased expression (**Figure 3C**). We also performed the mRNA expression validation, and the result was consistent with the analysis above (**Figure 3D**). Therefore, our results showed that *in vitro* maturation could give rise to increased expression of metabolic pathways.

From the KEGG analysis results above we found that several pathways related to environmental adaptation, the circulatory and excretory system were altered. While adaptive thermogenesis converts the energy into heat in response to environmental changes (Lynes et al., 2019), we then further analyzed the thermogenesis-related genes, and the results showed that more than 19 genes in the IVM oocytes showed a difference compared with IVO oocytes (**Supplementary Figure 1A**). To further confirm this, we examined the mRNA expression level of these genes, and the results showed that the genes, Atp5e, Cox6a1, Cox7b, etc., were all increased compared with IVO oocytes (**Supplementary Figure 1B**). Moreover, we also found that the cardiac muscle contraction-related genes, such as Cox6a1, Cox6b1, Cacnb3, Cox7b, Cox7c, which are related with the circulatory system also showed differences (**Supplementary Figure 1C**), and this was also confirmed by the quantitative real-time PCR results (**Supplementary Figure 1D**). The altered genes indicated that the oocyte capacity related to environmental adaption was activated during *in vitro* maturation compared with *in vivo* maturation.

FIGURE 2 | GO and KEGG analysis of DEGs for mouse IVM and IVO oocytes. **(A)** GO summary graph showing the summary of the top 20 enriched GO items. Different colors represent different GO categories. **(B)** The main biological process, cellular component, and molecular function of DEGs between mouse IVM and IVO oocytes. It shows the number of up- and down-regulated genes gathering in different classifications. **(C)** The KEGG analysis of DEGs based on classification by pathways. Each column represents a pathway, and the height of the column represents the number of genes that pathway contains. Legends indicate the pathway represented by different column colors. **(D)** The rich factors by the KEGG enrichment analysis for the differentially expressed genes of IVM treatment.

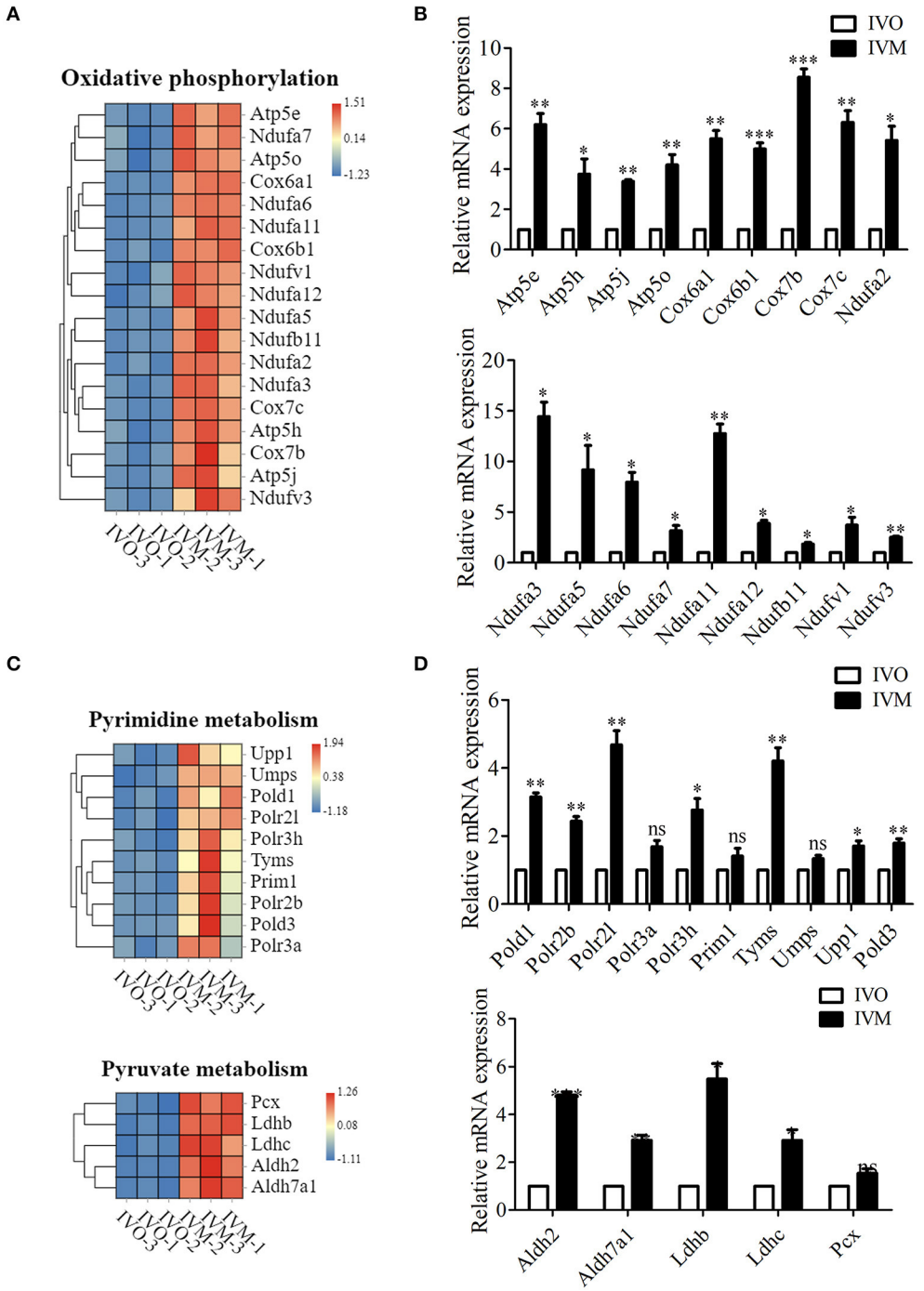

FIGURE 3 | Increased metabolic pathways in IVM oocytes compared with IVO oocytes. **(A)** The heat map for the gene expression level of oxidative phosphorylation pathway. **(B)** Relative mRNA expression levels of genes involved in oxidative phosphorylation in both IVM and IVO oocytes. *$p < 0.05$; **$p < 0.01$; ***$p < 0.001$. **(C)** The heat map for the gene expression level of pyrimidine metabolism and pyruvate metabolism pathways. **(D)** Relative mRNA expression levels of genes regulated the pyrimidine metabolism and pyruvate metabolism pathways in IVM and IVO oocytes. *$p < 0.05$; **$p < 0.01$; ***$p < 0.001$.

Increased Genetic Information Processing in IVM Oocytes Compared With IVO Oocytes

We next investigated the genetic expression-related genes. The KEGG pathway diagram showed that DNA replication and repair, protein synthesis and modification were affected. The analysis of ribosome and its biogenesis showed that more than 19 genes were up-regulated (**Figure 4A**), and the mRNA level of these genes were confirmed by the relative mRNA expression analysis (**Figure 4B**). Moreover, we also analyzed

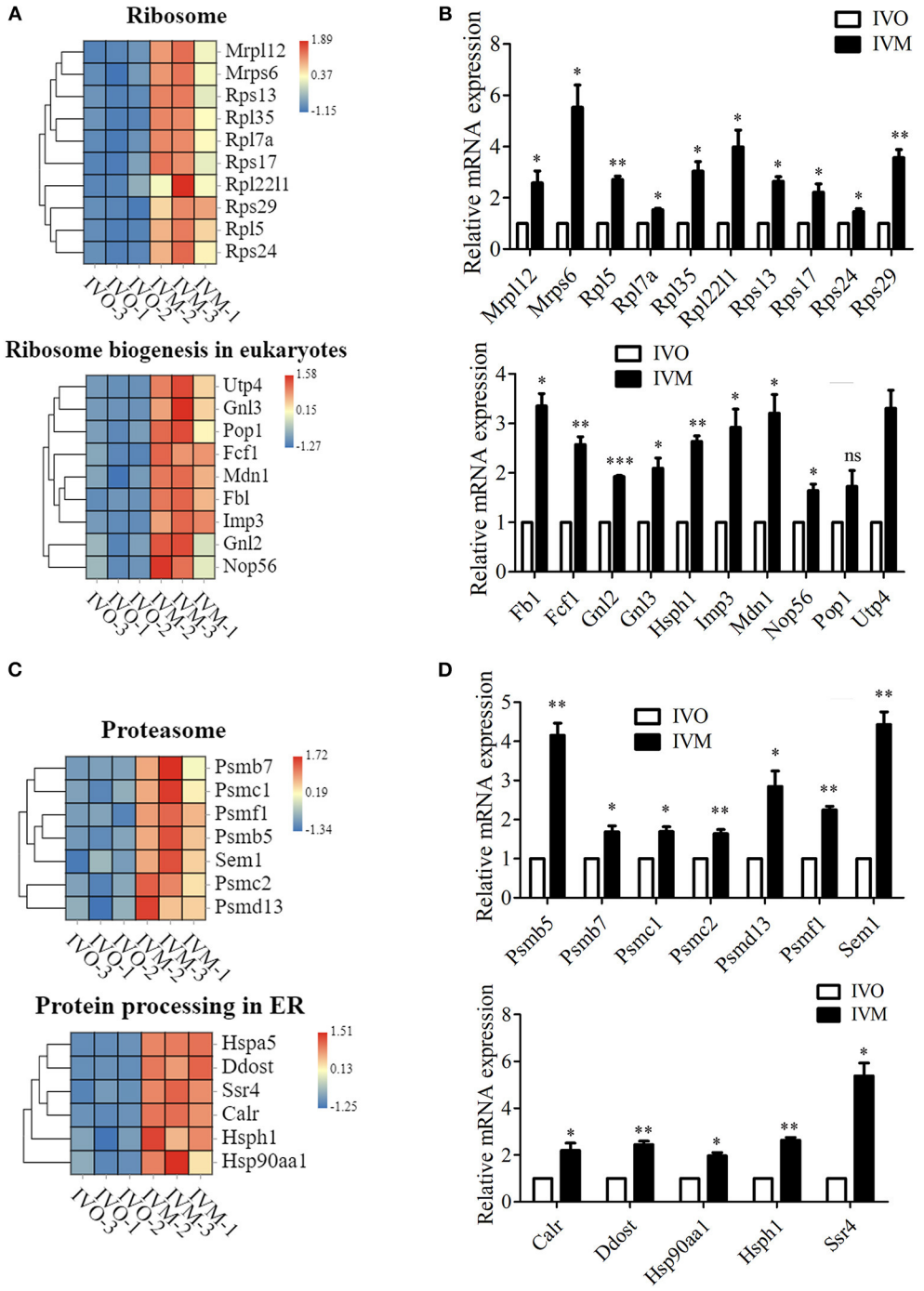

FIGURE 4 | Increased genetic information processing in IVM oocytes compared with IVO oocytes. **(A)** The heat map for the gene expression level of ribosome and ribosome biogenesis in eukaryotes pathway. **(B)** Relative mRNA expression levels of genes that involved in ribosome and ribosome biogenesis in eukaryotes in both IVM and IVO oocytes. $^{*}p < 0.05$; $^{**}p < 0.01$; $^{***}p < 0.001$. **(C)** The heat map for the gene expression level of proteasome and protein processing in ER. **(D)** The validation of mRNA expression level for proteasome and protein processing in ER. $^{*}p < 0.05$; $^{**}p < 0.01$; $^{***}p < 0.001$.

the protein degradation and modification processes, and the results showed that the expression of more than 13 genes were altered (**Figure 4C**). Real time RT-PCR data showed that the level of Psmb5, Psmb7, Psmc1, etc. expression increased in the IVM oocytes (**Figure 4D**). Afterwards, we performed statistical analysis of the DNA replication and repair-related genes, and the heat map showed that Rfc2, Ercc5, Top3a, Rpa2, etc. expressed differentially between these two groups (**Figure 5A**). We then carried out real time RT-PCR to confirm these results, and the mRNA expression level of Ercc2, Gtf2h5,

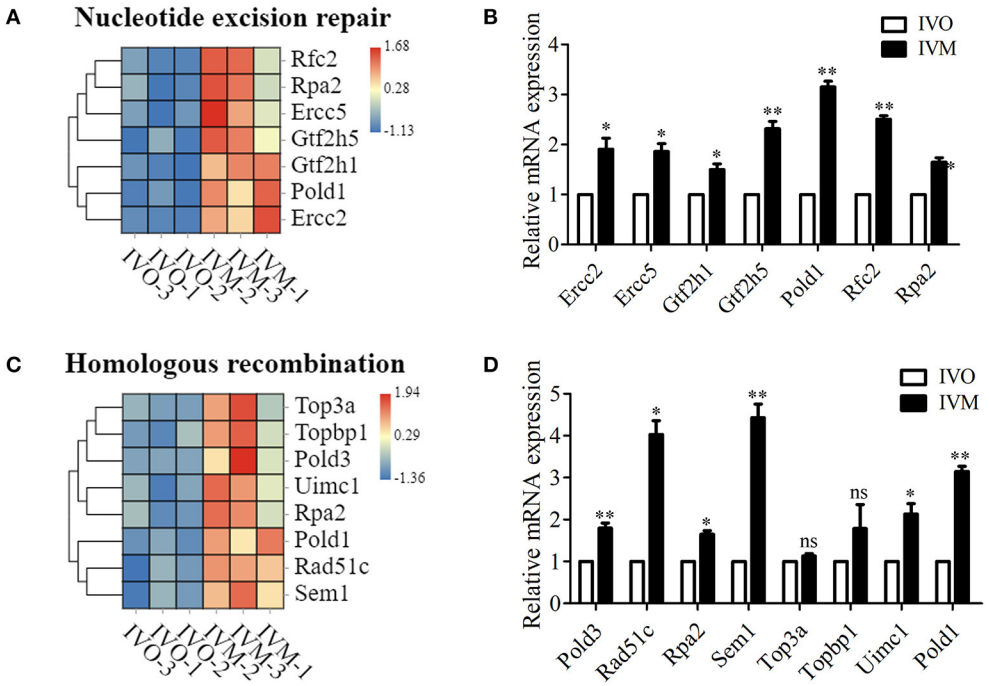

FIGURE 5 | Increased genetic information processing in IVM oocytes compared with IVO oocytes. **(A)** The heat map for the gene expression level of DNA repaired-related genes. **(B)** Relative mRNA expression levels of genes that involved in nucleotide excision repair in both IVM and IVO oocytes. $^{*}p < 0.05$; $^{**}p < 0.01$. **(C)** The heat map for the gene expression level of homologous recombination. **(D)** Relative mRNA expression levels of genes that participated in homologous recombination in both IVM and IVO oocytes. $^{*}p < 0.05$; $^{**}p < 0.01$.

and Pold1, which were related with DNA repair, showed the increase, which was consistent with the evaluation of the analysis results above (**Figure 5B**). Similarly, the mRNA expression level of Pold3, Rpa2, and Top3a, which were related with DNA replication, showed up-regulated characteristic, which conformed to the assessment of the analysis results above (**Figures 5C,D**). Therefore, we speculated that *in vitro* maturation affected the processing of genetic expression in mouse oocytes.

DISCUSSION

In this study we aimed to investigate the effects of *in vitro* maturation on mouse oocytes at the transcription level. We carried out our study by means of a transcriptome analysis to screen the differentially expressed genes. The genes were then grouped together to identify the biological processes that were affected. Our data showed that *in vitro* matured oocytes had multiple difference for the RNA expression compared with the *in vivo* maturation.

We first analyzed the dynamic changes in the global gene expression in mouse IVM and IVO oocytes. Our results showed that among the common differentially expressed genes of IVO and IVM groups, nearly 22% of the genes showed up-regulation expression in the IVM group, while only 3% was down-regulated. To further understand the influence of *in vitro* maturation on oocytes, we used the GO and KEGG analysis, starting with BP, MF, CC, and pathways respectively, to explore the issue. The analysis results showed that most genes related to environmental adaption were up-regulated, while metabolic processes were most affected, and the processes of genetic information, such as translation, folding, sorting and degradation, and replication and repair, were also altered. Compared with *in vivo* matured oocytes, the most striking difference of *in vitro* maturation processing was culturing conditions. As a result, we first detected the responses of oocytes to adapt environmental changes. Our results showed that thermogenesis, which was associated with the generation of energy, was answered more obviously. Previous studies showed that the environmental factors, such as light and culture medium composition, can induce metabolic alterations in the cytoplasm, resulting in mitochondrial dysfunction, augmentation of lipid peroxidation, and embryo growth arrest in cultured oocytes (Agarwal et al., 2006). While in human oocytes it was shown that *in vitro* maturation seemed to alter the mitochondrial membrane potential and endoplasmic reticulum (ER) compared with *in vivo* maturation (Ferrer-Vaquer et al., 2019). In addition, the mitochondrial activity was reduced in mature oocytes following 24 h of arrest and IVM (Santiquet et al., 2017). Part of the ultrastructure features in human oocytes shows abnormality *in vitro*, such as large mitochondria-vesicles (MV) complexes which partially replaced mitochondria-smooth endoplasmic reticulum (M-SER) aggregates in IVM oocytes (Coticchio et al., 2016). It has been demonstrated that *in vitro* culture conditions exert oxidative stress or an imbalance between oxidants and antioxidants, while the oxidative stress is generally resulted from mitochondrial dysfunction (Combelles et al., 2009). Our

data provided the molecular explanation for these previous studies and indicated that *in vitro* maturation might disturb oxidative phosphorylation processing in mouse oocytes. The pyrimidine pathway is a vital metabolic pathway which yields in the formation of pyrimidines, that are then integrated in nucleic acids (DNA and RNA) in sugars (UDP sugars) and lipids (CDP lipids) (Tiwari and Dubey, 2018). Our results indicated that several genes of the pyrimidine metabolism pathway were affected. Similar results were found for the genes of pyruvate metabolism. *In vitro* meiosis induction by gonadotropin is dependent upon the presence of glucose (Fagbohun and Downs, 1992), and the beneficial effect of glucose on oocyte maturation takes place through its glycolysis to pyruvate (Downs et al., 1996). Silencing mitochondrial pyruvate carrier 1 of cumulus-denuded oocytes (DOs) significantly impaired their maturation (Xie et al., 2018). Therefore, our data reveals that *in vitro* maturation may cause damage to metabolism pathways, resulting in increased gene expression.

We also found that the genetic information processing had significantly different expression levels between IVM and IVO oocytes. Genetic information processing in relation to transcription and translation of genes, regulates the synthesis of proteins for oocytes and indirectly control vital activities. The *in vitro* maturation procedure strongly affects the gene expression profile of human oocytes, including several genes involved in transcriptional regulation, embryogenesis, epigenetics, development, and the cell cycle (Virant-Klun et al., 2018). *In vitro*-produced fresh (IVF-F) bovine blastocysts, gene expression of ribosome, and its biogenesis was significantly up-regulated (Aksu et al., 2012). In cattle, *in vitro* production (IVP) embryos may display aberrations in ribosomal RNA gene activation (Hyttel et al., 2000). Our analysis results were consistent with previous studies, confirming that *in vitro* maturation could impair protein synthesis, and caused an increase in gene expression as compensation. Additionally, studies indicated that ER stress had been identified in mammalian oocytes and embryos produced *in vitro*, while functional proteins must be folded properly in the endoplasmic reticulum (ER) to maintain oocyte and embryo development (Lin et al., 2019). In human oocytes, *in vitro* maturation may cause dysregulation in either gene transcription or post-transcriptional modification of genes with the over-abundance of transcripts (Jones et al., 2008).

In conclusion, our data, through transcriptome analysis, indicated that *in vitro* maturation might induce errors through multiple pathways including the generation of energy and gene expression processing in mouse oocytes.

DATA AVAILABILITY STATEMENT

The original contributions presented in the study are included in the article/**Supplementary Material**, further inquiries can be directed to the corresponding author/s. The original data GEO Submission (GSE165546) (NCBI tracking system #21628819) could be found at the following link: https://www.ncbi.nlm.nih.gov/geo/query/acc.cgi?acc=GSE165546.

ETHICS STATEMENT

The animal study was reviewed and approved by Nanjing Agricultural University.

AUTHOR CONTRIBUTIONS

H-LZ and S-CS designed the study, wrote the manuscript, and analyzed the data. H-LZ performed the experiments. YX, Z-NP, and J-QJ contributed the materials. All the authors approved the final manuscript.

FUNDING

This work was supported by the National Key Research and Development Program of China (2018YFC1003802, 2018YFC1004003) and the Fundamental Research Funds for the Central Universities of China (KYGD202004).

ACKNOWLEDGMENTS

We are grateful for the sequencing platform and bioinformation analysis of Gene Denovo Biotechnology Co., Ltd (Guangzhou, China) and the Beijing Geek Gene Technology Co. Ltd.

SUPPLEMENTARY MATERIAL

The Supplementary Material for this article can be found online at: https://www.frontiersin.org/articles/10.3389/fcell.2021.642010/full#supplementary-material

Supplementary Figure 1 | Increased environmental adaptation in the IVM oocytes compared with IVO oocytes. **(A)** The heat map for the gene expression level of thermogenesis pathway. **(B)** The verification for the mRNA expression of differentially expressed genes from thermogenesis pathway. $^{*}p < 0.05$; $^{**}p < 0.01$; $^{***}p < 0.001$. **(C)** The heat map for the gene expression level of cardiac muscle contraction pathway. **(D)** The verification for the mRNA expression of differentially expressed genes from cardiac muscle contraction pathway. $^{*}p < 0.05$; $^{**}p < 0.01$; $^{***}p < 0.001$.

REFERENCES

Agarwal, A., Said, T. M., Bedaiwy, M. A., Banerjee, J., and Alvarez, J. G. (2006). Oxidative stress in an assisted reproductive techniques setting. *Fertil. Steril.* 86, 503–512. doi: 10.1016/j.fertnstert.2006.02.088

Aksu, D. A., Agca, C., Aksu, S., Bagis, H., Akkoc, T., Caputcu, A. T., et al. (2012). Gene expression profiles of vitrified *in vitro*- and *in vivo*-derived bovine blastocysts. *Mol. Reprod. Dev.* 79, 613–625. doi: 10.1002/mrd.22068

Borghol, N., Lornage, J., Blachere, T., Sophie Garret, A., and Lefevre, A. (2006). Epigenetic status of the H19 locus in human oocytes following *in vitro* maturation. *Genomics* 87, 417–426. doi: 10.1016/j.ygeno.2005.10.008

Budna, J., Chachula, A., Kazmierczak, D., Rybska, M., Ciesiolka, S., Bryja, A., et al. (2017). Morphogenesis-related gene-expression profile in porcine oocytes before and after *in vitro* maturation. *Zygote* 25, 331–340. doi: 10.1017/S096719941700020X

Cha, K. Y., and Chian, R. C. (1998). Maturation *in vitro* of immature human oocytes for clinical use. *Hum. Reprod. Update* 4, 103–120. doi: 10.1093/humupd/4.2.103

Chian, R. C., Xu, C. L., Huang, J. Y., and Ata, B. (2014). Obstetric outcomes and congenital abnormalities in infants conceived with oocytes matured *in vitro*. *Facts Views Vis. Obgyn.* 6, 15–18.

Combelles, C. M., Gupta, S., and Agarwal, A. (2009). Could oxidative stress influence the *in-vitro* maturation of oocytes? *Reprod. Biomed. Online* 18, 864–880. doi: 10.1016/S1472-6483(10)60038-7

Coticchio, G. (2016). IVM in need of clear definitions. *Hum. Reprod.* 31, 1387–1389. doi: 10.1093/humrep/dew110

Coticchio, G., Dal Canto, M., Fadini, R., Mignini Renzini, M., Guglielmo, M. C., Miglietta, S., et al. (2016). Ultrastructure of human oocytes after *in vitro* maturation. *Mol. Hum. Reprod.* 22, 110–118. doi: 10.1093/molehr/gav071

De Geyter, C. (2019). Assisted reproductive technology: Impact on society and need for surveillance. *Best Pract. Res. Clin. Endocrinol. Metab.* 33, 3–8. doi: 10.1016/j.beem.2019.01.004

Downs, S. M., Humpherson, P. G., Martin, K. L., and Leese, H. J. (1996). Glucose utilization during gonadotropin-induced meiotic maturation in cumulus cell-enclosed mouse oocytes. *Mol. Reprod. Dev.* 44, 121–131. doi: 10.1002/(SICI)1098-2795(199605)44:1<121::AID-MRD14>3.0.CO;2-7

Essers, P. B., Pereboom, T. C., Goos, Y. J., Paridaen, J. T., and Macinnes, A. W. (2014). A comparative study of nucleostemin family members in zebrafish reveals specific roles in ribosome biogenesis. *Dev. Biol.* 385, 304–315. doi: 10.1016/j.ydbio.2013.10.029

Fagbohun, C. F., and Downs, S. M. (1992). Requirement for glucose in ligand-stimulated meiotic maturation of cumulus cell-enclosed mouse oocytes. *J. Reprod. Fertil.* 96, 681–697. doi: 10.1530/jrf.0.0960681

Ferrer-Vaquer, A., Barragan, M., Rodriguez, A., and Vassena, R. (2019). Altered cytoplasmic maturation in rescued *in vitro* matured oocytes. *Hum. Reprod.* 34, 1095–1105. doi: 10.1093/humrep/dez052

Greenstein, D. (2005). Control of oocyte meiotic maturation and fertilization. *WormBook* 28, 1–12. doi: 10.1895/wormbook.1.53.1

Guerrero-Castillo, S., Cabrera-Orefice, A., Huynen, M. A., and Arnold, S. (2017). Identification and evolutionary analysis of tissue-specific isoforms of mitochondrial complex I subunit NDUFV3. *Biochim. Biophys. Acta Bioenerg.* 1858, 208–217. doi: 10.1016/j.bbabio.2016.12.004

Havlickova, V., Kaplanova, V., Nuskova, H., Drahota, Z., and Houstek, J. (2010). Knockdown of F1 epsilon subunit decreases mitochondrial content of ATP synthase and leads to accumulation of subunit c. *Biochim. Biophys. Acta* 1797, 1124–1129. doi: 10.1016/j.bbabio.2009.12.009

Hyttel, P., Viuff, D., Laurincik, J., Schmidt, M., Thomsen, P. D., Avery, B., et al. (2000). Risks of *in-vitro* production of cattle and swine embryos: aberrations in chromosome numbers, ribosomal RNA gene activation and perinatal physiology. *Hum. Reprod.* 15(Suppl. 5), 87–97. doi: 10.1093/humrep/15.suppl_5.87

Indrieri, A., Van Rahden, V. A., Tiranti, V., Morleo, M., Iaconis, D., Tammaro, R., et al. (2012). Mutations in COX7B cause microphthalmia with linear skin lesions, an unconventional mitochondrial disease. *Am. J. Hum. Genet.* 91, 942–949. doi: 10.1016/j.ajhg.2012.09.016

Jiang, N., Hu, L., Liu, C., Gao, X., and Zheng, S. (2015). 60S ribosomal protein L35 regulates beta-casein translational elongation and secretion in bovine mammary epithelial cells. *Arch. Biochem. Biophys.* 583, 130–139. doi: 10.1016/j.abb.2015.08.006

Jones, G. M., Cram, D. S., Song, B., Magli, M. C., Gianaroli, L., Lacham-Kaplan, O., et al. (2008). Gene expression profiling of human oocytes following *in vivo* or *in vitro* maturation. *Hum. Reprod.* 23, 1138–1144. doi: 10.1093/humrep/den085

Katz-Jaffe, M. G., Mccallie, B. R., Preis, K. A., Filipovits, J., and Gardner, D. K. (2009). Transcriptome analysis of *in vivo* and *in vitro* matured bovine MII oocytes. *Theriogenology* 71, 939–946. doi: 10.1016/j.theriogenology.2008.10.024

Lin, T., Lee, J. E., Kang, J. W., Shin, H. Y., Lee, J. B., and Jin, D. I. (2019). Endoplasmic reticulum (ER) stress and unfolded protein response (UPR) in mammalian oocyte maturation and preimplantation embryo development. *Int. J. Mol. Sci.* 20:409. doi: 10.3390/ijms20020409

Lu, C., Zhang, Y., Zheng, X., Song, X., Yang, R., Yan, J., et al. (2018). Current perspectives on *in vitro* maturation and its effects on oocyte genetic and epigenetic profiles. *Sci. China Life Sci.* 61, 633–643. doi: 10.1007/s11427-017-9280-4

Lynes, M. D., Kodani, S. D., and Tseng, Y. H. (2019). Lipokines and thermogenesis. *Endocrinology* 160, 2314–2325. doi: 10.1210/en.2019-00337

Nicolas, E., Golemis, E. A., and Arora, S. (2016). POLD1: Central mediator of DNA replication and repair, and implication in cancer and other pathologies. *Gene* 590, 128–141. doi: 10.1016/j.gene.2016.06.031

Rak, M., and Rustin, P. (2014). Supernumerary subunits NDUFA3, NDUFA5 and NDUFA12 are required for the formation of the extramembrane arm of human mitochondrial complex I. *FEBS Lett.* 588, 1832–1838. doi: 10.1016/j.febslet.2014.03.046

Rohlenova, K., Veys, K., Miranda-Santos, I., De Bock, K., and Carmeliet, P. (2018). Endothelial cell metabolism in health and disease. *Trends Cell Biol.* 28, 224–236. doi: 10.1016/j.tcb.2017.10.010

Santiquet, N. W., Greene, A. F., Becker, J., Barfield, J. P., Schoolcraft, W. B., and Krisher, R. L. (2017). A pre-*in vitro* maturation medium containing cumulus oocyte complex ligand-receptor signaling molecules maintains meiotic arrest, supports the cumulus oocyte complex and improves oocyte developmental competence. *Mol. Hum. Reprod.* 23, 594–606. doi: 10.1093/molehr/gax032

Son, W. Y., Henderson, S., Cohen, Y., Dahan, M., and Buckett, W. (2019). Immature oocyte for fertility preservation. *Front. Endocrinol.* 10:464. doi: 10.3389/fendo.2019.00464

Sutton-McDowall, M. L., Gilchrist, R. B., and Thompson, J. G. (2010). The pivotal role of glucose metabolism in determining oocyte developmental competence. *Reproduction* 139, 685–695. doi: 10.1530/REP-09-0345

Tiwari, K., and Dubey, V. K. (2018). Fresh insights into the pyrimidine metabolism in the trypanosomatids. *Parasit. Vectors* 11:87. doi: 10.1186/s13071-018-2660-8

Urbanska, K., and Orzechowski, A. (2019). Unappreciated role of LDHA and LDHB to control apoptosis and autophagy in tumor cells. *Int. J. Mol. Sci.* 20:2085. doi: 10.3390/ijms20092085

Virant-Klun, I., Bauer, C., Stahlberg, A., Kubista, M., and Skutella, T. (2018). Human oocyte maturation *in vitro* is improved by co-culture with cumulus cells from mature oocytes. *Reprod. Biomed. Online* 36, 508–523. doi: 10.1016/j.rbmo.2018.01.011

Wortmann, S. B., Chen, M. A., Colombo, R., Pontoglio, A., Alhaddad, B., Botto, L. D., et al. (2017). Mild orotic aciduria in UMPS heterozygotes: a metabolic finding without clinical consequences. *J. Inherit. Metab. Dis.* 40, 423–431. doi: 10.1007/s10545-017-0015-9

Xie, H. L., Zhu, S., Zhang, J., Wen, J., Yuan, H. J., Pan, L. Z., et al. (2018). Glucose metabolism during *in vitro* maturation of mouse oocytes: an study using RNA interference. *J. Cell. Physiol* 233, 6952–6964. doi: 10.1002/jcp.26484

Yang, Z. Y., and Chian, R. C. (2017). Development of *in vitro* maturation techniques for clinical applications. *Fertil. Steril.* 108, 577–584. doi: 10.1016/j.fertnstert.2017.08.020

Ye, M., Yang, Z. Y., Zhang, Y., Xing, Y. X., Xie, Q. G., Zhou, J. H., et al. (2020). Single-cell multiomic analysis of *in vivo* and *in vitro* matured human oocytes. *Hum. Reprod.* 35, 886–900. doi: 10.1093/humrep/deaa044

Yuan, H. X., Xiong, Y., and Guan, K. L. (2013). Nutrient sensing, metabolism, and cell growth control. *Mol. Cell* 49, 379–387. doi: 10.1016/j.molcel.2013.01.019

Zhao, H., Li, T., Zhao, Y., Tan, T., Liu, C., Liu, Y., et al. (2019). Single-cell transcriptomics of human oocytes: environment-driven metabolic competition and compensatory mechanisms during oocyte maturation. *Antioxid. Redox Signal.* 30, 542–559. doi: 10.1089/ars.2017.7151

Zhao, Y., Liao, X., Krysta, A. E., Bertoldo, M. J., Richani, D., and Gilchrist, R. B. (2020). Capacitation IVM improves cumulus function and oocyte quality in minimally stimulated mice. *J. Assist. Reprod. Genet.* 37, 77–88. doi: 10.1007/s10815-019-01610-x

Conflict of Interest: The authors declare that the research was conducted in the absence of any commercial or financial relationships that could be construed as a potential conflict of interest.

Copyright © 2021 Zhang, Xu, Ju, Pan, Liu and Sun. This is an open-access article distributed under the terms of the Creative Commons Attribution License (CC BY). The use, distribution or reproduction in other forums is permitted, provided the original author(s) and the copyright owner(s) are credited and that the original publication in this journal is cited, in accordance with accepted academic practice. No use, distribution or reproduction is permitted which does not comply with these terms.

frontiers in Cell and Developmental Biology

MINI REVIEW
published: 25 February 2021
doi: 10.3389/fcell.2021.638559

Critical Functions of PP2A-Like Protein Phosphotases in Regulating Meiotic Progression

*Wen-Long Lei[1], Wei-Ping Qian[1] and Qing-Yuan Sun[2]**

[1] Department of Reproductive Medicine, Peking University Shenzhen Hospital, Shenzhen, China, [2] Fertility Preservation Lab, Reproductive Medicine Center, Guangdong Second Provincial General Hospital, Guangzhou, China

Meiosis is essential to the continuity of life in sexually-reproducing organisms through the formation of haploid gametes. Unlike somatic cells, the germ cells undergo two successive rounds of meiotic divisions after a single cycle of DNA replication, resulting in the decrease in ploidy. In humans, errors in meiotic progression can cause infertility and birth defects. Post-translational modifications, such as phosphorylation, ubiquitylation and sumoylation have emerged as important regulatory events in meiosis. There are dynamic equilibrium of protein phosphorylation and protein dephosphorylation in meiotic cell cycle process, regulated by a conservative series of protein kinases and protein phosphatases. Among these protein phosphatases, PP2A, PP4, and PP6 constitute the PP2A-like subfamily within the serine/threonine protein phosphatase family. Herein, we review recent discoveries and explore the role of PP2A-like protein phosphatases during meiotic progression.

Keywords: protein phosphorylation, meiosis, PP2A, PP4, PP6

OPEN ACCESS

Edited by:
Wei Li,
Chinese Academy of Sciences (CAS), China

Reviewed by:
Jakob Nilsson,
University of Copenhagen, Denmark
Greg B. Moorhead,
University of Calgary, Canada
Xingzhi Xu,
Shenzhen University, China

****Correspondence:***
Qing-Yuan Sun
sunqy@gd2h.org.cn;
sunqy@ioz.ac.cn

Specialty section:
This article was submitted to Cell Growth and Division, a section of the journal Frontiers in Cell and Developmental Biology

Received: *07 December 2020*
Accepted: *08 February 2021*
Published: *25 February 2021*

Citation:
Lei W-L, Qian W-P and Sun Q-Y (2021) Critical Functions of PP2A-Like Protein Phosphotases in Regulating Meiotic Progression. Front. Cell Dev. Biol. 9:638559. doi: 10.3389/fcell.2021.638559

INTRODUCTION

In eukaryotes, reversible phosphorylation and dephosphorylation of proteins represents an prominent type of post-translational modification that has an crucial effect on controlling some cellular processes and events (Hunter, 1995). The state of protein phosphorylation can be adjusted by some highly conserved protein kinases and protein phosphatases (Mumby and Walter, 1993). In general, it is necessary for a number of critical biological events to keep a proper balance between protein kinases and protein phosphatases (Cassimeris, 1999). Disruption of this equilibrium can contribute to many pathological circumstances and even diseases. This spatial and temporal regulation of protein phosphorylation occurs not only in mitotic program, but also in meiotic progression.

Meiosis is a peculiar type of division in which one single round of DNA replication is followed by two sequential rounds of chromosome segregation (meiosis I and meiosis II), which is an important procedure for gamogenesis. Through this progression, diploid parent cells give rise to haploid gametes with the correct number of chromosomes. Similar to mitosis, meiotic division occurs in all eukaryotes and is an intricate event that is needed to change the cell cycle (Wolgemuth and Roberts, 2010). DNA replication and chromosome segregation both occur in meiosis. However, there are some other particular events in meiosis, such as homologous chromosome pairing, synaptonemal complex formation, double-strand break (DSB) repairing, meiotic recombination and a reductional division (Berchowitz and Copenhaver, 2010). Prior to the meiotic divisions, changing maternal and paternal chromosome behaviors including pairing, synapsis, and recombination must occur in a

highly adjusted manner during prophase (Sato-Carlton et al., 2014). Therefore, according to the different behaviors of chromosomes, the prophase I also can be divided into five stages which are named as leptotene, zygotene, pachytene, diplotene, diakinesis. These events result in the mutual exchange of DNA material between homologous chromosomes and increasing genetic diversity (Bishop and Zickler, 2004). During meiosis I, homologous chromosomes are segregated whereas sister chromatids are still interacted on each other. Then sister chromatids are fully segregated in the second meiotic division (Canela et al., 2003; Qi et al., 2013). Errors in any of these events attribute to failure of the gametogenesis. In this progress, human oocytes have an abnormally high chromosome error rate that significantly increases with age, with severe results for human fertility (Keating et al., 2020).

A battery of protein phosphorylation and protein dephosphorylation events, which are adjusted by protein kinases and protein phosphatases, are critical for meiotic process (Bornslaeger et al., 1986; Lu et al., 2001). Protein kinases shift a phosphoryl group from adenosine triphosphate (ATP) to the hydroxyl group of serine, threonine and tyrosine residues, while protein phosphatases dephosphorylate protein by phosphate group hydrolysis and thus oppose the actions of protein kinases (Lillo et al., 2014). Among the phosphorylation, almost 98% of protein phosphorylation occurs on serine and threonine residues (Pearlman et al., 2011; Hunter, 2014). In human genome, there are more than 500 protein kinases encoded that catalyze the phosphorylation (Subramani et al., 2013).These protein kinases can phosphorylate the specific sites of target proteins. Nevertheless, it is insufficient for protein kinases alone to control dynamic processes. Because the phosphorylation of serine and threonine sites is extraordinary stable, which has long half-life (Lad et al., 2003), protein phosphatases can ensure that protein phosphorylation is dynamic and reversible (Nilsson, 2019). For various reasons, compared with the rich knowledge on protein kinases, there is a relative lack of information about the functions of protein phosphatases (Afshar et al., 2016). Among these conserved phosphoprotein phosphatases, PP2A, PP4, and PP6 constitute the PP2A-like subfamily within the serine and threonine protein phosphatase family (Bielinski and Mumby, 2007). These phosphoprotein phosphatases play crucial roles in multiple series of fundamental cellular events. Recent studies have implicated that PP2A-like protein phosphatases play critical roles in regulating meiosis. In this review, we will summarize recent discoveries and explore the role of PP2A-like protein phosphatases during meiotic progression.

Classification of Protein Phosphatases

In the past decades, there are numerous studies about the biological roles of protein phosphatases, especially in meiosis. Generally, eukaryotic protein phosphatases can be divided into four major gene families based on specific substrate, catalytic activity and inhibitor sensitivity (Lillo et al., 2014). These families are phosphoprotein phosphatases (PPP), Mg^{2+}/Mn^{2+}-dependent protein phosphatases (PPM), aspartate-based protein phosphatases, and phosphotyrosine phosphatases (PTP) (Kerk et al., 2008). Among these families, the PPPs are the most comparatively conservative members across the whole eukaryotic species from yeast to human, indicating their "housekeeping" importance (Brautigan, 2013). In eukaryotic cells, almost 80% of the protein phosphatase activity is regulated by PPP family (Janssens and Goris, 2001). The PPP family includes seven members, namely PP1, PP2A, PP2B (also known as PP3), PP4, PP5, PP6, and PP7.

The Structure of PP2A-Like Protein Phosphatases

Within the PPP family, PP2A, PP4, and PP6 come into being an independent cluster, whose catalytic subunits are most closely related, suggestive of a common origin (Chen et al., 2017). The catalytic subunits combine with scaffolding and/or regulatory subunits to form heterotrimeric or heterodimeric holoenzyme complexes (Brautigan and Shenolikar, 2018). Although their catalytic subunits have high sequence similarity, they have their own special structural compositions (Nasa and Kettenbach, 2020). PP2A is a heterotrimer holoenzyme complex consisting of a catalytic subunit, a scaffold subunit, and a regulatory subunit. The heterodimeric holoenzyme also named as core enzyme, composing of the catalytic and scaffold subunit, which is indispensable for the function of the holoenzyme (Price and Mumby, 2000). In higher eukaryotes, there are two isoforms in PP2A catalytic subunit (PPP2ACα and PPP2ACβ), which have 97% sequence similarity with each other. There are also two isoforms in PP2A scaffold subunit (PPP2R1α and PPP2R1β), which have abmost 87% sequence similarity (Saurin, 2018). The PP2A regulatory subunit has multiple members, which belong to four different families: B (B55), B′ (B56), B′′ (B72), and B′′′ (Striatin) family (Janssens and Goris, 2001). Therefore, the different combination of subunits results in various PP2A holoenzyme, differing in subcellular localization and distinct substrate specificity. For PP4, catalytic subunit combines with different regulatory subunits to form heterodimers or heterotrimers. The PP4 regulatory subunit has five isoforms: PPP4R1, PPP4R2, PPP4R3A, PPP4R3B, and PPP4R4 (Kloeker and Wadzinski, 1999; Cohen et al., 2005). Like other type 2A serine/threonine protein phosphatases, PP6 also works as a holoenzyme, consisting of a catalytic subunit, PPP6C, one of the three regulatory subunits including PPP6R1, PPP6R2 and PPP6R3, and one of the three ankyrin subunits including ARS-A, -B, -C (Stefansson and Brautigan, 2006; Stefansson et al., 2008).

PP2A-Like Protein Phosphatases in Regulation of Meiotic Progression

PP2A

Among type 2A protein phosphatases, PP2A is the most famous and is widely researched. For a long time, accumulating evidence revealed its cellular and molecular importance. Studies also suggest that PP2A is involved in multiple steps of meiosis. In mouse oocytes, up-regulation of PP2A activity results in the meiotic arrest phenotype (Su et al., 2012). In *Oikopleura dioica*, PP2A is also necessary for meiotic arrest and precaution of parthenogenesis by restraining the abnormal Ca^{2+} burst

(Matsuo et al., 2020). These results indicate that the function of PP2A is highly conserved in different organisms.

PP2A is essential for chromosome segregation during meiosis (Kerr et al., 2016). Several *in vitro* experiments have indicated that PP2A can associate with shugoshins and hold back the phosphorylation of Rec8 at the centromeres, a member of the cohesin complex, and finally stop split of Rec8 and keep the cohesion of chromatids in meiosis I (Kitajima et al., 2006; Lee et al., 2008; Rattani et al., 2013). In addition, Sororin and Shugoshin-PP2A collaborates in the regulation of centromeric cohesion during meiosis (Gomez et al., 2016). In Drosophila meiosis, the Shugoshin MEI-S332 and PP2A reciprocally promote localization of the other to centromeres and together they thus function to ensure accurate segregation (Pinto and Orr-Weaver, 2017). Also, a new study indicated that SCF (Skp1–Cul1–F box) -Fbxo42 down-regulates the protein level of the PP2A-B56 during synaptonemal complex assembly and maintenance (Barbosa et al., 2021). In mice spermatocytes, Previato de Almeida et al. found that Sgo2 is essential to protect centromere pairing by recruiting PP2A, while Sgo1 regulates non-exchange segregation by recruiting PP2A to centromeres (Previato de Almeida et al., 2019). In meiosis II, sister chromatids disjoin upon cleavage of centromeric Rec8. One assumption is that PP2A is separated from Rec8 by bipolar spindle forces in metaphase II. A recent experiment suggested that PP2A is removed from centromeres by the ubiquitin-ligase APC/C^{Cdc20}, which can decrease the activity of Sgo1 and kinase Mps1 (Arguello-Miranda et al., 2017; Jonak et al., 2017).

Exact kinetochores-microtubule (KT-MT) is essential for correct chromosome segregation. In mitosis, correct KT-MT attachments are stabilized by inner sister KT stretching and the phosphorylation level of the KT. However, because of inherent property of the MI chromosomes, there is a difference between meiosis I and mitosis. This may explain the high incidence of KT-MT attachment errors in oocytes. In meiosis, PP2A-B56, which is regulated by the BubR1, is essential to determine the stability of KT-MT attachments independently of bivalent stretching (Yoshida et al., 2015). Overall, PP2A is targeted by Shugoshin and BubR1 to protect centromeric cohesion and stabilize KT-MT attachments in yeast and mouse meiosis. In *C. elegans* meiosis, the function of PP2A remains unclear. A recent study found that PP2A is necessary for female meiotic progression, such as spindle assembly and chromosome segregation. The mechanism is that BUB-1 targets PP2A-B′56 via a conserved LxxIxE motif and this regulation is necessary for correct meiotic progression (Bel Borja et al., 2020).

In addition, treatment with okadaic acid (OA) or calyculin-A (CL-A), which inhibits PP2A, caused an absence of microtubule polymerization and spindles. These studies have also showed that PP2A participated in microtubule organization and spindle formation (Lu et al., 2002). Protein phosphatase 2A regulatory subunit B55α (PP2A-B55α) is encoded by Ppp2r2a. Liang et al. found that PP2A-B55α was an important regulator of oocyte asymmetric division, chromosome congression, DNA damage response and spindle dynamics by RNA interference (Liang et al., 2017). In *Xenopus* oocytes,protein phosphatase 2A regulatory subunit B′56 (PP2A-B′56) and calcineurin (CaN) jointly contributes to APC/C^{Cdc20} activation by inhibiting phosphorylation of XErp1 (Heim et al., 2018). Two studies suggested that PP2A might be controlled by two distinct mechanisms in mouse oocytes. One is a post-translational modification by which MASTL (microtubule associated serine/threonine kinase-like), inhibit PP2A activity to promote anaphase (Adhikari et al., 2014). The other is CRL4-mediated degradation of the PP2A scaffold subunit, which reduces PP2A activity to facilitate non-reversible meiotic progression (Yu et al., 2015). These two regulation mechanisms of PP2A activity in conjunction with other meiotic regulators ensure precise meiotic progression in oocytes.

By using genetically modified mouse models, we further studied the functions of PP2A in oocyte meiosis We employed the conditional knockout method by using growth differentiation factor 9 (*Gdf9)-Cre* mice to gain mutant mice with depletion of PPP2R1α in oocytes in order to research its function in female meiosis. The results indicated that oocyte-specific depletion of PPP2R1α resulted in female subfertility because of production of aneuploid oocytes came from wrong separation of sister chromatids, but did not affect folliculogenesis, ovulation and spindle formation during meiosis II (Hu et al., 2014). Interestingly, another report generated conditional knockout mice by crossing *Ppp2ca*$^{f/f}$ and (or) *Ppp2cb*$^{f/f}$ with *Zp3-Cre* mice to study PP2A in female meiosis. They found that single knockout PPP2ACα females or PPP2ACβ females were fertile, indicating the paralogs were functionally redundant. Only the deficiency of both PPP2ACα and PPP2ACβ in oocytes finally resulted in female infertility (Tang et al., 2016). In this study, they also found that the PP2A can regulate chromosome behavior and bipolar spindle formation in meiosis I. PP2A counteracts Aurora kinase B/C to ensure bivalent stretching and KT-MT attachment stability (Tang et al., 2016). In contrast, PP2A is also essential for spermatogenesis, especially meiosis (Pan et al., 2015). However, the study is descriptive only, with a lack on mechanistic insight. It will be fascinating to reveal the deeply regulatory mechanism of PP2A in male meiosis.

PP4

PP4 has been widely studied over the past decade. However, there is a relative lack of information about PP4 in meiosis. In *C. elegans*, PP4 is indispensable for spindle formation during male meiosis, but it is not essential for female meiosis (Sumiyoshi et al., 2002). Moreover, at least four critical events in prophase require PP4, such as synapsis-independent chromosome pairing, prevention of non-homologous chromosome synapsis, DSB initiation, and crossover formation. The failure of these series of events eventually results in the failure of chiasmata formation (Sato-Carlton et al., 2014). In yeast, PP4 seems to be highly active during the whole meiotic progression. PP4 has an important role in single-end invasions, synaptonemal complex assembly, spindle formation and centromere pairing (Falk et al., 2010). To clarify whether PP4 has conserved functions in meiosis in mammalian species, we generated its catalytic subunit gene Ppp4c conditional knockout (*Ppp4c*$^{f/f}$) mouse strain using CRISPR/Cas9 technology, and showed that loss of PPP4C did not affect male germ cell meiosis, acrosome formation, nuclear

TABLE 1 | Consequences of deletions of PP2A-like protein phosphatases in mouse germ cells.

PP2A-like protein phosphatases	Subunit deleted	Cre recombinase	Phenotype	References
PP2A	PPP2R1α	Gdf9	Subfertile	Hu et al., 2014
	PPP2ACα	Zp3	Fertile	Tang et al., 2016
	PPP2ACβ	Zp3	Fertile	Tang et al., 2016
	PPP2ACα& PPP2ACβ	Zp3	Infertile	Tang et al., 2016
	PPP2ACα	DDx4	Infertile	Pan et al., 2015
PP4	PPP4C	Stra8	Infertile	Han et al., 2020
PP6	PPP6C	Zp3	Subfertile	Hu et al., 2015
	PPP6C	Gdf9	Infertile	Hu et al., 2016
	PPP6C	Stra8	Infertile	Lei et al., 2020

condensation and elongation, but caused the defect of cytoplasm removal, which in turn leads to the failure of spermiogenesis completion and male infertility (Han et al., 2020). Hence, the physiological roles and regulatory mechanism of PP4 in other organisms remain to be further studied.

PP6

Like other type 2A serine/threonine protein phosphatases, PP6 is also ubiquitously expressed in cells. However, PP6 has suffered less notice than its near relative PP2A and PP4, especially in meiosis. Until now, there only three papers about the functions of PP6 in meiosis. We showed that knockout of PP6 in oocytes from primary follicle stage resulted in female subfertility by disturbing MII spindle formation and MII exit after fertilization, indicating that PP6 can act as antagonizer to oocyte aneuploidy. But it is dispensable in oocyte meiotic maturation, follicle growth and ovulation (Hu et al., 2015). However, we showed that knockout of PP6 in oocytes from primordial follicle stage resulted in complete infertility of female mice. Deletion of PP6 caused meiotic prophase oocyte loss and abnormal folliculogenesis because of aberrant phosphorylation level of H2AX, which then led to lots of oocyte disappearance and eventually premature ovarian failure (POF). These results indicated that PP6 can also safeguard oocyte genomic integrity and regulate folliculogenesis during the long prophase I arrest (Hu et al., 2016). In male meiosis, our recent study by crossing *Ppp6c*$^{f/f}$ mice with *Stra8-Cre* mice to obtain genetically mutant mice with specific malformation of the *Ppp6c* in male germ cells. We discovered that the mutant mice were male infertile and male germ cells were blocked at the pachytene stage during meiosis. Further study found that the loss of PP6 in male germ cells affected chromatin relaxation owing to abnormal MAPK pathway activity, thus stopping the recruitment of DSB repair factors to the appropriate sites on chromosomes (Lei et al., 2020).

Perspectives

Undoubtedly, protein phosphorylation is one of the most significant post-translational modifications during meiotic progression. The phosphorylation state of a special protein is regulated by protein kinases and protein phosphatases. As a member of PPP family, these new researches on PP2A-like protein phosphatases reported in past decades enriched the list of functions in meiosis, especially by employing conditional knockout mice (**Table 1**). Nonetheless, the most studies are descriptive only, with a lack of deep mechanistic insight. The special substrates of the different PP2A-like protein phosphatases are still a remaining impediment. In meiosis, it is not hard to notice that all three members can play the same role in special stages or special biological events (**Figure 1**). Are they functionally redundant? In the future, these unanswered questions remain to be further studied. Quantitative mass spectrometry-based proteomic and phosphoprotoemic approaches maybe provide a solution for understanding regulatory functional mechanism of PP2A-like

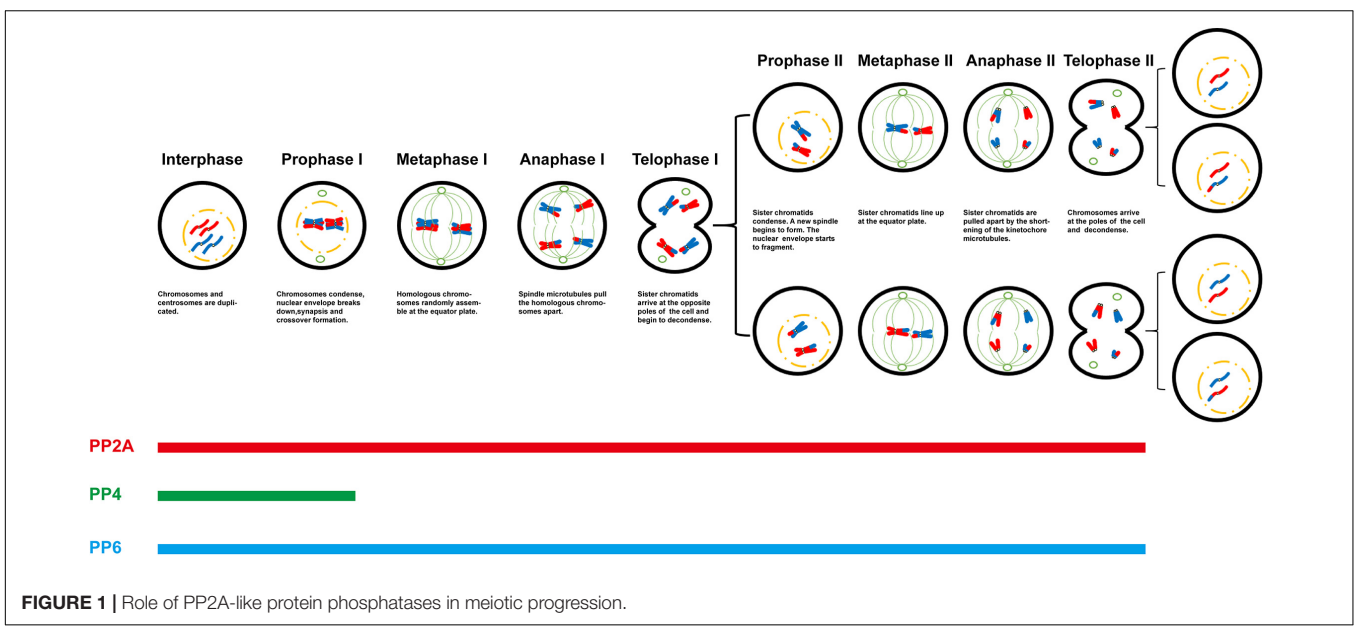

FIGURE 1 | Role of PP2A-like protein phosphatases in meiotic progression.

protein phosphatases in meiotic progress. In addition, the progress of short linear motifs (SLiM) also provides a method to study their biological functions and distinct substrates. These will fill the gaps in the regulation networks of phosphorylation.

AUTHOR CONTRIBUTIONS

W-LL collected the data, drew the picture and tables, and wrote the manuscript. W-PQ and Q-YS revised the manuscript. All authors contributed to the article and approved the submitted version.

FUNDING

This work was supported by grants from the National Natural Science Foundation of China (31530049) and the Guangdong Basic and Applied Basic Research Foundation (2020A1515011414).

REFERENCES

Adhikari, D., Diril, M. K., Busayavalasa, K., Risal, S., Nakagawa, S., Lindkvist, R., et al. (2014). Mastl is required for timely activation of APC/C in meiosis I and Cdk1 reactivation in meiosis II. *J. Cell Biol.* 206, 843–853. doi: 10.1083/jcb.201406033

Afshar, K., Werner, M. E., Tse, Y. C., Glotzer, M., and Gönczy, P. (2016). Regulation of cortical contractility and spindle positioning by the protein phosphatase 6 PPH-6 in one-cell stage C. elegans embryos. *Development* 143:2689. doi: 10.1242/dev.141515

Arguello-Miranda, O., Zagoriy, I., Mengoli, V., Rojas, J., Jonak, K., Oz, T., et al. (2017). Casein Kinase 1 Coordinates Cohesin Cleavage. Gametogenesis, and Exit from M Phase in Meiosis II. *Dev. Cell* 40, 37–52. doi: 10.1016/j.devcel.2016.11.021

Barbosa, P., Zhaunova, L., Debilio, S., Steccanella, V., Kelly, V., Ly, T., et al. (2021). SCF-Fbxo42 promotes synaptonemal complex assembly by downregulating PP2A-B56. *J.Cell Biol.* 220:202009167. doi: 10.1083/jcb.202009167

Bel Borja, L., Soubigou, F., Taylor, S. J. P., Fraguas Bringas, C., Budrewicz, J., Lara-Gonzalez, P., et al. (2020). BUB-1 targets PP2A:B56 to regulate chromosome congression during meiosis I in C. elegans oocytes. *eLife* 9:65307. doi: 10.7554/eLife.65307

Berchowitz, L. E., and Copenhaver, G. P. (2010). Genetic interference: don't stand so close to me. *Curr. Genomics* 11, 91–102. doi: 10.2174/138920210790886835

Bielinski, V. A., and Mumby, M. C. (2007). Functional analysis of the PP2A subfamily of protein phosphatases in regulating Drosophila S6 kinase. *Exp. Cell Res.* 313, 3117–3126. doi: 10.1016/j.yexcr.2007.05.008

Bishop, D. K., and Zickler, D. (2004). Early decision; meiotic crossover interference prior to stable strand exchange and synapsis. *Cell* 117, 9–15. doi: 10.1016/s0092-8674(04)00297-1

Bornslaeger, E. A., Mattei, P., and Schultz, R. M. (1986). Involvement of cAMP-dependent protein kinase and protein phosphorylation in regulation of mouse oocyte maturation. *Dev. Biol.* 114, 453–462. doi: 10.1016/0012-1606(86)90209-5

Brautigan, D. L. (2013). Protein Ser/Thr phosphatases–the ugly ducklings of cell signalling. *Febs* J. 280, 324–345. doi: 10.1111/j.1742-4658.2012.08609.x

Brautigan, D. L., and Shenolikar, S. (2018). Protein Serine/Threonine Phosphatases: Keys to Unlocking Regulators and Substrates. *Annu Rev Biochem* 87, 921–964. doi: 10.1146/annurev-biochem-062917-012332

Canela, N., Rodriguez-Vilarrupla, A., Estanyol, J. M., Diaz, C., Pujol, M. J., Agell, N., et al. (2003). The SET protein regulates G2/M transition by modulating cyclin B-cyclin-dependent kinase 1 activity. *J. Biol. Chem.* 278, 1158–1164. doi: 10.1074/jbc.M207497200

Cassimeris, L. (1999). Accessory protein regulation of microtubule dynamics throughout the cell cycle. *Curr. Opin. Cell Biol.* 11, 134–141. doi: 10.1016/s0955-0674(99)80017-9

Chen, M. J., Dixon, J. E., and Manning, G. (2017). Genomics and evolution of protein phosphatases. *Sci. Signal.* 10:aag1796. doi: 10.1126/scisignal.aag1796

Cohen, P. T., Philp, A., and Vazquez-Martin, C. (2005). Protein phosphatase 4–from obscurity to vital functions. *FEBS Lett.* 579, 3278–3286. doi: 10.1016/j.febslet.2005.04.070

Falk, J. E., Chan, A. C., Hoffmann, E., and Hochwagen, A. (2010). A Mec1- and PP4-dependent checkpoint couples centromere pairing to meiotic recombination. *Dev. Cell* 19, 599–611. doi: 10.1016/j.devcel.2010.09.006

Gomez, R., Felipe-Medina, N., Ruiz-Torres, M., Berenguer, I., Viera, A., Perez, S., et al. (2016). Sororin loads to the synaptonemal complex central region independently of meiotic cohesin complexes. *EMBO Rep.* 17, 695–707. doi: 10.15252/embr.201541060

Han, F., Dong, M. Z., Lei, W. L., Xu, Z. L., Gao, F., Schatten, H., et al. (2020). Oligoasthenoteratospermia and sperm tail bending in PPP4C-deficient mice. *Mol. Hum. Reprod* 2020:gaaa083. doi: 10.1093/molehr/gaaa083

Heim, A., Tischer, T., and Mayer, T. U. (2018). Calcineurin promotes APC/C activation at meiotic exit by acting on both XErp1 and Cdc20. *EMBO Rep.* 19:201846433. doi: 10.15252/embr.201846433

Hu, M. W., Meng, T. G., Jiang, Z. Z., Dong, M. Z., Schatten, H., Xu, X., et al. (2016). Protein Phosphatase 6 Protects Prophase I-Arrested Oocytes by Safeguarding Genomic Integrity. *PLoS Genet.* 12:e1006513. doi: 10.1371/journal.pgen.1006513

Hu, M. W., Wang, Z. B., Jiang, Z. Z., Qi, S. T., Huang, L., Liang, Q. X., et al. (2014). Scaffold subunit Aalpha of PP2A is essential for female meiosis and fertility in mice. *Biol. Reprod* 91:19. doi: 10.1095/biolreprod.114.120220

Hu, M. W., Wang, Z. B., Teng, Y., Jiang, Z. Z., Ma, X. S., Hou, N., et al. (2015). Loss of protein phosphatase 6 in oocytes causes failure of meiosis II exit and impaired female fertility. *J. Cell Sci.* 128, 3769–3780. doi: 10.1242/jcs.173179

Hunter, T. (1995). Protein kinases and phosphatases: the yin and yang of protein phosphorylation and signaling. *Cell* 80, 225–236. doi: 10.1016/0092-8674(95)90405-0

Hunter, T. (2014). The genesis of tyrosine phosphorylation. *Cold Spring Harb. Perspect. Biol.* 6:a020644. doi: 10.1101/cshperspect.a020644

Janssens, V., and Goris, J. (2001). Protein phosphatase 2A: a highly regulated family of serine/threonine phosphatases implicated in cell growth and signalling. *Biochem J.* 353(Pt 3), 417–439. doi: 10.1042/0264-6021:3530417

Jonak, K., Zagoriy, I., Oz, T., Graf, P., Rojas, J., Mengoli, V., et al. (2017). APC/C-Cdc20 mediates deprotection of centromeric cohesin at meiosis II in yeast. *Cell Cycle* 16, 1145–1152. doi: 10.1080/15384101.2017.1320628

Keating, L., Touati, S. A., and Wassmann, K. (2020). A PP2A-B56-Centered View on Metaphase-to-Anaphase Transition in Mouse Oocyte Meiosis I. *Cells* 9:9020390. doi: 10.3390/cells9020390

Kerk, D., Templeton, G., and Moorhead, G. B. (2008). Evolutionary radiation pattern of novel protein phosphatases revealed by analysis of protein data from the completely sequenced genomes of humans, green algae, and higher plants. *Plant Physiol.* 146, 351–367. doi: 10.1104/pp.107.111393

Kerr, G. W., Wong, J. H., and Arumugam, P. (2016). PP2A(Cdc55)'s role in reductional chromosome segregation during achiasmate meiosis in budding yeast is independent of its FEAR function. *Sci. Rep.* 6:30397. doi: 10.1038/srep30397

Kitajima, T. S., Sakuno, T., Ishiguro, K., Iemura, S., Natsume, T., Kawashima, S. A., et al. (2006). Shugoshin collaborates with protein phosphatase 2A to protect cohesin. *Nature* 441, 46–52. doi: 10.1038/nature04663

Kloeker, S., and Wadzinski, B. E. (1999). Purification and identification of a novel subunit of protein serine/threonine phosphatase 4. *J. Biol. Chem.* 274, 5339–5347. doi: 10.1074/jbc.274.9.5339

Lad, C., Williams, N. H., and Wolfenden, R. (2003). The rate of hydrolysis of phosphomonoester dianions and the exceptional catalytic proficiencies of protein and inositol phosphatases. *Proc. Natl. Acad. Sci. U S A* 100, 5607–5610. doi: 10.1073/pnas.0631607100

Lee, J., Kitajima, T. S., Tanno, Y., Yoshida, K., Morita, T., Miyano, T., et al. (2008). Unified mode of centromeric protection by shugoshin in mammalian oocytes and somatic cells. *Nat Cell Biol* 10, 42–52. doi: 10.1038/ncb1667

Lei, W. L., Han, F., Hu, M. W., Liang, Q. X., Meng, T. G., Zhou, Q., et al. (2020). Protein phosphatase 6 is a key factor regulating spermatogenesis. *Cell Death Differ* 27, 1952–1964. doi: 10.1038/s41418-019-0472-9

Liang, S., Guo, J., Choi, J. W., Shin, K. T., Wang, H. Y., Jo, Y. J., et al. (2017). Protein phosphatase 2A regulatory subunit B55alpha functions in mouse oocyte maturation and early embryonic development. *Oncotarget* 8, 26979–26991. doi: 10.18632/oncotarget.15927

Lillo, C., Kataya, A. R., Heidari, B., Creighton, M. T., Nemie-Feyissa, D., Ginbot, Z., et al. (2014). Protein phosphatases PP2A, PP4 and PP6: mediators and regulators in development and responses to environmental cues. *Plant. Cell Environ.* 37, 2631–2648. doi: 10.1111/pce.12364

Lu, Q., Dunn, R. L., Angeles, R., and Smith, G. D. (2002). Regulation of spindle formation by active mitogen-activated protein kinase and protein phosphatase 2A during mouse oocyte meiosis. *Biol. Reprod.* 66, 29–37. doi: 10.1095/biolreprod66.1.29

Lu, Q., Smith, G. D., Chen, D. Y., Yang, Z., Han, Z. M., Schatten, H., et al. (2001). Phosphorylation of mitogen-activated protein kinase is regulated by protein kinase C, cyclic 3′,5′-adenosine monophosphate, and protein phosphatase modulators during meiosis resumption in rat oocytes. *Biol. Reprod* 64, 1444–1450. doi: 10.1095/biolreprod64.5.1444

Matsuo, M., Onuma, T. A., Omotezako, T., and Nishida, H. (2020). Protein phosphatase 2A is essential to maintain meiotic arrest, and to prevent Ca(2+) burst at spawning and eventual parthenogenesis in the larvacean Oikopleura dioica. *Dev. Biol.* 460, 155–163. doi: 10.1016/j.ydbio.2019.12.005

Mumby, M. C., and Walter, G. (1993). Protein serine/threonine phosphatases: structure, regulation, and functions in cell growth. *Physiol. Rev.* 73, 673–699. doi: 10.1152/physrev.1993.73.4.673

Nasa, I., and Kettenbach, A. N. (2020). Effects of carboxyl-terminal methylation on holoenzyme function of the PP2A subfamily. *Biochem. Soc. Transac.* 48, 2015–2027. doi: 10.1042/bst20200177

Nilsson, J. (2019). Protein phosphatases in the regulation of mitosis. *J. Cell Biol.* 218, 395–409. doi: 10.1083/jcb.201809138

Pan, X., Chen, X., Tong, X., Tang, C., and Li, J. (2015). Ppp2ca knockout in mice spermatogenesis. *Reproduction* 149, 385–391. doi: 10.1530/REP-14-0231

Pearlman, S. M., Serber, Z., and Ferrell, J. E. Jr. (2011). A mechanism for the evolution of phosphorylation sites. *Cell* 147, 934–946. doi: 10.1016/j.cell.2011.08.052

Pinto, B. S., and Orr-Weaver, T. L. (2017). Drosophila protein phosphatases 2A B' Wdb and Wrd regulate meiotic centromere localization and function of the MEI-S332 Shugoshin. *Proc. Natl. Acad. Sci. U S A* 114, 12988–12993. doi: 10.1073/pnas.1718450114

Previato de Almeida, L., Evatt, J. M., Chuong, H. H., Kurdzo, E. L., Eyster, C. A., et al. (2019). Shugoshin protects centromere pairing and promotes segregation of nonexchange partner chromosomes in meiosis. *Proc. Natl. Acad. Sci. U S A* 116, 9417–9422. doi: 10.1073/pnas.1902526116

Price, N. E., and Mumby, M. C. (2000). Effects of regulatory subunits on the kinetics of protein phosphatase 2A. *Biochemistry* 39, 11312–11318. doi: 10.1021/bi0008478

Qi, S. T., Wang, Z. B., Ouyang, Y. C., Zhang, Q. H., Hu, M. W., Huang, X., et al. (2013). Overexpression of SETbeta, a protein localizing to centromeres, causes precocious separation of chromatids during the first meiosis of mouse oocytes. *J. Cell Sci.* 126(Pt 7), 1595–1603. doi: 10.1242/jcs.116541

Rattani, A., Wolna, M., Ploquin, M., Helmhart, W., Morrone, S., Mayer, B., et al. (2013). Sgol2 provides a regulatory platform that coordinates essential cell cycle processes during meiosis I in oocytes. *Elife* 2:e01133. doi: 10.7554/eLife.01133

Sato-Carlton, A., Li, X., Crawley, O., Testori, S., Martinez-Perez, E., Sugimoto, A., et al. (2014). Protein phosphatase 4 promotes chromosome pairing and synapsis, and contributes to maintaining crossover competence with increasing age. *PLoS Genet.* 10:e1004638. doi: 10.1371/journal.pgen.1004638

Saurin, A. T. (2018). Kinase and Phosphatase Cross-Talk at the Kinetochore. *Front. Cell Dev. Biol.* 6:62. doi: 10.3389/fcell.2018.00062

Stefansson, B., and Brautigan, D. L. (2006). Protein phosphatase 6 subunit with conserved Sit4-associated protein domain targets IkappaBepsilon. *J. Biol. Chem.* 281, 22624–22634. doi: 10.1074/jbc.M601772200

Stefansson, B., Ohama, T., Daugherty, A. E., and Brautigan, D. L. (2008). Protein phosphatase 6 regulatory subunits composed of ankyrin repeat domains. *Biochemistry* 47, 1442–1451. doi: 10.1021/bi7022877

Su, Y. Q., Sugiura, K., Sun, F., Pendola, J. K., Cox, G. A., Handel, M. A., et al. (2012). MARF1 regulates essential oogenic processes in mice. *Science* 335, 1496–1499. doi: 10.1126/science.1214680

Subramani, S., Jayapalan, S., Kalpana, R., and Natarajan, J. (2013). HomoKinase: A Curated Database of Human Protein Kinases. *ISRN Computational. Biol.* 2013:417634. doi: 10.1155/2013/417634

Sumiyoshi, E., Sugimoto, A., and Yamamoto, M. (2002). Protein phosphatase 4 is required for centrosome maturation in mitosis and sperm meiosis in C. elegans. *J. Cell Sci.* 115(Pt 7), 1403–1410.

Tang, A., Shi, P., Song, A., Zou, D., Zhou, Y., Gu, P., et al. (2016). PP2A regulates kinetochore-microtubule attachment during meiosis I in oocyte. *Cell Cycle* 15, 1450–1461. doi: 10.1080/15384101.2016.1175256

Wolgemuth, D. J., and Roberts, S. S. (2010). Regulating mitosis and meiosis in the male germ line: critical functions for cyclins. *Philos. Trans. R. Soc. Lond. B Biol. Sci.* 365, 1653–1662. doi: 10.1098/rstb.2009.0254

Yoshida, S., Kaido, M., and Kitajima, T. S. (2015). Inherent Instability of Correct Kinetochore-Microtubule Attachments during Meiosis I in Oocytes. *Dev. Cell* 33, 589–602. doi: 10.1016/j.devcel.2015.04.020

Yu, C., Ji, S. Y., Sha, Q. Q., Sun, Q. Y., and Fan, H. Y. (2015). CRL4-DCAF1 ubiquitin E3 ligase directs protein phosphatase 2A degradation to control oocyte meiotic maturation. *Nat. Commun.* 6:8017. doi: 10.1038/ncomms9017

Conflict of Interest: The authors declare that the research was conducted in the absence of any commercial or financial relationships that could be construed as a potential conflict of interest.

Copyright © 2021 Lei, Qian and Sun. This is an open-access article distributed under the terms of the Creative Commons Attribution License (CC BY). The use, distribution or reproduction in other forums is permitted, provided the original author(s) and the copyright owner(s) are credited and that the original publication in this journal is cited, in accordance with accepted academic practice. No use, distribution or reproduction is permitted which does not comply with these terms.

frontiers in Cell and Developmental Biology

REVIEW
published: 02 March 2021
doi: 10.3389/fcell.2021.642737

Mechanism and Control of Meiotic DNA Double-Strand Break Formation in *S. cerevisiae*

*Vikash Kumar Yadav and Corentin Claeys Bouuaert**

Louvain Institute of Biomolecular Science and Technology, Université catholique de Louvain, Louvain-La-Neuve, Belgium

Developmentally programmed formation of DNA double-strand breaks (DSBs) by Spo11 initiates a recombination mechanism that promotes synapsis and the subsequent segregation of homologous chromosomes during meiosis. Although DSBs are induced to high levels in meiosis, their formation and repair are tightly regulated to minimize potentially dangerous consequences for genomic integrity. In *S. cerevisiae*, nine proteins participate with Spo11 in DSB formation, but their molecular functions have been challenging to define. Here, we describe our current view of the mechanism of meiotic DSB formation based on recent advances in the characterization of the structure and function of DSB proteins and discuss regulatory pathways in the light of recent models.

Keywords: double-strand break, DNA recombination, meiosis, Spo11, phase separation

OPEN ACCESS

Edited by:
Akira Shinohara,
Osaka University, Japan

Reviewed by:
Bernard De Massy,
Université de Montpellier, France
Valérie Borde,
Centre National de la Recherche Scientifique (CNRS), France

***Correspondence:**
Corentin Claeys Bouuaert
corentin.claeys@uclouvain.be

Specialty section:
This article was submitted to Cell Growth and Division, a section of the journal Frontiers in Cell and Developmental Biology

Received: *16 December 2020*
Accepted: *01 February 2021*
Published: *02 March 2021*

Citation:
Yadav VK and Claeys Bouuaert C (2021) Mechanism and Control of Meiotic DNA Double-Strand Break Formation in S. cerevisiae. Front. Cell Dev. Biol. 9:642737. doi: 10.3389/fcell.2021.642737

INTRODUCTION

Genomes are continuously damaged by endogenous and exogenous factors and must be accurately repaired to maintain genome integrity and function (Ceccaldi et al., 2016; Kim et al., 2016). Homologous recombination is an ancient and universal mechanism that achieves accurate repair of DNA double-strand breaks (DSBs) by copying information from an intact template (Symington, 2016; Wright et al., 2018). This repair mechanism was hijacked early during eukaryotic evolution to achieve two key goals in meiosis. First, to exchange genetic material between chromosomes, thereby breaking up allelic linkage groups and promoting genetic diversity. Second, to provide physical connections between homologous chromosomes that allow their alignment along the meiotic spindle and their accurate segregation, thereby producing chromosomally balanced haploid gametes and maintain stable genomic contents between generations (Page and Hawley, 2003; Petronczki et al., 2003; Wilkins and Holliday, 2009; Hunter, 2015; **Figure 1A**). Meiotic cells trigger recombination by deliberately damaging their DNA, producing hundreds of DSBs per meiosis in yeast or mice (Sun et al., 1989; Keeney, 2008; Pan et al., 2011; Kauppi et al., 2013).

Meiotic DSBs are produced by the evolutionarily conserved topoisomerase-derived protein, Spo11, along with a cohort of partner subunits (Bergerat et al., 1997; Keeney et al., 1997; Keeney, 2008; Lam and Keeney, 2015). Following break formation, Spo11 remains covalently attached to the 5′-strands at both DNA ends and is released by an endonucleolytic cleavage reaction mediated by MRX (Mre11, Rad50, and Xrs2) and Sae2, which liberates Spo11 attached to a short oligonucleotide (Neale et al., 2005; **Figure 1B**). The 5′-strands are further resected by 5′-3′ exonucleases (Exo1 in yeast) to produce long single-stranded tails, which are coated with ssDNA-binding protein RPA (Sun et al., 1991; Zakharyevich et al., 2010; Garcia et al., 2011; Schiller et al., 2014; Symington, 2016; Mimitou et al., 2017). RPA is then replaced by recombinases Rad51 and Dmc1 that form a

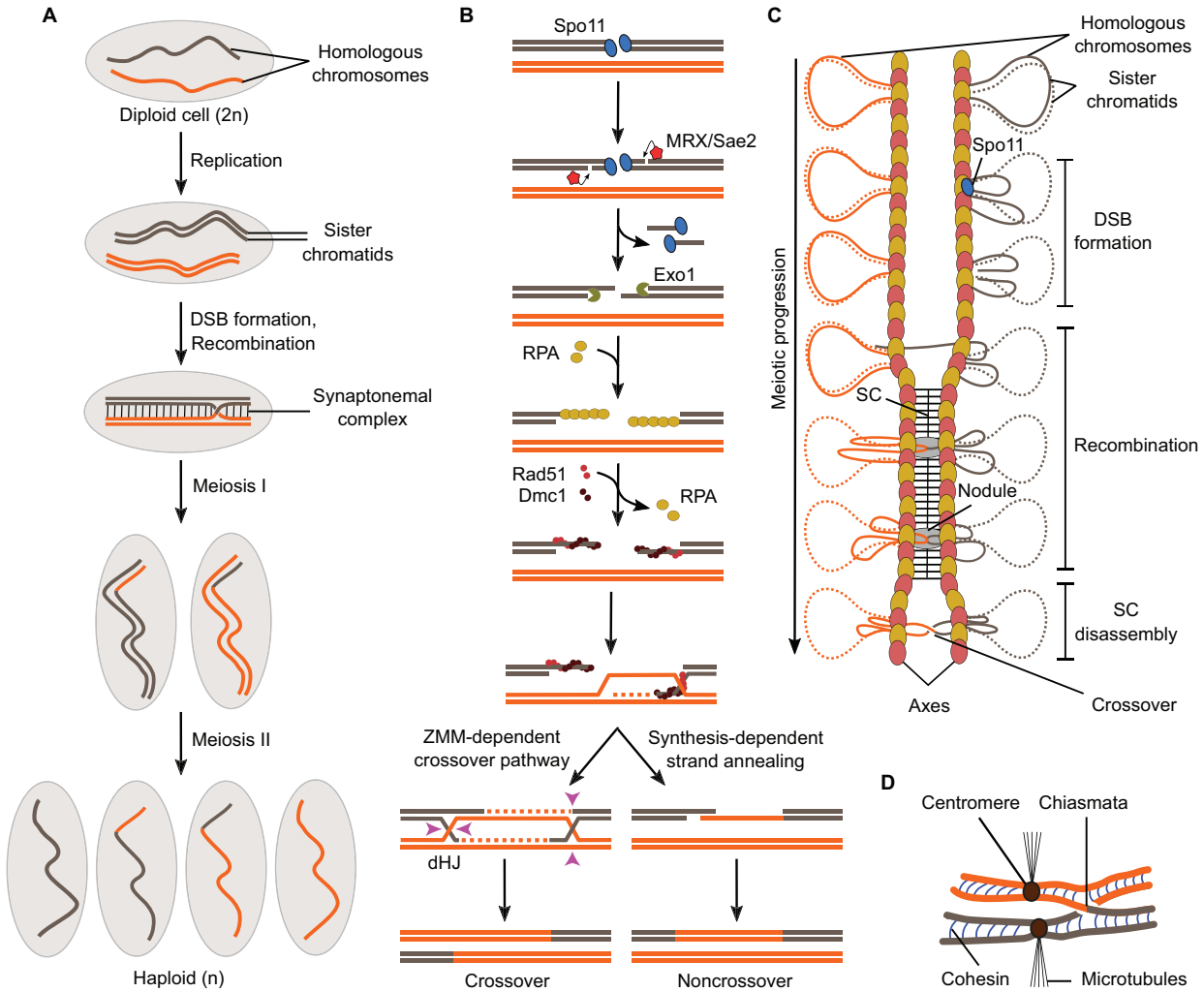

FIGURE 1 | Overview of meiosis and meiotic recombination. **(A)** Schematic of the formation of haploid gametes from a diploid cell with a single pair of homologous chromosomes. DSB formation and recombination promote homolog pairing and lead to the exchange of chromosomal fragments (crossovers) in the context of synapsed chromosomes. **(B)** Meiotic recombination is initiated by Spo11-mediated DSB formation and leads to the formation of crossovers via a ZMM-dependent double Holliday Junction (dHJ) resolution pathway or non-crossovers by synthesis-dependent strand annealing. **(C)** Relationships between meiotic recombination and higher-order chromosome structure. DSB formation happens in the context of the loop-axis structure. As recombination progresses, the SC polymerizes between the axes and is disassembled prior to chromosome segregation. Axis proteins Red1 (red ovals) and Hop1 (yellow ovals) are shown. **(D)** In metaphase I, homologs are held together through chiasmata and sister chromatid cohesion.

nucleoprotein filament and search for sequence similarity preferentially located on the homologous chromosome, producing D-loop structures (Hong et al., 2001; San Filippo et al., 2008; Brown and Bishop, 2015). Following DNA synthesis using the homolog as a repair template, the recombination structures experience one of two main outcomes (Allers and Lichten, 2001; Hunter and Kleckner, 2001; Bishop and Zickler, 2004; De Muyt et al., 2012; Pyatnitskaya et al., 2019; **Figure 1B**). The invading strand can be ejected from the donor by action of helicases, which provides an opportunity for the DNA ends to re-anneal. This process is referred to as synthesis-dependent strand annealing and produces non-crossovers, that is, products not associated with reciprocal exchanges of chromosome fragments, but with local transfer of genetic information from the repair template to the broken molecule (gene conversion) (Palmer et al., 2003; Martini et al., 2011). Alternatively, recombination structures are stabilized by the "ZMM" family of proteins and channeled through a pathway that produces mostly crossovers (Börner et al., 2004; Lynn et al., 2007; Pyatnitskaya et al., 2019). Here, both ends of the break engage the donor to form a double Holliday Junction intermediate, which is resolved through a crossover-specific pathway that involves MutLγ and Exo1 (Schwacha and Kleckner, 1995; Zakharyevich et al., 2012; Gray and Cohen, 2016; Pyatnitskaya et al., 2019).

Every aspect of meiotic recombination is tied to the structural organization of the chromosomes (**Figure 1C**). Early in meiotic prophase, chromosomes organize as series of DNA loops that are anchored along a nucleoprotein axis. DSB formation happens

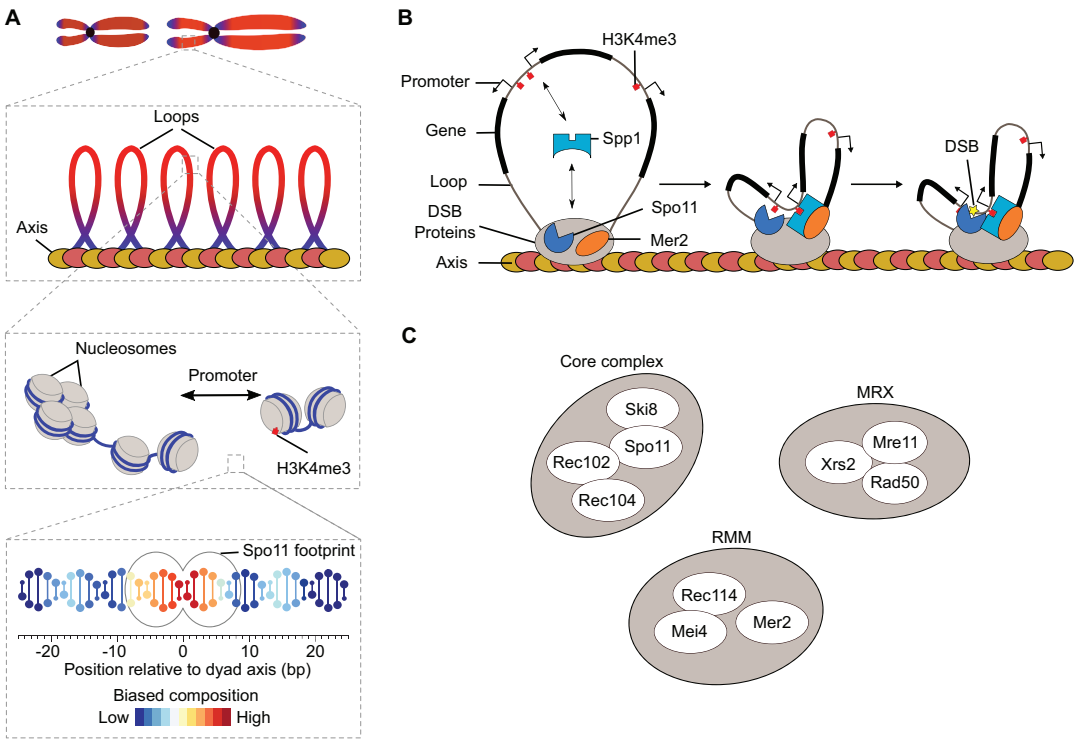

FIGURE 2 | DSB formation in *S. cerevisiae*. **(A)** The distribution of meiotic DSBs is influenced by a combination of factors that operates at various size scales (Pan et al., 2011). Spo11 footprint indicates the expected occupancy of Spo11 on DNA based on structural modeling. **(B)** The tethered loop-axis model for DSB formation. Spp1 binds to H3K4me2/3 enriched around DSB hotspots and connects it to the chromosome axis through interaction with Mer2. Axis proteins Red1 (red ovals) and Hop1 (yellow ovals) are shown. **(C)** Ten DSB proteins in *S. cerevisiae*.

in the context of this loop-axis structure. As recombination progresses, polymerization of a proteinaceous structure called the synaptonemal complex (SC) initiates between the two axes and elongates along their entire length (Kleckner, 2006; Zickler and Kleckner, 2015; **Figure 1C**). Recombination proceeds within the SC, inside a nodule embedded between the axes (Zickler and Kleckner, 1999). After recombination is completed, the SC disassembles and crossovers, now cytologically visible as chiasmata, provide physical connections between the homologs until their segregation at anaphase (**Figure 1D**).

Here, we discuss current models for meiotic DSB formation, focusing on the molecular mechanisms in *S. cerevisiae*. We present recent advances in deciphering the structure and function of proteins required for DSB formation, their interactions and relationships with chromosome organization, and discuss the mechanisms that regulate DSB formation in the light of these new models.

MEIOTIC DSB FORMATION IN *S. cerevisiae*

Meiotic DSBs are distributed non-randomly throughout the genome and concentrated within distinct regions of the chromosomes called hotspots, typically ∼50–300 base-pairs wide (Baudat and Nicolas, 1997; Petes, 2001; Buhler et al., 2007; Pan et al., 2011). The primary factor determining hotspot locations in yeast is chromatin accessibility (Baudat and Nicolas, 1997; Berchowitz et al., 2009; Pan et al., 2011). Indeed, the vast majority of the ∼3,600 *S. cerevisiae* hotspots localize within nucleosome-depleted regions at promoters (Pan et al., 2011). However, non-randomness, in terms of break distribution and intensity, can also be observed at the chromosomal scale and at the sequence level (Wu and Lichten, 1994; Lichten and Goldman, 1995; Berchowitz et al., 2009; Pan et al., 2011; **Figure 2A**). Indeed, chromosome size impacts DSB formation, with smaller chromosomes experiencing higher DSB densities (Pan et al., 2011; Murakami et al., 2020). DSBs are suppressed near telomeres and centromeres, and chromosomal domains with higher or lower DSB frequency alternate, correlating positively with GC content (Baudat and Nicolas, 1997; Borde et al., 1999; Gerton et al., 2000; Petes, 2001; Blat et al., 2002; Blitzblau et al., 2007; Buhler et al., 2007; Pan et al., 2011). Hotpots themselves tend to be AT-rich and are flanked by sequences enriched for the histone H3 lysine 4 trimethylation (H3K4me3) mark (Borde et al., 2009; Pan et al., 2011; Tischfield and Keeney, 2012). In addition, break formation displays sequence bias within and around the footprint of Spo11 and at the cleavage site, with a preference for cleavage 3′ of a C (Murakami and Nicolas, 2009; Pan et al., 2011; **Figure 2A**).

Although DSB formation happens primarily within chromatin loops, most of the DSB proteins are enriched along the chromosome axis (Kugou et al., 2009; Pan et al., 2011;

Panizza et al., 2011). The tethered loop-axis model reconciles these findings by suggesting that DSB formation involves the capture of a DNA loop by axis-bound DSB proteins, allowing Spo11 to cleave the loop (Blat et al., 2002; Kleckner, 2006; Kim et al., 2010; Panizza et al., 2011; **Figure 2B**). The COMPASS subunit Spp1 was identified as a key player that connects the loops to the axis via interactions with H3K4me3 marks located at gene promoters and the axis-bound DSB protein, Mer2 (Acquaviva et al., 2013; Sommermeyer et al., 2013).

THE MEIOTIC DSB PROTEINS

In *S. cerevisiae*, ten proteins collaborate to form DSBs, and they can be separated into three sub-groups (**Figure 2C**): the core complex (Spo11, Ski8, Rec102, and Rec104), the MRX complex, and the RMM proteins (Rec114, Mei4, and Mer2) (Lam and Keeney, 2015). All ten proteins are essential for DSB formation and their deletion lead to a similar meiotic phenotype in yeast: reduced homolog pairing, loss of meiotic recombination, failure to form the SC, and abnormal chromosomal segregation ultimately resulting in inviable spores (Game et al., 1980; Malone and Esposito, 1981; Klapholz et al., 1985; Menees and Roeder, 1989; Roeder et al., 1989; Malone et al., 1991; Engebrecht et al., 1991; Cool and Malone, 1992; Galbraith and Malone, 1992; Ivanov et al., 1992; Ajimura et al., 1993; Pittman et al., 1993; Rockmill et al., 1995; Gardiner et al., 1997; Lam and Keeney, 2015). Although the molecular mechanisms whereby DSB proteins collaborate during meiosis remain unclear, recent progress has been made to understand their structure, biochemical activities and regulation. Below, we provide an overview of meiotic DSB formation emphasizing some of these recent advances.

Spo11 and Topo VI

Spo11 evolved from the catalytic subunits of a type IIB topoisomerase, Topo VI (Bergerat et al., 1997; Keeney et al., 1997). Like other type II topoisomerases, Topo VI uses ATP binding and hydrolysis to coordinate the formation of a transient DSB to the passage of an intact duplex through the break, thereby modulating DNA topology (Corbett et al., 2007; Graille et al., 2008). Cleavage involves the coordinated action of two active-site tyrosines that attack opposite strands of the phosphoribose DNA backbone and produce 5′-phosphotyrosyl intermediates (**Figure 3A**). Both Topo VI and Spo11 produce staggered DSBs with 2-nucleotide 5′-overhangs (Liu et al., 1995; Buhler et al., 2001; Murakami and Nicolas, 2009). Spo11 can be thought of as a crippled topoisomerase in that it catalyzes break formation but is likely unable to perform strand passage and break re-sealing.

Topo VI has an A_2B_2 stoichiometry, where the A subunits perform DNA cleavage and the B subunits have ATP-binding and hydrolysis activities (Buhler et al., 2001; Corbett et al., 2007; Graille et al., 2008; **Figure 3B**). Although the relationship between Spo11 and Topo VIA has been recognized for over 20 years, whether Spo11 requires a B-type subunit for catalysis remained long a matter of conjecture (Bergerat et al., 1997; Buhler et al., 1998; Keeney, 2001). A few years ago, two studies eventually identified a B-type subunit in mice and plants and showed that they were essential for DSB formation (Robert et al., 2016; Vrielynck et al., 2016). This suggested that the meiotic DSB machinery is more similar to the ancestral topoisomerase than was previously appreciated. Nevertheless, while Spo11 is well-conserved and shares high sequence similarity with Topo VIA, the B-type subunits are very diverse between species and evolved almost beyond recognition from Topo VIB. Indeed, pairwise combinations of Spo11 and Topo VIA show typically 20–30% overall sequence identity with blocks that are much more conserved (Bergerat et al., 1997; Keeney et al., 1997). In contrast, conservation between the mouse Topo VIB-type subunit and *S. shibatae* Topo VIB is at best 11% identity over the most conserved 140 amino-acid block (Robert et al., 2016).

Topo VIA is composed of a 5Y-CAP domain (related to the DNA-binding domain of the catabolite activator protein) and a Toprim domain (also found in type IIA topoisomerases and in primase) (Bergerat et al., 1997; Nichols et al., 1999; Corbett et al., 2007; Graille et al., 2008; **Figure 3C**). Both domains participate in DNA binding and together form a groove that intimately engages the double helix (**Figure 3D**). The catalytic tyrosine is located in the 5Y-CAP domain and the Toprim domain coordinates Mg^{2+} ions important for catalysis. A composite active site is formed with the catalytic tyrosine and metal-ion binding pockets contributed by different subunits. Therefore, DNA cleavage necessarily requires dimerization of the A subunits. Topo VIB has an N-terminal GHKL-fold ATPase domain (found in DNA gyrase, Hsp90, Histidine Kinase, and MutL) responsible for nucleotide binding and ATP hydrolysis, a central helix two-turn helix (H2TH) fold and a C-terminal transducer domain with an extended α-helix that connects the B subunit to the 5Y-CAP domain of the A subunit (Corbett and Berger, 2003, 2005; Corbett et al., 2007; Graille et al., 2008; **Figures 3C,D**).

Topo VI functions through a two-gate mechanism (Corbett et al., 2007; Wendorff and Berger, 2018; **Figure 3E**). In its apo state, Topo VI dimerizes through the A subunits to form a U-shaped complex that can engage DNA. Topo VI binds two DNA segments, either sequentially or simultaneously (Wendorff and Berger, 2018). The G-segment (gate) binds within the DNA-binding grove formed by the A subunits and interactions between the B subunit and DNA facilitate G-segment bending (Wendorff and Berger, 2018). Engagement of the second duplex activates ATP-dependent dimerization of the GHKL domain, thereby trapping the T-segment (transfer) (Corbett et al., 2007). Dimerization of the GHKL domain is communicated to the A subunit by the transducer domain to activate DNA cleavage, whereupon ATP hydrolysis induces a conformational change that opens the DNA gate and allows strand passage (**Figure 3E**). Finally, the DSB is resealed, ADP in released, the ATP gate reverts to its open state, and the enzyme can dissociate from the substrate or directly engage in another round of catalysis without dissociation (Wendorff and Berger, 2018).

The Spo11 Core Complex

S. *cerevisiae* Spo11 has long been known to closely associate with Ski8, Rec102, and Rec104 based on genetic and cytological evidence. Indeed, yeast-two-hybrid (Y2H) experiments showed

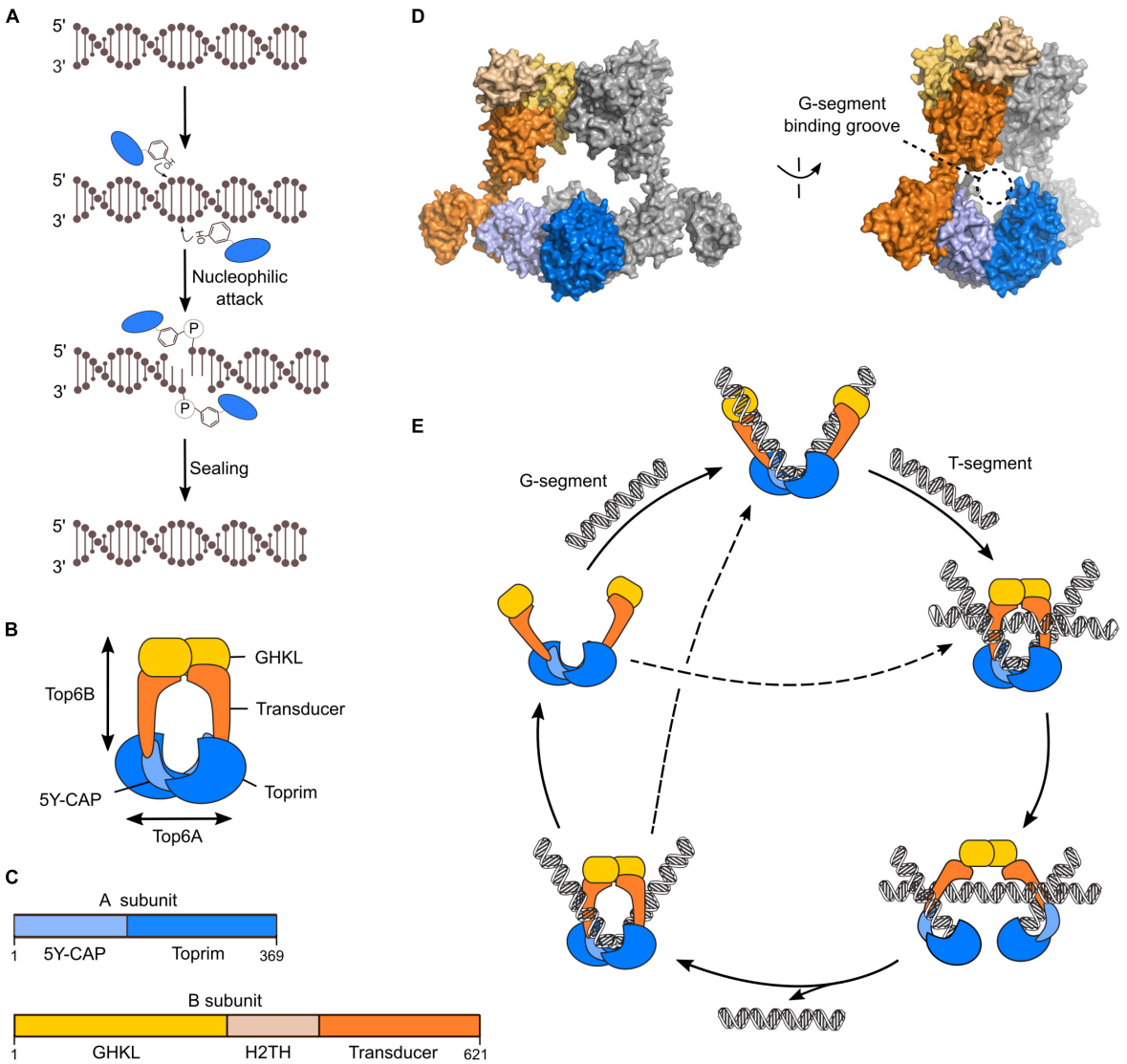

FIGURE 3 | Mechanism of Topo VI. **(A)** Chemistry of strand cleavage and re-sealing in Topo VI. **(B)** Cartoon of the Topo VI heterotetramer. **(C)** Domain structure of the A and B subunits of Topo VI. **(D)** Structure of Topo VI (PDB: 2Q2E) showing the expected position of the G-segment within the groove formed by the A subunits (Corbett et al., 2007). **(E)** Catalytic cycle of Topo VI through a two-gate mechanism. ATP-dependent dimerization of the GHKL domain upon sequential or simultaneous binding to gate (G) and transfer (T) DNA duplexes is communicated to the A subunit to activate DSB formation. Topo VI can undergo multiple catalytic cycles without dissociation from the G-segment.

strong interactions between Spo11 and Ski8, and between Rec102 and Rec104 (Arora et al., 2004; Kee et al., 2004; Maleki et al., 2007). Spo11 and Ski8 interaction is required for chromosomal localization of Rec102 and Rec104 (Arora et al., 2004; Kee et al., 2004). In addition, Rec102 and Rec104 are essential for the association of Spo11 to DSB hotspots and for Spo11 self-interaction (Prieler et al., 2005; Sasanuma et al., 2007). Furthermore, Y2H interactions with Rec114 suggested that Rec102/Rec104 may have a role to connect Spo11 with the RMM sub-group (Maleki et al., 2007).

Recent biochemical work has shown that Spo11 indeed interacts with Ski8, Rec102, and Rec104 to form a stoichiometric complex (Claeys Bouuaert et al., 2021; **Figure 4A**). This complex displays structural and functional similarities expected from its relationship with Topo VI, although with differences that presumably reflect their distinct biological functions (discussed below). Since DSB formation requires two Spo11 subunits and Topo VI has an A_2B_2 stoichiometry, the core complex was anticipated to form a dimer of tetramers. However, purified complexes turned out to have a 1:1:1:1 stoichiometry and are catalytically inactive *in vitro* (Claeys Bouuaert et al., 2021). Hence, Spo11 dimerization could be an important control mechanism for DSB formation. However, what triggers Spo11 dimerization and catalysis remains unclear.

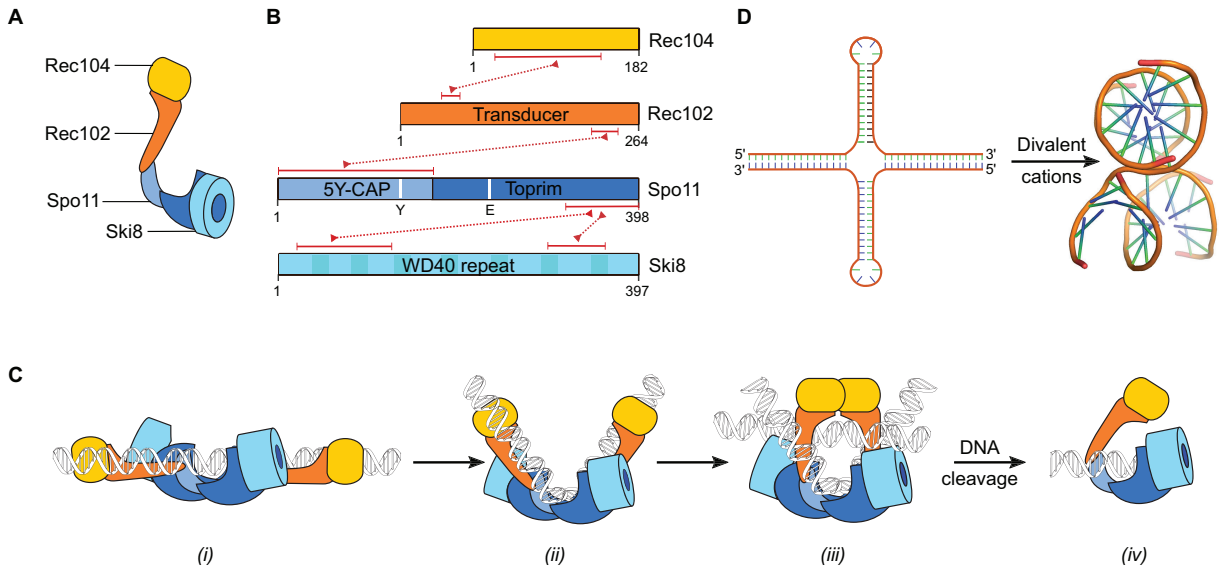

FIGURE 4 | The Spo11 core complex. **(A)** Cartoon illustrating the arrangement of the different subunits in the core complex. **(B)** Domain structure of Rec104, Rec102, Spo11, and Ski8. The red dotted lines connecting two proteins represent their respective interaction domains. The region of Rec104 that interacts with Rec102 is predicted based on crosslinking-mass spectrometry, other interaction regions were validated by mutagenesis (Arora et al., 2004; Cheng et al., 2009; Claeys Bouuaert et al., 2021). The position in Spo11 of the catalytic tyrosine Y135 and metal-ion coordinating residue E233 are shown. **(C)** Proposed dynamics of the interaction between the core complex and DNA based on *in vitro* binding activities and analogy with Topo VI (Claeys Bouuaert et al., 2021). After DSB formation, Spo11 remains bound to the DSB through covalent and non-covalent interactions. **(D)** Inverted repeat sequences form cruciforms that fold into three-dimensional structures that are similar to two overlapping DNA duplexes (PDB: 1DCW) (Eichman et al., 2000).

Remote homology search had previously identified Rec102 as the Topo VIB-like subunit in *S. cerevisiae* (Robert et al., 2016). However, in contrast to the B-type subunit in mice and plants, Rec102 lacks the GHKL domain essential for ATP-dependent dimerization in Topo VI (**Figure 4B**). Crosslinking coupled to mass spectrometry and mutagenesis provided evidence that Rec104 occupies the position of the GHKL domain in the core complex (Claeys Bouuaert et al., 2021). Structural predictions were consistent with the possibility that Rec104 adopts a cryptic GHKL-like fold, but whether this is indeed the case needs to be confirmed. Rec104 lacks recognizable ATP-binding and hydrolysis motifs, while the B-type subunit in mice and plants retained some, but not all, the sequences thought to be important for ATP binding and hydrolysis (Robert et al., 2016; Vrielynck et al., 2016). Whether ATP is involved in meiotic break formation remains therefore unclear and it is possible that the answer differs between organisms.

In addition to Spo11 and Rec102/Rec104 that jointly form the A and B subunits derived from Topo VI, the *S. cerevisiae* core complex has an additional subunit, Ski8, with as yet unknown functions (**Figure 4B**). In contrast to the other core complex proteins, Ski8 is not meiosis-specific. Indeed, Ski8 has a second, independent, function as part of the Ski complex, which is involved in mRNA decay via the exosome (Anderson and Parker, 1998; Halbach et al., 2013). In vegetative cells, Ski8 localizes to the cytoplasm, but in meiotic cells it localizes to the nucleus where it interacts with Spo11 and mediates its chromosomal localization (Arora et al., 2004; Claeys Bouuaert et al., 2021). Although the meiotic function of Ski8 is conserved in *S. pombe* (Evans et al., 1997) and *Sordaria* (Tessé et al., 2003), it is not conserved in *Arabidopsis* (Jolivet et al., 2006).

Ski8 contains tandem copies of WD repeats folded into a seven-bladed β-propeller (Madrona and Wilson, 2004; Cheng et al., 2009; **Figure 4B**). A conserved patch of hydrophobic residues located on the top surface of the β-propeller was implicated in the interactions with Ski3 and Spo11 (Cheng et al., 2009). Indeed, the crystal structure of the Ski complex showed that Ski3 interacts with two Ski8 subunits through a sequence motif (Q–R–x–x–Φ) also found in Spo11 (Halbach et al., 2013). Mutations within this motif abolish the Y2H interaction with Spo11 and meiotic recombination and compromises the integrity of the core complex *in vitro* (Arora et al., 2004; Claeys Bouuaert et al., 2021).

Analysis of the DNA-binding properties of the *S. cerevisiae* core complex showed that the presence of divalent metal ions and the metal-ion binding residues (E233) stabilize the interactions with DNA, but the catalytic tyrosine (Y135) does not impact DNA binding (Claeys Bouuaert et al., 2021). Binding specificities directed toward different DNA structures were observed and suggested that DSB formation may be preceded by a series of conformational transitions, similar to the mechanism of Topo VI (**Figure 4C**). The core complex binds with low-nanomolar affinity to DNA duplexes, its anticipated DNA substrate (**Figure 4C, *i***). Bound duplexes usually showed sharp ∼60° or ∼120° bends, and binding affinity was higher to pre-bent substrates than relaxed substrates, suggesting that Spo11 may bend its substrate prior to catalysis and/or bind preferentially to bendable sequences (**Figure 4C, *ii***). Core complexes had

particular affinity for positions where two DNA duplexes cross each other, such as plectonemic intertwinings of supercoiled DNA (Claeys Bouuaert et al., 2021). Binding to DNA junctions are reminiscent of other topoisomerases, including Topo VI (Corbett and Berger, 2005; Alonso-Sarduy et al., 2011; Wendorff and Berger, 2018), and suggest that core complexes dimerize in order to trap two duplexes (**Figure 4C, *iii***). However, the stoichiometry of this intermediate was not determined and alternative interpretations remain plausible, including that monomeric core complexes have two independent duplex-binding sites. Either way, the junction-binding activity of the core complex to DNA junctions is intriguing. If the complex has more than one duplex binding site, where is the second one located? If the complex traps two duplexes like Topo VI, what is the physiological relevance of this activity, since Spo11 activity presumably does not require strand passage?

An independent line of evidence provides potential support to the hypothesis that DSB formation happens in the context of trapped DNA junctions. Insertion of long palindromes (>50 bp) within the *S. cerevisiae* genome generate meiotic DSB hotspots (Nasar et al., 2000). Palindromic sequences can extrude as cruciform structures (Benham, 1982), which are structurally similar to two duplexes crossing each other (**Figure 4D**). Hence, perhaps palindromes generate DSB hotspots by providing a preferred binding substrate to Spo11 and/or by inducing Spo11 catalysis through signaling that two duplexes have been captured. Similarly, human topoisomerase IIβ recognizes and cleaves DNA substrates that form four-way junctions (West and Austin, 1999).

Finally, the core complex binds with high affinity to the ends of DNA duplexes *in vitro* (Claeys Bouuaert et al., 2021; **Figure 4C, *iv***). The end-binding activity was tightest with substrates that had a 2-nucleotide 5′-overhang identical to Spo11 cleavage products, suggesting that the core complex has intrinsic affinity for its product. Binding of Topo VI to the DSB intermediate has not been directly investigated, but in order for a topoisomerase to perform controlled strand passage, it must prevent swiveling of the DSB around the phosphotyrosyl bond and therefore hold on to both strands at both ends. Nevertheless, it is possible that Spo11 binds to DSB ends with much greater affinity than Topo VI. Indeed, since Spo11 does not turn over, increasing the stability of the complex from one intermediate to the next would help drive the reaction forward.

The significance of the end-binding activity is unclear, but it highlights the possibility that Spo11 binds strongly to DSBs after catalysis through covalent and non-covalent interactions. This may have implications regarding the first steps of DSB processing, since Spo11 could cap the DNA ends during resection and perhaps after strand invasion has initiated. Indeed, a recombination intermediate with Spo11-oligonucleotides capping the 3′-ends has been proposed to explain unanticipated patterns in genome-wide sequencing methods designed to map resection endpoints during meiosis in mice (Paiano et al., 2020; Yamada et al., 2020). In addition, scar-less repair by non-homologous end joining of meiotic DSBs that have undergone resection in a *Drosophila* strain with homolog pairing defects ($Mcm5^{A7}$) provided further support for end-capping by Spo11-oligonucleotides after resection had initiated (Hatkevich et al., 2020). Nevertheless, end-capping by Spo11-oligonucleotide complexes has not been formally demonstrated.

The MRX Complex

MRX is an evolutionarily-conserved complex that plays key functions in the maintenance of genomic integrity in somatic cells, including the recognition of DSBs, activation of the DNA-damage checkpoint, initiation of DSB resection, and telomere maintenance, in addition to essential roles during meiosis (Symington, 2016; Gnügge and Symington, 2017). In *S. cerevisiae*, MRX is essential for both the formation and processing of meiotic DSBs (Alani et al., 1990; Ivanov et al., 1992; Nairz and Klein, 1997; Keeney, 2001). The DSB-processing function of MRX depends on a single-strand endonuclease activity and a 3′-5′ exonuclease activity of Mre11 directed to the 5′-strand (**Figure 1B**; Paull and Gellert, 1998; Neale et al., 2005; Cannavo and Cejka, 2014). The endonuclease activity is controlled by phosphorylation of Sae2, which promotes its interaction with Rad50 (Cannavo et al., 2018). Indeed, a separation-of-function mutation of Rad50 (K81I) that supports DSB formation but blocks DSB processing abolishes the interaction with phosphorylated Sae2 (Alani et al., 1990; Cannavo et al., 2018).

While the function of MRX in processing DSBs is widely conserved, its role in promoting DSB formation has only been reported in budding yeast and *C. elegans* (Chin and Villeneuve, 2001). Indeed, MRX orthologs are not required for DSB formation in *A. thaliana* (Puizina et al., 2004) and *S. pombe* (Young et al., 2004), and whether they are required in mice remains unknown (Lam and Keeney, 2015). In *C. elegans*, MRE-11 and RAD-50 are important for DSB formation (Chin and Villeneuve, 2001; Hayashi et al., 2007), but NBS-1, the ortholog of Xrs2, is not (Girard et al., 2018).

In *S. cerevisiae*, MRX is thought to be recruited to the DSB machinery in part through interactions between Xrs2 and Mer2, based on Y2H experiments (Arora et al., 2004; Henderson et al., 2006). In addition, chromatin immunoprecipitation (ChIP) analyses show that Mre11 associates transiently to DSB sites independently of the catalytic activity of Spo11 (Borde et al., 2004). Mre11 binding to DSB hotspots requires all other DSB proteins, except Rad50, suggesting that MRX is the last component of the DSB machinery to be recruited. Perhaps MRX recruitment activates Spo11 catalysis, but how this may be achieved is unknown. It has been proposed that the requirement of the MRX complex prior to DSB formation ensures the coordination between DSB formation and subsequent repair to limit potential impacts on genomic instability (Borde et al., 2004). Indeed, breaks detected in wild-type cells are usually fully resected, indicating that they are processed faster than they accumulate, consistent with a coordination between DSB formation and repair (Bishop et al., 1992; Tran et al., 2002; Joshi et al., 2015; Mimitou et al., 2017).

Mre11 has an N-terminal nuclease domain containing five conserved phosphoesterase motifs that form the active site (**Figure 5A**; Arthur et al., 2004; Williams et al., 2008). Mre11 dimerizes via its phosphodiesterase domain, which is flanked by a capping domain and creates a U-shaped structure with a cleft

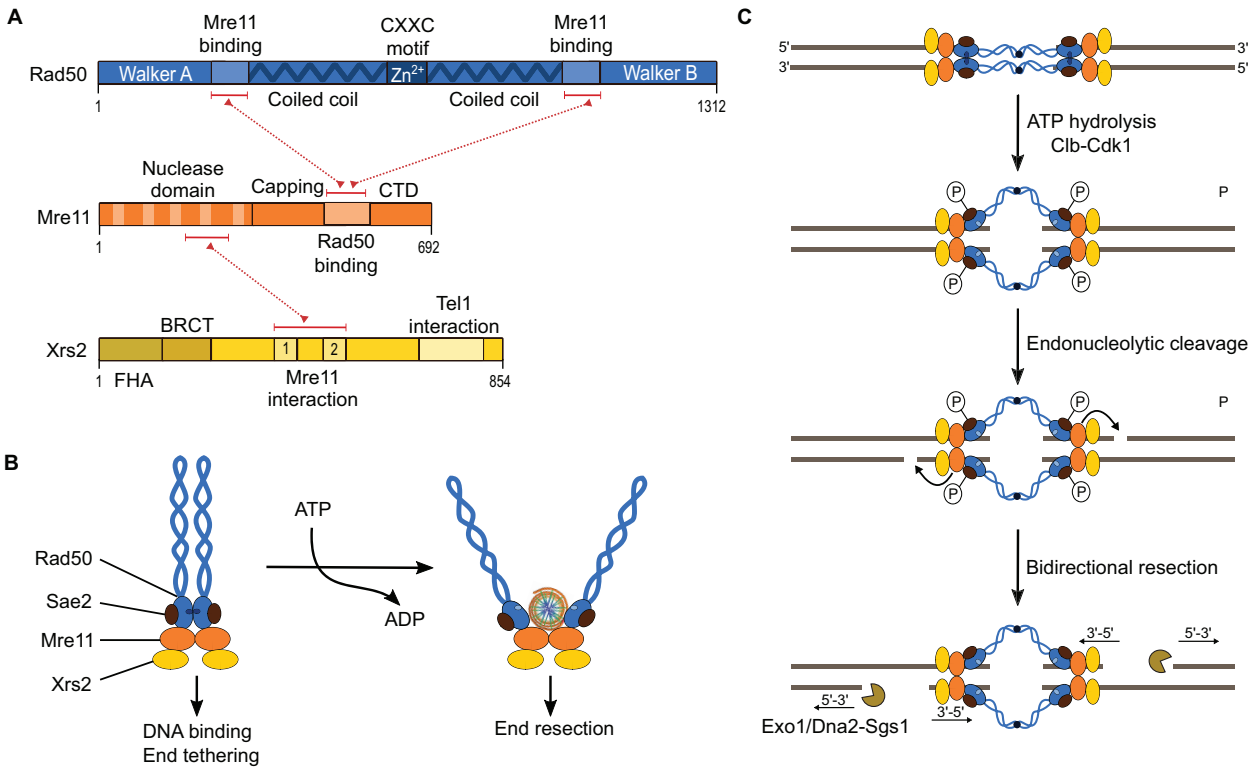

FIGURE 5 | The MRX complex. **(A)** Domain structure of Mre11, Rad50, and Xrs2, and their protein-protein interacting regions (red dotted lines). **(B)** Cartoon illustrating the structural arrangement of the MRX complex and the conformational dynamics upon ATP hydrolysis. In an ATP-bound state, the nuclease domain of Mre11 does not access DNA. However, after ATP hydrolysis by Rad50, a conformational change exposes the nuclease domain of Mre11 to DNA. Sae2 is illustrated here as interacting with Rad50 based on Cannavo et al. (2018), but interactions with Xrs2 have also been demonstrated (Liang et al., 2015). **(C)** Model for DSB resection by MRX. Endonuclease activity of Mre11 directed on the 5′-strand is followed by bi-directional resection through the 3′-5′ exonuclease activity of Mre11 and the 5′-3′ exonuclease activity of ExoI or Dna2-Sgs1 in vegetative conditions or ExoI in meiosis.

that binds DNA and Rad50 (**Figure 5B**). The capping domain is followed by a Rad50-interaction domain and a C-terminal domain with DNA-binding activity (Schiller et al., 2012). The C-terminal DNA-binding domain is dispensable for mitotic DNA repair but important for meiotic DSB formation (Furuse et al., 1998; Usui et al., 1998).

Rad50 is an ATPase with Walker A and B motifs located at its N- and C-termini, respectively (Hopfner et al., 2001; Gobbini et al., 2016; **Figure 5A**). These are separated by a long linker that folds into a dimeric coiled-coil with the ATP-binding domain at one end and a zinc-hook domain at the other (**Figure 5B**; Hopfner et al., 2002; Wiltzius et al., 2005). MRX complexes can tether the two ends of a DSB via Zn^{2+}-dependent dimerization of their hook domain (Hopfner et al., 2002; Hohl et al., 2010; Seifert et al., 2016; **Figure 5C**). Conformational changes within Rad50 upon ATP binding and hydrolysis control MRX function (Hopfner et al., 2001; Gobbini et al., 2016; Liu et al., 2016; Casari et al., 2019). In the presence of ATP, Rad50 adopts a closed dimeric conformation that occludes the nuclease domain of Mre11. Upon ATP hydrolysis, the Rad50 dimer dissociates, allowing the active site of Mre11 to access DNA (Hopfner et al., 2001; Liu et al., 2016; Casari et al., 2019; **Figures 5B,C**).

Xrs2 is thought to act as a molecular chaperone that connects Mre11 to other repair proteins, including Sae2 and the DNA-damage response kinase Tel1 (Oh et al., 2016). Xrs2 contains a fork-head associated (FHA) domain, a pair of BRCA1 C-terminus (BRCT) or BRCT-like domains, an Mre11-binding domain, and a Tel1-binding domain (Shima et al., 2005; **Figure 5A**). Xrs2 is essential for the nuclear localization of Mre11 (Tsukamoto et al., 2005). A mutation in Xrs2 that disrupts the interaction with Mre11 (K641E) abolishes its meiotic and vegetative functions (Tsukamoto et al., 2005). However, the Mre11-interaction domain alone (residues 630–662) is sufficient for Mre11 nuclear import and the DNA damage response but does not support meiotic recombination and telomere elongation. Although the FHA domain of Xrs2 was proposed to recruit Sae2 to the site of DNA damage (Liang et al., 2015), end resection remains Sae2-dependent in the absence of Xrs2 (Oh et al., 2016) and depends on interactions with Rad50 (Cannavo et al., 2018).

In vegetative cells, localization of Tel1 to the site of DNA damage is mediated by interactions between Tel1 and Xrs2 (Nakada et al., 2003; Iwasaki et al., 2016). Mutations in the Tel1-interaction motif of Xrs2 leads to DNA-damage signaling defects and short telomeres, similar to *tel1*Δ (Nakada et al., 2003). The FHA domain of Xrs2 has been shown to mediate robust Tel1

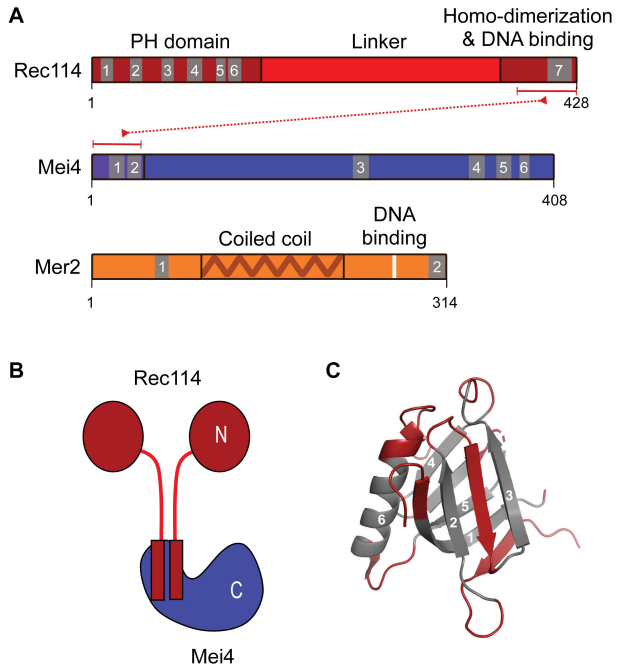

FIGURE 6 | The RMM proteins. **(A)** Domain structure of Rec114, Mei4, and Mer2 with regions involved in protein-protein and protein-DNA interactions (Claeys Bouuaert et al., 2021). Numbered blocks indicate conserved sequence motifs (Kumar et al., 2010; Tessé et al., 2017). **(B)** Schematic of the Rec114—Mei4 complex. **(C)** Structure of the Pleckstrin-homology domain of mouse REC114 (PDB: 6HFG) (Kumar et al., 2018). Residues in gray are the conserved motifs highlighted in **(A)**.

activation and to inhibit inaccurate DSB repair (Iwasaki et al., 2016). However, artificially tethering the Tel1-interaction domain of Xrs2 to an Mre11 construct containing a nuclear localization signal was sufficient for Tel1 activation (Oh et al., 2018), showing that the FHA domain was dispensable in that context.

The RMM Proteins

Rec114, Mei4, and Mer2 (RMM) form another sub-group of functionally conserved DSB proteins with enigmatic roles at the molecular level. Although they have long been recognized as meiotic DSB proteins in yeast, the identification of their homologs across the eukaryotic kingdom has been challenging because of sequence divergence. Nevertheless, RMM homologs have now been identified in many species, including mice and humans (Kumar et al., 2010, 2018; Stanzione et al., 2016; Tessé et al., 2017; Wang et al., 2019). While Rec114 and Mei4 are meiosis-specific, Mer2 is also expressed at low levels in vegetative *S. cerevisiae* cells and shows a unique regulation. The *MER2* transcript has an intron that is only spliced efficiently during meiosis in the presence of a meiosis-specific splicing factor, Mer1 (Engebrecht et al., 1991; Nandabalan and Roeder, 1995).

Rec114, Mei4, and Mer2 localize to chromosomes in leptonema prior to DSB formation and were proposed to act as a complex based on Y2H interactions, coimmunoprecipitation, and partial foci overlap and co-dependencies (Henderson et al., 2006; Li et al., 2006; Maleki et al., 2007; Steiner et al., 2010; Miyoshi et al., 2012). Nevertheless, the existence of a stoichiometric RMM complex has never been demonstrated. In fact, their mutual dependencies are not complete, suggesting that they could exist independently. For example, chromatin binding of Rec114 and Mei4 depend on Mer2, but Mer2 foci do not depend on Rec114 and Mei4 (Maleki et al., 2007; Panizza et al., 2011).

Recent biochemical data revealed that the RMM proteins form two sub-complexes (Claeys Bouuaert et al., 2021). Rec114—Mei4 forms a complex with a 2:1 stoichiometry where the C-terminus of Rec114 homodimerizes and interacts with the N-terminus of Mei4 (**Figures 6A,B**). These sequences are amongst the most conserved regions of the proteins, suggesting that the interactions are also conserved (Kumar et al., 2010, 2018). In addition, the C-terminal domain of Rec114 is important for DNA binding by Rec114—Mei4 (Claeys Bouuaert et al., 2021). The N-terminus of *Mus musculus* REC114 was crystallized and revealed a Pleckstrin Homology (PH)-like fold with an α-helix sandwiched between two anti-parallel β-sheets (**Figure 6C**; Kumar et al., 2018; Boekhout et al., 2019). Blocks of amino acids previously shown to share sequence similarities across kingdoms make up the core of the domain, providing a rationale for their conservation (Maleki et al., 2007; Kumar et al., 2010). Mer2 forms a homotetramer with a predicted coiled coil thought to arrange as pairs of parallel α-helices arranged in an anti-parallel configuration (Claeys Bouuaert et al., 2021; **Figure 6A**). The C-terminal domain of Mer2 contains residues important for DNA binding and DSB formation (Claeys Bouuaert et al., 2021).

ORGANIZATION OF THE MEIOTIC DSB MACHINERY

DSB Formation and the Chromosome Axis

It has long been appreciated that DSB formation is tied to chromosome organization (Keeney, 2001), but the relationships between local DNA-cleavage activity and higher-order structural assemblies remain poorly understood. A haploid *S. cerevisiae* genome contains approximately 700 loops, averaging about 15 kb each, with AT-rich sites that physically anchor a proteinaceous axis (Blat et al., 2002; Kleckner, 2006; Ito et al., 2014; Muller et al., 2018; Schalbetter et al., 2019). The loop-axis structure establishes in early prophase and plays important roles in DSB formation and inter-homolog repair (Carballo et al., 2008; Kim et al., 2010; Panizza et al., 2011; Zickler and Kleckner, 2015).

The chromosome axis in yeast includes a cohesin complex with the meiosis-specific kleisin subunit Rec8 (Klein et al., 1999), the HORMA-domain protein Hop1 (Hollingsworth et al., 1990), and the core axial protein Red1 (Smith and Roeder, 1997; **Figure 7A**). Axis sites are largely determined by Rec8, which localizes Red1 and Hop1 to gene ends (Panizza et al., 2011; Sun et al., 2015).

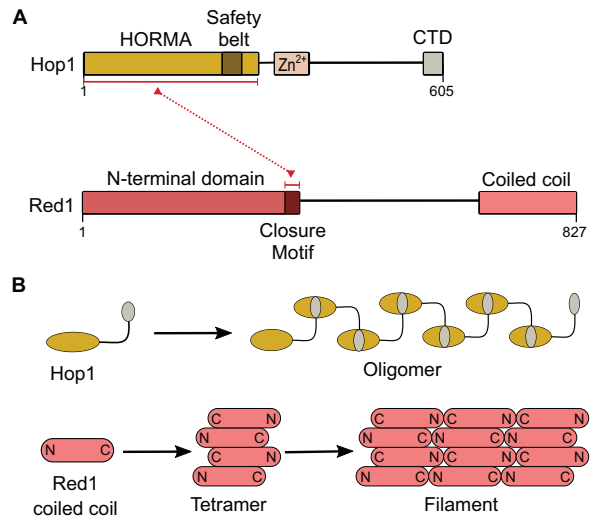

FIGURE 7 | Structural components of the meiotic chromosome axis. **(A)** Domain structure of Hop1 and Red1. The C-terminal-domain (CTD) of Hop1 contains a closure motif. **(B)** Hop1 forms an oligomer through intermolecular interactions between the HORMA domain and the closure motif (West et al., 2018). The Red1 coiled-coil domain forms a parallel-antiparallel tetramer that can form a filament structure by end-to-end polymerization (West et al., 2019).

The C-terminal coiled-coil domain of Red1 forms a tetrameric parallel-antiparallel α-helical bundle (West et al., 2019). End-to-end polymerization of the coiled-coil is thought to underlie axis assembly (West et al., 2019). Red1 is thought to recruit Hop1 via its closure motif located in its central region (West et al., 2018) and Hop1 may also multimerize on the chromosome axis through head-to-tail self-assembly between the N-terminal HORMA domain and a closure motif located at its C-terminus (Kim et al., 2014; West et al., 2019; **Figure 7B**).

The DSB machinery is recruited to the chromosome axis prior to DSB formation. ChIP-seq experiments reveal similar DNA-binding distributions between RMM proteins and axis proteins, and chromatin association of RMM depends on axis proteins (Panizza et al., 2011; Murakami et al., 2020). Consistently, deletion of Red1 causes a 2.5- to 5-fold reduction in DSB formation and deletion of Hop1 decreases DSB levels by at least 10-fold (Woltering et al., 2000; Blat et al., 2002; Niu et al., 2005; Kugou et al., 2009). Axis proteins are therefore important for DSB formation, but their relationships with DSB proteins remain poorly understood at the molecular level.

DNA-Dependent Condensation of RMM

Recent characterizations of the biochemical properties of *S. cerevisiae* RMM brought new insights into the relationship between DSB formation and higher-order chromatin organization. *In vitro*, Rec114—Mei4 and Mer2 complexes bind DNA with extremely high cooperativity and lead to the assembly of large nucleoprotein structures that contain hundreds or thousands of proteins, referred to as condensates (Claeys Bouuaert et al., 2021; **Figures 8A**, **10A**). DNA-dependent clustering is therefore an intrinsic property of Rec114—Mei4 and Mer2, suggesting that it may be important for their function. Accordingly, RMM foci are cytologically visible *in vivo*, implying the local accumulation of many proteins (Claeys Bouuaert et al., 2021). Nevertheless, the biophysical nature and the composition of the foci, or their relationship with break formation, remained unclear. Evidence for a direct link between foci assembly *in vivo* and DNA-driven condensation *in vitro* came from mutagenesis approaches. Mutations within Rec114 and Mer2 with mild effects on DNA binding strongly compromised DNA-driven condensation *in vitro* and foci formation *in vivo* and abolished Spo11-dependent break formation (Claeys Bouuaert et al., 2021).

Rec114—Mei4 and Mer2 nucleoprotein condensates share properties with systems that undergo phase-separation, including the capacity to fuse upon contact and reversibility (Claeys Bouuaert et al., 2021). In the past few years, phase separation has emerged as an important mechanism that promotes self-assembly of membrane-less intracellular compartments and exerts a variety of biological functions through local enrichment of specific biomolecules (Li et al., 2012; Banani et al.,

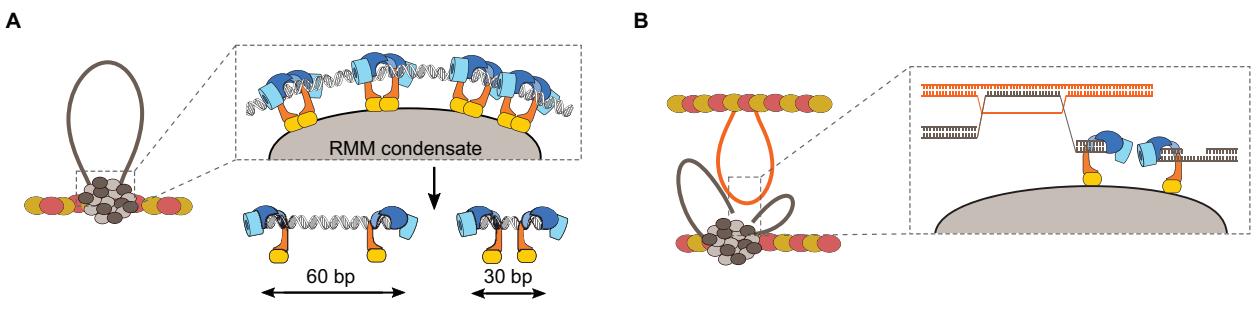

FIGURE 8 | Model for the assembly of the meiotic DSB machinery. **(A)** DNA-dependent condensation of Rec114—Mei4 and Mer2 leads to the formation of large mixed nucleoprotein structures along the chromosome axis. These condensates act as a platform to recruit the Spo11 core complex, MRX, and perhaps other regulatory proteins (Claeys Bouuaert et al., 2021). This model explains the observation that Spo11 often makes closely spaced double DSBs separated with a 10-bp periodicity (Johnson et al., 2021). **(B)** Condensate-embedded core complexes may assist DNA repair by holding broken ends in the vicinity of one another. The condensates could also hold the broken chromatids through association with the base of the loops, independently of whether the DNA ends themselves are embedded. Axis proteins Red1 (red ovals) and Hop1 (yellow ovals) are shown.

2017; Boeynaems et al., 2018). Phase separation is often driven by weak multivalent interactions involving intrinsically disordered proteins and/or RNA. In the nucleus, chromatin sub-compartments have been proposed to assemble through one of two potential mechanisms, through the self-association of a chromatin binder, or through chromatin scaffolding by a multivalent chromatin binder (Erdel and Rippe, 2018). Condensate assembly by Rec114—Mei4 and Mer2 is driven by electrostatic interactions between the negatively charged DNA and positively charged residues within RMM proteins and appears to involve a hybrid mechanism where complexes bind multiple sites simultaneously and also engage in protein-protein interactions (Claeys Bouuaert et al., 2021).

A recent study independently reported phase separation by Mer2 and its mouse homolog IHO1 (Tsai et al., 2020). In addition, Mer2 was shown to bind directly to histone octamers, suggesting the possibility that the condensates may involve chromatinized templates, not only naked DNA (Rousova et al., 2020).

Phase separation has previously been implicated in meiosis in the assembly of the SC in *C. elegans* and during homolog pairing in *S. pombe* (Rog et al., 2017; Ding et al., 2019). In *C. elegans*, interactions between SC proteins are promoted by weak hydrophobic interactions (Rog et al., 2017). This creates a SC structure with mobile constituents, which is thought to allow signal transmission at the interface between pairs of homologs and to regulate crossover distribution along chromosomes (Rog et al., 2017). In fission yeast, meiosis-specific lncRNAs-protein complexes with phase-separation properties promote robust pairing of homologous chromosomes at specific loci (Ding et al., 2019).

The biochemical properties of *S. cerevisiae* RMM suggest a model where condensates recruit Spo11 and other regulatory proteins to provide a coherent cluster for controlled DSB formation (**Figure 8A**). Indeed, *in vitro*, the core complex can be recruited to RMM condensates via at least two sets of interactions, one dependent on Mer2, the other dependent on contacts between the PH-fold domain of Rec114 and the Rec102—Rec104 subunits of the core complex (Claeys Bouuaert et al., 2021).

The coherence provided by the condensate could provide a mechanism to keep the broken chromatids in the vicinity of each other during repair, which may reduce the risks of gross chromosomal rearrangements. Indeed, the base of the cleaved loop would remain associated with the condensate after cleavage, and one or both ends of the DSB, capped by Spo11-oligonucleotide complexes (above), could also remain embedded within the condensate (Claeys Bouuaert et al., 2021; **Figure 8B**).

Hyperlocalized Formation of Coincident DSBs

Independent evidence providing strong support for a higher-order assembly model of the DSB machinery came from the analysis of break patterning in *S. cerevisiae* (Johnson et al., 2021). Sequencing of covalently bound Spo11-DNA complexes revealed short DNA molecules (ranging from 33 to >100 bp) that are independent of MRX/Sae2-mediated nuclease activity (*sae2*Δ, *mre11nd* (nuclease dead), or *rad50S*). These arise from situations where two Spo11 complexes catalyze break formation in close proximity from one another. Double-cuts account for ∼5–20% of total Spo11 activity in wild-type cells, much higher than expected if the DSBs were independent from one another. Therefore, a mechanism must explain the formation of hyper-localized DSBs.

An important clue came from their spatial patterning, which shows a periodicity of ∼10.5 bp corresponding to the helical pitch of DNA (Johnson et al., 2021). Therefore, Spo11 complexes cutting adjacent to one another must attack the same side of the double helix. This could arise if Spo11 complexes were immobilized on a surface, prior to engaging the DNA substrate (**Figure 8A**). Given the DNA-dependent condensation property of the RMM proteins, axis-embedded RMM condensates are a good candidate to provide this surface (Claeys Bouuaert et al., 2021). However, whether the core complex is only recruited to the surface, or only active at the surface, remains unknown.

REGULATION OF DSB FORMATION

Since DSB formation is potentially dangerous, the activity of Spo11 is controlled to ensure appropriate timing, number, and distribution of breaks (**Figure 9A**). Complementary mechanisms overlap to achieve controlled DSB formation: (i) Activation of DSB formation is controlled temporally by protein expression and by coordination with the cell cycle and DNA replication through the reliance on post-translational modifications; (ii) Positive and negative feedback loops provide homeostatic control of DSB levels; (iii) Locally, DSBs distribution is controlled by a pro-active mechanism of hotspot competition and a reactive mechanism of DSB interference; (iv) Finally, the window of opportunity of DSB formation is controlled at the chromosomal scale through a recombination-dependent feedback mechanism, and globally through pachytene exit.

Temporo-Spatial Regulation

Meiotic DSBs occur in a narrow window of time during early prophase I. This temporal regulation is achieved by a series of factors. One level of activation is implemented by meiosis-specific transcription of genes encoding DSB proteins (*SPO11, REC102*, *REC104*, *REC114*, and *MEI4*) and meiosis-specific splicing of *MER2* (Keeney, 2001, 2008). A second level is implemented through dependence of DSB formation on cell cycle progression and on coordination with DNA replication (Borde et al., 2000; Henderson et al., 2006; Wan et al., 2008; Murakami and Keeney, 2014).

S-phase cyclin-dependent kinase (CDK-S) and Dbf4-dependent kinase Cdc7 (DDK) are both essential for replication origin firing and later for DSB formation (Masai and Arai, 2002; Benjamin et al., 2003; Henderson et al., 2006; Matos et al., 2008; Wan et al., 2008). CDK-S and DDK sequentially phosphorylate Mer2 at S30 and S29, respectively, and this is important for the chromatin association of Rec114 and Mei4, and the interaction

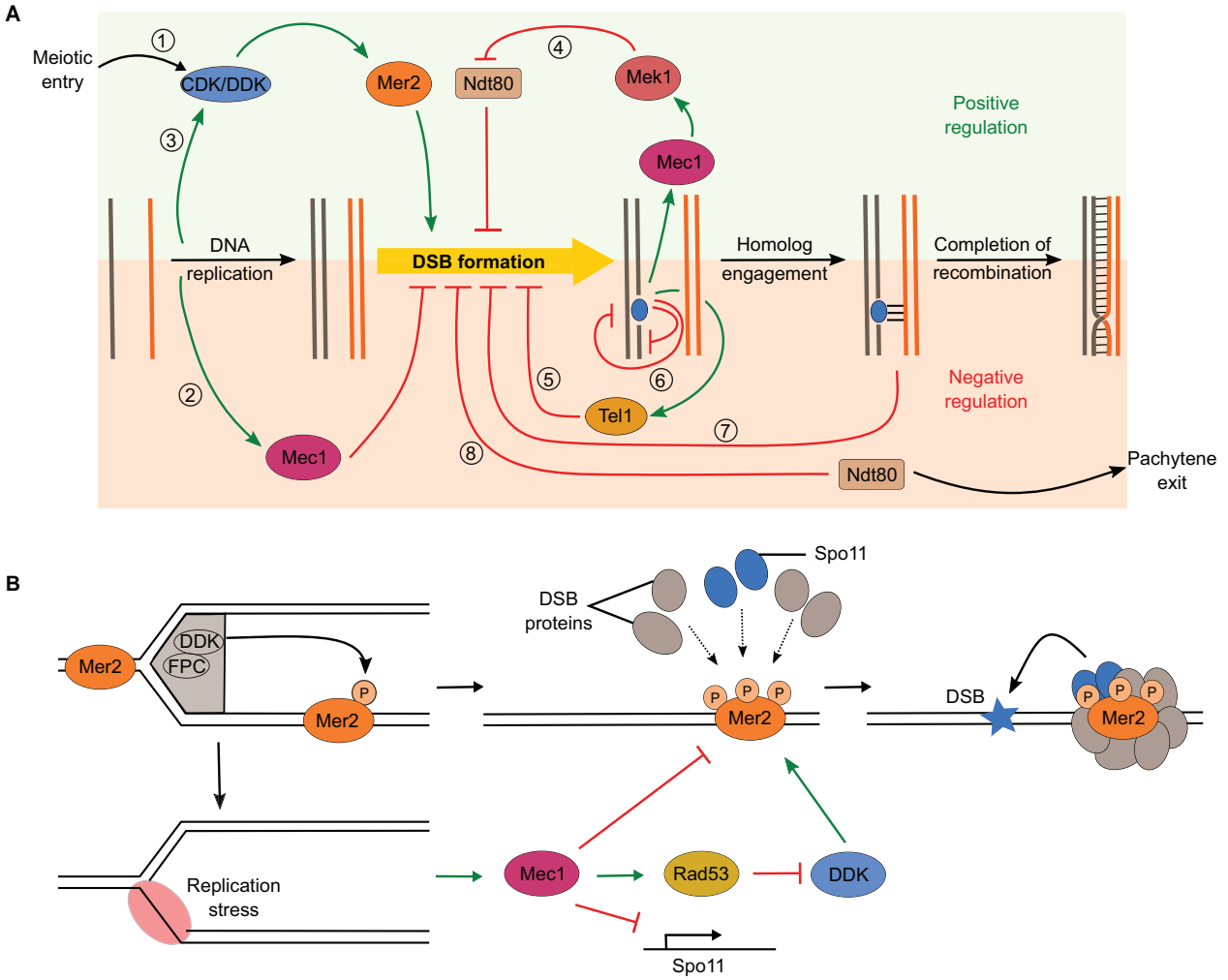

FIGURE 9 | Overlapping regulatory circuits control DSB formation. **(A)** (1) DSB formation is tied to cell cycle control through dependence on CDK and DDK phosphorylation of Mer2. (2) Replication stress inhibits DSB formation by different mechanisms through activation of the Mec1 checkpoint kinase. (3) Replication also positively impacts DSB formation by promoting Mer2 phosphorylation. (4) Recombination defects activate Mec1, which extends prophase by preventing Ndt80 activation, thereby producing a positive feedback loop. (5) Activation of the DNA-damage response kinase Tel1 inhibits further DSB formation, thereby creating a negative feedback loop. (6) Hotspot competition (Tel1-independent) and DSB interference (Tel1-dependent) impact spatial distribution of DSB formation, which limits the coincident formation of two DSBs in *cis* within a 100-kb range or in *trans* between allelic regions of sister chromatids or homologs. (7) Homolog engagement shuts down DSB formation through SC-dependent removal of DSB proteins. (8) Exit of pachytene following Ndt80 activation ends the DSB-permissive period. **(B)** Positive and negative impacts of DNA replication on DSB formation. DDK is bound to the replisome via interactions with the fork protection complex (FPC). Phosphorylation of Mer2 in regions that have undergone replication promotes the assembly of the DSB machinery and DSB formation (Murakami and Keeney, 2014). However, replication stress activates Mec1 and inhibits DSB formation by reducing Spo11 transcription, inhibiting DDK via Rad53, and independently inhibiting chromatin association of several DSB proteins (Blitzblau and Hochwagen, 2013).

between Mer2 and Xrs2 (Henderson et al., 2006; Wan et al., 2008; Panizza et al., 2011; **Figure 9A**, circuit 1).

Phosphorylation of Mer2 by DDK is temporally coordinated to DNA replication by tethering of DDK to the replisome component Tof1 (Matsumoto et al., 2005; Murakami and Keeney, 2014). Mer2 phosphorylation by DDK in the wake of the replication fork therefore serves as a mark to assemble the DSB machinery in chromatin regions that have completed DNA replication (**Figure 9A**, circuit 3 and **Figure 9B**, top). However, there is a lag of about 90 min between DNA replication and DSB formation (Borde et al., 2000; Murakami and Keeney, 2014). The events that must take place between Mer2 phosphorylation and DSB formation are unclear, but in the light of the DNA-driven condensation properties of Rec114—Mei4 and Mer2, this delay could be explained by the time required to assemble the condensates and recruit the core complex and MRX.

Replication stress downregulates DSB formation through Mec1 via three complementary mechanisms: (1) partial inhibition of Spo11 transcription, (2) inhibition of DDK

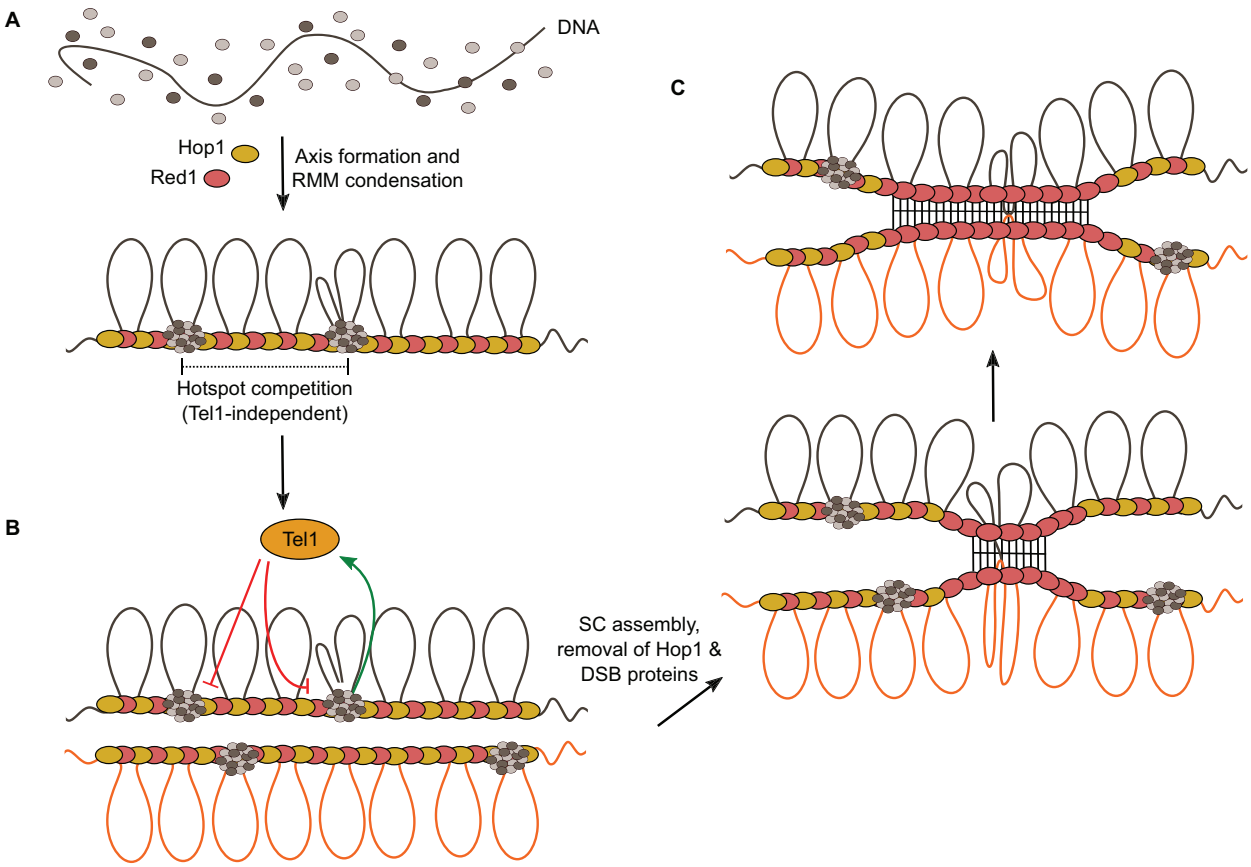

FIGURE 10 | The condensate model for hotspot competition, DSB interference, and homolog engagement. **(A)** The model suggests that hotspot competition is mediated prior to DSB formation through partitioning of RMM proteins into condensates, locally depleting pools of free DSB proteins. **(B)** DSB formation activates Tel1, which inhibits local DSB formation. **(C)** SC assembly leads to the removal of Hop1 and DSB proteins from the axis, thereby shutting down further DSB formation.

via Rad53 leading to hypophosphorylation of Mer2, and (3) inhibition of chromatin loading of Rec114 and Mre11 (Blitzblau and Hochwagen, 2013; Keeney et al., 2014; **Figure 9A**, circuit 2 and **Figure 9B**, bottom).

In *S. pombe*, blocking DNA replication also abolishes meiotic DSB formation (Ogino and Masai, 2006). In addition, early replicating regions are associated with higher DSB levels in *S. pombe* and in mice (Wu and Nurse, 2014; Pratto et al., 2020).

Hotspot Competition and DSB Interference

DSB formation is controlled to ensure non-random distribution of recombination events along the chromosomes (**Figure 9A**, circuits 5 and 6). The presence of a strong hotspot suppresses the DSB activity of an adjacent hotspot (Wu and Lichten, 1994; Xu et al., 1995; Keeney et al., 2014). This phenomenon, termed hotspot competition, is observed at a population level and can be explained by a competition between hotspots for a slowly diffusing factor that is limiting for DSB formation. Hotspot competition can therefore be implemented prior to DSB formation, and RMM proteins have been suggested to constitute this limiting factor based on the fact that they are bound to the chromosome axis, which would constrain their diffusion (Panizza et al., 2011). The condensation properties of RMM proteins provide a molecular framework to understand how this may be achieved. Partitioning of Rec114—Mei4 and Mer2 complexes within condensates lead to a local depletion of free proteins, which would reduce the probability of nucleation of other condensates nearby, leading to a non-random distribution of DSB-competent zones along the chromosomes (Claeys Bouuaert et al., 2021; **Figure 10A**). Consistently, in *Sordaria macrospora*, the Mer2 homolog Asy2 form regularly spaced foci along the chromosome axis throughout leptotene and zygotene (Tessé et al., 2017).

Hotspot competition is genetically separable from DSB interference, the phenomenon whereby the formation of a DSB at one locus reduces the chances of another break in its vicinity. Interference is observed at the level of individual chromatids and depends on the DNA-damage response kinase Tel1, but hotspot competition does not (Mohibullah and Keeney, 2017). Upon DSB formation, Tel1 suppresses further DSB formation via a negative feedback loop thought to be implemented in part through phosphorylation of Rec114 (Zhang et al., 2011; Carballo

et al., 2013; **Figure 10B**). Indeed, Rec114 subunit has eight [S/T]Q motifs, the known target of signal transduction kinases Tel1 and/or Mec1 (Sasanuma et al., 2007; Carballo et al., 2013), and mutation of all potential phosphorylation sites to alanine leads to elevated DSB formation, consistent with phosphorylation-dependent regulation of Rec114 (Carballo et al., 2013).

Tel1 and Mec1 mediate DSB interference in *cis* between different regions of the same molecule within about 100-kb range, and in *trans*, at allelic loci between sister chromatids (Zhang et al., 2011; Garcia et al., 2015; Fowler et al., 2018). In addition, DSB interference also occurs in *trans* between homologs, which must therefore depend on interhomolog contacts. Indeed, *trans* interference between homologs is reduced in the absence of Dmc1 (Zhang et al., 2011).

In the absence of Tel1, not only is *cis* interference abolished, but DSB formation shows negative interference within about a 10-kb range, meaning that coincident DSBs happen more often than predicted by chance (Garcia et al., 2015). Negative interference in the absence of Tel1 is explained by the condensate model of DSB formation since multiple Spo11 complexes are recruited within condensates, creating zones of high potential DSB activity that must be kept in check by Tel1 (**Figure 8**).

Hotspot competition and Tel1-dependent interference have been demonstrated in *S. pombe* (Fowler et al., 2018). In addition, $ATM^{-/-}$ mice show a high elevation of Spo11 breaks (Lange et al., 2011) and compromising ATM in *Drosophila* oocytes leads to increased levels of DNA damage (Joyce et al., 2011), showing that the Tel1/ATM-mediated negative feedback loop is conserved in mice and flies.

Homolog Engagement

In yeast, ZMM mutants defective for synapsis and crossing over experience persistent DSB formation (Thacker et al., 2014). This revealed that excessive DSB formation is controlled by a regulatory feedback mechanism that depends on interhomolog interactions (**Figure 9A**, circuit 7). Yeast strains with karyotype abnormalities show accumulation of DSBs specifically on the chromosomes that experience homolog engagement defects, showing that the feedback control operates in a chromosome-autonomous fashion (Mu et al., 2020). Smaller chromosomes also experience higher DSB levels, in part because they take more time to find each other, and as a consequence remain longer in a DSB-competent state due to the persistence of DSB proteins (Murakami et al., 2020).

Mutations in components of the SC central region (Gmc2 and Ecm11) that abolish SC elongation but not crossover formation show elevated DSBs (Humphryes and Hochwagen, 2014; Voelkel-Meiman et al., 2016; Lee et al., 2020; Mu et al., 2020). This indicates that homolog engagement feedback control operates at the level of SC assembly rather than recombination.

SC assembly removes Hop1 from the chromosome axis (Börner et al., 2008; Chen et al., 2014). This is thought to close the window of opportunity for DSB formation by triggering the dissociation of DSB proteins (Mu et al., 2020; **Figure 10C**). Indeed, many DSB proteins (Rec102, Rec104, Rec114, and Mei4) are removed from synapsed chromosomes (Kee et al., 2004; Li et al., 2006; Maleki et al., 2007; Panizza et al., 2011; Carballo et al., 2013). In addition, chromosomal regions ∼100 kb adjacent to telomeres retain Hop1 after synapsis and experience DSB formation in pachynema (Subramanian et al., 2019). Hop1 is removed from the axis by Pch2 that probably disrupts the interaction between Hop1 and the closure motif of Red1 (Chen et al., 2014; Kim et al., 2014; West et al., 2018).

In mice, reduced SPO11 dosage leads to synaptic defects, and unsynapsed regions display elevated DSB markers (Kauppi et al., 2013). In addition, the unsynapsed portion of the X chromosome also accumulates DSBs in wild-type male mice. Similar to yeast, synapsis leads to the removal by TRIP13 of HORMAD1 and HORMAD2, and of DSB proteins REC114 and MEI4 (Wojtasz et al., 2009; Acquaviva et al., 2020). Homolog engagement feedback control therefore appears to be conserved.

Pachytene Exit

In *S. cerevisiae*, exit from pachytene is controlled by the Ndt80 transcription factor (Xu et al., 1995). *NDT80* activation leads to the disassembly of the SC and the removal of DSB proteins, which ends the window of opportunity for DSB formation (**Figure 9A**, circuit 8). As a result, *ndt80* mutants accumulate more DSBs (Xu et al., 1995; Allers and Lichten, 2001; Keeney, 2001). In mutants with recombination or synapsis defects, checkpoint activation via Mec1 activates Mek1, which inhibits Ndt80 activity and leads to the extension of prophase (**Figure 9A**, circuit 4; Acosta et al., 2011; Gray et al., 2013; Prugar et al., 2017). Therefore, mutants that decrease Spo11 activity experience an extended window of time for DSB formation, effectively obscuring their catalytic defects. This is thought to provide homeostatic control of DSB formation.

While the negative feedback loop dependent on homolog engagement is chromosome autonomous, the Ndt80 feedback loop is nucleus-wide. The distinction was demonstrated by epistasis analysis showing that deletion of ZMM proteins in an *ndt80* mutant leads to a further increase in DSB levels (Thacker et al., 2014). Therefore, the extension of prophase and synaptic defects contribute independently to persistent DSB formation.

In *C. elegans* and *Drosophila* oocytes, suppression of crossing over on a single pair of chromosomes lead to nucleus-wide increase in the retention of DSB proteins (Carlton et al., 2006; Stamper et al., 2013) or crossover frequency (Joyce and Mckim, 2010), respectively, suggesting that recombination defects extends the DSB-permissive period, leading to global increase in DSB formation.

PERSPECTIVES

To conclude, recent studies have brought new insights into the mechanism and regulation of meiotic DSB formation. However, our understanding of the structure, biochemical properties, and regulation of DSB proteins remains limited, and many important questions are yet to be addressed. Why DSB formation requires the collaborative action of so many proteins has been enigmatic for a long time. Our current model provides a tentative and partial response to this question by highlighting the organizational role of Rec114—Mei4 and Mer2 in the assembly

of DSB-competent sites along chromosomes. As we have seen, the phase-separation model is consistent with, and explains, many long-standing observations regarding the behavior of DSB proteins. However, it also raises new questions regarding the biophysical properties of the condensates, their assembly and disassembly mechanisms, and how these might be controlled, perhaps through post-translational modifications. What are the minimal components required for DSB formation? In addition to known DSB proteins and essential phosphorylations, is something else needed to trigger Spo11 activity? What is the role of MRX? The rationale that its presence prior to break formation allows coordination with DSB repair is straightforward, but how is it recruited and how does it impact Spo11 activity? What is the relationship between DSB proteins and axis proteins? How are their spatial distributions controlled? Since Rec114—Mei4 and Mer2 bind DNA independently of axis proteins *in vitro*, why do their chromatin-association depend on the axis *in vivo*? Current models provide a molecular framework that will guide future experiments to better understand the mechanism of DSB formation.

AUTHOR CONTRIBUTIONS

VKY and CCB wrote the manuscript. Both authors approved the submitted version.

FUNDING

This work was supported by the European Research Council under the European Union's Horizon 2020 Research and Innovation Program (ERC Grant Agreement 802525) and by the Fonds National de la Recherche Scientifique (FNRS MIS-Ulysse Grant F.6002.20).

ACKNOWLEDGMENTS

We thank CCB lab members for feedback on the manuscript and Hajar Aït-Bella for help with figures.

REFERENCES

Acosta, I., Ontoso, D., and San-Segundo, P. A. (2011). The budding yeast polo-like kinase Cdc5 regulates the Ndt80 branch of the meiotic recombination checkpoint pathway. *Mol. Biol. Cell* 22, 3478–3490. doi: 10.1091/mbc.E11-06-0482

Acquaviva, L., Boekhout, M., Karasu, M. E., Brick, K., Pratto, F., Li, T., et al. (2020). Ensuring meiotic DNA break formation in the mouse pseudoautosomal region. *Nature* 582, 426–431. doi: 10.1038/s41586-020-2327-4

Acquaviva, L., Székvölgyi, L., Dichtl, B., Dichtl, B. S., Saint André, C. D. L. R., Nicolas, A., et al. (2013). The COMPASS subunit Spp1 links histone methylation to initiation of meiotic recombination. *Science* 339, 215–218. doi: 10.1126/science.1225739

Ajimura, M., Leem, S. H., and Ogawa, H. (1993). Identification of new genes required for meiotic recombination in Saccharomyces cerevisiae. *Genetics* 133, 51–66.

Alani, E., Padmore, R., and Kleckner, N. (1990). Analysis of wild-type and rad50 mutants of yeast suggests an intimate relationship between meiotic chromosome synapsis and recombination. *Cell* 61, 419–436. doi: 10.1016/0092-8674(90)90524-I

Allers, T., and Lichten, M. (2001). Differential timing and control of noncrossover and crossover recombination during meiosis. *Cell* 106, 47–57. doi: 10.1016/S0092-8674(01)00416-0

Alonso-Sarduy, L., Roduit, C., Dietler, G., and Kasas, S. (2011). Human topoisomerase II-DNA interaction study by using atomic force microscopy. *FEBS Lett.* 585, 3139–3145. doi: 10.1016/j.febslet.2011.08.051

Anderson, J. S. J., and Parker, R. (1998). The 3′ to 5′ degradation of yeast mRNAs is a general mechanism for mRNA turnover that requires the SK12 DEVH box protein and 3′ to 5′ exonucleases of the exosome complex. *EMBO J.* 17, 1497–1506. doi: 10.1093/emboj/17.5.1497

Arora, C., Kee, K., Maleki, S., and Keeney, S. (2004). Antiviral protein Ski8 is a direct partner of Spo11 in meiotic DNA break formation, independent of its cytoplasmic role in RNA metabolism. *Mol. Cell* 13, 549–559. doi: 10.1016/S1097-2765(04)00063-2

Arthur, L. M., Gustausson, K., Hopfner, K. P., Carson, C. T., Stracker, T. H., Karcher, A., et al. (2004). Structural and functional analysis of Mre11-3. *Nucleic Acids Res.* 32, 1886–1893. doi: 10.1093/nar/gkh343

Banani, S. F., Lee, H. O., Hyman, A. A., and Rosen, M. K. (2017). Biomolecular condensates: organizers of cellular biochemistry. *Nat. Rev. Mol. Cell Biol.* 18, 285–298. doi: 10.1038/nrm.2017.7

Baudat, F., and Nicolas, A. (1997). Clustering of meiotic double-strand breaks on yeast chromosome III. *Proc. Natl. Acad. Sci. U.S.A.* 94, 5213–5218. doi: 10.1073/pnas.94.10.5213

Benham, C. J. (1982). Stable cruciform formation at inverted repeat sequences in supercoiled DNA. *Biopolymers* 21, 679–696. doi: 10.1002/bip.360210314

Benjamin, K. R., Zhang, C., Shokat, K. M., and Herskowitz, I. (2003). Control of landmark events in meiosis by the CDK Cdc28 and the meiosis-specific kinase Ime2. *Genes Dev.* 17, 1524–1539. doi: 10.1101/gad.1101503

Berchowitz, L. E., Hanlon, S. E., Lieb, J. D., and Copenhaver, G. P. (2009). A positive but complex association between meiotic double-strand break hotspots and open chromatin in *Saccharomyces cerevisiae*. *Genome Res.* 19, 2245–2257. doi: 10.1101/gr.096297.109

Bergerat, A., De Massy, B., Gadelle, D., Varoutas, P. C., Nicolas, A., and Forterre, P. (1997). An atypical topoisomerase II from archaea with implications for meiotic recombination. *Nature* 386, 414–417. doi: 10.1038/386414a0

Bishop, D. K., Park, D., Xu, L., and Kleckner, N. (1992). DMC1: a meiosis-specific yeast homolog of *E. coli* recA required for recombination, synaptonemal complex formation, and cell cycle progression. *Cell* 69, 439–456. doi: 10.1016/0092-8674(92)90446-J

Bishop, D. K., and Zickler, D. (2004). Early decision: meiotic crossover interference prior to stable strand exchange and synapsis. *Cell* 117, 9–15. doi: 10.1016/S0092-8674(04)00297-1

Blat, Y., Protacio, R. U., Hunter, N., and Kleckner, N. (2002). Physical and functional interactions among basic chromosome organizational features govern early steps of meiotic chiasma formation. *Cell* 111, 791–802. doi: 10.1016/S0092-8674(02)01167-4

Blitzblau, H. G., Bell, G. W., Rodriguez, J., Bell, S. P., and Hochwagen, A. (2007). Mapping of meiotic single-stranded DNA reveals double-strand-break hotspots near centromeres and telomeres. *Curr. Biol.* 17, 2003–2012. doi: 10.1016/j.cub.2007.10.066

Blitzblau, H. G., and Hochwagen, A. (2013). ATR/Mec1 prevents lethal meiotic recombination initiation on partially replicated chromosomes in budding yeast. *Elife* 2:e00844. doi: 10.7554/eLife.00844.001

Boekhout, M., Karasu, M. E., Wang, J., Acquaviva, L., Pratto, F., Brick, K., et al. (2019). REC114 partner ANKRD31 controls number, timing, and location of meiotic DNA breaks. *Mol. Cell* 74, 1053.e8–1068.e8. doi: 10.1016/j.molcel.2019.03.023

Boeynaems, S., Alberti, S., Fawzi, N. L., Mittag, T., Polymenidou, M., Rousseau, F., et al. (2018). Protein phase separation: a new phase in cell biology. *Trends Cell Biol.* 28, 420–435. doi: 10.1016/j.tcb.2018.02.004

Borde, V., Goldman, A. S. H., and Lichten, M. (2000). Direct coupling between meiotic DNA replication and recombination initiation. *Science* 290, 806–809. doi: 10.1126/science.290.5492.806

Borde, V., Lin, W., Novikov, E., Petrini, J. H., Lichten, M., and Nicolas, A. (2004). Association of Mre11p with double-strand break sites during yeast meiosis. *Mol. Cell* 13, 389–401. doi: 10.1016/S1097-2765(04)00034-6

Borde, V., Robine, N., Lin, W., Bonfils, S., Géli, V., and Nicolas, A. (2009). Histone H3 lysine 4 trimethylation marks meiotic recombination initiation sites. *EMBO J.* 28, 99–111. doi: 10.1038/emboj.2008.257

Borde, V., Wu, T.-C., and Lichten, M. (1999). Use of a recombination reporter insert to define meiotic recombination domains on chromosome III of *Saccharomyces cerevisiae*. *Mol. Cell. Biol.* 19, 4832–4842. doi: 10.1128/mcb.19.7.4832

Börner, G. V., Barot, A., and Kleckner, N. (2008). Yeast Pch2 promotes domainal axis organization, timely recombination progression, and arrest of defective recombinosomes during meiosis. *Proc. Natl. Acad. Sci. U.S.A.* 105, 3327–3332. doi: 10.1073/pnas.0711864105

Börner, G. V., Kleckner, N., and Hunter, N. (2004). Crossover/noncrossover differentiation, synaptonemal complex formation, and regulatory surveillance at the leptotene/zygotene transition of meiosis. *Cell* 117, 29–45. doi: 10.1016/S0092-8674(04)00292-2

Brown, M. S., and Bishop, D. K. (2015). DNA strand exchange and RecA homologs in meiosis. *Cold Spring Harb. Perspect. Biol.* 7:a016659. doi: 10.1101/cshperspect.a016659

Buhler, C., Borde, V., and Lichten, M. (2007). Mapping meiotic single-strand DNA reveals a new landscape of DNA double-strand breaks in *Saccharomyces cerevisiae*. *PLoS Biol.* 5:e324. doi: 10.1371/journal.pbio.0050324

Buhler, C., Gadelle, D., Forterre, P., Wang, J. C., and Bergerat, A. (1998). Reconstitution of DNA topoisomerase VI of the thermophilic archaeon *Sulfolobus* shibatae from subunits separately overexpressed in *Escherichia coli*. *Nucleic Acids Res.* 26, 5157–5162. doi: 10.1093/nar/26.22.5157

Buhler, C., Lebbink, J. H. G., Bocs, C., Ladenstein, R., and Forterre, P. (2001). DNA topoisomerase VI generates ATP-dependent double-strand breaks with two-nucleotide overhangs. *J. Biol. Chem.* 276, 37215–37222. doi: 10.1074/jbc.M101823200

Cannavo, E., and Cejka, P. (2014). Sae2 promotes dsDNA endonuclease activity within Mre11-Rad50-Xrs2 to resect DNA breaks. *Nature* 514, 122–125. doi: 10.1038/nature13771

Cannavo, E., Johnson, D., Andres, S. N., Kissling, V. M., Reinert, J. K., Garcia, V., et al. (2018). Regulatory control of DNA end resection by Sae2 phosphorylation. *Nat. Commun.* 9:4016. doi: 10.1038/s41467-018-06417-5

Carballo, J. A., Johnson, A. L., Sedgwick, S. G., and Cha, R. S. (2008). Phosphorylation of the axial element protein Hop1 by Mec1/Tel1 ensures meiotic interhomolog recombination. *Cell* 132, 758–770. doi: 10.1016/j.cell.2008.01.035

Carballo, J. A., Panizza, S., Serrentino, M. E., Johnson, A. L., Geymonat, M., Borde, V., et al. (2013). Budding yeast ATM/ATR control meiotic double-strand break (DSB) levels by down-regulating Rec114, an essential component of the DSB-machinery. *PLoS Genet.* 9:e1003545. doi: 10.1371/journal.pgen.1003545

Carlton, P. M., Farruggio, A. P., and Dernburg, A. F. (2006). A link between meiotic prophase progression and crossover control. *PLoS Genet.* 2:e12. doi: 10.1371/journal.pgen.0020012

Casari, E., Rinaldi, C., Marsella, A., Gnugnoli, M., Colombo, C. V., Bonetti, D., et al. (2019). Processing of DNA double-strand breaks by the MRX complex in a chromatin context. *Front. Mol. Biosci.* 6:43. doi: 10.3389/fmolb.2019.00043

Ceccaldi, R., Rondinelli, B., and D'Andrea, A. D. (2016). Repair pathway choices and consequences at the double-strand break. *Trends Cell Biol.* 26, 52–64. doi: 10.1016/j.tcb.2015.07.009

Chen, C., Jomaa, A., Ortega, J., and Alani, E. E. (2014). Pch2 is a hexameric ring ATPase that remodels the chromosome axis protein Hop1. *Proc. Natl. Acad. Sci. U.S.A.* 111, E44–E53. doi: 10.1073/pnas.1310755111

Cheng, Z., Liu, Y., Wang, C., Parker, R., and Song, H. (2009). Crystal structure of Ski8p, a WD-repeat protein with dual roles in mRNA metabolism and meiotic recombination. *Protein Sci.* 13, 2673–2684. doi: 10.1110/ps.04856504

Chin, G. M., and Villeneuve, A. M. (2001). *C. elegans* mre-11 is required for meiotic recombination and DNA repair but is dispensable for the meiotic G2 DNA damage checkpoint. *Genes Dev.* 15, 522–534. doi: 10.1101/gad.864101

Claeys Bouuaert, C., Pu, S., Wang, J., Oger, C., Daccache, D., Xie, W., et al. (2021). DNA-driven condensation assembles the meiotic DNA break machinery. *Nature* (in press).

Claeys Bouuaert, C., Tischfield, S. E., Pu, S., Mimitou, E. P., Arias-Palomo, E., Berger, J. M., et al. (2021). Structural and functional characterization of the Spo11 core complex. *Nat. Struct. Mol. Biol.* 28, 92–102. doi: 10.1038/s41594-020-00534-w

Cool, M., and Malone, R. E. (1992). Molecular and genetic analysis of the yeast early meiotic recombination genes REC102 and REC107/MER2. *Mol. Cell. Biol.* 12, 1248–1256. doi: 10.1128/mcb.12.3.1248

Corbett, K. D., Benedetti, P., and Berger, J. M. (2007). Holoenzyme assembly and ATP-mediated conformational dynamics of topoisomerase VI. *Nat. Struct. Mol. Biol.* 14, 611–619. doi: 10.1038/nsmb1264

Corbett, K. D., and Berger, J. M. (2003). Structure of the topoisomerase VI-B subunit: implications for type II topoisomerase mechanism and evolution. *EMBO J.* 22, 151–163. doi: 10.1093/emboj/cdg008

Corbett, K. D., and Berger, J. M. (2005). Structural dissection of ATP turnover in the prototypical GHL ATPase TopoVI. *Structure* 13, 873–882. doi: 10.1016/j.str.2005.03.013

De Muyt, A., Jessop, L., Kolar, E., Sourirajan, A., Chen, J., Dayani, Y., et al. (2012). BLM helicase ortholog Sgs1 Is a central regulator of meiotic recombination intermediate metabolism. *Mol. Cell* 46, 43–53. doi: 10.1016/j.molcel.2012.02.020

Ding, D. Q., Okamasa, K., Katou, Y., Oya, E., Nakayama, J. I., Chikashige, Y., et al. (2019). Chromosome-associated RNA–protein complexes promote pairing of homologous chromosomes during meiosis in Schizosaccharomyces pombe. *Nat. Commun.* 10:5598. doi: 10.1038/s41467-019-13609-0

Eichman, B. F., Vargason, J. M., Mooers, B. H. M., and Ho, P. S. (2000). The Holliday junction in an inverted repeat DNA sequence: sequence effects on the structure of four-way junctions. *Proc. Natl. Acad. Sci. U.S.A.* 97, 3971–3976. doi: 10.1073/pnas.97.8.3971

Engebrecht, J. A., Voelkel-Meiman, K., and Roeder, G. S. (1991). Meiosis-specific RNA splicing in yeast. *Cell* 66, 1257–1268. doi: 10.1016/0092-8674(91)90047-3

Erdel, F., and Rippe, K. (2018). Formation of chromatin subcompartments by phase separation. *Biophys. J.* 114, 2262–2270. doi: 10.1016/j.bpj.2018.03.011

Evans, D. H., Li, Y. F., Fox, M. E., and Smith, G. R. (1997). A WD repeat protein, Rec14, essential for meiotic recombination in *Schizosaccharomyces* pombe. *Genetics* 146, 1253–1264.

Fowler, K. R., Hyppa, R. W., Cromie, G. A., and Smith, G. R. (2018). Physical basis for long-distance communication along meiotic chromosomes. *Proc. Natl. Acad. Sci. U.S.A.* 115, E9333–E9342. doi: 10.1073/pnas.1801920115

Furuse, M., Nagase, Y., Tsubouchi, H., Murakami-Murofushi, K., Shibata, T., and Ohta, K. (1998). Distinct roles of two separable in vitro activities of yeast Mre11 in mitotic and meiotic recombination. *EMBO J.* 17, 6412–6425. doi: 10.1093/emboj/17.21.6412

Galbraith, A. M., and Malone, R. E. (1992). Characterization ofREC104, a gene required for early meiotic recombination in the yeast *Saccharomyces cerevisiae*. *Dev. Genet.* 13, 392–402. doi: 10.1002/dvg.1020130603

Game, J. C., Zamb, T. J., Braun, R. J., Resnick, M., and Roth, R. M. (1980). The role of radiation (rad) genes in meiotic recombination in yeast. *Genetics* 94, 51–68.

Garcia, V., Gray, S., Allison, R. M., Cooper, T. J., and Neale, M. J. (2015). Tel1ATM-mediated interference suppresses clustered meiotic double-strand-break formation. *Nature* 520, 114–118. doi: 10.1038/nature13993

Garcia, V., Phelps, S. E. L., Gray, S., and Neale, M. J. (2011). Bidirectional resection of DNA double-strand breaks by Mre11 and Exo1. *Nature* 479, 241–244. doi: 10.1038/nature10515

Gardiner, J. M., Bullard, S. A., Chrome, C., and Malone, R. E. (1997). Molecular and genetic analysis of REC103, an early meiotic recombination gene in yeast. *Genetics* 146, 1265–1274.

Gerton, J. L., DeRisi, J., Shroff, R., Lichten, M., Brown, P. O., and Petes, T. D. (2000). Global mapping of meiotic recombination hotspots and coldspots in the yeast Saccharomyces cerevisiae. *Proc. Natl. Acad. Sci. U.S.A.* 97, 11383–11390. doi: 10.1073/pnas.97.21.11383

Girard, C., Roelens, B., Zawadzki, K. A., and Villeneuve, A. M. (2018). Interdependent and separable functions of *Caenorhabditis elegans* MRN-C

complex members couple formation and repair of meiotic DSBs. *Proc. Natl. Acad. Sci. U.S.A.* 115, E4443–E4452. doi: 10.1073/pnas.1719029115

Gnügge, R., and Symington, L. S. (2017). Keeping it real: MRX-Sae2 clipping of natural substrates. *Genes Dev.* 31, 2311–2312. doi: 10.1101/gad.310771.117

Gobbini, E., Cassani, C., Villa, M., Bonetti, D., and Longhese, M. P. (2016). Functions and regulation of the MRX complex at DNA double-strand breaks. *Microb. Cell* 3, 329–337. doi: 10.15698/mic2016.08.517

Graille, M., Cladière, L., Durand, D., Lecointe, F., Gadelle, D., Quevillon-Cheruel, S., et al. (2008). Crystal structure of an intact type II DNA topoisomerase: insights into DNA transfer mechanisms. *Structure* 16, 360–370. doi: 10.1016/j.str.2007.12.020

Gray, S., Allison, R. M., Garcia, V., Goldman, A. S. H., and Neale, M. J. (2013). Positive regulation of meiotic DNA double-strand break formation by activation of the DNA damage checkpoint kinase Mec1(ATR). *Open Biol.* 3:130019. doi: 10.1098/rsob.130019

Gray, S., and Cohen, P. E. (2016). Control of meiotic crossovers: from double-strand break formation to designation. *Annu. Rev. Genet.* 50, 175–210. doi: 10.1146/annurev-genet-120215-035111

Halbach, F., Reichelt, P., Rode, M., and Conti, E. (2013). The yeast ski complex: crystal structure and rna channeling to the exosome complex. *Cell* 154, 814–826. doi: 10.1016/j.cell.2013.07.017

Hatkevich, T., Miller, D. E., Turcotte, C. A., Miller, M. C., and Sekelsky, J. (2020). A pathway for error-free non-homologous end joining of resected meiotic double-strand breaks. *bioRxiv [Preprint]* doi: 10.1101/2020.06.17.157313

Hayashi, M., Chin, G. M., and Villeneuve, A. M. (2007). *C. elegans* germ cells switch between distinct modes of double-strand break repair during meiotic prophase progression. *PLoS Genet.* 3:e191. doi: 10.1371/journal.pgen.0030191

Henderson, K. A., Kee, K., Maleki, S., Santini, P. A., and Keeney, S. (2006). Cyclin-dependent kinase directly regulates initiation of meiotic recombination. *Cell* 125, 1321–1332. doi: 10.1016/j.cell.2006.04.039

Hohl, M., Kwon, Y., Galván, S. M., Xue, X., Tous, C., Aguilera, A., et al. (2010). The Rad50 coiled-coil domain is indispensable for Mre11 complex functions. *Nat. Struct. Mol. Biol.* 18, 1124–1131. doi: 10.1038/nsmb.2116

Hollingsworth, N. M., Goetsch, L., and Byers, B. (1990). The HOP1 gene encodes a meiosis-specific component of yeast chromosomes. *Cell* 61, 73–84. doi: 10.1016/0092-8674(90)90216-2

Hong, E. L., Shinohara, A., and Bishop, D. K. (2001). *Saccharomyces cerevisiae* Dmc1 protein promotes renaturation of single-strand DNA (ssDNA) and assimilation of ssDNA into homologous super-coiled duplex DNA. *J. Biol. Chem.* 276, 41906–41912. doi: 10.1074/jbc.M105563200

Hopfner, K. P., Craig, L., Moncalian, G., Zinkel, R. A., Usui, T., Owen, B. A. L., et al. (2002). The Rad50 zinc-hook is a structure joining Mre11 complexes in DNA recombination and repair. *Nature* 418, 562–566. doi: 10.1038/nature00922

Hopfner, K. P., Karcher, A., Craig, L., Woo, T. T., Carney, J. P., and Tainer, J. A. (2001). Structural biochemistry and interaction architecture of the DNA double-strand break repair Mre11 nuclease and Rad50-ATPase. *Cell* 105, 473–485. doi: 10.1016/S0092-8674(01)00335-X

Humphryes, N., and Hochwagen, A. (2014). A non-sister act: recombination template choice during meiosis. *Exp. Cell Res.* 329, 53–60. doi: 10.1016/j.yexcr.2014.08.024

Hunter, N. (2015). Meiotic recombination: the essence of heredity. *Cold Spring Harb. Perspect. Biol.* 7:a016618. doi: 10.1101/cshperspect.a016618

Hunter, N., and Kleckner, N. (2001). The single-end invasion: an asymmetric intermediate at the double-strand break to double-holliday junction transition of meiotic recombination. *Cell* 106, 59–70. doi: 10.1016/S0092-8674(01)00430-5

Ito, M., Kugou, K., Fawcett, J. A., Mura, S., Ikeda, S., Innan, H., et al. (2014). Meiotic recombination cold spots in chromosomal cohesion sites. *Genes Cells* 19, 359–373. doi: 10.1111/gtc.12138

Ivanov, E. L., Korolev, V. G., and Fabre, F. (1992). XRS2, a DNA repair gene of *Saccharomyces cerevisiae*, is needed for meiotic recombination. *Genetics* 132, 651–664.

Iwasaki, D., Hayashihara, K., Shima, H., Higashide, M., Terasawa, M., Gasser, S. M., et al. (2016). The MRX complex ensures NHEJ fidelity through multiple pathways including Xrs2-FHA–dependent tel1 activation. *PLoS Genet.* 12:e1005942. doi: 10.1371/journal.pgen.1005942

Johnson, D., Crawford, M., Cooper, T., Claeys Bouuaert, C., Keeney, S., Llorente, B., et al. (2021). Concerted cutting by Spo11 illuminates the mechanism of meiotic DNA break formation. *Nature* (in press).

Jolivet, S., Vezon, D., Froger, N., and Mercier, R. (2006). Non conservation of the meiotic function of the Ski8/Rec103 homolog in *Arabidopsis*. *Genes Cells* 11, 615–622. doi: 10.1111/j.1365-2443.2006.00972.x

Joshi, N., Brown, M. S., Bishop, D. K., and Börner, G. V. (2015). Gradual implementation of the meiotic recombination program via checkpoint pathways controlled by global DSB levels. *Mol. Cell* 57, 797–811. doi: 10.1016/j.molcel.2014.12.027

Joyce, E. F., and Mckim, K. S. (2010). Chromosome axis defects induce a checkpoint-mediated delay and interchromosomal effect on crossing over during drosophila meiosis. *PLoS Genet.* 6:e1001059. doi: 10.1371/journal.pgen.1001059

Joyce, E. F., Pedersen, M., Tiong, S., White-Brown, S. K., Paul, A., Campbell, S. D., et al. (2011). Drosophila ATM and ATR have distinct activities in the regulation of meiotic DNA damage and repair. *J. Cell Biol.* 195, 359–367.

Kauppi, L., Barchi, M., Lange, J., Baudat, F., Jasin, M., and Keeney, S. (2013). Numerical constraints and feedback control of double-strand breaks in mouse meiosis. *Genes Dev.* 27, 873–886. doi: 10.1101/gad.213652.113

Kee, K., Protacio, R. U., Arora, C., and Keeney, S. (2004). Spatial organization and dynamics of the association of Rec102 and Rec104 with meiotic chromosomes. *EMBO J.* 23, 1815–1824. doi: 10.1038/sj.emboj.7600184

Keeney, S. (2001). Mechanism and control of meiotic recombination initiation. *Curr. Top. Dev. Biol.* 52, 1–53. doi: 10.1016/s0070-2153(01)52008-6

Keeney, S. (2008). Spo11 and the formation of DNA double-strand breaks in meiosis. *Genome Dyn. Stab.* 2, 81–123. doi: 10.1007/7050_2007_026

Keeney, S., Giroux, C. N., and Kleckner, N. (1997). Meiosis-specific DNA double-strand breaks are catalyzed by Spo11, a member of a widely conserved protein family. *Cell* 88, 375–384. doi: 10.1016/S0092-8674(00)81876-0

Keeney, S., Lange, J., and Mohibullah, N. (2014). Self-organization of meiotic recombination initiation: general principles and molecular pathways. *Annu. Rev. Genet.* 48, 187–214. doi: 10.1146/annurev-genet-120213-092304

Kim, K. P., Weiner, B. M., Zhang, L., Jordan, A., Dekker, J., and Kleckner, N. (2010). Sister cohesion and structural axis components mediate homolog bias of meiotic recombination. *Cell* 143, 924–937. doi: 10.1016/j.cell.2010.11.015

Kim, S., Peterson, S. E., Jasin, M., and Keeney, S. (2016). Mechanisms of germ line genome instability. *Semin. Cell Dev. Biol.* 54, 177–187. doi: 10.1016/j.semcdb.2016.02.019

Kim, Y., Rosenberg, S. C., Kugel, C. L., Kostow, N., Rog, O., Davydov, V., et al. (2014). The chromosome axis controls meiotic events through a hierarchical assembly of HORMA domain proteins. *Dev. Cell* 31, 487–502. doi: 10.1016/j.devcel.2014.09.013

Klapholz, S., Waddell, C. S., and Esposito, R. E. (1985). The role of the Spo11 gene in meiotic recombination in yeast. *Genetics* 110, 187–216.

Kleckner, N. (2006). Chiasma formation: chromatin/axis interplay and the role(s) of the synaptonemal complex. *Chromosoma* 115, 175–194. doi: 10.1007/s00412-006-0055-7

Klein, F., Mahr, P., Galova, M., Buonomo, S. B. C., Michaelis, C., Nairz, K., et al. (1999). A central role for cohesins in sister chromatid cohesion, formation of axial elements, and recombination during yeast meiosis. *Cell* 98, 91–103. doi: 10.1016/S0092-8674(00)80609-1

Kugou, K., Fukuda, T., Yamada, S., Ito, M., Sasanuma, H., Mori, S., et al. (2009). Rec8 guides canonical Spo11 distribution along yeast meiotic chromosomes. *Mol. Biol. Cell* 20, 3064–3076. doi: 10.1091/mbc.E08-12-1223

Kumar, R., Bourbon, H. M., and De Massy, B. (2010). Functional conservation of Mei4 for meiotic DNA double-strand break formation from yeasts to mice. *Genes Dev.* 24, 1266–1280. doi: 10.1101/gad.571710

Kumar, R., Oliver, C., Brun, C., Juarez-Martinez, A. B., Tarabay, Y., Kadlec, J., et al. (2018). Mouse REC114 is essential for meiotic DNA double-strand break formation and forms a complex with MEI4. *Life Sci. Alliance* 1:e201800259. doi: 10.26508/lsa.201800259

Lam, I., and Keeney, S. (2015). Mechanism and regulation of meiotic recombination initiation. *Cold Spring Harb. Perspect. Biol.* 7:a016634. doi: 10.1101/cshperspect.a016634

Lange, J., Pan, J., Cole, F., Thelen, M. P., Jasin, M., and Keeney, S. (2011). ATM controls meiotic double-strand-break formation. *Nature* 479, 237–240. doi: 10.1038/nature10508

Lee, M.-S., Higashide, M. T., Choi, H., Li, K., Hong, S., Lee, K., et al. (2020). The synaptonemal complex central region modulates 2 crossover pathways and feedback control of meiotic double-strand break formation 4 5. *bioRxiv [Preprint]* doi: 10.1101/2020.07.10.198168

Li, J., Hooker, G. W., and Roeder, G. S. (2006). *Saccharomyces cerevisiae* Mer2, Mei4 and Rec114 form a complex required for meiotic double-strand break formation. *Genetics* 173, 1969–1981. doi: 10.1534/genetics.106.058768

Li, P., Banjade, S., Cheng, H. C., Kim, S., Chen, B., Guo, L., et al. (2012). Phase transitions in the assembly of multivalent signalling proteins. *Nature* 483, 336–340. doi: 10.1038/nature10879

Liang, J., Suhandynata, R. T., and Zhou, H. (2015). Phosphorylation of Sae2 mediates Forkhead-associated (FHA) domain-specific interaction and regulates its DNA repair function. *J. Biol. Chem.* 290, 10751–10763. doi: 10.1074/jbc.M114.625293

Lichten, M., and Goldman, A. S. H. (1995). Meiotic recombination hotspots. *Annu. Rev. Genet.* 29, 423–444. doi: 10.1146/annurev.ge.29.120195.002231

Liu, J., Wu, T. C., and Lichten, M. (1995). The location and structure of double-strand DNA breaks induced during yeast meiosis: evidence for a covalently linked DNA-protein intermediate. *EMBO J.* 14, 4599–4608. doi: 10.1002/j.1460-2075.1995.tb00139.x

Liu, Y., Sung, S., Kim, Y., Li, F., Gwon, G., Jo, A., et al. (2016). ATP -dependent DNA binding, unwinding, and resection by the Mre11/Rad50 complex. *EMBO J.* 35, 743–758. doi: 10.15252/embj.201592462

Lynn, A., Soucek, R., and Börner, G. V. (2007). ZMM proteins during meiosis: crossover artists at work. *Chromosom. Res.* 15, 591–605. doi: 10.1007/s10577-007-1150-1

Madrona, A. Y., and Wilson, D. K. (2004). The structure of Ski8p, a protein regulating mRNA degradation: implications for WD protein structure. *Protein Sci.* 13, 1557–1565. doi: 10.1110/ps.04704704

Maleki, S., Neale, M. J., Arora, C., Henderson, K. A., and Keeney, S. (2007). Interactions between Mei4, Rec114, and other proteins required for meiotic DNA double-strand break formation in *Saccharomyces cerevisiae*. *Chromosoma* 116, 471–486. doi: 10.1007/s00412-007-0111-y

Malone, R. E., Bullard, S., Hermiston, M., Rieger, R., Cool, M., and Galbraith, A. (1991). Isolation of mutants defective in early steps of meiotic recombination in the yeast *Saccharomyces cerevisiae*. *Genetics* 128, 79–88.

Malone, R. E., and Esposito, R. E. (1981). Recombinationless meiosis in *Saccharomyces cerevisiae*. *Mol. Cell. Biol.* 1, 891–901. doi: 10.1128/mcb.1.10.891

Martini, E., Borde, V., Legendre, M., Audic, S., Regnault, B., Soubigou, G., et al. (2011). Genome-wide analysis of heteroduplex DNA in mismatch repair–deficient yeast cells reveals novel properties of meiotic recombination pathways. *PLoS Genet.* 7:e1002305. doi: 10.1371/journal.pgen.1002305

Masai, H., and Arai, K. I. (2002). Cdc7 kinase complex: a key regulator in the initiation of DNA replication. *J. Cell. Physiol.* 190, 287–296. doi: 10.1002/jcp.10070

Matos, J., Lipp, J. J., Bogdanova, A., Guillot, S., Okaz, E., Junqueira, M., et al. (2008). Dbf4-dependent Cdc7 kinase links DNA replication to the segregation of homologous chromosomes in meiosis I. *Cell* 135, 662–678. doi: 10.1016/j.cell.2008.10.026

Matsumoto, S., Ogino, K., Noguchi, E., Russell, P., and Masai, H. (2005). Hsk1-Dfp1/Him1, the Cdc7-Dbf4 kinase in *Schizosaccharomyces* pombe, associates with Swi1, a component of the replication fork protection complex. *J. Biol. Chem.* 280, 42536–42542. doi: 10.1074/jbc.M510575200

Menees, T. M., and Roeder, G. S. (1989). MEI4, a yeast gene required for meiotic recombination. *Genetics* 123, 675–682.

Mimitou, E. P., Yamada, S., and Keeney, S. (2017). A global view of meiotic double-strand break end resection. *Science* 355, 40–45. doi: 10.1126/science.aak9704

Miyoshi, T., Ito, M., Kugou, K., Yamada, S., Furuichi, M., Oda, A., et al. (2012). A central coupler for recombination initiation linking chromosome architecture to s phase checkpoint. *Mol. Cell* 47, 722–733. doi: 10.1016/j.molcel.2012.06.023

Mohibullah, N., and Keeney, S. (2017). Numerical and spatial patterning of yeast meiotic DNA breaks by Tel1. *Genome Res.* 27, 278–288. doi: 10.1101/gr.213587.116

Mu, X., Murakami, H., Mohibullah, N., and Keeney, S. (2020). Chromosome-autonomous feedback down-regulates meiotic DNA break competence upon synaptonemal complex formation. *Genes Dev.* 34, 1605–1618. doi: 10.1101/gad.342873.120

Muller, H., Scolari, V. F., Agier, N., Piazza, A., Thierry, A., Mercy, G., et al. (2018). Characterizing meiotic chromosomes' structure and pairing using a designer sequence optimized for Hi-C. *Mol. Syst. Biol.* 14:e8293. doi: 10.15252/msb.20188293

Murakami, H., and Keeney, S. (2014). Temporospatial coordination of meiotic dna replication and recombination via DDK recruitment to replisomes. *Cell* 158, 861–873. doi: 10.1016/j.cell.2014.06.028

Murakami, H., Lam, I., Huang, P.-C., Song, J., van Overbeek, M., and Keeney, S. (2020). Multilayered mechanisms ensure that short chromosomes recombine in meiosis. *Nature* 582, 124–128. doi: 10.1038/s41586-020-2248-2

Murakami, H., and Nicolas, A. (2009). Locally, meiotic double-strand breaks targeted by Gal4BD-Spo11 occur at discrete sites with a sequence preference. *Mol. Cell. Biol.* 29, 3500–3516. doi: 10.1128/mcb.00088-09

Nairz, K., and Klein, F. (1997). mre11S - a yeast mutation that blocks double-strand-break processing and permits nonhomologous synapsis in meiosis. *Genes Dev.* 11, 2272–2290. doi: 10.1101/gad.11.17.2272

Nakada, D., Matsumoto, K., and Sugimoto, K. (2003). ATM-related Tel1 associates with double-strand breaks through an Xrs2-dependent mechanism. *Genes Dev.* 17, 1957–1962. doi: 10.1101/gad.1099003

Nandabalan, K., and Roeder, G. S. (1995). Binding of a cell-type-specific RNA splicing factor to its target regulatory sequence. *Mol. Cell. Biol.* 15, 1953–1960. doi: 10.1128/mcb.15.4.1953

Nasar, F., Jankowski, C., and Nag, D. K. (2000). Long palindromic sequences induce double-strand breaks during meiosis in yeast. *Mol. Cell. Biol.* 20, 3449–3458. doi: 10.1128/mcb.20.10.3449-3458.2000

Neale, M. J., Pan, J., and Keeney, S. (2005). Endonucleolytic processing of covalent protein-linked DNA double-strand breaks. *Nature* 436, 1053–1057. doi: 10.1038/nature03872

Nichols, M. D., DeAngelis, K., Keck, J. L., and Berger, J. M. (1999). Structure and function of an archaeal topoisomerase VI subunit with homology to the meiotic recombination factor Spo11. *EMBO J.* 18, 6177–6188. doi: 10.1093/emboj/18.21.6177

Niu, H., Wan, L., Baumgartner, B., Schaefer, D., Loidl, J., and Hollingsworth, N. M. (2005). Partner choice during meiosis is regulated by Hop1-promoted dimerization of Mek1. *Mol. Biol. Cell* 16, 5804–5818.

Ogino, K., and Masai, H. (2006). Rad3-Cds1 mediates coupling of initiation of meiotic recombination with DNA replication: Mei4-dependent transcription as a potential target of meiotic checkpoint. *J. Biol. Chem.* 281, 1338–1344. doi: 10.1074/jbc.M505767200

Oh, J., Al-Zain, A., Cannavo, E., Cejka, P., and Symington, L. S. (2016). Xrs2 dependent and independent functions of the Mre11-Rad50 complex. *Mol. Cell* 64, 405–415. doi: 10.1016/j.molcel.2016.09.011

Oh, J., Lee, S. J., Rothstein, R., and Symington, L. S. (2018). Xrs2 and tel1 independently contribute to MR-mediated DNA tethering and replisome stability. *Cell Rep.* 25, 1681.e4–1692.e4. doi: 10.1016/j.celrep.2018.10.030

Page, S. L., and Hawley, R. S. (2003). Chromosome choreography: the meiotic ballet. *Science* 301, 785–789. doi: 10.1126/science.1086605

Paiano, J., Wu, W., Yamada, S., Sciascia, N., Callen, E., Paola Cotrim, A., et al. (2020). ATM and PRDM9 regulate SPO11-bound recombination intermediates during meiosis. *Nat. Commun.* 11:857. doi: 10.1038/s41467-020-14654-w

Palmer, S., Schildkraut, E., Lazarin, R., Nguyen, J., and Nickoloff, J. A. (2003). Gene conversion tracts in Saccharomyces cerevisiae can be extremely short and highly directional. *Nucleic Acids Res.* 31, 1164–1173. doi: 10.1093/nar/gkg219

Pan, J., Sasaki, M., Kniewel, R., Murakami, H., Blitzblau, H. G., Tischfield, S. E., et al. (2011). A hierarchical combination of factors shapes the genome-wide topography of yeast meiotic recombination initiation. *Cell* 144, 719–731. doi: 10.1016/j.cell.2011.02.009

Panizza, S., Mendoza, M. A., Berlinger, M., Huang, L., Nicolas, A., Shirahige, K., et al. (2011). Spo11-accessory proteins link double-strand break sites to the chromosome axis in early meiotic recombination. *Cell* 146, 372–383. doi: 10.1016/j.cell.2011.07.003

Paull, T. T., and Gellert, M. (1998). The 3′ to 5′ exonuclease activity of Mre11 facilitates repair of DNA double-strand breaks. *Mol. Cell* 1, 969–979. doi: 10.1016/S1097-2765(00)80097-0

Petes, T. D. (2001). Meiotic recombination hot spots and cold spots. *Nat. Rev. Genet.* 2, 360–369. doi: 10.1038/35072078

Petronczki, M., Siomos, M. F., and Nasmyth, K. (2003). Un ménage à quatre: the molecular biology of chromosome segregation in meiosis. *Cell* 112, 423–440. doi: 10.1016/S0092-8674(03)00083-7

Pittman, D., Lu, W., and Malone, R. E. (1993). Genetic and molecular analysis of REC114, an early meiotic recombination gene in yeast. *Curr. Genet.* 23, 295–304. doi: 10.1007/BF00310890

Pratto, F., Brick, K., Cheng, G., Lam, G., Cloutier, J. M., Dahiya, D., et al. (2020). Germline DNA replication shapes the recombination landscape in mammals. *bioRxiv [Preprint]* doi: 10.1101/2020.09.23.308874

Prieler, S., Penkner, A., Borde, V., and Klein, F. (2005). The control of Spo11's interaction with meiotic recombination hotspots. *Genes Dev.* 19, 255–269. doi: 10.1101/gad.321105

Prugar, E., Burnett, C., Chen, X., and Hollingsworth, N. M. (2017). Coordination of double strand break repair and meiotic progression in yeast by a Mek1-Ndt80 negative feedback loop. *Genetics* 206, 497–512. doi: 10.1534/genetics.117.199703

Puizina, J., Siroky, J., Mokros, P., Schweizer, D., and Riha, K. (2004). Mre11 deficiency in Arabidopsis is associated with chromosomal instability in somatic cells and Spo11-dependent genome fragmentation during meiosis. *Plant Cell* 16, 1968–1978. doi: 10.1105/tpc.104.022749

Pyatnitskaya, A., Borde, V., and De Muyt, A. (2019). Crossing and zipping: molecular duties of the ZMM proteins in meiosis. *Chromosoma* 128, 181–198. doi: 10.1007/s00412-019-00714-8

Robert, T., Nore, A., Brun, C., Maffre, C., Crimi, B., Bourbon, H. M., et al. (2016). The topo VIB-Like protein family is required for meiotic DNA double-strand break formation. *Science* 351, 943–949. doi: 10.1126/science.aad5309

Rockmill, B., Engebrecht, J. A., Scherthan, H., Loidl, J., and Roeder, G. S. (1995). The yeast MER2 gene is required for chromosome synapsis and the initiation of meiotic recombination. *Genetics* 141, 49–59.

Roeder, G. S., Rockmill, B. M., Engebrecht, J., Thompson, E. A., and Menees, T. M. (1989). Isolation and characterization of yeast mutants defective in meiotic chromosome segregation. *Prog. Clin. Biol. Res.* 311, 303–326.

Rog, O., Köhler, S., and Dernburg, A. F. (2017). The synaptonemal complex has liquid crystalline properties and spatially regulates meiotic recombination factors. *Elife* 6:e21455. doi: 10.7554/eLife.21455

Rousova, D., Funk, S. K., Reichle, H., and Weir, J. R. (2020). Mer2 binds directly to both nucleosomes and axial proteins as the keystone of meiotic recombination. *bioRxiv [Preprint]* doi: 10.1101/2020.07.30.228908

San Filippo, J., Sung, P., and Klein, H. (2008). Mechanism of eukaryotic homologous recombination. *Annu. Rev. Biochem.* 77, 229–257. doi: 10.1146/annurev.biochem.77.061306.125255

Sasanuma, H., Murakami, H., Fukuda, T., Shibata, T., Nicolas, A., and Ohta, K. (2007). Meiotic association between Spo11 regulated by Rec102, Rec104 and Rec114. *Nucleic Acids Res.* 35, 1119–1133. doi: 10.1093/nar/gkl1162

Schalbetter, S. A., Fudenberg, G., Baxter, J., Pollard, K. S., and Neale, M. J. (2019). Principles of meiotic chromosome assembly revealed in *S. cerevisiae*. *Nat. Commun.* 10:4795. doi: 10.1038/s41467-019-12629-0

Schiller, C. B., Lammens, K., Guerini, I., Coordes, B., Feldmann, H., Schlauderer, F., et al. (2012). Structure of Mre11-Nbs1 complex yields insights into ataxia-telangiectasia- like disease mutations and DNA damage signaling. *Nat. Struct. Mol. Biol.* 19, 693–700. doi: 10.1038/nsmb.2323

Schiller, C. B., Seifert, F. U., Linke-Winnebeck, C., and Hopfner, K. P. (2014). Structural studies of DNA end detection and resection in homologous recombination. *Cold Spring Harb. Perspect. Biol.* 6:a017962. doi: 10.1101/cshperspect.a017962

Schwacha, A., and Kleckner, N. (1995). Identification of double holliday junctions as intermediates in meiotic recombination. *Cell* 83, 783–791

Seifert, F. U., Lammens, K., Stoehr, G., Kessler, B., and Hopfner, K. (2016). Structural mechanism of ATP -dependent DNA binding and DNA end bridging by eukaryotic Rad50. *EMBO J.* 35, 759–772. doi: 10.15252/embj.201592934

Shima, H., Suzuki, M., and Shinohara, M. (2005). Isolation and characterization of novel xrs2 mutations in Saccharomyces cerevisiae. *Genetics* 170, 71–85. doi: 10.1534/genetics.104.037580

Smith, A. V., and Roeder, G. S. (1997). The yeast Red1 protein localizes to the cores of meiotic chromosomes. *J. Cell Biol.* 136, 957–967. doi: 10.1083/jcb.136.5.957

Sommermeyer, V., Béneut, C., Chaplais, E., Serrentino, M. E., and Borde, V. (2013). Spp1, a member of the Set1 complex, promotes meiotic DSB formation in promoters by tethering histone H3K4 methylation sites to chromosome axes. *Mol. Cell* 49, 43–54. doi: 10.1016/j.molcel.2012.11.008

Stamper, E. L., Rodenbusch, S. E., Rosu, S., Ahringer, J., Villeneuve, A. M., and Dernburg, A. F. (2013). Identification of DSB-1, a protein required for initiation of meiotic recombination in *Caenorhabditis elegans*, illuminates a crossover assurance checkpoint. *PLoS Genet.* 9:e1003679. doi: 10.1371/journal.pgen.1003679

Stanzione, M., Baumann, M., Papanikos, F., Dereli, I., Lange, J., Ramlal, A., et al. (2016). Meiotic DNA break formation requires the unsynapsed chromosome axis-binding protein IHO1 (CCDC36) in mice. *Nat. Cell Biol.* 18, 1208–1220. doi: 10.1038/ncb3417

Steiner, S., Kohli, J., and Ludin, K. (2010). Functional interactions among members of the meiotic initiation complex in fission yeast. *Curr. Genet.* 56, 237–249. doi: 10.1007/s00294-010-0296-0

Subramanian, V. V., Zhu, X., Markowitz, T. E., Vale-Silva, L. A., San-Segundo, P. A., Hollingsworth, N. M., et al. (2019). Persistent DNA-break potential near telomeres increases initiation of meiotic recombination on short chromosomes. *Nat. Commun.* 10:970. doi: 10.1038/s41467-019-08875-x

Sun, H., Treco, D., Schultes, N. P., and Szostak, J. W. (1989). Double-strand breaks at an initiation site for meiotic gene conversion. *Nature* 338, 87–90. doi: 10.1038/338087a0

Sun, H., Treco, D., and Szostak, J. W. (1991). Extensive 3′-overhanging, single-stranded DNA associated with the meiosis-specific double-strand breaks at the ARG4 recombination initiation site. *Cell* 64, 1155–1161. doi: 10.1016/0092-8674(91)90270-9

Sun, X., Huang, L., Markowitz, T. E., Blitzblau, H. G., Chen, D., Klein, F., et al. (2015). Transcription dynamically patterns the meiotic chromosome-axis interface. *Elife* 4:e07424. doi: 10.7554/eLife.07424

Symington, L. S. (2016). Mechanism and regulation of DNA end resection in eukaryotes. *Crit. Rev. Biochem. Mol. Biol.* 51, 195–212. doi: 10.3109/10409238.2016.1172552

Tessé, S., Bourbon, H. M., Debuchy, R., Budin, K., Dubois, E., Liangran, Z., et al. (2017). Asy2/Mer2: an evolutionarily conserved mediator of meiotic recombination, pairing, and global chromosome compaction. *Genes Dev.* 31, 1880–1893. doi: 10.1101/gad.304543.117

Tessé, S., Storlazzi, A., Kleckner, N., Gargano, S., and Zickler, D. (2003). Localization and roles of Ski8p protein in Sordaria meiosis and delineation of three mechanistically distinct steps of meiotic homolog juxtaposition. *Proc. Natl. Acad. Sci. U.S.A.* 100, 12865–12870. doi: 10.1073/pnas.2034282100

Thacker, D., Mohibullah, N., Zhu, X., and Keeney, S. (2014). Homologue engagement controls meiotic DNA break number and distribution. *Nature* 510, 241–246. doi: 10.1038/nature13120

Tischfield, S. E., and Keeney, S. (2012). Scale matters. *Cell Cycle* 11, 1496–1503. doi: 10.4161/cc.19733

Tran, P. T., Erdeniz, N., Dudley, S., and Liskay, R. M. (2002). Characterization of nuclease-dependent functions of Exo1p in Saccharomyces cerevisiae. *DNA Repair.* 1, 895–912. doi: 10.1016/S1568-7864(02)00114-3

Tsai, B., Liu, W., Dong, D., Shi, K., Chen, L., and Gao, N. (2020). Phase separation of Mer2 organizes the meiotic loop-axis structure of chromatin during meiosis I. *bioRxiv [Preprint]* doi: 10.1101/2020.12.15.422856

Tsukamoto, Y., Mitsuoka, C., Terasawa, M., Ogawa, H., and Ogawa, T. (2005). Xrs2p regulates Mre11p translocation to the nucleus and plays a role in telomere elongation and meiotic recombination. *Mol. Biol. Cell* 16, 597–608. doi: 10.1091/mbc.E04-09-0782

Usui, T., Ohta, T., Oshiumi, H., Tomizawa, J. I., Ogawa, H., and Ogawa, T. (1998). Complex formation and functional versatility of Mre11 of budding yeast in recombination. *Cell* 95, 705–716. doi: 10.1016/S0092-8674(00)81640-2

Voelkel-Meiman, K., Cheng, S. Y., Morehouse, S. J., and Macqueen, A. J. (2016). Synaptonemal complex proteins of budding yeast define reciprocal roles in

MutSγ-mediated crossover formation. *Genetics* 203, 1091–1103. doi: 10.1534/genetics.115.182923

Vrielynck, N., Chambon, A., Vezon, D., Pereira, L., Chelysheva, L., De Muyt, A., et al. (2016). A DNA topoisomerase VI-like complex initiates meiotic recombination. *Science* 351, 939–943. doi: 10.1126/science.aad5196

Wan, L., Niu, H., Futcher, B., Zhang, C., Shokat, K. M., Boulton, S. J., et al. (2008). Cdc28-Clb5 (CDK-S) and Cdc7-Dbf4 (DDK) collaborate to initiate meiotic recombination in yeast. *Genes Dev.* 22, 386–397. doi: 10.1101/gad.1626408

Wang, W., Dong, J., Chen, B., Du, J., Kuang, Y., Sun, X., et al. (2019). Homozygous mutations in REC114 cause female infertility characterised by multiple pronuclei formation and early embryonic arrest. *J. Med. Genet.* 57, 187–194. doi: 10.1136/jmedgenet-2019-106379

Wendorff, T. J., and Berger, J. M. (2018). Topoisomerase VI senses and exploits both DNA crossings and bends to facilitate strand passage. *Elife* 7:e31724. doi: 10.7554/eLife.31724

West, A. M., Rosenberg, S. C., Ur, S. N., Lehmer, M. K., Ye, Q., Hagemann, G., et al. (2019). A conserved filamentous assembly underlies the structure of the meiotic chromosome axis. *Elife* 8:e40372. doi: 10.7554/eLife.40372

West, A. M. V., Komives, E. A., and Corbett, K. D. (2018). Conformational dynamics of the Hop1 HORMA domain reveal a common mechanism with the spindle checkpoint protein Mad2. *Nucleic Acids Res.* 46, 279–292. doi: 10.1093/nar/gkx1196

West, K. L., and Austin, C. A. (1999). Human DNA topoisomerase IIβ binds and cleaves four-way junction DNA in vitro. *Nucleic Acids Res.* 27, 984–992. doi: 10.1093/nar/27.4.984

Wilkins, A. S., and Holliday, R. (2009). The evolution of meiosis from mitosis. *Genetics* 181, 3–12. doi: 10.1534/genetics.108.099762

Williams, R. S., Moncalian, G., Williams, J. S., Yamada, Y., Limbo, O., Shin, D. S., et al. (2008). Mre11 dimers coordinate DNA end bridging and nuclease processing in double-strand-break repair. *Cell* 135, 97–109. doi: 10.1016/j.cell.2008.08.017

Wiltzius, J. J. W., Hohl, M., Fleming, J. C., and Petrini, J. H. J. (2005). The Rad50 hook domain is a critical determinant of Mre11 complex functions. *Nat. Struct. Mol. Biol.* 12, 403–407. doi: 10.1038/nsmb928

Wojtasz, L., Daniel, K., Roig, I., Bolcun-Filas, E., Xu, H., Boonsanay, V., et al. (2009). Mouse HORMAD1 and HORMAD2, two conserved meiotic chromosomal proteins, are depleted from synapsed chromosome axes with the help of TRIP13 AAA-ATPase. *PLoS Genet.* 5:e1000702. doi: 10.1371/journal.pgen.1000702

Woltering, D., Baumgartner, B., Bagchi, S., Larkin, B., Loidl, J., de los Santos, T., et al. (2000). Meiotic segregation, synapsis, and recombination checkpoint functions require physical interaction between the chromosomal proteins Red1p and Hop1p. *Mol. Cell. Biol.* 20, 6646–6658. doi: 10.1128/mcb.20.18.6646-6658.2000

Wright, W. D., Shah, S. S., and Heyer, W. D. (2018). Homologous recombination and the repair of DNA double-strand breaks. *J. Biol. Chem.* 293, 10524–10535. doi: 10.1074/jbc.TM118.000372

Wu, P. Y. J., and Nurse, P. (2014). Replication origin selection regulates the distribution of meiotic recombination. *Mol. Cell* 53, 655–662. doi: 10.1016/j.molcel.2014.01.022

Wu, T. C., and Lichten, M. (1994). Meiosis-induced double-strand break sites determined by yeast chromatin structure. *Science* 263, 515–518. doi: 10.1126/science.8290959

Xu, L., Ajimura, M., Padmore, R., Klein, C., and Kleckner, N. (1995). NDT80, a meiosis-specific gene required for exit from pachytene in *Saccharomyces cerevisiae*. *Mol. Cell. Biol.* 15, 6572–6581. doi: 10.1128/mcb.15.12.6572

Yamada, S., Hinch, A. G., Kamido, H., Zhang, Y., Edelmann, W., and Keeney, S. (2020). Molecular structures and mechanisms of DNA break processing in mouse meiosis. *Genes Dev.* 34, 806–818. doi: 10.1101/gad.336032.119

Young, J. A., Hyppa, R. W., and Smith, G. R. (2004). Conserved and nonconserved proteins for meiotic DNA breakage and repair in yeasts. *Genetics* 167, 593–605. doi: 10.1534/genetics.103.023762

Zakharyevich, K., Ma, Y., Tang, S., Hwang, P. Y. H., Boiteux, S., and Hunter, N. (2010). Temporally and biochemically distinct activities of exo1 during meiosis: double-strand break resection and resolution of double holliday junctions. *Mol. Cell* 40, 1001–1015. doi: 10.1016/j.molcel.2010.11.032

Zakharyevich, K., Tang, S., Ma, Y., and Hunter, N. (2012). Delineation of joint molecule resolution pathways in meiosis identifies a crossover-specific resolvase. *Cell* 149, 334–347. doi: 10.1016/j.cell.2012.03.023

Zhang, L., Kleckner, N. E., Storlazzi, A., and Kim, K. P. (2011). Meiotic double-strand breaks occur once per pair of (sister) chromatids and, via Mec1/ATR and Tel1/ATM, once per quartet of chromatids. *Proc. Natl. Acad. Sci. U. S. A.* 108, 20036–20041. doi: 10.1073/pnas.1117937108

Zickler, D., and Kleckner, N. (1999). Meiotic chromosomes: integrating structure and function. *Annu. Rev. Genet.* 33, 603–754. doi: 10.1146/annurev.genet.33.1.603

Zickler, D., and Kleckner, N. (2015). Recombination, pairing, and synapsis of homologs during meiosis. *Cold Spring Harb. Perspect. Biol.* 7:a016626. doi: 10.1101/cshperspect.a016626

Conflict of Interest: The authors declare that the research was conducted in the absence of any commercial or financial relationships that could be construed as a potential conflict of interest.

Copyright © 2021 Yadav and Claeys Bouuaert. This is an open-access article distributed under the terms of the Creative Commons Attribution License (CC BY). The use, distribution or reproduction in other forums is permitted, provided the original author(s) and the copyright owner(s) are credited and that the original publication in this journal is cited, in accordance with accepted academic practice. No use, distribution or reproduction is permitted which does not comply with these terms.

frontiers in Cell and Developmental Biology

MINI REVIEW
published: 05 March 2021
doi: 10.3389/fcell.2021.626020

Transcriptomics of Meiosis in the Male Mouse

Adriana Geisinger[1,2], Rosana Rodríguez-Casuriaga[2] and Ricardo Benavente[3]*

[1] *Biochemistry-Molecular Biology, Facultad de Ciencias, Universidad de la República (UdelaR), Montevideo, Uruguay,*
[2] *Department of Molecular Biology, Instituto de Investigaciones Biológicas Clemente Estable (IIBCE), Montevideo, Uruguay,*
[3] *Department of Cell and Developmental Biology, Biocenter, University of Würzburg, Würzburg, Germany*

Molecular studies of meiosis in mammals have been long relegated due to some intrinsic obstacles, namely the impossibility to reproduce the process *in vitro*, and the difficulty to obtain highly pure isolated cells of the different meiotic stages. In the recent years, some technical advances, from the improvement of flow cytometry sorting protocols to single-cell RNAseq, are enabling to profile the transcriptome and its fluctuations along the meiotic process. In this mini-review we will outline the diverse methodological approaches that have been employed, and some of the main findings that have started to arise from these studies. As for practical reasons most studies have been carried out in males, and mostly using mouse as a model, our focus will be on murine male meiosis, although also including specific comments about humans. Particularly, we will center on the controversy about gene expression during early meiotic prophase; the widespread existing gap between transcription and translation in meiotic cells; the expression patterns and potential roles of meiotic long non-coding RNAs; and the visualization of meiotic sex chromosome inactivation from the RNAseq perspective.

Keywords: meiosis, transcriptomics, RNAseq, meiotic prophase, spermatogenesis, lncRNAs, MSCI, spermatogenic cell sorting

OPEN ACCESS

Edited by:
Scott Keeney,
Memorial Sloan Kettering Cancer Center, United States

Reviewed by:
Sue Hammoud,
University of Michigan, United States
Satoshi H. Namekawa,
University of California, Davis, United States

****Correspondence:***
Adriana Geisinger
adriana.geisinger@gmail.com

Specialty section:
This article was submitted to Cell Growth and Division, a section of the journal Frontiers in Cell and Developmental Biology

Received: *04 November 2020*
Accepted: *15 February 2021*
Published: *05 March 2021*

Citation:
Geisinger A, Rodríguez-Casuriaga R and Benavente R (2021) Transcriptomics of Meiosis in the Male Mouse. Front. Cell Dev. Biol. 9:626020. doi: 10.3389/fcell.2021.626020

INTRODUCTION

The alteration of the meiotic program is at the basis of an important number of fertility problems (Handel and Schimenti, 2010; Hann et al., 2011; Geisinger and Benavente, 2016; Gheldof et al., 2019; Veitia, 2020) and other pathologies (e.g., Tsui and Crismani, 2019), including cancer (Feichtinger and McFarlane, 2019). Therefore, the need to improve the knowledge on the molecular groundwork of meiosis in mammals is obvious. However, the studies on the molecular bases of mammalian meiosis have been hampered by some intrinsic obstacles. In the first place, the lack of reliable and robust *in vitro* culture systems of mammalian meiotic cells (Handel et al., 2014; Sun et al., 2014; Komeya et al., 2018; Hayashi, 2019; Bharti et al., 2020) is an important drawback that raises the need to work with *in vivo* models. Besides, in females the main meiotic events take place during the embryonic phase, and the number of oocytes is scarce, which hinders molecular analyses (e.g., Hernández-López et al., 2020). Studies in males are more accessible as meiosis starts in the postnatal life, and the testes produce massive numbers of gametes; consequently, most studies have been performed in males. Notwithstanding this, male meiosis is part of the asynchronous and continuous spermatogenic process (Griswold, 2016), and therefore germ cells spanning all the different stages of spermatogenesis simultaneously coexist within adult testes, altogether with different types of testicular somatic cells. Testicular heterogeneity constitutes a challenge when trying to unravel the

molecular program of a specific stage or cell type, as a pre-requisite is the availability of methods to allow profiling that specific cell type separately from the whole mix. Particularly, pachytene spermatocytes (PS) comprise about 5% in adult mice testicular cell suspensions (Soumillon et al., 2013, and our own observations).

As mouse is the most popular mammalian model because of its relatively easy maintenance and manipulation, in addition to its highly curated genome, most transcriptomic studies on mammalian meiosis have been carried out in mice. Nevertheless, despite the extensive similarities with human meiosis, it must be recalled that some notorious between-species differences exist, including the histological organization of the testis, duration of the seminiferous epithelium cycle, and germline-niche interactions, among others (Guo et al., 2018, 2020; Shami et al., 2020). This being said, mouse studies are significantly contributing to increase our understanding about human meiosis and its associated pathologies.

Microarray-based studies have been employed for profiling the transcriptome along spermatogenesis (e.g., Schultz et al., 2003; Maratou et al., 2004; Rossi et al., 2004; Shima et al., 2004; Pang et al., 2006; Chalmel et al., 2007; Fallahi et al., 2010; Waldman Ben-Asher et al., 2010; Bao et al., 2013; Sun et al., 2013; Liang et al., 2014), albeit these are being largely replaced by RNAseq due to its increased sensitivity, and to its ability to identify previously unknown transcripts and novel isoforms (Roy et al., 2011; Mutz et al., 2013).

In this mini-review, we will outline some interesting features that are starting to arise from transcriptomic studies of murine meiotic cells, mostly based on RNAseq (although some microarray results will be also included). As due to the above-mentioned constraints the vast majority of reports correspond to males, we will focus on male meiosis. A number of recent studies have addressed the analysis of gene expression in mouse meiotic precursor cells, to evaluate spermatogonial differentiation and/or mitosis-to-meiosis transition (Green et al., 2018; Hermann et al., 2018; La et al., 2018; Ernst et al., 2019; Grive et al., 2019; Law et al., 2019; Liao et al., 2019; Velte et al., 2019; Tan et al., 2020). Here, due to space limitations, we will only focus on the meiotic phase itself. Overall, transcriptomic analyses have shown that male meiotic (and post-meiotic) cells have an extremely complex transcriptome (Soumillon et al., 2013), expressing a panoply of mRNAs and splice variants, long non-coding RNAs (lncRNAs), and small non-coding RNAs (sncRNAs). Far from aiming to cover all the knowledge in the field, our objective is to illustrate how the methodologies that allow to isolate different specific meiotic cell populations or to profile individual cells, in combination with transcriptomic techniques, are contributing to our understanding of the molecular bases of meiosis. In particular, we will center on the different approaches that have been employed to enable profiling the transcriptome of isolated/individual murine meiotic cells, and on some novel aspects we have selected to develop, specifically concerning coding genes and lncRNAs. On the other hand, sncRNAs – including miRNAs and piRNAs – play essential roles for the control of meiosis and spermiogenesis progression (e.g., Gou et al., 2014; Goh et al., 2015; Dai et al., 2019), and certainly would deserve a chapter. However, as exhaustive reviews about them have been published elsewhere, and in order not to extend further, we will not elaborate on the subject here (for revisions on meiotic sncRNAs, see Bortvin, 2013; de Mateo and Sassone-Corsi, 2014; Kotaja, 2014; Yadav and Kotaja, 2014; Wang and Xu, 2015; Luo et al., 2016; Dai et al., 2020, among others).

STRATEGIES FOR THE OBTAINMENT OF MEIOTIC CELLS FOR RNAseq

Different studies have addressed the complexity of mammalian testicular gene expression through RNAseq, by analyzing bulk RNA from testes of pre-pubertal animals at increasing ages along the semi-synchronous first spermatogenic wave, where the new transcripts are attributed to the newly appeared cell types (e.g., Gong et al., 2013; Laiho et al., 2013; Weng et al., 2017). The disadvantages of these studies are that they do not allow undoubtedly assigning specific RNAs to a certain cell type, and fail in the characterization of transcripts from poorly represented cell types such as those from early meiotic prophase stages. Besides, they do not take into account the intricate cell-cell interactions within the testis (e.g., between spermatogenic and somatic Sertoli cells), where some cell types can change their expression patterns in contact with the newly appeared cell types (Green et al., 2018; Guo et al., 2020; Tan et al., 2020). As an attempt to partially overcome these limitations, some studies have combined the use of testes of individuals at increasing ages with a computational approach, in order to de-convolve the temporal expression profiles into cell type-specific expression profiles (Margolin et al., 2014; Ball et al., 2016).

The alternative approach has been the use of isolated testicular cell populations or (more recently) individual cells, to more accurately profile the transcriptome of specific stages along the spermatogenic process. Beyond the fact that differences between the first spermatogenic round and the following ones have been reported (Yoshida et al., 2006; Grive et al., 2019), either adult or pre-pubertal individuals at increasing ages have been used. Historically, the most classical methods for obtaining stage-specific spermatogenic cell populations from rodent testicles, have been STA-PUT (i.e., a gravimetric decantation in an albumin gradient; Lam et al., 1970; Go et al., 1971; Romrell et al., 1976; Bellvé, 1993) and centrifugal elutriation (Meistrich, 1977). Both methods have been employed for the obtainment of enriched cell populations for RNAseq (e.g., Gan et al., 2013b; Soumillon et al., 2013; Chalmel et al., 2014; Hammoud et al., 2014; Sin et al., 2015; Lin et al., 2016; Wichman et al., 2017). However, these methods only allow the obtainment of highly enriched but not pure cell populations (Meistrich, 1977; Soumillon et al., 2013), and only of certain specific cell types, while other cell types are obtained at low purity levels (Meistrich, 1977). Particularly concerning meiosis, PS have been mostly taken as the representative meiotic stage, as they constitute the only meiotic cell type that can be obtained with a significant enrichment because of their relative abundance and larger size/density (Meistrich, 1977).

Multi-parametric flow cytometry (FCM) has been used to analyze and sort different testicular cell populations based on

DNA content together with differences in nuclear size, cellular size, complexity, and chromatin compaction (Geisinger and Rodríguez-Casuriaga, 2010). Besides the advantage of enabling the obtainment of highly pure stage-specific cell populations, it allows the discrimination and eventual classification of a higher number of cell populations (Malkov et al., 1998; Bastos et al., 2005). Taking advantage of the blue and red fluorescence of the vital dye Hoechst 33342 (Bastos et al., 2005; Getun et al., 2011), Fallahi et al. (2010) isolated spermatogonia, pre-leptotene (pre-L), leptotene-zygotene (L/Z), early-PS, middle-PS, late-PS, diplotene (D), and round spermatids (RS) from adult male mice with over 95% purity for each fraction, by fluorescence activated cell sorting (FACS). The sorted cell populations were used for transcriptome profiling by microarray analysis (Fallahi et al., 2010). In our laboratory, we have developed a protocol for the purification of testicular cell populations by FACS using Vybrant DyeCycle Green, a non-cytotoxic vital dye with the advantage over Hoechst 33342 that it is excited with a blue laser thus avoiding the need of a UV laser, which in turn minimizes potential damage to nucleic acids caused by UV light exposure (Rodríguez-Casuriaga et al., 2014; Geisinger and Rodríguez-Casuriaga, 2017). This protocol allowed the profiling of coding transcripts and lncRNAs along spermatogenesis through RNAseq, using highly pure (>95%) stage-specific cell populations (da Cruz et al., 2016; Trovero et al., 2020). These studies included the L/Z cell population, thus enabling for the first time to compare the transcriptomic profiles, as obtained through NGS, between early and medium/late meiotic prophase, and providing information on gene expression fluctuations along meiotic prophase (da Cruz et al., 2016). An optimized Hoechst-33342-based FCM protocol for sorting enriched leptotene (L) aside from zygotene (Z) cell populations (60–80% and 75–90% purity, respectively) from adult mouse testis has been described (Gaysinskaya et al., 2014) and used for genome-wide methylation analyses (Gaysinskaya et al., 2018), although no extensive transcriptome profiling studies using this protocol have been reported so far.

Fluorescence activated cell sorting can be combined with antibodies to sort additional cell types, mainly specific populations of spermatogonia. As an example, Zhu et al. (2016) used a combination of FACS and Magnetic Activated Cell Sorting (MACS) to classify spermatocytes, spermatids, and undifferentiated spermatogonia from human testicular biopsies, for RNAseq. Another strategy for generating germ cell-specific transcriptome profiles from human biopsies, where the amount of material is very limiting, has been individual-cell laser capture microdissection (LCM). This method allowed the selection and transcriptome profiling of six distinct germ cell subtypes based on morphology, location in the seminiferous tubular cross-section, and germ cell associations at the various stages of the seminiferous epithelium; concerning meiotic cells, L/Z, early PS, and late PS were profiled (Jan et al., 2017).

A completely different approach has been the use of "meiotic-like" immortalized mouse cell lines. GC-1 cells (American Type Culture Collection [ATCC], Manassas, VA, United States) were created by transformation of type B spermatogonia with pSV3-neo, and are claimed to exhibit the characteristics of a stage between type B spermatogonia and primary spermatocytes, while GC-2 cells (ATCC) originated by transformation of spermatocytes with SV40 large T antigen, are arrested at a pre-meiotic stage, and are claimed to exhibit the characteristics of primary spermatocytes. A couple of reports compared the transcriptomes of these cell lines (Zhang et al., 2013; Hong et al., 2018). Notwithstanding, to what extent their transcriptomic profiles resemble those of pre-meiotic and meiotic prophase cells, is highly doubtful. In fact, a microarray comparison with whole testis profiles showed that a very small proportion of the testis-specific mRNAs and lncRNAs were detected in these cell lines (Hong et al., 2018), thus indicating that they have a limited usefulness.

Recently, single cell RNA sequencing (scRNAseq) has gained much attention, as it enables to profile the transcriptome of thousands of single cells in a population. Pseudotime ordering allows arranging cells along a continuous path that represents the evolution of a process. Thus, scRNAseq permits to capture the continuity of spermatogenesis, rather than artificially chosen stages. Moreover, it allows characterize the existing heterogeneity at any given phase, as well as the RNA content of rare cell populations (Suzuki et al., 2019; Soraggi et al., 2020). Various laboratories have addressed the characterization of RNA fingerprints from human testicular samples (Guo et al., 2018; Hermann et al., 2018; Wang et al., 2018; Shami et al., 2020) and mouse testes (Green et al., 2018; Hermann et al., 2018; Lukassen et al., 2018; Ernst et al., 2019; Grive et al., 2019; Jung et al., 2019) through scRNAseq (for a revision on the different used methodologies for scRNAseq and data-analysis, see Suzuki et al., 2019; Soraggi et al., 2020). In general, these studies coincide that spermatogenesis progresses as a continuum, with no clear-cut changes between the transcriptomes of successive cell types (Green et al., 2018; Guo et al., 2018; Hermann et al., 2018; Lukassen et al., 2018; Jung et al., 2019). One aspect to note, is that while in the methods relying on the isolation of cell populations cell type-assignment is generally based on the analysis of an aliquot of each sorted population (microscopical observation, immune labeling for cell type-specific protein markers), in unsorted scRNAseq studies deduction of cell type/subtype is done through the expression of marker genes. However, due to the pronounced uncoupling between transcription and translation along spermatogenesis (see below), we consider that this criterion may be misleading for staging purposes. For a more accurate cell-type assignment, some have compared the expression profiles of single cells from total testis dissociation, to those of stage-specific cells purified by FACS or STA-PUT (Hermann et al., 2018; Jung et al., 2019) or to available data sets from isolated cells of known identity (e.g., Ernst et al., 2019).

Chen et al. (2018) combined transgenic labeling by means of Vasa-dTomato (expressed in spermatogenic cells) and Lin28-YFP (expressed in undifferentiated spermatogonia), with synchronization of the cycle of the seminiferous epithelium using WIN 18,446/retinoic acid (Hogarth et al., 2013) for FACS sorting and scRNAseq. This allowed the profiling of 20 different cell subtypes from synchronized testicular tissues. Thus far this has been the most complete RNAseq study in isolated cells, as it included some previously unpurified cell types. Concerning

meiotic cells, L, Z, early-PS, middle-PS, late-PS, D, metaphase I, and metaphase II were profiled (Chen et al., 2018). Anyway, it must be recalled that spermatogenesis was manipulated, and although no overt differences in appearance, fertility, or gene expression between synchronized and unsynchronized testes have been detected (Romer et al., 2018), some gene expression differences with the normal, asynchronous process cannot be excluded.

Altogether, despite the diversity of approaches and methodologies, the different studies are allowing to reach some common conclusions that shed light on the transcriptomic landscape of the complex meiotic process. On the other hand, in some other cases results are not conclusive as different studies have reached controversial results, leaving the questions remain open. In the next sections we will go over only a few of the many interesting aspects that are emerging from these studies, trying to highlight some of the common findings, as well as some of the controversial points where more research is still needed.

GENE EXPRESSION IN EARLY MEIOTIC PROPHASE

Early studies measuring the incorporation of [H^3]uridine or [H^3]cytidine had suggested null (Monesi, 1964) or very low (Kierszenbaum and Tres, 1974) transcription levels in mouse testes during early meiotic prophase (i.e., L and Z), and even during early pachytene (P), in comparison to later prophase stages. This was supported by Page et al. (2012), who observed low levels of RNA polymerase II and the active-chromatin marker H3K9ac (histone H3 acetylated at lysine 9) in L, Z, and early PS, but a strong increase in mid-PS, while the marker for gene silencing and heterochromatin H3K9me3 (histone H3 trimethylated at lysine 9), showed the opposite pattern.

As noted above, transcriptomic studies in the short L and Z stages have been long relegated compared to those in PS. Now, experiments including isolated early meiotic prophase cells are allowing to address gene expression during L/Z. In general, the different reports agree that murine early spermatocytes present a low complexity transcriptome (Chen et al., 2018; Ernst et al., 2019), and this would stand true for humans as well (Jan et al., 2017). In spite of that, the power of RNAseq technology in combination with the use of isolated L/Z spermatocytes, reveal that important genes are differentially expressed during early meiotic prophase.

Using a highly pure L/Z cell population, we have shown the existence of a set of genes that are upregulated in L/Z, with almost half of them exhibiting a marked expression peak in these early stages. This group of genes that peak in L/Z, to decay before the P stage, includes genes related to meiotic processes (gene ontology [GO] terms "meiosis," "synaptonemal complex," "meiotic recombination," "chromosome condensation," "meiotic chromosome segregation"), among others (da Cruz et al., 2016). The study by Chen et al. (2018), whose 20 different isolated spermatogenic cell types allowed very fine discrimination, also showed an expression peak during early prophase, and a decrease in PS, for the representative terms "meiotic DNA double-strand break formation" and "meiotic chromosome segregation." Moreover, differentially expressed genes in the categories "meiotic cell cycle," "DNA repair," and "DNA recombination," appeared downregulated after L/Z (Chen et al., 2018). This would be also the case for human testes, where the expression of genes involved in meiotic recombination, homologous synapsis, synaptonemal complex, and compaction of chromatin, were detected as upregulated in L/Z (Jan et al., 2017; Wang et al., 2018). Besides, germ cell-specific transcriptomic profiles indicated that the genes contained within the GO terms "reciprocal meiotic recombination" and "meiotic chromosome segregation" were highly conserved between mouse and human, and mainly expressed in human L/Z spermatocytes (Jan et al., 2017).

Of course, it is very likely that at least some of the transcripts we detect with a marked expression peak in L/Z were already present in a sub-population of spermatogonia/pre-L cells. In fact, different studies indicate that the commitment to meiosis takes place in pre-meiotic cells, with meiotic genes being turned on before meiosis onset (e.g., Evans et al., 2014; Jan et al., 2017; Chen et al., 2018), and it seems that this could be the case for female meiosis as well (Soh et al., 2015). Anyway, transcriptomic studies make it clear that a group of genes related to male meiotic processes present an expression peak during early prophase, to decay later on in PS.

THE LAG BETWEEN TRANSCRIPTION AND TRANSLATION

Post-transcriptional regulation and particularly translational delay are a hallmark of spermatogenesis; their massiveness can be evidenced through transcriptome profiling.

As stated above, we and others have reported an expression peak in L/Z for genes within GO terms related to early meiotic events, but also for others related to late meiotic events such as "meiotic chromosome segregation," both for mouse (da Cruz et al., 2016; Chen et al., 2018) and human (Jan et al., 2017). Furthermore, many of the significantly expressed genes within those categories, were already up in pre-L (Chen et al., 2018). Curiously, some genes whose protein products play their roles in post-meiotic stages, are also differentially expressed in L/Z (da Cruz et al., 2016), or even earlier. These include genes coding for proteins related to sperm function and motility such as *Hspa5*, *Tex101*, *Ly6k* (da Cruz et al., 2016), *Odf2*, *Cabyr*, *Tcp11*, and *Hook1* (Jan et al., 2017), to name a few. Notably, an RNAseq analysis of mice mutant for *Prdm9* (that encodes a histone methyltransferase expressed in L/Z and required for the activation of recombination), showed that although the mutant testes were cytologically arrested in a late-L/Z stage, they nevertheless developed gene expression signatures characteristic of later developmental substages (Fine et al., 2019).

Despite the uncoupling between transcription and translation in PS is known, especially striking is the finding that the P transcriptome reveals widespread early expression of genes related to post-meiotic processes. Concurring with a couple of previous microarray studies (Fallahi et al., 2010; Waldman Ben-Asher et al., 2010; **Figures 1A,a,b**), our RNAseq analyses detected

a global expression switch in the testicular transcriptome during the progression from Z to P (da Cruz et al., 2016; **Figure 1A,c**). Moreover, this switch coincides with the turning off of a high number of meiotic genes, and the turning on of spermiogenesis-related ones (da Cruz et al., 2016). Specifically, terms related to "spermatid differentiation and development," "fertilization," "cilium and flagellum assembly and motility," "sperm-egg recognition," and "binding of sperm to zona pellucida," were among the most significantly represented GO categories within the differentially expressed genes at the L/Z-to-P transition (da Cruz et al., 2016; see **Figure 1A,c**), thus indicating that the spermiogenesis programs are turned on as early as during meiotic prophase. This is consistent with the results from Soumillon et al. (2013), who found that a gene cluster strongly upregulated in spermatocytes and spermatids, was significantly enriched with genes involved in spermatogenesis, gamete generation, sperm motility, and fertilization. Similar results were reported in the scRNAseq study from Jung et al. (2019). Also coinciding with other reports, Hermann et al. (2018) observed that although the expression of some genes for products of the spermatozoon such as sperm-specific glycolytic isozymes (*Gapdhs*, *Ldhc*, *Pgk2*, etc.) peaks in RS, their transcription starts in primary spermatocytes. Even studies using whole testes of individuals of increasing ages, either with deconvolution (Ball et al., 2016) or without it (Laiho et al., 2013), showed an enrichment in the expression of genes related to microtubule and cilia, spermiogenesis, and fertilization, at ages corresponding to the appearance of P/D spermatocytes (**Figure 1A,d**). The expression of sperm-related genes in meiotic prophase, has been also reported for men (Jan et al., 2017; Hermann et al., 2018).

It is interesting that a transcriptome analysis of STA-PUT–fractionated cells from *Sox30*$^{-/-}$ infertile mice, revealed SOX30 as a testis-specific transcription factor essential for activating haploid differentiation programs during the later stages of meiotic prophase. Loss of SOX30 resulted in the downregulation of a set of genes in PS (**Figure 1A,e**), and these downregulated genes were related to spermatogenesis, spermatid development, sperm motility, fusion of sperm to egg plasma membrane, and sperm capacitation (Bai et al., 2018).

In the same line of evidence, a microarray study showed that loss of A-MYB (MYBL1) – a male-specific master regulator of several meiotic processes that is expressed in PS (Bolcun-Filas et al., 2011) and is essential for the production of piRNAs and piRNA-pathway proteins (Li et al., 2013) – not only results in misregulation of meiotic genes, but also in the downregulation of genes whose transcripts are translated post-meiotically and involved in post-meiotic functions (Bolcun-Filas et al., 2011). A novel finding indicates that A-MYB is a key regulator of meiotic super-enhancers (i.e., regions of the genome comprising multiple enhancers that regulate important genes for cell identity) (Maezawa et al., 2020). Interestingly, many genes that are adjacent to meiotic super-enhancers and would be regulated by A-MYB, are known to be critical for late spermatogenesis (Maezawa et al., 2020). One such critical genes is *PIWIL1*, for which a human transcriptomic study indicated that its expression peaks in PS (Jan et al., 2017), and whose product, besides functioning in transposon silencing, has been shown to exert a role in the post-transcriptional regulation of mRNAs encoding spermatid-specific proteins (e.g., Gou et al., 2014; Dai et al., 2019).

The switch in gene expression programs could be facilitated by genome-wide changes leading to the *de novo* formation of accessible chromatin (Maezawa et al., 2018), and the extensive reprogramming of chromatin 3D architecture that takes place in meiotic cells (Alavattam et al., 2019; Patel et al., 2019; Vara et al., 2019; Wang et al., 2019; Luo et al., 2020). An integration of Hi-C (high-throughput genome-wide chromatin conformation capture) and RNA-seq from purified mouse spermatogenic cell populations, showed a switching in a subset of B (inactive) compartments to A (active) compartments in the chromatin of PS; the number of genome regions in A compartments was higher in PS, suggesting that PS chromatin is in a more transcriptionally active state. Notably, a number of genes that were originally located in compartment B regions in primitive spermatogonia and switched to compartment A regions in PS, and at same time increased their expression, have a function in DNA DSBs repair, but also in cilium formation, critical for normal sperm physiology (Luo et al., 2020).

The temporal uncoupling between transcription and translation in testicular germ cells, would be related to the need for extensive post-transcriptional regulation. During the last stages of spermiogenesis, histones are sequentially replaced first by transition proteins and then by protamines (**Figure 1B**), which results in transcriptional silencing (e.g., Braun, 1998; Kleene, 2001; Legrand and Hobbs, 2018). Extensive early transcription and RNA sequestration for its delayed translation (that in some cases takes place several days, or even weeks, after transcription), are viewed as a strategy to regulate the time of synthesis for proteins required in the transcriptionally inert elongating and elongated spermatids. The mRNAs for transition proteins and protamines themselves, although attaining their expression peak in RS, would start to be transcribed as early as in P/D (da Cruz et al., 2016), thus being stored for weeks before translation. Moreover, it is known that their premature translation is related to spermiogenesis arrest and infertility (Lee et al., 1995; Tseden et al., 2007). Furthermore, contrasting the results from proteomic studies with those of transcriptomic studies also supports the widespread translational repression in PS (Gan et al., 2013a).

Meiotic and early post-meiotic cells have developed diverse regulatory mechanisms to achieve these unusually high levels of post-transcriptional regulation (Kleene, 2001, 2013). These mechanisms include binding of repressor proteins (e.g., Idler and Yan, 2012) and sequestration of mRNAs as free ribonucleoprotein particles (Iguchi et al., 2006); manipulation of the length of 3'UTRs (Li et al., 2016); regulation through sncRNAs (Yadav and Kotaja, 2014) and lncRNAs (see below): sequestration of mRNAs in the chromatoid body of post-meiotic cells (Meikar et al., 2011, 2014; de Mateo and Sassone-Corsi, 2014; Lehtiniemi and Kotaja, 2018), and others. Particularly, an RNAseq study of purified mouse male germ cells indicates that coordinated intron retention is a mechanism of male meiotic cells to produce stable, long-lived transcripts that are preserved for days before their timely translation in transcriptionally inert post-meiotic cells. Moreover, intron-retention genes were specifically enriched in functional categories related to the late spermiogenic phase,

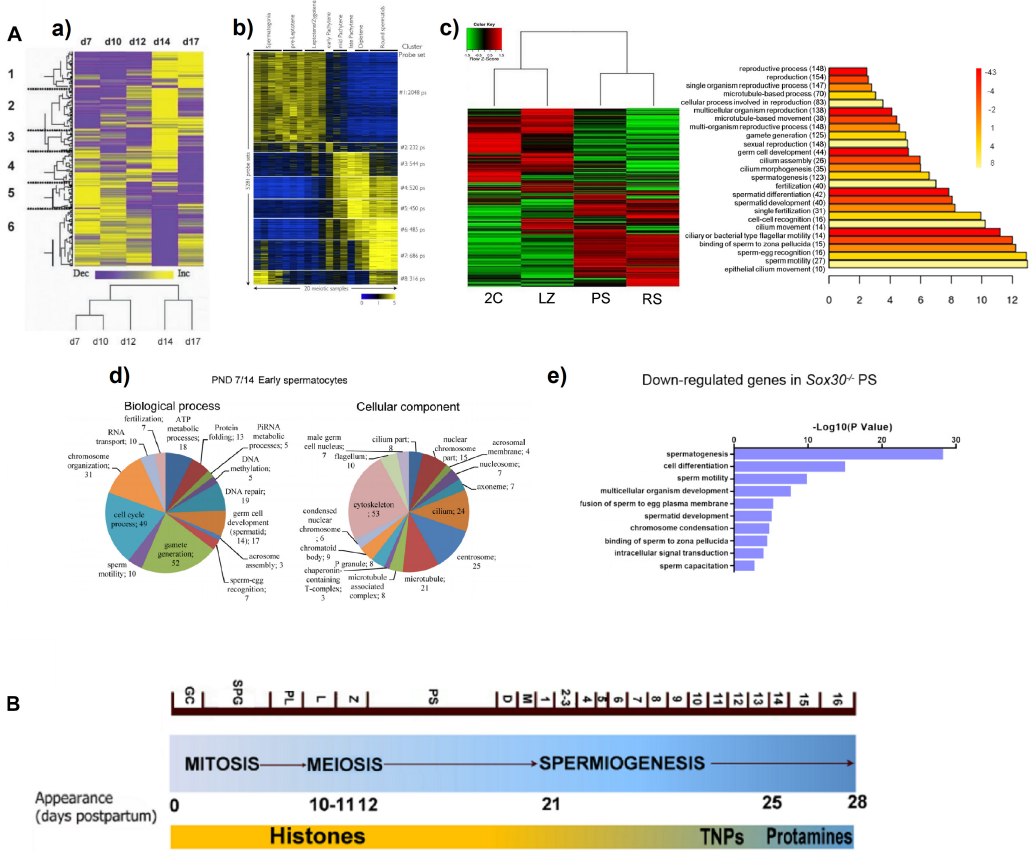

FIGURE 1 | (A) Examples from reports showing a switch in gene expression patterns, and the expression of spermiogenesis-specific programs during mouse meiotic prophase. **(a)** Heat map representing the clustering of 790 differentially expressed sequences derived from a microarray study in testes of animals of increasing age, from 7 days post-partum (d7) to 17 days post-partum (d17). Columns represent the expression profile of all the sequences for the indicated post-natal ages, while rows represent expression of specific genes over time (low expression levels are shown in purple, and high expression levels in yellow). Note the overall change from d12 to d14, coinciding with pachytene onset. A tree representing clustering by resemblance of expression profiles across the indicated post-natal ages is shown below. The figure is reproduced from Waldman Ben-Asher et al. (2010), with permission from John Wiley and Sons (license number 5014730359883). **(b)** Heat map showing the relative expression levels of 5,281 microarray probe sets divided into 8 K-means clusters, in different spermatogenic cell populations purified by FACS. Each horizontal line corresponds to a probe set (high expression in yellow, low expression in blue). The switch in the transcriptome between L/Z and mid-P is evident. Reprinted from Fallahi et al. (2010), under the Creative Commons Attribution License. **(c)** Heat map of expression levels and hierarchical clustering for the global differential gene expression in four FACS-sorted spermatogenic cell populations, profiled through RNAseq (2C, spermatogonia and somatic testicular cells; LZ, leptotene/zygotene; PS, pachytene spermatocytes; RS, round spermatids). High expression: red; low expression: green. To the right, the main enriched GO terms for biological process category (BP) of the upregulated genes in PS are shown. The heat map evidences a switch in gene expression patterns from L/Z to PS, while the GO analysis shows enrichment in spermiogenesis-related terms. Reproduced from da Cruz et al. (2016), under the Creative Commons Attribution License. **(d)** Pie charts showing enriched BP and cellular component (CC) GO terms among upregulated genes in the testes of animals at post-natal day 14 compared to those of post-natal day 7 (PND7/14), obtained from an RNAseq study. Note the upregulation of spermiogenesis-related terms both for BP and CC categories. The figure is reproduced from Laiho et al. (2013), under the Creative Commons Attribution License. **(e)** GO term enrichment analysis for downregulated transcripts in PS of *Sox30*$^{-/-}$ mice compared to WT, as assessed through RNAseq of STA-PUT-isolated stage-specific spermatogenic cells. Reprinted from Bai et al. (2018), with permission from The Company of Biologists Ltd.; permission conveyed through Copyright Clearance Center, Inc. **(B)** Diagram representing the three main spermatogenic phases, and the timing of mouse spermatogenesis. The different cell types and the onset of some of them (days postpartum) are indicated. The substitution of histones – first by transition proteins (TNPs) and then by protamines – is shown as well. GC, gonocytes; SPG, spermatogonia; PL, preleptotene; L, leptotene; Z, zygotene; PS, pachytene; D, diplotene; M, meiotic divisions; 1–16 represent the different spermatid stages. Adapted from Trovero et al. (2020), under the Creative Commons Attribution License.

thus revealing a meiosis-specific mechanism for the uncoupling between transcription and translation (Naro et al., 2017).

Finally, in the recent years an important role for post-transcriptional regulation has been also revealed at the transition from mitotic divisions to meiotic program, both in males and females, which would take place through a complex of MEIOC (Abby et al., 2016; Soh et al., 2017) and the RNA helicase YTHDC2 (Bailey et al., 2017; Hsu et al., 2017; Wojtas et al., 2017; Jain et al., 2018). Diverse approaches including microarrays (Abby et al., 2016) and different RNAseq studies (Bailey et al., 2017; Hsu et al., 2017; Soh et al., 2017; Wojtas et al., 2017; Jain et al., 2018) suggest that this – in turn mediated via a complex between the meiotic initiator MEIOSIN and STRA8 (Ishiguro et al., 2020) – would be accomplished by controlling mRNA

stability, either stabilizing meiotic transcripts (Abby et al., 2016), destabilizing transcripts of mitotic cell cycle genes (Bailey et al., 2017; Hsu et al., 2017; Soh et al., 2017; Wojtas et al., 2017), or maybe both (Jain et al., 2018).

MEIOTIC LONG NON-CODING RNAs (lncRNAs)

An RNAseq study indicated that the testes exhibit substantially higher expression of both genic and intergenic sequences than any other organ, in different mammalian species (Soumillon et al., 2013). Moreover, this widespread testicular transcription is especially prevalent in meiotic spermatocytes and post-meiotic RS, and has been proposed to be a consequence of the extensive chromatin remodeling, which would promote a permissive chromatin state (Soumillon et al., 2013). Remarkably, this higher expression in testis is especially notorious for lncRNAs (Cabili et al., 2011; Derrien et al., 2012; Soumillon et al., 2013; Necsulea et al., 2014; Hong et al., 2018; Darbellay and Necsulea, 2020); therefore, here we will specifically focus on lncRNAs.

By definition, lncRNAs are RNAs longer than 200 nucleotides (as opposed to sncRNAs) that lack protein-coding potential (Kapranov et al., 2007; Atkinson et al., 2012; Rinn and Chang, 2012), despite some of them might actually encode short functional peptides (Li et al., 2017). They are mostly transcribed by RNA polymerase II, in general show lower expression levels than coding genes, tend to be lowly conserved, and exhibit high tissue- and developmental-specific expression patterns (Cabili et al., 2011; Derrien et al., 2012; Ulitsky and Bartel, 2013; Necsulea et al., 2014; Quinn and Chang, 2016). LncRNAs have been implicated in the regulation of diverse biological processes (Ma et al., 2013; Fatica and Bozzoni, 2014; Wu and Du, 2017; Kopp and Mendell, 2018; Barman et al., 2019; Yao et al., 2019), and some of them have been related to the development of different diseases (Wu and Du, 2017; Sanchez Calle et al., 2018; Barman et al., 2019; Tsagakis et al., 2020), including ovarian and testicular pathologies (Lü et al., 2015; Liu et al., 2017; Das et al., 2018; Li et al., 2018; Zhang et al., 2018; Salemi et al., 2019).

Given its high numbers of expressed lncRNAs, the testis is an ideal system for their study. Moreover, it is believed that at least a subset of them may play important regulatory roles in spermatogenesis (e.g., Luk et al., 2014). A few transcriptomic studies have identified and partially characterized lncRNAs to variable extents in isolated spermatogenic cell types through microarrays (Liang et al., 2014) or strand-specific RNAseq (essential for the accurate identification of antisense lncRNAs), in mouse (Soumillon et al., 2013; Lin et al., 2016; Wichman et al., 2017; Chen et al., 2018; Trovero et al., 2020) and human (Rolland et al., 2019). Most of these studies reported the highest lncRNA numbers in meiotic, and mainly in post-meiotic cells (Soumillon et al., 2013; Lin et al., 2016; Chen et al., 2018; Rolland et al., 2019; Trovero et al., 2020). Interestingly, Chen et al. (2018), whose scRNAseq profiling of discrete cell subtypes was the only study to include D and metaphase I, found very high expression levels of lncRNAs in those cells, which allows to suspect that a high number of lncRNAs might be upregulated at those late meiotic stages.

Concerning meiotic lncRNAs, curiously Chalmel et al. (2014) reported that in rat they are longer than those differentially expressed in other stages due to greater exon length, and this was also reported for human (Rolland et al., 2019), although it was not corroborated for mouse (Trovero et al., 2020).

At least some of the meiotic lncRNAs would most probably be involved in the regulation of meiotic processes, despite few examples are available thus far. One such examples is *Mrhl* (*meiotic recombination hot-spot locus*), which is downregulated in spermatogonia upon the activation of the Wnt-signaling pathway (Arun et al., 2012). *Mrhl* inactivation would cause its release from the promoter of *Sox8* (that encodes a developmentally important transcription factor), thus leading to *Sox8* upregulation and the expression of genes required for meiotic commitment (Kataruka et al., 2017). LncRNA *Tesra*, which is transcribed from the *Prss/Tessp* locus mainly (although not exclusively) in PS, has been shown to bind the promoter of *Prss42/Tessp-2* – that encodes an important serine-protease for meiotic progression – and increase its activity (Satoh et al., 2019). *Gm2044*, which is transcriptionally activated by A-MYB (see above), has been shown to regulate the expression of the synaptonemal complex component-coding gene *Sycp1* by acting as a microRNA-sponge in mouse spermatocyte-derived GC-2 cells (Liang et al., 2020). *R53*, a SINE-containing lncRNA, is associated to meiotic metaphase chromatin and apparently would play an indispensable role for spermatogenesis progression, as its knockdown revealed a remarkable reduction of post-meiotic cells and irregular upregulation of several post-meiotic genes (Nakajima et al., 2017). Similarly, a role for meiosis progression has been suggested for *Tsx*, an X-linked lncRNA differentially expressed in PS, as knockout mice show increased PS apoptosis (Anguera et al., 2011). On the other hand, *2193* lncRNA has been identified by means of scRNAseq, and shown to play an important role in porcine oocyte maturation through epigenetic modification (Yang et al., 2020).

Of special interest, Ding et al. (2012, 2019) identified lncRNAs that accumulate at their respective gene *loci* in the fission yeast *Schizosaccharomyces pombe*, and mediate homologous recognition and robust pairing during meiotic prophase. So far, we ignore whether a similar mechanism may be operative in mammalian meiosis. No doubt, the years to come will shade light on the roles of lncRNAs, including their participation in the regulation of the unique meiotic processes.

MEIOTIC SEX CHROMOSOME INACTIVATION (MSCI) VIEWED FROM THE TRANSCRIPTOMIC PERSPECTIVE

Meiotic sex chromosome inactivation is the epigenetic silencing of the sex chromosomes that takes place in male mammals during meiotic prophase I. It is considered to avoid recombination between non-homologous regions of the sex chromosome pair, and is followed by partial transcriptional

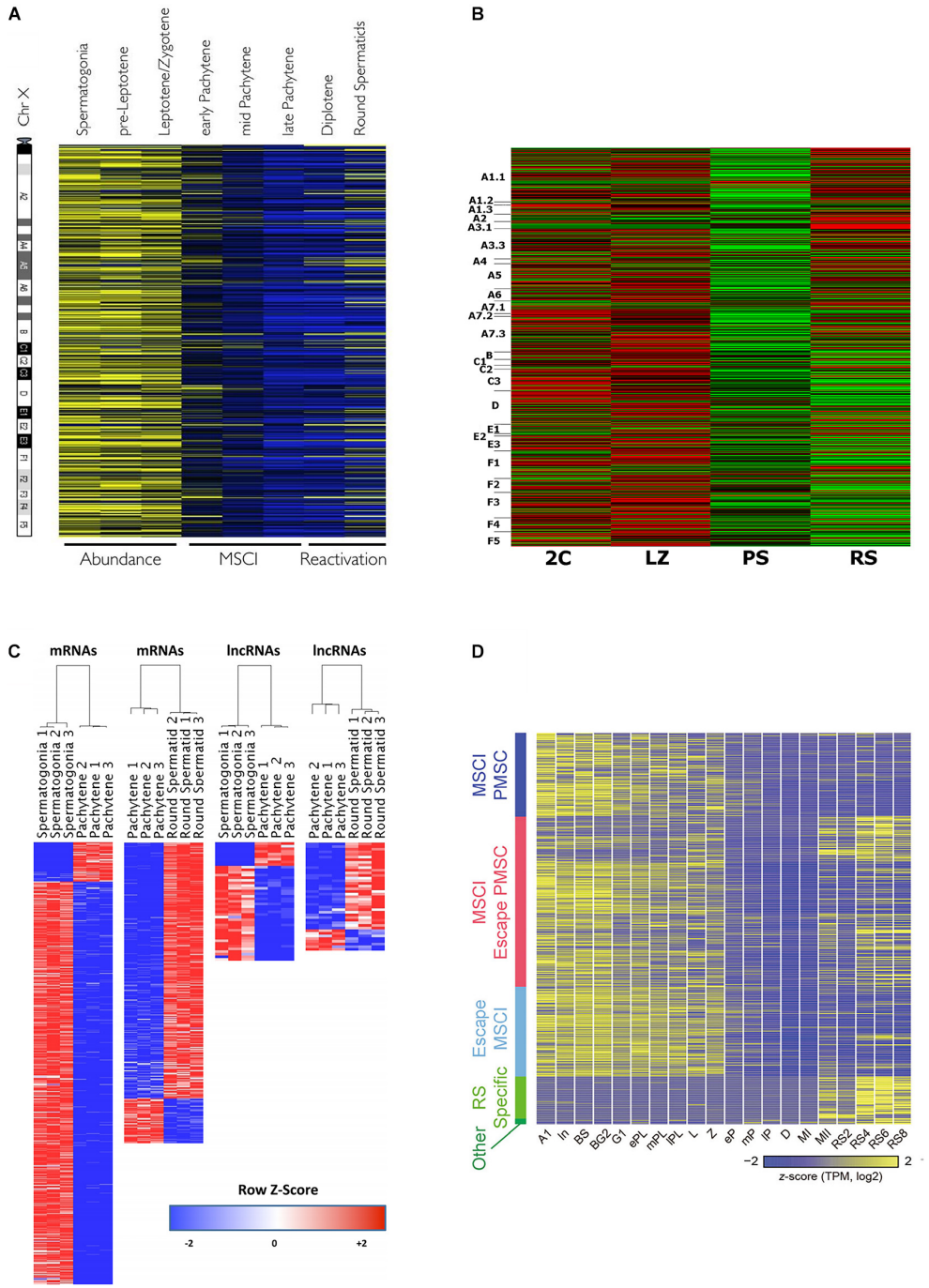

FIGURE 2 | Heat maps from different transcriptomic studies evidencing MSCI in mouse. **(A)** Relative expression levels of 874 X-linked genes, as obtained by microarray analysis, and ordered relative to their chromosome location from centromere to telomere. The different spermatogenic cell populations were purified by FACS. High expression is shown in yellow, and low expression in blue. The figure is reproduced from Fallahi et al. (2010), under the Creative Commons Attribution License. **(B)** Relative expression levels of X-linked protein-coding genes for FACS-sorted testicular cell populations, resulting from RNAseq analysis (cell-type abbreviations are the same as in **Figure 1A,c**). The genes are ordered according to their position on the chromosome from *p* to *q*. High expression: red; low expression: green. The figure is reproduced from da Cruz et al. (2016), under the Creative Commons Attribution License. **(C)** Differentially expressed X- and Y-linked mRNAs and lncRNAs between spermatogonia vs. PS, and PS vs. RS, on a red-to-blue scale. The cell populations were purified by STA-PUT, and transcriptomic profiles were obtained through RNAseq. Reprinted from Wichman et al. (2017), with permission from Oxford University Press (license number 4933230295359). **(D)** Expression patterns of sex chromosome-linked genes along 20 developmental stages, obtained through scRNAseq of synchronized spermatogenic cells (Concerning meiotic cells, L, leptotene; Z, zygotene; eP, early pachytene; mP, middle pachytene; lP, late pachytene; D, diplotene; MI, metaphase I; MII, metaphase II). The genes are grouped according to: MSCI PMSC (post-meiotic sex chromatin silencing), MSCI/escape PMSC, escape MSCI, RS-specific, and other. Colors from yellow to blue represent high to low relative expression levels. The figure is reproduced from Chen et al. (2018), under the Creative Commons Attribution License.

reactivation in RS (reviewed in Yan and McCarrey, 2009; Checchi and Engebrecht, 2011; Sin and Namekawa, 2013; Lu and Yu, 2015; Turner, 2015; Daish and Grützner, 2019).

Massive gene expression analyses allow to visualize MSCI in a very graphical way (**Figure 2**), and hence most transcriptomic studies along spermatogenesis have evaluated the dynamics of X chromosome inactivation and reactivation (Namekawa et al., 2006; Fallahi et al., 2010; Soumillon et al., 2013; Margolin et al., 2014; Sin et al., 2015; Ball et al., 2016; da Cruz et al., 2016; Wichman et al., 2017; Chen et al., 2018; Green et al., 2018; Lukassen et al., 2018; Ernst et al., 2019; Grive et al., 2019; Jung et al., 2019; Shami et al., 2020), which in turn is useful as a means to confirm the robustness of the employed cell-type classification methods and the reliability of the obtained transcriptomic data.

All the above-cited reports agree that gene expression from the sex chromosomes is massively silenced during the P stage. However, while it is accepted that MSCI in primates is less complete than in mice (de Vries et al., 2012; Shami et al., 2020), controversy exists about the extent of mouse MSCI. A number of transcriptomic studies have reported that a few X-linked mRNAs with high expression levels during late meiotic prophase I, would escape MSCI (Soumillon et al., 2013; da Cruz et al., 2016; Wichman et al., 2017; Chen et al., 2018). Contradicting these findings, a couple of recent scRNAseq analyses did not detect MSCI escapees during P/D in mouse (Jung et al., 2019; Shami et al., 2020). On the other hand, it is fairly accepted that a subset of microRNAs escape MSCI (Song et al., 2009; Sosa et al., 2015), albeit this has been controverted as well (Royo et al., 2015). Concerning lncRNAs, although no enough information is available yet, it has been suggested that X- and Y-linked lncRNAs would be mostly subject to MSCI, with a few of them escaping inactivation (Wichman et al., 2017).

In relation to MSCI and the partial post-meiotic reactivation (e.g., Namekawa et al., 2006; Mueller et al., 2008), an interesting finding is the establishment of active epigenetic marks on enhancers and promoters of silent sex chromosomes during meiosis, which would act as epigenetic memory, poising genes for their subsequent activation in RS (Sin et al., 2012; Adams et al., 2018). This would probably be in agreement with a previous observation that specific regions of the sex chromosomes during P retain active chromatin marks (Khalil and Driscoll, 2007). On the other hand, Ernst et al. (2019) reported that in PS, the promoters of spermatid-specific genes on the X chromosome carry high levels of the repressive chromatin mark H3K9me3, which would decrease in RS (observing at least for an analyzed example, a bivalent chromatin state), and suggested that these high H3K9me3 levels could be necessary to prevent premature transcription of X-linked spermatid-specific genes.

In addition, it has been reported that in spite of transcriptional silencing, MSCI would be accompanied by the massive *de novo* formation of accessible chromatin in the sex chromosomes in PS (Maezawa et al., 2018). In fact, genome-wide chromatin studies (Hi-C, ChIP-seq), some of them in combination with RNAseq, reveal a distinct higher-order chromatin structure in the sex chromosomes during MSCI (Alavattam et al., 2019; Patel et al., 2019; Vara et al., 2019; Wang et al., 2019).

CONCLUSION

Genome-wide characterization of the gene expression programs underlying the unique events that take place along meiotic prophase, and how they are regulated, is essential for the comprehensive understanding of meiosis groundwork. Deepening the knowledge of this extraordinary and highly complex process is indispensable for the development of therapeutic approaches, as the alteration of meiotic events is at the base of numerous pathologies including a high number of idiopathic infertility cases. Methodological advances to allow the analyses of specific cell types among the complex testicular tissue, together with modern omics techniques, provide a broad picture, while starting to disclose a detailed molecular landscape of the different stages of spermatogenesis in mouse, and also in human. These studies, carried out through different approaches and platforms, have often reached some confluent results, and revealed that meiotic spermatocytes, as well as post-meiotic spermatids, have highly complex transcriptomes. Here, we have focused on some of these results, and particularly concerning meiotic prophase gene expression. In synthesis, we highlight that despite early meiotic prophase cells have lower overall expression levels and a less complex transcriptome than other spermatogenic cell types, they differentially express a set of genes related to male meiosis, and in a few cases even to post-meiosis. We point out that transcriptomic analyses allow to appreciate the real magnitude of post-transcriptional regulation and translational delay along the process, showing their massiveness, as well as the switch in gene expression programs during meiotic prophase (particularly the P stage); in turn, this would be accompanied by extensive and sophisticated regulatory mechanisms to guarantee the perfect execution timing of the spermatogenic programs, which is essential for the production of healthy sperm. Transcriptomic studies have also provided an easy way to visualize massive meiotic-specific processes such as MSCI, and compare its extension between different species. Besides, transcriptomic studies have revealed the existence of a higher number of lncRNAs in spermatogenic cells than in any other analyzed cell type or tissue. Important regulatory roles are starting to be revealed for some of these lncRNAs in relation to meiosis, although, no doubt, we have only just begun to see the tip of the iceberg.

AUTHOR CONTRIBUTIONS

AG wrote most of the manuscript. RR-C and RB participated in the design, conception and writing, corrected the manuscript, and approved it for publication. All authors contributed to the article and approved the submitted version.

FUNDING

This work was supported by the Comisión Sectorial de Investigación Científica (CSIC), UDELAR (Uruguay), under an I + D Groups 2018 grant to AG and RB.

REFERENCES

Abby, E., Tourpin, S., Ribeiro, J., Daniel, K., Messiaen, S., Moison, D., et al. (2016). Implementation of meiosis prophase I programme requires a conserved retinoid-independent stabilizer of meiotic transcripts. *Nat. Commun.* 7:10324. doi: 10.1038/ncomms10324

Adams, S. R., Maezawa, S., Alavattam, K. G., Abe, H., Sakashita, A., Shroder, M., et al. (2018). RNF8 and SCML2 cooperate to regulate ubiquitination and H3K27 acetylation for escape gene activation on the sex chromosomes. *PLoS Genet.* 14:e1007233. doi: 10.1371/journal.pgen.1007233

Alavattam, K. G., Maezawa, S., Sakashita, A., Khoury, H., Barski, A., Kaplan, N., et al. (2019). Attenuated chromatin compartmentalization in meiosis and its maturation in sperm development. *Nat. Struct. Mol. Biol.* 26, 175–184. doi: 10.1038/s41594-019-0189-y

Anguera, M. C., Ma, W., Clift, D., Namekawa, S., Kelleher, R. J. I. I. I., and Lee, J. T. (2011). Tsx produces a long noncoding RNA and has general functions in the germline, stem cells, and brain. *PLoS Genet.* 7:e1002248. doi: 10.1371/journal.pgen.1002248

Arun, G., Akhade, V. S., Donakonda, S., and Rao, M. R. (2012). mrhl RNA, a long noncoding RNA, negatively regulates Wnt signaling through its protein partner Ddx5/p68 in mouse spermatogonial cells. *Mol. Cell. Biol.* 32, 3140–3152. doi: 10.1128/MCB.00006-12

Atkinson, S. R., Marguerat, S., and Bähler, J. (2012). Exploring long non-coding RNAs through sequencing. *Semin. Cell Dev. Biol.* 23, 200–205. doi: 10.1016/j.semcdb.2011.12.003

Bai, S., Fu, K., Yin, H., Cui, Y., Yue, Q., Li, W., et al. (2018). Sox30 initiates transcription of haploid genes during late meiosis and spermiogenesis in mouse testes. *Development* 146:dev179978. doi: 10.1242/dev.179978

Bailey, A. S., Batista, P. J., Gold, R. S., Chen, Y. G., de Rooij, D. G., Chang, H. Y., et al. (2017). The conserved RNA helicase YTHDC2 regulates the transition from proliferation to differentiation in the germline. *eLife* 6:e26116. doi: 10.7554/eLife.26116

Ball, R. L., Fujiwara, Y., Sun, F., Hu, J., Hibbs, M. A., Handel, M. A., et al. (2016). Regulatory complexity revealed by integrated cytological and RNA-seq analyses of meiotic substages in mouse spermatocytes. *BMC Genomics* 17:628. doi: 10.1186/s12864-016-2865-1

Bao, J., Wu, J., Schuster, A. S., Wu, J., Schuster, A. S., Hennig, G. W., et al. (2013). Expression profiling reveals developmentally regulated lncRNA repertoire in the mouse male germline. *Biol. Reprod.* 89:107. doi: 10.1095/biolreprod.113.113308

Barman, P., Reddy, D., and Bhaumik, S. R. (2019). Mechanisms of antisense transcription initiation with implications in gene expression, genomic integrity and disease pathogenesis. *Noncod. RNA* 5, 11. doi: 10.3390/ncrna5010011

Bastos, H., Lassalle, B., Chicheportiche, A., Riou, L., Testart, J., Allemand, I., et al. (2005). Flow cytometric characterization of viable meiotic and postmeiotic cells by Hoechst 33342 in mouse spermatogenesis. *Cytometry A* 65A, 40–49. doi: 10.1002/cyto.a.20129

Bellvé, A. R. (1993). Purification, culture, and fractionation of spermatogenic cells. *Methods Enzymol.* 225, 84–113. doi: 10.1016/0076-6879(93)25009-q

Bharti, D., Jang, S. J., Lee, S. Y., Lee, S. L., and Rho, G. J. (2020). In vitro generation of oocyte like cells and their in vivo efficacy: how far we have been succeeded. *Cells* 9:557. doi: 10.3390/cells9030557

Bolcun-Filas, E., Bannister, L. A., Barash, A., Schimenti, K. J., Hartford, S. A., Eppig, J. J., et al. (2011). A-MYB (MYBL1) transcription factor is a master regulator of male meiosis. *Development* 138, 3319–3330. doi: 10.1242/dev.067645

Bortvin, A. (2013). PIWI-interacting RNAs (piRNAs) - a mouse testis perspective. *Biochemistry* 78, 592–602. doi: 10.1134/S0006297913060059

Braun, R. E. (1998). Post-transcriptional control of gene expression during spermatogenesis. *Semin. Cell Dev. Biol.* 9, 483–489. doi: 10.1006/scdb.1998.0226

Cabili, M. N., Trapnell, C., Goff, L., Koziol, M., Tazon-Vega, B., Regev, A., et al. (2011). Integrative annotation of human large intergenic noncoding RNAs reveals global properties and specific subclasses. *Genes Dev.* 25, 1915–1927. doi: 10.1101/gad.17446611

Chalmel, F., Rolland, A. D., Niederhauser-Wiederkehr, C., Chung, S. S., Demougin, P., Gattiker, A., et al. (2007). The conserved transcriptome in human and rodent male gametogenesis. *Proc. Natl. Acad. Sci. U.S.A.* 104, 8346–8351. doi: 10.1073/pnas.0701883104

Chalmel, F., Lardenois, A., Evrard, B., Rolland, A. D., Sallou, O., Dumargne, M. C., et al. (2014). High-resolution profiling of novel transcribed regions during rat spermatogenesis. *Biol. Reprod.* 91:5. doi: 10.1095/biolreprod.114.118166

Checchi, P. M., and Engebrecht, J. (2011). Heteromorphic sex chromosomes: navigating meiosis without a homologous partner. *Mol. Reprod. Dev.* 78, 623–632. doi: 10.1002/mrd.21369

Chen, Y., Zheng, Y., Gao, Y., Lin, Z., Yang, S., Wang, T., et al. (2018). Single-cell RNA-seq uncovers dynamic processes and critical regulators in mouse spermatogenesis. *Cell Res.* 28, 879–896. doi: 10.1038/s41422-018-0074-y

da Cruz, I., Rodríguez-Casuriaga, R., Santiñaque, F. F., Farías, J., Curti, G., Capoano, C. A., et al. (2016). Transcriptome analysis of highly purified mouse spermatogenic cell populations: gene expression signatures switch from meiotic-to-postmeiotic-related processes at pachytene stage. *BMC Genomics* 17:294. doi: 10.1186/s12864-016-2618-1

Dai, P., Wang, X., Gou, L. T., Li, Z. T., Wen, Z., Chen, Z. G., et al. (2019). A translation-activating function of MIWI/piRNA during mouse spermiogenesis. *Cell* 179, 1566.e16–1581.e16. doi: 10.1016/j.cell.2019.11.022

Dai, P., Wang, X., and Liu, M. F. (2020). A dual role of the PIWI/piRNA machinery in regulating mRNAs during mouse spermiogenesis. *Sci. China Life Sci.* 63, 447–449. doi: 10.1007/s11427-020-1632-5

Daish, T., and Grützner, F. (2019). Evolution and meiotic organization of heteromorphic sex chromosomes. *Curr. Top. Dev. Biol.* 134, 1–48. doi: 10.1016/bs.ctdb.2019.01.009

Darbellay, F., and Necsulea, A. (2020). Comparative transcriptomics analyses across species, organs, and developmental stages reveal functionally constrained lncRNAs. *Mol. Biol. Evol.* 37, 240–259. doi: 10.1093/molbev/msz212

Das, M. K., Furu, K., Evensen, H. F., Haugen, ØP., and Haugen, T. B. (2018). Knockdown of SPRY4 and SPRY4-IT1 inhibits cell growth and phosphorylation of Akt in human testicular germ cell tumours. *Sci. Rep.* 8:2462. doi: 10.1038/s41598-018-20846-8

de Mateo, S., and Sassone-Corsi, P. (2014). Regulation of spermatogenesis by small non-coding RNAs: role of the germ granule. *Semin. Cell. Dev. Biol.* 29, 84–92. doi: 10.1016/j.semcdb.2014.04.021

de Vries, M., Vosters, S., Merkx, G., D'Hauwers, K., Wansink, D. G., Ramos, L., et al. (2012). Human male meiotic sex chromosome inactivation. *PLoS One* 7:e31485. doi: 10.1371/journal.pone.0031485

Derrien, T., Johnson, R., Bussotti, G., Tanzer, A., Djebali, S., Tilgner, H., et al. (2012). The GENCODE v7 catalog of human long noncoding RNAs: analysis of their gene structure, evolution, and expression. *Genome Res.* 22, 1775–1789. doi: 10.1101/gr.132159.111

Ding, D. Q., Okamasa, K., Katou, Y., Oya, E., Nakayama, J. I., Chikashige, Y., et al. (2019). Chromosome-associated RNA-protein complexes promote pairing of homologous chromosomes during meiosis in Schizosaccharomyces pombe. *Nat. Commun.* 10:5598. doi: 10.1038/s41467-019-13609-0

Ding, D. Q., Okamasa, K., Yamane, M., Tsutsumi, C., Haraguchi, T., Yamamoto, M., et al. (2012). Meiosis-specific noncoding RNA mediates robust pairing of homologous chromosomes in meiosis. *Science* 336, 732–736. doi: 10.1126/science.1219518

Ernst, C., Eling, N., Martinez-Jimenez, C. P., Marioni, J. C., and Odom, D. T. (2019). Staged developmental mapping and X chromosome transcriptional dynamics during mouse spermatogenesis. *Nat. Commun.* 10:1251. doi: 10.1038/s41467-019-09182-1

Evans, E., Hogarth, C., Mitchell, D., and Griswold, M. (2014). Riding the spermatogenic wave: profiling gene expression within neonatal germ and sertoli cells during a synchronized initial wave of spermatogenesis in mice. *Biol. Reprod.* 90:108. doi: 10.1095/biolreprod.114.118034

Fallahi, M., Getun, I. V., Wu, Z. K., and Bois, P. R. J. (2010). A global expression switch marks pachytene initiation during mouse male meiosis. *Genes* 1, 469–483. doi: 10.3390/genes1030469

Fatica, A., and Bozzoni, I. (2014). Long non-coding RNAs: new players in cell differentiation and development. *Nat. Rev. Genet.* 15, 7–21. doi: 10.1038/nrg3606

Feichtinger, J., and McFarlane, R. J. (2019). Meiotic gene activation in somatic and germ cell tumours. *Andrology* 7, 415–427. doi: 10.1111/andr.12628

Fine, A. D., Ball, R. L., Fujiwara, Y., Handel, M. A., and Carter, G. W. (2019). Uncoupling of transcriptomic and cytological differentiation in mouse spermatocytes with impaired meiosis. *Mol. Biol. Cell* 30, 717–728. doi: 10.1091/mbc.E18-10-0681

Gan, H., Cai, T., Lin, X., Wu, Y., Wang, X., Yang, F., et al. (2013a). Integrative proteomic and transcriptomic analyses reveal multiple post-transcriptional regulatory mechanisms of mouse spermatogenesis. *Mol. Cell. Proteomics* 12, 1144–1157. doi: 10.1074/mcp.M112.020123

Gan, H., Wen, L., Liao, S., Lin, X., Ma, T., Liu, J., et al. (2013b). Dynamics of 5-hydroxymethylcytosine during mouse spermatogenesis. *Nat. Commun*. 4:1995. doi: 10.1038/ncomms2995

Gaysinskaya, V., Miller, B. F., De Luca, C., van der Heijden, G. W., Hansen, K. D., and Bortvin, A. (2018). Transient reduction of DNA methylation at the onset of meiosis in male mice. *Epigenet. Chromatin* 11:15. doi: 10.1186/s13072-018-0186-0

Gaysinskaya, V., Soh, I. Y., van der Heijden, G. W., and Bortvin, A. (2014). Optimized flow cytometry isolation of murine spermatocytes. *Cytometry A* 85, 556–565. doi: 10.1002/cyto.a.22463

Geisinger, A., and Benavente, R. (2016). Mutations in genes coding for synaptonemal complex proteins and their impact on human fertility. *Cytogenet. Genome Res*. 150, 77–85. doi: 10.1159/000453344

Geisinger, A., and Rodríguez-Casuriaga, R. (2010). Flow cytometry for gene expression studies in mammalian spermatogenesis. *Cytogenet. Genome Res*. 128, 46–56. doi: 10.1159/000291489

Geisinger, A., and Rodríguez-Casuriaga, R. (2017). Flow cytometry for the isolation and characterization of rodent meiocytes. *Methods Mol. Biol.* 1471, 217–230. doi: 10.1007/978-1-4939-6340-9_11

Getun, I. V., Torres, B., and Bois, P. R. (2011). Flow cytometry purification of mouse meiotic cells. *J. Vis. Exp*. 50:2602. doi: 10.3791/2602

Gheldof, A., Mackay, D. J. G., Cheong, Y., and Verpoest, W. (2019). Genetic diagnosis of subfertility: the impact of meiosis and maternal effects. *J. Med. Genet*. 56, 271–282. doi: 10.1136/jmedgenet-2018-105513

Go, V. L. W., Vernon, R. G., and Fritz, I. B. (1971). Studies on spermatogenesis in rats. I. Application of the sedimentation velocity technique to an investigation of spermatogenesis. *Can. J. Biochem*. 49, 753–760. doi: 10.1139/o71-106

Goh, W. S., Falciatori, I., Tam, O. H., Burgess, R., Meikar, O., Kotaja, N., et al. (2015). piRNA-directed cleavage of meiotic transcripts regulates spermatogenesis. *Genes Dev*. 2, 1032–1044. doi: 10.1101/gad.260455.115

Gong, W., Linlin, P., Qiang, L., Yuanyuan, Z., Chengqi, X., Xiaomin, Y., et al. (2013). Transcriptome profiling of the developing postnatal mouse testis using next-generation sequencing. *Sci. China Life Sci*. 56, 1–12. doi: 10.1007/s11427-012-4411-y

Gou, L. T., Dai, P., Yang, J. H., Xue, Y., Hu, Y. P., Zhou, Y., et al. (2014). Pachytene piRNAs instruct massive mRNA elimination during late spermiogenesis. *Cell Res*. 24, 680–700. doi: 10.1038/cr.2014.41

Green, C. D., Ma, Q., Manske, G. L., Shami, A. N., Zheng, X., Marini, S., et al. (2018). A comprehensive roadmap of murine spermatogenesis defined by single-cell RNA-Seq. *Dev. Cell* 46, 651.e10–667.e10. doi: 10.1016/j.devcel.2018.07.025

Griswold, M. D. (2016). Spermatogenesis: the commitment to meiosis. *Physiol. Rev*. 96, 1–17. doi: 10.1152/physrev.00013.2015

Grive, K. J., Hu, Y., Shu, E., Grimson, A., Elemento, O., Grenier, J. K., et al. (2019). Dynamic transcriptome profiles within spermatogonial and spermatocyte populations during postnatal testis maturation revealed by single-cell sequencing. *PLoS Genet*. 15:e1007810. doi: 10.1371/journal.pgen.1007810

Guo, J., Grow, E. J., Mlcochova, H., Maher, G. J., Lindskog, C., Nie, X. C., et al. (2018). The adult human testis transcriptional cell atlas. *Cell Res*. 28, 1141–1157. doi: 10.1038/s41422-018-0099-2

Guo, J., Nie, X., Giebler, M., Mlcochova, H., Wang, Y., Grow, E. J., et al. (2020). The dynamic transcriptional cell atlas of testis development during human puberty. *Cell Stem Cell* 26, 262–276. doi: 10.1016/j.stem.2019.12.005

Hammoud, S. S., Low, D. H., Yi, C., Carrell, D. T., Guccione, E., and Cairns, B. R. (2014). Chromatin and transcription transitions of mammalian adult germline stem cells and spermatogenesis. *Cell Stem Cell* 15, 239–253. doi: 10.1016/j.stem.2014.04.006

Handel, M. A., and Schimenti, J. C. (2010). Genetics of mammalian meiosis: regulation, dynamics and impact on fertility. *Nat. Rev. Genet*. 11, 124–136. doi: 10.1038/nrg272

Handel, M. A., Eppig, J. J., and Schimenti, J. C. (2014). Applying "Gold Standards" to in vitro-derived germ cells. *Cell* 157, 1257–1261. doi: 10.1016/j.cell.2014.05.019

Hann, M. C., Lau, P. E., and Tempest, H. G. (2011). Meiotic recombination and male infertility: from basic science to clinical reality? *Asian J. Androl*. 13, 212–218. doi: 10.1038/aja.2011.1

Hayashi, K. (2019). In vitro reconstitution of germ cell development. *Biol. Reprod*. 101, 567–578. doi: 10.1093/biolre/ioz111

Hermann, B. P., Cheng, K., Singh, A., Roa-De, La Cruz, L., Mutoji, K. N., et al. (2018). The mammalian spermatogenesis single-cell transcriptome, from spermatogonial stem cells to spermatids. *Cell Rep*. 25, 1650.e8–1667.e8. doi: 10.1016/j.celrep.2018.10.026

Hernández-López, D., Geisinger, A., Trovero, M. F., Santiñaque, F. F., Brauer, M., Folle, G. A., et al. (2020). Familial primary ovarian failure associated with a *SYCE1* point mutation: defective meiosis elucidated in humanized mice. *Mol. Hum. Reprod.* 26, 485–497. doi: 10.1093/molehr/gaaa032

Hogarth, C. A., Evanoff, R., Mitchell, D., Kent, T., Small, C., Amory, J. K., et al. (2013). Turning a spermatogenic wave into a tsunami: synchronizing murine spermatogenesis using WIN 18,446. *Biol. Reprod*. 88:40. doi: 10.1095/biolreprod.112.105346

Hong, S. H., Kwon, J. T., Kim, J., Jeong, J., Kim, J., Lee, S., et al. (2018). Profiling of testis-specific long noncoding RNAs in mice. *BMC Genomics* 19:539. doi: 10.1186/s12864-018-4931-3

Hsu, P. J., Zhu, Y., Ma, H., Guo, Y., Shi, X., Liu, Y., et al. (2017). Ythdc2 is an N6-methyladenosine binding protein that regulates mammalian spermatogenesis. *Cell Res*. 27, 1115–1127. doi: 10.1038/cr.2017.99

Idler, R. K., and Yan, W. (2012). Control of messenger RNA fate by RNA-binding proteins: an emphasis on mammalian spermatogenesis. *J. Androl*. 33, 309–337. doi: 10.2164/jandrol.111.014167

Iguchi, N., Tobias, J. W., and Hecht, N. B. (2006). Expression profiling reveals meiotic male germ cell mRNAs that are translationally up- and down-regulated. *Proc. Natl. Acad. Sci. U.S.A*. 103, 7712–7717. doi: 10.1073/pnas.0510999103

Ishiguro, K. I., Matsuura, K., Tani, N., Takeda, N., Usuki, S., Yamane, M., et al. (2020). Meiosin directs the switch from mitosis to meiosis in mammalian germ cells. *Dev. Cell*. 52, 429–445. doi: 10.1016/j.devcel.2020.01.010

Jain, D., Puno, M. R., Meydan, C., Lailler, N., Mason, C. E., Lima, C. D., et al. (2018). Ketu mutant mice uncover an essential meiotic function for the ancient RNA helicase YTHDC2. *eLife* 7:e30919. doi: 10.7554/eLife.30919

Jan, S. J., Vormer, T. L., Jongejan, A., Röling, M. D., Silber, S. J., de Rooij, D. G., et al. (2017). Unraveling transcriptome dynamics in human spermatogenesis. *Development* 144, 3659–3673. doi: 10.1242/dev.152413

Jung, M., Wells, D., Rusch, J., Ahmed, S., Marchini, J., Myers, S., et al. (2019). Unified single-cell analysis of testis gene regulation and pathology in 5 mouse strains. *eLife* 8:e43966. doi: 10.7554/eLife.43966

Kapranov, P., Cheng, J., Dike, S., Nix, D. A., Duttagupta, R., Willingham, A. T., et al. (2007). RNA maps reveal new RNA classes and a possible function for pervasive transcription. *Science* 316, 1484–1488. doi: 10.1126/science.1138341

Kataruka, S., Akhade, V. S., Kayyar, B., and Rao, M. R. S. (2017). Mrhl long noncoding RNA mediates meiotic commitment of mouse spermatogonial cells by regulating Sox8 expression. *Mol. Cell Biol*. 37:e00632-16. doi: 10.1128/MCB.00632-16

Khalil, A. M., and Driscoll, D. J. (2007). Trimethylation of histone H3 lysine 4 is an epigenetic mark at regions escaping mammalian X inactivation. *Epigenetics* 2, 114–118. doi: 10.4161/epi.2.2.4612

Kierszenbaum, A. L., and Tres, L. L. (1974). Nucleolar and perichromosomal RNA synthesis during meiotic prophase in the mouse testis. *J. Cell Biol*. 60, 39–53. doi: 10.1083/jcb.60.1.39

Kleene, K. C. (2001). A possible meiotic function of the peculiar patterns of gene expression in mammalian spermatogenic cells. *Mech. Dev*. 106, 3–23. doi: 10.1016/s0925-4773(01)00413-0

Kleene, K. C. (2013). Connecting cis-elements and trans-factors with mechanisms of developmental regulation of mRNA translation in meiotic and haploid mammalian spermatogenic cells. *Reproduction* 146, R1–R19. doi: 10.1530/REP-12-0362

Komeya, M., Sato, T., and Ogawa, T. (2018). In vitro spermatogenesis: a century-long research journey, still half way around. *Reprod. Med. Biol.* 17, 407–420. doi: 10.1002/rmb2.12225

Kopp, F., and Mendell, J. T. (2018). Functional classification and experimental dissection of long noncoding RNAs. *Cell* 172, 393–407. doi: 10.1016/j.cell.2018.01.011

Kotaja, N. (2014). MicroRNAs and spermatogenesis. *Fertil. Steril.* 101, 1552–1562. doi: 10.1016/j.fertnstert.2014.04.025

La, H. M., Mäkelä, J. A., Chan, A. L., Rossello, F. J., Nefzger, C. M., Legrand, J. M. D., et al. (2018). Identification of dynamic undifferentiated cell states within the male germline. *Nat. Commun.* 9:2819. doi: 10.1038/s41467-018-04827-z

Laiho, A., Kotaja, N., Gyenesei, A., and Sironen, A. (2013). Transcriptome profiling of the murine testis during the first wave of spermatogenesis. *PLoS One* 8:e61558. doi: 10.1371/journal.pone.0061558

Lam, D. M. K., Furrer, R., and Bruce, W. R. (1970). The separation, physical characterization, and differentiation kinetics of spermatogonial cells of the mouse. *Proc. Natl. Acad. Sci. U.S.A.* 65, 192–199. doi: 10.1073/pnas.65.1.192

Law, N. C., Oatley, M. J., and Oatley, J. M. (2019). Developmental kinetics and transcriptome dynamics of stem cell specification in the spermatogenic lineage. *Nat. Commun.* 10:2787. doi: 10.1038/s41467-019-10596-0

Lee, K., Haugen, H. S., Clegg, C. H., and Braun, R. E. (1995). Premature translation of protamine 1 mRNA causes precocious nuclear condensation and arrests spermatid differentiation in mice. *Proc. Natl. Acad. Sci. U.S.A.* 92, 12451–12455. doi: 10.1073/pnas.92.26.12451

Legrand, J. M. D., and Hobbs, R. M. (2018). RNA processing in the male germline: mechanisms and implications for fertility. *Semin. Cell Dev. Biol.* 79, 80–91. doi: 10.1016/j.semcdb.2017.10.006

Lehtiniemi, T., and Kotaja, N. (2018). Germ granule-mediated RNA regulation in male germ cells. *Reproduction* 155, R77–R91. doi: 10.1530/REP-17-0356

Li, L. J., Leng, R. X., Fan, Y. G., Pan, H. F., and Ye, D. Q. (2017). Translation of noncoding RNAs: focus on lncRNAs, pri-miRNAs, and circRNAs. *Exp. Cell Res.* 361, 1–8. doi: 10.1016/j.yexcr.2017.10.010

Li, W., Ning, J. Z., Cheng, F., Yu, W. M., Rao, T., Ruan, Y., et al. (2018). MALAT1 Promotes cell apoptosis and suppresses cell proliferation in testicular ischemia-reperfusion injury by sponging miR-214 to modulate TRPV4 expression. *Cell. Physiol. Biochem.* 46, 802–814. doi: 10.1159/000488738

Li, W., Park, J. Y., Zheng, D., Hoque, M., Yehia, G., and Tian, B. (2016). Alternative cleavage and polyadenylation in spermatogenesis connects chromatin regulation with post-transcriptional control. *BMC Biol.* 14:6. doi: 10.1186/s12915-016-0229-6

Li, X. Z., Roy, C. K., Dong, X., Bolcun-Filas, E., Wang, J., Han, B. W., et al. (2013). An ancient transcription factor initiates the burst of piRNA production during early meiosis in mouse testes. *Mol. Cell* 50, 67–81. doi: 10.1016/j.molcel.2013.02.016

Liang, M., Li, W., Tian, H., Hu, T., Wang, L., Lin, Y., et al. (2014). Sequential expression of long noncoding RNA as mRNA gene expression in specific stages of mouse spermatogenesis. *Sci. Rep.* 4:5966. doi: 10.1038/srep05966

Liang, M., Wang, H., He, C., Zhang, K., and Hu, K. (2020). LncRNA-Gm2044 is transcriptionally activated by A-MYB and regulates Sycp1 expression as a miR-335-3p sponge in mouse spermatocyte-derived GC-2spd(ts) cells. *Differentiation* 114, 49–57. doi: 10.1016/j.diff.2020.05.004

Liao, J., Ng, S. H., Luk, A. C. S., Suen, A. H. C., Qian, Y., Tu, J., et al. (2019). Revealing cellular and molecular transitions in neonatal germ cell differentiation using single cell RNA sequencing. *Development* 146:dev174953. doi: 10.1242/dev.174953

Lin, X., Han, M., Cheng, L., Chen, J., Zhang, Z., Shen, T., et al. (2016). Expression dynamics, relationships, and transcriptional regulations of diverse transcripts in mouse spermatogenic cells. *RNA Biol.* 13, 1011–1024. doi: 10.1080/15476286.2016.1218588

Liu, Y. D., Li, Y., Feng, S. X., Ye, D. S., Chen, X., Zhou, X. Y., et al. (2017). Long noncoding RNAs: potential regulators involved in the pathogenesis of polycystic ovary syndrome. *Endocrinology* 158, 3890–3899. doi: 10.1210/en.2017-00605

Lu, L. Y., and Yu, X. (2015). Double-strand break repair on sex chromosomes: challenges during male meiotic prophase. *Cell Cycle* 14, 516–525. doi: 10.1080/15384101.2014.998070

Lü, M., Tian, H., Cao, Y. X., He, X., Chen, L., Song, X., et al. (2015). Downregulation of miR-320a/383- sponge-like long noncoding RNA NLC1-C (narcolepsy candidate-region 1 genes) is associated with male infertility and promotes testicular embryonal carcinoma cell proliferation. *Cell Death Dis.* 6:e1960. doi: 10.1038/cddis.2015.267

Luk, A. C., Chan, W. Y., Rennert, O. M., and Lee, T. L. (2014). Long noncoding RNAs in spermatogenesis: insights from recent high-throughput transcriptome studies. *Reproduction* 147, R131–R141. doi: 10.1530/REP-13-0594

Lukassen, S., Bosch, E., Ekici, A. B., and Winterpacht, A. (2018). Characterization of germ cell differentiation in the male mouse through single-cell RNA sequencing. *Sci. Rep.* 8:6521. doi: 10.1038/s41598-018-24725-0

Luo, L. F., Hou, C. C., and Yang, W. X. (2016). Small non-coding RNAs and their associated proteins in spermatogenesis. *Gene* 578, 141–157. doi: 10.1016/j.gene.2015.12.020

Luo, Z., Wang, X., Jiang, H., Wang, R., Chen, J., Chen, Y., et al. (2020). Reorganized 3D genome structures support transcriptional regulation in mouse spermatogenesis. *iScience* 23:101034. doi: 10.1016/j.isci.2020.101034

Ma, L., Bajic, V. B., and Zhang, Z. (2013). On the classification of long non-coding RNAs. *RNA Biol.* 10, 925–933. doi: 10.4161/rna.24604

Maezawa, S., Sakashita, A., Yukawa, M., Chen, X., Takahashi, K., Alavattam, K. G., et al. (2020). Super-enhancer switching drives a burst in gene expression at the mitosis-to-meiosis transition. *Nat. Struct. Mol. Biol.* 27, 978–988. doi: 10.1038/s41594-020-0488-3

Maezawa, S., Yukawa, M., Alavattam, K. G., Barski, A., and Namekawa, S. H. (2018). Dynamic reorganization of open chromatin underlies diverse transcriptomes during spermatogenesis. *Nucleic Acids Res.* 46, 593–608. doi: 10.1093/nar/gkx1052

Malkov, M., Fisher, Y., and Don, J. (1998). Developmental schedule of the postnatal rat testis determined by flow cytometry. *Biol. Reprod.* 59, 84–92. doi: 10.1095/biolreprod59.1.84

Maratou, K., Forster, T., Costa, Y., Taggart, M., Speed, R. M., Ireland, J., et al. (2004). Expression profiling of the developing testis in wild-type and Dazl knockout mice. *Mol. Reprod. Dev.* 67, 26–54. doi: 10.1002/mrd.20010

Margolin, G., Khil, P. P., Kim, J., Bellani, M. A., and Camerini-Otero, R. D. (2014). Integrated transcriptome analysis of mouse spermatogenesis. *BMC Genomics* 15:39. doi: 10.1186/1471-2164-15-39

Meikar, O., Da Ros, M., Korhonen, H., and Kotaja, N. (2011). Chromatoid body and small RNAs in male germ cells. *Reproduction* 142, 195–209. doi: 10.1530/REP-11-0057

Meikar, O., Vagin, V. V., Chalmel, F., Sõstar, K., Lardenois, A., Hammell, M., et al. (2014). An atlas of chromatoid body components. *RNA* 20, 483–495. doi: 10.1261/rna.043729.113

Meistrich, M. L. (1977). Separation of spermatogenic cells and nuclei from rodent testes. *Methods Cell Biol.* 15, 15–54. doi: 10.1016/s0091-679x(08)60207-1

Monesi, V. (1964). Ribonucleic acid synthesis during mitosis and meiosis in the mouse testis. *J. Cell Biol.* 22, 521–532. doi: 10.1083/jcb.22.3.521

Mueller, J. L., Mahadevaiah, S. K., Park, P. J., Warburton, P. E., Page, D. C., and Turner, J. M. (2008). The mouse X chromosome is enriched for multicopy testis genes showing postmeiotic expression. *Nat. Genet.* 40, 794–799. doi: 10.1038/ng.126

Mutz, K. O., Heilkenbrinker, A., Lönne, M., Walter, J. G., and Stahl, F. (2013). Transcriptome analysis using next-generation sequencing. *Curr. Opin. Biotechnol.* 24, 22–30. doi: 10.1016/j.copbio.2012.09.004

Nakajima, R., Sato, T., Ogawa, T., and Okano, H. (2017). A noncoding RNA containing a SINE-B1 motif associates with meiotic metaphase chromatin and has an indispensable function during spermatogenesis. *PLoS One* 12:e0179585. doi: 10.1371/journal.pone.0179585

Namekawa, S. H., Park, P. J., Zhang, L. F., Shima, J. E., McCarrey, J. R., Griswold, M. D., et al. (2006). Postmeiotic sex chromatin in the male germline of mice. *Curr. Biol.* 16, 660–667. doi: 10.1016/j.cub.2006.01.066

Naro, C., Jolly, A., Di Persio, S., Bielli, P., Setterblad, N., Alberdi, A. J., et al. (2017). An orchestrated intron retention program in meiosis controls timely usage of transcripts during germ cell differentiation. *Dev. Cell* 41, 82.e4–93.e4. doi: 10.1016/j.devcel.2017.03.003

Necsulea, A., Soumillon, M., Warnefors, M., Liechti, A., Daish, T., Zeller, U., et al. (2014). The evolution of lncRNA repertoires and expression patterns in tetrapods. *Nature* 505, 635–640. doi: 10.1038/nature12943

Page, J., de la Fuente, R., Manterola, M., Parra, M. T., Viera, A., Berríos, S., et al. (2012). Inactivation or non-reactivation: what accounts better for the silence of sex chromosomes during mammalian male meiosis? *Chromosoma* 121, 307–326. doi: 10.1007/s00412-012-0364-y

Pang, A. L., Johnson, W., Ravindranath, N., Dym, M., Rennert, O. M., and Chan, W. Y. (2006). Expression profiling of purified male germ cells: stage-specific expression patterns related to meiosis and postmeiotic development. *Physiol. Genomics* 24, 75–85. doi: 10.1152/physiolgenomics.00215.2004

Patel, L., Kang, R., Rosenberg, S. C., Qiu, Y., Raviram, R., Chee, S., et al. (2019). Dynamic reorganization of the genome shapes the recombination landscape in meiotic prophase. *Nat. Struct. Mol. Biol.* 26, 164–174. doi: 10.1038/s41594-019-0187-0

Quinn, J. J., and Chang, H. Y. (2016). Unique features of long non-coding RNA biogenesis and function. *Nat. Rev. Genet*. 17, 47–62. doi: 10.1038/nrg.2015.10

Rinn, J. L., and Chang, H. Y. (2012). Genome regulation by long noncoding RNAs. *Annu. Rev. Biochem*. 8, 145–166. doi: 10.1146/annurev-biochem-051410-092902

Rodríguez-Casuriaga, R., Santiñaque, F. F., Folle, G. A., Souza, E., López-Carro, B., and Geisinger, A. (2014). Rapid preparation of rodent testicular cell suspensions and spermatogenic stages purification by flow cytometry using a novel blue laser-excitable vital dye. *Methods X* 1, 239–243. doi: 10.1016/j.mex.2014.10.002

Rolland, A. D., Evrard, B., Darde, T. A., Le Béguec, C., Le Bras, Y., Bensalah, K., et al. (2019). RNA profiling of human testicular cells identifies syntenic lncRNAs associated with spermatogenesis. *Hum. Reprod*. 34, 1278–1290. doi: 10.1093/humrep/dez063

Romer, K. A., de Rooij, D. G., Kojima, M. L., and Page, D. C. (2018). Isolating mitotic and meiotic germ cells from male mice by developmental synchronization, staging, and sorting. *Dev. Biol*. 443, 19–34. doi: 10.1016/j.ydbio.2018.08.009

Romrell, L. J., Bellvé, A. R., and Fawcett, D. W. (1976). Separation of mouse spermatogenic cells by sedimentation velocity. A morphological characterization. *Dev. Biol.* 49, 119–131. doi: 10.1016/0012-1606(76)90262-1

Rossi, P., Dolci, S., Sette, C., Capolunghi, F., Pellegrini, M., Loiarro, M., et al. (2004). Analysis of the gene expression profile of mouse male meiotic germ cells. *Gene Exp. Patterns* 4, 267–281. doi: 10.1016/j.modgep.2003.11.003

Roy, N. C., Altermann, E., Park, Z. A., and McNabb, W. C. (2011). A comparison of analog and next-generation transcriptomic tools for mammalian studies. *Brief. Funct. Genomics* 10, 135–150. doi: 10.1093/bfgp/elr005

Royo, H., Seitz, H., ElInati, E., Peters, A. H., Stadler, M. B., and Turner, J. M. (2015). Silencing of X-linked microRNAs by meiotic sex chromosome inactivation. *PLoS Genet.* 11:e1005461. doi: 10.1371/journal.pgen.1005461

Salemi, M., Cannarella, R., Condorelli, R. A., Cimino, L., Ridolfo, F., Giurato, G., et al. (2019). Evidence for long noncoding RNA GAS5 up-regulation in patients with Klinefelter síndrome. *BMC Med. Genet*. 20:4. doi: 10.1186/s12881-018-0744-0

Sanchez Calle, A., Kawamura, Y., Yamamoto, Y., Takeshita, F., and Ochiya, T. (2018). Emerging roles of long non-coding RNA in cancer. *Cancer Sci.* 109, 2093–2100. doi: 10.1111/cas.13642

Satoh, Y., Takei, N., Kawamura, S., Takahashi, N., Kotani, T., and Kimura, A. P. (2019). A novel testis-specific long noncoding RNA, Tesra, activates the Prss42/Tessp-2 gene during mouse spermatogenesis. *Biol. Reprod*. 100, 833–848. doi: 10.1093/biolre/ioy230

Schultz, N., Hamra, F. K., and Garbers, D. L. (2003). A multitude of genes expressed solely in meiotic or postmeiotic spermatogenic cells offers a myriad of contraceptive targets. *Proc. Natl. Acad. Sci. U.S.A*. 100, 12201–12206. doi: 10.1073/pnas.1635054100

Shami, A. N., Zheng, X., Munyoki, S. K., Ma, Q., Manske, G. L., Green, C. D., et al. (2020). Single-cell RNA sequencing of human, macaque, and mouse testes uncovers conserved and divergent features of mammalian spermatogenesis. *Dev. Cell* 54, 529.e12–547.e12. doi: 10.1016/j.devcel.2020.05.010

Shima, J. E., McLean, D. J., McCarrey, J. R., and Griswold, M. D. (2004). The murine testicular transcriptome: characterizing gene expression in the testis during the progression of spermatogenesis. *Biol. Reprod.* 71, 319–330. doi: 10.1095/biolreprod.103.026880

Sin, H. S., Barski, A., Zhang, F., Kartashov, A. V., Nussenzweig, A., Chen, J., et al. (2012). RNF8 regulates active epigenetic modifications and escape gene activation from inactive sex chromosomes in post-meiotic spermatids. *Genes Dev*. 26, 2737–2748. doi: 10.1101/gad.202713.112

Sin, H. S., Kartashov, A. V., Hasegawa, K., Barski, A., and Namekawa, S. H. (2015). Poised chromatin and bivalent domains facilitate the mitosis-to-meiosis transition in the male germline. *BMC Biol*. 13:53. doi: 10.1186/s12915-015-0159-8

Sin, H. S., and Namekawa, S. H. (2013). The great escape: active genes on inactive sex chromosomes and their evolutionary implications. *Epigenetics* 8, 887–892. doi: 10.4161/epi.25672

Soh, Y. Q. S., Junker, J. P., Gill, M. E., Mueller, J. L., van Oudenaarden, A., and Page, D. C. (2015). A gene regulatory program for meiotic prophase in the fetal ovary. *PLoS Genet.* 11:e1005531. doi: 10.1371/ journal.pgen.1005531

Soh, Y. Q. S., Mikedis, M. M., Kojima, M., Godfrey, A. K., de Rooij, D. G., and Page, D. C. (2017). Meioc maintains an extended meiotic prophase I in mice. *PLoS Genet*. 13:e1006704. doi: 10.1371/journal.pgen.1006704

Song, R., Ro, S., Michaels, J. D., Park, C., McCarrey, J. R., and Yan, W. (2009). Many X-linked microRNAs escape meiotic sex chromosome inactivation. *Nat. Genet*. 41, 488–493. doi: 10.1038/ng.338

Soraggi, S., Riera, M., Rajpert-De Meyts, E., Schierup, M. H., and Almstrup, K. (2020). Evaluating genetic causes of azoospermia: what can we learn from a complex cellular structure and single-cell transcriptomics of the human testis? *Hum. Genet*. 140, 183–201. doi: 10.1007/s00439-020-02116-8

Sosa, E., Flores, L., Yan, W., and McCarrey, J. R. (2015). Escape of X-linked miRNA genes from meiotic sex chromosome inactivation. *Development* 142, 3791–3800. doi: 10.1242/dev.127191

Soumillon, M., Necsulea, A., Weier, M., Brawand, D., Zhang, X., Gu, H., et al. (2013). Cellular source and mechanisms of high transcriptome complexity in the mammalian testis. *Cell Rep.* 3, 2179–2190. doi: 10.1016/j.celrep.2013.05.031

Sun, J., Lin, Y., and Wu, J. (2013). Long non-coding RNA expression profiling of mouse testis during postnatal development. *PLoS One* 8:e75750. doi: 10.1371/journal.pone.0075750

Sun, Y. C., Cheng, S. F., Sun, R., Zhao, Y., and Shen, W. (2014). Reconstitution of gametogenesis in vitro: meiosis is the biggest obstacle. *J. Genet. Genomics* 41, 87–95. doi: 10.1016/j.jgg.2013.12.008

Suzuki, S., Diaz, V. D., and Hermann, B. P. (2019). What has single-cell RNA-seq taught us about mammalian spermatogenesis? *Biol. Reprod.* 101, 617–634. doi: 10.1093/biolre/ioz088

Tan, K., Song, H. W., and Wilkinson, M. F. (2020). Single-cell RNAseq analysis of testicular germ and somatic cell development during the perinatal period. *Development* 147:dev183251. doi: 10.1242/dev.183251

Trovero, M. F., Rodríguez-Casuriaga, R., Romeo, C., Santiñaque, F. F., Benavente, R., Folle, G. A., et al. (2020). Revealing stage-specific expression patterns of long noncoding RNAs along mouse spermatogenesis. *RNA Biol.* 17, 350–365. doi: 10.1080/15476286.2019.1700332

Tsagakis, I., Douka, K., Birds, I., and Aspden, J. L. (2020). Long non-coding RNAs in development and disease: conservation to mechanisms. *J. Pathol*. 250, 480–495. doi: 10.1002/path.5405

Tseden, K., Topaloglu, Ö, Meinhardt, A., Dev, A., Adham, I., Müller, C., et al. (2007). Premature translation of transition protein 2 mRNA causes sperm abnormalities and male infertility. *Mol. Reprod. Dev.* 74, 273–279. doi: 10.1002/mrd.20570

Tsui, V., and Crismani, W. (2019). The Fanconi anemia pathway and fertility. *Trends Genet*. 35, 199–214. doi: 10.1016/j.tig.2018.12.007

Turner, J. M. (2015). Meiotic silencing in mammals. *Annu. Rev. Genet*. 49, 395–412. doi: 10.1146/annurev-genet-112414-055145

Ulitsky, I., and Bartel, D. P. (2013). LincRNAs: genomics, evolution, and mechanisms. *Cell* 154, 26–46. doi: 10.1016/j.cell.2013.06.020

Vara, C., Paytuvi-Gallart, A., Cuartero, Y., Le Dily, F., Garcia, F., Salva-Castro, J., et al. (2019). Three-dimensional genomic structure and cohesin occupancy correlate with transcriptional activity during spermatogenesis. *Cell Rep*. 28, 352.e9–367.e9. doi: 10.1016/j.celrep.2019.06.037

Veitia, R. A. (2020). Primary ovarian insufficiency, meiosis and DNA repair. *Biomed. J*. 43, 115–123. doi: 10.1016/j.bj.2020.03.005

Velte, E. K., Niedenberger, B. A., Serra, N. D., Singh, A., Roa-DeLaCruz, L., Hermann, B. P., et al. (2019). Differential RA responsiveness directs formation of functionally distinct spermatogonial populations at the initiation of spermatogenesis in the mouse. *Development* 146:dev173088. doi: 10.1242/dev.173088

Waldman Ben-Asher, H., Shahar, I., Yitzchak, A., Mehr, R., and Don, J. (2010). Expression and chromosomal organization of mouse meiotic genes. *Mol. Reprod. Dev.* 77, 241–248. doi: 10.1002/mrd.21139

Wang, L., and Xu, C. (2015). Role of microRNAs in mammalian spermatogenesis and testicular germ cell tumors. *Reproduction* 149, R127–R137. doi: 10.1530/REP-14-0239

Wang, M., Liu, X., Chang, G., Chen, Y., An, G., Yan, L., et al. (2018). Single-Cell RNA sequencing analysis reveals sequential cell fate transition during human spermatogenesis. *Cell Stem Cell* 23, 599.e4–614.e4. doi: 10.1016/j.stem.2018.08.007

Wang, Y., Wang, H., Zhang, Y., Du, Z., Si, W., Fan, S., et al. (2019). Reprogramming of meiotic chromatin architecture during spermatogenesis. *Mol. Cell* 73, 547.e6–561.e6. doi: 10.1016/j.molcel.2018.11.019

Weng, B., Ran, M., Chen, B., He, C., Dong, L., and Peng, F. (2017). Genome-wide analysis of long non-coding RNAs and their role in postnatal porcine testis development. *Genomics* 109, 446–456. doi: 10.1016/j.ygeno.2017.07.001

Wichman, L., Somasundaram, S., Breindel, C., Valerio, D. M., McCarrey, J. R., Hodges, C. A., et al. (2017). Dynamic expression of long noncoding RNAs reveals their potential roles in spermatogenesis and fertility. *Biol. Reprod.* 97, 313–323. doi: 10.1093/biolre/iox084

Wojtas, M. N., Pandey, R. R., Mendel, M., Homolka, D., Sachidanandam, R., and Pillai, R. S. (2017). Regulation of m6A transcripts by the 3'/5' RNA helicase YTHDC2 is essential for a successful meiotic program in the mammalian germline. *Mol. Cell* 68, e312–e387. doi: 10.1016/j.molcel.2017.09.021

Wu, T., and Du, Y. (2017). LncRNAs: from basic research to medical application. *Int. J. Biol. Sci.* 13, 295–307. doi: 10.7150/ijbs.16968

Yadav, R. P., and Kotaja, N. (2014). Small RNAs in spermatogenesis. *Mol. Cell. Endocrinol.* 382, 498–508. doi: 10.1016/j.mce.2013.04.015

Yan, W., and McCarrey, J. R. (2009). Sex chromosome inactivation in the male. *Epigenetics* 4, 452–456. doi: 10.4161/epi.4.7.9923

Yang, C. X., Wang, P. C., Liu, S., Miao, J. K., Liu, X. M., Miao, Y. L., et al. (2020). Long noncoding RNA 2193 regulates meiosis through global epigenetic modification and cytoskeleton organization in pig oocytes. *J. Cell Physiol.* 235, 8304–8318. doi: 10.1002/jcp.29675

Yao, R. W., Wang, Y., and Chen, L. L. (2019). Cellular functions of long noncoding RNAs. *Nat.Cell Biol.* 21, 542–551. doi: 10.1038/s41556-019-0311-8

Yoshida, S., Sukeno, M., Nakagawa, T., Ohbo, K., Nagamatsu, G., Suda, T., et al. (2006). The first round of mouse spermatogenesis is a distinctive program that lacks the self-renewing spermatogonia stage. *Development* 133, 1495–1505. doi: 10.1242/dev.02316

Zhang, X., Hao, L., Meng, L., Liu, M., Zhao, L., Hu, F., et al. (2013). Digital gene expression tag profiling analysis of the gene expression patterns regulating the early stage of mouse spermatogenesis. *PLoS One* 8:e58680. doi: 10.1371/journal.pone.0058680

Zhang, X., Zhang, P., Song, D., Xiong, S., Zhang, H., Fu, J., et al. (2018). Expression profiles and characteristics of human lncRNAs in normal and asthenozoospermia sperm. *Biol. Reprod.* 100, 982–993. doi: 10.1093/biolre/ioy253

Zhu, Z., Li, C., Yang, S., Tian, R., Wang, J., Yuan, Q., et al. (2016). Dynamics of the transcriptome during human spermatogenesis: predicting the potential key genes regulating male gametes generation. *Sci. Rep.* 6:19069. doi: 10.1038/srep19069

Conflict of Interest: The authors declare that the research was conducted in the absence of any commercial or financial relationships that could be construed as a potential conflict of interest.

Copyright © 2021 Geisinger, Rodríguez-Casuriaga and Benavente. This is an open-access article distributed under the terms of the Creative Commons Attribution License (CC BY). The use, distribution or reproduction in other forums is permitted, provided the original author(s) and the copyright owner(s) are credited and that the original publication in this journal is cited, in accordance with accepted academic practice. No use, distribution or reproduction is permitted which does not comply with these terms.

frontiers in Cell and Developmental Biology

MINI REVIEW
published: 08 March 2021
doi: 10.3389/fcell.2021.652407

Meiotic Recombination Defects and Premature Ovarian Insufficiency

Chengzi Huang[1,2,3,4], *Ting Guo*[1,2,3,4]* *and Yingying Qin*[1,2,3,4]*

[1] Center for Reproductive Medicine, Cheeloo College of Medicine, Shandong University, Jinan, China, [2] National Research Center for Assisted Reproductive Technology and Reproductive Genetics, Shandong University, Jinan, China, [3] Key Laboratory of Reproductive Endocrinology of Ministry of Education, Shandong University, Jinan, China, [4] Shandong Provincial Clinical Medicine Research Center for Reproductive Health, Shandong University, Jinan, China

Premature ovarian insufficiency (POI) is the depletion of ovarian function before 40 years of age due to insufficient oocyte formation or accelerated follicle atresia. Approximately 1–5% of women below 40 years old are affected by POI. The etiology of POI is heterogeneous, including genetic disorders, autoimmune diseases, infection, iatrogenic factors, and environmental toxins. Genetic factors account for 20–25% of patients. However, more than half of the patients were idiopathic. With the widespread application of next-generation sequencing (NGS), the genetic spectrum of POI has been expanded, especially the latest identification in meiosis and DNA repair-related genes. During meiotic prophase I, the key processes include DNA double-strand break (DSB) formation and subsequent homologous recombination (HR), which are essential for chromosome segregation at the first meiotic division and genome diversity of oocytes. Many animal models with defective meiotic recombination present with meiotic arrest, DSB accumulation, and oocyte apoptosis, which are similar to human POI phenotype. In the article, based on different stages of meiotic recombination, including DSB formation, DSB end processing, single-strand invasion, intermediate processing, recombination, and resolution and essential proteins involved in synaptonemal complex (SC), cohesion complex, and fanconi anemia (FA) pathway, we reviewed the individual gene mutations identified in POI patients and the potential candidate genes for POI pathogenesis, which will shed new light on the genetic architecture of POI and facilitate risk prediction, ovarian protection, and early intervention for POI women.

Keywords: premature ovarian insufficiency, meiosis, homologous recombination, mutations, next-generation sequencing

OPEN ACCESS

Edited by:
Wei Li,
State Key Laboratory of Stem Cell and Reproductive Biology, Institute of Zoology, Chinese Academy of Sciences (CAS), China

Reviewed by:
Caixia Guo,
Key Laboratory of Genome and Precision Medicine, Beijing Institute of Genomics (CAS), China
Zhenbo Wang,
State Key Laboratory of Stem Cell and Reproductive Biology, Institute of Zoology, Chinese Academy of Sciences (CAS), China

***Correspondence:**
Yingying Qin
qinyingying1006@163.com
Ting Guo
gtlyp2008@126.com

Specialty section:
This article was submitted to Cell Growth and Division, a section of the journal Frontiers in Cell and Developmental Biology

Received: *12 January 2021*
Accepted: *05 February 2021*
Published: *08 March 2021*

Citation:
Huang C, Guo T and Qin Y (2021) Meiotic Recombination Defects and Premature Ovarian Insufficiency. Front. Cell Dev. Biol. 9:652407. doi: 10.3389/fcell.2021.652407

INTRODUCTION

Premature ovarian insufficiency (POI) is the depletion or dysfunction of ovarian follicles before the age of 40, which is characterized by menstrual disturbance (amenorrhea or oligomenorrhea) for at least 4 months, with raised gonadotrophins (FSH > 25 IU/I on two occasions > 4 weeks apart) and estrogen deficiency (European Society for Human et al., 2016). Approximately 1–5% of women under 40 years old are affected by POI, demonstrated with isolated or syndromic phenotype (Desai and Rajkovic, 2017). The etiologies of POI are heterogeneous, including genetic factors, autoimmune diseases, infection, iatrogenic factors, and environmental toxins. However, most of the

cases are still unexplained, known as idiopathic POI. Genetic defects account for approximately 20–25% of POI patients, including chromosomal abnormalities (10–15%) and monogenic mutations (Qin et al., 2015; Jiao et al., 2017). Until now, more than 75 genes have been found to cause POI, which were involved in various processes, including gonadal development, meiosis, DNA damage repair, follicle development, hormone metabolism, and mitochondrial function (Patino et al., 2017; Franca and Mendonca, 2020). Recently, advances in next-generation sequencing (NGS) allow more identification in DNA damage repair genes. Most of the newly identified genes play predominate roles in meiotic homologous recombination (HR), such as *STAG3* (Xiao et al., 2019), while other genes, although participating in DNA damage repair in somatic cells, are found to be essential for meiotic HR as well, such as *MCM8* (AlAsiri et al., 2015) and *BRCA2* (Weinberg-Shukron et al., 2018). Therefore, the role of meiotic HR genes in POI pathogenesis is indispensable.

Females are born with fixed number of oocytes within the ovaries. The fertile lifespan depends on the size of oocyte pool at birth and the rapidity of follicle depletion. The initial oocyte pool is determined by the number of primordial germs cells migrating to the genital ridge, followed by germ cell proliferation and functional meiosis, established as the number of primordial follicles at puberty. The human germ cells enter into meiosis from week 9 postconception, go through leptotene, zygotene, and pachytene, and then transitorily arrest at diplotene stage from the time of birth until puberty when primordial follicles are activated and meiosis continues secondary to FSH and LH secretion. During meiotic prophase I, the key processes are deliberate generation of DNA double-strand breaks (DSBs) and subsequent HR, which laid the foundations of stability and diversity of oocyte genome (Handel and Schimenti, 2010). Disturbance of meiotic HR leads to meiosis blocking before diplotene and DSB accumulation. Animal models defective at DSB formation and HR resulted in early exhaustion of follicle pool and infertility, which were similar to the phenotypes of human POI. While only a few genes have been identified with mutations in POI patients, such as *MSH4* (Carlosama et al., 2017) and *MSH5* (Guo et al., 2017), here, we categorized the genes participating in meiotic HR, candidate genes for human POI, and further reviewed the mutations in detail, Which have been identified in POI patients (**Figure 1** and **Table 1**).

SUBSECTIONS RELEVANT FOR THE SUBJECT

Programmed Double-Strand Break Formation

At the beginning of meiotic prophase I, accurate DSB localization and formation are the basis of homologous chromosome recognition and synapsis, and indispensable for crossover, which is crucial for chromosome segregation and formation of euploid gametes. The predominant protein determining potential DSB sites is PRDM9, which recognizes the DSB hotspots on the chromosome loops, catalyzes H3K4 trimethylation (Sun et al., 2015; Chen et al., 2020), and binds to the chromosome axis through interaction with protein CXXC1, HORMAD1 (Daniel et al., 2011), MEI4 (Kumar et al., 2010), REC114 (Kumar et al., 2018), and IHO1 (Stanzione et al., 2016; Kumar et al., 2018). Then, HELLS and PRDM9 form a pioneer complex to open chromatin at hotspots, permitting correct placement and repair of DSBs (Spruce et al., 2020). Then, the endonuclease SPO11 is recruited at PRDM9-binding sites before or after the loop axis interaction and catalyzes DSB formation at the hotspots (Romanienko and Camerini-Otero, 2000). Moreover, other proteins required along with SPO11 to generate DSBs including MEI1 (Reinholdt and Schimenti, 2005) and TOPOVIBL (Robert et al., 2016). The knockout mouse models of the above genes demonstrate female infertility and premature depletion of oocytes due to defective DSB formation and homologous synapsis, except for CXXC1 and HORMAD1. The conditional knockout mice of *Cxxc1* are fertile (Tian et al., 2018). *Hormad1* deficiency does not affect folliculogenesis but disrupts homologous chromosome segregation, resulting in infertility due to gemmate aneuploidy (Shin et al., 2010). Although most of the genes involving DSB formation might be candidate genes for human POI, no causative mutation has been identified in POI patients. Interestingly, there are findings that bi-allelic deleterious mutations of *TOROVIBL*, *MEI1*, and *REC114* could result in recurrent androgenetic complete hydatidiform moles due to extrusion of all maternal chromosomes with the spindles into the first polar body during meiosis metaphase I. These findings indicated that DSB-formed genes were essential for stabilization of gemmate genome. Defects in these genes might be pleiotropic and responsible for heterogeneous reproductive phenotypes (Nguyen et al., 2018).

DSB End Processing

After DSB formation, DNA ends are engaged in a process of maturation, involving the release of SPO11-oligonucleotide covalent complexes and exonucleolytic degradation on the same strand, which leads to extended overhanging of 3' single strands on both sides of the DSBs. This process is facilitated by the MRN complex, EXO1, CtIP, and RPA.

The multiprotein complex MRN is consisted of MRE11, RAD50, and NBS1, which are evolutionarily conserved in 5′-end resection of DSBs (Anand et al., 2019). Disruption of the N-terminal exons of *Nbs1* in mice resulted in female infertility due to oogenesis failure (Kang et al., 2002). The female mice with a mutation in *Mre11* exhibited premature oocyte elimination attributing to defects in homologous chromosome pairing and DSB repair during meiotic prophase I (Inagaki et al., 2016). *Rad50* heterozygous mutant mice demonstrated ovarian atrophy as well (Roset et al., 2014). These animal models indicated the essential role of the MRN complex in maintenance of the primordial follicle pool. In humans, mutations in MRN subunits caused Nijmegen Breakage Syndrome in recessive pattern, in which POI was one of the degenerative changes (Chrzanowska et al., 2012). Although they are potential causative genes for POI, no mutation has been identified in isolated POI yet. Besides that, CtIP is an important cofactor of MRN in catalyzing the 5′-end resection (Sartori et al., 2007). *CtIP* mutations cause Seckel

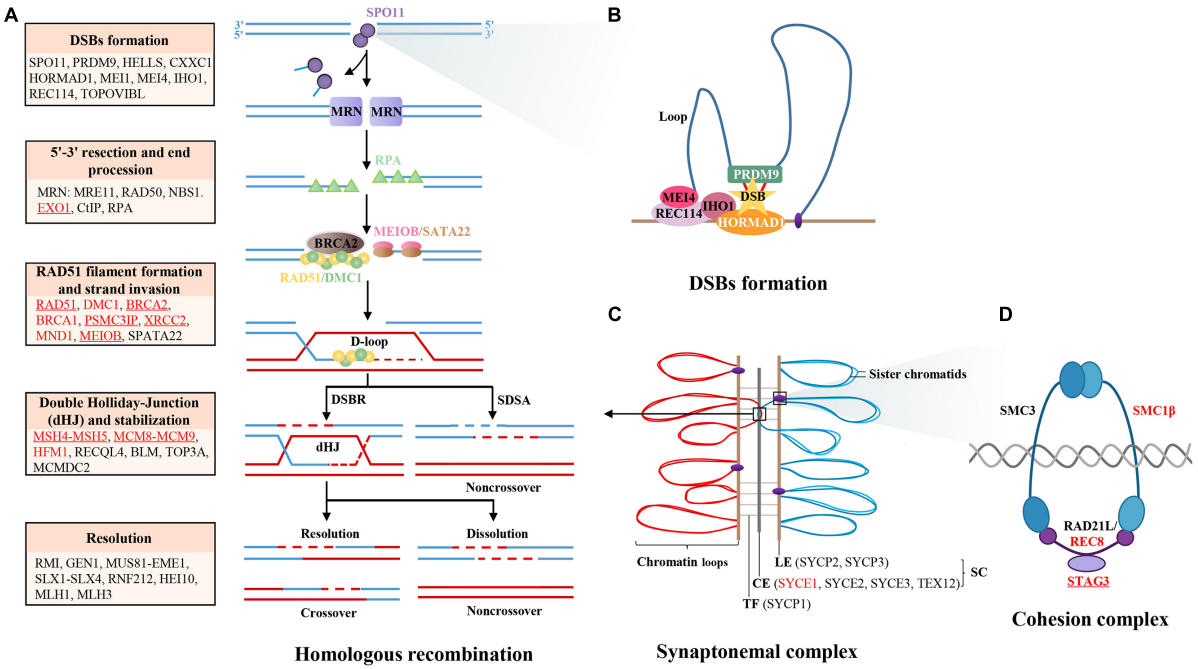

FIGURE 1 | Diagram of meiotic HR genes. **(A)** Major steps of meiotic prophase I, including DSBs formation, 5′-3′ resection, end procession, RAD51 filament formation, strand invasion, intermediates formation, and resolution. The key genes in different steps are labeled in the box, those genes that have been identified in POI patients are labeled with red color, and those that have been functionally validated are underlined. **(B)** The formation of DSBs is initiated by PRDM9, which binds to chromatin and catalyzes H3K4 trimethylation to mark hotspots. Then, the complex MEI4/REC114/IHO1 binds to HORMAD1 on the axis and activates SPO11 to cut chromatin to form DSBs. **(C)** The synapsis complex is installed by CE and LE with TF connections in each pair of homologous chromosomes, which establish the platform of HR. **(D)** The cohesion complex regulates sister chromatid cohesion and SC formation, which is consisted of meiosis-specific subunits STAG3, RAD21L, and SMC1B and non-specific subunits SMC3 and REC8. Notes: DSBs, double-strand breaks; SC, synaptonemal complex; LE, lateral element; CE, central element; TFs, transverse filaments; HR, homologous recombination.

and Jawad syndromes in a recessive manner, while no ovarian abnormality was noticed (Qvist et al., 2011). Therefore, although CtIP performs an important role in DSB end processing, it might not be a potential causative gene of POI.

EXO1 has 5′ to 3′ exonuclease activity, which is recruited to DSBs by MRN and promotes the formation of 3′-tailed single-strand DNA (ssDNA) (Garcia et al., 2011). *Exo1* knockout female mice were infertile due to dynamic loss of chiasmata during meiosis prophase I (Wei et al., 2003). A meta-analysis of 53 GWASs with nearly 70,000 women found EXO1 polymorphism associated with the age of natural menopause (Day et al., 2015). Recently, through whole-exome sequencing (WES) in 50 patients with POI, one heterozygous mutation in *EXO1* was identified, which impaired meiosis by disrupting recruitment of RPA and RAD51 onto DSB sites (Luo et al., 2020). These findings confirmed the role of EXO1 in POI, and discussed the dosage-dependent effect of oocyte-non-specific HR gene on ovarian function.

When 3′-tailed ssDNAs are established, RPA is recruited to prevent ssDNA degradation or formation of secondary structure (Soustelle et al., 2002). Recent study found that the loss of RPA completely abrogated the loading of recombinases RAD51 and DMC1 on DSBs sites, blocked strand invasion, and chromosome synapsis (Shi et al., 2019). However, because RPA is ubiquitously expressed, the *Rpa1* null mice showed embryonic lethality. Although the heterozygotes displayed defects in DSB repair, ovarian phenotype had not been observed (Wang et al., 2005). Therefore, the evidence of RPA participating in POI pathogenesis was insufficient yet.

Strand Invasion

As the proceeding of HR, RPA is replaced by the recombination proteins RAD51 and DMC1, which catalyze homology search and strand invasion, establishing the basis of synapsis (Brown and Bishop, 2014). Besides RAD51 and DMC1, the dynamic process is also regulated by other recombination factors, including BRCA2, PSMC3IP, MND1, MEIOB, and SPATA22.

RAD51 and its meiotic paralog DMC1 execute the critical step of strand invasion (Bishop et al., 1992; Park et al., 2008). In the *Dmc1*-deficient mice, gametogenesis arrested in meiotic prophase I, resulting in germ cell depletion in the adult ovaries and infertility. Recently, a homozygous mutation p.D36N in *DMC1* was identified in one consanguineous pedigree having one patient with POI and one patient with non-obstructive azoospermia (NOA) (He et al., 2018b). Histological study found that spermatogenesis was blocked at zygotene stage in the patient with NOA, indicating that POI in women might be caused by dysfunctional meiosis prophase I of oocytes (Pittman et al., 1998). Besides that, another homozygous mutation *DMC1* p.M200V was identified by Sanger sequencing in sporadic POI

TABLE 1 | Variants of meiosis HR genes identified in POI patients.

Gene	Aliases	Mechanism/function	Mutations found in POI pedigrees	Mutations found in sporadic POI patients	Phenotype	Inheritance	Ovarian phenotypes of mice model	Fertility of mice model
STAG3	–	Subunit of cohesion complex	p.F187*fs**7 (Caburet et al., 2014) p.S227* (Colombo et al., 2017) p.Y650S*fs**22 (Le Quesne Stabej et al., 2016) p.L490T*fs**10 (He et al., 2018a) p.N98Q*fs**2 and p.Y650* (Franca et al., 2019) p.H293_E295del; p.I297_E298insD (Xiao et al., 2019) p.R1018D*fs**14; p.L220R (Heddar et al., 2019)	–	PA	AR	Follicle are exhausted at 6 weeks of age (Winters et al., 2014)	Infertility
SYCE1	*POF12*	Central element of SC	p.Q205* (de Vries et al., 2014) Partial region deletion (~4 kb) (Zhe et al., 2020)	–	PA, SA	AR	Oocyte loss before reproductive age due to synapsis failure (Bolcun-Filas et al., 2009)	Infertility
SMC1β	*SMC1L2*	Subunit of cohesion complex	–	p.I221T; p.Q1177L (Bouilly et al., 2016)	PA, SA	Digenicity	Gradually follicle decrease from 4 to 8 weeks of age (Takabayashi et al., 2009)	Infertility
REC8	–	Subunit of cohesion complex	–	p.Q154R; p.R300L (Bouilly et al., 2016)	PA, SA	Di-genicity	Completely lack of oocytes at postnatal day 5 (Xu et al., 2005)	Infertility
RAD51	*FANCR*	Strand invasion	–	p.E68G (Luo et al., 2020)	PA	AD	–	Embryonic lethal (Tsuzuki et al., 1996)
DMC1	*LIM15*	Strand invasion	p.D36N (He et al., 2018b)	p.M200V (Mandon-Pepin et al., 2008)	SA	AR	Early oocyte exhausted in the adult ovaries (Pittman et al., 1998)	Infertility
FANCU	*XRCC2*	Strand invasion	p.L14P (Zhang et al., 2019)	–	SA	AR	Gradually follicles loss from postnatal days 21 to 180 (Yang et al., 2018)	Impaired fertility
PSMC3IP	*HOP2*	Strand invasion	p.Y163* (Al-Agha et al., 2018) p.E201del (Zangen et al., 2011)	p.R166A*fs*; p.L144* (Yang et al., 2019a)	PA	AR; AD	Absent follicle in the knockout ovaries (Petukhova et al., 2003)	Infertility
MND1	*GAJ*	Strand invasion	Partial region deletion (8.6 kb) (Jolly et al., 2019)	–	–	AR	Absent follicles and CL (Pezza et al., 2014)	Infertility

(Continued)

TABLE 1 | Continued

Gene	Aliases	Mechanism/function	Mutations found in POI pedigrees	Mutations found in sporadic POI patients	Phenotype	Inheritance	Ovarian phenotypes of mice model	Fertility of mice model
BRCA2	*FANCD1*	DNA DSBs repair	p.V2527* and p.S3231*fs*16* (Weinberg-Shukron et al., 2018)	New variations: p.I3312V; IVS-7T > A (Yilmaz et al., 2016)	PA	AR; AD	Absent follicle in adult ovaries (Connor et al., 1997); increased ovarian tumor incidence (Szabova et al., 2012)	Infertility
			c.68-1G > C and p.Y1480*; p.D2723V and p.C3233W*fs**15 (Qin et al., 2019)					
BRCA1	*FANCS*	DNA DSBs repair	–	New variations: p.T1246N; p.R1835Q (Yilmaz et al., 2016)	–	AD	Decreased primordial follicle number (Titus et al., 2013)	Impaired fertility
MEIOB	*SPGF22*	DSB repair/meiotic HR	p.T406 = (Caburet et al., 2019)	–	SA	AR	Completely lack of oocytes at postnatal day 2 (Luo et al., 2013)	Infertility
MSH4	–	Stabilization of double Holliday junction	p.I743_K785del (Carlosama et al., 2017)	–	SA	AR	Steady follicle loss soon after birth (Kneitz et al., 2000)	Infertility
MSH5	*POF13*	Stabilization of double Holliday junction	p.D487Y (Guo et al., 2017)	p.L353M; p.D487Y; p.I703V (Guo et al., 2017)	SA	AR; AD	Gradually follicle loss after birth and completely devoid at 2–3 months of age (de Vries et al., 1999)	Infertility
				p.P29S (Mandon-Pepin et al., 2008)				
MCM8	*POF10*	HR intermediate process	p.P149R (AlAsiri et al., 2015)	p.H317L; p.H601R (Dou et al., 2016)	PA, SA	AR; AD	Follicles were absent at 8 weeks post-partum; ovarian adenomas and sex cord stromal tumors developed in older females (Lutzmann et al., 2012)	Infertility
			p.H161P (Bouali et al., 2017)	p.C155Y; p.N183S; p.R445Q (Desai et al., 2017)				
			c.1954-1G > A; p.L491I*fs**88 (Tenenbaum-Rakover et al., 2015)					
			p.K118E*fs**5 (Zhang et al., 2020)					
			p.R309* (Heddar et al., 2020)					

(Continued)

TABLE 1 | Continued

Gene	Aliases	Mechanism/function	Mutations found in POI pedigrees	Mutations found in sporadic POI patients	Phenotype	Inheritance	Ovarian phenotypes of mice model	Fertility of mice model
MCM9	*ODG4*	HR intermediate process	P.R132*; c.1732+2T > C (Wood-Trageser et al., 2014)	p.T139A; p.T595R; p.V808I; p.Q551*; p.E670* (Desai et al., 2017)	PA, SA	AR; AD	Completely devoid of oocytes in adult ovaries (Lutzmann et al., 2012)	Infertility
			p.E495* (Fauchereau et al., 2016)	p.L475F; p.L974S; p.A1130T (Guo et al., 2020)				
			p.E225K*fs**4 (Goldberg et al., 2015)	p.T595R; c.905-1G > T (Yang et al., 2019a)				
			p.Q551* (Desai et al., 2017)					
HFM1	*POF9*	Crossover formation and proper synapsis	P.C1157Y (Zhe et al., 2019)	p.H414P; p.R1194C (Pu et al., 2016)	SA	AD; AR	Follicles are almost exhausted at 45 days (Guiraldelli et al., 2013)	Infertility
			p.I884S and c.1686-1G > C (Wang et al., 2014)	p.G736S and p.P1310R*fs**41 (Wang et al., 2014)				
EXO1	*HEX1*	Crossover resolution	–	p.T52S (Luo et al., 2020)	PA	AD	Small ovary with oocytes loss at 7 months of age (Wei et al., 2003)	Infertility
FANCM	*FAAP250*	HR intermediate process	p.Q1701* (Fouquet et al., 2017)	–	SA	AR	Depleted primary follicles and reduced developing follicles in ovaries (Bakker et al., 2009)	–
FANCL	*FAAP43,PHF9*	–	–	p.Q350V*fs**18; p.M247N*fs**4 (Yang et al., 2020)	PA, SA	AD	Reduced follicles at 4 weeks, germ cell-deficient (GCD) phenotype (Agoulnik et al., 2002)	Infertility
FANCA	*FAA*	–	–	p.R591Q; p.E1296G (Yang et al., 2019b)	PA, SA	AD	Significantly reduced follicles and obvious hypogonadism (Cheng et al., 2000; Wong et al., 2003)	Impaired fertility
SPIDR	–	HR intermediate process	p.W280* (Smirin-Yosef et al., 2017)	–	PA	AR	–	–
NUP107	–	Meiosis/DNA repair	p.R355C (Ren et al., 2018); p.D447N (Weinberg-Shukron et al., 2015)	–	PA	AR	–	–

DSBs, double-strand breaks; HR, homologous recombination; SC, synaptonemal complex; AD, autosomal dominant; AR, autosomal recessive; PA, primary amenorrhea; POI, premature ovarian insufficiency; SA, secondary amenorrhea; CL, corpora lutea; "–" unknown. ""means "stop codon".*

(Hikiba et al., 2008), while the point mutant mice showed normal ovarian morphology, highlighting the importance of functional studies in verifying the pathogenicity of variations (Hikiba et al., 2008; Tran and Schimenti, 2018). Absolutely, loss of RAD51 resulted in embryo lethality in mice (Tsuzuki et al., 1996). However, a WES study in sporadic POI patients found one heterozygous missense mutation of *RAD51*, which resisted the protein localization in the nucleus. *In vitro* experiments found that heterozygous mutation affected HR efficiency by haploinsufficiency, indicating that the pathogenic effect of *RAD51* on POI might be dosage dependent (Luo et al., 2020).

BRCA2 regulates the localization of RAD51 onto ssDNA to form an RAD51-ssDNA filament, promoting HR repair for DSBs both in somatic cells and in germ cells (Davies et al., 2001; Xia et al., 2001). Somatic *BRCA2* mutations impaired chromosome integrity, manifesting with an increased risk of tumor (Daum et al., 2018), whereas recent studies found its crucial role in ovarian development mediated by functional meiotic recombination (Miao et al., 2019). Until now, four pairs of compound heterozygous mutations and one homozygous mutation in *BRCA2* have been identified in POI pedigrees through WES analysis (Weinberg-Shukron et al., 2018; Qin et al., 2019; Caburet et al., 2020). Among them, four mutation carriers demonstrated with microcephaly, leukemia, thyroid cancer, or breast carcinoma, while other three carries presented with isolated POI. The widely varying severity of clinical profiles of bi-allelic *BRCA2* mutation carriers confirmed the complicated function of BRCA2, also highlighted the necessity of long-term follow-up for them. Recent studies in *Caenorhabditis elegans* found BRCA1 influenced RAD51 dynamics and combined with SYCP3 and MSH5 to promote synapsis and crossover resolution (Janisiw et al., 2018). Although its function in mammalian meiosis was unclear, *Brca1* mutant mice had impaired reproductive capacity and decreased primordial follicle counts (Titus et al., 2013). Women with *BRCA1* variations also presented with accelerated ovarian reserve decline (Lin et al., 2017; Porcu et al., 2020). Therefore, BRCA1 was a potential causative gene of POI, which required comprehensive evaluation of somatic characteristics like BRCA2.

PSMC3IP (also known as HOP2) and MND1 are meiosis-specific factors in all organisms expressing DMC1. PSMC3IP-MND1 complex facilitates strand invasion and D-loop formation by promoting DMC1/RAD51 capturing of double-strand DNA (dsDNA) (Chi et al., 2007; Pezza et al., 2007). Absence of them resulted in non-homologous synapses and DSB accumulation (Sansam and Pezza, 2015). *Psmc3ip* and *Mnd1* knockout mice showed severely reduced ovarian size and defective gametogenesis (Petukhova et al., 2003; Pezza et al., 2014). In previous studies, two-point mutations of *PSMC3IP* and one microdeletion of *MND1* inherited in recessive patterns have been identified in consanguineous pedigrees with POI or XX female gonadal dysgenesis (Zangen et al., 2011; Zhao and Sung, 2015; Al-Agha et al., 2018; Jolly et al., 2019), confirming their crucial roles in gametogenesis and POI pathogenesis.

MEIOB and SPATA22 are ssDNA-binding proteins predominately expressed in meiosis prophase I, which form a complex that interacts with RPA to recruit RAD51 and DMC1 to the ssDNA (La Salle et al., 2012; Luo et al., 2013; Souquet et al., 2013; Ishishita et al., 2014). Both *Meiob*-null mice and *Spata22*-null mice exhibited small ovaries devoid of oocytes in any developmental stage due to uncompleted meiotic HR (Luo et al., 2013; Hays et al., 2017). Recent WES study with a POI pedigree identified one homozygous splicing mutation in *MEIOB*, which resulted in a truncated MEIOB protein, thus interrupting the interaction with SPATA22 (Caburet et al., 2019). POI might be caused by defective MEIOB-SPATA22 complex-induced insufficient DNA single-strand invasion during meiotic HR. Although no mutation has been found in *SPATA22*, it still is a potential candidate gene of POI.

Intermediate Processing and Homologous Recombination

During strand invasion, the presynaptic filaments recognize the template strands, invade into the duplex DNA, displace the original strand, and bind to their complementary sequence, forming the intermediate of HR repair. The intermediate processing is performed by two pathways: synthesis-dependent strand annealing and double Holliday junction (dHJ). SDSA is a pathway for non-crossover repair, in which a D-loop intermediate is formed and the broken DNA is synthesized using the homologous chromosome as a template (Ranjha et al., 2018). In the dHJ pathway, two DSB ends participate in the invasion that forms a classic double junction intermediate, which facilitates crossover formation and resolution. During the process, MSH4–MSH5 heterodimer, MCM8–MCM9 helicase complex, HFM1, RECQL4, BLM, and MCMDC2 are involved.

The meiotic specially expressed proteins MSH4 and MSH5 form a heterodimeric complex (Acharya et al., 1996; Snowden et al., 2004), which clamps on homologous chromosomes to stabilize the Holliday junctions (Nishant et al., 2010). In the *Msh5/Msh4* deficient mice, chromosome pairing was failed and crossover was absent, resulting in atrophic ovaries, which were similar to the phenotype of human POI (de Vries et al., 1999; Kneitz et al., 2000). Through WES in two POI pedigrees, homozygous mutations of *MSH4* and *MSH5* were identified, pathogenicity of which was confirmed by *in vitro* studies and knock-in mice models (Carlosama et al., 2017; Guo et al., 2017). These results implied the recessive mode of inheritance for *MSH4* and *MSH5* in POI. Interestingly, four heterozygous mutations of *MSH5* have been reported in sporadic cases, indicating that their effects on meiosis and oogenesis might be dominated or dosage dependent as well (Mandon-Pepin et al., 2008; Guo et al., 2017).

MCM8 and MCM9 form a helicase complex regulating DNA repair and genome integrity both in somatic cells and in germ cells (Nishimura et al., 2012). They not only promote MRN-mediated ssDNA maturation, but also participate in intermediate processing of HR. *Mcm8* or *Mcm9* knockout mice suffered meiosis blocking at prophase I (Lutzmann et al., 2012). Bi-allelic mutations of *MCM8* and *MCM9* have been identified in POI patients with or without familial history (Wood-Trageser et al., 2014; AlAsiri et al., 2015; Goldberg et al., 2015; Tenenbaum-Rakover et al., 2015; Fauchereau et al., 2016; Bouali et al., 2017; Desai et al., 2017). The prevalence of bi-allelic mutations of

MCM9 in sporadic cases was variable among different studies, ranging from 1.6 to 6.1% (Yang et al., 2019a; Guo et al., 2020). However, heterozygous variations were also found in 1.0–4.6% of sporadic POI, making the inheritance pattern of *MCM8/MCM9* in recessive or dominate to be ambiguous (Dou et al., 2016; Desai et al., 2017; Guo et al., 2020). Interestingly, some patients were found to carry digenic heterozygous variants in both *MCM8* and *MCM9* or in *MCM8/MCM9* and other DNA repair genes (Desai et al., 2017). Moreover, researchers observed MCM8 had a dosage-dependent effect on the severity of POI phenotypes. These findings indicated that heterozygous variations of HR genes might establish a genetic background susceptive to DNA damage, which would affect meiosis when additional variations in the related genes or environmental toxin existed (Heddar et al., 2020; Wang et al., 2020). Besides the essential role in meiosis, MCM8 and MCM9 were involved in DNA replication, DNA damage response and cell cycle regulation in somatic cells. Some of the mutation carriers presented with short stature, and an *MCM8* carrier was reported to have pilomatricomas (Heddar et al., 2020). Mitomycin-induced DNA breaks and aberrant metaphases in the patient's lymphoblastoid cells suggested that the patients carrying *MCM8* or *MCM9* mutations were susceptive to tumor or growth retardation due to impaired DNA repair and genome instability in somatic cells. Therefore, long-term follow-up of cancers for those mutation carriers is needed.

HFM1 is a DNA helicase preferentially expressed in germline cells. Absence of HFM1 resulted in aberrant intermediate processing and reduced crossover formation (Guiraldelli et al., 2013). Two-compound heterozygous mutations of *HFM1* were identified in two familial POI and one sporadic case (Wang et al., 2014). Moreover, heterozygous pathogenic mutations were found in a POI pedigree and 1.5% of the sporadic case, indicating that *HFM1* mutants might cause POI through both recessive and dominate modes (Pu et al., 2016; Zhe et al., 2019).

RECQL4 and BLM are pleiotropic helicases expressed non-specifically, which unwind dsDNA into ssDNA during HR repair for DSBs (Singh et al., 2012). They are essential for maintenance of genome stability in both somatic and germline cells. Therefore, their defects mostly cause syndromic POI, such as Rothmund–Thomson syndrome (Siitonen et al., 2009) and Bloom syndrome (Arora et al., 2014), in which POI is one of the complicated symptoms.

Besides the helicases above, MCMDC2 is an atypical yet conserved MCM protein, which also plays an important role in ssDNA invasion that promotes homolog alignment and inter-homolog crossover formation. *Mcmdc2* knockout mice were infertile, demonstrated to have atrophic ovaries completely devoid of oocyte at 6 weeks post-natal (Finsterbusch et al., 2016). Although no mutation of *MCMDC2* has been reported in POI patient yet, it still is a potential causative gene for POI.

Synaptonemal Complex and Cohesion Complex

Throughout meiosis prophase I, the chromosomes are reorganized as linear arrays of chromatin loops anchored to a central axis. The chromosome axis forms a platform for the assembly of synaptonemal complex (SC), which plays a central role in homologous pairing, recombination, and chromosome segregation. The SC is installed by five central elements linked to two lateral elements by a transverse filament in each pair of homologous chromosomes.

The central elements of SC include SYCE1-3, C14ORF39, and TEX12. Female knockout mice of those genes were affected by infertility and oocyte loss before reproductive age due to different degrees of synapsis failure (Bolcun-Filas et al., 2007, 2009; Hamer et al., 2008; Schramm et al., 2011; Davies et al., 2012; Lu et al., 2014). In POI patients, except for one microdeletion and two homozygous mutations of *SYCE1* which have been identified (McGuire et al., 2011; Zhen et al., 2013; de Vries et al., 2014; Zhe et al., 2020), no causative mutation has been found in other genes, indicating that the mutations in central elements of SC might not be a common genetic causation for POI.

SYCP1 is the transverse filament of SC that connects central elements SYCE1–2 to the lateral elements localized in each homologous chromosome. Absence of *Sycp1* disturbed chromosomal synapsis, resulting in oocytes arrested at pachytene stage and apoptosis (de Vries et al., 2005). SYCP2 and SYCP3 are lateral elements of SC, which interact with each other (Winkel et al., 2009) and stabilize the linear array of chromatin loops during SC assembly (Yang et al., 2006; Syrjanen et al., 2014, 2017). The *Sycp2* and *Sycp3* mutant mice were subfertile (Yuan et al., 2000; Yang et al., 2006), which might be explained by insufficient SC formation, contrasting to the absolute loss of SC in *Sycp1* null mice (Yang et al., 2006). That dosage-dependent meiosis dysfunction could also be a potential explanation for heterogeneous clinical phenotypes of human POI. Furthermore, *Sycp3* mutant female mice exhibited increased aneuploidy in oocytes and embryos. In human beings, heterozygous variations of *SYCP3* were associated with miscarriage and increased predisposition to infertility (Bolor et al., 2009; Nishiyama et al., 2011). Therefore, although no *SYCP* mutation has been identified in POI patient yet, their roles in oogenesis and embryo development should be further explored.

The cohesion complex regulates sister chromatids cohesion and SC formation, which is composed of meiosis-specific subunits STAG3, RAD21L, and SMC1B and non-specific subunits SMC3 and REC8 (Ishiguro, 2019). Female mice deficient in *Stag3* were sterility and follicle exhausted at a young age (Caburet et al., 2014). To date, seven bi-allelic mutations of *STAG3* have been found in POI pedigrees. All the affected patients manifested with primary amenorrhea and streak ovaries (Caburet et al., 2014; Le Quesne Stabej et al., 2016; Colombo et al., 2017; He et al., 2018a; Franca et al., 2019; Heddar et al., 2019; Xiao et al., 2019), indicating that recessive mutations in *STAG3* were relatively common genetic causation for primary POI. Furthermore, mice deficient in other cohesion genes demonstrated with similar ovarian morphology of *Stag3* null mice (Xu et al., 2005; Takabayashi et al., 2009; Herran et al., 2011). Through target gene screening of sporadic POI patients, heterozygous mutations in *STAG3*, *SMC1B*, and *REC8* have been found (Bouilly et al., 2016), indicating that the recessive and dominate causative modes of cohesion genes in POI might coexist. Moreover, age-dependent decrease of cohesion protein

is associated with increased rate of aneuploidy oocytes, while mutations of *SMC3* were reported in Cornelia de Lange syndrome without ovarian abnormalities (Deardorff et al., 2007). Therefore, besides the indispensable contribution to POI, the pleiotropic effects of cohesion genes in reproductive and somatic diseases should be considered as well.

Resolution of Recombination Intermediates

In germ cells, the essential step for accurate separation of homologous chromosomes at the first meiotic division is resolution of recombination intermediates, including non-crossover pathway and crossover pathway. In the non-crossover pathway, the final products are generated by annealing the invaded strand to the complementary break end of single Holliday junction or dissolution of the dHJs (Bizard and Hickson, 2014; Daley et al., 2014). That process is the major route for dissipation of HR intermediate, which limits chromosomal rearrangements and heterozygosity of oocytes. This reaction requires the RecQ helicase BLM (Wu et al., 2000), topoisomerase TOP3A (Martin et al., 2018), RMI complex (Raynard et al., 2008), structure-selective endonucleases GEN1 (Shah Punatar et al., 2017), MUS81-EME1, and SLX1–SLX4 (Matos and West, 2014; Wyatt and West, 2014). Absence of the above genes resulted in syndromic disease or embryonic lethality. Therefore, their pleiotropic effect on meiosis and ovarian function was illusive and needs more detailed exploration.

Crossover pathway is the meiosis-specific resolution of dHJs that contributes to the genetic diversity of species. Although the process resolves less recombination than non-crossover pathway, the occurrence of at least one crossover in every pair of homologous chromosomes is essential for precise separation of chromosomes in the first meiotic division. Crossover pathway involves *RNF212* (Qiao et al., 2014), *HEI10* (Ward et al., 2007), *MLH1* (Baker et al., 1996), and *MLH3* (Lipkin et al., 2002). The knockout mice of the above genes had normal ovarian morphology; oocytes show proficient synapsis but deficient crossover, presenting with abnormal chromosome alignment at metaphase I and disturbed extrusion of polar bodies. Those female mice were infertile due to a decreased number of mature MII oocytes and increased number of aneuploidy embryos. Therefore, these gene defects are responsible for disorders of oocyte maturation or early embryo development rather than POI.

Fanconi Anemia Pathway Genes in Meiotic HR

Fanconi anemia (FA) is usually a recessive genetic disease associated with bone marrow failure, increased cancer susceptibility, and severe germline defects. There are 22 identified FA genes, which are involved in DNA interstrand crosslink repair, including the FA core complex which catalyzes the mono-ubiquitination of FANCD2 and FANCI, and DSB repair genes—*BRCA1* (*FANCS*), *BRCA2* (*FANCD1*), *BRIP1* (*FANCJ*), *PALB2* (*FANCN*), *RAD51C* (*FANCO*), *SLX4* (*FANCP*), *RAD51* (*FANCR*), and *XRCC2* (*FANCU*) (Tsui and Crismani, 2019). Although all mice models of FA genes reported to date have different degrees of reduction in fertility, the links between their roles in DNA repair and fertility have not been extensively explained. Recent studies found that BRCA2 promoted the localization of RAD51 and DMC1 to meiotic DSBs. As a member of RAD51 paralogs, FANCU (XRCC2) might be involved in the RAD51-mediated strand invasion during meiotic HR (Yang et al., 2018). Besides that, FA core factors FANCA, FANCB, and FANCC were reported to facilitate the recruitment of FANCD2 on sex chromosomes and regulate the histone modification during meiotic HR (Alavattam et al., 2016). FANCM has also been shown to limit crossover frequencies, which promoted the conservatism of gametes (Crismani et al., 2012). The increasing research of FA genes highlighted their roles in the resolution of meiotic DSBs, giving more indications of oogenesis as well. Up to date, several FA genes had identifications in POI, such as homozygous mutations in *FANCM* (Fouquet et al., 2017) and *FANCU* (Zhang et al., 2019) and heterozygous mutations in *FANCA* (Yang et al., 2019b) and *FANCL* (Yang et al., 2020). Interestingly, heterozygous *FANCA* knockout mice showed a declined follicle number and reduced fertility; *in vitro* studies found that single-allelic defects of *FANCA* and *FANCL* compromised DNA repair ability by haploinsufficiency, indicating that the adverse effects of FA gene variations on meiosis and ovarian function might be dosage dependent.

DISCUSSION

Identifying causative genes of POI and elucidating their molecular mechanisms are important for the genetic diagnosis of POI. As an increasing number of women prefer to conceive after their mid-30s, the genetic counseling of POI predisposition will be instructive for their childbearing plans. To date, more than 75 genes have been found to be responsible for POI, among which 24 genes were involved in meiotic HR process. With the widespread use of NGS and whole-genome sequencing, the identification of novel genes will be increased in the near future. Furthermore, with the development of data analysis strategies, more non-synonymous mutations with high risk of pathogenicity, microdeletion or interruption, and rearrangement of gene sequences will be identified, expanding the mutation spectrum and genetic architecture of POI.

Along with the increasing genes and variations identified, more challenges are emerging to determine the causative patterns of meiotic HR genes in POI. Most of the meiotic HR genes were found in familial POI by recessive modes, while heterozygous mutations were more common in sporadic cases, and the mutation frequencies varied significantly among different cohorts. These observations indicated that the genetic architecture of sporadic POI would be more complicated than that in familial cases. With more and more di-genetic or multigenetic variations reported and dosage-dependent effect confirmed by functional studies, sporadic POI seemed to be a complex disease, which occurred as a result of multiple genomic variants paired with environmental influences. Furthermore,

many HR genes had pleiotropic effects in proliferation and apoptosis of somatic cells. The relationships between pleiotropic genes and heterogeneous phenotypes of isolated or syndromic POI should be further explored as well.

Meiotic HR genes not only participate in oogenesis but also facilitate oocyte maturation, fertilization, and early embryo development. Dysfunction of several genes might be responsible for unexplained infertility or early pregnancy loss, such as members of SC and cohesion complex influenced chromosome separation and aneuploidy of oocytes. Therefore, besides the benefits of early diagnosis, intervention, and treatment of POI, further studies on the meiotic HR genes will give advice to other diseases of infertility and adverse pregnancy outcomes. Moreover, considering the increased cancer susceptibility of HR gene defects, long-term follow-up for cancer risks and healthcare should be suggested.

AUTHOR CONTRIBUTIONS

YQ and TG contributed to the conceptual idea. CH performed the data collection. TG and CH wrote the manuscript. YQ reviewed the manuscript. All authors contributed to the article and approved the submitted version.

FUNDING

This work was supported by the National Key Research and Developmental Program of China (2018YFC1003702); the Science Foundation for Distinguished Young Scholars of Shandong (JQ201720); the National Natural Science Foundation of China (32070847, 81771541, and 81671413); Basic Science Center Program of NFSC (31988101); and Shandong University Education Foundation Public Welfare Project (23460047102008).

REFERENCES

Acharya, S., Wilson, T., Gradia, S., Kane, M. F., Guerrette, S., Marsischky, G. T., et al. (1996). hMSH2 forms specific mispair-binding complexes with hMSH3 and hMSH6. *Proc. Natl. Acad. Sci. U.S.A.* 93, 13629–13634. doi: 10.1073/pnas.93.24.13629

Agoulnik, A. I., Lu, B., Zhu, Q., Truong, C., Ty, M. T., Arango, N., et al. (2002). A novel gene, Pog, is necessary for primordial germ cell proliferation in the mouse and underlies the germ cell deficient mutation, gcd. *Hum. Mol. Genet.* 11, 3047–3053. doi: 10.1093/hmg/11.24.3047

Al-Agha, A. E., Ahmed, I. A., Nuebel, E., Moriwaki, M., Moore, B., Peacock, K. A., et al. (2018). Primary ovarian insufficiency and azoospermia in carriers of a homozygous PSMC3IP stop gain mutation. *J. Clin. Endocrinol. Metab.* 103, 555–563. doi: 10.1210/jc.2017-01966

AlAsiri, S., Basit, S., Wood-Trageser, M. A., Yatsenko, S. A., Jeffries, E. P., Surti, U., et al. (2015). Exome sequencing reveals MCM8 mutation underlies ovarian failure and chromosomal instability. *J. Clin. Invest.* 125, 258–262. doi: 10.1172/JCI78473

Alavattam, K. G., Kato, Y., Sin, H. S., Maezawa, S., Kowalski, I. J., Zhang, F., et al. (2016). Elucidation of the fanconi anemia protein network in meiosis and its function in the regulation of histone modifications. *Cell Rep.* 17, 1141–1157. doi: 10.1016/j.celrep.2016.09.073

Anand, R., Jasrotia, A., Bundschuh, D., Howard, S. M., Ranjha, L., Stucki, M., et al. (2019). NBS1 promotes the endonuclease activity of the MRE11-RAD50 complex by sensing CtIP phosphorylation. *EMBO J.* 38:e101005. doi: 10.15252/embj.2018101005

Arora, H., Chacon, A. H., Choudhary, S., McLeod, M. P., Meshkov, L., Nouri, K., et al. (2014). Bloom syndrome. *Int. J. Dermatol.* 53, 798–802. doi: 10.1111/ijd.12408

Baker, S. M., Plug, A. W., Prolla, T. A., Bronner, C. E., Harris, A. C., Yao, X., et al. (1996). Involvement of mouse Mlh1 in DNA mismatch repair and meiotic crossing over. *Nat. Genet.* 13, 336–342. doi: 10.1038/ng0796-336

Bakker, S. T., van de Vrugt, H. J., Rooimans, M. A., Oostra, A. B., Steltenpool, J., Delzenne-Goette, E., et al. (2009). Fancm-deficient mice reveal unique features of Fanconi anemia complementation group M. *Hum. Mol. Genet.* 18, 3484–3495. doi: 10.1093/hmg/ddp297

Bishop, D. K., Park, D., Xu, L., and Kleckner, N. (1992). DMC1: a meiosis-specific yeast homolog of E. coli recA required for recombination, synaptonemal complex formation, and cell cycle progression. *Cell* 69, 439–456. doi: 10.1016/0092-8674(92)90446-j

Bizard, A. H., and Hickson, I. D. (2014). The dissolution of double Holliday junctions. *Cold Spring Harb. Perspect. Biol.* 6:a016477. doi: 10.1101/cshperspect.a016477

Bolcun-Filas, E., Costa, Y., Speed, R., Taggart, M., Benavente, R., De Rooij, D. G., et al. (2007). SYCE2 is required for synaptonemal complex assembly, double strand break repair, and homologous recombination. *J.Cell Biol.* 176, 741–747. doi: 10.1083/jcb.200610027

Bolcun-Filas, E., Hall, E., Speed, R., Taggart, M., Grey, C., de Massy, B., et al. (2009). Mutation of the mouse Syce1 gene disrupts synapsis and suggests a link between synaptonemal complex structural components and DNA repair. *PLoS Genet.* 5:e1000393. doi: 10.1371/journal.pgen.1000393

Bolor, H., Mori, T., Nishiyama, S., Ito, Y., Hosoba, E., Inagaki, H., et al. (2009). Mutations of the SYCP3 gene in women with recurrent pregnancy loss. *Am. J. Hum. Genet.* 84, 14–20. doi: 10.1016/j.ajhg.2008.12.002

Bouali, N., Francou, B., Bouligand, J., Imanci, D., Dimassi, S., Tosca, L., et al. (2017). New MCM8 mutation associated with premature ovarian insufficiency and chromosomal instability in a highly consanguineous Tunisian family. *Fertil. Steril.* 108, 694–702. doi: 10.1016/j.fertnstert.2017.07.015

Bouilly, J., Beau, I., Barraud, S., Bernard, V., Azibi, K., Fagart, J., et al. (2016). Identification of multiple gene mutations accounts for a new genetic architecture of primary ovarian insufficiency. *J. Clin. Endocrinol. Metab.* 101, 4541–4550. doi: 10.1210/jc.2016-2152

Brown, M. S., and Bishop, D. K. (2014). DNA strand exchange and RecA homologs in meiosis. *Cold Spring Harb. Perspect. Biol.* 7:a016659. doi: 10.1101/cshperspect.a016659

Caburet, S., Arboleda, V. A., Llano, E., Overbeek, P. A., Barbero, J. L., Oka, K., et al. (2014). Mutant cohesin in premature ovarian failure. *N. Engl. J. Med.* 370, 943–949. doi: 10.1056/NEJMoa1309635

Caburet, S., Heddar, A., Dardillac, E., Creux, H., Lambert, M., Messiaen, S., et al. (2020). Homozygous hypomorphic BRCA2 variant in primary ovarian insufficiency without cancer or Fanconi anaemia trait. *J. Med. Genet.* doi: 10.1136/jmedgenet-2019-106672 [Epub ahead of print].

Caburet, S., Todeschini, A. L., Petrillo, C., Martini, E., Farran, N. D., Legois, B., et al. (2019). A truncating MEIOB mutation responsible for familial primary ovarian insufficiency abolishes its interaction with its partner SPATA22 and their recruitment to DNA double-strand breaks. *EBioMedicine* 42, 524–531. doi: 10.1016/j.ebiom.2019.03.075

Carlosama, C., Elzaiat, M., Patino, L. C., Mateus, H. E., Veitia, R. A., and Laissue, P. (2017). A homozygous donor splice-site mutation in the meiotic gene MSH4 causes primary ovarian insufficiency. *Hum. Mol. Genet.* 26, 3161–3166.

Chen, Y., Lyu, R., Rong, B., Zheng, Y., Lin, Z., Dai, R., et al. (2020). Refined spatial temporal epigenomic profiling reveals intrinsic connection between PRDM9-mediated H3K4me3 and the fate of double-stranded breaks. *Cell Res.* 30, 256–268. doi: 10.1038/s41422-020-0281-1

Cheng, N. C., van de Vrugt, H. J., van der Valk, M. A., Oostra, A. B., Krimpenfort, P., de Vries, Y., et al. (2000). Mice with a targeted disruption of the Fanconi anemia homolog Fanca. *Hum. Mol. Genet.* 9, 1805–1811. doi: 10.1093/hmg/9.12.1805

Chi, P., San Filippo, J., Sehorn, M. G., Petukhova, G. V., and Sung, P. (2007). Bipartite stimulatory action of the Hop2-Mnd1 complex on the Rad51 recombinase. *Genes. Dev.* 21, 1747–1757. doi: 10.1101/gad.1563007

Chrzanowska, K. H., Gregorek, H., Dembowska-Baginska, B., Kalina, M. A., and Digweed, M. (2012). Nijmegen breakage syndrome (NBS). *Orphanet. J. Rare. Dis.* 7:13. doi: 10.1186/1750-1172-7-13

Colombo, R., Pontoglio, A., and Bini, M. (2017). A STAG3 missense mutation in two sisters with primary ovarian insufficiency. *Eur. J. Obstet. Gynecol. Reprod. Biol.* 216, 269–271. doi: 10.1016/j.ejogrb.2017.08.005

Connor, F., Bertwistle, D., Mee, P. J., Ross, G. M., Swift, S., Grigorieva, E., et al. (1997). Tumorigenesis and a DNA repair defect in mice with a truncating Brca2 mutation. *Nat. Genet.* 17, 423–430. doi: 10.1038/ng1297-423

Crismani, W., Girard, C., Froger, N., Pradillo, M., Santos, J. L., Chelysheva, L., et al. (2012). FANCM limits meiotic crossovers. *Science* 336, 1588–1590. doi: 10.1126/science.1220381

Daley, J. M., Gaines, W. A., Kwon, Y., and Sung, P. (2014). Regulation of DNA pairing in homologous recombination. *Cold Spring Harb. Perspect. Biol.* 6:a017954. doi: 10.1101/cshperspect.a017954

Daniel, K., Lange, J., Hached, K., Fu, J., Anastassiadis, K., Roig, I., et al. (2011). Meiotic homologue alignment and its quality surveillance are controlled by mouse HORMAD1. *Nat. Cell Biol.* 13, 599–610. doi: 10.1038/ncb2213

Daum, H., Peretz, T., and Laufer, N. (2018). BRCA mutations and reproduction. *Fertil. Steril.* 109, 33–38. doi: 10.1016/j.fertnstert.2017.12.004

Davies, A. A., Masson, J. Y., McIlwraith, M. J., Stasiak, A. Z., Stasiak, A., Venkitaraman, A. R., et al. (2001). Role of BRCA2 in control of the RAD51 recombination and DNA repair protein. *Mol. Cell* 7, 273–282. doi: 10.1016/s1097-2765(01)00175-7

Davies, O. R., Maman, J. D., and Pellegrini, L. (2012). Structural analysis of the human SYCE2-TEX12 complex provides molecular insights into synaptonemal complex assembly. *Open Biol.* 2:120099. doi: 10.1098/rsob.120099

Day, F. R., Ruth, K. S., Thompson, D. J., Lunetta, K. L., Pervjakova, N., Chasman, D. I., et al. (2015). Large-scale genomic analyses link reproductive aging to hypothalamic signaling, breast cancer susceptibility and BRCA1-mediated DNA repair. *Nat. Genet.* 47, 1294–1303. doi: 10.1038/ng.3412

de Vries, F. A., de Boer, E., van den Bosch, M., Baarends, W. M., Ooms, M., Yuan, L., et al. (2005). Mouse Sycp1 functions in synaptonemal complex assembly, meiotic recombination, and XY body formation. *Genes Dev.* 19, 1376–1389. doi: 10.1101/gad.329705

de Vries, L., Behar, D. M., Smirin-Yosef, P., Lagovsky, I., Tzur, S., and Basel-Vanagaite, L. (2014). Exome sequencing reveals SYCE1 mutation associated with autosomal recessive primary ovarian insufficiency. *J. Clin. Endocrinol. Metab.* 99, E2129–E2132. doi: 10.1210/jc.2014-1268

de Vries, S. S., Baart, E. B., Dekker, M., Siezen, A., de Rooij, D. G., de Boer, P., et al. (1999). Mouse MutS-like protein Msh5 is required for proper chromosome synapsis in male and female meiosis. *Genes Dev.* 13, 523–531. doi: 10.1101/gad.13.5.523

Deardorff, M. A., Kaur, M., Yaeger, D., Rampuria, A., Korolev, S., Pie, J., et al. (2007). Mutations in cohesin complex members SMC3 and SMC1A cause a mild variant of cornelia de Lange syndrome with predominant mental retardation. *Am. J. Hum. Genet.* 80, 485–494. doi: 10.1086/511888

Desai, S., and Rajkovic, A. (2017). Genetics of reproductive aging from gonadal dysgenesis through menopause. *Semin. Reprod. Med.* 35, 147–159. doi: 10.1055/s-0037-1599086

Desai, S., Wood-Trageser, M., Matic, J., Chipkin, J., Jiang, H., Bachelot, A., et al. (2017). MCM8 and MCM9 nucleotide variants in women with primary ovarian insufficiency. *J. Clin. Endocrinol. Metab.* 102, 576–582. doi: 10.1210/jc.2016-2565

Dou, X., Guo, T., Li, G., Zhou, L., Qin, Y., and Chen, Z. J. (2016). Minichromosome maintenance complex component 8 mutations cause primary ovarian insufficiency. *Fertil. Steril.* 106, 1485–1489e2. doi: 10.1016/j.fertnstert.2016.08.018

European Society for Human, R., Embryology Guideline Group on, P. O. I., Webber, L., Davies, M., Anderson, R., Bartlett, J., et al. (2016). ESHRE Guideline: management of women with premature ovarian insufficiency. *Hum. Reprod.* 31, 926–937. doi: 10.1093/humrep/dew027

Fauchereau, F., Shalev, S., Chervinsky, E., Beck-Fruchter, R., Legois, B., Fellous, M., et al. (2016). A non-sense MCM9 mutation in a familial case of primary ovarian insufficiency. *Clin. Genet.* 89, 603–607. doi: 10.1111/cge.12736

Finsterbusch, F., Ravindranathan, R., Dereli, I., Stanzione, M., Trankner, D., and Toth, A. (2016). Alignment of homologous chromosomes and effective repair of programmed DNA double-strand breaks during mouse meiosis require the minichromosome maintenance domain containing 2 (MCMDC2) protein. *PLoS Genet.* 12:e1006393. doi: 10.1371/journal.pgen.1006393

Fouquet, B., Pawlikowska, P., Caburet, S., Guigon, C., Makinen, M., Tanner, L., et al. (2017). A homozygous FANCM mutation underlies a familial case of non-syndromic primary ovarian insufficiency. *Elife* 6:e30490. doi: 10.7554/eLife.30490

Franca, M. M., and Mendonca, B. B. (2020). Genetics of primary ovarian insufficiency in the next-generation sequencing era. *J. Endocr. Soc.* 4:bvz037. doi: 10.1210/jendso/bvz037

Franca, M. M., Nishi, M. Y., Funari, M. F. A., Lerario, A. M., Baracat, E. C., Hayashida, S. A. Y., et al. (2019). Two rare loss-of-function variants in the STAG3 gene leading to primary ovarian insufficiency. *Eur. J. Med. Genet.* 62, 186–189. doi: 10.1016/j.ejmg.2018.07.008

Garcia, V., Phelps, S. E., Gray, S., and Neale, M. J. (2011). Bidirectional resection of DNA double-strand breaks by Mre11 and Exo1. *Nature* 479, 241–244. doi: 10.1038/nature10515

Goldberg, Y., Halpern, N., Hubert, A., Adler, S. N., Cohen, S., Plesser-Duvdevani, M., et al. (2015). Mutated MCM9 is associated with predisposition to hereditary mixed polyposis and colorectal cancer in addition to primary ovarian failure. *Cancer Genet.* 208, 621–624. doi: 10.1016/j.cancergen.2015.10.001

Guiraldelli, M. F., Eyster, C., Wilkerson, J. L., Dresser, M. E., and Pezza, R. J. (2013). Mouse HFM1/Mer3 is required for crossover formation and complete synapsis of homologous chromosomes during meiosis. *PLoS Genet.* 9:e1003383. doi: 10.1371/journal.pgen.1003383

Guo, T., Zhao, S., Zhao, S., Chen, M., Li, G., Jiao, X., et al. (2017). Mutations in MSH5 in primary ovarian insufficiency. *Hum. Mol. Genet.* 26, 1452–1457. doi: 10.1093/hmg/ddx044

Guo, T., Zheng, Y., Li, G., Zhao, S., Ma, J., and Qin, Y. (2020). Novel pathogenic mutations in minichromosome maintenance complex component 9 (MCM9) responsible for premature ovarian insufficiency. *Fertil. Steril.* 113, 845–852. doi: 10.1016/j.fertnstert.2019.11.015

Hamer, G., Wang, H., Bolcun-Filas, E., Cooke, H. J., Benavente, R., and Hoog, C. (2008). Progression of meiotic recombination requires structural maturation of the central element of the synaptonemal complex. *J. Cell Sci.* 121(Pt 15), 2445–2451. doi: 10.1242/jcs.033233

Handel, M. A., and Schimenti, J. C. (2010). Genetics of mammalian meiosis: regulation, dynamics and impact on fertility. *Nat. Rev. Genet.* 11, 124–136. doi: 10.1038/nrg2723

Hays, E., Majchrzak, N., Daniel, V., Ferguson, Z., Brown, S., Hathorne, K., et al. (2017). Spermatogenesis associated 22 is required for DNA repair and synapsis of homologous chromosomes in mouse germ cells. *Andrology* 5, 299–312. doi: 10.1111/andr.12315

He, W. B., Banerjee, S., Meng, L. L., Du, J., Gong, F., Huang, H., et al. (2018a). Whole-exome sequencing identifies a homozygous donor splice-site mutation in STAG3 that causes primary ovarian insufficiency. *Clin. Genet.* 93, 340–344. doi: 10.1111/cge.13034

He, W. B., Tu, C. F., Liu, Q., Meng, L. L., Yuan, S. M., Luo, A. X., et al. (2018b). DMC1 mutation that causes human non-obstructive azoospermia and premature ovarian insufficiency identified by whole-exome sequencing. *J. Med. Genet.* 55, 198–204. doi: 10.1136/jmedgenet-2017-104992

Heddar, A., Beckers, D., Fouquet, B., Roland, D., and Misrahi, M. (2020). A novel phenotype combining primary ovarian insufficiency growth retardation and pilomatricomas with MCM8 mutation. *J. Clin. Endocrinol. Metab.* 105:dgaa155. doi: 10.1210/clinem/dgaa155

Heddar, A., Dessen, P., Flatters, D., and Misrahi, M. (2019). Novel STAG3 mutations in a Caucasian family with primary ovarian insufficiency. *Mol. Genet. Genomics* 294, 1527–1534. doi: 10.1007/s00438-019-01594-4

Herran, Y., Gutierrez-Caballero, C., Sanchez-Martin, M., Hernandez, T., Viera, A., Barbero, J. L., et al. (2011). The cohesin subunit RAD21L functions in meiotic synapsis and exhibits sexual dimorphism in fertility. *EMBO J.* 30, 3091–3105. doi: 10.1038/emboj.2011.222

Hikiba, J., Hirota, K., Kagawa, W., Ikawa, S., Kinebuchi, T., Sakane, I., et al. (2008). Structural and functional analyses of the DMC1-M200V polymorphism found in the human population. *Nucleic Acids Res.* 36, 4181–4190. doi: 10.1093/nar/gkn362

Inagaki, A., Roset, R., and Petrini, J. H. (2016). Functions of the MRE11 complex in the development and maintenance of oocytes. *Chromosoma* 125, 151–162. doi: 10.1007/s00412-015-0535-8

Ishiguro, K. I. (2019). The cohesin complex in mammalian meiosis. *Genes Cells* 24, 6–30. doi: 10.1111/gtc.12652

Ishishita, S., Matsuda, Y., and Kitada, K. (2014). Genetic evidence suggests that Spata22 is required for the maintenance of Rad51 foci in mammalian meiosis. *Sci. Rep.* 4:6148. doi: 10.1038/srep06148

Janisiw, E., Dello Stritto, M. R., Jantsch, V., and Silva, N. (2018). BRCA1-BARD1 associate with the synaptonemal complex and pro-crossover factors and influence RAD-51 dynamics during Caenorhabditis elegans meiosis. *PLoS Genet.* 14:e1007653. doi: 10.1371/journal.pgen.1007653

Jiao, X., Zhang, H., Ke, H., Zhang, J., Cheng, L., Liu, Y., et al. (2017). Premature ovarian insufficiency: phenotypic characterization within different etiologies. *J. Clin. Endocrinol. Metab.* 102, 2281–2290. doi: 10.1210/jc.2016-3960

Jolly, A., Bayram, Y., Turan, S., Aycan, Z., Tos, T., Abali, Z. Y., et al. (2019). Exome sequencing of a primary ovarian insufficiency cohort reveals common molecular etiologies for a spectrum of disease. *J. Clin. Endocrinol. Metab.* 104, 3049–3067. doi: 10.1210/jc.2019-00248

Kang, J., Bronson, R. T., and Xu, Y. (2002). Targeted disruption of NBS1 reveals its roles in mouse development and DNA repair. *EMBO J.* 21, 1447–1455. doi: 10.1093/emboj/21.6.1447

Kneitz, B., Cohen, P. E., Avdievich, E., Zhu, L., Kane, M. F., Hou, H. Jr., et al. (2000). MutS homolog 4 localization to meiotic chromosomes is required for chromosome pairing during meiosis in male and female mice. *Genes Dev.* 14, 1085–1097.

Kumar, R., Bourbon, H. M., and de Massy, B. (2010). Functional conservation of Mei4 for meiotic DNA double-strand break formation from yeasts to mice. *Genes Dev.* 24, 1266–1280. doi: 10.1101/gad.571710

Kumar, R., Oliver, C., Brun, C., Juarez-Martinez, A. B., Tarabay, Y., Kadlec, J., et al. (2018). Mouse REC114 is essential for meiotic DNA double-strand break formation and forms a complex with MEI4. *Life Sci. Alliance* 1:e201800259. doi: 10.26508/lsa.201800259

La Salle, S., Palmer, K., O'Brien, M., Schimenti, J. C., Eppig, J., and Handel, M. A. (2012). Spata22, a novel vertebrate-specific gene, is required for meiotic progress in mouse germ cells. *Biol. Reprod.* 86:45. doi: 10.1095/biolreprod.111.095752

Le Quesne Stabej, P., Williams, H. J., James, C., Tekman, M., Stanescu, H. C., Kleta, R., et al. (2016). STAG3 truncating variant as the cause of primary ovarian insufficiency. *Eur. J. Hum. Genet.* 24, 135–138. doi: 10.1038/ejhg.2015.107

Lin, W., Titus, S., Moy, F., Ginsburg, E. S., and Oktay, K. (2017). Ovarian aging in women with BRCA germline mutations. *J. Clin. Endocrinol. Metab.* 102, 3839–3847. doi: 10.1210/jc.2017-00765

Lipkin, S. M., Moens, P. B., Wang, V., Lenzi, M., Shanmugarajah, D., Gilgeous, A., et al. (2002). Meiotic arrest and aneuploidy in MLH3-deficient mice. *Nat. Genet.* 31, 385–390. doi: 10.1038/ng931

Lu, J., Gu, Y., Feng, J., Zhou, W., Yang, X., and Shen, Y. (2014). Structural insight into the central element assembly of the synaptonemal complex. *Sci. Rep.* 4:7059. doi: 10.1038/srep07059

Luo, M., Yang, F., Leu, N. A., Landaiche, J., Handel, M. A., Benavente, R., et al. (2013). MEIOB exhibits single-stranded DNA-binding and exonuclease activities and is essential for meiotic recombination. *Nat. Commun.* 4:2788. doi: 10.1038/ncomms3788

Luo, W., Guo, T., Li, G., Liu, R., Zhao, S., Song, M., et al. (2020). Variants in homologous recombination genes EXO1 and RAD51 related with premature ovarian insufficiency. *J. Clin. Endocrinol. Metab.* 105:dgaa505. doi: 10.1210/clinem/dgaa505

Lutzmann, M., Grey, C., Traver, S., Ganier, O., Maya-Mendoza, A., Ranisavljevic, N., et al. (2012). MCM8- and MCM9-deficient mice reveal gametogenesis defects and genome instability due to impaired homologous recombination. *Mol. Cell* 47, 523–534. doi: 10.1016/j.molcel.2012.05.048

Mandon-Pepin, B., Touraine, P., Kuttenn, F., Derbois, C., Rouxel, A., Matsuda, F., et al. (2008). Genetic investigation of four meiotic genes in women with premature ovarian failure. *Eur. J. Endocrinol.* 158, 107–115. doi: 10.1530/EJE-07-0400

Martin, C. A., Sarlos, K., Logan, C. V., Thakur, R. S., Parry, D. A., Bizard, A. H., et al. (2018). Mutations in TOP3A cause a bloom syndrome-like disorder. *Am. J. Hum. Genet.* 103, 221–231. doi: 10.1016/j.ajhg.2018.07.001

Matos, J., and West, S. C. (2014). Holliday junction resolution: regulation in space and time. *DNA Repair (Amst)* 19, 176–181. doi: 10.1016/j.dnarep.2014.03.013

McGuire, M. M., Bowden, W., Engel, N. J., Ahn, H. W., Kovanci, E., and Rajkovic, A. (2011). Genomic analysis using high-resolution single-nucleotide polymorphism arrays reveals novel microdeletions associated with premature ovarian failure. *Fertil. Steril.* 95, 1595–1600. doi: 10.1016/j.fertnstert.2010.12.052

Miao, Y., Wang, P., Xie, B., Yang, M., Li, S., Cui, Z., et al. (2019). BRCA2 deficiency is a potential driver for human primary ovarian insufficiency. *Cell Death Dis.* 10:474. doi: 10.1038/s41419-019-1720-0

Nguyen, N. M. P., Ge, Z. J., Reddy, R., Fahiminiya, S., Sauthier, P., Bagga, R., et al. (2018). Causative mutations and mechanism of androgenetic hydatidiform moles. *Am. J. Hum. Genet.* 103, 740–751. doi: 10.1016/j.ajhg.2018.10.007

Nishant, K. T., Chen, C., Shinohara, M., Shinohara, A., and Alani, E. (2010). Genetic analysis of baker's yeast Msh4-Msh5 reveals a threshold crossover level for meiotic viability. *PLoS Genet.* 6:e1001083. doi: 10.1371/journal.pgen.1001083

Nishimura, K., Ishiai, M., Horikawa, K., Fukagawa, T., Takata, M., Takisawa, H., et al. (2012). Mcm8 and Mcm9 form a complex that functions in homologous recombination repair induced by DNA interstrand crosslinks. *Mol. Cell* 47, 511–522. doi: 10.1016/j.molcel.2012.05.047

Nishiyama, S., Kishi, T., Kato, T., Suzuki, M., Bolor, H., Nishizawa, H., et al. (2011). A rare synaptonemal complex protein 3 gene variant in unexplained female infertility. *Mol. Hum. Reprod.* 17, 266–271. doi: 10.1093/molehr/gaq098

Park, J. Y., Yoo, H. W., Kim, B. R., Park, R., Choi, S. Y., and Kim, Y. (2008). Identification of a novel human Rad51 variant that promotes DNA strand exchange. *Nucleic Acids Res.* 36, 3226–3234. doi: 10.1093/nar/gkn171

Patino, L. C., Beau, I., Carlosama, C., Buitrago, J. C., Gonzalez, R., Suarez, C. F., et al. (2017). New mutations in non-syndromic primary ovarian insufficiency patients identified via whole-exome sequencing. *Hum. Reprod.* 32, 1512–1520. doi: 10.1093/humrep/dex089

Petukhova, G. V., Romanienko, P. J., and Camerini-Otero, R. D. (2003). The Hop2 protein has a direct role in promoting interhomolog interactions during mouse meiosis. *Dev. Cell* 5, 927–936. doi: 10.1016/s1534-5807(03)00369-1

Pezza, R. J., Voloshin, O. N., Vanevski, F., and Camerini-Otero, R. D. (2007). Hop2/Mnd1 acts on two critical steps in Dmc1-promoted homologous pairing. *Genes Dev.* 21, 1758–1766. doi: 10.1101/gad.1562907

Pezza, R. J., Voloshin, O. N., Volodin, A. A., Boateng, K. A., Bellani, M. A., Mazin, A. V., et al. (2014). The dual role of HOP2 in mammalian meiotic homologous recombination. *Nucleic Acids Res.* 42, 2346–2357. doi: 10.1093/nar/gkt1234

Pittman, D. L., Cobb, J., Schimenti, K. J., Wilson, L. A., Cooper, D. M., Brignull, E., et al. (1998). Meiotic prophase arrest with failure of chromosome synapsis in mice deficient for Dmc1, a germline-specific RecA homolog. *Mol. Cell* 1, 697–705. doi: 10.1016/s1097-2765(00)80069-6

Porcu, E., Cillo, G. M., Cipriani, L., Sacilotto, F., Notarangelo, L., Damiano, G., et al. (2020). Impact of BRCA1 and BRCA2 mutations on ovarian reserve and fertility preservation outcomes in young women with breast cancer. *J. Assist. Reprod. Genet.* 37, 709–715. doi: 10.1007/s10815-019-01658-9

Pu, D., Wang, C., Cao, J., Shen, Y., Jiang, H., Liu, J., et al. (2016). Association analysis between HFM1 variation and primary ovarian insufficiency in Chinese women. *Clin. Genet.* 89, 597–602. doi: 10.1111/cge.12718

Qiao, H., Prasada Rao, H. B., Yang, Y., Fong, J. H., Cloutier, J. M., Deacon, D. C., et al. (2014). Antagonistic roles of ubiquitin ligase HEI10 and SUMO ligase RNF212 regulate meiotic recombination. *Nat. Genet.* 46, 194–199. doi: 10.1038/ng.2858

Qin, Y., Jiao, X., Simpson, J. L., and Chen, Z. J. (2015). Genetics of primary ovarian insufficiency: new developments and opportunities. *Hum. Reprod. Update* 21, 787–808. doi: 10.1093/humupd/dmv036

Qin, Y., Zhang, F., and Chen, Z. J. (2019). BRCA2 in ovarian development and function. *N. Engl. J. Med.* 380:1086. doi: 10.1056/NEJMc1813800

Qvist, P., Huertas, P., Jimeno, S., Nyegaard, M., Hassan, M. J., Jackson, S. P., et al. (2011). CtIP mutations cause seckel and jawad syndromes. *PLoS Genet.* 7:e1002310. doi: 10.1371/journal.pgen.1002310

Ranjha, L., Howard, S. M., and Cejka, P. (2018). Main steps in DNA double-strand break repair: an introduction to homologous recombination and related processes. *Chromosoma* 127, 187–214. doi: 10.1007/s00412-017-0658-1

Raynard, S., Zhao, W., Bussen, W., Lu, L., Ding, Y. Y., Busygina, V., et al. (2008). Functional role of BLAP75 in BLM-topoisomerase IIIalpha-dependent Holliday junction processing. *J. Biol. Chem.* 283, 15701–15708. doi: 10.1074/jbc.M802127200

Reinholdt, L. G., and Schimenti, J. C. (2005). Mei1 is epistatic to Dmc1 during mouse meiosis. *Chromosoma* 114, 127–134. doi: 10.1007/s00412-005-0346-4

Ren, Y., Diao, F., Katari, S., Yatsenko, S., Jiang, H., Wood-Trageser, M. A., et al. (2018). Functional study of a novel missense single-nucleotide variant of NUP107 in two daughters of Mexican origin with premature ovarian insufficiency. *Mol. Genet. Genomic. Med.* 6, 276–281. doi: 10.1002/mgg3.345

Robert, T., Nore, A., Brun, C., Maffre, C., Crimi, B., Bourbon, H. M., et al. (2016). The TopoVIB-Like protein family is required for meiotic DNA double-strand break formation. *Science* 351, 943–949. doi: 10.1126/science.aad5309

Romanienko, P. J., and Camerini-Otero, R. D. (2000). The mouse Spo11 gene is required for meiotic chromosome synapsis. *Mol. Cell* 6, 975–987. doi: 10.1016/s1097-2765(00)00097-6

Roset, R., Inagaki, A., Hohl, M., Brenet, F., Lafrance-Vanasse, J., Lange, J., et al. (2014). The Rad50 hook domain regulates DNA damage signaling and tumorigenesis. *Genes Dev.* 28, 451–462. doi: 10.1101/gad.236745.113

Sansam, C. L., and Pezza, R. J. (2015). Connecting by breaking and repairing: mechanisms of DNA strand exchange in meiotic recombination. *FEBS J.* 282, 2444–2457. doi: 10.1111/febs.13317

Sartori, A. A., Lukas, C., Coates, J., Mistrik, M., Fu, S., Bartek, J., et al. (2007). Human CtIP promotes DNA end resection. *Nature* 450, 509–514. doi: 10.1038/nature06337

Schramm, S., Fraune, J., Naumann, R., Hernandez-Hernandez, A., Hoog, C., Cooke, H. J., et al. (2011). A novel mouse synaptonemal complex protein is essential for loading of central element proteins, recombination, and fertility. *PLoS Genet.* 7:e1002088. doi: 10.1371/journal.pgen.1002088

Shah Punatar, R., Martin, M. J., Wyatt, H. D., Chan, Y. W., and West, S. C. (2017). Resolution of single and double Holliday junction recombination intermediates by GEN1. *Proc. Natl. Acad. Sci. U.S.A.* 114, 443–450. doi: 10.1073/pnas.1619790114

Shi, B., Xue, J., Yin, H., Guo, R., Luo, M., Ye, L., et al. (2019). Dual functions for the ssDNA-binding protein RPA in meiotic recombination. *PLoS Genet.* 15:e1007952. doi: 10.1371/journal.pgen.1007952

Shin, Y. H., Choi, Y., Erdin, S. U., Yatsenko, S. A., Kloc, M., Yang, F., et al. (2010). Hormad1 mutation disrupts synaptonemal complex formation, recombination, and chromosome segregation in mammalian meiosis. *PLoS Genet.* 6:e1001190. doi: 10.1371/journal.pgen.1001190

Siitonen, H. A., Sotkasiira, J., Biervliet, M., Benmansour, A., Capri, Y., Cormier-Daire, V., et al. (2009). The mutation spectrum in RECQL4 diseases. *Eur. J. Hum. Genet.* 17, 151–158. doi: 10.1038/ejhg.2008.154

Singh, D. K., Popuri, V., Kulikowicz, T., Shevelev, I., Ghosh, A. K., Ramamoorthy, M., et al. (2012). The human RecQ helicases BLM and RECQL4 cooperate to preserve genome stability. *Nucleic Acids Res.* 40, 6632–6648. doi: 10.1093/nar/gks349

Smirin-Yosef, P., Zuckerman-Levin, N., Tzur, S., Granot, Y., Cohen, L., Sachsenweger, J., et al. (2017). A biallelic mutation in the homologous recombination repair gene SPIDR is associated with human gonadal dysgenesis. *J. Clin. Endocrinol. Metab.* 102, 681–688. doi: 10.1210/jc.2016-2714

Snowden, T., Acharya, S., Butz, C., Berardini, M., and Fishel, R. (2004). hMSH4-hMSH5 recognizes Holliday Junctions and forms a meiosis-specific sliding clamp that embraces homologous chromosomes. *Mol. Cell* 15, 437–451. doi: 10.1016/j.molcel.2004.06.040

Souquet, B., Abby, E., Herve, R., Finsterbusch, F., Tourpin, S., Le Bouffant, R., et al. (2013). MEIOB targets single-strand DNA and is necessary for meiotic recombination. *PLoS Genet.* 9:e1003784. doi: 10.1371/journal.pgen.1003784

Soustelle, C., Vedel, M., Kolodner, R., and Nicolas, A. (2002). Replication protein A is required for meiotic recombination in Saccharomyces cerevisiae. *Genetics* 161, 535–547.

Spruce, C., Dlamini, S., Ananda, G., Bronkema, N., Tian, H., Paigen, K., et al. (2020). HELLS and PRDM9 form a pioneer complex to open chromatin at meiotic recombination hot spots. *Genes Dev.* 34, 398–412. doi: 10.1101/gad.333542.119

Stanzione, M., Baumann, M., Papanikos, F., Dereli, I., Lange, J., Ramlal, A., et al. (2016). Meiotic DNA break formation requires the unsynapsed chromosome axis-binding protein IHO1 (CCDC36) in mice. *Nat. Cell Biol.* 18, 1208–1220. doi: 10.1038/ncb3417

Sun, F., Fujiwara, Y., Reinholdt, L. G., Hu, J., Saxl, R. L., Baker, C. L., et al. (2015). Nuclear localization of PRDM9 and its role in meiotic chromatin modifications and homologous synapsis. *Chromosoma* 124, 397–415. doi: 10.1007/s00412-015-0511-3

Syrjanen, J. L., Heller, I., Candelli, A., Davies, O. R., Peterman, E. J., Wuite, G. J., et al. (2017). Single-molecule observation of DNA compaction by meiotic protein SYCP3. *Elife* 6:e22582. doi: 10.7554/eLife.22582

Syrjanen, J. L., Pellegrini, L., and Davies, O. R. (2014). A molecular model for the role of SYCP3 in meiotic chromosome organisation. *Elife* 3:e02963. doi: 10.7554/eLife.02963

Szabova, L., Yin, C., Bupp, S., Guerin, T. M., Schlomer, J. J., Householder, D. B., et al. (2012). Perturbation of Rb, p53, and Brca1 or Brca2 cooperate in inducing metastatic serous epithelial ovarian cancer. *Cancer Res.* 72, 4141–4153. doi: 10.1158/0008-5472.CAN-11-3834

Takabayashi, S., Yamauchi, Y., Tsume, M., Noguchi, M., and Katoh, H. (2009). A spontaneous smc1b mutation causes cohesin protein dysfunction and sterility in mice. *Exp. Biol. Med. (Maywood)* 234, 994–1001. doi: 10.3181/0808-RM-244

Tenenbaum-Rakover, Y., Weinberg-Shukron, A., Renbaum, P., Lobel, O., Eideh, H., Gulsuner, S., et al. (2015). Minichromosome maintenance complex component 8 (MCM8) gene mutations result in primary gonadal failure. *J. Med. Genet.* 52, 391–399. doi: 10.1136/jmedgenet-2014-102921

Tian, H., Billings, T., and Petkov, P. M. (2018). CXXC1 is not essential for normal DNA double-strand break formation and meiotic recombination in mouse. *PLoS Genet.* 14:e1007657. doi: 10.1371/journal.pgen.1007657

Titus, S., Li, F., Stobezki, R., Akula, K., Unsal, E., Jeong, K., et al. (2013). Impairment of BRCA1-related DNA double-strand break repair leads to ovarian aging in mice and humans. *Sci. Transl. Med.* 5:172ra21. doi: 10.1126/scitranslmed.3004925

Tran, T. N., and Schimenti, J. C. (2018). A putative human infertility allele of the meiotic recombinase DMC1 does not affect fertility in mice. *Hum. Mol. Genet.* 27, 3911–3918. doi: 10.1093/hmg/ddy286

Tsui, V., and Crismani, W. (2019). The fanconi anemia pathway and fertility. *Trends Genet.* 35, 199–214. doi: 10.1016/j.tig.2018.12.007

Tsuzuki, T., Fujii, Y., Sakumi, K., Tominaga, Y., Nakao, K., Sekiguchi, M., et al. (1996). Targeted disruption of the Rad51 gene leads to lethality in embryonic mice. *Proc. Natl. Acad. Sci. U.S.A.* 93, 6236–6240. doi: 10.1073/pnas.93.13.6236

Wang, F., Guo, S., and Li, P. (2020). Two novel mutations in the MCM8 gene shared by two Chinese siblings with primary ovarian insufficiency and short stature. *Mol. Genet. Genomic Med.* 8:e1396. doi: 10.1002/mgg3.1396

Wang, J., Zhang, W., Jiang, H., Wu, B. L., and Primary Ovarian Insufficiency, C. (2014). Mutations in HFM1 in recessive primary ovarian insufficiency. *N. Engl. J. Med.* 370, 972–974. doi: 10.1056/NEJMc1310150

Wang, Y., Putnam, C. D., Kane, M. F., Zhang, W., Edelmann, L., Russell, R., et al. (2005). Mutation in Rpa1 results in defective DNA double-strand break repair, chromosomal instability and cancer in mice. *Nat. Genet.* 37, 750–755. doi: 10.1038/ng1587

Ward, J. O., Reinholdt, L. G., Motley, W. W., Niswander, L. M., Deacon, D. C., Griffin, L. B., et al. (2007). Mutation in mouse hei10, an e3 ubiquitin ligase, disrupts meiotic crossing over. *PLoS Genet.* 3:e139. doi: 10.1371/journal.pgen.0030139

Wei, K., Clark, A. B., Wong, E., Kane, M. F., Mazur, D. J., Parris, T., et al. (2003). Inactivation of Exonuclease 1 in mice results in DNA mismatch repair defects, increased cancer susceptibility, and male and female sterility. *Genes Dev.* 17, 603–614. doi: 10.1101/gad.1060603

Weinberg-Shukron, A., Rachmiel, M., Renbaum, P., Gulsuner, S., Walsh, T., Lobel, O., et al. (2018). Essential role of BRCA2 in ovarian development and function. *N. Engl. J. Med.* 379, 1042–1049. doi: 10.1056/NEJMoa1800024

Weinberg-Shukron, A., Renbaum, P., Kalifa, R., Zeligson, S., Ben-Neriah, Z., Dreifuss, A., et al. (2015). A mutation in the nucleoporin-107 gene causes XX gonadal dysgenesis. *J. Clin. Invest.* 125, 4295–4304. doi: 10.1172/JCI83553

Winkel, K., Alsheimer, M., Ollinger, R., and Benavente, R. (2009). Protein SYCP2 provides a link between transverse filaments and lateral elements of mammalian synaptonemal complexes. *Chromosoma* 118, 259–267. doi: 10.1007/s00412-008-0194-0

Winters, T., McNicoll, F., and Jessberger, R. (2014). Meiotic cohesin STAG3 is required for chromosome axis formation and sister chromatid cohesion. *EMBO J.* 33, 1256–1270. doi: 10.1002/embj.201387330

Wong, J. C., Alon, N., McKerlie, C., Huang, J. R., Meyn, M. S., and Buchwald, M. (2003). Targeted disruption of exons 1 to 6 of the Fanconi Anemia group A gene leads to growth retardation, strain-specific microphthalmia, meiotic defects and primordial germ cell hypoplasia. *Hum. Mol. Genet.* 12, 2063–2076. doi: 10.1093/hmg/ddg219

Wood-Trageser, M. A., Gurbuz, F., Yatsenko, S. A., Jeffries, E. P., Kotan, L. D., Surti, U., et al. (2014). MCM9 mutations are associated with ovarian failure, short stature, and chromosomal instability. *Am. J. Hum. Genet.* 95, 754–762. doi: 10.1016/j.ajhg.2014.11.002

Wu, L., Davies, S. L., North, P. S., Goulaouic, H., Riou, J. F., Turley, H., et al. (2000). The Bloom's syndrome gene product interacts with topoisomerase III. *J. Biol. Chem.* 275, 9636–9644. doi: 10.1074/jbc.275.13.9636

Wyatt, H. D., and West, S. C. (2014). Holliday junction resolvases. *Cold Spring Harb. Perspect. Biol.* 6:a023192. doi: 10.1101/cshperspect.a023192

Xia, F., Taghian, D. G., DeFrank, J. S., Zeng, Z. C., Willers, H., Iliakis, G., et al. (2001). Deficiency of human BRCA2 leads to impaired homologous recombination but maintains normal nonhomologous end joining. *Proc. Natl. Acad. Sci. U.S.A.* 98, 8644–8649. doi: 10.1073/pnas.151253498

Xiao, W. J., He, W. B., Zhang, Y. X., Meng, L. L., Lu, G. X., Lin, G., et al. (2019). In-frame variants in STAG3 gene cause premature ovarian insufficiency. *Front. Genet.* 10:1016. doi: 10.3389/fgene.2019.01016

Xu, H., Beasley, M. D., Warren, W. D., van der Horst, G. T., and McKay, M. J. (2005). Absence of mouse REC8 cohesin promotes synapsis of sister chromatids in meiosis. *Dev. Cell* 8, 949–961. doi: 10.1016/j.devcel.2005.03.018

Yang, F., De La Fuente, R., Leu, N. A., Baumann, C., McLaughlin, K. J., and Wang, P. J. (2006). Mouse SYCP2 is required for synaptonemal complex assembly and chromosomal synapsis during male meiosis. *J. Cell Biol.* 173, 497–507. doi: 10.1083/jcb.200603063

Yang, X., Touraine, P., Desai, S., Humphreys, G., Jiang, H., Yatsenko, A., et al. (2019a). Gene variants identified by whole-exome sequencing in 33 French women with premature ovarian insufficiency. *J. Assist. Reprod. Genet.* 36, 39–45. doi: 10.1007/s10815-018-1349-4

Yang, X., Zhang, X., Jiao, J., Zhang, F., Pan, Y., Wang, Q., et al. (2019b). Rare variants in FANCA induce premature ovarian insufficiency. *Hum. Genet.* 138, 1227–1236. doi: 10.1007/s00439-019-02059-9

Yang, Y., Guo, J., Dai, L., Zhu, Y., Hu, H., Tan, L., et al. (2018). XRCC2 mutation causes meiotic arrest, azoospermia and infertility. *J. Med. Genet.* 55, 628–636. doi: 10.1136/jmedgenet-2017-105145

Yang, Y., Guo, T., Liu, R., Ke, H., Xu, W., Zhao, S., et al. (2020). FANCL gene mutations in premature ovarian insufficiency. *Hum. Mutat.* 41, 1033–1041. doi: 10.1002/humu.23997

Yilmaz, N. K., Karagin, P. H., Terzi, Y. K., Kahyaoglu, I., Yilmaz, S., Erkaya, S., et al. (2016). BRCA1 and BRCA2 sequence variations detected with next-generation sequencing in patients with premature ovarian insufficiency. *J. Turk. Ger. Gynecol. Assoc.* 17, 77–82. doi: 10.5152/jtgga.2016.16035

Yuan, L., Liu, J. G., Zhao, J., Brundell, E., Daneholt, B., and Hoog, C. (2000). The murine SCP3 gene is required for synaptonemal complex assembly, chromosome synapsis, and male fertility. *Mol. Cell* 5, 73–83. doi: 10.1016/s1097-2765(00)80404-9

Zangen, D., Kaufman, Y., Zeligson, S., Perlberg, S., Fridman, H., Kanaan, M., et al. (2011). XX ovarian dysgenesis is caused by a PSMC3IP/HOP2 mutation that abolishes coactivation of estrogen-driven transcription. *Am. J. Hum. Genet.* 89, 572–579. doi: 10.1016/j.ajhg.2011.09.006

Zhang, Y. X., He, W. B., Xiao, W. J., Meng, L. L., Tan, C., Du, J., et al. (2020). Novel loss-of-function mutation in MCM8 causes premature ovarian insufficiency. *Mol. Genet. Genomic Med.* 8:e1165. doi: 10.1002/mgg3.1165

Zhang, Y. X., Li, H. Y., He, W. B., Tu, C., Du, J., Li, W., et al. (2019). XRCC2 mutation causes premature ovarian insufficiency as well as non-obstructive azoospermia in humans. *Clin. Genet.* 95, 442–443. doi: 10.1111/cge.13475

Zhao, W., and Sung, P. (2015). Significance of ligand interactions involving Hop2-Mnd1 and the RAD51 and DMC1 recombinases in homologous DNA repair and XX ovarian dysgenesis. *Nucleic Acids Res.* 43, 4055–4066. doi: 10.1093/nar/gkv259

Zhe, J., Chen, S., Chen, X., Liu, Y., Li, Y., Zhou, X., et al. (2019). A novel heterozygous splice-altering mutation in HFM1 may be a cause of premature ovarian insufficiency. *J. Ovarian. Res.* 12:61. doi: 10.1186/s13048-019-0537-x

Zhe, J., Ye, D., Chen, X., Liu, Y., Zhou, X., Li, Y., et al. (2020). Consanguineous Chinese familial study reveals that a gross deletion that includes the SYCE1 gene region is associated with premature ovarian insufficiency. *Reprod. Sci.* 27, 461–467. doi: 10.1007/s43032-019-00037-0

Zhen, X. M., Sun, Y. M., Qiao, J., Li, R., Wang, L. N., and Liu, P. (2013). [Genome-wide copy number scan in Chinese patients with premature ovarian failure]. *Beijing Da Xue Xue Bao Yi Xue Ban* 45, 841–847.

Conflict of Interest: The authors declare that the research was conducted in the absence of any commercial or financial relationships that could be construed as a potential conflict of interest.

Copyright © 2021 Huang, Guo and Qin. This is an open-access article distributed under the terms of the Creative Commons Attribution License (CC BY). The use, distribution or reproduction in other forums is permitted, provided the original author(s) and the copyright owner(s) are credited and that the original publication in this journal is cited, in accordance with accepted academic practice. No use, distribution or reproduction is permitted which does not comply with these terms.

frontiers in Cell and Developmental Biology

ORIGINAL RESEARCH
published: 25 March 2021
doi: 10.3389/fcell.2021.635383

Rad9, a 53BP1 Ortholog of Budding Yeast, Is Insensitive to Spo11-Induced Double-Strand Breaks During Meiosis

*Takehiko Usui and Akira Shinohara**

Institute for Protein Research, Osaka University, Suita, Japan

Exogenous double-strand breaks (DSBs) induce a DNA damage response during mitosis as well as meiosis. The DNA damage response is mediated by a cascade involving Mec1/Tel1 (ATR/ATM) and Rad53 (Chk2) kinases. Meiotic cells are programmed to form DSBs for the initiation of meiotic recombination. In budding yeast, Spo11-mediated meiotic DSBs activate Mec1/Tel1, but not Rad53; however, the mechanism underlying the insensitivity of Rad53 to meiotic DSBs remains largely unknown. In this study, we found that meiotic cells activate Rad53 in response to exogenous DSBs and that this activation is dependent on an epigenetic marker, Dot1-dependent histone H3K79 methylation, which becomes a scaffold of an Rad53 mediator, Rad9, an ortholog of 53BP1. In contrast, Rad9 is insensitive to meiotic programmed DSBs. This insensitiveness of Rad9 derives from its inability to bind to the DSBs. Indeed, artificial tethering of Rad9 to the meiotic DSBs activated Rad53. The artificial activation of Rad53 kinase in meiosis decreases the repair of meiotic DSBs. These results suggest that the suppression of Rad53 activation is a key event in initiating a meiotic program that repairs programmed DSBs.

Keywords: Rad9/53BP1, Rad53, DDR (DNA damage response), checkpoint, meiosis, recombination

OPEN ACCESS

Edited by:
Eesin Chen,
National University of Singapore, Singapore

Reviewed by:
Marcus Smolka,
Cornell University, United States
Armin Michael Gamper,
University of Alberta, Canada

***Correspondence:**
Akira Shinohara
ashino@protein.osaka-u.ac.jp
orcid.org/0000-0003-4207-8247

Specialty section:
This article was submitted to Cell Growth and Division, a section of the journal Frontiers in Cell and Developmental Biology

Received: *30 November 2020*
Accepted: *25 February 2021*
Published: *25 March 2021*

Citation:
Usui T and Shinohara A (2021) Rad9, a 53BP1 Ortholog of Budding Yeast, Is Insensitive to Spo11-Induced Double-Strand Breaks During Meiosis. Front. Cell Dev. Biol. 9:635383. doi: 10.3389/fcell.2021.635383

INTRODUCTION

DNA double-strand breaks (DSBs) are accidentally formed in cells with endogenous and exogenous DNA damage. DSBs induce a DNA damage response enabling the cell to cope with the damage and to coordinate DNA damage tolerance, including the repair of DSBs, throughout progression in the cell cycle. Failure of the DNA damage response to DSBs leads to instability of the genome, which is often associated with the onset of cancer.

DNA damage response is a complex biological pathway that is accompanied by a signaling cascade involving multiple kinases. In mitotic dividing cells, DSBs activate 2 key kinases, Mec1 (ATR in humans), a member of the PI3-kinase family, and Tel1 (ATM in humans) [reviewed in Nyberg et al. (2002)]. Mec1 is recruited to single-stranded DNA (ssDNA) in a Ddc2 (ATRIP)-dependent manner. Ddc2 recognizes replication protein-A (RPA)-coated ssDNA (Paciotti et al., 2000; Zou and Elledge, 2003). Tel1 binds to the ends of DSBs through Xrs2/Nbs1

Abbreviations: ChIP, chromatin immuno-precipitation; DAPI, 4′,6-diamidino-2-phenylindole; DSBs, DNA double-strand breaks; ISA, *in situ* autophosphorylation; SC, synaptonemal complex; WCE, whole cell extract.

in the Mre11-Rad50-Xrs2/Nbs1 (MRX/N in humans) complex (Nakada et al., 2003). Activated Mec1/Tel1 then stimulates Rad53 kinase (Chk2 in humans) (Sanchez et al., 1996; Sun et al., 1996) and transduces a signal to downstream effector pathways (Allen et al., 1994). Rad9 (53BP1 in humans) is a key modulator of Rad53 activation (Sun et al., 1998; Schwartz et al., 2002). Rad9 is recruited to the DNA damage area using 2 distinct histone modifications, histone H2AS129 phosphorylation (γ-H2AX in humans) and H3K79 methylation (Giannattasio et al., 2005; Wysocki et al., 2005; Toh et al., 2006; Grenon et al., 2007; Hammet et al., 2007). H2AS129 phosphorylation and H3K79 methylation are recognized by 2 domains of Rad9, that is, BRCT and Tudor, respectively. Histone H2AS129 phosphorylation is DNA damage-dependent and is catalyzed by Mec1 and Tel1 (Shroff et al., 2004). On the other hand, H3K79 methylation is constitutive and is mediated by Dot1 methyltransferase. Rad9 recruited to DSBs is phosphorylated by Mec1/Tel1 (Vialard et al., 1998; Schwartz et al., 2002), leading to phosphorylation-dependent oligomerization of Rad9 (Usui et al., 2009). These upstream events promote a scaffold function of Rad9 for Mec1/Tel1-dependent Rad53 activation (Gilbert et al., 2001; Sweeney et al., 2005). Rad9 facilitates Mec1/Tel1 phosphorylation of Rad53 (Sweeney et al., 2005). This *trans*-phosphorylation by Mec1/Tel1 appears to function as a priming event for Rad53 activation. Rad9 also mediates the self-phosphorylation of Rad53 (Gilbert et al., 2001). The *cis*-phosphorylation induces the conversion of Rad53 into a fully activated form (Pellicioli et al., 1999; Gilbert et al., 2001; Sweeney et al., 2005). Moreover, Rad9 undergoes phosphorylation by cyclin-dependent kinase (CDK) to modulate the DNA damage response in a cell-cycle dependent manner (Bonilla et al., 2008; Granata et al., 2010; Pfander and Diffley, 2011). This phosphorylation promotes the binding of Rad9 to the other DDR mediator protein, Dpb11 (Pfander and Diffley, 2011; Puddu et al., 2011; di Cicco et al., 2017), whose recruitment to DSB sites is dependent of the Rad17-Ddc1-Mec3 checkpoint clamp (Rad9-Rad1-Hus1 in other organisms).

Although DSBs are usually an accidental event in cells, several somatic cells also introduce programmed DSBs in their genomes in order to promote cellular differentiation, such as mating type switching in fungi and antigen receptor rearrangement in the immune cells of vertebrates [reviewed in Haber (2012), Alt et al. (2013))]. Moreover, meiotic cells in sexually reproducing eukaryotes develop a program to induce hundreds of DSBs in their genomes (∼160 in the budding yeast, ∼300 in humans/mice, and more than ∼1,000 in the lily), which initiates meiotic recombination (Terasawa et al., 1995; Barlow et al., 1997; Buhler et al., 2007; Kauppi et al., 2011; Pan et al., 2011). Such recombination enables the exchange of paternal and maternal DNA molecules to form a crossover (CO) [reviewed in Bishop and Zickler (2004))]. The CO is converted into an exchange of homologous chromosome axes, which are cytologically visualized as chiasma. The chiasma promotes proper segregation of homologous chromosomes at meiosis I along with cohesion distal to chiasmata. The meiotic recombination is essential for meiosis, and thus gamete formation. Any defects in recombination result in mis-segregation of homologous chromosomes, leading to the formation of aneuploidy gametes.

The formation of meiotic DSBs is catalyzed by Spo11, a meiosis-specific topoisomerase VI-like protein (Bergerat et al., 1997; Keeney et al., 1997). Spo11-induced DSBs are processed to generate a 3′-overhanging ssDNA. This ssDNA is coated with RPA to become a template for homology search by 2 RecA homologs, Rad51 and meiosis-specific Dmc1 (Bishop et al., 1992; Shinohara et al., 1992). After homology search by Rad51 and Dmc1, the ssDNA invades homologous double-stranded DNAs (dsDNAs). The interaction between the ssDNA and dsDNA leads to the formation of a recombination intermediate, single-end invasion (SEI) (Allers and Lichten, 2001b; Hunter and Kleckner, 2001). The SEI is then converted into the next intermediate with double Holliday structures (dHJs) (Schwacha and Kleckner, 1995). The dHJ is predominantly resolved into reciprocal exchange molecules, COs (Allers and Lichten, 2001a; Hunter and Kleckner, 2001; Borner et al., 2004). In meiosis, recombination preferentially occurs between homologous chromosomes rather than between sister chromatids, as seen in mitotic cells (interhomolog bias) (Schwacha and Kleckner, 1997).

Recent studies have shown that canonical DNA damage signaling is non-responsive to ∼160 Spo11-induced DSBs in meiotic cells of the budding yeast (Lydall et al., 1996; Carballo et al., 2008; Cartagena-Lirola et al., 2008). This is quite different from the response of vegetatively growing cells, which are very sensitive even to a single DSB (Lee et al., 1998; Pellicioli et al., 2001). Spo11-induced DSBs are known to activate Mec1/Tel1, which in turn activates a meiosis-specific Rad53 paralog, Mek1/Mre4 kinase in the context of chromatin (Hollingsworth and Gaglione, 2019). Mec1/Tel1-dependent phosphorylation of a Mek1 adaptor protein, Hop1, provides the binding site of Mek1 for oligomerization for the activation (Niu et al., 2005; Carballo et al., 2008). Activated Mek1 promotes interhomolog recombination and CO formation as well as activates the recombination checkpoint during prophase I (Hollingsworth and Gaglione, 2019). Importantly, Spo11-induced DSBs do not activate Rad53 (Carballo et al., 2008; Cartagena-Lirola et al., 2008), suggesting that the upstream activation of the canonical pathway is turned on but that the downstream events are suppressed. Indeed, meiotic cells are not intrinsically inert to Rad53 activation; the treatment of *spo11* mutant cells with exogenous DNA damaging agents, such as phleomycin, stimulates Rad53 kinase activity (Cartagena-Lirola et al., 2008). Moreover, the artificial targeting of Rad53, through fusion to Ddc2 (Lee et al., 2004), to ssDNAs of Spo11-induced DSBs induces Rad53 activation in meiosis (Cartagena-Lirola et al., 2008). Previous study also showed that over-expression of Rad53 during meiosis activates Rad53 kinase activity (Usui and Kanehara, 2013). Therefore, it is postulated that meiotic cells develop a mechanism to make Rad53 insensitive to Spo11-dependent DSBs. The mechanism of this insensitiveness of Rad53 to meiotic DSBs remains unknown.

In this study, we showed that, compared to mitotic cells, meiotic cells rely more on Dot1-dependent histone H3K79 methylation to activate Rad53 in response to exogenous DSBs. Moreover, like Rad53 tethering (Cartagena-Lirola et al., 2008), the artificial tethering of Rad9 to meiotic Spo11-mediated DSBs by fusion with Ddc2 stimulated Rad53 kinase activity.

Consistent with this, a chromatin-immunoprecipitation (ChIP) assay revealed minimal binding of Rad9 to meiotic DSBs. These results suggest that meiotic DSBs are masked to Rad9 in order to downregulate Rad53 kinase activity in meiotic prophase I. Untimely activation of Rad53 in meiotic prophase I impairs chromosome events such as meiotic recombination. We propose that meiotic cells execute a program that suppresses a part of the DNA damage response to develop meiosis-specific DSB-induced chromosome metabolism.

MATERIALS AND METHODS

Strains and Plasmids

All the strains described here, with the exception of HO endonuclease-inducible strains, are derivatives of SK1 diploids. The strain list is provided in **Supplementary Table 1**. The pUS48 plasmid harbored *DDC2-3xHA-RAD9* fused with a 0.8-kb DNA fragment containing the *DMC1* 5′-UTR fragment followed by the *kan* gene from a pFA6a-KANMX6 plasmid (Longtine et al., 1998). Like the pUS48, the pUS49 plasmid harbored *3xHA-RAD9* fused with the DNA fragment containing the *DMC1* 5′-UTR fragment followed by the *kamMX6* gene. To integrate *DMC1p-DDC2-3xHA-RAD9* or *-3xHA-RAD9* into the yeast genome, SK1 wild-type cells were transformed with *Eco*RI-digested pUS48 or pUS49 and were grown on YPAD with 100 μg/mL of G418. The plasmids pUS50, pUS72, pUS73, and pUS70 were used to prepare *DDC2*-fusion strains carrying *rad9-7A* (*T390A T398A T410A T427A S435A T457A T603A*), *rad9-Y798A*, and *rad9-K1088M* mutations and a genomic *rad9-Y798A* mutant, respectively. Yeast strains carrying N-terminal 3xHA-tagged *RAD9* (Usui et al., 2009), C-terminal 6xFLAG-tagged *RAD53* (Usui and Petrini, 2007), *rad53-KD* (*K227A*) (Usui and Petrini, 2007), *hht1-K79R*, and *hht2-K79R* were prepared by the 2-step integration method (Kaiser et al., 1994) using the pRS406-based plasmids, pRS406-HA-RAD9, pTAP12, pTAP10, pUS52, and pUS53, respectively. Deletion mutants of the *DMC1*, *DOT1*, *RAD9*, and *SPO11* genes and a *DDC2-3xHA* strain were constructed using a polymerase chain reaction (PCR)-based method (Longtine et al., 1998). The sequences of primers used in the experiments are shown in **Supplementary Table 2**.

Antibodies

Anti-Flag (M2 Sigma or Wako), anti-HA (12CA5 for western blot, 16B12 for immunostaining, and F-7 for ChIP), anti-α-tubulin (Serotec), rabbit anti-Rad51 (Shinohara et al., 1992), anti-Dmc1 (Hayase et al., 2004), anti-Rad9 (Usui and Petrini, 2007), anti-Zip1 (Shinohara et al., 2008), and anti-H3K79-3me (Abcam) were used for western blot and immunostaining.

Meiotic Cell Analyses and DNA Damage Treatment

After SK1 diploid cells entered into meiosis, meiotic cell cycle progression was monitored by 4′,6-Diamidino-2-phenylindole (DAPI) staining as described previously (Hayase et al., 2004). The DNA content of fixed meiotic cells was examined with a FACS Calibur flow cytometer (BD Biosciences) after staining with propidium iodide. Physical analyses for meiotic DSBs and crossover recombinants at the *HIS4-LEU2* locus were performed as described previously (Storlazzi et al., 1995; Shinohara et al., 1997). To induce accidental DSBs in meiosis, cells were incubated with 5 μg/ml of phleomycin for 30 min at 3.5 h after incubation with sporulation media (SPM).

Cytological Analysis

Spreads of the meiotic nuclei was prepared as described previously (Bishop, 1994; Shinohara et al., 1997). Immunostained samples were observed as described previously (Shinohara et al., 2000) using an epifluorescent microscope (Olympus BX51 with a 100× objective; NA, 1.4), and images were captured with a CCD camera (Cool Snap, Roper) and processed using iVision (Silicon) and Photoshop (Adobe) applications.

Western Blotting and *in situ* Autophosphorylation (ISA) Assay

For western blot analysis, trichloroacetic acid (TCA)-precipitated cell extracts were prepared as follows: Meiotic cells (2×10^8) were fixed in 0.5 mL of 20% TCA and centrifuged. The cell pellets were disrupted with glass beads in 0.25 mL of 20% TCA using a bead shocker (5 cycles of 2500 rpm, 60 s ON/OFF, Yasui Kikai). TCA precipitates were collected by centrifugation (4,000 rpm, 3 min) and were suspended in 0.24 mL of the sodium dodecyl sulfate-polyacrylamide gel electrophoresis (SDS-PAGE) loading buffer supplemented with 0.33 M Tris-HCl (pH 8.0). The ISA assay was performed as described previously (Pellicioli et al., 1999). Briefly, TCA-precipitated cell extracts were fractionated by SDS-PAGE and transferred to a polyvinyldifluoride (PVDF) membrane (Immobilon P, Millipore). The membrane was sequentially treated by denaturation and renaturation solutions, followed by incubation with ^{32}P-γ-ATP. ^{32}P-incorporation to Rad53 was visualized and quantified with BAS2000 (Fujifilm).

HO Induction During Mitosis

To induce HO DSB, cells carrying a single unrepairable HO DSB site (Shroff et al., 2004) were arrested at G2/M by nocodazole (15 μg/mL) in YP-lactate. Galactose was added up to 2% to induce HO endonuclease.

Chromatin Immuno-Precipitation (ChIP) Assay

Meiotic induction was performed as described above. Cells were fixed with 1% formaldehyde for 15 min, and cell extracts were prepared as described previously (Hayase et al., 2004). Cell extracts was prepared using a bead shocker (5 cycles of 2,500 rpm, 60 s ON/OFF, Yasui Kikai). The extract corresponding to 3.6×10^8 cells in pertinent mitotic and meiotic conditions were subjected to immunoprecipitation (IP) using Protein-A coated magnetic beads pre-coated with anti-HA (F-7) or anti-Rad51. DNA precipitated with the immune complex was purified by phenol/chloroform extraction and ethanol precipitation after protease-K treatment and quantified by real-time quantitative PCR (Chromo 4, Bio-Rad) using

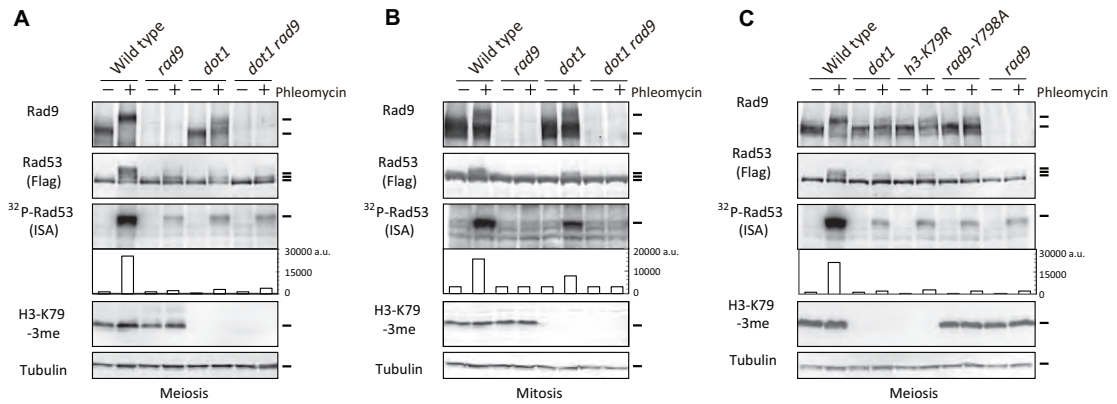

FIGURE 1 | H3K79me is required for Rad9-dependent Rad53 activation in meiosis after phleomycin treatment. **(A)** TCA-precipitated cell extracts were prepared from wild-type (USY543/544), *rad9* (USY524/525), *dot1* (USY526/527), and *dot1 rad9* (USY522/523) diploid strains, and were analyzed by western blotting using anti-Rad9, anti-Flag (for Rad53), anti-H3K79-3me, and anti-tubulin antibodies. "^{32}P-Rad53" represented ^{32}P-incorporation to Rad53 in the ISA assay. Band intensities were quantified and are shown as arbitrary units without normalization (fourth panels). Cell extracts derived from 4×10^6 cells were loaded for the ISA assay. **(A,C)** Cell extracts were prepared from 3.5-h meiotic cells before (labeled as "–") and after 30-min treatment with 5 μg/mL of phleomycin (labeled as "+"). **(B)** Diploid cells of the indicated strains were arrested at G2/M by nocodazole and treated with 5 μg/mL of phleomycin for 30 min, followed by TCA precipitation. Wild-type (USY543/544), *rad9* (USY524/525), *dot1* (USY526/527), and *dot1 rad9* (USY522/523) were used in the experiment. Results of an independent experiment are shown in **Supplementary Figure 1A**. **(C)** Rad53 activation was examined in various strains in meiosis as shown in **(A)**. Wild-type (USY543/544), *rad9* (USY524/525), *dot1* (USY526/527), *h3-K79R* (USY693/677), and *rad9-Y798A* (USY758/759) diploid strains were used. Results of an independent experiment are shown in **Supplementary Figure 1B**.

SyberGreen system (EvaGreen Supermix, Bio-Rad). The ChIP primers used were 5′-GGGTTTATAGTGGTGCCGTTC and 5′-ATGCAACGAAGCTTCCTGGC for *HIS4-LEU2*, 5′-ATGCTGAAGTACGTGGTGACGGAT and 5′-CCTCCGCC ACGACCACACTCT for 0.05 kb from HO-DSB, and 5′-GGTGTGCGGAGTAATCATTTGAGG and 5′-TTATAGGAGA CAGTTTTTCCATCAA for *SMC1*.

RESULTS

Histone H3K79 Methylation Is Necessary for Rad9-Dependent Rad53 Activation in Meiotic Cells After Phleomycin Treatment

Although Rad53 is not activated in response to endogenous Spo11-mediated DNA DSBs, Rad53 in meiotic cells is activated by exogenous DSBs (Cartagena-Lirola et al., 2008). Treatment of meiotic *spo11* mutant cells, which are defective in meiotic DSB formation (Bergerat et al., 1997; Keeney et al., 1997), with a radiomimetic agent, phleomycin, activates Rad53, and this activation depends on Rad9, as seen in vegetatively growing wild-type cells. This indicates that the Rad9-Rad53 axis is functional during meiosis in response to accidental DSBs (Cartagena-Lirola et al., 2008). We confirmed this by treating wild-type meiotic cells with phleomycin. Treatment of meiotic prophase cells grown in sporulation media (SPM) for 3.5 h with phleomycin for 30 min (by 4 h) induced band shifts of Rad53-Flag on western blots (**Figure 1A**). The band shifts of Rad53 corresponded with multiple phosphorylation of Rad53 accompanied with the activation of its kinase (Pellicioli et al., 1999). Rad53 kinase activity was tested for autophosphorylation activity of Rad53 using an *in situ* autophosphorylation (ISA) assay (Pellicioli et al., 1999). This finding suggests that Spo11-mediated endogenous DSBs do not interfere with the Rad53 activation by exogenous DSBs. Moreover, as shown previously (Cartagena-Lirola et al., 2008), untreated wild-type meiotic cells, which have ∼160 DSBs on their genomes, showed little band shifts or little autophosphorylation of Rad53 (**Figure 1A** and **Supplementary Figure 1A**).

As with mitotic cells, the treatment of meiotic wild-type cells with phleomycin leads to Rad53 activation in a Rad9-dependent manner. Meiotic *rad9* deletion cells showed reduced levels of Rad53 autophosphorylation with little band-shifts in response to phleomycin treatment (**Figure 1A**). This finding is consistent with the observed Rad9 dependency of Rad53 activation in meiotic *spo11* cells with DNA damage (Cartagena-Lirola et al., 2008). Moreover, the treatment of meiotic wild-type cells with phleomycin induced a band shift of Rad9 (**Figure 1A** and **Supplementary Figure 1A**), which is likely to be an activated form with multiple phosphorylation.

Methylation of histone H3K79 (H3K79me) by Dot1 methyltransferase is important, but not essential, for the ability of Rad9 to mediate Rad53 activation in mitosis (Giannattasio et al., 2005; Wysocki et al., 2005; Toh et al., 2006). In order to determine the involvement of Dot1 in Rad9-dependent Rad53 activation in meiosis, we analyzed Rad53 activation in meiotic *dot1* cells treated with phleomycin. The *dot1* deletion mutation, which abolished H3K79me, substantially decreased Rad53 activation in response to phleomycin; this decrease in activation was detected by reduced band shifts as well as decreased autophosphorylation levels (**Figure 1A** and **Supplementary Figure 1A**). This deficiency of Rad53 activation

in the *dot1* mutant was almost identical to that in the *rad9* mutant. Damage-induced Rad9 band shifts were also reduced in the *dot1* mutant. The *dot1 rad9* double mutant showed similar levels of reduced Rad53 activation to those of either single mutant (**Figure 1A**), suggesting that Dot1 and Rad9 function in the same pathway for phleomycin-dependent Rad53 activation in meiotic cells.

We confirmed that mitotic *dot1* mutant cells are capable of activating Rad53 in response to phleomycin. Previous studies have used only haploid cells, and therefore we used G2/M-arrested diploid cells for treatment with a microtubule polymerization inhibitor, nocodazole. As shown in **Figure 1B**, wild-type G2/M-arrested diploid cells activated Rad53 in response to phleomycin. In addition, the *rad9* deletion completely abolished the activation. The *dot1* mutant did show some activation of Rad53, but at half the level of that of the wild type, which was determined by the autophosphorylation activity (**Figure 1B** and **Supplementary Figure 1B**). Consistent with this result, like wild-type cells, the *dot1* mutant cells exhibited a Rad9 band shift after DNA damage treatment (**Figure 1B**).

To confirm the role of Dot1 through H3K79 methylation in Rad53 activation during meiosis, we created a histone *H3K79R* mutant strain (*hht1-K79R, hht2-K79R*; *h3-K79R* for simplicity) that was defective in Dot1-dependent methylation (Ontoso et al., 2013, Bani Ismail et al., 2014) (**Figure 1C**). In this strain, the histone H3 mutant proteins were expressed from the endogenous promoters of 2 copies of the histone H3 genes (*HHT1* and *HHT2*) on the genome. In meiosis, the *h3-K79R* mutant cells showed reduced Rad53 band shifts as well as reduced autophosphorylation when treated with phleomycin (**Figure 1C**). Decreased levels of activation in the *h3-K79R* mutant were similar to those observed in the absence of *DOT1*. In addition, the band shift of Rad9 was compromised in the *h3-K79R* mutant in a manner similar to that observed in the *dot1* mutant. These results suggest that Dot1-dependent H3K79 methylation is more critical for meiotic cells to activate Rad53 in response to exogenous DNA damage than it is for mitotic cells.

Histone H3K79 methylation is recognized by the Tudor domain of Rad9 (Grenon et al., 2007; Hammet et al., 2007). The *rad9-Y798A* mutation in the Rad9 Tudor domain is known to decrease the interaction between Rad9 Tudor and H3K79me. Therefore, we also investigated the effect of the *rad9-Y798A* mutation on Rad53 activation in meiotic cells. As shown in **Figure 1C**, *rad9-Y798A* mutant cells showed reduced Rad53 activation, as seen in the *rad9* null mutant. In addition, by itself, the Rad9-Y798A mutant protein showed minimal band shifting. This finding suggests that, in meiotic cells, Rad9 activates Rad53 in response to DNA damage through the Tudor domain of Rad9, which recognizes Dot1-dependent H3K79 methylation. It is important to stress that exogenous DNA damage slightly activated Rad53 even in the absence of Dot1 or Rad9; however, the residual activation was higher than that in the absence of exogenous DNA damage.

Although exogenous DSBs induce Rad53 activation in meiotic cells, Spo11-induced DSBs do not. Importantly, the *rad9*, *dot1*, *h3-K79R,* and *rad9-Y798A* mutants are all proficient in the activation of Mec1/Tel1 checkpoint kinases, which are upstream of Rad53-Rad9, in response to Spo11-DSBs (our unpublished results). These results suggest that meiotic cells show distinct responses to programmed and accidental DSBs with respect to activating Rad53 kinase. Moreover, it is likely that Spo11-dependent DSBs are masked for the activation of Rad53, but not for the activation of Mec1/Tel1.

The Ddc2-Rad9 Fusion Protein Activates Rad53 in Response to Meiotic DSBs

Rad53 activation in mitosis is under the control of a multilayered mechanism (Pellicioli and Foiani, 2005). The targeting of Rad9, as well as Rad53, at a DSB site is likely to be crucial for the activation. A previous study showed that tethering Rad53 to meiotic DSBs as a fusion protein to Ddc2 induced Rad53 activation in a Spo11-dependent manner (Cartagena-Lirola et al., 2008). Since Rad9 works upstream of Rad53 in the checkpoint pathway, we questioned whether the tethering of Rad9 to meiotic DSBs might also activate Rad53. To target Rad9 to meiotic DSBs, we placed the Ddc2-3HA-Rad9 fusion protein under the control of a meiosis-specific *DMC1* promoter (referred to as Ddc2-Rad9). The diploid strain (referred to as *DDC2-RAD9*) expressed the Ddc2-Rad9 fusion protein only in meiosis, together with the endogenous (non-tagged) Rad9 protein. Western blots showed that Ddc2-Rad9 was induced in meiotic prophase in a manner similar to the Dmc1 protein (**Figure 2A**). Ddc2-Rad9 started to appear at 1.5 h and reached a plateau at 3 h. At later periods, Ddc2-Rad9 showed smear bands, suggesting posttranslational modification of Ddc2-Rad9 during meiosis. The expression level of Ddc2-Rad9 from the *DMC1* promoter at 4 h was roughly comparable to that of HA-Rad9 from a native promoter (**Figure 2B** and **Supplementary Figure 4**). Concomitant with the expression of Ddc2-Rad9 during meiosis, endogenous Rad53 protein started to show reduced mobility, suggesting the activation of Rad53 (**Figure 2A** and **Supplementary Figure 2**). Indeed, the ISA assay confirmed robust autophosphorylation activity of Rad53 after 3-h incubation in meiosis, which was not observed at 0 and 1.5 h. The expression of the Ddc2-Rad9 fusion protein with kinase-dead Rad53, Rad53-KD, abolished the autophosphorylation activity, demonstrating that Rad53 activation by *DDC2-RAD9* was completely dependent on the Rad53 kinase activity. Interestingly, Ddc2-Rad9 induced a smaller, but significant band-shift of Rad53-KD at 4.5 h relative to wild-type Rad53. These results suggest that Ddc2-Rad9 induces Rad53-kinase independent modification of Rad53.

Activation of Rad53 by Ddc2-Rad9 fusion still requires meiotic DSBs. The *spo11* deletion greatly decreased the band shifts as well as the autophosphorylation activity of Rad53 (**Figure 2A**). Some band shifts of Rad53 were nonetheless apparent, and a low, but increase in Rad53 autophosphorylation was observed, even in the absence of Spo11. This finding indicates that there might be another mechanism for Rad53 activation by Ddc2-Rad9 in a meiotic-DSB independent manner, e.g., in the S phase, since a slight increase in Rad53 autophosphorylation was observed at 1.5 h, the point at which the meiotic S phase occurs.

An increased amount of Rad9 in the *DDC2-RAD9* strain could not explain the activation of Rad53. Expression of non-fusion

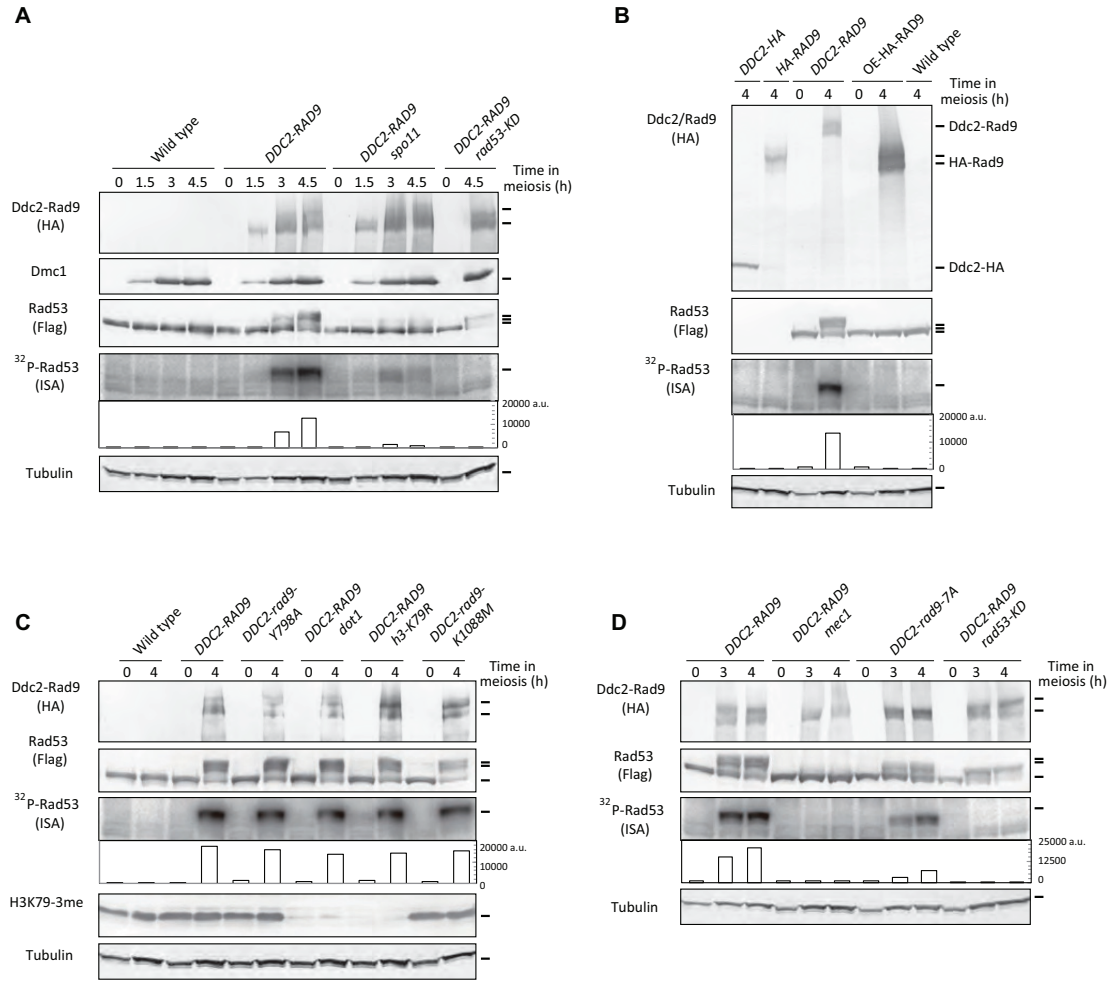

FIGURE 2 | Ddc2-Rad9 fusions activate Rad53 in meiosis. **(A)** TCA-precipitated meiotic cell extracts of the indicated strains were analyzed by western blotting using anti-HA, anti-Flag, anti-H3K79-3me (tri-methylation), anti-Dmc1, and anti–α-tubulin antibodies.^{32}P-Rad53 represented ^{32}P-incorporation to Rad53 in the ISA assay, and was quantified as shown **Figure 1A** (fifth panels). Cell extracts derived from 4×10^6 cells were loaded for the ISA assay. Wild-type (USY543/544), *DDC2-RAD9* (USY544/661), *DDC2-RAD9 spo11* (USY783/414), and *DDC2-RAD9 rad53-KD* (USY545/720) were examined. **(B)** Cell extracts were prepared from the strains expressing C-terminal 3x HA-tagged Ddc2 (USY83/84; *DDC2-HA*) and N-terminal 3x HA-tagged Rad9 (USY20/35; *HA-RAD9*) from their native promoters; Ddc2-Rad9 (USY544/671; *DDC2-RAD9*) and 3x HA-tagged Rad9 (USY544/661; *OE-HA-RAD9*) from the *DMC1* promoter; no HA-tagged wild-type strain (USY543/544); wild type. Rad53 was not tagged with Flag in *DDC2-HA* and *HA-RAD9* strains. Flag-Rad53 was expressed from the native promoter. **(C)** Rad53 activation was examined in various strains as in **(A)**. Wild-type (USY543/544), *DDC2-RAD9* (USY544/671), *DDC2-rad9-Y798A* (USY544/776), *DDC2-RAD9 dot1* (USY768/526), *DDC2-RAD9 h3-K79R* (USY770/693), and *DDC2-rad9-K1088M* (USY544/797) were examined. Results of an independent experiment are shown in **Supplementary Figure 2C**. **(D)** Rad53 activation was examined in various strains as in **(A)**. Wild-type (USY543/544), *DDC2-RAD9* (USY544/671), *DDC2-RAD9 mec1* (USY495/785), *DDC2-rad9-7A* (USY544/667), and *DDC2-RAD9 rad53-KD* (USY4520) were examined. Results of an independent experiment are shown in **Supplementary Figure 2D**.

HA-Rad9 from the *DMC1* promoter was approximately 10-fold higher than that from the endogenous promoter, which did not activate Rad53 (**Figure 2B** and **Supplementary Figure 2B**). This result reinforces the idea that the tethering of Rad9 to meiotic DSBs is a key event for inducing Rad53 activation in response to Spo11-induced meiotic DSBs.

We also confirmed the activation of Rad53 kinase activity by Ddc2-Rad9 fusion in the background of the *dmc1,* which is unable to repair meiotic DSBs (Bishop, 1994; Shinohara et al., 2000) and its genetic requirements (see below, with the *spo11*, *mec1*, and *rad53-KD* mutations; **Supplementary Figure 3**).

Genetic Requirements for Meiotic Rad53 Activation by Ddc2-Rad9

As shown above, in meiotic cells, exogenous DNA damage-dependent Rad53 activation largely relies on the interaction of Rad9's Tudor domain with Dot1-dependent H3K79me. Therefore, we questioned whether Rad53 activation by Ddc2-Rad9 in meiosis would also depend on the interaction. Even in the background of *dot1* deletion and *h3-K79R* mutants, Ddc2-Rad9 could still fully activate Rad53 (**Figure 2C** and **Supplementary Figure 2C**). The band shifts and autophosphorylation levels of Rad53 in the *dot1* deletion and *h3-K79R* mutants were

comparable to those in the wild type. Moreover, consistent with the above results, the introduction of a Tudor mutation, *rad9-Y798A,* in the fusion did not abolish its ability to facilitate the band shifts or autophosphorylation levels of Rad53 (**Figure 2C**).

In mitosis, in addition to H3K79me, Rad9 localizes to chromatin adjacent to DSBs via the interaction between the BRCT domain of Rad9 and phosphorylation of S129 of histone H2A by Mec1/Tel1 kinases (Hammet et al., 2007). Histone H2AS129 phosphorylation is induced during meiosis in response to Spo11-mediated DSBs (Eichinger and Jentsch, 2010). During meiosis, expression of the Ddc2-fusion of Rad9 with a BRCT domain mutation, *rad9-K1088M*, which impairs the binding of Rad9 to phosphorylated H2AS129 (Hammet et al., 2007), activated Rad53, as in the wild-type fusion protein (**Figure 2C**). Therefore, these data suggest that Rad53 activation by Ddc2-Rad9 does not require the ability of Rad9 to recognize 2 epigenetic markers that play a critical role in the Rad53 activation to exogenous DSBs in mitotic cells.

In mitosis, the kinase activity of Rad53 largely depends on a major DNA damage kinase, Mec1/ATR (Sanchez et al., 1996; Sun et al., 1996). *DDC2-RAD9*-dependent Rad53 activation in meiosis still requires Mec1. The *mec1 sml1* mutant (the *sml1* mutation suppresses a lethality of the *mec1* deletion) (Zhao et al., 1998) showed little stimulation of Rad53 kinase by *DDC2-RAD9* (**Figure 2D**). Interestingly, only a few band shifts of Rad53 were observed in the *mec1* mutant, which is in marked contrast to the results for the *DDC2-RAD9 RAD53-KD* strain, which showed a clear band shift with little Rad53 activation (**Figure 2A**). This finding suggests that Mec1-dependent Rad53 phosphorylation might be an initial key event for Rad53 activation by *DDC2-RAD9*.

Moreover, the Ddc2-Rad9 band shift was compromised in the *mec1* mutant. In the wild-type strain, Ddc2-Rad9 exhibited smear bands, often showing 2 major bands (**Figures 2C,D**), whereas the *mec1 (sml1)* mutant lacked the major upper band of the Rad9 fusion. Mec1 is known to phosphorylate Rad9 at multiple sites (Schwartz et al., 2002). The *rad9-7A* mutant, with mutations in the major Mec1-phosphorylation sites, T603, and an additional 6 S/T sites of the SQ/TQ cluster domain (SCD), showed decreased Rad53 band shifts and autophosphorylation activity in mitotic cells with exogenous DNA damage (Schwartz et al., 2002). When the Ddc2-Rad9 fusion protein with the *rad9-7A* mutation was expressed in meiosis, the band shift greatly decreased, and the autophosphorylation activity of Rad53 was diminished by ∼1/3 relative to that of the wild-type Ddc2-Rad9 protein at 4 h (**Figure 2D** and **Supplementary Figure 2D**). The residual activation of Rad53 might have originated from other, as yet unidentified, phosphorylation sites of Rad9 by Mec1/Tel1. The data suggest that Mec1-mediated phosphorylation of Rad9 remains important for Rad53 activation in *DDC2-RAD9* meiosis.

The Ddc2-Rad9 Fusion Protein Localizes to Meiotic Chromosomes

The Ddc2 protein shows punctate staining on meiotic chromosomes when ssDNAs are formed (Refolio et al., 2011). We tried to detect the localization of Ddc2-Rad9 on meiotic chromosomes by immunostaining. However, we did not detect any significant signals for the Ddc2-Rad9 fusion protein on meiotic chromosome spreads in the *DDC2-RAD9* cells by staining with the anti-HA antibody (**Figure 3A**). The *dmc1* mutant, which cannot repair and accumulate the ssDNA (Bishop et al., 1992), was used for efficient detection of the Ddc2 signal (Refolio et al., 2011). In parallel, staining for Rad51, a marker protein of processed meiotic DSBs (Bishop, 1994), was carried out together with HA-staining. At 6 h in *dmc1* meiosis, when Rad51 foci were formed in more than 94.7 ± 6.8% of nuclei, weak, but significant Ddc2-Rad9 signals as a focus were detectable on chromosomes (**Figure 3A** and **Supplementary Figure 5**).

Given that activated Rad53 kinase negatively regulates Rad9 assembly around DSBs (Usui et al., 2009), we further introduced a kinase-dead *rad53-KD* mutation, which may stabilize the Ddc2-Rad9 localization to chromatin. We detected brighter Ddc2-Rad9 foci on chromosomes of the *dmc1* mutant with the *rad53-KD* compared to those in the *dmc1* mutant with wild-type Rad53 (**Figure 3A** and **Supplementary Figure 5**). Ddc2-Rad9 localization to chromosomes was specific to meiotic prophase cells. At 0 and 2 h, there was little focus formation of the fusion in the *rad53-KD dmc1* (**Figure 3B**). Ddc2-Rad9 focus-positive cells appeared concomitantly with Rad51 focus-positive cells (**Figure 3B**). At 4.5 h, 80% of the cells were positive for Ddc2-Rad9 foci. The average numbers of Ddc2-Rad9 and Rad51 foci in the *rad53-KD dmc1* mutant were 59 ± 5.9 and 71 ± 6.8, respectively (n = 18), and 82 ± 4.7% (n = 18) of Ddc2-Rad9 was co-localized with Rad51. This supports the idea that Ddc2-Rad9 does indeed bind to ssDNAs for Rad53 activation.

The focus formation of Ddc2-Rad9 in the *dmc1 rad53-KD* mutant, like that of Rad51, once again depended on Spo11, and therefore on DSB formation (**Figure 3A**). Moreover, simple overexpression of the non-fusion version of HA-Rad9 in the *dmc1 rad53-KD* mutant did not support the localization of the HA-Rad9 protein on meiotic chromosomes (**Figure 3A**).

Binding of Rad9 to Meiotic DSBs Is Suppressed

The results described above suggested that meiotic cells lack the ability to recruit Rad9 or Rad53 to Spo11-induced DSBs. To confirm this hypothesis, we analyzed the binding of Rad9 to DSBs using a ChIP assay. First, as a control, we carried out ChIP to examine the localization of HA-Rad9 to an HO-endonuclease-induced DSB at the *MAT* locus in vegetative cells (Shroff et al., 2004; Usui et al., 2009). We used a haploid with *GAL1/10-HO*. After 1 h induction of the nuclease in G2/M arrested cells (by nocodazole) with the addition of galactose, increased binding of Rad9 to the DSB was observed at the *MAT* locus, but not at the control locus of *SMC1* (**Figure 4A**). At the same time, robust binding of Rad51 to the break was detected. Then, we analyzed the binding of HA-Rad9 to a strong meiotic recombination hotspot, the *HIS4-LEU2* locus. While robust binding of Rad51 to the hotspot was detected at 4 h in meiosis, we could detect little binding of Rad9 to the hotspot at 4 h at the same time (**Figure 4B**). This suggests that Rad9 is

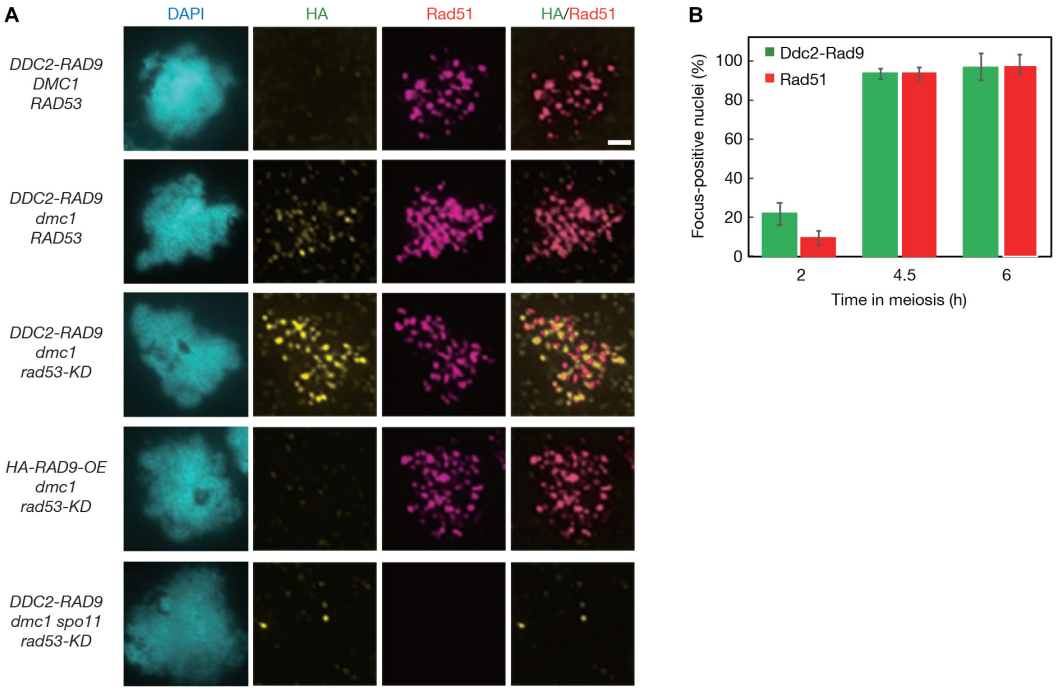

FIGURE 3 | Ddc2-Rad9 localizes to meiotic DSBs. **(A)** The representative images of anti-HA and anti-Rad51 double immunostaining of spread nuclei prepared from *DDC2-RAD9* (USY544/671), *DDC2-RAD9 dmc1 RAD53* (USY580/591), *DDC2-RAD9 dmc1 rad53-KD* (USY582/623), *HA-RAD9-OE dmc1 rad53-KD* (USY582/674), and *DDC2-RAD9 dmc1 spo11 rad53-KD* (USY559/666) strains are shown at 4.5 h in meiosis, except for *DDC2-RAD9 dmc1 RAD53*, which is shown at 6 h in meiosis. Typical DNA images stained with DAPI and merged images by HA- and Rad51-staining are presented. Bar equals 2 μm. **(B)** The percentage of *dmc1*Δ *rad53-KD DDC2-RAD9* nuclei that had more than 5 HA or Rad51 staining foci is presented at the indicated time points. At least 50 nuclei were counted at each time point. Error bars represent standard deviations obtained from 3 independent time courses.

insensitive to Spo11-mediated meiotic DSBs, different from the mitotic DSB.

Ddc2-Rad9 Fusion Delays DSB Repair and Cell Cycle Progression During Meiosis

We next examined the effect of Ddc2-Rad9 expression, and thus Rad53 activation, on meiosis. The *DDC2-RAD9* diploid showed wild-type spore viability levels (97.9% vs. 98.4% in the wild type; 48 asci). *DDC2-RAD9* cells delayed MI entry by approximately 2 h compared to the wild type (**Figure 5A**), without any delay in the pre-meiotic S phase (**Supplementary Figure 6A**).

We investigated meiotic DSB repair and CO formation at the *HIS4-LEU2,* by Southern blotting (**Figure 5B**) (Cao et al., 1990; Storlazzi et al., 1995). In the wild type, meiotic DSBs formed at 3 h, peaked at 4 h, and then gradually decreased after 5 h (**Figures 5C,D**). Concomitant with the disappearance of DSBs, COs started to appear at 5 h, and reached a plateau by 6 h in meiosis (**Figures 5E,F**). *DDC2-RAD9* cells formed DSBs in a manner similar to wild-type cells, but the disappearance of the DSBs was delayed by 1.5 h compared to the wild type (**Figures 5C,D**). Consistent with the kinetics of DSBs, COs in *DDC2-RAD9* started to appear at 6 h, and reached a plateau by 8 h (**Figures 5E,F**). Although delayed, the final level of COs in *DDC2-RAD9* cells was comparable to that in the wild type. These data suggest that meiotic DSB repair is delayed in *DDC2-RAD9* meiosis.

To confirm delayed DSB repair in *DDC2-RAD9* meiosis, we observed focus formation of Rad51 on meiotic chromosomes by immunostaining (Bishop, 1994; Shinohara et al., 2000). In the wild type, Rad51 focus-positive nuclei started to appear at 3 h in meiosis, reached a peak at 4 h, and disappeared gradually during further incubation with kinetics similar to those of meiotic DSBs (**Figures 5G,H**). Rad51 focus-positive nuclei in *DDC2-RAD9* appeared at 3 h and peaked at 5 h. However, the fusion induced a 2-h delay in the disappearance of Rad51 foci (**Figures 5G,H**). These data support the delay in DSB repair, particularly after Rad51 loading, in the *DDC2-RAD9* strain. Consistent with delayed repair, the average number of Rad51 foci in *DDC2-RAD9* was 30 ± 16 at 4 h (per total nucleus; n = 112; **Figure 5I**), which was higher than that observed in the wild type (24 ± 16, n = 113; P = 0.009, Mann–Whitney U test). Dmc1-focus kinetics were similar to those of the Rad51 focus in *DDC2-RAD9* meiosis (**Supplementary Figure 6B**). These data demonstrate that Ddc2-Rad9 expression impedes a recombination step after the loading of Rad51/Dmc1. The delayed DSB repair during meiosis of *DDC2-RAD9* cells is consistent with the result that the over-expression of Rad53 delays meiotic DSB repair (Usui and Kanehara, 2013).

Synaptonemal complex (SC) formation was also investigated in the *DDC2-RAD9* strain. We observed the localization of the

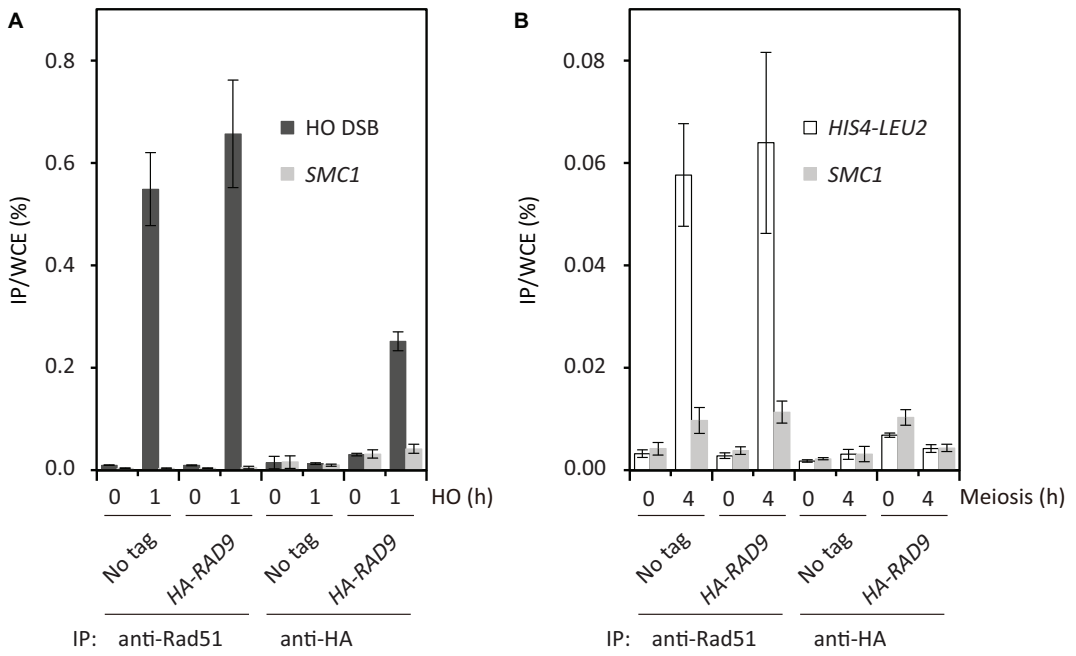

FIGURE 4 | Rad9 is insensitive to meiotic DSBs. Rad9 binding to chromatin adjacent to mitotic HO-induced DSBs **(A)** and to meiotic programmed DSBs at the *HIS4-LEU2* locus **(B)** was tested by ChIP. Formaldehyde-fixed chromatin extracts were prepared at 0 and 1 h after HO DSB induction in G2/M-arrested cells, and at 0 and 4 h after meiotic induction, followed by anti-HA and anti-Rad51 ChIP. Anti-HA- or anti-Rad51-bound DNAs were quantified by real-time PCR. Error bars represent standard deviations obtained from 3 independent cultures. The non-tagged wild-type and *HA-RAD9* strains examined were USY99 and USY100 in **(A)** and NKY1551 and USY2035 in **(B)**, respectively.

Zip1 protein, which is the central component of the SC (Sym et al., 1993). As shown in **Figures 5J,K**, in the wild type, dotty staining was initially observed for Zip1 (class I, leptonema), and the nuclei containing a mixture of dotty and short linear localizations of Zip1 increased (class II, zygonema). Finally, Zip1 was fully extended along chromosomes, which is indicative of a matured SC and complete synapsis (class III, pachynema), and then disappeared subsequently. In *DDC2-RAD9* cells, dotty-staining of Zip1 appeared at 2 h, similar to the wild type (**Figure 5K**). However, the appearance of short and long linear localization of Zip1 was delayed in *DDC2-RAD9* (**Figures 5K,L**). At 6 h, *DDC2-RAD9* showed a maximum fraction of Zip1-long lines, whereas the wild type showed the maximum at 4 h. Disassembly of Zip1 lines in the *DDC2-RAD9* strain was delayed by 2 h relative to the wild type. These results suggest that SC elongation is partially defective in *DDC2-RAD9.* Consistent with this, *DDC2-RAD9* cells showed an increased fraction of aggregates (polycomplex) of Zip1 (**Figures 5K,L**). These results indicate that Ddc2-Rad9 has negative impacts on SC assembly, probably due to delayed DSB repair.

DISCUSSION

Rad53 is the central effector kinase in the DNA damage checkpoint in mitosis but is not activated during meiosis (Cartagena-Lirola et al., 2008), even in the presence of ∼160 DSBs induced by Spo11 (Buhler et al., 2007; Pan et al., 2011), suggesting that Rad53 activation is masked in response to meiotic programmed DSBs. However, the molecular mechanism underlying the masking of Rad53 is largely unknown. Previous study showed that over-expression of Rad53 during meiosis delays DSB repair, thus the onset of meiosis I, suggesting the presence of silencing mechanism of Rad53 in meiotic cells (Usui and Kanehara, 2013). Here, we showed that Rad9, which mediates Mec1-dependent Rad53 activation (Gilbert et al., 2001; Schwartz et al., 2002; Sweeney et al., 2005), is a key regulator for this masking. Rad9 cannot bind to Spo11-mediated DSBs in meiosis, whereas it does bind to HO-induced DSBs in mitosis. Indeed, tethering of Rad9 to meiotic DSBs by Ddc2-fusion induces the activation of Rad53 kinase.

The inability of Rad9 to bind to meiotic DSB may result from meiosis-specific modulation of Rad9 in order to inhibit the activity, either by posttranslational modification or through interaction with a meiosis-specific inhibitor. However, this latter possibility is less likely, given that Ddc2-Rad9 can activate Rad53 in response to meiotic programmed DSBs. If meiotic cells impose inhibition on Rad9 directly, Ddc2-Rad9 would also be inhibited in meiosis. Alternatively, in contrast to exogenous DSBs as well as HO-mediated DSBs, meiotic DSBs are intrinsically inert to Rad9 binding. Rad9 binding to chromosomes is promoted by 2 epigenetic markers in mitosis, histone H2AS129 phosphorylation and H3K79 methylation, which are recognized by 2 domains of Rad9, that is, BRCT and Tudor, respectively (**Figure 6**). H2AS129 phosphorylation is DNA damage-dependent and is mediated by Mec1/Tel1 checkpoint kinases, whereas H3K79 methylation

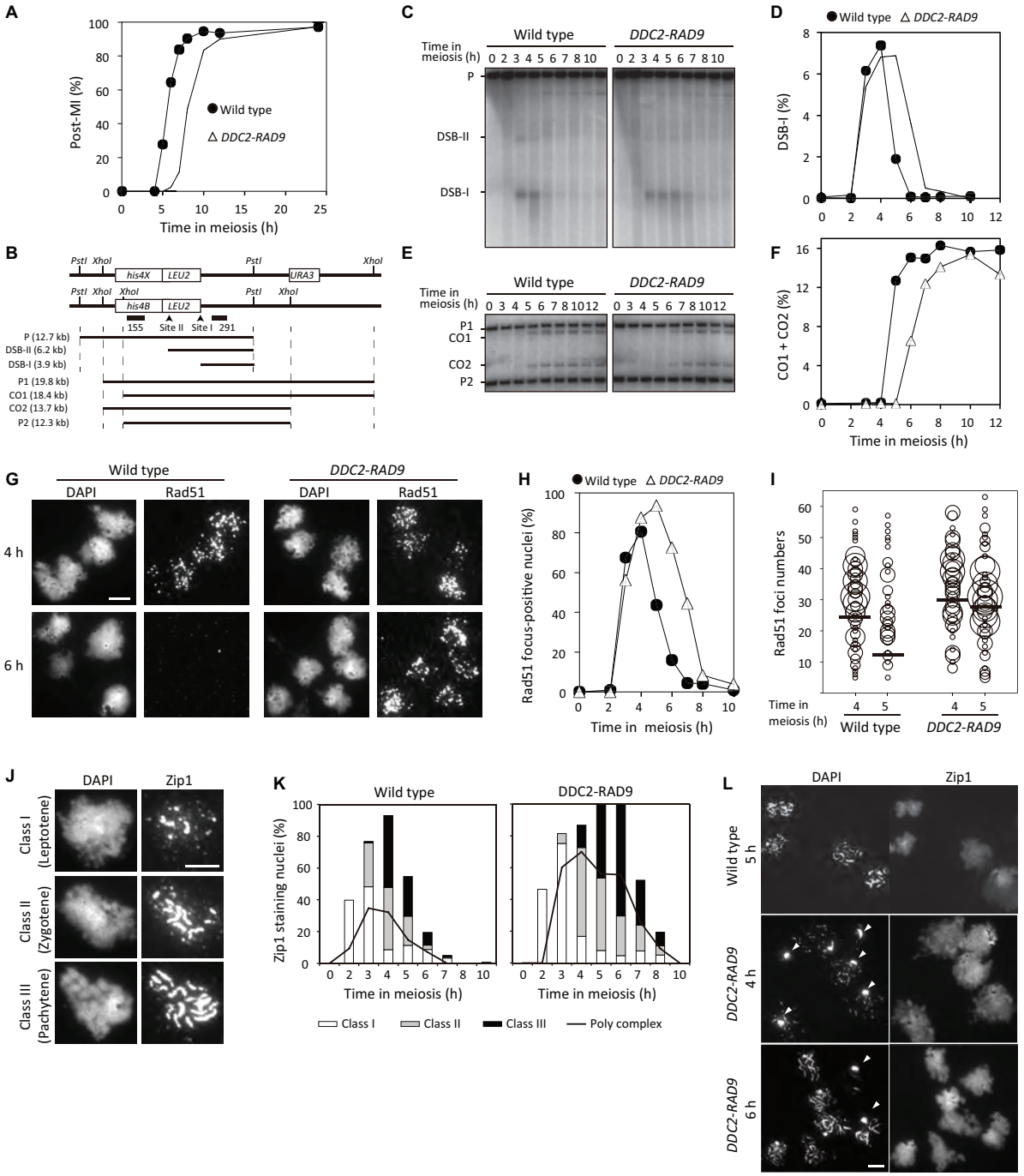

FIGURE 5 | *DDC2-RAD9* impedes cell cycle progression and meiotic recombination. **(A)** Meiotic nuclear divisions were monitored in wild-type (USY543/544) and *DDC2-RAD9* (USY544/671) strains by DAPI staining. The *y*-axis represents the percentage of cells that completed meiosis I and II (Post-MI). At least 200 cells were counted at each time point. **(B)** Schematic presentation of the *HIS4-LEU2* DSB site. **(C,E)** Genomic DNAs were prepared from the indicated strains during the meiotic time course. Meiotic DSBs (DSB-I and DSB-II) **(C)** or crossover recombinants (CO1 and CO2) **(E)** were detected by Southern blot using the probes pNK291 or pNKY155 after genomic DSBs were digested with *Pst*I or *Xho*I, respectively. **(D,F)** Quantitative data of DSB-I **(C)** and CO1 + CO2 **(E)** obtained from Southern blot are plotted. **(G–L)** *DDC2-RAD9* influences localization of Rad51 and Zip1 on meiotic chromosome. **(G)** The representative images of Rad51 immunostaining nuclear foci in spread nuclei prepared from the indicated strains at 4 and 6 h in meiosis are shown. **(H)** The percentage of the indicated cells' nuclei that had more than 5 Rad51 foci was plotted at the indicated time points. **(I)** Distribution of nuclei according to Rad51 foci number per nucleus at the indicated time is presented using the same data samples as in **(H)**. Only nuclei that had more than 5 Rad51 foci were plotted. The size of the bubbles reflects the percentage of nuclei that had a certain foci number of Rad51 among all nuclei examined. Bars represent the average numbers of Rad51 foci. **(J)** Representative images of Zip1 staining classification are shown. **(K)** Classifications of Zip1 staining at the indicated time in the indicated strains are shown. The line represents the Zip1 polycomplex (PC). At least 100 nuclei were examined at each time point. **(L)** Representative images of Zip1 staining in *DDC2-RAD9* at 4 h and 6 h are shown. Zip1 PCs are indicated by arrowheads. Experiments were performed at least twice, and representative data are shown. Bar equals 5 μm.

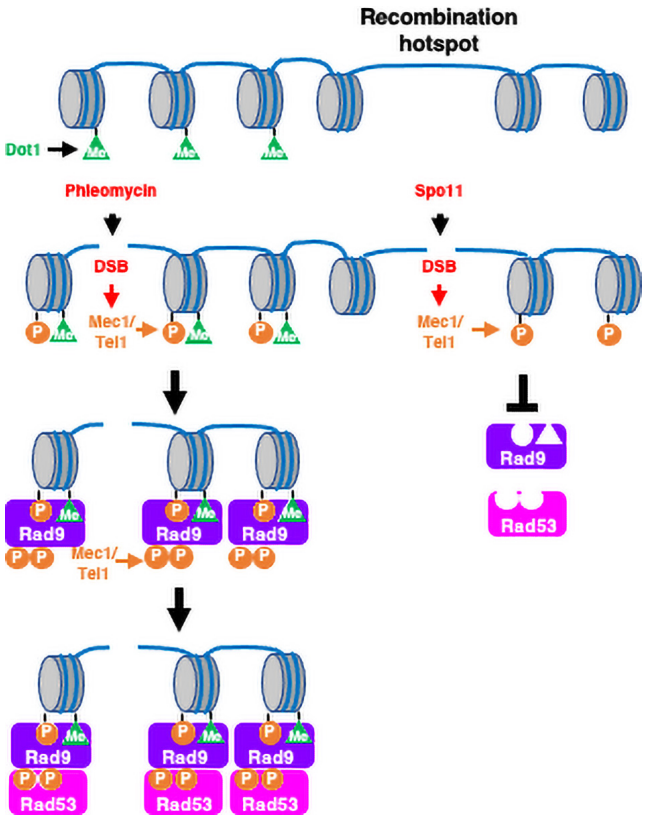

FIGURE 6 | Rad9 is incompetent to meiotic DSBs. Exogenous DSBs often occur in nucleosome-rich gene body where Dot1-mediated histone H3K79 methylation marks are enriched (left pathway). The DSBs activates Mec1/Tel1, which in turn phosphorylates histone H2AS129. The two epigenetics marks, H3K79 methylation and H129S phosphorylation, provides multiple binding sites to Rad9. Rad9 is phosphorylated by Mec1/Tel1 and activates Rad53 kinase. At recombination hotspots is located in nucleosome-free region, which shows less H3K79 methylation compared to gene bodies right pathway. This chromatin features make the region insensitive to Rad9 binding.

is constitutive and is catalyzed by Dot1 methyltransferase. H2AS129 phosphorylation is induced by Spo11-mediated DSBs in meiosis in a Mec1-dependent manner (Eichinger and Jentsch, 2010). Interestingly, recent genome-wide mapping of H3K79 methylation showed that promoter regions of the yeast genome, where most of the meiotic DSBs occur (Buhler et al., 2007; Pan et al., 2011), tend to exhibit reduced levels of this modification (Zhang et al., 2011). One likely possibility is that this reduction of H3K79 methylation around DSB sites may partially explain the weak binding of Rad9 to meiotic DSBs (**Figure 6**). Consistent with this hypothesis, Rad53 activation by artificial targeting of Rad9 to the DSBs is independent of Dot1 or H3K79 methylation. However, previous studies have shown that meiotic cell cycle arrest in the *zip1* mutant, which is defective in chromosome synapsis and meiotic recombination, requires Dot1-dependent H3K79 methylation, suggesting that the methylation plays a role in response to meiotic DSBs, at least in the *zip1* mutant (Ontoso et al., 2013). We propose a simple model in which meiosis-specific chromosome structures play a role in making meiotic DSBs insensitive to Rad9, and thus to Rad53. This model is supported by a previous study that showed that Rad53 was activated when DSBs escaped from the recombination checkpoint and were present in meiosis-II, where meiosis-specific chromosome structures are dismantled (Cartagena-Lirola et al., 2008).

Why do meiotic cells mask Rad53 activation in response to Spo11-mediated DSBs? In this study, we found that the untimely activation of Rad53 kinase during meiosis has a negative impact on meiotic chromosome metabolism. The Ddc2-Rad9 fusion delayed meiotic repair of DSBs, suggesting that Rad53 activation is inhibitory to meiotic DSB repair, and thus meiotic recombination. Meiotic recombination preferentially occurs between homologous chromosomes (Schwacha and Kleckner, 1997). On the other hand, intersister recombination is preferred in mitotic recombination (Kadyk and Hartwell, 1992; Bzymek et al., 2010). One simple idea is that Rad53 activation inhibits interhomolog recombination or activates intersister recombination. However, this is less likely since *DDC2-RAD9* cells, in which Rad53 is activated, still show normal levels of crossover formation in meiosis (**Figures 5E,F**).

Although Rad53 activation was inhibited in wild-type meiosis, we did not observe drastic defects in artificial activation of

the kinase by Ddc2-Rad9. The effect of Rad53 activation by Ddc2-Rad9 on meiotic events was weak. This finding might be attributable to the fusion protein restricting the activation of Rad53 very close to the DSBs. Rad9-Rad53 is generally more dynamic in nuclei for signaling, at least in mitotic cells with exogenous DSBs (Melo et al., 2001; Usui et al., 2009).

There are several downstream targets of the Rad53 pathway, including Dbf4-dependent Cdc7 kinase (DDK) (Lopez-Mosqueda et al., 2010; Zegerman and Diffley, 2010). In meiosis, DDK plays multiple roles such as in the formation of DSBs, expression of middle pachytene genes, monopolar spindle attachment, and efficient cleavage of meiosis-specific cohesion (Lo et al., 2008; Matos et al., 2008; Sasanuma et al., 2008; Katis et al., 2010). Thus, it is likely that, in meiosis, DDK should be constitutively activated during meiotic prophase-I by avoiding inhibitory Rad53 activation. Moreover, a recent study clearly showed that meiotic prophase develops a program to guarantee a longer prophase (G2) compared to the mitotic phase (Okaz et al., 2012). It is also possible that DSB-dependent Rad53 activation might inhibit the operation of this program in a timely manner. We speculate that meiotic cells ensure a longer prophase (G2) through the inactivation of the Rad53 checkpoint kinase.

In mitotic cells, in addition to Rad9, the other DDR mediator protein, Dpb11, plays a role for efficient activation of Rad53 (Pfander and Diffley, 2011; Puddu et al., 2011; di Cicco et al., 2017). The recruitment of Dpb11 to DSB sites is dependent of the phosphorylation of a C-terminal tail of Ddc1 in the Rad17-Ddc1-Mec3 checkpoint clamp (Rad9-Rad1-Hus1 in other organisms). Then, Dpb11 recruits Rad9 through CDK-dependent phosphorylation of Rad9. We have known little about the regulation of Dpb11 during meiosis. However, the involvement of the checkpoint clamp in meiotic DNA damage response is controversial (Shinohara et al., 2003; Shinohara et al., 2015).

In mammals, 53BP1, a Rad9 homolog, is recruited to DSB sites through multiple interactions, including various histone modifications (Huyen et al., 2004; Botuyan et al., 2006; Mailand et al., 2007; Stewart et al., 2009; Fradet-Turcotte et al., 2013). These interactions function in the positive regulation of 53BP1 recruitment. The present study suggests that negative control of Rad9 to the DSB is also a key process for modulating the DNA damage response under different physiological conditions.

DATA AVAILABILITY STATEMENT

The original contributions generated for this study are included in the article/**Supplementary Material**, further inquiries can be directed to the corresponding author.

AUTHOR CONTRIBUTIONS

TU and AS conceived and designed the experiments and prepared the manuscript. TU performed the experiments. Both authors contributed to the article and approved the submitted version.

FUNDING

This work was supported by a Grant-in-Aid from the JSPS KAKENHI Grant Numbers 22125001, 22125002, 15H05973, 16H04742, and 19H00981 to AS and 21770006 and 26440189 to TU.

ACKNOWLEDGMENTS

We thank Dr. John Petrini for the antibodies and strains. We are also indebted to the members of the Shinohara laboratory for the stimulating discussions.

SUPPLEMENTARY MATERIAL

The Supplementary Material for this article can be found online at: https://www.frontiersin.org/articles/10.3389/fcell.2021.635383/full#supplementary-material

Supplementary Figure 1 | H3K79me is required for Rad9-dependent Rad53 activation in meiosis after phleomycin treatment. **(A)** TCA-precipitated cell extracts from meiotic cells were prepared from wild-type (USY543/544), *dot1* (USY526/527), and *h3-K79R* (USY693/677) diploid strains, and were analyzed by western blotting using anti-Rad9, anti-Flag (for Rad53), anti-Histone H3K79-tri-methyl and anti-tubulin antibodies. "^{32}P-Rad53" represented ^{32}P-incorporation to Rad53 in the ISA assay. Cell extracts derived from 4×10^6 cells were loaded for the ISA assay. Cell extracts were prepared at indicated time points after the treatment of 3.5-h meiotic cells with 5 μg/mL of phleomycin. **(B)** Diploid cells of the indicated strains were arrested at G2/M by nocodazole and treated with 5 μg/mL of phleomycin for 30 min, followed by TCA precipitation. Wild-type (USY543/544), *rad9* (USY524/525), *dot1* (USY526/527), and *dot1 rad9* (USY522/523) were used in the experiment.

Supplementary Figure 2 | Ddc2-Rad9 fusions activate Rad53 in meiosis. **(A)** Cells in meiotic time course at indicated times were collected and TCA-precipitated meiotic cell extracts were analyzed by western blotting using anti-Flag, and anti–α-tubulin antibodies. Wild-type (USY543/544), *DDC2-RAD9* (USY544/661), *DDC2-rad9-7A* (USY544/667), and *DDC2-RAD9 rad53-KD* (USY545/720) were examined. **(B)** Cell extracts were prepared from the strains and analyzed by western blotting using anti-HA, anti-Flag and anti–α-tubulin antibodies; *DDC2-RAD9* (USY544/661), *DDC2-RAD9 rad53-KD* (USY545/720), 3x HA-tagged Rad9 (USY544/661; *OE-HA-RAD9*) from the *DMC1* promoter, and *DDC2-RAD9 spo11 rad53-KD* (USY545/720). **(C)** Cell extracts were prepared from the strains and analyzed by western blotting using anti-HA, anti-Flag, anti-histone H3K79-tri-methyl and anti–α-tubulin antibodies; Wild-type (USY543/544), *DDC2-RAD9* (USY544/661), *DDC2-rad9-Y798A* (USY544/776), *DDC2-RAD9 dot1* (USY768/526), and *DDC2-RAD9 h3-K79R* (USY770/693). **(D)** Cell extracts at 0, 3, and 4 h time points were prepared from the strains and analyzed by western blotting using anti-HA, anti-Flag, and anti–α-tubulin antibodies and also by ISA (third panel); Wild-type (USY543/544), *DDC2-RAD9* (USY544/661) and *DDC2-rad9-7A* (USY510/512). Cell extracts derived from 4×10^6 cells were loaded for the ISA assay.

Supplementary Figure 3 | Ddc2-Rad9 fusions activate Rad53 in *dmc1* meiosis. **(A)** Cell extracts at 0, 3, and 4.5 h time points of meiosis were prepared from the *dmc1*strains and analyzed by western blotting using anti-Flag and by ISA assay. Results from two independent time course are shown. Cell extracts derived from 4×10^6 cells were loaded for the ISA assay. HA-Rad9 and Ddc1-HA-Rad9 protein were expressed from the *DMC1* promoter. *HA-RAD9 dmc1* (USY528/529), *DDC2-RAD9 dmc1* (USY528/529), and *DDC2-RAD9 dmc1 rad53-KD* (USY508/509). **(B)** Cell extracts at 0, 3, and 4.5 h time points of meiosis of the *dmc1* mutant were prepared from the strains and analyzed by western blotting using anti-HA and anti-Flag, and by ISA assay. *HA-RAD9 dmc1* (USY528/529), *DDC2-RAD9 dmc1* (USY528/529), and *DDC2-RAD9 dmc1 mec1* (USY458/459).

(C,D) Cell extracts at 0, 1.5, 3, and 4.5 h time points of meiosis of the *dmc1* mutant were prepared from the strains and analyzed by western blotting using anti-HA and anti-Flag, and by ISA assay. **(C)** *DDC2-RAD9 dmc1* (USY528/529), and *DDC2-RAD9 dmc1 mec1* (USY458/459) and *DDC2-RAD9 dmc1 spo11* (USY514/515); **(D)** *HA-RAD9 dmc1* (USY528/529), *DDC2-RAD9 dmc1* (USY528/529), and *DDC2-RAD9 dmc1 rad53-KD* (USY508/509).

Supplementary Figure 4 | TCA-precipitated extracts prepared from cells expressing Ddc2-3xHA (USY8384) or 3xHA-Rad9 (USY2035) from their native promoter and the indicated dilutions of *DDC2-RAD9* (USY544/671) and *HA-RAD9-OE* (USY544/561) extracts were examined. All cell extracts were prepared from 4 h meiotic cells. Cell extracts derived from 1×10^7 or 4×10^6 cells were loaded for anti-HA or anti-Flag/tubulin Western blot, respectively. Dilutions were prepared accordingly.

Supplementary Figure 5 | The representative images of immunostaining of nuclear spreads prepared from *dmc1 RAD53 DDC2-RAD9* (USY580/591) at 6 h and *dmc1 rad53-KD DDC2-RAD9* (USY582/623) at 4.5 h in meiosis are shown with anti-HA and anti-Rad51. DNA images stained with DAPI are also presented. Bar equals 5 μm.

Supplementary Figure 6 | (A) DNA contents of wild type (USY543/544) and *DDC2-RAD9* (USY544/671) strains were examined by FACS analysis. The representative profiles were shown. **(B)** The percentage of nuclei of the indicated strains that had more than five Rad51 or Dmc1 foci was plotted each time point.

REFERENCES

Allen, J. B., Zhou, Z., Siede, W., Friedberg, E. C., and Elledge, S. J. (1994). The SAD1/RAD53 protein kinase controls multiple checkpoints and DNA damage-induced transcription in yeast. *Genes Dev.* 8, 2401–2415.

Allers, T., and Lichten, M. (2001a). Differential timing and control of noncrossover and crossover recombination during meiosis. *Cell* 106, 47–57.

Allers, T., and Lichten, M. (2001b). Intermediates of yeast meiotic recombination contain heteroduplex DNA. *Mol. Cell* 8, 225–231.

Alt, F. W., Zhang, Y., Meng, F. L., Guo, C., and Schwer, B. (2013). Mechanisms of programmed DNA lesions and genomic instability in the immune system. *Cell* 152, 417–429. doi: 10.1016/j.cell.2013.01.007

Bani Ismail, M., Shinohara, M., and Shinohara, A. (2014). Dot1-dependent histone H3K79 methylation promotes meiotic double-strand break formation in the absence of histone H3K4 methylation in budding yeast. *PLoS One* 9:e96648. doi: 10.1371/journal.pone.0096648

Barlow, A. L., Benson, F. E., West, S. C., and Hulten, M. A. (1997). Distribution of the Rad51 recombinase in human and mouse spermatocytes. *EMBO J.* 16, 5207–5215. doi: 10.1093/emboj/16.17.5207

Bergerat, A., de Massy, B., Gadelle, D., Varoutas, P. C., Nicolas, A., and Forterre, P. (1997). An atypical topoisomerase II from Archaea with implications for meiotic recombination. *Nature* 386, 414–417. doi: 10.1038/386414a0

Bishop, D. K. (1994). RecA homologs Dmc1 and Rad51 interact to form multiple nuclear complexes prior to meiotic chromosome synapsis. *Cell* 79, 1081–1092.

Bishop, D. K., Park, D., Xu, L., and Kleckner, N. (1992). DMC1: a meiosis-specific yeast homolog of E. coli recA required for recombination, synaptonemal complex formation, and cell cycle progression. *Cell* 69, 439–456.

Bishop, D. K., and Zickler, D. (2004). Early decision; meiotic crossover interference prior to stable strand exchange and synapsis. *Cell* 117, 9–15.

Bonilla, C. Y., Melo, J. A., and Toczyski, D. P. (2008). Colocalization of sensors is sufficient to activate the DNA damage checkpoint in the absence of damage. *Mol. Cell* 30, 267–276. doi: 10.1016/j.molcel.2008.03.023

Borner, G. V., Kleckner, N., and Hunter, N. (2004). Crossover/noncrossover differentiation, synaptonemal complex formation, and regulatory surveillance at the leptotene/zygotene transition of meiosis. *Cell* 117, 29–45.

Botuyan, M. V., Lee, J., Ward, I. M., Kim, J. E., Thompson, J. R., Chen, J., et al. (2006). Structural basis for the methylation state-specific recognition of histone H4-K20 by 53BP1 and Crb2 in DNA repair. *Cell* 127, 1361–1373. doi: 10.1016/j.cell.2006.10.043

Buhler, C., Borde, V., and Lichten, M. (2007). Mapping meiotic single-strand DNA reveals a new landscape of DNA double-strand breaks in *Saccharomyces cerevisiae*. *PLoS Biol.* 5:e324. doi: 10.1371/journal.pbio.0050324

Bzymek, M., Thayer, N. H., Oh, S. D., Kleckner, N., and Hunter, N. (2010). Double Holliday junctions are intermediates of DNA break repair. *Nature* 464, 937–941. doi: 10.1038/nature08868

Cao, L., Alani, E., and Kleckner, N. (1990). A pathway for generation and processing of double-strand breaks during meiotic recombination in *S. cerevisiae*. *Cell* 61, 1089–1101.

Carballo, J. A., Johnson, A. L., Sedgwick, S. G., and Cha, R. S. (2008). Phosphorylation of the axial element protein Hop1 by Mec1/Tel1 ensures meiotic interhomolog recombination. *Cell* 132, 758–770. doi: 10.1016/j.cell.2008.01.035

Cartagena-Lirola, H., Guerini, I., Manfrini, N., Lucchini, G., and Longhese, M. P. (2008). Role of the *Saccharomyces cerevisiae* Rad53 checkpoint kinase in signaling double-strand breaks during the meiotic cell cycle. *Mol. Cell Biol.* 28, 4480–4493. doi: 10.1128/MCB.00375-08

di Cicco, G., Bantele, S. C. S., Reusswig, K. U., and Pfander, B. (2017). A cell cycle-independent mode of the Rad9-Dpb11 interaction is induced by DNA damage. *Sci. Rep.* 7:11650. doi: 10.1038/s41598-017-11937-z

Eichinger, C. S., and Jentsch, S. (2010). Synaptonemal complex formation and meiotic checkpoint signaling are linked to the lateral element protein Red1. *Proc. Natl. Acad. Sci. U.S.A.* 107, 11370–11375. doi: 10.1073/pnas.1004248107

Fradet-Turcotte, A., Canny, M. D., Escribano-Diaz, C., Orthwein, A., Leung, C. C., Huang, H., et al. (2013). 53BP1 is a reader of the DNA-damage-induced H2A Lys 15 ubiquitin mark. *Nature* 499, 50–54. doi: 10.1038/nature12318

Giannattasio, M., Lazzaro, F., Plevani, P., and Muzi-Falconi, M. (2005). The DNA damage checkpoint response requires histone H2B ubiquitination by Rad6-Bre1 and H3 methylation by Dot1. *J. Biol. Chem.* 280, 9879–9886. doi: 10.1074/jbc.M414453200

Gilbert, C. S., Green, C. M., and Lowndes, N. F. (2001). Budding yeast Rad9 is an ATP-dependent Rad53 activating machine. *Mol. Cell* 8, 129–136.

Granata, M., Lazzaro, F., Novarina, D., Panigada, D., Puddu, F., Abreu, C. M., et al. (2010). Dynamics of Rad9 chromatin binding and checkpoint function are mediated by its dimerization and are cell cycle-regulated by CDK1 activity. *PLoS Genet.* 6:1001047. doi: 10.1371/journal.pgen.1001047

Grenon, M., Costelloe, T., Jimeno, S., O'Shaughnessy, A., Fitzgerald, J., Zgheib, O., et al. (2007). Docking onto chromatin via the *Saccharomyces cerevisiae* Rad9 Tudor domain. *Yeast* 24, 105–119. doi: 10.1002/yea.1441

Haber, J. E. (2012). Mating-type genes and MAT switching in *Saccharomyces cerevisiae*. *Genetics* 191, 33–64. doi: 10.1534/genetics.111.134577

Hammet, A., Magill, C., Heierhorst, J., and Jackson, S. P. (2007). Rad9 BRCT domain interaction with phosphorylated H2AX regulates the G1 checkpoint in budding yeast. *EMBO Rep.* 8, 851–857. doi: 10.1038/sj.embor.7401036

Hayase, A., Takagi, M., Miyazaki, T., Oshiumi, H., Shinohara, M., and Shinohara, A. (2004). A protein complex containing Mei5 and Sae3 promotes the assembly of the meiosis-specific RecA homolog Dmc1. *Cell* 119, 927–940. doi: 10.1016/j.cell.2004.10.031

Hollingsworth, N. M., and Gaglione, R. (2019). The meiotic-specific Mek1 kinase in budding yeast regulates interhomolog recombination and coordinates meiotic progression with double-strand break repair. *Curr. Genet.* 65, 631–641. doi: 10.1007/s00294-019-00937-3

Hunter, N., and Kleckner, N. (2001). The single-end invasion: an asymmetric intermediate at the double-strand break to double-holliday junction transition of meiotic recombination. *Cell* 106, 59–70.

Huyen, Y., Zgheib, O., Ditullio, R. A. Jr., Gorgoulis, V. G., Zacharatos, P., Petty, T. J., et al. (2004). Methylated lysine 79 of histone H3 targets 53BP1 to DNA double-strand breaks. *Nature* 432, 406–411. doi: 10.1038/nature03114

Kadyk, L. C., and Hartwell, L. H. (1992). Sister chromatids are preferred over homologs as substrates for recombinational repair in *Saccharomyces cerevisiae*. *Genetics* 132, 387–402.

Kaiser, C., Michaelis, S., Mitchell, A., and Cold Spring Harbor Laboratory (1994). *Methods in Yeast Genetics: a Cold Spring Harbor Laboratory Course Manual*. Cold Spring Harbor, NY: Cold Spring Harbor Laboratory Press.

Katis, V. L., Lipp, J. J., Imre, R., Bogdanova, A., Okaz, E., Habermann, B., et al. (2010). Rec8 phosphorylation by casein kinase 1 and Cdc7-Dbf4 kinase

regulates cohesin cleavage by separase during meiosis. *Dev. Cell* 18, 397–409. doi: 10.1016/j.devcel.2010.01.014

Kauppi, L., Barchi, M., Baudat, F., Romanienko, P. J., Keeney, S., and Jasin, M. (2011). Distinct properties of the XY pseudoautosomal region crucial for male meiosis. *Science* 331, 916–920. doi: 10.1126/science.1195774

Keeney, S., Giroux, C. N., and Kleckner, N. (1997). Meiosis-specific DNA double-strand breaks are catalyzed by Spo11, a member of a widely conserved protein family. *Cell* 88, 375–384.

Lee, S. E., Moore, J. K., Holmes, A., Umezu, K., Kolodner, R. D., and Haber, J. E. (1998). Saccharomyces Ku70, mre11/rad50 and RPA proteins regulate adaptation to G2/M arrest after DNA damage. *Cell* 94, 399–409.

Lee, S. J., Duong, J. K., and Stern, D. F. (2004). A Ddc2-Rad53 fusion protein can bypass the requirements for RAD9 and MRC1 in Rad53 activation. *Mol. Biol. Cell* 15, 5443–5455. doi: 10.1091/mbc.E04-07-0608

Lo, H. C., Wan, L., Rosebrock, A., Futcher, B., and Hollingsworth, N. M. (2008). Cdc7-Dbf4 regulates NDT80 transcription as well as reductional segregation during budding yeast meiosis. *Mol. Biol. Cell* 19, 4956–4967. doi: 10.1091/mbc.E08-07-0755

Longtine, M. S., McKenzie, A. III, Demarini, D. J., Shah, N. G., Wach, A., Brachat, A., et al. (1998). Additional modules for versatile and economical PCR-based gene deletion and modification in *Saccharomyces cerevisiae*. *Yeast* 14, 953–961.

Lopez-Mosqueda, J., Maas, N. L., Jonsson, Z. O., Defazio-Eli, L. G., Wohlschlegel, J., and Toczyski, D. P. (2010). Damage-induced phosphorylation of Sld3 is important to block late origin firing. *Nature* 467, 479–483. doi: 10.1038/nature09377

Lydall, D., Nikolsky, Y., Bishop, D. K., and Weinert, T. (1996). A meiotic recombination checkpoint controlled by mitotic checkpoint genes. *Nature* 383, 840–843. doi: 10.1038/383840a0

Mailand, N., Bekker-Jensen, S., Faustrup, H., Melander, F., Bartek, J., Lukas, C., et al. (2007). RNF8 ubiquitylates histones at DNA double-strand breaks and promotes assembly of repair proteins. *Cell* 131, 887–900. doi: 10.1016/j.cell.2007.09.040

Matos, J., Lipp, J. J., Bogdanova, A., Guillot, S., Okaz, E., Junqueira, M., et al. (2008). Dbf4-dependent CDC7 kinase links DNA replication to the segregation of homologous chromosomes in meiosis I. *Cell* 135, 662–678. doi: 10.1016/j.cell.2008.10.026

Melo, J. A., Cohen, J., and Toczyski, D. P. (2001). Two checkpoint complexes are independently recruited to sites of DNA damage in vivo. *Genes Dev.* 15, 2809–2821. doi: 10.1101/gad.903501

Nakada, D., Matsumoto, K., and Sugimoto, K. (2003). ATM-related Tel1 associates with double-strand breaks through an Xrs2-dependent mechanism. *Genes Dev.* 17, 1957–1962. doi: 10.1101/gad.1099003

Niu, H., Wan, L., Baumgartner, B., Schaefer, D., Loidl, J., and Hollingsworth, N. M. (2005). Partner choice during meiosis is regulated by Hop1-promoted dimerization of Mek1. *Mol. Biol. Cell* 16, 5804–5818. doi: 10.1091/mbc.e05-05-0465

Nyberg, K. A., Michelson, R. J., Putnam, C. W., and Weinert, T. A. (2002). Toward maintaining the genome: DNA damage and replication checkpoints. *Annu. Rev. Genet.* 36, 617–656. doi: 10.1146/annurev.genet.36.060402.113540

Okaz, E., Arguello-Miranda, O., Bogdanova, A., Vinod, P. K., Lipp, J. J., Markova, Z., et al. (2012). Meiotic prophase requires proteolysis of M phase regulators mediated by the meiosis-specific APC/CAma1. *Cell* 151, 603–618. doi: 10.1016/j.cell.2012.08.044

Ontoso, D., Acosta, I., van Leeuwen, F., Freire, R., and San-Segundo, P. A. (2013). Dot1-dependent histone H3K79 methylation promotes activation of the Mek1 meiotic checkpoint effector kinase by regulating the Hop1 adaptor. *PLoS Genet.* 9:e1003262. doi: 10.1371/journal.pgen.1003262

Paciotti, V., Clerici, M., Lucchini, G., and Longhese, M. P. (2000). The checkpoint protein Ddc2, functionally related to S. pombe Rad26, interacts with Mec1 and is regulated by Mec1-dependent phosphorylation in budding yeast. *Genes Dev.* 14, 2046–2059.

Pan, J., Sasaki, M., Kniewel, R., Murakami, H., Blitzblau, H. G., Tischfield, S. E., et al. (2011). A hierarchical combination of factors shapes the genome-wide topography of yeast meiotic recombination initiation. *Cell* 144, 719–731. doi: 10.1016/j.cell.2011.02.009

Pellicioli, A., and Foiani, M. (2005). Signal transduction: how rad53 kinase is activated. *Curr. Biol.* 15, R769–R771. doi: 10.1016/j.cub.2005.08.057

Pellicioli, A., Lee, S. E., Lucca, C., Foiani, M., and Haber, J. E. (2001). Regulation of *Saccharomyces* Rad53 checkpoint kinase during adaptation from DNA damage-induced G2/M arrest. *Mol. Cell* 7, 293–300.

Pellicioli, A., Lucca, C., Liberi, G., Marini, F., Lopes, M., Plevani, P., et al. (1999). Activation of Rad53 kinase in response to DNA damage and its effect in modulating phosphorylation of the lagging strand DNA polymerase. *EMBO J.* 18, 6561–6572. doi: 10.1093/emboj/18.22.6561

Pfander, B., and Diffley, J. F. (2011). Dpb11 coordinates Mec1 kinase activation with cell cycle-regulated Rad9 recruitment. *EMBO J.* 30, 4897–4907. doi: 10.1038/emboj.2011.345

Puddu, F., Piergiovanni, G., Plevani, P., and Muzi-Falconi, M. (2011). Sensing of replication stress and Mec1 activation act through two independent pathways involving the 9-1-1 complex and DNA polymerase ε. *PLoS Genet.* 7:e1002022. doi: 10.1371/journal.pgen.1002022

Refolio, E., Cavero, S., Marcon, E., Freire, R., and San-Segundo, P. A. (2011). The Ddc2/ATRIP checkpoint protein monitors meiotic recombination intermediates. *J. Cell Sci.* 124(Pt 14), 2488–2500. doi: 10.1242/jcs.081711

Sanchez, Y., Desany, B. A., Jones, W. J., Liu, Q., Wang, B., and Elledge, S. J. (1996). Regulation of RAD53 by the ATM-like kinases MEC1 and TEL1 in yeast cell cycle checkpoint pathways. *Science* 271, 357–360.

Sasanuma, H., Hirota, K., Fukuda, T., Kakusho, N., Kugou, K., Kawasaki, Y., et al. (2008). Cdc7-dependent phosphorylation of Mer2 facilitates initiation of yeast meiotic recombination. *Genes Dev.* 22, 398–410. doi: 10.1101/gad.1626608

Schwacha, A., and Kleckner, N. (1995). Identification of double Holliday junctions as intermediates in meiotic recombination. *Cell* 83, 783–791.

Schwacha, A., and Kleckner, N. (1997). Interhomolog bias during meiotic recombination: meiotic functions promote a highly differentiated interhomolog-only pathway. *Cell* 90, 1123–1135.

Schwartz, M. F., Duong, J. K., Sun, Z., Morrow, J. S., Pradhan, D., and Stern, D. F. (2002). Rad9 phosphorylation sites couple Rad53 to the *Saccharomyces cerevisiae* DNA damage checkpoint. *Mol. Cell* 9, 1055–1065.

Shinohara, A., Gasior, S., Ogawa, T., Kleckner, N., and Bishop, D. K. (1997). *Saccharomyces cerevisiae* recA homologues RAD51 and DMC1 have both distinct and overlapping roles in meiotic recombination. *Genes Cells* 2, 615–629.

Shinohara, A., Ogawa, H., and Ogawa, T. (1992). Rad51 protein involved in repair and recombination in *S. cerevisiae* is a RecA-like protein. *Cell* 69, 457–470.

Shinohara, M., Gasior, S. L., Bishop, D. K., and Shinohara, A. (2000). Tid1/Rdh54 promotes colocalization of rad51 and dmc1 during meiotic recombination. *Proc. Natl. Acad. Sci. U.S.A.* 97, 10814–10819.

Shinohara, M., Hayashihara, K., Grubb, J. T., Bishop, D. K., and Shinohara, A. (2015). DNA damage response clamp 9-1-1 promotes assembly of ZMM proteins for formation of crossovers and synaptonemal complex. *J. Cell Sci.* 128, 1494–1506. doi: 10.1242/jcs.161554

Shinohara, M., Oh, S. D., Hunter, N., and Shinohara, A. (2008). Crossover assurance and crossover interference are distinctly regulated by the ZMM proteins during yeast meiosis. *Nat. Genet.* 40, 299–309. doi: 10.1038/ng.83

Shinohara, M., Sakai, K., Ogawa, T., and Shinohara, A. (2003). The mitotic DNA damage checkpoint proteins Rad17 and Rad24 are required for repair of double-strand breaks during meiosis in yeast. *Genetics* 164, 855–865.

Shroff, R., Arbel-Eden, A., Pilch, D., Ira, G., Bonner, W. M., Petrini, J. H., et al. (2004). Distribution and dynamics of chromatin modification induced by a defined DNA double-strand break. *Curr. Biol.* 14, 1703–1711.

Stewart, G. S., Panier, S., Townsend, K., Al-Hakim, A. K., Kolas, N. K., Miller, E. S., et al. (2009). The RIDDLE syndrome protein mediates a ubiquitin-dependent signaling cascade at sites of DNA damage. *Cell* 136, 420–434. doi: 10.1016/j.cell.2008.12.042

Storlazzi, A., Xu, L., Cao, L., and Kleckner, N. (1995). Crossover and noncrossover recombination during meiosis: timing and pathway relationships. *Proc. Natl. Acad. Sci. U.S.A.* 92, 8512–8516.

Sun, Z., Fay, D. S., Marini, F., Foiani, M., and Stern, D. F. (1996). Spk1/Rad53 is regulated by Mec1-dependent protein phosphorylation in DNA replication and damage checkpoint pathways. *Genes Dev.* 10, 395–406.

Sun, Z., Hsiao, J., Fay, D. S., and Stern, D. F. (1998). Rad53 FHA domain associated with phosphorylated Rad9 in the DNA damage checkpoint. *Science* 281, 272–274.

Sweeney, F. D., Yang, F., Chi, A., Shabanowitz, J., Hunt, D. F., and Durocher, D. (2005). *Saccharomyces cerevisiae* Rad9 acts as a Mec1 adaptor to allow Rad53 activation. *Curr. Biol.* 15, 1364–1375. doi: 10.1016/j.cub.2005.06.063

Sym, M., Engebrecht, J. A., and Roeder, G. S. (1993). ZIP1 is a synaptonemal complex protein required for meiotic chromosome synapsis. *Cell* 72, 365–378.

Terasawa, M., Shinohara, A., Hotta, Y., Ogawa, H., and Ogawa, T. (1995). Localization of RecA-like recombination proteins on chromosomes of the lily at various meiotic stages. *Genes Dev.* 9, 925–934.

Toh, G. W., O'Shaughnessy, A. M., Jimeno, S., Dobbie, I. M., Grenon, M., Maffini, S., et al. (2006). Histone H2A phosphorylation and H3 methylation are required for a novel Rad9 DSB repair function following checkpoint activation. *DNA Repair.* 5, 693–703. doi: 10.1016/j.dnarep.2006.03.005

Usui, T., Foster, S. S., and Petrini, J. H. (2009). Maintenance of the DNA-damage checkpoint requires DNA-damage-induced mediator protein oligomerization. *Mol. Cell* 33, 147–159. doi: 10.1016/j.molcel.2008.12.022

Usui, T., and Kanehara, Y. (2013). Elevated Rad53 kinase activity influences formation and interhomolog repair of meiotic DNA double-strand breaks in budding yeast. *Biochem. Biophys. Res. Commun.* 441, 593–599. doi: 10.1016/j.bbrc.2013.10.111

Usui, T., and Petrini, J. H. (2007). The *Saccharomyces cerevisiae* 14-3-3 proteins Bmh1 and Bmh2 directly influence the DNA damage-dependent functions of Rad53. *Proc. Natl. Acad. Sci. U.S.A.* 104, 2797–2802. doi: 10.1073/pnas.0611259104

Vialard, J. E., Gilbert, C. S., Green, C. M., and Lowndes, N. F. (1998). The budding yeast Rad9 checkpoint protein is subjected to Mec1/Tel1-dependent hyperphosphorylation and interacts with Rad53 after DNA damage. *EMBO J.* 17, 5679–5688. doi: 10.1093/emboj/17.19.5679

Wysocki, R., Javaheri, A., Allard, S., Sha, F., Cote, J., and Kron, S. J. (2005). Role of Dot1-dependent histone H3 methylation in G1 and S phase DNA damage checkpoint functions of Rad9. *Mol. Cell Biol.* 25, 8430–8443. doi: 10.1128/MCB.25.19.8430-8443.2005

Zegerman, P., and Diffley, J. F. (2010). Checkpoint-dependent inhibition of DNA replication initiation by Sld3 and Dbf4 phosphorylation. *Nature* 467, 474–478. doi: 10.1038/nature09373

Zhang, L., Ma, H., and Pugh, B. F. (2011). Stable and dynamic nucleosome states during a meiotic developmental process. *Genome Res.* 21, 875–884. doi: 10.1101/gr.117465.110

Zhao, X., Muller, E. G., and Rothstein, R. (1998). A suppressor of two essential checkpoint genes identifies a novel protein that negatively affects dNTP pools. *Mol. Cell* 2, 329–340.

Zou, L., and Elledge, S. J. (2003). Sensing DNA damage through ATRIP recognition of RPA-ssDNA complexes. *Science* 300, 1542–1548. doi: 10.1126/science.1083430

Conflict of Interest: The authors declare that the research was conducted in the absence of any commercial or financial relationships that could be construed as a potential conflict of interest.

Copyright © 2021 Usui and Shinohara. This is an open-access article distributed under the terms of the Creative Commons Attribution License (CC BY). The use, distribution or reproduction in other forums is permitted, provided the original author(s) and the copyright owner(s) are credited and that the original publication in this journal is cited, in accordance with accepted academic practice. No use, distribution or reproduction is permitted which does not comply with these terms.

frontiers in Cell and Developmental Biology

ORIGINAL RESEARCH
published: 26 March 2021
doi: 10.3389/fcell.2021.664377

Sycp1 Is Not Required for Subtelomeric DNA Double-Strand Breaks but Is Required for Homologous Alignment in Zebrafish Spermatocytes

*Yukiko Imai[1], Kenji Saito[1], Kazumasa Takemoto[1], Fabien Velilla[1], Toshihiro Kawasaki[1,2], Kei-ichiro Ishiguro[3] and Noriyoshi Sakai[1,2]**

[1] Department of Gene Function and Phenomics, National Institute of Genetics, Mishima, Japan, [2] Department of Genetics, School of Life Sciences, SOKENDAI (The Graduate University for Advanced Studies), Mishima, Japan, [3] Department of Chromosome Biology, Institute of Molecular Embryology and Genetics, Kumamoto University, Kumamoto, Japan

In meiotic prophase I, homologous chromosomes are bound together by the synaptonemal complex, in which two axial elements are connected by transverse filaments and central element proteins. In human and zebrafish spermatocytes, homologous recombination and assembly of the synaptonemal complex initiate predominantly near telomeres. In mice, synapsis is not required for meiotic double-strand breaks (DSBs) and homolog alignment but is required for DSB repair; however, the interplay of these meiotic events in the context of peritelomeric bias remains unclear. In this study, we identified a premature stop mutation in the zebrafish gene encoding the transverse filament protein Sycp1. In *sycp1* mutant zebrafish spermatocytes, axial elements were formed and paired at chromosome ends between homologs during early to mid-zygonema. However, they did not synapse, and their associations were mostly lost in late zygotene- or pachytene-like stages. In *sycp1* mutant spermatocytes, γH2AX signals were observed, and Dmc1/Rad51 and RPA signals appeared predominantly near telomeres, resembling wild-type phenotypes. We observed persistent localization of Hormad1 along the axis in *sycp1* mutant spermatocytes, while the majority of Iho1 signals appeared and disappeared with kinetics similar to those in wild-type spermatocytes. Notably, persistent Iho1 foci were observed in *spo11* mutant spermatocytes, suggesting that Iho1 dissociation from axes occurs in a DSB-dependent manner. Our results demonstrated that Sycp1 is not required for peritelomeric DSB formation but is necessary for complete pairing of homologs in zebrafish meiosis.

Keywords: Sycp1, meiosis, recombination, zebrafish, synapsis, synaptonemal complex

OPEN ACCESS

Edited by:
Akira Shinohara,
Osaka University, Japan

Reviewed by:
Jibak Lee,
Kobe University, Japan
Xin Zhiguo Li,
University of Rochester, United States

***Correspondence:**
Noriyoshi Sakai
nosakai@nig.ac.jp

Specialty section:
This article was submitted to Cell Growth and Division, a section of the journal Frontiers in Cell and Developmental Biology

Received: *05 February 2021*
Accepted: *09 March 2021*
Published: *26 March 2021*

Citation:
Imai Y, Saito K, Takemoto K, Velilla F, Kawasaki T, Ishiguro K and Sakai N (2021) Sycp1 Is Not Required for Subtelomeric DNA Double-Strand Breaks but Is Required for Homologous Alignment in Zebrafish Spermatocytes. Front. Cell Dev. Biol. 9:664377. doi: 10.3389/fcell.2021.664377

INTRODUCTION

During meiosis, homologous chromosomes (homologs) undergo recombination that generates reciprocal DNA exchanges called crossovers. Since crossovers provide physical connections between homologs, meiotic recombination is essential for faithful segregation of chromosomes in most organisms (Hunter, 2015). This recombination is initiated in meiotic prophase I by the

programmed formation of DNA double-strand breaks (DSBs) that are repaired to ensure at least one crossover per homolog pair (Bolcun-Filas and Schimenti, 2012).

Meiotic recombination occurs in the context of a meiosis-specific loop-axis chromatin structure, where arrays of chromatin loops are tethered to a proteinaceous axis (Zickler and Kleckner, 2015). After DSB formation, homologous chromosomes are synapsed along the axis structure (axial element, AE) through the formation of the synaptonemal complex (SC). In the SC, two AEs (now called lateral elements, LEs) spanning the ∼100 nm distance are connected at the central region (CR), which comprises transverse filaments attached within the central element (CE) (Zickler and Kleckner, 2015). The tripartite structure of the SC is largely conserved among eukaryotes, while the amino acid sequences of individual components vary among organisms (Westergaard and von Wettstein, 1972; Grishaeva and Bogdanov, 2014). In mammals, eight SC components have been identified: AE proteins SYCP2 and SYCP3, the transverse filament (TF) protein SYCP1 (Meuwissen et al., 1992), and CE proteins SYCE1, SYCE2, SYCE3, SIX6OS1, and TEX12 (Costa et al., 2005; Hamer et al., 2006; Schramm et al., 2011; Gómez-H et al., 2016). SYCP1 is the main structural element of TFs and self-assembles into a supramolecular zipper-like lattice that mediates synapsis (Schramm et al., 2011; Dunce et al., 2018). The SC is thought to serve as a scaffold for recombination because most of the proteins required for DSB formation and repair localize to it (Baudat et al., 2013).

Meiotic DSB formation is catalyzed by the meiosis-specific endonuclease SPO11, which is widely conserved across eukaryotic lineages (Bergerat et al., 1997; Keeney et al., 1997; Malik et al., 2007), with the help of SPO11 accessory proteins reviewed in de Massy (2013). In mice, REC114, MEI4, IHO1, MEI1, and TOPO6BL, as well as SPO11, are essential for meiotic DSB formation (Keeney et al., 1997; Kumar et al., 2010, 2018, 2; Robert et al., 2016; Stanzione et al., 2016). IHO1 interacts with the axis-associated protein HORMAD1 and recruits REC114 and MEI4 onto axes (Stanzione et al., 2016; Kumar et al., 2018). These proteins are known to be excluded from synapsed axes, and HORMAD1 depletion is dependent on synapsis and the AAA-ATPase TRIP13 (Wojtasz et al., 2009; Kumar et al., 2010, 2018; Stanzione et al., 2016). Thus, synapses could be potentially involved in the regulation of DSB formation by removing DSB-promoting proteins, although the role of SCs remains largely unknown.

In mice, SYCP1 and all CE proteins are crucial for meiotic recombination as well as SC assembly, since their individual knockout leads to meiotic arrest with DSB repair defects (de Vries et al., 2005; Bolcun-Filas et al., 2007, 2009; Hamer et al., 2008; Schramm et al., 2011; Gómez-H et al., 2016). For example, in *Sycp1* knockout mice, AEs assemble normally and align homologously but do not synapse (de Vries et al., 2005). In *Sycp1*$^{-/-}$ mouse spermatocytes, γH2AX (the phosphorylated form of histone H2AX that appears in response to DSBs) appears normal in leptonema but remains in a number of discrete domains in pachynema; foci of RAD51, DMC1, and RPA (single-stranded DNA-binding proteins), as well as MSH4 (a MutS homolog protein stabilizing recombination intermediates), appear similarly as in wild-type spermatocytes but do not all disappear, and MLH1 and MLH3 (factors promoting crossover repair) foci are absent (de Vries et al., 2005). These observations indicate that SYCP1 is not required for the global formation of DSBs and for early recombinase recruitment but is necessary for the efficient repair of DSBs as crossovers in mice.

While meiosis has been studied extensively in mice as a mammalian model, differences in key meiotic features have been observed between humans and mice. In mice, meiotic DSBs visualized by single-stranded DNA-binding proteins (such as DMC1, RAD51, or RPA) are observed as a few hundred foci per nucleus that localize along the entire chromosome at both the cytological and sequence levels (Barlow et al., 1997; Mahadevaiah et al., 2001; Smagulova et al., 2011; Brick et al., 2018; Hinch et al., 2020). This chromosome-scale pattern of DSB distribution is similarly observed in both male and female mice (Brick et al., 2018). In humans, chromosome-scale distributions of DSBs in males are specific and strongly skewed toward telomeres (Pratto et al., 2014). The DSB frequency in human males correlates well with the crossover rate, which is also high in subtelomeric regions (Barlow and Hultén, 1998; Kong et al., 2002; Coop et al., 2008; Khil and Camerini-Otero, 2010; Lu et al., 2012; Wang et al., 2012; Kirkness et al., 2013; Pratto et al., 2014). In addition, SC formation also initiates at subtelomeric regions in human males, while in both male and female mice, it often initiates at multiple sites located along the entire chromosome, excluding centromeres (Bisig et al., 2012; Gruhn et al., 2016). Since reverse genetics approaches are difficult in humans, many features of meiotic recombination in the context of subtelomeric bias remain to be elucidated.

Zebrafish (*Danio rerio*) is an emerging model for studying meiotic recombination and has several characteristics similar to those of humans (Sansam and Pezza, 2015; Blokhina et al., 2019; Takemoto et al., 2020). In zebrafish spermatocytes, meiotic DSBs, crossovers, and initiation of homologous pairing and synapsis are predominantly observed near telomeres (Brown et al., 2005; Pratto et al., 2014; Saito et al., 2014; Blokhina et al., 2019; Takemoto et al., 2020). Thus, zebrafish have great potential for use to uncover the mechanisms underlying the subtelomeric bias of meiotic events, which are less obvious in mice. Both forward and reverse genetic approaches are accessible in zebrafish, and several meiotic mutant lines have been isolated (Feitsma et al., 2007; Rodríguez-Marí et al., 2010; Shive et al., 2010; Saito et al., 2011; Blokhina et al., 2019; Takemoto et al., 2020).

We previously isolated three mutant zebrafish lines generated by N-ethyl-N-nitrosourea (ENU) mutagenesis that present male sterile phenotypes (Saito et al., 2011). In this study, we identified the causal mutation of one of these mutant lines, named *iesada* (*isa*), in the *sycp1* gene. In zebrafish, Sycp1 has been reported to be expressed in early primary oocytes and primary spermatocytes and spermatids at the transcriptional level (Gautier et al., 2013) and in primary oocytes and primary spermatocytes at the protein level (Moens, 2006; Kochakpour and Moens, 2008). While Sycp1 staining patterns on zebrafish chromosome spreads suggest its function in meiotic SC formation (Moens, 2006; Kochakpour and Moens, 2008; Saito et al., 2014; Blokhina et al., 2019; Takemoto et al., 2020), its exact roles have not been verified in zebrafish by

loss-of-function approaches. Therefore, we further analyzed the meiotic phenotypes of this *sycp1* mutant zebrafish to understand Sycp1 functions and the interplay of meiotic events in the context of subtelomeric bias. Our data demonstrated that homologous pairing occurs only transiently at chromosome ends and cannot be formed over entire chromosomes in *sycp1* mutant zebrafish. Furthermore, meiotic DSBs occur predominantly near telomeres even in the absence of Sycp1, and Hormad1 but not Iho1 remains on axes.

RESULTS

A Premature Stop Mutation in *Sycp1* Is Responsible for *isa* Phenotypes

Previously, we reported ENU-induced mutant zebrafish lines associated with defective spermatogenesis (Saito et al., 2011). One of these mutant lines, called *iesada* (*isa*), was characterized by the accumulation of Sycp3-positive cells and a lack of haploid cells, suggesting defects in meiosis I. To identify the mutation responsible for the *isa* phenotypes, we performed screening with SSLP markers and identified a 544-kbp region containing the *sycp1* gene (see section "Materials and Methods," **Supplementary Figure 1**). Since *Sycp1* is known to be essential for the progression of meiotic prophase I in other species (Sym et al., 1993; Zickler and Kleckner, 1999; MacQueen et al., 2002; de Vries et al., 2005; Higgins et al., 2005; Osman et al., 2006; Fraune et al., 2012), we further examined its genomic sequence in *isa* and identified a premature stop mutation at the 1225th base of the coding sequence (A1225T, **Figure 1A**). This mutation, named $sycp1^{isa}$, potentially alters the lysine at position 409 to a stop codon and leads to aberrant Sycp1 protein expression (**Figure 1B**). Therefore, we analyzed the expression of the Sycp1 protein by western blotting, and we detected no Sycp1 protein in $sycp1^{isa/isa}$ testis extract (**Figure 1C**). Next, we carried out complementary tests using a *sycp1* knockout allele generated by CRISPR-Cas9 mutagenesis ($sycp1^{del5}$; see section "Materials and Methods"). The $sycp1^{del5}$ allele harbors a −5 bp frameshift mutation in exon 3 and is predicted to generate a protein of 87 amino-acids, in case of translation. After crossing $sycp1^{isa/+}$ and $sycp1^{del5/+}$ zebrafish, testis histology of $sycp1^{+/+}$, $sycp1^{isa/+}$, $sycp1^{del5/+}$, and $sycp1^{isa/del5}$ siblings was compared to examine whether the $sycp1^{del5}$ mutation can complement the spermatogenic defects caused by the *isa* mutation (**Figure 1D**). Strikingly, an accumulation of spermatocytes with neither spermatids nor spermatozoa was observed in $sycp1^{isa/del5}$ testes (**Figure 1D**; $sycp1^{isa/del5}$). We also observed spermatocysts with irregularly condensed nuclei (**Figure 1D**; broken lines), as observed in $sycp1^{isa/isa}$ and $sycp1^{del5/del5}$ testes (**Supplementary Figure 2**) (Saito et al., 2011). These phenotypes were in clear contrast with those of $sycp1^{+/+}$, $sycp1^{isa/+}$, and $sycp1^{del5/+}$ testes, where spermatids and accumulation of spermatozoa in the lumen of lobules were observed (**Figure 1D**; St and Sz). Therefore, the $sycp1^{del5}$ allele did not complement the *isa* phenotypes. Taken together, we confirmed that the absence of the Sycp1 protein caused by the A1225T non-sense mutation in the *sycp1* gene is responsible for *isa* phenotypes.

Sycp1 Is Required for the Ovarian Development of Zebrafish

We previously observed male-specific infertility among siblings obtained from intercrossing of *isa* heterozygote male and female zebrafish (Saito et al., 2011). This suggests that *sycp1* mutant females are fertile or that all mutants become male, similar to the case for other reported zebrafish mutants with germline defects (Slanchev et al., 2005; Draper et al., 2007; Houwing et al., 2007; Siegfried and Nüsslein-Volhard, 2008; Kamminga et al., 2010; Rodríguez-Marí et al., 2010; Shive et al., 2010; Takemoto et al., 2020). To examine whether females appear among $sycp1^{isa/isa}$ zebrafish, we analyzed the *sycp1* genotypes and sexual phenotypes of male and female offspring obtained from the intercrossing of $sycp1^{+/isa}$ fish (**Figure 2A**). Sexual phenotypes were determined by the morphology of adult gonads (≥4 months post fertilization) after dissection. While we detected male fish in all $sycp1^{+/+}$, $sycp1^{+/isa}$, and $sycp1^{isa/isa}$ fish (77%, 75% and 100% of each genotype, respectively), female fish were found only among $sycp1^{+/+}$ and $sycp1^{+/isa}$ fish (23% and 25% of each genotype, respectively). Since zebrafish sex is genetically determined with limited and secondary influences from the environment (Liew et al., 2012), the sex ratios could vary from 1:1 even in wild-type contexts. This result indicates that all $sycp1^{isa/isa}$ zebrafish developed as males. In zebrafish gametogenesis, all juvenile gonads first generate immature oocytes regardless of their definitive sex, and the individuals in which these immature oocytes degenerate develop as males (Uchida et al., 2002; Maack and Segner, 2003; Rodríguez-Marí et al., 2005). Thus, the absence of females in $sycp1^{isa/isa}$ fish (**Figure 2A**) implies that oocytes were eliminated during gametogenesis, most likely at the juvenile stage. To determine the stages of oocyte degeneration, we compared the histology of $sycp1^{+/+}$ and $sycp1^{isa/isa}$ gonads from 24 to 45 days post fertilization (dpf) (**Figures 2B,C**, **Supplementary Figure 3**). Since differences in environmental conditions affect the development of juvenile fish and lead to variations in zebrafish growth and gonad development (Elkouby and Mullins, 2017), we also measured the body sizes of the sampled fish. Gonads with previtellogenic dictyate (stage IB) (Selman et al., 1993) oocytes were found in both $sycp1^{+/+}$ and $sycp1^{isa/isa}$ fish (**Figure 2B**; images of all analyzed gonads are in **Supplementary Figure 3**). While gonads with oocytes up to ∼40 μm in diameter were found in both $sycp1^{isa/isa}$ and $sycp1^{+/+}$ fish (**Figure 2B**i, iii), gonads with oocytes larger than 40 μm were observed only among $sycp1^{+/+}$ fish (**Figure 2B**ii). In relatively large juvenile $sycp1^{isa/isa}$ fish (body size more than ∼13.5 mm), only gonads with spermatocysts were observed (**Figures 2B**iv, **C**, **Supplementary Figure 3**). These observations support the hypothesis that oocytes appear in juvenile $sycp1^{isa/isa}$ gonads but are lost during stage IB, and all $sycp1^{isa/isa}$ fish develop to males (**Figure 2A**).

Sycp1 Is Not Required for Axis Formation in Zebrafish Spermatocytes

The primary function of mammalian SYCP1 is to connect homologous chromosomal axes as a transverse filament component of the synaptonemal complex (de Vries et al., 2005).

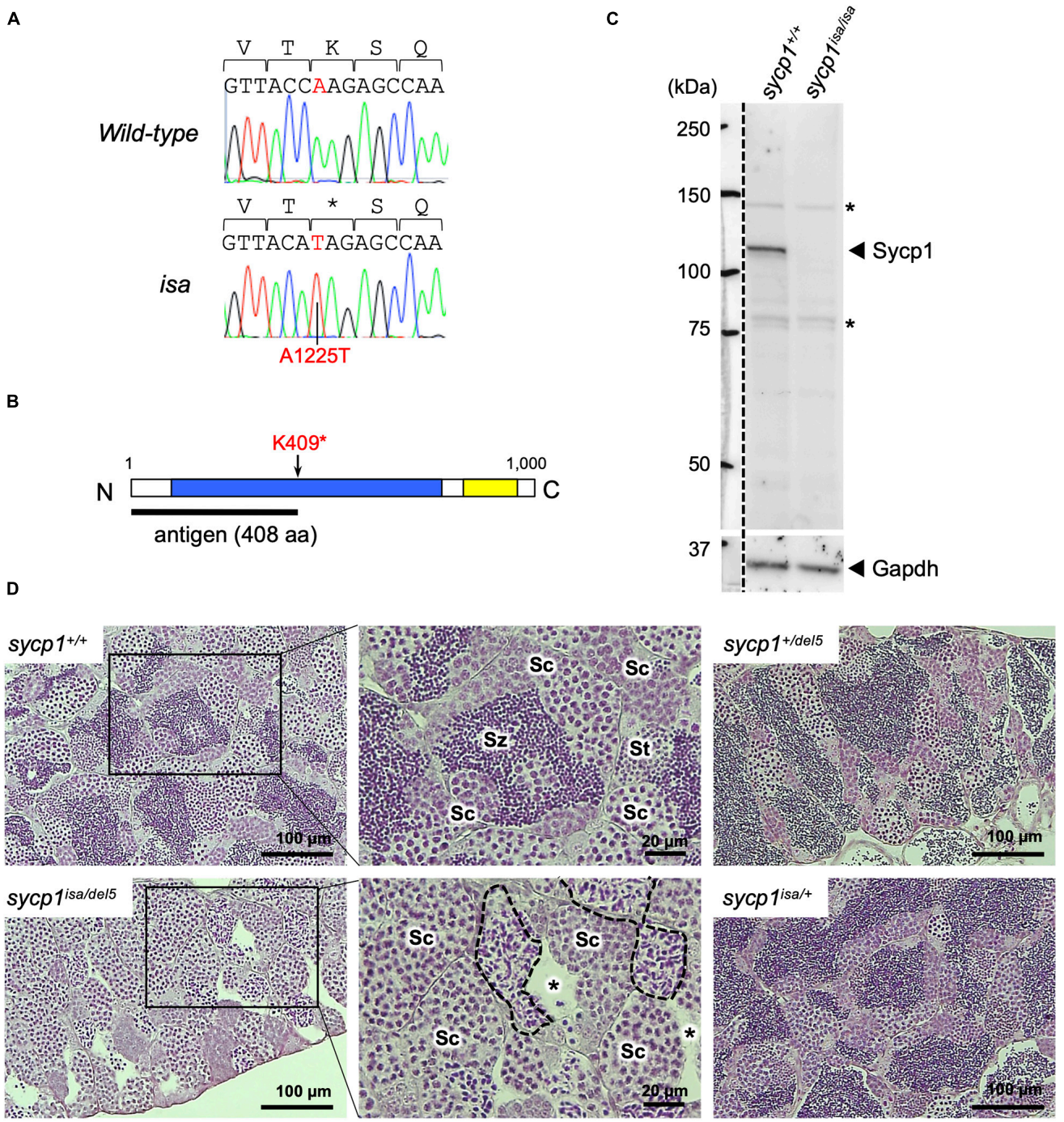

FIGURE 1 | A premature stop mutation of the *sycp1* gene in the *isa* mutant line. **(A)** Genomic sequences of a part of exon 15 in the *sycp1* gene. DNA sequences and peaks obtained from a wild-type and an *isa* mutant fish are shown with corresponding amino acids (above in 1-letter abbreviations). Positions of the *isa* mutation (base 1225 of the *sycp1* coding sequence) are shown in red letters. **(B)** A schematic presentation of the Sycp1 protein sequence. The *isa* mutation site is indicated with an arrow. The antigen region (amino acids 1 to 408) of the Sycp1 antibody used in this study is shown below as a black bar. N: N-terminus, C: C-terminus. Numbers indicate corresponding amino acid positions. **(C)** Western blotting of the Sycp1 protein. Testis protein extracts of wild-type (*sycp1*$^{+/+}$) and *isa* homozygote mutant (*sycp1*$^{isa/isa}$) adult fish were blotted with anti-Sycp1 antibody and anti-Gapdh antibody as an internal control. The left side of the broken line is a part labeled with a molecular ladder on the same membrane. The predicted molecular sizes of full-length Sycp1 and Gapdh proteins are 116 kDa and 35.8 kDa, respectively. Non-specific bands were marked with asterisks (*). **(D)** HE-stained sections of *sycp1*$^{+/+}$, *sycp1*$^{isa/del5}$, *sycp1*$^{isa/+}$ and *sycp1*$^{del5/+}$ testes. All samples were prepared from siblings at 4 mpf (months post fertilization). Representative results of 3 individual fish are shown for each genotype. Magnified images are shown for *sycp1*$^{+/+}$ and *sycp1*$^{isa/del5}$ sections. Sc: spermatocytes, St: spermatids, Sz: spermatozoa. In the *sycp1*$^{isa/del5}$ section, lumens with no spermatozoa (asterisks) and spermatocytes with irregular nuclei (inside broken lines) were observed.

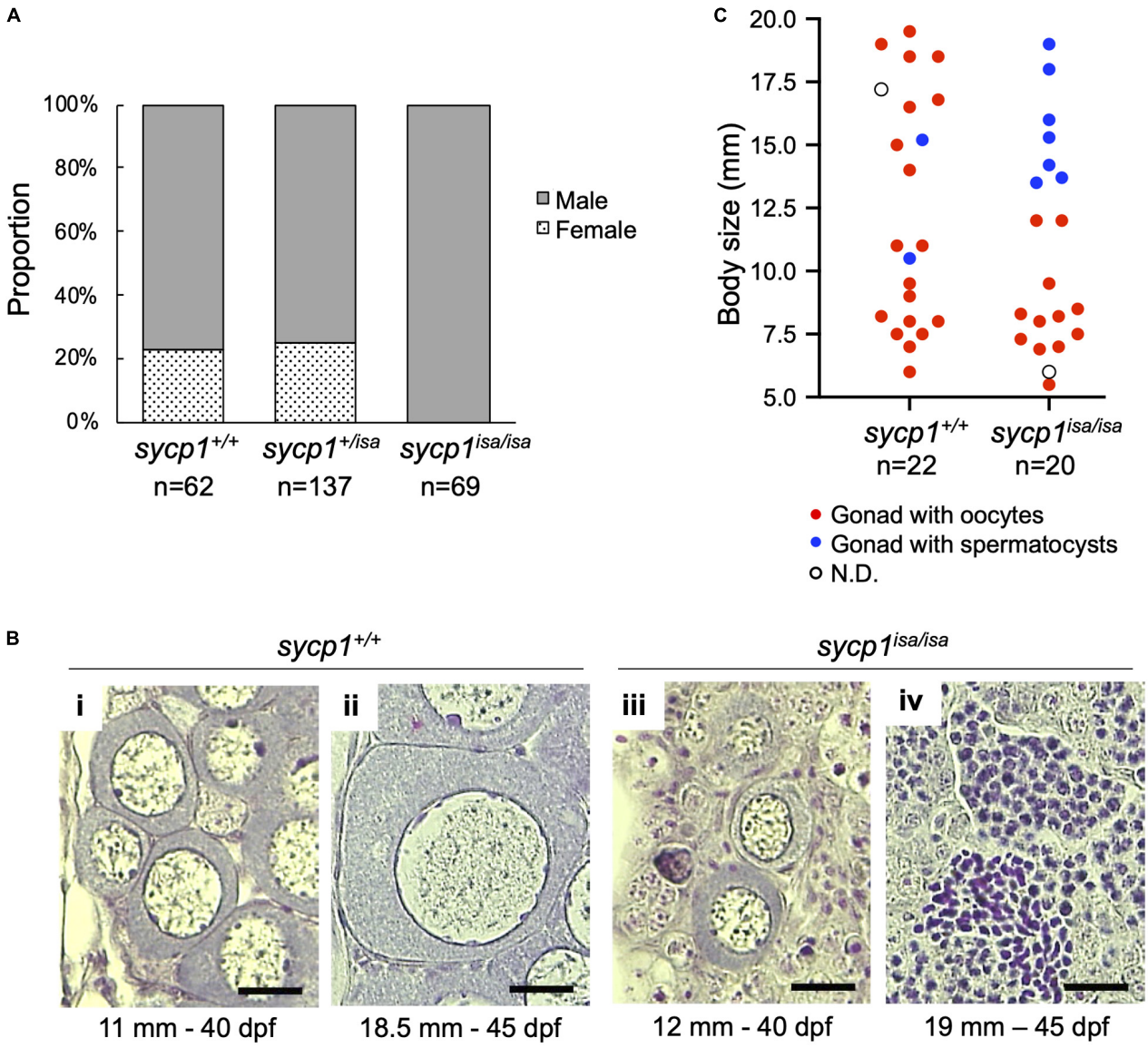

FIGURE 2 | Sexual phenotypes of *sycp1* mutant zebrafish. **(A)** Sexual phenotypes of offspring from *sycp1*$^{+/isa}$ incrosses. Proportions of offspring with testes (males) and ovaries (females) are shown for each genotype. The results of two incross matings were pooled and shown. **(B)** HE-stained sections of juvenile *sycp1*$^{+/+}$ and *sycp1*$^{isa/isa}$ gonads. Representative images of *sycp1*$^{+/+}$ (i and ii) and *sycp1*$^{isa/isa}$ (iii and iv) gonads with primary oocytes (i to iii) or spermatocysts (iv) are shown. Their body size (mm) and age (dpf: days post fertilization) are indicated below. Scale bars: 20 μm. **(C)** Phenotypes of juvenile *sycp1*$^{+/+}$ and *sycp1*$^{isa/isa}$ gonads. Phenotypes of gonads from 24 to 45 dpf of *sycp1*$^{+/+}$ and *sycp1*$^{isa/isa}$ fish were examined by HE staining and categorized into gonads with oocytes (red dots), gonads with spermatocysts (blue dots) and N.D. (not determined: open circle) and were plotted by their body size. Pooled results of siblings from two crosses are shown. Representative images are shown in **Figure 2B**. Histological images of all analyzed samples are shown in **Supplementary Figure 3**.

To examine whether Sycp1 has a conserved function in zebrafish, we analyzed the meiotic phenotypes of the *sycp1* mutant by immunostaining of spermatocyte spreads. First, we examined axis formation by costaining of axial elements Sycp2 and Sycp3, together with Sycp1, on wild-type (*sycp1*$^{+/+}$) and *sycp1* mutant (*sycp1*$^{isa/isa}$) spermatocytes (**Figure 3**). In *sycp1*$^{+/+}$ spermatocytes, Sycp2 and Sycp3 start to form short axis fragments together at leptonema (**Figure 3**i). This axis formation initiates near chromosome ends clustered as a telomere bouquet and progresses inwards (Saito et al., 2014; Blokhina et al., 2019; Takemoto et al., 2020, see below for telomere staining). At zygonema, Sycp1 appears as short fragments, colocalizing with Sycp2 and Sycp3 signals (**Figure 3**ii), and the entire length of homologous chromosomes was stained for these three proteins in pachynema (**Figure 3**iii), as we reported previously (Takemoto et al., 2020). Along the progression of zygonema, telomeres disperse from the bouquet (**Figure 3**ii, see below for telomere staining), and the bouquet structure is no longer evident in pachynema (**Figure 3**iii; Saito et al., 2014; Blokhina et al., 2019). We also marked that Sycp2 was not evenly stained along axes

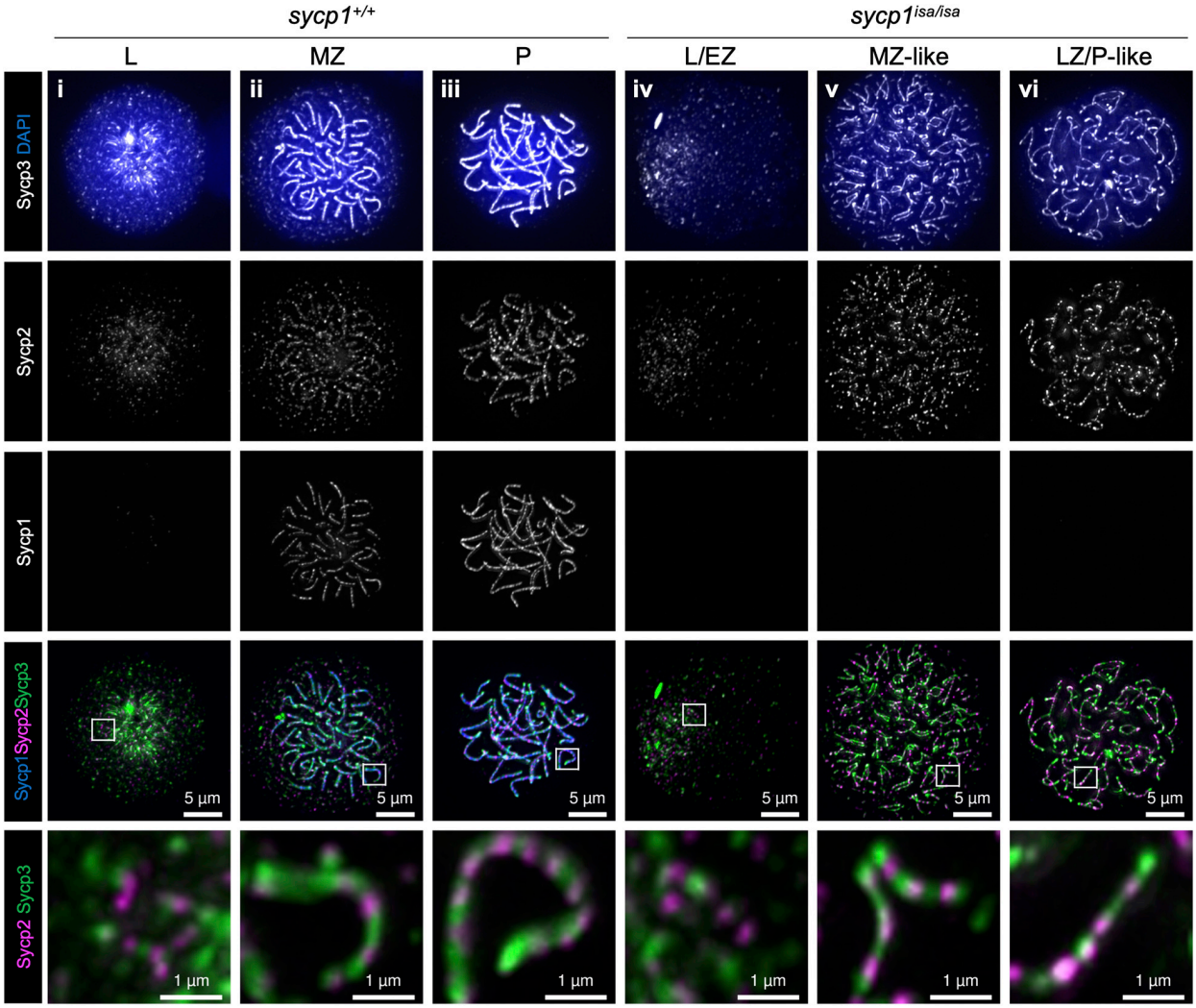

FIGURE 3 | Formation of chromosomal axes in *sycp1* mutant spermatocytes. Immunostaining of Sycp3, Sycp2 and Sycp1 components in wild-type ($sycp1^{+/+}$, i to iii) and $sycp1^{isa/isa}$ (iv to vii) spermatocyte chromosome spreads. Wild-type nuclei at leptotene (L, i), mid-zygotene (MZ, ii) and pachytene (P, iii) were staged according to the staining patterns of Sycp3, Sycp2 and Sycp1 (Blokhina et al., 2019). $sycp1^{isa/isa}$ nuclei at leptotene (L, iv), mid-zygotene-like (MZ-like, v) and late zygotene/pachytene-like (LZ/P-like, vi) stages were staged by axis staining patterns. Regions indicated in white rectangles are shown at the bottom at a higher magnification.

but rather appeared as discontinuous lines (**Figure 3**i–iii, bottom images). In $sycp1^{isa/isa}$ spermatocytes, no Sycp1 signals were observed (**Figure 3**iv–vi), as expected given the absence of Sycp1 protein by western blotting (**Figure 1C**). We observed Sycp2/Sycp3-stained axes in leptotene $sycp1^{isa/isa}$ spermatocytes that appeared similar to those of wild-type spermatocytes (**Figure 3**iv), as well as their extension in zygotene-like stages (**Figure 3**v,vi). Therefore, we staged $sycp1^{isa/isa}$ spermatocytes to preleptotene (PL, no axis), leptotene or early zygotene-like (L/EZ-like, punctate or short axes in a cluster), mid-zygotene-like (MZ-like, longer axes than L/EZ-like nuclei dissociating from a bouquet), or late zygotene/pachytene-like (LZ/P-like, axes similar to wild-type pachytene nuclei and axes ends are dispersed over nuclei) stages according to their axis staining patterns. Notably, we observed associations of two Sycp2-/Sycp3-stained axes in MZ-like $sycp1^{isa/isa}$ spermatocytes (**Figure 3**v, the bottom image). These associations were largely lost in LZ/P-like stages, and only a few paired ends were observed (**Figure 3**vi). Sycp2 was observed as discontinuous lines in $sycp1^{isa/isa}$ spermatocytes (**Figure 3**iv–vi, bottom images), similar to wild-type spermatocytes (**Figure 3**i–iii, bottom images). Thus, we concluded that axis formation occurs in the absence of Sycp1 in zebrafish spermatocytes.

Sycp1 Is Required for Complete Homolog Alignment in Zebrafish Spermatocytes

In $sycp1^{isa/isa}$ spermatocytes, we observed associations of two chromosomal axes in MZ-like stages (**Figure 3**v). Since axis

formation preferentially initiates near telomeres in zebrafish (Saito et al., 2014; Blokhina et al., 2019; Takemoto et al., 2020), we asked whether this pairing occurs near telomeres. To examine this, we visualized telomeres by telomere polyamide (TPA), a pyrrole–imidazole polyamide probe that binds to telomere sequences (Sasaki et al., 2016). After costaining of Sycp3 and telomeres by TPA, we found that axes emanated from telomeres, as observed in wild-type spermatocytes (**Figure 4A**i), even in the absence of Sycp1 (**Figure 4A**iii). In LZ/P-like *sycp1*$^{isa/isa}$ spermatocytes, we observed complete axis formation from telomeres to telomeres with some chromosomes (**Figure 4A**iv, arrowhead). Furthermore, the associations of two Sycp3-stained axes occurred in proximity to TPA-stained foci in MZ-like *sycp1*$^{isa/isa}$ spermatocytes (**Figure 4A**iii, the bottom image), indicating that the axes paired near telomeres even in the absence of Sycp1. Such pairing was observed with a few axes in later LZ/P-like stages (**Figure 4A**iv, arrow). To evaluate the pairing of chromosome ends, we compared the numbers of TPA foci in *sycp1*$^{+/+}$ and *sycp1*$^{isa/isa}$ spermatocytes (**Figure 4B**). Because zebrafish have 25 pairs of homologous chromosomes, 50 telomere foci are expected after tight axis associations by complete pairing. Consistent with this, 52 ± 3.1 (mean ± SD) foci were observed in LZ/P *sycp1*$^{+/+}$ spermatocytes, whereas far more than 50 foci were observed in L/EZ (62 ± 8.0) and MZ (57 ± 8.0) spermatocytes, because some homologs have yet to be paired at these stages (**Figure 4B**). In *sycp1*$^{isa/isa}$ spermatocytes, we observed more than 50 TPA foci in most spermatocytes at L/EZ-like (69 ± 12), MZ-like (69 ± 9.6) and LZ/P-like (81 ± 11) spermatocytes (**Figure 4B**), though at MZ-like stages, most TPA foci were observed in pairs (**Figure 4A**iii). The number of TPA foci in LZ/P-like *sycp1*$^{isa/isa}$ spermatocytes was significantly higher than that in wild-type LZ/P spermatocytes (**Figure 4B**). These data indicate that tight associations between homologous axes at chromosome ends were lost in the absence of Sycp1. However, it should be noted that non-homologous associations of telomeres occur independently of DSB in zebrafish (Blokhina et al., 2019). In addition, paired but not tightly associated telomeres, as observed in MZ-like *sycp1*$^{isa/isa}$ spermatocytes, cannot be evaluated by TPA quantification.

To further examine whether pairing of axis observed in MZ-like *sycp1*$^{isa/isa}$ spermatocytes (**Figure 3A**v, **4A**iii) occurred between homologs, we performed DNA fluorescence *in situ* hybridization (DNA FISH, **Figures 4C–E**). To assess homologous pairing, we used a DNA probe specific to a 35.9-kbp region close to a telomere on chromosome 3 (see section "Materials and Methods"). In wild-type spermatocytes, FISH foci were observed as two foci in the majority of early prophase I cells (**Figure 4C**i; 84% and 75% of PL and L/EZ cells, respectively; **Figure 4D**) and as one bright focus at the end of the Sycp3-stained axis in the majority of MZ (**Figure 4C**ii) and LZ/P (**Figure 4C**iii) cells (73% and 76%, respectively; **Figure 4D**). This indicates that the homologous sites at the end of chromosome 3 became closer during the progression of prophase I and remained paired throughout zygonema and pachynema in wild-type spermatocytes (**Figure 4E**). In *sycp1*$^{isa/isa}$ spermatocytes, we observed two foci in 82% and 63% of PL and L/EZ cells, respectively (**Figure 4C**iv, **D**), similar to the case in wild-type spermatocytes. Strikingly, we observed one or two closely paired foci in most MZ-like *sycp1*$^{isa/isa}$ spermatocytes (**Figure 4C**v, **D**), and the distances between the two FISH foci in those cells were not significantly different from those in wild-type MZ spermatocytes (0.98 ± 1.2 and 0.63 ± 0.71 in *sycp1*$^{isa/isa}$ and wild-type MZ spermatocytes, respectively; **Figure 4E**). In contrast, in the LZ/P-like stages, 78% of *sycp1*$^{isa/isa}$ spermatocytes showed two FISH foci (**Figures 4C**vi, **D**), and the distances between FISH foci were significantly higher than those in wild-type LZ/P spermatocytes (5.0 ± 4.3 and 0.51 ± 0.25, respectively; **Figure 4E**). These observations indicate that chromosome 3 paired at the probed site even in the absence of Sycp1, but this homologous association was mostly lost at LZ/P-like stages. Taken together, these data support the idea that homologous pairing of chromosome ends occurs but is not maintained in the absence of Sycp1.

Sycp1 Is Not Required for DSB Formation in Zebrafish Spermatocytes

Meiotic recombination is initiated with programmed DSBs (Baudat et al., 2013). To determine whether DSBs occur in *sycp1* mutant zebrafish, we examined γH2AX signals in *sycp1*$^{+/+}$ and *sycp1*$^{isa/isa}$ spermatocytes (**Figure 5**). γH2AX is a phosphorylated form of the histone variant H2AX, which appears in response to DSB formation (Scully and Xie, 2013). This histone mark is also observed in zebrafish meiosis, depending on the Spo11 nuclease (Saito et al., 2011; Blokhina et al., 2019; Takemoto et al., 2020). Consistent with previous reports, γH2AX signals appeared at the leptotene to EZ stages and diminished during zygonema. The majority of γH2AX signals disappeared, and only weak signals remained at pachynema in wild-type spermatocytes (**Figures 5A**i–iii, **B**). In *sycp1*$^{isa/isa}$ spermatocytes, γH2AX signals appeared at leptotene to L/EZ-like stages (**Figure 5A**iv), similar to the case in wild-type spermatocytes. However, γH2AX signals remained at significantly higher levels in MZ-like and LZ/P-like *sycp1*$^{isa/isa}$ spermatocytes (**Figure 5A**v, vi) than in wild-type MZ and LZ/P cells (**Figure 5B**). These results suggest that in the absence of Sycp1, meiotic DSBs occur but are not efficiently repaired and/or are initiated continuously in late prophase I.

DSBs Predominantly Occur at Subtelomeric Regions in *sycp1*$^{isa/isa}$ Zebrafish Spermatocytes

To further analyze early meiotic recombination in *sycp1* mutant fish, we examined the localization of RecA homolog proteins that bind to single-stranded DNAs during DSB repair (Gray and Cohen, 2016). We first performed immunostaining using an anti-Dmc1/Rad51 antibody raised against zebrafish Dmc1 (**Figures 6A,B**; Takemoto et al., 2020). In *sycp1*$^{+/+}$ spermatocytes, Dmc1/Rad51 foci appeared mostly near telomeres in L/EZ spermatocytes (**Figure 6A**i). Their numbers were reduced during zygonema (**Figure 6A**ii), and only a few or no Dmc1/Rad51 foci were observed at the LZ/P stages in *sycp1*$^{+/+}$ spermatocytes (**Figures 6A**iii, **B**), as observed previously (Sansam and Pezza, 2015; Blokhina et al., 2019; Takemoto et al., 2020). In *sycp1*$^{isa/isa}$ spermatocytes, Dmc1

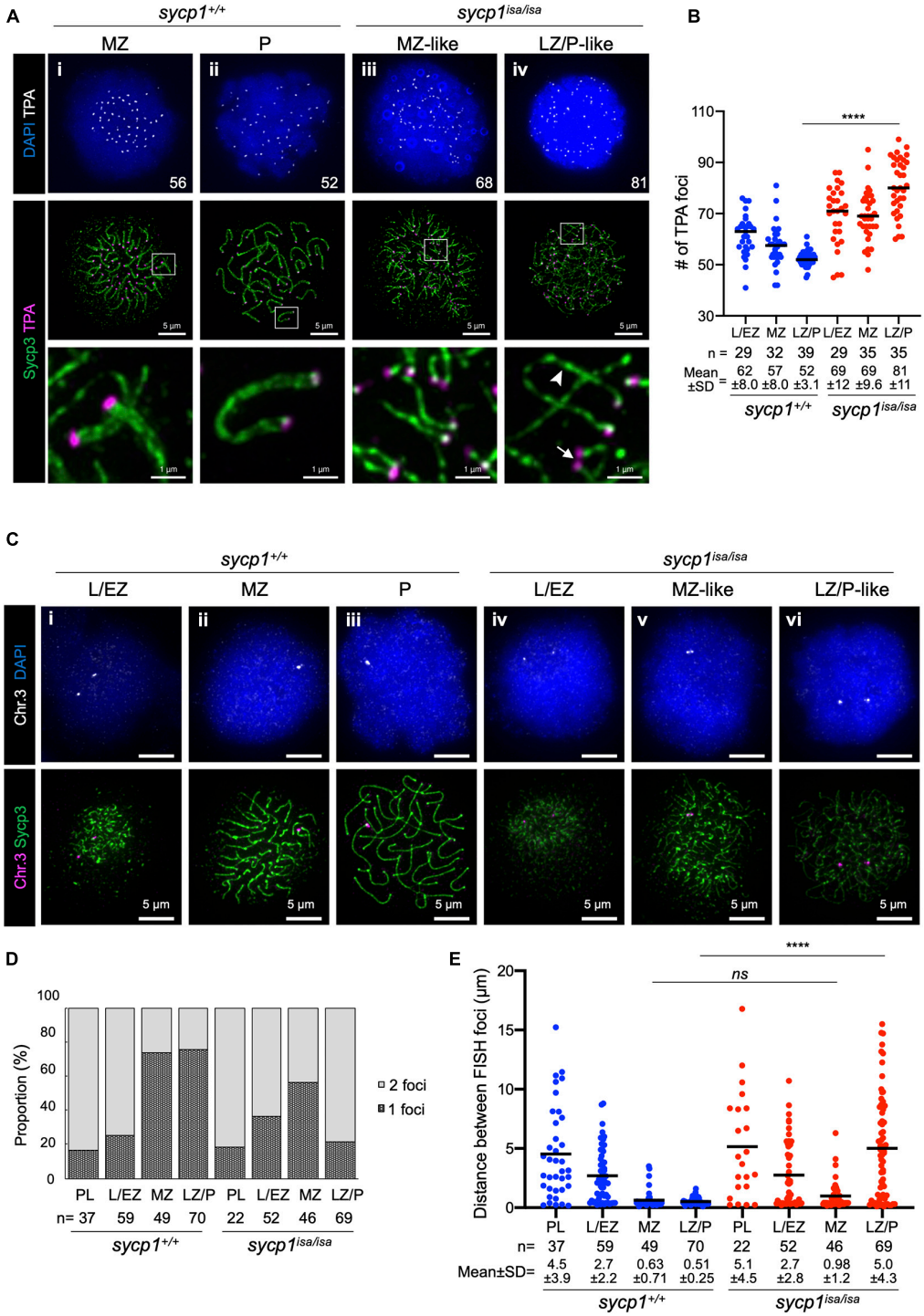

FIGURE 4 | Transient pairing of homologs at chromosome ends in *sycp1* mutant spermatocytes. **(A)** costaining of telomeres (TPA) and Sycp3 in *sycp1*$^{+/+}$ (i and ii) and *sycp1*$^{isa/isa}$ (iii and iv) spermatocytes. The arrowhead indicates complete axis formation between two telomeres, and the arrow indicates paired telomere foci in LZ/P-like *sycp1*$^{isa/isa}$ spermatocytes. Numbers in the top panels indicate counts of TPA foci. Regions indicated in white rectangles are shown at a higher magnification at the bottom. **(B)** quantification of telomere polyamide (TPA) foci in *sycp1*$^{+/+}$ and *sycp1*$^{isa/isa}$ spermatocytes. Black bars indicate means. Statistical significance was examined by a two-tailed Mann-Whitney test (****$P < 0.0001$; exact P value). **(C)** fish staining of a peritelomeric locus on chromosome 3 in *sycp1*$^{+/+}$ (i to iii) and *sycp1*$^{isa/isa}$ (iv to vi) spermatocytes. **(D)** Proportion of nuclei with one or two FISH foci in *sycp1*$^{+/+}$ and *sycp1*$^{isa/isa}$ spermatocytes. **(E)** quantification of distances between FISH foci of a peritelomeric locus on chromosome 3 in *sycp1*$^{+/+}$ and *sycp1*$^{isa/isa}$ spermatocytes. Distances between FISH foci observed in **Figure 4D**. For nuclei with only one FISH focus, the radius of the FISH-stained area was considered the distance between two FISH foci. Black bars indicate means. Statistical significance was examined by a two-tailed Mann-Whitney test (****$P < 0.0001$, ns, not significant; exact P value).

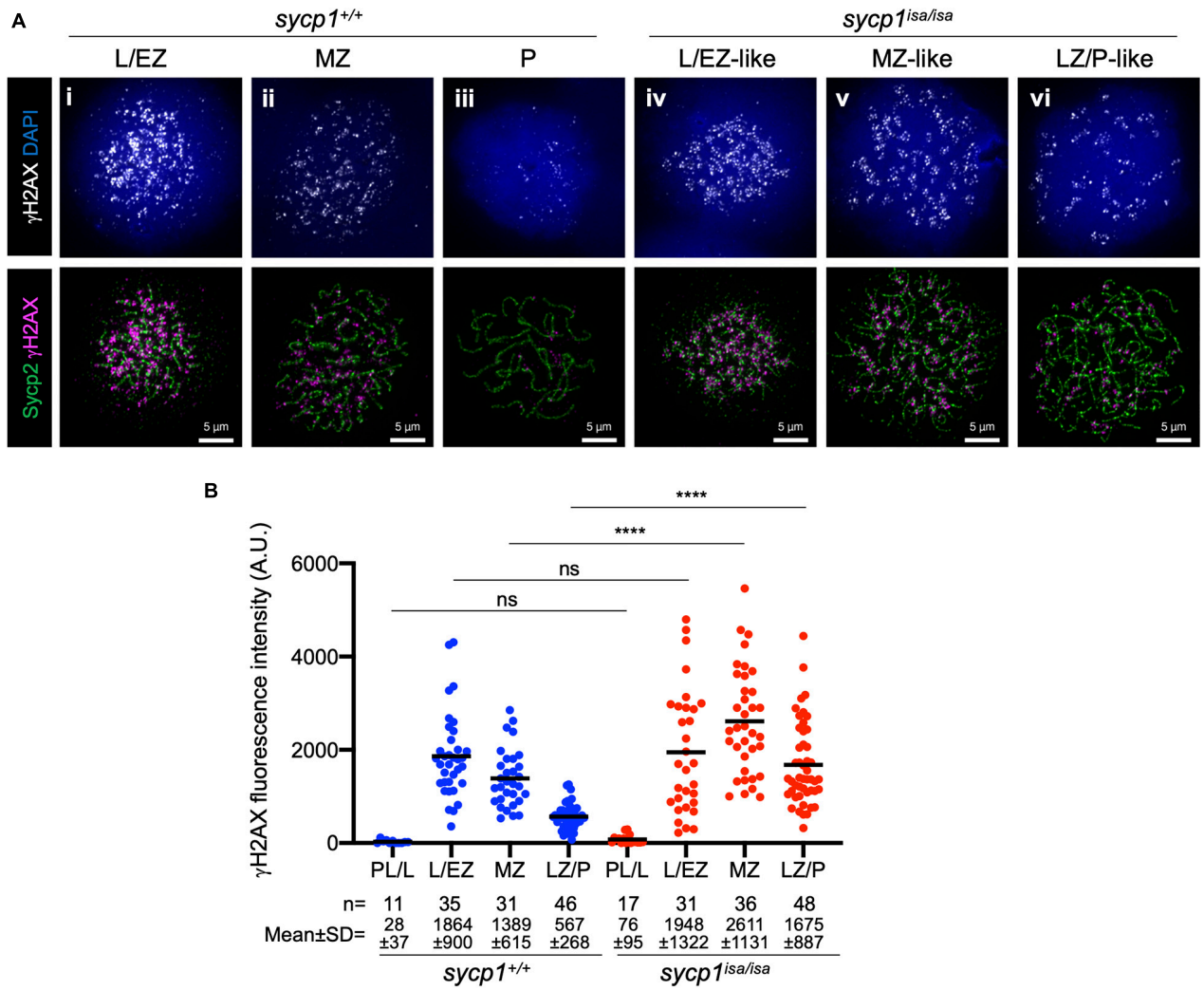

FIGURE 5 | Meiotic DSB formation in *sycp1* mutant spermatocytes. **(A)** costaining of γH2AX and Sycp2 in *sycp1*$^{+/+}$ (i to iii) and *sycp1*$^{isa/isa}$ (iv to vi) spermatocytes. **(B)** quantification of γH2AX signal intensity in *sycp1*$^{+/+}$ and *sycp1*$^{isa/isa}$ spermatocytes. Black bars indicate means. Statistical significance was examined by a two-tailed Mann-Whitney test (****$P < 0.0001$, ns, not significant; exact P value).

foci appeared at the L/EZ stages (**Figure 6A**iv) at lower numbers than in *sycp1*$^{+/+}$ spermatocytes (**Figure 6B**). The number of Dmc1/Rad51 foci reached the maximum level at MZ-like stages in *sycp1*$^{isa/isa}$ spermatocytes (**Figures 6A**v, **B**), and the number of Dmc1/Rad51 foci remained significantly higher at LZ/P-like stages (**Figure 6A**vi) than in wild-type LZ/P spermatocytes (**Figure 6B**). Notably, a majority of Dmc1/Rad51 foci in *sycp1*$^{isa/isa}$ spermatocytes were located near telomeres (**Figure 6A**iv–vi). We counted Dmc1/Rad51 foci in telomere-proximal regions (the 1 μm of axis adjacent to the TPA focus, see section "Materials and Methods"), and found that 65 ± 13% of Dmc1/Rad51 foci were in telomere-proximal regions in MZ-like *sycp1*$^{isa/isa}$ spermatocytes (**Supplementary Figure 4**). This result suggests that DSBs are limited to canonical sites even in the absence of Sycp1.

We also examined the localization of RPA (the replication protein A complex), which is required for the recruitment of DMC1/RAD51 and thus for strand invasion as well as efficient crossover formation during meiotic recombination (**Figures 6C,D**; Sugiyama et al., 1997; Soustelle et al., 2002; Shi et al., 2019; Hinch et al., 2020). In zebrafish spermatocytes, RPA appears as punctate foci at leptonema and forms short stretches mostly at chromosome ends in zygonema (Moens, 2006; Takemoto et al., 2020). We observed such localization of RPA in both wild-type MZ and *sycp1*$^{isa/isa}$ MZ-like spermatocytes (**Figure 6C**i, iii), and these signals decreased in wild-type LZ/P spermatocytes (**Figure 6B**ii) and in LZ/P-like *sycp1*$^{isa/isa}$ spermatocytes (**Figure 6B**iv). No significant difference was observed between the RPA signal intensities of wild-type and *sycp1*$^{isa/isa}$ spermatocytes at any stage (**Figure 6D**), although the number of RPA foci in MZ-like *sycp1*$^{isa/isa}$ spermatocytes was slightly lower than that in wild-type MZ spermatocytes (**Supplementary Figure 5**). Taken together, these results demonstrated that DSBs preferentially occur near telomeres in

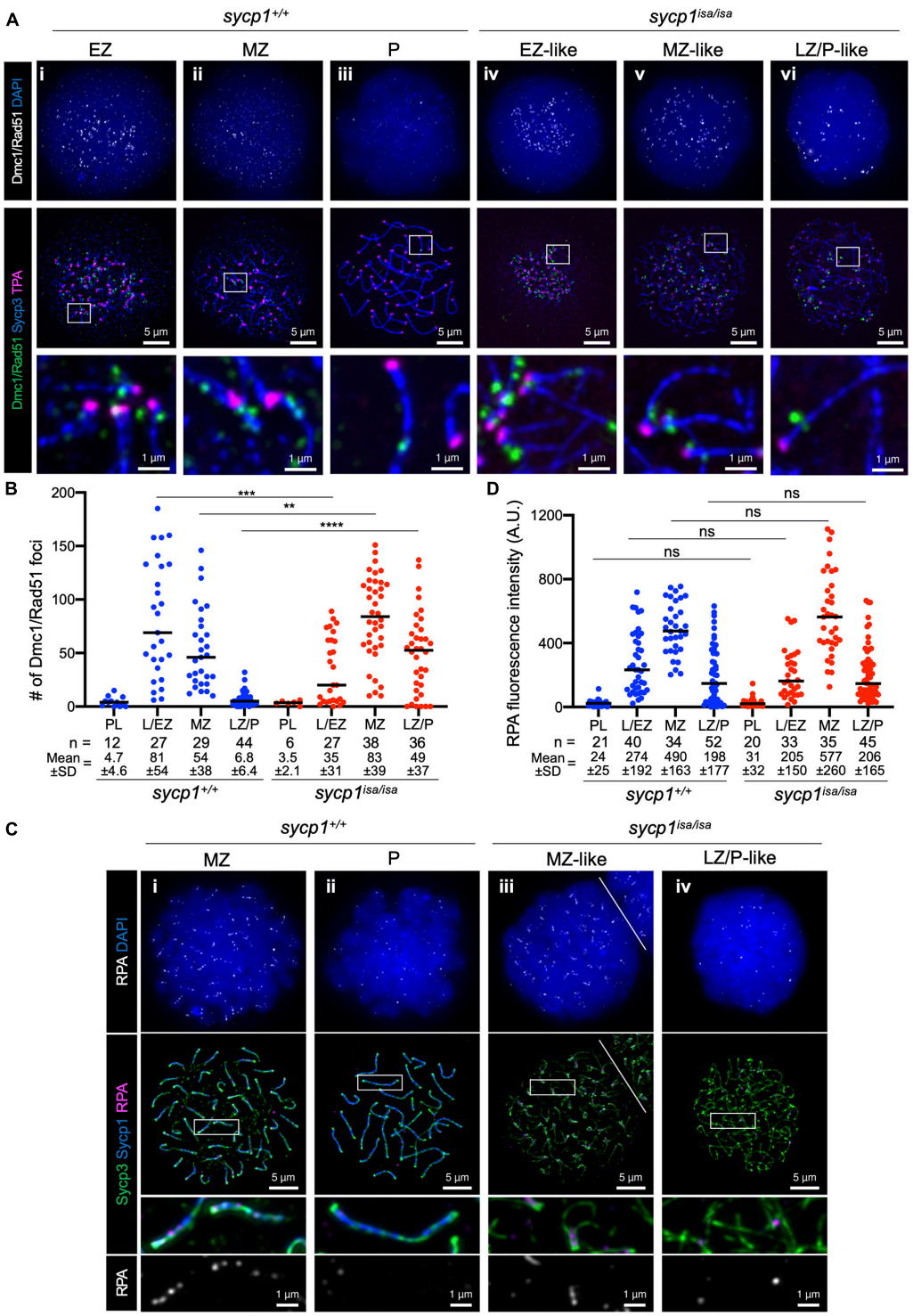

FIGURE 6 | DSB localization in *sycp1* mutant spermatocytes. **(A)** costaining of Dmc1/Rad51, telomeres and Sycp3 in *sycp1*$^{+/+}$ (i to iii) and *sycp1*$^{isa/isa}$ (iv to vi) spermatocytes. **(B)** quantification of Dmc1/Rad51 focus numbers in *sycp1*$^{+/+}$ and *sycp1*$^{isa/isa}$ spermatocytes. Black bars indicate means. Statistical significance was examined by a two-tailed Mann-Whitney test (**$P < 0.01$, ***$P < 0.001$, ****$P < 0.0001$; exact P value). **(C)** costaining of RPA, Sycp1 and Sycp3 in *sycp1*$^{+/+}$ (i and ii) and *sycp1*$^{isa/isa}$ (iii and iv) spermatocytes. Regions marked as a white rectangle in the middle panels are shown at a higher magnification at the bottom. The white line on (iii) indicates a border with another nucleus on the top right. **(D)** quantification of RPA signal intensity in *sycp1*$^{+/+}$ and *sycp1*$^{isa/isa}$ spermatocytes. Black bars indicate means. Statistical significance was examined by two-tailed Mann-Whitney test (ns, not significant; exact P value). Since RPA is observed as short stretches rather than discrete foci, signal intensity rather than the number of foci in a nucleus was quantified here. Quantification of RPA focus numbers is shown in **Supplementary Figure 5**.

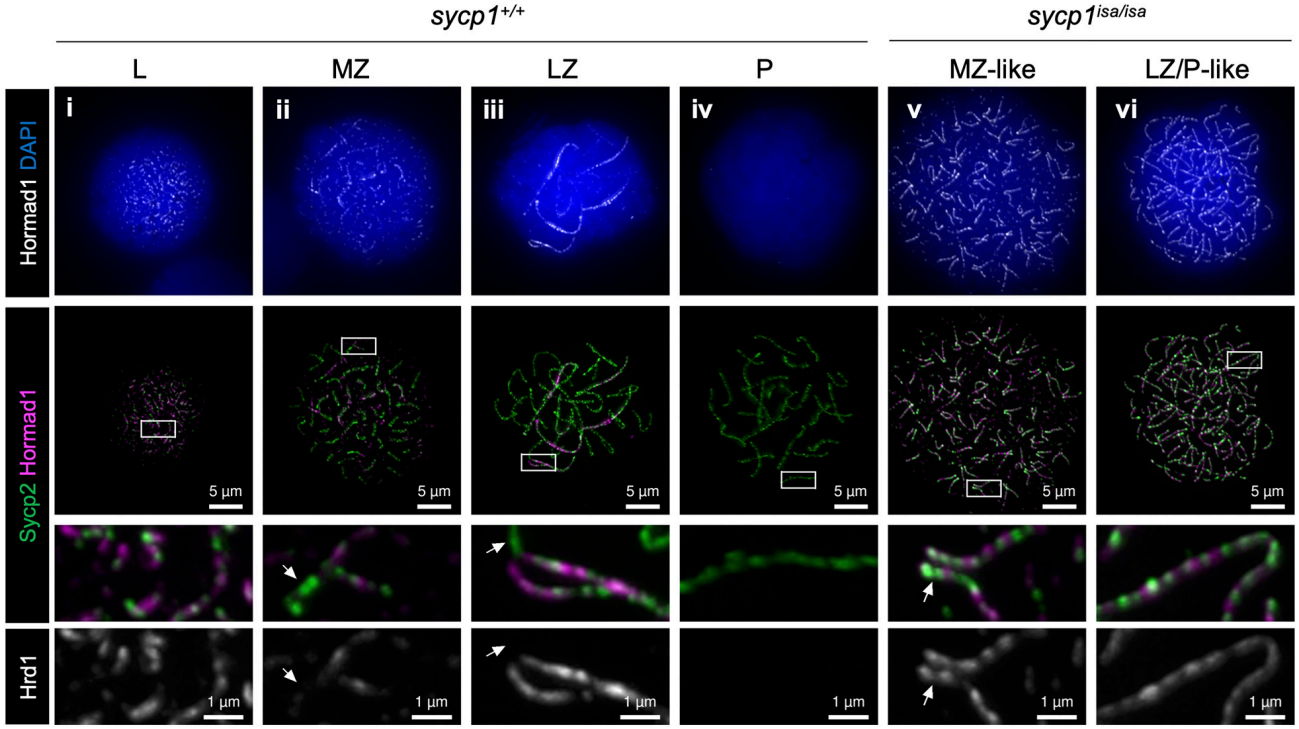

FIGURE 7 | Hormad1 localization in *sycp1* mutant spermatocytes. Costaining of Hormad1 and Sycp2 in *sycp1*$^{+/+}$ **(i to iv)** and *sycp1*$^{isa/isa}$ **(v and vi)** spermatocytes. Regions marked as a white rectangle are shown at a higher magnification at the bottom. Arrows indicate synapsed (*sycp1*$^{+/+}$) and paired (*sycp1*$^{isa/isa}$) regions of axes.

the absence of Sycp1 and that RPA and Dmc1/Rad51 are recruited to those DSB sites.

Depletion of Sycp1 Differentially Affects Hormad1 and Iho1 Localization on Chromosomal Axes

In mice, proteins promoting DSB formation, such as MEI4, REC114, IHO1, ANKRD31 and HORMAD1, are known to be absent from synapsed axes, implicating that synapsis is involved in DSB regulation (Wojtasz et al., 2009; Fukuda et al., 2010; Kumar et al., 2010; Shin et al., 2010; Stanzione et al., 2016; Boekhout et al., 2019; Papanikos et al., 2019). In *sycp1*$^{isa/isa}$ zebrafish, DSBs were still observed at canonical sites near telomeres by Dmc1/Rad51 and RPA staining (**Figure 6**). To examine the localization of DSB-promoting proteins in the *sycp1* mutant zebrafish, we generated antibodies against zebrafish Hormad1 and Iho1 (see section "Materials and Methods," **Supplementary Figure 6**). In mice, HORMAD1 is known as an axis-localizing protein that is required for robust recruitment of IHO1, which in turn recruits MEI4 and REC114 to unsynapsed axes (Stanzione et al., 2016). In wild-type zebrafish spermatocytes, we observed punctate and short filamentous Hormad1 signals partially colocalizing with Sycp2-stained axes at leptonema (**Figure 7**i). Hormad1 was costained with unsynapsed axes during zygonema (**Figure 7**ii, iii) and disappeared at pachynema upon complete synapsis of homologs (**Figure 7**iv). In *sycp1*$^{isa/isa}$ spermatocytes, however, we observed persistent localization of Hormad1 on axes at the MZ-like and LZ/P-like stages (**Figure 7**v, iv). Such Hormad1 localization on unsynapsed axes is similar to what has been observed in mice (Wojtasz et al., 2009; Fukuda et al., 2010; Shin et al., 2010). Notably, Hormad1 was also localized on paired regions of axes that were observed in EZ- to MZ-like *sycp1*$^{isa/isa}$ spermatocytes (**Figure 7**v, arrows). These results indicate that Sycp1 is required for the dissociation of Hormad1 from axes at late prophase I.

We next analyzed the localization of Iho1 (**Figure 8A**), the mouse ortholog of which is essential for meiotic DSB formation (Stanzione et al., 2016). In wild-type zebrafish spermatocytes, Iho1 foci were observed on axes at leptonema and zygonema (**Figure 8A**i–iii). In the MZ and LZ stages, Iho1 localized on unsynapsed axes as punctuate foci or short stretches (**Figure 8A**ii, iii) and disappeared from axes at pachynema (**Figure 8A**iv). Similarly, we observed bright Iho1 foci in leptotene and EZ-like *sycp1*$^{isa/isa}$ spermatocytes (**Figure 8A**v). These bright signals mostly disappeared in the LZ/P-like stage, and only a few weak signals were observed on some parts of the axes (**Figure 8A**vi). This was in contrast to Hormad1, in which strong signals persisted on the axes of LZ/P-like *sycp1*$^{isa/isa}$ spermatocytes (**Figure 7**vi). Since bright Iho1 signals disappear even in the absence of Sycp1, we suspected that Iho1 dissociation from axes might be promoted not by synapsis but rather by DSB formation. Thus, we analyzed Iho1 localization in *spo11*$^{-/-}$ spermatocytes that cannot form meiotic DSBs

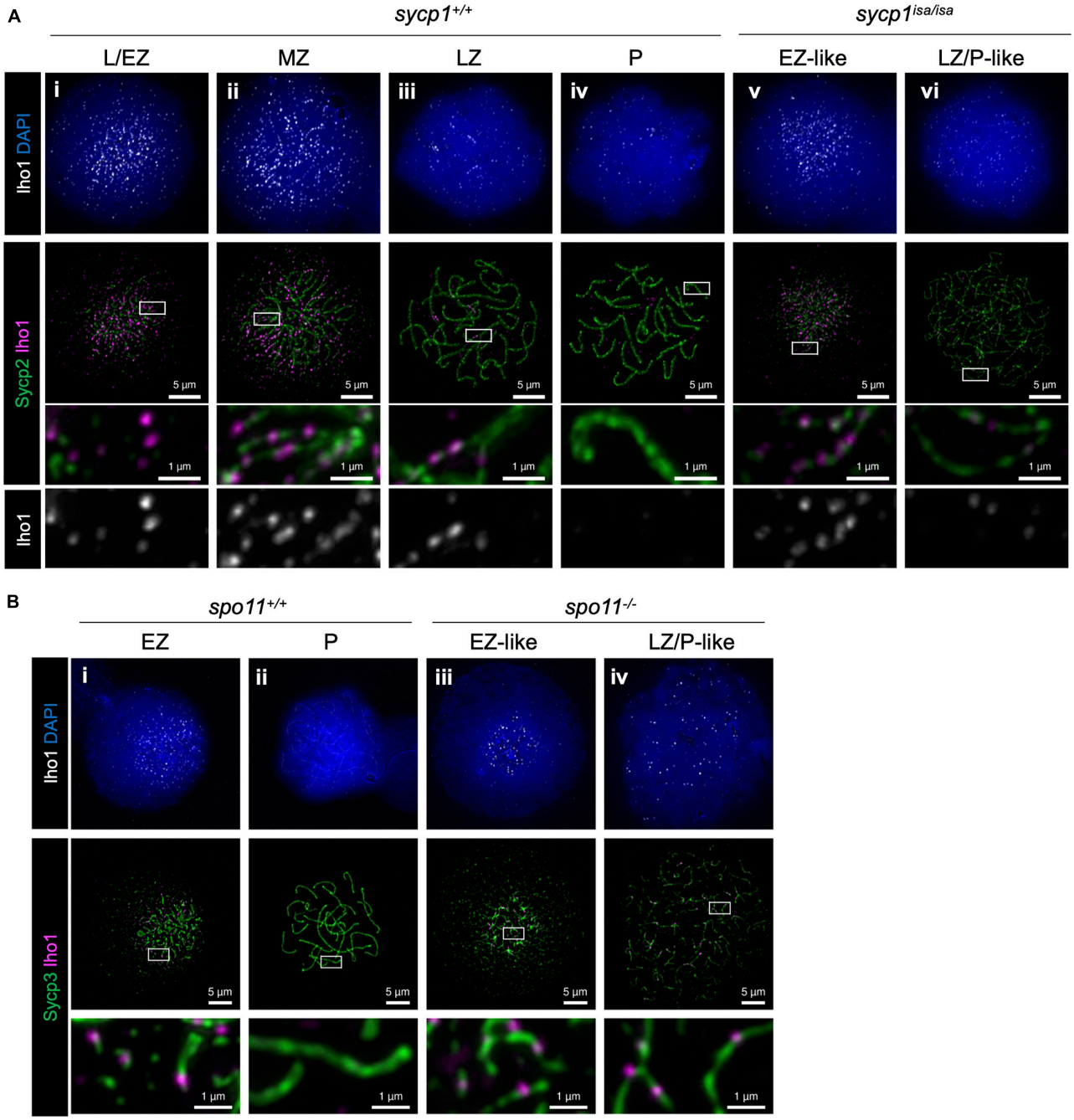

FIGURE 8 | Iho1 localization in *sycp1* and *spo11 m*utant spermatocytes. **(A)** costaining of Iho1 and Sycp2 in *sycp1*$^{+/+}$ (i to iv) and *sycp1*$^{isa/isa}$ (v and vi) spermatocytes. Regions marked in white rectangles are shown at a higher magnification at the bottom. **(B)** Costaining of Iho1 and Sycp3 in *spo11*$^{+/+}$ (i and ii) and *spo11*$^{-/-}$ (iii and iv) spermatocytes. Regions marked in white rectangles are shown at a higher magnification at the bottom.

(Blokhina et al., 2019; Takemoto et al., 2020) and observed bright foci of Iho1 in both EZ-like and LZ/P-like *spo11*$^{-/-}$ spermatocytes (**Figure 8B**iii, iv). This indicates that Iho1 remains associated with distinct sites on axes in the absence of meiotic DSBs. Altogether, our results demonstrated that the spatiotemporal localizations of Iho1 and Hormad1 are differentially affected by depletion of Sycp1.

DISCUSSION

Isolation of a *Sycp1* Null Mutant Zebrafish

In this study, we mapped the causal mutation of the *isa* mutant zebrafish line in the *sycp1* gene. Zebrafish *sycp1* is expressed in early primary oocytes and primary spermatocytes and spermatids

at the transcriptional level (Gautier et al., 2013) and in primary oocytes and primary spermatocytes at the protein level (Moens, 2006; Kochakpour and Moens, 2008). While zebrafish Sycp1 is known to localize to meiotic homologous chromosomes, as observed in other species (Moens, 2006; Kochakpour and Moens, 2008; Saito et al., 2014; Blokhina et al., 2019; Takemoto et al., 2020), its functions in meiosis have not been elucidated. The *isa* mutation appeared to be a non-sense mutation of the lysine at position 408 in Sycp1, which is 1000 amino acids at full length (**Figures 1A,B**). Although this mutation is located in the middle of the Sycp1 protein sequence, we did not detect truncated proteins of the expected size (47.7 kDa, **Figure 1C**). The absence of truncated Sycp1 protein could be explained by non-sense-mediated mRNA decay (NMD), by which mRNAs that contain a premature stop codon located more than 50 nucleotides upstream of the final exon are eliminated (Lewis et al., 2003; Baker and Parker, 2004). In support of this hypothesis, the *isa* mutation is 1632 nucleotides upstream of exon 31, the final exon of *sycp1*. We confirmed by complementation tests that the *sycp1* mutation is responsible for previously reported *isa* phenotypes: accumulation of spermatocytes and absence of spermatids and sperm (**Figure 1D**; Saito et al., 2011). Altogether, *isa* appeared to be a *sycp1* null mutant zebrafish that is suitable for analyzing the functions and roles of Sycp1 in synapsis in zebrafish meiosis.

Interdependency of Homologous Pairing, Recombination and Synapsis in Zebrafish Spermatocytes

A recent study in *spo11*-knockout zebrafish indicated that DSBs induced by Spo11 are required for the coalignment of axes and SC formation (Blokhina et al., 2019). Together with previous findings, our data provide evidence to clarify how key meiotic events—homologous pairing, recombination and synapsis—affect each other in zebrafish spermatocytes. In this study, we observed DSB formation in *sycp1* mutant spermatocytes, as indicated by γH2AX, Dmc1/Rad51 and RPA signals (**Figures 5**, **6**). Furthermore, local alignment of homologous axes was observed near telomeres in *sycp1* mutant spermatocytes (**Figures 3A**vii, **4B**v). These results demonstrated that DSB formation and homologous pairing occur independently of synapsis. However, homologous associations at chromosome ends were largely lost in LZ/P-like stages in the absence of Sycp1 (**Figures 3A**vi, **4C**vi, **D,E**). This is in clear contrast to what is observed in *Sycp1* and CE mutant mice, where most homologs remain aligned via parts of the chromosome at pachytene-like stages (Bolcun-Filas et al., 2007, 2009; Hamer et al., 2008; Schramm et al., 2011; de Vries et al., 2014; Gómez-H et al., 2016). This difference in pairing phenotypes might come from the difference between zebrafish and mouse DSB locations. In zebrafish spermatocytes, meiotic DSB formation is heavily biased toward the chromosome ends (Blokhina et al., 2019; Takemoto et al., 2020; **Figure 6A**i). In mouse spermatocytes, such peritelomeric bias is not evident (Brick et al., 2018), and the majority of DSBs occur at PRDM9-bound sites across chromosomes (Brick et al., 2012). In *Sycp1* mutant mice, foci of DSB repair proteins (RAD51, RPA and MSH4) are also distributed across the chromosomes (de Vries et al., 2005). Given that DSBs cluster at chromosome ends in zebrafish spermatocytes, homologous interactions at DSB sites (see below) might be unable to provide enough force to support homolog associations and full homolog alignment in the absence of synapsis. Alternatively, most DSBs at aligned axes might be repaired without crossovers, after which homolog associations are resolved at LZ/P-like stages in *sycp1*$^{isa/isa}$ zebrafish spermatocytes.

Meiotic Recombination Defects in *Sycp1* Mutant Zebrafish Spermatocytes

While meiotic DSB formation was observed in *sycp1* mutant zebrafish spermatocytes, these DSBs were unlikely to be repaired properly. In *sycp1* mutant zebrafish spermatocytes, γH2AX signals appeared at L/EZ-like stages, similar to wild-type spermatocytes, but peaked later, at MZ-like stages, and remained strong at LZ/P-like stages (**Figure 5B**). Accordingly, we observed delayed appearance of Dmc1/Rad51 foci in *sycp1*$^{isa/isa}$ spermatocytes compared to wild-type spermatocytes, and many Dmc1/Rad51 foci remained at LZ/P-like stages (**Figure 6B**). The kinetics of γH2AX and Dmc1/Rad51 signals suggest that early DSB repair is delayed in *sycp1*$^{isa/isa}$ spermatocytes (**Figures 5B**, **6B**), similar to what has been observed in *Sycp1* mutant mice (de Vries et al., 2005). In contrast, we observed similar kinetics in RPA intensities between wild-type and *sycp1*$^{isa/isa}$ spermatocytes (**Figures 6C,D**). Recent studies in mice revealed that RPA has dual functions: recruiting DMC1 and RAD51 to exposed ssDNA at DSB sites and binding to the repair template in a D-loop recombination intermediate (Shi et al., 2019; Hinch et al., 2020). In wild-type zebrafish spermatocytes, some RPA foci are observed as short stretches in mid-zygonema (Moens, 2006; Takemoto et al., 2020; **Figure 6C**i). These RPA signals may reflect localization on the repair template strand. We speculate that in *sycp1*$^{isa/isa}$ spermatocytes, RPA could accumulate at DSB sites because of inefficient loading of Dmc1/Rad51, but for the same reason, its binding to the repair template could be reduced. We might observe the sum of these two different effects which results in no apparent change in RPA signal intensities in *sycp1*$^{isa/isa}$ spermatocytes (**Figure 6D**).

Importantly, we observed short stretches of RPA between aligned axes in MZ-like *sycp1*$^{isa/isa}$ spermatocytes (**Figure 6C**iii), suggesting that a substantial portion of DSB sites undergo the strand invasion step and form recombination intermediates (Baudat et al., 2013; Brown and Bishop, 2015; Hunter, 2015). This is also supported by our observation that axis alignment at chromosome ends occurs between homologs (**Figures 4C–E**). The majority of these recombination intermediates are unlikely to form crossovers, since homolog associations at chromosome ends were largely lost in LZ/P-like *sycp1*$^{isa/isa}$ spermatocytes (**Figures 4D,E**). It is possible that those intermediates could be resolved without crossovers (non-crossovers). A minor fraction of intermediates might remain unresolved, since we detected several Dmc1/Rad51 and RPA foci in LZ/P-like *sycp1*$^{isa/isa}$ spermatocytes (**Figures 6A**vi, **C**iv). We cannot eliminate the possibility that DSBs are continuously formed at these sites with

Dmc1/Rad51 and RPA foci at LZ/P-like stages. However, given that Iho1 was mostly absent from these sites in the LZ/P-like stages (**Figure 8A**vi), this is less likely to be the case. Collectively, our data support the idea that Sycp1 is essential for homolog association via crossovers in zebrafish spermatocytes.

Meiotic DSB Regulations in Zebrafish Spermatocytes

In most species studied so far, meiotic DSBs are directed to distinct regions of the genome, called hotspots (Baudat et al., 2013). In this study, we demonstrated that Iho1 appears on axes at L/EZ stages around the telomere bouquet (**Figures 8A**i, **B**i), where DSBs predominantly occur, in zebrafish spermatocytes (**Figure 6A**; Blokhina et al., 2019; Takemoto et al., 2020). The initial loading of Iho1 most likely occurs prior to DSB formation, since Iho1 foci were observed in *spo11*$^{-/-}$ spermatocytes (**Figure 8B**iii, iv). This implies that these regions harbor properties to recruit DSB-promoting proteins through unknown mechanisms and become hotspots. IHO1 was first identified as a HORMAD1-interacting protein that promotes DSBs in mice (Stanzione et al., 2016). Although axis localization of IHO1 is largely lost in *Hormad1* mutant mice, a recent study indicated that HORMAD1 is not the sole factor required for axis recruitment of IHO1 (Fujiwara et al., 2020). Furthermore, another mouse study reported that DSB formation at the pseudoautosomal region and several chromosome ends are associated with a particular type of minisatellite repeat and HORMAD1-independent accumulation of DSB-promoting proteins, such as REC114, MEI4, IHO1 and MEI1 (Acquaviva et al., 2020). In zebrafish, it remains to be elucidated whether Hormad1 is required for Iho1 localization on axes. It will be of future interest to understand how DSB-promoting proteins are recruited to subtelomeric hotspots in zebrafish.

We demonstrated that the spatiotemporal localizations of Iho1 and Hormad1 are differentially affected by depletion of Sycp1 (**Figures 7**, **8**). This observation supports the idea that dissociation of Hormad1 and Iho1 from axes are regulated by different mechanisms. We observed Hormad1 localization on axes upon and after pairing in *sycp1* mutant spermatocytes (**Figure 7A**vi), suggesting that SC formation is required for the dissociation of Hormad1 from axes. This is consistent with observations in mice that HORMAD1 is enriched on unsynapsed axes in *Syce1* mutant spermatocytes (Wojtasz et al., 2009). In contrast to Hormad1, intense Iho1 foci mostly disappeared from axes in LZ/P-like *sycp1* mutant spermatocytes (**Figure 8A**vi), and subtelomeric DSBs were observed (**Figure 6**, **Supplementary Figure 4**). In addition, persistent Iho1 foci were observed in *spo11*$^{-/-}$ spermatocytes (**Figure 8**iv). Hence, the dissociation of Iho1 from axes seems to be promoted by DSB formation but not by synapsis. A recent report in mice showed that DSB-dependent IHO1 depletion is promoted locally in the vicinity of DSBs by the ATR kinase at pre-pachynema, and globally in all axes by the DNA damage response signaling pathway at pachynema (Dereli et al., 2021). It is presumable that Iho1 dissociation in *sycp1*$^{-/-}$ zebrafish occurs in similar pathways activated by DSBs, but all-axis depletion of Iho1 might occur prior to the pachytene stage, shortly after DSB formation around the telomere bouquet. Though further studies are required to unveil the complete picture of DSB regulation, our study provided the first insight into the feedback control of DSB protein in zebrafish.

MATERIALS AND METHODS

Ethics Statement

All experiments were conducted in accordance with Rules for Animal Experiments at the National Institute of Genetics, Research Organization of Information and Systems, Japan. The experimental plan using zebrafish was approved by the National Institute of Genetics official ethics committee (Approval Number 27–12, 28–13, 29–13, 30–14, 31–18, R2-8).

Fish

Zebrafish (*Danio rerio*) were maintained under standard conditions as described in The Zebrafish Book (Westerfield, 1995). The wild-type India line (see ZFIN at http://zfin.org/action/genotype/view/ZDB-GENO-980210-28) has been maintained in our laboratory for more than 20 generations. The *isa* fish have been described previously: *isa* mutant fish were derived from the wild-type Tübingen line and then crossed with the IM strain (wild-type inbred) (Shinya and Sakai, 2011) to obtain heterozygous mutant fish (Saito et al., 2011). The *sycp1*^{del5} line was generated by CRISPR-Cas9 mutagenesis based on published protocols (Hwang et al., 2013; Chen et al., 2017). Template DNA for single-guide RNA (sgRNA) synthesis was prepared by amplification with a primer specific to *sycp1* exon 3, a universal reverse primer (**Supplementary Table 1**) and T4 DNA polymerase. After purification of the template DNA, sgRNA was transcribed *in vitro* with a MEGAscript T7 kit (Ambion) and purified with a MEGA clean-up kit (Ambion). Wild-type India embryos were injected at the 1- or 2-cell stage with 2.3 nl of a mixture of 10 pmol/μl Cas9 NLS protein (abm) and 100 ng/μl *sycp1* sgRNA. Founders were backcrossed with India fish, and the F1 siblings were screened by genotyping. Heterozygous *sycp1* knockout fish carrying a −5 bp frameshift mutation in exon 3 (*sycp1*^{del5}, a 5-bp deletion affecting the codons for Leu78 and Pro79 that generates 10 amino acid residues from the wrong frame and stop codon after the 87th amino acid) were mated with heterozygous *isa* fish in complementation tests.

Mapping of the *isa* Mutation

We first analyzed 560 *isa* mutant fish with simple sequence polymorphism (SSLP) markers, and the causal genomic region was mapped to a 1197-kbp region on chromosome 6 containing 22 annotated genes. We further analyzed 676 (total 1236) *isa* mutant fish and narrowed it down to an ∼561-kbp region between the A4891 and z4950 markers (**Supplementary Figure 1**). Among 14 genes located in this region, we examined the genomic sequences of *tshb*, *vapb,* and *sycp1* genes and identified no mutation in *tshb* and *vapb* but a premature stop mutation in *sycp1*.

Genotyping

Genomic DNA was extracted from caudal fin clips (adult) or head (juvenile) tissue in lysis buffer at 65°C. DNA lysates were diluted 120 times in water and used for PCR with GoTaq Green Master Mix (Promega) using specific primers for each site (**Supplementary Table 1**). PCR products were examined by agarose or acrylamide gel electrophoresis. Genotyping of the *isa* mutation was performed by the dCAPS (derived cleaved amplified polymorphic sequences) method using *Kpn*I (Nippon Gene). For genotyping of *sycp1*^{del5} and the *spo11* mutation, PCR products were treated with ExoSAP-IT PCR Product Cleanup Reagent (Thermo Fisher Scientific) and analyzed by general Sanger sequencing.

Antibodies

All antibodies used in this study are listed in **Supplementary Table 2**. Our anti-Dmc1/Rad51 antibody was raised against recombinant Dmc1 protein, which shares high similarity with Rad51 at the amino acid sequence level, and thus the antibody potentially recognize Rad51 as well (Takemoto et al., 2020). Mouse polyclonal antibodies specific for zebrafish Hormad1 and Iho1 were generated in this study (**Supplementary Figure 6**). The *hormad1* and *iho1* cDNAs encoding amino acid residues Ser252 to Lys356 (UniProt ID: A2BF66) and Met1 to Pro306 (NCBI Reference: XP_021332557.1), respectively, were cloned into the pET-28a(+) vector (Novagen) using NEBuilder HiFi DNA Assembly (NEB). Primers used for cloning are shown in **Supplementary Table 1**. The cloned zebrafish Hormad1 region corresponds to a C-terminal region that was used for the generation of an anti-mouse HORMAD1 antibody to avoid cross-reaction with the HORMAD2 protein (Wojtasz et al., 2009). The recombinant Hormad1 and Iho1 proteins were expressed in *Escherichia coli* BL21C and purified by Ni-NTA agarose (Qiagen) under denaturing conditions (6 M HCl-guanidine, 20 mM Tris–HCl pH 7.5). After immunizing mice with the recombinant proteins, the obtained anti-Hormad1 antiserum was purified by Dynabeads protein G.

Western Blotting

Protein extracts were prepared from testes dissected from 3.5-month-old fish. A pair of testes was homogenized in 100 μl of extraction buffer (20 mM Tris; 150 mM NaCl; 2 mM EDTA; 1% NP-40; 0.1% SDS) complemented with cOmplete proteinase inhibitors (Roche). After sonication by a Bioruptor at high power for 5 cycles of 30 s on/30 s off, cell suspensions were incubated at 4°C for 30 minutes. Protein lysates were obtained by centrifugation at 14,500 rpm for 10 min at 4°C. Protein concentrations were determined by Bio-Rad Protein Assay (Bio-Rad), and 25 μg protein was loaded onto a 7.5% SuperSep(TM) Ace acrylamide gel (Wako) and migrated at 200 V for 75 min. The proteins were transferred onto a PVDF membrane by the Trans-Blot Turbo system (Bio-Rad), and then the membrane was blocked in 5% skim milk and TBST. The membrane was cut at ∼40 kDa as indicated by the position of protein markers and then incubated with anti-Sycp1 or anti-Gapdh antibodies. After washing 3 times in TBST, the membrane was blotted with HRP-conjugated secondary antibodies. The antibodies used in western blotting are listed in **Supplementary Table 2**. Signals were developed with ECL Prime reagent (Amersham) and detected by ChemiDoc XRS (Bio-Rad).

Histology

Adult testes and bodies of juvenile fish (24 to 45 dpf) were fixed in Bouin's solution (Sigma). For sampling of juvenile fish, total body size (from the snout to the end of the caudal fin) was measured, and either the fin clip or the head was kept for genotyping. The fixed samples were dehydrated in an ethanol series (70%, 80%, 90% and 100%), methyl benzoate, and Lemosol (Wako) and embedded in paraffin. Hematoxylin-eosin (HE) staining was performed with 5-μm-thick sections.

Immunostaining of Spermatocyte Chromosome Spreads

Zebrafish spermatocyte chromosome spreads were prepared from adult testes by a dry-down method as described previously (Takemoto et al., 2020). Blocking of the spread slides was performed with a solution of PBS containing 5% skimmed milk and 5% donkey serum. The slides were incubated at room temperature (RT) overnight with primary antibodies and at 37°C for 1 h with secondary antibodies. All antibodies and their dilutions at the time of use are listed in **Supplementary Table 2**. After each antibody incubation, slides were washed for 10 min each in 0.1% Tween 20-PBS, 0.1% Triton X-100-PBS, and 0.1% Tween 20-PBS. DAPI was added at 10 ng/ml in the last wash step. After washing the slides twice in distilled water, they were air dried and mounted using VECTASHIELD Antifade Mounting Medium (Vector Labs). For telomere staining, TEN buffer (100 mM NaCl, 20 mM Tris–HCl pH 7.4, 1 mM EDTA) or TE buffer (20 mM Tris–HCl pH 7.4, 1 mM EDTA, for the wash step before incubation with the secondary antibody mix) was used instead of PBS, and incubation with secondary antibodies was performed with 0.5 μg/ml DAPI and 15 nM TRed-HPTH59-A (telomere-targeting polyamide; HiPep Laboratories) (Sasaki et al., 2016) at RT for 3–4 h.

DNA FISH

The fosmid probe and Cot-1 DNAs were prepared as previously described using the fosmid clone CH1073-175H21 (BACPAC Genomics) and salmon sperm DNA (Wako), respectively (Blokhina et al., 2019). We confirmed that CH1073-175H21 contains a genomic region close to a telomere on chromosome 3 by PCR with a primer pair specific to the *sox9b* gene (**Supplementary Table 1**). The DNA probe staining protocol was adapted from Takemoto et al. (2020). After immunostaining of the chromosome spreads as described above, the slides were postfixed with 500 μl of 2% paraformaldehyde in PBS for 10 min at RT. The slides were then washed in PBS and dehydrated by placing in 70%, 85% and (twice) 100% ethanol. Dried slides were incubated with 10 μl of probe mixed with 25 μg of Cot-1 at 80°C for 5 min. After coming to temperature at ∼37°C, slides were incubated in a humid chamber at 37°C overnight. Slides were

then washed twice in 50% formamide in 2xSSC at 45°C for 5 min, twice in 2x SSC at 45°C for 5 min, once in 0.05% Tween20-4xSSC for at RT 8 min, once in 0.05% Tween20-1xSSC-0.5xPBS at RT for 5 min, and finally 3 times in 0.1% Tween 20-PBS at RT for 5 min. The slides were then stained with DAPI and mounted as described above.

Image Analysis

Histological images were captured with an Olympus BX51 microscope equipped with a Keyence VB7010 camera. Cytological images were captured with a DeltaVision Ultra fluorescence microscope equipped with a 1.45 NA 100x objective, and 20 images along the z-axis (section spacing: 0.1 μm) were deconvolved and projected using softWoRx software (GE Healthcare). All cytological images were processed using OMERO (OME) (Allan et al., 2012) and Fiji (Schindelin et al., 2012). All spread samples included in the same panel were prepared and stained at the same time, and the images were processed in the same manner. Quantifications were performed by Fiji macros using DAPI-positive areas as ROIs (programs available upon request). The same threshold was applied to all images in the same experiment to eliminate noise or background signals. The numbers of telomeres (TPA; **Figure 4B**) and Dmc1/Rad51 foci (**Figure 6B**) were counted by the FindMaxima tool in Fiji. The distance between two FISH foci was quantified as previously described (Blokhina et al., 2019). When only one FISH focus was detected in the nucleus, the radius of the FISH-stained area was considered to indicate the distance between two FISH foci. To quantify Dmc1/Rad51 foci in near telomeres, we defined telomere-proximal regions as the 1 μm of axis adjacent to the TPA focus, based on a criterion used for human DMC1 analysis (Pratto et al., 2014). We manually counted numbers of Dmc1/Rad51 foci in telomere-proximal regions in all MZ and MZ-like nuclei quantified in **Figure 6B**, and calculated proportion of Dmc1/Rad51 foci in telomere-proximal regions to total Dmc1/Rad51 foci in each nucleus.

Statistics

Two or more animals (or siblings in **Figure 2**) were analyzed as biological replicates for the same phenotypes, unless otherwise indicated. Each phenotype was compared between wild-type and mutant animals from the same brood (siblings). The significance of the numbers of TPA, Dmc1/Rad51 and RPA foci and intensities of γH2AX and RPA signals was calculated with the Mann–Whitney two-tailed test using GraphPad Prism 9 software.

DATA AVAILABILITY STATEMENT

The data generated for this study can be found within the article/**Supplementary Material**.

ETHICS STATEMENT

The animal study was reviewed and approved by Animal Experiments at the National Institute of Genetics, Research Organization of Information and Systems.

AUTHOR CONTRIBUTIONS

YI contributed to the conceptualization, investigation, formal analysis, visualization, writing of the original draft, and funding acquisition. KS contributed to the conceptualization, investigation, and formal analysis. KT and FV contributed to the investigation and formal analysis. TK contributed to project supervision. KI contributed to project supervision and resources for the project. NS contributed to the conceptualization, supervision, project administration, funding acquisition, and resources for the project. All authors revised, commented on, and approved the final manuscript.

FUNDING

This work was supported by JSPS KAKENHI (Grant Numbers JP19K16045 and JP18H06057 to YI) and partly supported by JSPS KAKENHI (Grant Numbers 25251034, 25114003, and 19K22437 to NS). The funders had no role in the study design, data collection and analysis, decision to publish, or preparation of the manuscript.

ACKNOWLEDGMENTS

We thank Miki Ohno and Kie Shioya for experimental support; Yukiko Yoshida, and Yoshimi Yamazaki for maintaining the zebrafish stocks; James Amatruda for the anti-γH2AX antibody; and Kellee R. Siegfreid for the *isa* mutant zebrafish line. The generation of the anti-Hormad1 and anti-Iho1 antibodies was supported by a program of the Joint Usage/Research Center for Developmental Medicine, Institute of Molecular Embryology and Genetics, Kumamoto University. We thank members of Bernard De Massy's laboratory at the Institute of Human Genetics, for discussions.

SUPPLEMENTARY MATERIAL

The Supplementary Material for this article can be found online at: https://www.frontiersin.org/articles/10.3389/fcell.2021.664377/full#supplementary-material

Supplementary Figure 1 | Mapping of the *isa* mutation with SSLP markers. The names of the SSLP markers used and their locations on chromosome 6 (in Mb, the Zv9 zebrafish reference genome) are shown with mapping results. Tu: Tubingen alleles associated with the ENU-mutated line)/IM: inbred India alleles associated with the wild-type line used for backcrossing. Sixteen genes found in an ∼561-kbp region between markers A4891 and z4950 are listed below.

Supplementary Figure 2 | HE-stained sections of *sycp1*$^{+/+}$, *sycp1*$^{isa/isa}$ and *sycp1*$^{del5/del5}$ testes. **(A)** images of *sycp1*$^{+/+}$ and *sycp1*$^{isa/isa}$ testes from siblings at 4 mpf. **(B)** images of *sycp1*$^{+/+}$ and *sycp1*$^{del5/del5}$ testes from siblings at 4 mpf. Representative results of two individual fish are shown for each genotype. Sc: spermatocytes, St: spermatids, Sz: spermatozoa. Lumens with no spermatozoa (asterisks) and spermatocytes with irregular nuclei (inside broken lines) were observed in the *sycp1*$^{isa/isa}$ section, as previously reported (Saito et al., 2014), as well as in the *sycp1*$^{del5/del5}$ section.

Supplementary Figure 3 | HE-stained sections of juvenile gonads. Images of *sycp1*$^{+/+}$ **(A)** and *sycp1*$^{isa/isa}$ **(B)** gonads are shown with fish ID, size (mm) and age (dpf). Samples were obtained from two different siblings indicated in red and black letters. The largest oocytes found on each section of gonads with oocytes are indicated with arrows. For gonads with spermatocysts, examples of spermatocysts are marked with white broken lines. Note that both oocytes and spermatocysts were observed in wt29 gonads (both images are shown here) and that neither oocytes nor spermatocysts were observed in mut14 gonads. These two fish were categorized as N.D. (not determined) in **Figure 2C**. Scale bars, 20 μm.

Supplementary Figure 4 | Proportion of Dmc1/Rad51 foci in telomere-proximal regions. The number of Dmc1/Rad51 foci in telomere-proximal regions was counted in the MZ and MZ-like nuclei quantified for total Dmc1/Rad51 foci in **Figure 6B**. Proportion of Dmc1/Rad51 foci in telomere-proximal regions to total Dmc1/Rad51 foci in a nucleus was plotted for MZ *sycp1*$^{+/+}$ and MZ-like *sycp1*$^{isa/isa}$ spermatocytes.

Supplementary Figure 5 | Quantification of RPA foci in *sycp1*$^{+/+}$ and *sycp1*$^{isa/isa}$ spermatocytes. The number of RPA foci was counted in the same nuclei quantified for RPA signal intensities, as shown in **Figure 6D**. Black bars indicate means. Statistical significance was examined by a two-tailed Mann-Whitney test (*$P < 0.1$, ***$P < 0.001$, ns, not significant; exact P value).

Supplementary Figure 6 | Generation of antibodies against zebrafish Hormad1 and Iho1. **(A)** Western blotting of wild-type testis protein extracts with anti-zebrafish Hormad1 antisera obtained from five immunized mice (M1 to M5), unimmunized mouse serum (Ctrl) and no-serum control (2nd Ab only). The blot image is superposed with a binary image of colorimetric capture of molecular ladders (in blue). The band indicated with a red arrowhead is close to the predicted size of the full-length Hormad1 protein (41 kDa). Each well was loaded with 50 μg protein. M1 serum was used for immunostaining in this study (red). **(B)** Western blotting of protein extracts from *Iho1*$^{+/+}$ and *Iho1*$^{-/-}$ testes with anti-zebrafish Iho1 antisera obtained from immunized mice. The predicted size of the full-length Iho1 protein is 61 kDa, and the band specific to the *Iho1*$^{+/+}$ sample is indicated with a red arrow. Each well was loaded with 50 μg protein. **(C)** Coimmunostaining of Iho1 and Sycp3 on *Iho1*$^{+/+}$ and *Iho1*$^{-/-}$ spermatocyte spreads. Iho1 signals were barely observed in *Iho1*$^{-/-}$ spermatocytes.

Supplementary Table 1 | List of primers used in this study.

Supplementary Table 2 | List of antibodies used in this study.

REFERENCES

Acquaviva, L., Boekhout, M., Karasu, M. E., Brick, K., Pratto, F., Li, T., et al. (2020). Ensuring meiotic DNA break formation in the mouse pseudoautosomal region. *Nature* 582, 426–431. doi: 10.1038/s41586-020-2327-4

Allan, C., Burel, J.-M., Moore, J., Blackburn, C., Linkert, M., Loynton, S., et al. (2012). OMERO: flexible, model-driven data management for experimental biology. *Nat. Methods* 9, 245–253. doi: 10.1038/nmeth.1896

Baker, K. E., and Parker, R. (2004). Nonsense-mediated mRNA decay: terminating erroneous gene expression. *Curr. Opin. Cell Biol.* 16, 293–299. doi: 10.1016/j.ceb.2004.03.003

Barlow, A. L., Benson, F. E., West, S. C., and Hultén, M. A. (1997). Distribution of the Rad51 recombinase in human and mouse spermatocytes. *EMBO J.* 16, 5207–5215. doi: 10.1093/emboj/16.17.5207

Barlow, A. L., and Hultén, M. A. (1998). Crossing over analysis at pachytene in man. *Eur. J. Hum. Genet.* 6, 350–358. doi: 10.1038/sj.ejhg.5200200

Baudat, F., Imai, Y., and de Massy, B. (2013). Meiotic recombination in mammals: localization and regulation. *Nat. Rev. Genet.* 14, 794–806. doi: 10.1038/nrg3573

Bergerat, A., de Massy, B., Gadelle, D., Varoutas, P.-C., Nicolas, A., and Forterre, P. (1997). An atypical topoisomerase II from archaea with implications for meiotic recombination. *Nature* 386, 414–417. doi: 10.1038/386414a0

Bisig, C. G., Guiraldelli, M. F., Kouznetsova, A., Scherthan, H., Höög, C., Dawson, D. S., et al. (2012). Synaptonemal complex components persist at centromeres and are required for homologous centromere pairing in mouse spermatocytes. *PLoS Genet.* 8:e1002701. doi: 10.1371/journal.pgen.1002701

Blokhina, Y. P., Nguyen, A. D., Draper, B. W., and Burgess, S. M. (2019). The telomere bouquet is a hub where meiotic double-strand breaks, synapsis, and stable homolog juxtaposition are coordinated in the zebrafish, *Danio rerio*. *PLoS Genet.* 15:e1007730. doi: 10.1371/journal.pgen.1007730

Boekhout, M., Karasu, M. E., Wang, J., Acquaviva, L., Pratto, F., Brick, K., et al. (2019). REC114 partner ANKRD31 controls number, timing and location of meiotic DNA breaks. *Mol. Cell* 74, 1053–1068.e8. doi: 10.1016/j.molcel.2019.03.023

Bolcun-Filas, E., Costa, Y., Speed, R., Taggart, M., Benavente, R., De Rooij, D. G., et al. (2007). SYCE2 is required for synaptonemal complex assembly, double strand break repair, and homologous recombination. *J. Cell Biol.* 176, 741–747. doi: 10.1083/jcb.200610027

Bolcun-Filas, E., and Schimenti, J. C. (2012). Genetics of meiosis and recombination in mice. *Int. Rev. Cell Mol. Biol.* 298, 179–227. doi: 10.1016/B978-0-12-394309-5.00005-5

Bolcun-Filas, E., Hall, E., Speed, R., Taggart, M., Grey, C., de Massy, B., et al. (2009). Mutation of the mouse syce1 gene disrupts synapsis and suggests a link between synaptonemal complex structural components and DNA repair. *PLoS Genet.* 5:e1000393. doi: 10.1371/journal.pgen.1000393

Brick, K., Smagulova, F., Khil, P., Camerini-Otero, R. D., and Petukhova, G. V. (2012). Genetic recombination is directed away from functional genomic elements in mice. *Nature* 485, 642–645. doi: 10.1038/nature11089

Brick, K., Thibault-Sennett, S., Smagulova, F., Lam, K.-W. G., Pu, Y., Pratto, F., et al. (2018). Extensive sex differences at the initiation of genetic recombination. *Nature* 561, 338–342. doi: 10.1038/s41586-018-0492-5

Brown, M. S., and Bishop, D. K. (2015). DNA strand exchange and RecA homologs in meiosis. *Cold Spring Harb. Perspect. Biol.* 7:a016659. doi: 10.1101/cshperspect.a016659

Brown, P. W., Judis, L., Chan, E. R., Schwartz, S., Seftel, A., Thomas, A., et al. (2005). Meiotic synapsis proceeds from a limited number of subtelomeric sites in the human male. *Am. J. Hum. Genet.* 77, 556–566. doi: 10.1086/468188

Chen, Y., Zeng, S., Hu, R., Wang, X., Huang, W., Liu, J., et al. (2017). Using local chromatin structure to improve CRISPR/Cas9 efficiency in zebrafish. *PLoS One* 12:e0182528. doi: 10.1371/journal.pone.0182528

Coop, G., Wen, X., Ober, C., Pritchard, J. K., and Przeworski, M. (2008). High-resolution mapping of crossovers reveals extensive variation in fine-scale recombination patterns among humans. *Science* 319, 1395–1398. doi: 10.1126/science.1151851

Costa, Y., Speed, R., Öllinger, R., Alsheimer, M., Semple, C. A., Gautier, P., et al. (2005). Two novel proteins recruited by synaptonemal complex protein 1 (SYCP1) are at the centre of meiosis. *J. Cell Sci.* 118, 2755–2762. doi: 10.1242/jcs.02402

de Massy, B. (2013). Initiation of meiotic recombination: how and where? conservation and specificities among eukaryotes. *Ann. Rev. Genet.* 47, 563–599. doi: 10.1146/annurev-genet-110711-155423

de Vries, F. A. T., de Boer, E., van den Bosch, M., Baarends, WM., Ooms, M., Yuan, L., et al. (2005). Mouse Sycp1 functions in synaptonemal complex assembly, meiotic recombination, and XY body formation. *Genes Dev.* 19, 1376–1389. doi: 10.1101/gad.329705

de Vries, L., Behar, D. M., Smirin-Yosef, P., Lagovsky, I., Tzur, S., and Basel-Vanagaite, L. (2014). Exome sequencing reveals SYCE1 mutation associated with autosomal recessive primary ovarian insufficiency. *J. Clin. Endocrinol. Metab.* 99, E2129–E2132. doi: 10.1210/jc.2014-1268

Dereli, I., Stanzione, M., Olmeda, F., Papanikos, F., Baumann, M., Demir, S., et al. (2021).pronged Four- negative feedback of DSB machinery in meiotic DNA-break control in mice. *Nucleic Acids Res.* doi: 10.1093/nar/gkab082 [Epub ahead of print].

Draper, B. W., McCallum, C. M., and Moens, C. B. (2007). nanos1 is required to maintain oocyte production in adult zebrafish. *Dev. Biol.* 305, 589–598. doi: 10.1016/j.ydbio.2007.03.007

Dunce, J. M., Dunne, O. M., Ratcliff, M., Millán, C., Madgwick, S., Usón, I., et al. (2018). Structural basis of meiotic chromosome synapsis through SYCP1 self-assembly. *Nat. Struct. Mol. Biol.* 25, 557–569. doi: 10.1038/s41594-018-0078-9

Elkouby, Y. M., and Mullins, M. C. (2017). Methods for the analysis of early oogenesis in zebrafish. *Dev. Biol.* 430, 310–324. doi: 10.1016/j.ydbio.2016.12.014

Feitsma, H., Leal, M. C., Moens, P. B., Cuppen, E., and Schulz, R. W. (2007). Mlh1 deficiency in zebrafish results in male sterility and aneuploid as well as triploid progeny in females. *Genetics* 175, 1561–1569. doi: 10.1534/genetics.106.068171

Fraune, J., Alsheimer, M., Volff, J.-N., Busch, K., Fraune, S., Bosch, T. C. G., et al. (2012). Hydra meiosis reveals unexpected conservation of structural synaptonemal complex proteins across metazoans. *Proc. Natl. Acad. Sci. U.S.A.* 109, 16588–16593. doi: 10.1073/pnas.1206875109

Fujiwara, Y., Horisawa-Takada, Y., Inoue, E., Tani, N., Shibuya, H., Fujimura, S., et al. (2020). Meiotic cohesins mediate initial loading of HORMAD1 to the chromosomes and coordinate SC formation during meiotic prophase. *PLoS Genet.* 16:e1009048. doi: 10.1371/journal.pgen.1009048

Fukuda, T., Daniel, K., Wojtasz, L., Toth, A., and Höög, C. (2010). A novel mammalian HORMA domain-containing protein, HORMAD1, preferentially associates with unsynapsed meiotic chromosomes. *Exp. Cell Res.* 316, 158–171. doi: 10.1016/j.yexcr.2009.08.007

Gautier, A., Goupil, A.-S., Le Gac, F., and Lareyre, J.-J. (2013). A promoter fragment of the sycp1 gene is sufficient to drive transgene expression in male and female meiotic germ cells in zebrafish. *Biol. Reprod.* 89, 1–14. doi: 10.1095/biolreprod.113.107706

Gómez-H, L., Felipe-Medina, N., Sánchez-Martín, M., Davies, O. R., Ramos, I., García-Tuñón, I., et al. (2016). C14ORF39/SIX6OS1 is a constituent of the synaptonemal complex and is essential for mouse fertility. *Nat. Commun.* 7:13298. doi: 10.1038/ncomms13298

Gray, S., and Cohen, P. E. (2016). Control of meiotic crossovers: from double-strand break formation to designation. *Annu. Rev. Genet.* 50, 175–210. doi: 10.1146/annurev-genet-120215-035111

Grishaeva, T. M., and Bogdanov, Y. F. (2014). Conservation and variability of synaptonemal complex proteins in phylogenesis of eukaryotes. *Int. J. Evol. Biol.* 2014:856230. doi: 10.1155/2014/856230

Gruhn, J. R., Al-Asmar, N., Fasnacht, R., Maylor-Hagen, H., Peinado, V., Rubio, C., et al. (2016). Correlations between synaptic initiation and meiotic recombination: a study of humans and Mice. *Am. J. Hum. Genet.* 98, 102–115. doi: 10.1016/j.ajhg.2015.11.019

Hamer, G., Gell, K., Kouznetsova, A., Novak, I., Benavente, R., and Höög, C. (2006). Characterization of a novel meiosis-specific protein within the central element of the synaptonemal complex. *J. Cell Sci.* 119, 4025–4032. doi: 10.1242/jcs.03182

Hamer, G., Wang, H., Bolcun-Filas, E., Cooke, H. J., Benavente, R., and Höög, C. (2008). Progression of meiotic recombination requires structural maturation of the central element of the synaptonemal complex. *J. Cell Sci.* 121, 2445–2451. doi: 10.1242/jcs.033233

Higgins, J. D., Sanchez-Moran, E., Armstrong, S. J., Jones, G. H., and Franklin, F. C. H. (2005). The *Arabidopsis* synaptonemal complex protein ZYP1 is required for chromosome synapsis and normal fidelity of crossing over. *Genes Dev.* 19, 2488–2500. doi: 10.1101/gad.354705

Hinch, A. G., Becker, P. W., Li, T., Moralli, D., Zhang, G., Bycroft, C., et al. (2020). The configuration of RPA, RAD51, and DMC1 binding in meiosis reveals the nature of critical recombination intermediates. *Mol. Cell* 79, 689–701.e10. doi: 10.1016/j.molcel.2020.06.015

Houwing, S., Kamminga, L. M., Berezikov, E., Cronembold, D., Girard, A., van den Elst, H., et al. (2007). A role for Piwi and piRNAs in germ cell maintenance and transposon silencing in zebrafish. *Cell* 129, 69–82. doi: 10.1016/j.cell.2007.03.026

Hunter, N. (2015). Meiotic recombination: the essence of heredity. *Cold Spring Harb. Perspect. Biol.* 7:a016618. doi: 10.1101/cshperspect.a016618

Hwang, W. Y., Fu, Y., Reyon, D., Maeder, M. L., Tsai, S. Q., Sander, J. D., et al. (2013). Efficient genome editing in zebrafish using a CRISPR-Cas system. *Nat. Biotech.* 31, 227–229. doi: 10.1038/nbt.2501

Kamminga, L. M., Luteijn, M. J., den Broeder, M. J., Redl, S., Kaaij, L. J. T., Roovers, E. K., et al. (2010). Hen1 is required for oocyte development and piRNA stability in zebrafish. *EMBO J.* 29, 3688–3700. doi: 10.1038/emboj.2010.233

Keeney, S., Giroux, C. N., and Kleckner, N. (1997). Meiosis-specific DNA double-strand breaks are catalyzed by Spo11, a member of a widely conserved protein family. *Cell* 88, 375–384. doi: 10.1016/S0092-8674(00)81876-0

Khil, P. P., and Camerini-Otero, R. D. (2010). Genetic crossovers are predicted accurately by the computed human recombination map. *PLoS Genet.* 6:e1000831. doi: 10.1371/journal.pgen.1000831

Kirkness, E. F., Grindberg, R. V., Yee-Greenbaum, J., Marshall, C. R., Scherer, S. W., Lasken, R. S., et al. (2013). Sequencing of isolated sperm cells for direct haplotyping of a human genome. *Genome Res.* 23, 826–832. doi: 10.1101/gr.144600.112

Kochakpour, N., and Moens, P. B. (2008). Sex-specific crossover patterns in Zebrafish (*Danio rerio*). *Heredity* 100, 489–495. doi: 10.1038/sj.hdy.6801091

Kong, A., Gudbjartsson, D. F., Sainz, J., Jonsdottir, G. M., Gudjonsson, S. A., Richardsson, B., et al. (2002). A high-resolution recombination map of the human genome. *Nat. Genet.* 31, 241–247. doi: 10.1038/ng917

Kumar, R., Bourbon, H.-M., and de Massy, B. (2010). Functional conservation of Mei4 for meiotic DNA double-strand break formation from yeasts to mice. *Genes Dev.* 24, 1266–1280. doi: 10.1101/gad.571710

Kumar, R., Oliver, C., Brun, C., Juarez-Martinez, A. B., Tarabay, Y., Kadlec, J., et al. (2018). Mouse REC114 is essential for meiotic DNA double-strand break formation and forms a complex with MEI4. *Life Sci. Alliance* 1:e201800259. doi: 10.26508/lsa.201800259

Lewis, B. P., Green, R. E., and Brenner, S. E. (2003). Evidence for the widespread coupling of alternative splicing and nonsense-mediated mRNA decay in humans. *Proc. Natl. Acad. Sci. U.S.A.* 100, 189–192. doi: 10.1073/pnas.0136770100

Liew, W. C., Bartfai, R., Lim, Z., Sreenivasan, R., Siegfried, K. R., and Orban, L. (2012). Polygenic sex determination system in zebrafish. *PLoS One* 7:e34397. doi: 10.1371/journal.pone.0034397

Lu, S., Zong, C., Fan, W., Yang, M., Li, J., Chapman, A. R., et al. (2012). Probing meiotic recombination and aneuploidy of single sperm cells by whole genome sequencing. *Science* 338, 1627–1630. doi: 10.1126/science.1229112

Maack, G., and Segner, H. (2003). Morphological development of the gonads in zebrafish. *J. Fish Biol.* 62, 895–906. doi: 10.1046/j.1095-8649.2003.00074.x

MacQueen, A. J., Colaiácovo, M. P., McDonald, K., and Villeneuve, A. M. (2002). Synapsis-dependent and -independent mechanisms stabilize homolog pairing during meiotic prophase in C. elegans. *Genes Dev.* 16, 2428–2442. doi: 10.1101/gad.1011602

Mahadevaiah, S. K., Turner, J. M. A., Baudat, F., Rogakou, E. P., de Boer, P., Blanco-Rodríguez, J., et al. (2001). Recombinational DNA double-strand breaks in mice precede synapsis. *Nat. Genet.* 27, 271–276. doi: 10.1038/85830

Malik, S.-B., Ramesh, M. A., Hulstrand, A. M., and Logsdon, J. M. (2007). Protist homologs of the meiotic Spo11 gene and topoisomerase VI reveal an evolutionary history of gene duplication and lineage-specific loss. *Mol. Biol. Evol.* 24, 2827–2841. doi: 10.1093/molbev/msm217

Meuwissen, R. L., Offenberg, H. H., Dietrich, A. J., Riesewijk, A., van Iersel, M., and Heyting, C. (1992). A coiled-coil related protein specific for synapsed regions of meiotic prophase chromosomes. *EMBO J.* 11, 5091–5100. doi: 10.1002/j.1460-2075.1992.tb05616.x

Moens, P. B. (2006). Zebrafish: chiasmata and interference. *Genome* 49, 205–208. doi: 10.1139/g06-021

Osman, K., Sanchez-Moran, E., Higgins, J. D., Jones, G. H., and Franklin, F. C. H. (2006). Chromosome synapsis in *Arabidopsis*: analysis of the transverse filament protein ZYP1 reveals novel functions for the synaptonemal complex. *Chromosoma* 115:212. doi: 10.1007/s00412-005-0042-4

Papanikos, F., Clément, J. A. J., Testa, E., Ravindranathan, R., Grey, C., Dereli, I., et al. (2019). Mouse ANKRD31 regulates spatiotemporal patterning of meiotic recombination initiation and ensures recombination between X and Y Sex chromosomes. *Mol. Cell* 74, 1069–1085.e11. doi: 10.1016/j.molcel.2019.03.022

Pratto, F., Brick, K., Khil, P., Smagulova, F., Petukhova, G. V., and Camerini-Otero, R. D. (2014). Recombination initiation maps of individual human genomes. *Science* 346, 1256442. doi: 10.1126/science.1256442

Robert, T., Nore, A., Brun, C., Maffre, C., Crimi, B., Guichard, V., et al. (2016). The TopoVIB-Like protein family is required for meiotic DNA double-strand break formation. *Science* 351, 943–949. doi: 10.1126/science.aad5309

Rodríguez-Marí, A., Cañestro, C., BreMiller, R. A., Nguyen-Johnson, A., Asakawa, K., Kawakami, K., et al. (2010). Sex reversal in zebrafish fancl mutants is caused by Tp53-mediated germ cell apoptosis. *PLoS Genet.* 6:e1001034. doi: 10.1371/journal.pgen.1001034

Rodríguez-Marí, A., Yan, Y.-L., BreMiller, R. A., Wilson, C., Cañestro, C., and Postlethwait, J. H. (2005). Characterization and expression pattern of zebrafish

anti-Müllerian hormone (amh) relative to sox9a, sox9b, and cyp19a1a, during gonad development. *Gene Expr. Patterns* 5, 655–667. doi: 10.1016/j.modgep.2005.02.008

Saito, K., Sakai, C., Kawasaki, T., and Sakai, N. (2014). Telomere distribution pattern and synapsis initiation during spermatogenesis in zebrafish. *Dev. Dyn.* 243, 1448–1456. doi: 10.1002/dvdy.24166

Saito, K., Siegfried, K. R., Nüsslein-Volhard, C., and Sakai, N. (2011). Isolation and cytogenetic characterization of zebrafish meiotic prophase I mutants. *Dev. Dyn.* 240, 1779–1792. doi: 10.1002/dvdy.22661

Sansam, C. L., and Pezza, R. J. (2015). Connecting by breaking and repairing: mechanisms of DNA strand exchange in meiotic recombination. *FEBS J.* 282, 2444–2457. doi: 10.1111/febs.13317

Sasaki, A., Ide, S., Kawamoto, Y., Bando, T., Murata, Y., Shimura, M., et al. (2016). Telomere visualization in tissue sections using pyrrole–imidazole polyamide probes. *Sci. Rep.* 6:29261. doi: 10.1038/srep29261

Schindelin, J., Arganda-Carreras, I., Frise, E., Kaynig, V., Longair, M., Pietzsch, T., et al. (2012). Fiji: an open-source platform for biological-image analysis. *Nat. Methods* 9, 676–682. doi: 10.1038/nmeth.2019

Schramm, S., Fraune, J., Naumann, R., Hernandez-Hernandez, A., Höög, C., Cooke, H. J., et al. (2011). A novel mouse synaptonemal complex protein is essential for loading of central element proteins, recombination, and fertility. *PLoS Genet.* 7:e1002088. doi: 10.1371/journal.pgen.1002088

Scully, R., and Xie, A. (2013). Double strand break repair functions of histone H2AX. *Mutat. Res.* 750, 5–14. doi: 10.1016/j.mrfmmm.2013.07.007

Selman, K., Wallace, R. A., Sarka, A., and Qi, X. (1993). Stages of oocyte development in the zebrafish, *Brachydanio rerio*. *J. Morphol.* 218, 203–224. doi: 10.1002/jmor.1052180209

Shi, B., Xue, J., Yin, H., Guo, R., Luo, M., Ye, L., et al. (2019). Dual functions for the ssDNA-binding protein RPA in meiotic recombination. *PLoS Genet.* 15:e1007952. doi: 10.1371/journal.pgen.1007952

Shin, Y.-H., Choi, Y., Erdin, S. U., Yatsenko, S. A., Kloc, M., Yang, F., et al. (2010). Hormad1 mutation disrupts synaptonemal complex formation, recombination, and chromosome segregation in mammalian meiosis. *PLoS Genet.* 6:e1001190. doi: 10.1371/journal.pgen.1001190

Shinya, M., and Sakai, N. (2011). Generation of highly homogeneous strains of zebrafish through full sib-pair mating. *G3(Bethesda)* 1, 377–386. doi: 10.1534/g3.111.000851

Shive, H. R., West, R. R., Embree, L. J., Azuma, M., Sood, R., Liu, P., et al. (2010). brca2 in zebrafish ovarian development, spermatogenesis, and tumorigenesis. *Proc. Natl. Acad. Sci. U.S.A.* 107, 19350–19355. doi: 10.1073/pnas.1011630107

Siegfried, K. R., and Nüsslein-Volhard, C. (2008). Germ line control of female sex determination in zebrafish. *Dev. Biol.* 324, 277–287. doi: 10.1016/j.ydbio.2008.09.025

Slanchev, K., Stebler, J., de la Cueva-Méndez, G., and Raz, E. (2005). Development without germ cells: the role of the germ line in zebrafish sex differentiation. *Proc. Natl. Acad. Sci. U.S.A.* 102, 4074–4079. doi: 10.1073/pnas.0407475102

Smagulova, F., Gregoretti, I. V., Brick, K., Khil, P., Camerini-Otero, R. D., and Petukhova, G. V. (2011). Genome-wide analysis reveals novel molecular features of mouse recombination hotspots. *Nature* 472, 375–378. doi: 10.1038/nature09869

Soustelle, C., Vedel, M., Kolodner, R., and Nicolas, A. (2002). Replication protein A is required for meiotic recombination in *Saccharomyces cerevisiae*. *Genetics* 161, 535–547.

Stanzione, M., Baumann, M., Papanikos, F., Dereli, I., Lange, J., Ramlal, A., et al. (2016). Meiotic DNA break formation requires the unsynapsed chromosome axis-binding protein IHO1 (CCDC36) in mice. *Nat. Cell Biol.* 18, 1208–1220. doi: 10.1038/ncb3417

Sugiyama, T., Zaitseva, E. M., and Kowalczykowski, S. C. (1997). A single-stranded DNA-binding protein is needed for efficient presynaptic complex formation by the Saccharomyces cerevisiae Rad51 protein. *J. Biol. Chem.* 272, 7940–7945. doi: 10.1074/jbc.272.12.7940

Sym, M., Engebrecht, J. A., and Roeder, G. S. (1993). ZIP1 is a synaptonemal complex protein required for meiotic chromosome synapsis. *Cell* 72, 365–378. doi: 10.1016/0092-8674(93)90114-6

Takemoto, K., Imai, Y., Saito, K., Kawasaki, T., Carlton, P. M., Ishiguro, K., et al. (2020). Sycp2 is essential for synaptonemal complex assembly, early meiotic recombination and homologous pairing in zebrafish spermatocytes. *PLoS Genet* 16:e1008640. doi: 10.1371/journal.pgen.1008640

Uchida, D., Yamashita, M., Kitano, T., and Iguchi, T. (2002). Oocyte apoptosis during the transition from ovary-like tissue to testes during sex differentiation of juvenile zebrafish. *J. Exp. Biol.* 205, 711–718.

Wang, J., Fan, H. C., Behr, B., and Quake, S. R. (2012). Genome-wide single-cell analysis of recombination activity and De novo mutation rates in human sperm. *Cell* 150, 402–412. doi: 10.1016/j.cell.2012.06.030

Westerfield, M. (1995). *The Zebrafish Book. A Guide for the Laboratory Use of Zebrafish (Danio rerio)*, 3rd Edn. Eugene, OR: University of Oregon Press.

Westergaard, M., and von Wettstein, D. (1972). The synaptinemal complex. *Annu. Rev. Genet.* 6, 71–110. doi: 10.1146/annurev.ge.06.120172.000443

Wojtasz, L., Daniel, K., Roig, I., Bolcun-Filas, E., Xu, H., Boonsanay, V., et al. (2009). Mouse HORMAD1 and HORMAD2, two conserved meiotic chromosomal proteins, are depleted from synapsed chromosome axes with the help of TRIP13 AAA-ATPase. *PLoS Genet.* 5:e1000702. doi: 10.1371/journal.pgen.1000702

Zickler, D., and Kleckner, N. (1999). Meiotic chromosomes: integrating structure and function. *Annu. Rev. Genet.* 33, 603–754. doi: 10.1146/annurev.genet.33.1.603

Zickler, D., and Kleckner, N. (2015). Recombination, pairing, and synapsis of homologs during meiosis. *Cold Spring Harb. Perspect. Biol.* 7:a016626. doi: 10.1101/cshperspect.a016626

Conflict of Interest: The authors declare that the research was conducted in the absence of any commercial or financial relationships that could be construed as a potential conflict of interest.

Copyright © 2021 Imai, Saito, Takemoto, Velilla, Kawasaki, Ishiguro and Sakai. This is an open-access article distributed under the terms of the Creative Commons Attribution License (CC BY). The use, distribution or reproduction in other forums is permitted, provided the original author(s) and the copyright owner(s) are credited and that the original publication in this journal is cited, in accordance with accepted academic practice. No use, distribution or reproduction is permitted which does not comply with these terms.

frontiers in Cell and Developmental Biology

ORIGINAL RESEARCH
published: 01 April 2021
doi: 10.3389/fcell.2021.646214

Dynamic Histone H3 Modifications Regulate Meiosis Initiation via Respiration

Jian Shi[1†], Yanjie Ma[1†], Hui Hua[2†], Yujiao Liu[1], Wei Li[1], Hongxiu Yu[3*] and Chao Liu[1*]*

[1] State Key Laboratory of Stem Cell and Reproductive Biology, Institute of Zoology, Chinese Academy of Sciences, College of Life Sciences, University of Chinese Academy of Sciences, Stem Cell and Regenerative Medicine Innovation Institute, Chinese Academy of Sciences, Beijing, China, [2] State Key Laboratory of Proteomics, National Center for Protein Sciences, Beijing Institute of Lifeomics, Beijing, China, [3] Shanghai Stomatological Hospital & Institutes of Biomedical Sciences, Fudan University, Shanghai, China

OPEN ACCESS

Edited by:
Biao Kong,
Fudan University, China

Reviewed by:
Klaas Schotanus,
Duke University, United States
Axel Imhof,
Ludwig Maximilians University of Munich, Germany

***Correspondence:**
Wei Li
leways@ioz.ac.cn
Hongxiu Yu
hongxiuyu@fudan.edu.cn
Chao Liu
liuchao@ioz.ac.cn

[†] *These authors have contributed equally to this work*

Specialty section:
This article was submitted to Cell Growth and Division, a section of the journal Frontiers in Cell and Developmental Biology

Received: *25 December 2020*
Accepted: *08 March 2021*
Published: *01 April 2021*

Citation:
Shi J, Ma Y, Hua H, Liu Y, Li W, Yu H and Liu C (2021) Dynamic Histone H3 Modifications Regulate Meiosis Initiation via Respiration. Front. Cell Dev. Biol. 9:646214. doi: 10.3389/fcell.2021.646214

Meiosis is essential for genetic stability and diversity during sexual reproduction in most eukaryotes. Chromatin structure and gene expression are drastically changed during meiosis, and various histone modifications have been reported to participate in this unique process. However, the dynamic of histone modifications during meiosis is still not well investigated. Here, by using multiple reaction monitoring (MRM) based LC-MS/MS, we detected dynamic changes of histone H3 lysine post-translational modifications (PTMs). We firstly quantified the precise percentage of H3 modifications on different lysine sites during mouse and yeast meiosis, and found H3 acetylation and methylation were dramatically changed. To further study the potential functions of H3 acetylation and methylation in meiosis, we performed histone H3 lysine mutant screening in yeast, and found that yeast strains lacking H3K18 acetylation (H3K18ac) failed to initiate meiosis due to insufficient *IME1* expression. Further studies showed that the absence of H3K18ac impaired respiration, leading to the reduction of Rim101p, which further upregulated a negative regulator of *IME1* transcription, Smp1p. Together, our studies reveal a novel meiosis initiation pathway mediated by histone H3 modifications.

Keywords: histone modifications, H3K18 acetylation, meiosis initiation, *RIM101*, *SMP1*

INTRODUCTION

To retain genetic stability and variety, most higher eukaryotes produce offspring through sexual reproduction, which includes the production and fusion of two haploid gametes (Smith et al., 2008; Fu et al., 2019). The production of haploid gamete is termed as gametogenesis, in which the diploid precursor germ cells halve the genome content to haploid through meiosis and subsequently develop into fertilization-competent gametes (Lesch and Page, 2012; Kracklauer et al., 2013). In some multicellular organisms, two types of gametes are produced through distinct differentiation processes, including oogenesis and spermatogenesis (Kracklauer et al., 2013; Sacks et al., 2018). Spermatogenesis is a continuous process that includes spermatogonial mitosis, spermatocytic meiosis and spermiogenesis (Roosen-Runge, 1962; Hess and Renato de Franca, 2008), whereas the differentiation of female germ cells is frequently arrested during oocyte maturation (Von Stetina and Orr-Weaver, 2011). Although the development of gametes often display some specialized differentiation processes (Lesch and Page, 2012), the key events of gametogenesis, especially for

meiosis, are relatively conserved from single cell organism yeast to multicellular organisms such as worms, flies and mice (Bolcun-Filas and Schimenti, 2012). As a widely used model organism, yeast plays crucial role in understanding mammalian gametogenesis and offers valuable knowledge of meiosis, such as meiotic DNA double-strand breaks (DSBs) formation, meiotic recombination, and synapsis. Many mammalian meiotic key regulators are identified based on the conserved domains in yeast (Bolcun-Filas and Schimenti, 2012). Yeast sporulation is similar to spermatogenesis to some extent. The early phase of yeast sporulation, meiosis itself and spore formation stages roughly correspond to the spermatogonia, spermatocytes and round spermatid stages during spermatogenesis in mouse (Cooper and Strich, 2011). Therefore, these two models build the way to understand the molecular mechanism underlying gametogenesis regulation.

Meiosis is an integral part of gametogenesis (Sacks et al., 2018). During meiosis, chromatin structure is dynamically changed, and a series of events takes place to ensure genetic stability and diversity, such as the programmed DSBs formation, meiotic recombination, homologous chromosomes synapsis and crossover formation (Zickler and Kleckner, 2015; Hillers et al., 2017). A number of mechanisms are used to ensure proper chromatin organization, including chromatin remodelers, non-coding regulatory RNAs (ncRNA), histone variants and histone modifications (Crespo et al., 2020). Any defects in these events may cause genome instability, which is associated with the failure of haploid gamete production and infertility (Wang et al., 2017, 2019).

Post-transcriptional modifications (PTMs) of histones are essential for regulating chromatin structure and gene expression, and extensively involved in many vital cellular processes (Bannister and Kouzarides, 2011; Tessarz and Kouzarides, 2014). Until now, various histone modifications, such as acetylation, methylation, phosphorylation and ubiquitination, have been reported to participate in meiosis (Grunstein, 1997; Tan et al., 2011; Zentner and Henikoff, 2013). These histone modifications could work individually or comprehensively as a "histone code" to regulate meiosis (Jenuwein and Allis, 2001; Koprinarova et al., 2016). For example, H2A.X phosphorylation on serine 139 (gamma H2A.X) could facilitate meiotic DSB repair and is essential for meiotic sex chromosome inactivation (MSCI) (Fernandez-Capetillo et al., 2003). H2BK120 mono-ubiquitination regulates meiotic recombination by promoting chromatin relaxation (Xu et al., 2016). H3K4 trimethylation is enriched at meiotic DSB sites to initiate meiotic recombination (Acquaviva et al., 2013). H4K44 acetylation could promote chromatin accessibility to facilitate meiotic recombination (Hu et al., 2015). Although a number of studies have been performed to decipher histone codes used during meiosis, the dynamics of histone modifications and their functional roles in meiosis are still not well investigated.

Here, we performed multiple reaction monitoring (MRM) based LC-MS/MS to examine the dynamic changes of histone H3 lysine post-translational modifications during meiosis in both mice and yeast. We found H3 acetylation and methylation were dramatically changed during meiosis. To further study their potential functions, we performed a systematic mutational screen on H3 lysine in yeast and found that H3K18 acetylation (H3K18ac) was critical for meiosis initiation. Further studies showed the absence of H3K18ac influenced yeast respiration, which further downregulated the expression of Rim101p. In addition, deficiency of Rim101p activated the expression of *SMP1*, an inhibitor of *IME1* transcription, which finally led to the failure of meiosis initiation. Therefore, our studies uncover a new relationship between histone H3 modifications and meiosis initiation.

MATERIALS AND METHODS

Strains and Plasmids

All strains and plasmids used in this study were described in **Supplementary Tables 1**, **2**, respectively. Histone shuffling strains were constructed using similar methods described in a previous study (Govin et al., 2010). Wild-type (WT) histone H3 and H4 were provided by *HHT1-HHF1* in plasmid pYES2 and then this plasmid was replaced with the pRS303 carrying mutant *HHT1-HHF1*. All deletion strains were homozygous, generated using a PCR-mediated gene replacement method as previously described (Govin et al., 2010). Overexpression plasmids were created by inserting genes into a pYC2-*CUP1* carrier.

Preparation of Standard Isotope-Labeled Histone Peptides

Standard isotope-labeled histone peptides (**Supplementary Tables 3**, **5**) were prepared as previously described (Gao et al., 2014). Briefly, stock solutions of isotope-labeled histone peptides were prepared at concentrations of 100 μM in 30% acetonitrile. The stock solutions were further diluted by sterile water to get a succession of working standards. Then moderate amounts of standard solution were mixed with 20 μL testing samples to final concentrations of 1, 5, 10, 50, 100, 500, and 1,000 nM as calibration standards. The same methods were used for quality control samples preparation, and the low, medium, and high concentrations were 3, 100, and 850 nM, respectively. All labeled-peptides were mixed at the final concentration of 100 nM in 30% acetonitrile. All prepared solutions and samples were kept at −80°C.

Histone Extraction and Purification

Samples for MRM-based LC-MS/MS were collected from mouse [spermatogonia (n = 4), spermatocytes (n = 4) and round spermatids (n = 3)] and yeast [incubating with sporulation medium at 0 h (n = 2), 4 h (n = 3), and 12 h (n = 3)]. Histone proteins were extracted and depurated as previously described (Shechter et al., 2007). Briefly, about 5×10^6 cells were pyrolyzed in 500 μL hypotonic lysis buffer (10 mM Tris-HCl pH 8.0, 1 mM KCl, 1.5 mM $MgCl_2$, 1 mM DTT, and cocktail of protease inhibitors) at 4°C for 40 min. Samples were then centrifuged for 10 min at 10,000 × g to deposit nuclei. Nuclei were digested with 0.4 M H_2SO_4, deposited with 100% (w/v) trichloroacetic acid (TCA), and washed twice with ice-cold acetone to retrieve

core histones. Histone proteins were further dephlegmated on a C8 column (150 mm × 4.6 mm, Agilent), using an Agilent series 1200 system (Waldbronn, Germany). Finally, histone H3 fractions were mixed together and exsiccated using a SpeedVac for further experiments.

Histones Derivatization and Digestion

The histone N-propionylation derivatization was performed as previously described (Liao et al., 2013; Gao et al., 2014). The extracted histone H3 fraction pool was redissolved in 100 μL sterile water, and 10 μL histone H3 solution was derivatized in the PD buffer (100 mM NHS acid, 25 mM NH_4HCO_3 and 50% acetonitrile) for 30 min at 50°C. Next, the histone H3 were concentrated to dryness with a SpeedVac and digested with trypsin in 25 mM NH_4HCO_3 overnight. Finally, the digested peptides were concentrated to dryness again and derivatized in the PD buffer. Before LC-MS analysis, the derivatized peptides were redissolved in 50 μL sterile water and then combined with 50 μL isotope labeled peptides mixture. 5 μL of the final solution was loaded onto the LC-MS/MS system for further analysis.

LC-MS/MS Analysis

Similar instruments and methods were used as previously described (Gao et al., 2014). Samples were analyzed using a configuration of high-performance liquid chromatography with a Shimadzu Prominence UFLC system (Shimadzu Scientific Instruments, Pleasanton, CA, United States), electrospray Ionization (ESI) with a TurboIonspray probe (AB Sciex, United States) and a QTRAP 5500 mass spectrometer (AB Sciex, United States). An Agilent Zorbax 300 SB-C18 column (150 mm × 4.6 mm, 5 μm; Agilent, United States) was used for chromatographic separation with 0.1% formic acid in sterile water as solvent A and 0.1% formic acid in acetonitrile (v/v) as solvent B. Samples were gradient eluted by a series of solvent: 2% B for 0-2.0 min; 2-30% B for 2.0-30 min; 30-90% B for 30-31 min, 90% B for 31-34 min, and were finally equilibrated to 2% B at a flow rate of 0.6 mL/min for 4 min. The infusion sample volume was 5 μL, the temperature of column was held at 25°C. The voltage of ion spray was set to 5000 V, and the temperature of the turbo spray was 550°C. 60 and 65 arbitrary units was set for nebulizer gas and heater gas, respectively. The curtain gas was set at 40 arbitrary units and turned on the interface heater. The collision energy and declustering potential for all isotope-labeled and endogenous peptides were adjusted to attain maximum MRM intensity. According to their retention times on the HPLC column, the isotope-labeled and endogenous histone peptides were separated in mass spectrometry. Dwell times for each MRM transition were 0.02 s. The AB Sciex analyst software 1.6.1 was used to control and synchronize all the data.

Quantification of Histone Modifications

The quantification of the histone modifications was performed as previously described (Gao et al., 2014). The concentration (C) of isotope labeled synthetic histone modification peptides were used as a standard, peak area $_{peptide}$ and peak area $_{labeled\ peptides}$ were achieved using LC-MS/MS analysis. The targeted endosome histone modification peptide concentration was calculated as below: $C_{peptide} = C_{labeled\ peptide} \times [\text{peak area}_{peptide}/\text{peak area}_{labeled\ peptide}]$. To achieve the relative quantitation of a specific kind of modification on the lysine site in H3, the concentration of the targeted modification divided by the concentrations of all peptides on this targeted site. Using H3K4me1 as an example, the amount of H3K4me1 was calculated as below: $\text{Percentage}_{H3K4me1} = \Sigma\ H3K4me1_{containing\ peptides}/[\Sigma\ H3K4_{containing\ peptides} + \Sigma\ H3K4me1_{containing\ peptides} + \Sigma\ H3K4me2_{containing\ peptides} + \Sigma\ H3K4me3_{containing\ peptides}] \times 100\%$. As some peptides were isobaric and difficult to be resolved by HPLC or precursor peptide ions, the b^{3+} fragment ions were selected in the MRM transitions to distinguish these peptides.

Isolation of Mouse Spermatogenic Cells

Testes from 7-day, 17-day, and 8-week old C57BL/6 mice were used to obtain spermatogonia, spermatocytes and round spermatids, respectively, following a method previously described (Xu et al., 2016). Briefly, testes were obtained and decapsulated. Seminiferous tubules were laniated with tweezers into small pieces and suspended by 8 ml PBS with 1 mg/ml hyaluronidase (Sigma, H3506, St. Louis, MO, United States) and 1 mg/ml collagenase (Sigma, C5138, St. Louis, MO, United States). Then, the samples were gently shaken in 37°C water bath for 5 min. After pipetting, the diffused seminiferous tubules and cells were kept at 37°C for another 5 min shaking softly. Then, the samples were centrifuged at 200 × *g* for 5 min at 4°C. After washed once by PBS, the sediments were re-suspended in 15 ml of PBS with 1 mg/ml DNase I and 0.25% Trypsin. Thereafter, the samples were shaking gently in 37°C water bath for 5 min. Then, the cells were assembled and washed by PBS with 0.5% BSA before filtrated through a 40 μm Nylon Cell Strainer. The cells were carefully loaded on a 2–4% BSA gradient in PBS and separated through sedimentation by gravity. The separate cells were collected into different tubes. The cells from each tube were examined with light microscopy to confirm cell-type and purity. The samples containing same cell type (spermatogonia, spermatocytes and round spermatids) with proper purity (≥90%) were collected together.

Sporulation Conditions

After growth in YPD medium (1% yeast extract, 2% peptone, and 2% glucose) or SD medium (synthetic complete medium with glucose without the corresponding essential amino acid) for 24 h, yeast was deliquesced with YPA medium (1% yeast extract, 2% peptone, and 2% potassium acetate) to OD_{600} = 0.3. Following growth for 10 h at 30°C, cells were gathered, washed, and resuspended in SPM (a sporulation medium, 2% potassium acetate) to OD_{600} = 1.9 and cultured at 30°C for sporulation. In addition, another method was used for WT and respiratory defective cells for sporulation, which was induced by rapamycin as previously depicted (Zheng and Schreiber, 1997). The strains were cultivated in YPD for 24 h shaking vigorously. When cells reached the G1 phase, they were aliquoted into two aliquots. One aliquot was cultivated with methanol as a control, and the other aliquot was treated with rapamycin at a final concentration of

100 nM. To evaluate the sporulation efficiency, meiotic nuclear divisions were used as a surrogate and observed by treating DNA with 1 mg/mL DAPI (4′, 6-diamidino-2-phenylindole). The cells were gathered at the designated times, and then fixed with 1 mL 70% ethanol for subsequent DAPI treating. A Nikon Eclipse Ti microscope (Eclipse Ti-S; Nikon, Tokyo, Japan) was used to obtain and analysis the images.

Flow Cytometry

About 1×10^7 cells were fixed overnight with 1 mL cold 70% ethanol, and then resuspended in 1 mL 50 mM sodium citrate for DNA content analysis. The cells were centrifuged at $845 \times g$ for 5 min, and the sediments were digested with RNase A (Sigma Aldrich, Shanghai, China) for 2 h at 37°C. After sonication for 2 s at 20% power, the samples were stained with 1 mM Sytox Green (Molecular Probes, Eugene, OR, United States). A BD FACS vantage SE Flow Cytometry System (BD, Franklin Lakes, NJ, United States) was used to analysis the results.

Yeast Growth Sensitivity

Yeast strains were cultured in YPD or SD medium to OD_{600} of 1.0 at 30°C. The cells were gathered, washed, and serially diluted. Each dilution was then spotted onto an auxotrophic plate containing glucose or glycerol and then cultured for 2 days at 30°C.

Immunoblotting

After mild alkaline treatment, cells were boiled in a standard electrophoresis loading buffer similar as previously described (Kushnirov, 2000). The protein samples were split by SDS-PAGE and then transferred to nitrocellulose membranes using a Bio-Rad *Trans*-Blot SD Semi-Dry Transfer Cell system. After incubation overnight at 4°C using a primary antibody, the blots were incubated with a secondary antibody (926-32211; LI-COR Biosciences, Lincoln, NE, United States). Then, an Odyssey infrared 740 imager (9120; LI-COR Biosciences) was used to scan the blots. H3K4me1, H3K4me2, H3K4me3, H3K9ac, H3K18me1, H3K23ac, H3K79me2, and H3K79me3 antibodies were obtained from EASYBIO (BE3281, BE3275, BE3224, BE3276, BE3291, BE3227, BE3301, and BE3302; Beijing, China). MYC and HA antibodies were purchased from Abmart (M20002 and M20003; Shanghai, China). FLAG antibodies were purchased from Bioregent Bio company (AB1027t; Beijing, China) and Abmart (M20008L; Shanghai, China). The Pgk1p polyclonal antibody was generated in rabbits.

Oxygen Consumption Measurement

The Seahorse XF96 Extracellular Flux Analyzer (Seahorse Bioscience, Agilent Technologies) was used to detect respirations of WT and mutant yeast cells. The methods were similar as previous description (Bradley et al., 2020). 25 μL 50 μg/mL Poly-D-Lysine were added to each well of the Seahorse plate and incubated for 30 min at room temperature. Then the solution was removed and the plate was dried overnight. The Seahorse XF96 Sensor Cartridge was hydrated with 200 μL water overnight at 37°C, and the Seahorse XF Calibrant Solution was also kept at 37°C overnight. Before experiments, the water was replaced by 200 μL Seahorse XF Calibrant Solution and incubated 1 h at 37°C.

Yeast cells were cultured in YPD overnight at 30°C. On the day of measurement, cells were diluted to OD_{600} = 0.2. After 4 h culture, the exponential phase cells were harvested and resuspended in YPD, YPA, YPG (1% yeast extract, 2% peptone, and 2% glycerol), and YPE (1% yeast extract, 2% peptone, and 2% ethanol), respectively. 175 μL of each kind of cultures were added into the treated Seahorse plate that each well contained about 1×10^5 cells. Then the plate was centrifuged for 3 min at $500 \times g$ and incubated for 30 min at 30°C before loaded into the analyzer. The measure times of basal oxygen consumption rates were 2.5 min, 30 s, and 2.5 min. And 10 cycles were detected.

Yeast Total RNA Extraction

Yeast total RNA extraction was accomplished using previously described methods (Schmitt et al., 1990). Briefly, corresponding sporulation samples were collected and mixed with 400 μL AE buffer (50 mM sodium acetate pH = 5.3 and 10 mM ethylene diamine tetraacetic acid), and 40 μL 10% SDS. After vibration 5 min using a vortex mixer (Scientific Industries, United States), 400 μL phenol was added and vibrated for another 5 min. Samples were next incubated for 4 min at 65°C and instantly cooled on ice. After centrifuged at 13,523 $\times g$ for 2 min, the supernatant was transferred to a new RNase free tube. The samples were then mixed with phenol and chloroform (1:1) and held at room temperature for 5 min, and the supernatant was again transferred to a new tube after centrifuging at 13,523 $\times g$ for 5 min. 2.5 × volume of ethanol and 40 μL 3M sodium acetate were added to the samples, which was finally centrifuged at 13,523 $\times g$ for 10 min to collect the RNA. 1 mL 80% ethanol was used to wash the RNA pellet and the supernatant was removed again after centrifuging at 13,523 $\times g$ for 10 min. Finally, the RNA pellet was dried, dissolved in 20 μL diethyl pyrocarbonate-treated water, and stored at −80°C.

Quantitative Real-Time PCR

A PrimeScript RT Reagent Kit (RR037A, TaKaRa, Kusatsu, Japan) was used to synthesize complementary DNA (cDNA). Amplification was performed in a 10 μl reaction containing 5 μL 2 × EvaGreen mix (Master Mix-S; Applied Biological Materials, Richmond, Canada), 0.5 μL each primer (10 nmol/L), 2 μL sample cDNA, and 2.5 μL ddH2O. A Roche Light Cycler 480II System (Roche Diagnostics, Mannheim, Germany) was used to perform real-time PCR. The PCR program was initiated at 95°C for 10 min, followed by 40 cycles of denaturation for 5 s at 95°C, annealing for 30 s at 60°C, and elongation for 60 s at 72°C. Fluorescence signals were detected at 72°C in the time of the elongation step. Three biological replicates were taken for each sample and normalized to housekeeping gene *TAF10*. A Light Cycle 480 software 1.5.1 was used to analyzed the results. All primers used are shown in **Supplementary Table 7**.

Statistical Analysis

All data were shown as the mean ± SD and statistic differences were calculated using a two-tailed Student's *t*-test. The data were

considered significant when the *P*-value was less than 0.05 (*), 0.01 (**), or 0.001 (***).

RESULTS

Histone H3 Acetylation and Methylation Are Dynamically Changed During Mouse Spermatogenesis

To assess the role of chromatin changes during gametogenesis, we detected the acetylation and methylation of H3 and its variants by using multiple reaction monitoring (MRM)-based LC-MS/MS of three crucial germ cell stages of spermatogenesis in mouse: spermatogonia, spermatocytes and round spermatids (**Figure 1A**). Proteins prepared from the separated cells were mixed with isotope-labeled histone peptides (**Supplementary Table 3**) and then analyzed using MRM-based LC-MS/MS. The concentration of the histones modifications during meiosis was measured by using isotope-labeled histone peptides as standards. Finally, we identified a total of 28 PTMs with 10 N-terminal lysine sites of acetylation, methylation in H3 and its variants, and found acetylation and methylation of H3 and its variants displayed dynamic change during spermatogenesis (**Figure 1B** and **Supplementary Table 4**).

These dynamically changed H3 modifications were clustered into three groups using Cluster 3.0 software (**Figure 1B**). Cluster I modifications showed an obvious decrease from spermatogonia to round spermatids, while cluster III modifications exhibited a gradual increase from spermatogonia to round spermatids (**Figure 1B**). Cluster II modifications showed decreases from spermatogonia to spermatocytes but increases in round spermatids (**Figure 1B**). The H3 modification trends in our data were similar to some previously reported, such as H3K4me1, H3K4me2, and H3K9me3 (Godmann et al., 2007; Iwamori et al., 2011), indicating our mass spec data could profile H3 acetylation and methylation during spermatogenesis quantitatively. To further confirm the data, we examined some H3 modification levels during spermatogenesis by using immunoblotting and found most of these H3 modifications were consistent with our MRM data (**Figures 1C,D**).

As MRM-based LC-MS/MS could determine the concentration of each histone modification, we attempted to quantify the precise percentage of H3 modifications at different lysine sites during spermatogenesis and found that modifications on different lysine sites in H3 or its variants were dramatically different from each other (**Figure 1E** and **Supplementary Table 4**). For example, rare modifications were found on H3K4, H3K18, and H3K79, whereas more than half the H3K9, H3.1K27, and H3.3K27 sites were modified by acetylation or methylation (**Figure 1E**). In these enriched modification sites, modifications were dramatically different between the three crucial stages of spermatogenesis (**Figure 1E**). We speculated that prevalent high percentage modifications might tend to have significant functions, like H3K9 methylation (**Figure 1E**). We also noticed that H3-variants modification were more prevalent than H3 modification (**Figure 1E**), indicating the H3 variants might play important roles in spermatogenesis. As the amount of histone were also dynamically changed during mouse spermatogenesis, the proportion of each kind of modifications on its own site might be different with the trend for the concentration of the histone modifications in **Figure 1B**. Taken together, our findings show MRM-based LC-MS/MS can profile H3 acetylation and methylation during spermatogenesis quantitatively, and H3 acetylation and methylation dynamically change during mouse spermatogenesis.

PTMs of Histone H3 Dynamically Change During Yeast Sporulation

Because we lack a direct way to manipulate histone modification sites in mice, it is difficult to directly assess the function of histone modification in mammals. Given yeast's genetic operability and conservatism with mammals, budding yeast is a powerful model to study the functions of histone modifications in meiosis (Jin and Neiman, 2016; Owens et al., 2018). To explore the functional roles of H3 acetylation and methylation during meiosis, we examined levels of H3 acetylation and methylation by MRM-based LC-MS/MS in yeast after incubating with sporulation medium (SPM) at 0, 4, and 12 h (**Figure 1A** and **Supplementary Table 5**). As these three time points successively represent the early phase, meiosis process and spore formation in sporulation, they roughly correspond to the stages of spermatogonia, spermatocyte and round spermatids in mouse spermatogenesis (Cooper and Strich, 2011). Together, we identified a total of 16 PTMs with 8 N-terminal lysine sites of acetylation and methylation in H3 and found that, similar to the mouse results, acetylation and methylation of H3 displayed dynamic changes during yeast sporulation (**Figure 2A** and **Supplementary Table 6**).

During yeast sporulation, four types of H3 modifications were identified using Cluster 3.0 software (**Figure 2A**). Cluster I modifications showed a strong presence at 4 h, while cluster III modifications exhibited an obvious decrease from 0 to 4 h but an increase at 12 h (**Figure 2A**). Cluster II modifications exhibited a gradual decrease from 0 to 12 h (**Figure 2A**). In contrast, cluster IV modifications showed a gradual increase from 0 to 12 h (**Figure 2A**). We further compared these modifications at different yeast sporulation stages, and found H3K4me1, H3K9ac, H3K14ac, H3K27ac, and H3K36me1 showed obvious dynamic changes during yeast sporulation (**Figures 2B–D**). To further confirm our findings, we examined some H3 modification levels by immunoblotting during yeast sporulation and found most of these H3 modifications were similar to our MRM data (**Figures 2E,F**), indicating our methods could quantitatively profile H3 acetylation and methylation during yeast sporulation.

Next, we quantified the precise percentage of H3 modifications at different lysine sites during yeast sporulation. Similar to our MRM-based LC-MS/MS results in mice, some H3 lysine sites showed rare modification (e.g., H3K9, H3K14, H3K18, and H3K27), whereas other H3 lysine sites showed that more than 50% of the regions could be modified by acetylation or methylation (**Figure 2G** and **Supplementary Table 6**). At these enriched modified lysine sites, modification percentages, as well as specific H3 acetylation and methylation markings,

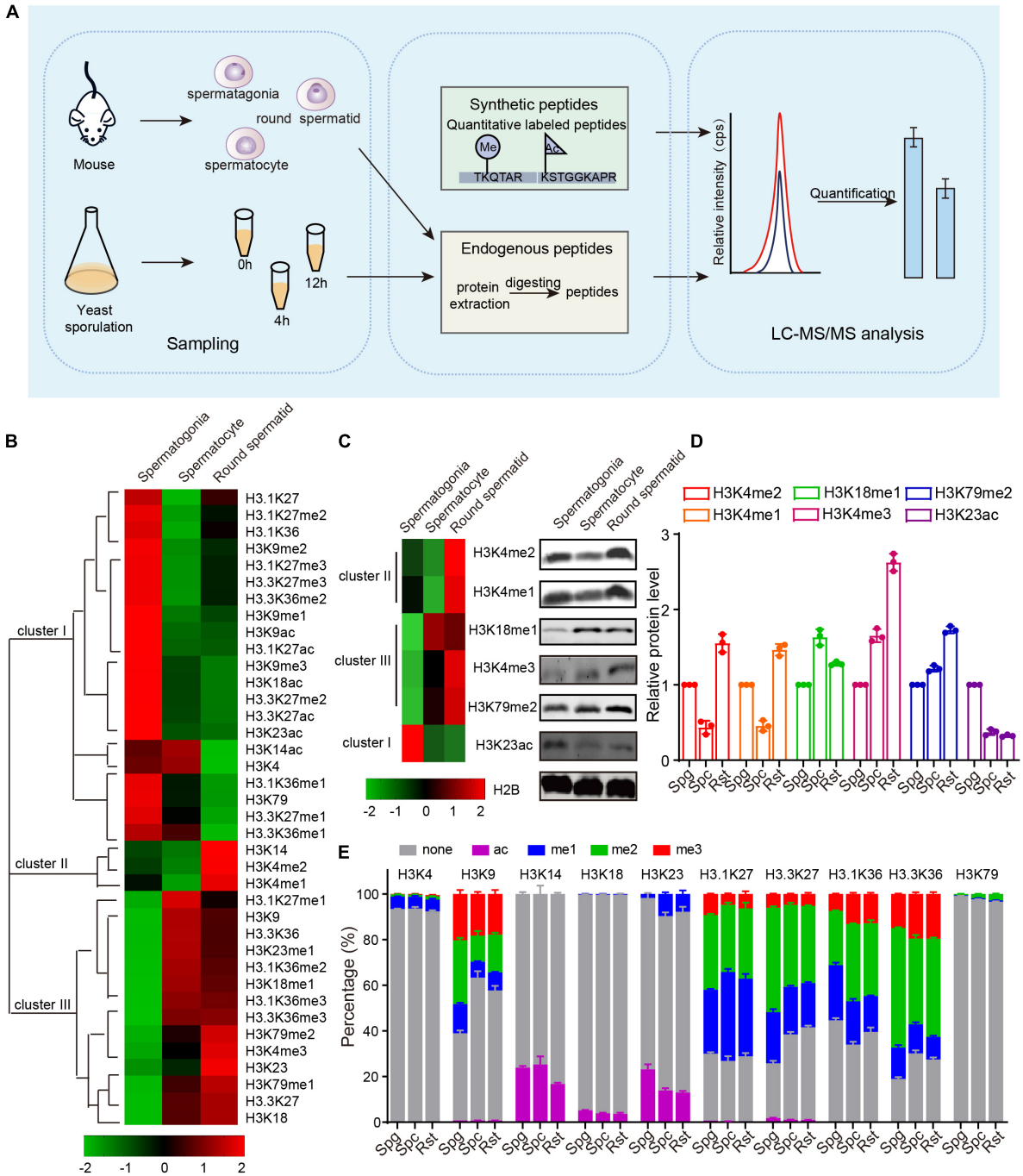

FIGURE 1 | Dynamic changes of mouse histone H3 modifications during spermatogenesis. **(A)** Schematic of MRM-based LC-MS/MS. **(B)** Hierarchical clustering analysis of histone H3 modifications during mouse spermatogenesis. **(C)** Western blot verification of MS data. Protein samples for both western blots and MS were extracted from mouse cells using the same methods. **(D)** Quantitative of the histone modifications level in **C**. The error bars indicate ± SD (n = 3). Spg, spermatogonia; Spc, spermatocytes; Rst, round spermatids. **(E)** Relative abundance of histone modifications at histone H3 lysine sites for mouse MS samples. The error bars indicate ± SD (spermatogonia, n = 4; spermatocytes, n = 4; round spermatids, n = 3). Spg, spermatogonia; Spc, spermatocytes; Rst, round spermatids.

showed dynamics changes during sporulation (**Figure 2G** and **Supplementary Table 6**).

To examine the conservation of H3 acetylation and methylation in mouse and yeast meiosis, we compared MRM-based LC-MS/MS results from mouse and yeast. Although some H3 modifications showed variable tendencies in mice and yeast, the dynamics of some H3 modifications during meiosis were conserved, such as H3K4me1, H3K4me2, and H3K18me1

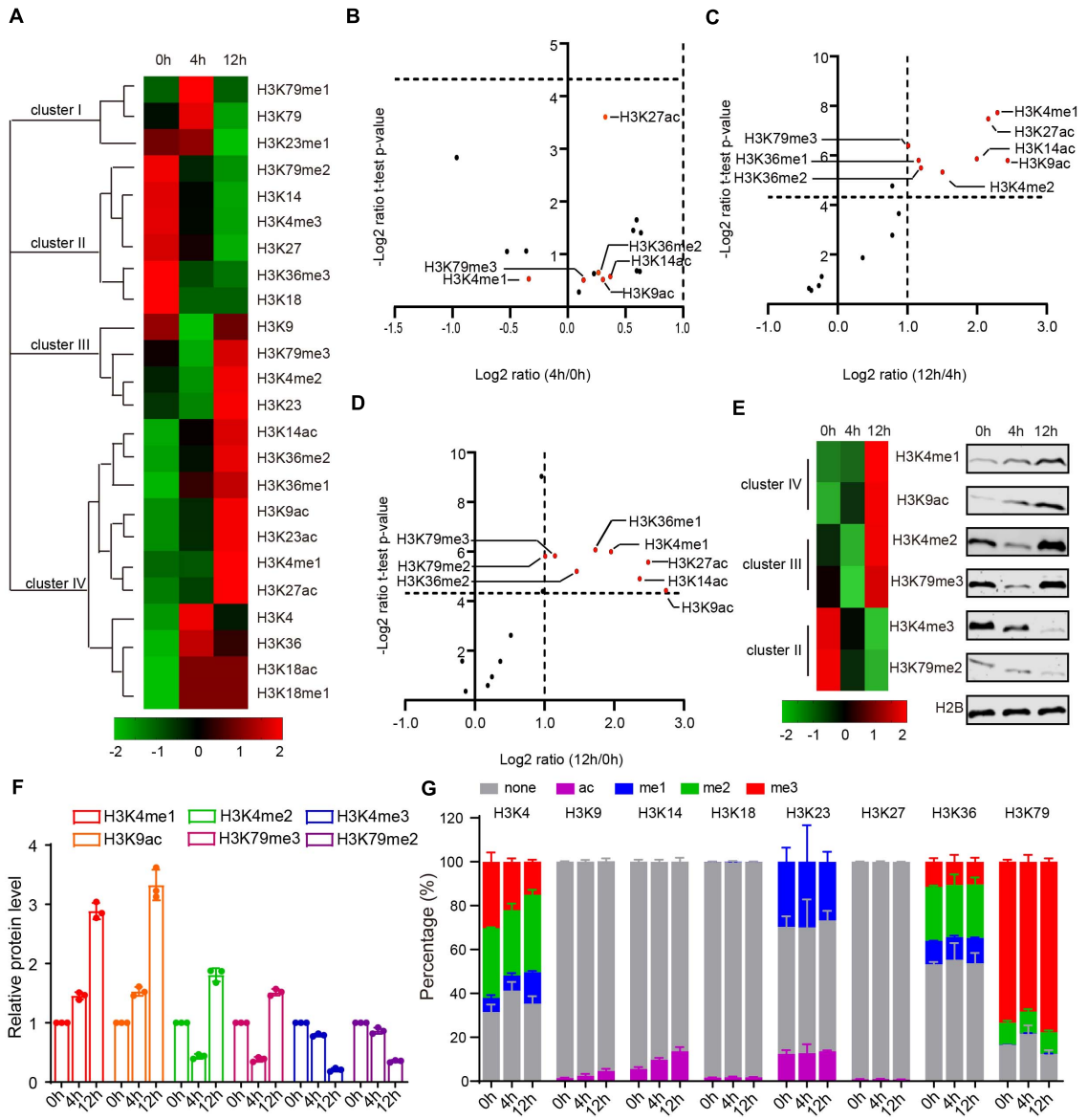

FIGURE 2 | Dynamic changes of yeast histone H3 modifications during sporulation. **(A)** Hierarchical clustering analysis of histone H3 modifications during yeast sporulation. **(B–D)** Volcano Plot indicates upregulated and downregulated histone H3 modifications comparing 4 h/0 h, 12 h/4 h, and 12 h/0 h, respectively. In **(C,D)**, histone H3 modifications with a fold change >2 and a *P*-value < 0.05 are shown in red. **(E)** Western blot verification of MS data. Protein samples for both western blots and MS were extracted from yeast cells using the same methods. **(F)** Quantitative results of **E**. The error bars indicate ± SD (*n* = 3). **(G)** Relative abundance of histone modifications at histone H3 lysine sites for yeast MS samples.

(**Supplementary Figure 1**). In summary, H3 acetylation and methylation were dynamically changed during mouse and yeast meiosis, and the variation tendency of some H3 modifications during gametogenesis were conserved in both mice and yeast.

Systematic Screening of H3 Lysine in Yeast

To further assess the functional role of H3 acetylation and methylation during meiosis, we performed a screen using systematic mutagenesis to substitute histone H3 lysine sites in yeast, based on a "histone shuffle" approach as previously described (Govin et al., 2010; **Figure 3A**). First, we deleted endogenous H3 and H4 genes (*HHF1*, *HHF2*, *HHT1*, and *HHT2*), and stabilized histone H3 and H4 protein levels by transforming a plasmid that contained *HHT1*, *HHF1*, and a *URA3* selectable marker (**Figure 3A**). Next, multiple H3 lysine mutations were included in a second plasmid (Lysine mutate to Alanine) included the WT promoter, making histone H3 protein expression similar to that of WT (**Figure 3A**). After the mutant plasmids were established, the original WT plasmid was removed using negative selection

of *URA3* with 5-Fluoroorotic Acid (5-FOA) (**Figure 3A** and **Supplementary Figure 2**). Examination of the shuffle yeast strain showed that endogenous H3 proteins were absent, which could be replaced by the FLAG-tagged versions of histone (**Supplementary Figure 2**). Importantly, the sporulation efficiency of the shuffle strain was comparable to that of the WT strain (**Figure 3B**).

Next, we performed sporulation of these H3 mutant strains and found that the sporulation efficiency of H3K4A, H3K18A, H3K27A, H3K42A, and H3K79A mutants showed significant decreases compared with that of the WT and shuffle strain (**Supplementary Figure 3** and **Figures 3B,C**), indicating the modifications on these sites might be very important to yeast sporulation. To further examine which modification types on these sites is important for yeast sporulation, we mutated Lysine (K) to Glutamine (Q) to mimic acetylation, to Leucine (L) to mimic mono-methylation, or to Methionine (M) to mimic di-methylation (Hyland et al., 2011; **Supplementary Figure 4**). We next determined the modification effects on sporulation efficiency. We found that H3K18Q and H3K18L could partially rescue impaired sporulation in H3K18A, indicating persistent H3K18ac and H3K18me were critical for yeast sporulation (**Figures 3D,E**). Similar results were observed for H3K27M, H3K42L, H3K42M, H3K42Q, H3K79L, and H3K79M, which suggest acetylation and methylation on H3K27, H3K42, and H3K79 might play important roles in yeast sporulation (**Figures 3D,E**). Given that the sporulation efficiency of H3K4L and H3K4M strains showed no significant differences compared with that of the H3K4A strain, H3K4me3 may be essential for proper meiosis progress, which is consistent with previous reported roles of H3K4me3 during meiosis (Adam et al., 2018). In addition, we also noticed that although H3K9A had no influence on yeast sporulation, H3K9M impaired sporulation progress (**Supplementary Figure 5**), indicating that persistent H3K9me2 might also influence yeast sporulation. Together, our results indicate that acetylation and methylation on H3K18, H3K27, H3K42, and H3K79 are very important to meiosis in yeast.

H3K18ac Facilitates Sporulation Initiation Through Respiration

Given that H3K18A absolutely blocked the sporulation progress (**Figures 3D**, **4A**) and that H3K18ac showed a higher proportion of K18 modification in H3 during yeast sporulation (**Figure 2G** and **Supplementary Table 6**), we selected H3K18ac for further analyze. To examine which stage was influenced during H3K18A mutant strain sporulation, we first used flow cytometry analysis to detect premeiotic DNA replication in the H3K18A mutant strain. In WT cells, premeiotic DNA replication was initiated at 2 h and finished at 4 h when cells were cultured in sporulation medium (**Figure 4B**). Contrarily, with the H3K18A mutant, premeiotic DNA replication did not even initiate at 10 h after the cells were cultured in SPM (**Figure 4B**). Thus, H3K18ac might be required for premeiotic DNA replication. To further confirm our findings, we generated H3K18R and H3K18Q strains which keeps the positive charge while mimic a non-acetylated state or a persistent H3K18ac state, respectively. We found that the sporulation of H3K18R mutant was blocked which is similar to that of the H3K18A mutant (**Figure 4C**), while the H3K18Q could partially rescue the sporulation progress (**Figures 4A,C**). Furthermore, the H3K18Q was sufficient to initiate premeiotic DNA replication (**Figure 4B**). Thus, our findings suggest that the absence of H3K18ac might perturb yeast sporulation by blocking premeiotic DNA replication.

As Ime1p serves as a master regulator to initiate yeast premeiotic DNA replication (Kassir et al., 1988; Vershon and Pierce, 2000), we evaluated the expression of Ime1p in H3K18A mutants. We found Ime1p expression was dramatically decreased in H3K18A mutants compared with that in WT strain, and the mimic H3K18ac in the H3K18Q mutant could partially rescue Ime1p protein levels (**Figure 4D**). Given that histone modifications commonly regulate gene expression (Fukuda et al., 2006; Rintisch et al., 2014), we speculated that H3K18ac might modulate Ime1p protein levels by regulating *IME1* expression. To test our speculation, we examined mRNA levels of *IME1* in WT, H3K18A and H3K18Q strains using quantitative real-time PCR and found that levels of *IME1* mRNA in WT, H3K18A, and H3K18Q strains correlated with their protein levels (**Figure 4E**), suggesting H3K18ac might modulate meiosis initiation by regulating *IME1* expression.

Many intrinsic and extrinsic signals have been reported to modulate the expression of *IME1* (Jaiswal et al., 2017), and among them, respiration has been shown to be required for *IME1* expression during meiosis (Jambhekar and Amon, 2008; Zhao et al., 2018). Therefore, we speculated that H3K18ac might regulate *IME1* expression via respiration. To test our hypothesis, we cultured WT and H3K18A mutant cells on YPG medium, which contains a non-fermentable carbon source that respiration-deficient cells cannot use. Compared to the WT strain, the H3K18A mutant strain displayed obvious growth defects (**Figure 4F**), whereas the H3K18Q mutant strain did not (**Figure 4F**). Moreover, the H3K18R mutant strain displayed obvious growth defects in YPG (**Figure 4F**), which further supports H3K18A effect can be attributed to acetylation. Therefore, H3K18ac might participate in respiration. To further confirm it, we measured the respiratory capacity of WT and mutant strains in different medium by detecting the oxygen consumption rate via Seahorse XF96 Extracellular Flux Analyzer. We found that the WT, H3K18A, and H3K18Q strains respired normally in YPD medium, when cultured in YPA, YPG, or YPE medium, only H3K18A strain displayed respiration defect, but not the WT or H3K18Q strains (**Figure 4G**). As respiration could also provide energy by using a non-fermentable carbon source during yeast sporulation, we sought to distinguish the effect of H3K18ac on energy supplement and *IME1* expression. To investigate, we induced the sporulation of WT and H3K18A mutant strains with rapamycin in YPD, in which glucose could supply an energy source (Zheng and Schreiber, 1997). We found the H3K18A mutant strain still failed to undergo sporulation compared with the WT strain,

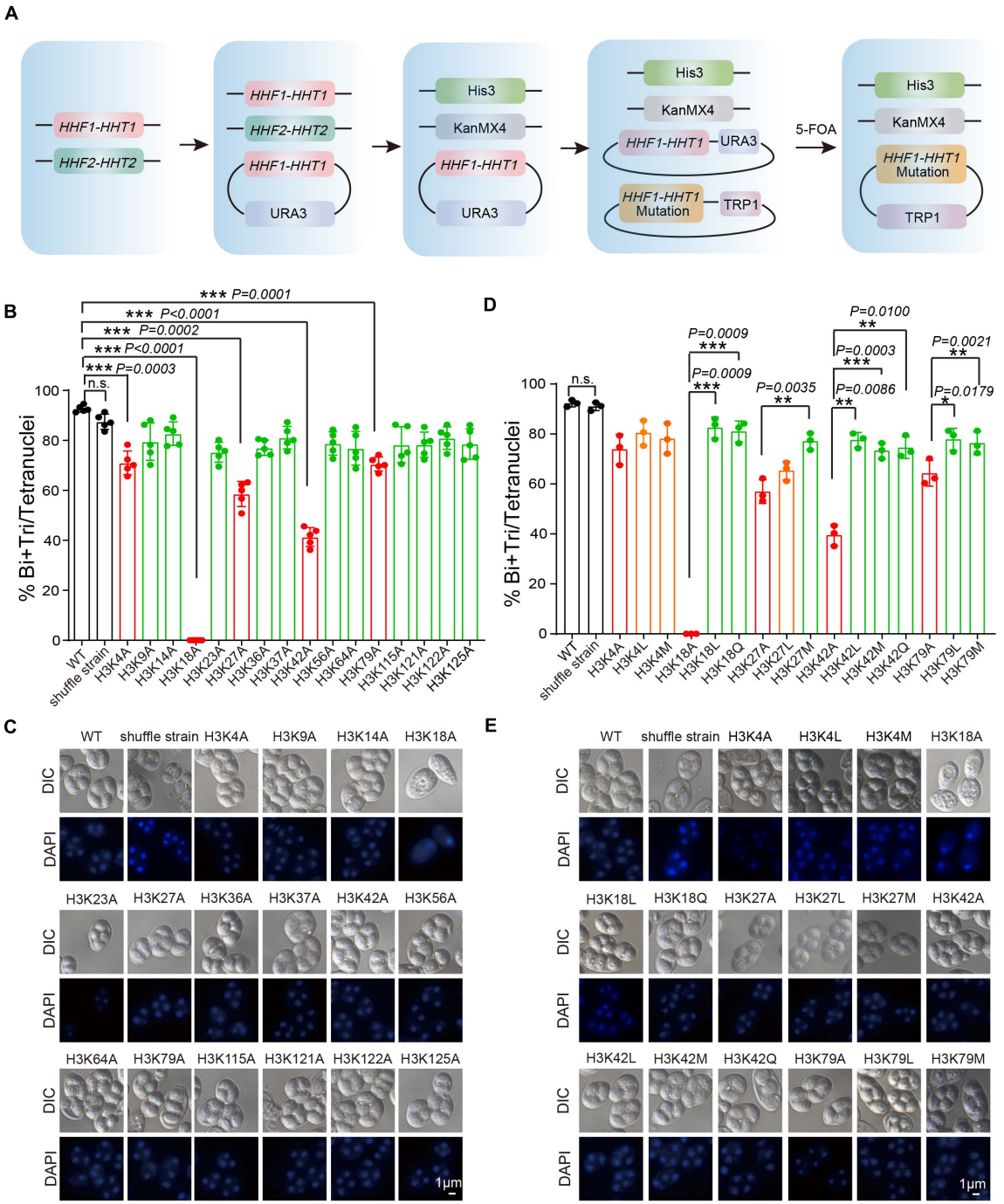

FIGURE 3 | Systematic screen of H3 lysine modifications needed for sporulation. **(A)** H3 mutant strains were generated using an SK1 background. Endogenous histone H3 and H4 genes were knocked out, and the cell (LW1599) was transfected with a plasmid which had an Myc-*HHF1-HHT1*-HA and a *URA3* selection marker. Then, another plasmid with histone H3 point mutation was transfected and 5-FOA negative selection was used to replace the original plasmid. **(B)** Sporulation efficiency of histone H3 K to A mutant strains. The error bars indicate ± SD ($n = 5$). ***$P < 0.001$. n.s. indicates no significant. WT: LW0066; shuffle strain: LW1599; H3K4A: LW1600; H3K9A: LW1601; H3K14A: LW1602; H3K18A: LW1603; H3K23A: LW1604; H3K27A: LW1605; H3K36A: LW1606; H3K37A: LW1607; H3K42A: LW1608; H3K56A: LW1609; H3K64A: LW1610; H3K79A: LW1611; H3K115A: LW1612; H3K121A: LW1613; H3K122A: LW1614; H3K125A: LW1615. **(C)** Images of nuclei from cells in **B**. **(D)** Sporulation efficiency of mutant cells mimic different histone modifications. The error bars indicate ± SD ($n = 3$). *$P < 0.05$, **$P < 0.01$, ***$P < 0.001$. n.s. indicates no significant. WT: LW0066; shuffle strain: LW1599; H3K4A: LW1601; H3K4L: LW1616; H3K4M: LW1617; H3K18A: LW1603; H3K18L: LW1622; H3K18Q: LW1623; H3K27A: LW1605; H3K27L: LW1624; H3K27M: LW1625; H3K42A: LW1608; H3K42L: LW1626; H3K42M: LW1627; H3K42Q: LW1628; H3K79A: LW1611; H3K79L: LW1629; H3K79M: LW1630. **(E)** Images of nuclei from cells in **D**.

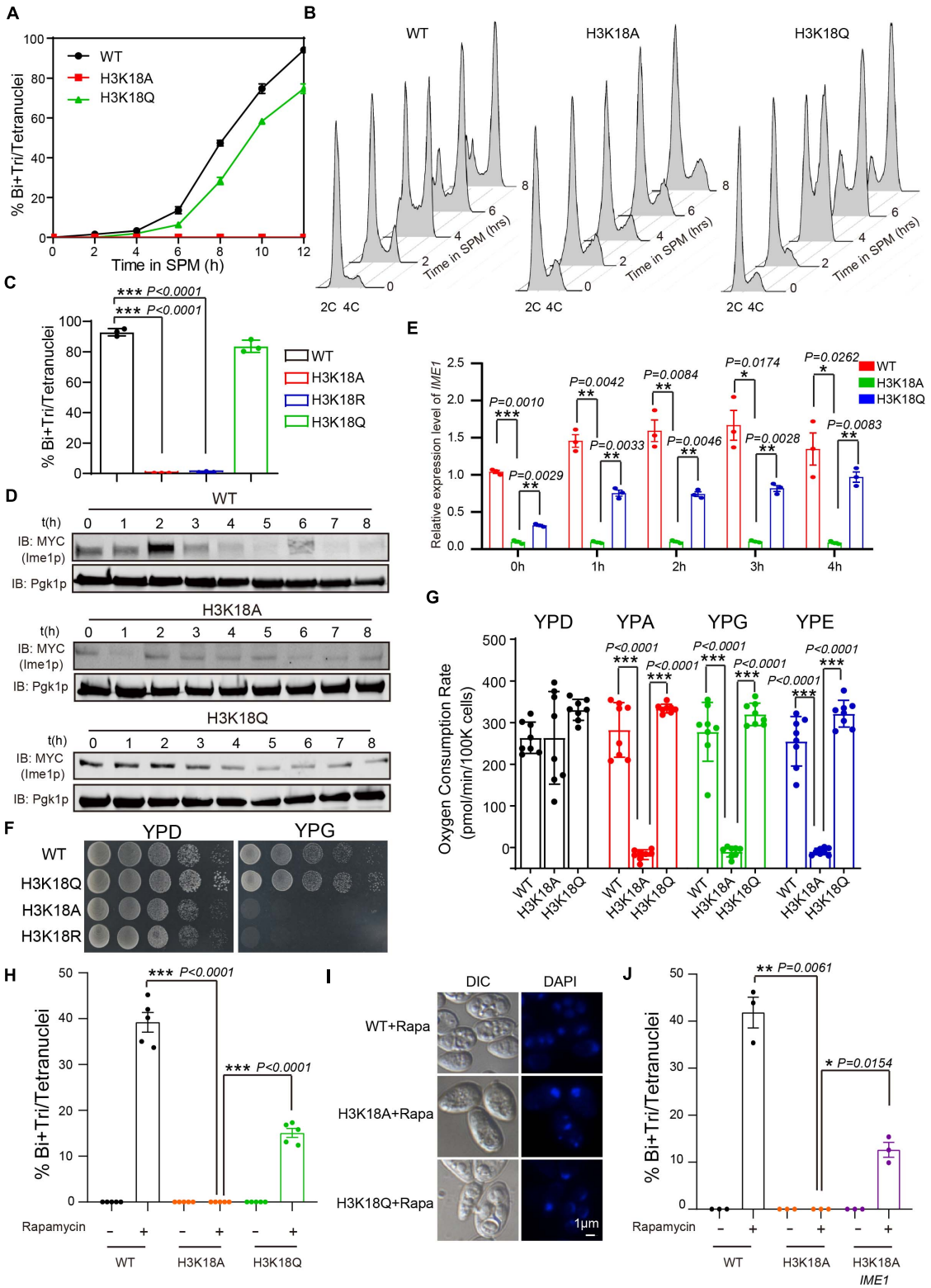

FIGURE 4 | Persistent H3K18ac state is sufficient to induce yeast sporulation. **(A)** Sporulation curve of WT, H3K18A and H3K18Q mutant strains in SPM from 0 h to 12 h. 300 μL samples were fixed with 1 mL 70% ethanol for at least 1 h and then stained with DAPI to calculate sporulation rates. The error bars indicate ± SD (n = 3). **(B)** Flow cytometry of the WT, H3K18A, and H3K18Q mutant strains. Samples were prepared at different times after being cultured in SPM to detect premeiotic DNA replication (2C-4C transition). Premeiotic DNA replication was blocked in the H3K18A mutant strain, whereas the H3K18Q mutant strain showed

(Continued)

FIGURE 4 | Continued
active premeiotic DNA replication. **(C)** Sporulation efficiencies of WT, H3K18A, H3K18R, and H3K18Q. The error bars indicate ± SD (n = 3). ***P < 0.001. H3K18R: LW1643. **(D)** Western blot of Ime1p expression in WT, H3K18A, and H3K18Q mutant strains during sporulation. *IME1* in all three strains was tagged with 9 × Myc. Pgk1p was used as a loading control. WT-*IME1*-9MYC: LW1631; H3K18A-*IME1*-9MYC: LW1632; H3K18Q-*IME1*-9MYC: LW1633. **(E)** Quantitative PCR analyzed *IME1* expression in WT, H3K18A, and H3K18Q mutant strains. Cells were harvested at the indicated times and then total RNA was extracted and reverse transcribed. *IME1* mRNA levels in the three strains were measured by quantitative PCR and normalized to the levels of the house keeping gene *TAF 10*. The error bars indicate ± SD (n = 3). *P < 0.05, **P < 0.01, ***P < 0.001. **(F)** Detection of respiration function of H3K18 mutant strains. Left panel: cells from WT and mutant strains were spotted on YPD plates as serial 10-fold dilutions. Right panel: cells from WT and mutant strains were also spotted on YPG plates (a medium using non-fermentable carbon source glycerol). **(G)** Oxygen consumption rates (OCR) of WT and mutant cells in fermentative and non-fermentative carbon source medium. Lack of H3K18ac showed respiration defect in YPA (yeast extract, peptone, potassium acetate), YPG (yeast extract, peptone, glycerol) and YPE medium (yeast extract, peptone, ethanol). The error bars indicate ± SD (n = 8). ***P < 0.001. **(H)** H3K18 acetylation played important roles in sporulation induced by rapamycin in YPD medium. The indicated cells were cultured in YPD for 24 h at 30°C and then induced by rapamycin or mock-induced by methanol. Sporulation efficiencies were analyzed at 36 h after treatment. The error bars indicate ± SD (n = 5). ***P < 0.001. **(I)** Images of nuclei from cells in **H**. **(J)** Overexpression of Ime1p in the H3K18A mutant strain could partly rescue sporulation induced by rapamycin in YPD medium. The indicated cells were cultured in YPD for 24 h at 30°C, then induced by rapamycin or mock-induced by methanol. Sporulation efficiencies were analyzed at 36 h after treatment. The error bars indicate ± SD (n = 3). *P < 0.05, **P < 0.01. H3K18A Ime1p: LW1640.

whereas the H3K18Q mutant strain could overcome this defect (**Figures 4H,I**). Our findings suggest H3K18ac might regulate meiosis initiation through respiration by modulating *IME1* expression, but not energy supplementation. To further confirm our results, in the H3K18A mutant strain, we overexpressed *IME1* under the *CUP1* promoter and found *IME1* overexpression could partially rescue the H3K18A sporulation defects (**Figure 4J**). Thus, H3K18ac might regulate *IME1* expression through respiration.

H3K18ac Regulates Ime1p Levels Through the Rim101p-Smp1p Pathway

Previously, we found respiration could promote *RIM101* expression to inhibit Smp1p, which further activates *IME1* expression to facilitate meiosis initiation (Zhao et al., 2018). Therefore, we speculated that H3K18ac might modulate respiration and initiate meiosis through the Rim101p-Smp1p-Ime1p pathway. To test this hypothesis, we first measured *RIM101* mRNA levels in WT, H3K18A, and H3K18Q mutant strains, and found that the *RIM101* level in H3K18A strain was significantly decreased compared with that of the WT and H3K18Q strains (**Figure 5A**). To further confirm it, we then detected the Rim101p levels in WT, H3K18A, and H3K18Q mutant strains during sporulation, and found that only the Rim101p in H3K18A mutant strain was dramatically downregulated (**Figure 5B**). Furthermore, the H3K18Q mutant strain showed recovered Rim101p protein levels (**Figure 5B**), indicating H3K18ac might regulate Rim101p expression through respiration. To further confirm this idea, in the H3K18A mutant strain, we overexpressed *RIM101* under the *CUP1* promoter and found *RIM101* overexpression could partially rescue sporulation defects in H3K18A mutant strain (**Figure 5C**). Thus, H3K18ac might regulate meiosis initiation through modulating Rim101p expression.

Given that Rim101p could activate *IME1* expression by down-regulating Smp1p (Zhao et al., 2018), we further examined the protein levels of Smp1p in WT, H3K18A, and H3K18Q mutant strains. We found Smp1p dramatically accumulated at the early stage of sporulation in the H3K18A mutant strain compared with the WT strain (**Figure 5D**), and the H3K18Q mutant strain showed recovered Smp1p protein levels (**Figure 5D**). In addition, the disruption of *SMP1* in the H3K18A mutant strain partially rescued sporulation defects (**Figure 5E**), suggesting H3K18ac might downregulate Smp1p through respiration. Thus, H3K18ac might modulate respiration and regulate meiosis initiation through the Rim101p-Smp1p-Ime1p pathway (**Figure 6**).

DISCUSSION

Histone modifications have been reported to be involved in many aspects of meiosis, including the generation of programmed DNA double-strand breaks (DSBs), homologous recombination, meiotic sex chromosome inactivation (MSCI) and crossover formation (Bannister and Kouzarides, 2011; Tan et al., 2011; Tessarz and Kouzarides, 2014). Although an appreciable number of studies have uncovered many histone modifications during meiosis, majority of the studies were descriptive and correlative. Our current study sought to elucidate how histone modifications directly or indirectly modulate meiosis. Quantitative analysis of prevalent histone proteins and their post-translational modifications (PTM) provided insight into understanding the mechanistic relationships between histone modifications and meiosis.

Based on our study, we speculated that highly prevalent modifications might tend to have significant functions, such as the H3K9 methylation that could be identified on more than half of the K9 sites in H3 during mouse spermatogenesis (**Figure 1E**). Indeed, impaired methylation of H3K9 (me1/3) led to abnormal meiosis homologous recombination, which could result in spermatogenesis failure (Tachibana et al., 2001). We also detected a high proportion of modifications on H3 variants (**Figure 1E**), suggesting important roles of PTMs during spermatogenesis. Indeed, some studies have revealed that H3 variants are essential for spermatogenesis (Jambhekar and Amon, 2008; Yuen et al., 2014), supported by findings that *H3f3b*-null male mice are complete infertile and show disrupted spermatogenesis-related genes expression in germ cells (Yuen et al., 2014). However, few works focused on the functional roles of H3 variants modifications, which need further investigation.

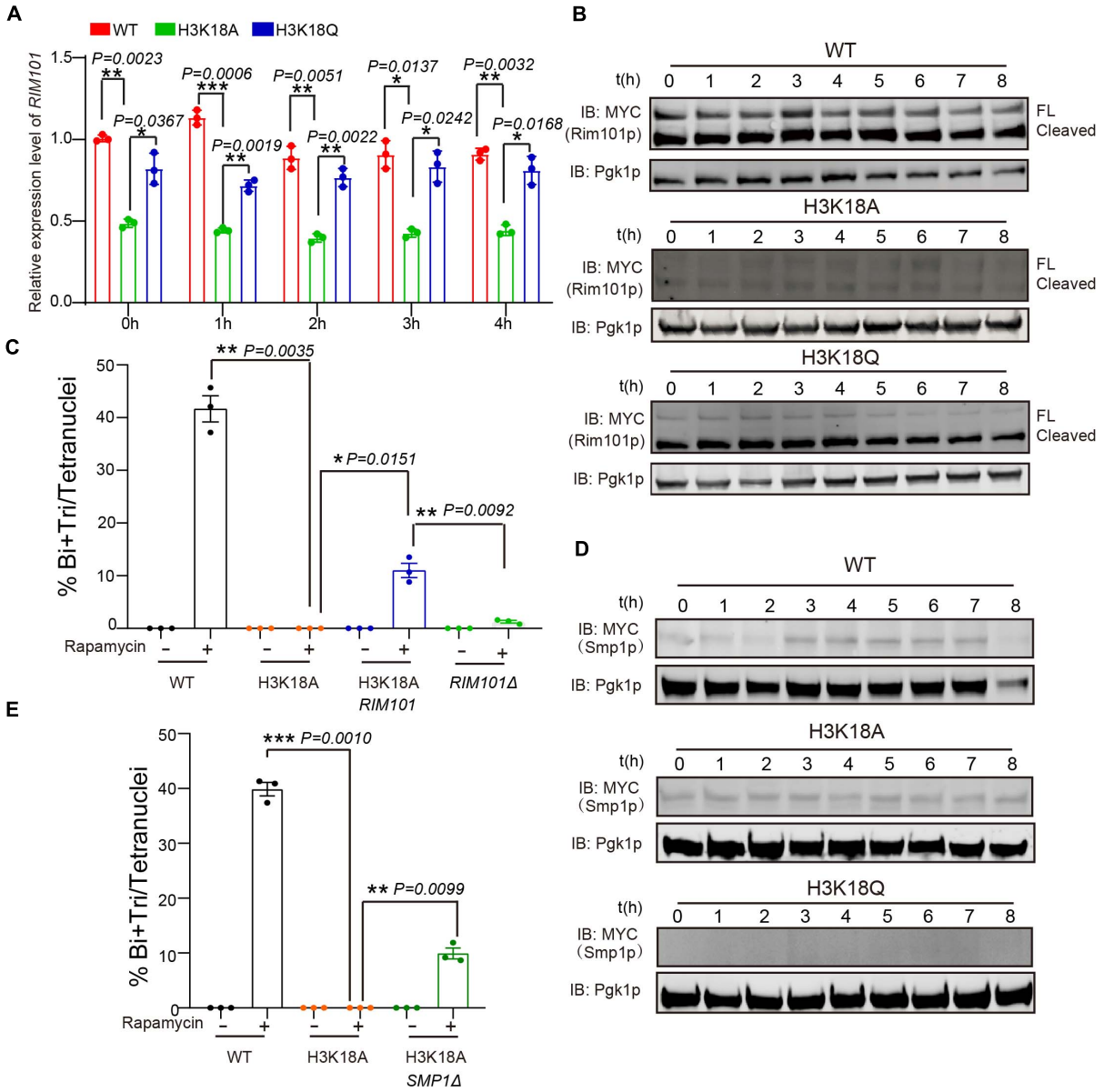

FIGURE 5 | H3K18ac influences meiosis initiation by regulating *RIM101* and *SMP1* expression. **(A)** Quantitative PCR analyzed *RIM101* expression in WT, H3K18A and H3K18Q mutant strains. Cells were harvested at the indicated times and then total RNA was extracted and reverse transcribed. *RIM101* mRNA levels in the three strains were measured by quantitative PCR and normalized to the levels of the house keeping gene *TAF10*. The error bars indicate ± SD ($n = 3$). $^{*}P < 0.05$, $^{**}P < 0.01$, $^{***}P < 0.001$. **(B)** Western blot of Rim101p expression in WT, H3K18A, and H3K18Q mutant strains during sporulation. *RIM101* in all three strains was tagged with 9 × Myc. Pgk1p was used as a loading control. WT-9MYC-*RIM101*: LW1634; H3K18A-9MYC-*RIM101*: LW1635; H3K18Q-9MYC-*RIM101*: LW1636. **(C)** Overexpression of *RIM101* in H3K18A mutant strain could partly rescue the sporulation induced by rapamycin in YPD medium. Indicated cells were cultured in YPD for 24 h at 30°C, then induced by rapamycin or methanol as control. Sporulation efficiency were analyzed at 36 h after treatment. Error bar indicate ± SD ($n = 3$). $^{*}P < 0.05$, $^{**}P < 0.01$. H3K18A Rim101p: LW1641; *RIM101*Δ: LW1560. **(D)** Western blot of Smp1p expression in WT, H3K18A and H3K18Q mutant strains during sporulation. *SMP1* in all three strains was tagged with 9 × Myc. Pgk1p was used as a loading control. WT-*SMP1*-9MYC: LW1637; H3K18A-*SMP1*-9MYC: LW1638; H3K18Q-*SMP1*-9MYC: LW1639. **(E)** Delete *SMP1* in H3K18A mutant strain could partly rescue the sporulation induced by rapamycin in YPD medium. Indicated cells were cultured in YPD for 24 h at 30°C, then induced by rapamycin or methanol as control. Sporulation efficiency were analyzed at 36 h after treatment. Error bar indicate ± SD ($n = 3$). $^{**}P < 0.01$, $^{***}P < 0.001$. H3K18A *SMP1*Δ: LW1642.

In the majority of eukaryotes, respiration is an important contributor of adenosine triphosphate (ATP), which supports a series of physiological function (Friedman and Nunnari, 2014). In budding yeast, a non-fermentable carbon source is critical for meiosis initiation (Zaman et al., 2008) and requires mitochondrial respiration to be utilized by the cell (Treinin and Simchen, 1993). In essence, the components of the mitochondrial respiratory chain are necessary for yeast

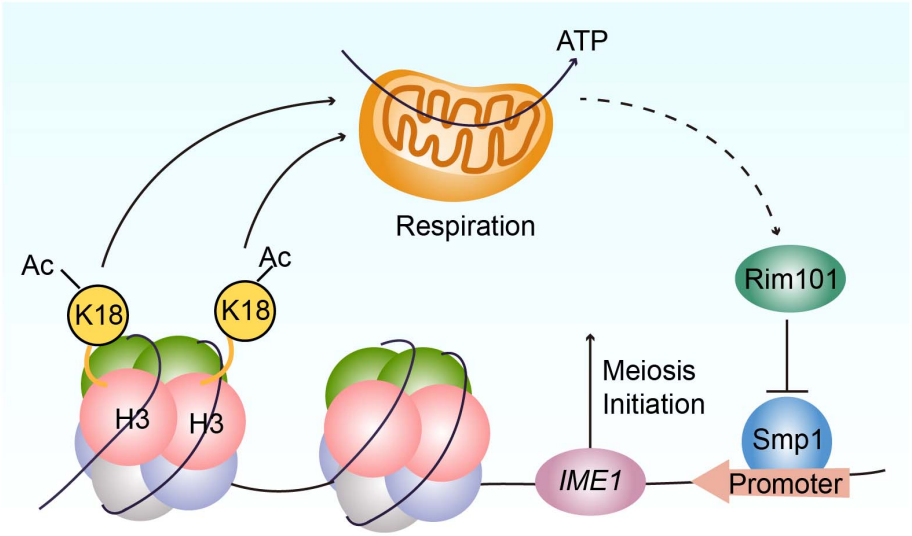

FIGURE 6 | Proposed model for the functional role of H3K18ac in meiosis initiation. H3K18ac influences the respiration to promote *RIM101* expression that down-regulates *SMP1* a repressor of *IME1* transcription, induces *IME1* expression, and finally leads to meiosis initiation.

sporulation (Treinin and Simchen, 1993; Zhao et al., 2018). In a previous study, we found respiration could activate *IME1* expression through the Rim101p-Smp1p pathway (Zhao et al., 2018). Because Ime1p is a master transcription regulator of yeast meiosis that activates early meiotic gene expression (van Werven and Amon, 2011), respiration could further promote meiosis initiation (Smith et al., 1990; Benjamin et al., 2003). Our current study finds that H3K18ac could modulate respiration to activate Rim101p expression, further downregulating a negative regulator of *IME1* transcription, Smp1p, to initiate meiosis (**Figure 6**).

According to our findings, H3K18ac plays important roles in meiosis initiation and histone acetylation is regulated by histone acetyl-transferase and deacetylase. Therefore, it is important to uncover how H3K18ac is regulated by enzymes during meiosis initiation. *SIRTUIN 7* (*SIRT7*) is known to be responsible for H3K18 deacetylation in mammals (Barber et al., 2012) and *SIR2* is the *SIRT7* homology in yeast (Paredes et al., 2018). SIRT7 methylated at R388 has been reported to lose its deacetylation activity on H3K18, and hyperacetylated H3K18 on SIRT7-target gene promoter has been reported to initiate mitochondria synthesis and maintain mitochondria respiration (Yan et al., 2018). Furthermore, a lack of Sir2p distinctly enhanced gluconeogenesis and respiration in yeast (Orlandi et al., 2017). Gcn5p-Ada2p-Ada3p was the catalytic subunit of the Ada2-Gcn5-Ada3 transcription activator (ADA) and Spt-Ada-Gcn5-acetyltransferase (SAGA) complexes, which showed acetylation activity on H3K18 (Cieniewicz et al., 2014), and Gcn5p was reported to play a central role in yeast meiosis initiation through histone H3 acetylation (Burgess et al., 1999). Given that H3K18ac was dynamically changed during meiosis in both mice and yeast (**Figures 1**, **2**) albeit their trends are different from each other, more efforts should be made to understand the functional role of H3K18ac on spermatogenesis.

DATA AVAILABILITY STATEMENT

The data presented in the study are deposited in the PeptideAtlas repository, accession number (PASS01662).

ETHICS STATEMENT

The animal study was reviewed and approved by the Animal Research Panel of the Committee on Research Practice of the Institute of Zoology, Chinese Academy of Sciences (#08-133).

AUTHOR CONTRIBUTIONS

WL, HY, and CL conceived and designed the experiments. JS, YM, and HH performed most of the experiments. YL performed some of the experiments. HY performed LC-MS/MS. JS, YM, CL, and WL wrote the article. All authors contributed to the article and approved the submitted version.

FUNDING

This study was supported by the National Key R&D Program of China (Grant No. 2018YFC1004202).

ACKNOWLEDGMENTS

We thank Dr. Jun Gao for conducting LC-MS/MS analysis. We also thank Tracey Baas for critical editing of the manuscript.

SUPPLEMENTARY MATERIAL

The Supplementary Material for this article can be found online at: https://www.frontiersin.org/articles/10.3389/fcell.2021.646214/full#supplementary-material

Supplementary Figure 1 | The comparison of histone modifications which show similar dynamic trends in mouse spermatogenesis and yeast sporulation. H3K4me1, H3K4me2, and H3K18me1 showed similar changes in both mouse and yeast during meiosis.

Supplementary Figure 2 | Western blot verification of the construction of histone H3 K to A mutant strains. **(A)** The K to A mutant histone H3 could be expressed. Pgk1p was used as a loading control. **(B)** The original histone H3 could not be detected. 5-FOA was used to remove the plasmid expressing wild-type histone H3. Pgk1p was used as a loading control.

Supplementary Figure 3 | Less zoomed-in versions of the sporulation images about the representative sporulation defect strains in **Figure 3B**.

Supplementary Figure 4 | Western blot verification of the generated of histone H3 mimic strains. **(A–G)** The modification mimic histone H3 could be expressed and the original wild-type histone H3 plasmid was removed using negative section with 5-FOA. Pgk1p was used as a loading control.

Supplementary Figure 5 | Modifications mimic strains to rescue the sporulation rate of H3K9A and H3K14A mutant strains. **(A)** Sporulation efficiencies of mutant cells mimic different histone modifications. The error bars indicate ± SD ($n = 3$). $^{*}P < 0.05$, $^{**}P < 0.01$. WT: LW0066; H3K9A: LW1601; H3K9L: LW1618; H3K9M: LW1619; H3K9Q: LW1620; H3K14A: LW1602; H3K14Q: LW1621. **(B)** Images of nuclei of cells in **A**.

REFERENCES

Acquaviva, L., Drogat, J., Dehé, P. M., de La Roche Saint-André, C., and Géli, V. (2013). Spp1 at the crossroads of h3k4me3 regulation and meiotic recombination. *Epigenetics* 8, 355–360. doi: 10.4161/epi.24295

Adam, C., Guérois, R., Citarella, A., Verardi, L., Adolphe, F., Béneut, C., et al. (2018). The phd finger protein spp1 has distinct functions in the set1 and the meiotic dsb formation complexes. *PLoS Genet.* 14:e1007223. doi: 10.1371/journal.pgen.1007223

Bannister, A. J., and Kouzarides, T. (2011). Regulation of chromatin by histone modifications. *Cell Res.* 21, 381–395. doi: 10.1038/cr.2011.22

Barber, M. F., Michishita-Kioi, E., Xi, Y., Tasselli, L., Kioi, M., Moqtaderi, Z., et al. (2012). Sirt7 links h3k18 deacetylation to maintenance of oncogenic transformation. *Nature* 487, 114–118. doi: 10.1038/nature11043

Benjamin, K. R., Zhang, C., Shokat, K. M., and Herskowitz, I. (2003). Control of landmark events in meiosis by the cdk cdc28 and the meiosis-specific kinase ime2. *Genes Dev.* 17, 1524–1539. doi: 10.1101/gad.1101503

Bolcun-Filas, E., and Schimenti, J. C. (2012). Genetics of meiosis and recombination in mice. *Int. Rev. Cell Mol. Biol.* 298, 179–227. doi: 10.1016/b978-0-12-394309-5.00005-5

Bradley, M. C., Yang, K., Fernández-Del-Río, L., Ngo, J., Ayer, A., Tsui, H. S., et al. (2020). Coq11 deletion mitigates respiratory deficiency caused by mutations in the gene encoding the coenzyme q chaperone protein coq10. *J. Biol. Chem.* 295, 6023–6042. doi: 10.1074/jbc.RA119.012420

Burgess, S. M., Ajimura, M., and Kleckner, N. (1999). Gcn5-dependent histone h3 acetylation and rpd3-dependent histone h4 deacetylation have distinct, opposing effects on ime2 transcription, during meiosis and during vegetative growth, in budding yeast. *Proc. Natl. Acad. Sci. U.S.A.* 96, 6835–6840. doi: 10.1073/pnas.96.12.6835

Cieniewicz, A. M., Moreland, L., Ringel, A. E., Mackintosh, S. G., Raman, A., Gilbert, T. M., et al. (2014). The bromodomain of gcn5 regulates site specificity of lysine acetylation on histone h3. *Mol. Cell. Proteomics* 13, 2896–2910. doi: 10.1074/mcp.M114.038174

Cooper, K. F., and Strich, R. (2011). Meiotic control of the apc/c: similarities & differences from mitosis. *Cell Div.* 6:16. doi: 10.1186/1747-1028-6-16

Crespo, M., Luense, L. J., Arlotto, M., Hu, J., Dorsey, J., García-Oliver, E., et al. (2020). Systematic genetic and proteomic screens during gametogenesis identify h2bk34 methylation as an evolutionary conserved meiotic mark. *Epigenetics Chromatin* 13:35. doi: 10.1186/s13072-020-00349-5

Fernandez-Capetillo, O., Mahadevaiah, S. K., Celeste, A., Romanienko, P. J., Camerini-Otero, R. D., Bonner, W. M., et al. (2003). H2ax is required for chromatin remodeling and inactivation of sex chromosomes in male mouse meiosis. *Dev. Cell* 4, 497–508. doi: 10.1016/s1534-5807(03)00093-5

Friedman, J. R., and Nunnari, J. (2014). Mitochondrial form and function. *Nature* 505, 335–343. doi: 10.1038/nature12985

Fu, C., Coelho, M. A., David-Palma, M., Priest, S. J., and Heitman, J. (2019). Genetic and genomic evolution of sexual reproduction: echoes from leca to the fungal kingdom. *Curr. Opin. Genet. Dev.* 5, 70–75. doi: 10.1016/j.gde.2019.07.008

Fukuda, H., Sano, N., Muto, S., and Horikoshi, M. (2006). Simple histone acetylation plays a complex role in the regulation of gene expression. *Brief Funct. Genomic Proteomic* 5, 190–208. doi: 10.1093/bfgp/ell032

Gao, J., Liao, R., Yu, Y., Zhai, H., Wang, Y., Sack, R., et al. (2014). Absolute quantification of histone ptm marks by mrm-based lc-ms/ms. *Anal. Chem.* 86, 9679–9686. doi: 10.1021/ac502333a

Godmann, M., Auger, V., Ferraroni-Aguiar, V., Di Sauro, A., Sette, C., Behr, R., et al. (2007). Dynamic regulation of histone h3 methylation at lysine 4 in mammalian spermatogenesis. *Biol. Reprod.* 77, 754–764. doi: 10.1095/biolreprod.107.062265

Govin, J., Dorsey, J., Gaucher, J., Rousseaux, S., Khochbin, S., and Berger, S. L. (2010). Systematic screen reveals new functional dynamics of histones h3 and h4 during gametogenesis. *Genes Dev.* 24, 1772–1786. doi: 10.1101/gad.1954910

Grunstein, M. (1997). Histone acetylation in chromatin structure and transcription. *Nature* 389, 349–352. doi: 10.1038/38664

Hess, R. A., and Renato de Franca, L. (2008). Spermatogenesis and cycle of the seminiferous epithelium. *Adv. Exp. Med. Biol.* 636, 1–15. doi: 10.1007/978-0-387-09597-4_1

Hillers, K. J., Jantsch, V., Martinez-Perez, E., and Yanowitz, J. L. (2017). Meiosis. *WormBook* 2017, 1–43. doi: 10.1895/wormbook.1.178.1

Hu, J., Donahue, G., Dorsey, J., Govin, J., Yuan, Z., Garcia, B. A., et al. (2015). H4k44 acetylation facilitates chromatin accessibility during meiosis. *Cell Rep.* 13, 1772–1780. doi: 10.1016/j.celrep.2015.10.070

Hyland, E. M., Molina, H., Poorey, K., Jie, C., Xie, Z., Dai, J., et al. (2011). An evolutionarily 'young' lysine residue in histone h3 attenuates transcriptional output in *Saccharomyces cerevisiae*. *Genes Dev.* 25, 1306–1319. doi: 10.1101/gad.2050311

Iwamori, N., Zhao, M., Meistrich, M. L., and Matzuk, M. M. (2011). The testis-enriched histone demethylase, kdm4d, regulates methylation of histone h3 lysine 9 during spermatogenesis in the mouse but is dispensable for fertility. *Biol. Reprod.* 84, 1225–1234. doi: 10.1095/biolreprod.110.088955

Jaiswal, D., Turniansky, R., and Green, E. M. (2017). Choose your own adventure: the role of histone modifications in yeast cell fate. *J. Mol. Biol.* 429, 1946–1957. doi: 10.1016/j.jmb.2016.10.018

Jambhekar, A., and Amon, A. (2008). Control of meiosis by respiration. *Curr. Biol.* 18, 969–975. doi: 10.1016/j.cub.2008.05.047

Jenuwein, T., and Allis, C. D. (2001). Translating the histone code. *Science* 293, 1074–1080. doi: 10.1126/science.1063127

Jin, L., and Neiman, A. M. (2016). Post-transcriptional regulation in budding yeast meiosis. *Curr. Genet.* 62, 313–315. doi: 10.1007/s00294-015-0546-2

Kassir, Y., Granot, D., and Simchen, G. (1988). Ime1, a positive regulator gene of meiosis in s. Cerevisiae. *Cell* 52, 853–862. doi: 10.1016/0092-8674(88)90427-8

Koprinarova, M., Schnekenburger, M., and Diederich, M. (2016). Role of histone acetylation in cell cycle regulation. *Curr. Top. Med. Chem.* 16, 732–744. doi: 10.2174/1568026615666150825140822

Kracklauer, M. P., Link, J., and Alsheimer, M. (2013). Lincing the nuclear envelope to gametogenesis. *Curr. Top. Dev. Biol.* 102, 127–157. doi: 10.1016/b978-0-12-416024-8.00005-2

Kushnirov, V. V. (2000). Rapid and reliable protein extraction from yeast. *Yeast* 16, 857–860. doi: 10.1002/1097-0061(20000630)16:9<857::Aid-yea561<3.0.Co;2-b

Lesch, B. J., and Page, D. C. (2012). Genetics of germ cell development. *Nat. Rev. Genet.* 13, 781–794. doi: 10.1038/nrg3294

Liao, R., Wu, H., Deng, H., Yu, Y., Hu, M., Zhai, H., et al. (2013). Specific and efficient n-propionylation of histones with propionic acid n-hydroxysuccinimide ester for histone marks characterization by lc-ms. *Anal. Chem.* 85, 2253–2259. doi: 10.1021/ac303171h

Orlandi, I., Pellegrino Coppola, D., Strippoli, M., Ronzulli, R., and Vai, M. (2017). Nicotinamide supplementation phenocopies sir2 inactivation by modulating carbon metabolism and respiration during yeast chronological aging. *Mech. Ageing Dev.* 161, 277–287. doi: 10.1016/j.mad.2016.06.006

Owens, S., Tang, S., and Hunter, N. (2018). Monitoring recombination during meiosis in budding yeast. *Methods Enzymol.* 601, 275–307. doi: 10.1016/bs.mie.2017.12.005

Paredes, S., Angulo-Ibanez, M., Tasselli, L., Carlson, S. M., Zheng, W., Li, T. M., et al. (2018). The epigenetic regulator sirt7 guards against mammalian cellular senescence induced by ribosomal DNA instability. *J. Biol. Chem.* 293, 11242–11250. doi: 10.1074/jbc.AC118.003325

Rintisch, C., Heinig, M., Bauerfeind, A., Schafer, S., Mieth, C., Patone, G., et al. (2014). Natural variation of histone modification and its impact on gene expression in the rat genome. *Genome Res.* 24, 942–953. doi: 10.1101/gr.169029.113

Roosen-Runge, E. C. (1962). The process of spermatogenesis in mammals. *Biol. Rev. Camb. Philos. Soc.* 37, 343–377. doi: 10.1111/j.1469-185x.1962.tb01616.x

Sacks, D., Baxter, B., Campbell, B. C. V., Carpenter, J. S., Cognard, C., Dippel, D., et al. (2018). Multisociety consensus quality improvement revised consensus statement for endovascular therapy of acute ischemic stroke. *Int. J. Stroke* 13, 612–632. doi: 10.1177/1747493018778713

Schmitt, M. E., Brown, T. A., and Trumpower, B. L. (1990). A rapid and simple method for preparation of rna from saccharomyces cerevisiae. *Nucleic Acids Res.* 18, 3091–3092. doi: 10.1093/nar/18.10.3091

Shechter, D., Dormann, H. L., Allis, C. D., and Hake, S. B. (2007). Extraction, purification and analysis of histones. *Nat. Protoc.* 2, 1445–1457. doi: 10.1038/nprot.2007.202

Smith, C. A., Roeszler, K. N., Bowles, J., Koopman, P., and Sinclair, A. H. (2008). Onset of meiosis in the chicken embryo; evidence of a role for retinoic acid. *BMC Dev. Biol.* 8:85. doi: 10.1186/1471-213X-8-85

Smith, H. E., Su, S. S., Neigeborn, L., Driscoll, S. E., and Mitchell, A. P. (1990). Role of ime1 expression in regulation of meiosis in *Saccharomyces cerevisiae*. *Mol. Cell. Biol.* 10, 6103–6113. doi: 10.1128/mcb.10.12.6103

Tachibana, M., Sugimoto, K., Fukushima, T., and Shinkai, Y. (2001). Set domain-containing protein, g9a, is a novel lysine-preferring mammalian histone methyltransferase with hyperactivity and specific selectivity to lysines 9 and 27 of histone h3. *J. Biol. Chem.* 276, 25309–25317. doi: 10.1074/jbc.M101914200

Tan, M., Luo, H., Lee, S., Jin, F., Yang, J. S., Montellier, E., et al. (2011). Identification of 67 histone marks and histone lysine crotonylation as a new type of histone modification. *Cell* 146, 1016–1028. doi: 10.1016/j.cell.2011.08.008

Tessarz, P., and Kouzarides, T. (2014). Histone core modifications regulating nucleosome structure and dynamics. *Nat. Rev. Mol. Cell Biol.* 15, 703–708. doi: 10.1038/nrm3890

Treinin, M., and Simchen, G. (1993). Mitochondrial activity is required for the expression of ime1, a regulator of meiosis in yeast. *Curr. Genet.* 23, 223–227. doi: 10.1007/bf00351500

van Werven, F. J., and Amon, A. (2011). Regulation of entry into gametogenesis. *Philos. Trans. R. Soc. Lond. B Biol. Sci.* 366, 3521–3531. doi: 10.1098/rstb.2011.0081

Vershon, A. K., and Pierce, M. (2000). Transcriptional regulation of meiosis in yeast. *Curr. Opin. Cell Biol.* 12, 334–339. doi: 10.1016/s0955-0674(00)00104-6

Von Stetina, J. R., and Orr-Weaver, T. L. (2011). Developmental control of oocyte maturation and egg activation in metazoan models. *Cold Spring Harb. Perspect. Biol.* 3:a005553. doi: 10.1101/cshperspect.a005553

Wang, L., Xu, Z., Khawar, M. B., Liu, C., and Li, W. (2017). The histone codes for meiosis. *Reproduction* 154, R65–R79. doi: 10.1530/REP-17-0153

Wang, T., Gao, H., Li, W., and Liu, C. (2019). Essential role of histone replacement and modifications in male fertility. *Front. Genet.* 10:962. doi: 10.3389/fgene.2019.00962

Xu, Z., Song, Z., Li, G., Tu, H., Liu, W., Liu, Y., et al. (2016). H2b ubiquitination regulates meiotic recombination by promoting chromatin relaxation. *Nucleic Acids Res.* 44, 9681–9697. doi: 10.1093/nar/gkw652

Yan, W. W., Liang, Y. L., Zhang, Q. X., Wang, D., Lei, M. Z., Qu, J., et al. (2018). Arginine methylation of sirt7 couples glucose sensing with mitochondria biogenesis. *EMBO Rep.* 19:e46377. doi: 10.15252/embr.201846377

Yuen, B. T., Bush, K. M., Barrilleaux, B. L., Cotterman, R., and Knoepfler, P. S. (2014). Histone h3.3 regulates dynamic chromatin states during spermatogenesis. *Development* 141, 3483–3494. doi: 10.1242/dev.106450

Zaman, S., Lippman, S. I., Zhao, X., and Broach, J. R. (2008). How *Saccharomyces* responds to nutrients. *Annu. Rev. Genet.* 42, 27–81. doi: 10.1146/annurev.genet.41.110306.130206

Zentner, G. E., and Henikoff, S. (2013). Regulation of nucleosome dynamics by histone modifications. *Nat. Struct. Mol. Biol.* 20, 259–266. doi: 10.1038/nsmb.2470

Zhao, H., Wang, Q., Liu, C., Shang, Y., Wen, F., Wang, F., et al. (2018). A role for the respiratory chain in regulating meiosis initiation in *Saccharomyces cerevisiae*. *Genetics* 208, 1181–1194. doi: 10.1534/genetics.118.300689

Zheng, X. F., and Schreiber, S. L. (1997). Target of rapamycin proteins and their kinase activities are required for meiosis. *Proc. Natl. Acad. Sci. U.S.A.* 94, 3070–3075. doi: 10.1073/pnas.94.7.3070

Zickler, D., and Kleckner, N. (2015). Recombination, pairing, and synapsis of homologs during meiosis. *Cold Spring Harb. Perspect. Biol.* 7:a016626. doi: 10.1101/cshperspect.a016626

Conflict of Interest: The authors declare that the research was conducted in the absence of any commercial or financial relationships that could be construed as a potential conflict of interest.

Copyright © 2021 Shi, Ma, Hua, Liu, Li, Yu and Liu. This is an open-access article distributed under the terms of the Creative Commons Attribution License (CC BY). The use, distribution or reproduction in other forums is permitted, provided the original author(s) and the copyright owner(s) are credited and that the original publication in this journal is cited, in accordance with accepted academic practice. No use, distribution or reproduction is permitted which does not comply with these terms.

frontiers in Cell and Developmental Biology

REVIEW
published: 08 April 2021
doi: 10.3389/fcell.2021.660322

Tell the Difference Between Mitosis and Meiosis: Interplay Between Chromosomes, Cytoskeleton, and Cell Cycle Regulation

Masamitsu Sato[1,2,3]*, *Yasutaka Kakui*[1,4] *and Mika Toya*[1,2,5]

[1] *Laboratory of Cytoskeletal Logistics, Center for Advanced Biomedical Sciences (TWIns), Waseda University, Tokyo, Japan,* [2] *Institute for Advanced Research of Biosystem Dynamics, Waseda Research Institute for Science and Engineering, Graduate School of Advanced Science and Engineering, Waseda University, Tokyo, Japan,* [3] *Institute for Medical-Oriented Structural Biology, Waseda University, Tokyo, Japan,* [4] *Waseda Institute for Advanced Study, Waseda University, Tokyo, Japan,* [5] *Major in Bioscience, Global Center for Science and Engineering, Faculty of Science and Engineering, Waseda University, Tokyo, Japan*

OPEN ACCESS

Edited by:
Akira Shinohara, Osaka University, Japan

Reviewed by:
Takashi Toda, Hiroshima University, Japan
Manuel Mendoza, INSERM U964 Institut de Génétique et de Biologie Moléculaire et Cellulaire (IGBMC), France
Alfonso Fernández-Álvarez, Universidad Pablo de Olavide, Spain

***Correspondence:**
Masamitsu Sato
masasato@waseda.jp

Specialty section:
This article was submitted to Cell Growth and Division, a section of the journal Frontiers in Cell and Developmental Biology

Received: *29 January 2021*
Accepted: *02 March 2021*
Published: *08 April 2021*

Citation:
Sato M, Kakui Y and Toya M (2021) Tell the Difference Between Mitosis and Meiosis: Interplay Between Chromosomes, Cytoskeleton, and Cell Cycle Regulation. Front. Cell Dev. Biol. 9:660322. doi: 10.3389/fcell.2021.660322

Meiosis is a specialized style of cell division conserved in eukaryotes, particularly designed for the production of gametes. A huge number of studies to date have demonstrated how chromosomes behave and how meiotic events are controlled. Yeast substantially contributed to the understanding of the molecular mechanisms of meiosis in the past decades. Recently, evidence began to accumulate to draw a perspective landscape showing that chromosomes and microtubules are mutually influenced: microtubules regulate chromosomes, whereas chromosomes also regulate microtubule behaviors. Here we focus on lessons from recent advancement in genetical and cytological studies of the fission yeast *Schizosaccharomyces pombe*, revealing how chromosomes, cytoskeleton, and cell cycle progression are organized and particularly how these are differentiated in mitosis and meiosis. These studies illuminate that meiosis is strategically designed to fulfill two missions: faithful segregation of genetic materials and production of genetic diversity in descendants through elaboration by meiosis-specific factors in collaboration with general factors.

Keywords: mitosis, meiosis, microtubule, kinetochore, cell cycle, fission yeast (*Schizosaccharomyces pombe*), chromosome

INTRODUCTION

Eukaryotic cells undergo two styles of cell division. Mitosis is a type of cell division for somatic cells and for the asexual reproduction of unicellular eukaryotic cells. Meiosis is the type of cell division for the production of gametes in sexual reproduction. How mitosis and meiosis are differentially designed and conducted is a long-standing key question in the field of cell biology. Yeast cells undergo both types of divisions that can be switched according to environmental conditions, and therefore yeast cells have been studied to reveal underlying molecular mechanisms. In the last few decades, a considerable number of studies revealed that cells exploit meiosis-specific factors to shift the division style from the standard mitotic one to the specialized meiotic one. We, in this review,

focus on how such meiosis-specific factors dramatically modulate the way of divisions, featuring fission yeast as an example.

OVERVIEW OF CHROMOSOME CONFIGURATION IN MITOSIS AND MEIOSIS

As one of the most evident and essential differences in mitosis and meiosis is configuration of chromosomes, we briefly give an overview on how chromosomes differ in those divisions. In both divisions, chromosomes are duplicated in the S phase of the cell cycle, resulting in forming a pair of the replicated chromosomes defined as sister chromatids (**Figure 1A**). During DNA replication, cohesion between sister chromatids is established by the cohesin complex, which forms a proteinaceous ring comprised of two coiled-coil components, Psm1^{SMC1} and Psm3^{SMC3}, kleisin/Rad21, and HEAT repeat Psc3^{SCC3}.

The molecular basis constituting meiosis-specific chromosome configuration is largely attributed to meiotic cohesin, in which kleisin subunit Rad21 is replaced by Rec8 (Parisi et al., 1999; Watanabe and Nurse, 1999). Rec8 is a cohesin expressed specifically during meiosis, and both cohesins are conserved in all eukaryotes from yeast to human [reviewed in Ishiguro (2019)]. In meiosis, meiotic Rec8-cohesin, in addition to mitotic Rad21-cohesin, decorates chromosomes to connect sister chromatids as well as homologous chromosomes which are linked by chiasmata. The difference of Rec8-cohesin and Rad21-cohesin is their chromosomal localization. Rec8-cohesin can localize at the core centromeric region but Rad21-cohesin cannot in both mitosis and meiosis. Furthermore, Rec8-cohesin forms two distinct complexes, one with Psc3 for centromeric cohesion and the other with arm cohesion (Kitajima et al., 2003).

The kinetochore is assembled at the centromere of a chromosome, which serves as a dock site for spindle microtubule emanated from the spindle pole (**Figure 1B**). In mitosis, homologous chromosomes (a pair of maternal and paternal chromosomes) in diploid cells behave independently upon segregation, whereas in meiosis, homologous chromosomes are paired and a part of them are physically connected by chiasmata.

In mitosis, sister kinetochores built on core centromeres of sister chromatids are oppositely oriented in a back-to-back manner (bi-oriented; **Figure 1B**). On the other hand, the orientation in meiosis is converted to mono-orientation, in which the sister kinetochores are united in a side-by-side manner (**Figure 1B**). The mono-orientation is constructed by Rec8-cohesin and monopolin proteins (Moa1 in fission yeast; Spo13 and Mam1 in budding yeast) (Lee et al., 2002; Shonn et al., 2002; Katis et al., 2004; Yokobayashi and Watanabe, 2005; Monje-Casas et al., 2007; Kim et al., 2015; Galander et al., 2019).

Moa1 is a meiosis-specific kinetochore protein and is later found to be a member of the Meikin family together with Spo13 in budding yeast (Kim et al., 2015). Moa1 together with the Rec8-cohesin located at core centromeres ties up kinetochores of sister chromatids facing toward the same direction so that the sister kinetochores can be mono-oriented (meiosis, **Figure 1B**; Yokobayashi and Watanabe, 2005; Kim et al., 2015). The mono-orientation of sister kinetochores is maintained until anaphase of meiosis I (anaphase I) to ensure reductional division but is resolved to the mitotic bi-oriented style by the onset of meiosis II (equational division).

In mutants lacking Rec8 or Moa1, sister kinetochores are split and bi-oriented, and the division pattern of meiosis I results in equational division, as is seen in wild-type mitosis and meiosis II. Thus, mono-orientation of kinetochores mediated by Rec8 and Moa1 is essential for the establishment of reductional division in meiosis I (**Figure 1B**).

In the absence of Moa1 (or Meikin), localization of the Shugoshin protein (Sgo1 in fission yeast meiosis and SGO2 or SGOL2 in mouse meiosis) diminished (Kim et al., 2015). As shugoshin protein protects the cleavage of meiotic cohesin Rec8 during meiosis I, *moa1*Δ (the *moa1* deletion mutant) cells lose Rec8 at centromeres as a result. Thus, meiotic kinetochore protein Meikin constitutes the mono-orientation of sister kinetochores as well as protects meiotic cohesin at centromeres through the recruitment of shugoshin. Shugoshin recruits PP2A to counteract the phosphorylation of the kleisin subunit of the cohesin complex to prevent cleavage (Kitajima et al., 2006; Riedel et al., 2006).

These two functions of Meikin are conducted *via* Polo kinase. Polo kinase is one of the mitotic kinases which mainly localize to spindle poles [reviewed in Nigg (2001) and Zitouni et al. (2014)]. Plo1, the *Schizosaccharomyces pombe* Polo kinase, also localizes to SPBs during mitosis but localizes to meiotic kinetochores using Moa1 as a platform (**Figure 1A**; Kakui et al., 2013; Kim et al., 2015). Polo kinase at meiotic kinetochores with Moa1 thus dictates the mono-orientation of sister kinetochores *via* Rec8 (or monopolin in budding yeast) as well as the protection of centromeric cohesin *via* shugoshin. In addition to those dual functions of Moa1–Plo1, we will later discuss additional roles regarding interaction with microtubules.

ALTERATION OF CHROMOSOME ARRANGEMENT IN THE NUCLEUS UPON SEXUAL DIFFERENTIATION

A number of studies revealed that the geographical arrangement of chromosomes in the nucleus affects the behaviors of chromosomes essential to accomplish meiotic events. Most importantly, the location of the chromosomes in the nucleus directly affects the efficiency of meiotic recombination. A brief schematic overview of chromosome allocation in the nucleus of the fission yeast is summarized in **Figures 1C–E**.

In the interphase of mitotic cell cycles, the centromeres of all chromosomes are clustered near SPBs (the centrosome equivalent in yeast species) located at the nuclear periphery (Rabl orientation, **Figure 1C**; Funabiki et al., 1993). *S. pombe* cells undergo sexual differentiation when cells are starved under nitrogen depletion and when the ploidy of cells is in a diploid state originated from a pair of haploid cells with two distinct mating types (Yamamoto et al., 1997). Zygotic meiosis occurs when a

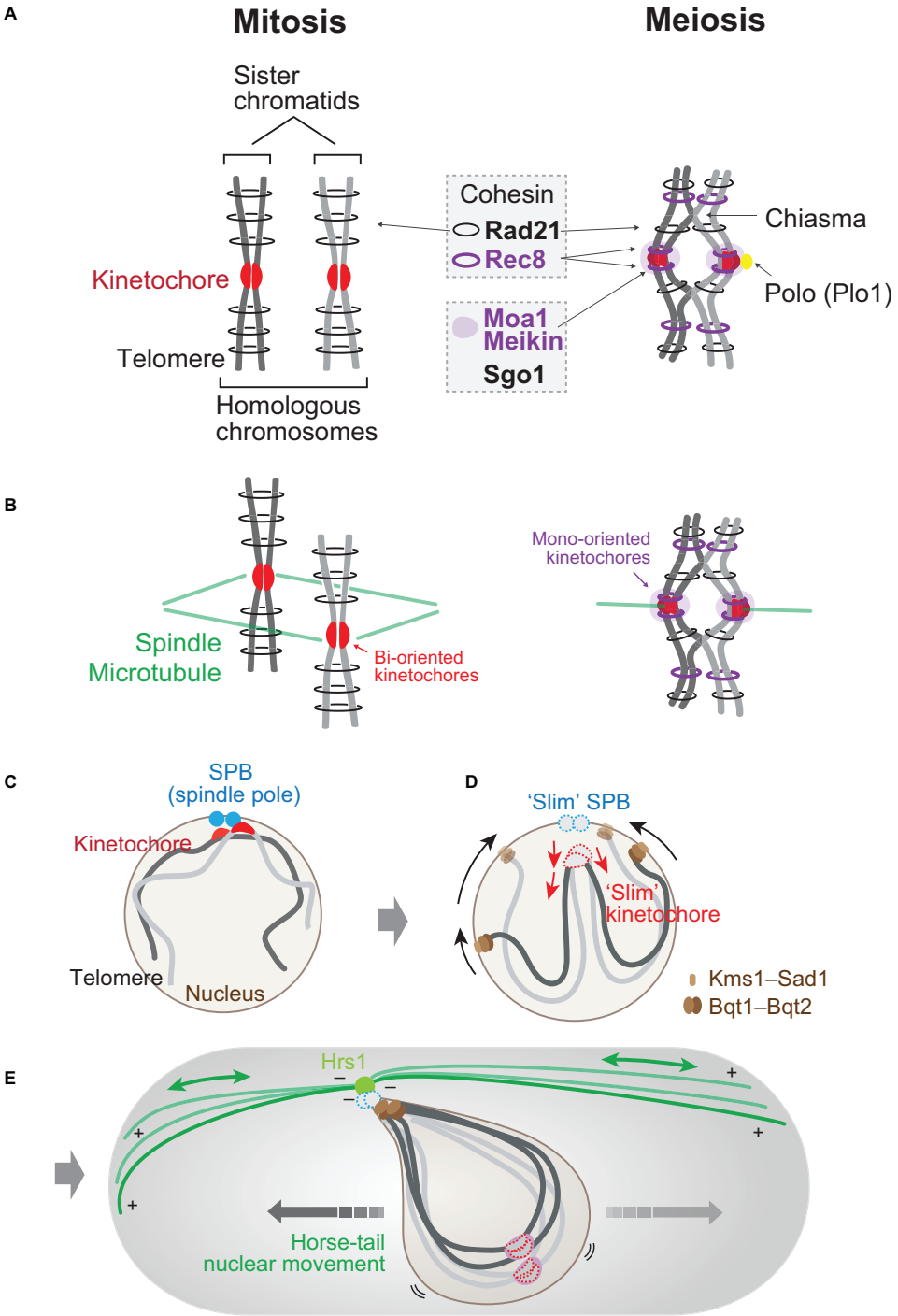

FIGURE 1 | Chromosomes in mitosis and in meiosis. **(A)** Chromosomes in mitosis and in meiosis. During mitotic cell cycles (left), homologous chromosomes behave independently. Sister chromatids are connected by mitotic cohesin Rad21 (Scc1). In meiosis I (right), homologous chromosomes are paired and crossed *via* chiasmata. Rad21 locates in the arm region of chromosomes in both divisions, whereas meiotic cohesin Rec8 (purple ring) locates in both the arm and centromeric regions. Moa1 (Meikin) is a meiosis-specific kinetochore protein that protects centromeric Rec8 cohesin through the recruitment of shugoshin (Sgo1) to centromeres and regulates attachment to microtubules through the recruitment of Polo kinase (Plo1). **(B)** Orientation of kinetochores. In mitosis (left), sister kinetochores are bi-oriented in a back-to-back position. In meiosis I, sister kinetochores are oriented in a side-by-side position. Spindle microtubules, green. **(C–E)** Conversion of chromosome arrangement upon sexual differentiation in fission yeast. In interphase (e.g., G1 phase) of mitotic cycles **(C)**, centromeres (kinetochores; red) are clustered at spindle pole bodies (SPBs; blue). In reaction to mating pheromone **(D)**, telomeres get clustered to SPBs. Telomeres slide on the nuclear envelope toward SPBs *via* interaction with meiosis-specific bouquet proteins (Bqt1 and Bqt2) and nuclear membrane proteins (Kms1/2–Sad1). Kinetochores are dissociated off SPBs. A number of kinetochore and SPB components are dissociated in this stage (slim SPBs and kinetochores). During meiotic prophase **(E)**, a cytoplasmic array of microtubules is tethered by Hrs1 at SPBs, thereby shaking the nucleus. The SPB-led back-and-forth movement of the nucleus is called horse-tail nuclear movement.

pair of haploid cells is fused through the mating process to form a diploid cell right before entry into meiosis. In contrast, azygotic meiosis occurs when proliferating cells in a diploid state start meiosis without the mating process (Cipak et al., 2014).

Both in zygotic and azygotic meiosis the mating pheromones are secreted and received on the cell surface to induce differentiation *via* the MAP kinase cascade.

The mating pheromone–MAPK pathway affects chromosome positioning at the initial stage of sexual differentiation. First, as illustrated in **Figure 1D**, telomeres are clustered in reaction to the mating pheromone. Then, centromeres are dissociated from the SPBs after cell conjugation in the case of zygotic meiosis (Chikashige et al., 1997; Jin et al., 1998). This means that the chromosome arrangement in the nucleus becomes upside-down from the original state (Rabl orientation): telomeres are clustered at SPBs, whereas centromeres (kinetochores) are located far from SPBs (**Figure 1E**). This state is called "bouquet" arrangement, and the upside-down allocation of chromosomes hung from SPBs is essential to promote pairing and meiotic recombination of homologous chromosomes in meiotic prophase. The bouquet configuration of chromosomes is highly conserved throughout eukaryotes, which is essential to promote meiotic recombination [reviewed in Scherthan (2001)].

A cytoplasmic array of microtubules is assembled particularly during meiotic prophase, and the minus ends of such microtubules are tethered at the SPBs. A meiosis-specific coiled-coil protein, Hrs1 (also known as Mcp6), localizes to SPBs and anchors the cytoplasmic array of microtubules at their minus ends (**Figure 1E**), which serves as a fulcrum at the SPBs that transmit the dynamic motion of microtubules to the oscillatory nuclear movement (Saito et al., 2005; Tanaka et al., 2005a; Funaya et al., 2012). The SPB-led microtubule array is dynamically reformed to pull and push the SPBs and the accompanying nucleus in the cytoplasm, by which the nucleus repeats a back-and-forth movement in the cytoplasm during meiotic prophase (Chikashige et al., 1994; Ding et al., 1998; Yamamoto et al., 1999; Hiraoka et al., 2000). The microtubule-driven "horse-tail nuclear movement" aligns the upside-down chromosome bouquet and is thus essential for promotion of pairing and recombination (Yamamoto et al., 1999; Niwa et al., 2000).

The molecular mechanisms for clustering of telomeres have been intensively studied, and meiosis-specific telomere proteins Bqt1 and Bqt2 (bouquet proteins) play central roles for telomere clustering. Bqt1–Bqt2 binds to the constitutive telomere protein Rap1 and also associates nuclear membrane proteins Sad1–Kms1 (and Kms2) (**Figure 1D**; Chikashige et al., 2006). Sad1 is an inner nuclear membrane protein containing the SUN domain, whereas Kms1/2 are outer ones with the KASH domain, and both domains are widely conserved among eukaryotes (Hagan and Yanagida, 1995; Shimanuki et al., 1997; Wälde and King, 2014).

The whole complex is called linker of nucleoskeleton and cytoskeleton (LINC), and it brings all the telomeres toward SPBs by sliding along the nuclear envelope using the cytoplasmic microtubules tethered at SPBs. The LINC complex in *S. pombe* includes the γ-tubulin complex, a base for microtubule nucleation, and the dynein motor protein complex [composed of heavy (Dhc1) and light (Dlc1) chains as well as dynactin (Ssm4)] (Yamashita et al., 1997; Yamamoto et al., 1999; Miki et al., 2002; Yoshida et al., 2013).

Systems to rearrange chromosome positions in eukaryotes are generally conserved: cytoskeleton such as actin (in the budding yeast *Saccharomyces cerevisiae*) or microtubule (in *S. pombe*, *Caenorhabditis elegans* and mice, and partly in *Drosophila melanogaster*) plays functions in the reorganization of chromosome states into the telomere-led bouquet arrangement (reviewed in Rubin et al., 2020). The function of the LINC complex (SUN-KASH proteins) is also conserved in eukaryotes. For instance, in mice germ cells, Majin serves as a related function in the linkage of telomeres and the nuclear envelope as a functional homolog of Bqt4, another transmembrane bouquet protein connecting telomeres and inner nuclear membrane (Chikashige et al., 2009). The transmembrane protein Majin interacts with SUN1-KASH5 proteins as well as with telomere-binding proteins TERB2-TERB1, thereby enhancing the association of telomeres to the nuclear envelope upon meiotic entry (Shibuya et al., 2015). Thus, SUN-KASH proteins are widely employed among eukaryotes to dynamically alter chromosome arrangement inside the nucleus during meiosis [reviewed in Chikashige et al. (2007) and Rubin et al. (2020)].

In addition, the telomere bouquet may regulate spindle functions. The first report described that if the bouquet formation is defective (e.g., in *bqt1*Δ or in *taz1*Δ; Taz1 is a telomere-binding protein), SPBs are fragmented, which results in defective spindles such as monopolar and multipolar ones (Tomita and Cooper, 2007). This is mostly due to the SPB-led horse-tail nuclear movement: SPBs are often apart from the main nuclear body after frequent shaking by cytoplasmic microtubules because the spindle phenotype can be rescued by interrupting the nuclear movement (Chikashige et al., 2014). In mitosis and meiosis, the association of centromeres to SPBs promote mitotic spindle formation (Fennell et al., 2015; Fernández-Álvarez et al., 2016). Taking this knowledge together, we can generalize that chromosome configuration controls the spindle.

Another study reported that bouquet formation contributes to the correct attachment of kinetochores and microtubules in subsequent meiosis I. The bouquet-deficient strains (e.g., *bqt1*Δ) tend to lose CENP-A (the centromere-specific variant of histone H3) and Swi6 [the heterochromatin protein 1 (HP1) ortholog] at centromeres, indicating that the telomere bouquet is required for the maintenance of heterochromatin during meiosis (Klutstein et al., 2015).

It is also reported that telomere bouquet is required to activate the cyclin-dependent kinase-cyclin B (CDK-cyclin B) at SPBs at the later stage of meiotic prophase (Moiseeva et al., 2017). Bouquet-deficient cells also show defects in the detachment of centromeres from SPBs (illustrated in **Figure 1D**), indicating that the detachment of centromeres and the collection of telomeres toward SPBs are linked to each other by the LINC complex and microtubules (Katsumata et al., 2016).

Further investigation to address the biological meaning of telomere bouquet, except for pairing of homologous

chromosomes, will clarify how the conserved chromosomes' behavior functions for the production of gametes.

COMPOSITION OF KINETOCHORES AND SPINDLE POLES IS ALTERED IN MEIOSIS

Another essential phenomenon seen during the initial stage of meiotic events is reorganization of kinetochore and SPB components.

In fission yeast, most of the kinetochore components, including both inner and outer factors, stably constitute kinetochores throughout the mitotic cell cycle. There are only few exceptions: the Dam1 complex is a mitosis-specific kinetochore component, while the Mis18 complex disappears in mitosis (Hayashi et al., 2004, 2014; Liu et al., 2005; Hirai et al., 2014; Subramanian et al., 2014). Components of fission yeast tend to be constitutive in contrast to those of metazoans. The modification of kinetochore proteins by mitotic kinases might have been developed during the evolution from yeast to metazoans. In meiotic prophase, however, most of the outer kinetochore components dismiss, including the Ndc80 (also known as Hec1) complex, the Mis12/MIND complex and Spc7 (KNL1), whereas inner factors remain intact ("slim" kinetochores; **Figure 1D**; Goshima et al., 1999; Wigge and Kilmartin, 2001; Kerres et al., 2004; Asakawa et al., 2005; Hayashi et al., 2006; Meyer et al., 2015).

Signaling *via* the mating pheromone–MAPK pathway in the early stage of meiosis is responsible for the disappearance of the kinetochore components. A reason for making slim kinetochores is for the detachment of centromeres from SPBs (**Figure 1D**), through which chromosomes get inverted to promote pairing and recombination.

In budding yeast meiosis, kinetochores detach from the SPB as in fission yeast meiosis. Although kinetochore detachment in fission yeast is mediated by the delocalization of outer kinetochore complexes, that in budding yeast is controlled through the degradation of Ndc80/Hec1 (Chen et al., 2020). It is suggested that the dissociation of outer kinetochore components may trigger the recruitment of Mam1 (monopolin) to kinetochores for mono-orientation at meiosis I (Meyer et al., 2015).

It is intriguing to point out that many of SPB components including Polo kinase alter its localization during meiotic prophase as is observed for kinetochores ("slim SPB" in **Figure 1D**; Ohta et al., 2012). SPB components are categorized into three groups: (i) disappeared from SPBs during prophase: Cut12, Pcp1, and Spo15. Although Plo1 is not a constitutive component of SPBs (Ohkura et al., 1995; Mulvihill et al., 1999; Tanaka et al., 2001), Plo1 predominantly localizes to SPBs during mitosis, whereas not during meiotic prophase. Plo1 localizes instead to kinetochores as mentioned above. It gets localized to SPBs later, upon entry into meiosis I. Therefore, Plo1 can be categorized to (i); (ii) reduced amount of proteins at SPBs: Sid4 and Cdc11 (Tomlin et al., 2002; Morrell et al., 2004); and (iii) constantly localized to SPBs: Cdc31, Sfi1, Sad1, and Ppc89—those mainly function for SPB duplication as SPB half-bridge factors (Hagan and Yanagida, 1995; Kilmartin, 2003; Paoletti et al., 2003; Rosenberg et al., 2006; Bouhlel et al., 2015).

The slimming down of SPB components shares similarities with that of kinetochore components. For example, the timing of dis/re-appearance of both factors is synchronized, and particularly the disappearance of both factors is dependent on the mating pheromone–MAPK pathway. One of the physiological meanings of SPB reorganization is to avoid overduplication of meiotic SPBs by temporarily reducing Plo1 from SPBs, as enforced localization of Plo1 to meiotic SPBs results in an excess of the SPB number (Ohta et al., 2012; Agarwal et al., 2018). Slim SPB might uncouple SPB duplication with DNA replication in meiosis, which potentially explains how cells secure two rounds of SPB duplication with oscillation of CDK activity in meiosis. Another advantage for dynamic SPB reorganization is to temporarily deposit Plo1 to kinetochores at meiosis I onset: reducing Plo1 at SPBs to get priority to depositing it at kinetochores. The kinetochore localization of Plo1 plays crucial roles in the collection of dispersed kinetochores before meiosis I entry (see below).

The slimming down of SPBs is not evident in budding yeast meiosis, although only a small number of SPB-associated proteins fluctuate: for instance, a meiosis-specific *S. cerevisiae* protein Ndj1 dissociates from SPBs in meiotic prophase (Li et al., 2015). The discrepancy in yeast species might be due to SPB structures. A budding yeast SPB is a three-layered structure and is embedded to the nuclear envelope throughout the cell cycle, whereas a fission yeast SPB has an amorphous structure and is inserted into the nuclear envelope prior to M phase entry (Ding et al., 1997; Jaspersen and Winey, 2004). It is possible that fission yeast SPB is structurally flexible compared to that of budding yeast and that the plasticity may allow a reorganization of the components.

Thus, in mitosis, the components of kinetochores and SPBs are almost constitutive, whereas there are a number of reorganizations taking place probably to streamline cellular machineries to adapt for divisions specialized for the production of gametes. Data remain elusive regarding molecular mechanisms as to how slimmed kinetochores and SPBs are rebuilt right before entry into meiosis I. Previous studies indicated the requirement of activities of cell cycle kinases. Re-accumulation of SPB components including Plo1 at meiosis I onset requires elevation of the CDK activity (Ohta et al., 2012). In budding yeast, the activity of the Aurora B kinase Ipl1 is required for the reappearance of Ndc80 to kinetochores before meiosis I (Kim et al., 2013; Meyer et al., 2015). It is possible that those kinases phosphorylate some key components that are required for further recruitment of other components to reconstitute SPBs and kinetochores before entry into meiosis I.

ENTRY INTO MEIOSIS I: POSITION OF CHROMOSOMES IS ALTERED BY MEIOTIC MICROTUBULES

Next, we compare the chromosome arrangement in the nucleus upon entry into mitosis and into meiosis I. As discussed

above, centromeres (kinetochores) are located close to SPBs in the interphase of the mitotic cell cycle (**Figure 1C**). This allocation is suitable for easy connection between microtubules and kinetochores upon entry into mitosis, as microtubules are nucleated from two SPBs, where kinetochores have been clustered even during interphase (**Figure 2A**).

The SPBs, duplicated in interphase, are separated from each other on the surface of the nucleus, as microtubules emanated from each of the SPBs start to overlap and interdigitate upon mitotic entry (**Figure 2B**). Finally, those two SPBs are separated to opposite sides so that the bipolar spindle can be assembled by metaphase (**Figure 2C**).

On the contrary, in cells entering meiosis I, positioning of chromosomes is completely upside-down as a result of centromere dissociation and telomere clustering. In addition, chromosomes are duplicated as sister chromatids, and homologous chromosomes are paired with chiasmata as a result of meiotic recombination during the horse-tail nuclear movement, as illustrated in **Figure 2D**. The upside-down positioning of chromosomes could be a potential risk for the subsequent chromosome segregation in meiosis I because kinetochores are located distal from the microtubule nucleation site, unlike that in mitosis.

When cells enter meiosis I, the horse-tail nuclear movement ceases, and microtubules are nucleated from SPBs toward inside the nucleus as observed at mitotic entry. In contrast to mitotic entry, meiotic cells, at this stage, start to nucleate an extensive radial array of microtubules from SPBs (**Figure 2D**; Kakui et al., 2013).

The extended microtubules then capture kinetochores scattered in the nucleus and then shrink to retrieve the attached kinetochores toward SPBs (**Figure 2E**). The retrieval of kinetochores mostly relies on depolymerization of microtubules rather than sliding of kinetochores on microtubules. First, a kinetochore may attach to the lateral surface of a microtubule, and this can then be converted to end-on pulling when the plus end of the shrinking microtubule reaches the kinetochore. End-on pulling motion in meiotic kinetochore retrieval relies on the Dam1 complex, which forms oligomeric rings around microtubules (Westermann et al., 2005). In contrast, budding yeast kinetochores are mainly collected by sliding on the surface of microtubules in mitosis (Tanaka et al., 2005b). Homologous kinetochores are retrieved as a pair by microtubules, and mathematical modeling indicated that the dynamic instability of microtubules is essential for efficient retrieval and that paired configuration of kinetochores accelerates the capture by pivoting microtubules (Cojoc et al., 2016; Blackwell et al., 2017).

When homologous kinetochores are captured and pulled by microtubules, the mode of attachment may be mostly monopolar, the state in which both kinetochores are pulled by microtubules emanated from the same spindle pole. This may be resolved by Aurora B kinase, as budding yeast meiotic kinetochores retrieved in a monopolar manner are converted to bipolar attachment through phosphorylation by the Aurora B kinase Ipl1 (Meyer et al., 2013). The kinetochore protein Dam1 is also shown to promote chromosome bi-orientation through phosphorylation by the Mps1 kinase (Meyer et al., 2018).

During retrieval of kinetochores by pivoting monopolar microtubules, formation of the bipolar spindle (separation of two SPBs) should be repressed, although the system that surveys the completion of the scattered kinetochores does not appear very strict, as occasionally bipolar spindle starts to assemble even before the completion of kinetochore retrieval (Kakui et al., 2013). At least in budding yeast meiosis, the Aurora B Ipl1 localizes to SPBs during meiotic prophase and is involved in delaying the assembly of bipolar formation driven by S-CDK (Kim et al., 2013; Newnham et al., 2013).

Regarding regulation of SPB separation, a meiosis-specific telomere-associated protein, Ndj1, is known to localize to SPBs together with Mps3 (a SUN-domain protein) in budding yeast meiosis to suppress the premature separation of SPBs (Li et al., 2015, 2017). Polo kinase Cdc5 removes Ndj1 from the half-bridge structure connecting two SPBs, thereby promoting SPB separation in meiosis I. As Ndj1, Mps3, and Csm4 are also involved in telomere positioning and motility in meiotic prophase, loss of Ndj1 in meiosis I brings two consequences: SPB separation and telomere dissociation from the nuclear envelope (Conrad et al., 2008; Kosaka et al., 2008; Wanat et al., 2008; Li et al., 2015), indicating that these factors may play central roles to coordinate mitotic progression and chromosome configuration.

In summary, the extensive microtubules are assembled to relocate chromosomes to the original position as seen in mitotic entry, thereby minimizing the potential risk of segregation errors in meiosis I.

In addition to the assembly of radial microtubules, cells at meiosis I onset take the second strategy, namely, cells utilize Alp7 (also known as Mia1), the *S. pombe* ortholog of the microtubule-associated protein transforming acidic coiled-coil protein (TACC) for this purpose. Alp7 primarily localizes to SPBs and microtubules. Alp7 also localizes to mitotic kinetochores once captured by spindle microtubules, which means that Alp7 is delivered to kinetochores by microtubules and stabilizes kinetochore–microtubule attachment in mitosis (Oliferenko and Balasubramanian, 2002; Sato et al., 2003, 2004; Sato and Toda, 2007). Although Alp7 localizes also to meiotic kinetochores, it is of note that Alp7 localizes there even before microtubule attachment (**Figure 2D**). Alp7 precociously localized to scattered kinetochores promotes capture by radial microtubules (Kakui et al., 2013).

Thus, cells employ two machineries—extension of radial microtubules and precious localization of Alp7 to kinetochores—to synergistically promote relocation of chromosomes. Do these machineries operate also during mitosis or only during meiosis? The radial array of microtubules is not evident in cells at mitotic onset, in which kinetochores are constantly located in the vicinity of SPBs. When kinetochores are artificially detached from SPBs upon entry into mitosis, for example, by the use of transient exposure to microtubule poisons, similar long microtubules are assembled after drug washout to capture and collect the scattered kinetochores. Thus, the machinery utilizing extending microtubules may also operate during mitosis as a backup system to respond to the unexpected risk, although it has not been clarified if the molecular mechanisms for microtubule extension are identical in mitosis and in meiosis. Alternatively, either SPB

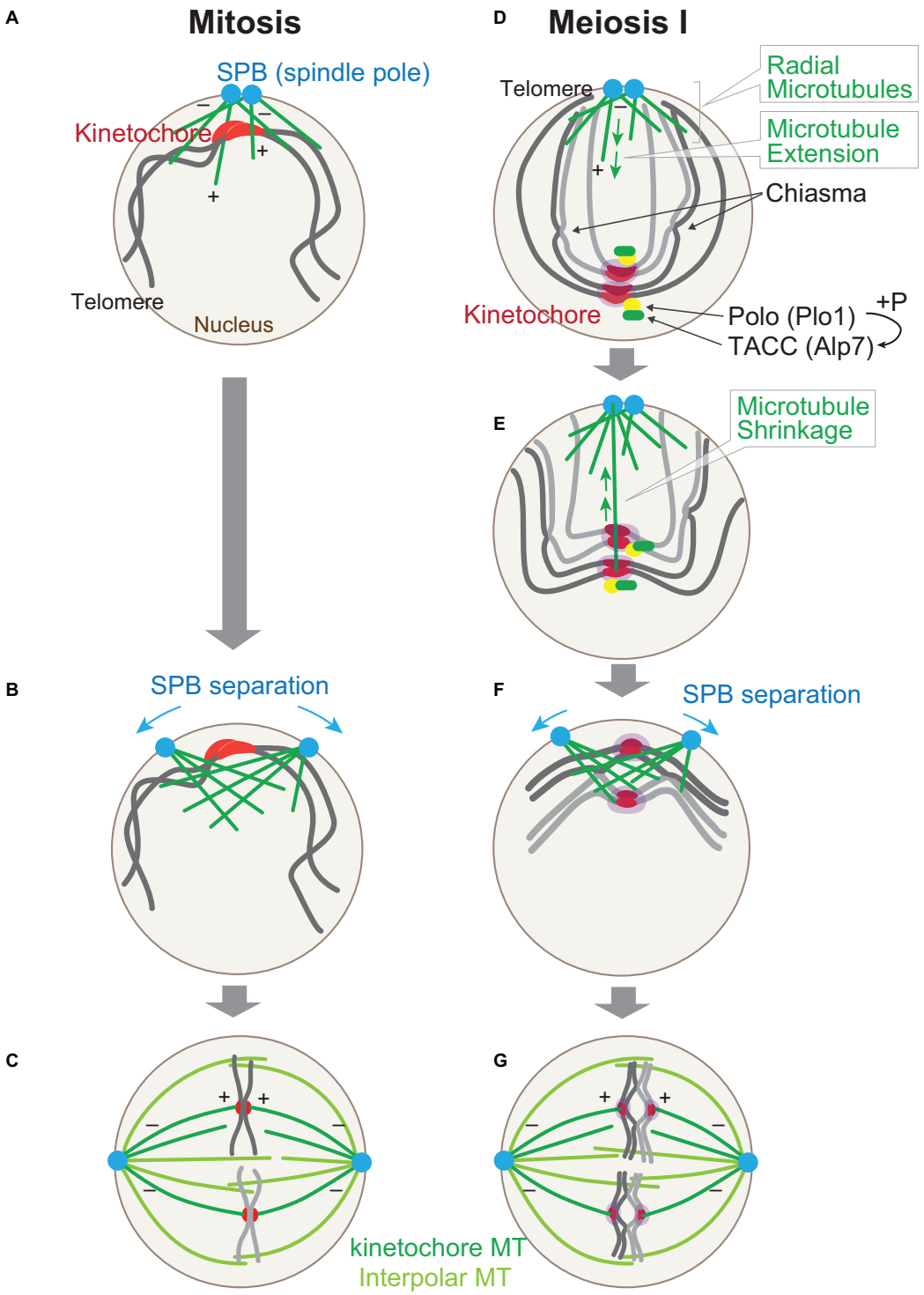

FIGURE 2 | Chromosome arrangement changes upon sexual differentiation. Chromosome positioning upon entry into mitosis. At the onset of mitosis **(A)**, kinetochores (red) are clustered at spindle pole bodies (SPBs; blue), where microtubules (green) start to nucleate. The polarity of a microtubule is indicated (+, –). SPBs start to separate as the microtubules grow **(B)**, and in metaphase **(C)**, kinetochore microtubules (MTs) and interpolar MTs comprise the nuclear spindle. **(D–G)** Chromosomes are re-arranged upon entry into meiosis I right after the horse-tail nuclear movement is ceased **(D)**. Microtubules are nucleated from SPBs, but kinetochores are scattered in the nucleus. Kinetochores are mono-oriented by Moa1 (Meikin, purple), which recruits Polo kinase (Plo1). Plo1 then recruits Alp7 (TACC) to pre-attached kinetochores. A radial array of microtubules is formed from SPBs **(E)** and capture kinetochores and retrieve them toward SPBs. Telomeres are dissociated from SPBs. At the timing when kinetochore retrieval is completed **(F)**, SPBs start to separate to assemble the bipolar spindle **(G)**. Note that homologous chromosomes are independently attached to microtubules in mitosis **(C)**, whereas they are paired in meiosis I **(G)**.

separation or maturation in meiosis I could be repressed by slim SPBs during meiotic prophase to efficiently form a radial microtubule array.

In meiosis, however, extension of microtubules is observed in cells at the stage without exception, and the microtubules complete kinetochore retrieval mostly by the time SPBs start to separate (**Figures 2F,G**), suggesting that the scheme in meiosis is programmed as a physiological system rather than as a reflex action to the contingency. The second strategy, namely, the precocious deposition of Alp7 to microtubule-free kinetochores, is exclusively observed in this stage, and a similar localization cannot be observed in mitotic cells. Thus, deposition of Alp7 to pre-attached kinetochores is programmed specifically for meiosis. This is indeed evidenced by the molecular mechanism underlying the precocious localization of Alp7 to meiotic kinetochores: the meiosis-specific localization of Alp7 is dependent on the Polo kinase Plo1, which is also located to pre-attached kinetochores in meiosis (**Figure 2D**).

As mentioned above, Plo1 localizes to pre-attached kinetochores using Moa1 (Meikin) as a platform; therefore, Alp7 localization to the kinetochores is also a meiosis-specific event. Taken together, we consider that Moa1–Plo1 plays the third function in meiosis—at the onset of meiosis I, kinetochores are highlighted as center for microtubule control: Moa1 (Meikin) recruits Plo1 (Polo kinase), which deposits Alp7 (TACC) to stably capture microtubules emanated radially from spindle poles.

Moa1–Plo1 has an additional role: Plo1 at meiotic kinetochores also phosphorylates Spc7 (KNL1) of the outer kinetochore components. This affects the localization of Bub1 kinase which is known as a checkpoint kinase and phosphorylates histone H2A to recruit shugoshin at centromeres (Tang et al., 2004; Kawashima et al., 2010). In mitosis, the kinetochore localization of Bub1 is transient, whereas Bub1 in meiosis persists at kinetochores until anaphase of meiosis I because Spc7, the platform for Bub1, is phosphorylated by Plo1 specifically in meiosis (Miyazaki et al., 2017).

Thus, Moa1–Plo1 plays a central role to dictate a number of meiosis-specific events regarding the interaction of kinetochores and microtubules, thereby differentiating meiosis from mitosis.

The progression of kinetochore–microtubule association is monitored by the spindle assembly checkpoint (SAC) machinery in mitosis and meiosis. Briefly, kinetochores unattached to microtubules are recognized by the Mad1–Mad2 complex, the main components of SAC. When chromosomes are repositioned at the onset of meiosis I, the unattached kinetochores are not recognized by Mad1–Mad2. This is probably due to a lack of sufficient CDK activity, which is a prerequisite for the localization of Mad1–Mad2 to unattached kinetochores (Aoi et al., 2014).

For an entire resolution of the bouquet arrangement, telomeres that have been clustered around SPBs during meiotic prophase are detached from SPBs upon entry (**Figure 2E**), although the molecular mechanism remains elusive. Resolution of telomere clustering occurs almost at the same timing with kinetochore retrieval, albeit slightly later than the retrieval. The resolution requires elevation of the cyclin-dependent kinase activity by Cdc25 phosphatase, which is transcriptionally activated by the meiosis-specific transcription factor Mei4 (Murakami-Tonami et al., 2007; Kakui et al., 2011, 2013). Cdc13 (cyclin B) predominantly accumulates at bouquet telomeres for the resolution of telomere clustering (Moiseeva et al., 2017).

POWER BALANCE FOR SPINDLE POLE SEPARATION IN MITOSIS AND MEIOSIS

It has been recently shown that difference in chromosome configuration in mitosis and meiosis affects bipolar spindle organization using their kinetic properties.

The assembly of bipolar spindle is based on the elongation of microtubules and their mutual and physical interaction. Spindle microtubules are emanated from both of the two SPBs, and they interact with each other to separate the SPBs outward, which is the major driving force for bipolar spindle formation.

As illustrated in **Figure 3A**, a couple of kinesin motor proteins are involved in the separation of two SPBs. Kinesin-5 is a conserved subfamily of the kinesin superfamily motor proteins that move to plus-ends and functions as a homo-tetramer (Hagan and Yanagida, 1990, 1992; Kapoor et al., 2000). Cut7, the fission yeast ortholog of kinesin-5 subfamily members, is an essential protein required for outward SPB separation that functions as a tetramer (Hagan and Yanagida, 1990, 1992; Akera et al., 2015). Cut7 captures the lateral surface of a pair of interpolar microtubules emanating from both SPBs, and it moves toward their plus-ends along the microtubules. The motion consequently pushes two SPBs outward (**Figures 3A,B**).

On the contrary, members belonging to another subfamily kinesin-14 (Pkl1 and Klp2) are minus-end-directed and generate inward forces for SPBs (**Figure 3A**). Pkl1 preferentially localizes to SPBs and the spindle as well as the nucleoplasm during mitosis, and Klp2 localizes to spindle microtubules (Pidoux et al., 1996; Troxell et al., 2001; Simeonov et al., 2009).

The knock-out of Cut7 (*cut7*Δ) is lethal with an adjacent pair of SPBs, which extend the monopolar spindle therefrom. The lethality of *cut7*Δ and *cut7*-ts (temperature sensitive) mutants is suppressed by a simultaneous knock-out of pkl1 (Rodriguez et al., 2008; Syrovatkina et al., 2013; Olmsted et al., 2014; Syrovatkina and Tran, 2015). This can be explained in such a way that, in the absence of Cut7, the major force operating between two SPBs is inward force generated by Pkl1 and Klp2, which hampers SPB separation (**Figure 3B**). In the absence of two antagonistic kinesins Cut7 and Pkl1, the outward force wins again to consequently separate the SPBs (mitosis, **Figure 3C**).

This also indicates that there are additional factors that generate the outward force to separate SPBs other than Cut7. One of such factors is the microtubule-associated protein Ase1 (human PRC1), which is known to connect a pair of interdigitating microtubules as an anti-parallel bundle (Pellman et al., 1995; Loïodice et al., 2005; Yamashita et al., 2005). This indicates that Ase1 connects interpolar microtubules in *cut7*Δ *pkl1*Δ mitosis (**Figure 3C**), and microtubule polymerization by Alp14 (a member of the ch-TOG/XMAP215/Dis1 microtubule-associated protein family) together with Alp7 (TACC) pushes the SPB of the other side outward (Yukawa et al., 2017). Similarly,

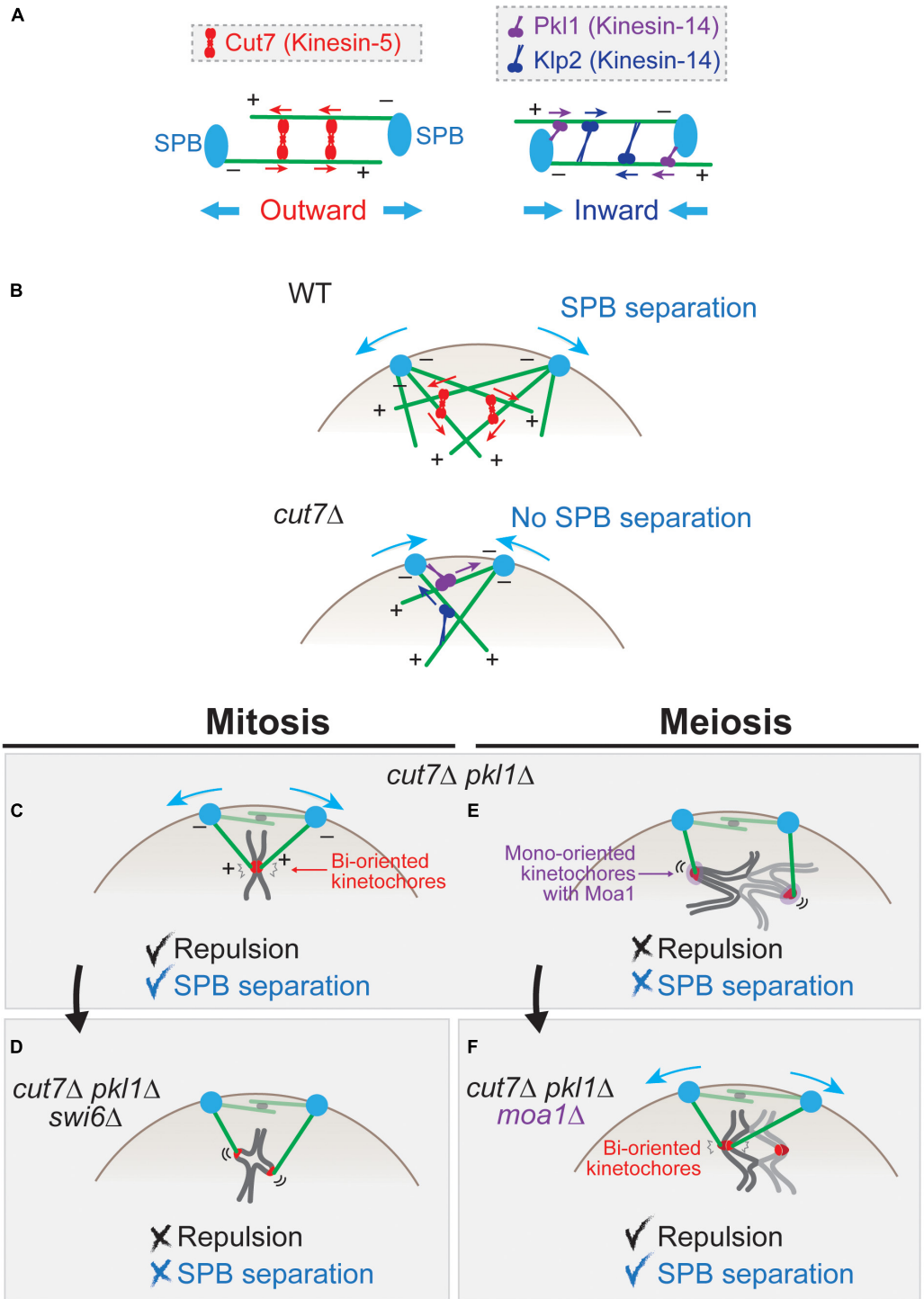

FIGURE 3 | Force balance affects spindle pole body (SPB) separation in mitosis and meiosis. **(A)** Schematics for functions of Cut7 (kinesin-5) and Pkl1 and Klp2 (kinesin-14) for the inter-SPB distance. A tetramer of Cut7 (red) captures two bundles of microtubules. When they are aligned in an anti-parallel manner, the plus-end-directed Cut7 generates the outward force that consequently separates two SPBs. The polarity of microtubules (+, –) is indicated. Microtubules are tethered to SPBs at their minus ends. Pkl1 localizes to SPBs and Klp2 to the microtubules. Those minus-end-directed motors generate the inward force. **(B)** SPB separation in prometaphase of mitosis. In wild-type cells, the microtubules nucleated from two SPBs are linked by Cut7 and separate the SPBs. In the *cut7* deletion (*cut7*Δ) mutant, SPBs fail to separate because of the inward force generated by Pkl1 and Klp2. **(C)** In mitotic *cut7*Δ *pkl1*Δ cell, SPBs are separated by repulsive forces generated by sister kinetochores. **(D)** When Swi6 (HP1) is deleted, the structure of sister kinetochores is loosened, which does not generate a sufficient repulsive force to separate SPBs. **(E)** In contrast to mitosis **(C)**, *cut7*Δ *pkl1*Δ cells in meiosis I cannot generate a sufficient repulsive force to separate SPBs. **(F)** When kinetochores are artificially bi-oriented by depleting Moa1 (*cut7*Δ *pkl1*Δ *moa1*Δ), sister kinetochores generate a repulsive force that causes SPB separation.

other microtubule-associated proteins promote outward force generation in the absence of Cut7 (Yukawa et al., 2019).

In addition to microtubule-associated proteins, chromosome is another factor that generates outward force for SPB separation. In *cut7*Δ *pkl1*Δ mitosis (**Figure 3C**), a pair of sister chromatids mediate pole-to-pole connection through kinetochore–microtubule attachment (Shirasugi and Sato, 2019). The microtubules use the sister kinetochores as the fulcrum to generate the repulsive force which separates SPBs.

This is evidenced by genetic analyses; for instance, SPB separation is inhibited when the mitotic cohesin Rad21 is removed (i.e., in the *cut7*Δ *pkl1*Δ *rad21-ts* triple mutant). Moreover, when the sister kinetochores are unfastened by reduction of centromeric cohesion using deletion of Swi6 (HP1) (Ekwall et al., 1995; Bernard et al., 2001; Nonaka et al., 2002; Kitajima et al., 2003), the outward force is significantly diminished (**Figure 3D**; Shirasugi and Sato, 2019). These results altogether demonstrate that centromeric cohesion and functional sister kinetochores are required for generation of the outward force in the absence of Cut7 and Pkl1.

In contrast to mitosis, *cut7*Δ *pkl1*Δ cells are not able to separate SPBs in meiosis I (Shirasugi and Sato, 2019). This is due to the loosened connection between homologous kinetochores instead of a tight sister kinetochore connection of mitotic cells (**Figure 3E**). When mono-orientation of sister chromatids is converted to bi-orientation by deletion of Moa1 (i.e., *cut7*Δ *pkl1*Δ *moa1*Δ cells), SPBs are separated (**Figure 3F**).

This provides us two concepts. First, the rigidity of the kinetochore connection matters because it determines whether an additional outward force for SPB separation is generated in mitosis and in meiosis. Second, the kinetochore-mediated outward force is weaker in meiosis I than in mitosis, owing to meiotic kinetochore mono-orientation. This may lead to a delay in SPB separation in meiosis I, unless the Cut7-mediated force is somehow augmented or the opposing inward force by kinesin-14 motors decreases. Alternatively, SPB separation may be suspended until scattered kinetochores are retrieved near SPBs. When kinetochores are retrieved to the close vicinity of SPBs, it may be able to generate a rigid repulsive force by short microtubules that is sufficient for SPB separation. This may be reasonable for cells at this stage, as they need to earn some additional time until all the scattered kinetochores are collected to SPBs. Thus, the kinetochore-mediated repulsive force may modulate the balance of mechanical forces, through which meiosis-specific cell cycle progression and chromosomal events may be timely coordinated.

In general, either in mitosis or meiosis, fission yeast microtubules do not complete end-on attachment to kinetochores by the timing of SPB separation. Therefore, the kinetochore-mediated SPB separation may not rely on the end-on attachment; rather, a pair of bi-oriented kinetochores serves as a glue factor that connects two anti-parallel microtubules through attachment to their lateral surfaces, similarly to the microtubule-associated bundling factor Ase1.

Kinetochore-driven centrosome separation has also been observed in HeLa cells. When a kinetochore protein, either CENP-O (Mcm21) or CENP-L, is depleted, separation of centrosomes is delayed albeit partially, and this is due to defects in the formation of kinetochore microtubules (kinetochore fibers or k-fibers) (Toso et al., 2009; McHedlishvili et al., 2012).

There are two major pathways for centrosome separation in HeLa mitosis: the aurora A-dependent pathway, which is presumably for centrosomal microtubule-mediated separation, and the kinetochore-dependent pathway (Toso et al., 2009). The kinetochore-mediated pathway does not exert a significant influence on mitotic progression when centrosomes have already been separated before nuclear envelope breakdown (∼50% of total mitotic cells), suggesting that the kinetochore-driven machinery is a backup for efficient centrosome separation in HeLa mitosis.

When the nuclear envelope breakdown precedes centrosome separation in prometaphase, lateral attachment and kinetochores to microtubules and their lateral transport are promoted to form a ring-like alignment of chromosomes, called prometaphase rosette (Nagele et al., 1995; Bolzer et al., 2005). The prometaphase rosette is gradually converted to metaphase congression through the transport of laterally attached kinetochores by the kinesin-7 motor CENP-E and the chromokinesin Kid (Tokai et al., 1996; Funabiki and Murray, 2000). Kinetochore-driven centrosome separation may occur during the conversion and establishment of the metaphase alignment. These observations imply that the way of kinetochore-mediated SPB separation is an analogous phenomenon to the similar centrosome separation.

During acentrosomal meiosis I of mouse oocytes, the Ndc80 complex of outer kinetochores accumulate the microtubule crosslinker Prc1 (yeast Ase1) to kinetochores, which becomes a center for microtubule bundling to assemble the functional bipolar spindle even without positional cues at spindle poles (Yoshida et al., 2020). Thus, the kinetochore-mediated force generation, as well as the Ase1/Prc1-dependent cross-linking pathway in yeast mitosis, may be an evolutionary origin for spindle organization in female acentrosomal meiosis. In line with this, it is recently found that acentrosomal spindle microtubules containing Ase1/Prc1 can be induced in fission yeast meiosis (Pineda-Santaella and Fernández-Álvarez, 2019).

ANAPHASE EVENTS: SPINDLE ELONGATION AND RESOLUTION OF RECOMBINATION

As mentioned above, the SAC machinery monitors the state of kinetochore–microtubule interaction, and in the case of problems, SAC arrests cell cycle progression in metaphase. SAC detects two types of erroneous interactions: an improper attachment and a lack of tension between kinetochores (Nezi and Musacchio, 2009). The overall functions of SAC are common in mitosis and in meiosis, but tension is generated in a different manner. In mitosis, tension by microtubules is generated between sister kinetochores (left, **Figure 1B**), whereas it is generated between homologous kinetochores (right).

In anaphase I, homologous chromosomes with chiasmata are segregated; hence, chiasmata need to be resolved by

anaphase onset. The resolution of meiotic recombination intermediates is promoted by the Skp1–Cul1-F–box (SCF) complex. SCF constitutes a conserved ubiquitin ligase family and contributes a number of cellular phenomena, and the fission yeast orthologs of the components are Skp1, Cul1, and at least 18 F-box proteins [reviewed in Toda et al. (1999)]. In the temperature-sensitive mutant of SCF–Skp1 (*skp1*-ts), the anaphase spindle becomes abnormally bent in the nucleus, both in mitotic and meiotic anaphase (Lehmann and Toda, 2004; Okamoto et al., 2012).

The bend spindle in anaphase I is due to unresolved meiotic recombination intermediates that remained until anaphase as evidenced by the prolonged foci of Rad51 (the RecA homolog) indicating sites of meiotic recombination (Muris et al., 1993; Shinohara et al., 1993). When meiotic cohesin Rec8 or the meiotic endonuclease Spo11 (the fission yeast ortholog is named Rec12) is deleted, the bent spindle phenotype is suppressed, verifying that entangled chromosomes by prolonged recombination intermediates attached to microtubules hamper the full elongation of the anaphase spindle; therefore, the spindle is bent.

In conclusion, Skp1 and the F-box helicase Fbh1 are required for the resolution of meiotic recombination intermediates, although it remains to be elucidated which protein is targeted by SCF-Skp1–Fbh1 for degradation for the resolution (Okamoto et al., 2012; Tsutsui et al., 2014).

The function of SCF–Skp1 in the resolution process appears conserved in eukaryotes: the *Arabidopsis ask1* mutant (Ask1 is the Skp1 ortholog) has the spindle which displays an overall normal structure but somewhat longer than that of WT cells during meiosis I (Yang et al., 1999; Yang and Ma, 2001; Wang et al., 2004). The difference in spindle morphology (bent or long) in these two organisms could be simply due to whether the spindle poles are embedded in the nuclear envelope and whether the spindle is assembled in the compartmentalized nucleus in closed mitosis (**Figure 4A**), and the function in resolution of meiotic intermediates is likely to be conserved.

EXIT FROM MEIOSIS I AND ENTRY INTO MEIOSIS II

One of the most enigmatic mechanisms of meiosis is two consecutive rounds of cell division: meiosis I (MI) and meiosis II (MII) without replicating DNAs, which is a clear contrast to the single M phase per cell cycle in mitotically growing cells. The interval between MI and MII is called the interkinesis period.

After segregation of homologous chromosomes and spindle elongation in anaphase I of fission yeast (**Figure 4A**), the spindle is disorganized once, and after a while (∼30 min at 25°C), the spindle for meiosis II starts to assemble (prophase of MII, **Figure 4A**; Sato et al., 2009). Specialized regulation of CDK is essential for the interkinesis period, followed by the initiation of meiosis II. Earlier genetic studies have demonstrated that the CDK activity is essential to start meiosis II, as the *cdc2/tws1* mutant cannot enter meiosis II, and terminates meiosis with the formation of the spore wall (Nakaseko et al., 1984; Grallert and Sipiczki, 1990; Iino et al., 1995).

The drug-sensitive mutant *cdc2-as* (analog-sensitive) (Dischinger et al., 2008) contains a mutation in the gatekeeper residue, which causes a reduction of the Cdc2 activity. The *cdc2-as* mutant is deficient in meiosis II initiation and terminates meiosis in a binucleate state even without exposure to the ATP analog. The activity of the mutant protein can be regained by the introduction of a suppressor mutation into the Cdc2-as protein. The *cdc2-asM17* mutant has additional mutations to improve the Cdc2-as activity and proceeds meiosis normally to produce normal spores (Aoi et al., 2014).

The *mes1* mutant has been isolated as a *mes* (meiosis second) mutant defective in meiosis II, although the *mes1* mutant does not display the spore wall unlike *cdc2/tws1* (Bresch et al., 1968; Shimoda et al., 1985). The *mes1* gene is expressed specifically during meiosis and encodes an inhibitor of the anaphase promoting complex/cyclosome (APC/C) (Kishida et al., 1994; Izawa et al., 2005; Kimata et al., 2008), the mega-complex serving as a conserved E3 ubiquitin ligase [reviewed in Yamano (2019)]. In WT cells entering anaphase I, the CDK activity is maintained by Mes1, which blocks the full activation of APC/C to a moderate level that is sufficient to initiate anaphase I (top, **Figure 4B**).

The APC/C is, in general, activated by the coactivator Cdc20 (Slp1 in fission yeast) both in mitosis and meiosis, but in meiosis, Fzr1 (also known as Mfr1 and Sms1) also assists the activation of APC/C (Asakawa et al., 2001; Blanco et al., 2001; Kimata et al., 2011; Aoi et al., 2013). In WT meiocytes, Slp1 is the main coactivator for anaphase I onset, whereas Fzr1 is mainly for anaphase II onset and completion of meiosis. Mes1 binds and initially inhibits Fzr1 and Slp1 as a competitive substrate to prevent premature APC/C activation until anaphase I. Mes1 is a competitive substrate but not a pseudosubstrate for Slp1; therefore, Slp1 eventually overcomes the inhibition by Mes1 and triggers anaphase I onset (Kimata et al., 2008).

On the contrary, Mes1 serves as a pseudosubstrate for Fzr1; therefore, Fzr1 remains inactive possibly until Mes1 is somehow diminished. In the absence of Mes1 (*mes1*Δ), APC/C is prematurely activated by Fzr1 in anaphase I, which terminates meiosis early, right after anaphase I, without initiating meiosis II (middle, **Figure 4B**). In line with this, the early termination of *mes1*Δ can be substantially suppressed by the simultaneous deletion of Fzr1: the *mes1*Δ *fzr1*Δ double mutant initiates meiosis II and produces spores (Aoi et al., 2013).

The *fzr1*Δ single mutant can initiate anaphase I and anaphase II, as Slp1 functions as the major APC/C coactivator for both divisions, but for complete exit from meiosis II, Fzr1 is essential in addition to Slp1, as *fzr1*Δ meiocytes do not exit from meiosis even after anaphase II; cyclin B reaccumulates later instead (bottom, **Figure 4B**). The *fzr1*Δ mutant thus initiates "meiosis III", although the division is incomplete in terms of insufficient materials such as SPBs and chromosomes.

The checkpoint (SAC) functions twice, namely, at meiosis I and II. The activity of SAC during two sequential divisions may be regulated in a continuous manner. When the first division is delayed by SAC, the anaphase onset of meiosis II is advanced,

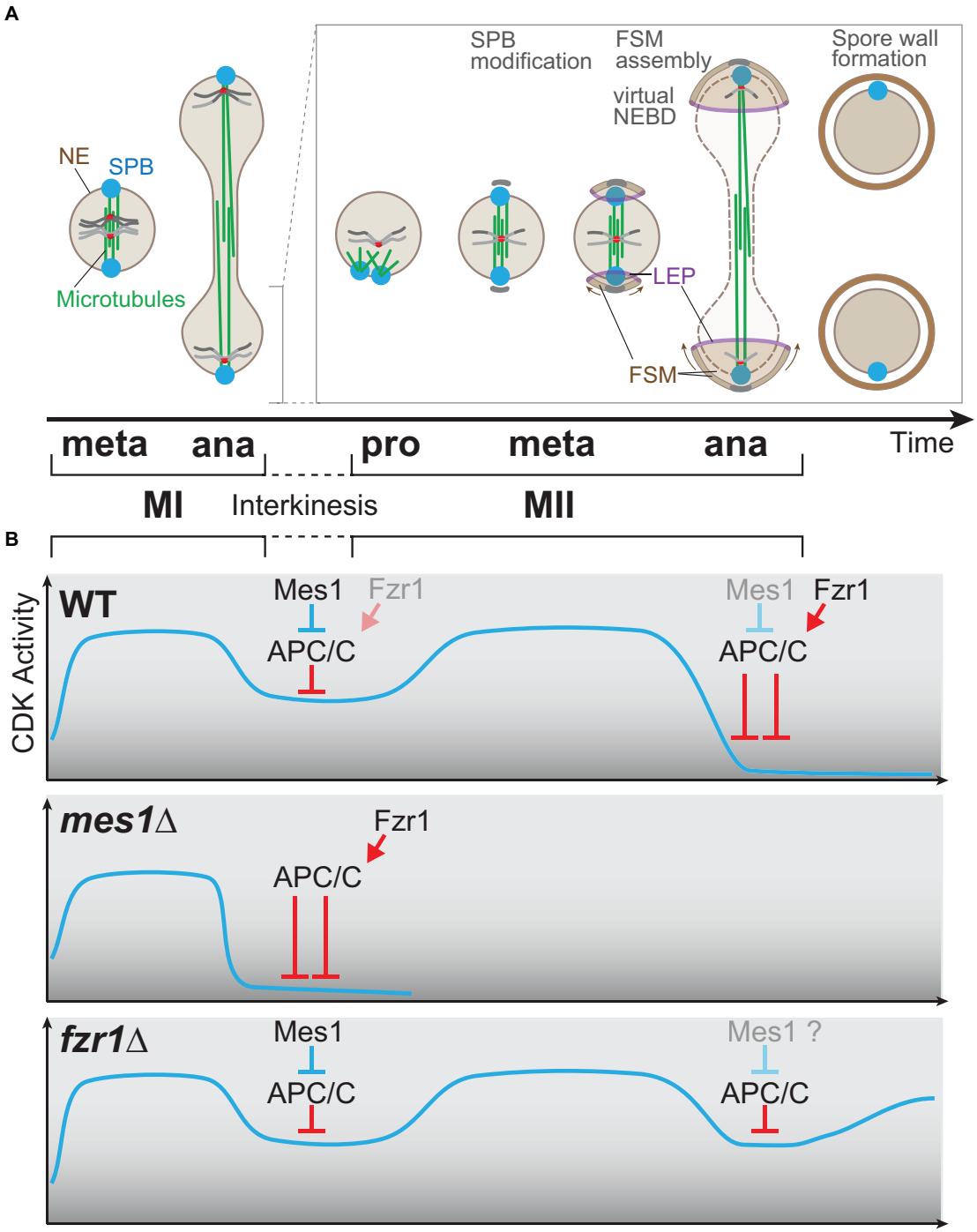

FIGURE 4 | Meiosis-specific cell cycle progression from meiosis I to meiosis II. **(A)** A graphical view of meiotic progression from metaphase of meiosis I (MI) to anaphase of meiosis II (MII). After anaphase I, only one of two nuclei is chosen for drawing to illustrate MII progression. In prophase II, the microtubules are nucleated from spindle pole bodies (SPBs) and form the bipolar spindle for meiosis II as in mitosis and MI. At the transition stage of metaphase to anaphase, each SPB is modified, and the globular forespore membrane (FSM) begins to grow to surround the nucleus. The leading edge of the FSM opening is decorated by leading edge proteins. During anaphase II, the barrier function of the nuclear envelope is invalidated, which is an incident called virtual nuclear envelope breakdown. After completion of MII, the rigid spore wall is assembled. **(B)** The kinetics of the CDK activity during meiosis. The horizontal axis (time) is shared with the time scale in **(A)**. In wild-type cells (top), the CDK activity elevates until metaphase I and drops at anaphase I onset, which is triggered by APC/C. The APC/C inhibitor Mes1 modulates the activity of APC/C to a moderate level so that cells can enter anaphase I and to restart meiosis II, which requires re-accumulation of the CDK activity. In *mes1*Δ cells (middle), Fzr1, an APC/C coactivator, is prematurely activated to fully activate APC/C, and the cells cannot enter meiosis II, and terminates meiosis early instead. In *fzr1*Δ cells (bottom), meiosis I proceeds almost normally, but CDK repression after anaphase II onset is not sufficient as APC/C cannot be fully activated in the absence of Fzr1. The cells then start the aberrant third division albeit incomplete.

which means that the SAC effect was reduced at meiosis II to compensate the previous delay that occurred in meiosis I (Yamamoto et al., 2008).

In conclusion, the number of meiotic divisions is exclusively determined as two, neither one nor three. This biological rule strictly conserved and complied among eukaryotes is defined by the repetitive battles of the "CDK–APC/C derby", which is reinforced by meiosis-specific factors Mes1 and Fzr1.

Although the seesaw battle is commonly seen in meiocytes of any species, the underlying molecular mechanisms may be divergent. The functional homologs of *S. pombe* Mes1 are OSD1 in plants and Erp1/Emi2 in vertebrates (Liu et al., 2006; Ohe et al., 2007; d'Erfurth et al., 2010; Cromer et al., 2012). In oocyte meiosis of vertebrates, Erp1 functions as a cytostatic factor that arrests the meiotic cell cycle in metaphase II (Masui and Markert, 1971; Inoue et al., 2007; Nishiyama et al., 2007), although fission yeast meiosis does not particularly arrest at metaphase II.

Arabidopsis OSD1 (*OMISSION OF SECOND DIVISION 1*) is also an APC/C inhibitor, which ensures initiation of meiosis II together with TAM (Cyclin A; *TARDY ASYNCHRONOUS MEIOSIS*), and the *tam osd1* double mutant cannot initiate meiosis II (d'Erfurth et al., 2010). *Arabidopsis* TDM1/MS5 (*THREE DIVISION MUTANT 1/MALE STERILE 5*) is the functional homolog of Fzr1 and is required for exit from meiosis. The *tdm1/ms5* mutant exhibits the aberrant third meiosis similar to the *S. pombe fzr1*Δ mutant (Ross et al., 1997; Glover et al., 1998). Although the players for the CDK–APC seesaw battle appears conserved in fission yeast and plant cells, the way of molecular regulation seems distinct. For meiotic exit, the active level of fission yeast Fzr1 may be regulated transcriptionally, but the plant TDM1 is post-translationally regulated through phosphorylation (Cifuentes et al., 2016).

The other *S. pombe mes* mutant *mes2* is allelic to the *spo5* mutant, and the *spo5* gene encodes a meiosis-specific RNA-binding protein (Bresch et al., 1968; Kasama et al., 2006; Okuzaki et al., 2010). Spo5 promotes progression of meiosis II through regulation of cyclin B (Arata et al., 2014; Togashi et al., 2014). At the moment, the *mes* mutants isolated to date are only two, and many things still remain to be elucidated: e.g., how the *mes1* expression is controlled. It is reported that the *mes1* gene is spliced only during meiosis (Kishida et al., 1994; Shimoseki and Shimoda, 2001; Malapeira et al., 2005). Although the mechanism remains unclear, this may be dependent on the meiosis-specific splicing machinery particularly driven by the promoter region and transcription factors belonging to the forkhead family (Averbeck et al., 2005; Moldón et al., 2008).

MEIOSIS II IS NOT JUST AN ANALOGOUS EVENT TO MITOSIS

Forespore Membrane Formation

An *S. pombe* diploid meiocyte produces two nuclei after anaphase I; each of the nuclei is next divided into two in meiosis II to finally produce four haploid spores (**Figure 4A**). The second division of meiosis is similar to mitosis regarding the pattern of chromosome segregation (equational division), in which sister chromatids are segregated. Besides that, meiosis II is generally linked with gametogenesis, which corresponds to sporulation in yeast species.

The detailed processes of sporulation and underlying molecular mechanisms are comprehensively reviewed in Shimoda (2004); therefore, here we briefly summarize the general picture of sporulation events.

In pro-prometaphase of meiosis II, SPBs separate to form the bipolar spindle. At the same time, SPBs get modified by the SPB component Spo15 so that the forespore membrane can be assembled from the modified SPBs (Ikemoto et al., 2000; **Figure 4A**). The forespore membrane gradually grows to surround and cover the nucleus from both SPBs, and the edge of the opening region of the forespore membrane is entirely decorated by the leading edge proteins (LEPs) including Meu14 (Okuzaki et al., 2003; **Figure 4A**). Growth of the forespore membrane is guided by LEPs and septins over the anaphase nucleus, and the opening closes by contraction, thereby completely surrounding the divided nuclei (Onishi et al., 2010; Yang et al., 2020; **Figure 4A**). The hard spore wall is then formed after completion of the forespore membrane.

Virtual NEBD in Meiosis II

Observations in the last decade revealed that the sporulation events give some unexpected impacts on the progression of meiosis II. Here we focus on an interesting behavior of the nuclear envelope: virtual nuclear envelope breakdown (vNEBD). Both *S. pombe* and the budding yeast *S. cerevisiae* undergo closed mitosis in which the nuclear envelope persists in mitosis, in contrast to open mitosis seen in higher eukaryotes (Boettcher and Barral, 2013; Dey et al., 2020), but in meiosis II, this "closed" rule seems to be obscure: the nuclear envelope in anaphase II shows both aspects of open and close mitoses; therefore, this phenomenon has been termed "virtual nuclear envelope breakdown (vNEBD)" (Asakawa et al., 2016). In anaphase II, nucleoplasmic proteins mostly dispersed, although observation of the nuclear envelope and the nuclear pore complex indicated that the nuclear envelope itself is not particularly disrupted or fragmented at least in fluorescence microscopy and in transmission electron microscopy (Arai et al., 2010; Asakawa et al., 2010).

One of the triggers of vNEBD in anaphase II may be related to the formation of the forespore membrane, which is also assembled at the same timing. The dispersal of nuclear proteins to the cytoplasm during anaphase II can be blocked in several *spo* gene mutants, which are involved in the assembly of the forespore membrane. When the nuclear envelope expands in anaphase II, the lipid components constituting the nuclear envelope may be in a shortage because the components may need to be preferentially used for the assembly of the forespore membrane. This idea is based on the fact that vNEBD does not occur when the vesicle transport pathway that conveys membrane components from Golgi to endoplasmic reticulum is inhibited by a drug (Arai et al., 2010). This implies the possibility that vNEBD may be caused by a shortage of nuclear envelope components,

which results in an increase of membrane permeability only during anaphase II.

Interestingly, vNEBD accompanies nuclear entry of the cytoplasmic RanGAP protein (Asakawa et al., 2010, 2011). RanGAP (Rna1 in *S. pombe*) is expected to localize constantly to the cytoplasm to govern the Ran GTPase-dependent nucleocytoplasmic transport. The aberrant nuclear entry of RanGAP indicates that the nucleocytoplasmic transport is invalidated during meiosis II. Even when the nuclear envelope seemingly persists as in closed meiosis II, the nuclear conditions can be temporarily neutralized as is seen in open mitosis of higher eukaryotes.

The biological roles of vNEBD had been undefined, but recently it was shown to promote the maturation of spores through redistribution of the nuclear proteasome subunit Rpn11 to the cytoplasm (Yang et al., 2020). This means that vNEBD can be induced by sporulation events, which in turn feedbacks to promote spore maturation.

Further studies will illuminate the molecular mechanisms to trigger vNEBD as well as the biological significance of the phenomenon. As the interplay between the nuclear envelope and the genome contributes to the determination of cell fate [reviewed in Talamas and Capelson (2015)], it would be tempting to investigate the role of (v)NEBD for differentiation of cells in yeast and other species.

Dispensable Interpolar Microtubules

Another unexpected aspect of sporulation events is the effect of the forespore membrane on the spindle of meiosis II.

In general, the spindle comprises three types of microtubules: kinetochore microtubules (kinetochore fibers, k-fibers) as mentioned earlier (see **Figures 2C,G**), interpolar microtubules connecting two spindle poles in an antiparallel manner, and astral microtubules extending outward of the spindle from the poles. In fission yeast, the majority of astral microtubules are formed in the cytoplasm from SPBs, and some bundles are in the nucleus (Zimmerman et al., 2004). Other two types are in the nucleus. Both kinetochore microtubules and interpolar microtubules are essential in mitosis and meiosis I, but interpolar microtubules are dispensable for the bi-directional segregation of chromosomes only in meiosis II (Akera et al., 2012). When interpolar microtubules are disrupted by microtubule poisons, the globular forespore membrane serves as an interpolar structure on their behalf to separate SPBs to assemble a bipolar apparatus and to separate two nuclei. The forespore membrane is guided by LEPs and septin proteins and grows from two SPBs, and two globular structures make a physical contact with each other in the middle of the nucleus in anaphase II, when the interpolar microtubules are destroyed by microtubule poisons. As a pair of the contacted forespore membrane grows, they gradually cleave and separate the anaphase nucleus into two, even though there is no spindle elongation in the conditions.

The forespore membrane-mediated nuclear division partly contributes to physiological meiosis II in the presence of normal microtubules, as SPB separation is perturbed in the *spo15* mutant lacking meiosis II-specific SPB modification as well as in the *meu14*Δ *spn6*Δ double mutant, showing the disorganized forespore membrane by depletion of both LEP and septin structures (Akera et al., 2012). Data remained elusive on whether kinetochore microtubules are also dispensable in meiosis II, although it is technically impossible at the moment to remove even the last traces of kinetochore microtubules, as some microtubules are resistant to canonical drugs [benzimidazole compounds such as MBC (carbendazim) and TBZ (thiabendazole)].

It is also reported that, in mitosis, microtubule-independent nuclear fission also occurs (Castagnetti et al., 2010). SPBs can separate in the absence of spindle microtubules when *cdc11* mutant cells (defective in cytokinesis) are exposed to microtubule poisons. It is also possible that a constant increase of the nuclear membrane components, which are supposed to be used for nuclear elongation in anaphase, caused an abundance in surplus in the absence of spindle elongation, resulting in aberrant nuclear fission (Castagnetti et al., 2010), given the case of vNEBD (Arai et al., 2010). Interestingly, nuclear fission requires F-actin. This is reminiscent of animal cells in which F-actin-dependent mechanisms promote spindle positioning and orientation [reviewed in Sandquist et al. (2011)].

The study strikingly showed that chromosome segregation is also fine to some degree. This might be also due to actin-dependent mechanisms as in bacterial cells in which chromosome segregation is driven by actin-like cytoskeleton. It is also possible that the segregation system utilizes any nucleoplasmic factors such as Csi1, as a material that connects mitotic SPBs and kinetochores even in the absence of microtubules, because Csi1 has been shown to connect SPBs and centromeres constantly in interphase (Hou et al., 2012).

It should be noted that no specific systems have been so far identified that ensure the equal segregation of sister chromatids in eukaryotes besides spindle microtubules. Currently, it is hard to completely rule out the possibility that very tiny residual microtubule seeds remain at SPBs even in the presence of the drug, as such tiny microtubule seeds might be able to connect SPBs and kinetochores clustered altogether at the mitotic onset. Once such attachments were made, kinetochore-mediated SPB separation might take place (similar to the situation in **Figure 3C**) to separate SPBs and segregate sister chromatids. It has been impossible to completely disrupt microtubules and inhibit regrowth by existing drugs; it would be intriguing to revisit these phenomena again when more effective drugs are invented in the future.

PERSPECTIVES

The evolutionary origin of meiosis has been discussed from the viewpoint of the phenomena for a long period, and one of the most reasonable ideas must be that meiosis was evolved from mitosis (Simchen and Hugerat, 1993). Although meiosis is different from mitosis in many ways, one of the most essential characteristics in meiosis could be pairing of homologous chromosomes. Meiosis might have first evolved from mitosis

through the acquisition of homolog pairing as an additional step (Wilkins and Holliday, 2009). As the molecular mechanisms have been illuminated in the last decades, the idea is getting realistic as evidenced by the genes involved in key events in meiosis. Most of the key events in meiosis appear to be conducted by meiosis-specific genes that are paralogous to those used in mitosis. Assuming that paralogous genes are generated *via* gene duplication in the long history of evolution, Spo11 (*S. pombe* Rec12) might have evolved from other topoisomerase genes as a copy specific for homolog pairing in meiosis, and this could be a key incident to acquire meiotic recombination and the following reductional division in meiosis I.

The meiotic cohesin Rec8 could likewise be originated from a duplicated copy of the mitotic cohesin Rad21. Fzr1, a meiosis-specific activator of APC/C, might have evolved from the mitotic one Slp1 (Cdc20). Those key factors might have defined the outline of meiosis as a newly acquired division system. In addition to those copied genes, meiosis-specific genes whose ancestors are currently unknown are also created to fine-tune meiotic events to the current state.

On the other hand, we also know that molecules or detailed molecular mechanisms in meiosis have been differentiated depending on species, although the whole system of meiosis *per se* is common among eukaryotes. The molecular mechanisms are thought to be fine-tuned in each organism depending on internal and external reasons such as the lifestyle and surrounding environment. Considering similarities and differences among species and in between two types of divisions, we will be able to converge the divergent mechanisms to explore the ultimate origin in the future.

AUTHOR CONTRIBUTIONS

MS conceived the framework of the entire manuscript. MS, YK, and MT wrote the manuscript. MS prepared the figures. All the authors contributed to the article and approved the submitted version.

FUNDING

This study was supported by JSPS KAKENHI JP18K19347 to MS, JP20K22635 to YK, and JP20K06645 to MT. This study was also supported by Ohsumi Frontier Science Foundation, Daiichi Sankyo Foundation of Life Science to MS, Dr. Yoshifumi Jigami Memorial Fund, The Society of Yeast Scientists to YK, and Waseda University grants for Special Research Projects 2019C-570 and 2020R-038 to MS and 2020C-738 to YK.

ACKNOWLEDGMENTS

We thank the members of the Masayuki Yamamoto laboratory for the inspiring discussion and support and Yutaka Shirasugi, Naoko Nishizawa, and Rio Fukuchi for their helpful comments.

REFERENCES

Agarwal, M., Jin, H., McClain, M., Fan, J., Koch, B. A., Jaspersen, S. L., et al. (2018). The half-bridge component Kar1 promotes centrosome separation and duplication during budding yeast meiosis. *Mol. Biol. Cell* 29, 1798–1810. doi: 10.1091/mbc.E18-03-0163

Akera, T., Goto, Y., Sato, M., Yamamoto, M., and Watanabe, Y. (2015). Mad1 promotes chromosome congression by anchoring a kinesin motor to the kinetochore. *Nat. Cell Biol.* 17, 1124–1133. doi: 10.1038/ncb3219

Akera, T., Sato, M., and Yamamoto, M. (2012). Interpolar microtubules are dispensable in fission yeast meiosis II. *Nat. Commun.* 3, 695–698. doi: 10.1038/ncomms1725

Aoi, Y., Arai, K., Miyamoto, M., Katsuta, Y., Yamashita, A., Sato, M., et al. (2013). Cuf2 boosts the transcription of APC/C activator Fzr1 to terminate the meiotic division cycle. *EMBO Rep.* 14, 553–560. doi: 10.1038/embor.2013.52

Aoi, Y., Kawashima, S. A., Simanis, V., Yamamoto, M., and Sato, M. (2014). Optimization of the analogue-sensitive Cdc2/Cdk1 mutant by *in vivo* selection eliminates physiological limitations to its use in cell cycle analysis. *Open Biol.* 4:140063. doi: 10.1098/rsob.140063

Arai, K., Sato, M., Tanaka, K., and Yamamoto, M. (2010). Nuclear compartmentalization is abolished during fission yeast meiosis. *Curr. Biol.* 20, 1913–1918. doi: 10.1016/j.cub.2010.09.004

Arata, M., Sato, M., Yamashita, A., and Yamamoto, M. (2014). The RNA-binding protein Spo5 promotes meiosis II by regulating cyclin Cdc13 in fission yeast. *Genes Cells* 19, 225–238. doi: 10.1111/gtc.12133

Asakawa, H., Hayashi, A., Haraguchi, T., and Hiraoka, Y. (2005). Dissociation of the Nuf2-Ndc80 complex releases centromeres from the spindle-pole body during meiotic prophase in fission yeast. *Mol. Biol. Cell* 16, 2325–2338. doi: 10.1091/mbc.E04-11-0996

Asakawa, H., Hiraoka, Y., and Haraguchi, T. (2011). Physical breakdown of the nuclear envelope is not necessary for breaking its barrier function. *Nucleus* 2, 523–526. doi: 10.4161/nucl.2.6.16117

Asakawa, H., Kitamura, K., and Shimoda, C. (2001). A novel Cdc20-related WD-repeat protein, Fzr1, is required for spore formation in *Schizosaccharomyces pombe*. *Mol. Genet. Genomics* 265, 424–435. doi: 10.1007/s004380000429

Asakawa, H., Kojidani, T., Mori, C., Osakada, H., Sato, M., Ding, D.-Q., et al. (2010). Virtual breakdown of the nuclear envelope in fission yeast meiosis. *Curr. Biol.* 20, 1919–1925. doi: 10.1016/j.cub.2010.09.070

Asakawa, H., Yang, H.-J., Hiraoka, Y., and Haraguchi, T. (2016). Virtual nuclear envelope breakdown and its regulators in fission yeast meiosis. *Front. Cell Dev. Biol.* 4:5. doi: 10.3389/fcell.2016.00005

Averbeck, N., Sunder, S., Sample, N., Wise, J. A., and Leatherwood, J. (2005). Negative control contributes to an extensive program of meiotic splicing in fission yeast. *Mol. Cell* 18, 491–498. doi: 10.1016/j.molcel.2005.04.007

Bernard, P., Maure, J. F., and Javerzat, J. P. (2001). Fission yeast Bub1 is essential in setting up the meiotic pattern of chromosome segregation. *Nat. Cell Biol.* 3, 522–526. doi: 10.1038/35074598

Blackwell, R., Sweezy-Schindler, O., Edelmaier, C., Gergely, Z. R., Flynn, P. J., Montes, S., et al. (2017). Contributions of microtubule dynamic instability and rotational diffusion to kinetochore capture. *Biophys. J.* 112, 552–563. doi: 10.1016/j.bpj.2016.09.006

Blanco, M. A., Pelloquin, L., and Moreno, S. (2001). Fission yeast mfr1 activates APC and coordinates meiotic nuclear division with sporulation. *J. Cell Sci.* 114, 2135–2143.

Boettcher, B., and Barral, Y. (2013). The cell biology of open and closed mitosis. *Nucleus* 4, 160–165. doi: 10.4161/nucl.24676

Bolzer, A., Kreth, G., Solovei, I., Koehler, D., Saracoglu, K., Fauth, C., et al. (2005). Three-dimensional maps of all chromosomes in human male fibroblast nuclei and prometaphase rosettes. *PLoS Biol.* 3:e0030157. doi: 10.1371/journal.pbio.0030157

Bouhlel, I. B., Ohta, M., Mayeux, A., Bordes, N., Dingli, F., Boulanger, J., et al. (2015). Cell cycle control of spindle pole body duplication and splitting by Sfi1 and Cdc31 in fission yeast. *J. Cell Sci.* 128, 1481–1493. doi: 10.1242/jcs.159657

Bresch, C., Muller, G., and Egel, R. (1968). Genes involved in meiosis and sporulation of a yeast. *Mol. Gen. Genet.* 102, 301–306. doi: 10.1007/bf00433721

Castagnetti, S., Oliferenko, S., and Nurse, P. (2010). Fission yeast cells undergo nuclear division in the absence of spindle microtubules. *PLoS Biol.* 8:e1000512. doi: 10.1371/journal.pbio.1000512

Chen, J., Liao, A., Powers, E. N., Liao, H., Kohlstaedt, L. A., Evans, R., et al. (2020). Aurora B-dependent Ndc80 degradation regulates kinetochore composition in meiosis. *Genes Dev.* 34, 209–225. doi: 10.1101/gad.333997.119

Chikashige, Y., Ding, D. Q., Funabiki, H., Haraguchi, T., Mashiko, S., Yanagida, M., et al. (1994). Telomere-led premeiotic chromosome movement in fission yeast. *Science* 264, 270–273. doi: 10.1126/science.8146661

Chikashige, Y., Ding, D. Q., Imai, Y., Yamamoto, M., Haraguchi, T., and Hiraoka, Y. (1997). Meiotic nuclear reorganization: switching the position of centromeres and telomeres in the fission yeast *Schizosaccharomyces pombe*. *EMBO J.* 16, 193–202. doi: 10.1093/emboj/16.1.193

Chikashige, Y., Haraguchi, T., and Hiraoka, Y. (2007). Another way to move chromosomes. *Chromosoma* 116, 497–505. doi: 10.1007/s00412-007-0114-8

Chikashige, Y., Tsutsumi, C., Yamane, M., Okamasa, K., Haraguchi, T., and Hiraoka, Y. (2006). Meiotic proteins bqt1 and bqt2 tether telomeres to form the bouquet arrangement of chromosomes. *Cell* 125, 59–69. doi: 10.1016/j.cell.2006.01.048

Chikashige, Y., Yamane, M., Okamasa, K., Mori, C., Fukuta, N., Matsuda, A., et al. (2014). Chromosomes rein back the spindle pole body during horsetail movement in fission yeast meiosis. *Cell Struct. Funct.* 39, 93–100. doi: 10.1247/csf.14007

Chikashige, Y., Yamane, M., Okamasa, K., Tsutsumi, C., Kojidani, T., Sato, M., et al. (2009). Membrane proteins Bqt3 and -4 anchor telomeres to the nuclear envelope to ensure chromosomal bouquet formation. *J. Cell Biol.* 187, 413–427. doi: 10.1083/jcb.200902122

Cifuentes, M., Jolivet, S., Cromer, L., Harashima, H., Bulankova, P., Renne, C., et al. (2016). TDM1 regulation determines the number of meiotic divisions. *PLoS Genet.* 12:e1005856. doi: 10.1371/journal.pgen.1005856

Cipak, L., Polakova, S., Hyppa, R. W., Smith, G. R., and Gregan, J. (2014). Synchronized fission yeast meiosis using an ATP analog-sensitive Pat1 protein kinase. *Nat. Protoc.* 9, 223–231. doi: 10.1038/nprot.2014.013

Cojoc, G., Florescu, A.-M., Krull, A., Klemm, A. H., Pavin, N., Jülicher, F., et al. (2016). Paired arrangement of kinetochores together with microtubule pivoting and dynamics drive kinetochore capture in meiosis I. *Sci. Rep.* 6:25736. doi: 10.1038/srep25736

Conrad, M. N., Lee, C.-Y., Chao, G., Shinohara, M., Kosaka, H., Shinohara, A., et al. (2008). Rapid telomere movement in meiotic prophase is promoted by *NDJ1*, *MPS3*, and *CSM4* and is modulated by recombination. *Cell* 133, 1175–1187. doi: 10.1016/j.cell.2008.04.047

Cromer, L., Heyman, J., Touati, S., Harashima, H., Araou, E., Girard, C., et al. (2012). OSD1 promotes meiotic progression via APC/C inhibition and forms a regulatory network with TDM and CYCA1;2/TAM. *PLoS Genet.* 8:e1002865. doi: 10.1371/journal.pgen.1002865

d'Erfurth, I., d'Erfurth, I., Cromer, L., Jolivet, S., Girard, C., Horlow, C., et al. (2010). The cyclin-A CYCA1;2/TAM is required for the meiosis I to meiosis II transition and cooperates with OSD1 for the prophase to first meiotic division transition. *PLoS Genet.* 6:e1000989. doi: 10.1371/journal.pgen.1000989

Dey, G., Culley, S., Curran, S., Schmidt, U., Henriques, R., Kukulski, W., et al. (2020). Closed mitosis requires local disassembly of the nuclear envelope. *Nature* 585, 119–123. doi: 10.1038/s41586-020-2648-3

Ding, D., Ding, D. Q., Chikashige, Y., Haraguchi, T., and Hiraoka, Y. (1998). Oscillatory nuclear movement in fission yeast meiotic prophase is driven by astral microtubules, as revealed by continuous observation of chromosomes and microtubules in living cells. *J. Cell Sci.* 111(Pt 6), 701–712.

Ding, R., West, R. R., Morphew, D. M., Oakley, B. R., and McIntosh, J. R. (1997). The spindle pole body of *Schizosaccharomyces pombe* enters and leaves the nuclear envelope as the cell cycle proceeds. *Mol. Biol. Cell* 8, 1461–1479.

Dischinger, S., Krapp, A., Xie, L., Paulson, J. R., and Simanis, V. (2008). Chemical genetic analysis of the regulatory role of Cdc2p in the *S. pombe* septation initiation network. *J. Cell Sci.* 121, 843–853. doi: 10.1242/jcs.021584

Ekwall, K., Javerzat, J. P., Lorentz, A., Schmidt, H., Cranston, G., and Allshire, R. (1995). The chromodomain protein Swi6: a key component at fission yeast centromeres. *Science* 269, 1429–1431. doi: 10.1126/science.7660126

Fennell, A., Fernández-Álvarez, A., Tomita, K., and Cooper, J. P. (2015). Telomeres and centromeres have interchangeable roles in promoting meiotic spindle formation. *J. Cell Biol.* 208, 415–428. doi: 10.1083/jcb.201409058

Fernández-Álvarez, A., Bez, C., O'Toole, E. T., Morphew, M., and Cooper, J. P. (2016). Mitotic nuclear envelope breakdown and spindle nucleation are controlled by interphase contacts between centromeres and the nuclear envelope. *Dev. Cell* 39, 544–559. doi: 10.1016/j.devcel.2016.10.021

Funabiki, H., Hagan, I., Uzawa, S., and Yanagida, M. (1993). Cell cycle-dependent specific positioning and clustering of centromeres and telomeres in fission yeast. *J. Cell Biol.* 121, 961–976. doi: 10.1083/jcb.121.5.961

Funabiki, H., and Murray, A. W. (2000). The *Xenopus* chromokinesin Xkid is essential for metaphase chromosome alignment and must be degraded to allow anaphase chromosome movement. *Cell* 102, 411–424. doi: 10.1016/S0092-8674(00)00047-7

Funaya, C., Samarasinghe, S., Pruggnaller, S., Ohta, M., Connolly, Y., Müller, J., et al. (2012). Transient structure associated with the spindle pole body directs meiotic microtubule reorganization in *S. pombe*. *Curr. Biol.* 22, 562–574. doi: 10.1016/j.cub.2012.02.042

Galander, S., Barton, R. E., Borek, W. E., Spanos, C., Kelly, D. A., Robertson, D., et al. (2019). Reductional Meiosis I chromosome segregation is established by coordination of key meiotic kinases. *Dev. Cell* 49, 526.e5–541.e5. doi: 10.1016/j.devcel.2019.04.003

Glover, J., Grelon, M., Craig, S., Chaudhury, A., and Dennis, E. (1998). Cloning and characterization of *MS5* from *Arabidopsis*: a gene critical in male meiosis. *Plant J.* 15, 345–356. doi: 10.1046/j.1365-313x.1998.00216.x

Goshima, G., Saitoh, S., and Yanagida, M. (1999). Proper metaphase spindle length is determined by centromere proteins Mis12 and Mis6 required for faithful chromosome segregation. *Genes Dev.* 13, 1664–1677. doi: 10.1101/gad.13.13.1664

Grallert, B., and Sipiczki, M. (1990). Dissociation of meiotic and mitotic roles of the fission yeast *cdc2* gene. *Mol. Gen. Genet.* 222, 473–475. doi: 10.1007/BF00633860

Hagan, I., and Yanagida, M. (1990). Novel potential mitotic motor protein encoded by the fission yeast *cut7*$^{+}$ gene. *Nature* 347, 563–566. doi: 10.1038/347563a0

Hagan, I., and Yanagida, M. (1992). Kinesin-related cut7 protein associates with mitotic and meiotic spindles in fission yeast. *Nature* 356, 74–76. doi: 10.1038/356074a0

Hagan, I., and Yanagida, M. (1995). The product of the spindle formation gene *sad1*$^{+}$ associates with the fission yeast spindle pole body and is essential for viability. *J. Cell Biol.* 129, 1033–1047. doi: 10.1083/jcb.129.4.1033

Hayashi, A., Asakawa, H., Haraguchi, T., and Hiraoka, Y. (2006). Reconstruction of the kinetochore during meiosis in fission yeast *Schizosaccharomyces pombe*. *Mol. Biol. Cell* 17, 5173–5184. doi: 10.1091/mbc.E06-05-0388

Hayashi, T., Ebe, M., Nagao, K., Kokubu, A., Sajiki, K., and Yanagida, M. (2014). *Schizosaccharomyces pombe* centromere protein Mis19 links Mis16 and Mis18 to recruit CENP-A through interacting with NMD factors and the SWI/SNF complex. *Genes Cells* 19, 541–554. doi: 10.1111/gtc.12152

Hayashi, T., Fujita, Y., Iwasaki, O., Adachi, Y., Takahashi, K., and Yanagida, M. (2004). Mis16 and Mis18 are required for CENP-A loading and histone deacetylation at centromeres. *Cell* 118, 715–729. doi: 10.1016/j.cell.2004.09.002

Hirai, H., Arai, K., Kariyazono, R., Yamamoto, M., and Sato, M. (2014). The kinetochore protein Kis1/Eic1/Mis19 ensures the integrity of mitotic spindles through maintenance of kinetochore factors Mis6/CENP-I and CENP-A. *PLoS One* 9:e111905. doi: 10.1371/journal.pone.0111905

Hiraoka, Y., Ding, D. Q., Yamamoto, A., Tsutsumi, C., and Chikashige, Y. (2000). Characterization of fission yeast meiotic mutants based on live observation of meiotic prophase nuclear movement. *Chromosoma* 109, 103–109. doi: 10.1007/s004120050417

Hou, H., Zhou, Z., Wang, Y., Wang, J., Kallgren, S. P., Kurchuk, T., et al. (2012). Csi1 links centromeres to the nuclear envelope for centromere clustering. *J. Cell Biol.* 199, 735–744. doi: 10.1083/jcb.201208001

Iino, Y., Hiramine, Y., and Yamamoto, M. (1995). The role of *cdc2* and other genes in meiosis in *Schizosaccharomyces pombe*. *Genetics* 140, 1235–1245.

Ikemoto, S., Nakamura, T., Kubo, M., and Shimoda, C. (2000). *S. pombe* sporulation-specific coiled-coil protein Spo15p is localized to the spindle pole body and essential for its modification. *J. Cell Sci.* 113(Pt 3), 545–554.

Inoue, D., Ohe, M., Kanemori, Y., Nobui, T., and Sagata, N. (2007). A direct link of the Mos-MAPK pathway to Erp1/Emi2 in meiotic arrest of *Xenopus laevis* eggs. *Nature* 446, 1100–1104. doi: 10.1038/nature05688

Ishiguro, K.-I. (2019). The cohesin complex in mammalian meiosis. *Genes Cells* 24, 6–30. doi: 10.1111/gtc.12652

Izawa, D., Goto, M., Yamashita, A., Yamano, H., and Yamamoto, M. (2005). Fission yeast Mes1p ensures the onset of meiosis II by blocking degradation of cyclin Cdc13p. *Nature* 434, 529–533. doi: 10.1038/nature03406

Jaspersen, S. L., and Winey, M. (2004). The budding yeast spindle pole body: structure, duplication, and function. *Annu. Rev. Cell Dev. Biol.* 20, 1–28. doi: 10.1146/annurev.cellbio.20.022003.114106

Jin, Q., Trelles-Sticken, E., Scherthan, H., and Loidl, J. (1998). Yeast nuclei display prominent centromere clustering that is reduced in nondividing cells and in meiotic prophase. *J. Cell Biol.* 141, 21–29.

Kakui, Y., Sato, M., Okada, N., Toda, T., and Yamamoto, M. (2013). Microtubules and Alp7-Alp14 (TACC-TOG) reposition chromosomes before meiotic segregation. *Nat. Cell Biol.* 15, 786–796. doi: 10.1038/ncb2782

Kakui, Y., Sato, M., Tanaka, K., and Yamamoto, M. (2011). A novel fission yeast *mei4* mutant that allows efficient synchronization of telomere dispersal and the first meiotic division. *Yeast* 28, 467–479. doi: 10.1002/yea.1851

Kapoor, T. M., Mayer, T. U., Coughlin, M. L., and Mitchison, T. J. (2000). Probing spindle assembly mechanisms with monastrol, a small molecule inhibitor of the mitotic kinesin. Eg5. *J. Cell Biol.* 150, 975–988. doi: 10.1083/jcb.150.5.975

Kasama, T., Shigehisa, A., Hirata, A., Saito, T. T., Tougan, T., Okuzaki, D., et al. (2006). Spo5/Mug12, a putative meiosis-specific RNA-binding protein, is essential for meiotic progression and forms Mei2 dot-like nuclear foci. *Eukaryotic Cell* 5, 1301–1313. doi: 10.1128/EC.00099-06

Katis, V. L., Galova, M., Rabitsch, K. P., Gregan, J., and Nasmyth, K. (2004). Maintenance of cohesin at centromeres after meiosis I in budding yeast requires a kinetochore-associated protein related to MEI-S332. *Curr. Biol.* 14, 560–572. doi: 10.1016/j.cub.2004.03.001

Katsumata, K., Hirayasu, A., Miyoshi, J., Nishi, E., Ichikawa, K., Tateho, K., et al. (2016). A Taz1- and microtubule-dependent regulatory relationship between telomere and centromere positions in bouquet formation secures proper meiotic divisions. *PLoS Genet.* 12:e1006304. doi: 10.1371/journal.pgen.1006304

Kawashima, S. A., Yamagishi, Y., Honda, T., Ishiguro, K.-I., and Watanabe, Y. (2010). Phosphorylation of H2A by Bub1 prevents chromosomal instability through localizing shugoshin. *Science* 327, 172–177. doi: 10.1126/science.1180189

Kerres, A., Vietmeier-Decker, C., Ortiz, J., Karig, I., Beuter, C., Hegemann, J., et al. (2004). The fission yeast kinetochore component Spc7 associates with the EB1 family member Mal3 and is required for kinetochore-spindle association. *Mol. Biol. Cell* 15, 5255–5267. doi: 10.1091/mbc.E04-06-0443

Kilmartin, J. V. (2003). Sfi1p has conserved centrin-binding sites and an essential function in budding yeast spindle pole body duplication. *J. Cell Biol.* 162, 1211–1221. doi: 10.1083/jcb.200307064

Kim, J., Ishiguro, K.-I., Nambu, A., Akiyoshi, B., Yokobayashi, S., Kagami, A., et al. (2015). Meikin is a conserved regulator of meiosis-I-specific kinetochore function. *Nature* 517, 466–471. doi: 10.1038/nature14097

Kim, S., Kim, S., Meyer, R., Meyer, R., Chuong, H., Chuong, H., et al. (2013). Dual mechanisms prevent premature chromosome segregation during meiosis. *Genes Dev.* 27, 2139–2146. doi: 10.1101/gad.227454.113

Kimata, Y., Kitamura, K., Fenner, N., and Yamano, H. (2011). Mes1 controls the meiosis I to meiosis II transition by distinctly regulating the anaphase-promoting complex/cyclosome coactivators Fzr1/Mfr1 and Slp1 in fission yeast. *Mol. Biol. Cell* 22, 1486–1494. doi: 10.1091/mbc.E10-09-0774

Kimata, Y., Trickey, M., Izawa, D., Gannon, J., Yamamoto, M., and Yamano, H. (2008). A mutual inhibition between APC/C and its substrate Mes1 required for meiotic progression in fission yeast. *Dev. Cell* 14, 446–454. doi: 10.1016/j.devcel.2007.12.010

Kishida, M., Nagai, T., Nakaseko, Y., and Shimoda, C. (1994). Meiosis-dependent mRNA splicing of the fission yeast *Schizosaccharomyces pombe mes1*$^{+}$ gene. *Curr. Genet.* 25, 497–503. doi: 10.1007/BF00351668

Kitajima, T. S., Sakuno, T., Ishiguro, K.-I., Iemura, S.-I., Natsume, T., Kawashima, S. A., et al. (2006). Shugoshin collaborates with protein phosphatase 2A to protect cohesin. *Nature* 441, 46–52. doi: 10.1038/nature04663

Kitajima, T. S., Yokobayashi, S., Yamamoto, M., and Watanabe, Y. (2003). Distinct cohesin complexes organize meiotic chromosome domains. *Science* 300, 1152–1155. doi: 10.1126/science.1083634

Klutstein, M., Fennell, A., Fernández-Álvarez, A., and Cooper, J. P. (2015). The telomere bouquet regulates meiotic centromere assembly. *Nat. Cell Biol.* 17, 458–469. doi: 10.1038/ncb3132

Kosaka, H., Shinohara, M., and Shinohara, A. (2008). Csm4-dependent telomere movement on nuclear envelope promotes meiotic recombination. *PLoS Genet.* 4:e1000196. doi: 10.1371/journal.pgen.1000196

Lee, B. H., Amon, A., and Prinz, S. (2002). Spo13 regulates cohesin cleavage. *Genes Dev.* 16, 1672–1681. doi: 10.1101/gad.989302

Lehmann, A., and Toda, T. (2004). Fission yeast Skp1 is required for spindle morphology and nuclear membrane segregation at anaphase. *FEBS Lett.* 566, 77–82. doi: 10.1016/j.febslet.2004.04.022

Li, P., Jin, H., Koch, B. A., Abblett, R. L., Han, X., Yates, J. R., et al. (2017). Cleavage of the SUN-domain protein Mps3 at its N-terminus regulates centrosome disjunction in budding yeast meiosis. *PLoS Genet.* 13:e1006830. doi: 10.1371/journal.pgen.1006830

Li, P., Shao, Y., Jin, H., and Yu, H.-G. (2015). Ndj1, a telomere-associated protein, regulates centrosome separation in budding yeast meiosis. *J. Cell Biol.* 209, 247–259. doi: 10.1083/jcb.201408118

Liu, J., Grimison, B., Lewellyn, A. L., and Maller, J. L. (2006). The anaphase-promoting complex/cyclosome inhibitor Emi2 is essential for meiotic but not mitotic cell cycles. *J. Biol. Chem.* 281, 34736–34741. doi: 10.1074/jbc.M606607200

Liu, X., McLeod, I., Anderson, S., Yates, J. R., and He, X. (2005). Molecular analysis of kinetochore architecture in fission yeast. *EMBO J.* 24, 2919–2930. doi: 10.1038/sj.emboj.7600762

Loïodice, I., Staub, J., Setty, T. G., Nguyen, N.-P. T., Paoletti, A., and Tran, P. T. (2005). Ase1p organizes antiparallel microtubule arrays during interphase and mitosis in fission yeast. *Mol. Biol. Cell* 16, 1756–1768. doi: 10.1091/mbc.e04-10-0899

Malapeira, J., Moldón, A., Hidalgo, E., Smith, G. R., Nurse, P., and Ayté, J. (2005). A meiosis-specific cyclin regulated by splicing is required for proper progression through meiosis. *Mol. Cell Biol.* 25, 6330–6337. doi: 10.1128/MCB.25.15.6330-6337.2005

Masui, Y., and Markert, C. L. (1971). Cytoplasmic control of nuclear behavior during meiotic maturation of frog oocytes. *J. Exp. Zool.* 177, 129–145. doi: 10.1002/jez.1401770202

McHedlishvili, N., Wieser, S., Holtackers, R., Mouysset, J., Belwal, M., Amaro, A. C., et al. (2012). Kinetochores accelerate centrosome separation to ensure faithful chromosome segregation. *J. Cell Sci.* 125, 906–918. doi: 10.1242/jcs.091967

Meyer, R. E., Brown, J., Beck, L., and Dawson, D. S. (2018). Mps1 promotes chromosome meiotic chromosome biorientation through Dam1. *Mol. Biol. Cell* 29, 479–489. doi: 10.1091/mbc.E17-08-0503

Meyer, R. E., Chuong, H. H., Hild, M., Hansen, C. L., Kinter, M., and Dawson, D. S. (2015). Ipl1/Aurora-B is necessary for kinetochore restructuring in meiosis I in *Saccharomyces cerevisiae*. *Mol. Biol. Cell* 26, 2986–3000. doi: 10.1091/mbc.E15-01-0032

Meyer, R. E., Kim, S., Obeso, D., Straight, P. D., Winey, M., and Dawson, D. S. (2013). Mps1 and Ipl1/Aurora B act sequentially to correctly orient chromosomes on the meiotic spindle of budding yeast. *Science* 339, 1071–1074. doi: 10.1126/science.1232518

Miki, F., Okazaki, K., Shimanuki, M., Yamamoto, A., Hiraoka, Y., and Niwa, O. (2002). The 14-kDa dynein light chain-family protein Dlc1 is required for regular oscillatory nuclear movement and efficient recombination during meiotic prophase in fission yeast. *Mol. Biol. Cell* 13, 930–946. doi: 10.1091/mbc.01-11-0543

Miyazaki, S., Kim, J., Yamagishi, Y., Ishiguro, T., Okada, Y., Tanno, Y., et al. (2017). Meikin-associated polo-like kinase specifies Bub1 distribution in meiosis I. *Genes Cells* 22, 552–567. doi: 10.1111/gtc.12496

Moiseeva, V., Amelina, H., Collopy, L. C., Armstrong, C. A., Pearson, S. R., and Tomita, K. (2017). The telomere bouquet facilitates meiotic prophase progression and exit in fission yeast. *Cell Discov.* 3:17041. doi: 10.1038/celldisc.2017.41

Moldón, A., Malapeira, J., Gabrielli, N., Gogol, M., Gómez-Escoda, B., Ivanova, T., et al. (2008). Promoter-driven splicing regulation in fission yeast. *Nature* 455, 997–1000. doi: 10.1038/nature07325

Monje-Casas, F., Monje-Casas, F., Prabhu, V. R., Prabhu, V. R., Lee, B. H., Lee, B. H., et al. (2007). Kinetochore orientation during meiosis is controlled by Aurora B and the monopolin complex. *Cell* 128, 477–490. doi: 10.1016/j.cell.2006.12.040

Morrell, J. L., Tomlin, G. C., Rajagopalan, S., Venkatram, S., Feoktistova, A. S., Tasto, J. J., et al. (2004). Sid4p-Cdc11p assembles the septation initiation network and its regulators at the *S. pombe* SPB. *Curr. Biol.* 14, 579–584. doi: 10.1016/j.cub.2004.03.036

Mulvihill, D. P., Petersen, J., Ohkura, H., Glover, D. M., and Hagan, I. M. (1999). Plo1 kinase recruitment to the spindle pole body and its role in cell division in *Schizosaccharomyces pombe*. *Mol. Biol. Cell* 10, 2771–2785. doi: 10.1091/mbc.10.8.2771

Murakami-Tonami, Y., Yamada-Namikawa, C., Tochigi, A., Hasegawa, N., Kojima, H., Kunimatsu, M., et al. (2007). Mei4p coordinates the onset of meiosis I by regulating *cdc25*$^{+}$ in fission yeast. *Proc. Natl. Acad. Sci. U.S.A.* 104, 14688–14693. doi: 10.1073/pnas.0702906104

Muris, D. F., Vreeken, K., Carr, A. M., Broughton, B. C., Lehmann, A. R., Lohman, P. H., et al. (1993). Cloning the RAD51 homologue of *Schizosaccharomyces pombe*. *Nucleic Acids Res.* 21, 4586–4591. doi: 10.1093/nar/21.19.4586

Nagele, R., Nagele, R., Freeman, T., Freeman, T., McMorrow, L., McMorrow, L., et al. (1995). Precise spatial positioning of chromosomes during prometaphase: evidence for chromosomal order. *Science* 270, 1831–1835. doi: 10.1126/science.270.5243.1831

Nakaseko, Y., Niwa, O., and Yanagida, M. (1984). A meiotic mutant of the fission yeast *Schizosaccharomyces pombe* that produces mature asci containing two diploid spores. *J. Bacteriol.* 157, 334–336. doi: 10.1128/JB.157.1.334-336.1984

Newnham, L., Jordan, P. W., Carballo, J. A., Newcombe, S., and Hoffmann, E. (2013). Ipl1/Aurora kinase suppresses S-CDK-driven spindle formation during prophase I to ensure chromosome integrity during meiosis. *PLoS One* 8:e83982. doi: 10.1371/journal.pone.0083982

Nezi, L., and Musacchio, A. (2009). Sister chromatid tension and the spindle assembly checkpoint. *Curr. Opin. Cell Biol.* 21, 785–795. doi: 10.1016/j.ceb.2009.09.007

Nigg, E. A. (2001). Mitotic kinases as regulators of cell division and its checkpoints. *Nat. Rev. Mol. Cell Biol.* 2, 21–32. doi: 10.1038/35048096

Nishiyama, T., Ohsumi, K., and Kishimoto, T. (2007). Phosphorylation of Erp1 by p90rsk is required for cytostatic factor arrest in *Xenopus laevis* eggs. *Nature* 446, 1096–1099. doi: 10.1038/nature05696

Niwa, O., Shimanuki, M., and Miki, F. (2000). Telomere-led bouquet formation facilitates homologous chromosome pairing and restricts ectopic interaction in fission yeast meiosis. *EMBO J.* 19, 3831–3840. doi: 10.1093/emboj/19.14.3831

Nonaka, N., Kitajima, T., Yokobayashi, S., Xiao, G., Yamamoto, M., Grewal, S. I. S., et al. (2002). Recruitment of cohesin to heterochromatic regions by Swi6/HP1 in fission yeast. *Nat. Cell Biol.* 4, 89–93. doi: 10.1038/ncb739

Ohe, M., Inoue, D., Kanemori, Y., and Sagata, N. (2007). Erp1/Emi2 is essential for the meiosis I to meiosis II transition in *Xenopus* oocytes. *Dev. Biol.* 303, 157–164. doi: 10.1016/j.ydbio.2006.10.044

Ohkura, H., Hagan, I. M., and Glover, D. M. (1995). The conserved *Schizosaccharomyces pombe* kinase plo1, required to form a bipolar spindle, the actin ring, and septum, can drive septum formation in G1 and G2 cells. *Genes Dev.* 9, 1059–1073. doi: 10.1101/gad.9.9.1059

Ohta, M., Sato, M., and Yamamoto, M. (2012). Spindle pole body components are reorganized during fission yeast meiosis. *Mol. Biol. Cell* 23, 1799–1811. doi: 10.1091/mbc.E11-11-0951

Okamoto, S.-Y., Sato, M., Toda, T., and Yamamoto, M. (2012). SCF ensures meiotic chromosome segregation through a resolution of meiotic recombination intermediates. *PLoS One* 7:e30622. doi: 10.1371/journal.pone.0030622

Okuzaki, D., Kasama, T., Hirata, A., Ohtaka, A., Kakegawa, R., and Nojima, H. (2010). Spo5 phosphorylation is essential for its own timely degradation and for successful meiosis in *Schizosaccharomyces pombe*. *Cell Cycle* 9, 3751–3760.

Okuzaki, D., Satake, W., Hirata, A., and Nojima, H. (2003). Fission yeast *meu14*$^{+}$ is required for proper nuclear division and accurate forespore membrane formation during meiosis II. *J. Cell Sci.* 116, 2721–2735. doi: 10.1242/jcs.00496

Oliferenko, S., and Balasubramanian, M. K. (2002). Astral microtubules monitor metaphase spindle alignment in fission yeast. *Nat. Cell Biol.* 4, 816–820. doi: 10.1038/ncb861

Olmsted, Z. T., Colliver, A. G., Riehlman, T. D., and Paluh, J. L. (2014). Kinesin-14 and kinesin-5 antagonistically regulate microtubule nucleation by γ-TuRC in yeast and human cells. *Nat. Commun.* 5:5339. doi: 10.1038/ncomms6339

Onishi, M., Koga, T., Hirata, A., Nakamura, T., Asakawa, H., Shimoda, C., et al. (2010). Role of septins in the orientation of forespore membrane extension during sporulation in fission yeast. *Mol. Cell Biol.* 30, 2057–2074. doi: 10.1128/MCB.01529-09

Paoletti, A., Bordes, N., Haddad, R., Schwartz, C. L., Chang, F., and Bornens, M. (2003). Fission yeast cdc31p is a component of the half-bridge and controls SPB duplication. *Mol. Biol, Cell* 14, 2793–2808. doi: 10.1091/mbc.E02-10-0661

Parisi, S., McKay, M. J., Molnar, M., Thompson, M. A., van der Spek, P. J., van Drunen-Schoenmaker, E., et al. (1999). Rec8p, a meiotic recombination and sister chromatid cohesion phosphoprotein of the Rad21p family conserved from fission yeast to humans. *Mol. Cell Biol.* 19, 3515–3528. doi: 10.1128/mcb.19.5.3515

Pellman, D., Bagget, M., Tu, Y. H., Tu, H., and Fink, G. R. (1995). Two microtubule-associated proteins required for anaphase spindle movement in *Saccharomyces cerevisiae*. *J. Cell Biol.* 130, 1373–1385. doi: 10.1083/jcb.130.6.1373

Pidoux, A. L., LeDizet, M., and Cande, W. Z. (1996). Fission yeast pkl1 is a kinesin-related protein involved in mitotic spindle function. *Mol. Biol. Cell* 7, 1639–1655.

Pineda-Santaella, A., and Fernández-Álvarez, A. (2019). Spindle assembly without spindle pole body insertion into the nuclear envelope in fission yeast meiosis. *Chromosoma* 128, 267–277. doi: 10.1007/s00412-019-00710-y

Riedel, C. G., Katis, V. L., Katou, Y., Mori, S., Itoh, T., Helmhart, W., et al. (2006). Protein phosphatase 2A protects centromeric sister chromatid cohesion during meiosis I. *Nature* 441, 53–61. doi: 10.1038/nature04664

Rodriguez, A. S., Batac, J., Killilea, A. N., Filopei, J., Simeonov, D. R., Lin, I., et al. (2008). Protein complexes at the microtubule organizing center regulate bipolar spindle assembly. *Cell Cycle* 7, 1246–1253. doi: 10.4161/cc.7.9.5808

Rosenberg, J. A., Tomlin, G. C., McDonald, W. H., Snydsman, B. E., Muller, E. G., Yates, J. R., et al. (2006). Ppc89 links multiple proteins, including the septation initiation network, to the core of the fission yeast spindle-pole body. *Mol. Biol. Cell* 17, 3793–3805. doi: 10.1091/mbc.E06-01-0039

Ross, K. J., Fransz, P., Armstrong, S. J., Vizir, I., Mulligan, B., Franklin, F. C., et al. (1997). Cytological characterization of four meiotic mutants of *Arabidopsis* isolated from T-DNA-transformed lines. *Chromosome Res.* 5, 551–559. doi: 10.1023/a:1018497804129

Rubin, T., Macaisne, N., and Huynh, J.-R. (2020). Mixing and matching chromosomes during female meiosis. *Cells* 9:696. doi: 10.3390/cells9030696

Saito, T. T., Tougan, T., Okuzaki, D., Kasama, T., and Nojima, H. (2005). Mcp6, a meiosis-specific coiled-coil protein of *Schizosaccharomyces pombe*, localizes to the spindle pole body and is required for horsetail movement and recombination. *J. Cell Sci.* 118, 447–459. doi: 10.1242/jcs.01629

Sandquist, J. C., Kita, A. M., and Bement, W. M. (2011). And the dead shall rise: actin and myosin return to the spindle. *Dev. Cell* 21, 410–419. doi: 10.1016/j.devcel.2011.07.018

Sato, M., Koonrugsa, N., Toda, T., Vardy, L., Tournier, S., and Millar, J. B. A. (2003). Deletion of Mia1/Alp7 activates Mad2-dependent spindle assembly checkpoint in fission yeast. *Nat. Cell Biol.* 5, 764–766. doi: 10.1038/ncb0903-764 author reply 766

Sato, M., and Toda, T. (2007). Alp7/TACC is a crucial target in Ran-GTPase-dependent spindle formation in fission yeast. *Nature* 447, 334–337. doi: 10.1038/nature05773

Sato, M., Toya, M., and Toda, T. (2009). Visualization of fluorescence-tagged proteins in fission yeast: the analysis of mitotic spindle dynamics using GFP-tubulin under the native promoter. *Methods Mol. Biol.* 545, 185–203. doi: 10.1007/978-1-60327-993-2_11

Sato, M., Vardy, L., Angel Garcia, M., Koonrugsa, N., and Toda, T. (2004). Interdependency of fission yeast Alp14/TOG and coiled coil protein Alp7 in microtubule localization and bipolar spindle formation. *Mol. Biol. Cell* 15, 1609–1622. doi: 10.1091/mbc.E03-11-0837

Scherthan, H. (2001). A bouquet makes ends meet. *Nat. Rev. Mol. Cell Biol.* 2, 621–627. doi: 10.1038/35085086

Shibuya, H., Hernández-Hernández, A., Morimoto, A., Negishi, L., Höög, C., and Watanabe, Y. (2015). MAJIN links telomeric DNA to the nuclear membrane

by exchanging telomere cap. *Cell* 163, 1252–1266. doi: 10.1016/j.cell.2015.10.030

Shimanuki, M., Miki, F., Ding, D. Q., Chikashige, Y., Hiraoka, Y., Horio, T., et al. (1997). A novel fission yeast gene, *kms1*$^{+}$, is required for the formation of meiotic prophase-specific nuclear architecture. *Mol. Gen. Genet.* 254, 238–249. doi: 10.1007/s004380050412

Shimoda, C. (2004). Forespore membrane assembly in yeast: coordinating SPBs and membrane trafficking. *J. Cell Sci.* 117, 389–396. doi: 10.1242/jcs.00980

Shimoda, C., Hirata, A., Kishida, M., Hashida, T., and Tanaka, K. (1985). Characterization of meiosis-deficient mutants by electron microscopy and mapping of four essential genes in the fission yeast *Schizosaccharomyces pombe*. *Mol. Gen. Genet.* 200, 252–257. doi: 10.1007/BF00425432

Shimoseki, M., and Shimoda, C. (2001). The 5′ terminal region of the *Schizosaccharomyces pombe mes1* mRNA is crucial for its meiosis-specific splicing. *Mol. Genet. Genomics* 265, 673–682. doi: 10.1007/s004380100462

Shinohara, A., Ogawa, H., Matsuda, Y., Ushio, N., Ikeo, K., and Ogawa, T. (1993). Cloning of human, mouse and fission yeast recombination genes homologous to *RAD51* and *recA*. *Nat. Genet.* 4, 239–243. doi: 10.1038/ng0793-239

Shirasugi, Y., and Sato, M. (2019). Kinetochore-mediated outward force promotes spindle pole separation in fission yeast. *Mol. Biol. Cell* 30, 2802–2813. doi: 10.1091/mbc.E19-07-0366

Shonn, M. A., McCarroll, R., and Murray, A. W. (2002). Spo13 protects meiotic cohesin at centromeres in meiosis I. *Genes Dev.* 16, 1659–1671. doi: 10.1101/gad.975802

Simchen, G., and Hugerat, Y. (1993). What determines whether chromosomes segregate reductionally or equationally in meiosis? *Bioessays* 15, 1–8. doi: 10.1002/bies.950150102

Simeonov, D. R., Kenny, K., Seo, L., Moyer, A., Allen, J., and Paluh, J. L. (2009). Distinct Kinesin-14 mitotic mechanisms in spindle bipolarity. *Cell Cycle* 8, 3563–3575.

Subramanian, L., Toda, N. R. T., Rappsilber, J., and Allshire, R. C. (2014). Eic1 links Mis18 with the CCAN/Mis6/Ctf19 complex to promote CENP-A assembly. *Open Biol.* 4:140043. doi: 10.1098/rsob.140043

Syrovatkina, V., Fu, C., and Tran, P. T. (2013). Antagonistic spindle motors and MAPs regulate metaphase spindle length and chromosome segregation. *Curr. Biol.* 23, 2423–2429. doi: 10.1016/j.cub.2013.10.023

Syrovatkina, V., and Tran, P. T. (2015). Loss of kinesin-14 results in aneuploidy via kinesin-5-dependent microtubule protrusions leading to chromosome cut. *Nat. Commun.* 6:7322. doi: 10.1038/ncomms8322

Talamas, J. A., and Capelson, M. (2015). Nuclear envelope and genome interactions in cell fate. *Front. Genet.* 6:95. doi: 10.3389/fgene.2015.00095

Tanaka, K., Kohda, T., Yamashita, A., Nonaka, N., and Yamamoto, M. (2005a). Hrs1p/Mcp6p on the meiotic SPB organizes astral microtubule arrays for oscillatory nuclear movement. *Curr. Biol.* 15, 1479–1486. doi: 10.1016/j.cub.2005.07.058

Tanaka, K., Mukae, N., Dewar, H., van Breugel, M., James, E. K., Prescott, A. R., et al. (2005b). Molecular mechanisms of kinetochore capture by spindle microtubules. *Nature* 434, 987–994. doi: 10.1038/nature03483

Tanaka, K., Petersen, J., MacIver, F., Mulvihill, D. P., Glover, D. M., and Hagan, I. M. (2001). The role of Plo1 kinase in mitotic commitment and septation in *Schizosaccharomyces pombe*. *EMBO J.* 20, 1259–1270. doi: 10.1093/emboj/20.6.1259

Tang, Z., Sun, Y., Harley, S. E., Zou, H., and Yu, H. (2004). Human Bub1 protects centromeric sister-chromatid cohesion through Shugoshin during mitosis. *Proc. Natl. Acad. Sci. U.S.A.* 101, 18012–18017. doi: 10.1073/pnas.0408600102

Toda, T., Ochotorena, I., and Kominami, K. (1999). Two distinct ubiquitin-proteolysis pathways in the fission yeast cell cycle. *Philos. Trans. R. Soc. Lond. B Biol. Sci.* 354, 1551–1557. doi: 10.1098/rstb.1999.0498

Togashi, N., Yamashita, A., Sato, M., and Yamamoto, M. (2014). Functional significance of nuclear export and mRNA binding of meiotic regulator Spo5 in fission yeast. *BMC Microbiol.* 14:188. doi: 10.1186/1471-2180-14-188

Tokai, N., Fujimoto-Nishiyama, A., Toyoshima, Y., Yonemura, S., Tsukita, S., Inoue, J., et al. (1996). Kid, a novel kinesin-like DNA binding protein, is localized to chromosomes and the mitotic spindle. *EMBO J.* 15, 457–467. doi: 10.1002/j.1460-2075.1996.tb00378.x

Tomita, K., and Cooper, J. P. (2007). The telomere bouquet controls the meiotic spindle. *Cell* 130, 113–126. doi: 10.1016/j.cell.2007.05.024

Tomlin, G. C., Morrell, J. L., and Gould, K. L. (2002). The spindle pole body protein Cdc11p links Sid4p to the fission yeast septation initiation network. *Mol. Biol. Cell* 13, 1203–1214. doi: 10.1091/mbc.01-09-0455

Toso, A., Winter, J. R., Garrod, A. J., Amaro, A. C., Meraldi, P., and McAinsh, A. D. (2009). Kinetochore-generated pushing forces separate centrosomes during bipolar spindle assembly. *J. Cell Biol.* 184, 365–372. doi: 10.1083/jcb.200809055

Troxell, C. L., West, R. R., Reed, K. D., Cande, W. Z., and McIntosh, J. R. (2001). *pkl1*$^{+}$and *klp2*$^{+}$: two kinesins of the Kar3 subfamily in fission yeast perform different functions in both mitosis and meiosis. *Mol. Biol. Cell* 12, 3476–3488. doi: 10.1091/mbc.12.11.3476

Tsutsui, Y., Kurokawa, Y., Ito, K., Siddique, M. S. P., Kawano, Y., Yamao, F., et al. (2014). Multiple regulation of Rad51-Mediated homologous recombination by fission yeast Fbh1. *PLoS Genet.* 10:e1004542. doi: 10.1371/journal.pgen.1004542

Wälde, S., and King, M. C. (2014). The KASH protein Kms2 coordinates mitotic remodeling of the spindle pole body. *J. Cell Sci.* 127, 3625–3640. doi: 10.1242/jcs.154997

Wanat, J. J., Kim, K. P., Koszul, R., Zanders, S., Weiner, B., Kleckner, N., et al. (2008). Csm4, in collaboration with Ndj1, mediates telomere-led chromosome dynamics and recombination during yeast meiosis. *PLoS Genet.* 4:e1000188. doi: 10.1371/journal.pgen.1000188

Wang, Y., Wu, H., Liang, G., and Yang, M. (2004). Defects in nucleolar migration and synapsis in male prophase I in the *ask1-1* mutant of *Arabidopsis*. *Sex. Plant Reprod.* 16, 273–282. doi: 10.1007/s00497-004-0206-z

Watanabe, Y., and Nurse, P. (1999). Cohesin Rec8 is required for reductional chromosome segregation at meiosis. *Nature* 400, 461–464. doi: 10.1038/22774

Westermann, S., Avila-Sakar, A., Wang, H.-W., Niederstrasser, H., Wong, J., Drubin, D. G., et al. (2005). Formation of a dynamic kinetochore- microtubule interface through assembly of the Dam1 ring complex. *Mol. Cell* 17, 277–290. doi: 10.1016/j.molcel.2004.12.019

Wigge, P. A., and Kilmartin, J. V. (2001). The Ndc80p complex from *Saccharomyces cerevisiae* contains conserved centromere components and has a function in chromosome segregation. *J. Cell Biol.* 152, 349–360. doi: 10.1083/jcb.152.2.349

Wilkins, A. S., and Holliday, R. (2009). The evolution of meiosis from mitosis. *Genetics* 181, 3–12. doi: 10.1534/genetics.108.099762

Yamamoto, A., Kitamura, K., Hihara, D., Hirose, Y., Katsuyama, S., and Hiraoka, Y. (2008). Spindle checkpoint activation at meiosis I advances anaphase II onset via meiosis-specific APC/C regulation. *J. Cell Biol.* 182, 277–288. doi: 10.1083/jcb.200802053

Yamamoto, A., West, R., McIntosh, J., and Hiraoka, Y. (1999). A cytoplasmic dynein heavy chain is required for oscillatory nuclear movement of meiotic prophase and efficient meiotic recombination in fission yeast. *J. Cell Biol.* 145, 1233–1249.

Yamamoto, M., Imai, Y., and Watanabe, Y. (1997). "12 Mating and Sporulation in *Schizosaccharomyces pombe*," in *The Molecular and Cellular Biology of the Yeast Saccharomyces Cell Cycle Cell Biology*, Vol. III, eds J. R. Broach, J. Pringle, J. R. Pringle, and E. W. Jones (Cold Spring Harbor, NY: Cole Spring Harbor Laboratory Press).

Yamano, H. (2019). APC/C: current understanding and future perspectives. *F1000Res.* 8:F1000 Faculty Rev-725. doi: 10.12688/f1000research.18582.1

Yamashita, A., Sato, M., Fujita, A., Yamamoto, M., and Toda, T. (2005). The roles of fission yeast Ase1 in mitotic cell division, meiotic nuclear oscillation, and cytokinesis checkpoint signaling. *Mol. Biol. Cell* 16, 1378–1395. doi: 10.1091/mbc.e04-10-0859

Yamashita, A., Watanabe, Y., and Yamamoto, M. (1997). Microtubule-associated coiled-coil protein Ssm4 is involved in the meiotic development in fission yeast. *Genes Cells* 2, 155–166. doi: 10.1046/j.1365-2443.1997.1100307.x

Yang, H.-J., Asakawa, H., Ohtsuki, C., Haraguchi, T., and Hiraoka, Y. (2020). Transient breakage of the nucleocytoplasmic barrier controls spore maturation via mobilizing the proteasome subunit Rpn11 in the Fission Yeast *Schizosaccharomyces pombe*. *J. Fungi* 6, 1–10. doi: 10.3390/jof6040242

Yang, M., Hu, Y., Lodhi, M., McCombie, W. R., and Ma, H. (1999). The *Arabidopsis SKP1-LIKE1* gene is essential for male meiosis and may control homologue

separation. *Proc. Natl. Acad. Sci. U.S.A.* 96, 11416–11421. doi: 10.1073/pnas.96.20.11416

Yang, M., and Ma, H. (2001). Male meiotic spindle lengths in normal and mutant *Arabidopsis* cells. *Plant Physiol.* 126, 622–630. doi: 10.1104/pp.126.2.622

Yokobayashi, S., and Watanabe, Y. (2005). The kinetochore protein Moa1 enables cohesion-mediated monopolar attachment at meiosis I. *Cell* 123, 803–817. doi: 10.1016/j.cell.2005.09.013

Yoshida, M., Katsuyama, S., Tateho, K., Nakamura, H., Miyoshi, J., Ohba, T., et al. (2013). Microtubule-organizing center formation at telomeres induces meiotic telomere clustering. *J. Cell Biol.* 200, 385–395. doi: 10.1083/jcb.201207168

Yoshida, S., Nishiyama, S., Lister, L., Hashimoto, S., Mishina, T., Courtois, A., et al. (2020). Prc1-rich kinetochores are required for error-free acentrosomal spindle bipolarization during meiosis I in mouse oocytes. *Nat. Commun.* 11:2652. doi: 10.1038/s41467-020-16488-y

Yukawa, M., Kawakami, T., Okazaki, M., Kume, K., Tang, N. H., and Toda, T. (2017). A microtubule polymerase cooperates with the kinesin-6 motor and a microtubule cross-linker to promote bipolar spindle assembly in the absence of kinesin-5 and kinesin-14 in fission yeast. *Mol. Biol. Cell* 28, 3647–3659. doi: 10.1091/mbc.E17-08-0497

Yukawa, M., Yamada, Y., and Toda, T. (2019). Suppressor analysis uncovers That MAPs and microtubule dynamics balance with the Cut7/Kinesin-5 motor for mitotic spindle assembly in *Schizosaccharomyces pombe*. *G3* 9, 269–280. doi: 10.1534/g3.118.200896

Zimmerman, S., Daga, R. R., and Chang, F. (2004). Intra-nuclear microtubules and a mitotic spindle orientation checkpoint. *Nat. Cell Biol.* 6, 1245–1246. doi: 10.1038/ncb1200

Zitouni, S., Nabais, C., Jana, S. C., Guerrero, A., and Bettencourt-Dias, M. (2014). Polo-like kinases: structural variations lead to multiple functions. *Nat. Rev. Mol. Cell Biol.* 15, 433–452. doi: 10.1038/nrm3819

Conflict of Interest: The authors declare that the research was conducted in the absence of any commercial or financial relationships that could be construed as a potential conflict of interest.

Copyright © 2021 Sato, Kakui and Toya. This is an open-access article distributed under the terms of the Creative Commons Attribution License (CC BY). The use, distribution or reproduction in other forums is permitted, provided the original author(s) and the copyright owner(s) are credited and that the original publication in this journal is cited, in accordance with accepted academic practice. No use, distribution or reproduction is permitted which does not comply with these terms.

frontiers in Cell and Developmental Biology

REVIEW
published: 13 April 2021
doi: 10.3389/fcell.2021.667073

Phospho-Regulation of Meiotic Prophase

*Funda M. Kar and Andreas Hochwagen**

Department of Biology, New York University, New York, NY, United States

Germ cells undergoing meiosis rely on an intricate network of surveillance mechanisms that govern the production of euploid gametes for successful sexual reproduction. These surveillance mechanisms are particularly crucial during meiotic prophase, when cells execute a highly orchestrated program of chromosome morphogenesis and recombination, which must be integrated with the meiotic cell division machinery to ensure the safe execution of meiosis. Dynamic protein phosphorylation, controlled by kinases and phosphatases, has emerged as one of the main signaling routes for providing readout and regulation of chromosomal and cellular behavior throughout meiotic prophase. In this review, we discuss common principles and provide detailed examples of how these phosphorylation events are employed to ensure faithful passage of chromosomes from one generation to the next.

Keywords: meiosis, prophase, recombination, synapsis, checkpoint, kinase, phosphatase

OPEN ACCESS

Edited by:
Liangran Zhang,
Shandong University, China

Reviewed by:
Valérie Borde,
Centre National de la Recherche Scientifique (CNRS), France
Amy MacQueen,
Wesleyan University, United States

***Correspondence:**
Andreas Hochwagen
andi@nyu.edu

Specialty section:
This article was submitted to Cell Growth and Division, a section of the journal Frontiers in Cell and Developmental Biology

Received: *11 February 2021*
Accepted: *22 March 2021*
Published: *13 April 2021*

Citation:
Kar FM and Hochwagen A (2021) Phospho-Regulation of Meiotic Prophase. Front. Cell Dev. Biol. 9:667073. doi: 10.3389/fcell.2021.667073

INTRODUCTION

The central function of meiosis is to produce haploid genomes that can be packaged into gametes for sexual reproduction. Going from a diploid germ cell progenitor to haploid meiotic products involves a modified cell division program, in which a single round of DNA replication is followed by two rounds of chromosome segregation, meiosis I and meiosis II. These two segregation phases separate homologous chromosomes and sister chromatids, respectively (Petronczki et al., 2003; Hunter, 2013). The spatiotemporal regulation of meiotic events is highly complex and this complexity is accompanied by rates of chromosome missegregation that are orders of magnitude higher than during mitosis. Errors in meiotic chromosome segregation account for the naturally high rate of spontaneous pregnancy loss in humans and are the main cause of chromosomal birth defects, including Down syndrome (Nagaoka et al., 2012; Geisinger and Benavente, 2016; Potapova and Gorbsky, 2017; Webster and Schuh, 2017).

The complexities of meiosis arise primarily from the need to faithfully identify and connect homologous chromosome pairs and to ensure their proper separation during meiosis I. Unlike sister chromatids, which are connected by sister chromatid cohesion from the moment they are synthesized, homologous chromosomes originate from different organisms (mom and dad). As a result, meiotic germ cells spend an inordinate amount of time and energy to properly identify and connect pairs of homologous chromosomes (Zickler and Kleckner, 2015, 2016). This process occurs after premeiotic DNA replication in a period called meiotic prophase and, in most organisms, involves the physical rewiring of homologous chromosomes by meiotic crossover recombination. Crossover recombination is important evolutionarily for creating new allele combinations but also has an important mechanical function during meiosis. Together with the existing sister chromatid

cohesion, crossovers create physical links between homologous chromosome pairs that support proper chromosome alignment and separation during meiosis I (Hunter, 2015).

Crossover recombination involves the controlled introduction and repair of numerous DNA double-strand breaks (DSBs) (**Figure 1**). Meiotic DSBs are formed by SPO11, a conserved meiosis-specific enzyme related to topoisomerases that remains covalently attached to DSB ends and must be nucleolytically removed to allow repair (Lam and Keeney, 2015). Once removed, DSBs are resected to expose single-stranded DNA (ssDNA). These ssDNA tails provide the substrate for recombinases including RAD51 and DMC1, which scan the genome for homology and catalyze strand invasion of a donor duplex to initiate repair (Brown and Bishop, 2015). Depending on the processing of the resulting displacement loops, these intermediates are either stabilized and further processed to form crossovers, or they are dissolved after limited repair synthesis to yield non-crossover products (Hunter, 2015). To prevent genomic instability, DSBs must be repaired by the time cells initiate meiosis I.

Alongside these DNA-based events occur large-scale changes in chromosome architecture and dynamics (Zickler and Kleckner, 2015, 2016; **Figure 1**). Chromosomes assemble into longitudinally compacted arrays of chromatin loops that emanate from the axial element, a meiosis-specific nucleoprotein axis that dynamically adapts to ongoing transcription and recombination. As meiotic prophase progresses, axial elements of homologous chromosomes align to form the lateral elements of the synaptonemal complex (SC), a dynamic structure that progressively connects homologous chromosome pairs in a zipper-like arrangement (Zickler and Kleckner, 2015; Lake and Hawley, 2021). The chromosomal compaction and organization mediated by the SC are tightly coupled to the progression of crossover recombination and play numerous roles in controlling all stages of meiotic recombination. They also lead to gross morphological changes in chromosome architecture that underlie the cytologically defined stages of meiotic prophase, leptonema, zygonema, pachynema, and diplonema, which describe the progressive compaction and ultimate decompaction of prophase chromosomes. Alongside SC formation, chromosomes cluster with their telomeres in the nuclear envelope to form the telomere bouquet (Scherthan, 2001; Zickler and Kleckner, 2016). Telomeric attachment to the nuclear envelope also creates chromosomal linkages with the cytoplasmic cytoskeleton, which powers rapid chromosomal movements during pachynema.

The programmed formation of meiotic DSBs in the context of a highly dynamic genome creates a substantial hazard for genomic integrity. Meiotic checkpoints and surveillance mechanisms serve to safely navigate this developmental process and ensure that DSBs form at the right time and are appropriately repaired before cells initiate the meiotic divisions (MacQueen and Hochwagen, 2011; Subramanian and Hochwagen, 2014). These mechanisms ensure that DNA replication is largely complete before DSBs start to form, they help to locally downregulate DSB formation once a chromosome pair has initiated productive crossover recombination, and they stop DSB formation as cells exit prophase. In addition, signaling events suppress inappropriate repair patterns, control crossover maturation, and create dependent relationships between DSB repair and

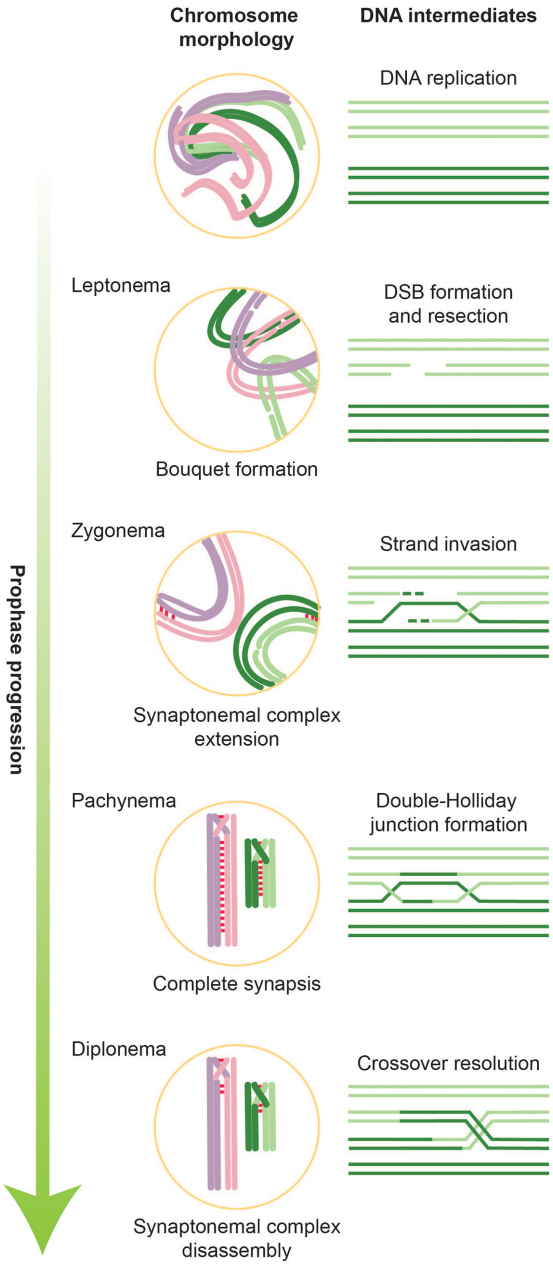

FIGURE 1 | Overview of stages of meiotic prophase along with corresponding DNA intermediates. During leptonema, the first stage of meiotic prophase, chromatin condenses and forms attachments with the nuclear envelope. It is also during this stage that DSBs are introduced. In parallel with ongoing DNA repair, homologous chromosomes pair and formation of the SC is initiated. Partial SCs define the next meiotic stage, zygonema. When all chromosomes are synapsed along their axes, cells are in pachynema, which is when the bulk of double-Holliday junctions form. During late pachynema/early diplonema, double-Holliday junctions are resolved into crossovers and SC disassembly begins. Cells then exit meiotic prophase and prepare for the first meiotic division.

chromosome morphogenesis. Our understanding of this network has grown substantially as more connections are being uncovered and dissected at the molecular level, although available data suggest that this network is likely significantly more complex.

Dynamic protein phosphorylation has emerged as a major mediator of this signaling during meiotic prophase. Protein phosphorylation is a very versatile way of communication mediated by kinases and phosphatases. Kinases catalyze the transfer of the gamma-phosphate group of ATP onto suitable targets (in eukaryotes primarily the hydroxyl groups of serine, threonine, and tyrosine). Phosphatases reverse this process by hydrolyzing the resulting phosphoesters. Both classes of enzymes have important roles in the regulation of meiotic prophase, although research has primarily focused on the role of kinases (**Figure 2**). In part this bias arises because eukaryotic genomes encode more kinases than phosphatases (Smoly et al., 2017). However, phosphatases have crucial roles in controlling signaling dynamics and in executing large transitions during meiotic prophase.

FUNCTIONS OF PHOSPHORYLATION

Research over the past two decades has greatly improved our understanding of how phosphorylation events regulate meiotic prophase. It has also revealed a number of recurrent regulatory modes that create dependencies, allow local decision-making, and integrate signals. We would like to highlight some of these modes before discussing the regulation of individual prophase processes in more detail.

Creating Dependent Relationships

A key function of kinase signaling in meiotic prophase is the establishment of dependent relationships, whereby the ongoing activity of one process, such as the presence of DSBs, is communicated to other metabolically independent processes, such as centromere coupling or cell-cycle progression (Lydall et al., 1996; Falk et al., 2010). These dependent relationships can promote the co-occurrence of processes, or they can create a "wait" signal to ensure that one process is completed before the next process initiates (MacQueen and Hochwagen, 2011; Subramanian and Hochwagen, 2014). The creation of a wait signal is often referred to as a checkpoint (Hartwell and Weinert, 1989). Many of the known dependent relationships in meiotic prophase are established by a core kinase signaling network, consisting of the DNA-damage sensor kinases ATM and ATR and the transducer kinase CHK2 (Pereira et al., 2020). ATM and ATR sense protein-linked DNA ends and RPA-coated single-stranded DNA, respectively (Marechal and Zou, 2013; Awasthi et al., 2015). CHK2 gets activated by ATM/ATR and targets an additional set of substrates (Stracker et al., 2009). In meiotic prophase, all three kinases have an expanded substrate spectrum that includes numerous meiosis-specific proteins (Carballo et al., 2008, 2013; Falk et al., 2010; Kim et al., 2015; Penedos et al., 2015). In addition, the architecture of the signaling cascade appears to be rewired in multiple ways. All three kinases display altered (DSB-independent) modalities of activation in at least some organisms (Barchi et al., 2005; Bellani et al., 2005; Bhalla and Dernburg, 2005; Blanco-Rodríguez, 2012; Widger et al., 2018). In addition, several cell-cycle kinases, including Dbf4-dependent kinase (DDK) and Polo-like kinases (PLKs), have been tied into this network to establish dependencies (Clyne et al., 2003; Sasanuma et al., 2008; Sourirajan and Lichten, 2008; Wan et al., 2008; Labella et al., 2011; Murakami and Keeney, 2014; Nadarajan et al., 2017). On the other hand, several well-known mediators of canonical DNA-damage signaling, including the *Saccharomyces cerevisiae* adaptor protein Rad9^{53BP1} and the metazoan effector protein p53 appear to have less pronounced roles (Lydall et al., 1996; Odorisio et al., 1998; Murakami and Nurse, 1999; Ward et al., 2003; Ashley et al., 2004).

Local Versus Global Signaling

The inherent asynchrony of DNA metabolism within the genome of each nucleus during meiotic prophase, including differences in the local timing of DNA replication, DSB formation, and repair kinetics, necessitates spatially restricted communication to coordinate processes at individual loci or on individual chromosomes. For example, DSB formation in yeast is locally licensed by DDK, which is thought to ride along with the DNA replication machinery and thus promote DSB formation specifically in DNA regions where replication is completed (Murakami and Keeney, 2014). Spatially constrained signaling is also inherent to ATM and ATR. Their damage dependency ensures that both kinases are principally active when tethered to DSB sites (Marechal and Zou, 2013; Awasthi et al., 2015; Paull, 2015) and helps establish local signaling hubs around DSB sites (Cimprich and Cortez, 2008; Blackford and Jackson, 2017). In mammalian spermatocytes, ATR is also activated independently of meiotic DSBs through the recruitment to unpaired chromosome axes (Keegan et al., 1996; Moens et al., 1999; Turner, 2015), thereby constraining kinase activity to specific chromosomal regions. An analogous situation occurs in *S. cerevisiae* where the meiotic CHK2-like transducer kinase, Mek1, depends on interactions with axis components to become active (Carballo et al., 2008). With kinase activity confined to these regions, it depends on the diffusibility of the respective kinase substrates whether signaling is locally constrained as seen for chromatin-associated phosphorylation events (Rogakou et al., 1999; He et al., 2020; Raina and Vader, 2020) or whether the signal is able to spread through the nucleus or the whole cell. Finally, dephosphorylation can also be spatially constrained. For example, meiotic cohesin is retained around centromeres during and after meiosis I due to localized activity of protein phosphatase 2A (PP2A) in these regions (Wassmann, 2013). These localized mechanisms allow signaling to occur independently at multiple locations despite their presence in a common nuclear space.

Signal Amplification and Integration

A number of instances have been described in meiotic prophase where phosphorylation of one residue by an initiator kinase primes the protein for additional phosphorylation events mediated by another kinase. Such priming events can help amplify a signal by creating a larger region of phosphorylation (Wan et al., 2008; Falk et al., 2010; Chen et al., 2015). They

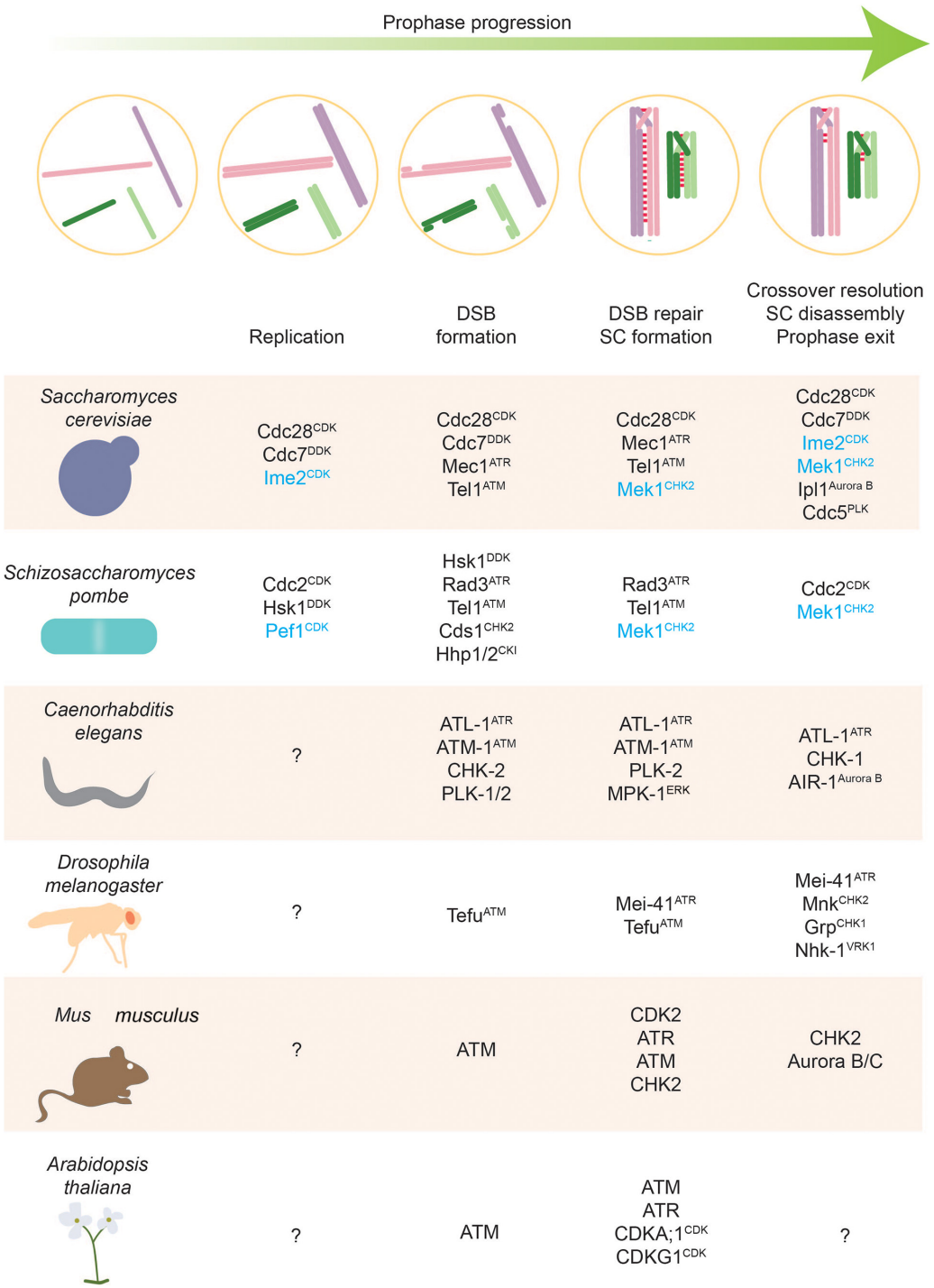

FIGURE 2 | Stages of meiosis and kinases that regulate them. Kinases along with phosphatases are the main actors of phosphorylation-based regulatory control. This figure highlights kinases with defined roles in different meiotic stages. Meiosis-specific kinases are colored blue.

also provide an opportunity to integrate multiple signals if the two kinases are differentially regulated. For example, DSB formation in *S. cerevisiae* requires priming phosphorylation of the DSB activator Mer2 by cyclin-dependent kinase (CDK) (Henderson et al., 2006; Sasanuma et al., 2008; Wan et al., 2008). This phosphorylation event creates a substrate recognition site for DDK, which subsequently phosphorylates additional sites (Sasanuma et al., 2008; Wan et al., 2008). Both of these phosphorylation events have to occur for DSB formation to initiate, but the two kinases are independently regulated. DDK

is commonly observed as a responder to priming events, because it preferentially phosphorylates serines and threonines that are followed by residues with a negative charge, which can also be provided by phosphorylation. Several kinases, including DDK, CHK2, and PLK, also have phospho-binding domains that allow binding to specific phosphorylated targets and stimulate further phosphorylation. In addition, signal integration can also occur if two different kinases simply phosphorylate the same substrate. This pattern has emerged in a number of cases where a protein is phosphorylated by general cell cycle kinases with a wide spectrum of substrates, such as CDK, but also by a signal response kinase, such as ATM/ATR or CHK2 (Sopko et al., 2002; Callender et al., 2016; Chen et al., 2018). In these cases, phosphorylation by the cell-cycle kinase may communicate the appropriate cell cycle state and thus license the protein for regulation by the response kinase (or phosphatase).

CONTROL OF MEIOTIC PROPHASE

This review intends to provide a solid overview of our current understanding of phospho-regulation of meiotic prophase in common model organisms of meiosis. However, given the wide spectrum of available examples, we apologize if space constraints prevented us from including all examples of this regulation.

DNA REPLICATION

Premeiotic S phase, though not formally part of meiotic prophase, is the first stage of meiosis-associated DNA metabolism and appears tightly integrated with subsequent prophase events. The phospho-regulation of premeiotic S phase has so far primarily been studied in *S. cerevisiae* and *Schizosaccharomyces pombe*, and, similar to mitotically proliferating cells, relies heavily on the activity of CDKs (MacKenzie and Lacefield, 2020). In *S. cerevisiae*, S-CDK ($Cdc28^{CDK}$ bound to the cyclins Clb5 and Clb6) is essential for initiating premeiotic DNA replication (Stuart and Wittenberg, 1998; Benjamin et al., 2003). In *S. pombe*, the cyclin Cig2 bound to $Cdc2^{CDK}$ similarly promotes premeiotic S phase, although *cig2* mutants only have a partial replication defect, because altered expression of later cyclins substitutes for the necessary CDK activity (Borgne et al., 2002; Malapeira et al., 2005). Cyclin gene expression patterns are consistent with CDKs also driving premeiotic S phase in mammals (Chotiner et al., 2019). One unusual feature of premeiotic S phase in both yeasts is the additional involvement of non-canonical CDKs. In *S. cerevisiae*, efficient S-CDK activation requires the meiosis-specific CDK2-like kinase Ime2, which promotes degradation of the CDK inhibitor Sic1 (Dirick et al., 1998; Benjamin et al., 2003; Sedgwick et al., 2006; Szwarcwort-Cohen et al., 2009). Like CDKs, Ime2 activation requires phosphorylation in its T-loop by the CDK-activating kinase Cak1 (Schindler et al., 2003). However, it does not require binding of a canonical cyclin (Honigberg, 2004). Ime2 likely has additional roles in activating DNA replication, because deletion of Sic1 does not rescue the DNA replication defects conferred by the absence of Ime2 (Dirick et al., 1998; Clifford et al., 2004). Although a large number of Ime2-dependent phosphorylation sites have been defined (Clifford et al., 2004; Holt et al., 2007), the relevant targets for premeiotic S phase activation remain to be determined. It is possible that the effect on S-phase activation occurs in part through Ime2's role in promoting the meiotic gene expression program (Brush et al., 2012). A similar situation is observed in *S. pombe* where the CDK5-like kinase Pef1 promotes premeiotic DNA replication by inducing the expression of key replication factors (Matsuda et al., 2021). In both *S. cerevisiae* and *S. pombe*, timely activation of premeiotic DNA replication also requires DDK (Ogino and Masai, 2006; Valentin et al., 2006). In mitotically dividing cells, S-CDK and DDK phosphorylate numerous components of the pre-replicative complex to activate replication (Bell and Labib, 2016), although whether the same or additional targets become phosphorylated in meiosis remains to be determined.

DSB FORMATION

Connecting DSB Formation to DNA Replication

Meiotic DSB formation must be delayed until premeiotic DNA replication is largely complete because Spo11-induced DSBs on unreplicated DNA are difficult to repair and also interfere with the completion of DNA replication (Blitzblau and Hochwagen, 2013). Initiation of premeiotic DNA replication requires substantially lower levels of DDK activity than DSB formation (Wan et al., 2006), providing a basal mechanism to temporally separate the two processes. In addition, evidence suggests that formation of DSBs is coordinated with DNA replication in a local manner, as a delay in DNA replication in one region of a chromosome leads to a delay in DSB formation specifically in that region (Borde et al., 2000; Murakami and Keeney, 2014). However, the dependence of DSB formation on the completion of DNA replication is not strict, as both *S. cerevisiae* and *S. pombe*, can form DSBs in the absence of DNA replication (Hochwagen et al., 2005; Tonami et al., 2005; Ogino and Masai, 2006; Blitzblau et al., 2012). In *S. cerevisiae*, coordination between DNA replication and DSB formation involves phosphorylation of the Spo11-accessory protein Mer2. Mer2 is phosphorylated on S30 by CDK, which primes phosphorylation on S29 by DDK (Henderson et al., 2006; Sasanuma et al., 2008; Wan et al., 2008). Phosphorylation of these sites is required for formation of DSBs (Henderson et al., 2006; Sasanuma et al., 2008; Wan et al., 2008) and promotes localization of other components of the meiotic DSB machinery to chromosome axes (Panizza et al., 2011). Additional DDK-dependent phosphorylation events in the N-terminus of Mer2 also contribute to DSB formation, albeit more weakly (Sasanuma et al., 2008).

Double-strand break formation is thought to be connected to local completion of DNA replication through the activity of DDK. According to this model, DDK is recruited to replisomes and phosphorylates chromatin-bound Mer2 as replisomes pass through replicating DNA (Murakami and Keeney, 2014). Mer2 may not be the only target of this control mechanism as

phospho-mimetic mutants of S29 or S30 cannot bypass the need for DDK or CDK for DSB formation (Wan et al., 2008), although it is also possible that the phospho-mimetic substitutions did not fully substitute for the lack of phosphorylation. The DSB factor Rec104 is phosphorylated during meiosis in a Spo11-independent manner and has a different electrophoretic mobility when DNA replication is blocked (Kee et al., 2004; Blitzblau and Hochwagen, 2013). Thus, it is possible that Rec104 provides a further link between replication and DSB formation. However, this model can still not explain how DSB formation can happen in the absence of DNA replication. A potential answer is suggested by the observations that DDK activity progressively increases in meiotic prophase (Matos et al., 2008; Wan et al., 2008) and that induced overexpression of DDK abrogates local differences in DSB timing (Murakami and Keeney, 2014). We therefore speculate that replication fork passage facilitates Mer2 phosphorylation, but that this barrier can also be overcome independently of replication once nuclear DDK activity is sufficiently high.

Whether and how DSB formation is linked to DNA replication in other organisms is less clear. Perhaps the most intriguing link comes from analysis of *Caenorhabditis elegans* CHK-2^{CHK2}, which has emerged as a master regulator of meiotic recombination in this organism. *chk-2* mutants are defective in numerous aspects of meiotic recombination, including chromosome pairing and nuclear organization (MacQueen and Villeneuve, 2001; Oishi et al., 2001). CHK-2 is also essential for meiotic DSB formation through controlling chromatin association of the DSB regulator DSB-1 (Stamper et al., 2013). It has been proposed that CHK-2 activity provides a link between DNA replication and recombination (MacQueen and Villeneuve, 2001), although inhibiting premeiotic DNA replication compromises meiotic progression in both wild-type and *chk-2* mutants (MacQueen and Villeneuve, 2001). It also remains puzzling is how CHK-2 would be activated in this model because mutants lacking both canonical activators of CHK2 kinases (*atl-1*^{ATR} and *atm-1*^{ATM}) have less severe recombination defects than *chk-2* mutants (Li and Yanowitz, 2019). Perhaps other kinases substitute for ATM/ATR. Alternatively, CHK-2 activity may be primarily regulated at the level of gene expression (Mohammad et al., 2018).

Role of the Replication Checkpoint

Research in *S. cerevisiae* and *S. pombe* has also revealed a mechanism that further delays DSB formation in response to persistent blocks in replication fork progression. In *S. cerevisiae*, the checkpoint kinases Mec1^{ATR} and Rad53^{CHK2} attenuate DDK activity in response to replication problems, thereby providing a mechanism to block DSB formation during replication stress (Blitzblau and Hochwagen, 2013). Mer2 phosphorylation happens independently of replication in *mec1*^{ATR} and *rad53*^{CHK2} mutants, suggesting that DDK's association with replisomes is not essential for its ability to target and phosphorylate Mer2 (Blitzblau and Hochwagen, 2013). In addition to inhibiting DDK, replication stress controls DSB formation by downregulating Spo11 transcript levels (Blitzblau and Hochwagen, 2013), but how the replication checkpoint intersects with transcriptional regulation has not been investigated. In *S. pombe*, Rad3^{ATR} along with Cds1^{CHK2} is similarly required for preventing DSB formation in response to replication stress by downregulating expression of the transcription factor Mei4 (Tonami et al., 2005; Ogino and Masai, 2006). One key factor affected by this regulation is Mde2, which tethers the DSB machinery to the meiotic chromosome axis and is essential for DSB formation (Abe and Shimoda, 2000; Miyoshi et al., 2012, 2013). In addition, Mei4 downregulation leads to prolonged nuclear movement (Ruan et al., 2015). Whether similar regulation exists in mammals remains unclear. One potential candidate for checkpoint-dependent regulation is the protein ANKRD31, which interacts with the DSB factor REC114 (Boekhout et al., 2019; Papanikos et al., 2019). Mouse *Ankrd31−/−* mutants experience a delay in DSB formation along with other defects in recombination, including DSB patterning (Boekhout et al., 2019; Papanikos et al., 2019). ANKRD31 harbors 24 ATM/ATR consensus sites and thus has the potential to be a target for ATM/ATR-dependent regulation for DSB formation (Boekhout et al., 2019).

Control of DSB Numbers

The number of meiotic DSBs per cell must be carefully titrated to ensure sufficient DSB formation for successful meiotic recombination while minimizing the risk of chromosome abnormalities associated with excessive DSB numbers. ATM mutants in various organisms exhibit increased DSB formation, suggesting a universal role for ATM in the regulation of DSB levels (Joyce et al., 2011; Lange et al., 2011; Checchi et al., 2014; Garcia et al., 2015; Mohibullah and Keeney, 2017; Fowler et al., 2018; Kurzbauer et al., 2021). In *S. cerevisiae* and *S. pombe*, ATM regulates DSB numbers by preventing double-cutting in proximity of DSBs (Garcia et al., 2015; Fowler et al., 2018). The activity of *S. cerevisiae* Tel1^{ATM} also limits DSB formation at a given locus to one DSB per quartet of chromatids (Zhang et al., 2011). Conversely, Mec1^{ATR} is suggested to promote DSB formation by blocking prophase exit until enough DSBs are made (Gray et al., 2013). Antagonistic roles of ATM and ATR in DSB formation have also been observed in *C. elegans* (Li and Yanowitz, 2019).

The definition of the relevant ATM substrates remains incomplete. In the protist *Tetrahymena thermophila*, the DSB factor Pars11 gets phosphorylated by ATR upon DSB formation (this organism lacks ATM) and is removed from chromatin and degraded (Tian and Loidl, 2018). Mutants lacking ATR during meiosis or expressing non-phosphorylatable versions of Pars11 exhibit elevated DSB numbers (Tian and Loidl, 2018), suggesting that Pars11 is a major mediator of feedback control in this organism. In *S. cerevisiae*, negative feedback of DSB formation is suggested to be partially achieved through the essential DSB factor Rec114, which gets phosphorylated by Tel1^{ATM}/Mec1^{ATR} at multiple sites after DSB formation (Carballo et al., 2013). These phosphorylation events were found to reduce binding of Rec114 at DSB hotspots and reduce DSB levels (Carballo et al., 2013). However, altering Rec114 phosphorylation had little effect on DSB numbers in another study and did not recapitulate the increased DSB numbers or double cutting observed in ATM mutants (Garcia et al., 2015; Mohibullah and Keeney, 2017).

It has been suggested that Rec114 might be only one of the targets of Tel1^{ATM}, with each target contributing slightly to DSB-number regulation (Garcia et al., 2015; Mohibullah and Keeney, 2017). In *C. elegans*, the proteins DSB-1 and DSB-2 are required for DSB formation, and are suggested to be involved in a negative feedback regulation of DSB formation (Rosu et al., 2013; Stamper et al., 2013). DSB-1 and DSB-2 have clustered ATM/ATR phosphorylation sites, a feature that is also seen in other meiotic ATM/ATR targets like Rec114 (Carballo et al., 2013; Rosu et al., 2013; Stamper et al., 2013). Whether ATM/ATR function through these proteins to modulate DSB levels remains to be determined. Notably, feedback on DSB numbers in *C. elegans* also involves the polo-like kinases PLK-1 and PLK-2, which phosphorylate the SC protein SYP-4 on S269 (Nadarajan et al., 2017). This phosphorylation event takes place after a DSB site is designated as a crossover, connecting crossover designation to preventing further DSB formation in this organism (Nadarajan et al., 2017).

Other kinases also contribute to DSB formation. For example, casein kinase I (CKI) regulates DSB formation in fission yeast (Phadnis et al., 2015; Sakuno and Watanabe, 2015) by phosphorylating the meiosis specific cohesin subunit Rec11^{STAG3}, which regulates loading of the DSB-promoting axis protein Rec10 (Phadnis et al., 2015; Sakuno and Watanabe, 2015). STAG3 is also phosphorylated in a *SPO11*-independent manner in mouse but the role of this phosphorylation has not been explored (Fukuda et al., 2012).

CHROMOSOME DYNAMICS

Protein phosphorylation has several key functions in controlling nuclear organization, chromosome movement, pairing, and synapsis in meiotic prophase.

Nuclear Organization and Chromosome Movement

Meiotic chromosomes form connections with the nuclear envelope (Scherthan, 2001) and move to facilitate homolog pairing and resolution of chromosome entanglements (Zickler and Kleckner, 2016). These movements are mediated by SUN and KASH domain-containing proteins, which span the nuclear envelope and connect the chromosomes to the cytoskeleton (Hiraoka and Dernburg, 2009). In *C. elegans*, meiotic chromosome pairing and movement is initiated by the CHK-2-dependent phosphorylation and recruitment of chromosome-specific pairing proteins to subtelomeric pairing centers (Phillips and Dernburg, 2006; Kim et al., 2015; **Figure 3**). Some of the CHK-2-dependent phosphorylation sites (e.g., phosphorylation of HIM-8 on T64) occur in polo-box motifs and lead to the recruitment of PLK-2 (Kim et al., 2015). One output of this signaling is the CHK-2 and PLK-2 dependent phosphorylation of the SUN-domain protein SUN-1 (Penkner et al., 2009; Harper et al., 2011; Labella et al., 2011). SUN-1 phosphorylation stabilizes PLK-2 binding and promotes chromosome synapsis (Woglar et al., 2013), but there are likely additional substrates, because PLK-2 also promotes other processes, including chromosome pairing and movement, which were not disrupted by mutating

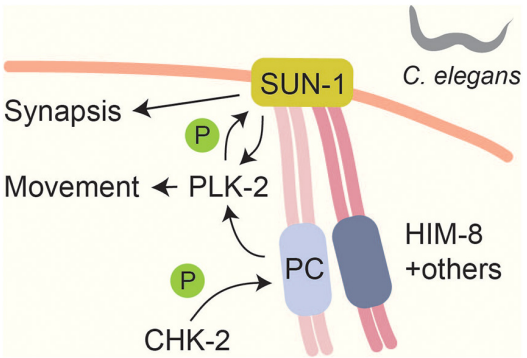

FIGURE 3 | Linking chromosome movements and synapsis in *Caenorhabditis elegans*. A CHK-2 mediated signal localizes pairing centers (PCs) to the nuclear envelope. CHK-2 phosphorylates PC proteins like HIM-8 at PLK binding motifs (Kim et al., 2015). This phosphorylation leads to PLK-2 localization to PCs and promotes SUN-1 phosphorylation (Penkner et al., 2009; Harper et al., 2011; Labella et al., 2011). Phosphorylation of SUN-1 stabilizes PLK-2 at PCs and is thought to be part of a checkpoint that responds to synapsis and recombination defects (Woglar et al., 2013). SUN-1 phosphorylation promotes efficient SC formation (Woglar et al., 2013).

SUN-1 phosphorylation sites (Harper et al., 2011; Labella et al., 2011; Woglar et al., 2013). Interestingly, CHK-2 itself appears to respond to phosphorylation, because its phospho-binding FHA domain is required for binding to pairing centers (Kim et al., 2015). However, the nature of the CHK-2 docking site remains to be determined.

Phospho-regulation also contributes to telomere tethering in mammals because mice lacking CDK2 or the atypical CDK activator Speedy A are defective in tethering telomeres to the nuclear envelope (Viera et al., 2015; Tu et al., 2017). CDK2 is required for the proper distribution of SUN1 in the nuclear envelope and can phosphorylate SUN1 *in vitro* (Viera et al., 2015), but whether this phosphorylation takes place *in vivo* and whether it is necessary for SUN1 distribution remains to be determined.

Finally, protein kinases also regulate the characteristic nuclear reorganization seen in several organisms during meiotic prophase. In *C. elegans*, CHK-2 and PLK-2 signaling organizes meiotic chromatin into a crescent shaped domain within the nucleus (MacQueen and Villeneuve, 2001; Harper et al., 2011; Labella et al., 2011), whereas the dramatic elongation of the meiotic micronucleus in the ciliate *T. thermophila* is induced by ATR in response to meiotic DSB induction (Mochizuki et al., 2008; Loidl and Mochizuki, 2009). In both instances the relevant kinase targets are currently unknown.

Chromosome Pairing and Synapsis

As chromosomes undergo recombination at the DNA level, their axes pair up and, in many organisms, become stably aligned by the SC. This process is regulated by phosphorylation at multiple levels (Gao and Colaiácovo, 2018; Kim and Choi, 2019). In *Arabidopsis thaliana*, CDKA;1 phosphorylates the axis protein ASY1^{HORMAD}, which is required for its recruitment to the axial element (Yang et al., 2020). Loss of another CDK, CDKG1, causes incomplete synapsis in male meiosis in a temperature-dependent

manner (Zheng et al., 2014). In *S. cerevisiae*, reduced CDK activity also leads to defects in the formation of full-length SCs but the relevant phosphorylation targets remain to be determined (Zhu et al., 2010). In *C. elegans*, CDK-dependent phosphorylation of the SC protein SYP-1 primes recruitment of the PLK-2 to the SC (Sato-Carlton et al., 2018; Brandt et al., 2020). Interestingly, PLK-2 is prevented from binding to these primed sites until a chromosome undergoes crossover designation, whereupon CDK-1 dependent PLK-2 recruitment helps partition the holocentric chromosomes of *C. elegans* into short and long arms in preparation for the meiotic divisions (Sato-Carlton et al., 2018; Brandt et al., 2020).

Phosphorylation of SC proteins also helps break chromosomal interactions. In *S. cerevisiae*, the SC protein Zip1 connects pairs of centromeres independently of homology (Tsubouchi and Roeder, 2005). This association occurs separately from SC formation and is thought to provide a backup system for chromosomes that failed to undergo crossover formation (Obeso et al., 2014). $Mec1^{ATR}$-dependent phosphorylation of Zip1 on S75 leads to the transient disruption of centromere coupling during meiotic prophase, presumably to enable homology-dependent pairing (Falk et al., 2010; Obeso et al., 2014). In the process, S75 phosphorylation primes Zip1 for phosphorylation on multiple additional residues that may amplify the effect of the initial phosphorylation event (Falk et al., 2010), but the nature and role of these additional events remains unknown.

Other kinases also impact SC formation and stability. In *C. elegans*, the ERK kinase MPK-1 is highly active in early-mid pachytene when it phosphorylates the SC proteins HTP-1 and SYP-2 (Lee et al., 2007; Nadarajan et al., 2016; Das et al., 2020). HTP-1 phosphorylation on S325 is essential for complete synapsis, as large stretches of chromosomes remain asynapsed in S325A mutants (Das et al., 2020). On the other hand, phosphorylation of SYP-2 prevents breakdown of SC on long chromosome arms (Nadarajan et al., 2016). A phospho-mimetic mutant of SYP-2 for this phosphorylation fails to disassemble its SC, similar to what is seen in mutants with sustained MPK-1 activity (Nadarajan et al., 2016). Pro-crossover proteins help to downregulate MPK-1 in late pachytene, thereby maintaining SC stability until after crossover formation has occurred (Nadarajan et al., 2016).

DSB REPAIR AND CROSSOVER FORMATION

Crossover formation is a multi-step process with several decision points. Following break resection, DSBs must be targeted to the appropriate homologous repair template. A subset of DSBs is then designated to form joint molecules and double-Holliday junctions that are ultimately resolved as crossovers when cells exit meiotic prophase. Many of these processes and decision points are regulated by phosphorylation.

Resection

Following DSB formation, SPO11 remains covalently linked to DSB ends. Processing of these protein-linked ends as well as the subsequent production of ssDNA ends by resection depends on the MRN complex and its activator CtIP. In *S. cerevisiae*, $Sae2^{CtIP}$ tetramerization as well as its interaction with MRX^{MRN} is controlled by CDK-dependent phosphorylation of Sae2 S267, which is required for efficient resection (Huertas et al., 2008; Manfrini et al., 2010; Cannavo et al., 2018). Sae2 is also phosphorylated in a DSB-dependent manner by $Mec1^{ATR}$ /$Tel1^{ATM}$ (Baroni et al., 2004; Terasawa et al., 2008), but these modifications appear to be specifically required for Spo11 release from DSB ends and do not affect resection *in vitro* (Baroni et al., 2004; Terasawa et al., 2008; Cannavo et al., 2018).

Suppression of Sister Repair

To encourage crossover recombination between homologous chromosomes, the use of the more readily available sister chromatid as a repair template must be suppressed. This suppression involves the combined action of the meiotic chromosome axes and specialized recombinase activities (Hollingsworth, 2010; Lao and Hunter, 2010; Humphryes and Hochwagen, 2014; Brown and Bishop, 2015; Rinaldi et al., 2017). In *S. cerevisiae*, phospho-regulation of repair template choice requires ATM/ATR-dependent phosphorylation of $Hop1^{HORMAD}$ on T318 (Carballo et al., 2008). This phosphorylation event occurs specifically in the context of the axial element (Lin et al., 2010; Raina and Vader, 2020) and recruits the phospho-binding FHA domain of $Mek1^{CHK2}$, resulting in the stabilization of phospho-T318 and $Mek1^{CHK2}$ activation (Carballo et al., 2008; Chuang et al., 2012). Structural studies suggested that the FHA domain of $Mek1^{CHK2}$ prefers hydrophobic amino acids at +2 and +3 positions from the phosphorylated residue (Xie et al., 2018), and the amino acids surrounding T318 fit this description. Whether any other phosphorylation events recruit $Mek1^{CHK2}$ in a similar manner as $Hop1^{HORMAD}$ is not yet known. Once activated, $Mek1^{CHK2}$ phosphorylates at least two targets to suppress Rad51-mediated intersister repair. These include Rad54, a Rad51-interacting protein that stimulates Rad51 activity (Niu et al., 2009), and Hed1, a meiosis-specific protein that binds to Rad51 and displaces Rad54 (Callender et al., 2016). $Mek1^{CHK2}$-dependent phosphorylation of Rad54 on T132 reduces its interaction with Rad51 (Niu et al., 2009), whereas phosphorylation of Hed1 T40 stabilizes Hed1 and thus downregulates Rad51 activity (Callender et al., 2016). $Mek1^{CHK2}$ may phosphorylate additional meiotic factors to establish repair template choice because elimination of Rad54 phosphorylation and Hed1 together leads only to a two-fold decrease in homolog bias, whilst suppression of intersister repair is completely lost in the absence of $Mek1^{CHK2}$ (Goldfarb and Lichten, 2010; Kim et al., 2010; Liu et al., 2014), but the relevant factors remain to be determined. ATM/ATR-dependent phosphorylation of the N-terminus of Rad51 may also contribute because it stabilizes Rad51 and is important for inter-homolog bias under certain conditions (Woo et al., 2020). A role for ATM in promoting interhomolog repair has also been suggested in *C. elegans* (Li and Yanowitz, 2019).

In several organisms, the suppression of sister repair is ultimately alleviated to promote repair of persisting meiotic

DSBs. In *S. cerevisiae*, the recruitment of the AAA-ATPase Pch2^{TRIP13} to synapsing chromosomes leads to the removal of phospho-Hop1^{HORMAD}-T318, partial inactivation of Mek1^{CHK2}, and increased inter-sister repair (Subramanian et al., 2016). A transition of repair patterns during pachynema has also been reported for mouse spermatogenesis (Enguita-Marruedo et al., 2019). In *C. elegans*, ATM/ATR redundantly promote inter-sister repair in response to persistent DSBs (Garcia-Muse et al., 2019). A similar function has also been proposed for ATM in *Arabidopsis* (Yao et al., 2020). Notably, *Arabidopsis atr* mutants do not exhibit any meiotic phenotypes but exacerbate the meiotic defects of *atm* mutants, thus ATR likely plays a supporting role (Culligan and Britt, 2008; Yao et al., 2020).

One of the downstream phosphorylation targets of this response in *C. elegans* is the SC protein SYP-1, which is phosphorylated at six sites, none of which are in consensus ATM/ATR motifs, suggesting catalysis by other kinases (Garcia-Muse et al., 2019). Of note, one of these residues, T452, has also been implicated in crossover patterning and synapsis (Sato-Carlton et al., 2018). Puzzlingly, phospho-dead *syp-1 T452A* exhibit lower rates of embryo survival (∼60%) than *syp-1 6A* mutants (∼80%) (Sato-Carlton et al., 2018; Garcia-Muse et al., 2019), but whether mutation of the additional sites in the 6A mutant masks the effects of T452A remains to be investigated.

Regulation of Crossover Designation

Once DSBs have encountered the homologous chromosome, repair intermediates that give rise to well-spaced (interfering) crossovers are stabilized by pro-crossover proteins. ATR mutants show defects in crossover patterning in multiple organisms (Brady et al., 2018; Li and Yanowitz, 2019; Shinohara et al., 2019). In *S. cerevisiae*, two key pro-crossover proteins, the SC protein Zip1 and the SUMO ligase Zip3^{RNF212} are both phosphorylated in this process. Phosphorylation on up to four consecutive serines in the C-terminus of Zip1 is important to promote crossover formation and to ensure efficient chromosome synapsis (Chen et al., 2015). One of these sites, S816, is phosphorylated by DDK in a DSB and Mek1^{CHK2}-dependent manner (Chen et al., 2015). Since DDK uses prior phosphorylation events to recognize its targets, it is possible that there are other kinases that prime Zip1 at S817 or S818 to recruit DDK (Chen et al., 2015). As this region does not contain a canonical Mek1^{CHK2} motif, DDK-dependent phosphorylation might be primed by a different kinase than Mek1^{CHK2} or by Mek1^{CHK2} in a non-canonical manner (Chen et al., 2015). Zip3^{RNF212}, which marks crossover sites, is phosphorylated in a Mec1^{ATR}/Tel1^{ATM}-dependent manner (Serrentino et al., 2013) and mutation of ATM/ATM consensus sites leads to a reduction of Zip3^{RNF212} recruitment to DSB sites and lower crossover frequency (Serrentino et al., 2013).

Phosphorylation of the SC protein SYP-1 also contributes to regulation of crossovers in *C. elegans*. Phosphorylation on SYP-1 T452 is required for wild-type crossover levels and patterning (Sato-Carlton et al., 2018). T452 is located in a polo-recognition motif and its phosphorylation promotes recruitment of PLK-2 to the short arms of chromosomes where phosphorylated SYP-1 is localized (Sato-Carlton et al., 2018).

Other phosphorylation events have been implicated in crossover formation in *S. cerevisiae*, although their exact mechanism and effect on crossover formation remain elusive. Like mutation of Zip3^{RNF212}, mutation of phospho-sites in the meiotic cohesin Rec8 also causes a reduction in Zip3^{RNF212} foci (Yoon et al., 2016). In addition, Rfa2^{RPA} is phosphorylated at S122 by Mec1^{ATR} both in mitosis and meiosis, and a phosphomimetic mutant exhibits changes in crossover patterning in some intervals but not in others (Bartrand et al., 2006). However, how these phosphorylation events impact crossover-related phenomena has not been studied in detail.

One novel form of phospho-regulation was recently identified for the MutSγ complex, which contributes to formation of crossovers in many organisms (Hunter, 2015; Gray and Cohen, 2016). In *S. cerevisiae*, Msh4, one of the subunits of MutSγ, is phosphorylated in its N-terminus by DDK in a DSB-dependent manner (He et al., 2020). Phosphorylated Msh4 is enriched in the chromatin-bound fraction of Msh4 and depends on pro-crossover factors, suggesting that Msh4 phosphorylation occurs at sites of recombination (He et al., 2020). The activities of ATM/ATR and Mek1^{CHK2} are also required for this phosphorylation, although it is not clear whether their roles are direct (He et al., 2020). Intriguingly, Msh4 phosphorylation disrupts a degron sequence that would lead to proteasome-mediated degradation and thus may selectively stabilize Msh4 at crossover designated DSBs (He et al., 2020).

A Role for CDKs

Cyclin-dependent kinases regulate crossover formation in mice and *Arabidopsis*. In *Arabidopsis*, reduction in CDKA;1 activity leads to a reduction in the number of crossovers and to changes in crossover distribution in certain genomic regions (Wijnker et al., 2019). In mice, CDK2 localizes to crossover sites (Ashley et al., 2001) and is required for completion of DSB repair (Viera et al., 2009). In hyperactive CDK2 mutants, the number of chromosomal foci of MHL1, a subunit of the pro-crossover MutLγ complex, increases although the number of crossovers does not change (Palmer et al., 2020). On the other hand, reduction of CDK2 activity blocks formation of crossovers (Palmer et al., 2020). How and through which targets CDKs promote crossover formation in these organisms remains to be answered, but they might be acting through similar pathways. Interestingly, a cyclin-related protein, COSA-1/Cntd1, marks crossover sites and is required for crossover formation in *C. elegans* and mice (Yokoo et al., 2012; Holloway et al., 2014; Gray et al., 2020). COSA-1/Cntd1 might partner up with CDK to promote crossover formation, although co-immunoprecipitation experiments in mice argue against a stable interaction between Cndt1 and CDK2 (Bondarieva et al., 2020; Gray et al., 2020).

Regulation of Joint Molecule Resolution and Dissolution

In *S. cerevisiae*, Cdc5^{PLK} and its kinase activity are required for joint-molecule resolution into crossovers at the end of meiotic prophase (Clyne et al., 2003; Sourirajan and Lichten, 2008; Sanchez et al., 2020). Recent work has shed light on how different

repair pathways are regulated by Cdc5^{PLK} to accomplish the appropriate processing of these repair intermediates.

Resolution of repair intermediates that were subject to crossover interference requires the interaction of Cdc5^{PLK} with the nuclease Exo1 (Sanchez et al., 2020). During meiosis, Exo1 forms a complex with the repair complex MutLγ, which is required for crossover formation and marks crossover sites (Zakharyevich et al., 2012). Unlike other examples involving PLK discussed in this review, the interaction between Exo1 and Cdc5^{PLK} does not depend on phosphorylation of Exo1 by another kinase (Sanchez et al., 2020). Since kinase activity of Cdc5^{PLK} is required for crossover formation independently of its interaction with Exo1, it is proposed that Cdc5^{PLK} phosphorylates yet unidentified targets to promote crossover resolution (Sanchez et al., 2020). The Mus81-Mms4 endonuclease complex also promotes joint-molecule resolution and is responsible for formation of non-interfering crossovers (de los Santos et al., 2003; Jessop and Lichten, 2008). Phosphorylation of Mms4 by Cdc5^{PLK} boosts Mus81-Mms4 activity in late pachynema, and this boost is required for timely resolution of repair intermediates (Matos et al., 2011). By contrast the endonuclease Yen1 is inhibited by Cdc28^{CDK} until the onset of meiosis II and likely serves only as a last resort to resolve persistent repair intermediates (Matos et al., 2011; Arter et al., 2018). Indeed, phosphorylation-resistant Yen1 is constitutively active, and this abnormal activation leads to early resolution of repair intermediates and aberrant crossover patterning (Arter et al., 2018).

The BLM helicase Sgs1 mediates the dissolution of joint molecules and is also regulated via phosphorylation by Cdc28^{CDK} (Grigaitis et al., 2020). Contrary to Yen1, Sgs1 activity is upregulated by Cdc28^{CDK}-dependent phosphorylation, which is required for resolving some repair intermediates into non-crossovers (Grigaitis et al., 2020). In late pachynema, Sgs1 becomes hyper-phosphorylated by Cdc5^{PLK}, and this phosphorylation is dependent on prior CDK phosphorylation (Grigaitis et al., 2020). Cdc5^{PLK}-dependent phosphorylation of Sgs1 has been suggested to reduce its activity, thereby favoring joint-molecule resolution into crossovers in late pachynema (Grigaitis et al., 2020).

THE PACHYTENE CHECKPOINT

Many organisms delay meiotic progression in response to problems in meiotic DSB repair or defects in chromosome synapsis. These delays are similar to the cell-cycle delays observed in the canonical DNA-damage response and help to ensure that cells do not initiate the meiotic divisions with broken chromosomes (Mei et al., 2015; ElInati et al., 2020). The pachytene checkpoint employs the canonical DNA-damage sensor kinases ATR and ATM in most organisms (Hochwagen and Amon, 2006; Subramanian and Hochwagen, 2014). However, there are differences in downstream targets and effectors of this checkpoint.

In budding yeast, where this checkpoint is best understood, Mec1^{ATR}/Tel1^{ATM} phosphorylate the axis protein Hop1^{HORMAD} at T318 as well as other sites (Carballo et al., 2008). Phosphorylated Hop1 recruits and activates Mek1^{CHK2} (Carballo et al., 2008) by mediating Mek1^{CHK2} dimerization and autophosphorylation (Niu et al., 2005, 2007). Phosphorylation of a different Mec1^{ATR} / Tel1^{ATM} site on Hop1, S298, is important to stabilize this interaction especially under checkpoint-activating conditions (Penedos et al., 2015). Mek1^{CHK2} phosphorylates a large number of downstream targets (Suhandynata et al., 2016), one of which is the meiosis-specific transcription factor Ndt80 (Prugar et al., 2017; Chen et al., 2018). Phosphorylation of Ndt80 attenuates its DNA binding and transcriptional activity and prevents expression of Cdc5^{PLK} (Chen et al., 2018), thereby blocking resolution of joint molecules and completion of meiotic prophase (Clyne et al., 2003; Sourirajan and Lichten, 2008; **Figure 4**). In *S. pombe*, Mek1^{CHK2} instead delays meiotic progression by phosphorylating the CDK-activating phosphatase Cdc25 and blocking its localization to the nucleus (Pérez-Hidalgo et al., 2003, 2008). Cdc25 promotes cell-cycle progression by removing the Wee1-dependent inhibitory phosphorylation on Cdc2^{CDK} Y15 (Pérez-Hidalgo et al., 2003, 2008). A role for tyrosine phosphorylation of CDK is also seen in *S. cerevisiae* (Leu and Roeder, 1999), although its regulation is not understood. In mice, ATM and CHK2 are also involved in the establishment of a checkpoint arrest in response to recombination defects (Bolcun-Filas et al., 2014; Pacheco et al., 2015; Rinaldi et al., 2017). Several chromosomal proteins are phosphorylated in a DSB-dependent manner in mice, including the Hop1 homologs HORMAD1/2 (Fukuda et al., 2012), but whether these phosphorylation events are important for checkpoint regulation remains to be investigated.

In multicellular organisms, the pachytene checkpoint also activates apoptosis to eliminate germ cells that exhibit repair defects (Gartner et al., 2000; Barchi et al., 2005; ElInati et al., 2020). In *Drosophila melanogaster*, unrepaired breaks activate Mei-41^{ATR} and lead to the phosphorylation of Mnk^{CHK2} (Ghabrial and Schüpbach, 1999; Abdu et al., 2002; **Figure 5**). Brca2 is also involved in the activation of this checkpoint, presumably through its interaction with the checkpoint protein Rad9 (Klovstad et al., 2008). Mnk^{CHK2} in turn activates the pro-apoptosis protein p53 in response to persistent DSBs (Lu et al., 2010). Genetic experiments also identified a function for ATM and parallel roles for p53 and the p53-like regulator TAp63 in activating apoptosis during mouse spermatogenesis (Marcet-Ortega et al., 2017). In *C. elegans*, induction of apoptosis requires activation of the transducer kinase CHK-1 by ATL-1^{ATR} (Jaramillo-Lambert et al., 2010). The regulation in worms shows pronounced differences between hermaphrodites and males, possibly related to the inherent asynapsis of the monosomic X chromosome in *C. elegans* males (Gartner et al., 2000; Jaramillo-Lambert et al., 2010; Woglar et al., 2013). Moreover, the cell-death response varies depending on the mode of checkpoint activation (Ye et al., 2014).

Intriguingly, the pachytene checkpoint can also affect subsequent germline development. In *Drosophila,* this pathway reduces the levels of the developmental regulator Gurken, leading to impaired egg chamber polarization (Abdu et al., 2002),

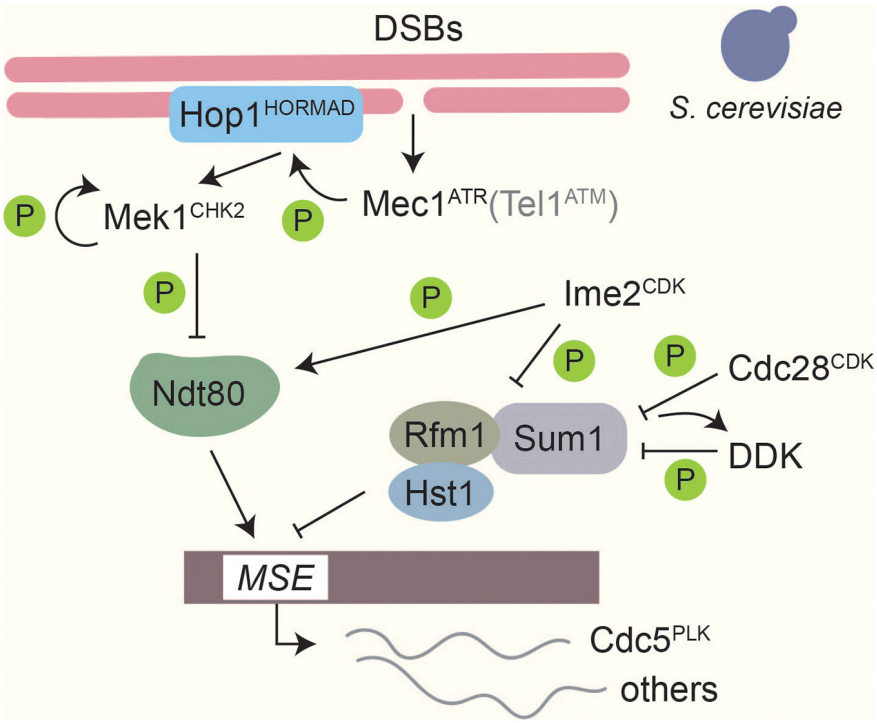

FIGURE 4 | Phosphorylation-based regulation of middle gene transcription in *Saccharomyces cerevisiae*. Transcriptional control of middle genes in *S. cerevisiae* is under the control of several kinases. Formation of DSBs activates Mec1^{ATR}, which in turn activates Mek1^{CHK2} through Hop1 phosphorylation and Mek1^{CHK2} autophosphorylation. Tel1^{ATM} contributes only weakly (Carballo et al., 2008). Ndt80 binding to middle sporulation elements (MSEs) is downregulated by Mek1^{CHK2} phosphorylation (Chen et al., 2018). Thus, when DSBs are present expression of middle sporulation genes is blocked. On the other hand, Ime2^{CDK}-dependent phosphorylation promotes Ndt80 activity and facilitates competition with the Sum1 transcriptional repressor complex on MSEs (Sopko et al., 2002; Benjamin et al., 2003). Ime2^{CDK}, along with Cdc28^{CDK} and Cdc7^{DDK}, also phosphorylates Sum1 to promote dissociation of the repressor complex from MSEs (Lo et al., 2008; Sasanuma et al., 2008; Ahmed et al., 2009; Corbi et al., 2014).

whereas the combined activity of CHK1 and CHK2 is required to reduce oocyte number and promote folliculogenesis in mice (Martínez-Marchal et al., 2020).

The Role of Chromosome Architecture in Checkpoint Activation

Research in a number of organisms has led to the realization that the pachytene checkpoint senses more than just the accumulation of unrepaired DSBs. Although ATM/ATR clearly respond to DSB formation using canonical DNA damage response factors (Subramanian and Hochwagen, 2014), a number of observations indicate additional dependencies for full ATM/ATR activation. For example, the strong arrest response seen in *S. cerevisiae* mutants lacking the Dmc1 recombinase is weakened in mutants that also lack the second recombinase, Rad51, even though both mutants are severely defective in DSB repair (Shinohara et al., 2003). Similarly, the crossover factors MSH-4/5 and ZHP-3^{RNF212} are required for full checkpoint activation in *C. elegans*, raising the possibility that a downstream DNA repair intermediate helps activate the pachytene checkpoint (Silva et al., 2013). Perhaps most strikingly, research in mouse spermatocytes indicates that ATM/ATR are activated by unsynapsed chromosomal regions because the ATM/ATR-dependent γ-H2AX epitope is observed on unpaired X and Y chromosomes even in the absence of SPO11-induced DSBs (Mahadevaiah et al., 2001). Perhaps this activation is related to persistent SPO11-independent damage on asynaptic meiotic chromosomes as seen in mouse oocytes (Rinaldi et al., 2017).

Although the mechanisms of meiotic ATM/ATR activation remain enigmatic, available evidence suggests an important role for chromosome-structure proteins in stimulating full checkpoint activity. Components of the SC are required for checkpoint activation in *S. cerevisiae, C. elegans,* and mice (Xu et al., 1997; Daniel et al., 2011; Kogo et al., 2012; Wojtasz et al., 2012; Kim et al., 2015; Bohr et al., 2016), and altering the relative levels of individual SC components can lead to a severely disrupted checkpoint response without affecting other meiotic processes (Ontoso et al., 2013; Herruzo et al., 2016; Markowitz et al., 2017; Castellano-Pozo et al., 2020; Raina and Vader, 2020). Work in *S. cerevisiae, C. elegans,* and mouse has strongly implicated meiotic HORMAD proteins and their regulator Pch2/TRIP13 in this response. HORMAD proteins are very dynamic chromosomal constituents (Borner et al., 2008; Wojtasz et al., 2009; Subramanian et al., 2016) whose HORMA domain transitions between closed and unbuckled states, a behavior akin to the closed and open conformations of the essential spindle-checkpoint component

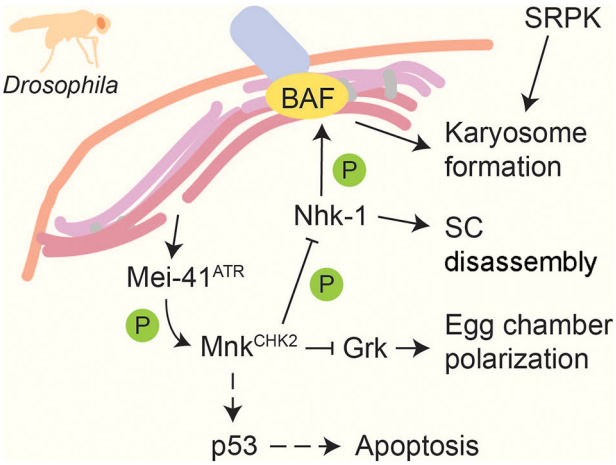

FIGURE 5 | Recombination and meiotic progression in *Drosophila*. DSBs activate the DNA-damage sensor kinase Mei-41^{ATR}, which in turn activates the effector kinase Mnk^{CHK2} (Ghabrial and Schüpbach, 1999; Abdu et al., 2002). Mnk^{CHK2} triggers p53-dependent apoptosis in response to persistent repair defects (Lu et al., 2010). Mnk^{CHK2} also suppresses translation of Gurken (Grk), which promotes egg chamber polarization (Abdu et al., 2002). In addition, Mnk^{Chk2} prevents meiotic progression by inhibiting Nhk-1, which normally prompts SC disassembly and induces karyosome formation by phosphorylating BAF (Ivanovska et al., 2005; Lancaster et al., 2007, 2010). Another kinase, SRPK, positively regulates karyosome formation in a Mnk^{CHK2}- independent manner (Loh et al., 2012). Dashed lines indicate activation in response to persistent DNA damage signal.

MAD2 (Mapelli et al., 2007; Kim et al., 2014; West et al., 2018). The AAA+-ATPase Pch2/TRIP13 facilitates the formation of the unbuckled conformation (Ye et al., 2015; West et al., 2018).

Synapsis defects and recombination defects are signaled through a shared signaling network in several organisms (Hochwagen and Amon, 2006; Kim et al., 2015; Rinaldi et al., 2017). Early work in *C. elegans* suggested that Pch2^{TRIP13} specifically mediates the response to synapsis defects (Bhalla and Dernburg, 2005), and analyses in *S. cerevisiae* indicated the existence of Pch2^{TRIP13}-dependent and Pch2^{TRIP13}-independent checkpoint signaling (Wu and Burgess, 2006), which had been interpreted as separate synapsis and DNA damage sensing pathways (MacQueen and Hochwagen, 2011; Subramanian and Hochwagen, 2014). However, Pch2 responds to defects in DSB repair in *Drosophila* (Joyce and McKim, 2009), and *S. cerevisiae* mutants with defects in both synapsis and DNA repair show more severe Pch2^{TRIP13}-dependent delays than mutants that only affect synapsis (San-Segundo and Roeder, 1999; Humphryes et al., 2013; Herruzo et al., 2016), indicating that Pch2^{TRIP13} acts in the response to DNA repair defects.

Intriguingly, the mode of Pch2^{TRIP13} checkpoint function depends on its binding to the SC (Raina and Vader, 2020). A plausible model is that Pch2^{TRIP13}-mediated accumulation of unbuckled Hop1^{HORMAD} in the nucleoplasm leads to a cell cycle delay whereas an accumulation of unbuckled Hop1^{HORMAD} on chromosomes leads to a checkpoint silencing (Raina and Vader, 2020). Consistent with this model Pch2^{TRIP13} executes its checkpoint-activating function when not bound to chromosomes (Herruzo et al., 2019), and Pch2^{TRIP13}-dependent action on chromosomal Hop1^{HORMAD} silences Mek1^{CHK2}-dependent signaling (Subramanian et al., 2016). The proposed action of Pch2^{TRIP13} on Hop1^{HORMAD} is reminiscent of the function of TRIP13 and MAD2 in the spindle checkpoint (Vader, 2015), and nicely explains why *pch2* mutations tend to alleviate arrests caused by synapsis defects but often strengthen arrests caused by DNA repair defects (Raina and Vader, 2020). What remains unclear is how Hop1^{HORMAD} conformation is interpreted to create the appropriate checkpoint response. Hop1^{HORMAD} phosphorylation is specifically detected on the chromosome-bound pool of Hop1^{HORMAD} (Herruzo et al., 2016; Raina and Vader, 2020), which polymerizes along chromosomes (West et al., 2019). By contrast Hop1 in the nucleoplasm is unphosphorylated and may be monomeric. Notably, Pch2 is necessary for preventing the phosphorylation of nucleoplasmic Hop1 (Lo et al., 2014), perhaps by keeping the HORMA domain unbuckled. However, which receptor interprets this form of Hop1 as a checkpoint signal is unknown. Pch2^{TRIP13} physically interacts with the phospho-binding BRCT domain of the DNA-damage response factor Xrs2^{NBS1}, and this domain is required for pachytene checkpoint function (Ho and Burgess, 2011). Thus, perhaps the BRCT domain provides a mechanism to distinguish phosphorylated chromosomal and unphosphorylated non-chromosomal Hop1^{HORMAD}.

FORMATION OF NUCLEAR BODIES

Several organisms form distinct nuclear bodies in the course of meiotic prophase, including the XY body in mammals and the karyosome in *Drosophila*. The formation of these structures is coordinated with meiotic progression and is regulated by protein phosphorylation.

XY-Body Formation

Failure of chromosome synapsis leads to transcriptional silencing of asynaptic chromosomes in mammals, a phenomenon named meiotic silencing of unsynapsed chromatin (Schimenti, 2005; Turner et al., 2005). An example of this process in action is meiotic sex-chromosome inactivation, which is a regular occurrence during meiosis in spermatocytes (Schimenti, 2005; Turner et al., 2005). As mammalian X and Y sex chromosomes only share sequence homology in their pseudo-autosomal regions, they are mostly asynaptic during meiosis. Asynaptic sex chromosomes become transcriptionally silenced and form a cytologically detectable structure called the sex-body or XY-body through meiotic sex-chromosome inactivation (Solari, 1974; McKee and Handel, 1993).

The XY-body is strongly enriched for the canonical DNA damage mark, γH2AX (histone H2AX phosphorylated on S139), which localizes to the axes and chromatin loops of the asynaptic X and Y chromosomes in spermatocytes (Mahadevaiah et al., 2001). Knockout studies have shown that the H2AX histone variant is required for the establishment of the XY-body, although whether the γH2AX epitope is required has not been answered (Fernandez-Capetillo et al., 2003; Ichijima et al., 2011).

γH2AX accumulation on the XY-body requires the DNA-damage response protein BRCA1, which recruits ATR to asynaptic chromosomes (Keegan et al., 1996; Turner et al., 2004; Bellani et al., 2005; Royo et al., 2013). The other canonical DNA-damage kinases ATM and DNA-PK are dispensable (Turner et al., 2004; Bellani et al., 2005). ATR-dependent phosphorylation of H2AX on the XY axes initially recruits the DNA-damage checkpoint factor MDC1, which mediates the expansion of γH2AX throughout the X and Y chromatin (Ichijima et al., 2011). Mutating a nearby phosphorylatable residue on H2AX, Y142, impairs expansion of the γH2AX signal similar to the loss of MDC1 (Abe et al., 2020). Interestingly, this failure in XY body formation caused a high level of ATR binding and accumulation of other DNA-damage marks on autosomes despite largely normal DSB levels (Abe et al., 2020). This observation led to the proposal that the XY body may provide a sink for DNA-damage signaling molecules, thereby allowing meiotic progression once repair has occurred (Abe et al., 2020). However, it is unclear why no such sink would be necessary during oogenesis, which involves similar levels of recombination but lacks a domain comparable to the XY body. DSB levels, as inferred from RAD51 foci, were elevated on the sex chromosomes in *H2ax-Y142A* but not *Mdc1*KO spermatocytes (Abe et al., 2020), which may point to a role for this residue in regulating DSB repair on asynaptic chromosomes, presumably by inter-sister repair. Interestingly, recruitment of the FHA domain of NBS1 to XY axes requires protein phosphorylation but not MDC1 (Zhang et al., 2020), and may thus be influenced by these histone marks.

In addition to ATR, sex chromosome silencing and XY body formation also requires CDK2 (Viera et al., 2009; Wang et al., 2014), which localizes to the XY body in its activated T160-phosphorylated form (Wang et al., 2014). The T160 phosphorylation enhances the interaction between γH2AX and CDK2 (Wang et al., 2014), but it is likely needed at later stages of XY body formation and gene silencing, because γH2AX localization to XY chromatin was unaffected in the CDK2 T160A mutant (Palmer et al., 2020).

Karyosome Formation

Following recombination in *Drosophila* oocytes, chromosomes cluster into a spherical body called the karyosome, which subsequently nucleates acentrosomal spindle formation for the first meiotic division. A number of mutants with meiotic DSB-repair defects show abnormal karyosome formation (Ghabrial et al., 1998), which can be rescued by inactivation of the checkpoint kinase Mnk^{CHK2} (Abdu et al., 2002), indicating a dependent relationship between karyosome formation and meiotic recombination (**Figure 5**). Mnk^{CHK2} impairs the activity of the nucleosomal histone kinase Nhk-1, which phosphorylates the anchoring factor BAF to release chromosomes from the nuclear envelope (Lancaster et al., 2007, 2010). In addition, karyosome formation is regulated by the conserved kinase SRPK, which is required for heterochromatin clustering (Loh et al., 2012). A spherical chromosome assembly has also been reported in other organisms, including maturing human oocytes (Bogolyubov, 2018), but whether this structure is regulated in a similar manner remains to be determined.

MEIOTIC PROGRESSION

Upon completion of meiotic recombination, meiocytes transition out of meiotic prophase by disassembling their SC and initiating the next steps of the meiotic program. These steps must be coordinated with meiotic recombination to prevent premature prophase exit or persistent SC during the meiotic divisions.

SC Disassembly

Synaptonemal complex disassembly is regulated by phosphorylation in several organisms. SC disassembly in *Drosophila* requires Nhk-1 (Ivanovska et al., 2005), whose regulation by Mnk^{CHK2} helps tie SC disassembly to meiotic DNA repair (Lancaster et al., 2010; **Figure 5**). A similar dependence exists in *C. elegans*, where pro-crossover factors promote the downregulation of MPK-1, leading to the loss of SYP-2 phosphorylation and SC disassembly (Nadarajan et al., 2016). In *S. cerevisiae*, several kinases have been implicated in SC disassembly, including CDK, DDK, $Cdc5^{PLK}$, and $Ipl1^{AuroraB}$ (Sourirajan and Lichten, 2008; Jordan et al., 2009; Argunhan et al., 2017). PLK and Aurora B and C kinases are also required for desynapsis in mammals (Jordan et al., 2012; Wellard et al., 2020). SC disassembly in *S. cerevisiae* is tied to the successful completion of meiotic DSB repair through the control of $Cdc5^{PLK}$ expression, which is maintained at a low level by proteasome-dependent degradation during meiotic prophase (Okaz et al., 2012) and whose expression is regulated at the transcriptional level by $Mek1^{CHK2}$ (Tung et al., 2000; Pak and Segall, 2002b; Chen et al., 2018). However, the targets of $Cdc5^{PLK}$ in promoting SC disassembly remain to be identified.

Transcriptional Regulation of Prophase Exit

In *S. cerevisiae*, exit from meiotic prophase is marked by a strong shift in gene expression, which activates the "middle" genes necessary for completion of the meiotic divisions and spore maturation (Chu and Herskowitz, 1998). Expression of middle genes is under the control of the meiosis-specific transcription factor Ndt80 and the transcriptional repressor complex Sum1/Rfm1/Hst1 (Chu and Herskowitz, 1998; Xie et al., 1999; McCord et al., 2003), which compete for binding to a shared middle-sporulation element in the promoters of target genes. Three kinases are known to regulate Sum1 during meiosis (**Figure 4**). $Ime2^{CDK}$ phosphorylates Sum1 at T306, which interferes with Hst1 binding and promotes Sum1's dissociation from middle-sporulation elements (Moore et al., 2007; Ahmed et al., 2009). In addition, CDK^{Cdc28} phosphorylates Sum1 at multiple sites, including S379 and S512, which prime Sum1 to be phosphorylated by DDK (Lo et al., 2008; Sasanuma et al., 2008; Corbi et al., 2014). Phosphorylation promotes Sum1 removal from middle sporulation elements (MSEs) and is essential for the initiation of *NDT80* transcription (Pak and Segall, 2002a; Ahmed et al., 2009). Once Ndt80 production starts, Ndt80 can compete with Sum1 to bind to MSEs (Pierce et al., 2003). Ime2-dependent phosphorylation of Ndt80 promotes the ability of Ndt80 to bind DNA, and thus increases its activity (Sopko et al., 2002;

Benjamin et al., 2003). Conversely, phosphorylation of Ndt80 by Mek1^{CHK2} reduces its ability to bind to DNA, and thus connects completion of DSB repair to exit from meiotic prophase (Chen et al., 2018; Hollingsworth and Gaglione, 2019).

REVERSAL OF PHOSPHORYLATION

Several phosphatases have been implicated in the regulation of meiotic prophase, although their functions in many cases remain poorly defined. Perhaps the best understood among these is protein phosphatase 4 (PP4), which acts to reverse ATR/ATM-dependent phosphorylation events similar to its function in the canonical DNA damage response (Nakada et al., 2008; Falk et al., 2010; Hustedt et al., 2015). Inactivation of PP4 leads to a number of meiotic defects in *S. cerevisiae* and *C. elegans*, including problems with chromosome synapsis and impaired crossover recombination (Falk et al., 2010; Sato-Carlton et al., 2014). However, so far only a small number of substrates have been identified in *S. cerevisiae*, including γH2AX, Hop1-T318, and Zip1-S75 (Falk et al., 2010; Chuang et al., 2012; Subramanian et al., 2016). PP4 appears to be continuously active during meiotic prophase and may thus require that ATR/ATM repeatedly phosphorylate the same substrates to maintain the DSB response (Falk et al., 2010). This arrangement would permit rapid removal of ATM/ATR-dependent phospho-marks once DSBs are repaired, and ATM and ATR are no longer active. In line with such dynamic regulation of phosphorylation events, binding of the FHA domain of Mek1^{CHK2} stabilizes the phosphorylation of Hop1-T318 (Chuang et al., 2012), possibly by blocking PP4 access. The rapid turnover of phosphorylated histone H2AV during meiotic prophase in *Drosophila* (Joyce et al., 2011) may result from a similar balance of kinase and phosphatase activities. In addition, continued PP4 activity may also help remove spurious or very transient phosphorylation events, as seen for the mitotic checkpoint kinase Rad53^{CHK2}, which accumulates in a phosphorylated form in *pp4* mutants, but is not detectably phosphorylated in response to meiotic DSBs in wild-type cells (Cartagena-Lirola et al., 2008; Falk et al., 2010).

Protein phosphatase 1 (PP1) is another phosphatase implicated in the regulation of meiotic prophase, although its function may differ among organisms. In *C. elegans*, the PP1-interacting protein LAB-1 helps recruit PP1 to chromosomes to restrict the activity of AIR-1^{AuroraB} and promote SC assembly and DSB repair (Tzur et al., 2012). By contrast, PP1 activity is kept low in *S. cerevisiae* through binding of the FK506-binding protein Fpr3, which is important to maintain the activity of the pachytene checkpoint, as premature activation of PP1, or PP1 overexpression, allows DSB-repair mutants to enter the meiotic divisions (Bailis and Roeder, 2000; Hochwagen et al., 2005). Phosphatase inhibition is also important in *Drosophila* where overexpression of Wrd, a B56 subunit of protein phosphatase 2A, leads to delayed assembly and precocious disassembly of the SC, as well as karyosome defects (Barbosa et al., 2021). In this case, low Wrd levels in meiotic prophase depend on the ubiquitin ligase SCF (Barbosa et al., 2021), which presumably targets Wrd for proteasome-mediated degradation. Disruption of PP2A-Cdc55 has also been shown to affect premeiotic DNA replication and interhomolog recombination in *S. cerevisiae* (Nolt et al., 2011). Finally, the transient activation of the phosphatase LIP-1 is thought to counteract the activity of MPK-1, to create a window for damage-dependent germ cell apoptosis in *C. elegans* (Hajnal and Berset, 2002; Rutkowski et al., 2011).

CHALLENGES AHEAD

Research over the past two decades has revealed many profound roles for protein phosphorylation in coordinating the processes of meiotic prophase. However, the rate at which new signaling connections are reported has not slowed, indicating that there are still many regulatory connections that remain to be uncovered before we can gain a systematic understanding of this impressive signaling network. The extent of the unknown is highlighted by a recent phospho-proteomic study, which identified a large number of novel phosphorylation events that were differentially regulated between wild-type and *mek1*^{CHK2} mutants in *S. cerevisiae* (Suhandynata et al., 2016). Although this study also identified many events that resulted from premature prophase exit in *mek1* mutants, a substantial number of novel phosphorylation events of unknown function could be attributed to Mek1 based on consensus sequences. Further targeted and stage-specific proteomic analyses therefore promise to provide a wealth of new information on the phospho-proteome of meiotic prophase.

With identification of phosphorylation sites becoming easier, pinpointing which ones are functionally important will be the difficult question to answer. Kinases can have somewhat promiscuous activity leading to "accidental" phosphorylation events (Levy et al., 2012). These accidental events can be influenced by several factors, including high concentration of a target protein in the proximity to the kinase (Levy et al., 2012). It has been suggested that integration of absolute protein abundance data with phosphorylation data or using stoichiometry of phosphorylation can help prioritize sites for characterization (Levy et al., 2012). However, even mutation of high-confidence sites frequently fails to yield an easily observable phenotype. For example, γH2AX and Mek1-dependent phosphorylation of histone H3 T11 are well-characterized chromatin marks that nevertheless appear to be dispensable for meiotic prophase in *S. cerevisiae* (Shroff et al., 2004; Kniewel et al., 2017). Some phosphorylation events may be unnecessary under standard laboratory conditions but have functions in specific environments or mutant situations. Others may have redundant activities. For example, in *S. cerevisiae* the cohesin Rec8 is phosphorylated at many sites, and the general level of phosphorylation rather than phosphorylation of any individual site is required for function (Brar et al., 2006). Such multi-site phosphorylations can mediate progressive charge accumulation or activate multiple low affinity sites to establish thresholds rather than switches, which can also be established by single phosphorylation events (Nash et al., 2001; Gunawardena, 2005; Salazar and Höfer, 2009). However, in the case of the

abundantly phosphorylated *S. cerevisiae* axis protein Red1, even large-scale mutational sweeps of phosphorylation sites have failed to yield a detectable phenotype (Lai et al., 2011).

Evolutionary conservation is one of the predictors for functional importance of phosphorylation sites (Beltrao et al., 2012; Studer et al., 2016). Implementation of this predictor for meiotic phosphorylation events may be challenging as many meiotic proteins have very little sequence conservation across species (Cole et al., 2010; Kumar et al., 2010). In line with this, there are several examples for phosphorylation events that are important for meiosis but whose sites are not well conserved. These include Hop1 T318, which is essential for meiosis in *S. cerevisiae* but only conserved in yeasts and plants (Carballo et al., 2008) and Mer2 S30, which is absolutely required for formation of DSBs in *S. cerevisiae* but only conserved in yeasts (Wan et al., 2008). Even so, the general mechanisms by which these phosphorylation events act may be conserved even when exact sites are not. For example, mouse HORMAD1 and HORMAD2 contain S/TQ sites, and HORMAD1 is phosphorylated in an ATM/ATR dependent manner like Hop1 (Fukuda et al., 2012). It has been suggested that phosphorylation events that promote interactions through phosphopeptide binding domains (as is the case for Hop1 T318) may evolve more rapidly and may be less dependent on exact location for their function, while phosphorylation events that promote conformational changes may be more conserved (Holt et al., 2009). Similarly, clusters of target sites may show functional redundancy and thus, conservation of some of these sites may be enough to maintain function without a requirement for conservation of the exact position (Holt et al., 2009; Freschi et al., 2014).

A better understanding of phospho-regulation of meiotic prophase will also require a more detailed analysis of the spatial relationships of phosphorylation events. A number of experiments have demonstrated the power of phospho-specific antibodies in dissecting regulatory connections in *C. elegans* and other organisms (Carballo et al., 2008; Penkner et al., 2009; Labella et al., 2011; Woglar et al., 2013; Herruzo et al., 2016; Subramanian et al., 2016; Nadarajan et al., 2017), although the use of these reagents has often been limited to cytological analyses of fixed samples. Using the same antibodies in ChIP-seq experiments could provide complementary information at high genomic resolution, but this experimental route remains comparatively underused. In addition phospho-specific nanobodies and FRET-based kinase sensors (Oldach and Zhang, 2014; Traenkle and Rothbauer, 2017) may provide an opportunity to follow *in vivo* phospho-dynamics, which remains a key frontier in understanding the regulation of meiotic prophase. Finally, it will also be important to understand the crosstalk between protein phosphorylation with other signaling modes and protein modifications, including ubiquitylation and sumoylation, which are abundantly present in meiotic prophase (Cheng et al., 2006; Watts and Hoffmann, 2011; Nottke et al., 2017; Rao et al., 2017; Bhagwat et al., 2021), and to integrate nuclear events with regulation outside of the nucleus. For example, B-type cyclins in *S. cerevisiae* are translationally regulated by phosphorylation of an RNA-binding protein (Berchowitz et al., 2015; Carpenter et al., 2018) and mitochondrial localization is controlled by Ime2 kinase (Sawyer et al., 2019). Thus, notwithstanding the impressive progress in understanding the phospho-regulation of meiotic prophase, much remains to be discovered about this intricate signaling network that ensures the faithful passage of genetic material from one generation to the next.

AUTHOR CONTRIBUTIONS

FMK and AH performed the research and wrote the manuscript. Both authors contributed to the article and approved the submitted version.

FUNDING

This research was funded in part by NIH grant GM111715 to AH. FMK acknowledges funding from the Chair's Graduate Fellowship (NYU). The funders had no role in the assembly of this manuscript.

REFERENCES

Abdu, U., Brodsky, M., and Schüpbach, T. (2002). Activation of a meiotic checkpoint during *Drosophila* oogenesis regulates the translation of gurken through Chk2/Mnk. *Curr. Biol.* 12, 1645–1651. doi: 10.1016/S0960-9822(02)01165-X

Abe, H., Alavattam, K. G., Hu, Y.-C., Pang, Q., Andreassen, P. R., Hegde, R. S., et al. (2020). The initiation of meiotic sex chromosome inactivation sequesters DNA damage signaling from autosomes in mouse spermatogenesis. *Curr. Biol.* 30, 408.e5–420.e5. doi: 10.1016/j.cub.2019.11.064

Abe, H., and Shimoda, C. (2000). Autoregulated expression of Schizosaccharomyces pombe meiosis-specific transcription factor Mei4 and a genome-wide search for its target genes. *Genetics* 154, 1497–1508.

Ahmed, N. T., Bungard, D., Shin, M. E., Moore, M., and Winter, E. (2009). The Ime2 protein kinase enhances the disassociation of the Sum1 repressor from middle meiotic promoters. *Mol. Cell. Biol.* 29, 4352–4362. doi: 10.1128/MCB.00305-09

Argunhan, B., Leung, W., Afshar, N., Terentyev, Y., Subramanian, V. V., Murayama, Y., et al. (2017). Fundamental cell cycle kinases collaborate to ensure timely destruction of the synaptonemal complex during meiosis. *EMBO J.* 36, 2488–2509. doi: 10.15252/embj.201695895

Arter, M., Hurtado-Nieves, V., Oke, A., Zhuge, T., Wettstein, R., Fung, J. C., et al. (2018). Regulated crossing-over requires inactivation of Yen1/GEN1 resolvase during meiotic prophase I. *Dev. Cell* 45, 785.e6–800.e6. doi: 10.1016/j.devcel.2018.05.020

Ashley, T., Walpita, D., and de Rooij, D. G. (2001). Localization of two mammalian cyclin dependent kinases during mammalian meiosis. *J. Cell Sci.* 114(Pt 4), 685–693.

Ashley, T., Westphal, C., Plug-de Maggio, A., and de Rooij, D. G. (2004). The mammalian mid-pachytene checkpoint: meiotic arrest in spermatocytes with a mutation in Atm alone or in combination with a Trp53 (p53) or Cdkn1a (p21/cip1) mutation. *Cytogenet. Genome. Res.* 107, 256–262. doi: 10.1159/000080603

Awasthi, P., Foiani, M., and Kumar, A. (2015). ATM and ATR signaling at a glance. *J. Cell Sci.* 128, 4255–4262. doi: 10.1242/jcs.169730

Bailis, J. M., and Roeder, G. S. (2000). Pachytene exit controlled by reversal of Mek1-dependent phosphorylation. *Cell* 101, 211–221. doi: 10.1016/S0092-8674(00)80831-4

Barbosa, P., Zhaunova, L., Debilio, S., Steccanella, V., Kelly, V., Ly, T., et al. (2021). SCF-Fbxo42 promotes synaptonemal complex assembly by downregulating PP2A-B56. *J. Cell Biol.* 220:e202009167. doi: 10.1083/jcb.202009167

Barchi, M., Mahadevaiah, S., Di Giacomo, M., Baudat, F., de Rooij, D. G., Burgoyne, P. S., et al. (2005). Surveillance of different recombination defects in mouse spermatocytes yields distinct responses despite elimination at an identical developmental stage. *Mol. Cell. Biol.* 25, 7203–7215. doi: 10.1128/MCB.25.16.7203-7215.2005

Baroni, E., Viscardi, V., Cartagena-Lirola, H., Lucchini, G., and Longhese, M. P. (2004). The functions of budding yeast Sae2 in the DNA damage response require Mec1- and Tel1-dependent phosphorylation. *Mol. Cell. Biol.* 24, 4151–4165. doi: 10.1128/MCB.24.10.4151-4165.2004

Bartrand, A. J., Iyasu, D., Marinco, S. M., and Brush, G. S. (2006). Evidence of meiotic crossover control in *Saccharomyces cerevisiae* through Mec1-mediated phosphorylation of replication protein A. *Genetics* 172, 27–39. doi: 10.1534/genetics.105.047845

Bell, S. P., and Labib, K. (2016). Chromosome duplication in *Saccharomyces cerevisiae*. *Genetics* 203, 1027–1067. doi: 10.1534/genetics.115.186452

Bellani, M. A., Romanienko, P. J., Cairatti, D. A., and Camerini-Otero, R. D. (2005). SPO11 is required for sex-body formation, and Spo11 heterozygosity rescues the prophase arrest of Atm-/- spermatocytes. *J. Cell Sci.* 118, 3233–3245. doi: 10.1242/jcs.02466

Beltrao, P., Albanèse, V., Kenner, L. R., Swaney, D. L., Burlingame, A., Villén, J., et al. (2012). Systematic functional prioritization of protein posttranslational modifications. *Cell* 150, 413–425. doi: 10.1016/j.cell.2012.05.036

Benjamin, K. R., Zhang, C., Shokat, K. M., and Herskowitz, I. (2003). Control of landmark events in meiosis by the CDK Cdc28 and the meiosis-specific kinase Ime2. *Genes Dev.* 17, 1524–1539. doi: 10.1101/gad.1101503

Berchowitz, L. E., Kabachinski, G., Walker, M. R., Carlile, T. M., Gilbert, W. V., Schwartz, T. U., et al. (2015). Regulated formation of an amyloid-like translational repressor governs gametogenesis. *Cell* 163, 406–418. doi: 10.1016/j.cell.2015.08.060

Bhagwat, N. R., Owens, S. N., Ito, M., Boinapalli, J. V., Poa, P., Ditzel, A., et al. (2021). SUMO is a pervasive regulator of meiosis. *ELife* 10:e57720. doi: 10.7554/eLife.57720

Bhalla, N., and Dernburg, A. F. (2005). A conserved checkpoint monitors meiotic chromosome synapsis in *Caenorhabditis elegans*. *Science* 310, 1683–1686. doi: 10.1126/science.1117468

Blackford, A. N., and Jackson, S. P. (2017). ATM, ATR, and DNA-PK: the trinity at the heart of the DNA damage response. *Mol. Cell.* 66, 801–817. doi: 10.1016/j.molcel.2017.05.015

Blanco-Rodríguez, J. (2012). Programmed phosphorylation of histone H2AX precedes a phase of DNA double-strand break-independent synapsis in mouse meiosis. *Reproduction* 144, 699–712. doi: 10.1530/REP-12-0326

Blitzblau, H. G., Chan, C. S., Hochwagen, A., and Bell, S. P. (2012). Separation of DNA replication from the assembly of break-competent meiotic chromosomes. *PLoS Genet.* 8:e1002643. doi: 10.1371/journal.pgen.1002643

Blitzblau, H. G., and Hochwagen, A. (2013). ATR/Mec1 prevents lethal meiotic recombination initiation on partially replicated chromosomes in budding yeast. *ELife* 2:e00844. doi: 10.7554/eLife.00844

Boekhout, M., Karasu, M. E., Wang, J., Acquaviva, L., Pratto, F., Brick, K., et al. (2019). REC114 Partner ANKRD31 controls number, timing, and location of meiotic DNA breaks. *Mol. Cell.* 74, 1053.e8–1068.e8. doi: 10.1016/j.molcel.2019.03.023

Bogolyubov, D. S. (2018). Karyosphere (Karyosome): a peculiar structure of the oocyte nucleus. *Int. Rev. Cell Mol. Biol.* 337, 1–48. doi: 10.1016/bs.ircmb.2017.12.001

Bohr, T., Ashley, G., Eggleston, E., Firestone, K., and Bhalla, N. (2016). Synaptonemal complex components are required for meiotic checkpoint function in *Caenorhabditis elegans*. *Genetics* 204, 987–997. doi: 10.1534/genetics.116.191494

Bolcun-Filas, E., Rinaldi, V. D., White, M. E., and Schimenti, J. C. (2014). Reversal of female infertility by Chk2 ablation reveals the oocyte DNA damage checkpoint pathway. *Science* 343, 533–536. doi: 10.1126/science.1247671

Bondarieva, A., Raveendran, K., Telychko, V., Rao, H. B. D. P., Ravindranathan, R., Zorzompokou, C., et al. (2020). Proline-rich protein PRR19 functions with cyclin-like CNTD1 to promote meiotic crossing over in mouse. *Nat. Commun.* 11:3101. doi: 10.1038/s41467-020-16885-3

Borde, V., Goldman, A. S., and Lichten, M. (2000). Direct coupling between meiotic DNA replication and recombination initiation. *Science* 290, 806–809. doi: 10.1126/science.290.5492.806

Borgne, A., Murakami, H., Ayté, J., and Nurse, P. (2002). The G1/S Cyclin Cig2p during meiosis in fission yeast. *Mol. Biol. Cell* 13, 2080–2090. doi: 10.1091/mbc.01-10-0507

Borner, G. V., Barot, A., and Kleckner, N. (2008). Yeast Pch2 promotes domainal axis organization, timely recombination progression, and arrest of defective recombinosomes during meiosis. *Proc. Natl. Acad. Sci. U.S.A.* 105, 3327–3332. doi: 10.1073/pnas.0711864105

Brady, M. M., McMahan, S., and Sekelsky, J. (2018). Loss of *Drosophila* Mei-41/ATR alters meiotic crossover patterning. *Genetics* 208, 579–588. doi: 10.1534/genetics.117.300634

Brandt, J. N., Hussey, K. A., and Kim, Y. (2020). Spatial and temporal control of targeting Polo-like kinase during meiotic prophase. *J. Cell Biol.* 219:e202006094. doi: 10.1083/jcb.202006094

Brar, G. A., Kiburz, B. M., Zhang, Y., Kim, J.-E., White, F., and Amon, A. (2006). Rec8 phosphorylation and recombination promote the step-wise loss of cohesins in meiosis. *Nature* 441, 532–536. doi: 10.1038/nature04794

Brown, M. S., and Bishop, D. K. (2015). DNA strand exchange and reca homologs in meiosis. *Cold Spring Harb. Perspect. Biol.* 7:a016659. doi: 10.1101/cshperspect.a016659

Brush, G. S., Najor, N. A., Dombkowski, A. A., Cukovic, D., and Sawarynski, K. E. (2012). Yeast IME2 functions early in meiosis upstream of cell cycle-regulated SBF and MBF targets. *PLoS One* 7:e31575. doi: 10.1371/journal.pone.0031575

Callender, T. L., Laureau, R., Wan, L., Chen, X., Sandhu, R., Laljee, S., et al. (2016). Mek1 down regulates Rad51 activity during yeast meiosis by phosphorylation of Hed1. *PLoS Genet.* 12:e1006226. doi: 10.1371/journal.pgen.1006226

Cannavo, E., Johnson, D., Andres, S. N., Kissling, V. M., Reinert, J. K., Garcia, V., et al. (2018). Regulatory control of DNA end resection by Sae2 phosphorylation. *Nat. Commun.* 9:4016. doi: 10.1038/s41467-018-06417-5

Carballo, J. A., Johnson, A. L., Sedgwick, S. G., and Cha, R. S. (2008). Phosphorylation of the axial element protein Hop1 by Mec1/Tel1 ensures meiotic interhomolog recombination. *Cell* 132, 758–770. doi: 10.1016/j.cell.2008.01.035

Carballo, J. A., Panizza, S., Serrentino, M. E., Johnson, A. L., Geymonat, M., Borde, V., et al. (2013). Budding yeast atm/atr control meiotic double-strand break (DSB) levels by down-regulating Rec114, an essential component of the DSB-machinery. *PLoS Genet.* 9:e1003545. doi: 10.1371/journal.pgen.1003545

Carpenter, K., Bell, R. B., Yunus, J., Amon, A., and Berchowitz, L. E. (2018). Phosphorylation-mediated clearance of amyloid-like assemblies in meiosis. *Dev. Cell* 45, 392.e6–405.e6. doi: 10.1016/j.devcel.2018.04.001

Cartagena-Lirola, H., Guerini, I., Manfrini, N., Lucchini, G., and Longhese, M. P. (2008). Role of the *Saccharomyces cerevisiae* Rad53 checkpoint kinase in signaling double-strand breaks during the meiotic cell cycle. *Mol. Cell. Biol.* 28, 4480–4493. doi: 10.1128/MCB.00375-08

Castellano-Pozo, M., Pacheco, S., Sioutas, G., Jaso-Tamame, A. L., Dore, M. H., Karimi, M. M., et al. (2020). Surveillance of cohesin-supported chromosome structure controls meiotic progression. *Nat. Commun.* 11:4345. doi: 10.1038/s41467-020-18219-9

Checchi, P. M., Lawrence, K. S., Van, M. V., Larson, B. J., and Engebrecht, J. (2014). Pseudosynapsis and decreased stringency of meiotic repair pathway choice on the hemizygous sex chromosome of *Caenorhabditis elegans* males. *Genetics* 197, 543–560. doi: 10.1534/genetics.114.164152

Chen, X., Gaglione, R., Leong, T., Bednor, L., de los Santos, T., Luk, E., et al. (2018). Mek1 coordinates meiotic progression with DNA break repair by directly

phosphorylating and inhibiting the yeast pachytene exit regulator Ndt80. *PLoS Genet.* 14:e1007832. doi: 10.1371/journal.pgen.1007832

Chen, X., Suhandynata, R. T., Sandhu, R., Rockmill, B., Mohibullah, N., Niu, H., et al. (2015). Phosphorylation of the synaptonemal complex protein zip1 regulates the crossover/noncrossover decision during yeast meiosis. *PLoS Biol.* 13:e1002329. doi: 10.1371/journal.pbio.1002329

Cheng, C. H., Lo, Y. H., Liang, S. S., Ti, S. C., Lin, F. M., Yeh, C. H., et al. (2006). SUMO modifications control assembly of synaptonemal complex and polycomplex in meiosis of *Saccharomyces cerevisiae*. *Genes Dev.* 20, 2067–2081. doi: 10.1101/gad.1430406

Chotiner, J. Y., Wolgemuth, D. J., and Wang, P. J. (2019). Functions of cyclins and CDKs in mammalian gametogenesis†. *Biol. Reprod.* 101, 591–601. doi: 10.1093/biolre/ioz070

Chu, S., and Herskowitz, I. (1998). Gametogenesis in yeast is regulated by a transcriptional cascade dependent on Ndt80. *Mol. Cell.* 1, 685–696.

Chuang, C.-N., Cheng, Y.-H., and Wang, T.-F. (2012). Mek1 stabilizes Hop1-Thr318 phosphorylation to promote interhomolog recombination and checkpoint responses during yeast meiosis. *Nucleic Acids Res.* 40, 11416–11427. doi: 10.1093/nar/gks920

Cimprich, K. A., and Cortez, D. (2008). ATR: an essential regulator of genome integrity. *Nat. Rev. Mol. Cell Biol.* 9, 616–627. doi: 10.1038/nrm2450

Clifford, D. M., Marinco, S. M., and Brush, G. S. (2004). The meiosis-specific protein kinase Ime2 directs phosphorylation of replication protein A. *J. Biol. Chem.* 279, 6163–6170. doi: 10.1074/jbc.M306943200

Clyne, R. K., Katis, V. L., Jessop, L., Benjamin, K. R., Herskowitz, I., Lichten, M., et al. (2003). Polo-like kinase Cdc5 promotes chiasmata formation and cosegregation of sister centromeres at meiosis I. *Nat. Cell Biol.* 5, 480–485. doi: 10.1038/ncb977

Cole, F., Keeney, S., and Jasin, M. (2010). Evolutionary conservation of meiotic DSB proteins: more than just Spo11. *Genes Dev.* 24, 1201–1207. doi: 10.1101/gad.1944710

Corbi, D., Sunder, S., Weinreich, M., Skokotas, A., Johnson, E. S., and Winter, E. (2014). Multisite phosphorylation of the Sum1 transcriptional repressor by S-phase kinases controls exit from meiotic prophase in yeast. *Mol. Cell. Biol.* 34, 2249–2263. doi: 10.1128/MCB.01413-13

Culligan, K. M., and Britt, A. B. (2008). Both ATM and ATR promote the efficient and accurate processing of programmed meiotic double-strand breaks. *Plant J.* 55, 629–638. doi: 10.1111/j.1365-313X.2008.03530.x

Daniel, K., Lange, J., Hached, K., Fu, J., Anastassiadis, K., Roig, I., et al. (2011). Meiotic homologue alignment and its quality surveillance are controlled by mouse HORMAD1. *Nat. Cell Biol.* 13, 599–610. doi: 10.1038/ncb2213

Das, D., Chen, S.-Y., and Arur, S. (2020). ERK phosphorylates chromosomal axis component HORMA domain protein HTP-1 to regulate oocyte numbers. *Sci. Adv.* 6:eabc5580. doi: 10.1126/sciadv.abc5580

de los Santos, T., Hunter, N., Lee, C., Larkin, B., Loidl, J., and Hollingsworth, N. M. (2003). The Mus81/Mms4 endonuclease acts independently of double-Holliday junction resolution to promote a distinct subset of crossovers during meiosis in budding yeast. *Genetics* 164, 81–94.

Dirick, L., Goetsch, L., Ammerer, G., and Byers, B. (1998). Regulation of meiotic s phase by Ime2 and a Clb5,6-associated kinase in *Saccharomyces cerevisiae*. *Science* 281, 1854–1857. doi: 10.1126/science.281.5384.1854

ElInati, E., Zielinska, A. P., McCarthy, A., Kubikova, N., Maciulyte, V., Mahadevaiah, S., et al. (2020). The BCL-2 pathway preserves mammalian genome integrity by eliminating recombination-defective oocytes. *Nat. Commun.* 11:2598. doi: 10.1038/s41467-020-16441-z

Enguita-Marruedo, A., Martín-Ruiz, M., García, E., Gil-Fernández, A., Parra, M. T., Viera, A., et al. (2019). Transition from a meiotic to a somatic-like DNA damage response during the pachytene stage in mouse meiosis. *PLoS Genet.* 15:e1007439. doi: 10.1371/journal.pgen.1007439

Falk, J. E., Chan, A. C., Hoffmann, E., and Hochwagen, A. (2010). A Mec1- and PP4-dependent checkpoint couples centromere pairing to meiotic recombination. *Dev. Cell* 19, 599–611. doi: 10.1016/j.devcel.2010.09.006

Fernandez-Capetillo, O., Mahadevaiah, S. K., Celeste, A., Romanienko, P. J., Camerini-Otero, R. D., Bonner, W. M., et al. (2003). H2AX Is required for chromatin remodeling and inactivation of sex chromosomes in male mouse meiosis. *Dev. Cell* 4, 497–508. doi: 10.1016/S1534-5807(03)00093-5

Fowler, K. R., Hyppa, R. W., Cromie, G. A., and Smith, G. R. (2018). Physical basis for long-distance communication along meiotic chromosomes. *Proc. Natl. Acad. Sci. U.S.A.* 115, E9333–E9342. doi: 10.1073/pnas.1801920115

Freschi, L., Osseni, M., and Landry, C. R. (2014). Functional divergence and evolutionary turnover in mammalian *Phosphoproteomes*. *PLoS Genet.* 10:e1004062. doi: 10.1371/journal.pgen.1004062

Fukuda, T., Pratto, F., Schimenti, J. C., Turner, J. M. A., Camerini-Otero, R. D., and Höög, C. (2012). Phosphorylation of chromosome core components may serve as axis marks for the status of chromosomal events during mammalian meiosis. *PLoS Genet.* 8:e1002485. doi: 10.1371/journal.pgen.1002485

Gao, J., and Colaiácovo, M. P. (2018). Zipping and unzipping: protein modifications regulating synaptonemal complex dynamics. *Trends Genet.* 34, 232–245. doi: 10.1016/j.tig.2017.12.001

Garcia, V., Gray, S., Allison, R. M., Cooper, T. J., and Neale, M. J. (2015). Tel1ATM-mediated interference suppresses clustered meiotic double-strand-break formation. *Nature* 520, 114–118. doi: 10.1038/nature13993

Garcia-Muse, T., Galindo-Diaz, U., Garcia-Rubio, M., Martin, J. S., Polanowska, J., O'Reilly, N., et al. (2019). A meiotic checkpoint alters repair partner bias to permit inter-sister repair of persistent DSBs. *Cell Rep.* 26, 775.e5–787.e5. doi: 10.1016/j.celrep.2018.12.074

Gartner, A., Milstein, S., Ahmed, S., Hodgkin, J., and Hengartner, M. O. (2000). A conserved checkpoint pathway mediates DNA damage–induced *Apoptosis* and cell cycle arrest in *C. elegans*. *Mol. Cell* 5, 435–443. doi: 10.1016/S1097-2765(00)80438-4

Geisinger, A., and Benavente, R. (2016). Mutations in genes coding for synaptonemal complex proteins and their impact on human fertility. *Cytogenet. Genome. Res* 150, 77–85. doi: 10.1159/000453344

Ghabrial, A., Ray, R. P., and Schupbach, T. (1998). Okra and spindle-B encode components of the RAD52 DNA repair pathway and affect meiosis and patterning in *Drosophila* oogenesis. *Genes Dev.* 12, 2711–2723. doi: 10.1101/gad.12.17.2711

Ghabrial, A., and Schüpbach, T. (1999). Activation of a meiotic checkpoint regulates translation of Gurken during *Drosophila* oogenesis. *Nat. Cell Biol.* 1, 354–357. doi: 10.1038/14046

Goldfarb, T., and Lichten, M. (2010). Frequent and efficient use of the sister chromatid for DNA double-strand break repair during budding yeast meiosis. *PLoS Biol.* 8:e1000520. doi: 10.1371/journal.pbio.1000520

Gray, S., Allison, R. M., Garcia, V., Goldman, A. S. H., and Neale, M. J. (2013). Positive regulation of meiotic DNA double-strand break formation by activation of the DNA damage checkpoint kinase Mec1(ATR). *Open Biol.* 3:130019. doi: 10.1098/rsob.130019

Gray, S., and Cohen, P. E. (2016). Control of meiotic crossovers: from double-strand break formation to designation. *Annu. Rev. Genet.* 50, 175–210. doi: 10.1146/annurev-genet-120215-035111

Gray, S., Santiago, E. R., Chappie, J. S., and Cohen, P. E. (2020). Cyclin N-terminal domain-containing-1 coordinates meiotic crossover formation with cell-cycle progression in a cyclin-independent manner. *Cell Rep.* 32:107858. doi: 10.1016/j.celrep.2020.107858

Grigaitis, R., Ranjha, L., Wild, P., Kasaciunaite, K., Ceppi, I., Kissling, V., et al. (2020). Phosphorylation of the RecQ Helicase Sgs1/BLM controls Its DNA unwinding activity during meiosis and mitosis. *Dev. Cell* 53, 706.e5–723.e5. doi: 10.1016/j.devcel.2020.05.016

Gunawardena, J. (2005). Multisite protein phosphorylation makes a good threshold but can be a poor switch. *Proc. Natl. Acad. Sci. U.S.A.* 102, 14617–14622. doi: 10.1073/pnas.0507322102

Hajnal, A., and Berset, T. (2002). The C.elegans MAPK phosphatase LIP-1 is required for the G2/M meiotic arrest of developing oocytes. *EMBO J.* 21, 4317–4326. doi: 10.1093/emboj/cdf430

Harper, N. C., Rillo, R., Jover-Gil, S., Assaf, Z. J., Bhalla, N., and Dernburg, A. F. (2011). Pairing centers recruit a polo-like kinase to orchestrate meiotic chromosome dynamics in *C. elegans*. *Dev. Cell* 21, 934–947. doi: 10.1016/j.devcel.2011.09.001

Hartwell, L., and Weinert, T. (1989). Checkpoints: controls that ensure the order of cell cycle events. *Science* 246, 629–634. doi: 10.1126/science.2683079

He, W., Rao, H. B. D. P., Tang, S., Bhagwat, N., Kulkarni, D. S., Ma, Y., et al. (2020). Regulated proteolysis of MutSγ controls meiotic crossing over. *Mol. Cell.* 78, 168.e5–183.e5. doi: 10.1016/j.molcel.2020.02.001

Henderson, K. A., Kee, K., Maleki, S., Santini, P. A., and Keeney, S. (2006). Cyclin-dependent kinase directly regulates initiation of meiotic recombination. *Cell* 125, 1321–1332. doi: 10.1016/j.cell.2006.04.039

Herruzo, E., Ontoso, D., González-Arranz, S., Cavero, S., Lechuga, A., and San-Segundo, P. A. (2016). The Pch2 AAA+ ATPase promotes phosphorylation of the Hop1 meiotic checkpoint adaptor in response to synaptonemal complex defects. *Nucleic Acids Res.* 44, 7722–7741. doi: 10.1093/nar/gkw506

Herruzo, E., Santos, B., Freire, R., Carballo, J. A., and San-Segundo, P. A. (2019). Characterization of Pch2 localization determinants reveals a nucleolar-independent role in the meiotic recombination checkpoint. *Chromosoma* 128, 297–316. doi: 10.1007/s00412-019-00696-7

Hiraoka, Y., and Dernburg, A. F. (2009). The sun rises on meiotic chromosome dynamics. *Dev. Cell* 17, 598–605. doi: 10.1016/j.devcel.2009.10.014

Ho, H.-C., and Burgess, S. M. (2011). Pch2 acts through Xrs2 and Tel1/ATM to modulate interhomolog bias and checkpoint function during meiosis. *PLoS Genet.* 7:e1002351. doi: 10.1371/journal.pgen.1002351

Hochwagen, A., and Amon, A. (2006). Checking your breaks: surveillance mechanisms of meiotic recombination. *Curr. Biol.* 16, R217–R228. doi: 10.1016/j.cub.2006.03.009

Hochwagen, A., Tham, W.-H., Brar, G. A., and Amon, A. (2005). The FK506 binding protein Fpr3 counteracts protein phosphatase 1 to maintain meiotic recombination checkpoint activity. *Cell* 122, 861–873. doi: 10.1016/j.cell.2005.07.010

Hollingsworth, N. M. (2010). Phosphorylation and the creation of interhomolog bias during meiosis in yeast. *Cell Cycle* 9, 436–437. doi: 10.4161/cc.9.3.10773

Hollingsworth, N. M., and Gaglione, R. (2019). The meiotic-specific Mek1 kinase in budding yeast regulates interhomolog recombination and coordinates meiotic progression with double-strand break repair. *Curr. Genet.* 65, 631–641. doi: 10.1007/s00294-019-00937-3

Holloway, J. K., Sun, X., Yokoo, R., Villeneuve, A. M., and Cohen, P. E. (2014). Mammalian CNTD1 is critical for meiotic crossover maturation and deselection of excess precrossover sites. *J. Cell Biol.* 205, 633–641. doi: 10.1083/jcb.201401122

Holt, L. J., Hutti, J. E., Cantley, L. C., and Morgan, D. O. (2007). Evolution of Ime2 phosphorylation sites on Cdk1 substrates provides a mechanism to limit the effects of the phosphatase Cdc14 in meiosis. *Mol. Cell.* 25, 689–702. doi: 10.1016/j.molcel.2007.02.012

Holt, L. J., Tuch, B. B., Villen, J., Johnson, A. D., Gygi, S. P., and Morgan, D. O. (2009). Global analysis of Cdk1 substrate phosphorylation sites provides insights into evolution. *Science* 325, 1682–1686. doi: 10.1126/science.1172867

Honigberg, S. M. (2004). Ime2p and Cdc28p: co-pilots driving meiotic development. *J. Cell. Biochem.* 92, 1025–1033. doi: 10.1002/jcb.20131

Huertas, P., Cortés-Ledesma, F., Sartori, A. A., Aguilera, A., and Jackson, S. P. (2008). CDK targets Sae2 to control DNA-end resection and homologous recombination. *Nature* 455, 689–692. doi: 10.1038/nature07215

Humphryes, N., and Hochwagen, A. (2014). A non-sister act: recombination template choice during meiosis. *Exp. Cell Res.* 329, 53–60. doi: 10.1016/j.yexcr.2014.08.024

Humphryes, N., Leung, W.-K., Argunhan, B., Terentyev, Y., Dvorackova, M., and Tsubouchi, H. (2013). The Ecm11-Gmc2 complex promotes synaptonemal complex formation through assembly of transverse filaments in budding yeast. *PLoS Genet.* 9:e1003194. doi: 10.1371/journal.pgen.1003194

Hunter, N. (2013). "Meiosis," in *Encyclopedia of Biological Chemistry*, eds William J. Lennarz and M. Daniel Lane, 2nd Edn. (Waltham, MA: Academic Press), 17–23. doi: 10.1016/B978-0-12-378630-2.00474-6

Hunter, N. (2015). Meiotic recombination: the essence of heredity. *Cold Spring Harb. Perspect. Biol.* 7:a016618. doi: 10.1101/cshperspect.a016618

Hustedt, N., Seeber, A., Sack, R., Tsai-Pflugfelder, M., Bhullar, B., Vlaming, H., et al. (2015). Yeast PP4 interacts with ATR homolog Ddc2-Mec1 and regulates checkpoint signaling. *Mol. Cell.* 57, 273–289. doi: 10.1016/j.molcel.2014.11.016

Ichijima, Y., Ichijima, M., Lou, Z., Nussenzweig, A., Camerini-Otero, R. D., Chen, J., et al. (2011). MDC1 directs chromosome-wide silencing of the sex chromosomes in male germ cells. *Genes Dev.* 25, 959–971. doi: 10.1101/gad.2030811

Ivanovska, I., Khandan, T., Ito, T., and Orr-Weaver, T. L. (2005). A histone code in meiosis: the histone kinase, NHK-1, is required for proper chromosomal architecture in *Drosophila* oocytes. *Genes Dev.* 19, 2571–2582. doi: 10.1101/gad.1348905

Jaramillo-Lambert, A., Harigaya, Y., Vitt, J., Villeneuve, A., and Engebrecht, J. (2010). Meiotic errors activate checkpoints that improve gamete quality without triggering *Apoptosis* in male germ cells. *Curr. Biol.* 20, 2078–2089. doi: 10.1016/j.cub.2010.10.008

Jessop, L., and Lichten, M. (2008). Mus81/Mms4 endonuclease and sgs1 helicase collaborate to ensure proper recombination intermediate metabolism during meiosis. *Mol. Cell.* 31, 313–323. doi: 10.1016/j.molcel.2008.05.021

Jordan, P. W., Copsey, A., Newnham, L., Kolar, E., Lichten, M., and Hoffmann, E. (2009). Ipl1/Aurora B kinase coordinates synaptonemal complex disassembly with cell cycle progression and crossover formation in budding yeast meiosis. *Genes Dev.* 23, 2237–2251. doi: 10.1101/gad.536109

Jordan, P. W., Karppinen, J., and Handel, M. A. (2012). Polo-like kinase is required for synaptonemal complex disassembly and phosphorylation in mouse spermatocytes. *J. Cell Sci.* 125, 5061–5072. doi: 10.1242/jcs.105015

Joyce, E. F., and McKim, K. S. (2009). *Drosophila* PCH2 is required for a pachytene checkpoint that monitors double-strand-break-independent events leading to meiotic crossover formation. *Genetics* 181, 39–51. doi: 10.1534/genetics.108.093112

Joyce, E. F., Pedersen, M., Tiong, S., White-Brown, S. K., Paul, A., Campbell, S. D., et al. (2011). *Drosophila* ATM and ATR have distinct activities in the regulation of meiotic DNA damage and repair. *J. Cell Biol.* 195, 359–367. doi: 10.1083/jcb.201104121

Kee, K., Protacio, R. U., Arora, C., and Keeney, S. (2004). Spatial organization and dynamics of the association of Rec102 and Rec104 with meiotic chromosomes. *EMBO J.* 23, 1815–1824. doi: 10.1038/sj.emboj.7600184

Keegan, K. S., Holtzman, D. A., Plug, A. W., Christenson, E. R., Brainerd, E. E., Flaggs, G., et al. (1996). The Atr and Atm protein kinases associate with different sites along meiotically pairing chromosomes. *Genes Dev.* 10, 2423–2437. doi: 10.1101/gad.10.19.2423

Kim, J., and Choi, K. (2019). Signaling-mediated meiotic recombination in plants. *Curr. Opin. Plant Biol.* 51, 44–50. doi: 10.1016/j.pbi.2019.04.001

Kim, K. P., Weiner, B. M., Zhang, L., Jordan, A., Dekker, J., and Kleckner, N. (2010). Sister cohesion and structural axis components mediate homolog bias of meiotic recombination. *Cell* 143, 924–937. doi: 10.1016/j.cell.2010.11.015

Kim, Y., Kostow, N., and Dernburg, A. F. (2015). The chromosome axis mediates feedback control of CHK-2 to ensure crossover formation in *C. elegans*. *Dev. Cell* 35, 247–261. doi: 10.1016/j.devcel.2015.09.021

Kim, Y., Rosenberg, S. C., Kugel, C. L., Kostow, N., Rog, O., Davydov, V., et al. (2014). The chromosome axis controls meiotic events through a hierarchical assembly of HORMA domain proteins. *Dev. Cell* 31, 487–502. doi: 10.1016/j.devcel.2014.09.013

Klovstad, M., Abdu, U., and Schüpbach, T. (2008). *Drosophila* brca2 is required for mitotic and meiotic DNA repair and efficient activation of the meiotic recombination checkpoint. *PLoS Genet.* 4:e31. doi: 10.1371/journal.pgen.0040031

Kniewel, R., Murakami, H., Liu, Y., Ito, M., Ohta, K., Hollingsworth, N. M., et al. (2017). Histone H3 threonine 11 phosphorylation is catalyzed directly by the meiosis-specific kinase Mek1 and provides a molecular readout of Mek1 activity in vivo. *Genetics* 207, 1313–1333. doi: 10.1534/genetics.117.300359

Kogo, H., Tsutsumi, M., Inagaki, H., Ohye, T., Kiyonari, H., and Kurahashi, H. (2012). HORMAD2 is essential for synapsis surveillance during meiotic prophase via the recruitment of ATR activity. *Genes Cells* 17, 897–912. doi: 10.1111/gtc.12005

Kumar, R., Bourbon, H.-M., and de Massy, B. (2010). Functional conservation of Mei4 for meiotic DNA double-strand break formation from yeasts to mice. *Genes Dev.* 24, 1266–1280. doi: 10.1101/gad.571710

Kurzbauer, M.-T., Janisiw, M. P., Paulin, L. F., Prusén Mota, I., Tomanov, K., Krsicka, O., et al. (2021). ATM controls meiotic DNA double-strand break formation and recombination and affects synaptonemal complex organization in plants. *Plant Cell* doi: 10.1093/plcell/koab045

Labella, S., Woglar, A., Jantsch, V., and Zetka, M. (2011). Polo kinases establish links between meiotic chromosomes and cytoskeletal forces essential for homolog pairing. *Dev. Cell* 21, 948–958. doi: 10.1016/j.devcel.2011.07.011

Lai, Y.-J., Lin, F.-M., Chuang, M.-J., Shen, H.-J., and Wang, T.-F. (2011). Genetic requirements and meiotic function of phosphorylation of the yeast axial element protein Red1. *Mol. Cell. Biol.* 31, 912–923. doi: 10.1128/MCB.00895-10

Lake, C. M., and Hawley, R. S. (2021). Synaptonemal complex. *Curr. Biol.* 31, R225–R227. doi: 10.1016/j.cub.2021.01.015

Lam, I., and Keeney, S. (2015). Mechanism and regulation of meiotic recombination initiation. *Cold Spring Harb. Perspect. Biol.* 7:a016634. doi: 10.1101/cshperspect.a016634

Lancaster, O. M., Breuer, M., Cullen, C. F., Ito, T., and Ohkura, H. (2010). The meiotic recombination checkpoint suppresses NHK-1 kinase to prevent reorganisation of the oocyte nucleus in *Drosophila*. *PLoS Genet.* 6:e1001179. doi: 10.1371/journal.pgen.1001179

Lancaster, O. M., Cullen, C. F., and Ohkura, H. (2007). NHK-1 phosphorylates BAF to allow karyosome formation in the *Drosophila* oocyte nucleus. *J. Cell Biol.* 179, 817–824. doi: 10.1083/jcb.200706067

Lange, J., Pan, J., Cole, F., Thelen, M. P., Jasin, M., and Keeney, S. (2011). ATM controls meiotic double-strand-break formation. *Nature* 479, 237–240. doi: 10.1038/nature10508

Lao, J. P., and Hunter, N. (2010). Trying to avoid your sister. *PLoS Biol.* 8:e1000519. doi: 10.1371/journal.pbio.1000519

Lee, M.-H., Ohmachi, M., Arur, S., Nayak, S., Francis, R., Church, D., et al. (2007). Multiple functions and dynamic activation of MPK-1 extracellular signal-regulated kinase signaling in *Caenorhabditis elegans* germline development. *Genetics* 177, 2039–2062. doi: 10.1534/genetics.107.081356

Leu, J.-Y., and Roeder, G. S. (1999). The pachytene checkpoint in *S. cerevisiae* depends on Swe1-Mediated phosphorylation of the cyclin-dependent kinase Cdc28. *Mol. Cell* 4, 805–814. doi: 10.1016/S1097-2765(00)80390-1

Levy, E. D., Michnick, S. W., and Landry, C. R. (2012). Protein abundance is key to distinguish promiscuous from functional phosphorylation based on evolutionary information. *Philos. Trans. R. Soc. B Biol. Sci.* 367, 2594–2606. doi: 10.1098/rstb.2012.0078

Li, W., and Yanowitz, J. L. (2019). ATM and ATR influence meiotic crossover formation through antagonistic and overlapping functions in *Caenorhabditis elegans*. *Genetics* 212, 431–443. doi: 10.1534/genetics.119.302193

Lin, F.-M., Lai, Y.-J., Shen, H.-J., Cheng, Y.-H., and Wang, T.-F. (2010). Yeast axial-element protein, Red1, binds SUMO chains to promote meiotic interhomologue recombination and chromosome synapsis. *EMBO J.* 29, 586–596. doi: 10.1038/emboj.2009.362

Liu, Y., Gaines, W. A., Callender, T., Busygina, V., Oke, A., Sung, P., et al. (2014). Down-regulation of Rad51 activity during meiosis in yeast prevents competition with Dmc1 for repair of double-strand breaks. *PLoS Genet.* 10:e1004005. doi: 10.1371/journal.pgen.1004005

Lo, H.-C., Wan, L., Rosebrock, A., Futcher, B., and Hollingsworth, N. M. (2008). Cdc7-Dbf4 regulates NDT80 transcription as well as reductional segregation during budding yeast meiosis. *Mol. Biol. Cell* 19, 4956–4967. doi: 10.1091/mbc.e08-07-0755

Lo, Y.-H., Chuang, C.-N., and Wang, T.-F. (2014). Pch2 prevents Mec1/Tel1-mediated Hop1 phosphorylation occurring independently of Red1 in budding yeast meiosis. *PLoS One* 9:e85687. doi: 10.1371/journal.pone.0085687

Loh, B. J., Cullen, C. F., Vogt, N., and Ohkura, H. (2012). The conserved kinase SRPK regulates karyosome formation and spindle microtubule assembly in *Drosophila* oocytes. *J. Cell Sci.* 125, 4457–4462. doi: 10.1242/jcs.107979

Loidl, J., and Mochizuki, K. (2009). Tetrahymena meiotic nuclear reorganization is induced by a checkpoint kinase–dependent response to DNA damage. *Mol. Biol. Cell* 20, 2428–2437. doi: 10.1091/mbc.e08-10-1058

Lu, W.-J., Chapo, J., Roig, I., and Abrams, J. M. (2010). Meiotic recombination provokes functional activation of the p53 Regulatory network. *Science* 328, 1278–1281. doi: 10.1126/science.1185640

Lydall, D., Nikolsky, Y., Bishop, D. K., and Weinert, T. (1996). A meiotic recombination checkpoint controlled by mitotic checkpoint genes. *Nature* 383, 840–843. doi: 10.1038/383840a0

MacKenzie, A. M., and Lacefield, S. (2020). CDK Regulation of meiosis: lessons from *S. cerevisiae* and *S. pombe*. *Genes* 11:723. doi: 10.3390/genes11070723

MacQueen, A. J., and Villeneuve, A. M. (2001). Nuclear reorganization and homologous chromosome pairing during meiotic prophase require *C. elegans* chk-2. *Genes Dev.* 15, 1674–1687. doi: 10.1101/gad.902601

MacQueen, A. J., and Hochwagen, A. (2011). Checkpoint mechanisms: the puppet masters of meiotic prophase. *Trends Cell Biol.* 21, 393–400. doi: 10.1016/j.tcb.2011.03.004

Mahadevaiah, S. K., Turner, J. M. A., Baudat, F., Rogakou, E. P., de Boer, P., Blanco-Rodríguez, J., et al. (2001). Recombinational DNA double-strand breaks in mice precede synapsis. *Nat. Genet.* 27, 271–276. doi: 10.1038/85830

Malapeira, J., Moldón, A., Hidalgo, E., Smith, G. R., Nurse, P., and Ayté, J. (2005). A meiosis-specific cyclin regulated by splicing is required for proper progression through meiosis. *Mol. Cell. Biol.* 25, 6330–6337. doi: 10.1128/MCB.25.15.6330-6337.2005

Manfrini, N., Guerini, I., Citterio, A., Lucchini, G., and Longhese, M. P. (2010). Processing of meiotic DNA double strand breaks requires cyclin-dependent kinase and multiple nucleases*. *J. Biol. Chem.* 285, 11628–11637. doi: 10.1074/jbc.M110.104083

Mapelli, M., Massimiliano, L., Santaguida, S., and Musacchio, A. (2007). The Mad2 conformational dimer: structure and implications for the spindle assembly checkpoint. *Cell* 131, 730–743. doi: 10.1016/j.cell.2007.08.049

Marcet-Ortega, M., Pacheco, S., Martínez-Marchal, A., Castillo, H., Flores, E., Jasin, M., et al. (2017). P53 and TAp63 participate in the recombination-dependent pachytene arrest in mouse spermatocytes. *PLoS Genet.* 13:e1006845. doi: 10.1371/journal.pgen.1006845

Marechal, A., and Zou, L. (2013). DNA Damage Sensing by the ATM and ATR Kinases. *Cold Spring Harb. Perspect. Biol.* 5:a012716. doi: 10.1101/cshperspect.a012716

Markowitz, T. E., Suarez, D., Blitzblau, H. G., Patel, N. J., Markhard, A. L., MacQueen, A. J., et al. (2017). Reduced dosage of the chromosome axis factor Red1 selectively disrupts the meiotic recombination checkpoint in *Saccharomyces cerevisiae*. *PLoS Genet.* 13:e1006928. doi: 10.1371/journal.pgen.1006928

Martínez-Marchal, A., Huang, Y., Guillot-Ferriols, M. T., Ferrer-Roda, M., Guixé, A., Garcia-Caldés, M., et al. (2020). The DNA damage response is required for oocyte cyst breakdown and follicle formation in mice. *PLoS Genet.* 16:e1009067. doi: 10.1371/journal.pgen.1009067

Matos, J., Blanco, M. G., Maslen, S., Skehel, J. M., and West, S. C. (2011). Regulatory control of the resolution of dna recombination intermediates during meiosis and mitosis. *Cell* 147, 158–172. doi: 10.1016/j.cell.2011.08.032

Matos, J., Lipp, J. J., Bogdanova, A., Guillot, S., Okaz, E., Junqueira, M., et al. (2008). Dbf4-dependent Cdc7 kinase links DNA replication to the segregation of homologous chromosomes in meiosis I. *Cell* 135, 662–678. doi: 10.1016/j.cell.2008.10.026

Matsuda, S., Kikkawa, U., and Nakashima, A. (2021). The *S. pombe* CDK5 orthologue Pef1 cooperates with three cyclins, Clg1, Pas1 and Psl1, to promote pre-meiotic DNA replication. *Biomolecules* 11:89. doi: 10.3390/biom11010089

McCord, R., Pierce, M., Xie, J., Wonkatal, S., Mickel, C., and Vershon, A. K. (2003). Rfm1, a novel tethering factor required to recruit the Hst1 histone deacetylase for repression of middle sporulation genes. *Mol. Cell. Biol.* 23, 2009–2016. doi: 10.1128/MCB.23.6.2009-2016.2003

McKee, B. D., and Handel, M. A. (1993). Sex chromosomes, recombination, and chromatin conformation. *Chromosoma* 102, 71–80. doi: 10.1007/BF00356023

Mei, F., Chen, P. F., Dombecki, C. R., Aljabban, I., and Nabeshima, K. (2015). A defective meiotic outcome of a failure in homologous pairing and synapsis is masked by meiotic quality control. *PLoS One* 10:e0134871. doi: 10.1371/journal.pone.0134871

Miyoshi, T., Ito, M., Kugou, K., Yamada, S., Furuichi, M., Oda, A., et al. (2012). A central coupler for recombination initiation linking chromosome architecture to s phase checkpoint. *Mol. Cell.* 47, 722–733. doi: 10.1016/j.molcel.2012.06.023

Miyoshi, T., Ito, M., and Ohta, K. (2013). Spatiotemporal regulation of meiotic recombination by Liaisonin. *BioArchitecture* 3, 20–24. doi: 10.4161/bioa.23966

Mochizuki, K., Novatchkova, M., and Loidl, J. (2008). DNA double-strand breaks, but not crossovers, are required for the reorganization of meiotic nuclei in *Tetrahymena*. *J. Cell Sci.* 121, 2148–2158. doi: 10.1242/jcs.031799

Moens, P. B., Tarsounas, M., Morita, T., Habu, T., Rottinghaus, S. T., Freire, R., et al. (1999). The association of ATR protein with mouse meiotic chromosome cores. *Chromosoma* 108, 95–102. doi: 10.1007/s004120050356

Mohammad, A., Vanden Broek, K., Wang, C., Daryabeigi, A., Jantsch, V., Hansen, D., et al. (2018). Initiation of meiotic development is controlled by three post-transcriptional pathways in *Caenorhabditis elegans*. *Genetics* 209, 1197–1224. doi: 10.1534/genetics.118.300985

Mohibullah, N., and Keeney, S. (2017). Numerical and spatial patterning of yeast meiotic DNA breaks by Tel1. *Genome Res.* 27, 278–288. doi: 10.1101/gr.213587.116

Moore, M., Shin, M. E., Bruning, A., Schindler, K., Vershon, A., and Winter, E. (2007). Arg-Pro-X-Ser/Thr is a Consensus phosphoacceptor sequence for the

meiosis-specific Ime2 protein kinase in *Saccharomyces cerevisiae* †. *Biochemistry* 46, 271–278. doi: 10.1021/bi061858p

Murakami, H., and Keeney, S. (2014). Temporospatial coordination of meiotic DNA replication and recombination via DDK recruitment to replisomes. *Cell* 158, 861–873. doi: 10.1016/j.cell.2014.06.028

Murakami, H., and Nurse, P. (1999). Meiotic DNA replication checkpoint control in fission yeast. *Genes Dev.* 13, 2581–2593. doi: 10.1101/gad.13.19.2581

Nadarajan, S., Lambert, T. J., Altendorfer, E., Gao, J., Blower, M. D., Waters, J. C., et al. (2017). Polo-like kinase-dependent phosphorylation of the synaptonemal complex protein SYP-4 regulates double-strand break formation through a negative feedback loop. *ELife* 6:e23437. doi: 10.7554/eLife.23437

Nadarajan, S., Mohideen, F., Tzur, Y. B., Ferrandiz, N., Crawley, O., Montoya, A., et al. (2016). The MAP kinase pathway coordinates crossover designation with disassembly of synaptonemal complex proteins during meiosis. *ELife* 5:e12039. doi: 10.7554/eLife.12039

Nagaoka, S. I., Hassold, T. J., and Hunt, P. A. (2012). Human aneuploidy: mechanisms and new insights into an age-old problem. *Nat. Rev. Genet.* 13, 493–504. doi: 10.1038/nrg3245

Nakada, S., Chen, G. I., Gingras, A., and Durocher, D. (2008). PP4 is a γH2AX phosphatase required for recovery from the DNA damage checkpoint. *EMBO Rep.* 9, 1019–1026. doi: 10.1038/embor.2008.162

Nash, P., Tang, X., Orlicky, S., Chen, Q., Gertler, F. B., Mendenhall, M. D., et al. (2001). Multisite phosphorylation of a CDK inhibitor sets a threshold for the onset of DNA replication. *Nature* 414, 514–521. doi: 10.1038/35107009

Niu, H., Li, X., Job, E., Park, C., Moazed, D., Gygi, S. P., et al. (2007). Mek1 kinase is regulated to suppress double-strand break repair between sister chromatids during budding yeast meiosis. *Mol. Cell. Biol.* 27, 5456–5467. doi: 10.1128/MCB.00416-07

Niu, H., Wan, L., Baumgartner, B., Schaefer, D., Loidl, J., and Hollingsworth, N. M. (2005). Partner choice during meiosis is regulated by Hop1-promoted dimerization of Mek1. *Mol. Biol. Cell* 16, 5804–5818. doi: 10.1091/mbc.e05-05-0465

Niu, H., Wan, L., Busygina, V., Kwon, Y., Allen, J. A., Li, X., et al. (2009). Regulation of meiotic recombination via Mek1-mediated Rad54 phosphorylation. *Mol. Cell.* 36, 393–404. doi: 10.1016/j.molcel.2009.09.029

Nolt, J. K., Rice, L. M., Gallo-Ebert, C., Bisher, M. E., and Nickels, J. T. (2011). PP2A Cdc55 is required for multiple events during meiosis I. *Cell Cycle* 10, 1420–1434. doi: 10.4161/cc.10.9.15485

Nottke, A. C., Kim, H.-M., and Colaiácovo, M. P. (2017). "Wrestling with chromosomes: the roles of SUMO during meiosis," in *SUMO Regulation of Cellular Processes*, Vol. 963, ed. V. G. Wilson (Berlin: Springer International Publishing), 185–196. doi: 10.1007/978-3-319-50044-7_11

Obeso, D., Pezza, R. J., and Dawson, D. (2014). Couples, pairs, and clusters: mechanisms and implications of centromere associations in meiosis. *Chromosoma* 123, 43–55. doi: 10.1007/s00412-013-0439-4

Odorisio, T., Rodriguez, T. A., Evans, E. P., Clarke, A. R., and Burgoyne, P. S. (1998). The meiotic checkpoint monitoring sypapsis eliminates spermatocytes via p53-independent *apoptosis*. *Nat. Genet.* 18, 257–261. doi: 10.1038/ng0398-257

Ogino, K., and Masai, H. (2006). Rad3-Cds1 mediates coupling of initiation of meiotic recombination with DNA Replication: mei4-dependent transcription as a potential target of meiotic checkpoint. *J. Biol Chem.* 281, 1338–1344. doi: 10.1074/jbc.M505767200

Oishi, I., Iwai, K., Kagohashi, Y., Fujimoto, H., Kariya, K.-I., Kataoka, T., et al. (2001). Critical Role of *Caenorhabditis elegans* homologs of Cds1 (Chk2)-related kinases in meiotic recombination. *Mol. Cell. Biol.* 21, 1329–1335. doi: 10.1128/MCB.21.4.1329-1335.2001

Okaz, E., Argüello-Miranda, O., Bogdanova, A., Vinod, P. K., Lipp, J. J., Markova, Z., et al. (2012). Meiotic prophase requires proteolysis of m phase regulators mediated by the meiosis-specific APC/CAma1. *Cell* 151, 603–618. doi: 10.1016/j.cell.2012.08.044

Oldach, L., and Zhang, J. (2014). Genetically encoded fluorescent biosensors for live-cell visualization of protein phosphorylation. *Chem. Biol.* 21, 186–197. doi: 10.1016/j.chembiol.2013.12.012

Ontoso, D., Acosta, I., van Leeuwen, F., Freire, R., and San-Segundo, P. A. (2013). Dot1-dependent histone H3K79 methylation promotes activation of the Mek1 meiotic checkpoint effector kinase by regulating the Hop1 adaptor. *PLoS Genet.* 9:e1003262. doi: 10.1371/journal.pgen.1003262

Pacheco, S., Marcet-Ortega, M., Lange, J., Jasin, M., Keeney, S., and Roig, I. (2015). The ATM signaling cascade promotes recombination-dependent pachytene arrest in mouse *Spermatocytes*. *PLoS Genet.* 11:e1005017. doi: 10.1371/journal.pgen.1005017

Pak, J., and Segall, J. (2002a). Regulation of the premiddle and middle phases of expression of the NDT80 gene during sporulation of *Saccharomyces cerevisiae*. *Mol. Cell. Biol.* 22, 6417–6429. doi: 10.1128/MCB.22.18.6417-6429.2002

Pak, J., and Segall, J. (2002b). Role of Ndt80, Sum1, and Swe1 as targets of the meiotic recombination checkpoint that control exit from pachytene and spore formation in *Saccharomyces cerevisiae*. *Mol. Cell. Biol.* 22, 6430–6440. doi: 10.1128/MCB.22.18.6430-6440.2002

Palmer, N., Talib, S. Z. A., Singh, P., Goh, C. M. F., Liu, K., Schimenti, J. C., et al. (2020). A novel function for CDK2 activity at meiotic crossover sites. *PLoS Biol.* 18:e3000903. doi: 10.1371/journal.pbio.3000903

Panizza, S., Mendoza, M. A., Berlinger, M., Huang, L., Nicolas, A., Shirahige, K., et al. (2011). Spo11-accessory proteins link double-strand break sites to the chromosome axis in early meiotic recombination. *Cell* 146, 372–383. doi: 10.1016/j.cell.2011.07.003

Papanikos, F., Clément, J. A. J., Testa, E., Ravindranathan, R., Grey, C., Dereli, I., et al. (2019). Mouse ANKRD31 regulates spatiotemporal patterning of meiotic recombination initiation and ensures recombination between X and Y Sex chromosomes. *Mol. Cell.* 74, 1069.e11–1085.e11. doi: 10.1016/j.molcel.2019.03.022

Paull, T. T. (2015). Mechanisms of ATM activation. *Annu. Rev. Biochem.* 84, 711–738. doi: 10.1146/annurev-biochem-060614-034335

Penedos, A., Johnson, A. L., Strong, E., Goldman, A. S., Carballo, J. A., and Cha, R. S. (2015). Essential and checkpoint functions of budding yeast ATM and ATR during meiotic prophase are facilitated by differential phosphorylation of a meiotic adaptor protein Hop1. *PLoS One* 10:e0134297. doi: 10.1371/journal.pone.0134297

Penkner, A. M., Fridkin, A., Gloggnitzer, J., Baudrimont, A., Machacek, T., Woglar, A., et al. (2009). Meiotic chromosome homology search involves modifications of the nuclear envelope protein Matefin/SUN-1. *Cell* 139, 920–933. doi: 10.1016/j.cell.2009.10.045

Pereira, C., Smolka, M. B., Weiss, R. S., and Brieño-Enríquez, M. A. (2020). ATR signaling in mammalian meiosis: from upstream scaffolds to downstream signaling. *Environ. Mol. Mutagen.* 61, 752–766. doi: 10.1002/em.22401

Pérez-Hidalgo, L., Moreno, S., and San-Segundo, P. A. (2003). Regulation of meiotic progression by the meiosis-specific checkpoint kinase Mek1 in fission yeast. *J. Cell Sci.* 116, 259–271. doi: 10.1242/jcs.00232

Pérez-Hidalgo, L., Moreno, S., and San-Segundo, P. A. (2008). The fission yeast meiotic checkpoint kinase Mek1 regulates nuclear localization of Cdc25 by phosphorylation. *Cell Cycle* 7, 3720–3730. doi: 10.4161/cc.7.23.7177

Petronczki, M., Siomos, M. F., and Nasmyth, K. (2003). Un ménage à quatre. *Cell* 112, 423–440. doi: 10.1016/S0092-8674(03)00083-7

Phadnis, N., Cipak, L., Polakova, S., Hyppa, R. W., Cipakova, I., Anrather, D., et al. (2015). Casein kinase 1 and phosphorylation of cohesin subunit rec11 (SA3) promote meiotic recombination through linear element formation. *PLoS Genet.* 11:e1005225. doi: 10.1371/journal.pgen.1005225

Phillips, C. M., and Dernburg, A. F. (2006). A family of zinc-finger proteins is required for chromosome-specific pairing and synapsis during meiosis in *C. elegans*. *Dev. Cell* 11, 817–829. doi: 10.1016/j.devcel.2006.09.020

Pierce, M., Benjamin, K. R., Montano, S. P., Georgiadis, M. M., Winter, E., and Vershon, A. K. (2003). Sum1 and Ndt80 proteins compete for binding to middle sporulation element sequences that control meiotic gene expression. *Mol. Cell. Biol.* 23, 4814–4825. doi: 10.1128/MCB.23.14.4814-4825.2003

Potapova, T., and Gorbsky, G. (2017). The consequences of chromosome segregation errors in mitosis and meiosis. *Biology* 6:12. doi: 10.3390/biology6010012

Prugar, E., Burnett, C., Chen, X., and Hollingsworth, N. M. (2017). Coordination of double strand break repair and meiotic progression in yeast by a Mek1-Ndt80 negative feedback loop. *Genetics* 206, 497–512. doi: 10.1534/genetics.117.199703

Raina, V. B., and Vader, G. (2020). Homeostatic control of meiotic prophase checkpoint function by Pch2 and Hop1. *Curr. Biol.* 30, 4413.e5–4424.e5. doi: 10.1016/j.cub.2020.08.064

Rao, H. B. D. P., Qiao, H., Bhatt, S. K., Bailey, L. R. J., Tran, H. D., Bourne, S. L., et al. (2017). A SUMO-ubiquitin relay recruits proteasomes to chromosome axes to regulate meiotic recombination. *Science* 355, 403–407. doi: 10.1126/science.aaf6407

Rinaldi, V. D., Bolcun-Filas, E., Kogo, H., Kurahashi, H., and Schimenti, J. C. (2017). The DNA damage checkpoint eliminates mouse oocytes with chromosome synapsis failure. *Mol. Cell.* 67, 1026.e2–1036.e2. doi: 10.1016/j.molcel.2017.07.027

Rogakou, E. P., Boon, C., Redon, C., and Bonner, W. M. (1999). Megabase chromatin domains involved in DNA double-strand breaks in vivo. *J. Cell Biol.* 146, 905–916. doi: 10.1083/jcb.146.5.905

Rosu, S., Zawadzki, K. A., Stamper, E. L., Libuda, D. E., Reese, A. L., Dernburg, A. F., et al. (2013). The *C. elegans* DSB-2 protein reveals a regulatory network that controls competence for meiotic DSB formation and promotes crossover assurance. *PLoS Genet.* 9:e1003674. doi: 10.1371/journal.pgen.1003674

Royo, H., Prosser, H., Ruzankina, Y., Mahadevaiah, S. K., Cloutier, J. M., Baumann, M., et al. (2013). ATR acts stage specifically to regulate multiple aspects of mammalian meiotic silencing. *Genes Dev.* 27, 1484–1494. doi: 10.1101/gad.219477.113

Ruan, K., Yamamoto, T. G., Asakawa, H., Chikashige, Y., Masukata, H., Haraguchi, T., et al. (2015). Meiotic nuclear movements in fission yeast are regulated by the transcription factor Mei4 downstream of a Cds1-dependent replication checkpoint pathway. *Genes Cells* 20, 160–172. doi: 10.1111/gtc.12207

Rutkowski, R., Dickinson, R., Stewart, G., Craig, A., Schimpl, M., Keyse, S. M., et al. (2011). Regulation of *Caenorhabditis elegans* p53/CEP-1–dependent germ cell *Apoptosis* by Ras/MAPK signaling. *PLoS Genet.* 7:e1002238. doi: 10.1371/journal.pgen.1002238

Sakuno, T., and Watanabe, Y. (2015). Phosphorylation of cohesin Rec11/SA3 by casein kinase 1 promotes homologous recombination by assembling the meiotic chromosome axis. *Dev. Cell* 32, 220–230. doi: 10.1016/j.devcel.2014.11.033

Salazar, C., and Höfer, T. (2009). Multisite protein phosphorylation—from molecular mechanisms to kinetic models. *FEBS J.* 276, 3177–3198. doi: 10.1111/j.1742-4658.2009.07027.x

Sanchez, A., Adam, C., Rauh, F., Duroc, Y., Ranjha, L., Lombard, B., et al. (2020). Exo1 recruits Cdc5 polo kinase to MutLγ to ensure efficient meiotic crossover formation. *Proc. Natl. Acad. Sci. U.S.A.* 2020:13012. doi: 10.1073/pnas.2013012117

San-Segundo, P. A., and Roeder, G. S. (1999). Pch2 links chromatin silencing to meiotic checkpoint control. *Cell* 97, 313–324. doi: 10.1016/S0092-8674(00)80741-2

Sasanuma, H., Hirota, K., Fukuda, T., Kakusho, N., Kugou, K., Kawasaki, Y., et al. (2008). Cdc7-dependent phosphorylation of Mer2 facilitates initiation of yeast meiotic recombination. *Genes Dev.* 22, 398–410. doi: 10.1101/gad.1626608

Sato-Carlton, A., Li, X., Crawley, O., Testori, S., Martinez-Perez, E., Sugimoto, A., et al. (2014). Protein phosphatase 4 promotes chromosome pairing and synapsis, and contributes to maintaining crossover competence with increasing age. *PLoS Genet.* 10:e1004638. doi: 10.1371/journal.pgen.1004638

Sato-Carlton, A., Nakamura-Tabuchi, C., Chartrand, S. K., Uchino, T., and Carlton, P. M. (2018). Phosphorylation of the synaptonemal complex protein SYP-1 promotes meiotic chromosome segregation. *J. Cell Biol.* 217, 555–570. doi: 10.1083/jcb.201707161

Sawyer, E. M., Joshi, P. R., Jorgensen, V., Yunus, J., Berchowitz, L. E., and Ünal, E. (2019). Developmental regulation of an organelle tether coordinates mitochondrial remodeling in meiosis. *J. Cell Biol.* 218, 559–579. doi: 10.1083/jcb.201807097

Scherthan, H. (2001). A bouquet makes ends meet. *Nat. Rev. Mol. Cell Biol.* 2, 621–627. doi: 10.1038/35085086

Schimenti, J. (2005). Synapsis or silence. *Nat. Genet.* 37, 11–13. doi: 10.1038/ng0105-11

Schindler, K., Benjamin, K. R., Martin, A., Boglioli, A., Herskowitz, I., and Winter, E. (2003). The Cdk-activating kinase Cak1p promotes meiotic S phase through Ime2p. *Mol. Cell. Biol.* 23, 8718–8728. doi: 10.1128/MCB.23.23.8718-8728.2003

Sedgwick, C., Rawluk, M., Decesare, J., Raithatha, S., Wohlschlegel, J., Semchuk, P., et al. (2006). *Saccharomyces cerevisiae* Ime2 phosphorylates Sic1 at multiple PXS/T sites but is insufficient to trigger Sic1 degradation. *Biochem. J.* 399, 151–160. doi: 10.1042/BJ20060363

Serrentino, M.-E., Chaplais, E., Sommermeyer, V., and Borde, V. (2013). Differential association of the conserved SUMO ligase Zip3 with meiotic double-strand break sites reveals regional variations in the outcome of meiotic recombination. *PLoS Genet.* 9:e1003416. doi: 10.1371/journal.pgen.1003416

Shinohara, A., Gasior, S., Ogawa, T., Kleckner, N., and Bishop, D. K. (2003). *Saccharomyces cerevisiae* recA homologues RAD51 and DMC1 have both distinct and overlapping roles in meiotic recombination. *Genes Cells* 2, 615–629. doi: 10.1046/j.1365-2443.1997.1480347.x

Shinohara, M., Bishop, D. K., and Shinohara, A. (2019). Distinct functions in regulation of meiotic crossovers for DNA damage response clamp loader Rad24(Rad17) and Mec1(ATR) kinase. *Genetics* 213, 1255–1269. doi: 10.1534/genetics.119.302427

Shroff, R., Arbel-Eden, A., Pilch, D., Ira, G., Bonner, W. M., Petrini, J. H., et al. (2004). Distribution and dynamics of chromatin modification induced by a defined DNA double-strand break. *Curr. Biol.* 14, 1703–1711. doi: 10.1016/j.cub.2004.09.047

Silva, N., Adamo, A., Santonicola, P., Martinez-Perez, E., and La Volpe, A. (2013). Pro-crossover factors regulate damage-dependent *apoptosis* in the *Caenorhabditis elegans* germ line. *Cell Death Differ.* 20, 1209–1218. doi: 10.1038/cdd.2013.68

Smoly, I., Shemesh, N., Ziv-Ukelson, M., Ben-Zvi, A., and Yeger-Lotem, E. (2017). An asymmetrically balanced organization of kinases versus phosphatases across eukaryotes determines their distinct impacts. *PLoS Comput. Biol.* 13:e1005221. doi: 10.1371/journal.pcbi.1005221

Solari, A. J. (1974). The behavior of the XY pair in mammals. *Int. Rev. Cytol.* 38, 273–317. doi: 10.1016/S0074-7696(08)60928-6

Sopko, R., Raithatha, S., and Stuart, D. (2002). Phosphorylation and maximal activity of *Saccharomyces cerevisiae* meiosis-specific transcription factor Ndt80 is dependent on Ime2. *Mol. Cell. Biol.* 22, 7024–7040. doi: 10.1128/MCB.22.20.7024-7040.2002

Sourirajan, A., and Lichten, M. (2008). Polo-like kinase Cdc5 drives exit from pachytene during budding yeast meiosis. *Genes Dev.* 22, 2627–2632. doi: 10.1101/gad.1711408

Stamper, E. L., Rodenbusch, S. E., Rosu, S., Ahringer, J., Villeneuve, A. M., and Dernburg, A. F. (2013). Identification of DSB-1, a protein required for initiation of meiotic recombination in *Caenorhabditis elegans*, illuminates a crossover assurance checkpoint. *PLoS Genet.* 9:e1003679. doi: 10.1371/journal.pgen.1003679

Stracker, T. H., Usui, T., and Petrini, J. H. J. (2009). Taking the time to make important decisions: the checkpoint effector kinases Chk1 and Chk2 and the DNA damage response. *DNA Repair.* 8, 1047–1054. doi: 10.1016/j.dnarep.2009.04.012

Stuart, D., and Wittenberg, C. (1998). CLB5 and CLB6 are required for premeiotic DNA replication and activation of the meiotic S/M checkpoint. *Genes Dev.* 12, 2698–2710. doi: 10.1101/gad.12.17.2698

Studer, R. A., Rodriguez-Mias, R. A., Haas, K. M., Hsu, J. I., Vieitez, C., Sole, C., et al. (2016). Evolution of protein phosphorylation across 18 fungal species. *Science* 354, 229–232. doi: 10.1126/science.aaf2144

Subramanian, V. V., and Hochwagen, A. (2014). The meiotic checkpoint network: step-by-step through meiotic prophase. *Cold Spring Harb. Perspect. Biol.* 6:a016675. doi: 10.1101/cshperspect.a016675

Subramanian, V. V., MacQueen, A. J., Vader, G., Shinohara, M., Sanchez, A., Borde, V., et al. (2016). Chromosome synapsis alleviates Mek1-dependent suppression of Meiotic DNA Repair. *PLoS Biol.* 14:e1002369. doi: 10.1371/journal.pbio.1002369

Suhandynata, R. T., Wan, L., Zhou, H., and Hollingsworth, N. M. (2016). Identification of putative Mek1 substrates during meiosis in *Saccharomyces cerevisiae* using quantitative phosphoproteomics. *PLoS One* 11:e0155931. doi: 10.1371/journal.pone.0155931

Szwarcwort-Cohen, M., Kasulin-Boneh, Z., Sagee, S., and Kassir, Y. (2009). Human Cdk2 is a functional homolog of budding yeast Ime2, the meiosis-specific Cdk-like kinase. *Cell Cycle* 8, 647–654. doi: 10.4161/cc.8.4.7843

Terasawa, M., Ogawa, T., Tsukamoto, Y., and Ogawa, H. (2008). Sae2p phosphorylation is crucial for cooperation with Mre11p for resection of DNA double-strand break ends during meiotic recombination in *Saccharomyces cerevisiae*. *Genes Genet. Syst.* 83, 209–217. doi: 10.1266/ggs.83.209

Tian, M., and Loidl, J. (2018). A chromatin-associated protein required for inducing and limiting meiotic DNA double-strand break formation. *Nucleic Acids Res.* 46, 11822–11834. doi: 10.1093/nar/gky968

Tonami, Y., Murakami, H., Shirahige, K., and Nakanishi, M. (2005). A checkpoint control linking meiotic S phase and recombination initiation in fission yeast. *Proc. Natl. Acad. Sci. U.S.A.* 102, 5797–5801. doi: 10.1073/pnas.0407236102

Traenkle, B., and Rothbauer, U. (2017). Under the microscope: single-domain antibodies for live-cell imaging and super-resolution microscopy. *Front. Immunol.* 8:1030. doi: 10.3389/fimmu.2017.01030

Tsubouchi, T., and Roeder, G. S. (2005). A synaptonemal complex protein promotes homology-independent centromere coupling. *Science* 308, 870–873. doi: 10.1126/science.1108283

Tu, Z., Bayazit, M. B., Liu, H., Zhang, J., Busayavalasa, K., Risal, S., et al. (2017). Speedy A–Cdk2 binding mediates initial telomere–nuclear envelope attachment during meiotic prophase I independent of Cdk2 activation. *Proc. Natl. Acad. Sci. U.S.A.* 114, 592–597. doi: 10.1073/pnas.1618465114

Tung, K.-S., Hong, E.-J. E., and Roeder, G. S. (2000). The pachytene checkpoint prevents accumulation and phosphorylation of the meiosis-specific transcription factor Ndt80. *Proc. Natl. Acad. Sci. U.S.A.* 97, 12187–12192. doi: 10.1073/pnas.220464597

Turner, J. M. A. (2015). Meiotic silencing in mammals. *Annu. Rev. Genet.* 49, 395–412. doi: 10.1146/annurev-genet-112414-055145

Turner, J. M. A., Aprelikova, O., Xu, X., Wang, R., Kim, S., Chandramouli, G. V. R., et al. (2004). BRCA1, histone H2AX phosphorylation, and male meiotic sex chromosome inactivation. *Curr. Biol.* 14, 2135–2142. doi: 10.1016/j.cub.2004.11.032

Turner, J. M. A., Mahadevaiah, S. K., Fernandez-Capetillo, O., Nussenzweig, A., Xu, X., Deng, C.-X., et al. (2005). Silencing of unsynapsed meiotic chromosomes in the mouse. *Nat. Genet.* 37, 41–47. doi: 10.1038/ng1484

Tzur, Y. B., Egydio de Carvalho, C., Nadarajan, S., Van Bostelen, I., Gu, Y., Chu, D. S., et al. (2012). LAB-1 targets PP1 and restricts aurora B kinase upon entrance into meiosis to promote sister chromatid cohesion. *PLoS Biol.* 10:e1001378. doi: 10.1371/journal.pbio.1001378

Vader, G. (2015). Pch2TRIP13: controlling cell division through regulation of HORMA domains. *Chromosoma* 124, 333–339. doi: 10.1007/s00412-015-0516-y

Valentin, G., Schwob, E., and Seta, F. D. (2006). Dual role of the Cdc7-regulatory Protein Dbf4 during yeast meiosis. *J. Biol. Chem.* 281, 2828–2834. doi: 10.1074/jbc.M510626200

Viera, A., Alsheimer, M., Gomez, R., Berenguer, I., Ortega, S., Symonds, C. E., et al. (2015). CDK2 regulates nuclear envelope protein dynamics and telomere attachment in mouse meiotic prophase. *J. Cell Sci.* 128, 88–99. doi: 10.1242/jcs.154922

Viera, A., Rufas, J. S., Martinez, I., Barbero, J. L., Ortega, S., and Suja, J. A. (2009). CDK2 is required for proper homologous pairing, recombination and sex-body formation during male mouse meiosis. *J. Cell Sci.* 122, 2149–2159. doi: 10.1242/jcs.046706

Wan, L., Niu, H., Futcher, B., Zhang, C., Shokat, K. M., Boulton, S. J., et al. (2008). Cdc28-Clb5 (CDK-S) and Cdc7-Dbf4 (DDK) collaborate to initiate meiotic recombination in yeast. *Genes Dev.* 22, 386–397. doi: 10.1101/gad.1626408

Wan, L., Zhang, C., Shokat, K. M., and Hollingsworth, N. M. (2006). Chemical inactivation of Cdc7 kinase in budding yeast results in a reversible arrest that allows efficient cell synchronization prior to meiotic recombination. *Genetics* 174, 1767–1774. doi: 10.1534/genetics.106.064303

Wang, L., Liu, W., Zhao, W., Song, G., Wang, G., Wang, X., et al. (2014). Phosphorylation of CDK2 on threonine 160 influences silencing of sex chromosome during male meiosis. *Biol. Reprod.* 90:138. doi: 10.1095/biolreprod.113.116624

Ward, I. M., Minn, K., van Deursen, J., and Chen, J. (2003). P53 binding protein 53BP1 is required for DNA damage responses and tumor suppression in mice. *Mol. Cell. Biol.* 23, 2556–2563. doi: 10.1128/MCB.23.7.2556-2563.2003

Wassmann, K. (2013). Sister chromatid segregation in meiosis II: deprotection through phosphorylation. *Cell Cycle* 12, 1352–1359. doi: 10.4161/cc.24600

Watts, F. Z., and Hoffmann, E. (2011). SUMO meets meiosis: an encounter at the synaptonemal complex: sUMO chains and sumoylated proteins suggest that heterogeneous and complex interactions lie at the centre of the synaptonemal complex. *BioEssays* 33, 529–537. doi: 10.1002/bies.201100002

Webster, A., and Schuh, M. (2017). Mechanisms of aneuploidy in human eggs. *Trends Cell Biol.* 27, 55–68. doi: 10.1016/j.tcb.2016.09.002

Wellard, S. R., Schindler, K., and Jordan, P. W. (2020). Aurora B and C kinases regulate chromosome desynapsis and segregation during mouse and human spermatogenesis. *J. Cell Sci.* 133:jcs248831. doi: 10.1242/jcs.248831

West, A. M., Komives, E. A., and Corbett, K. D. (2018). Conformational dynamics of the Hop1 HORMA domain reveal a common mechanism with the spindle checkpoint protein Mad2. *Nucleic Acids Res.* 46, 279–292. doi: 10.1093/nar/gkx1196

West, A. M., Rosenberg, S. C., Ur, S. N., Lehmer, M. K., Ye, Q., Hagemann, G., et al. (2019). A conserved filamentous assembly underlies the structure of the meiotic chromosome axis. *ELife* 8:e40372. doi: 10.7554/eLife.40372

Widger, A., Mahadevaiah, S. K., Lange, J., ElInati, E., Zohren, J., Hirota, T., et al. (2018). ATR is a multifunctional regulator of male mouse meiosis. *Nat. Commun.* 9:2621. doi: 10.1038/s41467-018-04850-0

Wijnker, E., Harashima, H., Müller, K., Parra-Nuñez, P., de Snoo, C. B., van de Belt, J., et al. (2019). The Cdk1/Cdk2 homolog CDKA;1 controls the recombination landscape in *Arabidopsis*. *Proc. Natl. Acad. Sci. U.S.A.* 116, 12534–12539. doi: 10.1073/pnas.1820753116

Woglar, A., Daryabeigi, A., Adamo, A., Habacher, C., Machacek, T., La Volpe, A., et al. (2013). Matefin/SUN-1 phosphorylation is part of a surveillance mechanism to coordinate chromosome synapsis and recombination with meiotic progression and chromosome movement. *PLoS Genet.* 9:e1003335. doi: 10.1371/journal.pgen.1003335

Wojtasz, L., Cloutier, J. M., Baumann, M., Daniel, K., Varga, J., Fu, J., et al. (2012). Meiotic DNA double-strand breaks and chromosome asynapsis in mice are monitored by distinct HORMAD2-independent and -dependent mechanisms. *Genes Dev.* 26, 958–973. doi: 10.1101/gad.187559.112

Wojtasz, L., Daniel, K., Roig, I., Bolcun-Filas, E., Xu, H., Boonsanay, V., et al. (2009). Mouse HORMAD1 and HORMAD2, two conserved meiotic chromosomal proteins, are depleted from synapsed chromosome axes with the help of TRIP13 AAA-ATPase. *PLoS Genet.* 5:e1000702. doi: 10.1371/journal.pgen.1000702

Woo, T.-T., Chuang, C.-N., Higashide, M., Shinohara, A., and Wang, T.-F. (2020). Dual roles of yeast Rad51 N-terminal domain in repairing DNA double-strand breaks. *Nucleic Acids Res.* 48, 8474–8489. doi: 10.1093/nar/gkaa587

Wu, H.-Y., and Burgess, S. M. (2006). Two distinct surveillance mechanisms monitor meiotic chromosome metabolism in budding yeast. *Curr. Biol.* 16, 2473–2479. doi: 10.1016/j.cub.2006.10.069

Xie, C., He, C., Jiang, Y., Yu, H., Cheng, L., Nshogoza, G., et al. (2018). Structural insights into the recognition of phosphorylated Hop1 by Mek1. *Acta Crystallogr. D Struct. Biol.* 74, 1027–1038. doi: 10.1107/S2059798318011993

Xie, J., Pierce, M., Gailus-Durner, V., Wagner, M., Winter, E., and Vershon, A. K. (1999). Sum1 and Hst1 repress middle sporulation-specific gene expression during mitosis in *Saccharomyces cerevisiae*. *EMBO J.* 18, 6448–6454. doi: 10.1093/emboj/18.22.6448

Xu, L., Weiner, B. M., and Kleckner, N. (1997). Meiotic cells monitor the status of the interhomolog recombination complex. *Genes Dev.* 11, 106–118. doi: 10.1101/gad.11.1.106

Yang, C., Sofroni, K., Wijnker, E., Hamamura, Y., Carstens, L., Harashima, H., et al. (2020). The *Arabidopsis* Cdk1/Cdk2 homolog CDKA?;1 controls chromosome axis assembly during plant meiosis. *EMBO J.* 39:e101625. doi: 10.15252/embj.2019101625

Yao, Y., Li, X., Chen, W., Liu, H., Mi, L., Ren, D., et al. (2020). ATM promotes RAD51-mediated meiotic DSB repair by inter-sister-chromatid recombination in Arabidopsis. *Front. Plant Sci.* 11:839. doi: 10.3389/fpls.2020.00839

Ye, A. L., Ragle, J. M., Conradt, B., and Bhalla, N. (2014). Differential regulation of germline *Apoptosis* in response to meiotic checkpoint activation. *Genetics* 198, 995–1000. doi: 10.1534/genetics.114.170241

Ye, Q., Rosenberg, S. C., Moeller, A., Speir, J. A., Su, T. Y., and Corbett, K. D. (2015). TRIP13 is a protein-remodeling AAA+ ATPase that catalyzes MAD2 conformation switching. *ELife* 4:e07367. doi: 10.7554/eLife.07367

Yokoo, R., Zawadzki, K. A., Nabeshima, K., Drake, M., Arur, S., and Villeneuve, A. M. (2012). COSA-1 reveals robust homeostasis and separable licensing and reinforcement steps governing meiotic crossovers. *Cell* 149, 75–87. doi: 10.1016/j.cell.2012.01.052

Yoon, S.-W., Lee, M.-S., Xaver, M., Zhang, L., Hong, S.-G., Kong, Y.-J., et al. (2016). Meiotic prophase roles of Rec8 in crossover recombination and chromosome structure. *Nucleic Acids Res.* 44, 9296–9314. doi: 10.1093/nar/gkw682

Zakharyevich, K., Tang, S., Ma, Y., and Hunter, N. (2012). Delineation of joint molecule resolution pathways in meiosis identifies a crossover-specific resolvase. *Cell* 149, 334–347. doi: 10.1016/j.cell.2012.03.023

Zhang, B., Tang, Z., Li, L., and Lu, L.-Y. (2020). NBS1 is required for SPO11-linked DNA double-strand break repair in male meiosis. *Cell Death Differ.* 27, 2176–2190. doi: 10.1038/s41418-020-0493-4

Zhang, L., Kim, K. P., Kleckner, N. E., and Storlazzi, A. (2011). Meiotic double-strand breaks occur once per pair of (sister) chromatids and, via Mec1/ATR and Tel1/ATM, once per quartet of chromatids. *Proc. Natl. Acad. Sci. U.S.A.* 108, 20036–20041. doi: 10.1073/pnas.1117937108

Zheng, T., Nibau, C., Phillips, D. W., Jenkins, G., Armstrong, S. J., and Doonan, J. H. (2014). CDKG1 protein kinase is essential for synapsis and male meiosis at high ambient temperature in *Arabidopsis thaliana*. *Proc. Natl. Acad. Sci. U.S.A.* 111, 2182–2187. doi: 10.1073/pnas.1318460111

Zhu, Z., Mori, S., Oshiumi, H., Matsuzaki, K., Shinohara, M., and Shinohara, A. (2010). Cyclin-dependent kinase promotes formation of the synaptonemal complex in yeast meiosis: cDK on meiotic chromosomes. *Genes Cells* 15, 1036–1050. doi: 10.1111/j.1365-2443.2010.01440.x

Zickler, D., and Kleckner, N. (2015). Recombination, pairing, and synapsis of homologs during meiosis. *Cold Spring Harb. Perspect. Biol.* 7:a016626. doi: 10.1101/cshperspect.a016626

Zickler, D., and Kleckner, N. (2016). A few of our favorite things: pairing, the bouquet, crossover interference and evolution of meiosis. *Semin. Cell Dev. Biol.* 54, 135–148. doi: 10.1016/j.semcdb.2016.02.024

Conflict of Interest: The authors declare that the research was conducted in the absence of any commercial or financial relationships that could be construed as a potential conflict of interest.

Copyright © 2021 Kar and Hochwagen. This is an open-access article distributed under the terms of the Creative Commons Attribution License (CC BY). The use, distribution or reproduction in other forums is permitted, provided the original author(s) and the copyright owner(s) are credited and that the original publication in this journal is cited, in accordance with accepted academic practice. No use, distribution or reproduction is permitted which does not comply with these terms.

frontiers in Cell and Developmental Biology

REVIEW
published: 23 April 2021
doi: 10.3389/fcell.2021.668309

BRCA1 and BRCA2 Tumor Suppressor Function in Meiosis

*Qianyan Li and JoAnne Engebrecht**

Department of Molecular and Cellular Biology, and Biochemistry, Molecular, Cellular and Developmental Biology Graduate Group, University of California, Davis, Davis, CA, United States

Meiosis is a specialized cell cycle that results in the production of haploid gametes for sexual reproduction. During meiosis, homologous chromosomes are connected by chiasmata, the physical manifestation of crossovers. Crossovers are formed by the repair of intentionally induced double strand breaks by homologous recombination and facilitate chromosome alignment on the meiotic spindle and proper chromosome segregation. While it is well established that the tumor suppressors BRCA1 and BRCA2 function in DNA repair and homologous recombination in somatic cells, the functions of BRCA1 and BRCA2 in meiosis have received less attention. Recent studies in both mice and the nematode *Caenorhabditis elegans* have provided insight into the roles of these tumor suppressors in a number of meiotic processes, revealing both conserved and organism-specific functions. BRCA1 forms an E3 ubiquitin ligase as a heterodimer with BARD1 and appears to have regulatory roles in a number of key meiotic processes. BRCA2 is a very large protein that plays an intimate role in homologous recombination. As women with no indication of cancer but carrying BRCA mutations show decreased ovarian reserve and accumulated oocyte DNA damage, studies in these systems may provide insight into why BRCA mutations impact reproductive success in addition to their established roles in cancer.

Keywords: BARD1, BRCA1, BRCA2, DSBs, meiosis, MSCI, recombination

OPEN ACCESS

Edited by:
Akira Shinohara,
Osaka University, Japan

Reviewed by:
Sarit Smolikove,
The University of Iowa, United States
Anton Gartner,
IBS Center for Genomic Integrity, Ulsan National Institute of Science and Technology, South Korea

***Correspondence:**
JoAnne Engebrecht
jengebrecht@ucdavis.edu

Specialty section:
This article was submitted to Cell Growth and Division, a section of the journal Frontiers in Cell and Developmental Biology

Received: *16 February 2021*
Accepted: *19 March 2021*
Published: *23 April 2021*

Citation:
Li Q and Engebrecht J (2021) BRCA1 and BRCA2 Tumor Suppressor Function in Meiosis. Front. Cell Dev. Biol. 9:668309. doi: 10.3389/fcell.2021.668309

INTRODUCTION

Homologous recombination (HR) is a high-fidelity pathway that mediates error-free repair of DNA double strand breaks (DSBs) and is essential for maintaining genome integrity. In somatic cells, DSBs can arise when DNA replication is impeded or following exposure to irradiation or other genotoxic stress. Cells deficient for HR show genomic instability including chromosome rearrangements, characteristic of most cancers (Negrini et al., 2010). In contrast to somatic cells, where DSBs pose a risk to genome integrity, during meiosis, hundreds of DSBs are purposely introduced by the topoisomerase-like protein SPO11 in early meiotic prophase and these meiotic DSBs must be accurately repaired for the production of euploid gametes (Lam and Keeney, 2014). As meiosis proceeds, meiotic DSBs are processed by DNA end resection to reveal 3′ overhangs (Garcia et al., 2011). The RAD51 recombinase as well as the meiosis-specific paralog DMC1 assemble on the resulting single strand DNA to form nucleoprotein filaments that mediate strand invasion and homology search for accurate repair (Shinohara and Shinohara, 2004). Meiotic DSB repair occurs concomitantly with the assembly of the synaptonemal complex (SC), the meiosis-specific multi-protein structure that forms between homologous chromosomes. In many

organisms, SC assembly is driven by HR (Zickler and Kleckner, 2015). In the context of full length SC at the pachytene stage of meiotic prophase, a subset of recombination intermediates is processed into inter-homolog crossovers, which are essential for accurate separation of homologous chromosomes at meiosis I (Neale and Keeney, 2006; Baudat and de Massy, 2007). A large number of proteins are critical for HR, including the tumor suppressors BRCA1 and BRCA2, whose functions have been well characterized in somatic cells in the context of DNA damage and carcinogenesis. However, the roles of BRCA1 and BRCA2 during meiotic recombination have received less attention. Although the processing of DSBs by HR is similar in somatic cells and meiosis, meiotic recombination is unique in that SPO11 remains attached to the DNA end following DSB formation. Additionally, meiotic recombination occurs in the context of the SC and both sister and non-sister chromatids can serve as templates for repair. Thus, BRCA1 and BRCA2 function may be modified in meiosis to ensure accurate repair of meiotic DSBs. Studies in model organisms have provided insights into the roles of BRCA1 and BRCA2 in meiosis. This review will summarize the conserved and organism-specific meiotic functions of BRCA1 and BRCA2, focusing on recent studies in mice and *C. elegans*.

BRCA1 IN COMPLEX WITH BARD1 IS AN E3 UBIQUITIN LIGASE CRITICAL FOR GENOME INTEGRITY

Breast cancer susceptibility gene 1 (BRCA1) is a tumor suppressor gene, germline mutations of which are linked to familial breast and ovarian cancers (Hall et al., 1990; Futreal et al., 1994; Godwin et al., 1994; Miki et al., 1994). More than two decades of research has implicated BRCA1 function in multiple cellular pathways, including transcriptional regulation, DNA damage signaling, cell cycle checkpoints, centrosome regulation and in the repair of DNA DSBs through HR (Moynahan et al., 1999; Xu et al., 1999; Deng, 2002, 2006; Yarden et al., 2002; Caestecker and Van de Walle, 2013; Hill et al., 2014; Hatchi et al., 2015). Of critical importance, its role in promoting HR is directly linked to maintenance of genome integrity (Roy et al., 2011; Prakash et al., 2015).

In humans, the 1,863 amino acid BRCA1 protein has an N-terminal RING (Really Interesting New Gene) domain that coordinates two zinc cations in a cross-braced arrangement, a largely unstructured central region encoded by exon11, followed by a coiled coil domain and two C-terminal BRCT repeats (**Figure 1**). RING domains create a platform for binding to E2 ubiquitin conjugating enzymes and facilitate the transfer of ubiquitin from the E2 to substrates, thereby specifying E3 ubiquitin ligase activity (Deshaies and Joazeiro, 2009). The BRCT repeats are phosphopeptide interaction modules for binding to phosphorylated proteins (Manke et al., 2003; Rodriguez et al., 2003; Yu et al., 2003). BRCA1 forms a heterodimer with its obligate binding partner BARD1 (BRCA1-Associated RING Domain protein 1) through their N-terminal regions and the heterodimer exhibits efficient ubiquitin transfer activity (Wu et al., 1996; Meza et al., 1999; Brzovic et al., 2001; Hashizume et al., 2001; Baer and Ludwig, 2002). The BARD1 protein is 777 amino acids in length and similar to BRCA1, contains a RING domain at its N-terminus and two BRCT repeats at its C-terminus (**Figure 1**). In addition, four ankyrin repeats involved in chromatin recognition of newly replicated sister chromatids are present in the middle of the protein (FoxIII, Le Trong et al., 2008; Nakamura et al., 2019). Most studies indicate that BARD1 is indispensable for BRCA1 function and depletion of BARD1 leads to highly similar phenotypes as observed for BRCA1 mutants. Mutations in BARD1 have been identified in patients with breast, ovarian and other cancer types, although at a lower frequency than BRCA1 mutations (Thai et al., 1998; Ghimenti et al., 2002). Further, as with BRCA1, loss of BARD1 results in embryonic lethality in mice as well as defects in HR leading to chromosomal instability (McCarthy et al., 2003).

The mechanisms by which BRCA1-BARD1 promotes HR during DSB repair involve multiple steps. First, BRCA1 promotes DNA end resection by antagonizing 53BP1, a DNA damage response protein that promotes error-prone non-homologous end joining (NHEJ) (Bunting et al., 2010; Daley and Sung, 2014). Two, BRCA1 regulates the MRE11-RAD50-NBS1-CtIP complex essential for DNA end processing (Cruz-Garcia et al., 2014; Aparicio et al., 2016). There is also evidence that BRCA1 removes a chromatin barrier for DNA resection through ubiquitylation of histone H2A (Densham et al., 2016). In addition to promoting resection, BRCA1-BARD1 binds to DNA and interacts with RAD51 directly, enhancing RAD51 recombinase activity by promoting homologous strand invasion and synaptic complex formation (Zhao et al., 2017). However, whether BRCA1 functions by similar mechanisms to promote HR during meiosis for the repair of SPO11-induced DSBs has remained elusive.

BRCA1 FUNCTION IN MOUSE MEIOSIS

Mice homozygous for *Brca1* null alleles are embryonic lethal, excluding the possibility to assess BRCA1 function during meiosis (Gowen et al., 1996; Hakem et al., 1996; Liu et al., 1996; Ludwig et al., 1997). To circumvent this limitation, meiosis has been analyzed in mice carrying a hypomorphic mutation that deletes the large exon11 in the heterozygous *Trp53* (encoding p53) mutant background ($Brca1^{\Delta 11/\Delta 11}$ $Trp53^{+/-}$) (Xu et al., 2003; **Figure 1**). These mice develop and survive to adulthood; lethality likely bypassed by the reduced expression of *Trp53* (Cressman et al., 1999).

BRCA1 Is Essential for Meiotic Sex Chromosome Inactivation During Spermatogenesis

Although *Trp53* heterozygosity rescues the embryonic lethality of $Brca1^{\Delta 11/\Delta 11}$ mice, males are infertile as a result of pachytene arrest and apoptotic removal of germ cells (Xu et al., 2003). This observation revealed an essential role of BRCA1 in meiotic sex chromosome inactivation (MSCI). MSCI is a repressive mechanism that occurs during meiotic prophase I and involves elaboration of heterochromatin and transcriptional silencing of non-homologous regions of sex chromosomes (Turner, 2007).

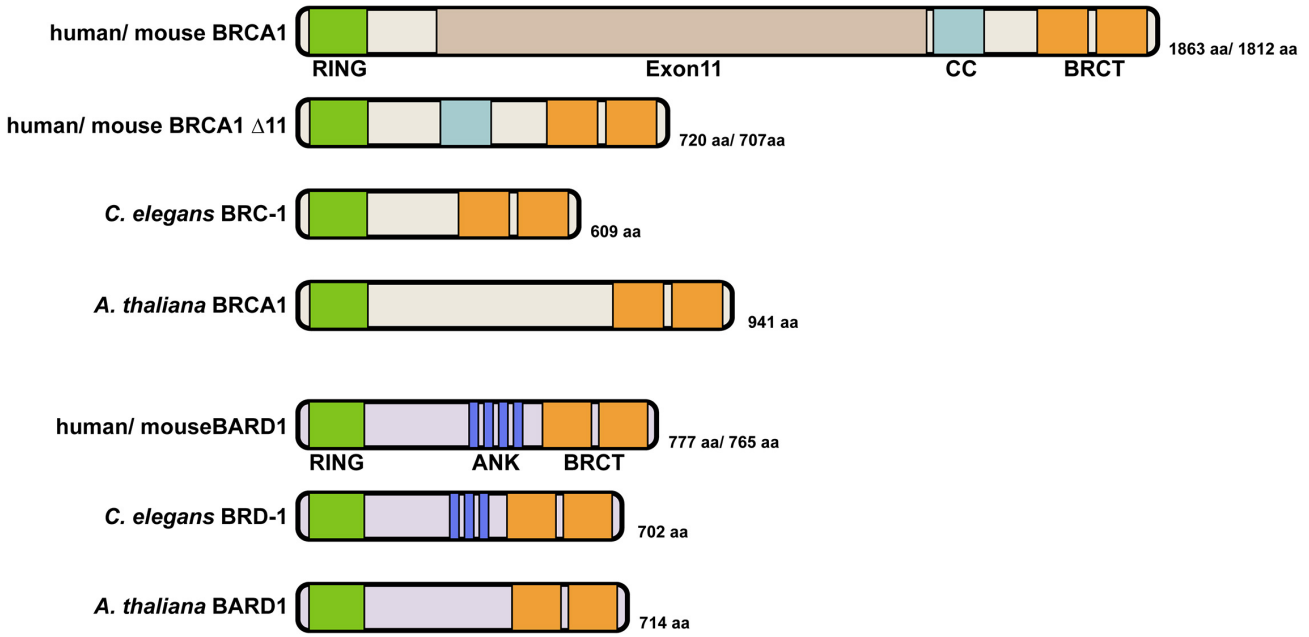

FIGURE 1 | Domain structure of BRCA1 and BARD1 proteins. Human BRCA1 contains an N-terminal RING domain, an unstructured central region encoded by the large exon11 followed by a coiled coil (CC) domain and two BRCA1 C-terminal (BRCT) repeats. Both human and mouse express an alternatively spliced variant BRCA1Δ11 that contains the N-terminal RING domain and C-terminal BRCT repeats but lacks the unstructured central region (Thakur et al., 1997; Huber et al., 2001). This truncated protein is expressed in the hypomorphic *Brca1*$^{\Delta 11/\Delta 11}$ mouse. *C. elegans* BRC-1 is structurally similar to the BRCA1Δ11 splicing variant with the presence of an N-terminal RING domain and two BRCT repeats at its C terminus. *A. thaliana* encodes a similarly structured BRCA1 ortholog that has a N-terminal RING and two C-terminal BRCT repeats. Human BARD1 and *C. elegans* BRD-1 are similar in size and domain structure, containing an N-terminal RING domain, ankyrin repeats in the middle and two C-terminal BRCT repeats. *A. thaliana* BARD-1 has a similar domain structure but appears to lack ankyrin repeats, which were not predicted by sequence alignment. BRCA1 interacts with BARD1 through their RING domains to form a heterodimer with E3 ubiquitin ligase activity.

MSCI is required for efficient meiotic progression in males as failure to repress the X and Y chromosomes results in elevated germline apoptosis (**Figure 2**).

In wild-type spermatocytes, BRCA1 localizes to asynapsed chromosome axes, including the mostly unsynapsed X and Y sex chromosomes (Scully et al., 1997). BRCA1 recruits the checkpoint kinase ataxia telangiectasia and Rad3-related protein (ATR) to the hemizygous regions of sex chromosomes; ATR phosphorylates a histone variant, H2AX, to form γH2AX, leading to sex chromosome compaction and transcriptional silencing (Fernandez-Capetillo et al., 2003; Turner et al., 2004). In the absence of full length BRCA1, ATR and γH2AX localization is disrupted, formation of XY sex body fails, and transcriptional silencing is abolished, leading to ectopic gene transcription from the hemizygous regions of the sex chromosomes (Xu et al., 2003; Turner et al., 2004; Broering et al., 2014). The inability to execute successful MSCI in the *Brca1*$^{\Delta 11/\Delta 11}$ mutant has been attributed to a direct role of BRCA1 in establishing heterochromatin on the X and Y chromosomes and XY body morphogenesis, rather than an indirect consequence of defective meiotic recombinational repair in the absence of full-length BRCA1 (Broering et al., 2014).

The related process of meiotic silencing of unsynapsed chromatin (MSUC) also requires BRCA1 and operates in both male and female germ cells (Mahadevaiah et al., 2008; Kouznetsova et al., 2009). As with MSCI, MSUC leads to accumulation of repressive chromatin and transcriptional silencing on any asynapsed chromosomal regions. MSUC promotes the elimination of gametes with chromosome asynapsis and is initiated by the recruitment of BRCA1 to unsynapsed chromosomes through the interaction with the SC axial component SYCP3. Interestingly, oocytes have a limited capacity to silence unsynapsed chromosomes and this appears to be a consequence of the amount of BRCA1 available to accumulate on unsynapsed chromosomes. Thus, the role of BRCA1 in transcriptional silencing contributes to ensuring the production of euploid gametes.

Potential BRCA1 Role in Meiotic Recombination

In addition to MSCI failure, spermatocytes from *Brca1*$^{\Delta 11/\Delta 11}$ Trp53$^{+/-}$ mice exhibited a prolonged autosomal γH2AX signal with greatly reduced numbers of RAD51 (but not DMC1) and MLH1 foci, suggesting that BRCA1 plays a role in meiotic DSBs repair and crossover formation (Xu et al., 2003). In contrast, a separate study utilizing Cre/LoxP mediated conditional germline-specific deletion of *Brca1* exon11 in the presence of both wild-type *Trp53* alleles showed that RAD51 foci were not reduced, although decreased numbers of MSH4 foci and delayed appearance of MLH1 foci were observed. These authors concluded that while BRCA1 is not essential for meiotic DSB repair, BRCA1 might be involved in the regulation of the

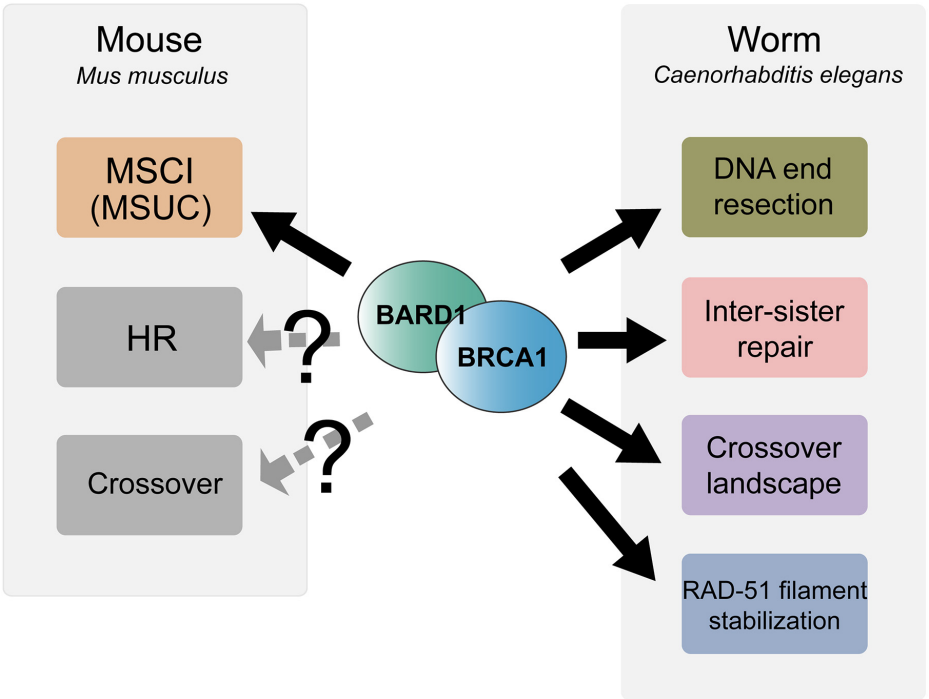

FIGURE 2 | Summary of meiotic functions of BRCA1-BARD1 in mouse and *C. elegans*. BRCA1-BARD1 is critical for meiotic sex chromosome inactivation (MSCI) and meiotic silencing of unsynapsed chromatin (MUSC) during mouse meiosis while it remains an open question as to whether it functions in meiotic recombination and crossover regulation. In contrast to mouse, *C. elegans* BRC-1-BRD-1 is dispensable for MSCI but functions in DNA end resection, inter-sister recombinational repair, RAD-51 filament stabilization and regulation of the crossover landscape.

timing of crossover formation (Broering et al., 2014). In a recent study using END-seq on mouse spermatocytes that allows direct examination of meiotic DSB processing at the single nucleotide level, hypomorphic *Brca1*$^{\Delta 11/\Delta 11}$ Trp53$^{+/-}$ mice did not exhibit a reduction in resection track length, suggesting that BRCA1 does not promote DNA resection in meiotic DSB repair as in somatic cells (Paiano et al., 2020). Together these results suggest that the critical meiotic role for BRCA1 is in transcriptional silencing; however, it is possible that BRCA1 function in meiotic recombination is obscured by the use of the hypomorphic *Brca1*$^{\Delta 11/\Delta 11}$ mutant (**Figure 2**).

Analysis of female meiosis in the hypomorphic *Brca1*$^{\Delta 11/\Delta 11}$ mutation revealed no observable phenotypes. Female *Brca1* mutants are fertile and the number of MLH1 foci are comparable to that observed in wild-type oogenesis, suggesting that the region deleted in *Brca1*$^{\Delta 11/\Delta 11}$ is not required for meiotic recombination during female meiosis (Xu et al., 2003; Broering et al., 2014). Therefore, the observed sex-specific phenotypes in the hypomorphic *Brca1*$^{\Delta 11/\Delta 11}$ mutant are likely a consequence of the presence of unsynapsed sex chromosomes in males. It is also important to note that the region encoded by exon11 is thought to be unstructured with no resemblance to known domain structures (Li and Greenberg, 2012). Future studies focusing on the RING domain, which confers E3 ubiquitin ligase activity, and the BRCT repeats, are necessary to reveal whether these domains play important roles in the repair of meiotic DSBs in both male and female meiosis. Finally, to the best of our knowledge a functional role of BARD1 in mice gametogenesis has not been examined.

BRCA1 FUNCTION IN *C. ELEGANS* MEIOSIS

The *C. elegans* Germ Line as a Model for Studying Meiosis and BRCA1-BARD1 Function

Caenorhabditis elegans has emerged as an excellent model for investigating meiosis: many genes required for meiotic recombination are conserved in this metazoan and the animals possess prominent gonads that exhibit a spatial temporal organization of germ cells undergoing meiotic prophase I (**Figure 3A**). At the distal tip, germline stem cells divide to produce cells that will advance down the gonad and enter meiosis. In transition zone (corresponding to leptotene/zygotene), homologous chromosomes are paired together, facilitated by Zn-finger ZIM-1/2/3 and HIM-8 proteins that bind to special sequences present on each homolog pair. Beginning at this stage, SPO-11 induces meiotic DSBs, which are processed and bound by RAD-51 for homologous recombinational repair. In pachytene, the SC is fully assembled between the homologs and within this context strictly one crossover forms between each chromosome pair in late pachytene. Upon crossover formation, the SC

disassembles and homologs undergo remodeling and compaction to reveal six bivalents at diakinesis stage, representing the six pairs of homologs connected by chiasmata (**Figure 3B**; Lui and Colaiacovo, 2013; Hillers et al., 2017). Although the overall process is very similar to other systems, it is important to note that there are differences unique to *C. elegans* meiosis. These include the absence of DMC1 in this organism, thus RAD-51 is the sole recombinase acting during both mitotic and meiotic recombination (Brown and Bishop, 2014). Interestingly, *C. elegans* RAD-51 contains three amino acids conserved in the DMC1 lineage that stabilize mismatch-containing heteroduplex DNA, critical for meiotic recombinase function (Steinfeld et al., 2019). Another unique feature of *C. elegans* meiosis is that chromosome synapsis does not depend on meiotic recombination initiation (Dernburg et al., 1998). Nevertheless, the availability of molecular markers combined with genetic and genomic approaches has made the *C. elegans* germ line a powerful system that provides a unique opportunity to dissect gene function at any particular sub-stage of meiotic prophase. Most importantly, proteins with conserved domain structure and sequence similarity to BRCA1 and BARD1, referred to as BRC-1 and BRD-1, are encoded in the *C. elegans* genome. *brc-1* and *brd-1* null mutants exhibit elevated IR sensitivity and a higher incidence of males among self-progeny (a readout of X chromosome non-disjunction) compared to wild type, but are mostly fertile, allowing analysis of meiotic outcomes in the absence of functional BRCA1 and BARD1 (Boulton et al., 2004; Li et al., 2018). Similar to *C. elegans*, *Arabidopsis AtBRCA1* and *AtBARD1* mutants are also fertile, suggesting that the essentiality of mammalian BRCA1-BARD1 is not broadly conserved (Reidt et al., 2006).

C. elegans brc-1 encodes a 609 amino acid protein with highly conserved N-terminal RING domain and C terminal BRCT repeats, similar to the human protein. Structurally, *C. elegans* BRC-1 is analogous to the BRCA1Δ11 splicing variant (**Figure 1**). AtBRCA1 with 941 amino acids is also considerably smaller than the human protein. The *C. elegans* BRD-1 and AtBARD1 proteins are similar in both size and domain architecture to the human protein, although AtBARD1 does not have recognizable ankyrin repeats (**Figure 1**). Interestingly, *C. elegans* BRC-1-BRD-1 exhibits dynamic localization throughout meiotic prophase. Discrete foci of BRC-1-BRD-1 that partially colocalize with RAD-51 are present in both proliferative/mitotic region and early meiotic prophase, from leptotene to early pachytene (Li et al., 2018, 2020). As meiotic prophase progresses, BRC-1-BRD-1 localizes with the SC between the maternal and paternal chromosomes (Polanowska et al., 2006; Janisiw et al., 2018; Li et al., 2018). This localization is in contrast to BRCA1 localization in mammalian meiocytes, where BRCA1 is found on the axes of asynapsed chromosomes (Turner et al., 2004). In late pachytene upon crossover maturation, BRC-1-BRD-1 concentrates on one subdomain of the chromosome pair termed the "short arm", suggesting an intimate connection of BRC-1-BRD-1 to crossover sites and potential involvement in crossover regulation.

BRC-1-BRD-1 Is Not Essential for Meiotic Sex Chromosome Inactivation but Promotes HR in Spermatogenesis

C. elegans BRC-1-BRD-1 is absent from the single asynapsed X chromosome in male germ cells, and consistent with

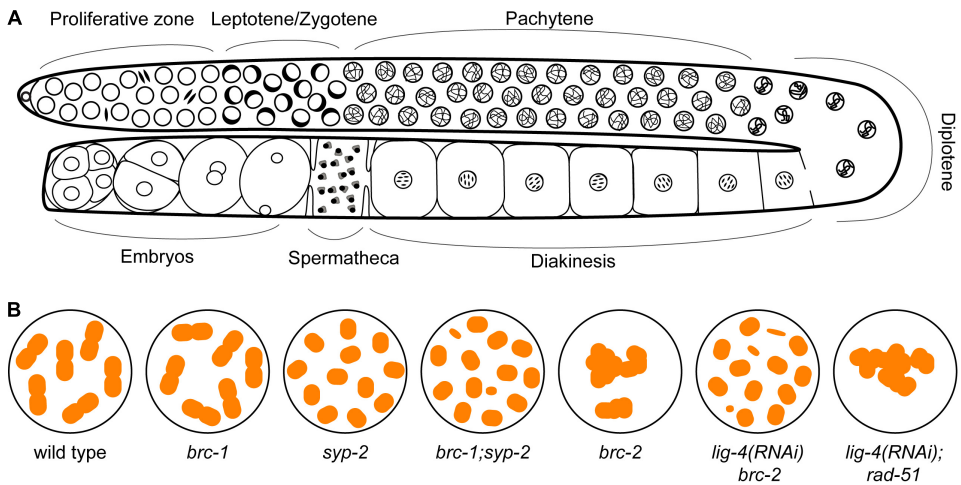

FIGURE 3 | The *C. elegans* germ line presents a spatial temporal organization of events during meiotic prophase I. **(A)** At the distal proliferative zone, germline stem cells mitotically divide to produce cells that will advance down the gonad and enter meiosis. Chromosome pairing and DSBs induction by SPO-11 occur in leptotene/zygotene (transition zone), which is characterized by the presence of clustered chromatin on one side of the nuclei. DSBs are processed and bound by RAD-51 for homologous recombinational repair, which are visible as RAD-51 foci by immunostaining starting in leptotene through pachytene. The synaptonemal complex (SC) is fully assembled between the homologs in pachytene and strictly one crossover forms between each chromosome pair in late pachytene. Upon crossover formation, the SC disassembles and homologs undergo remodeling and compaction to reveal six bivalents at diakinesis stage. **(B)** Cartoon of chromosome structure observed in diakinesis nuclei in WT (6 bivalents), *brc-1* (6 bivalents), *syp-2* (12 univalents), *brc1; syp-2* (> 12 univalents/DNA fragments) (Adamo et al., 2008), *brc-2* (aggregation), *lig-4* (RNAi) *brc-2* (12 univalents with some DNA fragments) and *lig-4* (RNAi); *rad-51* (aggregation) (Martin et al., 2005) mutants.

this observation, BRC-1-BRD-1 is not required for MSCI during spermatogenesis. In *brc-1* and *brd-1* null mutants, deposition of the repressive chromatin mark H3K9me2 and the absence of Pol2-S2P (actively transcribing RNA polymerase II) signal on the X chromosome are indistinguishable from wild-type animals, suggesting that MSCI is successful in these mutants. As such, the null mutants do not exhibit pachytene arrest and germ cells complete meiotic prophase in preparation for the meiotic divisions (Li et al., 2020).

Analysis of RAD-51 immunostaining in the *brc-1* and *brd-1* null male germ lines showed reduced levels of RAD-51 foci in early meiotic prophase and this reduction was suppressed by inhibiting the NHEJ pathway. Moreover, quantification of GFP:RPA-1 foci, indicative of single stranded DNA, showed a significant reduction in overall foci number and intensity in the absence of BRC-1-BRD-1, suggesting that BRC-1-BRD-1 favors HR at the expense of NHEJ through promoting resection of DSBs during male meiosis (Li et al., 2020; **Figure 2**). This role is similar to what is proposed for BRCA1 function in promoting HR in somatic cells.

BRC-1-BRD-1 Promotes Inter-Sister Recombination and Stabilizes the RAD-51 Filament Under Checkpoint Activation in Oogenesis

In contrast to male meiosis, *brc-1* and *brd-1* null mutants exhibited an increased number of RAD-51 foci at late pachytene in oogenic germ lines, with no obvious difference in RAD-51 kinetics in early meiotic prophase as compared to wild-type animals (Adamo et al., 2008; Janisiw et al., 2018; Li et al., 2018). The elevated RAD-51 foci observed in late pachytene suggests that the repair of a subset of DSBs is delayed in the absence of BRC-1-BRD-1. The high fertility and presence of six bivalents, representing the six homologs connected by chiasmata, at diakinesis in *brc-1* and *brd-1* mutants (**Figure 3B**) suggest that BRC-1-BRD-1 is not essential for crossover formation. To test the hypothesis that BRC-1 promotes repair of DSBs by the inter-sister recombination pathway, Adamo and coworkers disrupted SC assembly and thereby inter-homolog crossovers by mutation of *syp-2* (one of six components in the central region of the SC) in the *brc-1* mutant. *syp-2* mutants have twelve intact univalents at diakinesis (**Figure 3B**), suggesting efficient repair of DSBs by the inter-sister pathway. On the other hand, in the *brc-1; syp-2* double mutant more than twelve DAPI staining bodies were often observed (**Figure 3B**), indicating the presence of chromosome fragmentation and failure in inter-sister repair. These results are consistent with BRC-1 playing an important role in inter-sister repair during oogenesis (Adamo et al., 2008). A recent study extended these findings by showing that mutation of *brc-1* enhanced the phenotype of phosphorylation defective mutants in *syp-1* (another component of the central region of the SC), presumably through impairment of inter-sister recombination (Garcia-Muse et al., 2019; **Figure 2**). Importantly, BRC-1-dependent inter-sister repair prevents erroneous recombination (recombination between heterologous sequences) in meiosis, suggesting one mechanism by which BRC-1 prevents genome instability (Leon-Ortiz et al., 2018).

In addition to promoting inter-sister repair, BRC-1 is required to stabilize the RAD-51 filament from premature disassembly in late pachytene under meiotic checkpoint activation conditions. In *zim-1/2/3* or *syp-1* mutants, which lack crossovers on a subset or all chromosomes, respectively, and activate meiotic checkpoints, extensive RAD-51 foci are present throughout meiotic prophase (Yu et al., 2016). Removing BRC-1 in these mutant backgrounds results in a region in late pachytene with significantly reduced RAD-51 levels, with high levels of RAD-51 both prior to and after this region. Both the number of RAD-51 foci as well as the fluorescence intensity of residual foci was greatly diminished in this region and thus this pattern has been referred to as a RAD-51 "dark zone". Taking advantage of the spatial temporal organization of the germ line, time course analysis of *spo-11; brc-1; syp-1* mutants exposed to irradiation (IR) was performed. The *spo-11* mutant was used so that breaks could be induced uniformly in the germ line at a single point in time by IR and as nuclei moved through the germ line no new breaks were formed. This analysis revealed that RAD-51 installed on processed DSBs in nuclei residing in early prophase at the time of DSB induction was dismantled once the nuclei reached late pachytene, suggesting that BRC-1 promotes the stability of the RAD-51 filament under these conditions (Li et al., 2018). The mechanism underlying BRC-1-dependent RAD-51 stabilization is currently unknown and could be either through direct interaction with RAD-51 to reduce its ATP hydrolysis and/or regulation of helicases which dismantle the RAD-51 filament. Interestingly, the requirement for BRC-1 to stabilize RAD-51 filaments under checkpoint activation conditions is oogenesis-specific, as a RAD-51 dark zone was not observed in the male germ line (Li et al., 2020; **Figure 2**).

Recent studies examining the mutational signatures of *brc-1* and *brd-1* mutants propagated over multiple generations revealed elevated levels of small deletions, deletions-insertions, single nucleotide variants and tandem repeats (Kamp et al., 2020; Volkova et al., 2020). Analysis of *brc-1* and *brd-1* mutants in combination with mutations in different repair pathways provided evidence that theta-mediated end joining (TMEJ), but not NHEJ, was responsible for the mutational profiles observed. TMEJ anneals short regions of microhomology and catalyzes template-dependent DNA synthesis to repair the broken DNA molecule. These results suggest that in the absence of BRC-1-BRD-1, TMEJ repairs inefficiently resected DSBs. It will be important to distinguish whether the mutations are a consequence of repair of meiotic DSBs, or repair of breaks generated during replication prior to meiotic entry or during embryogenesis, to understand the complete spectrum of BRC-1-BRD-1 function in both the soma and in meiosis. Nonetheless, the mutational profile of *C. elegans brc-1* and *brd-1* mutants is very similar to that found in BRCA1-deficient tumor cells, suggesting that TMEJ repair in the absence of BRCA1 contributes to carcinogenesis (Kamp et al., 2020; Volkova et al., 2020).

BRC-1-BRD-1 Regulates Crossover Patterning

Given that there are many more DSBs than crossovers, a subset of processed DSBs is chosen to be resolved as crossovers in a process referred to as crossover designation (Gray and Cohen, 2016). To investigate whether BRC-1 plays a role in crossover designation and/or resolution, genetic linkage analysis on meiotic products of *brc-1* mutants was performed and revealed an altered crossover landscape. Although the genetic map length was not significantly different between wild type and *brc-1* mutants, there was a shift in crossover distribution from chromosome arms, which are most often observed in wild-type animals, to more central regions on chromosomes (Li et al., 2018, 2020). Altered crossover distribution to the chromosome center has been observed in many other *C. elegans* mutants defective for various aspects of meiotic recombination (Zetka and Rose, 1995; Wagner et al., 2010; Meneely et al., 2012; Saito et al., 2012, 2013; Chung et al., 2015; Hong et al., 2016; Jagut et al., 2016). While the underlying mechanisms are currently unknown, it has been suggested that this could result from an altered chromatin landscape (Saito and Colaiacovo, 2017). Thus, BRCA1 may regulate chromatin structure in *C. elegans* meiosis, as it does in mouse meiosis (Broering et al., 2014; Densham et al., 2016), although the specific types of chromatin modification regulated by BRCA1 may not be identical in *C. elegans* and mouse.

Surprisingly, in the *zim-1* mutant where two chromosomes fail to pair and synapse, BRC-1-BRD-1 promoted the formation of extra COSA-1 marked crossover designation events on the remaining chromosome pairs during oogenesis. COSA-1 (CrossOver Site Associated protein 1) is generally accepted to mark canonical crossovers in *C. elegans* meiosis (Yokoo et al., 2012); therefore, the number of COSA-1 foci has been used as a cytological readout of the number of genetic crossovers. The reduced COSA-1 foci in the *brc-1; zim-1* double mutant, however, was not accompanied by a smaller genetic map distance, measured by SNP marker-based linkage analysis. These results suggest that not all crossovers are marked by COSA-1 in the *brc-1; zim-1*double mutant. Further, while the map length was similar in the absence of BRC-1, CO patterning was altered such that there were elevated levels of single crossovers (SCOs) with a concomitant reduction in double crossovers (DCOs). As a crossover can form between any two non-sister chromatids within paired homologs, two, three or four-strand DCOs are possible outcomes of elevated crossover formation. However, only DCOs between the same two chromatids can be detected as DCOs in SNP marker-based analysis, because only one sister chromatid is inherited in the product of meiosis. DCOs involving three or four chromatids will be detected as SCOs. Therefore, the aforementioned observation is consistent with a model whereby inactivation of BRC-1 in the *zim-1* mutant results in a shift from two-strand DCOs that are marked by COSA-1 and observed in the DCO class, to three- and four-strand DCOs that lack the COSA-1 marker and are detected as SCOs (Li et al., 2018). In contrast to oogenesis, BRC-1 inhibits the formation of extra COSA-1 marked crossover precursors in spermatogenesis. Elevated levels of COSA-1 foci were observed in the *brc-1; zim-1* double mutant as compared to *zim-1*. Additionally, the genetic map distance was enlarged in the *brc-1*; *zim-1* double mutant, suggesting that BRC-1 inhibits the formation of extra canonical crossovers in spermatogenesis (Li et al., 2020). Together, these results suggest that BRC-1 plays a role in CO patterning, perhaps through regulating both canonical and non-canonical CO pathways under conditions of meiotic dysfunction (**Figure 2**).

Why does *brc-1* and *brd-1* mutation exhibit sex-specific phenotypes? One hypothesis is that BRC-1-BRD-1 interacts with unique partners to form different complexes during male and female meiosis. This would be analogous to what has been established for BRCA1 function in somatic cells, where it forms three different complexes with distinct functions under different physiological conditions (Li and Greenberg, 2012). Alternatively, or in addition, the sex-specific phenotypes could be a consequence of BRC-1-BRD-1 being differentially regulated by post-translational modifications in the diverging environments of male and female meiosis. Future studies on BRC-1-BRD-1 interacting proteins and the regulation of complex(es) will provide insight into the functions of BRC-1-BRD-1 during spermatogenesis and oogenesis. These studies may also shed light on the sex-specific regulation of the BRCA1-BARD1 complex in mammals.

BRCA2 FUNCTIONS AS AN ESSENTIAL MEDIATOR FOR HR

Breast cancer susceptibility gene 2 (BRCA2) is an essential mediator of HR (Jensen et al., 2010; Liu et al., 2010; Kowalczykowski, 2015). Similar to *BRCA1,* germline mutations in *BRCA2* predispose patients to breast and ovarian cancer and genome instability (Wooster et al., 1995; Yu et al., 2000; Venkitaraman, 2002; King et al., 2003). Biochemical, cell biological and genetic studies have supported a role of BRCA2 in recruiting the RAD51 recombinase to resected single strand DNA at DSBs and promoting nucleoprotein filament assembly to mediate homology search and strand exchange (Sharan et al., 1997; Wong et al., 1997; Abbott et al., 1998; Chen et al., 1999; Tutt et al., 1999; Yuan et al., 1999; Moynahan et al., 2001; Xu et al., 2001; Jensen et al., 2010; Liu et al., 2010; Thorslund et al., 2010).

Human BRCA2 encodes an exceptionally large protein consisting of 3,418 amino acids with multiple functional domains: an N-terminal domain that facilitates binding with Partner And Localizer of BRCA2 (PALB2), eight BRC repeats that define the RAD51 binding motif, a DSS1 and DNA binding domain (DBD, composed of one helix-rich domain (HD), three oligonucleotide/oligosaccharide binding (OB) folds and a tower domain), and a C terminal RAD51 binding domain (CTRB) (**Figure 4**; Yang et al., 2002; Esashi et al., 2005; Xia et al., 2006; Carreira et al., 2009; Shivji et al., 2009). Given its essential role in HR, it is not surprising that BRCA2 is conserved in fungi, plants and metazoans. While overall similar, BRCA2 orthologs possess different numbers of BRC repeats and OB folds, which are signature domains of BRCA2, and vary considerably in size (Gudmundsdottir and Ashworth, 2004; **Figure 4**). For example, Brh2, the BRCA2 ortholog in the fungus *Ustilago maydis,* contains a single BRC repeat and

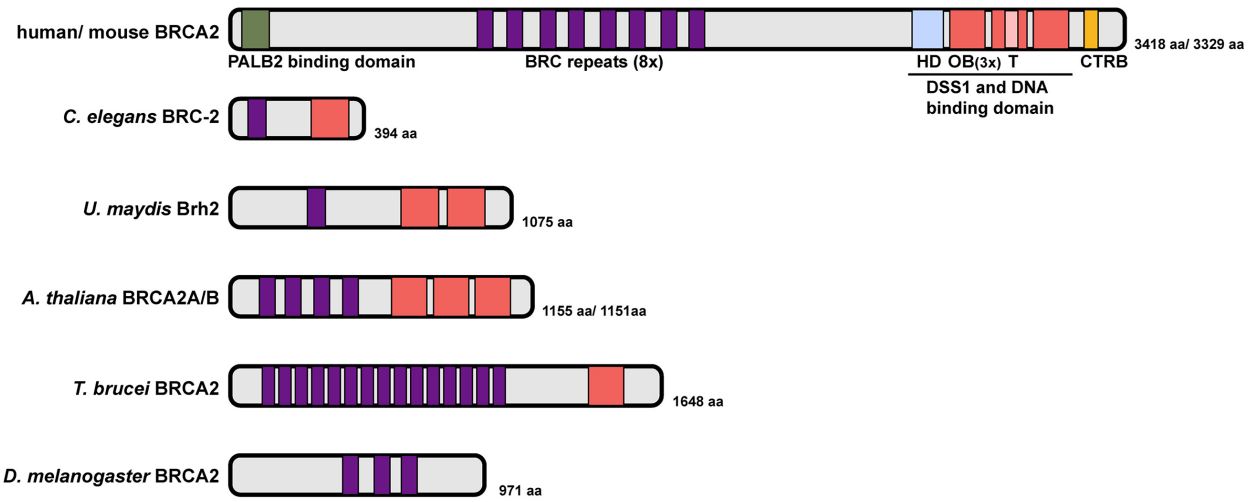

FIGURE 4 | Domain structure of BRCA2 proteins. Human BRCA2 encodes an exceptionally large protein with an N-terminal PALB2 binding domain, eight BRC repeats, a DSS1 and DNA binding domain (DBD) composed of one helix-rich domain (HD), three oligonucleotide/oligosaccharide binding (OB) folds and a tower domain, and a C terminal RAD51 binding domain (CTRB). *C. elegans* BRC-2 represents a simplified version with a single BRC repeat and OB fold. The number of BRC repeats and OB fold domains vary greatly in different organisms (*U. maydis* Brh2, *A. thaliana* BRCA2A/B, *T. brucei* BRCA2 and *D. melanogaster* BRCA2). Sequence alignment did not identify a putative OB fold/DNA binding domain in *Drosophila* BRCA2 (Yang et al., 2002).

two OB folds (Kojic et al., 2002, 2005). *Drosophila melanogaster* BRCA2 contains three BRC repeats but no recognizable OB fold (Klovstad et al., 2008). Two almost identical BRCA2 orthologs were identified in *Arabidopsis thaliana*, each containing four BRC repeats (Siaud et al., 2004). In contrast, the parasite *Trypanosoma brucei* possess a single BRCA2 ortholog with 15 BRC repeats (Hartley and McCulloch, 2008). The BRC repeat is highly conserved among species; despite the different number of repeats, BRC domains in all BRCA2 orthologs examined so far have been shown to bind RAD51 directly and to promote RAD51 nucleoprotein filament formation on ssDNA, which is essential for homology search and strand exchange during HR. In addition, BRCA2 interaction with the highly conserved DSS1 protein also contributes to HR through promoting RAD51-recruitment activity and stability of BRCA2 (Li et al., 2006; Liu et al., 2010; Siaud et al., 2011). The CTRB domain, while conferring RAD51 binding and stabilizing RAD51 filaments on ssDNA, is not essential for HR (Davies and Pellegrini, 2007; Esashi et al., 2007; Prakash et al., 2015).

C. elegans BRCA2 (BRC-2) contains domain signatures similar to mammalian BRCA2 but is approximately 1/8 the size, with just 394 amino acids. BRC-2 contains a single BRC repeat that directly interacts with RAD51 and a single OB fold that preferentially binds to ssDNA (Martin et al., 2005; Petalcorin et al., 2006; **Figure 4**). The single BRC repeat is comprised of two RAD-51 interaction regions, one that preferentially binds to free RAD-51, and the other to the RAD-51-DNA nucleoprotein filament that exhibits inhibitory activity on RAD-51 ATPase hydrolysis. Together, these two RAD-51 interaction regions within the BRC repeat are proposed to coordinate the activity of BRC-2 for promoting RAD-51 nucleation on ssDNA and stabilizing existing RAD51 filament from disassembly through inhibiting ATP hydrolysis (Petalcorin et al., 2007). Recent single-molecule analysis has revealed that BRC-2 acts primarily as a RAD-51 nucleation factor on RPA-coated ssDNA (Belan et al., 2021).

BRCA2 Role in Meiotic Recombination

In addition to a role of promoting RAD51 mediated HR in somatic cells, studies on BRCA2 orthologs have revealed a requirement for BRCA2 during meiosis. In *Ustilago maydis,* mutation of Brh2 led to a failure in the formation of meiotic spore products (Kojic et al., 2002). Null mutants of BRCA2 ortholog in *Drosophila* led to sterility in both male and female flies (Klovstad et al., 2008; Weinberg-Shukron et al., 2018). A transgenic mouse line expressing low levels of human BRCA2 in the gonad showed reduced RAD51 and DMC1 foci formation and prophase arrest of spermatocytes, due to the inability to complete meiotic recombination (Sharan et al., 2004). Depletion of *A. thaliana* BRCA2 by RNAi showed meiotic defects similar to *rad51; dmc1* double mutants (Siaud et al., 2004) and *C. elegans brc-2* mutant produced completely inviable progeny (Martin et al., 2005), suggesting an indispensable role of BRCA2 during meiosis. Studies on human and *Arabidopsis* BRCA2 proteins demonstrated that BRCA2 directly binds to the meiosis-specific recombinase DMC1, which functions together with RAD51 to promote strand invasion and joint molecule formation during meiotic recombination (Dray et al., 2006; Thorslund et al., 2007; Jensen et al., 2010; Martinez et al., 2016). As with RAD51, the BRC repeats facilitate binding between BRCA2 and DMC1, although binding affinities for each individual BRC repeat differ between RAD51 and DMC1 (Martinez et al., 2016). Moreover, different mechanisms have been proposed for BRCA2 stimulation of RAD51 versus DMC1 recombinase activity. In the context of RAD51 mediated recombination, BRCA2 and its eight BRC repeats function by a combination of inhibiting RAD51 ATPase activity, promoting RAD51 filament formation

on ssDNA but not dsDNA, and enhancing strand exchange activity of RAD51. In contrast, stabilization of DMC1 filament on ssDNA was proposed to be the major mechanism by which BRCA2 functions with DMC1 (Martinez et al., 2016; **Figure 5**).

BRCA2 localization to DSBs in somatic cells depends on PALB2 (Xia et al., 2006). It has remained mysterious until recently, how BRCA2 is recruited to DSBs during meiosis. The Shibuya group identified a BRCA2 localizer in mice, which they named meiotic localizer of BRCA2 (MEILB2). MEILB2 is specifically expressed in germ cells and localizes to meiotic recombination sites on the chromosome axis. In the absence of MEILB2, the recruitment of DMC1 and RAD51 recombinase to meiotic DSBs is abolished, leading to sterility in male mice. Furthermore, MEILB2 directly binds to BRCA2 *in vitro* and is a physiological binding partner of BRCA2 *in vivo*. Removing MEILB2 impairs BRCA2 localization to resected ssDNA in spermatocytes, suggesting that MEILB2 recruits BRCA2 to sites undergoing meiotic recombination (Zhang et al., 2019). In contrast to males, female *Meilb2*$^{-/-}$ mice show only a ∼50% reduction in the localization of DMC1 and RAD51, and are sub-fertile, suggesting that redundant mechanisms exist to localize BRAC2 in oogenesis. One possibility is that PALB2 functions in concert with MEILB2 in female meiosis to localize BRCA2. Interestingly, PALB2 knockout mice show reduced male, but not female, fertility. This reduction in fertility is likely due to PALB2 interaction with BRCA1 (Simhadri et al., 2014). Future studies addressing the roles, redundancies and interconnections between PALB2, BRCA1 and BRCA2 will be important for understanding how meiotic DSBs are processed in male and female meiosis. Recently a third component of the BRCA2 complex, BRCA2 and MEILB2-associating protein 1 (BRME1), was identified. BRME1 forms a ternary complex with BRCA2 and MEILB2 and in the absence of BRME1, meiotic DSB repair, homologous chromosome synapsis and crossover formation were impaired in spermatogenesis (Takemoto et al., 2020; Zhang et al., 2020). MEILB2 is conserved among vertebrate taxa; whether binding partners promote meiotic regulation of BRCA2 in organisms such as worms and plants remain to be investigated.

Non-conserved Role of BRCA2 in *C. elegans* Meiosis

BRCA2's role in promoting RAD51/DMC1 nucleoprotein filament formation for homology search and strand exchange in meiotic recombination is conserved among all organisms where it has been examined. A RAD-51 independent, non-conserved role of BRC-2 was uncovered in *C. elegans* meiosis (Martin et al., 2005; Petalcorin et al., 2006). Without BRC-2, SPO-11 induced DSBs are resected, but RAD-51 is not recruited to the single stranded DNA, blocking strand invasion for error-free repair. As the presence of DSBs is extremely deleterious, alternative repair pathways are engaged to remove any remaining breaks before cells exit meiotic prophase I. In *rad-51* or *brc-2* single mutant, oogenic diakinesis nuclei exhibit aggregated DAPI staining chromosome structures, in contrast to the six

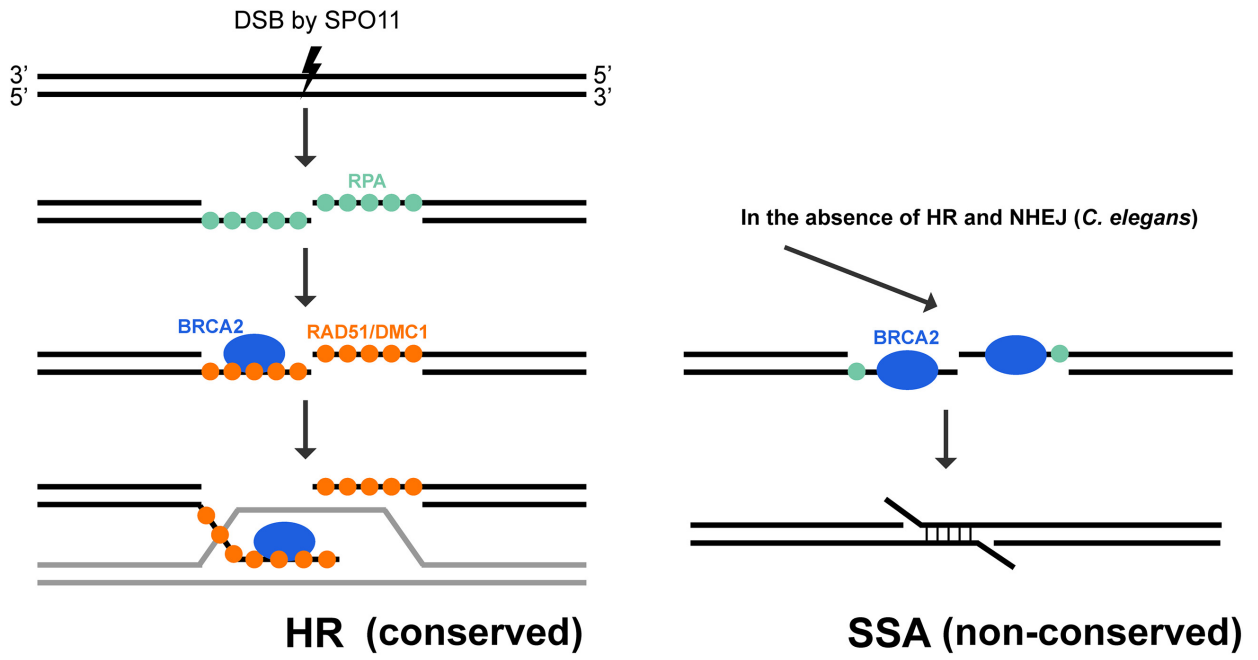

FIGURE 5 | Conserved and non-conserved roles of BRCA2 during meiosis. BRCA2 is an essential mediator of homologous recombination in meiosis. After SPO-11 induced DSB is resected, the 3′ ssDNA is coated with RPA. BRCA2 is critical for recruiting DMC1/RAD51 recombinases to displace RPA molecules on the ssDNA, promoting the formation and stabilization of nucleoprotein filaments to mediate homology search and strand exchange. This function of BRCA2 is highly conserved during meiosis among a large variety of organisms, including *C. elegans*. However, *C. elegans* BRC-2 also exhibits a non-conserved role in promoting single strand annealing when HR (*rad-51* mutant) and NHEJ (*lig-4* knock down) are not available for repair (Martin et al., 2005).

morphologically distinct bivalent structures in wild-type animals (**Figure 3B**). Inactivating NHEJ (*lig-4*) in the *brc-2* mutant resulted in mostly twelve DAPI bodies (**Figure 3B**), suggesting that the aggregation observed in *brc-2* is due to inappropriate repair of meiotic DSBs by NHEJ. However, when a functional BRC-2 was present, as in the case of the *lig-4; rad-51* double mutant, diakinesis nuclei contained clumped DAPI structures as seen in *brc-2* and *rad-51* single mutants (**Figure 3B**; Martin et al., 2005). This observation suggests that BRC-2 promotes an alternative repair pathway when both HR and NHEJ fail to be executed in meiocytes. A possible candidate for this repair pathway is single strand annealing (SSA). Indeed, *in vitro* experiments showed that purified *C. elegans* BRC-2 protein promoted annealing of single strand oligonucleotide coated with RPA (Petalcorin et al., 2006), an activity that mammalian BRCA2 does not possess (Jensen et al., 2010; **Figure 5**). It is likely that *C. elegans* BRC-2 has acquired this function to promote SSA during meiosis, as an ortholog of RAD52, which mediates SSA, is missing.

CONCLUSION

That organisms such as mice, *C. elegans*, and *A. thaliana* carrying mutations in their respective BRCA1 and BRCA2 orthologs exhibit meiotic phenotypes is consistent with BRCA1 and BRCA2 playing critical roles in meiosis. While important for meiotic recombination, BRCA1 and BRCA2 orthologs have acquired divergent functions throughout evolution. BRCA1 together with BARD1 functions as an E3 ubiquitin ligase that promotes ubiquitin transfer to a number of substrates and therefore plays regulatory roles in various processes. Not surprisingly, BRCA1 function during meiosis is quite diverse in different organisms (**Figure 2**). For example, BRCA1 is essential for MSCI in mice but is dispensable for MSCI in *C. elegans*, while *C. elegans* BRC-1 promotes DNA end resection, stabilizes the RAD-51 filament and regulates the crossover landscape. It remains an open question whether BRCA1-BARD1 functions in any of these aspects of meiotic recombination in mammals. Future studies taking advantage of conditional expression and genome editing tools should facilitate analyses on the role of E3 ligase activity, including identification of substrates, and the conserved BRCT domains. In contrast to BRCA1, BRCA2 plays a fundamental and conserved role in HR as a mediator to recruit RAD51 and DMC1 for nucleoprotein filament formation and strand invasion. However, *C. elegans* BRC-2 also uniquely promotes the alternative SSA pathway, perhaps as a consequence of a streamlined set of repair proteins (e.g., absence of DMC1 and RAD52) (**Figure 5**). While not identical, knowledge on meiotic roles of BRCA1 and BRCA2 from model organisms will continue to provide valuable insights into the mechanisms by which these two genes function during human meiosis. Clinical data has shown a correlation between the presence of BRCA1 and BRCA2 mutations in healthy carriers and ovarian aging, which is measured by elevated accumulation of DNA damage in oocytes and reduced primordial follicle reserve (Oktay et al., 2010; Lin et al., 2017; Lambertini et al., 2018). This indicates that the functions of BRCA1 and BRCA2 during human meiosis are likely to influence sperm and egg quality. Interestingly, some cancers inappropriately express meiotic genes and recent evidence suggests that this may lead to altered BRCA2 function (Hosoya et al., 2011; Zhang et al., 2020). HR was inhibited in somatic cells when the SC protein SYCP3 and the meiotic partners of BRCA2, MEILB2 and BRME1, were aberrantly expressed, presumably as a result of BRCA2 protein being sequestered when bound by the meiotic proteins. Future studies focusing on meiotic aspects of BRCA1 and BRCA2 may advance our knowledge in human reproduction as well as tumorigenesis to provide tools for improving fertility and health.

AUTHOR CONTRIBUTIONS

QL wrote the manuscript with content and editorial input from JE. Both authors contributed to the article and approved the submitted version.

FUNDING

Work in the Engebrecht lab is supported by National Institutes of Health GM103860.

ACKNOWLEDGMENTS

We are grateful to members of the Engebrecht lab for thoughtful discussions. We also acknowledge the meiosis research community and apologize to those researchers whose work we were unable to include.

REFERENCES

Abbott, D. W., Freeman, M. L., and Holt, J. T. (1998). Double-strand break repair deficiency and radiation sensitivity in BRCA2 mutant cancer cells. *J. Natl. Cancer Inst.* 90, 978–985. doi: 10.1093/jnci/90.13.978

Adamo, A., Montemauri, P., Silva, N., Ward, J. D., Boulton, S. J., and La Volpe, A. (2008). BRC-1 acts in the inter-sister pathway of meiotic double-strand break repair. *EMBO Rep.* 9, 287–292. doi: 10.1038/sj.embor.7401167

Aparicio, T., Baer, R., Gottesman, M., and Gautier, J. (2016). MRN, CtIP, and BRCA1 mediate repair of topoisomerase II-DNA adducts. *J. Cell Biol.* 212, 399–408. doi: 10.1083/jcb.201504005

Baer, R., and Ludwig, T. (2002). The BRCA1/BARD1 heterodimer, a tumor suppressor complex with ubiquitin E3 ligase activity. *Curr. Opin. Genet. Dev.* 12, 86–91. doi: 10.1016/s0959-437x(01)00269-6

Baudat, F., and de Massy, B. (2007). Regulating double-stranded DNA break repair towards crossover or non-crossover during mammalian meiosis. *Chromosome Res.* 15, 565–577. doi: 10.1007/s10577-007-1140-3

Belan, O., Barroso, C., Kaczmarczyk, A., Anand, R., Federico, S., O'reilly, N., et al. (2021). Single-molecule analysis reveals cooperative stimulation of Rad51 filament nucleation and growth by mediator proteins. *Mol. Cell* 81, 1058.e7–1073.e7.

Boulton, S. J., Martin, J. S., Polanowska, J., Hill, D. E., Gartner, A., and Vidal, M. (2004). BRCA1/BARD1 orthologs required for DNA repair in

Caenorhabditis elegans. *Curr. Biol.* 14, 33–39. doi: 10.1016/j.cub.2003.11.029

Broering, T. J., Alavattam, K. G., Sadreyev, R. I., Ichijima, Y., Kato, Y., Hasegawa, K., et al. (2014). BRCA1 establishes DNA damage signaling and pericentric heterochromatin of the X chromosome in male meiosis. *J. Cell Biol.* 205, 663–675. doi: 10.1083/jcb.201311050

Brown, M. S., and Bishop, D. K. (2014). DNA strand exchange and RecA homologs in meiosis. *Cold Spring Harb. Perspect. Biol.* 7:a016659. doi: 10.1101/cshperspect.a016659

Brzovic, P. S., Rajagopal, P., Hoyt, D. W., King, M. C., and Klevit, R. E. (2001). Structure of a BRCA1-BARD1 heterodimeric RING-RING complex. *Nat. Struct. Biol.* 8, 833–837.

Bunting, S. F., Callen, E., Wong, N., Chen, H. T., Polato, F., Gunn, A., et al. (2010). 53BP1 inhibits homologous recombination in Brca1-deficient cells by blocking resection of DNA breaks. *Cell* 141, 243–254. doi: 10.1016/j.cell.2010.03.012

Caestecker, K. W., and Van de Walle, G. R. (2013). The role of BRCA1 in DNA double-strand repair: past and present. *Exp. Cell Res.* 319, 575–587. doi: 10.1016/j.yexcr.2012.11.013

Carreira, A., Hilario, J., Amitani, I., Baskin, R. J., Shivji, M. K., Venkitaraman, A. R., et al. (2009). The BRC repeats of BRCA2 modulate the DNA-binding selectivity of RAD51. *Cell* 136, 1032–1043. doi: 10.1016/j.cell.2009.02.019

Chen, C. F., Chen, P. L., Zhong, Q., Sharp, Z. D., and Lee, W. H. (1999). Expression of BRC repeats in breast cancer cells disrupts the BRCA2-Rad51 complex and leads to radiation hypersensitivity and loss of G(2)/M checkpoint control. *J. Biol. Chem.* 274, 32931–32935. doi: 10.1074/jbc.274.46.32931

Chung, G., Rose, A. M., Petalcorin, M. I., Martin, J. S., Kessler, Z., Sanchez-Pulido, L., et al. (2015). REC-1 and HIM-5 distribute meiotic crossovers and function redundantly in meiotic double-strand break formation in *Caenorhabditis elegans*. *Genes Dev.* 29, 1969–1979. doi: 10.1101/gad.266056.115

Cressman, V. L., Backlund, D. C., Avrutskaya, A. V., Leadon, S. A., Godfrey, V., and Koller, B. H. (1999). Growth retardation, DNA repair defects, and lack of spermatogenesis in BRCA1-deficient mice. *Mol. Cell Biol.* 19, 7061–7075. doi: 10.1128/mcb.19.10.7061

Cruz-Garcia, A., Lopez-Saavedra, A., and Huertas, P. (2014). BRCA1 accelerates CtIP-mediated DNA-end resection. *Cell Rep.* 9, 451–459. doi: 10.1016/j.celrep.2014.08.076

Daley, J. M., and Sung, P. (2014). 53BP1, BRCA1, and the choice between recombination and end joining at DNA double-strand breaks. *Mol. Cell Biol.* 34, 1380–1388. doi: 10.1128/mcb.01639-13

Davies, O. R., and Pellegrini, L. (2007). Interaction with the BRCA2 C terminus protects RAD51-DNA filaments from disassembly by BRC repeats. *Nat. Struct. Mol. Biol.* 14, 475–483. doi: 10.1038/nsmb1251

Deng, C. X. (2002). Roles of BRCA1 in centrosome duplication. *Oncogene* 21, 6222–6227. doi: 10.1038/sj.onc.1205713

Deng, C. X. (2006). BRCA1: cell cycle checkpoint, genetic instability, DNA damage response and cancer evolution. *Nucleic Acids Res.* 34, 1416–1426. doi: 10.1093/nar/gkl010

Densham, R. M., Garvin, A. J., Stone, H. R., Strachan, J., Baldock, R. A., Daza-Martin, M., et al. (2016). Human BRCA1-BARD1 ubiquitin ligase activity counteracts chromatin barriers to DNA resection. *Nat. Struct. Mol. Biol.* 23, 647–655. doi: 10.1038/nsmb.3236

Dernburg, A. F., Mcdonald, K., Moulder, G., Barstead, R., Dresser, M., and Villeneuve, A. M. (1998). Meiotic recombination in *C. elegans* initiates by a conserved mechanism and is dispensable for homologous chromosome synapsis. *Cell* 94, 387–398. doi: 10.1016/s0092-8674(00)81481-6

Deshaies, R. J., and Joazeiro, C. A. (2009). RING domain E3 ubiquitin ligases. *Annu. Rev. Biochem.* 78, 399–434. doi: 10.1146/annurev.biochem.78.101807.093809

Dray, E., Siaud, N., Dubois, E., and Doutriaux, M. P. (2006). Interaction between *Arabidopsis* Brca2 and its partners Rad51, Dmc1, and Dss1. *Plant Physiol.* 140, 1059–1069. doi: 10.1104/pp.105.075838

Esashi, F., Christ, N., Gannon, J., Liu, Y., Hunt, T., Jasin, M., et al. (2005). CDK-dependent phosphorylation of BRCA2 as a regulatory mechanism for recombinational repair. *Nature* 434, 598–604. doi: 10.1038/nature03404

Esashi, F., Galkin, V. E., Yu, X., Egelman, E. H., and West, S. C. (2007). Stabilization of RAD51 nucleoprotein filaments by the C-terminal region of BRCA2. *Nat. Struct. Mol. Biol.* 14, 468–474. doi: 10.1038/nsmb1245

Fernandez-Capetillo, O., Mahadevaiah, S. K., Celeste, A., Romanienko, P. J., Camerini-Otero, R. D., Bonner, W. M., et al. (2003). H2AX is required for chromatin remodeling and inactivation of sex chromosomes in male mouse meiosis. *Dev. Cell* 4, 497–508. doi: 10.1016/s1534-5807(03)00093-5

Fox, D. III, Le Trong, I., Rajagopal, P., Brzovic, P. S., Stenkamp, R. E., and Klevit, R. E. (2008). Crystal structure of the BARD1 ankyrin repeat domain and its functional consequences. *J. Biol. Chem.* 283, 21179–21186. doi: 10.1074/jbc.m802333200

Futreal, P. A., Liu, Q., Shattuck-Eidens, D., Cochran, C., Harshman, K., Tavtigian, S., et al. (1994). BRCA1 mutations in primary breast and ovarian carcinomas. *Science* 266, 120–122. doi: 10.1126/science.7939630

Garcia, V., Phelps, S. E., Gray, S., and Neale, M. J. (2011). Bidirectional resection of DNA double-strand breaks by Mre11 and Exo1. *Nature* 479, 241–244. doi: 10.1038/nature10515

Garcia-Muse, T., Galindo-Diaz, U., Garcia-Rubio, M., Martin, J. S., Polanowska, J., O'reilly, N., et al. (2019). A meiotic checkpoint alters repair partner bias to permit inter-sister repair of persistent DSBs. *Cell Rep.* 26, 775.e5–787.e5.

Ghimenti, C., Sensi, E., Presciuttini, S., Brunetti, I. M., Conte, P., Bevilacqua, G., et al. (2002). Germline mutations of the BRCA1-associated ring domain (BARD1) gene in breast and breast/ovarian families negative for BRCA1 and BRCA2 alterations. *Genes Chromosomes Cancer* 33, 235–242. doi: 10.1002/gcc.1223

Godwin, A. K., Vanderveer, L., Schultz, D. C., Lynch, H. T., Altomare, D. A., Buetow, K. H., et al. (1994). A common region of deletion on chromosome 17q in both sporadic and familial epithelial ovarian tumors distal to BRCA1. *Am. J. Hum. Genet.* 55, 666–677.

Gowen, L. C., Johnson, B. L., Latour, A. M., Sulik, K. K., and Koller, B. H. (1996). Brca1 deficiency results in early embryonic lethality characterized by neuroepithelial abnormalities. *Nat. Genet.* 12, 191–194. doi: 10.1038/ng0296-191

Gray, S., and Cohen, P. E. (2016). Control of meiotic crossovers: from double-strand break formation to designation. *Annu. Rev. Genet.* 50, 175–210. doi: 10.1146/annurev-genet-120215-035111

Gudmundsdottir, K., and Ashworth, A. (2004). BRCA2 in meiosis: turning over a new leaf. *Trends Cell Biol.* 14, 401–404. doi: 10.1016/j.tcb.2004.07.002

Hakem, R., De La Pompa, J. L., Sirard, C., Mo, R., Woo, M., Hakem, A., et al. (1996). The tumor suppressor gene Brca1 is required for embryonic cellular proliferation in the mouse. *Cell* 85, 1009–1023. doi: 10.1016/s0092-8674(00)81302-1

Hall, J. M., Lee, M. K., Newman, B., Morrow, J. E., Anderson, L. A., Huey, B., et al. (1990). Linkage of early-onset familial breast cancer to chromosome 17q21. *Science* 250, 1684–1689. doi: 10.1126/science.2270482

Hartley, C. L., and McCulloch, R. (2008). Trypanosoma brucei BRCA2 acts in antigenic variation and has undergone a recent expansion in BRC repeat number that is important during homologous recombination. *Mol. Microbiol.* 68, 1237–1251. doi: 10.1111/j.1365-2958.2008.06230.x

Hashizume, R., Fukuda, M., Maeda, I., Nishikawa, H., Oyake, D., Yabuki, Y., et al. (2001). The RING heterodimer BRCA1-BARD1 is a ubiquitin ligase inactivated by a breast cancer-derived mutation. *J. Biol. Chem.* 276, 14537–14540. doi: 10.1074/jbc.c000881200

Hatchi, E., Skourti-Stathaki, K., Ventz, S., Pinello, L., Yen, A., Kamieniarz-Gdula, K., et al. (2015). BRCA1 recruitment to transcriptional pause sites is required for R-loop-driven DNA damage repair. *Mol. Cell* 57, 636–647. doi: 10.1016/j.molcel.2015.01.011

Hill, S. J., Rolland, T., Adelmant, G., Xia, X., Owen, M. S., Dricot, A., et al. (2014). Systematic screening reveals a role for BRCA1 in the response to transcription-associated DNA damage. *Genes Dev.* 28, 1957–1975. doi: 10.1101/gad.241620.114

Hillers, K. J., Jantsch, V., Martinez-Perez, E., and Yanowitz, J. L. (2017). Meiosis. *WormBook* 2017, 1–43. doi: 10.1016/b978-0-12-503365-7.50005-5

Hong, Y., Sonneville, R., Agostinho, A., Meier, B., Wang, B., Blow, J. J., et al. (2016). The SMC-5/6 complex and the HIM-6 (BLM) helicase synergistically promote meiotic recombination intermediate processing and chromosome maturation during *Caenorhabditis elegans* Meiosis. *PLoS Genet.* 12:e1005872. doi: 10.1371/journal.pgen.1005872

Hosoya, N., Okajima, M., Kinomura, A., Fujii, Y., Hiyama, T., Sun, J., et al. (2011). Synaptonemal complex protein SYCP3 impairs mitotic recombination

by interfering with BRCA2. *EMBO Rep.* 13, 44–51. doi: 10.1038/embor.2011.221

Huber, L. J., Yang, T. W., Sarkisian, C. J., Master, S. R., Deng, C. X., and Chodosh, L. A. (2001). Impaired DNA damage response in cells expressing an exon 11-deleted murine Brca1 variant that localizes to nuclear foci. *Mol. Cell Biol.* 21, 4005–4015. doi: 10.1128/mcb.21.12.4005-4015.2001

Jagut, M., Hamminger, P., Woglar, A., Millonigg, S., Paulin, L., Mikl, M., et al. (2016). Separable roles for a *Caenorhabditis elegans* RMI1 homolog in promoting and antagonizing meiotic crossovers ensure faithful chromosome inheritance. *PLoS Biol.* 14:e1002412. doi: 10.1371/journal.pbio.1002412

Janisiw, E., Dello Stritto, M. R., Jantsch, V., and Silva, N. (2018). BRCA1-BARD1 associate with the synaptonemal complex and pro-crossover factors and influence RAD-51 dynamics during *Caenorhabditis elegans* meiosis. *PLoS Genet.* 14:e1007653. doi: 10.1371/journal.pgen.1007653

Jensen, R. B., Carreira, A., and Kowalczykowski, S. C. (2010). Purified human BRCA2 stimulates RAD51-mediated recombination. *Nature* 467, 678–683. doi: 10.1038/nature09399

Kamp, J. A., Van Schendel, R., Dilweg, I. W., and Tijsterman, M. (2020). BRCA1-associated structural variations are a consequence of polymerase theta-mediated end-joining. *Nat. Commun.* 11:3615.

King, M. C., Marks, J. H., Mandell, J. B., and New York Breast Cancer Study Group (2003). Breast and ovarian cancer risks due to inherited mutations in BRCA1 and BRCA2. *Science* 302, 643–646. doi: 10.1126/science.1088759

Klovstad, M., Abdu, U., and Schupbach, T. (2008). Drosophila brca2 is required for mitotic and meiotic DNA repair and efficient activation of the meiotic recombination checkpoint. *PLoS Genet.* 4:e31. doi: 10.1371/journal.pgen.0040031

Kojic, M., Kostrub, C. F., Buchman, A. R., and Holloman, W. K. (2002). BRCA2 homolog required for proficiency in DNA repair, recombination, and genome stability in *Ustilago maydis*. *Mol. Cell* 10, 683–691. doi: 10.1016/s1097-2765(02)00632-9

Kojic, M., Zhou, Q., Lisby, M., and Holloman, W. K. (2005). Brh2-Dss1 interplay enables properly controlled recombination in *Ustilago maydis*. *Mol. Cell Biol.* 25, 2547–2557. doi: 10.1128/mcb.25.7.2547-2557.2005

Kouznetsova, A., Wang, H., Bellani, M., Camerini-Otero, R. D., Jessberger, R., and Hoog, C. (2009). BRCA1-mediated chromatin silencing is limited to oocytes with a small number of asynapsed chromosomes. *J. Cell Sci.* 122, 2446–2452. doi: 10.1242/jcs.049353

Kowalczykowski, S. C. (2015). An overview of the molecular mechanisms of recombinational DNA repair. *Cold Spring Harb. Perspect. Biol.* 7:a016410. doi: 10.1101/cshperspect.a016410

Lam, I., and Keeney, S. (2014). Mechanism and regulation of meiotic recombination initiation. *Cold Spring Harb. Perspect. Biol.* 7:a016634. doi: 10.1101/cshperspect.a016634

Lambertini, M., Goldrat, O., Ferreira, A. R., Dechene, J., Azim, H. A. Jr., Desir, J., et al. (2018). Reproductive potential and performance of fertility preservation strategies in BRCA-mutated breast cancer patients. *Ann. Oncol.* 29, 237–243. doi: 10.1093/annonc/mdx639

Leon-Ortiz, A. M., Panier, S., Sarek, G., Vannier, J. B., Patel, H., Campbell, P. J., et al. (2018). A distinct class of genome rearrangements driven by heterologous recombination. *Mol. Cell* 69, 292.e6–305.e6.

Li, J., Zou, C., Bai, Y., Wazer, D. E., Band, V., and Gao, Q. (2006). DSS1 is required for the stability of BRCA2. *Oncogene* 25, 1186–1194. doi: 10.1038/sj.onc.1209153

Li, M. L., and Greenberg, R. A. (2012). Links between genome integrity and BRCA1 tumor suppression. *Trends Biochem. Sci.* 37, 418–424. doi: 10.1016/j.tibs.2012.06.007

Li, Q., Hariri, S., and Engebrecht, J. (2020). Meiotic double-strand break processing and crossover patterning are regulated in a sex-specific manner by BRCA1-BARD1 in *Caenorhabditis elegans*. *Genetics* 216, 359–379. doi: 10.1534/genetics.120.303292

Li, Q., Saito, T. T., Martinez-Garcia, M., Deshong, A. J., Nadarajan, S., Lawrence, K. S., et al. (2018). The tumor suppressor BRCA1-BARD1 complex localizes to the synaptonemal complex and regulates recombination under meiotic dysfunction in *Caenorhabditis elegans*. *PLoS Genet.* 14:e1007701. doi: 10.1371/journal.pgen.1007701

Lin, W., Titus, S., Moy, F., Ginsburg, E. S., and Oktay, K. (2017). Ovarian aging in women with BRCA germline mutations. *J. Clin. Endocrinol. Metab.* 102, 3839–3847. doi: 10.1210/jc.2017-00765

Liu, C. Y., Flesken-Nikitin, A., Li, S., Zeng, Y., and Lee, W. H. (1996). Inactivation of the mouse Brca1 gene leads to failure in the morphogenesis of the egg cylinder in early postimplantation development. *Genes Dev.* 10, 1835–1843. doi: 10.1101/gad.10.14.1835

Liu, J., Doty, T., Gibson, B., and Heyer, W. D. (2010). Human BRCA2 protein promotes RAD51 filament formation on RPA-covered single-stranded DNA. *Nat. Struct. Mol. Biol.* 17, 1260–1262. doi: 10.1038/nsmb.1904

Ludwig, T., Chapman, D. L., Papaioannou, V. E., and Efstratiadis, A. (1997). Targeted mutations of breast cancer susceptibility gene homologs in mice: lethal phenotypes of Brca1, Brca2, Brca1/Brca2, Brca1/p53, and Brca2/p53 nullizygous embryos. *Genes Dev.* 11, 1226–1241. doi: 10.1101/gad.11.10.1226

Lui, D. Y., and Colaiacovo, M. P. (2013). Meiotic development *in Caenorhabditis elegans*. *Adv. Exp. Med. Biol.* 757, 133–170. doi: 10.1007/978-1-4614-4015-4_6

Mahadevaiah, S. K., Bourc'his, D., De Rooij, D. G., Bestor, T. H., Turner, J. M., and Burgoyne, P. S. (2008). Extensive meiotic asynapsis in mice antagonises meiotic silencing of unsynapsed chromatin and consequently disrupts meiotic sex chromosome inactivation. *J. Cell Biol.* 182, 263–276. doi: 10.1083/jcb.200710195

Manke, I. A., Lowery, D. M., Nguyen, A., and Yaffe, M. B. (2003). BRCT repeats as phosphopeptide-binding modules involved in protein targeting. *Science* 302, 636–639. doi: 10.1126/science.1088877

Martin, J. S., Winkelmann, N., Petalcorin, M. I., Mcilwraith, M. J., and Boulton, S. J. (2005). RAD-51-dependent and -independent roles of a *Caenorhabditis elegans* BRCA2-related protein during DNA double-strand break repair. *Mol. Cell Biol.* 25, 3127–3139. doi: 10.1128/mcb.25.8.3127-3139.2005

Martinez, J. S., Von Nicolai, C., Kim, T., Ehlen, A., Mazin, A. V., Kowalczykowski, S. C., et al. (2016). BRCA2 regulates DMC1-mediated recombination through the BRC repeats. *Proc. Natl. Acad. Sci. U.S.A.* 113, 3515–3520. doi: 10.1073/pnas.1601691113

McCarthy, E. E., Celebi, J. T., Baer, R., and Ludwig, T. (2003). Loss of Bard1, the heterodimeric partner of the Brca1 tumor suppressor, results in early embryonic lethality and chromosomal instability. *Mol. Cell Biol.* 23, 5056–5063. doi: 10.1128/mcb.23.14.5056-5063.2003

Meneely, P. M., Mcgovern, O. L., Heinis, F. I., and Yanowitz, J. L. (2012). Crossover distribution and frequency are regulated by him-5 in *Caenorhabditis elegans*. *Genetics* 190, 1251–1266. doi: 10.1534/genetics.111.137463

Meza, J. E., Brzovic, P. S., King, M. C., and Klevit, R. E. (1999). Mapping the functional domains of BRCA1. Interaction of the ring finger domains of BRCA1 and BARD1. *J. Biol. Chem.* 274, 5659–5665.

Miki, Y., Swensen, J., Shattuck-Eidens, D., Futreal, P. A., Harshman, K., Tavtigian, S., et al. (1994). A strong candidate for the breast and ovarian cancer susceptibility gene BRCA1. *Science* 266, 66–71. doi: 10.1126/science.7545954

Moynahan, M. E., Chiu, J. W., Koller, B. H., and Jasin, M. (1999). Brca1 controls homology-directed DNA repair. *Mol. Cell* 4, 511–518. doi: 10.1016/s1097-2765(00)80202-6

Moynahan, M. E., Pierce, A. J., and Jasin, M. (2001). BRCA2 is required for homology-directed repair of chromosomal breaks. *Mol. Cell* 7, 263–272. doi: 10.1016/s1097-2765(01)00174-5

Nakamura, K., Saredi, G., Becker, J. R., Foster, B. M., Nguyen, N. V., Beyer, T. E., et al. (2019). H4K20me0 recognition by BRCA1-BARD1 directs homologous recombination to sister chromatids. *Nat. Cell Biol.* 21, 311–318. doi: 10.1038/s41556-019-0282-9

Neale, M. J., and Keeney, S. (2006). Clarifying the mechanics of DNA strand exchange in meiotic recombination. *Nature* 442, 153–158. doi: 10.1038/nature04885

Negrini, S., Gorgoulis, V. G., and Halazonetis, T. D. (2010). Genomic instability–an evolving hallmark of cancer. *Nat. Rev. Mol. Cell Biol.* 11, 220–228. doi: 10.1038/nrm2858

Oktay, K., Kim, J. Y., Barad, D., and Babayev, S. N. (2010). Association of BRCA1 mutations with occult primary ovarian insufficiency: a possible explanation for the link between infertility and breast/ovarian cancer risks. *J. Clin. Oncol.* 28, 240–244. doi: 10.1200/jco.2009.24.2057

Paiano, J., Wu, W., Yamada, S., Sciascia, N., Callen, E., Paola Cotrim, A., et al. (2020). ATM and PRDM9 regulate SPO11-bound recombination intermediates during meiosis. *Nat. Commun.* 11:857.

Petalcorin, M. I., Galkin, V. E., Yu, X., Egelman, E. H., and Boulton, S. J. (2007). Stabilization of RAD-51-DNA filaments via an interaction domain in *Caenorhabditis elegans* BRCA2. *Proc. Natl. Acad. Sci. U.S.A.* 104, 8299–8304. doi: 10.1073/pnas.0702805104

Petalcorin, M. I., Sandall, J., Wigley, D. B., and Boulton, S. J. (2006). CeBRC-2 stimulates D-loop formation by RAD-51 and promotes DNA single-strand annealing. *J Mol. Biol.* 361, 231–242. doi: 10.1016/j.jmb.2006.06.020

Polanowska, J., Martin, J. S., Garcia-Muse, T., Petalcorin, M. I., and Boulton, S. J. (2006). A conserved pathway to activate BRCA1-dependent ubiquitylation at DNA damage sites. *EMBO J.* 25, 2178–2188. doi: 10.1038/sj.emboj.7601102

Prakash, R., Zhang, Y., Feng, W., and Jasin, M. (2015). Homologous recombination and human health: the roles of BRCA1, BRCA2, and associated proteins. *Cold Spring Harb. Perspect. Biol.* 7:a016600. doi: 10.1101/cshperspect.a016600

Reidt, W., Wurz, R., Wanieck, K., Chu, H. H., and Puchta, H. (2006). A homologue of the breast cancer-associated gene BARD1 is involved in DNA repair in plants. *EMBO J.* 25, 4326–4337. doi: 10.1038/sj.emboj.7601313

Rodriguez, M., Yu, X., Chen, J., and Songyang, Z. (2003). Phosphopeptide binding specificities of BRCA1 COOH-terminal (BRCT) domains. *J. Biol. Chem.* 278, 52914–52918. doi: 10.1074/jbc.c300407200

Roy, R., Chun, J., and Powell, S. N. (2011). BRCA1 and BRCA2: different roles in a common pathway of genome protection. *Nat. Rev. Cancer* 12, 68–78. doi: 10.1038/nrc3181

Saito, T. T., and Colaiacovo, M. P. (2017). Regulation of crossover frequency and distribution during meiotic recombination. *Cold Spring Harb. Symp. Quant. Biol.* 82, 223–234. doi: 10.1101/sqb.2017.82.034132

Saito, T. T., Lui, D. Y., Kim, H. M., Meyer, K., and Colaiacovo, M. P. (2013). Interplay between structure-specific endonucleases for crossover control during *Caenorhabditis elegans* meiosis. *PLoS Genet.* 9:e1003586. doi: 10.1371/journal.pgen.1003586

Saito, T. T., Mohideen, F., Meyer, K., Harper, J. W., and Colaiacovo, M. P. (2012). SLX-1 is required for maintaining genomic integrity and promoting meiotic noncrossovers in the *Caenorhabditis elegans* germline. *PLoS Genet.* 8:e1002888. doi: 10.1371/journal.pgen.1002888

Scully, R., Chen, J., Plug, A., Xiao, Y., Weaver, D., Feunteun, J., et al. (1997). Association of BRCA1 with Rad51 in mitotic and meiotic cells. *Cell* 88, 265–275. doi: 10.1016/s0092-8674(00)81847-4

Sharan, S. K., Morimatsu, M., Albrecht, U., Lim, D. S., Regel, E., Dinh, C., et al. (1997). Embryonic lethality and radiation hypersensitivity mediated by Rad51 in mice lacking Brca2. *Nature* 386, 804–810. doi: 10.1038/386804a0

Sharan, S. K., Pyle, A., Coppola, V., Babus, J., Swaminathan, S., Benedict, J., et al. (2004). BRCA2 deficiency in mice leads to meiotic impairment and infertility. *Development* 131, 131–142. doi: 10.1242/dev.00888

Shinohara, A., and Shinohara, M. (2004). Roles of RecA homologues Rad51 and Dmc1 during meiotic recombination. *Cytogenet. Genome Res.* 107, 201–207. doi: 10.1159/000080598

Shivji, M. K., Mukund, S. R., Rajendra, E., Chen, S., Short, J. M., Savill, J., et al. (2009). The BRC repeats of human BRCA2 differentially regulate RAD51 binding on single- versus double-stranded DNA to stimulate strand exchange. *Proc. Natl. Acad. Sci. U.S.A.* 106, 13254–13259. doi: 10.1073/pnas.0906208106

Siaud, N., Barbera, M. A., Egashira, A., Lam, I., Christ, N., Schlacher, K., et al. (2011). Plasticity of BRCA2 function in homologous recombination: genetic interactions of the PALB2 and DNA binding domains. *PLoS Genet.* 7:e1002409. doi: 10.1371/journal.pgen.1002409

Siaud, N., Dray, E., Gy, I., Gerard, E., Takvorian, N., and Doutriaux, M. P. (2004). Brca2 is involved in meiosis in *Arabidopsis thaliana* as suggested by its interaction with Dmc1. *EMBO J.* 23, 1392–1401. doi: 10.1038/sj.emboj.7600146

Simhadri, S., Peterson, S., Patel, D. S., Huo, Y., Cai, H., Bowman-Colin, C., et al. (2014). Male fertility defect associated with disrupted BRCA1-PALB2 interaction in mice. *J. Biol. Chem.* 289, 24617–24629. doi: 10.1074/jbc.m114.566141

Steinfeld, J. B., Belan, O., Kwon, Y., Terakawa, T., Al-Zain, A., Smith, M. J., et al. (2019). Defining the influence of Rad51 and Dmc1 lineage-specific amino acids on genetic recombination. *Genes Dev.* 33, 1191–1207. doi: 10.1101/gad.328062.119

Takemoto, K., Tani, N., Takada-Horisawa, Y., Fujimura, S., Tanno, N., Yamane, M., et al. (2020). Meiosis-Specific C19orf57/4930432K21Rik/BRME1 Modulates Localization of RAD51 and DMC1 to DSBs in mouse meiotic recombination. *Cell Rep.* 31:107686. doi: 10.1016/j.celrep.2020.107686

Thai, T. H., Du, F., Tsan, J. T., Jin, Y., Phung, A., Spillman, M. A., et al. (1998). Mutations in the BRCA1-associated RING domain (BARD1) gene in primary breast, ovarian and uterine cancers. *Hum. Mol. Genet.* 7, 195–202. doi: 10.1093/hmg/7.2.195

Thakur, S., Zhang, H. B., Peng, Y., Le, H., Carroll, B., Ward, T., et al. (1997). Localization of BRCA1 and a splice variant identifies the nuclear localization signal. *Mol. Cell Biol.* 17, 444–452. doi: 10.1128/mcb.17.1.444

Thorslund, T., Esashi, F., and West, S. C. (2007). Interactions between human BRCA2 protein and the meiosis-specific recombinase DMC1. *EMBO J.* 26, 2915–2922. doi: 10.1038/sj.emboj.7601739

Thorslund, T., Mcilwraith, M. J., Compton, S. A., Lekomtsev, S., Petronczki, M., Griffith, J. D., et al. (2010). The breast cancer tumor suppressor BRCA2 promotes the specific targeting of RAD51 to single-stranded DNA. *Nat. Struct. Mol. Biol.* 17, 1263–1265. doi: 10.1038/nsmb.1905

Turner, J. M. (2007). Meiotic sex chromosome inactivation. *Development* 134, 1823–1831. doi: 10.1242/dev.000018

Turner, J. M., Aprelikova, O., Xu, X., Wang, R., Kim, S., Chandramouli, G. V., et al. (2004). BRCA1, histone H2AX phosphorylation, and male meiotic sex chromosome inactivation. *Curr. Biol.* 14, 2135–2142. doi: 10.1016/j.cub.2004.11.032

Tutt, A., Gabriel, A., Bertwistle, D., Connor, F., Paterson, H., Peacock, J., et al. (1999). Absence of Brca2 causes genome instability by chromosome breakage and loss associated with centrosome amplification. *Curr. Biol.* 9, 1107–1110. doi: 10.1016/s0960-9822(99)80479-5

Venkitaraman, A. R. (2002). Cancer susceptibility and the functions of BRCA1 and BRCA2. *Cell* 108, 171–182. doi: 10.1016/s0092-8674(02)00615-3

Volkova, N. V., Meier, B., Gonzalez-Huici, V., Bertolini, S., Gonzalez, S., Vohringer, H., et al. (2020). Mutational signatures are jointly shaped by DNA damage and repair. *Nat. Commun.* 11:2169.

Wagner, C. R., Kuervers, L., Baillie, D. L., and Yanowitz, J. L. (2010). xnd-1 regulates the global recombination landscape in *Caenorhabditis elegans*. *Nature* 467, 839–843. doi: 10.1038/nature09429

Weinberg-Shukron, A., Rachmiel, M., Renbaum, P., Gulsuner, S., Walsh, T., Lobel, O., et al. (2018). Essential role of BRCA2 in ovarian development and function. *N. Engl. J. Med.* 379, 1042–1049.

Wong, A. K., Pero, R., Ormonde, P. A., Tavtigian, S. V., and Bartel, P. L. (1997). RAD51 interacts with the evolutionarily conserved BRC motifs in the human breast cancer susceptibility gene brca2. *J. Biol. Chem.* 272, 31941–31944. doi: 10.1074/jbc.272.51.31941

Wooster, R., Bignell, G., Lancaster, J., Swift, S., Seal, S., Mangion, J., et al. (1995). Identification of the breast cancer susceptibility gene BRCA2. *Nature* 378, 789–792.

Wu, L. C., Wang, Z. W., Tsan, J. T., Spillman, M. A., Phung, A., Xu, X. L., et al. (1996). Identification of a RING protein that can interact in vivo with the BRCA1 gene product. *Nat. Genet.* 14, 430–440. doi: 10.1038/ng1296-430

Xia, B., Sheng, Q., Nakanishi, K., Ohashi, A., Wu, J., Christ, N., et al. (2006). Control of BRCA2 cellular and clinical functions by a nuclear partner. PALB2. *Mol. Cell* 22, 719–729. doi: 10.1016/j.molcel.2006.05.022

Xu, X., Aprelikova, O., Moens, P., Deng, C. X., and Furth, P. A. (2003). Impaired meiotic DNA-damage repair and lack of crossing-over during spermatogenesis in BRCA1 full-length isoform deficient mice. *Development* 130, 2001–2012. doi: 10.1242/dev.00410

Xu, X., Qiao, W., Linke, S. P., Cao, L., Li, W. M., Furth, P. A., et al. (2001). Genetic interactions between tumor suppressors Brca1 and p53 in apoptosis, cell cycle and tumorigenesis. *Nat. Genet.* 28, 266–271. doi: 10.1038/90108

Xu, X., Weaver, Z., Linke, S. P., Li, C., Gotay, J., Wang, X. W., et al. (1999). Centrosome amplification and a defective G2-M cell cycle checkpoint induce genetic instability in BRCA1 exon 11 isoform-deficient cells. *Mol. Cell* 3, 389–395. doi: 10.1016/s1097-2765(00)80466-9

Yang, H., Jeffrey, P. D., Miller, J., Kinnucan, E., Sun, Y., Thoma, N. H., et al. (2002). BRCA2 function in DNA binding and recombination from a BRCA2-DSS1-ssDNA structure. *Science* 297, 1837–1848. doi: 10.1126/science.297.5588.1837

Yarden, R. I., Pardo-Reoyo, S., Sgagias, M., Cowan, K. H., and Brody, L. C. (2002). BRCA1 regulates the G2/M checkpoint by activating Chk1 kinase upon DNA damage. *Nat. Genet.* 30, 285–289. doi: 10.1038/ng837

Yokoo, R., Zawadzki, K. A., Nabeshima, K., Drake, M., Arur, S., and Villeneuve, A. M. (2012). COSA-1 reveals robust homeostasis and separable licensing and

reinforcement steps governing meiotic crossovers. *Cell* 149, 75–87. doi: 10.1016/j.cell.2012.01.052

Yu, V. P., Koehler, M., Steinlein, C., Schmid, M., Hanakahi, L. A., Van Gool, A. J., et al. (2000). Gross chromosomal rearrangements and genetic exchange between nonhomologous chromosomes following BRCA2 inactivation. *Genes Dev.* 14, 1400–1406.

Yu, X., Chini, C. C., He, M., Mer, G., and Chen, J. (2003). The BRCT domain is a phospho-protein binding domain. *Science* 302, 639–642. doi: 10.1126/science.1088753

Yu, Z., Kim, Y., and Dernburg, A. F. (2016). Meiotic recombination and the crossover assurance checkpoint in *Caenorhabditis elegans*. *Semin. Cell Dev. Biol.* 54, 106–116. doi: 10.1016/j.semcdb.2016.03.014

Yuan, S. S., Lee, S. Y., Chen, G., Song, M., Tomlinson, G. E., and Lee, E. Y. (1999). BRCA2 is required for ionizing radiation-induced assembly of Rad51 complex in vivo. *Cancer Res.* 59, 3547–3551.

Zetka, M. C., and Rose, A. M. (1995). Mutant rec-1 eliminates the meiotic pattern of crossing over in *Caenorhabditis elegans*. *Genetics* 141, 1339–1349. doi: 10.1093/genetics/141.4.1339

Zhang, J., Fujiwara, Y., Yamamoto, S., and Shibuya, H. (2019). A meiosis-specific BRCA2 binding protein recruits recombinases to DNA double-strand breaks to ensure homologous recombination. *Nat. Commun.* 10:722.

Zhang, J., Gurusaran, M., Fujiwara, Y., Zhang, K., Echbarthi, M., Vorontsov, E., et al. (2020). The BRCA2-MEILB2-BRME1 complex governs meiotic recombination and impairs the mitotic BRCA2-RAD51 function in cancer cells. *Nat. Commun.* 11:2055.

Zhao, W., Steinfeld, J. B., Liang, F., Chen, X., Maranon, D. G., Jian Ma, C., et al. (2017). BRCA1-BARD1 promotes RAD51-mediated homologous DNA pairing. *Nature* 550, 360–365. doi: 10.1038/nature24060

Zickler, D., and Kleckner, N. (2015). Recombination, pairing, and synapsis of homologs during meiosis. *Cold Spring Harb. Perspect. Biol.* 7:a016626. doi: 10.1101/cshperspect.a016626

Conflict of Interest: The authors declare that the research was conducted in the absence of any commercial or financial relationships that could be construed as a potential conflict of interest.

Copyright © 2021 Li and Engebrecht. This is an open-access article distributed under the terms of the Creative Commons Attribution License (CC BY). The use, distribution or reproduction in other forums is permitted, provided the original author(s) and the copyright owner(s) are credited and that the original publication in this journal is cited, in accordance with accepted academic practice. No use, distribution or reproduction is permitted which does not comply with these terms.

frontiers in Cell and Developmental Biology

REVIEW
published: 10 May 2021
doi: 10.3389/fcell.2021.670599

Sexual Dimorphism in Mouse Meiosis

*Rong Hua and Mingxi Liu**

State Key Laboratory of Reproductive Medicine, Department of Histology and Embryology, School of Basic Medical Sciences, Nanjing Medical University, Nanjing, China

Meiosis is a highly conserved and essential process in gametogenesis in sexually reproducing organisms. However, there are substantial sex-specific differences within individual species with respect to meiosis-related chromatin reorganization, recombination, and tolerance for meiotic defects. A wide range of murine models have been developed over the past two decades to study the complex regulatory processes governing mammalian meiosis. The present review article thus provides a comprehensive overview of the knockout mice that have been employed to study meiosis, with a particular focus on gene- and gametogenesis-related sexual dimorphism observed in these model animals. In so doing, we aim to provide a firm foundation for the future study of sex-specific differences in meiosis at the molecular level.

OPEN ACCESS

Edited by:
Wei Li,
Chinese Academy of Sciences (CAS), China

Reviewed by:
Shuiqiao Yuan,
Huazhong University of Science and Technology, China
Jeremy Wang,
University of Pennsylvania, United States

***Correspondence:**
Mingxi Liu
mingxi.liu@njmu.edu.cn

Specialty section:
This article was submitted to Cell Growth and Division, a section of the journal Frontiers in Cell and Developmental Biology

Received: *22 February 2021*
Accepted: *19 April 2021*
Published: *10 May 2021*

Citation:
Hua R and Liu M (2021) Sexual Dimorphism in Mouse Meiosis. Front. Cell Dev. Biol. 9:670599. doi: 10.3389/fcell.2021.670599

Keywords: meiosis, sexual dimorphism, knockout mice, spermatocyte, oocyte

INTRODUCTION

For mammalian species, life begins when haploid egg and sperm cells fuse with one another. These two types of gametes are generated from diploid precursor cells through tightly regulated processes including an initial round of DNA replication and two subsequent rounds of cellular division (meiosis I and II). Meiosis is a specialized form of cell division that occurs only in the context of gametogenesis wherein diploid cells give rise to genetically diversified haploid progeny (Bolcun-Filas and Handel, 2018). During the initial meiotic prophase I, sister chromatids undergo proteinaceous axial element (AE) structural organization along the chromosome axis to facilitate synaptonemal complex (SC) assembly (Zickler and Kleckner, 1999), after which homologous chromosome pairing (Gerton and Hawley, 2005; Barzel and Kupiec, 2008; Bhalla and Dernburg, 2008), synapsis (Cahoon and Hawley, 2016), and meiotic recombination occur to generate physical chiasmatic linkages between paired chromosomes (Handel and Schimenti, 2010; Baudat et al., 2013; Keeney et al., 2014; Lam and Keeney, 2014). These processes are subject to spatiotemporal regulation by telomeres anchored on the nuclear membrane (Ding et al., 2007). The end result of this process is the physical connection of homologous chromosomes by chiasmata that aid in subsequent chromosomal capture by microtubules from the opposing cellular poles during subsequent metaphase I (MI) (Sakuno et al., 2011). The chromosomes are then separated from one another during anaphase I, segregating to opposite cellular poles following chiasmatic dissolution (Buonomo et al., 2000; Kudo et al., 2006), thereby reducing the number of chromosomes by half in the daughter cells generated at the end of meiosis I (Watanabe, 2012).

While these processes are highly conserved, they also differ significantly in the context of male and female gametogenesis, a phenomenon known as sexual dimorphism in the mammalian meiosis (Hunt and Hassold, 2002). Such sexual dimorphism in meiosis has been studied in many previous reports, including a review prepared by Handel et al. highlighting sexual dimorphism as it pertains to the regulation of cell cycle progression and kinetics during meiosis (Handel and Eppig, 1998).

Mammalian oocytes undergo synchronous meiosis during fetal development, followed by two rounds of arrest and resumption of these meiotic processes. In contrast, meiosis in males is a continuous process that occurs in waves throughout adulthood, with new germ cell populations being regularly recruited to undergo meiosis (Handel and Eppig, 1998). Sex chromosomes also impact patterns of meiosis-related transcriptional activity in males and females. In females, sex chromosomes undergo normal recombination and transcription, whereas meiotic sex chromosome inactivation (MSCI) occurs in males in the context of meiosis, as has been reviewed previously (Turner, 2015).

Sexually dimorphic regulatory processes also manifest during mammalian gametogenesis. For example, Morelli et al. have previously reviewed sex-specific differences in the processes of recombination, double-strand break (DSB) repair, and synapsis (Morelli and Cohen, 2005), detailing essential proteins known to be associated with these processes. Many recent advances in gene-editing technologies, however, have led to important breakthroughs in the study of meiotic processes in recent years. The present review was therefore formulated by searching the Pubmed database using "meiosis" and "knockout" as keywords to identify over 700 articles which were then surveyed to identify all proteins that play functionally important roles during meiosis (**Supplementary Table 1**). While many of these proteins have been studied in detail, mice in which others have been knocked out exhibit sex-specific differences in meiotic phenotypes that have not been discussed at length in prior reviews. By surveying these proteins and associated murine knockout model systems, we herein seek to provide novel insight into the sexual dimorphism of meiosis in order to guide future research efforts.

THE ONSET OF MEIOTIC PROPHASE

The onset and regulation of meiosis differ significantly between male and female mice (**Figure 1**; Handel and Eppig, 1998). Oocyte meiosis begins by embryonic day 13 in these animals, whereas testicular germ cell division at this same time point exhibits stagnation in the mitotic phase. Factors that ultimately govern these sexually dimorphic meiotic initiation phenotypes include retinoic acid (RA) inhibition in male germ cells and the regulation of germ cell entry into a meiosis-competent state.

Both germ cell-intrinsic factors and somatic cell-derived external factors ultimately influence meiotic initiation in mice. In order to enter into meiosis, germ cells must first enter a meiosis-competent state. This state, in turn, is regulated by the *Dazl* gene (Nicholls et al., 2019), which encodes a highly conserved RNA-binding protein that is specifically expressed within germ cells (Seligman and Page, 1998). In murine embryos lacking DAZL expression, primordial germ cells (PGCs) arrive at the gonad but do not undergo appropriate developmental differentiation, instead proliferating and persisting in their expression of pluripotency factors without initiating spermatogenesis or oogenesis at the proper time points (Lin et al., 2008; Chen et al., 2014; Nicholls et al., 2019). While the loss of DAZL interferes with meiosis in both male and female mice, the effects of knocking out this protein were sex-specific. The loss of DAZL disrupted oogenesis prior to the onset of meiosis, whereas spermatogenesis was arrested during the G0 phase of meiosis, with limited SYCP3 expression being evident at this time point (Lin et al., 2008). This suggests that different regulatory mechanisms ultimately govern the entry of male and female germ cells into a meiosis-competent state. Prior work has shown BCAS2 to function as a post-transcriptional regulator of spermatocyte meiosis initiation such that the conditional knockout of BCAS2 in male germ cells results in impaired spermatogenesis and male infertility. While spermatagonia in these *Bcas2* conditional knockout mice appear normal, they rarely enter meiosis prophase I or subsequent phases of meiosis (Liu et al., 2017). The alternative splicing of 245 genes, including *Dazl*, has also been detected in *Bcas2* -null testes. Despite its central role in spermatocyte meiosis, BCAS2 is dispensable in the context of oocyte meiosis (Liu et al., 2017).

The vitamin A derivative RA is produced by somatic cells in the kidneys and gonads, and functions as an important external regulator of meiotic initiation (van Pelt and de Rooij, 1991; Anderson et al., 2008; Endo et al., 2017), serving as a key inducer of meiosis in many contexts (Bowles et al., 2006; Koubova et al., 2006). Stra8 is a protein that is upregulated in response to RA (Baltus et al., 2006), and that is expressed at high levels in germ cells immediately following the initiation of meiosis only to be rapidly downregulated during subsequent stages of this process. As a transcriptional regulator, STRA8 can bind to the promoter regions of thousands of different genes including those associated with meiotic prophase I, the G1-S cell cycle transition, and mitotic program inhibition thereby regulating their expression to orchestrate appropriate meiotic cell division (Kojima et al., 2019). While both spermatogonial cells and oocytes are exposed to RA during embryonic development, such exposure is not sufficient to initiate meiosis in male germ cells. This is believed to be due to the presence of certain meiosis-preventing factors within the fetal and neonatal testis, and experimental studies using testicular extracts and organ cultures lend credence to such a hypothesis (Moor and Warnes, 1979; Gondos et al., 1996). Indeed, recent work has shown that CYP26B1, which is expressed in the fetal testes, can degrade RA and thereby prevent STRA8 upregulation and consequent meiotic initiation (Koubova et al., 2006). The expression of CYP26B1 has been detected in developing seminiferous cord tissues (Bowles et al., 2006; Koubova et al., 2006; Sedlmeier et al., 2014), and *Cyp26b1*-deficient embryos exhibit ectopic STRA8 expression and meiotic initiation within germ cells in the fetal testis (Bowles et al., 2006; MacLean et al., 2007; Sedlmeier et al., 2014). These data thus suggest that CYP26B1-expressing cells serve as a barrier to the exogenous RA-mediated initiation of germ cell meiosis in male mice.

The highly conserved DMRT family of transcription factors harbor the unique DM domain DNA binding motif, and serve as key regulators of meiotic initiation. Specifically, DMRT1 can simultaneously suppress the initiation of meiosis while promoting mitotic proliferation, as evidenced by the results of chromatin immunoprecipitation (ChIP) and transcriptomic studies of mutant cells demonstrating the ability of this

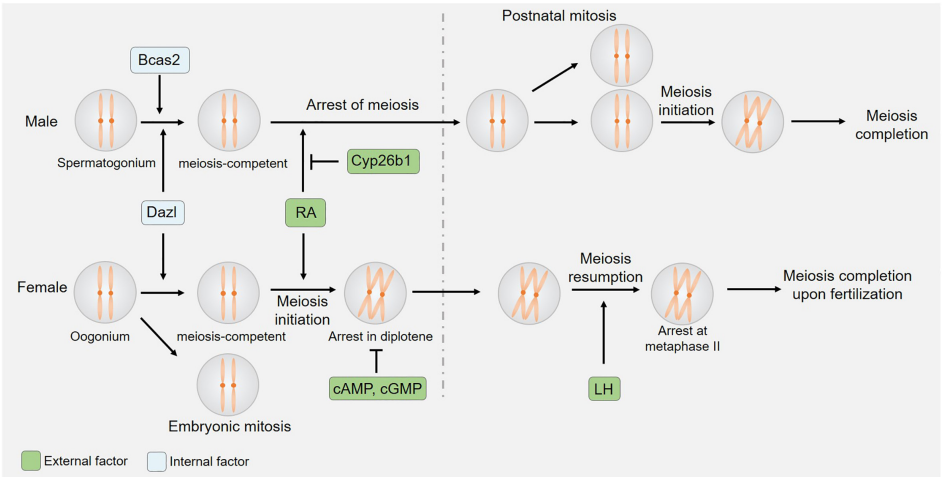

FIGURE 1 | Sexual dimorphism in the initiation and kinetics of meiosis. Both germ cell-derived internal factors and somatic cell-derived external factors regulate meiotic initiation. The expression of CYP26B1 by somatic cells of the embryonic testis suppresses RA-induced meiotic entry, while cAMP/cGMP and LH control oocyte-specific meiotic arrest and resumption.

transcription factor to regulate STRA8 and CYP26B1 expression (Matson et al., 2010). The expression of DMRT6 is also evident in type A, intermediate, and type B differentiating spermatogonia wherein it coordinates the differentiation of these cells by orchestrating the appropriate transition from the mitotic spermatogonial program to a meiotic spermatocytic program (Zhang et al., 2016). While the DNA binding characteristics and genetic targets of DMRT6 are very similar to those of DMRT1, these two transcription factors have opposing impacts on gene expression. While DMRT1 can promote spermatogonial division and differentiation, DMRT6 instead functions by terminating mitotic division and promoting meiotic entry (Zhang et al., 2014). Notably, DMRT1/6 function as regulators of these meiotic processes specifically in testicular tissues (Zhang and Zarkower, 2017), underscoring the sexually dimorphic regulatory roles of these transcription factors in the context of murine gametogenesis.

Both internal and external factors ultimately regulate germ cell entry into meiosis. The observed sex-specific differences in *Dazl*-knockout-related phenotypes and in the testicular-specific expression of BCAS2 underscore the sexually dimorphic regulation of germ cell entry into a meiosis-competent state. Somatic cell-derived RA, in contrast, serves as an external factor that promotes meiotic entry, whereas DMRT1/CYP26B1 suppress these RA-induced effects in spermatogonia but not oocytes, thereby disrupting the initiation of meiosis in a sex-specific manner (**Figure 1**).

OOCYTE MEIOSIS ARREST AND RESUMPTION DURING PROPHASE I

Spermatocyte meiosis is a continuous and ongoing process in mammals, but the same is not true for oocytes, which undergo initial meiotic progression during embryonic development, only to arrest at the diplotene stage of prophase I (**Figure 1**). Such arrest persists until immediately prior to ovulation, at which time a preovulatory luteinizing hormone (LH) surge induces oocyte maturation by promoting meiotic resumption and progression to metaphase II (MII). After the reinitiation of meiosis I in these cells, organized nuclear envelope breakdown occurs through a process known as germinal vesicle breakdown (GVBD), after which chromosome condensation, spindle formation, and first polar body (PB) extrusion occur. Oocytes then enter meiosis II only to arrest at MII until fertilization occurs.

The orchestration of oocyte maturation upon gonadotropin stimulation is tightly regulated through bidirectional signaling between oocytes and somatic cells (Hsieh et al., 2007; Conti et al., 2012). The accumulation of cyclic AMP (cAMP) generated through GPR3/12 signaling suppresses maturation-promoting factor expression and thereby promotes oocyte arrest at meiotic prophase I (Conti et al., 2012). The knockout of *Gpr3* interferes with this arrest, resulting in premature oocyte meiosis and a consequent reduction of the oocyte reserve. The absence of GPR3 expression in aging mice leads to markedly reduced fertility as evidenced by an increase in the observed numbers of non-developing embryos following spontaneous ovulation and the large quantities of fragmented oocytes detected following the induction of superovulation (Ledent et al., 2005). The production of follicle-stimulating hormone (FSH) prior to the LH surge served to additionally promote mural granulosa cells (mGCs) to secrete natriuretic peptide precursor type C (CNP/NPPC), which regulates cumulus cell-mediated cyclic GMP (cGMP) production to maintain meiotic arrest in oocytes (Zhang et al., 2010). By entering these cells through gap junctions, cGMP inhibits the activity of the cAMP-degrading enzyme PDE3A in oocytes, thereby furthering meiotic arrest (Richard et al., 2001; Vaccari et al., 2009). The knockout of *Pde3a* can rescue GPR3

deficiency-related abnormal meiotic arrest and premature follicular failure (Vaccari et al., 2008).

An LH surge that occurs proximal to the time of birth can suppress the expression of NPPC/NPR2, thus disrupting the synthesis of cGMP (Sun et al., 2009). LH can also induce the production of key epidermal growth factor (EGF)-like growth factors by mGCs including amphiregulin, beta-cellulin, and epiregulin, which in turn activate cumulus cell EGF receptor signaling and promote the degradation of cGMP in response to the activation of PDE5 and the inactivation of NPR2. These regulatory changes facilitate subsequent oocyte maturation. LH additionally activates ERK1/2 signaling to prevent GC proliferation while inducing GC luteinization (Park et al., 2004). While abnormal meiotic recovery typically results in female infertility (**Supplementary Table 1**), few studies regarding the role of LH regulation in this process have been conducted using knockout mouse models, highlighting promising directions for future research.

TELOMERE ATTACHMENT AND MOVEMENT

Telomere attachment to the nuclear envelope (NE) is a relatively conserved meiotic process. Chromosomal movement during meiotic prophase I, homologous chromosome pairing, synapsis, and recombination all depend on appropriate telomere attachment, which is therefore regulated by multiple telomere binding protein complexes (Zickler and Kleckner, 2016). A shelterin complex covers the chromatin telomeres of most eukaryotic cells (Palm and de Lange, 2008), protecting these structures from degradation, which would trigger irreversible checkpoint activation, senescence, and/or apoptotic death (Palm and de Lange, 2008). The primary protein components of the shelterin complex include TRF1, TRF2, TIN2, POT1, TPP1, and RAP1 (Palm and de Lange, 2008). Of these, TRF1/2 serve as the core shelterin complex proteins. Conditional TRF1 deletion in spermatocytes has been shown to result in a failure of telomere attachment and fusion between telomeres (Wang et al., 2018). Reductions in TRF2 expression can similarly drive abnormal telomere attachment (Hua et al., 2019). In contrast, *Rap1* knockout does not adversely impact telomere attachment or bouquet formation (Scherthan et al., 2011). Further research is necessary to determine whether the other protein components of the shelterin complex play an important role in telomere anchoring during meiosis.

In addition to the shelterin complex, the TERB1-TERB2-MAJIN protein complex is important for the establishment of a second physical linkage for telomere attachment to the NE (Shibuya et al., 2014, 2015). Mutated of these three proteins impairs telomere attachment to the NE and causes infertility in both male and female mice (Shibuya et al., 2014, 2015). TERB1 serves as a molecular scaffold, interacting with both TERB2 as well as the shelterin complex protein TRF1 (Shibuya et al., 2014, 2015; Long et al., 2017). MAJIN is predicted to be a transmembrane protein that localizes to the inner NE surface where it can bind to the SUN Domain protein (Shibuya et al., 2015). The SUN Domain protein, together with the KASH Domain protein, in turn form the linker of nucleoskeleton and cytoskeleton (LINC) complex (Ding et al., 2007), which provides sites for telomere anchoring at the NE and permits NE linkage to the cytoplasm in order to facilitate the force generation necessary to achieve chromosomal movement (Hiraoka and Dernburg, 2009; Tapley and Starr, 2013). By interacting with one another, these proteins generate a robust telomere anchoring complex. Cyclin-dependent kinase 2 (Cdk2) is also known to be important for telomere binding to the inner NE during meiosis (Viera et al., 2015), as is the atypical Cdk activator Speedy A/RingoA, which rapidly induces G2/M progression in oocytes (Mikolcevic et al., 2016; Tu et al., 2017). However, further research will be necessary to understand the precise mechanisms whereby these kinases regulate this stage of meiotic progression.

FBXO47 is an F-box protein that regulates the telomeric shelterin complex necessary for telomere-NE attachment during meiotic prophase I. FBXO47 binds to TRF2 and thereby localizes to telomeres anchored to the nuclear membrane, thereby suppressing TRF2 ubiquitination and degradation. The expression of FBXO47 is testis-specific, suggesting that it plays no role in regulating meiotic prophase I in oocytes and that other compensatory proteins may play a similar role in this context (Hua et al., 2019). Ubiquitination during telomere attachment and movement also differ between the sexes as a consequence of this sex-specific FBXO47 expression pattern.

Overall, patterns of telomere attachment and movement are largely similar in males and females, but data pertaining to FBXO47 suggest that further research into sexual dimorphism during this stage of the meiotic process is warranted.

DNA DOUBLE-STRAND BREAK AND REPAIR

DSB formation and DSB repair are key processes that occur during prophase I over the course of 7–8 or 4–5 days in murine spermatocytes and oocytes, respectively (Baudat et al., 2013). Such DSB repair depends upon the initial alignment and recombination of homologous chromosomes, which are governed by homologous DNA recombination and by the synaptonemal complex (SC). Many prior articles have already discussed meiotic recombination in detail, and this topic will thus not be discussed at length in the present review (Zickler and Kleckner, 1999; Roig and Keeney, 2008; Lichten and de Massy, 2011; Baudat et al., 2013). Interestingly, significant sexual dimorphism has been reported with respect to the regulation of chromatin organization, recombination, and meiotic defect tolerance in male and female germ cells (**Figure 2**). Complete meiotic failure typically arises in male mice harboring mutations that interfere with synapsis or recombination such that cells are unable to progress past the zygotene or pachytene stages, thereby causing spermatocyte apoptosis and consequent infertility. In contrast, these same mutations can result in a spectrum of phenotypes in females ranging from decreased fertility to

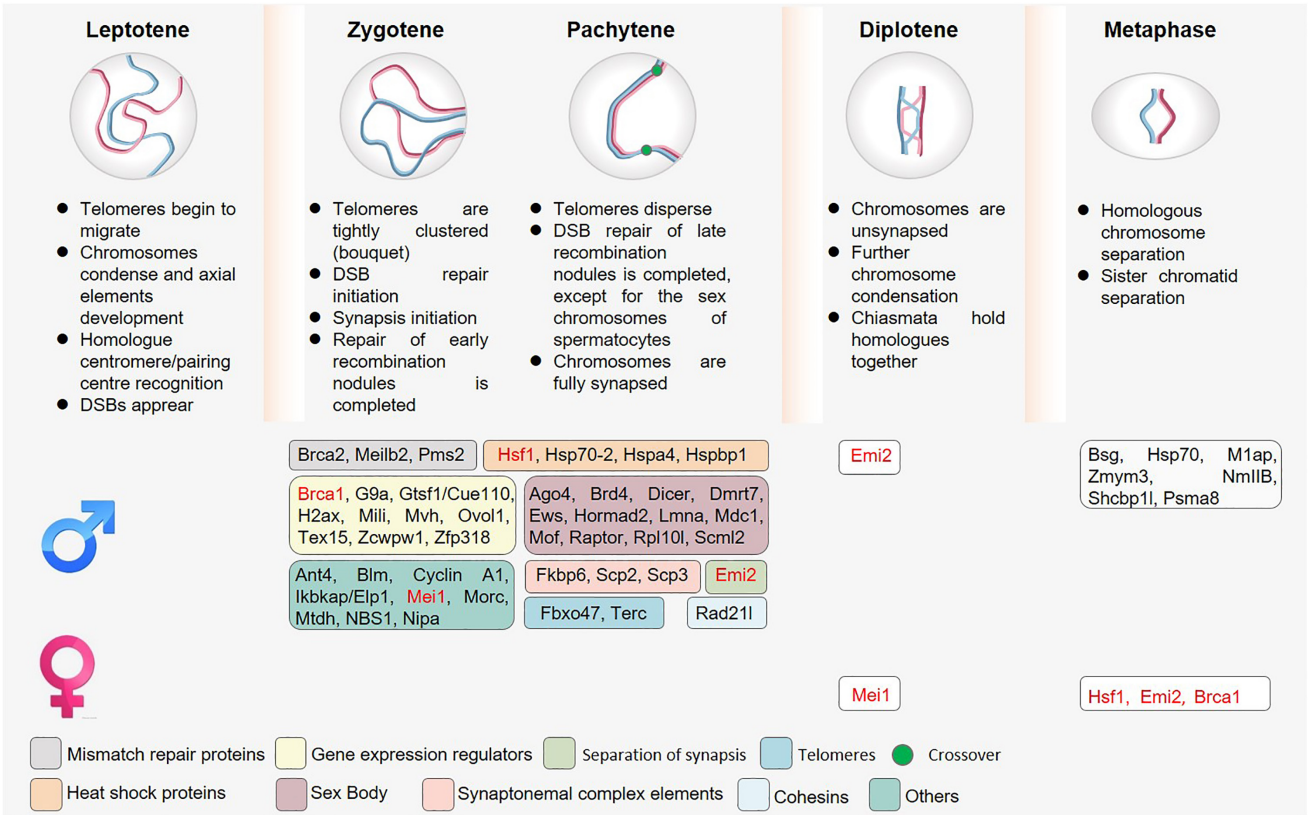

FIGURE 2 | The roles of sex-specific regulatory proteins in meiosis. Owing to overlap in the timing of telomere attachment and movement, double-strand break (DSB) repair, and MSCI, the knockout of proteins associated with these meiotic processes often results in multiple complex phenotypes. Spermatocytes have additionally evolved to express many different sex-specific proteins (shown in boxes). Proteins marked in red indicate the presence of a meiotic phenotype after knockout in both spermatocytes and oocytes, although these phenotypes are not consistent in these two cell types.

infertility, ovarian dysgenesis, or embryo loss, likely as a consequence of aneuploidy.

A wide array of proteins serve as essential regulators of DSB formation and repair in the context of meiosis, including SPO11, which is specifically expressed during prophase I and is thought to exert type II DNA topoisomerase-like activity to form DSBs (Keeney et al., 1997). These DSB sites then undergo further processing, potentially through the activity of other regulatory proteins, to generate overhangs that serve as substrates for the RECA homolog single-stranded binding proteins DMC1 and RAD51, which in turn facilitate strand invasion and the formation of double Holliday junctions (Masson and West, 2001). This leads to the interaction of homologous chromosomes. The RAD51 paralog XRCC2 has also been identified as a key driver of RAD51-mediated homologous recombination (Chun et al., 2013). In both humans and mice, a recessive mutation (c.41T > C/p.Leu14Pro) in XRCC2 results in meiotic arrest, azoospermia, and infertility. Notably, however, studies of $Xrcc2^{L14P/rmL14P}$ mice revealed that while these meiotic and fertility defects were universal in male mice, they affected only half of $Xrcc2^{L14P/rmL14P}$ female mice, with the remainder of these animals instead exhibiting reduced reproductive capacity (Yang et al., 2018).

After homologous chromosomes interact with one another, a series of structural proteins promote their further stabilization and the initiation of SC formation. The cohesion complex is a ring-shaped structural protein complex that entraps pairs of sister chromatids following replication until the initiation of anaphase at which time the separase-mediated cleavage of the α-kleisin subunits RAD21 or REC8 (during mitosis and meiosis, respectively) results in the opening of the ring structure. This complex serves as an essential recombination scaffold, and is critical for appropriate recombination, synapsis, and chiasmata formation during meiosis. The α-kleisin RAD21L is highly conserved even in non-mammalian species, and is able to interact with the cohesion subunits SMC1, SMC3, and STAG3. The knockout of *Rad21l* in male mice results in defective synapsis during prophase I, in turn causing zygotene arrest, complete azoospermia, and consequent infertility. In contrast, *Rad21l* -deficient females suffer from an age-dependent loss of fertility. SYCE1 and SYCE3 also connect lateral elements via SYCP1 at zygonema, after which TEX12 and SYCE2 loading promotes SC propagation (Fraune et al., 2012). The SC component protein FKBP6 is exclusively expressed in males such that the knockout of this protein impairs spermatocyte meiosis and causes zygotene-like stage arrest in these cells, whereas oocytes are

unaffected by the loss of its expression (Crackower et al., 2003; Noguchi et al., 2008).

Yeast model assays have revealed that following strand invasion by one end, strand displacement occurs followed by D-loop formation and invading 3′-end elongation. The other end is then able to interact with the D-loop or the elongated invading strand in respective crossover and non-crossover pathways. PMS2 is a DNA mismatch repair gene homolog, and stabilizing MLH1 levels prior to its critical crossing over function with MLH3. When PMS2 is deleted, complete spermatocyte arrest is similarly observed without any corresponding impact on the development of oocytes (Baker et al., 1995).

A wide range of other DSB-related proteins have been shown to exhibit sexually dimorphic functionality in mammals. For example, TEX15 is an essential regulator of chromosomal synapsis and meiotic recombination, but the knockout of this protein only results in meiotic arrest in male mice without having a corresponding effect on females (Yang et al., 2008). The F-box-like NIPA protein is an E3 ligase and SCF complex member that results in male sterility in conditional knockout models as a consequence of spermatogenesis arrest during meiotic prophase due to improper synapsis, disrupted DSB repair, and abnormal SC formation. In contrast, female *Nipa*$^{-/-}$ mice remain fertile albeit with a ∼50% reduction in litter size (Illert et al., 2012). Meiosis-related sexual dimorphism also extends to epigenetic regulatory processes. For example, the H3K4me3-responsive ZCWPW1 protein is necessary for the progression of prophase I in male mice whereas it is dispensable in the context of female murine gametogenesis. *Zcwpw1* knockout in male mice results in the complete disruption of synapsis, causing meiotic arrest at the zygotene/pachytene stage, impaired DSP repair, crossover failure, and infertility. Knockout of ZCWPW1 in oocytes, in contrast, only partially slows the progression of meiotic prophase I, and *Zcwpw1*$^{-/-}$ female mice retail normal fertility through mid-adulthood (Li et al., 2019). As the loss of many proteins can result in multi-faceted impacts on meiotic processes, it is important to note that it can be challenging to clearly distinguish between the key regulators of these processes. As such, additional in-depth molecular analyses of these putative regulatory proteins and their targets will be essential to fully appreciate their roles in the context of gametogenesis.

MEIOTIC METAPHASE

Following the completion of diploid meiotic recombination, germ cells enter a state of transient diakinesis after which spermatocytes/oocytes enter meiotic metaphase to complete the process of meiotic division. Chromosomal alignment at the metaphase plate and subsequent segregation during the initial round of meiotic division are essential to ensure successful meiosis. Several proteins exhibit sexual dimorphism during metaphase. For example, ZMYM3 is a member of the MYM-type zinc finger protein family and a component of an LSD1-containing transcriptional repressor complex. Spermatogenesis in *Zmym3*-knockout mice was arrested during the metaphase of the first meiotic division (MI). ZMYM3 knockout resulted in elevated numbers of apoptotic germ cells and MI spermatocytes that are positive for BUB3, which is a key factor associated with the spindle assembly checkpoint (SAC). In contrast, female *Zmym3*-knockout mice remain fertile (Hu et al., 2017).

The SAC serves as the central regulator of appropriate chromosomal segregation. In a previously published review, Lane et al. have discussed the sexual dimorphism of the meiotic SAC (Lane and Kauppi, 2019), highlighting multiple important proteins that have been studied in the context of metaphase in spermatocytes or/and oocytes. Lower levels of some SAC proteins and more SAC permissiveness in females may result in a higher incidence of meiotic aneuploidy in oocytes relative to spermatocytes.

After the separation of homologous chromosomes, spermatocytes undergo a second round of meiotic division, resulting in the production of four spermatids. However, after the first polar body (PB) is extruded into the space under the zona pellucida, oocytes arrest at MII until fertilization, at which time the second phase of meiotic division is triggered and the extrusion of the second PB occurs. Owing to these phases of regulated meiotic arrest, oocytes are never truly haploid given that their second meiotic division occurs only following fusion with a male germ cell harboring a haploid genome (Bolcun-Filas and Handel, 2018). Several phosphorylation signaling pathway proteins have been found to play important roles in maintaining MII phase arrest in oocytes. For example, MOS is an upstream activator of mitogen-activated protein kinase (MAPK) and, in mouse oocytes, and is responsible for MII arrest (Colledge et al., 1994; Hashimoto et al., 1994). The extracellular regulated kinase-1 and -2 (ERK1/2) cascade plays pivotal roles in regulating oocyte meiotic cell cycle progression. Ovulated *Erk1/2*-knockout oocytes exhibited poorly-assembled MII spindles, spontaneous PB 2 release, and were arrested at metaphase III (MIII). In addition, ERK1/2 deletion prevented male pronuclear formation after fertilization, resulting in female infertility (Zhang et al., 2015). *Ppp2r1a* encodes the scaffold subunit Aalpha of protein phosphatase 2A (PP2A), which is an important and ubiquitously expressed serine-threonine phosphatase family member. Depletion of PP2A-Aalpha facilitates germinal vesicle breakdown, causing elongation of the MII spindle and precocious separation of sister chromatids (Hu et al., 2014). As spermatocytes do not have a MII arrest, these proteins play a specific role only in oocytes.

SUMMARY

Meiosis is a tightly conserved mammalian biological process that is essential to the generation of male and female gametes, but a high degree of sexual dimorphism exists in the specific regulation of such gametogenesis. Clear differences in the regulation and characteristics of meiotic onset and duration are observed between the sexes (**Figure 1**). In addition, spermatocytes and oocytes regulate conserved processes through distinct mechanisms, and further exhibit differences in functional processes including unequal follicular cytoplasm differentiation and MSCI that ultimately give rise to these respective

gametes (**Figure 2**). Studying specific proteins using knockout models offers a robust means of exploring their roles in the context of meiotic regulation, and the advent of novel gene-editing technologies has facilitated the identification of a wide array of sexually dimorphic phenotypes exhibited by particular knockout mice.

In this review, we have surveyed over 200 proteins related to meiosis and highlighted those that are functionally sexually dimorphic. However, there are still many other proteins the functions of which have only been reported in a single sex. As meiosis is a sexually dimorphic process, further study of these sex-related differences is warranted. Of the 200+ proteins discovered in this context to date, the molecular functions of many remain to be fully clarified. For example, some of the proteins that cause meiotic arrest in the zygotene and pachytene phases may lead to abnormalities in SC, repair, and telomere attachment. However, differentiation between causes and effects remains challenging. As protein profiling techniques continue to rapidly develop, further screening for protein-protein interactions, small molecule metabolites, and the construction of molecular interaction networks will be beneficial to our understanding of the molecular mechanisms governing meiosis.

By analyzing these sexually dimorphic proteins, we found that a number of spermatocyte-specific proteins are involved in the regulation of gene expression, including histone acetylation mediators, methylation mediators, and transcriptional enhancers/inhibitors. Interestingly, after these genes are mutated, spermatocytes primarily undergo arrest in the early pachytene phase. During the zygotene to pachytene transition, an autosomal transition from transcriptional inhibition to activation occurs. The specific gene expression regulatory proteins involved in the regulation of meiotic processes in spermatocytes suggest that there are distinct and complex gene expression regulatory mechanisms engaged in spermatocytes and oocytes. In addition, it is important to note that the spermatocyte-specific piRNA proteins and associated piRNA/mRNA modifications represent a further dimension regulating spermatocyte gene expression. Despite these advances, defining the purpose underlying observed mechanisms of mammalian germline sexual dimorphism remains challenging. Recent studies have described increasingly intricate technologies allowing for analyses of the regulation of gene expression, such as high-throughput/resolution chromosome conformation capture (Hi-C), Assay for Targeting Accessible-Chromatin with high-throughout sequencing (ATAC-seq), and Full-Length Isoform Sequencing. Additional comprehensive studies leveraging these technologies will aid in more thoroughly elucidating the mechanisms governing meiosis.

AUTHOR CONTRIBUTIONS

RH prepared figures and tables, authored draft of the manuscript, and approved the final draft. ML reviewed, revised draft of the manuscript, and approved the final draft. Both authors contributed to the article and approved the submitted version.

FUNDING

This work was supported by the National Key Research and Development Program of China 2016YFA0500902 (to ML); the Natural Science Foundation of China (32070842, and 31771654 to ML; 32000584 to RH); the Natural Science Foundation of Jiangsu Province (Grants No. BK20190081 to ML); and the Qing Lan Project (to ML).

SUPPLEMENTARY MATERIAL

The Supplementary Material for this article can be found online at: https://www.frontiersin.org/articles/10.3389/fcell.2021.670599/full#supplementary-material

REFERENCES

Anderson, E., Baltus, A., Roepers-Gajadien, H., Hassold, T., De Rooij, D., Van Pelt, A., et al. (2008). Stra8 and its inducer, retinoic acid, regulate meiotic initiation in both spermatogenesis and oogenesis in mice. *Proc. Natl. Acad. Sci. USA* 105, 14976–14980. doi: 10.1073/pnas.0807297105

Baker, S., Bronner, C., Zhang, L., Plug, A., Robatzek, M., Warren, G., et al. (1995). Male mice defective in the DNA mismatch repair gene PMS2 exhibit abnormal chromosome synapsis in meiosis. *Cell* 82, 309–319. doi: 10.1016/0092-8674(95)90318-6

Baltus, A., Menke, D., Hu, Y., Goodheart, M., Carpenter, A., De Rooij, D., et al. (2006). In germ cells of mouse embryonic ovaries, the decision to enter meiosis precedes premeiotic DNA replication. *Nat. Genet.* 38, 1430–1434. doi: 10.1038/ng1919

Barzel, A., and Kupiec, M. (2008). Finding a match: how do homologous sequences get together for recombination? *Nat. Rev. Genet.* 9, 27–37. doi: 10.1038/nrg2224

Baudat, F., Imai, Y., and De Massy, B. (2013). Meiotic recombination in mammals: localization and regulation. *Nat. Rev. Genet.* 14, 794–806. doi: 10.1038/nrg3573

Bhalla, N., and Dernburg, A. (2008). Prelude to a division. *Annu. Rev. Cell Dev. Biol.* 24, 397–424.

Bolcun-Filas, E., and Handel, M. A. (2018). Meiosis: the chromosomal foundation of reproduction. *Biol. Reprod.* 99, 112–126. doi: 10.1093/biolre/ioy021

Bowles, J., Knight, D., Smith, C., Wilhelm, D., Richman, J., Mamiya, S., et al. (2006). Retinoid signaling determines germ cell fate in mice. *Science* 312, 596–600. doi: 10.1126/science.1125691

Buonomo, S., Clyne, R., Fuchs, J., Loidl, J., Uhlmann, F., and Nasmyth, K. (2000). Disjunction of homologous chromosomes in meiosis i depends on proteolytic cleavage of the meiotic cohesin Rec8 by separin. *Cell* 103, 387–398. doi: 10.1016/s0092-8674(00)00131-8

Cahoon, C., and Hawley, R. (2016). Regulating the construction and demolition of the synaptonemal complex. *Nat. Struct. Mol. Biol.* 23, 369–377. doi: 10.1038/nsmb.3208

Chen, H., Welling, M., Bloch, D., Muñoz, J., Mientjes, E., Chen, X., et al. (2014). DAZL limits pluripotency, differentiation, and apoptosis in developing primordial germ cells. *Stem Cell Rep.* 3, 892–904. doi: 10.1016/j.stemcr.2014.09.003

Chun, J., Buechelmaier, E., and Powell, S. (2013). Rad51 paralog complexes BCDX2 and CX3 act at different stages in the BRCA1-BRCA2-dependent homologous recombination pathway. *Mol. Cell. Biol.* 33, 387–395. doi: 10.1128/mcb.00465-12

Colledge, W., Carlton, M., Udy, G., and Evans, M. (1994). Disruption of c-mos causes parthenogenetic development of unfertilized mouse eggs. *Nature* 370, 65–68. doi: 10.1038/370065a0

Conti, M., Hsieh, M., Zamah, A., and Oh, J. (2012). Novel signaling mechanisms in the ovary during oocyte maturation and ovulation. *Mol. Cell. Endocrinol.* 356, 65–73. doi: 10.1016/j.mce.2011.11.002

Crackower, M., Kolas, N., Noguchi, J., Sarao, R., Kikuchi, K., Kaneko, H., et al. (2003). Essential role of Fkbp6 in male fertility and homologous chromosome pairing in meiosis. *Science* 300, 1291–1295. doi: 10.1126/science.1083022

Ding, X., Xu, R., Yu, J., Xu, T., Zhuang, Y., and Han, M. (2007). SUN1 is required for telomere attachment to nuclear envelope and gametogenesis in mice. *Dev. Cell* 12, 863–872. doi: 10.1016/j.devcel.2007.03.018

Endo, T., Freinkman, E., De Rooij, D., and Page, D. (2017). Periodic production of retinoic acid by meiotic and somatic cells coordinates four transitions in mouse spermatogenesis. *Proc. Natl. Acad. Sci. USA* 114, E10132–E10141.

Fraune, J., Schramm, S., Alsheimer, M., and Benavente, R. (2012). The mammalian synaptonemal complex: protein components, assembly and role in meiotic recombination. *Exp. Cell Res.* 318, 1340–1346. doi: 10.1016/j.yexcr.2012.02.018

Gerton, J., and Hawley, R. (2005). Homologous chromosome interactions in meiosis: diversity amidst conservation. *Nat. Rev. Genet.* 6, 477–487. doi: 10.1038/nrg1614

Gondos, B., Byskov, A., and Hansen, J. (1996). Regulation of the onset of meiosis in the developing testis. *Ann. Clin. Lab. Sci.* 26, 421–425.

Handel, M. A., and Schimenti, J. C. (2010). Genetics of mammalian meiosis: regulation, dynamics and impact on fertility. *Nat. Rev. Genet.* 11, 124–136. doi: 10.1038/nrg2723

Handel, M., and Eppig, J. (1998). Sexual dimorphism in the regulation of mammalian meiosis. *Curr. Top. Dev. Biol.* 37, 333–358. doi: 10.1016/s0070-2153(08)60179-9

Hashimoto, N., Watanabe, N., Furuta, Y., Tamemoto, H., Sagata, N., Yokoyama, M., et al. (1994). Parthenogenetic activation of oocytes in c-mos-deficient mice. *Nature* 370, 68–71. doi: 10.1038/370068a0

Hiraoka, Y., and Dernburg, A. F. (2009). The SUN rises on meiotic chromosome dynamics. *Dev. Cell* 17, 598–605. doi: 10.1016/j.devcel.2009.10.014

Hsieh, M., Lee, D., Panigone, S., Horner, K., Chen, R., Theologis, A., et al. (2007). Luteinizing hormone-dependent activation of the epidermal growth factor network is essential for ovulation. *Mol. Cell. Biol.* 27, 1914–1924. doi: 10.1128/mcb.01919-06

Hu, M., Wang, Z., Jiang, Z., Qi, S., Huang, L., Liang, Q., et al. (2014). Scaffold subunit Aalpha of PP2A is essential for female meiosis and fertility in mice. *Biol. Reprod.* 9:19.

Hu, X., Shen, B., Liao, S., Ning, Y., Ma, L., Chen, J., et al. (2017). Gene knockout of Zmym3 in mice arrests spermatogenesis at meiotic metaphase with defects in spindle assembly checkpoint. *Cell Death Dis.* 8:e2910. doi: 10.1038/cddis.2017.228

Hua, R., Wei, H., Liu, C., Zhang, Y., Liu, S., Guo, Y., et al. (2019). FBXO47 regulates telomere-inner nuclear envelope integration by stabilizing TRF2 during meiosis. *Nucleic Acids Res.* 47, 11755–11770.

Hunt, P., and Hassold, T. (2002). Sex matters in meiosis. *Science* 296, 2181–2183. doi: 10.1126/science.1071907

Illert, A., Kawaguchi, H., Antinozzi, C., Bassermann, F., Quintanilla-Martinez, L., Von Klitzing, C., et al. (2012). Targeted inactivation of nuclear interaction partner of ALK disrupts meiotic prophase. *Development* 139, 2523–2534. doi: 10.1242/dev.073072

Keeney, S., Giroux, C., and Kleckner, N. (1997). Meiosis-specific DNA double-strand breaks are catalyzed by Spo11, a member of a widely conserved protein family. *Cell* 88, 375–384. doi: 10.1016/s0092-8674(00)81876-0

Keeney, S., Lange, J., and Mohibullah, N. (2014). Self-organization of meiotic recombination initiation: general principles and molecular pathways. *Annu. Rev. Genet.* 48, 187–214. doi: 10.1146/annurev-genet-120213-092304

Kojima, M., De Rooij, D., and Page, D. (2019). Amplification of a broad transcriptional program by a common factor triggers the meiotic cell cycle in mice. *eLife* 8:e43738

Koubova, J., Menke, D., Zhou, Q., Capel, B., Griswold, M., and Page, D. (2006). Retinoic acid regulates sex-specific timing of meiotic initiation in mice. *Proc. Natl. Acad. Sci. USA* 103, 2474–2479. doi: 10.1073/pnas.0510813103

Kudo, N., Wassmann, K., Anger, M., Schuh, M., Wirth, K., Xu, H., et al. (2006). Resolution of chiasmata in oocytes requires separase-mediated proteolysis. *Cell* 126, 135–146. doi: 10.1016/j.cell.2006.05.033

Lam, I., and Keeney, S. (2014). Mechanism and regulation of meiotic recombination initiation. *Cold Spring Harb. Perspect. Biol.* 7:a016634. doi: 10.1101/cshperspect.a016634

Lane, S., and Kauppi, L. (2019). Meiotic spindle assembly checkpoint and aneuploidy in males versus females. *Cell. Mol. Life Sci.* 76, 1135–1150. doi: 10.1007/s00018-018-2986-6

Ledent, C., Demeestere, I., Blum, D., Petermans, J., Hämäläinen, T., Smits, G., et al. (2005). Premature ovarian aging in mice deficient for Gpr3. *Proc. Natl. Acad. Sci. USA* 102, 8922–8926. doi: 10.1073/pnas.0503840102

Li, M., Huang, T., Li, M., Zhang, C., Yu, X., Yin, Y., et al. (2019). The histone modification reader ZCWPW1 is required for meiosis prophase I in male but not in female mice. *Sci. Adv.* 5:eaax1101. doi: 10.1126/sciadv.aax1101

Lichten, M., and de Massy, B. (2011). The impressionistic landscape of meiotic recombination. *Cell* 147, 267–270. doi: 10.1016/j.cell.2011.09.038

Lin, Y., Gill, M., Koubova, J., and Page, D. (2008). Germ cell-intrinsic and -extrinsic factors govern meiotic initiation in mouse embryos. *Science* 322, 1685–1687. doi: 10.1126/science.1166340

Liu, W., Wang, F., Xu, Q., Shi, J., Zhang, X., Lu, X., et al. (2017). BCAS2 is involved in alternative mRNA splicing in spermatogonia and the transition to meiosis. *Nat. Commun.* 8:14182.

Long, J., Huang, C., Chen, Y., Zhang, Y., Shi, S., Wu, L., et al. (2017). Telomeric TERB1-TRF1 interaction is crucial for male meiosis. *Nat. Struct. Mol. Biol.* 24, 1073–1080. doi: 10.1038/nsmb.3496

MacLean, G., Li, H., Metzger, D., Chambon, P., and Petkovich, M. (2007). Apoptotic extinction of germ cells in testes of Cyp26b1 knockout mice. *Endocrinology* 148, 4560–4567. doi: 10.1210/en.2007-0492

Masson, J., and West, S. (2001). The Rad51 and Dmc1 recombinases: a non-identical twin relationship. *Trends Biochem. Sci.* 26, 131–136. doi: 10.1016/s0968-0004(00)01742-4

Matson, C., Murphy, M., Griswold, M., Yoshida, S., Bardwell, V., and Zarkower, D. (2010). The mammalian doublesex homolog DMRT1 is a transcriptional gatekeeper that controls the mitosis versus meiosis decision in male germ cells. *Dev. Cell* 19, 612–624. doi: 10.1016/j.devcel.2010.09.010

Mikolcevic, P., Isoda, M., Shibuya, H., Del Barco Barrantes, I., Igea, A., Suja, J., et al. (2016). Essential role of the Cdk2 activator RingoA in meiotic telomere tethering to the nuclear envelope. *Nat. Commun.* 7:11084.

Moor, R., and Warnes, G. (1979). Regulation of meiosis in mammalian oocytes. *Br. Med. Bull.* 35, 99–103. doi: 10.1093/oxfordjournals.bmb.a071578

Morelli, M., and Cohen, P. (2005). Not all germ cells are created equal: aspects of sexual dimorphism in mammalian meiosis. *Reproduction* 130, 761–781. doi: 10.1530/rep.1.00865

Nicholls, P., Schorle, H., Naqvi, S., Hu, Y., Fan, Y., Carmell, M., et al. (2019). Mammalian germ cells are determined after PGC colonization of the nascent gonad. *Proc. Natl. Acad. Sci. USA* 116, 25677–25687. doi: 10.1073/pnas.1910733116

Noguchi, J., Ozawa, M., Nakai, M., Somfai, T., Kikuchi, K., Kaneko, H., et al. (2008). Affected homologous chromosome pairing and phosphorylation of testis specific histone, H2AX, in male meiosis under FKBP6 deficiency. *J. Reprod. Dev.* 54, 203–207. doi: 10.1262/jrd.19158

Palm, W., and de Lange, T. (2008). How shelterin protects mammalian telomeres. *Annu. Rev. Genet.* 42, 301–334. doi: 10.1146/annurev.genet.41.110306.130350

Park, J., Su, Y., Ariga, M., Law, E., Jin, S., and Conti, M. (2004). EGF-like growth factors as mediators of LH action in the ovulatory follicle. *Science* 303, 682–684. doi: 10.1126/science.1092463

Richard, F., Tsafriri, A., and Conti, M. (2001). Role of phosphodiesterase type 3A in rat oocyte maturation. *Biol. Reprod.* 65, 1444–1451. doi: 10.1095/biolreprod65.5.1444

Roig, I., and Keeney, S. (2008). Probing meiotic recombination decisions. *Dev. Cell* 15, 331–332. doi: 10.1016/j.devcel.2008.08.009

Sakuno, T., Tanaka, K., Hauf, S., and Watanabe, Y. (2011). Repositioning of aurora B promoted by chiasmata ensures sister chromatid mono-orientation in meiosis I. *Dev. Cell* 21, 534–545. doi: 10.1016/j.devcel.2011.08.012

Scherthan, H., Sfeir, A., and De Lange, T. (2011). Rap1-independent telomere attachment and bouquet formation in mammalian meiosis. *Chromosoma* 120, 151–157. doi: 10.1007/s00412-010-0295-4

Sedlmeier, E. M., Brunner, S., Much, D., Pagel, P., Ulbrich, S. E., and Meyer, H. H. (2014). Human placental transcriptome shows sexually dimorphic gene expression and responsiveness to maternal dietary n-3 long-chain polyunsaturated fatty acid intervention during pregnancy. *BMC Genomics* 15:941. doi: 10.1186/1471-2164-15-941

Seligman, J., and Page, D. (1998). The Dazh gene is expressed in male and female embryonic gonads before germ cell sex differentiation. *Biochem. Biophys. Res. Commun.* 245, 878–882. doi: 10.1006/bbrc.1998.8530

Shibuya, H., Hernandez-Hernandez, A., Morimoto, A., Negishi, L., Hoog, C., and Watanabe, Y. (2015). MAJIN links telomeric DNA to the nuclear membrane by exchanging telomere cap. *Cell* 163, 1252–1266. doi: 10.1016/j.cell.2015.10.030

Shibuya, H., Ishiguro, K., and Watanabe, Y. (2014). The TRF1-binding protein TERB1 promotes chromosome movement and telomere rigidity in meiosis. *Nat. Cell Biol.* 16, 145–156. doi: 10.1038/ncb2896

Sun, Q., Miao, Y., and Schatten, H. (2009). Towards a new understanding on the regulation of mammalian oocyte meiosis resumption. *Cell Cycle* 8, 2741–2747. doi: 10.4161/cc.8.17.9471

Tapley, E., and Starr, D. (2013). Connecting the nucleus to the cytoskeleton by SUN-KASH bridges across the nuclear envelope. *Curr. Opin. Cell Biol.* 25, 57–62. doi: 10.1016/j.ceb.2012.10.014

Tu, Z., Bayazit, M., Liu, H., Zhang, J., Busayavalasa, K., Risal, S., et al. (2017). Speedy A-Cdk2 binding mediates initial telomere-nuclear envelope attachment during meiotic prophase I independent of Cdk2 activation. *Proc. Natl. Acad. Sci. USA* 114, 592–597. doi: 10.1073/pnas.1618465114

Turner, J. (2015). Meiotic silencing in mammals. *Annu. Rev. Genet.* 49, 395–412. doi: 10.1146/annurev-genet-112414-055145

Vaccari, S., Horner, K., Mehlmann, L., and Conti, M. (2008). Generation of mouse oocytes defective in cAMP synthesis and degradation: endogenous cyclic AMP is essential for meiotic arrest. *Dev. Biol.* 316, 124–134. doi: 10.1016/j.ydbio.2008.01.018

Vaccari, S., Weeks, J., Hsieh, M., Menniti, F., and Conti, M. (2009). Cyclic GMP signaling is involved in the luteinizing hormone-dependent meiotic maturation of mouse oocytes. *Biol. Reprod.* 81, 595–604. doi: 10.1095/biolreprod.109.077768

van Pelt, A., and de Rooij, D. (1991). Retinoic acid is able to reinitiate spermatogenesis in vitamin a-deficient rats and high replicate doses support the full development of spermatogenic cells. *Endocrinology* 128, 697–704. doi: 10.1210/endo-128-2-697

Viera, A., Alsheimer, M., Gómez, R., Berenguer, I., Ortega, S., Symonds, C., et al. (2015). CDK2 regulates nuclear envelope protein dynamics and telomere attachment in mouse meiotic prophase. *J. Cell Sci.* 128, 88–99. doi: 10.1242/jcs.154922

Wang, L., Tu, Z., Liu, C., Liu, H., Kaldis, P., Chen, Z., et al. (2018). Dual roles of TRF1 in tethering telomeres to the nuclear envelope and protecting them from fusion during meiosis. *Cell Death. Differ.* 25, 1174–1188. doi: 10.1038/s41418-017-0037-8

Watanabe, Y. (2012). Geometry and force behind kinetochore orientation: lessons from meiosis. *Nat. Rev. Mol. Cell Biol.* 13, 370–382. doi: 10.1038/nrm3349

Yang, F., Eckardt, S., Leu, N., Mclaughlin, K., and Wang, P. (2008). Mouse TEX15 is essential for DNA double-strand break repair and chromosomal synapsis during male meiosis. *J. Cell Biol.* 180, 673–679. doi: 10.1083/jcb.200709057

Yang, Y., Guo, J., Dai, L., Zhu, Y., Hu, H., Tan, L., et al. (2018). XRCC2 mutation causes meiotic arrest, azoospermia and infertility. *J. Med. Genet.* 55, 628–636. doi: 10.1136/jmedgenet-2017-105145

Zhang, M., Su, Y., Sugiura, K., Xia, G., and Eppig, J. (2010). Granulosa cell ligand NPPC and its receptor NPR2 maintain meiotic arrest in mouse oocytes. *Science* 330, 366–369. doi: 10.1126/science.1193573

Zhang, T., and Zarkower, D. (2017). DMRT proteins and coordination of mammalian spermatogenesis. *Stem Cell Res.* 24, 195–202. doi: 10.1016/j.scr.2017.07.026

Zhang, T., Murphy, M., Gearhart, M., Bardwell, V., and Zarkower, D. (2014). The mammalian Doublesex homolog DMRT6 coordinates the transition between mitotic and meiotic developmental programs during spermatogenesis. *Development* 141, 3662–3671. doi: 10.1242/dev.113936

Zhang, T., Oatley, J., Bardwell, V., and Zarkower, D. (2016). DMRT1 is required for mouse spermatogonial stem cell maintenance and replenishment. *PLoS Genet.* 12:e1006293. doi: 10.1371/journal.pgen.1006293

Zhang, Y., Liu, X., Ji, S., Sha, Q., Zhang, J., and Fan, H. (2015). ERK1/2 activities are dispensable for oocyte growth but are required for meiotic maturation and pronuclear formation in mouse. *J. Genet. Genomics* 42, 477–485. doi: 10.1016/j.jgg.2015.07.004

Zickler, D., and Kleckner, N. (1999). Meiotic chromosomes: integrating structure and function. *Annu. Rev. Genet.* 33, 603–754. doi: 10.1146/annurev.genet.33.1.603

Zickler, D., and Kleckner, N. (2016). A few of our favorite things: pairing, the bouquet, crossover interference and evolution of meiosis. *Semin. Cell Dev. Biol.* 54, 135–148. doi: 10.1016/j.semcdb.2016.02.024

Conflict of Interest: The authors declare that the research was conducted in the absence of any commercial or financial relationships that could be construed as a potential conflict of interest.

Copyright © 2021 Hua and Liu. This is an open-access article distributed under the terms of the Creative Commons Attribution License (CC BY). The use, distribution or reproduction in other forums is permitted, provided the original author(s) and the copyright owner(s) are credited and that the original publication in this journal is cited, in accordance with accepted academic practice. No use, distribution or reproduction is permitted which does not comply with these terms.

frontiers in Cell and Developmental Biology

ORIGINAL RESEARCH
published: 19 May 2021
doi: 10.3389/fcell.2021.672590

Podophyllotoxin Exposure Affects Organelle Distribution and Functions in Mouse Oocyte Meiosis

*Ping-Shuang Lu†, Lan-Ping Xie†, Xiao-Han Kong, Yi Xu and Shao-Chen Sun**

College of Animal Science and Technology, Nanjing Agricultural University, Nanjing, China

Podophyllotoxin (POD) is one of the most characterized lignans that is commonly found in podophyllum, and its preparations and derivatives are widely used in clinical treatment due to strong antitumor and antivirus activities. POD has been reported for its neurotoxicity, liver toxicity, and potential reproductive toxicity. In the present study, we investigated the effects of POD on the organelles of mouse oocytes during meiosis. Our results showed that exposure to POD significantly reduced the developmental competence of mouse oocytes. Further analysis revealed that the endoplasmic reticulum (ER) failed to accumulate to the spindle periphery, suggesting that POD exposure might affect protein synthesis during oocyte meiotic maturation. Similarly, abnormal Golgi apparatus distribution was found after POD exposure, which could be confirmed by the aberrant localization of Rab11a-related vesicles, indicating that POD induced vesicle-based protein transport disorder. We also found the aberrant accumulation of lysosomes in the cytoplasm of POD-exposed oocytes, which implied that POD might lead to aberrant protein degradation. Moreover, the perinuclear distribution of mitochondria was also significantly disturbed, indicating the mitochondrial dysfunction after POD exposure. In all, our study illustrated that exposure to POD might disrupt protein synthesis, transport, degradation, and ATP production by its effects on the distribution and functions of organelles during mouse oocyte meiotic maturation.

Keywords: podophyllotoxin, oocyte, meiosis, organelles, mitochondria

OPEN ACCESS

Edited by:
Liangran Zhang,
Shandong University, China

Reviewed by:
Yi-Liang Miao,
Huazhong Agricultural University, China
Cheng-guang Liang,
Inner Mongolia University, China
Qiang Wang,
Nanjing Medical University, China

***Correspondence:**
Shao-Chen Sun
sunsc@njau.edu.cn

†These authors have contributed equally to this work

Specialty section:
This article was submitted to Cell Growth and Division, a section of the journal Frontiers in Cell and Developmental Biology

Received: *26 February 2021*
Accepted: *30 March 2021*
Published: *19 May 2021*

Citation:
Lu P-S, Xie L-P, Kong X-H, Xu Y and Sun S-C (2021) Podophyllotoxin Exposure Affects Organelle Distribution and Functions in Mouse Oocyte Meiosis. Front. Cell Dev. Biol. 9:672590. doi: 10.3389/fcell.2021.672590

INTRODUCTION

Lignans, as one of the secondary metabolites of plants, are a kind of polyphenols that are widely present in plant tissues such as rhizomes, flowers, leaves, fruits, etc. (Cui et al., 2020). The diversity of the lignan family exhibits a variety of pharmacological activities, such as anti-inflammatory, antioxidant, antitumor, and antivirus effects (Ardalani et al., 2017; Rodríguez-García et al., 2019). Podophyllotoxin (POD) is one of the most characterized lignans that is commonly found in the *Podophyllum* genus, *Dysosma, Diphylleia, Jeffersonia and Catharanthus* etc. (Ardalani et al., 2017). The alcoholic solution of podophyllin was first proven to be an effective treatment for genital warts in 1942 (Giri and Lakshmi Narasu, 2000). However, it has been mostly replaced by POD preparations, 0.5% solution or 0.15% cream, and other alternative therapies due to its

Abbreviations: POD, podophyllotoxin; GVBD, germinal vesicle breakdown; MI, metaphase I; MII, metaphase II; PB1, first polar body.

high recurrence rate, poor stability, and toxicity (von Krogh and Longstaff, 2001; Wiley et al., 2002; Lacey et al., 2003). In addition, POD is recognized as a potent antitumor factor, and its synthetic derivatives, etoposide and teniposide, have already been used in the clinical treatment of lymphocytic leukemia, certain brain tumors, and lung tumors (Zálešák et al., 2019). Studies have shown that POD is potentially toxic to the nervous and respiratory system since the neurons are swollen and the Nissl substance (RNA/ribosome) reduced significantly after 72-h treatment with POD in adult rats (Chang et al., 1992a). It also has been reported that POD can affect hepatocellular respiration by altering mitochondrial electron flow and inhibiting the synthesis of DNA, RNA, and proteins (Horrum et al., 1986; Yang et al., 1994). Besides, radiolabeled POD reaches a higher concentration in fetal than maternal tissues after giving it to pregnant mice by the oral or intravenous route, and it is still noted to avoid POD therapy during pregnancy or pregnancy planning, indicating the potential effects of POD on reproduction (von Krogh and Longstaff, 2001; Yanofsky et al., 2012). Indeed, the toxicity of POD to the reproductive system especially on germ cells is already reported. In males, exposure to POD causes the mice testicular seminiferous tubules atrophy and degeneration at a certain dose (Chang et al., 1992b). Similarly, POD has harmful effects on rat sperm maturation or fertility due to epididymal epithelial cell apoptosis induced by activating TNF-α and the caspase signaling pathway (Xie et al., 2017). In females, *in vitro* tests confirm that exposure to POD can inhibit microtubule dynamics and meiotic spindle formation, which leads to low oocyte maturing rates and early embryonic developmental competence (Hu et al., 2018). Moreover, porcine oocytes exposed to POD are also subjected to oxidative stress, apoptosis, abnormal spindle formation, and chromosome abnormality (Jiang et al., 2020). However, the toxin effects of POD on the organelle functions of mammalian oocytes have not been studied.

Oocyte quality is important for fertilization in all mammalian species. To ensure the high developmental potential of oocytes, the organelles of oocytes, such as the endoplasmic reticulum (ER), Golgi apparatus, lysosomes, and mitochondria, must have appropriate spatial and temporal dynamics (Sirard et al., 2006). The ER is a complex organelle involved in protein and lipid synthesis, calcium regulation, and interactions with other organelles (Schwarz and Blower, 2016). The Golgi apparatus is the central hub of the secretory pathway where proteins are processed, sorted, and distributed to different destinations (Li et al., 2019). Rab GTPases play vital roles in vesicle formation and trafficking of oocytes (Duan and Sun, 2019), and Rab11 is a modulator of membrane delivery, acting as the intersection between the endocytic and exocytic trafficking pathways (Welz et al., 2014). Previous studies also show that Rab11a-positive vesicles could recruit the myosin Vb and further contribute to oocyte asymmetric spindle orientation during cytokinesis (Holubcová et al., 2013). Lysosomes are membrane-bound organelles that degrade macromolecules through endocytosis, phagocytosis, and autophagy pathways (Luzio et al., 2014). Moreover, mitochondria synthesize adenosine triphosphate (ATP), which is an essential energy currency for many cellular processes (Nunnari and Suomalainen, 2012). Dysfunctional organelles cannot reorganize and store enough mRNAs, proteins, and transcription factors, which are important to oocyte maturation, fertilization, and early embryogenesis (Watson, 2007). It has been found that ER stress has negative effect on oocyte maturation (Lin et al., 2019). Furthermore, intact, functional Golgi membranes are required for germinal vesicle breakdown (GVBD), which is the morphological feature of meiotic resumption (Mao et al., 2014; Pan and Li, 2019). It is also verified that the gradual increase in lysosomal autophagy significantly reduces the fertilization and developmental potential of mature oocytes *in vitro* (McGinnis et al., 2014). Moreover, the stress-induced changes in the mitochondrial function can lead to reduced oocyte maturation (Roth, 2018). Environmental toxins can disrupt oocyte maturation by affecting organelle functions. For example, decabromodiphenyl ethane (DBDPE) is a new brominated flame retardant and an emerging environmental pollutant that induces mitochondrial dysfunction and blocks oocyte maturation (Shi et al., 2021), and a synthetic lactone antibiotic, brefeldin A, has been reported to affect porcine oocyte meiotic maturation by blocking protein transport from the ER to the Golgi apparatus (Cui et al., 2019). Our recent study also shows that citrinin, which is widely found in vegetable-derived foods, impairs the functions of organelles of mouse oocytes and thus affects oocyte maturation (Sun et al., 2020).

In this study, we adopt mouse as the model to explore the potential toxic effects of POD on organelles, including the ER, Golgi apparatus, lysosome, and mitochondria of mammalian oocytes. Our results indicate that POD causes the disruption of the ER, Golgi apparatus, and lysosome distribution in oocytes, which might disturb protein synthesis, transport, and degradation. We also show that POD has adverse effects on mitochondria functions in oocytes. Therefore, our study provides important evidence for the toxicity of POD on organelle functions of mouse oocytes.

MATERIALS AND METHODS

Ethics Statement and Oocyte Culture

Four-week-old female ICR mice were used in the study, and the guidelines of the Animal Research Committee of Nanjing Agriculture University in China were followed. This study was specifically approved by the Animal Research Committee of Nanjing Agriculture University. The mice were kept at a constant temperature of 24°C and with a 12-h light/dark cycle and were provided with adequate food and water. We collected the ovaries to acquire the germinal vesicle stage oocytes in an M2 medium (Sigma, MO, United States). Moreover, the oocytes after washing three times were cultured in an M16 medium for 8.5 h (metaphase I, MI) or 12 h (metaphase II, MII) under paraffin oil at 37°C in 5% CO_2 atmosphere.

Antibodies and Chemicals

Rabbit polyclonal anti-Rab11a antibody was from Cell Signaling Technology (Danvers, MA, United States). Alexa Fluor 488 goat anti-rabbit antibody was from

Invitrogen (Carlsbad, CA, United States). Hoechst 33342 and all other unstated chemicals and reagents were from Sigma-Aldrich Corp.

Podophyllotoxin Treatment

Podophyllotoxin (CAS: 518-28-5) was purchased from J&K Corp. (Shanghai, China). It was dissolved in DMSO to 1 μM solution and then diluted in an M16 medium to final concentrations of 0.5 and 1.0 nM. The final concentration of DMSO in the culture medium was less than 0.1%. The oocytes were exposed to different concentrations of POD at 37 °C, 5% CO_2, and were cultured for 8.5 or 12 h.

Immunofluorescence Staining and Confocal Microscopy

The oocytes were immobilized in 4% paraformaldehyde for 30 min at room temperature and then permeated with 0.5% Triton X-100 (in PBS) for 20 min. After that, the oocytes were blocked in 1% BSA-supplemented PBS for 1 h. Then we incubated the oocytes with primary antibodies (1:100 for Rab11a) at 4°C overnight or room temperature for 8 h and washed three times with PBS lotion (0.1% Tween and 0.01% Triton X-100) 4 min each time. Next, samples were incubated with the secondary antibodies (Alexa Fluor 488 goat anti-rabbit, 1:100) at room temperature for 1 h. Finally, the oocytes were stained with Hoechst 33342 for 15 min and were sealed and examined by a confocal laser scanning microscope (Zeiss LSM 800 META, Jena, Germany).

Fluorescence Intensity Analysis

The fluorescence intensity of the samples was analyzed using Image J software. We fixed the control and treated oocytes in a different area on the same glass slide. Moreover, we detected the mean fluorescence intensity per unit area in the region of interest and then statistically analyzed the mean values of the control group and the treatment group.

Mitochondria and ER Detection

The distribution of mitochondria and the ER in living oocytes was detected by Mito-Tracker Red CMRos (1:600) (Cat# M7512, Invitrogen, Eugene, OR, United States) or ER-Tracker Red (1:500) (C1041 Beyotime Biotechnology Shanghai, China) in an M2 medium at 37°C for 30 min. Then we washed the oocytes three times and scanned the live oocytes with a laser confocal microscope by Zeiss LSM 800 META.

Golgi Apparatus Detection

For the detection of the Golgi apparatus, we first incubated the oocytes with 1% pronase for 4 min to remove the zona pellucida. Then the living oocytes were incubated with Golgi-Tracker Red (1:100) (C1043 Beyotime Biotechnology Shanghai, China) in an M16 medium at 4°C for 30 min. After washing three times with a fresh culture medium, we incubated the oocytes with M2 at 37°C for 30 min. Finally, we immediately examined the oocytes by a confocal laser-scanning microscope (Zeiss LSM 800 META, Germany).

Lysosome Detection

Lysosome Red (1:10,000) (C1046 Beyotime Biotechnology Shanghai, China) was used to detect the distribution of lysosome in living oocytes, which were incubated with an M2 medium at 37°C for 30 min. The oocytes were washed three times and then examined by a confocal laser-scanning microscope (Zeiss LSM 800 META, Germany).

Statistical Analysis

Data were analyzed using the GraphPad Prism 5 software (GraphPad, San Diego, CA, United States), and independent sample *t*-test was used for statistical analysis. We repeated each experiment at least three times. Data were expressed as mean ± SEM. $P < 0.05$ was considered statistically significant.

RESULTS

Effects of POD on the Developmental Competence of Mouse Oocytes

We first examined the oocyte maturation with increased concentrations (0.5 and 1 nM) of POD after 12 h in culture. As shown in **Figure 1A**, the majority of the oocytes in the control group could extrude the first polar body (PB1) and reached the stage of metaphase II (MII) (74.18 ± 4.59%, $n = 146$). However, a large number of oocytes failed to extrude PB1 in the POD treatment group, and the maturation rate was significantly reduced compared with the control group (0.5 nM, 19.80 ± 2.72%, $n = 142$, $P < 0.01$; 1 nM, 13.13 ± 3.64%, $n = 171$, $P < 0.01$) (**Figure 1B**). Therefore, our results showed that POD exposure could reduce the developmental capacity of mouse oocytes, and 0.5 nM POD was selected in our following experiments.

Effects of POD on ER Distribution in Mouse Oocytes

The ER is the major site for protein biosynthesis. We then used ER-Tracker to examine the distribution of the ER after POD exposure in mouse oocytes. In the control group, the ER in the MI stage was mainly distributed around the spindle, while oocytes exposed to POD mostly showed a homogenous distribution rather than a perinuclear distribution (**Figure 2A**). The statistical analysis data also confirmed that the abnormal rate of the ER distribution increased markedly after POD exposure (control group, 6.23 ± 3.14%, $n = 58$; POD group, 74.47 ± 7.72%, $n = 49$, $P < 0.01$) (**Figure 2B**). To further determine the effects of POD on the ER, we calculated the fluorescence intensities of ER-Tracker and found that it was much weaker in the treatment group than the control oocytes (control group, 45.59 ± 4.88, $n = 23$; POD group, 26.06 ± 8.56, $n = 22$, $P < 0.05$) (**Figure 2C**). These results demonstrated that POD exposure affected the distribution and function of the ER of mouse oocytes.

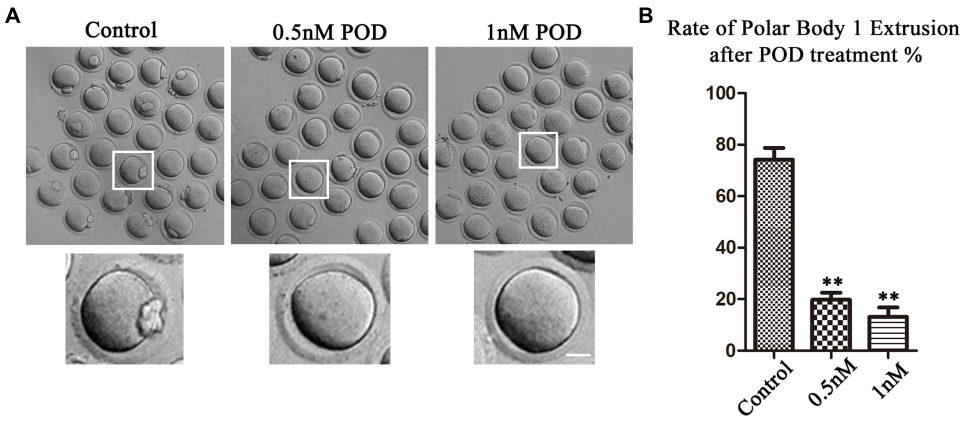

FIGURE 1 | Effects of POD on maturation competence of mouse oocytes. **(A)** The typical picture for the oocyte polar body extrusion in the control and POD-treated group. Bar = 20 μm. **(B)** The rate of polar body extrusion was significantly lower than that in the control group after POD exposure. $^{**}P < 0.01$.

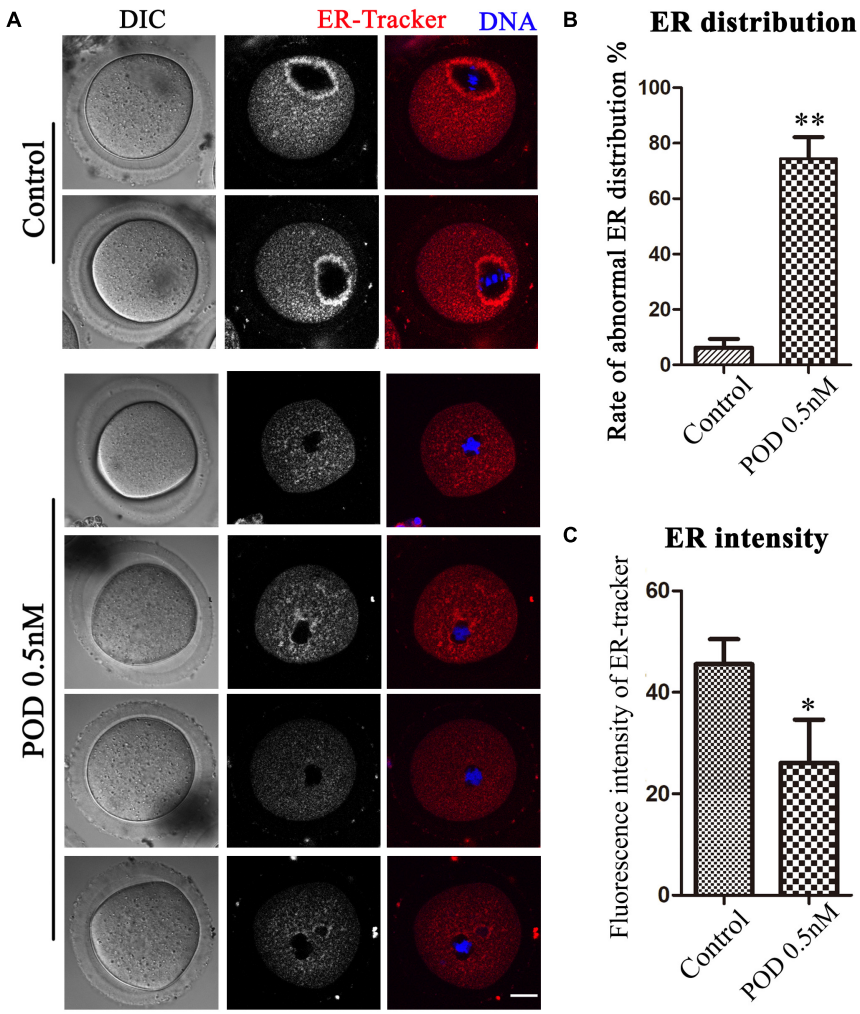

FIGURE 2 | Effects of POD on ER distribution in mouse oocytes. **(A)** The typical picture for the ER distribution in the control and POD-treated groups. Red, ER-Tracker. Blue, DNA. Bar = 20 μm. **(B)** The rate of the abnormal ER distribution was significantly increased in the 0.5 nM POD group compared with the control group. $^{**}P < 0.01$. **(C)** The fluorescence intensity of ER-Tracker was reduced markedly in the 0.5 nM POD group. $^{*}P < 0.05$.

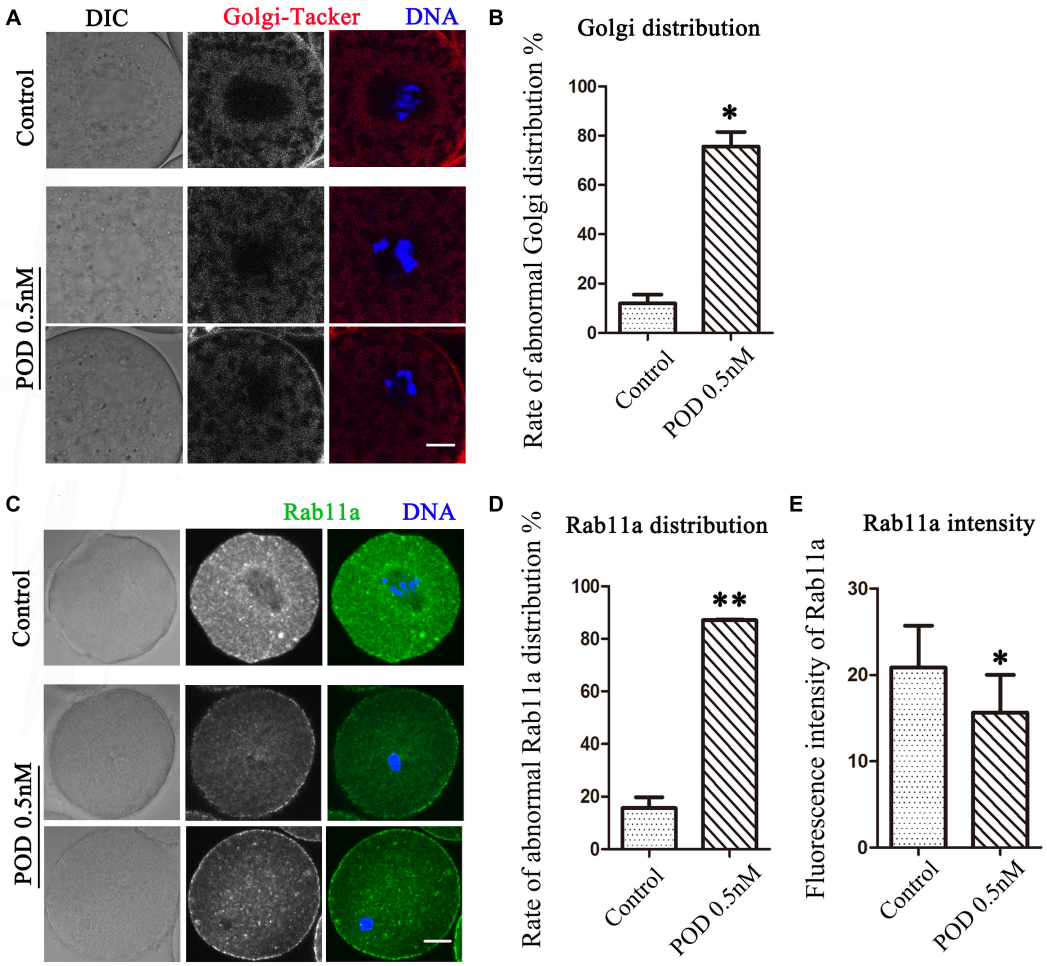

FIGURE 3 | Effects of POD on the Golgi apparatus in mouse oocytes. **(A)** The typical picture for the Golgi distribution after POD exposure in mice. Red, Golgi-Tracker. Blue, DNA. Bar = 10 μm. **(B)** The rate of abnormal Golgi distribution was significantly increased in the 0.5 nM POD group. $^{*}P < 0.05$. **(C)** The typical picture for Rab11a after POD exposure in mouse oocytes. Green, Rab11a. Blue, DNA. Bar = 20 μm. **(D)** The rate of the abnormal Rab11a distribution was significantly increased in the 0.5 nM POD group. $^{**}P < 0.01$. **(E)** The relative fluorescence intensity of Rab11a in the 0.5 nM POD group was significantly weaker than the control group $^{*}P < 0.05$.

Effects of POD on Golgi Apparatus Distribution in Mouse Oocytes

The Golgi apparatus, which acts as the docking station for cargo transportations, is closely related to protein synthesis and transportation. We then detected the distribution of the Golgi apparatus by using Golgi-Tracker. As shown in **Figure 3A**, similar to the ER, the Golgi apparatus of oocytes in the control group was also distributed around the spindle; however, in the treatment group, the Golgi apparatus failed to accumulate to the spindle periphery. In addition, compared with the control group, the abnormal distribution rate of the Golgi apparatus was significantly increased after POD treatment (control group, 11.98 ± 3.56%, $n = 50$; POD group, 75.63 ± 5.88%, $n = 43$, $P < 0.05$) (**Figure 3B**). Based on the vesicle transport function of the Golgi apparatus, we also examined the distribution of Rab11a, which was related to the vesicle transport. We found that the accumulation of Rab11a around the spindle was reduced in oocytes exposed to POD (**Figure 3C**). Compared with the control group, the rate of the abnormal distribution of Rab11a in the treatment group was significantly increased (control group, 15.59 ± 4.10%, $n = 44$; POD group, 87.14 ± 0.25%, $n = 47$, $P < 0.01$) (**Figure 3D**). And the intensity of Rab11a was markedly reduced in the POD-treated oocytes (control group, 20.85 ± 4.86, $n = 44$; POD group, 15.64 ± 7.56, $n = 47$, $P < 0.05$) (**Figure 3E**). These results suggested that POD exposure disrupted the distribution and function of the Golgi apparatus in mouse oocytes.

Effects of POD on Lysosome Distribution in Mouse Oocytes

We also detected lysosomes to further confirm the effects of POD on oocyte organelles. As shown in **Figure 4A**, we found that the distribution of lysosomes in the control group was homogeneous but agglutinated in the treatment group. In

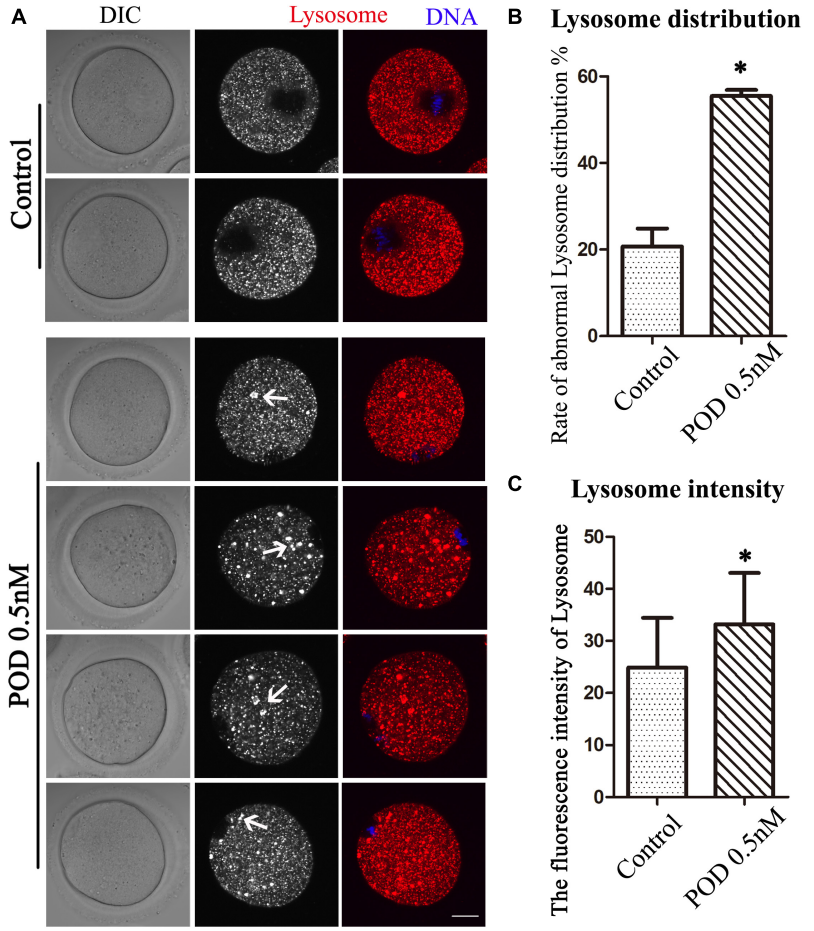

FIGURE 4 | Effects of POD on the lysosome distribution in mouse oocytes. **(A)** The typical picture for the lysosome distribution after POD exposure in mouse oocytes. Red, lysosome. Blue, DNA. Bar = 20 μm. **(B)** The rate of the abnormal lysosome distribution was significantly increased in the 0.5 nM POD group. *$P < 0.05$. **(C)** The relative fluorescence intensity of lysosome was significantly increased in the 0.5 nM POD group compared with the control group. *$P < 0.05$.

addition, compared with the control group, the rate of the abnormal distribution of lysosome in the treatment group was significantly increased (control group, 20.72 ± 4.18%, $n = 55$; POD group, 55.46 ± 1.43%, $n = 54$, $P < 0.05$) (**Figure 4B**). Similarly, we also found that the fluorescence intensity of lysosome in the cytoplasm of oocytes was markedly increased in the treatment group compared with the control group (control group, 24.88 ± 16.54, $n = 40$; POD group, 33.17 ± 9.90, $n = 40$, $P < 0.05$) (**Figure 4C**). These results indicated that POD exposure impaired the function of lysosomes in mouse oocytes.

Effects of POD on Mitochondria Distribution in Mouse Oocytes

Mitochondria can provide ATP, which is a key factor to ensure oocyte maturation. Thus, we investigated the mitochondria by Mito-Tracker staining. We classified the mitochondria distribution of MI oocytes into three types: perinuclear phenotype, homogeneous phenotype, and clustering phenotype (**Figure 5A**). As shown in **Figure 5B**, a perinuclear distribution (73.61 ± 7.64%), with small proportion of homogenous (10.58 ± 7.47%) and clustering distribution (15.97 ± 1.84%), was observed in the control group ($n = 44$), whereas the proportion of clustering mitochondria (64.99 ± 9.08%, $P < 0.01$) was much higher in the POD-exposed oocytes, showing with a few perinuclear distributions (12.18 ± 3.04%, $P < 0.01$); moreover, there was no significance between the control and the POD group for the homogenous distribution (22.83 ± 10.21%, $P > 0.1$) ($n = 48$). Therefore, these results indicated that POD exposure led to oocyte mitochondrial dysfunction in mice.

DISCUSSION

With its antivirus and antitumor activities, POD preparations are wildly used in the treatment of genital warts, and its derivatives have also been adopted as a novel natural anticancer agent. POD, a unique lignan, has certain toxic effects on the reproductive system of mammals. In this study, we investigated the distribution of the ER, Golgi apparatus, lysosomes, and

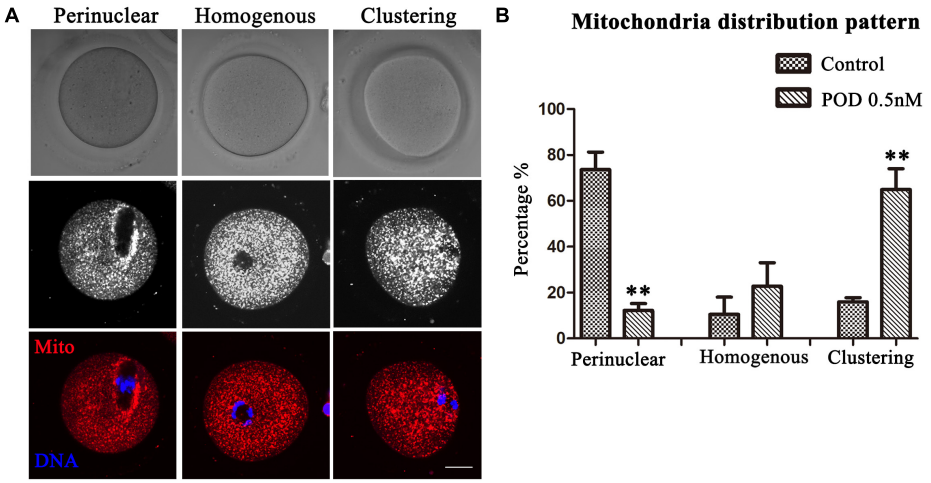

FIGURE 5 | Effects of POD on the mitochondria distribution in mouse oocytes. **(A)** The typical picture for the mitochondria distribution in the control and POD-treated group. Red, Mito-Tracker. Blue, DNA. Bar = 20 μm. **(B)** The perinuclear localization pattern was decreased in the POD-treated group compared with the control group; the clustering localization pattern was increased in the POD-treated group compared with the control group. $^{**}P < 0.01$.

mitochondria in mouse oocytes after POD exposure. The results showed that the POD exposure had wide-ranging adverse effects on organelle distribution and functions, which might further lead to declined oocyte quality in mice.

Oocyte maturity and quality are critical for fertilization in mammals. Successful extrusion of PB1 is the last step of oocyte nuclear maturation (Reyes and Ross, 2016). Our results suggest that POD exposure significantly causes declined oocyte quality in mice, showing with a reduction of the PB1 extrusion rate, which is similar to a previous report (Hu et al., 2018). During oocyte maturation, the demand for new proteins that are accomplished by proper protein synthesis, folding, modification, and trafficking is increasing (Guzel et al., 2017). The ER, a multifunctional organelle in eukaryotic cells, is the major store of intracellular calcium and plays a vital role in protein and lipid synthesis (Schwarz and Blower, 2016). To ensure the normal oocyte development, maintaining ER homeostasis is an important issue (Lin et al., 2019). Many studies have reported that the ER is affected after POD derivative exposure, which may imply the potential toxicity of POD on the ER. For example, the epimer of POD can result in esophageal squamous cell carcinoma apoptosis by ER stress and increased ROS level (Kwak et al., 2020). Etoposide, a semisynthetic POD derivative, causes focally extensive dilation of the rough ER in the ganglion cell bodies of female CD-1 mice (Bregman et al., 1994; Wang et al., 2020). Moreover, Ching001 is the structural analog of POD, which partly induces apoptosis *via* the activation of the ER stress signaling pathway, showing with increased expression of p-PREK, p-eIF2α, p-JNK, GADD153, and caspase-4 (Chen et al., 2013). Similarly, our data show that the distribution of the ER is significantly affected after POD exposure, indicating that the protein synthesis is disturbed in mouse oocytes.

The Golgi apparatus acts as a docking station for cargo transportation in which the *cis* face receives the new synthesized molecules from the ER while the *trans* face represents the exit site to a lot of destinations (Wei and Seemann, 2017). Due to its central role, the abnormal structure and function of the Golgi apparatus dramatically influence the cell processes (Kulkarni-Gosavi et al., 2019). Disrupting the Golgi complex by Brefeldin A, a membrane trafficking inhibitor that blocks the anterograde transport of proteins from the ER to the Golgi apparatus, has been suggested to impair oocyte maturation (Moreno et al., 2002; Cui et al., 2019). And the depletion of GM130, a *cis*-Golgi protein, could disturb spindle organization, migration, and asymmetric division during mouse oocyte maturation (Zhang et al., 2011). Moreover, the Golgi apparatus is often affected by the ER due to its role in post-translational modifications and transport of newly synthesized proteins and lipids (Passemard et al., 2019). Our results show that POD led to a failure of spindle periphery accumulation of the Golgi apparatus in mouse oocytes. It is shown that Golgi morphology is changed, and trafficking function is suppressed after exposure to etoposide, which refers to a derivative of POD (Dinsdale et al., 1999; Torii et al., 2020). Besides, aberrant distribution and weak fluorescence intensities of Rab11a are also observed in the POD treatment group oocytes, indicating the decrease in the Rab11a-positive vesicle, which might induce the failure of spindle migration and polar body extrusions (Duan and Sun, 2019). These findings suggest that POD could affect protein and vesicle transportation by Golgi apparatus damage in mouse oocytes.

As protein demand increases, the levels of unfolded or misfolded proteins are enhancing (Guzel et al., 2017), which probably induces ER stress and ultimately causes apoptosis (Lin et al., 2019). Lysosome, the major catabolic center, degrades macromolecules delivered *via* endocytic, phagocytic, and autophagic pathways (Luzio et al., 2014). And this function depends on its more than 50 different hydrolases, which are, respectively, synthesized and transported in the ER and Golgi apparatus (Darios and Stevanin, 2020). The dysfunctional lysosomes can cause various diseases including

cancer, neurodegenerative, and autoimmune diseases (Cabukusta and Neefjes, 2018; Darios and Stevanin, 2020). Furthermore, lysosomal dysfunction probably destroys porcine oocyte maturation and developmental capacity by disturbing chromosome and activating autophagy (Miao et al., 2019). POD can inhibit lysosomes to degrade asialo-orosomucoid in rat hepatocytes and prevent the radial redistribution of lysosomes in mouse macrophages (Phaire-Washington et al., 1980; Oka and Weigel, 1983). Our results illustrate that POD inhibits lysosome distribution and function, showing with large lysosomes and strong fluorescence intensities. The enlarged lysosomes likely indicate the occurrence of autophagy, which is considered as a mechanism of defense against oxidative and environmental stress (McGinnis et al., 2014). Therefore, our results demonstrate that POD impairs the function of lysosomes in mouse oocytes.

Mitochondria are the main organelles that produce ATP and are essential to meeting the energy requirements of oocytes. Dysfunction of mitochondria decreases oocyte quality and interferes with embryonic development (Babayev and Seli, 2015). Abnormal structure and function of mitochondria are found in oocytes and cumulus cells from diabetic mice, which may explain the adverse effects of maternal diabetes on embryo development and pregnancy outcomes (Wang et al., 2009, 2010). Our data also show that POD causes significant damage to mitochondria distribution, which may ultimately lead to mitochondria dysfunction in mouse oocytes. Previous studies have shown that POD exposure increases the ROS level and leads to oxidative stress (Jiang et al., 2020), which is interconnected with mitochondrial dysfunction (Willems et al., 2015; Kudryavtseva et al., 2016). We speculate that POD affects the oocyte developmental capacity by inducing mitochondrial damage-mediated insufficient energy supply and oxidative stress. Similarly, it has been reported that POD can induce the change of mitochondrial membrane potential and raise the ROS level in green monkey kidney cells (Li et al., 2013). And the inhibition of coupled and uncoupled respiration of both FAD and NAD-linked substrates is still found in isolated and digitonin-permeabilized hepatocytes after POD exposure (Horrum et al., 1986). These previous findings, together with our work, indicate the general conserved effects of POD on the function of mitochondria among different models. It should be noted that our study is adopted with an *in vitro* model, and whether POD has similar effects on oocytes *in vivo* needs further study.

We speculate that there are two possible causes for the aberrant distribution of organelles in oocytes: one is that POD could prevent the assembly of tubulin into microtubules, which serve as a scaffold for organelle transport and positioning (Ardalani et al., 2017; Meiring et al., 2020); another is that the disrupted spindle structure by microtubule disassembly may affect organelle location and function since they accumulate at the spindle periphery at the MI stage, and POD exposure can disrupt the spindle formation (Coticchio et al., 2015; Hu et al., 2018). However, the deeper explanation for the alteration of the distribution after POD exposure still needs further mechanism study.

In summary, our study illustrates that POD exposure disrupts the distribution and functions of organelles in mouse oocytes, including the ER, Golgi apparatus, lysosome, and mitochondria, which further leads to the defects of oocyte meiotic maturation.

DATA AVAILABILITY STATEMENT

The original contributions presented in the study are included in the article/supplementary material, further inquiries can be directed to the corresponding author/s.

ETHICS STATEMENT

The animal study was reviewed and approved by Animal Research Committee of Nanjing Agriculture University in China.

AUTHOR CONTRIBUTIONS

S-CS designed the experiments. P-SL, L-PX, X-HK, and YX performed the experiments. P-SL, L-PX, and YX contributed to the materials. P-SL and L-PX analyzed the data. P-SL, L-PX, and S-CS wrote the manuscript. All authors approved the submission of the manuscript.

FUNDING

This work was supported by the National Undergraduate Innovation and Entrepreneurship Training Program of China (202010307023Z/202010307041), the National Key Research and Development Program of China (2018YFC1003802, 2018YFC1004003), and the Fundamental Research Funds for the Central Universities of China (KYGD202004).

REFERENCES

Ardalani, H., Avan, A., and Ghayour-Mobarhan, M. (2017). Podophyllotoxin: a novel potential natural anticancer agent. *Avicenna J. Phytomed.* 7, 285–294.

Babayev, E., and Seli, E. (2015). Oocyte mitochondrial function and reproduction. *Curr. Opin. Obstet. Gynecol.* 27, 175–181. doi: 10.1097/gco.0000000000000164

Bregman, C. L., Buroker, R. A., Hirth, R. S., Crosswell, A. R., and Durham, S. K. (1994). Etoposide- and BMY-40481-induced sensory neuropathy in mice. *Toxicol. Pathol.* 22, 528–535. doi: 10.1177/019262339402200508

Cabukusta, B., and Neefjes, J. (2018). Mechanisms of lysosomal positioning and movement. *Traffic* 19, 761–769. doi: 10.1111/tra.12587

Chang, L. W., Yang, C. M., Chen, C. F., and Deng, J. F. (1992a). Experimental podophyllotoxin (bajiaolian) poisoning: I. Effects on the nervous system. *Biomed. Environ. Sci.* 5, 283–292.

Chang, L. W., Yang, C. M., Chen, C. F., and Deng, J. F. (1992b). Experimental podophyllotoxin (bajiaolian) poisoning: II. Effects on the liver, intestine, kidney, pancreas and testis. *Biomed. Environ. Sci.* 5, 293–302.

Chen, J. Y., Tang, Y. A., Li, W. S., Chiou, Y. C., Shieh, J. M., and Wang, Y. C. (2013). A synthetic podophyllotoxin derivative exerts anti-cancer effects by inducing mitotic arrest and pro-apoptotic ER stress in lung cancer preclinical models. *PLoS One* 8:e62082. doi: 10.1371/journal.pone.0062082

Coticchio, G., Dal Canto, M., Mignini Renzini, M., Guglielmo, M. C., Brambillasca, F., Turchi, D., et al. (2015). Oocyte maturation: gamete-somatic cells interactions, meiotic resumption, cytoskeletal dynamics and cytoplasmic reorganization. *Hum. Reprod. Update.* 21, 427–454. doi: 10.1093/humupd/dmv011

Cui, Q., Du, R., Liu, M., and Rong, L. (2020). Lignans and their derivatives from plants as antivirals. *Molecules* 25:183. doi: 10.3390/molecules25010183

Cui, Z., Yu, L., Shi Yang, X., Zhang, Y., Shi, X., Li, Y., et al. (2019). Brefeldin a impairs porcine oocyte meiotic maturation via interruption of organelle dynamics. *J. Cell Physiol.* 234, 20111–20117. doi: 10.1002/jcp.28611

Darios, F., and Stevanin, G. (2020). Impairment of lysosome function and autophagy in rare neurodegenerative diseases. *J. Mol. Biol.* 432, 2714–2734. doi: 10.1016/j.jmb.2020.02.033

Dinsdale, D., Zhuang, J., and Cohen, G. M. (1999). Redistribution of cytochrome c precedes the caspase-dependent formation of ultracondensed mitochondria, with a reduced inner membrane potential, in apoptotic monocytes. *Am. J. Pathol.* 155, 607–618. doi: 10.1016/s0002-9440(10)65156-5

Duan, X., and Sun, S. C. (2019). Actin cytoskeleton dynamics in mammalian oocyte meiosis. *Biol. Reprod.* 100, 15–24. doi: 10.1093/biolre/ioy163

Giri, A., and Lakshmi Narasu, M. (2000). Production of podophyllotoxin from *Podophyllum hexandrum*: a potential natural product for clinically useful anticancer drugs. *Cytotechnology* 34, 17–26.

Guzel, E., Arlier, S., Guzeloglu-Kayisli, O., Tabak, M. S., Ekiz, T., Semerci, N., et al. (2017). Endoplasmic reticulum stress and homeostasis in reproductive physiology and pathology. *Int. J. Mol. Sci.* 18:792. doi: 10.3390/ijms18040792

Holubcová, Z., Howard, G., and Schuh, M. (2013). Vesicles modulate an actin network for asymmetric spindle positioning. *Nat. Cell Biol.* 15, 937–947. doi: 10.1038/ncb2802

Horrum, M. A., Jennett, R. B., Ecklund, R. E., and Tobin, R. B. (1986). Inhibition of respiration in mitochondria and in digitonin-treated rat hepatocytes by podophyllotoxin. *Mol. Cell Biochem.* 71, 79–85.

Hu, L. L., Zhou, X., Zhang, H. L., Wu, L. L., Tang, L. S., Chen, L. L., et al. (2018). Exposure to podophyllotoxin inhibits oocyte meiosis by disturbing meiotic spindle formation. *Sci. Rep.* 8:10145.

Jiang, W. J., Hu, L. L., Ren, Y. P., Lu, X., Luo, X. Q., Li, Y. H., et al. (2020). Podophyllotoxin affects porcine oocyte maturation by inducing oxidative stress-mediated early apoptosis. *Toxicon* 176, 15–20. doi: 10.1016/j.toxicon.2020.01.006

Kudryavtseva, A. V., Krasnov, G. S., Dmitriev, A. A., Alekseev, B. Y., Kardymon, O. L., Sadritdinova, A. F., et al. (2016). Mitochondrial dysfunction and oxidative stress in aging and cancer. *Oncotarget* 7, 44879–44905.

Kulkarni-Gosavi, P., Makhoul, C., and Gleeson, P. A. (2019). Form and function of the Golgi apparatus: scaffolds, cytoskeleton and signalling. *FEBS Lett.* 593, 2289–2305. doi: 10.1002/1873-3468.13567

Kwak, A. W., Yoon, G., Lee, M. H., Cho, S. S., Shim, J. H., and Chae, J. I. (2020). Picropodophyllotoxin, an epimer of podophyllotoxin, causes apoptosis of human esophageal squamous cell carcinoma cells through ROS-Mediated JNK/P38 MAPK pathways. *Int. J. Mol. Sci.* 21:4640. doi: 10.3390/ijms21134640

Lacey, C. J., Goodall, R. L., Tennvall, G. R., Maw, R., Kinghorn, G. R., Fisk, P. G., et al. (2003). Randomised controlled trial and economic evaluation of podophyllotoxin solution, podophyllotoxin cream, and podophyllin in the treatment of genital warts. *Sex. Transm. Infect.* 79, 270–275. doi: 10.1136/sti.79.4.270

Li, J., Ahat, E., and Wang, Y. (2019). Golgi structure and function in health, stress, and diseases. *Results Probl. Cell Differ.* 67, 441–485. doi: 10.1007/978-3-030-23173-6_19

Li, J., Sun, H., Jin, L., Cao, W., Zhang, J., Guo, C. Y., et al. (2013). Alleviation of podophyllotoxin toxicity using coexisting flavonoids from *Dysosma versipellis*. *PLoS One* 8:e72099. doi: 10.1371/journal.pone.0072099

Lin, T., Lee, J. E., Kang, J. W., Shin, H. Y., Lee, J. B., and Jin, D. I. (2019). Endoplasmic reticulum (ER) stress and unfolded protein response (UPR) in mammalian oocyte maturation and preimplantation embryo development. *Int. J. Mol. Sci.* 20:409. doi: 10.3390/ijms20020409

Luzio, J. P., Hackmann, Y., Dieckmann, N. M., and Griffiths, G. M. (2014). The biogenesis of lysosomes and lysosome-related organelles. *Cold Spring Harb. Perspect. Biol.* 6:a016840. doi: 10.1101/cshperspect.a016840

Mao, L., Lou, H., Lou, Y., Wang, N., and Jin, F. (2014). Behaviour of cytoplasmic organelles and cytoskeleton during oocyte maturation. *Reprod. Biomed. Online* 28, 284–299. doi: 10.1016/j.rbmo.2013.10.016

McGinnis, L. K., Pelech, S., and Kinsey, W. H. (2014). Post-ovulatory aging of oocytes disrupts kinase signaling pathways and lysosome biogenesis. *Mol. Reprod. Dev.* 81, 928–945. doi: 10.1002/mrd.22413

Meiring, J. C. M., Shneyer, B. I., and Akhmanova, A. (2020). Generation and regulation of microtubule network asymmetry to drive cell polarity. *Curr. Opin. Cell Biol.* 62, 86–95. doi: 10.1016/j.ceb.2019.10.004

Miao, J. K., Liu, Y. H., Liu, S., Liu, X. M., Wang, P. C., Du, Z. Q., et al. (2019). Lysosomal dysfunction disturbs porcine oocyte maturation and developmental capacity by disorganizing chromosome/cytoskeleton and activating autophagy/apoptosis. *Theriogenology* 140, 44–51. doi: 10.1016/j.theriogenology.2019.08.019

Moreno, R. D., Schatten, G., and Ramalho-Santos, J. (2002). Golgi apparatus dynamics during mouse oocyte in vitro maturation: effect of the membrane trafficking inhibitor brefeldin A. *Biol. Reprod.* 66, 1259–1266. doi: 10.1095/biolreprod66.5.1259

Nunnari, J., and Suomalainen, A. (2012). Mitochondria: in sickness and in health. *Cell* 148, 1145–1159. doi: 10.1016/j.cell.2012.02.035

Oka, J. A., and Weigel, P. H. (1983). Microtubule-depolymerizing agents inhibit asialo-orosomucoid delivery to lysosomes but not its endocytosis or degradation in isolated rat hepatocytes. *Biochim. Biophys. Acta* 763, 368–376. doi: 10.1016/0167-4889(83)90098-8

Pan, B., and Li, J. (2019). The art of oocyte meiotic arrest regulation. *Reprod. Biol. Endocrinol.* 17:8.

Passemard, S., Perez, F., Gressens, P., and El Ghouzzi, V. (2019). Endoplasmic reticulum and Golgi stress in microcephaly. *Cell Stress* 3, 369–384. doi: 10.15698/cst2019.12.206

Phaire-Washington, L., Silverstein, S. C., and Wang, E. (1980). Phorbol myristate acetate stimulates microtubule and 10-nm filament extension and lysosome redistribution in mouse macrophages. *J. Cell Biol.* 86, 641–655. doi: 10.1083/jcb.86.2.641

Reyes, J. M., and Ross, P. J. (2016). Cytoplasmic polyadenylation in mammalian oocyte maturation. *Wiley Interdiscip. Rev. RNA* 7, 71–89. doi: 10.1002/wrna.1316

Rodríguez-García, C., Sánchez-Quesada, C., Toledo, E., Delgado-Rodríguez, M., and Gaforio, J. J. (2019). Naturally lignan-rich foods: a dietary tool for health promotion? *Molecules* 24:917. doi: 10.3390/molecules24050917

Roth, Z. (2018). Symposium review: Reduction in oocyte developmental competence by stress is associated with alterations in mitochondrial function. *J. Dairy Sci.* 101, 3642–3654. doi: 10.3168/jds.2017-13389

Schwarz, D. S., and Blower, M. D. (2016). The endoplasmic reticulum: structure, function and response to cellular signaling. *Cell. Mol. Life Sci.* 73, 79–94. doi: 10.1007/s00018-015-2052-6

Shi, F., Qiu, J., Zhang, J., Wang, S., Zhao, X., and Feng, X. (2021). The toxic effects and possible mechanisms of decabromodiphenyl ethane on mouse oocyte. *Ecotoxicol. Environ. Saf.* 207:111290. doi: 10.1016/j.ecoenv.2020.111290

Sirard, M. A., Richard, F., Blondin, P., and Robert, C. (2006). Contribution of the oocyte to embryo quality. *Theriogenology* 65, 126–136. doi: 10.1016/j.theriogenology.2005.09.020

Sun, M. H., Li, X. H., Xu, Y., Xu, Y., Pan, Z. N., and Sun, S. C. (2020). Citrinin exposure disrupts organelle distribution and functions in mouse oocytes. *Environ. Res.* 185, 109476. doi: 10.1016/j.envres.2020.109476

Torii, S., Yamaguchi, H., Nakanishi, A., Arakawa, S., Honda, S., Moriwaki, K., et al. (2020). Identification of a phosphorylation site on Ulk1 required for genotoxic stress-induced alternative autophagy. *Nat. Commun.* 11:1754.

von Krogh, G., and Longstaff, E. (2001). Podophyllin office therapy against condyloma should be abandoned. *Sex. Transm. Infect.* 77, 409–412. doi: 10.1136/sti.77.6.409

Wang, Q., Frolova, A. I., Purcell, S., Adastra, K., Schoeller, E., Chi, M. M., et al. (2010). Mitochondrial dysfunction and apoptosis in cumulus cells of type I diabetic mice. *PLoS One* 5:e15901. doi: 10.1371/journal.pone.0015901

Wang, Q., Ratchford, A. M., Chi, M. M., Schoeller, E., Frolova, A., Schedl, T., et al. (2009). Maternal diabetes causes mitochondrial dysfunction and meiotic defects in murine oocytes. *Mol. Endocrinol.* 23, 1603–1612. doi: 10.1210/me.2009-0033

Wang, Y., Wang, S., Xu, Y., Wang, P., Li, S., Liu, L., et al. (2020). Etoposide amorphous nanopowder for improved oral bioavailability: formulation development, optimization, in vitro and in vivo evaluation. *Int. J. Nanomedicine* 15, 7601–7613. doi: 10.2147/ijn.s265817

Watson, A. J. (2007). Oocyte cytoplasmic maturation: a key mediator of oocyte and embryo developmental competence. *J. Anim. Sci.* 85, E1–E3.

Wei, J. H., and Seemann, J. (2017). Golgi ribbon disassembly during mitosis, differentiation and disease progression. *Curr. Opin. Cell Biol.* 47, 43–51. doi: 10.1016/j.ceb.2017.03.008

Welz, T., Wellbourne-Wood, J., and Kerkhoff, E. (2014). Orchestration of cell surface proteins by Rab11. *Trends Cell Biol.* 24, 407–415. doi: 10.1016/j.tcb.2014.02.004

Wiley, D. J., Douglas, J., Beutner, K., Cox, T., Fife, K., Moscicki, A. B., et al. (2002). External genital warts: diagnosis, treatment, and prevention. *Clin. Infect. Dis.* 35, S210–S224.

Willems, P. H., Rossignol, R., Dieteren, C. E., Murphy, M. P., and Koopman, W. J. (2015). Redox homeostasis and mitochondrial dynamics. *Cell Metab.* 22, 207–218. doi: 10.1016/j.cmet.2015.06.006

Xie, S., Li, G., Qu, L., Zhong, R., Chen, P., Lu, Z., et al. (2017). Podophyllotoxin Extracted from *Juniperus sabina* fruit inhibits rat sperm maturation and fertility by promoting epididymal epithelial cell apoptosis. *Evid. Based Complement Alternat. Med.* 2017:6958982.

Yang, C. M., Deng, J. F., Chen, C. F., and Chang, L. W. (1994). Experimental podophyllotoxin (bajiaolian) poisoning: III. Biochemical bases for toxic effects. *Biomed. Environ. Sci.* 7, 259–265.

Yanofsky, V. R., Patel, R. V., and Goldenberg, G. (2012). Genital warts: a comprehensive review. *J. Clin. Aesthet. Dermatol.* 5, 25–36.

Zálešák, F., Bon, D. J. D., and Pospíšil, J. (2019). Lignans and Neolignans: Plant secondary metabolites as a reservoir of biologically active substances. *Pharmacol. Res.* 146:104284. doi: 10.1016/j.phrs.2019.104284

Zhang, C. H., Wang, Z. B., Quan, S., Huang, X., Tong, J. S., Ma, J. Y., et al. (2011). GM130, a cis-Golgi protein, regulates meiotic spindle assembly and asymmetric division in mouse oocyte. *Cell Cycle* 10, 1861–1870. doi: 10.4161/cc.10.11.15797

Conflict of Interest: The authors declare that the research was conducted in the absence of any commercial or financial relationships that could be construed as a potential conflict of interest.

Copyright © 2021 Lu, Xie, Kong, Xu and Sun. This is an open-access article distributed under the terms of the Creative Commons Attribution License (CC BY). The use, distribution or reproduction in other forums is permitted, provided the original author(s) and the copyright owner(s) are credited and that the original publication in this journal is cited, in accordance with accepted academic practice. No use, distribution or reproduction is permitted which does not comply with these terms.

frontiers in Cell and Developmental Biology

ORIGINAL RESEARCH
published: 21 May 2021
doi: 10.3389/fcell.2021.673258

PRMT5 Is Involved in Spermatogonial Stem Cells Maintenance by Regulating *Plzf* Expression via Modulation of Lysine Histone Modifications

Fangfang Dong[1,2,3†], Min Chen[1,3†], Min Chen[4], Lin Jiang[5], Zhiming Shen[1,2,3], Longfei Ma[1,2,3], Chunsheng Han[1,2,3], Xudong Guo[6*] and Fei Gao[1,2,3*]*

[1] State Key Laboratory of Stem Cell and Reproductive Biology, Institute of Zoology, Chinese Academy of Sciences, Beijing, China, [2] University of Chinese Academy of Sciences, Beijing, China, [3] Institute for Stem Cell and Regeneration, Chinese Academy of Sciences, Beijing, China, [4] Guangdong and Shenzhen Key Laboratory of Male Reproductive Medicine and Genetics, Institute of Urology, Peking University Shenzhen Hospital, Shenzhen Peking University-Hong Kong University of Science and Technology Medical Center, Shenzhen, China, [5] School of Basic Medical Sciences, Zunyi Medical University, Zunyi, China, [6] State Key Laboratory of Reproductive Regulation and Breeding of Grassland Livestock, Inner Mongolia University, Hohhot, China

Protein arginine methyltransferase 5 (PRMT5) catalyzes the formation of mono- or symmetric dimethylarginine residues on histones and non-histone substrates and has been demonstrated to play important roles in many biological processes. In the present study, we observed that PRMT5 is abundantly expressed in spermatogonial stem cells (SSCs) and that *Prmt5* deletion results in a progressive loss of SSCs and male infertility. The proliferation of *Prmt5*-deficient SSCs cultured *in vitro* exhibited abnormal proliferation, cell cycle arrest in G0/G1 phase and a significant increase in apoptosis. Furthermore, PLZF expression was dramatically reduced in *Prmt5*-deficient SSCs, and the levels of H3K9me2 and H3K27me2 were increased in the proximal promoter region of the *Plzf* gene in *Prmt5*-deficient SSCs. Further study revealed that the expression of lysine demethylases (JMJD1A, JMJD1B, JMJD1C, and KDM6B) was significantly reduced in *Prmt5*-deficient SSCs and that the level of permissive arginine methylation H3R2me2s was significantly decreased at the upstream promoter region of these genes in *Prmt5*-deficient SSCs. Our results demonstrate that PRMT5 regulates spermatogonial stem cell development by modulating histone H3 lysine modifications.

Keywords: PRMT5, spermatogonial stem cells, histone lysine modification, lysine demethylase, PLZF

OPEN ACCESS

Edited by:
Liangran Zhang,
Shandong University, China

Reviewed by:
Wei Shen,
Qingdao Agricultural University, China
Qi-En Yang,
Northwest Institute of Plateau Biology, Chinese Academy of Sciences (CAS), China

****Correspondence:***
Chunsheng Han
hancs@ioz.ac.cn
Xudong Guo
bixdguo@imu.edu.cn
Fei Gao
gaof@ioz.ac.cn

† These authors have contributed equally to this work

Specialty section:
This article was submitted to Cell Growth and Division, a section of the journal Frontiers in Cell and Developmental Biology

Received: *27 February 2021*
Accepted: *26 April 2021*
Published: *21 May 2021*

Citation:
Dong F, Chen M, Chen M, Jiang L, Shen Z, Ma L, Han C, Guo X and Gao F (2021) PRMT5 Is Involved in Spermatogonial Stem Cells Maintenance by Regulating Plzf Expression via Modulation of Lysine Histone Modifications. Front. Cell Dev. Biol. 9:673258. doi: 10.3389/fcell.2021.673258

INTRODUCTION

Spermatogenesis is a highly precise cellular process, which consists of the self-renewal and differentiation of spermatogonial stem cells, spermatocyte meiosis and post-meiotic development of spermatids (He et al., 2008; Wu et al., 2016). Spermatogonia contain a small population of germline-specific stem cells with the ability to self-renew and differentiation. The differentiation of spermatogonia is stimulated by both intrinsic and extrinsic factors, which subsequently

generate differentiating spermatogonia, spermatocytes, spermatids, and mature sperm (Chen and Liu, 2015; Mäkelä and Hobbs, 2019). In mammals, both genetic and epigenetic modifications are involved in the development of male germ cells. *Plzf*, *Gfra1*, *Pou5f1*, *Lin28A*, and *Nanos3* are expressed in undifferentiated spermatogonia, and *c-Kit* is considered a marker gene of differentiating spermatogonia. Several Sertoli cell-produced growth factors, such as glial cell line-derived neurotrophic factor (GDNF), fibroblast growth factor (FGF2), and insulin-like growth factor (IGF), are also crucial for the maintenance and proliferation of spermatogonial stem cells (SSCs) (Oatley and Brinster, 2008; Zhang et al., 2012; Wang et al., 2016; Chen et al., 2017). Homozygous deletion of *Gdnf* leads to major defects in neonatal death. The function of *Gdnf* in SSC maintenance was first discovered in *Gdnf* heterozygous mutant (Meng et al., 2000).

Plzf (also known as *Zfp145*, *Zbtb16*, and promyelocytic leukemia zinc-finger) belongs to the Kruppel family and is expressed in hematopoietic stem/progenitor cells (Reid et al., 1995; Liu et al., 2016; Hai et al., 2019; Poplineau et al., 2019), bone marrow progenitor cells (Shaknovich et al., 1998), mesenchymal stem cells (Agrawal Singh et al., 2019) and other somatic cells (Cook et al., 1995; Barna et al., 2000). In mammalian testes, PLZF was first detected in prospermatogonia at E17.5 and is continually expressed in SSCs and spermatogonial progenitor cells (SPCs) at the adult stage (Avantaggiato et al., 1995; Buaas et al., 2004; Costoya et al., 2004). PLZF has been reported to play an essential role in SSCs pool maintenance and in regulating the self-renewal of SSCs. *Plzf* knockout leads to progressive germ cell loss after birth, and the spermatogonia are visible in only a few seminiferous tubules of adult mice (Buaas et al., 2004; Costoya et al., 2004).

PRMT5, a type II protein arginine methyltransferase, catalyzes the transfer of a methyl group from S-adenosylmethionine (SAM or AdoMet) to histones and non-histone substrates to form mono- or symmetric dimethylarginine (MMA or sDMA, respectively) (Rho et al., 2001; Bedford, 2007; Stopa et al., 2015). PRMT5 plays important roles in diverse cellular processes, such as cell differentiation, cell cycle, apoptosis, tumorigenesis and spliceosome assembly (Pahlich et al., 2006; Stopa et al., 2015; Hamard et al., 2018; Raposo and Piller, 2018). Previous studies have demonstrated that PRMT5 is required for germ cell development, as the loss of *Prmt5* in primordial germ cells (PGCs) causes male and female sterility. PRMT5 represses the activation of LINEs and IAP transposons via symmetric dimethylation of arginine 3 on histone H2A and H4 (H2A/H4R3me2s) (Kim et al., 2014). PRMT5 is also required for PGC survival by promoting methylation of Sm spliceosomal proteins (Li et al., 2015). The results of our previous study demonstrated that inactivation of *Prmt5* in male germ cells using *Stra8-Cre* causes aberrant spermatogenesis and male infertility (Wang et al., 2015c), suggesting that PRMT5 is essential for the development of male germ cells. PRMT5 is also expressed in mouse spermatogonial stem cells (SSCs). However, whether PRMT5 is involved in the development of SSCs is unknown. In the present study, we demonstrated that the deletion of *Prmt5* in germ cells resulted in loss of spermatogonial stem cells (SSCs) and male infertility. *Prmt5*-deficient SSCs cultured *in vitro* exhibited abnormal proliferation, and the cell cycle was arrested in G0/G1 phase. Further study revealed that the expression of PLZF was dramatically reduced in *Prmt5*-deficient SSCs. We also observed that inactivation of *Prmt5* resulted in enrichment of H3K9me2 and H3K27me2 in the promoter region of the *Plzf* gene, which in turn caused downregulation of *Plzf* expression and defects in SSC development.

RESULTS

Deletion of *Prmt5* in Spermatogonia Causes Germ Cell Loss and Male Infertility

PRMT5 was previously reported to be expressed in PGCs during the embryonic stage (Ancelin et al., 2006; Kim et al., 2014; Li et al., 2015) and in spermatocytes postnatally (Wang et al., 2015c; Dong et al., 2019). In the present study, PRMT5 expression in spermatogonia was examined by immunofluorescence and western blot assays. As shown in **Supplementary Figure 1**, PRMT5 was primarily detected in the cytoplasm of PLZF-positive germ cells (**Supplementary Figure 1C**, white arrowheads). PRMT5 was also detected in both the nucleus and cytoplasm of SSCs cultured *in vitro* by both immunofluorescence (**Supplementary Figure 1D**, white arrows) and western blot analysis. Lamin a/c and GAPDH served as loading controls for the nuclear and cytoplasmic extracts, respectively (**Supplementary Figure 1G**).

To assess the functions of PRMT5 in the development of SSCs, *Prmt5* was deleted in prospermatogonia from E15 by crossing with *Mvh-Cre* transgenic mice (Gallardo et al., 2007). The immunofluorescence showed that PRMT5 was completely deleted in the PLZF-positive germ cells of $Prmt5^{\Delta/flox}$;*Mvh-Cre* testes (**Supplementary Figures 2D–F**, white arrows). No obvious developmental abnormalities were observed in adult $Prmt5^{\Delta/flox}$;*Mvh-Cre* mice (**Figure 1A**), and their body weights were comparable to those of control littermates (**Figure 1B**). However, the size of testes from $Prmt5^{\Delta/flox}$;*Mvh-Cre* mice was significantly reduced (**Figures 1C,D**). The histological results showed that germ cells at different developmental stages were observed in control testes (**Figure 1E**), whereas most of the seminiferous tubules in adult $Prmt5^{\Delta/flox}$;*Mvh-Cre* testes lacked germ cells (**Figure 1F**, asterisks). The cauda epididymis of control males was filled with mature sperm (**Figure 1G**), but no mature sperm were observed in *Prmt5*-deficient males (**Figure 1H**, asterisks). PLZF-positive spermatogonia were located at the peripheral region of the seminiferous tubules in control mice (**Figure 1I**, black arrows), whereas no PLZF-positive spermatogonia were observed in $Prmt5^{\Delta/flox}$;*Mvh-Cre* mice (**Figure 1J**, asterisks). SOX9-positive Sertoli cells were observed in the seminiferous tubules of both control (**Figure 1K**, black arrows) and $Prmt5^{\Delta/flox}$;*Mvh-Cre* mice (**Figure 1L**, black arrows). These results indicate that

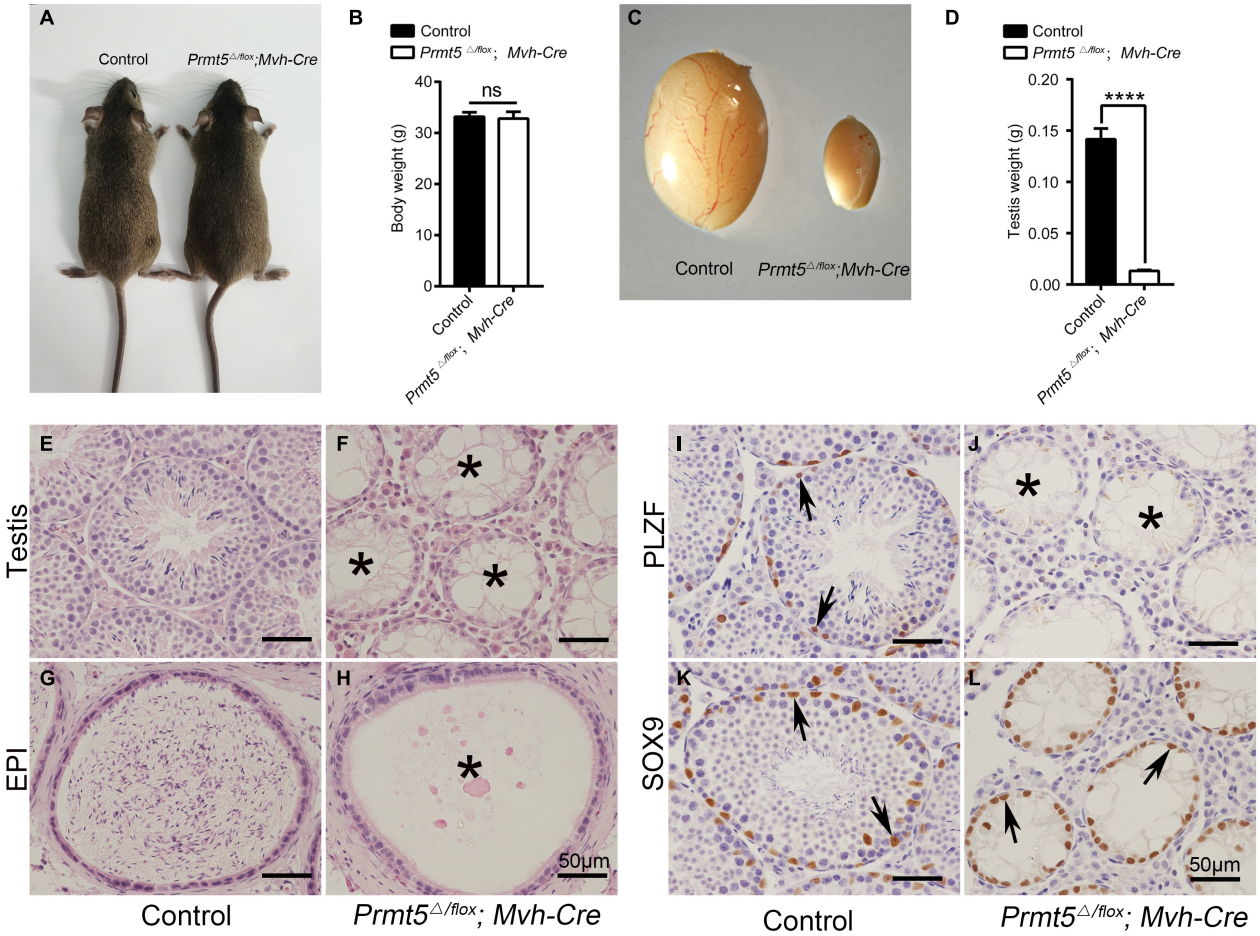

FIGURE 1 | Deletion of *Prmt5* causes germ cell loss and male infertility. No obvious developmental abnormalities were observed in adult *Prmt5*$^{\Delta/flox}$*;Mvh-Cre* mice **(A)**, and the body weights were comparable to those of control littermates **(B)**. The size of testes from *Prmt5*$^{\Delta/flox}$*;Mvh-Cre* mice was significantly smaller than that of control littermates **(C,D)**. Germ cells at different developmental stages were observed in control testes **(E)**, whereas most seminiferous tubules were empty in adult *Prmt5*$^{\Delta/flox}$*;Mvh-Cre* testes **(F**, asterisks). The cauda epididymis of control males was filled with mature sperm **(G)**, but no mature sperm were observed in the epididymis of *Prmt5*-deficient males **(H)**. PLZF-positive spermatogonia were located at the peripheral region of the seminiferous tubules in control mice [**(I)**, black arrows], whereas no PLZF-positive spermatogonia were observed in *Prmt5*$^{\Delta/flox}$*;Mvh-Cre* mice **(J)**. SOX9-positive Sertoli cells were observed in the seminiferous tubules of both control [**(K)**, black arrows] and *Prmt5*$^{\Delta/flox}$*;Mvh-Cre* mice [**(L)**, black arrows]. Error bars represent the SEM of triplicate results. ****$P < 0.00001$ indicates a significant difference (*t*-test).

PRMT5 is important for the survival and maintenance of spermatogonial stem cells.

The Germ Cells in *Prmt5*$^{\Delta/flox}$*;Mvh-Cre* Mice Were Gradually Lost From P10

Testes from *Prmt5*$^{\Delta/flox}$*;Mvh-Cre* mice (**Supplementary Figure 3B**) were grossly normal at P7 compared to those of control testes (**Supplementary Figure 3A**). Aberrant seminiferous tubules were first noted in *Prmt5*$^{\Delta/flox}$*;Mvh-Cre* testes at P10 (**Supplementary Figure 3D**, asterisks). Empty tubules were observed in *Prmt5*-deficient testes at 2 weeks (**Supplementary Figure 3F**, asterisks), 3 weeks (**Supplementary Figure 3H**, asterisks), 4 weeks (**Supplementary Figure 3J**, asterisks) and 6 weeks (**Supplementary Figure 3L**, asterisks). The development of germ cells at different developmental stages was also examined by immunohistochemistry. MVH-positive germ cells were observed in both control (**Figure 2A**, black arrows) and *Prmt5*$^{\Delta/flox}$*;Mvh-Cre* mice (**Figure 2B**, black arrows) at P7, and no difference was noted. The number of germ cells in *Prmt5*$^{\Delta/flox}$*;Mvh-Cre* mice (**Figure 2D**, black arrows) was significantly reduced at P10 than that in control mice (**Figure 2C**, black arrows), while the number of germ cells was significantly increased from 2 to 6 weeks in these mice (**Figures 2E,G,I,K**, black arrows). In contrast, the number of germ cells in *Prmt5*$^{\Delta/flox}$*;Mvh-Cre* mice was gradually reduced from 2 to 4 weeks (**Figures 2F,H,J**, black arrows), and they were completely absent at 6 weeks of age (**Figure 2L**, asterisks). PLZF-positive spermatogonia (green) were observed in the seminiferous tubules of control mice at 3 weeks (**Supplementary Figure 4A**, white arrows), 4 weeks (**Supplementary Figure 4B**, white arrows), and 6 weeks (**Supplementary Figure 4C**, white

arrows). PLZF-positive spermatogonia were also observed in the seminiferous tubules of *Prmt5*$^{\Delta/flox}$*;Mvh-Cre* mice at 3 weeks (**Supplementary Figure 4D**, white arrows) and 4 weeks (**Supplementary Figure 4E**, white arrows) but not at 6 weeks (**Supplementary Figure 4F**, asterisks). The quantitative results showed that the number of PLZF-positive germ cells was dramatically reduced in *Prmt5*$^{\Delta/flox}$*;Mvh-Cre* mice at 3 weeks (**Supplementary Figure 4G**) and 4 weeks (**Supplementary Figure 4H**), and no germ cells were counted at 6 weeks (**Supplementary Figure 4I**). These results indicate that PRMT5 is required for the maintenance of the SSC pool.

Prmt5-Deficient Germ Cells Were Defective for Meiosis

To test whether the process of meiosis is affected after *Prmt5* depletion, the expression of STRA8, SYCP3 and γH2AX at P10 was analyzed by immunofluorescence and western blot assays. A strong STRA8 signal was detected in the germ cells of control testes at P10 (**Figure 3A**, white arrows), whereas only very weak STRA8 expression was observed in the germ cells of *Prmt5*$^{\Delta/flox}$*;Mvh-Cre* testes (**Figure 3B**, white arrows). SYCP3-positive germ cells were observed in control testes (**Figure 3C**, white arrows), but no SYCP3 signal was detected in the germ cells of *Prmt5*$^{\Delta/flox}$*;Mvh-Cre* testes at P10 (**Figure 3D**, white asterisks). The western blot results showed that the expression of the meiosis-associated proteins STRA8, SYCP3 and SYCP1 was significantly reduced in *Prmt5*$^{\Delta/flox}$*; Mvh-Cre* testes at P10 (**Figures 3E,F**). These results indicate that meiosis is blocked in *Prmt5*-deficient germ cells.

Prmt5-Deficient Spermatogonial Stem Cells Exhibited Abnormal Proliferation

In the present study, we observed that PLZF-positive spermatogonial stem cells were gradually lost in *Prmt5* knockout mice. To test whether PRMT5 is involved in the proliferation or self-renewal of SSCs, germ cells were labeled with Ki67 and PH3. Ki67 and PH3 were detected in MVH-positive germ cells in both control (**Figures 4A,D**, white arrows) and *Prmt5*$^{\Delta/flox}$*;Mvh-Cre* testes (**Figures 4B,E**, white arrows) at P10. The quantitative results showed that the percentage of Ki67- and PH3-positive germ cells was dramatically reduced in *Prmt5*$^{\Delta/flox}$*;Mvh-Cre* mice (**Figures 4C,F**). These results indicate that the deletion of *Prmt5* leads to defects in germ cell proliferation. To further confirm these results, SSCs from *Prmt5*$^{flox/flox}$*;Cre-ER*^{TM} mice were cultured *in vitro*, and *Prmt5* was deleted by treatment with 1 μM tamoxifen. Bright-field images showed that the clone size of *Prmt5*-deficient SSCs was significantly smaller (**Figures 4Gc,d**) than that of SSCs treated with ethanol (**Figures 4Ga,b**). In addition, the MTT assay results also showed that knockout of *Prmt5* resulted in a significant decrease in cell proliferation (**Figure 4H**). The flow cytometry results showed that the loss of *Prmt5* resulted in G0/G1 phase arrest with a concomitant decrease in S phase (**Figures 4I,J**). These results indicate that deletion of *Prmt5* results in cell cycle arrest of SSCs cultured *in vitro*.

Prmt5-Deficient Spermatogonial Stem Cells Exhibited Differentially Expressed Genes

The differentially expressed genes associated with stemness maintenance, proliferation and the cell cycle in both control and *Prmt5*-deficient SSCs were examined by real-time PCR and western blot analysis. *Plzf*, *Oct4*, *Nanos3*, and *Gfra1* are well-characterized pluripotent factors that are important for the maintenance of SSC stemness (Oatley and Brinster, 2008; Chen et al., 2017; Mäkelä and Hobbs, 2019). As shown in **Figure 5**, the expression of *Prmt5* was dramatically reduced in *Prmt5*$^{flox/flox}$*;Cre-ER*^{TM} SSCs treated with 1 μM tamoxifen compared to those treated with ethanol. Both the mRNA and protein levels of stemness-related genes, such as *Oct4* and *Plzf*, were significantly decreased in *Prmt5* knockout SSCs. We also observed that the expression of the germ cell marker gene *Mvh* was significantly decreased in *Prmt5*-deficient SSCs. The mRNA level of *c-Myc* was decreased in *Prmt5*-deficient SSCs (**Figure 5A**), whereas the protein level was not changed (**Figures 5B,C**). The expression of cell cycle-associated genes was also examined. As shown in **Figures 5D–F**, the mRNA and protein levels of A-type cyclins (*Ccna1* and *Ccna2*) and B-type cyclins (*Ccnb1*, *Ccnb2*, and *Ccnb3*) were all significantly reduced in *Prmt5*-deficient SSCs. In contrast, the expression of *cyclin-D*, *cyclin-E1*, and *cyclin-G* was not altered after *Prmt5* inactivation. It is worth noting that *p21* and *p53* expression dramatically increased after inactivation *Prmt5* at both the mRNA and protein levels. These results indicate that PRMT5 is important for stemness maintenance and the proliferation of spermatogonial stem cells.

H3K9me2 and H3K27me2 Levels Were Significantly Increased in *Prmt5*-Deficient SSCs

PRMT5 has been shown to regulate the expression of target genes such as *Blimp1* (Ancelin et al., 2006), *c-Myc* (Liu M. et al., 2020), *p21* (Zhang et al., 2015), and androgen receptor (Deng et al., 2017) via symmetric dimethylation of arginine residues of histones H4 (H4R3), H3 (H3R2 and H3R8), and H2A (H2AR3). The western blot results showed that loss of *Prmt5* led to a dramatic decrease in H4R3me2s, H3R2me2s, and H2AR3me2s levels. Interestingly, the levels of the repressive histone lysine modifications H3K9me2 and H3K27me2 were significantly increased (**Figures 6A,B**). Previous studies have reported that histone H3 lysine modifications, especially the methylation of H3K9 and H3K27, play important roles in the prospermatogonia to spermatogonia transition and in the development of SPCs/SSCs (Mu et al., 2014; Tseng et al., 2015; Kuroki et al., 2020). To test whether the downregulation of PLZF in *Prmt5*-deficient SSCs is due to a decrease in H4R3me2s, H3R2me2s, and H2AR3me2s levels or an increase in H3K9me2 and H3K27me2, ChIP assays were performed to analyze the enrichment of H4R3me2s, H3R2me2s, H2AR3me2s, H3K9me2, and H3K27me2 at the promoter region (TSS-1 kb upstream of TSS) of the *Plzf* gene. The ChIP-qPCR results showed

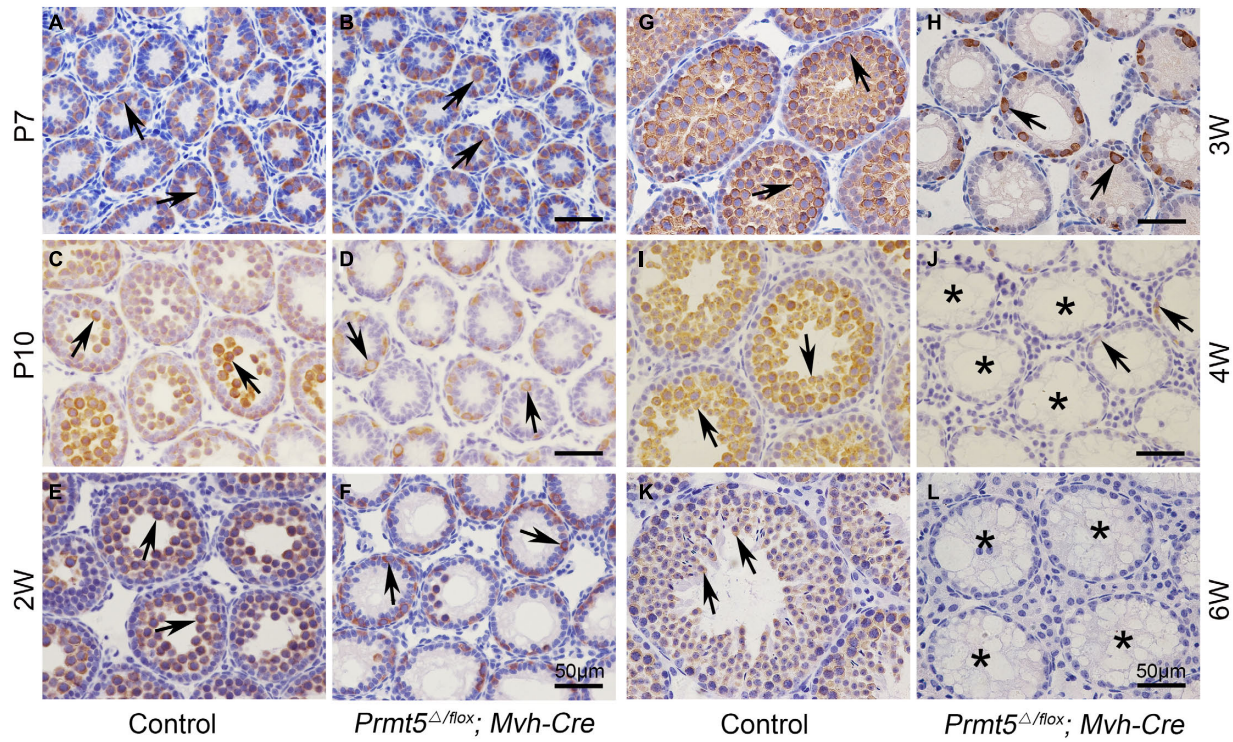

FIGURE 2 | Germ cells from *Prmt5*$^{\Delta/flox}$*;Mvh-Cre* mice are gradually lost from P10. The germ cells in control and *Prmt5*$^{\Delta/flox}$*;Mvh-Cre* mice were labeled with an anti-MVH antibody. MVH-positive germ cells were observed in both control [**(A)**, black arrows] and *Prmt5*$^{\Delta/flox}$*;Mvh-Cre* mice [**(B)**, black arrows] at P7, and no difference was noted. The number of germ cells in *Prmt5*$^{\Delta/flox}$*;Mvh-Cre* mice [**(D)**, black arrows] was significantly reduced at P10 compared to that observed in control mice [**(C)**, black arrows]. The number of germ cells was significantly increased from 2 to 6 weeks in control mice [**(E,G,I,K)**, black arrows]. In contrast, the number of germ cells in *Prmt5*$^{\Delta/flox}$*;Mvh-Cre* mice was gradually reduced from 2 to 4 weeks [**(F,H,J)**, black arrows] and was completely absent at 6 weeks of age [**(L)**, asterisks].

that H4R3me2s, H3R2me2s, and H2AR3me2s levels remained unchanged (data not shown), whereas those of H3K27me2 and H3K9me2 were significantly increased at the proximal promoter region (Site 2: −175∼−347 bp) of *Plzf* in *Prmt5*-deficient SSCs (**Figures 6C,D**). These results indicate that the downregulation of *Plzf* in *Prmt5*-deficient SSCs is not directly regulated by *Prmt5* via histone arginine methylation, which is most likely caused by increased H3K27me2 and H3K9me2 levels.

Expression of Lysine Demethylases of H3K9me2 and H3K27me2 Was Regulated by PRMT5 via Histone Arginine Modifications

To assess the underlying mechanisms that cause the increase in H3K9me2 and H3K27me2 in *Prmt5*-deficient SSCs, we analyzed the expression of lysine methylases and demethylases for H3K9me2 and H3K27me2 by real-time PCR and western blot analysis. As shown in **Figure 7**, the mRNA level of lysine demethylase for H3K9me2 (JMJD1A, JMJD1B, and JMJD1C) was significantly decreased after *Prmt5* inactivation, whereas the expression of lysine methylases for H3K9me2 (KMT1A, KMT1B, KMT1E, and KMT1F) remained unchanged. The mRNA levels of lysine methylases for H3K27me2 (NSD3, EZH2, and NSD2) were not increased in *Prmt5*-deficient SSCs, while the expression of demethylase for H3K27me2 (KDM6B) was significantly deceased (**Figures 7A,B**). The western blot results further demonstrated that the expression of the demethylases for H3K9me2 or H3K27me2 was dramatically reduced in *Prmt5*-deficient SSCs (**Figures 7C,D**). These results suggest that the increase in H3K9me2 and H3K27me2 in *Prmt5*-deficient SSCs is most likely due to the downregulation of demethylases.

To further examine whether the downregulation of lysine demethylase for H3K9me2 (JMJD1A, JMJD1B, and JMJD1C) and H3K27me2 (KDM6B) is caused by changes in histone arginine methylation in *Prmt5*-deficient SSCs, we analyzed the level of H4R3me2s or H3R2me2s at the promoter regions (TSS-1 kb upstream of TSS) of JMJD1A, JMJD1B, JMJD1C, and KDM6B. The ChIP-qPCR results showed that inactivation of *Prmt5* led to a significant increase in the repressive histone modification H4R3me2s at the promoter region (−417 ∼−546 bp) of JMJD1C (**Figure 7G**), whereas the occupancy of H4R3me2s at the upstream promoters of JMJD1A, JMJD1B, KDM6B was not changed (**Figures 7E,F,H**). Moreover, the occupancy of permissive histone modification H3R2me2s at the upstream regions (TSS-1 kb upstream of TSS) of the JMJD1A, JMJD1B, and KDM6B genes was significantly reduced in *Prmt5*-deficient SSCs (**Figures 7I,J,L**). The level of H3R2me2s at the proximal promoter region of JMJD1C was not decreased (**Figure 7K**). These results

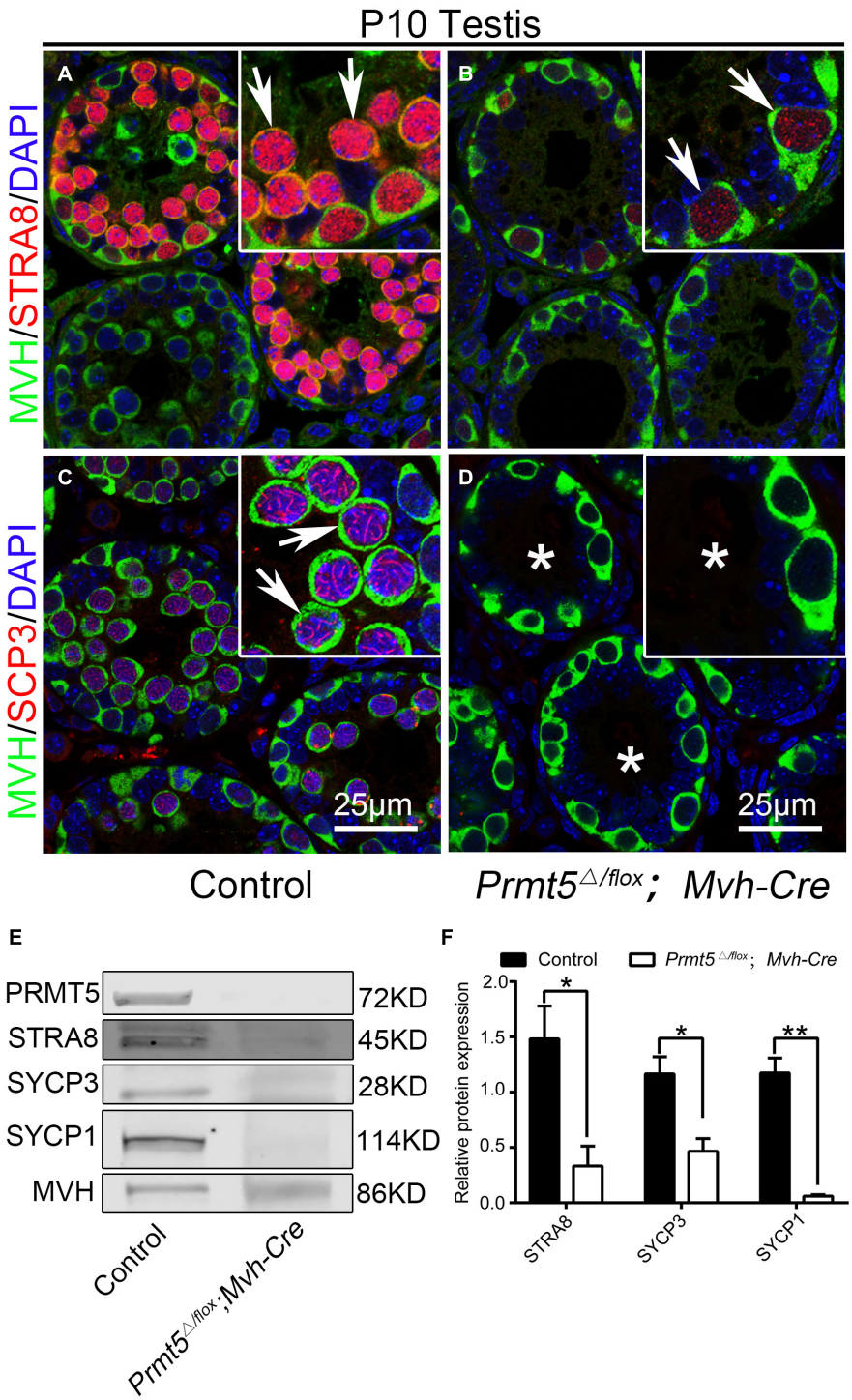

FIGURE 3 | *Prmt5*-deficient germ cells exhibit a defect in meiosis initiation. A strong STRA8 signal was detected in the germ cells of control testes [**(A)**, white arrows], whereas only a weak STRA8 signal was detected in the germ cells of *Prmt5*$^{\Delta/flox}$*;Mvh-Cre* testes [**(B)**, white arrows]. SYCP3-positive germ cells were observed in control testes [**(C)**, white arrows], but no SYCP3 signal was detected in the germ cells of *Prmt5*$^{\Delta/flox}$*;Mvh-Cre* testes [**(D)**, asterisks]. The expression of meiosis-associated genes (STRA8, SYCP3 and SYCP1) was significantly reduced in *Prmt5*$^{\Delta/flox}$*;Mvh-Cre* testes at P10 **(E,F)**, The total protein detected from control testes was 10 μg, and the total protein detected from *Prmt5*$^{\Delta/flox}$*;Mvh-Cre* testes was 40 μg. MVH was used as a loading control in **(E)**, protein values were normalized to MVH and expressed as the mean ± SEM (n = 3), $^{*}P < 0.01$, $^{**}P < 0.001$ indicates a significant difference (t-test).

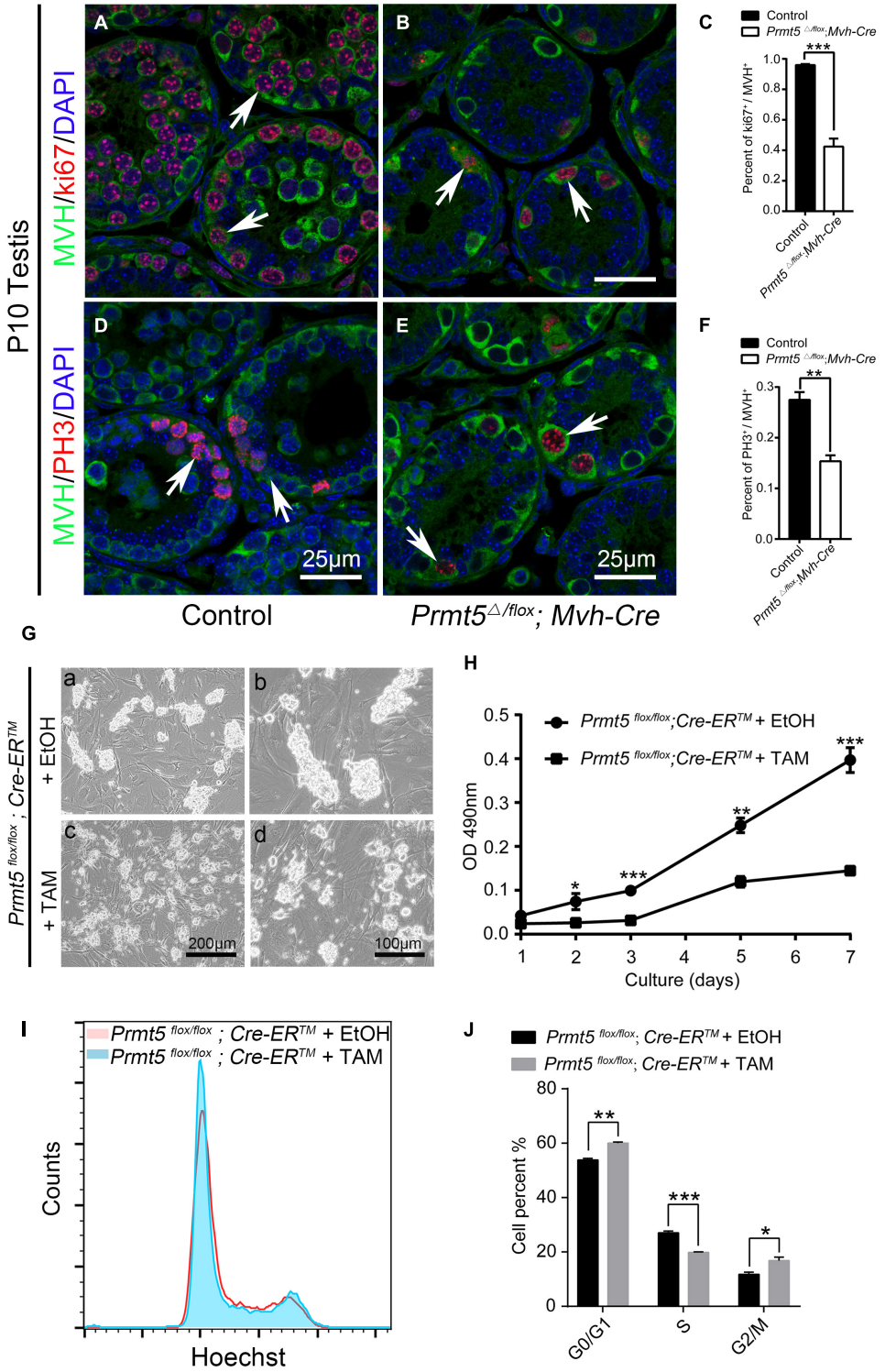

FIGURE 4 | *Prmt5*-deficient spermatogonial stem cells exhibit abnormal proliferation. Ki67-positive (red) germ cells were detected in both control [**(A)**, white arrows] and *Prmt5*$^{\Delta/flox}$*;Mvh-Cre* testes [**(B)**, white arrows] at P10. The percentage of Ki67-positive germ cells was dramatically reduced in *Prmt5*$^{\Delta/flox}$*;Mvh-Cre* mice **(C)**. PH3 (red) was detected in MVH-positive germ cells of both control [**(D)**, white arrows] and *Prmt5*$^{\Delta/flox}$*;Mvh-Cre* testes [**(E)**, white arrows] at P10. The percentage of PH3-positive germ cells was dramatically reduced in *Prmt5*$^{\Delta/flox}$*;Mvh-Cre* mice **(F)**. **(G)** Bright-field images of control and *Prmt5*-deficient SSCs cultured *in vitro*. *Prmt5*$^{flox/flox}$*;Cre-ER*^{TM} SSCs were treated with ethanol or 1 μM tamoxifen to induce *Cre* activation. **(H)** MTT assay of cultured control and *Prmt5*-deficient SSCs. **(I)** FACS analysis of cultured control and *Prmt5*-deficient SSCs. **(J)** Quantitative analysis of cells in G0/G1, S, and G2 phase. Error bars represent the SEM of triplicate results. **P* < 0.05, ***P* < 0.005, ****P* < 0.0005 indicates a significant difference (*t*-test).

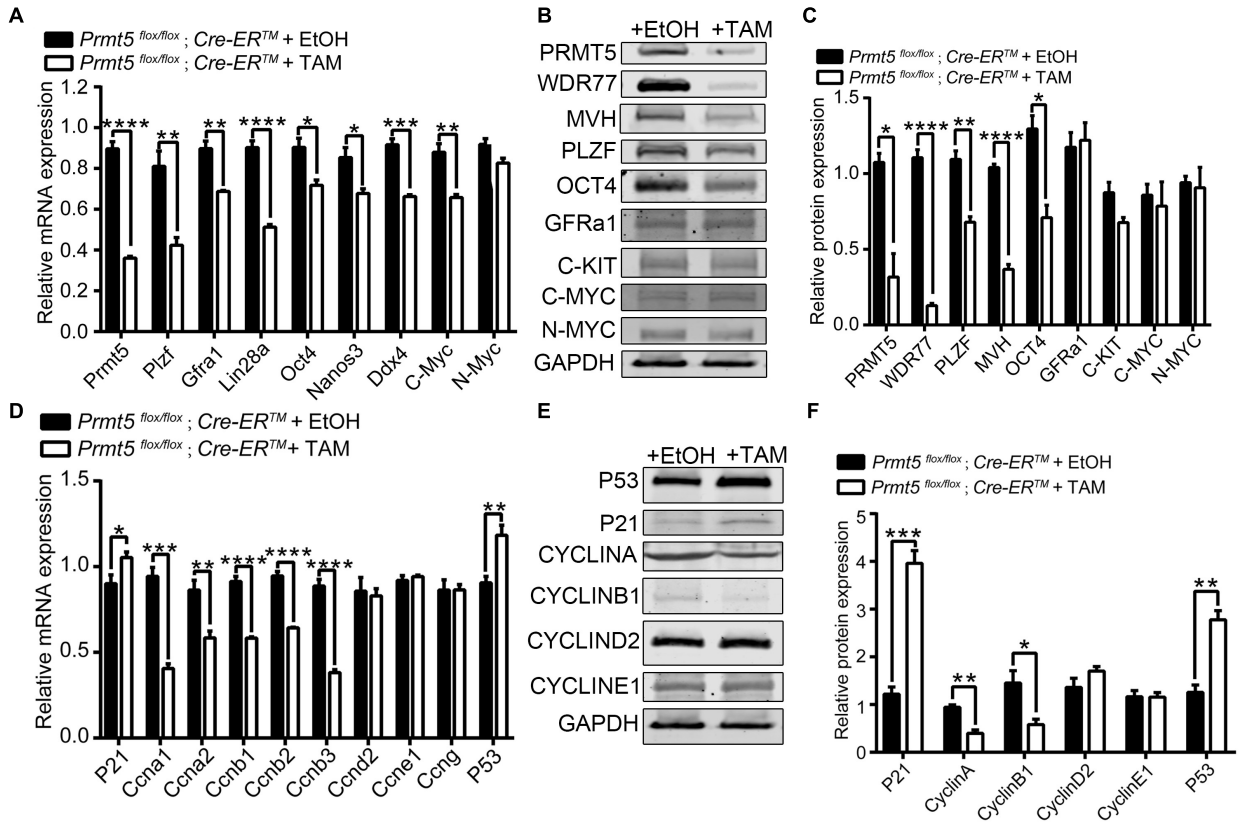

FIGURE 5 | Differentially expressed genes in *Prmt5*-deficient spermatogonial stem cells. The expression of genes related to self-renewal and proliferation was analyzed by real-time PCR **(A)** and western blotting **(B)** in *Prmt5*$^{flox/flox}$;*Cre-ER*^{TM} SSCs treated with ethanol or 1 μM tamoxifen. The quantitative results of western blot analysis **(C)**. The expression of cell cycle-associated genes was analyzed by real-time PCR **(D)** and western blot **(E)**. The quantitative results of western blot analysis **(F)**. GAPDH was used as a loading control, and the protein values were normalized. Error bars represent the SEM of triplicate results. *$P < 0.05$, **$P < 0.005$, ***$P < 0.0005$, ****$P < 0.0005$ indicates a significant difference (*t*-test).

suggest that the expression of histone lysine demethylases for H3K9me2 and H3K27me2 is regulated by PRMT5 via histone arginine modifications.

DISCUSSION

As an epigenetic modifier, PRMT5 has been demonstrated to play important roles in PGC development, and inactivation of this gene caused loss of germ cells during the embryonic stage (Kim et al., 2014; Li et al., 2015; Wang et al., 2015b). The results of our previous study revealed that the postnatal knockout of *Prmt5* in male germ cells using *Stra8-Cre* led to defects in meiosis and male infertility (Wang et al., 2015c). However, the functions of PRMT5 in SSC development have not been previously investigated. In the present study, we demonstrated that PRMT5 is essential for the survival and maintenance of SSCs. The inactivation of *Prmt5* resulted in cell cycle arrest and progressive loss of SSCs at 3 weeks of age.

PLZF has been reported to play important roles in the regulation of diverse cellular processes, including stemness maintenance, differentiation, cell cycle, proliferation and apoptosis (Suliman et al., 2012; Liu et al., 2016). PLZF is also highly expressed in spermatogonial stem cells and is considered a marker gene for undifferentiated spermatogonial stem cells. The deletion of *Plzf* was shown to lead to a progressive loss of spermatogonial stem cells in a mouse model (Buaas et al., 2004; Costoya et al., 2004). Moreover, *Plzf* is considered a cell cycle regulator, and PLZF overexpression in hematopoietic stem cells or the hematopoietic cell line 32Dcl3 was observed to block cells in G1/S phase, resulting in defects in cell growth and differentiation with an increase in apoptosis (Shaknovich et al., 1998; Yeyati et al., 1999; Vincent-Fabert et al., 2016). In the present study, we showed that the expression was dramatically reduced after the loss of *Prmt5*. Based on these results, we speculated that the defect in SSC development in *Prmt5*-deficient mice is most likely due to the downregulation of PLZF.

As a protein arginine methyltransferase, PRMT5 catalyzes MMA or sDMA in histones and non-histone substrates (Rho et al., 2001; Bedford, 2007). Interestingly, we observed that the level of global histone lysine modifications (H3K9me2 and H3K27me2) was significantly increased in *Prmt5*-deficient SSCs. PRMT5-induced H4R3 methylation has been reported to regulate lysine methylation modification (H3K27) via recruitment

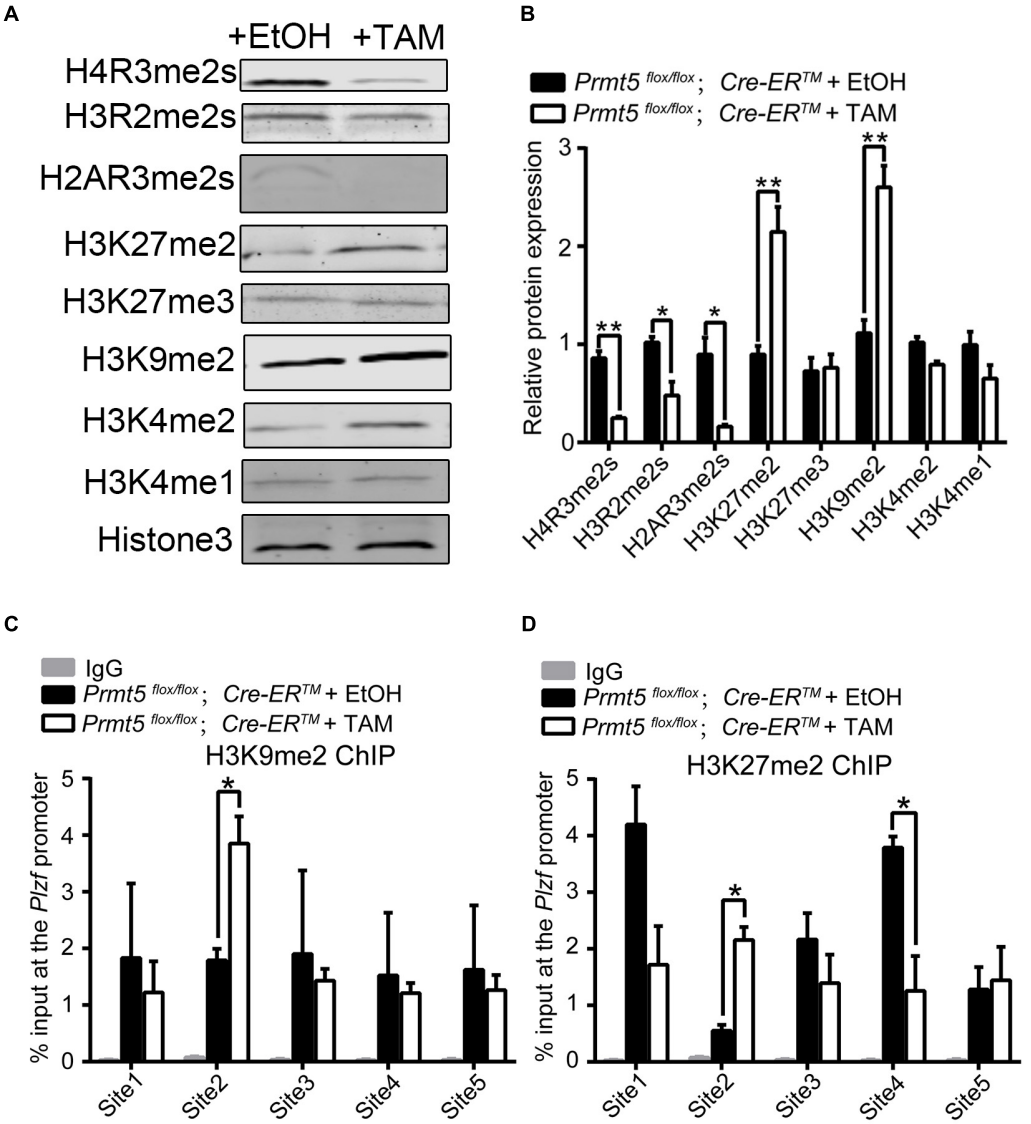

FIGURE 6 | H3K9me2 and H3K27me2 levels are significantly increased in *Prmt5*-deficient spermatogonial stem cells. **(A)** The level of histone modification in control and *Prmt5*-deficient spermatogonial stem cells was examined by western blot. **(B)** Quantitative results of western blot analysis. ChIP assays were performed to analyze the enrichment of H3K27me2 **(C)** and H3K9me2 **(D)** modifications in the promoter regions (TSS-1 kb upstream of TSS) of the *Plzf* (site 1∼ site 5) gene in control and *Prmt5*-deficient SSCs. The relative enrichment of the *Plzf* promoter region was examined by real-time PCR using sequence-specific primer sets. IgG was used as a negative control. Site 1: −114∼−284 bp, Site 2: −175∼−347 bp, Site 3: −381∼−552 bp, Site 4: −573∼−743 bp, Site 5: −755∼−948 bp. Quantitative data are presented as the enrichment of the ChIP to the input DNA. TSS, transcription start site. Error bars present SEM of three ChIP experiments. $^{*}P < 0.05$, $^{**}P < 0.005$ indicates a significant difference (*t*-test).

of Polycomb protein in a Pax2/Grg4-dependent manner (Patel et al., 2012). In hematopoietic cells, *Prmt5* depletion resulted in the upregulation of global H3K27 dimethylation and trimethylation (Liu F. et al., 2020). In the present study, the global level of H3K27me2 was significantly increased, whereas the level of H3K27me3 was not increased in *Prmt5*-deficient SSCs (**Figures 6A,B**). Moreover, unlike in a previous study (Tae et al., 2011; Patel et al., 2012; Li et al., 2018), the expression of methylases for H3K9me2 and H3K27me2 was not increased in *Prmt5*-deficient SSCs. However, the expression of demethylases (JMJD1A, JMJD1B, JMJD1C, and KDM6B) was significantly reduced at both the protein and mRNA levels, indicating that the increase in H3K9me2 and H3K27me2 was most likely due to the downregulation of histone H3 lysine demethylase expression. These results suggested that the expression of target genes regulated by PRMT5 is cell context dependent.

The functions of histone lysine methylation in SSCs development have been previously reported. The histone lysine demethylase JMJD1 isozymes targeting H3K9me2 play essential roles in the development of SSCs and spermatogenesis. The depletion of both JMJD1A and JMJD1B results in defects in the prospermatogonia to spermatogonia transition and causes

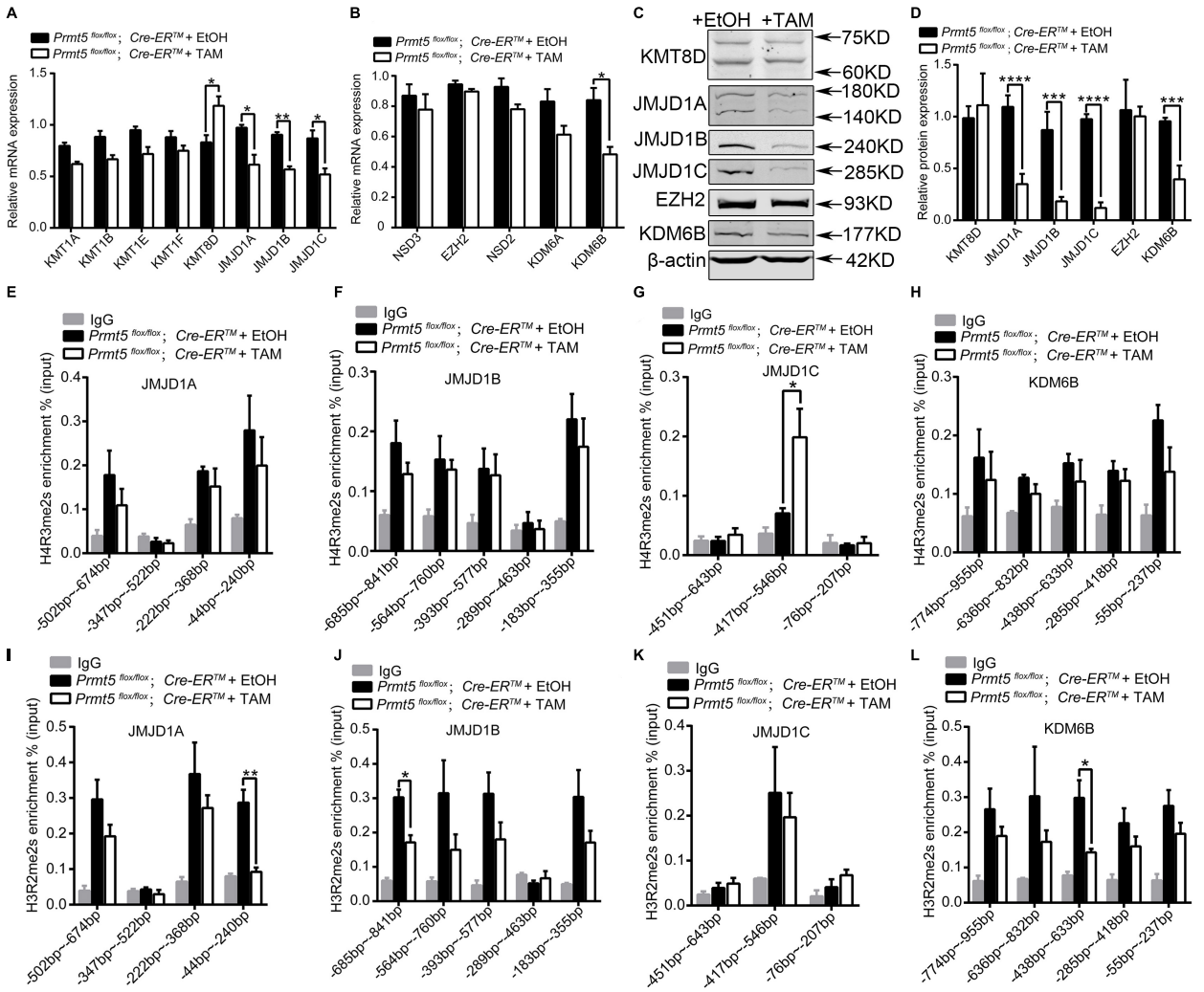

FIGURE 7 | The expression of lysine demethylases of H3K9me2 and H3K27me2 is regulated by PRMT5 via histone arginine modifications. The differential expression of lysine methylases and demethylases of H3K9me2 and H3K27me2 in *Prmt5*-deficient SSCs was analyzed by real-time PCR **(A,B)** and western blot **(C,D)**. β-Actin was used as a loading control, and the protein values were normalized. ChIP-qPCR assays were performed to examine the enrichment of H4R3me2s or H3R2me2s modifications at the upstream regions of JMJD1A **(E,I)**, JMJD1B **(F,J)**, JMJD1C **(G,K)**, and KDM6B **(H,L)** in *Prmt5*-deficient SSCs. The immunoprecipitated DNA fragments were analyzed by real-time PCR with sequence-specific primer sets. IgG was used as a negative control. Quantitative data are presented as the enrichment of the ChIP to the input DNA. Error bars represent the SEM of triplicate results. $^{*}P < 0.05$, $^{**}P < 0.005$, $^{***}P < 0.0005$, $^{****}P < 0.00005$ indicates a significant difference (*t*-test).

abnormal spermatogenesis (Kuroki et al., 2020). The loss of JMJD1C also results in a progressive reduction of SSCs/SPCs and male infertility (Kuroki et al., 2013). The histone H3K27 demethylase KDM6B is involved in regulating the fragmentation of spermatogonial cysts, but the differentiation of SSCs is not affected (Iwamori et al., 2013). EED is a core subunit of Polycomb-repressive complex (PRC2), which is responsible for catalyzing H3K27me2/H3K27me3, and deletion of EED by *Mvh-Cre* leads to defects in SSC maintenance (Mu et al., 2014). Therefore, appropriate epigenetic modification is crucial for the maintenance of the SSC pool and the support of long-term sperm production. In the present study, we concluded that aberrant histone H3 lysine methylation leads to the downregulation of PLZF, which in turn causes defects in SSC maintenance. However, other unknown mechanisms that are regulated by histone modification are probably also involved in this process.

H4R3me2s is a repressive histone arginine modification that is catalyzed by PRMT5 (Zhao et al., 2009; Xu et al., 2010; Deng et al., 2017; Li et al., 2018; Liu M. et al., 2020). The global level of H4R3me2s was dramatically reduced in *Prmt5*-deficient SSCs, consistent with the results of previous studies (Zhao et al., 2009; Wang et al., 2015c; Zhu et al., 2019). Surprisingly, H4R3me2s was enriched at the promoter region of the JMJD1C gene in *Prmt5*-deficient SSCs. These results suggest that H4R3me2s is probably also catalyzed by other arginine methyltransferases and that the increase in H4R3me2s at the promoter region of the

JMJD1C gene is probably not directly regulated by PRMT5. H3R2me2s is a permissive histone arginine modification that is also catalyzed by PRMT5 (Kirmizis et al., 2007; Migliori et al., 2012; Yuan et al., 2012; Chiang et al., 2017; Yang et al., 2020). The global level of H3R2me2s was dramatically reduced in *Prmt5*-deficient SSCs, and the levels of H3R2me2s at the promoter regions of JMJD1A, JMJD1B, and KDM6B were all significantly decreased. Based on these results, we concluded that the change in histone arginine methylation in *Prmt5*-deficient SSCs causes the downregulation of histone lysine demethylases. The downregulation of histone lysine demethylase expression causes an increase in H3K9me2 and H3K27me2.

In the present study, we also observed that meiosis was completely blocked in *Prmt5*-deficient germ cells, and no SYCP3 signal was detected in $Prmt5^{\Delta/flox}$;*Mvh-Cre* mice at P10. The results of our previous study revealed that deletion of *Prmt5* in male germ cells using *Stra8-Cre* (∼P3) results in aberrant meiotic progression. However, the expression of meiosis-associated genes, such as *Stra8*, *Sycp3*, *Dmc1*, and *γH2AX*, was not affected (Wang et al., 2015c). Although meiosis was blocked in *Prmt5*-deficient germ cells, we could not conclude that PRMT5 is required for meiosis initiation. The defect of meiosis is probably a consequence of cell cycle arrest of *Prmt5*-deficient SSCs, and the underlying mechanism needs further investigation.

Taken together, the results of the present study reveal that PRMT5 is involved in regulating the development of spermatogonia and that deletion of *Prmt5* results in depletion of the spermatogonial stem cells pool. We also demonstrated that loss of *Prmt5* caused downregulation of demethylases for H3K9me2 and H3K27me2, which in turn led to an increase in H3K9me2 and H3K27me2 and downregulation of the *Plzf* gene (**Figure 8**). Our results demonstrated that the crosstalk between histone arginine methylations and histone lysine methylation plays an important role in regulating SSCs development.

MATERIALS AND METHODS

Mice

All mice experiments were carried out in accordance with institutional animal care and the use committee regulations of Institute of Zoology, CAS. All mice were maintained in a C57BL/6;129/SvEv mixed background. $Prmt5^{flox}$ mice were obtained from the European Conditional Mouse Mutagenesis Program (EUCOMM; $Prmt5^{tm2a(EUCOMM)Wtsi}$) (Bezzi et al., 2013), $Prmt5^{+/\Delta}$ mice were obtained by crossing with *ZP3-Cre* mice. $Prmt5^{\Delta/flox}$;*Mvh-Cre* mice were obtained by crossing $Prmt5^{+/\Delta}$;*Mvh-Cre* males with $Prmt5^{flox/flox}$ females. Genotyping was performed by PCR as described previously using DNA isolated from tail tips (Gao et al., 2006; Bezzi et al., 2013; Gao et al., 2014).

Tissue Collection and Histological Analysis

Testes were dissected from $Prmt5^{+/\Delta}$;*Mvh-Cre* and control mice immediately after euthanasia, fixed in 4% paraformaldehyde for up to 24 h, stored in 70% ethanol, and embedded in paraffin. Five-micrometer-thick sections were cut and mounted on glass slides. Then, the tissue sections were processed for immunohistochemistry and immunofluorescence.

Immunohistochemistry (IHC), Immunofluorescence (IF), and TUNEL Assay

IHC and IF procedures were performed as described previously (Chen et al., 2019; Qin et al., 2019). Antibodies were diluted as follows: MVH (1:500, Abcam, ab13840), PLZF (1:100, R&D, AF2944), PRMT5 (1:200, Millipore, 07-405), SOX9 (1:500, Millipore, AB5535), STRA8 (1:200, Abcam, ab49405), SYCP3

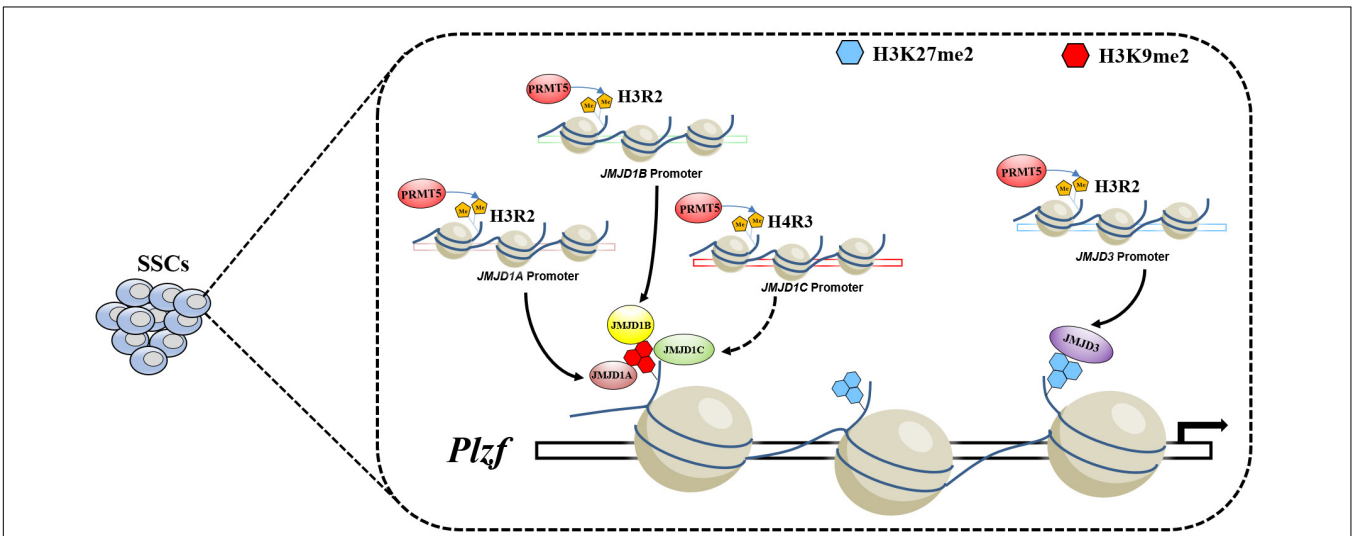

FIGURE 8 | Model of PRMT5 regulating *Plzf* expression via histone modifications in SSCs. In SSCs, PRMT5 promotes the expression of demethylases for H3K9me2 and H3K27me2 by catalyzing permissive histone H3R2me2s. The high expression of the corresponding lysine demethylases leads to low levels of H3K9me2 and H3K27me2 at the upstream promoter of *Plzf*, which in turn leads to the upregulation of the *Plzf* gene.

(1:200, Abcam, ab15093), Ki67 (1:400, Abcam, ab15580), and PH3 (1:400, Millipore, 2605439). After staining, the sections were examined with a Nikon microscopy, and images were captured with a Nikon DS-Ri1 CCD camera. The IF sections were examined using a confocal laser scanning microscope (Carl Zeiss Inc., Thornwood, NY, United States). TUNEL assay was performed using the Dead-End Fluorometric TUNEL System (Promega, G3250).

Spermatogonial Stem Cells *in vitro* Culture

Establishment and maintenance of SSCs were performed as previously described (Wang et al., 2015a; Chen et al., 2017). In brief, seminiferous tubules from *Prmt5*$^{flox/flox}$;*Cre-ER*^{TM} mice at 5–7 days postpartum (dpp) were digested with collagenase IV and DNase I for 5 min into small fragments and then centrifuged at 400 rpm for 2 min. The seminiferous fragments were suspended in mouse embryo fibroblast (MEF) medium containing 10% FBS (fetal bovine serum). Twenty-four hours later, the SSCs were collected and then transferred to mitomycin C-treated MEF feeder cells. The specific medium for SSCs contained GDNF and FGF2 for later culture. *Prmt5*$^{flox/flox}$;*Cre-ER*^{TM} SSCs treated with ethanol or 1 μM tamoxifen were harvested for western blot, real-time PCR or MTT assay.

Western Blotting and Antibodies

Western blotting procedures were performed as described previously (Zhou et al., 2018). Tissues and cells were lysed in cold RIPA buffer, supplemented with 1 mM phenylmethylsulfonyl fluoride and protease inhibitor cocktail (Roche, Indianapolis, IN, United States). The protein lysates were subjected to SDS-PAGE, transferred onto a nitrocellulose membrane and probed with the primary antibodies. The images were captured with the ODYSSEY Sa Infrared Imaging System (LI-COR Biosciences, Lincoln, NE, United States). Primary antibodies used were shown in **Supplementary Table 1**.

Nucleic Acid Isolation and Quantitative Real-Time PCR

For Real-Time PCR, RNA was isolated from cultured SSCs using EASYspin Plus Tissue/Cells RNA Rapid Extraction kit following manufacturer's instructions. The relative expression level was calculated using the formula $2^{-\Delta\Delta CT}$. *Gapdh* was used as an internal control for quantification. The primers used were listed in **Supplementary Table 2**.

Cell Proliferation Assay

The relative number and viability of SSCs were evaluated by MTT assays. In brief, SSCs seeded in 24-well plates were washed with PBS twice and incubated with MTT solution (0.5 mg/ml) for at least 4 h at 37°C in a CO_2 incubator. Then, the medium containing MTT was removed, and 750 μl DMSO was added. After an incubation for 10 min on a shaking table at 75 rpm/min, the OD value at 490 nm was measured.

ChIP-qPCR Assay

ChIP assays were conducted using a SimpleChIP® Plus Sonication Chromatin IP Kit (# 56383) following the manufacturer's instructions. For ChIP-qPCR, the input genomic DNA or immunoprecipitated DNA was used as a template. Quantitative real-time PCR was performed according to the manufacturer's instructions. The input DNA was used as a normalization control. The primers used are listed in **Supplementary Table 2**.

Statistics Analysis

Experiments were repeated at least three times. GraphPad Prism7 software was used for analysis of *P*-values based on three to six independent experiments in PCR reactions or western blotting assay. Multiple *t*-test-one per row was used to compare the differences between two groups. $P < 0.05$ or $P < 0.01$ was considered statistically significant.

DATA AVAILABILITY STATEMENT

The original contributions presented in the study are included in the article/**Supplementary Material**, further inquiries can be directed to the corresponding author/s.

ETHICS STATEMENT

The animal study was reviewed and approved by the Institutional Animal Care and Use Committee (IACUC) of the Institute of Zoology, CAS (AEI-09-02-2014).

AUTHOR CONTRIBUTIONS

FD and MC (co-first author): formal analysis and investigation. FG: funding acquisition. FD, MC (co-first author), MC (third author), LJ, ZS, LM, CH, and XG: methodology. FG: project administration. MC (co-first author) and LM: resources. FD: writing—original draft. FD and FG: writing—review and editing.

FUNDING

This work was supported by the National Key R&D Program of China (2016YFA0500901, 2018YFA0107702, and 2018YFC1004200), Strategic Priority Research Program of the Chinese Academy of Sciences (XDB19000000), the National Science Fund for Distinguished Young Scholars (81525011), and the National Natural Science Foundation of China (31970785 and 31671496).

SUPPLEMENTARY MATERIAL

The Supplementary Material for this article can be found online at: https://www.frontiersin.org/articles/10.3389/fcell.2021.673258/full#supplementary-material

REFERENCES

Agrawal Singh, S., Lerdrup, M., Gomes, A. R., van de Werken, H. J., Vilstrup Johansen, J., Andersson, R., et al. (2019). PLZF targets developmental enhancers for activation during osteogenic differentiation of human mesenchymal stem cells. *Elife* 8:e40364. doi: 10.7554/eLife.40364

Ancelin, K., Lange, U. C., Hajkova, P., Schneider, R., Bannister, A. J., Kouzarides, T., et al. (2006). Blimp1 associates with Prmt5 and directs histone arginine methylation in mouse germ cells. *Nat. Cell Biol.* 8, 623–630. doi: 10.1038/ncb1413

Avantaggiato, V., Pandolfi, P. P., Ruthardt, M., Hawe, N., Acampora, D., Pelicci, P. G., et al. (1995). Developmental Analysis of Murine Promyelocyte Leukemia Zinc Finger (PLZF) gene expression_ implications for the neuromeric model of the forebrain organization. *J. Neurosci.* 15(7 Pt. 1), 4927–4942. doi: 10.1523/JNEUROSCI.15-07-04927.1995

Barna, M., Hawe, N., Niswander, L., and Pandolfi, P. P. (2000). Plzf regulates limb and axial skeletal patterning. *Nat. Genet.* 25, 166–172. doi: 10.1038/76014

Bedford, M. T. (2007). Arginine methylation at a glance. *J. Cell Sci.* 120, 4243–4246. doi: 10.1242/jcs.019885

Bezzi, M., Teo, S. X., Muller, J., Mok, W. C., Sahu, S. K., Vardy, L. A., et al. (2013). Regulation of constitutive and alternative splicing by PRMT5 reveals a role for Mdm4 pre-mRNA in sensing defects in the spliceosomal machinery. *Genes Dev.* 27, 1903–1916. doi: 10.1101/gad.219899.113

Buaas, F. W., Kirsh, A. L., Sharma, M., McLean, D. J., Morris, J. L., Griswold, M. D., et al. (2004). Plzf is required in adult male germ cells for stem cell self-renewal. *Nat. Genet.* 36, 647–652. doi: 10.1038/ng1366

Chen, J., Cai, T., Zheng, C., Lin, X., Wang, G., Liao, S., et al. (2017). MicroRNA-202 maintains spermatogonial stem cells by inhibiting cell cycle regulators and RNA binding proteins. *Nucleic Acids Res.* 45, 4142–4157. doi: 10.1093/nar/gkw1287

Chen, M., Chen, M., Chen, S., Zhou, J., Dong, F., Shen, Z., et al. (2019). Abnormal meiosis initiation in germ cell caused by aberrant differentiation of gonad somatic cell. *Oxid. Med. Cell. Longev.* 2019:8030697. doi: 10.1155/2019/8030697

Chen, S. R., and Liu, Y. X. (2015). Regulation of spermatogonial stem cell self-renewal and spermatocyte meiosis by Sertoli cell signaling. *Reproduction* 149, R159–R167. doi: 10.1530/REP-14-0481

Chiang, K., Zielinska, A. E., Shaaban, A. M., Sanchez-Bailon, M. P., Jarrold, J., Clarke, T. L., et al. (2017). PRMT5 is a critical regulator of breast cancer stem cell function via histone methylation and FOXP1 expression. *Cell Rep.* 21, 3498–3513. doi: 10.1016/j.celrep.2017.11.096

Cook, M., Gould, A., Brand, N., Davies, J., Strutt, P., Shaknovich, R., et al. (1995). Expression of the zinc-finger gene PLZF at rhombomere boundaries in the vertebrate hindbrain. *Proc. Natl. Acad. Sci. U.S.A.* 92, 2249–2253. doi: 10.1073/pnas.92.6.2249

Costoya, J. A., Hobbs, R. M., Barna, M., Cattoretti, G., Manova, K., Sukhwani, M., et al. (2004). Essential role of Plzf in maintenance of spermatogonial stem cells. *Nat. Genet.* 36, 653–659. doi: 10.1038/ng1367

Deng, X., Shao, G., Zhang, H. T., Li, C., Zhang, D., Cheng, L., et al. (2017). Protein arginine methyltransferase 5 functions as an epigenetic activator of the androgen receptor to promote prostate cancer cell growth. *Oncogene* 36, 1223–1231. doi: 10.1038/onc.2016.287

Dong, J., Wang, X., Cao, C., Wen, Y., Sakashita, A., Chen, S., et al. (2019). UHRF1 suppresses retrotransposons and cooperates with PRMT5 and PIWI proteins in male germ cells. *Nat. Commun.* 10:4705. doi: 10.1038/s41467-019-12455-4

Gallardo, T., Shirley, L., John, G. B., and Castrillon, D. H. (2007). Generation of a germ cell-specific mouse transgenic Cre line, Vasa-Cre. *Genesis* 45, 413–417. doi: 10.1002/dvg.20310

Gao, F., Maiti, S., Alam, N., Zhang, Z., Deng, J. M., Behringer, R. R., et al. (2006). The Wilms tumor gene, Wt1, is required for Sox9 expression and maintenace of tubular architecture in the developing testis. *Proc. Natl. Acad. Sci. U.S.A.* 103, 11987–11992. doi: 10.1073/pnas.0600994103

Gao, F., Zhang, J., Wang, X., Yang, J., Chen, D., Huff, V., et al. (2014). Wt1 functions in ovarian follicle development by regulating granulosa cell differentiation. *Hum. Mol. Genet.* 23, 333–341. doi: 10.1093/hmg/ddt423

Hai, L., Szwarc, M. M., Lanza, D. G., Heaney, J. D., and Lydon, J. P. (2019). Using CRISPR/Cas9 engineering to generate a mouse with a conditional knockout allele for the promyelocytic leukemia zinc finger transcription factor. *Genesis* 57:e23281. doi: 10.1002/dvg.23281

Hamard, P. J., Santiago, G. E., Liu, F., Karl, D. L., Martinez, C., Man, N., et al. (2018). PRMT5 regulates DNA repair by controlling the alternative splicing of histone-modifying enzymes. *Cell Rep.* 24, 2643–2657. doi: 10.1016/j.celrep.2018.08.002

He, Z., Jiang, J., Kokkinaki, M., Golestaneh, N., Hofmann, M. C., and Dym, M. (2008). Gdnf upregulates c-Fos transcription via the Ras/Erk1/2 pathway to promote mouse spermatogonial stem cell proliferation. *Stem Cells* 26, 266–278. doi: 10.1634/stemcells.2007-0436

Iwamori, N., Iwamori, T., and Matzuk, M. M. (2013). H3K27 demethylase, JMJD3, regulates fragmentation of spermatogonial cysts. *PLoS One* 8:e72689. doi: 10.1371/journal.pone.0072689

Kim, S., Gunesdogan, U., Zylicz, J. J., Hackett, J. A., Cougot, D., Bao, S., et al. (2014). PRMT5 protects genomic integrity during global DNA demethylation in primordial germ cells and preimplantation embryos. *Mol. Cell* 56, 564–579. doi: 10.1016/j.molcel.2014.10.003

Kirmizis, A., Santos-Rosa, H., Penkett, C. J., Singer, M. A., Vermeulen, M., Mann, M., et al. (2007). Arginine methylation at histone H3R2 controls deposition of H3K4 trimethylation. *Nature* 449, 928–932. doi: 10.1038/nature06160

Kuroki, S., Akiyoshi, M., Tokura, M., Miyachi, H., Nakai, Y., Kimura, H., et al. (2013). JMJD1C, a JmjC domain-containing protein, is required for long-term maintenance of male germ cells in mice. *Biol. Reprod.* 89:93. doi: 10.1095/biolreprod.113.108597

Kuroki, S., Maeda, R., Yano, M., Kitano, S., Miyachi, H., Fukuda, M., et al. (2020). H3K9 demethylases JMJD1A and JMJD1B control prospermatogonia to spermatogonia transition in mouse germline. *Stem Cell Rep.* 15, 424–438. doi: 10.1016/j.stemcr.2020.06.013

Li, S., Ali, S., Duan, X., Liu, S., Du, J., Liu, C., et al. (2018). JMJD1B demethylates H4R3me2s and H3K9me2 to facilitate gene expression for development of hematopoietic stem and progenitor cells. *Cell Rep.* 23, 389–403. doi: 10.1016/j.celrep.2018.03.051

Li, Z., Yu, J., Hosohama, L., Nee, K., Gkountela, S., Chaudhari, S., et al. (2015). The Sm protein methyltransferase PRMT5 is not required for primordial germ cell specification in mice. *EMBO J.* 34, 748–758. doi: 10.15252/embj.201489319

Liu, F., Xu, Y., Lu, X., Hamard, P. J., Karl, D. L., Man, N., et al. (2020). PRMT5-mediated histone arginine methylation antagonizes transcriptional repression by polycomb complex PRC2. *Nucleic Acids Res.* 48, 2956–2968. doi: 10.1093/nar/gkaa065

Liu, M., Yao, B., Gui, T., Guo, C., Wu, X., Li, J., et al. (2020). PRMT5-dependent transcriptional repression of c-Myc target genes promotes gastric cancer progression. *Theranostics* 10, 4437–4452. doi: 10.7150/thno.42047

Liu, T. M., Lee, E. H., Lim, B., and Shyh-Chang, N. (2016). Concise Review: balancing stem cell self-renewal and differentiation with PLZF. *Stem Cells* 34, 277–287. doi: 10.1002/stem.2270

Mäkelä, J. A., and Hobbs, R. M. (2019). Molecular regulation of spermatogonial stem cell renewal and differentiation. *Reproduction* 158, R169–R187. doi: 10.1530/REP-18-0476

Meng, X., Lindahl, M., Hyvönen, M. E., Parvinen, M., de Rooij, D. G., Hess, M. W., et al. (2000). Regulation of cell fate decision of undifferentiated spermatogonia by GDNF. *Science* 287, 1489–1493. doi: 10.1126/science.287.5457.1489

Migliori, V., Muller, J., Phalke, S., Low, D., Bezzi, M., Mok, W. C., et al. (2012). Symmetric dimethylation of H3R2 is a newly identified histone mark that supports euchromatin maintenance. *Nat. Struct. Mol. Biol.* 19, 136–144. doi: 10.1038/nsmb.2209

Mu, W., Starmer, J., Fedoriw, A. M., Yee, D., and Magnuson, T. (2014). Repression of the soma-specific transcriptome by Polycomb-repressive complex 2 promotes male germ cell development. *Genes Dev.* 28, 2056–2069. doi: 10.1101/gad.246124.114

Oatley, J. M., and Brinster, R. L. (2008). Regulation of spermatogonial stem cell self-renewal in mammals. *Annu. Rev. Cell Dev. Biol.* 24, 263–286. doi: 10.1146/annurev.cellbio.24.110707.175355

Pahlich, S., Zakaryan, R. P., and Gehring, H. (2006). Protein arginine methylation: cellular functions and methods of analysis. *Biochim. Biophys. Acta* 1764, 1890–1903. doi: 10.1016/j.bbapap.2006.08.008

Patel, S. R., Bhumbra, S. S., Paknikar, R. S., and Dressler, G. R. (2012). Epigenetic mechanisms of Groucho/Grg/TLE mediated transcriptional repression. *Mol. Cell* 45, 185–195. doi: 10.1016/j.molcel.2011.11.007

Poplineau, M., Vernerey, J., Platet, N., N'Guyen, L., Herault, L., Esposito, M., et al. (2019). PLZF limits enhancer activity during hematopoietic progenitor aging. *Nucleic Acids Res.* 47, 4509–4520. doi: 10.1093/nar/gkz174

Qin, Y., Zhou, Y., Shen, Z., Xu, B., Chen, M., Li, Y., et al. (2019). WDR62 is involved in spindle assembly by interacting with CEP170 in spermatogenesis. *Development* 146:dev174128. doi: 10.1242/dev.174128

Raposo, A. E., and Piller, S. C. (2018). Protein arginine methylation: an emerging regulator of the cell cycle. *Cell Div.* 13:3. doi: 10.1186/s13008-018-0036-2

Reid, A., Gould, A., Brand, N., Cook, M., Strutt, P., Li, J., et al. (1995). Leukemia translocation gene, PLZF, is expressed with a speckled nuclear pattern in early hematopoietic progenitors. *Blood* 86, 4544–4552. doi: 10.1182/blood.V86.12.4544.bloodjournal86124544

Rho, J., Choi, S., Seong, Y. R., Cho, W. K., Kim, S. H., and Im, D. S. (2001). Prmt5, which forms distinct homo-oligomers, is a member of the protein-arginine methyltransferase family. *J. Biol. Chem.* 276, 11393–11401. doi: 10.1074/jbc.M008660200

Shaknovich, R., Yeyati, P. L., Ivins, S., Melnick, A., Lempert, C., Waxman, S., et al. (1998). The promyelocytic leukemia zinc finger protein affects myeloid cell growth, differentiation, and apoptosis. *Mol. Cell. Biol.* 18, 5533–5545. doi: 10.1128/MCB.18.9.5533

Stopa, N., Krebs, J. E., and Shechter, D. (2015). The PRMT5 arginine methyltransferase: many roles in development, cancer and beyond. *Cell Mol. Life Sci.* 72, 2041–2059. doi: 10.1007/s00018-015-1847-9

Suliman, B. A., Xu, D., and Williams, B. R. (2012). The promyelocytic leukemia zinc finger protein: two decades of molecular oncology. *Front. Oncol.* 2:74. doi: 10.3389/fonc.2012.00074

Tae, S., Karkhanis, V., Velasco, K., Yaneva, M., Erdjument-Bromage, H., Tempst, P., et al. (2011). Bromodomain protein 7 interacts with PRMT5 and PRC2, and is involved in transcriptional repression of their target genes. *Nucleic Acids Res.* 39, 5424–5438. doi: 10.1093/nar/gkr170

Tseng, Y. T., Liao, H. F., Yu, C. Y., Mo, C. F., and Lin, S. P. (2015). Epigenetic factors in the regulation of prospermatogonia and spermatogonial stem cells. *Reproduction* 150, R77–R91. doi: 10.1530/REP-14-0679

Vincent-Fabert, C., Platet, N., Vandevelde, A., Poplineau, M., Koubi, M., Finetti, P., et al. (2016). PLZF mutation alters mouse hematopoietic stem cell function and cell cycle progression. *Blood* 127, 1881–1885. doi: 10.1182/blood-2015-09-666974

Wang, S., Wang, X., Ma, L., Lin, X., Zhang, D., Li, Z., et al. (2016). Retinoic acid is sufficient for the in vitro induction of mouse spermatocytes. *Stem Cell Rep.* 7, 80–94. doi: 10.1016/j.stemcr.2016.05.013

Wang, S., Wang, X., Wu, Y., and Han, C. (2015a). IGF-1R signaling is essential for the proliferation of cultured mouse spermatogonial stem cells by promoting the G2/M progression of the cell cycle. *Stem Cells Dev.* 24, 471–483. doi: 10.1089/scd.2014.0376

Wang, Y., Li, Q., Liu, C., Han, F., Chen, M., Zhang, L., et al. (2015b). Protein arginine methyltransferase 5 (Prmt5) is required for germ cell survival during mouse embryonic development. *Biol. Reprod.* 92:104. doi: 10.1095/biolreprod.114.127308

Wang, Y., Zhu, T., Li, Q., Liu, C., Han, F., Chen, M., et al. (2015c). Prmt5 is required for germ cell survival during spermatogenesis in mice. *Sci. Rep.* 5:11031. doi: 10.1038/srep11031

Wu, Y., Hu, X., Li, Z., Wang, M., Li, S., Wang, X., et al. (2016). Transcription factor RFX2 is a key regulator of mouse spermiogenesis. *Sci. Rep.* 6:20435. doi: 10.1038/srep20435

Xu, X., Hoang, S., Mayo, M. W., and Bekiranov, S. (2010). Application of machine learning methods to histone methylation ChIP-Seq data reveals H4R3me2 globally represses gene expression. *BMC Bioinformatics* 11:396. doi: 10.1186/1471-2105-11-396

Yang, M., Lin, X., Segers, F., Suganthan, R., Hildrestrand, G. A., Rinholm, J. E., et al. (2020). OXR1A, a coactivator of PRMT5 regulating histone arginine methylation. *Cell Rep.* 30, 4165–4178.e7. doi: 10.1016/j.celrep.2020.02.063

Yeyati, P. L., Shaknovich, R., Boterashvili, S., Li, J., Ball, H. J., Waxman, S., et al. (1999). Leukemia translocation protein PLZF inhibits cell growth and expression of cyclin A. *Oncogene* 18, 925–934. doi: 10.1038/sj.onc.1202375

Yuan, C. C., Matthews, A. G., Jin, Y., Chen, C. F., Chapman, B. A., Ohsumi, T. K., et al. (2012). Histone H3R2 symmetric dimethylation and histone H3K4 trimethylation are tightly correlated in eukaryotic genomes. *Cell Rep.* 1, 83–90. doi: 10.1016/j.celrep.2011.12.008

Zhang, T., Gunther, S., Looso, M., Kunne, C., Kruger, M., Kim, J., et al. (2015). Prmt5 is a regulator of muscle stem cell expansion in adult mice. *Nat. Commun.* 6:7140. doi: 10.1038/ncomms8140

Zhang, Y., Wang, S., Wang, X., Liao, S., Wu, Y., and Han, C. (2012). Endogenously produced FGF2 is essential for the survival and proliferation of cultured mouse spermatogonial stem cells. *Cell Res.* 22, 773–776. doi: 10.1038/cr.2012.17

Zhao, Q., Rank, G., Tan, Y. T., Li, H., Moritz, R. L., Simpson, R. J., et al. (2009). PRMT5-mediated methylation of histone H4R3 recruits DNMT3A, coupling histone and DNA methylation in gene silencing. *Nat. Struct. Mol. Biol.* 16, 304–311. doi: 10.1038/nsmb.1568

Zhou, Y., Qin, Y., Qin, Y., Xu, B., Guo, T., Ke, H., et al. (2018). Wdr62 is involved in female meiotic initiation via activating JNK signaling and associated with POI in humans. *PLoS Genet.* 14:e1007463. doi: 10.1371/journal.pgen.1007463

Zhu, J., Zhang, D., Liu, X., Yu, G., Cai, X., Xu, C., et al. (2019). Zebrafish prmt5 arginine methyltransferase is essential for germ cell development. *Development* 146:dev179572. doi: 10.1242/dev.179572

Conflict of Interest: The authors declare that the research was conducted in the absence of any commercial or financial relationships that could be construed as a potential conflict of interest.

Copyright © 2021 Dong, Chen, Chen, Jiang, Shen, Ma, Han, Guo and Gao. This is an open-access article distributed under the terms of the Creative Commons Attribution License (CC BY). The use, distribution or reproduction in other forums is permitted, provided the original author(s) and the copyright owner(s) are credited and that the original publication in this journal is cited, in accordance with accepted academic practice. No use, distribution or reproduction is permitted which does not comply with these terms.

frontiers in Cell and Developmental Biology

MINI REVIEW
published: 24 May 2021
doi: 10.3389/fcell.2021.672191

High Resolution View on the Regulation of Recombinase Accumulation in Mammalian Meiosis

*Aditya N. Mhaskar[1], Lieke Koornneef[1,2], Alex N. Zelensky[3], Adriaan B. Houtsmuller[4,5] and Willy M. Baarends[1]**

[1] Department of Developmental Biology, Erasmus MC, Rotterdam, Netherlands, [2] Oncode Institute, Utrecht, Netherlands, [3] Department of Molecular Genetics, Erasmus MC, Rotterdam, Netherlands, [4] Erasmus Optical Imaging Centre, Department of Pathology, Erasmus MC, Rotterdam, Netherlands, [5] Department of Pathology, Erasmus MC, Rotterdam, Netherlands

OPEN ACCESS

Edited by:
Wei Li,
State Key Laboratory of Stem Cell and Reproductive Biology, Institute of Zoology, Chinese Academy of Sciences (CAS), China

Reviewed by:
Xiaoyang Zhao,
Southern Medical University, China
Judith Yanowitz,
Magee-Womens Research Institute, United States
Jesus Page,
Universidad Autómoma de Madrid, Spain

***Correspondence:**
Willy M. Baarends
w.baarends@erasmusmc.nl

Specialty section:
This article was submitted to Cell Growth and Division, a section of the journal Frontiers in Cell and Developmental Biology

Received: *25 February 2021*
Accepted: *19 April 2021*
Published: *24 May 2021*

Citation:
Mhaskar AN, Koornneef L, Zelensky AN, Houtsmuller AB and Baarends WM (2021) High Resolution View on the Regulation of Recombinase Accumulation in Mammalian Meiosis. Front. Cell Dev. Biol. 9:672191. doi: 10.3389/fcell.2021.672191

A distinguishing feature of meiotic DNA double-strand breaks (DSBs), compared to DSBs in somatic cells, is the fact that they are induced in a programmed and specifically orchestrated manner, which includes chromatin remodeling prior to DSB induction. In addition, the meiotic homologous recombination (HR) repair process that follows, is different from HR repair of accidental DSBs in somatic cells. For instance, meiotic HR involves preferred use of the homolog instead of the sister chromatid as a repair template and subsequent formation of crossovers and non-crossovers in a tightly regulated manner. An important outcome of this distinct repair pathway is the pairing of homologous chromosomes. Central to the initial steps in homology recognition during meiotic HR is the cooperation between the strand exchange proteins (recombinases) RAD51 and its meiosis-specific paralog DMC1. Despite our understanding of their enzymatic activity, details on the regulation of their assembly and subsequent molecular organization at meiotic DSBs in mammals have remained largely enigmatic. In this review, we summarize recent mouse data on recombinase regulation *via* meiosis-specific factors. Also, we reflect on bulk "omics" studies of initial meiotic DSB processing, compare these with studies using super-resolution microscopy in single cells, at single DSB sites, and explore the implications of these findings for our understanding of the molecular mechanisms underlying meiotic HR regulation.

Keywords: super-resolution microscopy, meiosis, DSB repair, recombinase, ChIP-seq

INTRODUCTION

Meiotic prophase I in vertebrates begins with programmed induction of DNA double-strand breaks (DSBs) in leptotene [reviewed by Lam and Keeney (2015)]. Somewhat later, coalignment, or pairing, of the homologous chromosomal axes (axial elements) at a distance of ∼400 nm from each other can be observed [reviewed by Zickler and Kleckner (2015)]. As prophase progresses to zygotene, these paired homologs are drawn closer to each other through the assembly of the synaptonemal complex (SC), which physically connects the chromosomal axes at a distance of approximately ∼200 nm (Schücker et al., 2015). The progression of homologous chromosome pairing and synapsis is functionally linked to the concomitant progression of DSBs repair by the specialized meiotic homologous recombination (HR) pathway. By pachytene, the SC assembly

(synapsis) along the homologs is complete, and toward the end of pachytene (almost) all meiotic DSBs have been repaired.

Until now, the molecular details of the precise events that lead from meiotic DSB repair to homologous chromosome synapsis have remained obscure. However, advancements in whole-genome analyses and the complementary application of super-resolution microscopy have revealed a plethora of novel information regarding the localization and function of several proteins that are critical to meiotic HR repair and subsequent chromosome pairing in mice (Hinch et al., 2019; Shi et al., 2019; Paiano et al., 2020; Slotman et al., 2020). In this review, we aim to integrate these novel findings to better understand the initial steps of meiotic HR in mice.

RECOMBINATION INITIATION DURING MEIOTIC PROPHASE I

In mouse, recombination initiation is triggered by the generation of DSBs by SPO11 and TOPOVIBL in early leptotene (Bergerat et al., 1997; Keeney et al., 1997; Robert et al., 2016a,b). This topoisomerase complex requires several accessory proteins (HORMAD1/REC114/MEI4/MEI1/IHO1/ANKRD31) to ensure (efficient) DSB formation (Kumar et al., 2015, 2018; Stanzione et al., 2016; Boekhout et al., 2019; Papanikos et al., 2019; Acquaviva et al., 2020). According to the model proposed by Kleckner (2006), DSBs occur in chromatin loops after they have become tethered to the chromosomal axis. This axis association of DSB formation is thought to be critical for converting local DNA repair interactions to whole chromosome coalignment during pairing (Zickler and Kleckner, 2015).

Recombination initiation by SPO11/TOPOVIBL is non-random, as was clearly shown by ChIP-seq analyses of meiotic recombinases along with SPO11-oligo sequencing (DNA fragments covalently attached to SPO11 after initial DSB-processing), which have revealed the locations of the many recombination hotspots (Smagulova et al., 2011; Brick et al., 2012). These hotspots are defined by H3K4me3/H3K36me3 signatures, induced by the meiosis-specific histone methyltransferase PRDM9 (Hayashi et al., 2005; Baudat et al., 2010; Berg et al., 2010; Parvanov et al., 2010; Powers et al., 2016). In *Prdm9* knockout mice, DSBs are still induced at other H3K4me3 modified sites, such as enhancers, and the chromatin environment at these aberrant locations may contribute to the impaired DSB repair, causing sterility or reduced fertility depending on genetic background (Hayashi et al., 2005; Brick et al., 2012; Mihola et al., 2019).

END PROCESSING AND ASSEMBLY OF ssDNA BINDING PROTEINS AT THE BREAK SITE

Our understanding of break processing following SPO11-mediated recombinase initiation is based on yeast data, in which, Mre11-Rad50-Xrs2 (MRE11-RAD50-NBS1 in *M. musculus* or so-called the MRX/MRN complex) along with Sae2 endonuclease nick the Spo11 bound strand (Mimitou and Symington, 2008; Cannavo and Cejka, 2014). This serves as an entry point for Mre11 mediated 3′–5′ resection and Exo1 and Dna2 mediated 5′–3′ resection, resulting in the release of Spo11 bound oligos and generation of 3′ resected single-stranded DNA (ssDNA) (Neale et al., 2005; Mimitou and Symington, 2008; Zhu et al., 2008; Zakharyevich et al., 2010; Garcia et al., 2011; Keelagher et al., 2011; Cannavo and Cejka, 2014; Mimitou et al., 2017). In mice, DSB processing is thought to be similar with a conserved role for MRN/MRX complex. However, EXO1 appears to be redundant with other long range resection mechanisms (Zhang B. et al., 2020; Paiano et al., 2020; Yamada et al., 2020).

The resulting ssDNA is then bound by the RPA complex and meiosis-specific ssDNA binding proteins SPATA22 and MEIOB (La Salle et al., 2012; Luo et al., 2013; Souquet et al., 2013; Hays et al., 2017). These proteins colocalize extensively when foci first appear in leptotene, their numbers peak in zygotene, and subsequently decline in early pachytene (Souquet et al., 2013; Ishishita et al., 2014; Hays et al., 2017). In fact, MEIOB and SPATA22 form an obligate complex, which facilitates its interaction with subunits of the RPA complex (Xu et al., 2017). However, the functional significance of these interactions is not completely clear, and the recruitment of both RPA and MEIOB/SPATA22 to DSB foci can occur independently (Shi et al., 2019). Interestingly, the absence of MEIOB/SPATA22 has no impact on recombinase recruitment in leptotene (Luo et al., 2013; Ishishita et al., 2014), while in absence of RPA, recombinase loading at meiotic breaks is completely abrogated (Shi et al., 2019). Thus, of these ssDNA binding proteins, only the RPA complex is indispensable for initial recombinase assembly at meiotic DSBs. However, despite normal recombinase recruitment in leptotene, the absence of MEIOB/SPATA22 is associated with a dramatic reduction in RAD51 and DMC1 foci numbers in late zygotene (Souquet et al., 2013; Ishishita et al., 2014). This phenotype is most likely due to a failure to maintain recombinase proteins at the DSBs and not because of faster repair, since the number of RPA foci remains high in *Meiob* and *Spata22* knockout spermatocytes (Luo et al., 2013; Ishishita et al., 2014).

REGULATION OF RECOMBINASE ASSEMBLY AT MEIOTIC DSBs

As meiosis progresses, ssDNA binding proteins at meiotic DSBs are gradually replaced by the recombinases RAD51 and DMC1 (Moens et al., 2002). Homology search and strand exchange in meiosis are thought to be performed by the meiosis-specific DMC1 while RAD51 plays an accessory role (Cloud et al., 2012; Da Ines et al., 2013; Hong et al., 2013). This idea is mainly based on functional genetic analyses in yeast. Similarly, in mouse, knockout of *Dmc1* leads to a failure to repair meiotic DSBs, causing aberrant and incomplete synapsis in both sexes. Still, RAD51 foci accumulation appears normal (Pittman et al., 1998; Yoshida et al., 1998). Knockout of RAD51 leads to an embryonic lethal phenotype (Lim and Hasty, 1996; Tsuzuki et al., 1996), but an *in vivo* knockdown approach provided indications that DMC1

plays a more dominant role in meiotic DSB repair compared to RAD51 (Dai et al., 2017).

Loading of meiotic recombinase at DSBs sites require several proteins in both somatic and meiotic cells. Here, we restrict ourselves to the components that are most directly involved in the actual transfer of the recombinases onto the ssDNA. Similar to HR in mitotic cells, recombinase loading in meiosis is thought to be directly mediated by BRCA2 (reviewed by Zelensky et al., 2014). However, details of the precise meiotic roles of BRCA2 are missing as knockout of the gene is embryonic lethal (Hakem et al., 1998; Gudmundsdottir and Ashworth, 2004). Nevertheless, *Brca2* knockout mice expressing human BRCA2 rescues embryonic lethality, but the lack of expression in meiotic cells impairs recombinase recruitment and synapsis (Sharan et al., 2004). This confirms the critical role of BRCA2 in recombinase loading in meiosis. In addition, *in vitro* analyses have shown direct interaction between BRCA2 and DMC1 (Dray et al., 2006; Thorslund et al., 2007; Martinez et al., 2016). Thus, it is plausible that the mediator model established in somatic HR is applicable in meiotic HR: BRCA2 delivers RAD51 and DMC1 to meiotic DSBs and facilitates orderly replacement of the ssDNA-binding proteins with the recombinase nucleoprotein filaments. Still, it is unclear how the mediator function of BRCA2 extends to the meiosis-specific ssDNA binding proteins MEIOB/SPATA22 and even to DMC1, as a *Brca2* point mutation affecting the residue essential for BRCA2-DMC1 interaction *in vitro* did not result in the expected meiotic defect (Biswas et al., 2012). Another BRCA2 interactor, SWSAP1, and its partner in the Shu complex SWS1, are both essential for mouse meiosis (Matsuzaki et al., 2019). In absence of either Shu component, RAD51 and DMC1 foci numbers are strongly reduced, which may well be due to reduced stability of the filaments (Abreu et al., 2018; Matsuzaki et al., 2019).

In somatic cells, stable accumulation of RAD51 also requires direct interactions of BRCA2 with its "partner and localizer" PALB2 (Xia et al., 2006). Mouse spermatocytes with a *Brca2* mutation impairing PALB2-BRCA2 interaction displayed a reduced number of RAD51 foci (Hartford et al., 2016). PALB2 forms a complex with the tumor suppressor protein BRCA1, which is thought to help in the accumulation of PALB2 at damage sites (Zhang et al., 2009a,b). Indeed, recombinase accumulation is also impaired in *Brca1* mutant mice (Xu et al., 2003). We and others have recently identified a novel, germ cell specific BRCA2 associated protein complex comprising HSF2BP (or MEILB2) and BRME1 (or MEIOK21/C19orf57), and proposed that this complex functions as meiotic BRCA2 localizer, analogous to the function of PALB2 (Zhang et al., 2019; Brandsma et al., 2019; Felipe-Medina et al., 2020; Shang et al., 2020; Takemoto et al., 2020; Zhang J. et al., 2020). Consistent with this hypothesis, *Hsf2bp* (Brandsma et al., 2019; Zhang et al., 2019) and (to a lesser extent) *Brme1* knockout mice (Zhang J. et al., 2020; Felipe-Medina et al., 2020; Shang et al., 2020) show a strong reduction in meiotic recombinase RAD51/DMC1 foci numbers, associated with severe meiotic defects in males. Interestingly, these proteins are critical only for male fertility while their absence in females has only minor consequences (Zhang et al., 2019; Brandsma et al., 2019; Felipe-Medina et al., 2020; Shang et al., 2020; Takemoto et al., 2020; Zhang J. et al., 2020). This suggests that recombinase loading might be differentially regulated in female mice.

Detection of RPA, SPATA22 and MEIOB in HSF2BP and/or BRME1 co-immunoprecipitates has led to the suggestion that HSF2BP and BRME1 may act as adaptors between BRCA2 and the ssDNA binding protein-coated 3′ overhang of the resected DSB, again not unlike the PALB2 paradigm (Murphy et al., 2014). How PALB2, HSF2BP, and BRME1 divide their BRCA2 localizer roles in meiosis among each other, and how these combine with the intrinsic DNA-binding activity of BRCA2, and its ability to autonomously stimulate recombinases *in vitro* remains to be established. Alternatively, an observed inhibitory effect of HSF2BP on somatic HR caused by its stimulation of proteasomal degradation of BRCA2 (Sato et al., 2020), suggests that HSF2BP (also) affects BRCA2 turnover. The precise functions and regulation of BRCA2 in meiosis may be revealed when better antibodies or other (live) imaging tools for reliable monitoring of BRCA2 abundance and localization in meiocytes become available. An obviously required specialization of BRCA2 in meiosis is the need to assemble RAD51 as well as DMC1 in functional filaments, so it might be speculated that HSF2BP and BRME1 are involved in regulating the meiosis-specific transition from RPA/MEIOB/SPATA22 loaded ssDNA to appropriately assembled RAD51 and DMC1 filaments. But what is the precise molecular organization of these proteins on the ssDNA?

MOLECULAR ARRANGEMENT OF RPA, RAD51, and DMC1 FILAMENTS IN NANOFOCI AT MEIOTIC DSBs

RPA and the recombinases RAD51 and DMC1 are sequentially loaded on the processed ssDNA ends of a DSBs. In this process, the recombinases are thought to replace RPA in the first steps toward strand invasion events. In addition, once strand invasion has been successful, RPA is thought to accumulate on the displaced strand (D-loop). The organization of RPA, RAD51 and DMC1 on meiotic repair intermediates has been analyzed using two different approaches in the mouse. On the one hand, specific ChIP-seq approaches (Smagulova et al., 2011; Hinch et al., 2019, 2020) have been used to study, in bulk cell data, the accumulation of these proteins on ssDNA. On the other hand, there is single cell, and even single repair focus data from fluorescent super-resolution microscopy approaches (Brown et al., 2015; Yoon et al., 2018; Slotman et al., 2020). Fluorescent super-resolution microscopy techniques (for example SIM, STED, dSTORM, and expansion microscopy) bypass the diffraction limit, which restricts the resolution of light microscopy to ∼250 nm (see **Figure 1**).

In meiosis, initial super-resolution microscopy data was mostly focused on the molecular platform of meiotic DSB repair; the SC (Schücker et al., 2015; Agostinho et al., 2018; Zwettler et al., 2020) and the associated meiotic cohesion components (Agostinho et al., 2016; Ishiguro and Watanabe, 2016; Rong et al., 2016). Structured illumination microscopy (SIM), with a resolution of ∼115 nm (Gustafsson, 2005), is a perfect tool to resolve the lateral elements of the SC, which was not possible with

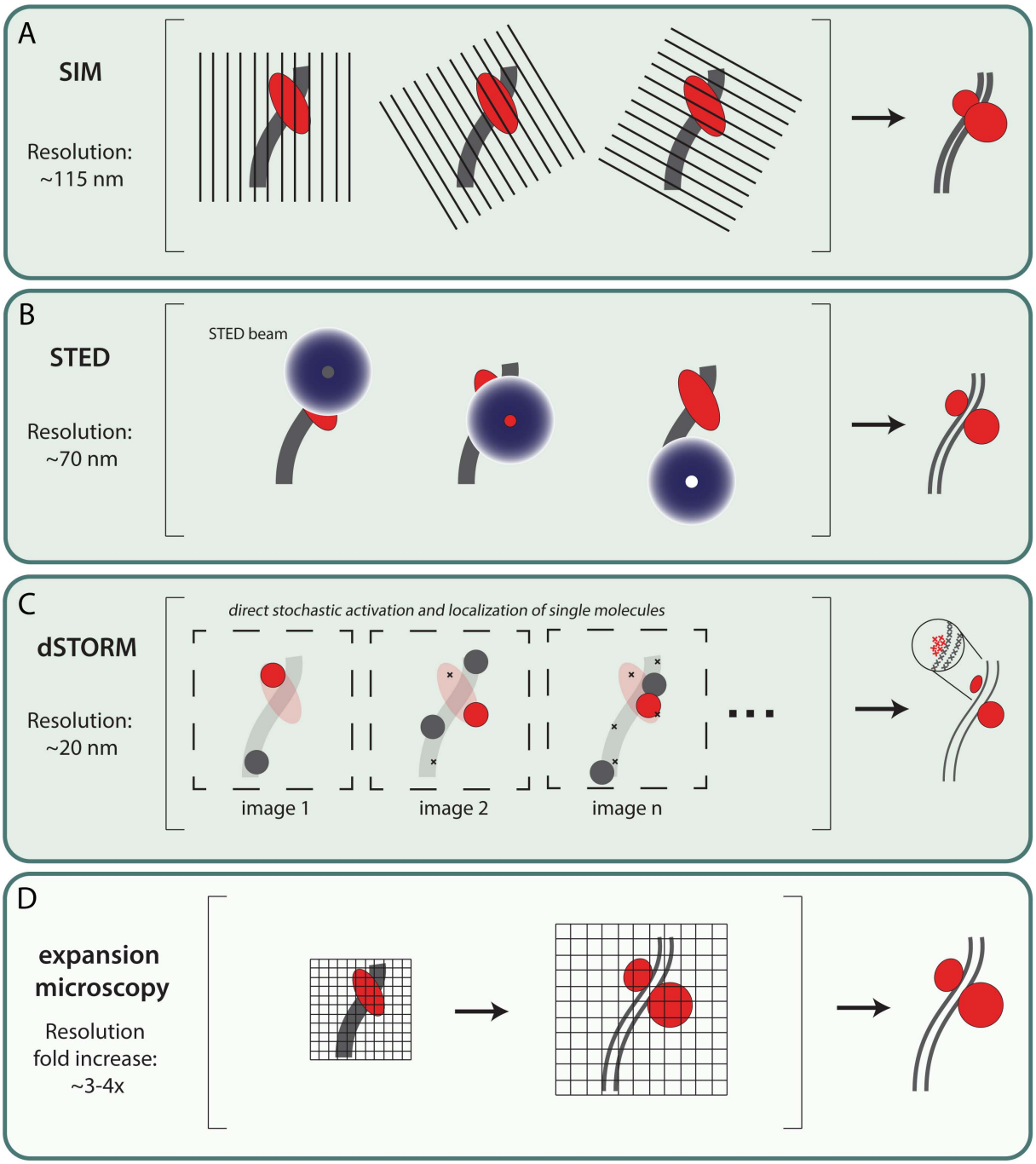

FIGURE 1 | Most commonly used fluorescent super-resolution microscopy techniques in meiosis research. **(A)** Structured illumination microscopy (SIM) – SIM uses a movable diffraction grating in combination with widefield microscopy. By exciting the sample and simultaneously translating and rotating the grid, an interference pattern—also called a Moiré pattern—occurs which contains more detailed information. Using mathematical tools these images are converted to one image with a lateral resolution up to ~115 nm (Guerra, 1995; Gustafsson, 2000). **(B)** Stimulated emission depletion (STED) – In addition to the excitation laser, STED microscopy includes a second laser that generates a donut shaped STED beam of a longer wavelength that induces stimulated emission of any fluorophore that is not located at the center of the STED beam. This physically narrows the point spread function and therefore increases the lateral resolution up to ~70 nm (Galbraith and Galbraith, 2011). **(C)** Direct Stochastic optical reconstruction microscopy(dSTORM) – dSTORM microscopy can provide high resolution images with a lateral resolution of ~20 nm. Fluorophores are stochastically activated by increasing the switch between active and dark-state using an oxygen-reducing buffer and high laser power. Images are generated by combining individual localization signals which are recorded over time (Rust et al., 2006). It should be noted that although single molecules can be detected, the exact number of target proteins present cannot be quantified due to the indirect detection method, using fluorescent antibodies. **(D)** Expansion microscopy (ExM) – Expansion microscopy is a method to increase resolution by enlargement of the sample. This enlargement makes use of a swelling polymer that expand (swelling polymer) samples directly or indirectly (Chen et al., 2015). ExM can be combined with other microscopy techniques resulting in ExM-SIM, ExSTORM or ExSTED with a resolution increase of ~3–4x fold (Gao et al., 2018; Wang et al., 2018; Xu et al., 2019; Zwettler et al., 2020).

confocal microscopy but earlier shown with electron microscopy (Solari and Moses, 1973; Moses et al., 1975). Using this technique, RPA localization relative to the axial (unsynapsed) and lateral elements of the SC was analyzed by Yoon et al. (2018). They observed that in zygotene, many of the RPA foci localized on the inner side of the still unsynapsed SYCP3 axial elements, and between the synapsed lateral elements in pachytene. These were proposed to represent sites where RPA is associated with D-loops, as also suggested from the ChIP-seq analyses of ssDNA by Hinch et al. (2020). The SIM analyses also allowed a more precise measurement of the foci size which was estimated between 170–270 nm (Yoon et al., 2018). Other super-resolution techniques like STED and dSTORM can obtain even higher resolution, and can visualize relative protein distributions inside the classical repair foci (Hell and Wichmann, 1994; Rust et al., 2006). A further ∼3–4 fold increase in resolution can be achieved by combining expansion microscopy with the above mentioned super-resolution techniques (see **Figure 1**; Gao et al., 2018; Wang et al., 2018; Xu et al., 2019).

Localization patterns of RAD51 and DMC1 have been investigated in different species, using different methods. Standard widefield and confocal microscopy imaging have indicated colocalization of RAD51 and DMC1 in mouse meiocytes (Tarsounas et al., 1999; Moens et al., 2002; Carofiglio et al., 2018), but in *A. thaliana,* non-overlapping RAD51/DMC1 foci were observed (Kurzbauer et al., 2012). This has led to the hypothesis that RAD51 and DMC1 were loaded on opposite ends of DSBs. In *C. elegans*, that lacks DMC1, ∼60% of RAD51 was observed in paired foci using 3D-SIM (Woglar and Villeneuve, 2018). Interestingly, in yeast, the appearance of partially overlapping RAD51-DMC1 co-foci has been reported (Brown et al., 2015). Subsequent analyses of RAD51 and DMC1 nanofoci using single color dSTORM, indicated that variable combinations of relatively short (∼100 nm length) RAD51 and DMC1 filaments might be present within a single focus (Brown et al., 2015). However, in mice, high resolution ssDNA ChIP-seq of DMC1 and RAD51 indicated highly organized and symmetric loading of DMC1 near the 3′ ends and RAD51 signal closer to the dsDNA (Hinch et al., 2020). This spatial organization of RAD51 and DMC1 agreed with the SIM data reported by the same group, which showed partially overlapping RAD51-DMC1 foci in close proximity to the SC, where RAD51 was closest (Hinch et al., 2020). Dual color dSTORM analyses in combination with 3D-SIM of mouse spermatocytes also showed that DMC1 is further away from the axis than RAD51 (Slotman et al., 2020). In yeast, this organization was already suggested by the inferred preference of RAD51 to form filaments in 3′–5′ direction, while that of DMC1 would be in 5′–3′ (see **Figure 2A**, left) from *in vitro* data analysis of directionality in a four-strand reaction (reviewed in Brown and Bishop, 2014). Although the microscopy data at present cannot be translated into an actual organization of filaments on the DNA, combined with the ssDNA ChIP-seq analyses it might be speculated that DMC1 coated ssDNA end has more freedom of movement compared to the RAD51 coated region closer to the dsDNA (and thus to the SC), when searching for homology (Zickler and Kleckner, 2015; Hinch et al., 2020; Slotman et al., 2020). However, contrary to the ChIP-seq data, our super-resolution analysis revealed much less strict-organized RAD51 and DMC1 structures. A bit more than half of the foci in leptotene contain a single DMC1 and a single RAD51 nanofocus (termed D1R1). The second most frequent structure (∼20%) contained two DMC1 nanofoci, and a single, more elongated RAD51 structure (termed D2R1). In addition, the pairing of two RAD51-DMC1 co-foci (two D1R1,D2R1, or other, in any combination) was hardly observed (Slotman et al., 2020). Still, a lack of clear observation of co-foci might be explained if two ends of a DSB are at variable distances. This interpretation would best fit with the expected occurrence of co-foci that each consist of a single DMC1 and RAD51 nanofocus based on the ssDNA ChIP-seq analyses. In addition, or alternatively, (some of the) foci might represent one end of a DSB while the other end is "invisible" because it is still unresected, or associated with other DNA repair factors such as RPA (Paiano et al., 2020). We also cannot exclude that in some foci, the two ends of the DSBs are too close together to be separated even by dSTORM (see **Figure 2B**). It might be that recombinase loading patterns as described by Hinch et al. (2020) are a consequence of the signal averaging effect that bulk cell analysis could yield (see **Figure 2A**, combine hypothetical variable recombinase loading patterns shown on the left, with the subsequent expected outcome of ChIP-seq analyses shown on the right). The actual RAD51 and DMC1 loading patterns at individual sites might be more stochastic and thus highly variable (see **Figures 2A,B**). Nonetheless, both microscopic and omic approaches are consistent with the observation that RAD51 and DMC1 generally form spatially separate structures (Brown et al., 2015; Hinch et al., 2020; Slotman et al., 2020). This implies that BRCA2 somehow loads separate cargos of these proteins on the resected ends. However, the precise mechanism driving this process is still elusive.

Based on *in vitro* analysis and (non-fluorescent) super-resolution imaging in somatic cells, both RAD51 and DMC1 nucleoprotein filament sizes on resected ssDNA could be measured (Lee et al., 2005; Sheridan et al., 2008; Hilario et al., 2009; van Mameren et al., 2009; Candelli et al., 2014; Sanchez et al., 2017; Haas et al., 2018). This data suggests that RAD51 and DMC1 nucleoprotein filaments would occupy ∼100 nt each in yeast meiocytes, which is only a fraction of the estimated 800 nt resected DNA (Brown et al., 2015). Likewise, in mice, simulations based on dSTORM data estimated the average length of RAD51 and DMC1 filaments to be around 140 nm (Slotman et al., 2020). Given the fact that primary and secondary antibodies decorating the underlying protein may add up to 20–40 nm to the resulting image (Mikhaylova et al., 2015; Pleiner et al., 2018), the actual length of each RAD51 and DMC1 filaments would be around 100 nm. Since each nm of recombinase foci corresponds to 2 nt (Ristic et al., 2005; Sheridan et al., 2008; Short et al., 2016), recombinase filaments in mice would occupy around 400 nt of resected DNA. This suggests that only part of 1–2 kb of resected DNA is covered by recombinases (Hinch et al., 2020; Paiano et al., 2020; Yamada et al., 2020). Assuming that the occupation of resected DNA by meiotic recombinase is partial, it can be speculated that RPA, or the other meiosis-specific ssDNA binding proteins (MEIOB/SPATA22) might be simultaneously bound to the rest of ssDNA (Brown et al., 2015;

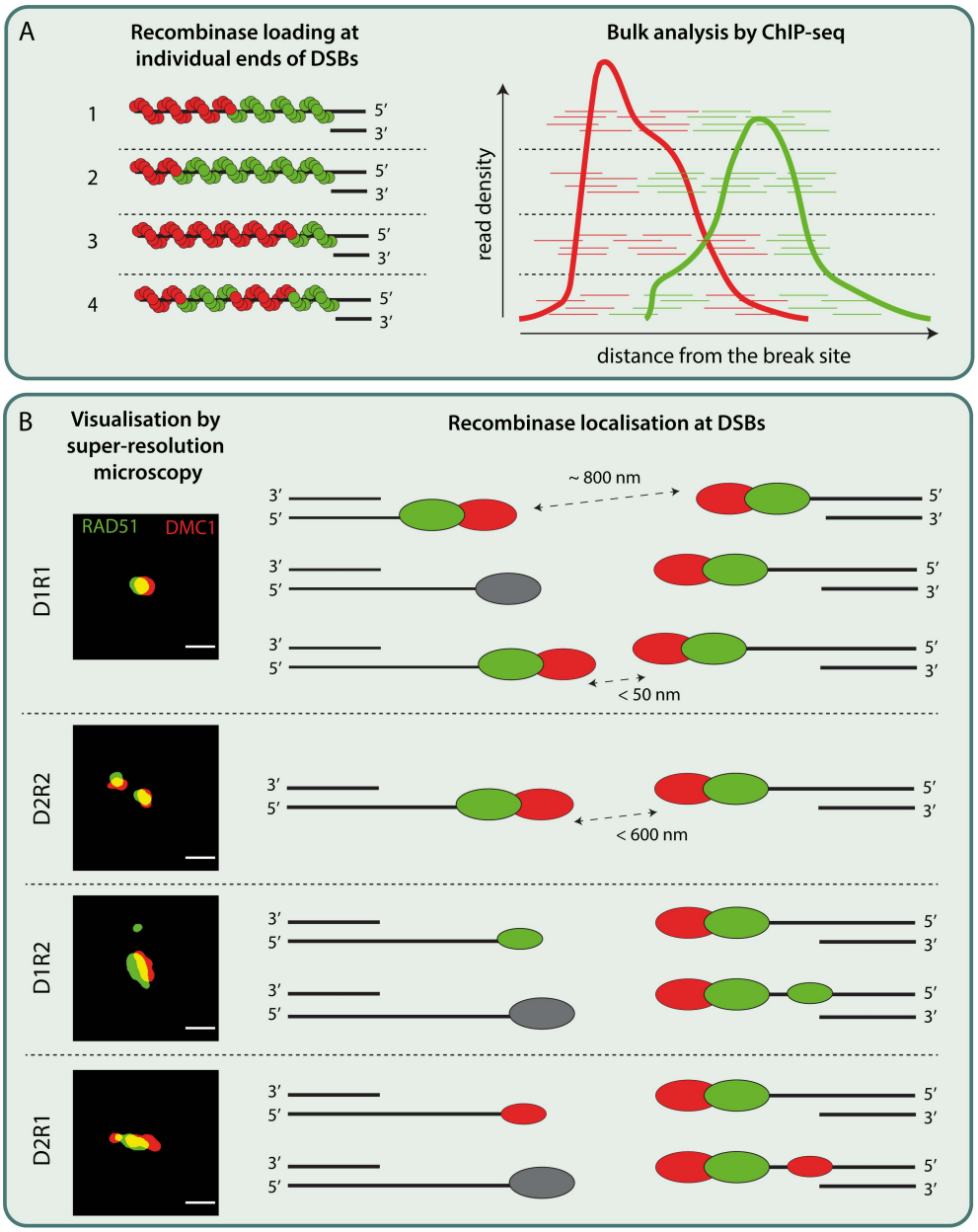

FIGURE 2 | Schematic models interpreting bulk and single-cell data on recombinase loading at individual DSBs in mouse meiosis. **(A)** (left)The location of initial RAD51 and DMC1 loading on ssDNA might be random. The suggested directionality to their filament formation (Brown and Bishop, 2014) could subsequently lead to the RAD51 filaments extending in 3′–5′ direction while DMC1 filaments extending in 5′–3′ direction. The resulting ssDNA would then be occupied with a varying composition of RAD51 and DMC1 recombinases as represented in 1–3. It is equally possible that multiple short stretches of RAD51 and DMC1 filaments are assembled on ssDNA as shown in 4. (right) is a schematic drawing of putative RAD51 and DMC1 ChIP-seq reads corresponding to their loading on individual break sites as depicted in 1–4. The bulk cell nature of ChIP-seq analysis would then yield density plots as indicated in the cartoon, inspired from the RAD51 and DMC1 ChIP-seq analysis from Hinch et al. (2020). **(B)** Super-resolution imaging of DSB repair foci in mice revealed various configurations of DMC1 (D, red oval) and RAD51 (R, green oval). The most frequent configuration, D1R1, can be interpreted in three ways: Assuming that the recombinase foci with a preferred nearest neighbor distance of around ∼800 nm (Slotman et al., 2020) represent two ends of DSB, D1R1 can be interpreted as DMC1-RAD51 pairs loaded symmetrically across two ends of DSB. Alternatively, D1R1 configuration might also be the result of two ends of DSB each loaded with DMC1-RAD51 pairs that end up so close (<50 nm) that they could not be resolved even with super-resolution microscopy. It is equally possible that one end of DSB might be occupied by other ssDNA binding proteins or is being processed while the other end is loaded with DMC1-RAD51 pair. Secondly, based on the paired foci observed in other species and according to ChIP-seq data, a D2R2 can be interpreted as a subset of D1R1 loaded ends of a DSB that lie within the ROI (<600 nm). However, this configuration is rare. Besides these configurations, other configurations such as D2R1 and D1R2 (of which D2R1 is the second most frequent configuration) consisting of a smaller DMC1 or RAD51 foci along with a D1R1 have been observed rather frequently. These configurations may be interpreted as the presence of a single DMC1 or RAD51 focus on the other end of DSB occupied by a D1R1, or an extra focus on the same ssDNA accommodating a D1R1. Other interpretations of these recombinase configurations are also possible. ROI: region of interest Scale bar representing 250 nm. Binary super-resolution images of RAD51 and DMC1 configurations are derived from Slotman et al. (2020).

Slotman et al., 2020). However, it cannot be excluded that the actual filament length might be underestimated due to its 3D organization of chromatin in the cell. Measurements related to recombinase occupancy *in vitro* on ssDNA filaments (Sheridan et al., 2008) perhaps cannot be directly "translated" to what is observed *in vivo*, where RAD51 and/or DMC1 loaded DNA might adopt a higher order, or different configuration.

CONCLUDING REMARKS

In this review, we provide an overview of recent data on RAD51 and DMC1 recruitment, which raises several key issues. First, the recently discovered meiotic proteins HSF2BP and BRME1 are critical for BRCA2-mediated loading of RAD51 and DMC1 (Zhang et al., 2019; Zhang J. et al., 2020; Brandsma et al., 2019; Felipe-Medina et al., 2020; Shang et al., 2020; Takemoto et al., 2020). However, key evidence that directly couples BRCA2 localization and activity to that of HSF2BP and BRME1 is still missing. High-resolution imaging of endogenous BRCA2 localization in relation to its proposed recruiters (HSF2BP and BRME1), or genetic experiments that specifically remove interactions between BRCA2 and these proteins are therefore essential.

Second, despite their proposed role in BRCA2 recruitment, the fact that the absence of BRME1 and HSF2BP have only minor consequences in female meiosis is puzzling. This asks for further genetic, biochemical and microscopic analyses of early recombination intermediates in mouse oocytes and comparison with observations in mouse spermatocytes. Third, regarding the differential loading of RAD51 and DMC1, the seemingly strict organization of one DMC1 filament at the 3′ end, and one RAD51 filament further upstream, on both sides of the DSB observed in ChIP-seq data by Hinch et al. (2020), is at odds with the huge diversity of RAD51 and DMC1 nanofoci configurations in super-resolution microscopy (dSTORM) analyses in yeast (Brown et al., 2015) and mice (Slotman et al., 2020). However, the super-resolution microscopy data discussed above is limited by being a 2D snapshot of a dynamic 3D process. Further analysis of recombinases in combination with synaptonemal complex components or even ssDNA using 3D super-resolution techniques could help. Also, it is expected that single cell omics technology involving protein-DNA analyses, will become available, allowing a better comparison of these two types of data. Finally, the development of systems to track a single DSB over time would be another crucial next step to truly unravel the dynamics of the repair process. A recent example of such an approach in somatic cells involved precisely timed and targeted induction of a single DSB, followed by live imaging of repair protein accumulation (Liu et al., 2020). Together, these technical innovations and new approaches will help to make important steps toward our understanding of meiotic recombinase recruitment mechanisms and their functions.

AUTHOR CONTRIBUTIONS

AM wrote the draft of the manuscript and designed **Figure 2**. LK critically reviewed the draft, added text, designed **Figure 1**, and improved **Figure 2**. AZ critically reviewed the draft and added text. ABH contributed to the concepts and critically reviewed and adapted the manuscript. WB supervised writing of the draft, and critically reviewed and adapted the manuscript. All authors agreed on the final version of the manuscript.

REFERENCES

Abreu, C. M., Prakash, R., Romanienko, P. J., Roig, I., Keeney, S., and Jasin, M. (2018). Shu complex SWS1-SWSAP1 promotes early steps in mouse meiotic recombination. *Nat. Commun.* 9:3961. doi: 10.1038/s41467-018-06384-x

Acquaviva, L., Boekhout, M., Karasu, M. E., Brick, K., Pratto, F., Li, T., et al. (2020). Ensuring meiotic DNA break formation in the mouse pseudoautosomal region. *Nature* 582, 426–431. doi: 10.1038/s41586-020-2327-4

Agostinho, A., Kouznetsova, A., Hernandez-Hernandez, A., Bernhem, K., Blom, H., Brismar, H., et al. (2018). Sexual dimorphism in the width of the mouse synaptonemal complex. *J. Cell Sci.* 131:jcs212548. doi: 10.1242/jcs.212548

Agostinho, A., Manneberg, O., Van Schendel, R., Hernandez-Hernandez, A., Kouznetsova, A., Blom, H., et al. (2016). High density of REC8 constrains sister chromatid axes and prevents illegitimate synaptonemal complex formation. *EMBO Rep.* 17, 901–913. doi: 10.15252/embr.201642030

Baudat, F., Buard, J., Grey, C., Fledel-Alon, A., Ober, C., Przeworski, M., et al. (2010). PRDM9 is a major determinant of meiotic recombination hotspots in humans and mice. *Science* 327, 836–840. doi: 10.1126/science.1183439

Berg, I. L., Neumann, R., Lam, K. W., Sarbajna, S., Odenthal-Hesse, L., May, C. A., et al. (2010). PRDM9 variation strongly influences recombination hot-spot activity and meiotic instability in humans. *Nat. Genet.* 42, 859–863. doi: 10.1038/ng.658

Bergerat, A., De Massy, B., Gadelle, D., Varoutas, P. C., Nicolas, A., and Forterre, P. (1997). An atypical topoisomerase II from archaea with implications for meiotic recombination. *Nature* 386, 414–417. doi: 10.1038/386414a0

Biswas, K., Das, R., Eggington, J. M., Qiao, H., North, S. L., Stauffer, S., et al. (2012). Functional evaluation of BRCA2 variants mapping to the PALB2-binding and C-terminal DNA-binding domains using a mouse ES cell-based assay. *Hum. Mol. Genet.* 21, 3993–4006. doi: 10.1093/hmg/dds222

Boekhout, M., Karasu, M. E., Wang, J., Acquaviva, L., Pratto, F., Brick, K., et al. (2019). REC114 partner ANKRD31 controls number, timing, and location of meiotic DNA breaks. *Mol. Cell* 74, 1053–1068. doi: 10.1016/j.molcel.2019.03.023

Brandsma, I., Sato, K., Van Rossum-Fikkert, S. E., Van Vliet, N., Sleddens, E., Reuter, M., et al. (2019). HSF2BP interacts with a conserved domain of BRCA2 and is required for mouse spermatogenesis. *Cell Rep.* 27, 3790–3798. doi: 10.1016/j.celrep.2019.05.096

Brick, K., Smagulova, F., Khil, P., Camerini-Otero, R. D., and Petukhova, G. V. (2012). Genetic recombination is directed away from functional genomic elements in mice. *Nature* 485, 642–645. doi: 10.1038/nature11089

Brown, M. S., and Bishop, D. K. (2014). DNA strand exchange and RecA homologs in meiosis. *Cold Spring Harb. Perspect. Biol.* 7:a016659. doi: 10.1101/cshperspect.a016659

Brown, M. S., Grubb, J., Zhang, A., Rust, M. J., and Bishop, D. K. (2015). Small Rad51 and Dmc1 complexes often Co-occupy both ends of a meiotic DNA double strand break. *PLoS Genet.* 11:e1005653. doi: 10.1371/journal.pgen.1005653

Candelli, A., Holthausen, J. T., Depken, M., Brouwer, I., Franker, M. A., Marchetti, M., et al. (2014). Visualization and quantification of nascent RAD51 filament formation at single-monomer resolution. *Proc. Natl. Acad. Sci. U. S. A.* 111, 15090–15095. doi: 10.1073/pnas.1307824111

Cannavo, E., and Cejka, P. (2014). Sae2 promotes dsDNA endonuclease activity within Mre11-Rad50-Xrs2 to resect DNA breaks. *Nature* 514, 122–125. doi: 10.1038/nature13771

Carofiglio, F., Sleddens-Linkels, E., Wassenaar, E., Inagaki, A., Van Cappellen, W. A., Grootegoed, J. A., et al. (2018). Repair of exogenous DNA double-strand breaks promotes chromosome synapsis in SPO11-mutant mouse meiocytes, and is altered in the absence of HORMAD1. *DNA Repair (Amst.)* 63, 25–38. doi: 10.1016/j.dnarep.2018.01.007

Chen, F., Tillberg, P. W., and Boyden, E. S. (2015). Optical imaging. Expansion microscopy. *Science* 347, 543–548. doi: 10.1126/science.1260088

Cloud, V., Chan, Y. L., Grubb, J., Budke, B., and Bishop, D. K. (2012). Rad51 is an accessory factor for Dmc1-mediated joint molecule formation during meiosis. *Science* 337, 1222–1225. doi: 10.1126/science.1219379

Da Ines, O., Degroote, F., Goubely, C., Amiard, S., Gallego, M. E., and White, C. I. (2013). Meiotic recombination in Arabidopsis is catalysed by DMC1, with RAD51 playing a supporting role. *PLoS Genet.* 9:e1003787. doi: 10.1371/journal.pgen.1003787

Dai, J., Voloshin, O., Potapova, S., and Camerini-Otero, R. D. (2017). Meiotic knockdown and complementation reveals essential role of RAD51 in mouse spermatogenesis. *Cell Rep.* 18, 1383–1394. doi: 10.1016/j.celrep.2017.01.024

Dray, E., Siaud, N., Dubois, E., and Doutriaux, M. P. (2006). Interaction between Arabidopsis Brca2 and its partners Rad51, Dmc1, and Dss1. *Plant Physiol.* 140, 1059–1069. doi: 10.1104/pp.105.075838

Felipe-Medina, N., Caburet, S., Sanchez-Saez, F., Condezo, Y. B., De Rooij, D. G., Gomez, H. L., et al. (2020). A missense in HSF2BP causing primary ovarian insufficiency affects meiotic recombination by its novel interactor C19ORF57/BRME1. *Elife* 9:e56996. doi: 10.7554/eLife.56996

Galbraith, C. G., and Galbraith, J. A. (2011). Super-resolution microscopy at a glance. *J. Cell Sci.* 124, 1607–1611. doi: 10.1242/jcs.080085

Gao, M., Maraspini, R., Beutel, O., Zehtabian, A., Eickholt, B., Honigmann, A., et al. (2018). Expansion stimulated emission depletion microscopy (ExSTED). *ACS Nano* 12, 4178–4185. doi: 10.1021/acsnano.8b00776

Garcia, V., Phelps, S. E., Gray, S., and Neale, M. J. (2011). Bidirectional resection of DNA double-strand breaks by Mre11 and Exo1. *Nature* 479, 241–244. doi: 10.1038/nature10515

Gudmundsdottir, K., and Ashworth, A. (2004). BRCA2 in meiosis: turning over a new leaf. *Trends Cell Biol.* 14, 401–404. doi: 10.1016/j.tcb.2004.07.002

Guerra, J. M. (1995). Super-resolution through illumination by diffraction-born evanescent waves. *Appl. Phys. Lett.* 66:3555. doi: 10.1063/1.113814

Gustafsson, M. G. (2000). Surpassing the lateral resolution limit by a factor of two using structured illumination microscopy. *J. Microsc.* 198, 82–87. doi: 10.1046/j.1365-2818.2000.00710.x

Gustafsson, M. G. (2005). Nonlinear structured-illumination microscopy: wide-field fluorescence imaging with theoretically unlimited resolution. *Proc. Natl. Acad. Sci. U. S. A.* 102, 13081–13086. doi: 10.1073/pnas.0406877102

Haas, K. T., Lee, M., Esposito, A., and Venkitaraman, A. R. (2018). Single-molecule localization microscopy reveals molecular transactions during RAD51 filament assembly at cellular DNA damage sites. *Nucleic Acids Res.* 46, 2398–2416. doi: 10.1093/nar/gkx1303

Hakem, R., De La Pompa, J. L., and Mak, T. W. (1998). Developmental studies of Brca1 and Brca2 knock-out mice. *J. Mammary Gland Biol. Neoplasia* 3, 431–445. doi: 10.1023/a:1018792200700

Hartford, S. A., Chittela, R., Ding, X., Vyas, A., Martin, B., Burkett, S., et al. (2016). Interaction with PALB2 Is essential for maintenance of genomic integrity by BRCA2. *PLoS Genet.* 12:e1006236. doi: 10.1371/journal.pgen.1006236

Hayashi, K., Yoshida, K., and Matsui, Y. (2005). A histone H3 methyltransferase controls epigenetic events required for meiotic prophase. *Nature* 438, 374–378. doi: 10.1038/nature04112

Hays, E., Majchrzak, N., Daniel, V., Ferguson, Z., Brown, S., Hathorne, K., et al. (2017). Spermatogenesis associated 22 is required for DNA repair and synapsis of homologous chromosomes in mouse germ cells. *Andrology* 5, 299–312. doi: 10.1111/andr.12315

Hell, S. W., and Wichmann, J. (1994). Breaking the diffraction resolution limit by stimulated emission: stimulated-emission-depletion fluorescence microscopy. *Opt. Lett.* 19, 780–782. doi: 10.1364/ol.19.000780

Hilario, J., Amitani, I., Baskin, R. J., and Kowalczykowski, S. C. (2009). Direct imaging of human Rad51 nucleoprotein dynamics on individual DNA molecules. *Proc. Natl. Acad. Sci. U. S. A.* 106, 361–368. doi: 10.1073/pnas.0811965106

Hinch, A. G., Becker, P. W., Li, T., Moralli, D., Zhang, G., Bycroft, C., et al. (2020). The configuration of RPA, RAD51, and DMC1 binding in meiosis reveals the nature of critical recombination intermediates. *Mol. Cell* 79, 689–701. doi: 10.1016/j.molcel.2020.06.015

Hinch, A. G., Zhang, G., Becker, P. W., Moralli, D., Hinch, R., Davies, B., et al. (2019). Factors influencing meiotic recombination revealed by whole-genome sequencing of single sperm. *Science* 363:eaau8861. doi: 10.1126/science.aau8861

Hong, S., Sung, Y., Yu, M., Lee, M., Kleckner, N., and Kim, K. P. (2013). The logic and mechanism of homologous recombination partner choice. *Mol. Cell* 51, 440–453. doi: 10.1016/j.molcel.2013.08.008

Ishiguro, K., and Watanabe, Y. (2016). The cohesin REC8 prevents illegitimate inter-sister synaptonemal complex assembly. *EMBO Rep.* 17, 783–784. doi: 10.15252/embr.201642544

Ishishita, S., Matsuda, Y., and Kitada, K. (2014). Genetic evidence suggests that Spata22 is required for the maintenance of Rad51 foci in mammalian meiosis. *Sci. Rep.* 4:6148. doi: 10.1038/srep06148

Keelagher, R. E., Cotton, V. E., Goldman, A. S., and Borts, R. H. (2011). Separable roles for Exonuclease I in meiotic DNA double-strand break repair. *DNA Repair (Amst.)* 10, 126–137. doi: 10.1016/j.dnarep.2010.09.024

Keeney, S., Giroux, C. N., and Kleckner, N. (1997). Meiosis-specific DNA double-strand breaks are catalyzed by Spo11, a member of a widely conserved protein family. *Cell* 88, 375–384. doi: 10.1016/s0092-8674(00)81876-0

Kleckner, N. (2006). Chiasma formation: chromatin/axis interplay and the role(s) of the synaptonemal complex. *Chromosoma* 115, 175–194. doi: 10.1007/s00412-006-0055-7

Kumar, R., Ghyselinck, N., Ishiguro, K., Watanabe, Y., Kouznetsova, A., Hoog, C., et al. (2015). MEI4 – a central player in the regulation of meiotic DNA double-strand break formation in the mouse. *J. Cell Sci.* 128, 1800–1811. doi: 10.1242/jcs.165464

Kumar, R., Oliver, C., Brun, C., Juarez-Martinez, A. B., Tarabay, Y., Kadlec, J., et al. (2018). Mouse REC114 is essential for meiotic DNA double-strand break formation and forms a complex with MEI4. *Life Sci. Alliance* 1:e201800259. doi: 10.26508/lsa.201800259

Kurzbauer, M. T., Uanschou, C., Chen, D., and Schlogelhofer, P. (2012). The recombinases DMC1 and RAD51 are functionally and spatially separated during meiosis in Arabidopsis. *Plant Cell* 24, 2058–2070. doi: 10.1105/tpc.112.098459

La Salle, S., Palmer, K., O'brien, M., Schimenti, J. C., Eppig, J., and Handel, M. A. (2012). Spata22, a novel vertebrate-specific gene, is required for meiotic progress in mouse germ cells. *Biol. Reprod.* 86:45. doi: 10.1095/biolreprod.111.095752

Lam, I., and Keeney, S. (2015). Mechanism and regulation of meiotic recombination initiation. *Cold Spring Harb. Perspect. Biol.* 7:a016634. doi: 10.1101/cshperspect.a016634

Lee, M. H., Chang, Y. C., Hong, E. L., Grubb, J., Chang, C. S., Bishop, D. K., et al. (2005). Calcium ion promotes yeast Dmc1 activity via formation of long and fine helical filaments with single-stranded DNA. *J. Biol. Chem.* 280, 40980–40984. doi: 10.1074/jbc.M505896200

Lim, D. S., and Hasty, P. (1996). A mutation in mouse rad51 results in an early embryonic lethal that is suppressed by a mutation in p53. *Mol. Cell Biol.* 16, 7133–7143. doi: 10.1128/mcb.16.12.7133

Liu, Y., Zou, R. S., He, S., Nihongaki, Y., Li, X., Razavi, S., et al. (2020). Very fast CRISPR on demand. *Science* 368, 1265–1269. doi: 10.1126/science.aay8204

Luo, M., Yang, F., Leu, N. A., Landaiche, J., Handel, M. A., Benavente, R., et al. (2013). MEIOB exhibits single-stranded DNA-binding and exonuclease activities and is essential for meiotic recombination. *Nat. Commun.* 4:2788. doi: 10.1038/ncomms3788

Martinez, J. S., Von Nicolai, C., Kim, T., Ehlen, A., Mazin, A. V., Kowalczykowski, S. C., et al. (2016). BRCA2 regulates DMC1-mediated recombination through the BRC repeats. *Proc. Natl. Acad. Sci. U. S. A.* 113, 3515–3520. doi: 10.1073/pnas.1601691113

Matsuzaki, K., Kondo, S., Ishikawa, T., and Shinohara, A. (2019). Human RAD51 paralogue SWSAP1 fosters RAD51 filament by regulating the anti-recombinase FIGNL1 AAA+ ATPase. *Nat. Commun.* 10:1407. doi: 10.1038/s41467-019-09190-1

Mihola, O., Pratto, F., Brick, K., Linhartova, E., Kobets, T., Flachs, P., et al. (2019). Histone methyltransferase PRDM9 is not essential for meiosis in male mice. *Genome Res.* 29, 1078–1086. doi: 10.1101/gr.244426.118

Mikhaylova, M., Cloin, B. M., Finan, K., Van Den Berg, R., Teeuw, J., Kijanka, M. M., et al. (2015). Resolving bundled microtubules using anti-tubulin nanobodies. *Nat. Commun.* 6:7933. doi: 10.1038/ncomms8933

Mimitou, E. P., and Symington, L. S. (2008). Sae2, Exo1 and Sgs1 collaborate in DNA double-strand break processing. *Nature* 455, 770–774. doi: 10.1038/nature07312

Mimitou, E. P., Yamada, S., and Keeney, S. (2017). A global view of meiotic double-strand break end resection. *Science* 355, 40–45. doi: 10.1126/science.aak9704

Moens, P. B., Kolas, N. K., Tarsounas, M., Marcon, E., Cohen, P. E., and Spyropoulos, B. (2002). The time course and chromosomal localization of recombination-related proteins at meiosis in the mouse are compatible with models that can resolve the early DNA-DNA interactions without reciprocal recombination. *J. Cell Sci.* 115, 1611–1622.

Moses, M. J., Counce, S. J., and Paulson, D. F. (1975). Synaptonemal complex complement of man in spreads of spermatocytes, with details of the sex chromosome pair. *Science* 187, 363–365.

Murphy, A. K., Fitzgerald, M., Ro, T., Kim, J. H., Rabinowitsch, A. I., Chowdhury, D., et al. (2014). Phosphorylated RPA recruits PALB2 to stalled DNA replication forks to facilitate fork recovery. *J. Cell Biol.* 206, 493–507. doi: 10.1083/jcb.201404111

Neale, M. J., Pan, J., and Keeney, S. (2005). Endonucleolytic processing of covalent protein-linked DNA double-strand breaks. *Nature* 436, 1053–1057. doi: 10.1038/nature03872

Paiano, J., Wu, W., Yamada, S., Sciascia, N., Callen, E., Paola Cotrim, A., et al. (2020). ATM and PRDM9 regulate SPO11-bound recombination intermediates during meiosis. *Nat. Commun.* 11:857. doi: 10.1038/s41467-020-14654-w

Papanikos, F., Clement, J. A. J., Testa, E., Ravindranathan, R., Grey, C., Dereli, I., et al. (2019). Mouse ANKRD31 regulates spatiotemporal patterning of meiotic recombination initiation and ensures recombination between X and Y sex chromosomes. *Mol. Cell* 74, 1069–1085.e11. doi: 10.1016/j.molcel.2019.03.022

Parvanov, E. D., Petkov, P. M., and Paigen, K. (2010). Prdm9 controls activation of mammalian recombination hotspots. *Science* 327:835. doi: 10.1126/science.1181495

Pittman, D. L., Cobb, J., Schimenti, K. J., Wilson, L. A., Cooper, D. M., Brignull, E., et al. (1998). Meiotic prophase arrest with failure of chromosome synapsis in mice deficient for Dmc1, a germline-specific RecA homolog. *Mol. Cell* 1, 697–705. doi: 10.1016/s1097-2765(00)80069-6

Pleiner, T., Bates, M., and Gorlich, D. (2018). A toolbox of anti-mouse and anti-rabbit IgG secondary nanobodies. *J. Cell Biol.* 217, 1143–1154. doi: 10.1083/jcb.201709115

Powers, N. R., Parvanov, E. D., Baker, C. L., Walker, M., Petkov, P. M., and Paigen, K. (2016). The meiotic recombination activator PRDM9 trimethylates Both H3K36 and H3K4 at recombination hotspots in vivo. *PLoS Genet.* 12:e1006146. doi: 10.1371/journal.pgen.1006146

Ristic, D., Modesti, M., Van Der Heijden, T., Van Noort, J., Dekker, C., Kanaar, R., et al. (2005). Human Rad51 filaments on double- and single-stranded DNA: correlating regular and irregular forms with recombination function. *Nucleic Acids Res.* 33, 3292–3302. doi: 10.1093/nar/gki640

Robert, T., Nore, A., Brun, C., Maffre, C., Crimi, B., Bourbon, H. M., et al. (2016a). The TopoVIB-Like protein family is required for meiotic DNA double-strand break formation. *Science* 351, 943–949. doi: 10.1126/science.aad5309

Robert, T., Vrielynck, N., Mezard, C., De Massy, B., and Grelon, M. (2016b). A new light on the meiotic DSB catalytic complex. *Semin. Cell Dev. Biol.* 54, 165–176. doi: 10.1016/j.semcdb.2016.02.025

Rong, M., Matsuda, A., Hiraoka, Y., and Lee, J. (2016). Meiotic cohesin subunits RAD21L and REC8 are positioned at distinct regions between lateral elements and transverse filaments in the synaptonemal complex of mouse spermatocytes. *J. Reprod. Dev.* 62, 623–630. doi: 10.1262/jrd.2016-127

Rust, M. J., Bates, M., and Zhuang, X. (2006). Sub-diffraction-limit imaging by stochastic optical reconstruction microscopy (STORM). *Nat. Methods* 3, 793–795. doi: 10.1038/nmeth929

Sanchez, H., Paul, M. W., Grosbart, M., Van Rossum-Fikkert, S. E., Lebbink, J. H. G., Kanaar, R., et al. (2017). Architectural plasticity of human BRCA2-RAD51 complexes in DNA break repair. *Nucleic Acids Res.* 45, 4507–4518. doi: 10.1093/nar/gkx084

Sato, K., Brandsma, I., Van Rossum-Fikkert, S. E., Verkaik, N., Oostra, A. B., Dorsman, J. C., et al. (2020). HSF2BP negatively regulates homologous recombination in DNA interstrand crosslink repair. *Nucleic Acids Res.* 48, 2442–2456. doi: 10.1093/nar/gkz1219

Schücker, K., Holm, T., Franke, C., Sauer, M., and Benavente, R. (2015). Elucidation of synaptonemal complex organization by super-resolution imaging with isotropic resolution. *Proc. Natl. Acad. Sci. U. S. A.* 112, 2029–2033. doi: 10.1073/pnas.1414814112

Shang, Y., Huang, T., Liu, H., Liu, Y., Liang, H., Yu, X., et al. (2020). MEIOK21: a new component of meiotic recombination bridges required for spermatogenesis. *Nucleic Acids Res.* 48, 6624–6639. doi: 10.1093/nar/gkaa406

Sharan, S. K., Pyle, A., Coppola, V., Babus, J., Swaminathan, S., Benedict, J., et al. (2004). BRCA2 deficiency in mice leads to meiotic impairment and infertility. *Development* 131, 131–142. doi: 10.1242/dev.00888

Sheridan, S. D., Yu, X., Roth, R., Heuser, J. E., Sehorn, M. G., Sung, P., et al. (2008). A comparative analysis of Dmc1 and Rad51 nucleoprotein filaments. *Nucleic Acids Res.* 36, 4057–4066. doi: 10.1093/nar/gkn352

Shi, B., Xue, J., Yin, H., Guo, R., Luo, M., Ye, L., et al. (2019). Dual functions for the ssDNA-binding protein RPA in meiotic recombination. *PLoS Genet.* 15:e1007952. doi: 10.1371/journal.pgen.1007952

Short, J. M., Liu, Y., Chen, S., Soni, N., Madhusudhan, M. S., Shivji, M. K., et al. (2016). High-resolution structure of the presynaptic RAD51 filament on single-stranded DNA by electron cryo-microscopy. *Nucleic Acids Res.* 44, 9017–9030. doi: 10.1093/nar/gkw783

Slotman, J. A., Paul, M. W., Carofiglio, F., De Gruiter, H. M., Vergroesen, T., Koornneef, L., et al. (2020). Super-resolution imaging of RAD51 and DMC1 in DNA repair foci reveals dynamic distribution patterns in meiotic prophase. *PLoS Genet.* 16:e1008595. doi: 10.1371/journal.pgen.1008595

Smagulova, F., Gregoretti, I. V., Brick, K., Khil, P., Camerini-Otero, R. D., and Petukhova, G. V. (2011). Genome-wide analysis reveals novel molecular features of mouse recombination hotspots. *Nature* 472, 375–378. doi: 10.1038/nature09869

Solari, A. J., and Moses, M. J. (1973). The structure of the central region in the synaptonemal complexes of hamster and cricket spermatocytes. *J. Cell Biol.* 56, 145–152. doi: 10.1083/jcb.56.1.145

Souquet, B., Abby, E., Herve, R., Finsterbusch, F., Tourpin, S., Le Bouffant, R., et al. (2013). MEIOB targets single-strand DNA and is necessary for meiotic recombination. *PLoS Genet.* 9:e1003784. doi: 10.1371/journal.pgen.1003784

Stanzione, M., Baumann, M., Papanikos, F., Dereli, I., Lange, J., Ramlal, A., et al. (2016). Meiotic DNA break formation requires the unsynapsed chromosome axis-binding protein IHO1 (CCDC36) in mice. *Nat. Cell Biol.* 18, 1208–1220. doi: 10.1038/ncb3417

Takemoto, K., Tani, N., Takada-Horisawa, Y., Fujimura, S., Tanno, N., Yamane, M., et al. (2020). Meiosis-specific C19orf57/4930432K21Rik/BRME1 modulates localization of RAD51 and DMC1 to DSBs in mouse meiotic recombination. *Cell Rep.* 31:107686. doi: 10.1016/j.celrep.2020.107686

Tarsounas, M., Morita, T., Pearlman, R. E., and Moens, P. B. (1999). RAD51 and DMC1 form mixed complexes associated with mouse meiotic chromosome cores and synaptonemal complexes. *J. Cell Biol.* 147, 207–220. doi: 10.1083/jcb.147.2.207

Thorslund, T., Esashi, F., and West, S. C. (2007). Interactions between human BRCA2 protein and the meiosis-specific recombinase DMC1. *EMBO J.* 26, 2915–2922. doi: 10.1038/sj.emboj.7601739

Tsuzuki, T., Fujii, Y., Sakumi, K., Tominaga, Y., Nakao, K., Sekiguchi, M., et al. (1996). Targeted disruption of the Rad51 gene leads to lethality in embryonic mice. *Proc. Natl. Acad. Sci. U. S. A.* 93, 6236–6240. doi: 10.1073/pnas.93.13.6236

van Mameren, J., Gross, P., Farge, G., Hooijman, P., Modesti, M., Falkenberg, M., et al. (2009). Unraveling the structure of DNA during overstretching by using multicolor, single-molecule fluorescence imaging. *Proc. Natl. Acad. Sci. U. S. A.* 106, 18231–18236. doi: 10.1073/pnas.0904322106

Wang, Y., Yu, Z., Cahoon, C. K., Parmely, T., Thomas, N., Unruh, J. R., et al. (2018). Combined expansion microscopy with structured illumination microscopy for analyzing protein complexes. *Nat. Protoc.* 13, 1869–1895. doi: 10.1038/s41596-018-0023-8

Woglar, A., and Villeneuve, A. M. (2018). Dynamic architecture of DNA repair complexes and the synaptonemal complex at sites of meiotic recombination. *Cell* 173, 1678–1691.e16. doi: 10.1016/j.cell.2018.03.066

Xia, B., Sheng, Q., Nakanishi, K., Ohashi, A., Wu, J., Christ, N., et al. (2006). Control of BRCA2 cellular and clinical functions by a nuclear partner, PALB2. *Mol. Cell* 22, 719–729. doi: 10.1016/j.molcel.2006.05.022

Xu, H., Tong, Z., Ye, Q., Sun, T., Hong, Z., Zhang, L., et al. (2019). Molecular organization of mammalian meiotic chromosome axis revealed by expansion STORM microscopy. *Proc. Natl. Acad. Sci. U. S. A.* 116, 18423–18428. doi: 10.1073/pnas.1902440116

Xu, X., Aprelikova, O., Moens, P., Deng, C. X., and Furth, P. A. (2003). Impaired meiotic DNA-damage repair and lack of crossing-over during spermatogenesis in BRCA1 full-length isoform deficient mice. *Development* 130, 2001–2012. doi: 10.1242/dev.00410

Xu, Y., Greenberg, R. A., Schonbrunn, E., and Wang, P. J. (2017). Meiosis-specific proteins MEIOB and SPATA22 cooperatively associate with the single-stranded DNA-binding replication protein A complex and DNA double-strand breaks. *Biol. Reprod.* 96, 1096–1104. doi: 10.1093/biolre/iox040

Yamada, S., Hinch, A. G., Kamido, H., Zhang, Y., Edelmann, W., and Keeney, S. (2020). Molecular structures and mechanisms of DNA break processing in mouse meiosis. *Genes Dev.* 34, 806–818. doi: 10.1101/gad.336032.119

Yoon, S., Choi, E. H., Kim, J. W., and Kim, K. P. (2018). Structured illumination microscopy imaging reveals localization of replication protein A between chromosome lateral elements during mammalian meiosis. *Exp. Mol. Med.* 50:112. doi: 10.1038/s12276-018-0139-5

Yoshida, K., Kondoh, G., Matsuda, Y., Habu, T., Nishimune, Y., and Morita, T. (1998). The mouse RecA-like gene Dmc1 is required for homologous chromosome synapsis during meiosis. *Mol. Cell* 1, 707–718. doi: 10.1016/s1097-2765(00)80070-2

Zakharyevich, K., Ma, Y., Tang, S., Hwang, P. Y., Boiteux, S., and Hunter, N. (2010). Temporally and biochemically distinct activities of Exo1 during meiosis: double-strand break resection and resolution of double holliday junctions. *Mol. Cell* 40, 1001–1015. doi: 10.1016/j.molcel.2010.11.032

Zelensky, A., Kanaar, R., and Wyman, C. (2014). Mediators of homologous DNA pairing. *Cold Spring Harb. Perspect. Biol.* 6:a016451. doi: 10.1101/cshperspect.a016451

Zhang, B., Tang, Z., Li, L., and Lu, L. Y. (2020). NBS1 is required for SPO11-linked DNA double-strand break repair in male meiosis. *Cell Death Differ.* 27, 2176–2190. doi: 10.1038/s41418-020-0493-4

Zhang, F., Fan, Q., Ren, K., and Andreassen, P. R. (2009a). PALB2 functionally connects the breast cancer susceptibility proteins BRCA1 and BRCA2. *Mol. Cancer Res.* 7, 1110–1118. doi: 10.1158/1541-7786.MCR-09-0123

Zhang, F., Ma, J., Wu, J., Ye, L., Cai, H., Xia, B., et al. (2009b). PALB2 links BRCA1 and BRCA2 in the DNA-damage response. *Curr. Biol.* 19, 524–529. doi: 10.1016/j.cub.2009.02.018

Zhang, J., Fujiwara, Y., Yamamoto, S., and Shibuya, H. (2019). A meiosis-specific BRCA2 binding protein recruits recombinases to DNA double-strand breaks to ensure homologous recombination. *Nat. Commun.* 10:722. doi: 10.1038/s41467-019-08676-2

Zhang, J., Gurusaran, M., Fujiwara, Y., Zhang, K., Echbarthi, M., Vorontsov, E., et al. (2020). The BRCA2-MEILB2-BRME1 complex governs meiotic recombination and impairs the mitotic BRCA2-RAD51 function in cancer cells. *Nat. Commun.* 11:2055. doi: 10.1038/s41467-020-15954-x

Zhu, Z., Chung, W. H., Shim, E. Y., Lee, S. E., and Ira, G. (2008). Sgs1 helicase and two nucleases Dna2 and Exo1 resect DNA double-strand break ends. *Cell* 134, 981–994. doi: 10.1016/j.cell.2008.08.037

Zickler, D., and Kleckner, N. (2015). Recombination, pairing, and synapsis of homologs during meiosis. *Cold Spring Harb. Perspect. Biol.* 7:a016626. doi: 10.1101/cshperspect.a016626

Zwettler, F. U., Spindler, M. C., Reinhard, S., Klein, T., Kurz, A., Benavente, R., et al. (2020). Tracking down the molecular architecture of the synaptonemal complex by expansion microscopy. *Nat. Commun.* 11:3222. doi: 10.1038/s41467-020-17017-7

Conflict of Interest: The authors declare that the research was conducted in the absence of any commercial or financial relationships that could be construed as a potential conflict of interest.

Copyright © 2021 Mhaskar, Koornneef, Zelensky, Houtsmuller and Baarends. This is an open-access article distributed under the terms of the Creative Commons Attribution License (CC BY). The use, distribution or reproduction in other forums is permitted, provided the original author(s) and the copyright owner(s) are credited and that the original publication in this journal is cited, in accordance with accepted academic practice. No use, distribution or reproduction is permitted which does not comply with these terms.

frontiers in Cell and Developmental Biology

ORIGINAL RESEARCH
published: 28 May 2021
doi: 10.3389/fcell.2021.687522

Echinoderm Microtubule Associated Protein Like 1 Is Indispensable for Oocyte Spindle Assembly and Meiotic Progression in Mice

*Hong Yin[1], Teng Zhang[1], Hao Wang[1], Xin Hu[1], Xuan Hou[1], Xianbao Fang[1], Yaoxue Yin[1], Hui Li[2], Lanying Shi[2] and You-Qiang Su[1,2,3,4]**

[1] State Key Laboratory of Reproductive Medicine, Nanjing Medical University, Nanjing, China, [2] Shandong Provincial Key Laboratory of Animal Cells and Developmental Biology, School of Life Sciences, Shandong University, Qingdao, China, [3] Women's Hospital of Nanjing Medical University, Nanjing Maternity and Child Health Hospital, Nanjing Medical University, Nanjing, China, [4] Collaborative Innovation Center of Genetics and Development, Fudan University, Shanghai, China

OPEN ACCESS

Edited by:
Wei Li,
State Key Laboratory of Stem Cell and Reproductive Biology, Institute of Zoology, Chinese Academy of Sciences (CAS), China

Reviewed by:
Shao-Chen Sun,
Nanjing Agricultural University, China
Koji Sugiura,
The University of Tokyo, Japan

***Correspondence:**
You-Qiang Su
youqiang.su@sdu.edu.cn

Specialty section:
This article was submitted to Cell Growth and Division, a section of the journal Frontiers in Cell and Developmental Biology

Received: *29 March 2021*
Accepted: *04 May 2021*
Published: *28 May 2021*

Citation:
Yin H, Zhang T, Wang H, Hu X, Hou X, Fang X, Yin Y, Li H, Shi L and Su Y-Q (2021) Echinoderm Microtubule Associated Protein Like 1 Is Indispensable for Oocyte Spindle Assembly and Meiotic Progression in Mice. Front. Cell Dev. Biol. 9:687522. doi: 10.3389/fcell.2021.687522

Completion of the first meiosis is an essential prerequisite for producing a functionally normal egg for fertilization and embryogenesis, but the precise mechanisms governing oocyte meiotic progression remains largely unclear. Here, we report that echinoderm microtubule associated protein (EMAP) like 1 (EML1), a member of the conserved EMAP family proteins, plays a crucial role in the control of oocyte meiotic progression in the mouse. Female mice carrying an ENU-induced nonsense mutation (c.1956T > A; p.Tyr652*) of *Eml1* are infertile, and the majority of their ovulated oocytes contain abnormal spindles and misaligned chromosomes. In accordance with the mutant oocyte phenotype, we find that EML1 is colocalized with spindle microtubules during the process of normal oocyte meiotic maturation, and knockdown (KD) of EML1 by specific morpholinos in the fully grown oocytes (FGOs) disrupts the integrity of spindles, and delays meiotic progression. Moreover, EML1-KD oocytes fail to progress to metaphase II (MII) stage after extrusion of the first polar body, but enter into interphase and form a pronucleus containing decondensed chromatins. Further analysis shows that EML1-KD impairs the recruitment of γ-tubulin and pericentrin to the spindle poles, as well as the attachment of kinetochores to microtubules and the proper inactivation of spindle assembly checkpoint at metaphase I (MI). The loss of EML1 also compromises the activation of maturation promoting factor around the time of oocyte resumption and completion of the first meiosis, which, when corrected by WEE1/2 inhibitor PD166285, efficiently rescues the phenotype of oocyte delay of meiotic resumption and inability of reaching MII. Through IP- mass spectrometry analysis, we identified that EML1 interacts with nuclear distribution gene C (NUDC), a critical mitotic regulator in somatic cells, and EML1-KD disrupts the specific localization of NUDC at oocyte spindles. Taken together, these data suggest that EML1 regulates acentrosomal spindle formation and the progression of meiosis to MII in mammalian oocytes, which is likely mediated by distinct mechanisms.

Keywords: EML1, oocyte, spindle, meiosis, CDK1, female fertility

INTRODUCTION

Completion of the first meiosis is an essential step toward producing a mature oocyte (commonly known as "egg") competent for fertilization and supporting preimplantation development. In oocytes of most mammalian species, meiosis stops at diplotene stage around birth, and keeps arrested at this stage until puberty and onward when the surge of preovulatory luteinizing hormone (LH) emerges. Under the stimulation of the LH signaling, meiosis in the fully grown oocyte (FGO) of preovulatory follicles reinitiates, which is manifested by the dissolution of the nuclear envelope and disappearance of the nucleolus, a process also commonly referred to as germinal vesicle breakdown (GVBD). After GVBD, meiosis enters a protracted prometaphase (Pro-MI), during which microtubules nucleate around the condensed chromosomes, and gradually assemble into the bipolar spindles at metaphase I (MI). MI to anaphase I (AI) transition takes place when stable attachment between the kinetochore and microtubule is established, and all homologous chromosomes are aligned at the spindle equator. Homologous chromosome separation starts at AI when the spindle moved to the cortex, and complete segregation is achieved following cytokinesis in telophase I (TI). Meiosis then proceeds to metaphase II (MII) without an intervening interphase in between. In the end, the oocyte first meiosis is completed by formation of a large egg and a small polar body with each of them containing the same number of chromosomes (Eppig et al., 2004; Conti and Franciosi, 2018).

Oocyte meiotic progression is a complex process controlled by sophisticated mechanisms. Central to this process are the correct assembly of bipolar spindles and the establishment of stable attachment between kinetochores and microtubules at MI. These are the key events that ensure the precise timing of meiotic progression and the fidelity of chromosome segregation (Vogt et al., 2008; Mullen et al., 2019). However, in oocytes of most mammalian species, centrosomes are lost during the early stage of oogenesis, and spindles are formed in the absence of centrioles (Szollosi et al., 1972; Manandhar et al., 2005; Schuh and Ellenberg, 2007). The oocyte specialized acentrosomal spindles are assembled with the aid of multiple microtubule organizing centers (MTOCs) containing essential pericentriolar materials (e.g., TUBG/γ-tubulin and PCNT/pericentrin) (Raynaud-Messina and Merdes, 2007; Baumann et al., 2017). This is in contrast to somatic cells and spermatocytes in which spindles are formed under the guidance of centrioles. In addition, unlike in mitotic cells where the sister chromatids are bi-oriented to the opposite spindles poles; in the oocytes, it is the paired homologous chromosomes held together by chiasmata in the bivalents that are bi-oriented at MI. Sister chromatids in the homologous chromosomes are mono-oriented to the same pole in oocytes, which ensures the separation of homologous chromosomes at AI/TI (Holt and Jones, 2009). Therefore, meiotic division in oocytes differs largely from that of spermatocytes and mitotic division in somatic cells, and the oocyte is deemed to use distinct mechanisms to control spindle morphogenesis and chromosome congression. However, these mechanisms remain largely undefined.

Nevertheless, three centrosome-independent pathways are reported to be involved in oocyte microtubule nucleation and spindle assembly: the Ras-like nuclear protein (Ran) GTP-dependent, kinetochore chromosome passenger complex (CPC)-dependent, and Augmin-dependent pathways (Bennabi et al., 2016). The former two pathways mediate the chromosome-based microtubule nucleation and assembly, while the latter pathway drives microtubule amplification through a microtubule-dependent microtubule nucleation mechanism. In the RanGTP pathway, RanGTP produced by the chromosome-bound Ran guanosine exchange factor RCC1 (regulator of chromosome condensation 1) forms a gradient around the chromosome. This RanGTP gradient promotes the release of Importin-bound spindle assembly factors, such as TPX2 and NuMA (Brunet et al., 2008; Kolano et al., 2012), and allow them to regulate oocyte spindle morphogenesis. Although the RanGTP pathway is initially found to be indispensable for only human oocyte spindle assembly (Holubcova et al., 2015), a recent study demonstrates that it is also crucial for mouse oocyte spindle formation (Drutovic et al., 2020). The CPC is composed of the Aurora B/C, INCENP (inner centromeric protein), Survin, and Borealin, which are localized at the kinetochore and are all crucial for the formation of normal bipolar spindles and meiotic progression in oocytes (Sharif et al., 2010; Sun et al., 2010; Jiang et al., 2014; Nguyen et al., 2018). Augmin is a hetero-octameric protein complex comprised of HAUS 1–8, which triggers new microtubule growth by recruiting γ-tubulin to pre-existing microtubules. Augmin is reported to be crucial for microtubule nucleation and bipolar spindle formation in *Xenopus* egg extracts and *Drosophila* oocytes (Petry et al., 2011; Colombie et al., 2013), but its function in mammalian oocytes remains largely unclear. Given the enormous size difference between somatic cells and oocytes (∼40 μm in diameter of Hela cells vs. 85 and 120 μm in diameter of mouse and human oocytes), these spatial restricted microtubule nucleation and assembly pathways are critical for the oocyte to manage the progression of meiosis within such a large volume. It is therefore not surprising that the oocyte adopt a meiosis-specific mechanism to regulate these pathways. Indeed, a conserved liquid-like meiotic spindle domain (LISD) is identified recently in mammalian oocytes that specifically regulate meiotic spindle assembly (So et al., 2019). This oocyte-specific LISD is formed by multiple microtubule regulatory factors (e.g., microtubule nucleation and stability regulator TACC3 and CHC17) through phase separation, disruption of which causes severe spindle assembly defects. Formation of such a LISD may be of particular advantage to the oocyte with such a large volume to enrich microtubule regulatory factors in local proximity to the spindle.

Fine-tuned interactions between factors that regulate microtubule dynamics and function are essential for oocyte spindle morphogenesis and chromosome segregation (Greaney et al., 2018; So et al., 2019). As a major type of microtubule regulatory factors, microtubule-associated proteins (MAPs) are frequently found to be expressed in oocytes and considered to play a crucial role in the control of oocyte acentriolar spindle assembly and meiotic progression (Han et al., 2010; Goodson and Jonasson, 2018). Interestingly, an ever-growing number of MAPs

has been identified in oocytes of several model organisms (Gache et al., 2010; Han et al., 2010). However, the identity of the MAPs that are critical for oocyte meiotic maturation and the extent to which these essential MAPs contribute to the regulation of oocyte spindle morphogenesis remain largely unclear. Nevertheless, a recent study in our laboratories indicated that the echinoderm microtubule associated protein (EMAP) like (EML) family proteins are probably such essential MAPs that are crucial for oocyte meiotic spindle formation and meiotic progression in the mouse (Yin et al., 2020).

EMLs are a highly conserved family of MAPs, with 6 members (*i.e.*, EML1-6) found in mammals (Suprenant et al., 2000). They are considered to be a unique and important class of MAPs owing to lower sequence homology with other commonly known MAPs. The founding member of this family protein, *i.e.*, EMAP, was initially discovered as the principal components of the microtubule cytoskeleton in sea urchin eggs and embryos in the early 1990s (Suprenant et al., 1993; Hamill et al., 1998). Since then, for quite a long time, the only common features recognized for this family of proteins had remained to be decorating spindles and regulating microtubule stability *in vitro* (Suprenant et al., 1993; Eichenmuller et al., 2002; Tegha-Dunghu et al., 2008; Kielar et al., 2014; Chen et al., 2015; Richards et al., 2015). Until recently, the physiological role of this family protein was starting to be appreciated, as the disease- and developmental disorder causing-mutations and deletions of the EML encoding genes were gradually discovered (De Keersmaecker et al., 2005; Lin et al., 2009; Sun et al., 2015). Of particularly, for instance, deletions or losses of function of EML1 in mouse, rat, and human cause subcortical heterotopia in the brain or disorganization of retina architecture in the eye, which is probably brought by defects in primary cilia formation, mitotic spindle length/positioning and proliferation of neuronal progenitors, and lamination of the inner retina (Eudy et al., 1997; Kielar et al., 2014; Bizzotto et al., 2017; Collins et al., 2019; Oegema et al., 2019; Uzquiano et al., 2019; Collin et al., 2020; Grosenbaugh et al., 2020). Unfortunately, these interesting new findings were all on somatic cells, the function of EMLs in oocytes remained virtually unknown. Nevertheless, we found recently that all the six members of EML family were expressed in the ovarian follicles although their abundance varies in the oocyte and granulosa cells. Knockdown of EML6, the mostly preferentially expressed EML protein by oocytes, impaired spindle integrity and the fidelity of chromosome segregation (Yin et al., 2020). Therefore, EMLs are crucial for the control of oocyte spindle morphogenesis and meiotic division. Here, as a continuation of our recent effort to unraveling the role of EMLs in mammalian oogenesis, we show that EML1, another member of the EML family, is also essential for oocyte maturation and female fertility by regulating oocyte spindle assembly and the progression of meiosis to MII via distinct mechanisms.

MATERIALS AND METHODS

Ethics Statement

All animal procedures and experiments were approved by the Ethical Committee of Laboratory Animals and the Animal Care and Use Committee of Nanjing Medical University (NJMU), and were carried out in accordance with the institutional guidelines of Animal Care and Use.

Animals

The ENU-induced *Eml1*^{tvrm360} point mutant mice were provided by Dr. Patsy Nishina at The Jackson Laboratory. These mice were imported to the investigator's colony at NJMU, and were maintained on identical C57BL/6J genetic background. Mice were genotyped by PCR using primers P1 (CCCATGACAACTGCATCTACATATGA), P2 (GCAATCGGCTGGCATGACAACTGCATCTACATGTAT) and P3 (GGTAAGTTTCTCTTGCCTTTCTGA), with P1 + P3 amplifying a 168-bp product specific to the mutant allele, and P2 + P3 amplifying a 178-bp wildtype allele. Normal wildtype ICR mice were purchased from the Animal Core Facility of Nanjing Medical University, while the C57BL/6JXDBA2 (B6D2) F1 mice were produced at the investigator's own colony.

Chemicals and Reagents

Unless otherwise specified, all chemicals and reagents were purchased from Sigma-Aldrich (United States). Antibodies used in this study include: rabbit polyclonal anti-EML1 (1:100, Proteintech, #12765-AP), rabbit polyclonal anti-EML4 (1:500, Cell Signaling Technology, #2428), rabbit polyclonal anti-Gamma Tubulin (1:200, Proteintech, #15176-AP), rabbit polyclonal anti-Pericentrin (1:200, Abcam, # ab4448), rabbit polyclonal anti-Phospho-cdc2 (Tyr15) (1:500, CST, #9111); rabbit monoclonal anti-BubR1(1:250, Abcam, #ab3305), rabbit polyclonal anti-tRFP/mKate (1:500, evrogen, #AB234), mouse monoclonal anti-Cyclin B1 (1:100, abcam, #ab72), mouse monoclonal anti-Cdk1/Cdk2 (1:100, Santa Cruz, #sc-53219), mouse monoclonal anti-NUDC (1:100, Santa Cruz, #sc-365782), human anti-Centromere (1:500, Antibodies Incorporated, #15-234), and Alexa flour 594/488-conjugated secondary antibodies (Thermo Fisher Scientific, United States). Rhodamine Phalloidin (1:750, #R415) and PD166285 (#3785) were purchased from Thermo Fisher Scientific and Tocris Bioscience, respectively.

Fertility Test

To assess the reproductive potential, 8-week-old wide type (WT) control (n = 3) and *Eml1*^{tvrm360} mutant (n = 3) female mice were mated with normal adult B6D2F1 males at the ratio of 1:1. Although most of the *Eml1*^{tvrm360} mutant mice died at about 4 months of age, mating pairs were continuously caged together for a period of 2 months. The number of pups for each litter was recorded at birth, and the average accumulating number of pups per female was calculated at the end of the fertility test.

Oocyte Isolation and Culture

Fully grown oocytes (FGOs) were isolated from large antral follicles of 22-days old female mice that were initially primed with equine chorionic gonadotropin (eCG, Ningbo Second Hormone Factory) for 46 h, and were matured in culture as described previously (Yin et al., 2020). The medium used for

oocyte collection and culture was bicarbonate-buffered minimum essential medium with Earle's salts (Thermo Fisher Scientific) supplemented with 75 μg/ml penicillin G, 50 μg/ml streptomycin sulfate, 0.23 mM pyruvate, and 3 mg/ml bovine serum albumin (BSA). Oocyte culture was carried out at 37°C in an Eppendorf NewBrunswick Galaxy170R incubator (Hamburg) infused with 5% O_2, 5% CO_2 and 90% N_2. During the culture, resumption and completion of the first meiosis were assessed by scoring the oocytes that have undergone germinal vesicle breakdown (GVB) and first polar body (PB1) extrusion, respectively. To study the subcellular localization of EML1 in oocytes during meiotic maturation, oocytes were collected at the individual timepoint of 0, 4, 6, 8, 10, and 14 h that corresponds to the meiotic stages of GV, Pro Metaphase I (Pro-M I), M I, Anaphase I (A I), Telophase I (T I), and Metaphase II (M II), respectively, and processed for immunofluorescence (IF) analysis. For Western Blot analysis of EML1 at GV, M I and M II stages, oocyte samples were collected at 0, 6 and 14 h respectively.

To examine the meiotic status of the ovulated oocytes, 7 weeks old WT and *Eml1*^{tvrm360} mutant female mice were subjected to a standard superovulation regimen as described previously and the oocytes were collected from the ampulla of oviducts 14 h after human chorionic gonadotropin (hCG) injection (Li et al., 2020).

Cloning and Expression of *Eml1* and *Nudc*

Mouse *Eml1* and *Nudc* ORF were amplified by PCR using the cDNA derived from the normal WT GV-stage oocytes, and cloned into the pCMV6-AC-3DDK and pCMV6-AN-mkate vector (Origene), respectively. Ectopic expression of the EML1-3DDK and NUDC-mKate fusion proteins in HEK293T cells was then achieved by transfection with 10 μg of the plasmid DNA using the Megatran1.0 (Origene) transfection reagent. Successful expression of the fusion protein was confirmed by either IF staining or WB analysis using the anti- FLAG (DDK) or tRFP (mKate) antibody.

Microinjection of *Eml1*-MO and *Eml1*-3DDK mRNA

Morpholino oligomers for EML1 (EML1-MO, 5′-TAG CTGGAGAAGCCGTCCTCCATGC-3′) and the Standard Control (Control-MO, 5′-CCTCTTACCTCAGTTACAATTT ATA-3′) were purchased from Gene Tools, LLC, and were dissolved in sterile water to a final concentration of 2 mM. *Eml1*-3DDK mRNA was synthesized as described previously (Guo et al., 2018), and diluted to a final concentration of 500 ng/μl for microinjection. Approximately 10 pl of MOs or mRNA was microinjected into the cytoplasm of one normal WT- FGO that was plating in the M2 medium containing 10% FBS. After microinjection, the oocytes were first maintained at GV-stage by incubation in 5 μM milrinone-containing medium for 20 h and 12 h, respectively, in order to let the MOs and mRNA fully function. The oocytes were then released from the milrinone medium, and cultured in maturation medium for up to 14 h.

Assessment of Oocyte Microtubule Dynamics and Kinetochore-Microtubule Attachments

To investigate whether the subcellular localization of EML1 is dependent on the stability of microtubules, M I oocytes were treated with reagents that interfere with microtubule stability at 37°C, i.e., 20 mg/ml of Nocodazole for 10-15 min and 10 mM of Taxol (Selleck, #S1150) for 45 min, respectively, and the localization of EML1 was then examined by IF analysis. MI oocytes that were treated with the same concentration of DMSO under the same culture conditions served as Controls. To assess kinetochore-microtubule attachment, M I oocytes were subjected to cold treatment on ice for about 10 min, and then immediately fixed in 4% PFA for 30 min at room temperature. These oocytes were subsequently stained by IF for kinetochores and microtubules as described previously (Li et al., 2020).

Immunofluorescence Analysis

Oocytes were fixed in 4% PFA in PBS for 30 min at room temperature, or subjected to treatment in PHEM buffer (60 mM PIPES, 25 mM HEPES, 10 mM EGTA and 2 mM MgCl2, pH 6.9) containing 1% (v/v) Triton X-100 for 10 min before fixation, followed by permeabilization and blocking for 1 h in PBS containing 0.1% Triton X-100 and 10% fetal bovine serum (FBS). The samples were subsequently incubated with primary antibodies (4°C, overnight) and Alexa flour 594/488-conjugated secondary antibodies (room temperature, 1 h), respectively, according to experimental design, and counterstained with Hoechst 33342 for 10 min to label chromosomes. All images were taken under a LSM710 META confocal laser-scanning microscope (Zeiss) with the same settings. Data analysis was performed using ZEN 2.6 (blue edtion) LSM and ImageJ software (National Institutes of Health, United States) under the same processing parameters.

Western Blot Analysis

Western Blot (WB) analysis was performed as described previously (Guo et al., 2018). Briefly, oocyte samples were lysed in 2 × Laemmli sample buffer, and heated at 108°C for 5 min to be denatured. The proteins were separated by SDS-PAGE and transferred onto polyvinylidene difluoride (PVDF) membranes for probing the proteins under examination. The expression of β-actin (ACTB) served as internal control of each sample. Quantification of the intensity of the protein band of interest detected by WB was accomplished using Image J software according to the instructions provided by the manufacturer.

Co-immunoprecipitation and Mass Spectrometry

HEK293T cells transfected with *Eml1*-3DDK and *Nudc*-mKate plasmid DNAs were harvested and lysed using the lysis buffer that comes with the Pierce^{TM} Crosslink Immunoprecipitation Kit (Thermo Fisher Scientific, #26147). Immunoprecipitation (IP) was then carried out on these cell lysates using the anti-FLAG (DDK) M2 and anti-tRFP/mKate antibodies, respectively. The IP products were then subjected to WB validation followed by

Mass Spectrometry analysis. For Mass Spectrometry analysis, the IP products from two independent experiments were resolved simultaneously on 10% SDS-PAGE and visualized with Coomassie blue. The lanes corresponding to each IP product were sliced out and sent to the proteomics core facility of the Institute of Biomedical Sciences at Fudan University (Shanghai, China) for Mass Spectrometry analysis.

Mass Spectrometry analysis was carried out using the same exact protocols as detailed in the previous studies (Zhang et al., 2007; Wu et al., 2018). Briefly, the gel slices were cut into 1 mm^3 particles, destained, reduced, and alkylated, followed by the overnight Trypsin in-gel digestion at 37°C. LC-ESI-MS/MS analysis was performed using a nanoflow EASY-nLC 1000 system (Thermo Fisher Scientific, Odense, Denmark) coupled to an LTQ Orbitrap Elite mass spectrometer (Thermo Fisher Scientific Bremen, Germany). The raw data were analyzed by Proteome Discoverer (version 1.4, Thermo Fisher Scientific) using an in-house Mascot Server (version 2.3, Matrix Science, London, United Kingdom) (Perkins et al., 1999). Human database (20160213, 20,186 sequences) was downloaded from UniProt. Data were searched using the following parameters: trypsin/P as the enzyme; up to two missed cleavage sites were allowed; 10 ppm mass tolerance for MS and 0.05 Da for MS/MS fragment ions; propionamidation on cysteine as fixed modification; oxidation on methionine as variable modification. The incorporated Target Decoy PSM Validator in Proteome Discoverer and the Mascot expectation value was used to validate the search results and only the hits with FDR $\leq$ 0.01 and MASCOT expected value $\leq$ 0.05 were accepted for discussion.

Statistical Analysis

Statistical analysis was performed using GraphPad Prism 7.0 software (GraphPad Software, Inc, United States). Student's *t*-test was conducted to compare differences between two groups. $P < 0.05$ was defined to be significantly different. Data presented are presented as Mean ± SEM of at least three independent experiments.

RESULTS

Forward Genetics Identified EML1 as an Essential Regulator of Oocyte Meiotic Progression and Female Fertility in Mice

The *Eml1*^{tvrm360} mutant mice were created by the ENU-induced mutagenesis in the Translational Vision Research Model (TVRM) program led by Dr. Patsy Nishina at The Jackson Laboratory. This ENU-induced mutant allele bears a nonsense point mutation (c.1956T > A; pTyr652*) of *Eml1*, which creates a premature stop codon after pTyr652*, and leads to the nonsense-mediated decay of *Eml1* mRNA (Collin et al., 2020). Therefore, these mutant mice present a nice model for addressing the role of EML1 in the regulation of oocyte meiotic progression and female fertility. Consistent with the reported low postnatal viability, we found that the *Eml1*^{tvrm360} mutant females are extremely small in size (6.55 ± 0.60g), with the body weight only about half of the wild type (WT) littermates (11.44 ± 0.59g, $P < 0.01$) at the age of 3 weeks. For those mutant females that survived to 7 weeks and beyond (14.68 ± 0.70g), the difference from the WT (18.04 ± 0.57g, $P < 0.01$) in body weight was significantly minimized (**Figure 1A**).

Using these precious 7-week and plus old mutant female mice, we analyzed the phenotypes of the oocytes and female fertility. We found that the *Eml1*^{tvrm360} mutant mice could ovulate following a standard superovulation regimen, *i.e.*, injection with 5IU/mouse eCG followed 5IU/mouse hCG within a 48-h interval. The ovulated cumulus-oocyte complexes (COC) appeared normal, with the well expanded cumulus oophori surrounding the mature oocytes (**Figure 1B**). Although most of the *Eml1*^{tvrm360} mutant mice died at about 4 months of age, fertility test by mating with normal B6D2F1 males indicated that the *Eml1*^{tvrm360} mutant females did not produce any pups or have any signs of pregnancy during the entire period of testing when they were still alive. In contrast, the female WT littermates of the *Eml1*^{tvrm360} mutants produced normally in the same period with an average of 7.5 pups/litter (**Figure 1C**). Whole mount immunofluorescene (IF) analysis of the spindle morphology and chromosome configuration indicated that near 60% (57.8 ± 7.25%, $P < 0.01$) of the oocytes ovulated by *Eml1*^{tvrm360} mutant females was abnormal. They displayed various abnormalities including partial or complete depolymerization of the microtubules and incomplete cytokinesis coupled with chromosome misalignment or failure of segregation (**Figure 1D**).

Stable Expression and Subcellular Colocalization of EML1 With Meiotic Spindles in Oocytes During Meiotic Division

The spindle and chromosome defects observed in the *Eml1*^{tvrm360} mutant oocytes suggest that EML1 may have specific subcellular localization during the process of meiotic division. We therefore examined the expression and subcellular localization of EML1 protein in mouse oocytes. As shown in **Figure 2A**, western blotting (WB) analysis showed that EML1 protein is expressed in the fully grown oocytes (FGO), and is maintained at stable levels during the process of meiotic progression. No apparent changes were observed among the immature germinal vesicle (GV), maturing metaphase I (MI), and matured MII stages oocytes. To investigate the subcellular distribution of EML1, whole mount IF was carried out on oocytes at various stages of meiotic division (**Figure 2B**). In the immature GV-stage oocyte, EML1 was ubiquitously distributed in the cytoplasm with no specific localization was observed. After the resumption of meiosis, EML1 was found to be colocalized with the nucleated microtubules, and enriched exclusively on the meiotic spindles at MI, anaphase/telophase I (AI/TI), and MII stages.

To test whether the specialized localization of EML1 within the maturing oocytes is dependent upon the integrity of the meiotic spindles, oocytes at MI stage were treated with either the microtubule depolymerization reagent, nocodazole,

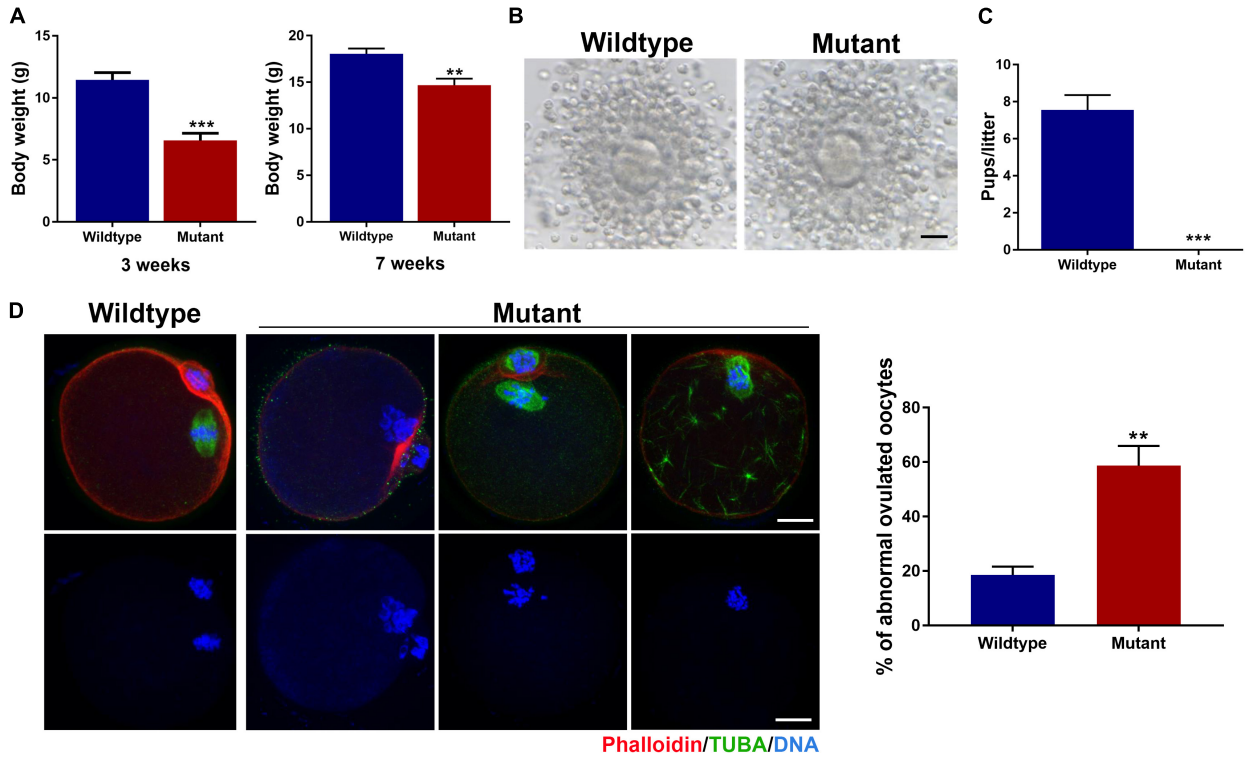

FIGURE 1 | Growth and fertility defects in female mice carrying the ENU-induced nonsense mutation of *Eml1*. **(A)** Comparison of body weight between wildtype and *Eml1*-mutant (Mutant) female mice at the age of 3 and 7 weeks. **(B)** Microphotographs showing the ovulated cumulus-oocyte complexes by Wildtype and Mutant females. Scale bars indicate 10 μm. **(C)** Fecundity (pups/litter) of WT (n = 3) and Mutant (n = 3) female mice during the 2 month fertility test period. ***$P < 0.005$, compared with the Wildtype. **(D)** Assessment of spindle morphology and chromosome alignment in the Wildtype and Mutant ovulated oocytes. The left panel shows the representative micrographs of the IF stained oocytes. Spindles are stained in green, chromosomes and F-actins are stained in blue and red, respectively. Scale bars indicate 20 μm. The right bar graph shows the percentage of the oocytes with abnormal spindles and/or misaligned chromosomes. **$P < 0.05$, compared with the Wildtype.

or microtubule stabilizer, Taxol, and the localization of EML1 was then examined. As indicated by **Figure 2C**, under the treatment with Nocodazole, oocyte spindles were shrinked and disappeared gradually, so did the specific localization of EML1 on the spindles. In contrast, taxol treatment stabilized the spindles, and accordingly, EML1 was persistently stayed on the enlarged meiotic spindles.

In order to verify whether the staining patterns by the EML1 antibody in oocytes were specific to EML1 protein, we microinjected the mRNA encoding C-terminal tagged EML1-3DDK fusion protein into oocytes and examined its expression and localization using the DDK antibody. Prior to this experiment, we first validated that *Eml1*-3DDK was correctly cloned and expressed using the HEK293 cell line. As shown in **Supplementary Figure 1**, WB analysis of the lysate from cells transfected with *Eml1*-3DDK plasmid DNA detected the expression of the fusion protein; while IF staining with the DDK antibody indicated that the fusion protein was localized on the mitotic spindles. In the oocytes that were injected with the *Eml1*-3DDK mRNA, IF staining with DDK antibody revealed the same specific localization pattern of EML1-3DDK with that directly detected by the EML1 antibody (**Supplementary Figure 2**).

Knockdown of *EML1* in Oocytes Causes the Delay of Oocyte Resumption and Completion of the First Meiosis

Because the severe rarity of obtaining sufficient number of viable *Eml1*^{tvrm360} mutant mice for experimentation, we turned to use the *in vitro* knockdown approaches to investigate the role of EML1 in the regulation of oocyte meiotic maturation. We knocked down the expression of EML1 in FGOs of normal WT females with the specific ATG-morpholino oligos (MO) that block translation (see **Figure 3A** for the illustration of the experimental design). WB analysis indicated that 22 h after microinjection, the levels of EML1 protein in the oocytes receiving EML1-MO were reduced by 57.1 ± 0.44%, which was significantly lower than the control group ($P < 0.05$; **Figure 3B**). When these injected oocytes were released from milrinone medium to undergo *in vitro* maturation (IVM), there was a significant delay in the kinetics of both the resumption and completion of the first meiosis, as indicated by germinal vesicle breakdown (GVBD) and extrusion of the first polar body (PBE) (**Figure 3C**). GVBD took place between 30-60 min after the initiation of IVM, and completed by 90-120 min (99.17 ± 0.83%) in the control group that receiving

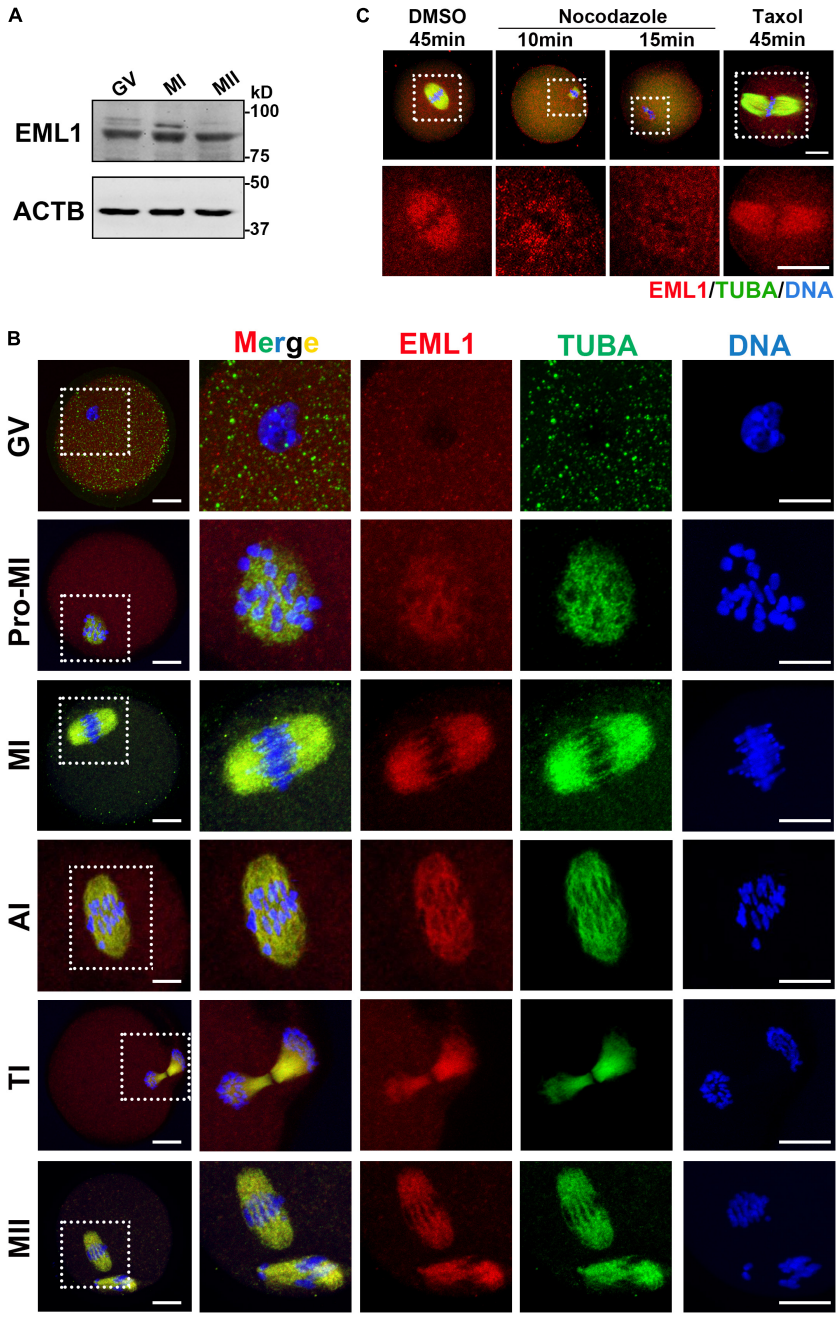

FIGURE 2 | Stable expression and specific localization of EML1 in mouse oocyte during meiotic progression. **(A)** Western Blot (WB) analysis of the expression of EML1 and ACTB (internal control) protein in oocytes at different stages of maturation. Lysate of 200 oocytes that were collected at 0, 8, and 14 h of IVM corresponding to GV-, MI-, and MII- stage, respectively, was load in each lane. **(B)** Confocal micrographs showing the dynamic co-localization of EML1 protein with meiotic spindles in oocytes at various stages (i.e., GV, Pro-MI, MI, AI, TI, and MII) of maturation. EML1 and α-tubulin were stained in red and green, respectively, while chromosomes were stained in blue. The far left panel shows the whole-oocyte view of the staining. The magnified view of the boxed area within the oocyte at each stage is listed on the right side. Scale Bar = 20 μm. **(C)** Confocal micrographs demonstrating the changes of localization of EML1 and tubulin in MI- stage oocytes treated with microtubule-interfering drugs. MI- oocytes were treated with 20 μg/ml nocodazole for 10 and 15 min, respectively, or with 10 μM Taxol for 45 min, and then processed for IF analysis of EML1 and α-tubulin localization. EML1, α-tubulin, and chromosomes are shown in red, green, and blue, respectively. The first row indicates the whole-oocyte view of the staining. The magnified view of the boxed area within the oocyte is shown in the second row. Scale Bar = 20 μm.

control morpholino (Conrol-MO). However, in the EML1-MO group, GVB wouldn't occur until 60-90 min after IVM, and at all the time points been examined, the rate of GVB was much lower than that of the control groups. Moreover, for those oocytes that have already undergone GVB, PBE was also delayed in the EML1-MO group, with the rate at 7-11 h after GVBD being significantly lower than that in the controls.

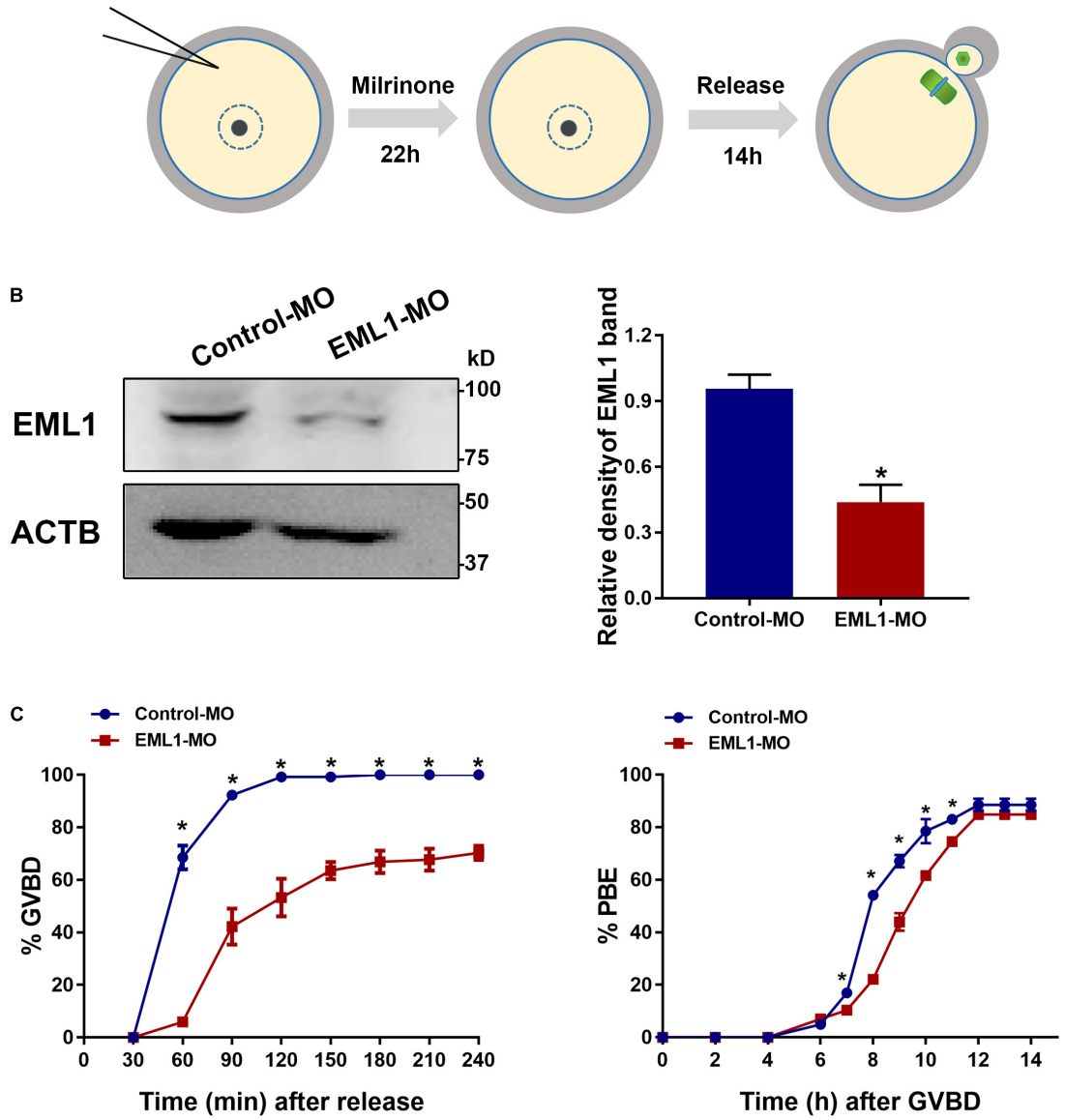

FIGURE 3 | Knockdown of EML1 expression in oocytes causes the delay of meiotic progression. **(A)** Schematic illustration of the experimental design for examining the effect of EML1 knockdown on oocyte meiotic maturation. **(B)** WB analysis of the efficiency of knocking down EML1 in oocytes by EML1-morpholino oligos (MO). Lysate from 200 oocytes was loaded in each lane. ACTB serves as internal control. Representative gel image is shown in the left panel, whereas quantification of the WB result is shown in the right panel. *$P < 0.05$, compared with the Control-MO. **(C)** Effect of knockdown of EML1 in oocytes on the kinetics of GVB (left graph) and PBE (right graph). *$P < 0.05$, compared with the EML1-MO groups.

EML1 Depletion Impairs Spindle Assembly and Chromosome Alignment in MI Oocytes

The formation of bipolar spindles and correct congression of chromosomes at MI stage is critical for normal progression and completion of the first meiosis. The significant delay of oocyte PBE after EML1 knockdown prompted us to assess whether spindle assembly and chromosome alignment were impaired in these oocytes. IF staining of α-tubulins in oocytes that have undergone IVM for 8 h revealed that 88.93 ± 3.07% of the oocytes in the control group formed normal appearing MI spindles with the homologous chromosomes all nicely aligned at the equator. However, in the EML1-MO treated group, only 34.73 ± 10.16% of them had normal spindles with well aligned chromosomes. In the rest of the EML1-MO treated oocytes, the spindles were either stunted in size or deformed with the spindle pole area extremely flat and some of the misaligned chromosomes stretched-out

far away from the spindle equator (**Figure 4A**). This spindle and chromosome defect was further characterized by careful measurements of the length and width of the spindles, as well as the distance between the bivalents that fall farest apart, defined as "chromosome displacement." These geometric measurements demonstrated that both the length and width of the spindles were reduced, while the chromosome displacement was significantly increased, in the EML1-knockdown oocytes (**Figures 4B,C**).

EML1 Knockdown Disrupted the Normal Assembly of Microtubule Organization Center (MTOC) Onto the Spindle Pole

Since the most typical phenotypes of EML1-delepted MI oocytes were small spindle and aberrant spindle pole, we speculated that the absence of EML1 may interrupt the normal function of MTOC in oocytes during meiotic progression. We hence examined the effect of EML1 knockdown on the intracellular distribution of the key MTOC components, *i.e.*, γ-tubulin and pericentrin, in oocytes. Consistent with previous reports by others, IF analysis showed that γ-tubulin was positively stained on the MI-spindle in the control oocytes, with prominent punctate foci concentrating at the spindle poles; while the staining pattern of pericentrin was more unique, with crescent- or horseshoe-shaped discrete foci detected exclusively at the spindle pole region. After the oocytes were treated with EML1-MO, the discrete foci of γ-tubulin staining at the spindle pole area was lost, and a more diffused distribution on the entire spindle area was formed (**Figure 5A**). The spindle pole area restricted pattern of localization for pericentrin was also disrupted by EML1-knockdown, with the positive foci either scattered around the pole area or diffused onto the body of the spindle (**Figure 5B**). This happened in 61.9 ± 8.60% of the EML1-MO treated MI-stage oocytes (**Figure 5C**).

EML1 Depletion Interfered With the Attachment of Kinetochore to Microtubules and the Checkpoint of Spindle Assembly

The preceding observations of the delayed PBE and defects in spindle assembly and chromosome alignment in EML1-knocked down oocytes indicates that the kinetochore-microtubule (K-M) attachment and the spindle assembly checkpoint are probably also compromised in these oocytes. Indeed, we observed that the rate of kinetochores forming stable "end-on" type of attachment with spindle microtubules was reduced (Control-MO 95.36 ± 1.15% vs. EML1-MO 88.82 ± 1.92%, $P < 0.01$), while that having no microtubule attached was increased in EML1-MO treated oocytes (Control-MO 3.47 ± 0.76% vs. EML1-MO 8.27 ± 1.41%, $P < 0.01$) after cold treatment (**Figure 6A**). Also, IF staining of BubR1 on kinetochore revealed the aberrant inactivation of SAC in MI-stage EML1-knockdown oocytes. There were more oocytes stained positively by BubR1 antibody at the kinetochore region following EML1-MO treatment (Control-MO 23.62 ± 0.69% vs. EML1-MO 58.63 ± 2.04%, $P < 0.01$; **Figure 6B**).

EML1-Deficiency Caused Spontaneous Formation of Pronucleus in Matured Oocytes After the First Meiotic Division

Oocytes that were injected with EML1-MO extruded PB1 as normally as those receiving the Control-MO injection. However, almost all of the EML1 knocked down oocytes that have extruded PB1 contained a visible pronucleus (**Figure 7A**). IF staining revealed that 83.25 ± 3.34% of the EML1 knocked oocytes did not form the MII spindle after the first meiotic division, they instead entered interphase with the DNA completely de-condensed and the resulting secondary oocyte and the PB1 still connected by the central spindle (**Figure 7B**).

Depletion of EML1 Compromised the Expression of CCNB1 and Phosphorylation of CDK1 in Oocytes

Given the indispensable role of MPF in the control of oocyte meiotic resumption and progression, we tested the possibility whether depletion of EML1 affects the activation of MPF. Because MPF activity is determined by the steady-state levels of its regulatory subunit CCNB1 and the phosphorylation status of its catalytic subunit CDK1, we measured the levels of CCNB1 and the phosphorylated form of CDK1 by Western blot analysis. As shown in **Figures 8A,B**, after the oocytes were microinjected with EML1-MO and further cultured in milrinone-supplemented medium for 24 h, the levels of CCNB1 were slightly reduced (12.15 ± 0.08%, $P < 0.05$), while those of pY15-CDK1, the inactive form of CDK1, were increased (18.31 ± 0.09%, $P < 0.05$). When the oocytes were released from the milrinone medium and subjected for *in vitro* maturation, the differences between the control-MO and EML1-MO treated oocytes in the levels of CCNB1 (37.41 ± 0.15%, $P < 0.05$) and pY15-CDK1 (52.55 ± 0.09%, $P < 0.05$) became larger. Near complete dephosphorylation of pY15-CDK1 occurred concurrently with GVBD in the control oocytes, whereas in the EML1-MO group, this was significantly delayed. At the time (12 h after GVBD) when PB1 was normally extruded, pY15-CDK1 remained undetectable while CCNB1 stayed at a relatively high level in the control oocytes. However, in the EML1-MO treated oocytes, the levels of CCNB1 were still lower (0.8088 ± 0.01706 in the control vs 0.3803 ± 0.01874 in the EML1-MO, $P < 0.05$), while those of pY15-CDK1 were bounced back staying at a level higher than the control's (2.018 ± 0.1465 fold of the control group, $P < 0.05$) (**Figures 8C,D**).

Inhibition of WEE1/2 Kinases Partially Rescued the Defects of Meiotic Progression in EML1-MO Treated Oocytes

Results of the preceding experiments suggest that lower levels of MPF activity is probably the major causes of the meiotic defects observed in EML1-MO treated oocytes. We therefore tested this possibility by treating the EML1-knockdown oocytes with PD166285, a small molecule compound proven to be a

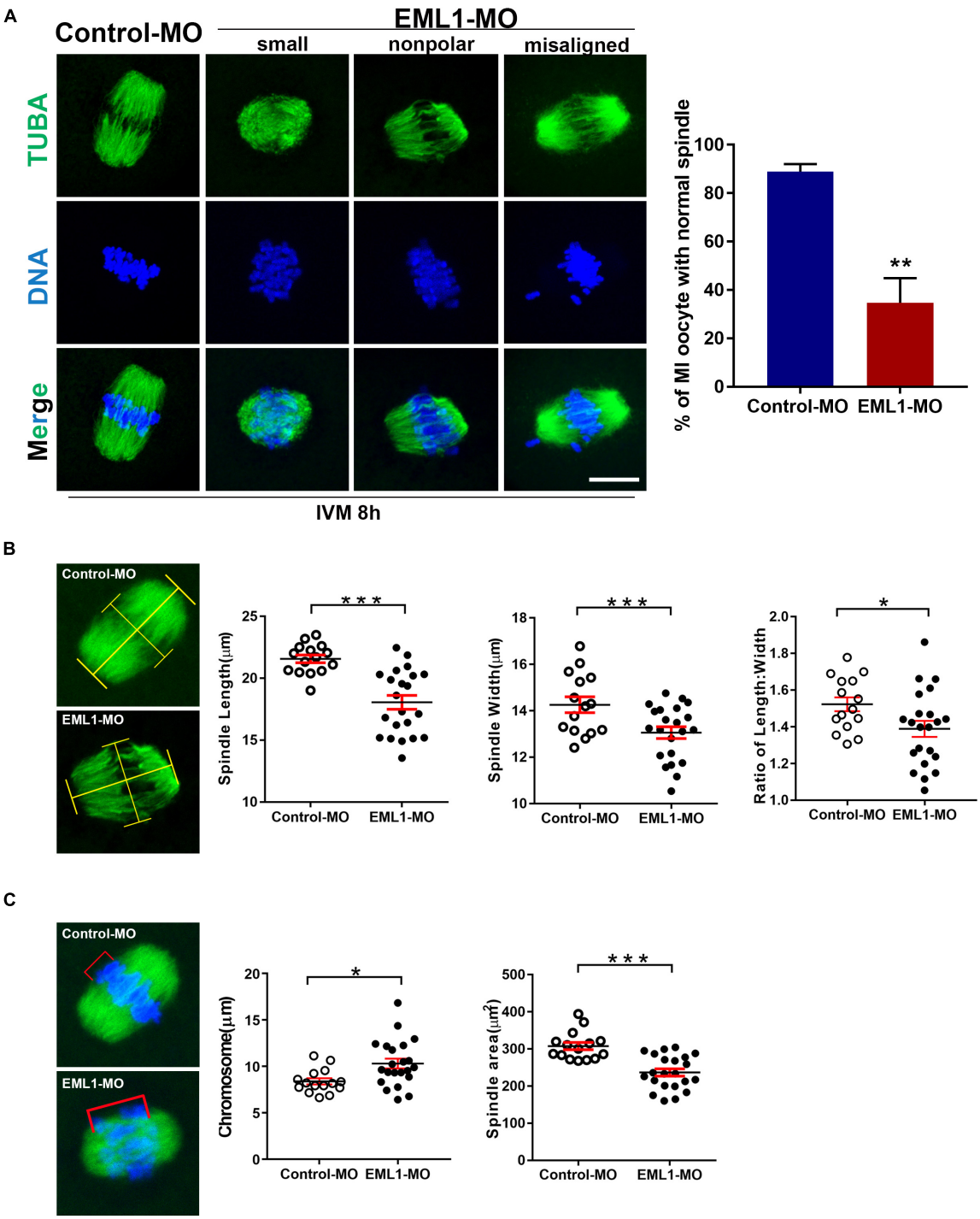

FIGURE 4 | Knockdown of EML1 in oocytes impairs MI- spindle assembly and chromosome alignment. **(A)** Oocytes microinjected with the MOs were first maintained at GV-stage in milrinone-containing for 24 h, and then transferred to milrinone-free medium for IVM. After 8-h IVM, the oocytes were subjected to IF staining of spindles and chromosomes. The left panel is the representative micrographs of the IF staining, with the α-tubulin and chromosomes stained in green and blue, respectively. Arrows point to misaligned chromosomes. Scale Bar = 20 μm. The right bar graph shows the quantification of the percentage of the oocyte with normal spindles as revealed by the IF analysis. $^{**}P < 0.01$, compared with the Control-MO group. **(B)** Geometric analysis of the MI- spindles in oocytes that were treated with Control-MO and EML1-MO and EML1-MO. Spindle (stained in green) length and width were measured as illustrated in the left micrographs, and plotted into dot graphs as shown in the right panels. $^{*}P < 0.05$, $^{***}P < 0.005$. **(C)** Geometric analysis of chromosome alignment in MI- oocytes that were treated with Control-MO and EML1-MO. Chromosome displacement was measured according to the illustration in the left panel, and the quantification was shown in the right graph. The spindle was shown in green and chromosomes in blue. $^{*}P < 0.05$, $^{***}P < 0.005$.

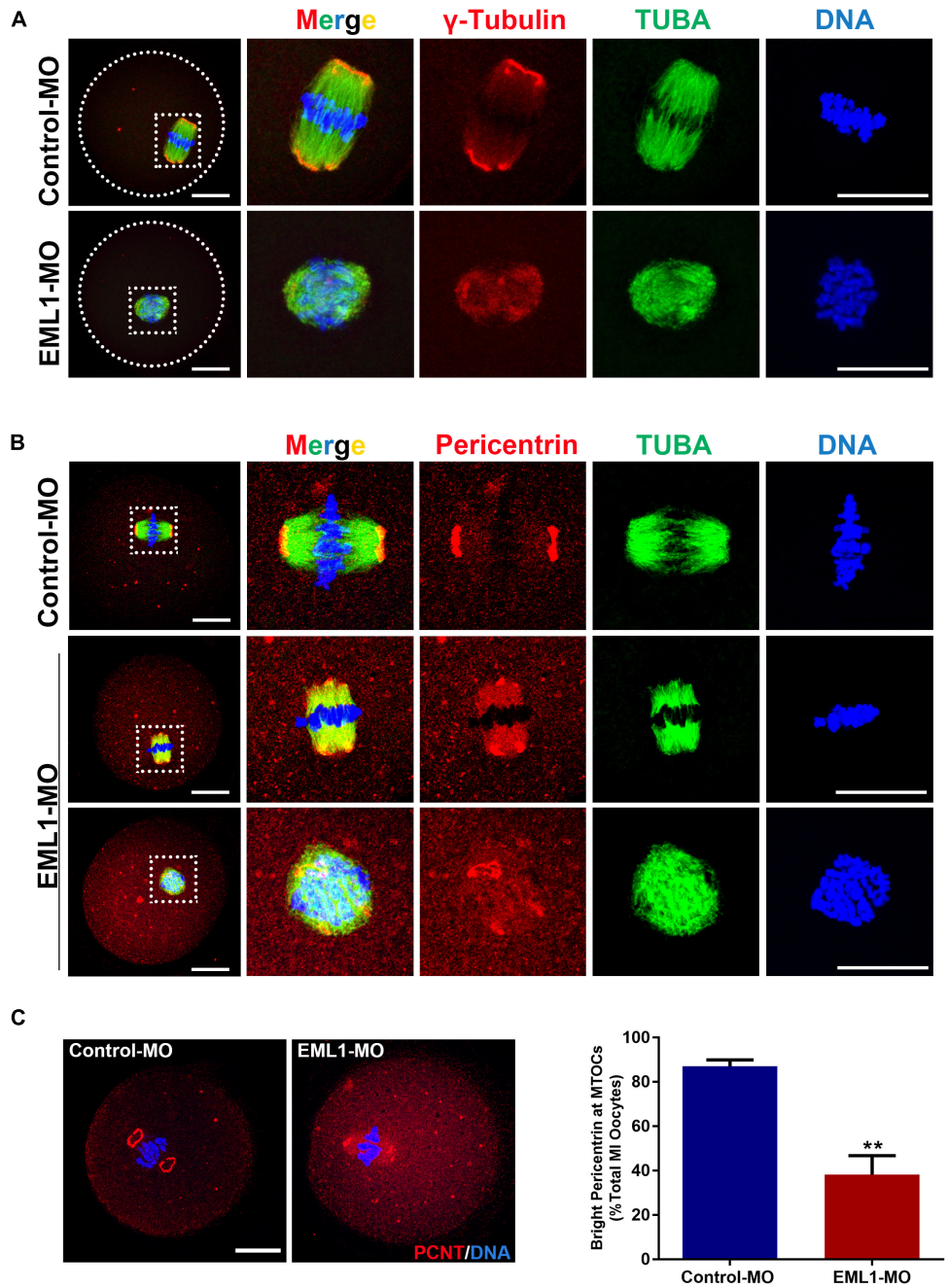

FIGURE 5 | Knockdown of EML1 in oocytes disrupts the normal localization of a MTOC-associated proteins to the spindle pole. **(A)** Representative images of MO-injected oocytes labeled with anti-γ-Tubulin (red) and anti-α-Tubulin (green). DNA was counterstained with Hochest 33342 (blue). **(B)**. Representative images of MO-injected oocytes labeled with anti-Pericentrin (red) and anti-α-Tubulin (green). DNA was counterstained with Hochest 33342 (blue). In both **(A,B)**, the far left panel indicate the whole-oocyte view of the staining. The magnified images of the boxed areas within the oocyte are listed on the right side. Scale Bar = 20 μm. **(C)** Quantification of the percentage of oocytes with correct spindle pole Pericentrin (PCNT). $^{**}P < 0.01$, compared with the Control-MO group.

specific inhibitor of WEE1 and 2 kinases, and shown to be able to activate MPF in mouse oocytes (Adhikari et al., 2014; Hanna et al., 2019). The result showed that treatment with 10 μM PD166285 effectively prevented the delay of GVBD in EML1-MO treated oocytes (**Figure 9A**). More interestingly, PD166285 even promoted the resumption of meiosis in EML1-knocked down oocytes, with the rate of GVBD already reaching 89.02 ± 4.17% within 1 h of IVM, which is significantly higher than that in the controls. Western blot analysis revealed that PD166285 treatment did not affect the expression of CCNB1

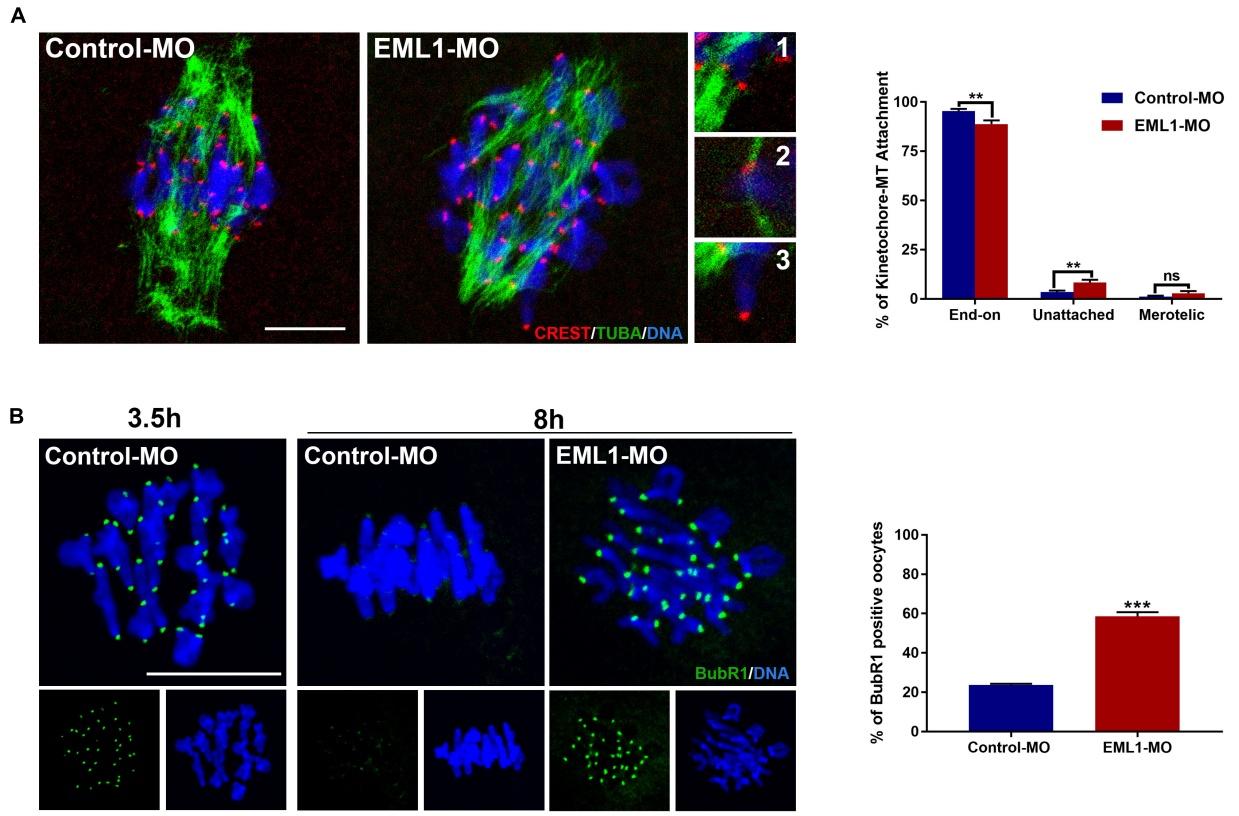

FIGURE 6 | Increased kinetochore-microtubule attachment error and abnormal activation of spindle assembly checkpoint in EML1-Knocked down MI-stage oocytes. **(A)** Assessment of kinetochore–microtubule attachments in MO-injected oocytes that were matured *in vitro* for 8 h by IF staining. Microtubules, kinetochores, and chromosomes were stained in green, red, and blue, respectively. Representative images of end-on (1), unattached (2), and merotelic (3) attachments are shown. A total of 349 and 247 attachments were assessed, respectively, in the Control-MO and EML1-MO treated oocytes. $^{**}P < 0.01$, ns denotes no significant difference. compared with the Control-MO and EML1-MO group. **(B)** Assessment of the activation of SAC in MO-injected oocytes that were matured *in vitro* for 8 h by IF staining of BubR1. Oocytes that were normally matured *in vitro* for 3.5 h served as positive control. BubR1 and chromosomes are stained in green and blue, respectively. $^{***}P < 0.005$, compared with the EML1-MO group.

and CDK1, but dramatically reduced the levels of pY15-CDK1 in EML1-knocked down oocytes at the end of 14 h- IVM (**Figure 9B**). Coincidently, treating the EML1-knocked down oocytes with PD166285 at the beginning of IVM when the oocytes were still at GV stage, or 14 h after IVM when the oocytes already formed PN, effectively drove meiosis in these oocytes to progress to MII by the end of 20 h culture (**Figures 9C,D**). However, IF staining demonstrated that few of these PD166285 treated oocytes formed normal MII spindles with the chromosomes well aligned on the spindle equator (**Figures 9C,E**).

Interaction and Co-localization of EML1 With NUDC

To unravel the molecular mechanism of EML1 function, immunoprecipitation (IP) of EML1 protein followed by mass spectrometry (MS) analysis was carried to identify the potential interacting partners of EML1 using HEK293 cells expressing 3DDK tagged EML1. This resulted in the identification of a total of 514 proteins that were presumably partners of EML1 (Table S1). Gene enrichment analysis revealed that these proteins are mainly involved in "processes of RNA or mRNA metabolism/splicing/localization," "composition of cytoplasmic ribosomal subunit and CDC5L complex," and "protein folding and translation" (**Figure 10A**). Further mining of the protein list revealed that in addition to the proteins commonly known to be involved in the regulation of cytoskeleton dynamics, *i.e.*, tubulin protein TUBA1, TUBB, TUBB2, and TUBB4, actin polymerizion regulator ARPC3, ARPC4, and CDC42, as well as other members of the EML family (*i.e.*, EML2 and EML4), EML1 also interacts with NUDC (nuclear distribution C), an evolutionarily conserved *Nudc* gene product essential for cell division (Fu et al., 2016; **Figure 10B**). NUDC was recently reported to be highly expressed in mouse oocytes, and was suggested to be involved in the regulation of oocyte development (Cao et al., 2020). We therefore validated the interaction of EML1 with NUDC, and examined the potential co-localization of these two proteins in oocytes. The result of Co-IP experiment indicated that EML1 indeed interacts with NUDC (**Figure 10C**). IF staining showed that NUDC was co-localized with EML1on the spindles of MI-stage oocytes, and was dislodged from the spindles in

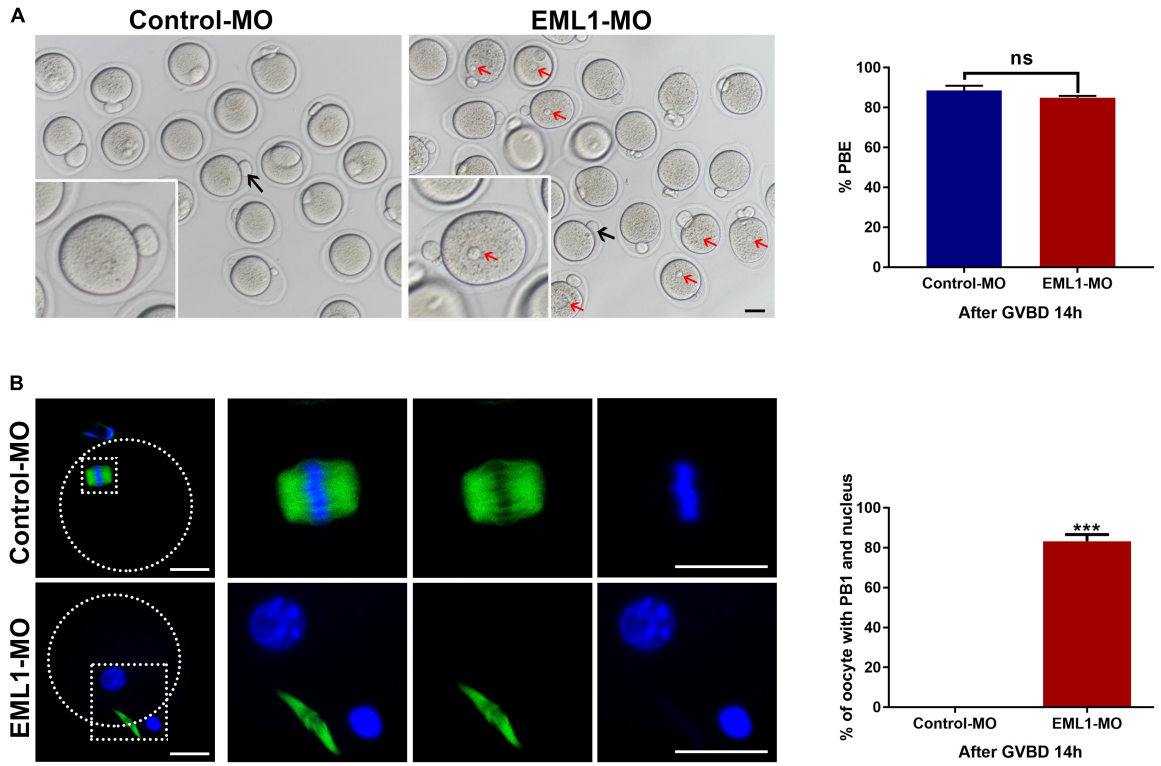

FIGURE 7 | Knockdown of EML1 causes the spontaneous formation of pronucleus and failure to enter into the second metaphase by the matured oocytes after completion of the first meiotic division. Oocytes microinjected with Control-MO and EML1-MO were first maintained at GV stage for 24 h, and then transferred to maturation medium to allow for IVM. Oocytes that had undergone GVB within 2 h of IVM were selected and further cultured for additional 14 h. At the end of the culture, PBE and formation of pronucleus in oocytes were assessed. **(A)** Scoring PBE in cultured oocyte under light microscope. Representative bright field images of cultured oocytes are shown in the left panel, and the quantification of the rate of PBE are shown in the right bar graph. Red arrows denote pronucleus (PN), black arrows indicate PB1. Scale Bar = 10 μm. ns: non-significant. **(B)** Examining the formation of PN by fluorescent staining of tubulin (green) and DNA (blue) in the matured oocytes. The left panel is the representative images of the stained oocytes, with the magnified view of the circled area are listed on the right side. The right bar graph shows the quantification of the percentage of oocytes that have both the emitted PB1 and the PN. Scale Bar = 20 μm. ***$P < 0.005$, compared with the Control-MO group. ns denote no significant difference between the two groups compared.

EML1-knocked down oocytes (**Figure 10E**). Nevertheless, the expression of NUDC was not changed by EML1-knockdown in oocytes (**Figure 10D**).

DISCUSSION

Despite of the initial finding of the founding member of EMLs in the eggs and early embryos of the echinoderm species, the functional roles of the EML family proteins in the oocyte were heretofore largely undefined. We revealed here that EML1 is a bona fide MAP in mouse oocytes that is indispensable for the correct assembly of acentriolar bipolar spindles and the normal progression of the first meiosis to MII. These critical roles of EML1 seems to be mediated by different mechanism, with the former likely via interactions with other important factors for spindle morphogenesis and organization of the MTOC component at the spindle pole, whereas the latter possibly through a distinct mechanism involving the regulation of the activation of MPF.

Decoration of microtubules is a well-recognized feature common to the EML family proteins. Consistent with this notion, we observed in the present study that EML1 protein is steadily expressed and specifically localized on the spindles during the process of oocytes meiotic maturation in the mouse. The specificity of the spindle localization was demonstrated by IF staining of both the endogenous EML1 using the EML1 antibody and the ectopically expressed DDK-tagged EML1 using the DDK antibody in the oocytes. The association of EML1 with the spindle microtubules was also supported by the observation that EML1 changes its localization in the same way as the microtubules when the stability of oocyte spindles was interfered with Nocodazole and Taxol. Interestingly, we found that, unlike EML3, EML4 and sea urchin EMAP that were reported to be hyperphosphorylated in mitosis (Brisch et al., 1996; Pollmann et al., 2006), EML1 seems to be not phosphorylated during oocyte maturation since no apparent shift in its mobility was observed on the WB gel. This result suggests that the association of EML1 with meiotic spindles is probably not regulated by phosphorylation event postulated previously for this family of proteins. EML1 may hence have distinct roles in oocyte meiosis and function via different molecular mechanisms. Indeed, we observed that knockdown of EML1 in the fully grown oocytes *in vitro* causes the delay of both GVB and PBE, thus suggesting that part

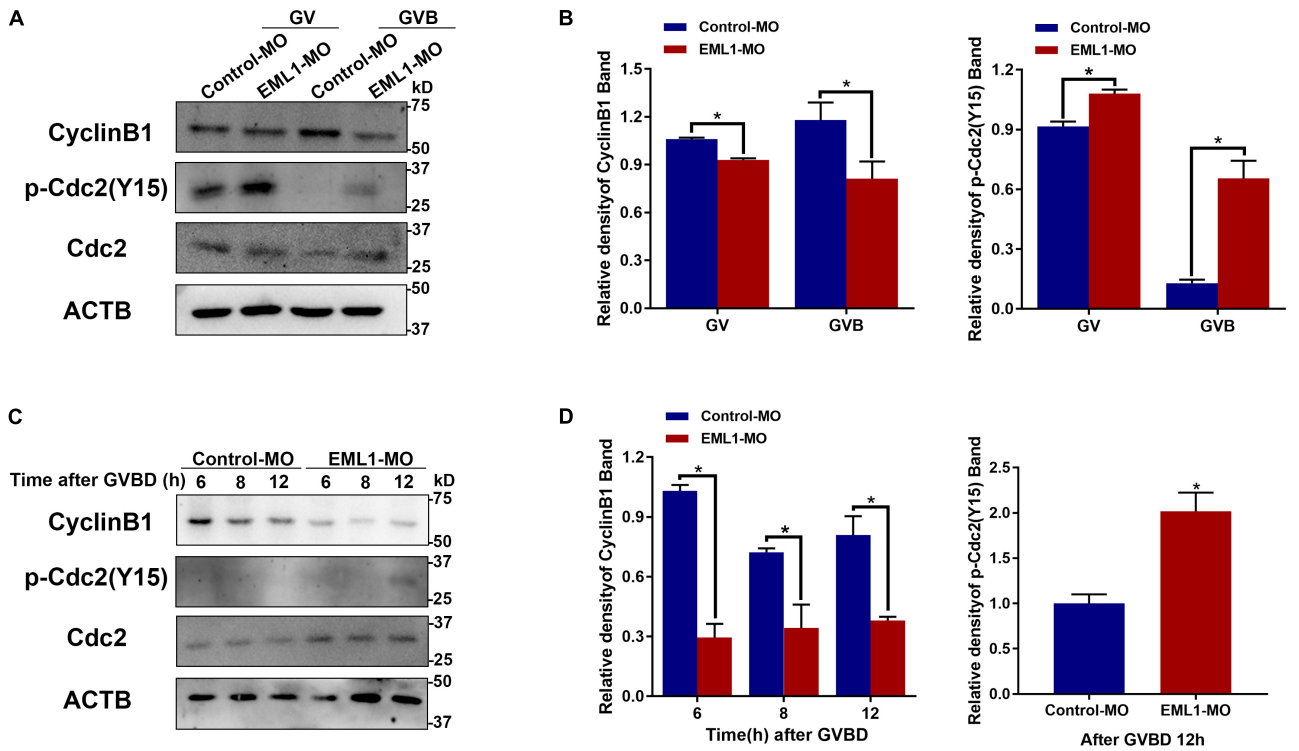

FIGURE 8 | Depletion of EML1 in oocytes impairs the activation of MPF. Dynamic changes in the levels of CCNB1, pCDK1-Y15, and CDK1 in the oocytes during the period of oocytes meiosis resumption **(A,B)** and MI-to-MII transition **(C,D)** were assessed by Western Blot analysis, with the level of ACTB used as internal control. Lysate from 50 oocytes was loaded in each lane. The representative gel images of three independent experiments are shown in panels **(A,C)**, and the quantification of the Western Blot results are shown in panels **(B,D)**. *$P < 0.05$, compared with the Control-MO group.

of the function of EML1 in oocytes is to ensure the precise timing of oocyte meiotic re-initiation and completion of the first meiotic division. More strikingly, we found that coincident with completion of the first meiotic division, EML1 knocked down oocytes fail to proceed to MII stage, but instead enter into the interphase and form PN. Chromosomes are decondensed in both the oocytes and the extruded first PBs. Therefore, EML1 is also essential for maintaining the dyads at condensed state after the segregation of the homologous bivalents, and preventing the secondary oocytes from entering into the interphase.

MPF is a cell cycle master regulator, its activation at late GV stage and reactivation at the end of first meiotic division are essential for oocyte meiotic resumption, and the transition into and arrest at MII, respectively (Adhikari and Liu, 2014; Adhikari et al., 2014). MPF activity is determined in large part by the levels of CCNB1 regulatory subunit and the phosphorylated forms of CDK1 catalytic subunit, with high levels of CCNB1 and low levels of p-CDK1 (Y14, Y15) beneficial to its activation (Adhikari and Liu, 2014). Our WB analysis of the CCNB1 and pCDK1-Y15 revealed that the levels of CCNB1 are significantly reduced in EML1 knocked down oocytes, especially after the resumption of meiosis. Also, a dramatic increase in the levels of pCDK1-Y15 is detected in the EML1 knocked down oocytes shortly after GVB, as well as at the time when oocytes normally reached the stage of MII. These changes in the levels of CCNB1 and pCDK1-Y15 in the EML1 knocked down oocytes are strong indicative of the reduction of MPF activity. It is therefore rational to believe that the presence of EML1 is required for maintaining the activity of MPF at optimal levels crucial for oocyte meiotic resumption and progression to MII. This inference is further buttressed by the observation that WEE1/2 kinases inhibitor, PD166285, effectively prevented the phosphorylation of CDK1 at Tyr15 residue and the formation of PN in the EML1 knocked down oocytes, and drove the oocytes entering to MII stage. WEE2 is the oocyte-specific isoform of WEE kinases, which acts as the direct upstream negative regulator of MPF through phosphorylation of CDK1 at the Thr14 and Tyr15 residues (Han et al., 2005). WEE2 plays an essential role in the maintenance of oocyte meiotic arrest before the LH surge and in the oocyte exit from the MII arrest upon fertilization (Han and Conti, 2006; Oh et al., 2010, 2011).

It is not clear how EML1 may regulate the activity of MPF in mouse oocytes. Since both the levels of CCNB1 and pCDK1-Y15 were significantly changed in the EML1 knocked down oocytes, EML1 may regulate the activation of MPF by interaction with the MPF subunits CCNB1 and CDK1, or the upstream regulators of CDK1. Interestingly, sea urchin EMAP was reported to interact with CDK1 in the unfertilized eggs (Brisch et al., 1996), which makes this postulated "interaction model" a more

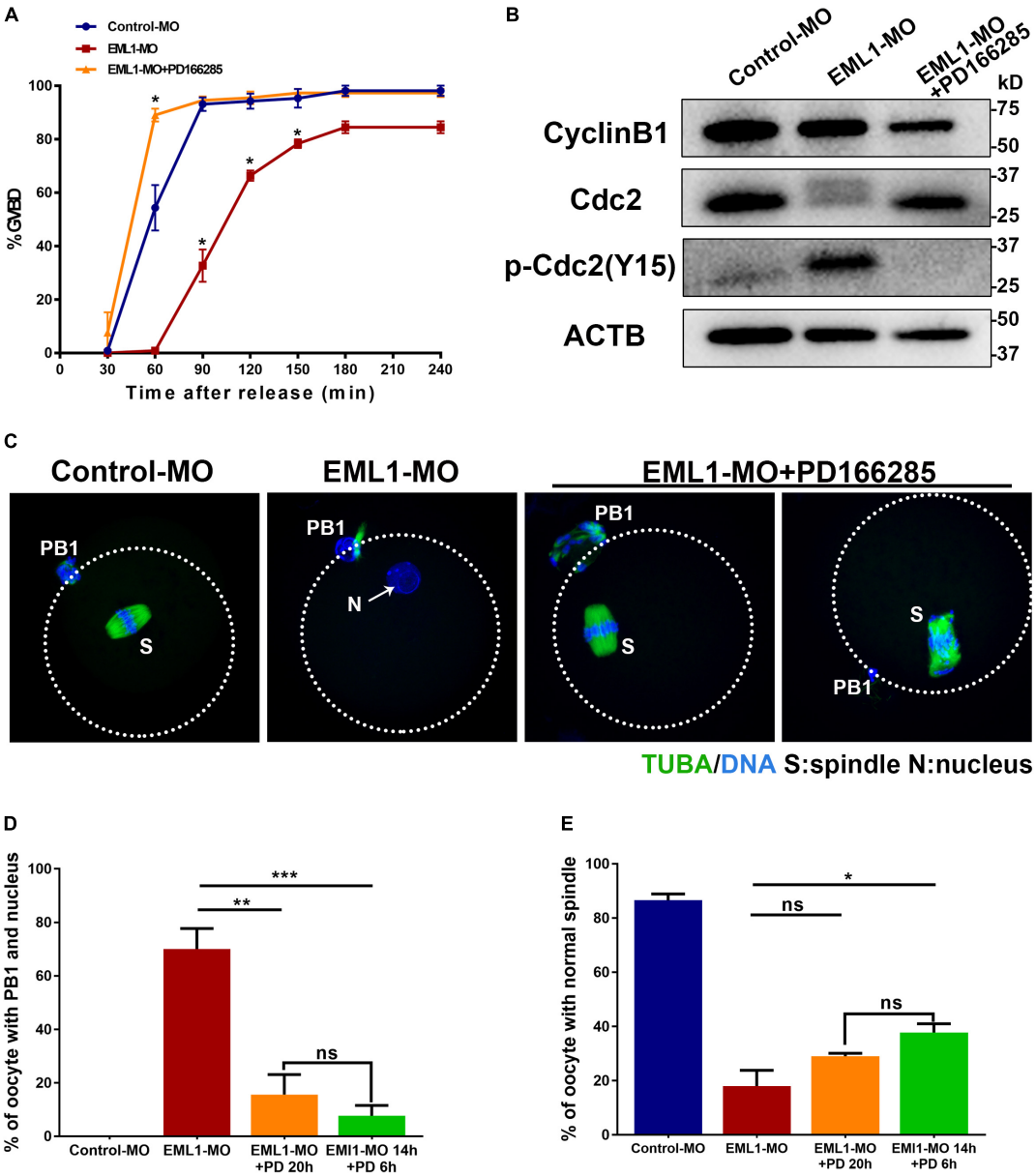

FIGURE 9 | Activation of MPF by inhibitors of WEE1/2 kinases rescues the defects of meiotic progression in EML1-knocked down oocytes. **(A)** Oocytes microinjected with Control-MO and EML1-MO were first maintained at GV stage for 20 h, and then transferred to maturation medium with (for EML1-MO group) or without (for Control-MO group) the supplementation of the inhibitor of WEE1/2 kinases, PD166285, to allow for maturation. Oocyte GVB was scored during the culture. *$P < 0.05$, compared with the Control-MO group. **(B)** Western Blot analysis of the changes in the levels of CCNB1, pCDK1-Y15, and CDK1 in the EML1-knocked down oocytes that were treated with PD166285. ACTB was used as the loading control. Lysate from 50 oocytes was loaded in each lane. The representative gel images of three independent experiments are shown. (**C–E**) Assessment of the effect of PD166285 on the progression of meiosis to MII in EML1-knocked down oocytes. Oocytes microinjected with Control-MO and EML1-MO were first maintained at GV stage for 24 h. Then the EML1-MO oocytes were split into two groups, one of which was transferred to maturation medium supplemented with PD16628S and directly cultured for 20 h, while the other one was first transferred to maturation medium without PD166285 for 14 h, and then in the PD166285-supplemented medium for another 4 h culture. PBE, PN formation, and spindle morphology were then scored and analyzed. Representative images of the oocytes with the microtubules labeled with anti-tubulin antibody (green) and DNA stained with Hochest (blue) are shown in panel **(C)**. Scale Bar = 20 μm. Quantification of the percentages of oocytes with PB1 and PN, and those with normal MII-spindles are shown in panels **(D,E)**, respectively. *$P < 0.05$, **$P < 0.01$, ***$P < 0.005$, compared with the EML1-MO group. ns denote no significant difference between the two groups compared.

attractive candidate mechanism. There are several cases in the literature that also demonstrated the spontaneous formation of PN in the oocytes. These include oocytes from the LT/Sv and related mouse strains, the *Mos*-knockout, and the oocyte-specific *Ccnb1* and *Mastl* knockout (Colledge et al., 1994; Hashimoto et al., 1994; Eppig et al., 1996, 2000; Adhikari et al., 2014;

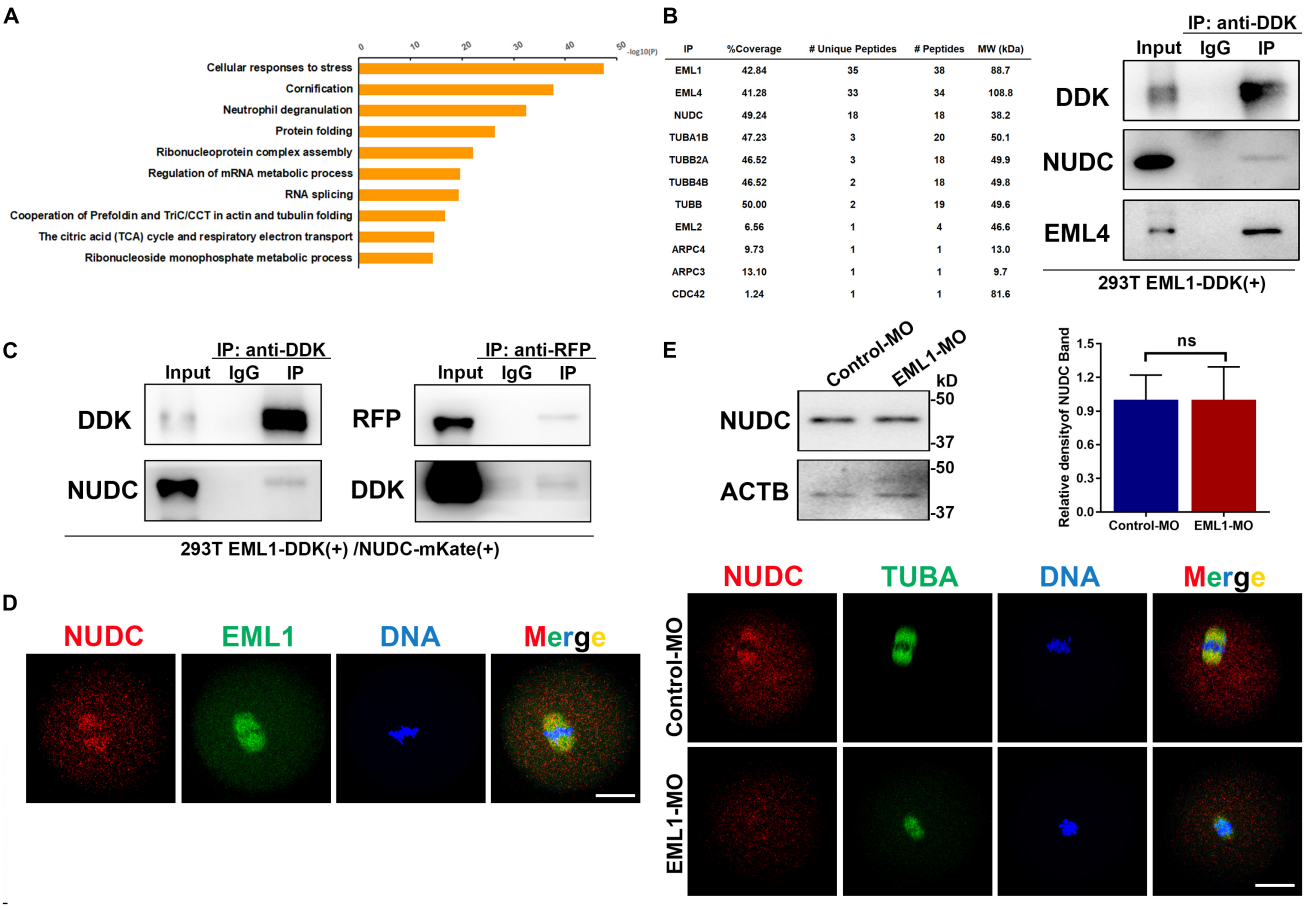

IP	%Coverage	# Unique Peptides	# Peptides	MW (kDa)
EML1	42.84	35	38	88.7
EML4	41.28	33	34	108.8
NUDC	49.24	18	18	38.2
TUBA1B	47.23	3	20	50.1
TUBB2A	46.52	3	18	49.9
TUBB4B	46.52	2	18	49.8
TUBB	50.00	2	19	49.6
EML2	6.56	1	4	46.6
ARPC4	9.73	1	1	13.0
ARPC3	13.10	1	1	9.7
CDC42	1.24	1	1	81.6

FIGURE 10 | Potential interacting partners identified for EML1. **(A)** Gene enrichment analysis of the interacting proteins of EML1 identified by IP-MS. **(B)** List of IP-MS identified EML1interacting proteins that are involved in spindle morphogenesis and actin polymerization (left table), and the validation of the presence of NUDC and EML4 in the EML1-IP product by WB analysis (right panel). **(C)** WB validation of the interaction between EML1 and NUDC. Expression of 3DDK-tagged EML1 and mKate-tagged NUDC proteins was achieved by simultaneously transfecting HEK293T cells with the corresponding plasmids. Co-IP and WB analysis were then carried out with the anti-DDK and anti-mKate antibodies. **(D)** IF staining images showing the co-localization of NUDC with EML1 on the spindles of MI-stage oocytes. **(E)** Knockdown of EML1 did not affect the expression levels of NUDC in the oocyte as indicated by the WB analysis in the top panel, but dislodged the localization of NUDC from the spindles in oocytes (bottom IF images). ns, denote no significant difference between the two groups compared. Scale Bar = 20 μm.

Li et al., 2018). The formation of PN in the former two mouse models differs from the latter's; it actually belongs to spontaneous parthenogenetic activation, *i.e.*, exit from MII arrest (Colledge et al., 1994; Hashimoto et al., 1994; Eppig et al., 1996, 2000). *Ccnb1* and *Mastl* knockout oocytes failed to mature to MII but rather enter into interphase and form PN, the same phenotype as what we have observed here (Adhikari et al., 2014; Li et al., 2018). Given that MASTL regulates the activity of MPF by antagonizing the activity of protein phosphatase PP2A, it is plausible to speculate that, in addition to CCNB1, EML1 may interact with MASTL to regulate the activity of MPF. Interestingly, EML1 was found by the pulldown assay in a very recent study to interact with MASTL in the embryonic brain extract (Bizzotto et al., 2017). This report adds more excitement to targeting MASTL as the potential interacting factor for EML1 to regulate MPF activity. Whether or not EML1 interact with MASTL, CCNB1, and CDK1 in mouse oocyte warrants further exploration.

Another important role that we revealed for EML1 is the regulation of the correct assembly of meiotic spindles in mouse oocytes, which is demonstrated by both the *in vivo* mutant model and the *in vitro* knockdown system. *In vitro*, knockdown of EML1 expression in the FGOs caused severe defects in spindle assembly at MI stage. The defects were reflected by small-sized spindles, flat spindle poles with disorganized localization of γ-tubulin and pericentrin, unattached kinetochores and misaligned chromosomes, and the abnormal activation of SAC. Therefore, EML1 is crucial for MI spindle assembly in oocytes. The sequentially connected defects in K-M attachment, chromosome alignment, and SAC activation may cumulate in the delay of anaphase I onset and the extrusion of the PB1 in the EML1 knocked down oocytes. Analysis of the oocytes ovulated by EML1-mutants revealed that EML1 is also essential for the formation and integrity maintenance of MII spindles. About 60% of the mutant ovulated oocytes are abnormal, with the chromosomes severely misaligned and the microtubules poorly

organized. Because of the extreme scarcity of viable homozygous animals for experimentation, we were unable to use the *Eml1*-mutant mouse model to carry out detailed analysis of all stages of oocyte other than just focusing on the ovulated eggs. It is also important to note that phenotypic variations exist between the *Eml1*-mutant mouse oocytes and the *in vitro* EML1-knockdown oocytes. The discrepancy in the phenotype could be caused by the fundamental difference in the two model systems used. The *in vivo* mutant mouse model could reflect the systemic effect of *Eml1* mutation on oocyte throughout the entire process of oocyte and follicle development. While the *in vitro* EML1-knockdown in the normal fully grown oocytes could only reveal the acute effect of loss of EML1 during the specific process of oocyte development, *i.e.*, meiotic maturation. Given that all six members of the EML family proteins are expressed in the oocytes and/or granulosa cells, some functions of EML1 that are critical for oocyte meiotic progression to MII could be compensated by the other EML family members during the growth phase of the mutant oocytes. This compensation could probably happen at the levels of transcription in the growing oocytes *in vivo*, which could not be done by the fully grown oocytes *in vitro* upon EML1 is knocked down since these oocytes are transcriptional quiescent. Nevertheless, the mutant model complement well with the *in vitro* knockdown experiment in which the oocytes are unable to progress to MII. Further dissection of the physiological role of EML1 in the entire process of oocyte meiotic progression necessitates the creation of a female germ cell-specific knockout allele of *Eml1* in the future studies.

In a spontaneous mouse mutant model where the expression of *Eml1* was disrupted by a transposon insertion, the localization of γ-tubulin and the length of metaphase spindles were also found to be altered in the apical progenitors of the developing cerebral cortex (Kielar et al., 2014; Collins et al., 2019). But the spindles in this mutant brain cells were abnormally long, which was opposite to what we observed here in the oocytes with EML1 knocked down. This discrepancy might be due to the lack of centrioles in the oocytes since the astral microtubules nucleated at the centrosomes in the mitotic somatic cells can interact with the cell cortex and orient the mitotic spindles (Szollosi et al., 1972; Gonczy, 2002; Roubinet and Cabernard, 2014). Despite of this difference, it is clear that EML1 participates in the regulation of microtubule dynamics and spindle assembly in both mitosis and meiosis. The extremely flat spindle poles and the increased incidence of unattached kinetochores observed in the EML1 knocked down oocytes indicate that EML1 might be required for the nucleation and assembly of both the minus- and plus- end microtubules of the spindle. Knockdown of EML1 also disrupted the correct aggregation of γ-tubulin and pericentrin, two key components of the aMTOC in mouse oocytes. Given the indispensable roles of γ-tubulin and pericentrin in the control of microtubule nucleation and the recruitment of other key pericentriolar materials (*e.g.,* γ-tubulin, NEDD and CEP125) to the aMTOC, respectively, in mouse oocytes (Ma et al., 2010; Ma and Viveiros, 2014; Baumann et al., 2017), it is tempting to speculate that EML1 may regulate the assembly of oocyte acentriolar spindles by cooperation with γ-tubulin and/or pericentrin.

We identified here through IP-MS and validated by Co-IP analysis that EML1 interacts with NUDC, an evolutionally conserved gene product that is phosphorylated by PLK1 and Aurora kinase B, and is critical for K-M attachment, chromosome congression, spindle organization and cytokinesis during mitosis in mammalian somatic cells (Aumais et al., 2003; Nishino et al., 2006; Weiderhold et al., 2016). We found that, in the oocytes, EML1 and NUDC were colocalized to the spindle in MI oocytes, and knockdown of EML1 disrupted the spindle-specific localization of NUDC without affecting its expression levels. This result suggests that the function of EML1 in the regulation of oocyte meiotic spindle assembly is probably mediated, at least in part, by interaction with NUDC. Similar results were also found for EML4 in Hela cells, where the association of EML4 with NUDC is required for the localization of NUDC to the mitotic spindle (Chen et al., 2015). Interestingly, our IP-MS analysis in this study also revealed that EML1 binds to EML4 and EML2. Furthermore, NUDC was recently reported to be highly expressed in mouse oocytes, and was suggested to be involved in the regulation of oocyte development (Cao et al., 2020). These data together make it more likely that EML1 cooperates with NUDC to regulate oocyte meiotic spindle assembly.

Although MAPs were initially discovered as proteins that bind to and stabilize microtubules, they are now believed to exert a large variety of functions through interaction with a plethora of proteins (Bodakuntla et al., 2019). This may exactly be the case for EML1 since its N-terminal TAPE (Tandem atypical propeller in EML) domain contains both the unique HELP (hydrophobic EML protein) motif and several WD40 repeats (Richards et al., 2014). The HELP motif binds to tubulins, while the WD40 repeats are presumed to mediate protein-protein interactions for many biological functions (Stirnimann et al., 2010). In addition to its direct regulation of microtubule dynamics, EML1 may act as a scaffold to recruit other regulators essential for spindle assembly and oocyte meiotic progression. The identity and function of the factors that interact with EML1, as well as the ways through which they cooperate with each other, await further studies. This study therefore provides new insights into the understanding of how MAPs regulate spindle morphogenesis and meiotic progression in mammalian oocytes.

DATA AVAILABILITY STATEMENT

The datasets presented in this study can be found in online repositories. The names of the repository/repositories and accession number(s) can be found below: ProteomeXchange PXD025159.

ETHICS STATEMENT

The animal study was reviewed and approved by the Ethical Committee of Laboratory Animals and Animal Care and Use Committee of the Nanjing Medical University (NJMU).

AUTHOR CONTRIBUTIONS

Y-QS and HY conceived the study. HY, TZ, HW, XiH, XuH, XF, YY, HL, and LS performed the research. HY and Y-QS analyzed the data and wrote the manuscript. All authors contributed to the article and approved the submitted version.

FUNDING

This research was supported by grants from the National Key Research and Development Program of China (2018YFC1003800), the National Natural Science Foundation of China (31871507, 31471351, and 31271538), the National Basic Research (973) Program of China (2014CB943200 and 2013CB945500), and the Natural Science Foundation of Jiangsu Province (BK20140061) to Y-QS.

ACKNOWLEDGMENTS

The authors thank Prof. Patsy Nishina at The Jackson Laboratory for providing the *Eml1* point mutant mice, Prof. Xumin Zhang and Miss Lin Huang at the State Key Laboratory of Genetic Engineering, School of Life Sciences, Fudan University, for the help with LC-MS/MS analysis, and all the other members at the Su laboratory for the help on this project.

SUPPLEMENTARY MATERIAL

The Supplementary Material for this article can be found online at: https://www.frontiersin.org/articles/10.3389/fcell.2021.687522/full#supplementary-material

Supplementary Figure 1 | Expression and localization of C-terminal tagged EML1-3DDK fusion protein in HEK293T cell line during mitosis. **(A)** Western Blot (WB) analysis of the expression of EML1, FLAG and ACTB (internal control) protein in lysate from HEK293T cells transfected with *Eml1*-3DDK plasmid DNA for 24 h. **(B)** Confocal micrographs showing the dynamic co-localization of EML1-3DDK fusion protein with spindles in HET293T cells during mitosis. FLAG and α-tubulin were stained in Red and green, respectively, while chromosomes were stained in blue. Scale Bar = 10 μm.

Supplementary Figure 2 | C-terminal tagged EML1-3DDK fusion protein showed the same special localization in mouse oocyte during meiosis progression with EML1 antibody. Oocytes microinjected with *Eml1*-3DDK mRNA were first maintained at GV stage for 12 h, and then transferred to maturation medium. Confocal micrographs showing the dynamic co-localization of EML1-3DDK protein with meiotic spindles in oocytes at various stages (i.e., GV, Pro-MI, MI, AI, TI, and MII) of maturation. FLAG and α-tubulin were stained in Red and green, respectively, while chromosomes were stained in blue. The far left panel shows the whole-oocyte view of the staining. The magnified view of the boxed area within the oocyte at each stage is listed on the right side. Scale Bar = 20 μm.

REFERENCES

Adhikari, D., and Liu, K. (2014). The regulation of maturation promoting factor during prophase I arrest and meiotic entry in mammalian oocytes. *Mol. Cell Endocrinol.* 382, 480–487. doi: 10.1016/j.mce.2013.07.027

Adhikari, D., Diril, M. K., Busayavalasa, K., Risal, S., Nakagawa, S., Lindkvist, R., et al. (2014). Mastl is required for timely activation of APC/C in meiosis I and Cdk1 reactivation in meiosis II. *J. Cell Biol.* 206, 843–853. doi: 10.1083/jcb.201406033

Aumais, J. P., Williams, S. N., Luo, W., Nishino, M., Caldwell, K. A., Caldwell, G. A., et al. (2003). Role for NudC, a dynein-associated nuclear movement protein, in mitosis and cytokinesis. *J. Cell Sci.* 116, 1991–2003. doi: 10.1242/jcs.00412

Baumann, C., Wang, X., Yang, L., and Viveiros, M. M. (2017). Error-prone meiotic division and subfertility in mice with oocyte-conditional knockdown of pericentrin. *J. Cell Sci.* 130, 1251–1262. doi: 10.1242/jcs.196188

Bennabi, I., Terret, M. E., and Verlhac, M. H. (2016). Meiotic spindle assembly and chromosome segregation in oocytes. *J. Cell Biol.* 215, 611–619. doi: 10.1083/jcb.201607062

Bizzotto, S., Uzquiano, A., Dingli, F., Ershov, D., Houllier, A., Arras, G., et al. (2017). Eml1 loss impairs apical progenitor spindle length and soma shape in the developing cerebral cortex. *Sci. Rep.* 7:17308.

Bodakuntla, S., Jijumon, A. S., Villablanca, C., Gonzalez-Billault, C., and Janke, C. (2019). Microtubule-Associated Proteins: Structuring the Cytoskeleton. *Trends Cell Biol.* 29, 804–819. doi: 10.1016/j.tcb.2019.07.004

Brisch, E., Daggett, M. A., and Suprenant, K. A. (1996). Cell cycle-dependent phosphorylation of the 77 kDa echinoderm microtubule-associated protein (EMAP) in vivo and association with the p34cdc2 kinase. *J. Cell Sci.* 109(Pt 12), 2885–2893. doi: 10.1242/jcs.109.12.2885

Brunet, S., Dumont, J., Lee, K. W., Kinoshita, K., Hikal, P., Gruss, O. J., et al. (2008). Meiotic regulation of TPX2 protein levels governs cell cycle progression in mouse oocytes. *PLoS One* 3:e3338. doi: 10.1371/journal.pone.0003338

Cao, S., Huang, S., Guo, Y., Zhou, L., Lu, Y., and Lai, S. (2020). Proteomic-based identification of oocyte maturation-related proteins in mouse germinal vesicle oocytes. *Reprod. Domest. Anim.* 55, 1607–1618. doi: 10.1111/rda.13819

Chen, D., Ito, S., Yuan, H., Hyodo, T., Kadomatsu, K., Hamaguchi, M., et al. (2015). EML4 promotes the loading of NUDC to the spindle for mitotic progression. *Cell Cycle* 14, 1529–1539. doi: 10.1080/15384101.2015.1026514

Colledge, W. H., Carlton, M. B., Udy, G. B., and Evans, M. J. (1994). Disruption of c-mos causes parthenogenetic development of unfertilized mouse eggs. *Nature* 370, 65–68. doi: 10.1038/370065a0

Collin, G. B., Won, J., Krebs, M. P., Hicks, W. J., Charette, J. R., Naggert, J. K., et al. (2020). Disruption in murine Eml1 perturbs retinal lamination during early development. *Sci. Rep.* 10:5647.

Collins, S. C., Uzquiano, A., Selloum, M., Wendling, O., Gaborit, M., Osipenko, M., et al. (2019). The neuroanatomy of Eml1 knockout mice, a model of subcortical heterotopia. *J. Anat.* 235, 637–650. doi: 10.1111/joa.13013

Colombie, N., Gluszek, A. A., Meireles, A. M., and Ohkura, H. (2013). Meiosis-specific stable binding of augmin to acentrosomal spindle poles promotes biased microtubule assembly in oocytes. *PLoS Genet.* 9:e1003562. doi: 10.1371/journal.pgen.1003562

Conti, M., and Franciosi, F. (2018). Acquisition of oocyte competence to develop as an embryo: integrated nuclear and cytoplasmic events. *Hum. Reprod. Update* 24, 245–266. doi: 10.1093/humupd/dmx040

De Keersmaecker, K., Graux, C., Odero, M. D., Mentens, N., Somers, R., Maertens, J., et al. (2005). Fusion of EML1 to ABL1 in T-cell acute lymphoblastic leukemia with cryptic t(9;14)(q34;q32). *Blood* 105, 4849–4852. doi: 10.1182/blood-2004-12-4897

Drutovic, D., Duan, X., Li, R., Kalab, P., and Solc, P. (2020). RanGTP and importin beta regulate meiosis I spindle assembly and function in mouse oocytes. *EMBO J.* 39:e101689.

Eichenmuller, B., Everley, P., Palange, J., Lepley, D., and Suprenant, K. A. (2002). The human EMAP-like protein-70 (ELP70) is a microtubule destabilizer that localizes to the mitotic apparatus. *J. Biol. Chem.* 277, 1301–1309. doi: 10.1074/jbc.m106628200

Eppig, J. J., Viveiros, M. M., Marin Bivens, C., and De La Fuente, R. (2004). *Regulation of mammalian oocyte maturation*. Amsterdam: Elsevier.

Eppig, J. J., Wigglesworth, K., and Hirao, Y. (2000). Metaphase I arrest and spontaneous parthenogenetic activation of strain LTXBO oocytes: chimeric reaggregated ovaries establish primary lesion in oocytes. *Dev. Biol.* 224, 60–68. doi: 10.1006/dbio.2000.9764

Eppig, J. J., Wigglesworth, K., Varnum, D. S., and Nadeau, J. H. (1996). Genetic regulation of traits essential for spontaneous ovarian teratocarcinogenesis in strain LT/Sv mice: aberrant meiotic cell cycle, oocyte activation, and parthenogenetic development. *Cancer Res.* 56, 5047–5054.

Eudy, J. D., Ma-Edmonds, M., Yao, S. F., Talmadge, C. B., Kelley, P. M., Weston, M. D., et al. (1997). Isolation of a novel human homologue of the gene coding for echinoderm microtubule-associated protein (EMAP) from the Usher syndrome type 1a locus at 14q32. *Genomics* 43, 104–106. doi: 10.1006/geno.1997.4779

Fu, Q., Wang, W., Zhou, T., and Yang, Y. (2016). Emerging roles of NudC family: from molecular regulation to clinical implications. *Sci. China Life Sci.* 59, 455–462. doi: 10.1007/s11427-016-5029-2

Gache, V., Waridel, P., Winter, C., Juhem, A., Schroeder, M., Shevchenko, A., et al. (2010). Xenopus meiotic microtubule-associated interactome. *PLoS One* 5:e9248. doi: 10.1371/journal.pone.0009248

Gonczy, P. (2002). Mechanisms of spindle positioning: focus on flies and worms. *Trends Cell Biol.* 12, 332–339. doi: 10.1016/s0962-8924(02)02306-1

Goodson, H. V., and Jonasson, E. M. (2018). Microtubules and Microtubule-Associated Proteins. *Cold Spring Harb. Perspect. Biol.* 10:a022608.

Greaney, J., Wei, Z., and Homer, H. (2018). Regulation of chromosome segregation in oocytes and the cellular basis for female meiotic errors. *Hum. Reprod. Update* 24, 135–161. doi: 10.1093/humupd/dmx035

Grosenbaugh, D. K., Joshi, S., Fitzgerald, M. P., Lee, K. S., Wagley, P. K., Koeppel, A. F., et al. (2020). A deletion in Eml1 leads to bilateral subcortical heterotopia in the tish rat. *Neurobiol. Dis.* 140:104836. doi: 10.1016/j.nbd.2020.104836

Guo, J., Zhang, T., Guo, Y., Sun, T., Li, H., Zhang, X., et al. (2018). Oocyte stage-specific effects of MTOR determine granulosa cell fate and oocyte quality in mice. *Proc. Natl. Acad. Sci. U S A.* 115, E5326–E5333.

Hamill, D. R., Howell, B., Cassimeris, L., and Suprenant, K. A. (1998). Purification of a WD repeat protein, EMAP, that promotes microtubule dynamics through an inhibition of rescue. *J. Biol. Chem.* 273, 9285–9291. doi: 10.1074/jbc.273.15.9285

Han, S. J., and Conti, M. (2006). New pathways from PKA to the Cdc2/cyclin B complex in oocytes: Wee1B as a potential PKA substrate. *Cell Cycle* 5, 227–231. doi: 10.4161/cc.5.3.2395

Han, S. J., Chen, R., Paronetto, M. P., and Conti, M. (2005). Wee1B is an oocyte-specific kinase involved in the control of meiotic arrest in the mouse. *Curr. Biol.* 15, 1670–1676. doi: 10.1016/j.cub.2005.07.056

Han, Z., Liang, C. G., Cheng, Y., Duan, X., Zhong, Z., Potireddy, S., et al. (2010). Oocyte spindle proteomics analysis leading to rescue of chromosome congression defects in cloned embryos. *J. Proteome Res.* 9, 6025–6032. doi: 10.1021/pr100827j

Hanna, C. B., Yao, S., Martin, M., Schonbrunn, E., Georg, G. I., Jensen, J. T., et al. (2019). Identification and Screening of Selective WEE2 Inhibitors to Develop Non-Hormonal Contraceptives that Specifically Target Meiosis. *ChemistrySelect* 4, 13363–13369. doi: 10.1002/slct.201903696

Hashimoto, N., Watanabe, N., Furuta, Y., Tamemoto, H., Sagata, N., Yokoyama, M., et al. (1994). Parthenogenetic activation of oocytes in c-mos-deficient mice. *Nature* 370, 68–71. doi: 10.1038/370068a0

Holt, J. E., and Jones, K. T. (2009). Control of homologous chromosome division in the mammalian oocyte. *Mol. Hum. Reprod.* 15, 139–147. doi: 10.1093/molehr/gap007

Holubcova, Z., Blayney, M., Elder, K., and Schuh, M. (2015). Human oocytes. Error-prone chromosome-mediated spindle assembly favors chromosome segregation defects in human oocytes. *Science* 348, 1143–1147. doi: 10.1126/science.aaa9529

Jiang, Z. Z., Hu, M. W., Wang, Z. B., Huang, L., Lin, F., Qi, S. T., et al. (2014). Survivin is essential for fertile egg production and female fertility in mice. *Cell Death Dis.* 5:e1154. doi: 10.1038/cddis.2014.126

Kielar, M., Tuy, F. P., Bizzotto, S., Lebrand, C., de Juan Romero, C., Poirier, K., et al. (2014). Mutations in Eml1 lead to ectopic progenitors and neuronal heterotopia in mouse and human. *Nat. Neurosci.* 17, 923–933. doi: 10.1038/nn.3729

Kolano, A., Brunet, S., Silk, A. D., Cleveland, D. W., and Verlhac, M. H. (2012). Error-prone mammalian female meiosis from silencing the spindle assembly checkpoint without normal interkinetochore tension. *Proc. Natl. Acad. Sci. U S A.* 109, E1858–E1867.

Li, H., You, L., Tian, Y., Guo, J., Fang, X., Zhou, C., et al. (2020). DPAGT1-Mediated Protein N-Glycosylation Is Indispensable for Oocyte and Follicle Development in Mice. *Adv. Sci.* 7:2000531. doi: 10.1002/advs.202000531

Li, J., Tang, J. X., Cheng, J. M., Hu, B., Wang, Y. Q., Aalia, B., et al. (2018). Cyclin B2 can compensate for Cyclin B1 in oocyte meiosis I. *J. Cell Biol.* 217, 3901–3911. doi: 10.1083/jcb.201802077

Lin, E., Li, L., Guan, Y., Soriano, R., Rivers, C. S., Mohan, S., et al. (2009). Exon array profiling detects EML4-ALK fusion in breast, colorectal, and non-small cell lung cancers. *Mol. Cancer Res.* 7, 1466–1476. doi: 10.1158/1541-7786.mcr-08-0522

Ma, W., and Viveiros, M. M. (2014). Depletion of pericentrin in mouse oocytes disrupts microtubule organizing center function and meiotic spindle organization. *Mol. Reprod. Dev.* 81, 1019–1029. doi: 10.1002/mrd.22422

Ma, W., Baumann, C., and Viveiros, M. M. (2010). NEDD1 is crucial for meiotic spindle stability and accurate chromosome segregation in mammalian oocytes. *Dev. Biol.* 339, 439–450. doi: 10.1016/j.ydbio.2010.01.009

Manandhar, G., Schatten, H., and Sutovsky, P. (2005). Centrosome reduction during gametogenesis and its significance. *Biol. Reprod.* 72, 2–13. doi: 10.1095/biolreprod.104.031245

Mullen, T. J., Davis-Roca, A. C., and Wignall, S. M. (2019). Spindle assembly and chromosome dynamics during oocyte meiosis. *Curr. Opin. Cell Biol.* 60, 53–59. doi: 10.1016/j.ceb.2019.03.014

Nguyen, A. L., Drutovic, D., Vazquez, B. N., El Yakoubi, W., Gentilello, A. S., Malumbres, M., et al. (2018). Genetic Interactions between the Aurora Kinases Reveal New Requirements for AURKB and AURKC during Oocyte Meiosis. *Curr. Biol.* 28, 3458–3468e3455.

Nishino, M., Kurasawa, Y., Evans, R., Lin, S. H., Brinkley, B. R., and Yu-Lee, L. Y. (2006). NudC is required for Plk1 targeting to the kinetochore and chromosome congression. *Curr. Biol.* 16, 1414–1421. doi: 10.1016/j.cub.2006.05.052

Oegema, R., McGillivray, G., Leventer, R., Le Moing, A. G., Bahi-Buisson, N., Barnicoat, A., et al. (2019). EML1-associated brain overgrowth syndrome with ribbon-like heterotopia. *Am. J. Med. Genet. C Semin. Med. Genet.* 181, 627–637. doi: 10.1002/ajmg.c.31751

Oh, J. S., Han, S. J., and Conti, M. (2010). Wee1B, Myt1, and Cdc25 function in distinct compartments of the mouse oocyte to control meiotic resumption. *J. Cell Biol.* 188, 199–207. doi: 10.1083/jcb.200907161

Oh, J. S., Susor, A., and Conti, M. (2011). Protein tyrosine kinase Wee1B is essential for metaphase II exit in mouse oocytes. *Science* 332, 462–465. doi: 10.1126/science.1199211

Perkins, D. N., Pappin, D. J. C., Creasy, D. M., and Cottrell, J. S. (1999). Probability-based protein identification by searching sequence databases using mass spectrometry data. *Electrophoresis* 20, 3551–3567. doi: 10.1002/(sici)1522-2683(19991201)20:18<3551::aid-elps3551>3.0.co;2-2

Petry, S., Pugieux, C., Nedelec, F. J., and Vale, R. D. (2011). Augmin promotes meiotic spindle formation and bipolarity in Xenopus egg extracts. *Proc. Natl. Acad. Sci. U S A.* 108, 14473–14478. doi: 10.1073/pnas.1110412108

Pollmann, M., Parwaresch, R., Adam-Klages, S., Kruse, M. L., Buck, F., and Heidebrecht, H. J. (2006). Human EML4, a novel member of the EMAP family, is essential for microtubule formation. *Exp. Cell Res.* 312, 3241–3251. doi: 10.1016/j.yexcr.2006.06.035

Raynaud-Messina, B., and Merdes, A. (2007). Gamma-tubulin complexes and microtubule organization. *Curr. Opin. Cell Biol.* 19, 24–30. doi: 10.1016/j.ceb.2006.12.008

Richards, M. W., Law, E. W., Rennalls, L. P., Busacca, S., O'Regan, L., Fry, A. M., et al. (2014). Crystal structure of EML1 reveals the basis for Hsp90 dependence of oncogenic EML4-ALK by disruption of an atypical beta-propeller domain. *Proc. Natl. Acad. Sci. U S A.* 111, 5195–5200. doi: 10.1073/pnas.1322892111

Richards, M. W., O'Regan, L., Roth, D., Montgomery, J. M., Straube, A., Fry, A. M., et al. (2015). Microtubule association of EML proteins and the EML4-ALK variant 3 oncoprotein require an N-terminal trimerization domain. *Biochem. J.* 467, 529–536. doi: 10.1042/bj20150039

Roubinet, C., and Cabernard, C. (2014). Control of asymmetric cell division. *Curr. Opin. Cell Biol.* 31, 84–91. doi: 10.1016/j.ceb.2014.09.005

Schuh, M., and Ellenberg, J. (2007). Self-organization of MTOCs replaces centrosome function during acentrosomal spindle assembly in live mouse oocytes. *Cell* 130, 484–498. doi: 10.1016/j.cell.2007.06.025

Sharif, B., Na, J., Lykke-Hartmann, K., McLaughlin, S. H., Laue, E., Glover, D. M., et al. (2010). The chromosome passenger complex is required for fidelity of

chromosome transmission and cytokinesis in meiosis of mouse oocytes. *J. Cell Sci.* 123, 4292–4300. doi: 10.1242/jcs.067447

So, C., Seres, K. B., Steyer, A. M., Monnich, E., Clift, D., Pejkovska, A., et al. (2019). A liquid-like spindle domain promotes acentrosomal spindle assembly in mammalian oocytes. *Science* 364:eaat9557. doi: 10.1126/science.aat9557

Stirnimann, C. U., Petsalaki, E., Russell, R. B., and Muller, C. W. (2010). WD40 proteins propel cellular networks. *Trends Biochem. Sci.* 35, 565–574. doi: 10.1016/j.tibs.2010.04.003

Sun, J. J., Huang, M., Xiao, F., and Xi, Z. Q. (2015). Echinoderm microtubule-associated protein -like protein 5 in anterior temporal neocortex of patients with intractable epilepsy. *Iran J. Basic Med. Sci.* 18, 1008–1013.

Sun, S. C., Lin, S. L., Zhang, D. X., Lu, S. S., Sun, Q. Y., and Kim, N. H. (2010). Borealin regulates bipolar spindle formation but may not act as chromosomal passenger during mouse oocyte meiosis. *Front. Biosci.* 2, 991–1000. doi: 10.2741/e158

Suprenant, K. A., Dean, K., McKee, J., and Hake, S. (1993). EMAP, an echinoderm microtubule-associated protein found in microtubule-ribosome complexes. *J. Cell Sci.* 104, 445–450. doi: 10.1242/jcs.104.2.445

Suprenant, K. A., Tuxhorn, J. A., Daggett, M. A., Ahrens, D. P., Hostetler, A., Palange, J. M., et al. (2000). Conservation of the WD-repeat, microtubule-binding protein, EMAP, in sea urchins, humans, and the nematode C. elegans. *Dev. Genes Evol.* 210, 2–10. doi: 10.1007/pl00008183

Szollosi, D., Calarco, P., and Donahue, R. P. (1972). Absence of centrioles in the first and second meiotic spindles of mouse oocytes. *J. Cell Sci.* 11, 521–541. doi: 10.1242/jcs.11.2.521

Tegha-Dunghu, J., Neumann, B., Reber, S., Krause, R., Erfle, H., Walter, T., et al. (2008). EML3 is a nuclear microtubule-binding protein required for the correct alignment of chromosomes in metaphase. *J. Cell Sci.* 121, 1718–1726. doi: 10.1242/jcs.019174

Uzquiano, A., Cifuentes-Diaz, C., Jabali, A., Romero, D. M., Houllier, A., Dingli, F., et al. (2019). Mutations in the Heterotopia Gene Eml1/EML1 Severely Disrupt the Formation of Primary Cilia. *Cell Rep.* 28, 1596–1611e10.

Vogt, E., Kirsch-Volders, M., Parry, J., and Eichenlaub-Ritter, U. (2008). Spindle formation, chromosome segregation and the spindle checkpoint in mammalian oocytes and susceptibility to meiotic error. *Mutat. Res.* 651, 14–29. doi: 10.1016/j.mrgentox.2007.10.015

Weiderhold, K. N., Fadri-Moskwik, M., Pan, J., Nishino, M., Chuang, C., Deeraksa, A., et al. (2016). Dynamic Phosphorylation of NudC by Aurora B in Cytokinesis. *PLoS One* 11:e0153455. doi: 10.1371/journal.pone.0153455

Wu, Z., Huang, J., Huang, J., Li, Q., and Zhang, X. (2018). Lys-C/Arg-C, a More Specific and Efficient Digestion Approach for Proteomics Studies. *Anal. Chem.* 90, 9700–9707. doi: 10.1021/acs.analchem.8b02448

Yin, H., Hou, X., Zhang, T., Shi, L., and Su, Y. Q. (2020). Participation of EML6 in the regulation of oocyte meiotic progression in mice. *J. Biomed. Res.* 34:10.

Zhang, X., Shi, L., Shu, S., Wang, Y., Zhao, K., Xu, N., et al. (2007). An improved method of sample preparation on AnchorChip targets for MALDI-MS and MS/MS and its application in the liver proteome project. *Proteomics* 7, 2340–2349. doi: 10.1002/pmic.200600184

Conflict of Interest: The authors declare that the research was conducted in the absence of any commercial or financial relationships that could be construed as a potential conflict of interest.

Copyright © 2021 Yin, Zhang, Wang, Hu, Hou, Fang, Yin, Li, Shi and Su. This is an open-access article distributed under the terms of the Creative Commons Attribution License (CC BY). The use, distribution or reproduction in other forums is permitted, provided the original author(s) and the copyright owner(s) are credited and that the original publication in this journal is cited, in accordance with accepted academic practice. No use, distribution or reproduction is permitted which does not comply with these terms.

frontiers in Cell and Developmental Biology

REVIEW
published: 03 June 2021
doi: 10.3389/fcell.2021.688878

Chromosome Organization in Early Meiotic Prophase

Corinne Grey and Bernard de Massy**

Institut de Génétique Humaine, Centre National de la Recherche Scientifique, Université de Montpellier, Montpellier, France

One of the most fascinating aspects of meiosis is the extensive reorganization of the genome at the prophase of the first meiotic division (prophase I). The first steps of this reorganization are observed with the establishment of an axis structure, that connects sister chromatids, from which emanate arrays of chromatin loops. This axis structure, called the axial element, consists of various proteins, such as cohesins, HORMA-domain proteins, and axial element proteins. In many organisms, axial elements are required to set the stage for efficient sister chromatid cohesion and meiotic recombination, necessary for the recognition of the homologous chromosomes. Here, we review the different actors involved in axial element formation in *Saccharomyces cerevisiae* and in mouse. We describe the current knowledge of their localization pattern during prophase I, their functional interdependence, their role in sister chromatid cohesion, loop axis formation, homolog pairing before meiotic recombination, and recombination. We also address further challenges that need to be resolved, to fully understand the interplay between the chromosome structure and the different molecular steps that take place in early prophase I, which lead to the successful outcome of meiosis I.

Keywords: meiosis, HiC, synapsis, loops, DNA double-strand breaks, recombination, prophase, cohesin

OPEN ACCESS

Edited by:
Liangran Zhang,
Shandong University, China

Reviewed by:
Valérie Borde,
Centre National de la Recherche Scientifique (CNRS), France
Kei-ichiro Ishiguro,
Kumamoto University, Japan

****Correspondence:***
Corinne Grey
corinne.grey@igh.cnrs.fr
Bernard de Massy
bernard.de-massy@igh.cnrs.fr
orcid.org/0000-0002-0950-2758

Specialty section:
This article was submitted to Cell Growth and Division, a section of the journal Frontiers in Cell and Developmental Biology

Received: *31 March 2021*
Accepted: *10 May 2021*
Published: *03 June 2021*

Citation:
Grey C and de Massy B (2021) Chromosome Organization in Early Meiotic Prophase. Front. Cell Dev. Biol. 9:688878. doi: 10.3389/fcell.2021.688878

INTRODUCTION

Meiosis is a specialized cell cycle in which diploid cells are converted into haploid cells.
During meiosis, diploid cells proceed through an S phase, also called premeiotic S phase, and then enter an extended prophase to reach the first division or meiosis I. The unique mode of chromosome segregation at meiosis I, called reductional segregation, requires the establishment of connections between homologous chromosomes (homologs) to allow their proper alignment and separation (Hunter, 2015). Multiple events occur during prophase I to allow the interaction between homologs and the formation of at least one crossing over (CO) per homolog pair, by homologous recombination. At the DNA level, exchanges are highly regulated in time, space, and choice of recombination partner. The homologous recombination pathway is initiated by the formation of DNA double-strand breaks (DSBs) at the onset of prophase I (i.e., leptotene) in most species, and their repair is completed at the end of pachytene. DSBs are not randomly distributed along the genome, and the choice of the sister chromatid or the homologous chromosome during their repair is regulated. At the chromosomal level, the pairing process allows each homolog to find and interact with its partner, and recombination (i.e., DSB formation and repair) stabilizes the interactions through non-reciprocal and reciprocal exchanges. This process is ensured in parallel for all chromosome pairs within the meiotic nucleus (Zickler and Kleckner, 2015).

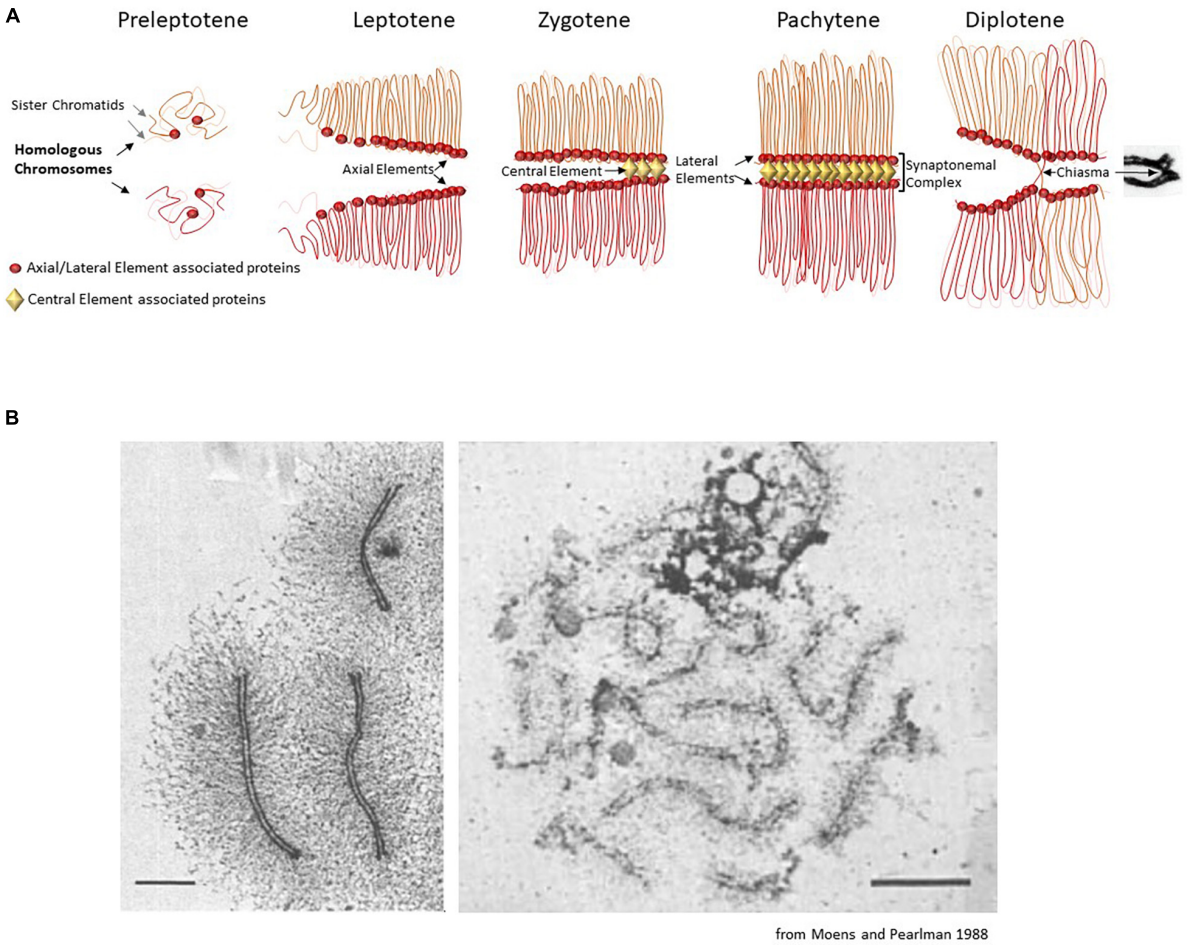

FIGURE 1 | (A) Schematic description of the chromosomal organization during the first meiotic prophase. The first meiosis-specific proteins of the axial element are loaded on chromosomes during meiotic S-phase at the preleptotene stage. At leptotene stage, the elongating axial elements serve as scaffolds along which sister chromatids attach and begin to form an array of loops. At the zygotene stage, the proteins of the central element start to load and to initiate the formation of the synaptonemal complex that associates homologous chromosomes (homologous synapsis). In most organisms, homologous synapsis depends on meiotic DNA double-strand break formation and repair. During the pachytene stage, homologous chromosomes are fully synapsed and the chromatin is organized in a tight loop-axis array. Meiotic double-strand break repair is completed during this stage. The proteins of the central element unload and the synaptonemal complex dissolves during the diplotene stage, while homologous chromosomes remain connected only at centromeres and at chiasmata (the cytological manifestation of crossing-over sites). **(B)** Chromosome loops and axis visualized by electron microscopy. Left panel: chromosome spread of a pachytene nucleus in the moth *Hyalophora columbia*. The chromatin loops extend about 3 μm from the parallel-aligned chromosome cores, which together form the synaptonemal complex. Scale bar = 2 μm. Right panel: chromosome spread of a pachytene nucleus in *S. cerevisiae*, presenting a smaller loop size to axis ratio. Scale bar 2 μm.

Cytology was crucial for identifying the connections between homologs that were named chiasma by Janssens in 1909 (Janssens et al., 2012). Since then, a large number of cytological studies have described and analyzed the chromosomal architecture and organization during meiotic prophase I, particularly the specific loop-axis organization of meiotic chromosomes that appears at prophase I onset, after the premeiotic S phase (Zickler and Kleckner, 1999), and the specific anchoring of telomeres to the nuclear envelope (Klutstein and Cooper, 2014). Both features are dynamic during prophase I, and play important roles in recombination and prophase progression, and thus in the proper execution of meiosis I.

The loop-axis organization can be observed in early prophase I, by electron microscopy and immunocytochemistry in many species, where two adjacent sister chromatids are organized as an array of loops anchored to a proteinaceous axis (Zickler and Kleckner, 1999; **Figure 1**). Several proteins are part of this axial structure: the cohesin complex(es) (Ishiguro, 2019), type II DNA topoisomerase (TopoII) (Moens and Earnshaw, 1989; Klein et al., 1992), condensins (Yu and Koshland, 2003; Mets and Meyer, 2009; Wood et al., 2010; Lee, 2013), and other proteins that are expressed specifically in meiotic cells (described below).

This review presents the current knowledge on the organization of meiotic chromosomes at the onset of meiotic prophase when the axial structure, also called the axial element, forms and before it engages into interaction with the homolog where additional structural components

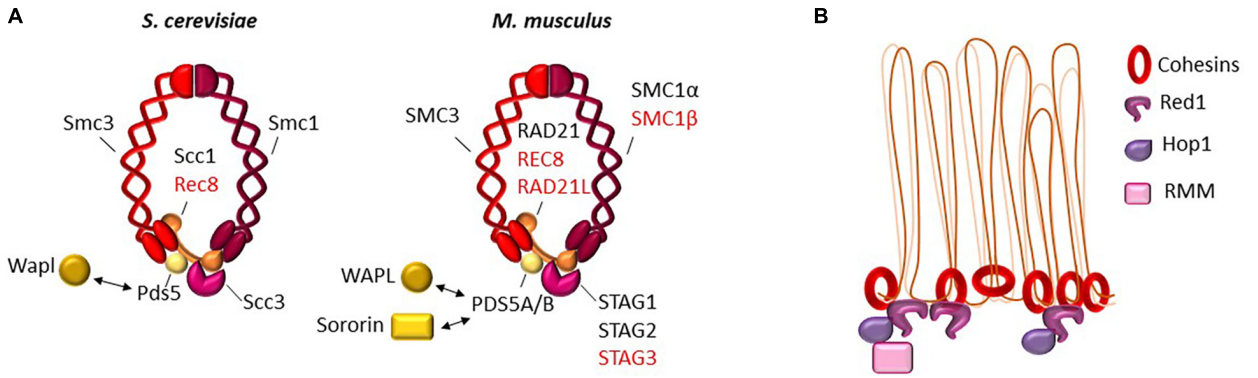

FIGURE 2 | (A) The cohesin complex. Schematic presentation of the ring-like structure of the cohesin complex (red, pink, and orange), and the main regulators of its stability (yellow) in *S. cerevisiae* (left) and in mouse (right). Sororin-Pds5 interaction promotes stabilization of the cohesin complex and Wapl-Pds5 interaction promotes unloading of the cohesin complex. During meiosis in *S. cerevisiae*, the somatic α-kleisin subunit Scc1 (also called Rad21) is replaced by Rec8 (red). In mouse, several meiosis specific subunits exist (indicated in red), and differently combined lead to various cohesin complexes. Constitutive and meiotic orthologs of the various subunits are also listed in **Table 1**. **(B)** 2D localization of the cohesin complex and main partners in *S. cerevisiae*. *In S. cerevisiae*, cohesins and its main meiotic partners localize at axial elements at the basis of chromatin loops, where they contribute to loop-axis formation and sister chromatid cohesion. RMM is Rec114/Mei4/Mer2.

come into play for the formation of the synaptonemal complex (**Figure 1**). We present the associated proteins, how they contribute to this organization, and their roles in the execution of the meiotic recombination program during meiotic prophase.

The first part describes the knowledge gained in *Saccharomyces cerevisiae* where the identified proteins and functions provide a framework for understanding this organization. Then, it focuses on the main currently known players, the cohesin complex and the axis proteins Hop1 and Red1. This is followed by the second part that presents data obtained in mammals on the proteins that build and organize meiotic chromosomes with a detailed description of the best characterized components: the cohesin complexes and HORMAD1 and SYCP2 (orthologs of *S. cerevisiae* Hop1 and Red1, respectively). Then, the various identified or postulated functions of these proteins in the initiation of the meiotic recombination program are discussed. Insights gained from other species that provide complementary information from those obtained in yeast and mammals are included, to outline the evolutionary conservation of this functional organization among eukaryotes.

ORGANIZATION OF THE CHROMOSOME AXIAL ELEMENT IN *S. cerevisiae*

In *S. cerevisiae*, genetic and cytological studies allowed identifying the key components of meiotic chromosomes and their roles, among which the meiotic cohesin complex and the Hop1/Red1 axis- associated proteins are central players.

The Meiotic Cohesin Complex, With the Specific α-Kleisin Rec8

The cohesin protein complex includes coiled-coil proteins with an SMC (Structural Maintenance of Chromosome) domain connected by an α-kleisin (hereafter named kleisin) subunit, and accessory proteins involved in loading/unloading of the complex onto/from chromatin. Cohesins play an essential role in sister chromatid cohesion and centromere organization for chromosome segregation during mitosis (Yatskevich et al., 2019). Cohesins have a major role in chromosome organization by mediating contacts between different chromosomal regions through potential different mechanisms, one of which is loop extrusion, as demonstrated by *in vitro* and *in vivo* studies in somatic cells (Fudenberg et al., 2016; Goloborodko et al., 2016; Davidson et al., 2019; Kim et al., 2019).

In *S. cerevisiae*, during vegetative growth, the cohesin complex is composed of four mains subunits, Smc1, Smc3, Rad21 (Scc1), and Scc3. During meiosis, Scc1 is expressed at very low levels, and a meiotic specific kleisin, Rec8, is expressed and ensures functions unique to meiotic cells (**Figure 2**). At the onset of meiosis, Rec8 is loaded on chromatin and forms the meiotic cohesin complex together with Smc1, Smc3, and Scc3. In addition to its role in sister chromatid cohesion at centromeres for ensuring chromosome segregation, Rec8 plays an essential role in meiotic chromosome structure and recombination (Klein et al., 1999). In the absence of Rec8, the axial structure of meiotic chromosomes is defective as observed by electron microscopy and Red1, one of the components of this structure, does not localize as linear structures (Klein et al., 1999). Genome-wide mapping showed that Rec8 localizes mostly around centromeres before meiotic S phase, but becomes enriched during meiotic prophase in intergenic regions of convergent genes, together with Red1 and Hop1, the structural proteins of axial elements (see below) (Kugou et al., 2009; Panizza et al., 2011; Sun et al., 2015). Rec8 localization coincides with regions of contacts, detected by HiC in yeast meiotic cells, that represent the bases of chromatin loops (Muller et al., 2018; Schalbetter et al., 2019).

Based on the interactions between Rec8 and Red1, it is thought that Rec8 recruits Red1/Hop1 to form chromosomal axis sites at the onset of meiotic prophase I (Sun et al., 2015; **Figure 2**).

Similar interactions between cohesin and structural axis proteins have been observed in *Schizosaccharomyces pombe*, although it is Rec11, the meiotic-specific Scc3 subunit, and not Rec8 that interacts with the axial protein Rec10 (ortholog of Red1) (Sakuno and Watanabe, 2015).

The absence of Rec8 leads to defective axial structures of meiotic chromosomes and to changes in Red1 and Hop1 chromatin localization, but not to their loss (Panizza et al., 2011). In the absence of Rec8, Hop1/Red1 levels are decreased in some, but not all genomic regions. This indicates that Hop1 and Red1 can bind to chromatin in a cohesin-independent manner, but the determinants are not known. Interestingly, Red1 and Hop1 are less affected at small chromosomes in the absence of Rec8 (Panizza et al., 2011; Sun et al., 2015). Consistent with the view of Rec8 as a platform for Red1/Hop1 loading, in the absence of Red1, Rec8 chromatin loading is not affected (Sun et al., 2015).

The Meiotic Axis Proteins Hop1 and Red1

The two chromosome axis proteins Hop1 and Red1 interact and form an evolutionarily conserved complex that can be recruited by cohesins. Hop1 and Red1 are required for homolog pairing and synapsis in *S. cerevisiae*, localize to meiotic chromosome axes (Hollingsworth and Byers, 1989; Rockmill and Roeder, 1990; Smith and Roeder, 1997), and are required for wild type level of meiotic DSBs and meiotic recombination (Mao-Draayer et al., 1996; Schwacha and Kleckner, 1997; Blat et al., 2002; Kim et al., 2010; Murakami et al., 2020). The formation of the Hop1 and Red1 complex is stimulated by the Mek1 kinase (delosSantos and Hollingsworth, 1999). These features are shared also by their orthologs in *S. pombe* (Hop1 and Rec10, respectively) (Lorenz et al., 2004; Kariyazono et al., 2019). Hop1 is a meiotic protein containing the HORMA domain. This domain, which was named after three proteins that harbor it (Hop1, Rev7, and Mad2), undergoes a regulated conformation change providing an alternative status for homo- and hetero-interactions (Rosenberg and Corbett, 2015). Structural analyses of the interaction between Hop1 and Red1 have identified an important feature: the interaction between a short domain called the closure motif, present on both Hop1 and Red1, and the HORMA domain. Red1 also oligomerizes to form protein filaments *in vitro* (West et al., 2018, 2019). The interaction features between Hop1 and Red1 are evolutionarily conserved in budding yeast, mammals, plants, and nematodes (Kim et al., 2014; West et al., 2019). Hop1 has DNA binding activity *in vitro* (Kironmai et al., 1998; Khan et al., 2012), but its direct implication *in vivo* remains to be demonstrated.

Hop1 and Red1 play a role in DSB formation by serving as a platform for the Mer2/Mei4/Rec114 DSB proteins (Panizza et al., 2011; **Figure 2**) that then promote Spo11 catalytic activity through direct or indirect interactions with Spo11 (Yadav and Claeys Bouuaert, 2021). This Hop1/Red1 function is mediated by the direct interaction between Hop1 and Mer2 in *S. cerevisiae* (Rousova et al., 2020), and between their orthologs Hop1 and Rec15 in *S. pombe* (Kariyazono et al., 2019). In the absence of Rec8, Hop1/Red1 and Rec114 still colocalize, but their positioning is altered (Panizza et al., 2011). DSB localization is also altered (Kugou et al., 2009), and DSBs are concentrated in regions enriched for Red1 and Hop1 (Sun et al., 2015). Hop1 or Red1 depletion does not have the same consequences. In the absence of Red1, Hop1 is not detected on chromatin, but DSB activity is still observed although at reduced levels. In the absence of Hop1, Red1 localization is not affected (Sun et al., 2015), but DSB activity is strongly reduced. Rec114 chromatin binding is strongly reduced in both cases (Panizza et al., 2011; Murakami et al., 2020).

Later during meiotic prophase I (i.e., after DSB formation), Rec8, Hop1 and Red1 play important roles in regulating the partner choice, homolog versus sister chromatid for DSB repair and by regulating DSB levels through the Tel1 kinase, and by switching off DSB activity upon Hop1/Red1 depletion from chromosomes concomitant with the formation of the synaptonemal complex (SC) that initiates at sites of DSB repair designed to mature as crossing overs (Keeney et al., 2014). Several structural changes take place to establish the tripartite structure of the SC composed of the two axes of each homolog and a central element (Zickler and Kleckner, 2015).

Overall, cohesin, Red1 and Hop1, by organizing chromosomes, have a key role in meiotic prophase. Two additional components of chromosome axis with direct and/or indirect role on meiotic recombination, DSB formation and/or repair are DNA Topoisomerase II (TopoII) (Klein et al., 1992; Zhang et al., 2014; Heldrich et al., 2020) and condensins (Yu and Koshland, 2003; Yu and Koshland, 2005; Hong et al., 2015).

LOCALIZATION OF THE CHROMOSOME AXIAL ELEMENT IN MAMMALS

In this section, we present the components of the mammalian axial element, involved in organizing meiotic chromosomes in early prophase I before the formation of the synaptonemal complex (**Figure 1**). These components include the cohesin complexes with somatic and meiotic-specific subunits (SMC1 α and SMC1β, SMC3, STAG3, RAD21, RAD21L, REC8) and their associated regulatory proteins (PDS5A, PDS5B, WAPL, and Sororin), the structural and regulatory proteins HORMAD1 and HORMAD2 and the axial element proteins SYCP2 and SYCP3 (**Table 1**).

Cohesins

Like their mitotic counterparts and similarly to *S. cerevisiae*, mammalian meiotic cohesin complexes are composed of four core units that form a ring-like structure: two subunits of the SMC family, one α-kleisin, and one stromal antigen protein subunit (**Table 1**). In meiosis, there are three main cohesin complexes. All contain the two subunits SMC3 and SMC1β (Revenkova et al., 2001) and the accessory subunit STAG3 (or SA3), orthologous to *S. cerevisiae* Scc3 (Pezzi et al., 2000; Bayes et al., 2001; Prieto et al., 2004). Conversely, each of the three complexes contains a distinct kleisin subunit: RAD21 (Parra et al., 2004), RAD21L (Gutierrez-Caballero et al., 2011; Ishiguro et al., 2011; Lee and Hirano, 2011), or REC8 (Parisi et al., 1999; Eijpe et al., 2003; Lee et al., 2003). SMC1β (Revenkova et al., 2001;

TABLE 1 | Evolutionary conservation of axis components.

	S. cerevisiae		*M. musculus*		*C. elegans*		*A. thaliana*		*D. melanogaster*	
	Constitutive	***Meiosis specific***	***Constitutive***	***Meiosis specific***	***Constitutive***	***Meiosis specific***	***Constitutive***	***Meiosis specific***	***Constitutive***	***Meiosis specific***
Horma domain proteins		Hop1		HORMAD1/2		HIM-3		ASY1/2		
						HTP-1/2/3				
Axis associated proteins		Red1		SYCP2				ASY3		
				SYCP3				ASY4		
Cohesin complex subunits										
α-Kleisins	Rad21 (Scc1)	Rec8	RAD21	REC8	SCC-1	REC8	RAD21.1/.2/.3 (SYN2/3/4)	REC8 (SYN1)	Rad21 (Scc1)	c(2)M
				RAD21L		COH-3/4				
Coiled-coil domain proteins	Smc1		SMC1α	SMC1β	HIM-1 (SMC-1)		SMC1		Smc1	
	Smc3		SMC3		SMC-3		SMC3		Smc3	
Adapters, kleisin binding	Scc3		STAG1/2	STAG3	SCC-3		SCC3		SA	
Cohesin regulators	Wapl		WAPL		WAPL-1		WAPl1/2		Wapl	
	Pds5		PDS5A/B		PDS-5 (Evl-14)		PDS5A/B/ C/D/E		Pds5	
	Eco1 (Ctf7p)		ESCO1/2 Sororin		F08F8.4		CTF7			
Cohesin loaders	Scc2		NIPBL		PQN-85 (SCC-2)		SCC2		Nipped-B	
	Scc4		MAU2		MAU-2		SCC4		Mau2	

The homologs of meiotic axis components in five different species (S. cerevisiae, M. musculus, C. elegans, A. thaliana, and D. melanogaster) are indicated, their expression is either constitutive or meiotic specific. Note that whether the constitutive components are also expressed in meiotic cells has not been always determined. The level of conservation varies: the subunits of the cohesin complexes, the cohesin regulators and loaders are relatively well conserved. The Horma domain allows the identification of homologs in the different species excepted for D. melanogaster. The axis associated proteins are poorly conserved at the amino-acid sequence level and were identified as homologs based on in vivo and in vitro data.

Eijpe et al., 2003), RAD21L (Herran et al., 2011; Ishiguro et al., 2011), REC8 and STAG3 are meiosis-specific proteins. In addition, the SMC1α subunit, present in the somatic cohesin complex, is also present in meiosis, leading to more complexity (Eijpe et al., 2003; Revenkova et al., 2004). In mice, deficiency for either of the meiotic-specific subunits leads to severe defects in meiotic prophase I, with variable phenotypes according to the subunit. Such defects are for example the impairment of sister chromatid cohesion, aberrant axis formation, defective recombination and homologous synapsis, and compromised telomere integrity, all of which ultimately lead to male and female sterility (Revenkova et al., 2004; Xu et al., 2005; Adelfalk et al., 2009; Herran et al., 2011; Biswas et al., 2013; Fukuda et al., 2014; Llano et al., 2014; Winters et al., 2014; Biswas et al., 2018).

The α-Kleisin Subunits of Cohesin

The first germ-cell specific cohesin complex that localizes on meiotic chromosomes contains REC8. In mouse male meiosis, where most of the observations were made, REC8 is detected early before the premeiotic S phase, when it starts to form foci, visible by immunostaining (Eijpe et al., 2003). Shortly afterward, in premeiotic S phase, the RAD21L-cohesin complex also starts forming foci all over the nucleus (Lee and Hirano, 2011; Ishiguro et al., 2014; Fujiwara et al., 2020). After premeiotic S phase, REC8 cohesin and RAD21L cohesin complexes show differences in localization on meiotic chromosomes. From the beginning of leptotene, REC8 cohesin complexes form foci that coincide with the staining of axial elements. On the other hand, RAD21L cohesin complexes are mainly detected around heterochromatin, where they form aggregates of bright foci. By mid-leptotene, RAD21L cohesin complexes change their pattern and form short axial structures (Ishiguro et al., 2011; Fukuda et al., 2014). Then, foci or short stretches of both REC8- and RAD21L-containing complexes progressively become almost continuous segments by zygotene (Eijpe et al., 2003; Herran et al., 2011; Ishiguro et al., 2011; Lee and Hirano, 2011; Fukuda et al., 2014). Subtle differences in localizations may also be due to distinct properties (sensitivity and specificity) of the antibodies used in such assays. At the beginning of pachytene, both complexes remain associated with the synapsed autosomal axis, and on the unsynapsed XY-bivalent (Ishiguro et al., 2011). REC8 co-localizes with the lateral elements of the SC, and RAD21L shows a more central localization in the SC, suggesting a distinct activity (Rong et al., 2016). The RAD21L signal starts to dissociate from the axis around mid-pachytene, partially producing self-assembled poly-complexes or aggregates. REC8 cohesin complexes remain strongly associated with synapsed and unsynapsed axes until diplotene, and then progressively disassemble to be detected

as discontinuous foci along the chromosome arms and at centromeric regions (Ishiguro et al., 2011; Biswas et al., 2013; Fukuda et al., 2014). After prophase I, some residual RAD21L signal can be detected on chromosome arms (Herran et al., 2011; Ishiguro et al., 2011), but it is mostly restricted to centromeric regions and the unsynapsed sex chromosomes (Herran et al., 2011; Ishiguro et al., 2011; Lee and Hirano, 2011).

Through prophase I, the localization of RAD21L and REC8 on chromosomes is mostly mutually exclusive, suggesting that they may have distinct roles in axial element formation and sister chromatid cohesion (Ishiguro et al., 2011; Lee and Hirano, 2011; Vara et al., 2019). Interestingly, in zygotene, both complexes can be found in a symmetrical localization pattern between the two homologous unsynapsed regions of a given pair of chromosomes. This suggests the existence of intrinsic loading sites for cohesin-enriched domains featuring REC8 or RAD21L (Ishiguro et al., 2011; Lee and Hirano, 2011). However, a genome-wide chromatin immunoprecipitation (ChIP) study in pachytene cells, and thus the evaluation of the binding average of both proteins in a cell population, showed that most REC8 and RAD21L sites overlap and are located to active promoters (Vara et al., 2019).

Other Cohesin Complex Components

The somatic subunit SMC1α, present at premeiotic S-phase disappears at leptotene, and then reappears at late zygotene. At this stage, its phosphorylated form is detected as discontinuous stretches on synapsed chromosomes, including in the pseudo-autosomal region (PAR) of the sex chromosomes X and Y, and its non-phosphorylated form marks the chromatin loops of the XY-bivalent. By the end of diplotene, both phosphorylated and non-phosphorylated SMC1α disappear completely (Eijpe et al., 2000, 2003; Biswas et al., 2013; Hopkins et al., 2014). After premeiotic S phase, SMC1β largely replaces the somatic subunit SMC1α (Revenkova et al., 2001). From leptotene, SMC1β localizes along the forming axial elements, rather uniformly along unsynapsed and synapsed autosomes, as well as on the unsynapsed XY-bivalent at pachytene. From leptotene to early pachytene, SMC1β is detected also at telomeres (Adelfalk et al., 2009). At the beginning of diplotene, SMC1β initially stays on desynapsed chromosomes, but also starts to accumulate at centromeric regions. Then, it progressively dissociates from the chromosome arms, and remains only at the centromeric regions until the metaphase II–anaphase II transition (Revenkova et al., 2001). In agreement with their distinct spatiotemporal localization, SMC1α and SMC1β do not interact within the same complex, but they both associate with SMC3, as indicated by immunoprecipitation (Ishiguro et al., 2011; Lee and Hirano, 2011). SMC3 is present at all stages of meiosis, and its staining pattern is compatible with both isoforms (Eijpe et al., 2003). Thus, during the axial element formation in early prophase I, the vast majority of meiotic cohesin complexes contain SMC3 and the meiosis-specific SMC1β isoform.

The meiosis-specific stromalin subunit STAG3 appears first at preleptotene when it localizes to telomeres and chromocenters (Shibuya et al., 2014). From leptotene, STAG3 expression completely overlaps with that of SMC1β in time and space (Prieto et al., 2001). This suggests that at this time point of axial element formation, cohesin complexes contain SMC1β, SMC3, and STAG3.

The third cohesin complex present during meiosis contains the somatic RAD21 subunit. Some studies reported RAD21 presence on chromosome axes and centromeres from leptotene to diplotene (Xu et al., 2004; Herran et al., 2011; Llano et al., 2012), whereas others detected RAD21 only from late pachytene onward (Ishiguro et al., 2011; Lee and Hirano, 2011). At pachytene and diplotene, RAD21 rarely colocalizes with RAD21L or REC8 (Ishiguro et al., 2011; Lee and Hirano, 2011; Fukuda et al., 2014). This could indicate that RAD21 either binds to distinct sites, or replaces the meiosis-specific RAD21L and REC8 cohesin complexes when they dissociate from the chromosome arms by the end of pachytene and diplotene, respectively. Later, from diakinesis until anaphase II, RAD21 is only detected at inner centromeres (Parra et al., 2003, 2004; Xu et al., 2004).

The stability and persistence time of cohesin complexes on chromosomes are regulated by pro- and anti-cohesion factors (e.g., Sororin, ESCO1, ESCO2, WAPL, and PDS5) and several posttranslational modifications (Schmitz et al., 2007; Shintomi and Hirano, 2009; Nasmyth, 2011; Losada, 2014; McNicoll et al., 2020). In somatic cells, cohesins can be actively released by two pathways: the Separase and the WAPL-PDS5 pathways (Nasmyth et al., 2000; Peters and Nishiyama, 2012). Separase catalyzes the proteolytic cleavage of the kleisin subunit of cohesins during metaphase–anaphase transition. On the other hand, WAPL promotes cohesin unloading during mitotic prophase, and to some extent during interphase, through an antagonistic mechanism that involves the competition with Sororin for binding to PDS5 (Gandhi et al., 2006; Kueng et al., 2006; Haarhuis et al., 2013; Tedeschi et al., 2013; Ouyang et al., 2016). Thus, Sororin-PDS5 promote the loading and stabilization of cohesins, and WAPL-PDS5 mediate their unloading.

In prophase I, pro-and anti-cohesin factors have similar functions as in somatic cells, but they face additional challenges due to the different constraints that are related to the presence of other axis associated proteins such as HORMADs, SYCP2, and SYCP3 (see below, also **Figure 3A**). At that stage, the unloading of cohesin complexes is regulated by WAPL and the two orthologs, PDS5A and PDS5B, both strongly expressed in mouse testes and ovaries (Kuroda et al., 2005; Losada et al., 2005; Zhang et al., 2008; Fukuda et al., 2010). WAPL is detected at lateral axial elements of zygotene and pachytene spermatocytes, and colocalizes with SYCP2 (Kuroda et al., 2005; Zhang et al., 2008). Similarly, PDS5A is detected on axial and lateral elements from zygotene until early pachytene. By mid-pachytene PDS5A disperses on the chromatin, with no staining detected on lateral axial elements. Later, at metaphase I and II, PDS5A reappears at centromeres (Viera et al., 2020). PDS5B has a partly different localization pattern, it is detected earlier (early leptotene) and remains longer (late pachytene) at axial elements where it colocalizes with REC8, and partially with SYCP3 (Viera et al., 2020). Co-immunoprecipitation assays corroborate this finding, showing that PDS5B interacts with the axis-related proteins SMC1β, SYCP2, and HORMAD1 (Fukuda et al., 2010). PDS5B

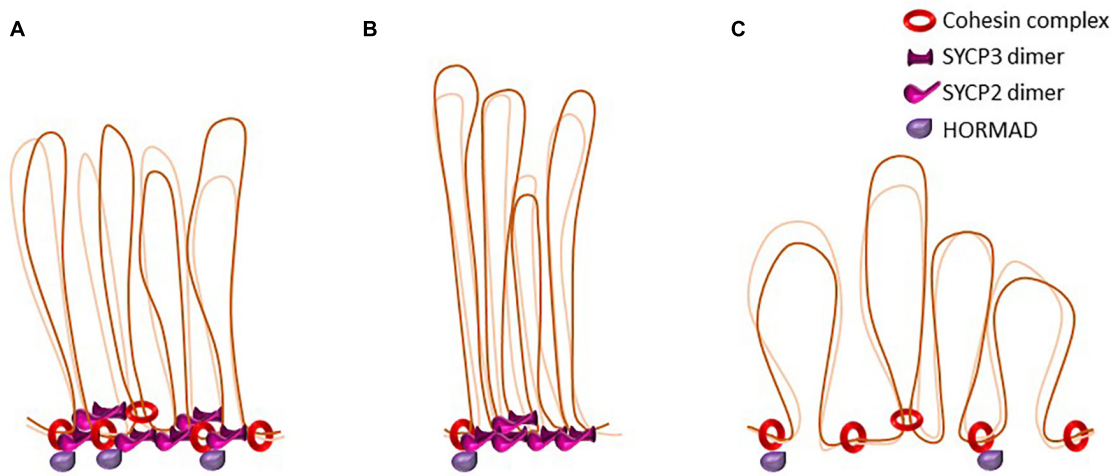

FIGURE 3 | The dynamics of loop-axis organization. Schematic representation of axial elements in the mouse. Cohesins form the axial core onto which other axial element proteins such HORMADs, SYCP2, and SYCP3 bind. Some cohesin complexes are involved in sister cohesion, others might be involved in the formation of the loop axis-structure. SYCP3 and SYCP2 form an antiparallel heterotetramer. **(A)** representation of wild type axial elements. **(B)** Representation of loop-axis structure in mouse mutants for the cohesin subunit SMC1β. Axes are twofold shorter and loops appear longer and less homogenous in size. In this mutant, HORMAD is able to load on axes. **(C)** Representation of loop-axis structure in mice deficient for SYCP3. Cohesin axis core is formed but axes are almost twofold longer and loops appear shorter, irregular, and denser. SYCP2 is not detected on axes in the absence of SYCP3.

also colocalizes with telomeres in all stages of prophase I (Viera et al., 2020). Conditional depletion of either PDS5A or PDS5B does not alter progression through prophase I. However, the simultaneous depletion of both proteins leads to severe defects in axial element formation (see below) and telomere integrity. This indicates that albeit their different localization pattern, PDS5A and PDS5B have redundant functions (Viera et al., 2020).

Rather surprisingly, the WAPL antagonist Sororin localizes only in the central region of the synaptonemal complex, whereas the other subunits of the cohesin complex do not localize in this region, and its presence on meiotic chromosome axes correlates with the appearance of the central element protein SYCP1. This suggests that in meiosis, Sororin might have different functions from what described in mitosis (Gomez et al., 2016; Jordan et al., 2017). ESCO1 role in meiosis has not been investigated yet, but ESCO2 and acetylated SMC3 are mostly detected upon synapsis formation in zygotene (McNicoll et al., 2020). Both proteins remain associated with the chromosome axes until desynapsis in diplonema, suggesting that acetylated SMC3-stabilized cohesion is required during prophase I, and likely during synaptonemal complex formation or maintenance. Germ cell-specific conditional ablation of *Esco2*, resulting in ESCO2 hypomorphism in spermatocytes, leads to a delay in synaptonemal complex formation, a slight defect of autosome synapsis, and a clear defect in sister chromatid cohesion of unsynapsed sex chromosomes that appears transiently in pachynema, adjacent to the XY PAR. This suggests a role of ESCO2 in sister chromatid cohesion of unsynapsed regions in addition to supporting autosomal synaptonemal complex synapsis (McNicoll et al., 2020).

The role of ESPL1 Separase has been investigated in mouse oocytes only, and specific depletion of ESPL1 in metaphase arrested oocytes shows that ESPL1 promotes the release of REC8 from chromosome arms and allows chiasma resolution (Kudo et al., 2006; Tachibana-Konwalski et al., 2010). In oocytes, the REC8 cohesin complex is mostly resistant to WAPL-mediated release. This is reminiscent of what observed in *Caenorhabditis elegans*, where WAPL releases COH-3/4 but not REC8 cohesin complexes, and COH-3/4 is functionally linked to RAD21L (Severson and Meyer, 2014; Silva et al., 2020).

The HORMA Domain Proteins HORMAD1 and HORMAD2

HORMA domain-containing proteins are conserved in yeast (Hop1), plants (ASY1), nematodes (HTP-1–3 and HIM-3) and in mammals (**Table 1**). *Hormad1* and *Hormad2* were discovered as genes that are specifically upregulated in female and male mouse gonads during prophase I (Wojtasz et al., 2009; Fukuda et al., 2010; Shin et al., 2010). Mouse HORMAD1 and HORMAD2 are closely related, and both have human homologs. Their HORMA domains are highly conserved; the HORMA domain of mouse HORMAD1 shares 28 and 89% of amino acids with the HORMA domain of *S. cerevisiae* Hop1 and human HORMAD1, respectively. Mouse HORMAD1 is a 44kDa protein; a slightly shorter isoform is weakly expressed and lacks the nuclear localization signal at its C-terminus (Fukuda et al., 2010). HORMAD2 is a 35 kDa protein with no other documented isoforms in the mouse. HORMAD1 and HORMAD2 show slightly different dynamics during prophase I (see below). In mouse, deficiency of HORMAD1 leads to sterility in male and female due to defects in recombination and in homologous synapsis, leading to an impairment of chromosome segregation. This indicates an important role of this protein in early prophase

I events (Shin et al., 2010; Daniel et al., 2011). HORMAD2 deficiency leads to sterility in males only, likely due to a role of this protein in the surveillance of asynapsis upon synaptonemal complex formation (Kogo et al., 2012; Wojtasz et al., 2012).

In vivo, immunofluorescence and proximity ligation assays demonstrated that HORMAD1 appears as distinct foci at preleptotene, when it mostly co-localizes with REC8 and RAD21L cohesins. Super-resolution microscopy showed that RAD21L tends to colocalize more frequently with HORMAD1 than REC8 (Fujiwara et al., 2020). At leptotene, both HORMAD proteins form short stretches that overlap with RAD21L, REC8 and the axial element proteins SYCP3 and SYCP2 (see below) (Wojtasz et al., 2009; Shin et al., 2010; Fujiwara et al., 2020). At this stage, the chromosomal localization of HORMAD1 is slightly reduced in the absence of SYCP2, suggesting that this protein might be involved in HORMAD1 stabilization on chromosomes (Fujiwara et al., 2020).

During zygotene, HORMAD1 and HORMAD2 staining is stronger on unsynapsed than synapsed axes, and the signal intensity is weaker close to centromeres. Synapsed regions show some residual HORMAD signal the intensity of which is anti-correlated with that of synaptonemal complex proteins, such as SYCP1, indicating HORMAD1 and HORMAD2 depletion upon synaptonemal complex formation. The depletion of HORMADs from synapsed regions is independent of meiotic recombination but depends on TRIP13, an ortholog of *S. cerevisiae* Pch2, and on the formation of the synaptonemal complex (Wojtasz et al., 2009; Dereli et al., 2021). In *S. cerevisiae*, Pch2 is also involved in Hop1 depletion from synapsed axes (Borner et al., 2008). In pachytene, the signal for both HORMAD proteins is strongest on the unsynapsed XY-bivalent (in males), but some punctuate signal remains along synapsed chromosomes. At this stage, HORMAD1 is present as two distinct forms: phosphorylated and non-phosphorylated (Wojtasz et al., 2009; Shin et al., 2010). Although HORMAD1 and HORMAD2 mostly overlap until pachytene, they show slightly distinct distribution patterns. In zygotene, HORMAD2 signal spreads further in the synapsed regions than HORMAD1, indicating that HORMAD1 is depleted faster from the forming synaptonemal complexes than HORMAD2. During pachytene, HORMAD1 is clearly detectable on centromeres of synapsed chromosomes, whereas HORMAD2 shows only a very faint signal in these regions. In spermatocytes during diplotene, HORMAD1 and HORMAD2 show distinct patterns on the axes of desynapsing autosomal chromosomes. HORMAD1 signal increases, whereas HORMAD2 remains restricted to the unsynapsed XY-bivalent. Conversely, in diplotene oocytes, both are detected on desynapsed axes. During diakinesis, only HORMAD1 strongly accumulates at inner centromeres and remains between sister-kinetochores until interkinesis, perfectly overlapping with the SYCP3 signal (see below) (Wojtasz et al., 2009; Fukuda et al., 2010).

The Axial Proteins SYCP2 and SYCP3

Synaptonemal complex protein 3 (SYCP3, also called SCP3 and Cor1) was first described as a component of rat and hamster axial elements (Heyting et al., 1985, 1987; Dobson et al., 1994; Lammers et al., 1995). No ortholog has been identified in yeasts, but orthologs were found in many metazoans, including in early branching lineages, such as *Cnidaria* (Fraune et al., 2012). In almost all studied species, the *Sycp3* gene encodes a single protein product, except in the mouse and rat, where it encodes an additional longer isoform, with an N-terminal extension. It is not clear whether this isoform has additional properties (Alsheimer et al., 2010). Mammalian SYCP3 is a fibrillar 30 kDa molecule that is composed of a central α-helical domain that is flanked by non-helical N- and C-termini, and that interacts with double-stranded DNA *via* its N-terminal DNA binding domain (Syrjanen et al., 2014). A crystallographic analysis showed that the N-terminal regions are located at both ends of a SYCP3-tetramer, composed of a helical core, which folds in an elongated rod-like structure. Single molecule fluorescent microscopy provided *in vitro* evidence that this structural feature allows SYCP3 to hold distant DNA regions together via a non-sequence specific bridging reaction (Syrjanen et al., 2017). However, *in vivo*, SYCP3 might show some sequence specificity, because ChIP and DNA sequencing in macaque, mouse and rat demonstrated that it associates with a specific subfamily of active short-interspersed elements (SINE) (i.e., AluY and B1). SYCP3 might use these sequences as anchoring points, while repressing their retrotransposition activity (Hernandez-Hernandez et al., 2008; Johnson et al., 2013). In female mice, deficiency of SYCP3 promotes aneuploidy due to segregation defects in oocytes, leading to non-viable offspring (Yuan et al., 2002; Kouznetsova et al., 2005; Wang and Hoog, 2006). In male, the absence of SYCP3 compromises the maintenance of the integrity of axial elements and the efficiency of the repair of meiotic double strand breaks, leading to a prophase I arrest (Yuan et al., 2000; Pelttari et al., 2001).

In vitro assays showed that SYCP3 forms tetramers, bind DNA and can self-assemble into regular superstructures that are reminiscent of the structure of axial elements (Syrjanen et al., 2014; West et al., 2019). Those studies further indicated that this self-assembly property does not depend on the presence of DNA. However the SYCP3 fiber structure can interact with DNA through the N-terminal tail (Syrjanen et al., 2014; Bollschweiler et al., 2019). It was proposed that the structural properties of SYCP3 fibers are compatible with those of a liquid crystal (Rog et al., 2017), and that SYCP3 might form a protein layer, coating the surface of the existing chromosome structure established by cohesins (Bollschweiler et al., 2019). SYCP3 physical properties might also explain the evolutionarily conserved density of chromatin loops (∼20 loops per μm) on meiotic chromosomes (Kleckner, 2006), because molecular modeling predicts one loop for every two repeating units of the SYCP3 fiber (Syrjanen et al., 2014). It is unclear what determines the length of the loops and in turn the length of the chromosome axis. Cohesins might be involved in regulating loop length, and also in axis length together with other axis components (see below section "Axis Formation and Axis-Loop Organization").

In vivo, it is likely that SYCP3 assembles on the pre-existing chromosome axis, determined to a large extent by cohesins (see below). Immunostaining of spermatocyte spreads showed that SYCP3 first appears at preleptotene/early leptotene, where

it forms small stretches of axial-like structures that colocalize with REC8 and RAD21L cohesins, HORMADs and SYCP2 (see below). The association of SYCP3 with axial elements might be stabilized by SYCP2, because in its absence SYCP3 signal is reduced (Fujiwara et al., 2020). At this early stage, most centromere regions also co-localize with SYCP3 (Bisig et al., 2012). Like cohesins, SYCP3 then forms increasingly longer stretches of axial structures that become progressively more continuous and form the lateral elements of the synaptonemal complex in pachytene. Like all axial element components, SYCP3 localizes on unsynapsed and synapsed chromosomes and the XY-bivalent. Super-resolution imagining of SYCP3 staining in mouse spermatocytes showed that in pachytene, the lateral elements form a helicoidal structure around the central element of the synaptonemal complex (Schucker et al., 2015). In late diplotene, SYCP3 starts to dissociate from the chromosome arms and accumulates during diakinesis at the inner domain of centromeres. At metaphase I and interkinesis, SYCP3 is completely lost from the chromosome arms, and is detected as a bar-like structure between sister kinetochores. In telophase I, when sister kinetochores are separated, SYCP3 is released from kinetochores (Dobson et al., 1994; Parra et al., 2004, 2006, 2009; Bisig et al., 2012).

Synaptonemal complex protein 2 (SYCP2, also called SCP2) was first identified as a component of rat axial elements. Its sequence shows limited homology over a short region with the yeast protein Red1 (Offenberg et al., 1998). Biochemical and structural studies found similarities between HORMAD1-SYCP2, Hop1-Red1 in yeast and ASY1-ASY3 in *Arabidopsis thaliana*, thus indicating the evolutionary conservation of this pathway of axis assembly (**Table 1**; West et al., 2019). Mouse SYCP2 is a 172 kDa protein harboring different potential DNA binding motifs and several distinct domains. The crystal structure of the ordered N-terminal domain revealed two separate subdomains, ARLD and SLD. The ARLD domain might function as a protein-interacting platform, because it can associate with various proteins, such as the two centromere-associated proteins CENP J and F. The SLD domain structurally resembles the Spt16M subunit of the FACT complex, a chaperone involved in the assembly and disassembly of histones H2A and H2B. This domain might be implicated in SYCP2 binding to chromatin (Feng et al., 2017). The N-terminal region of SYCP2 is followed by an extended disordered region. A short region, directly following the ordered region of the N-terminal domain shows homology with HORMAD1 and HORMAD2 closure motif. This putative closure motif, the position of which is equivalent to the closure motif in Red1, interacts with the HORMA domain of HORMAD2 and competes with the HORMAD2 closure motif to bind to the HORMA domain of HORDMAD2. It is predicted (not demonstrated yet) that the SYCP2 closure motif also binds to HORMAD1 (West et al., 2019). The C-terminal of SYCP2 contains a coiled-coil domain. Unlike Red1 that self-associates through its coiled-coil domain, SYCP2 interacts with the coiled-coil domain of SYCP3 (Tarsounas et al., 1997; Yang et al., 2006; Winkel et al., 2009; West et al., 2019). Although SYCP3 can exist as a homo-tetramer (Syrjanen et al., 2014; West et al., 2019), antiparallel SYCP2:SYCP3-heterotetramer formation appears to be the preferred state when both proteins are present (West et al., 2019).

In vivo, SYCP2 first appears at meiotic axial elements in early leptotene (Schalk et al., 1998). Until metaphase I, SYCP2 co-localizes with SYCP3 (Kouznetsova et al., 2005; Shin et al., 2010). High-resolution stochastic optical reconstruction microscopy revealed that the C-terminal, coiled-coil domain of SYCP2 preferentially co-localizes with SYCP3, compared with the N-terminus, as predicted by interaction data (Xu et al., 2019). SYCP2 localization on chromosomes depends on SYCP3 and cohesins (see below) (Pelttari et al., 2001; Fujiwara et al., 2020). In mouse, absence of SYCP2 leads to male sterility and female subfertility, due to their incapacity of forming fully functional axial elements (Yang et al., 2006; Fujiwara et al., 2020).

FUNCTIONAL ROLES OF THE MEIOTIC AXIS ORGANIZATION IN EARLY MEIOTIC PROPHASE I

Axis Components and the Control of Sister Chromatid Cohesion

The general principles of the establishment and maintenance of sister chromatin cohesion (SCC) also apply to the meiotic stages. The complexity of SCC establishment and maintenance at chromosome arms during early prophase I results from the presence of different kleisin subunits that in agreement with their differential spatiotemporal localization, appear to have different properties. FISH analysis in spermatocytes that lack REC8 and RAD21L (the two meiotic kleisins) shows proper SCC at prophase I entry, suggesting that the somatic RAD21 cohesin complexes are sufficient to establish SCC during premeiotic S phase (Llano et al., 2012). It is likely that RAD21L has no or only a minor role in SCC along chromosome arms, because in its absence their cohesion is established and maintained through prophase I (Herran et al., 2011; Ishiguro et al., 2014). On the other hand, REC8 cohesin complexes play an important role in SCC at chromosome arms early in prophase I (**Figure 4**). In REC8 absence, cohesion is established but sister chromatids partially lose their tight association and split, although RAD21L cohesin complexes can load onto chromosome axes (Bannister et al., 2004; Xu et al., 2005; Agostinho et al., 2016). In STAG3-deficient mice, in which REC8 levels are reduced, it appears that REC8 density along chromosome arms is crucial for SCC maintenance. If the spacing of REC8 foci is larger than 15% of the total chromosome length, the tight association is lost (Agostinho et al., 2016). SMC1β absence also leads to the local loss of the tight association between sister chromatids on a proportion of chromosomes from early prophase. The relatively milder SCC phenotype, compared with what observed in the absence of REC8, may be due to the presence of SMC1α that can compensate for SMC1β role in SCC at chromosome arms (Revenkova et al., 2004; Biswas et al., 2013; Agostinho et al., 2016). Absence or reduction of STAG3 partially phenocopies the loss of REC8 because the amount of REC8 cohesin complexes is strongly reduced in these mice (Caburet et al., 2014; Fukuda et al., 2014;

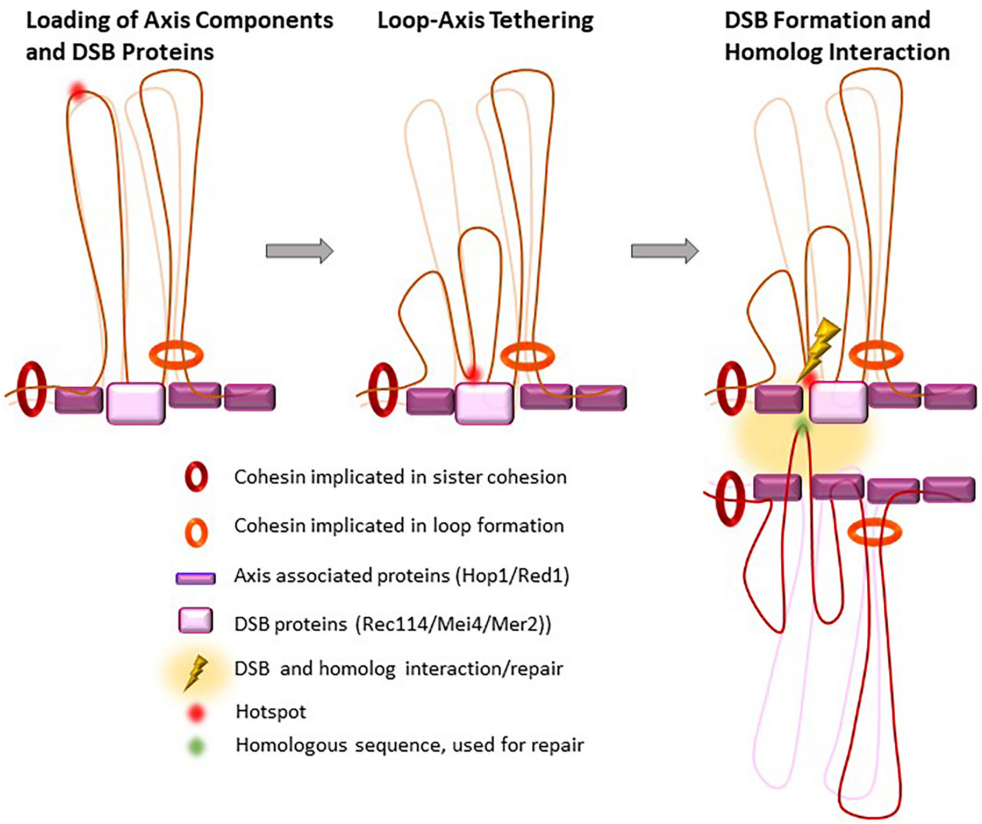

FIGURE 4 | Proposed loop re-organization at leptonema upon and after DSB formation. In early prophase I, meiotic hotspots localize in loops and the DSB formation proteins (DSB pre-recombinosome) localize on the axis. Before DSB formation, hotspots contact the DSB pre-recombinosome, reorganizing the loops that contain hotspots where DSB will form.

Hopkins et al., 2014; Llano et al., 2014; Winters et al., 2014). However, unlike REC8 mutants (Bannister et al., 2004), the cohesion of centromeres and telomeres is partially lost, showing the important role of STAG3 in SCC maintenance, which is not compensated by the somatic STAG1 and STAG2 isoforms even though they are detected in meiosis (Fukuda et al., 2014; Llano et al., 2014; Winters et al., 2014).

Interestingly, all cohesin mutants that lead to loss of SCC at chromosome arms (SMC1β, REC8 and STAG3) present loading of synaptonemal complex proteins (SYCP1, SYCE1, SYCE2 and TEX12) between sister chromatids instead of homologs (Bannister et al., 2004; Xu et al., 2005; Agostinho et al., 2016; Biswas et al., 2016). It is not clear whether the loss of the tight association between sister chromatids allows the formation of inter-sister synaptonemal complexes, or whether the binding of REC8 cohesin complexes prevents the binding of synaptonemal complex proteins to specific sites on axial elements (Bannister et al., 2004; Xu et al., 2005; Caburet et al., 2014; Fukuda et al., 2014; Hopkins et al., 2014; Llano et al., 2014). The role of RAD21L is not known. RAD21L cohesin complexes do not mediate SCC, but may promote contacts and loop organization on single chromatids or between recombinant chromatids. This duality of function between REC8 and RAD21L is observed also for the *Drosophila melanogaster* Rad21 and C(2)M proteins (Cahoon and Hawley, 2016; Gyuricza et al., 2016) and in *C. elegans* where REC8 and COH-3, COH-4 (RAD21L orthologs) (Severson et al., 2009) show distinct localizations on chromosome axes (Kohler et al., 2017; Woglar et al., 2020). However, this separation of tasks between REC8 and RAD21L homologs is not a general rule as some species have either REC8 only (*S. cerevisiae*; *A. thaliana*), as RAD21L is only found in deuterostomia, or RAD21L only (birds), as meiotic-specific kleisin (Gutierrez-Caballero et al., 2011).

Axis Formation and Loop-Axis Organization

Contribution of Axis Components

Extensive studies in single and double mutant mice demonstrated that cohesins are not only the first building blocks of axial elements, by forming an axial chromosome core upon which the remaining axial element proteins can build, but they also determine their structure, and specifically their length. Their role in axis formation seems not to be linked to their function in SCC, because the axis can form normally in a *Coprinus cinereus* mutant that lacks sister chromatids or in mutants where the premeiotic S-phase does not occur (Merino et al., 2000; Blitzblau et al., 2012). The most striking phenotype, which shows the importance of

cohesins in axis formation, is observed in STAG3-deficient mice, where the axis does not form, and only dot-like structures remain that might just contain SYCP3 aggregates (Ishiguro et al., 2014; Winters et al., 2014). The presence of cohesin subunits on axis in a distinct *Stag3* mutant background may be due to residual level of STAG3 and/or expression of STAG1/2 (Caburet et al., 2014; Fukuda et al., 2014; Hopkins et al., 2014; Llano et al., 2014).

Absence of SMC1β also dramatically alters the axis structure with almost a twofold reduction of its length in *Smc1*β–/– mice compared with wild type mice (Revenkova et al., 2004; Biswas et al., 2016). The different kleisin proteins show distinct functions during axis formation. Concomitant absence of REC8 and RAD21L leads to a similar phenotype as in STAG3-deficient mice, suggesting that somatic RAD21 contributes only little, or not at all, to the formation of the chromosomal axial core (Llano et al., 2012; Biswas et al., 2016). However, absence of REC8 or RAD21L alone only partially affects axis length, with a length reduction of about one third compared with wild type (Biswas et al., 2016). Genetic studies using mice that lack SMC1β and one of the two kleisins brought more information on their relative involvement. The combined loss of SMC1β and REC8 reduces axis length to one third of the wild type length. Conversely, the simultaneous loss of SMC1β and RAD21L is almost as dramatic as the loss of STAG3, with a seven-fold reduction of the axis length compared with wild type. These data show that axis formation is mainly supported by the meiotic cohesin components SMC1α/RAD21L, SMC1β/REC8 and to a lower extent by SMC1α/REC8 (Biswas et al., 2016). Interestingly, axis length can also be impacted by the dynamic behavior of cohesin complexes. Indeed, the concomitant depletion of the cohesin regulators PDS5A and PDS5B leads to a severe shortening of axial elements, despite the presence of all tested cohesin subunits in those spermatocytes (Viera et al., 2020). This role of Pds5 in controlling axis length as also been observed in *S. cerevisiae* (Jin et al., 2009; Song et al., 2021) and even in the absence of the sister chromatid (Hong et al., 2019). Although this may indicate an increase in loop lengths, this may result from the consequences of the absence of Pds5 on loop expansion and on sister chromatid cohesion as clearly observed by HiC in yeast vegetative cells (Dauban et al., 2020).

The severe defects of axis formation observed in mutants for cohesins and their regulators, illustrate the importance for forming a functional cohesin core that provides the structural basis for the loading of other proteins such as HORMADs, SYCP2, and SYCP3 to complete axial element formation. Yet, not all cohesin complexes present in prophase I have equivalent roles for the recruitment of other axis-associated proteins. REC8 deficiency, for example only slightly affects HORMAD1 foci formation, as shown by immunostaining. Conversely, the number of preleptotene and early leptotene HORMAD1 foci is drastically reduced in RAD21L mutants, suggesting, at least at early stages, the involvement of RAD21L in HORMAD1 loading to chromosomes (Fujiwara et al., 2020). The lack of a definite DNA binding domain in both HORMAD proteins and the fact that HORMAD1 co-immunoprecipitates with all meiotic cohesin subunits, corroborate this possibility (Fujiwara et al., 2020). It has also been suggested, that HORMAD1 and RAD21L stabilize each other for their mutual loading on chromatin, because RAD21L axis localization also is slightly reduced in the absence of HORMAD1, without any obvious effect on cohesin axial core formation or SYCP3 or SYCP2 loading (Shin et al., 2010; Daniel et al., 2011; Fujiwara et al., 2020). Thus, HORMAD1 loading depends on cohesin components and might be coordinated with RAD21L loading or stabilization. Additionally, even though HORMAD1 is loaded independently of axial element proteins, as shown by genetic studies in mice lacking SYCP2 or SYCP3 (Fukuda et al., 2010; Fujiwara et al., 2020), those proteins may play a role in stabilizing HORMAD1 interaction with the axial core because cohesin-HORMAD1 co-localization is reduced in SYCP2-deficient mice (Fujiwara et al., 2020).

SYCP2 and SYCP3 are not essential for the formation of the cohesin core (Yuan et al., 2000, 2002; Pelttari et al., 2001; Fujiwara et al., 2020), but have an important role in determining its compaction and thereby the size of axial elements. In SYCP3-deficient oocytes, the residual axis is twice as long as in wild type cells (Yuan et al., 2002; Novak et al., 2008). The respective contribution of each protein is difficult to address because the loading of one protein on the axial core depends on the other (Pelttari et al., 2001; Yang et al., 2006; Fujiwara et al., 2020). This default in axis compaction can be partly rescued by the simultaneous absence of SMC1β and SYCP3, leading to the hypothesis that the interplay between the compaction exerted by axial element proteins and the restriction of this compaction mediated by cohesin complexes determines the final length of axial elements in meiosis (Novak et al., 2008).

The Loop-Axis Configuration

The loop-axis organization of prophase I chromosomes is a very fascinating aspect of meiosis. The first description of the loop-axis organization in the mouse was based on light microscopy observations in which pachytene chromosomes were described as axes from which emanate fuzzy lateral projections, interpreted as DNA loops (Monesi, 1965), as previously suggested in rat and insect spermatocytes (Sotelo and Trujillo-Cenoz, 1960). The lamp brush-like loop-axis shape of meiotic chromosomes in the mouse was later confirmed by electron microscopy (Kierszenbaum and Tres, 1974). The general nature of the loop-axis setup of meiotic chromosomes is extremely conserved in different species (Zickler and Kleckner, 1999). However, the fine-scale loop-axis organization may vary greatly, even within species. An example of this variation can be observed in male and female mammals. Immunofluorescence studies and electron microscopy serial sections (von Wettstein et al., 1984) in mouse and human, have shown that axes are in average twofold longer in female than in male gametocytes with variations between chromosomes (Tease and Hulten, 2004; Gruhn et al., 2013; Wang et al., 2017). The mouse PAR region on the XY chromosomes further illustrates variability between chromosomes. In early prophase, the PAR axis is longer compared with that of autosomal regions of similar size and then shortens as prophase I progresses. In both examples, staining of chromatin loops by immuno-FISH shows that longer axes (female and early PAR) feature more compact loops, that appear closer to the axis, whereas shorter axes (male and late PAR) feature more decompacted loops, that appear further away from

the axis (Kauppi et al., 2011; Acquaviva et al., 2020). Similar observations were made in mutant mice where axes are shorter (Cohesin and PDS5, see above) or longer (SYCP3, see above) (Novak et al., 2008; Viera et al., 2020; **Figure 3**). Taken together, these observations led to the suggestion that in mouse and human, axis-lengthening leads to loop shortening and *vice-versa*, as it was proposed in other organisms (Zickler and Kleckner, 1999; Tease and Hulten, 2004; Kleckner, 2006). However, it is difficult to infer loop length from Immuno-FISH experiments on chromosome spreads. Loops that appear shorter, might contain the same amount of chromatin as loops that appear longer, but simply stretch out laterally due to a longer and less compact axis. Ideally, one would need to measure the amount of DNA present within loops. In addition, a change in axis length is expected to be associated to a change in loop length, only if one assumes that the density of loops per unit length is constant.

Loop organization has been analyzed by direct molecular approaches in particular by chromosome conformation capture (HiC). In *S. cerevisiae* HiC experiments showed that pachytene chromosomes feature a punctuate contact pattern in which contact points partially overlap with Rec8 binding sites (Muller et al., 2018; Schalbetter et al., 2019). This contact pattern is lost in the absence of Rec8 (Schalbetter et al., 2019), suggesting that cohesin is responsible for shaping the loop-axis conformation of prophase I chromosomes in yeast. *In silico* simulation experiments, in which chromatin is modeled as a polymer, best fit with the experimental data when Rec8 is localized at the basis of chromatin loops that are progressively extruded, until stopped by another extruder or an unknown barrier, for example a large protein complex, such as the transcription machinery. The best fitting model suggests that in a given cell, only few Rec8 sites, not necessarily adjacent, are occupied, leading to the heterogeneous loop size distribution observed along chromosomes. In this scenario, loop distribution is expected to be mostly stochastic, and thus, to vary from cell to cell, and possibly between sister chromatids and homologs. In these experiments, the loop size was estimated to be in the range of 10–50 kb, with a mean value of about 26 kb (Muller et al., 2018; Schalbetter et al., 2019). This estimation is consistent with the loop size of 20kb proposed by electron microscopy experiments (Moens and Pearlman, 1988).

In the mouse, HiC experiments using purified zygotene and pachytene spermatocytes show contact probability patterns that are compatible with chromosome individualization, and that are similar to what observed in mitotic cells, namely a pattern of a linear compressed array of consecutive loops along a scaffold axis (Gibcus et al., 2018). The establishment of the loop-axis configuration in the mouse is accompanied by a progressive loss of contacts of topologically associated domains (TADs), with similarity to mitosis. TAD boundaries are preferentially occupied by CTCF that can provide anchors for cohesin-mediated loop extrusion (Bonev and Cavalli, 2016). Intriguingly, unlike in mitosis where CTCF is largely evicted from chromosomes, CTCF remains bound to TAD boundaries in pachytene chromosomes (Oomen et al., 2019; Vara et al., 2019; Luo et al., 2020). Another feature lost in mitosis, but conserved in prophase I chromosomes, is the maintenance of a substantial amount of refined compartmentalization of large-scale, gene-dense *versus* gene-poor compartments, also called A and B compartments. These compartments are maintained in meiotic chromosomes possibly due to active transcription (Alavattam et al., 2019; Patel et al., 2019; Vara et al., 2019; Wang et al., 2019; Luo et al., 2020). Unlike in *S. cerevisiae*, in the mouse and monkey there is no evidence of distinct loop-basis interaction sites. This suggests that loops are mainly anchored randomly along axial elements, yielding only very low-frequency contact sites, which remain undetectable at the sensitivity of the experiments performed until now (Alavattam et al., 2019; Patel et al., 2019; Vara et al., 2019; Wang et al., 2019; Luo et al., 2020). If distinct loop interaction sites exist in the mouse, CTCF-bound sites, which colocalize with about half of all REC8 and RAD21L binding sites found in pachytene cells, would be good candidate regions (Vara et al., 2019; Luo et al., 2020).

In silico modeling using HiC data estimated the mean loop size of mouse zygotene and pachytene chromosomes to be between 0.8 and 2 Mbps (Alavattam et al., 2019; Patel et al., 2019). This value may, however, mask variability that is detected when separating A and B compartments and revealing shorter predicted loop sizes in A compartments (Jin et al., 2021). Electron microscopy and immuno-FISH experiments using female and male meiotic chromosome spreads estimated the loop size on several autosomes to be about 2.2 mm in leptotene, and about 6 μm in pachytene (Novak et al., 2008; Kauppi et al., 2011). Considering an estimated DNA density of about 40 kb to 94 kb/μm of chromatin loops (Moens and Pearlman, 1988; Kauppi et al., 2011; Ito et al., 2014), loop size would be expected to be smaller than what deduced from HiC data: about 250–500 Kb. However, as mentioned above, Immuno-FISH experiments on chromosome spreads have several limitations and do not take into account loop extension in space. This could be one of the reasons, why cytological measures do not fit Hi-C data. These differences need to be investigated more thoroughly. Both REC8 and RAD21L could participate in loop extrusion, and loop boarders could be potentially defined by CTCF sites and sites of meiotic DSBs. Indeed, DSBs in vegetative cells are enriched in cohesins (Strom et al., 2004; Unal et al., 2004) and DSBs have recently been shown to anchor cohesins at loop bases both in human cells (Arnould et al., 2021) and *S. cerevisiae* (Piazza et al., 2020).

The Role of Axis Components in Homolog Pairing Before Meiotic Recombination

In several studies in *S. cerevisiae* and mammals, homolog pairing is detected even in the absence of meiotic recombination (Cha et al., 2000; Boateng et al., 2013; Ishiguro et al., 2014). Obviously, this is also a well-established property of meiosis in species (e.g., *D. melanogaster* and *C. elegans)* where pairing and homologous synapsis take place before DSB formation (Gerton and Hawley, 2005). The molecular mechanism of this pairing process is unknown and different species may adopt distinct strategies. In the context of the meiotic chromosome structure, one hypothesis is that cohesins mediates homologous pairing. This is based on two observations. First, in mouse spermatocytes, REC8 and

RAD21L form distinct foci that can be at similar positions on both homologs. Each homolog would then have a specific bar code defined by these cohesin complexes, and this would allow a specific interhomolog interaction (Ishiguro et al., 2011). Second, recombination-independent (i.e., in *Spo11* mutants) homologous pairing detected by immuno-FISH assays (Boateng et al., 2013; Ishiguro et al., 2014), is defective in *Rad21L*$^{-/-}$ but not in *Rec8*$^{-/-}$ mice, suggesting a direct or indirect role for the RAD21L cohesin complex (Ishiguro et al., 2014). In *S. pombe*, where recombination-independent pairing has been analyzed in detail (Ding et al., 2012, 2019), cohesins are required (Ding et al., 2016). This could indicate a direct role of cohesins in pairing, or a more indirect role through the establishment of proper chromosome organization.

The Axis Role in Meiotic Recombination

The chromosome axis is a platform for regulating meiotic recombination and specially to regulate DSB formation, interhomolog bias and CO formation during DSB repair. The contribution of the axis structure to DSB repair involves several additional components, namely the proteins that organize the central element of the synaptonemal complex for synapsis starting at zygonema. This aspect of the regulation of DSB repair and synapsis involves many factors and molecular pathways, will not be reviewed here, and only a few points will be highlighted below.

Impact of the Axis Structure on DSB Activity

Double-strand breaks repair takes place in the context of the chromosome axis, as shown by the many studies that described the axial localization of proteins involved in the early steps of DSB repair, such as RPA, RAD51, and DMC1 (Bishop, 1994). Meiotic DSBs might thus be introduced on genomic DNA sequences localized near the axis. It is thought that this is ensured, at least in part, by the axis-specific localization of the RMM complex, or Rec114/Mei4/Mer2 (REC114/MEI4/IHO1 in mammals), a protein complex that is essential for DSB activity. Indeed, the axis-associated proteins, cohesins, HORMADs, SYCP2 and SYCP3 in mammals, constitute a basis for loading the RMM complex (Winters et al., 2014; Kumar et al., 2015; Stanzione et al., 2016; Bhattacharyya et al., 2019; Papanikos et al., 2019; Acquaviva et al., 2020; Fujiwara et al., 2020; **Figure 4**). Such control also implies the tethering of potential DSB sites to the axis, as proposed by N. Kleckner (Blat et al., 2002). Indeed, in *S. cerevisiae*, DNA sequences that are constitutively axis-associated and interact with Rec8 or Red1 are not DSB sites, possibly because the DNA is not accessible to Spo11. In fact, it has been suggested that Rec8 antagonizes DSB formation in yeast and *A. thaliana* (Ito et al., 2014; Nambiar and Smith, 2018; Lambing et al., 2020). As described earlier (see section "The Meiotic Cohesin Complex, With the Specific α-Kleisin Rec8"), in *S. cerevisiae*, Rec8 is enriched near the 3′ ends of convergent genes. Thus, the potential DSB sites, which are promoter regions and have accessible chromatin, are brought, or stabilized to the axis thanks to the partly characterized interactions of H3K4me3 with Spp1 and of Spp1 with Mer2 (Acquaviva et al., 2013; Sommermeyer et al., 2013; Adam et al., 2018). How the RMM complex is localized remains to be understood and the interaction detected between HORMAD1 and IHO1 (Stanzione et al., 2016) and between Hop1 and Mer2 (Rousova et al., 2020) is one determinant for this localization.

Disrupting or changing Hop1 or Red1 localization directly by mutations or indirectly by altering cohesin localization has a direct consequence on DSB activity. This has been shown in *S. cerevisiae*, with changes of DSB localization in the Rec8 mutant (Kugou et al., 2009; Sun et al., 2015). When Red1 or Hop1 is disrupted, the overall DSB activity is slightly or strongly reduced, respectively (Mao-Draayer et al., 1996; Schwacha and Kleckner, 1997). Similarly, DSB activity is reduced in *Hormad1*$^{-/-}$ mice (Daniel et al., 2011). Moreover, the chromosome axis has additional roles by ensuring feedback controls of DSB activity *in cis*. DSB formation leads to ATM (Tel1) kinase activation that negatively regulates locally and remotely DSB activity (Garcia et al., 2015). This local effect is likely to be explained by the chromosomal organization around DSB sites. It has been proposed that chromatin loops are physical units than can be targeted by the DSB machinery. This is consistent with the observation that increasing loop density, such as in the mouse PAR region, increases the potential for DSB activity (Kauppi et al., 2011). Long distance effects of ATM regulation could involve axis and chromatin components. One well known ATM dependent-chromatin modification that is observed also away from DSB sites (50 Kb in yeast, a few Mb in mammals) is the phosphorylation of the H2A variant H2AX, named as gH2AX (Mahadevaiah et al., 2001). As reported in somatic cells upon DSB induction, gH2AX spreads over large domains around the DSB sites, but its spreading is constrained at TADs in a process that requires cohesin-mediated loop extrusion (Caron et al., 2012; Arnould et al., 2021).

On chromosome axes, the Hop1/HORMAD1 protein also plays a role in inhibiting DSB activity and in checkpoint signaling. One pathway for this regulation is mediated by the displacement of Hop1/HORMAD1 from the chromosome axis upon synapsis triggered by homologous DSB repair. Hop1/HORMAD1 displacement leads to delocalization of the RMM complex, and thus downregulation of DSB activity. Additional regulations for signaling meiotic progression involve axis interactions and the ATR kinase (Daniel et al., 2011; Widger et al., 2018; Dereli et al., 2021).

Impact on DSB Repair

Although regulation of DSB repair is a wide and complex process beyond the scope of this review, few notable observations link chromosome axis to DSB repair. Hop1/Red1 ensures the bias of DSB repair toward the homolog, at the expenses of inter-sister repair. Indeed, Hop1/Red1 counteracts the activity of Rec8 that promotes sister chromatid cohesion (Kim et al., 2010). The underlying mechanism is not known, but it may occur through the regulation of one or several DSB repair steps, such as strand invasion, the activity of strand exchange proteins, or 3′ end extension. Interestingly, this also implies the uncoupling of the two DSB ends, one to be engaged in interaction with the sister chromatid, the other one excluded from this interaction. Additional chromosome axis structural components

that are implicated in DSB repair through formation of the central element of the synaptonemal complex upon synapsis, play important roles in the decision of repair toward CO or non-CO. This control ensures that each homolog pair has undergone at least one CO.

CONCLUDING REMARKS

Main Properties and Functions

- The highly specialized organization of meiotic chromosomes is put in place at the onset of meiotic prophase I with some early components already bound to chromatin during the meiotic S phase.
- This organization is characterized by chromatin loops anchored to a protein axis. The main structural components and their roles are evolutionarily conserved. These components include cohesins, meiotic HORMA domain proteins, and structural components (Red1 in *S. cerevisiae*, SYCP2 in mammals, HTP-1/2, -3, HIM-3 in *C. elegans*, ASY3 in plants). Cohesin complexes recruit the other components, although these may also bind to chromatin independently from cohesins. Cohesin-mediated recruitment might be important to initiate axis formation. As shown *in vitro*, some axis structural components can multimerize and form filaments (e.g., Red1, SYCP2 and ASY3 with their partners) and are thus predicted to promote elongation of the axial structure. This structure is not static, and loop size and axis length can vary in an anti-correlated manner.
- Several meiotic specific cohesin complexes can co-exist in several species and differ by their α-kleisin subunits. The somatic cohesin complex may also be expressed in meiocytes. Those cohesin complexes achieve several functions, sister chromatid cohesion, loop organization and partner choice for DSB repair. The RAD21L (or COH-3/4) cohesin complex has no detectable sister chromatid cohesion activity. The function of this complex remains to be understood, but it might promote chromatid interactions during meiotic DSB repair.
- The axis forms a platform for loading other components, among which there is the RMM (Rec114, Mei4, Mer2/IHO1) complex that is essential for meiotic DSB formation. The axis-component Hop1/HORMAD1 plays a central role in turning on and off DSB activity with several additional consequences for recombination and meiotic progression. Hop1/HORMAD1 are regulated by conformational changes, mediated by Pch2/PCH2.
- Loops define domains that contribute to DSB activity regulation.
- Anchoring DSB formation to the chromosome axis allows organizing DSB repair regulation, specifically for controlling the inter-homolog bias and the crossover/non-crossover choice.

Future Challenges

What are the determinants of chromatin loop organization? Although cohesins are likely to promote the formation of these loops, how their activities are regulated, how loops are spatially organized along the axis, what is the variability in loop size, and how are loops from the two sisters and from the two homologs organized remain to be determined.

Does this organization participate in homolog pairing and if yes, how?
How are these structural components organized relative to the genomic DNA sequence?
What are the role and activity of the meiotic RAD21L cohesin complex?
Does a loop define a domain for DSB activation? How are the borders defined?
How does the loop/axis from one homolog interact with the loop/axis from its partner upon DSB formation?

AUTHOR CONTRIBUTIONS

Both authors listed have made a substantial, direct and intellectual contribution to the work, and approved it for publication.

FUNDING

BM was funded by grants from the Centre National pour la Recherche Scientifique (CNRS), the European Research Council (ERC) under the European Union's Horizon 2020 research and innovation programme (grant agreement No. 883605), and the Agence Nationale de la Recherche (ANR-18-CE11-0024-01/Topobreaks) and MSDAVENIR.

ACKNOWLEDGMENTS

We thank Denise Zickler, Alberto Pendas, and Attila Toth for their insightful comments on the manuscript. We apologize for those whose work could not be cited as we could not include all aspects of meiotic prophase and could not include data from all species.

REFERENCES

Acquaviva, L., Boekhout, M., Karasu, M. E., Brick, K., Pratto, F., Li, T., et al. (2020). Ensuring meiotic DNA break formation in the mouse pseudoautosomal region. *Nature* 582, 426–431. doi: 10.1038/s41586-020-2327-4

Acquaviva, L., Szekvolgyi, L., Dichtl, B., Dichtl, B. S., de La Roche Saint Andre, C., Nicolas, A., et al. (2013). The compass subunit Spp1 links histone methylation to initiation of meiotic recombination. *Science* 339, 215–218. doi: 10.1126/science.1225739

Adam, C., Guerois, R., Citarella, A., Verardi, L., Adolphe, F., Beneut, C., et al. (2018). The PHD finger protein Spp1 has distinct functions in the Set1 and

the meiotic DSB formation complexes. *PLoS Genet* 14:e1007223. doi: 10.1371/journal.pgen.1007223

Adelfalk, C., Janschek, J., Revenkova, E., Blei, C., Liebe, B., Gob, E., et al. (2009). Cohesin SMC1beta protects telomeres in meiocytes. *J. Cell. Biol.* 187, 185–199. doi: 10.1083/jcb.200808016

Agostinho, A., Manneberg, O., van Schendel, R., Hernandez-Hernandez, A., Kouznetsova, A., Blom, H., et al. (2016). High density of REC8 constrains sister chromatid axes and prevents illegitimate synaptonemal complex formation. *EMBO Rep.* 17, 901–913. doi: 10.15252/embr.201642030

Alavattam, K. G., Maezawa, S., Sakashita, A., Khoury, H., Barski, A., Kaplan, N., et al. (2019). Attenuated chromatin compartmentalization in meiosis and its maturation in sperm development. *Nat. Struct. Mol. Biol.* 26, 175–184. doi: 10.1038/s41594-019-0189-y

Alsheimer, M., Baier, A., Schramm, S., Schutz, W., and Benavente, R. (2010). Synaptonemal complex protein SYCP3 exists in two isoforms showing different conservation in mammalian evolution. *Cytogenet. Genome Res.* 128, 162–168. doi: 10.1159/000303341

Arnould, C., Rocher, V., Finoux, A. L., Clouaire, T., Li, K., Zhou, F., et al. (2021). Loop extrusion as a mechanism for formation of DNA damage repair foci. *Nature* 590, 660–665. doi: 10.1038/s41586-021-03193-z

Bannister, L. A., Reinholdt, L. G., Munroe, R. J., and Schimenti, J. C. (2004). Positional cloning and characterization of mouse mei8, a disrupted allele of the meiotic cohesin Rec8. *Genesis* 40, 184–194. doi: 10.1002/gene.20085

Bayes, M., Prieto, I., Noguchi, J., Barbero, J. L., and Perez Jurado, L. A. (2001). Evaluation of the Stag3 gene and the synaptonemal complex in a rat model (as/as) for male infertility. *Mol. Rep. Dev.* 60, 414–417. doi: 10.1002/mrd.1104

Bhattacharyya, T., Walker, M., Powers, N. R., Brunton, C., Fine, A. D., Petkov, P. M., et al. (2019). Prdm9 and meiotic cohesin proteins cooperatively promote DNA double-strand break formation in mammalian spermatocytes. *Curr. Biol.* 29, 1002–1018.e1007.

Bishop, D. K. (1994). RecA homologs Dmc1 and Rad51 interact to form multiple nuclear complexes prior to meiotic chromosome synapsis. *Cell* 79, 1081–1092. doi: 10.1016/0092-8674(94)90038-8

Bisig, C. G., Guiraldelli, M. F., Kouznetsova, A., Scherthan, H., Hoog, C., Dawson, D. S., et al. (2012). Synaptonemal complex components persist at centromeres and are required for homologous centromere pairing in mouse spermatocytes. *PLoS Genet* 8:e1002701. doi: 10.1371/journal.pgen.1002701

Biswas, U., Hempel, K., Llano, E., Pendas, A., and Jessberger, R. (2016). Distinct roles of meiosis-specific cohesin complexes in mammalian spermatogenesis. *PLoS Genet* 12:e1006389. doi: 10.1371/journal.pgen.1006389

Biswas, U., Stevense, M., and Jessberger, R. (2018). SMC1alpha substitutes for many meiotic functions of smc1beta but cannot protect telomeres from damage. *Curr. Biol.* 28:e244.

Biswas, U., Wetzker, C., Lange, J., Christodoulou, E. G., Seifert, M., Beyer, A., et al. (2013). Meiotic cohesin SMC1beta provides prophase I centromeric cohesion and is required for multiple synapsis-associated functions. *PLoS Genet* 9:e1003985. doi: 10.1371/journal.pgen.1003985

Blat, Y., Protacio, R. U., Hunter, N., and Kleckner, N. (2002). Physical and functional interactions among basic chromosome organizational features govern early steps of meiotic chiasma formation. *Cell* 111, 791–802. doi: 10.1016/s0092-8674(02)01167-4

Blitzblau, H. G., Chan, C. S., Hochwagen, A., and Bell, S. P. (2012). Separation of DNA replication from the assembly of break-competent meiotic chromosomes. *PLoS Genet* 8:e1002643. doi: 10.1371/journal.pgen.1002643

Boateng, K. A., Bellani, M. A., Gregoretti, I. V., Pratto, F., and Camerini-Otero, R. D. (2013). Homologous pairing preceding SPO11-mediated double-strand breaks in mice. *Dev. Cell.* 24, 196–205. doi: 10.1016/j.devcel.2012.12.002

Bollschweiler, D., Radu, L., Joudeh, L., Plitzko, J. M., Henderson, R. M., Mela, I., et al. (2019). Molecular architecture of the SYCP3 fibre and its interaction with DNA. *Open biology* 9:190094. doi: 10.1098/rsob.190094

Bonev, B., and Cavalli, G. (2016). Organization and function of the 3D genome. *Nat. Rev. Genet.* 17, 661–678. doi: 10.1038/nrg.2016.112

Borner, G. V., Barot, A., and Kleckner, N. (2008). Yeast Pch2 promotes domainal axis organization, timely recombination progression, and arrest of defective recombinosomes during meiosis. *Proc. Natl. Acad. Sci. U.S.A.* 105, 3327–3332. doi: 10.1073/pnas.0711864105

Caburet, S., Arboleda, V. A., Llano, E., Overbeek, P. A., Barbero, J. L., Oka, K., et al. (2014). Mutant cohesin in premature ovarian failure. *N. Engl. J. Med.* 370, 943–949. doi: 10.1056/nejmoa1309635

Cahoon, C. K., and Hawley, R. S. (2016). Meiosis: cohesins are not just for sisters any more. *Curr. Biol.* 26, R523–R525.

Caron, P., Aymard, F., Iacovoni, J. S., Briois, S., Canitrot, Y., Bugler, B., et al. (2012). Cohesin protects genes against gammaH2AX induced by DNA double-strand breaks. *PLoS Genet* 8:e1002460. doi: 10.1371/journal.pgen.1002460

Cha, R. S., Weiner, B. M., Keeney, S., Dekker, J., and Kleckner, N. (2000). Progression of meiotic DNA replication is modulated by interchromosomal interaction proteins, negatively by Spo11p and positively by Rec8p. *Genes Dev.* 14, 493–503.

Daniel, K., Lange, J., Hached, K., Fu, J., Anastassiadis, K., Roig, I., et al. (2011). Meiotic homologue alignment and its quality surveillance are controlled by mouse HORMAD1. *Nat. Cell. Biol.* 13, 599–610. doi: 10.1038/ncb2213

Dauban, L., Montagne, R., Thierry, A., Lazar-Stefanita, L., Bastie, N., Gadal, O., et al. (2020). Regulation of cohesin-mediated chromosome folding by eco1 and other partners. *Mol. Cell.* 77, 1279–1293.e1274.

Davidson, I. F., Bauer, B., Goetz, D., Tang, W., Wutz, G., and Peters, J. M. (2019). DNA loop extrusion by human cohesin. *Science* 366, 1338–1345. doi: 10.1126/science.aaz3418

delosSantos, T., and Hollingsworth, N. M. (1999). Red1p, a MEK1-dependent phosphoprotein that physically interacts with Hop1p during meiosis in yeast. *J. Biol. Chem.* 274, 1783–1790. doi: 10.1074/jbc.274.3.1783

Dereli, I., Stanzione, M., Olmeda, F., Papanikos, F., Baumann, M., Demir, S., et al. (2021). Four-pronged negative feedback of DSB machinery in meiotic DNA-break control in mice. *Nucleic Acids Res.* 49, 2609–2628. doi: 10.1093/nar/gkab082

Ding, D. Q., Matsuda, A., Okamasa, K., Nagahama, Y., Haraguchi, T., and Hiraoka, Y. (2016). Meiotic cohesin-based chromosome structure is essential for homologous chromosome pairing in Schizosaccharomyces pombe. *Chromosoma* 125, 205–214. doi: 10.1007/s00412-015-0551-8

Ding, D. Q., Okamasa, K., Katou, Y., Oya, E., Nakayama, J. I., Chikashige, Y., et al. (2019). Chromosome-associated RNA-protein complexes promote pairing of homologous chromosomes during meiosis in Schizosaccharomyces pombe. *Nat. Commun.* 10:5598.

Ding, D. Q., Okamasa, K., Yamane, M., Tsutsumi, C., Haraguchi, T., Yamamoto, M., et al. (2012). Meiosis-specific noncoding RNA mediates robust pairing of homologous chromosomes in meiosis. *Science* 336, 732–736. doi: 10.1126/science.1219518

Dobson, M. J., Pearlman, R. E., Karaiskakis, A., Spyropoulos, B., and Moens, P. B. (1994). Synaptonemal complex proteins: occurrence, epitope mapping and chromosome disjunction. *J. Cell Sci.* 107, 2749–2760. doi: 10.1242/jcs.107.10.2749

Eijpe, M., Heyting, C., Gross, B., and Jessberger, R. (2000). Association of mammalian SMC1 and SMC3 proteins with meiotic chromosomes and synaptonemal complexes. *J. Cell Sci.* 113, 673–682. doi: 10.1242/jcs.113.4.673

Eijpe, M., Offenberg, H., Jessberger, R., Revenkova, E., and Heyting, C. (2003). Meiotic cohesin REC8 marks the axial elements of rat synaptonemal complexes before cohesins SMC1{beta} and SMC3. *J. Cell Biol.* 160, 657–670. doi: 10.1083/jcb.200212080

Feng, J., Fu, S., Cao, X., Wu, H., Lu, J., Zeng, M., et al. (2017). Synaptonemal complex protein 2 (SYCP2) mediates the association of the centromere with the synaptonemal complex. *Protein Cell* 8, 538–543. doi: 10.1007/s13238-016-0354-6

Fraune, J., Alsheimer, M., Volff, J. N., Busch, K., Fraune, S., Bosch, T. C., et al. (2012). Hydra meiosis reveals unexpected conservation of structural synaptonemal complex proteins across metazoans. *Proc. Natl. Acad. Sci. U.S.A.* 109, 16588–16593. doi: 10.1073/pnas.1206875109

Fudenberg, G., Imakaev, M., Lu, C., Goloborodko, A., Abdennur, N., and Mirny, L. A. (2016). Formation of chromosomal domains by loop extrusion. *Cell Rep.* 15, 2038–2049. doi: 10.1016/j.celrep.2016.04.085

Fujiwara, Y., Horisawa-Takada, Y., Inoue, E., Tani, N., Shibuya, H., Fujimura, S., et al. (2020). Meiotic cohesins mediate initial loading of HORMAD1 to the chromosomes and coordinate SC formation during meiotic prophase. *PLoS Genet* 16:e1009048. doi: 10.1371/journal.pgen.1009048

Fukuda, T., Daniel, K., Wojtasz, L., Toth, A., and Hoog, C. (2010). A novel mammalian HORMA domain-containing protein, HORMAD1, preferentially associates with unsynapsed meiotic chromosomes. *Exp. Cell Res.* 316, 158–171. doi: 10.1016/j.yexcr.2009.08.007

Fukuda, T., Fukuda, N., Agostinho, A., Hernandez-Hernandez, A., Kouznetsova, A., and Hoog, C. (2014). STAG3-mediated stabilization of REC8 cohesin complexes promotes chromosome synapsis during meiosis. *EMBO J.* 33, 1243–1255. doi: 10.1002/embj.201387329

Gandhi, R., Gillespie, P. J., and Hirano, T. (2006). Human Wapl is a cohesin-binding protein that promotes sister-chromatid resolution in mitotic prophase. *Curr. Biol.* 16, 2406–2417. doi: 10.1016/j.cub.2006.10.061

Garcia, V., Gray, S., Allison, R. M., Cooper, T. J., and Neale, M. J. (2015). Tel1(ATM)-mediated interference suppresses clustered meiotic double-strand-break formation. *Nature* 520, 114–118. doi: 10.1038/nature13993

Gerton, J. L., and Hawley, R. S. (2005). Homologous chromosome interactions in meiosis: diversity amidst conservation. *Nat. Rev. Genet.* 6, 477–487. doi: 10.1038/nrg1614

Gibcus, J. H., Samejima, K., Goloborodko, A., Samejima, I., Naumova, N., Nuebler, J., et al. (2018). A pathway for mitotic chromosome formation. *Science* 359:eaao6135.

Goloborodko, A., Imakaev, M. V., Marko, J. F., and Mirny, L. (2016). Compaction and segregation of sister chromatids via active loop extrusion. *eLife* 5:e14864.

Gomez, R., Felipe-Medina, N., Ruiz-Torres, M., Berenguer, I., Viera, A., Perez, S., et al. (2016). Sororin loads to the synaptonemal complex central region independently of meiotic cohesin complexes. *EMBO Rep.* 17, 695–707. doi: 10.15252/embr.201541060

Gruhn, J. R., Rubio, C., Broman, K. W., Hunt, P. A., and Hassold, T. (2013). Cytological studies of human meiosis: sex-specific differences in recombination originate at, or prior to, establishment of double-strand breaks. *PLoS One* 8:e85075. doi: 10.1371/journal.pone.0085075

Gutierrez-Caballero, C., Herran, Y., Sanchez-Martin, M., Suja, J. A., Barbero, J. L., Llano, E., et al. (2011). Identification and molecular characterization of the mammalian alpha-kleisin RAD21L. *Cell Cycle* 10, 1477–1487. doi: 10.4161/cc.10.9.15515

Gyuricza, M. R., Manheimer, K. B., Apte, V., Krishnan, B., Joyce, E. F., McKee, B. D., et al. (2016). Dynamic and stable cohesins regulate synaptonemal complex assembly and chromosome segregation. *Curr. Biol.* 26, 1688–1698. doi: 10.1016/j.cub.2016.05.006

Haarhuis, J. H., Elbatsh, A. M., van den Broek, B., Camps, D., Erkan, H., Jalink, K., et al. (2013). WAPL-mediated removal of cohesin protects against segregation errors and aneuploidy. *Curr. Biol.* 23, 2071–2077. doi: 10.1016/j.cub.2013.09.003

Heldrich, J., Sun, X., Vale-Silva, L. A., Markowitz, T. E., and Hochwagen, A. (2020). Topoisomerases modulate the timing of meiotic DNA breakage and chromosome morphogenesis in *Saccharomyces cerevisiae*. *Genetics* 215, 59–73. doi: 10.1534/genetics.120.303060

Hernandez-Hernandez, A., Rincon-Arano, H., Recillas-Targa, F., Ortiz, R., Valdes-Quezada, C., Echeverria, O. M., et al. (2008). Differential distribution and association of repeat DNA sequences in the lateral element of the synaptonemal complex in rat spermatocytes. *Chromosoma* 117, 77–87. doi: 10.1007/s00412-007-0128-2

Herran, Y., Gutierrez-Caballero, C., Sanchez-Martin, M., Hernandez, T., Viera, A., Barbero, J. L., et al. (2011). The cohesin subunit RAD21L functions in meiotic synapsis and exhibits sexual dimorphism in fertility. *EMBO J.* 30, 3091–3105. doi: 10.1038/emboj.2011.222

Heyting, C., Dietrich, A. J., Redeker, E. J., and Vink, A. C. (1985). Structure and composition of synaptonemal complexes, isolated from rat spermatocytes. *Eur. J. Cell Biol.* 36, 307–314.

Heyting, C., Moens, P. B., van Raamsdonk, W., Dietrich, A. J., Vink, A. C., and Redeker, E. J. (1987). Identification of two major components of the lateral elements of synaptonemal complexes of the rat. *Eur. J. Cell Biol.* 43, 148–154.

Hollingsworth, N. M., and Byers, B. (1989). HOP1: a yeast meiotic pairing gene. *Genetics* 121, 445–462. doi: 10.1093/genetics/121.3.445

Hong, S., Choi, E. H., and Kim, K. P. (2015). Ycs4 is required for efficient double-strand break formation and homologous recombination during meiosis. *J. Microbiol. Biotechnol.* 25, 1026–1035. doi: 10.4014/jmb.1504.04013

Hong, S., Joo, J. H., Yun, H., Kleckner, N., and Kim, K. P. (2019). Recruitment of Rec8, Pds5 and Rad61/Wapl to meiotic homolog pairing, recombination, axis formation and S-phase. *Nucleic Acids Res.* 47, 11691–11708.

Hopkins, J., Hwang, G., Jacob, J., Sapp, N., Bedigian, R., Oka, K., et al. (2014). Meiosis-specific cohesin component, Stag3 is essential for maintaining centromere chromatid cohesion, and required for DNA repair and synapsis between homologous chromosomes. *PLoS Genet* 10:e1004413. doi: 10.1371/journal.pgen.1004413

Hunter, N. (2015). Meiotic recombination: the essence of heredity. *Cold Spring Harb. Perspect. Biol.* 7:a016618. doi: 10.1101/cshperspect.a016618

Ishiguro, K., Kim, J., Fujiyama-Nakamura, S., Kato, S., and Watanabe, Y. (2011). A new meiosis-specific cohesin complex implicated in the cohesin code for homologous pairing. *EMBO Rep.* 12, 267–275. doi: 10.1038/embor.2011.2

Ishiguro, K., Kim, J., Shibuya, H., Hernandez-Hernandez, A., Suzuki, A., Fukagawa, T., et al. (2014). Meiosis-specific cohesin mediates homolog recognition in mouse spermatocytes. *Genes Dev.* 28, 594–607. doi: 10.1101/gad.237313.113

Ishiguro, K. I. (2019). The cohesin complex in mammalian meiosis. *Genes Cells* 24, 6–30. doi: 10.1111/gtc.12652

Ito, M., Kugou, K., Fawcett, J. A., Mura, S., Ikeda, S., Innan, H., et al. (2014). Meiotic recombination cold spots in chromosomal cohesion sites. *Genes Cells* 19, 359–373. doi: 10.1111/gtc.12138

Janssens, F. A., Koszul, R., and Zickler, D. (2012). The chiasmatype theory. a new interpretation of the maturation divisions. 1909. *Genetics* 191, 319–346.

Jin, H., Guacci, V., and Yu, H. G. (2009). Pds5 is required for homologue pairing and inhibits synapsis of sister chromatids during yeast meiosis. *J. Cell Biol.* 186, 713–725. doi: 10.1083/jcb.200810107

Jin, X., Fudenberg, G., and Pollard, K. S. (2021). Genome-wide variability in recombination activity is associated with meiotic chromatin organization. *bioRxiv[preprint]* doi: 10.1101/2021.01.06.425599

Johnson, M. E., Rowsey, R. A., Shirley, S., Vandevoort, C., Bailey, J., and Hassold, T. (2013). A specific family of interspersed repeats (SINEs) facilitates meiotic synapsis in mammals. *Mol. Cytogenet.* 6:1. doi: 10.1186/1755-8166-6-1

Jordan, P. W., Eyster, C., Chen, J., Pezza, R. J., and Rankin, S. (2017). Sororin is enriched at the central region of synapsed meiotic chromosomes. *Chromosome Res.* 25, 115–128. doi: 10.1007/s10577-016-9542-8

Kariyazono, R., Oda, A., Yamada, T., and Ohta, K. (2019). Conserved HORMA domain-containing protein Hop1 stabilizes interaction between proteins of meiotic DNA break hotspots and chromosome axis. *Nucleic Acids Res.* 47, 10166–10180. doi: 10.1093/nar/gkz754

Kauppi, L., Barchi, M., Baudat, F., Romanienko, P. J., Keeney, S., and Jasin, M. (2011). Distinct properties of the XY pseudoautosomal region crucial for male meiosis. *Science* 331, 916–920. doi: 10.1126/science.1195774

Keeney, S., Lange, J., and Mohibullah, N. (2014). Self-organization of meiotic recombination initiation: general principles and molecular pathways. *Annu. Rev. Genet.* 48, 187–214. doi: 10.1146/annurev-genet-120213-092304

Khan, K., Karthikeyan, U., Li, Y., Yan, J., and Muniyappa, K. (2012). Single-molecule DNA analysis reveals that yeast Hop1 protein promotes DNA folding and synapsis: implications for condensation of meiotic chromosomes. *ACS Nano* 6, 10658–10666. doi: 10.1021/nn3038258

Kierszenbaum, A. L., and Tres, L. L. (1974). Transcription sites in spread meiotic prophase chromosomes from mouse spermatocytes. *J. Cell Biol.* 63, 923–935. doi: 10.1083/jcb.63.3.923

Kim, K. P., Weiner, B. M., Zhang, L., Jordan, A., Dekker, J., and Kleckner, N. (2010). Sister cohesion and structural axis components mediate homolog bias of meiotic recombination. *Cell* 143, 924–937. doi: 10.1016/j.cell.2010.11.015

Kim, Y., Rosenberg, S. C., Kugel, C. L., Kostow, N., Rog, O., Davydov, V., et al. (2014). The chromosome axis controls meiotic events through a hierarchical assembly of HORMA domain proteins. *Dev. Cell* 31, 487–502. doi: 10.1016/j.devcel.2014.09.013

Kim, Y., Shi, Z., Zhang, H., Finkelstein, I. J., and Yu, H. (2019). Human cohesin compacts DNA by loop extrusion. *Science* 366, 1345–1349. doi: 10.1126/science.aaz4475

Kironmai, K. M., Muniyappa, K., Friedman, D. B., Hollingsworth, N. M., and Byers, B. (1998). DNA-binding activities of HOP1 protein, a synaptonemal complex component from *Saccharomyces cerevisiae*. *Mol. Cell Biol.* 18, 1424–1435. doi: 10.1128/mcb.18.3.1424

Kleckner, N. (2006). Chiasma formation: chromatin/axis interplay and the role(s) of the synaptonemal complex. *Chromosoma* 115, 175–194. doi: 10.1007/s00412-006-0055-7

Klein, F., Laroche, T., Cardenas, M. E., Hofmann, J. F., Schweizer, D., and Gasser, S. M. (1992). Localization of RAP1 and topoisomerase II in nuclei and meiotic chromosomes of yeast. *J. Cell Biol.* 117, 935–948. doi: 10.1083/jcb.117.5.935

Klein, F., Mahr, P., Galova, M., Buonomo, S. B. C., Michaelis, C., Nairz, K., et al. (1999). A central role for cohesions in sister chromatid cohesion, formation of axial elements, and recombination during yeast meiosis. *Cell* 98, 91–103. doi: 10.1016/s0092-8674(00)80609-1

Klutstein, M., and Cooper, J. P. (2014). The chromosomal courtship dance-homolog pairing in early meiosis. *Curr. Opin. Cell. Biol.* 26C, 123–131. doi: 10.1016/j.ceb.2013.12.004

Kogo, H., Tsutsumi, M., Inagaki, H., Ohye, T., Kiyonari, H., and Kurahashi, H. (2012). HORMAD2 is essential for synapsis surveillance during meiotic prophase via the recruitment of ATR activity. *Genes Cells* 17, 897–912. doi: 10.1111/gtc.12005

Kohler, S., Wojcik, M., Xu, K., and Dernburg, A. F. (2017). Superresolution microscopy reveals the three-dimensional organization of meiotic chromosome axes in intact *Caenorhabditis elegans* tissue. *Proc. Natl. Acad. Sci. U.S.A.* 114, E4734–E4743.

Kouznetsova, A., Novak, I., Jessberger, R., and Hoog, C. (2005). SYCP2 and SYCP3 are required for cohesin core integrity at diplotene but not for centromere cohesion at the first meiotic division. *J. Cell Sci.* 118, 2271–2278. doi: 10.1242/jcs.02362

Kudo, N. R., Wassmann, K., Anger, M., Schuh, M., Wirth, K. G., Xu, H., et al. (2006). Resolution of chiasmata in oocytes requires separase-mediated proteolysis. *Cell* 126, 135–146. doi: 10.1016/j.cell.2006.05.033

Kueng, S., Hegemann, B., Peters, B. H., Lipp, J. J., Schleiffer, A., Mechtler, K., et al. (2006). Wapl controls the dynamic association of cohesin with chromatin. *Cell* 127, 955–967. doi: 10.1016/j.cell.2006.09.040

Kugou, K., Fukuda, T., Yamada, S., Ito, M., Sasanuma, H., Mori, S., et al. (2009). Rec8 guides canonical Spo11 distribution along yeast meiotic chromosomes. *Mol. Biol. Cell.* 20, 3064–3076. doi: 10.1091/mbc.e08-12-1223

Kumar, R., Ghyselinck, N., Ishiguro, K., Watanabe, Y., Kouznetsova, A., Hoog, C., et al. (2015). MEI4 - a central player in the regulation of meiotic DNA double-strand break formation in the mouse. *J. Cell. Sci.* 128, 1800–1811. doi: 10.1242/jcs.165464

Kuroda, M., Oikawa, K., Ohbayashi, T., Yoshida, K., Yamada, K., Mimura, J., et al. (2005). A dioxin sensitive gene, mammalian WAPL, is implicated in spermatogenesis. *FEBS Lett.* 579, 167–172. doi: 10.1016/j.febslet.2004.11.070

Lambing, C., Tock, A. J., Topp, S. D., Choi, K., Kuo, P. C., Zhao, X., et al. (2020). Interacting genomic landscapes of REC8-cohesin, chromatin, and meiotic recombination in arabidopsis. *Plant Cell* 32, 1218–1239. doi: 10.1105/tpc.19.00866

Lammers, J. H., van Aalderen, M., Peters, A. H., van Pelt, A. A., de Rooij, D. G., de Boer, P., et al. (1995). A change in the phosphorylation pattern of the 30000-33000 Mr synaptonemal complex proteins of the rat between early and mid-pachytene. *Chromosoma* 104, 154–163. doi: 10.1007/s00412005 0103

Lee, J. (2013). Roles of cohesin and condensin in chromosome dynamics during *Mammalian meiosis*. *J. Reproduc. Dev.* 59, 431–436. doi: 10.1262/jrd.2013-068

Lee, J., and Hirano, T. (2011). RAD21L, a novel cohesin subunit implicated in linking homologous chromosomes in mammalian meiosis. *J. Cell Biol.* 192, 263–276. doi: 10.1083/jcb.201008005

Lee, J., Iwai, T., Yokota, T., and Yamashita, M. (2003). Temporally and spatially selective loss of Rec8 protein from meiotic chromosomes during mammalian meiosis. *J. Cell Sci.* 116, 2781–2790. doi: 10.1242/jcs.00495

Llano, E., Gomez, H. L., Garcia-Tunon, I., Sanchez-Martin, M., Caburet, S., Barbero, J. L., et al. (2014). STAG3 is a strong candidate gene for male infertility. *Hum. Mol. Genet.* 23, 3421–3431. doi: 10.1093/hmg/ddu051

Llano, E., Herran, Y., Garcia-Tunon, I., Gutierrez-Caballero, C., de Alava, E., Barbero, J. L., et al. (2012). Meiotic cohesin complexes are essential for the formation of the axial element in mice. *J. Cell Biol.* 197, 877–885. doi: 10.1083/jcb.201201100

Lorenz, A., Wells, J. L., Pryce, D. W., Novatchkova, M., Eisenhaber, F., McFarlane, R. J., et al. (2004). S. pombe meiotic linear elements contain proteins related to synaptonemal complex components. *J. Cell. Sci.* 117, 3343–3351. doi: 10.1242/jcs.01203

Losada, A. (2014). Cohesin in cancer: chromosome segregation and beyond. *Nat. Rev. Cancer* 14, 389–393. doi: 10.1038/nrc3743

Losada, A., Yokochi, T., and Hirano, T. (2005). Functional contribution of Pds5 to cohesin-mediated cohesion in human cells and xenopus egg extracts. *J. Cell Sci.* 118, 2133–2141. doi: 10.1242/jcs.02355

Luo, Z., Wang, X., Jiang, H., Wang, R., Chen, J., Chen, Y., et al. (2020). Reorganized 3D genome structures support transcriptional regulation in mouse spermatogenesis. *Science* 23:101034. doi: 10.1016/j.isci.2020.101034

Mahadevaiah, S. K., Turner, J. M., Baudat, F., Rogakou, E. P., de Boer, P., Blanco-Rodriguez, J., et al. (2001). Recombinational DNA double-strand breaks in mice precede synapsis. *Nat. Genet.* 27, 271–276. doi: 10.1038/85830

Mao-Draayer, Y., Galbraith, A. M., Pittman, D. L., Cool, M., and Malone, R. E. (1996). Analysis of meiotic recombination pathways in the yeast *Saccharomyces cerevisiae*. *Genetics* 144, 71–86. doi: 10.1093/genetics/144.1.71

McNicoll, F., Kuhnel, A., Biswas, U., Hempel, K., Whelan, G., Eichele, G., et al. (2020). Meiotic sex chromosome cohesion and autosomal synapsis are supported by Esco2. *Life Sci. Alliance* 3:e201900564. doi: 10.26508/lsa.201900564

Merino, S. T., Cummings, W. J., Acharya, S. N., and Zolan, M. E. (2000). Replication-dependent early meiotic requirement for Spo11 and Rad50. *Proc. Natl. Acad. Sci. U.S.A.* 97, 10477–10482. doi: 10.1073/pnas.190346097

Mets, D. G., and Meyer, B. J. (2009). Condensins regulate meiotic DNA break distribution, thus crossover frequency, by controlling chromosome structure. *Cell* 139, 73–86. doi: 10.1016/j.cell.2009.07.035

Moens, P. B., and Earnshaw, W. C. (1989). Anti-topoisomerase II recognizes meiotic chromosome cores. *Chromosoma* 98, 317–322. doi: 10.1007/bf00292383

Moens, P. B., and Pearlman, R. E. (1988). Chromatin organization at meiosis. *Bioessays* 9, 151–153. doi: 10.1002/bies.950090503

Monesi, V. (1965). Differential rate of ribonucleic acid synthesis in the autosomes and sex chromosomes during male meiosis in the mouse. *Chromosoma* 17, 11–21.

Muller, H., Scolari, V. F., Agier, N., Piazza, A., Thierry, A., Mercy, G., et al. (2018). Characterizing meiotic chromosomes' structure and pairing using a designer sequence optimized for Hi-C. *Mol. Syst. Biol.* 14:e8293.

Murakami, H., Lam, I., Huang, P. C., Song, J., van Overbeek, M., and Keeney, S. (2020). Multilayered mechanisms ensure that short chromosomes recombine in meiosis. *Nature* 582, 124–128. doi: 10.1038/s41586-020-2248-2

Nambiar, M., and Smith, G. R. (2018). Pericentromere-specific cohesin complex prevents meiotic pericentric DNA double-strand breaks and lethal crossovers. *Mol. Cell* 71, 540–553.e544.

Nasmyth, K. (2011). Cohesin: a catenase with separate entry and exit gates? *Nat. Cell Biol.* 13, 1170–1177. doi: 10.1038/ncb2349

Nasmyth, K., Peters, J. M., and Uhlmann, F. (2000). Splitting the chromosome: cutting the ties that bind sister chromatids. *Science* 288, 1379–1385. doi: 10.1126/science.288.5470.1379

Novak, I., Wang, H., Revenkova, E., Jessberger, R., Scherthan, H., and Hoog, C. (2008). Cohesin Smc1beta determines meiotic chromatin axis loop organization. *J. Cell Biol.* 180, 83–90. doi: 10.1083/jcb.200706136

Offenberg, H. H., Schalk, J. A., Meuwissen, R. L., van Aalderen, M., Kester, H. A., Dietrich, A. J., et al. (1998). SCP2: a major protein component of the axial elements of synaptonemal complexes of the rat. *Nucleic Acids Res.* 26, 2572–2579. doi: 10.1093/nar/26.11.2572

Oomen, M. E., Hansen, A. S., Liu, Y., Darzacq, X., and Dekker, J. (2019). CTCF sites display cell cycle-dependent dynamics in factor binding and nucleosome positioning. *Genome Res.* 29, 236–249. doi: 10.1101/gr.241547.118

Ouyang, Z., Zheng, G., Tomchick, D. R., Luo, X., and Yu, H. (2016). Structural Basis and IP6 requirement for Pds5-dependent cohesin dynamics. *Mol. Cell.* 62, 248–259. doi: 10.1016/j.molcel.2016.02.033

Panizza, S., Mendoza, M. A., Berlinger, M., Huang, L., Nicolas, A., Shirahige, K., et al. (2011). Spo11-accessory proteins link double-strand break sites to the chromosome axis in early meiotic recombination. *Cell* 146, 372–383. doi: 10.1016/j.cell.2011.07.003

Papanikos, F., Clement, J. A. J., Testa, E., Ravindranathan, R., Grey, C., Dereli, I., et al. (2019). Mouse ANKRD31 regulates spatiotemporal patterning of meiotic recombination initiation and ensures recombination between X and Y sex chromosomes. *Mol. Cell.* 74, 1069–1085.e1011.

Parisi, S., McKay, M. J., Molnar, M., Thompson, M. A., vanderSpek, P. J., vanDrunenSchoenmaker, E., et al. (1999). Rec8p, a meiotic recombination and sister chromatid cohesion phosphoprotein of the Rad21p family conserved from fission yeast to humans. *Mol. Cell. Biol.* 19, 3515–3528. doi: 10.1128/mcb.19.5.3515

Parra, M. T., Gomez, R., Viera, A., Llano, E., Pendas, A. M., Rufas, J. S., et al. (2009). Sequential assembly of centromeric proteins in male mouse meiosis. *PLoS Genet* 5:e1000417. doi: 10.1371/journal.pgen.1000417

Parra, M. T., Gomez, R., Viera, A., Page, J., Calvente, A., Wordeman, L., et al. (2006). A perikinetochoric ring defined by MCAK and aurora-B as a novel centromere domain. *PLoS Genet* 2:e84. doi: 10.1371/journal.pgen.0020084

Parra, M. T., Viera, A., Gomez, R., Page, J., Benavente, R., Santos, J. L., et al. (2004). Involvement of the cohesin Rad21 and SCP3 in monopolar attachment of sister kinetochores during mouse meiosis I. *J. Cell Sci.* 117, 1221–1234. doi: 10.1242/jcs.00947

Parra, M. T., Viera, A., Gomez, R., Page, J., Carmena, M., Earnshaw, W. C., et al. (2003). Dynamic relocalization of the chromosomal passenger complex proteins inner centromere protein (INCENP) and aurora-B kinase during male mouse meiosis. *J. Cell Sci.* 116, 961–974. doi: 10.1242/jcs.00330

Patel, L., Kang, R., Rosenberg, S. C., Qiu, Y., Raviram, R., Chee, S., et al. (2019). Dynamic reorganization of the genome shapes the recombination landscape in meiotic prophase. *Nat. Struct. Mol. Biol.* 26, 164–174. doi: 10.1038/s41594-019-0187-0

Pelttari, J., Hoja, M. R., Yuan, L., Liu, J. G., Brundell, E., Moens, P., et al. (2001). A meiotic chromosomal core consisting of cohesin complex proteins recruits DNA recombination proteins and promotes synapsis in the absence of an axial element in mammalian meiotic cells. *Mol. Cell Biol.* 21, 5667–5677. doi: 10.1128/mcb.21.16.5667-5677.2001

Peters, J. M., and Nishiyama, T. (2012). Sister chromatid cohesion. *Cold Spring Harb. Perspect. Biol.* 4:a011130.

Pezzi, N., Prieto, I., Kremer, L., Perez Jurado, L. A., Valero, C., Del Mazo, J., et al. (2000). STAG3, a novel gene encoding a protein involved in meiotic chromosome pairing and location of STAG3-related genes flanking the Williams-Beuren syndrome deletion. *FASEB J.* 14, 581–592. doi: 10.1096/fasebj.14.3.581

Piazza, A., Bordelet, H., Dumont, A., Thierry, A., Savocco, J., Girard, F., et al. (2020). Cohesin regulates homology search during recombinational DNA repair. *bioRxiv[preprint]* doi: 10.1101/2020.12.17.423195

Prieto, I., Suja, J. A., Pezzi, N., Kremer, L., Martinez, A. C., Rufas, J. S., et al. (2001). Mammalian STAG3 is a cohesin specific to sister chromatid arms in meiosis I. *Nat. Cell Biol.* 3, 761–766. doi: 10.1038/35087082

Prieto, I., Tease, C., Pezzi, N., Buesa, J. M., Ortega, S., Kremer, L., et al. (2004). Cohesin component dynamics during meiotic prophase I in mammalian oocytes. *Chromosome Res.* 12, 197–213. doi: 10.1023/b:chro.0000021945.83198.0e

Revenkova, E., Eijpe, M., Heyting, C., Gross, B., and Jessberger, R. (2001). Novel meiosis-specific isoform of mammalian SMC1. *Mol. Cell Biol.* 21, 6984–6998. doi: 10.1128/mcb.21.20.6984-6998.2001

Revenkova, E., Eijpe, M., Heyting, C., Hodges, C. A., Hunt, P. A., Liebe, B., et al. (2004). Cohesin SMC1 beta is required for meiotic chromosome dynamics, sister chromatid cohesion and DNA recombination. *Nat. Cell Biol.* 6, 555–562. doi: 10.1038/ncb1135

Rockmill, B., and Roeder, G. S. (1990). Meiosis in asynaptic yeast. *Genetics* 126, 563–574. doi: 10.1093/genetics/126.3.563

Rog, O., Kohler, S., and Dernburg, A. F. (2017). The synaptonemal complex has liquid crystalline properties and spatially regulates meiotic recombination factors. *eLife* 6:e21455.

Rong, M., Matsuda, A., Hiraoka, Y., and Lee, J. (2016). Meiotic cohesin subunits RAD21L and REC8 are positioned at distinct regions between lateral elements and transverse filaments in the synaptonemal complex of mouse spermatocytes. *J. Reproduc. Dev.* 62, 623–630. doi: 10.1262/jrd.2016-127

Rosenberg, S. C., and Corbett, K. D. (2015). The multifaceted roles of the HORMA domain in cellular signaling. *J. Cell Biol.* 211, 745–755. doi: 10.1083/jcb.201509076

Rousova, D., Funk, S. K., Reichle, H., and Weir, J. R. (2020). Mer2 binds directly to both nucleosomes and axial proteins as the keystone of meiotic recombination. *bioRxiv[preprint]*. doi: 10.1101/2020.07.30.228908

Sakuno, T., and Watanabe, Y. (2015). Phosphorylation of cohesin Rec11/SA3 by casein kinase 1 promotes homologous recombination by assembling the meiotic chromosome axis. *Dev. Cell.* 32, 220–230. doi: 10.1016/j.devcel.2014.11.033

Schalbetter, S. A., Fudenberg, G., Baxter, J., Pollard, K. S., and Neale, M. J. (2019). Principles of meiotic chromosome assembly revealed in S. cerevisiae. *Nat. Commun.* 10:4795.

Schalk, J. A. C., Dietrich, A. J. J., Vink, A. C. G., Offenberg, H. H., vanAalderen, M., and Heyting, C. (1998). Localization of SCP2 and SCP3 protein molecules within synaptonemal complexes of the rat. *Chromosoma* 107, 540–548. doi: 10.1007/s004120050340

Schmitz, J., Watrin, E., Lenart, P., Mechtler, K., and Peters, J. M. (2007). Sororin is required for stable binding of cohesin to chromatin and for sister chromatid cohesion in interphase. *Curr. Biol.* 17, 630–636. doi: 10.1016/j.cub.2007.02.029

Schucker, K., Holm, T., Franke, C., Sauer, M., and Benavente, R. (2015). Elucidation of synaptonemal complex organization by super-resolution imaging with isotropic resolution. *Proc. Natl. Acad. Sci. U.S.A.* 112, 2029–2033. doi: 10.1073/pnas.1414814112

Schwacha, A., and Kleckner, N. (1997). Interhomolog bias during meiotic recombination: meiotic functions promote a highly differentiated interhomolog- only pathway. *Cell* 90, 1123–1135. doi: 10.1016/s0092-8674(00)80378-5

Severson, A. F., Ling, L., van Zuylen, V., and Meyer, B. J. (2009). The axial element protein HTP-3 promotes cohesin loading and meiotic axis assembly in C. elegans to implement the meiotic program of chromosome segregation. *Genes Dev.* 23, 1763–1778. doi: 10.1101/gad.1808809

Severson, A. F., and Meyer, B. J. (2014). Divergent kleisin subunits of cohesin specify mechanisms to tether and release meiotic chromosomes. *eLife* 3:e03467.

Shibuya, H., Ishiguro, K., and Watanabe, Y. (2014). The TRF1-binding protein TERB1 promotes chromosome movement and telomere rigidity in meiosis. *Nat. Cell. Biol.* 16, 145–156. doi: 10.1038/ncb2896

Shin, Y. H., Choi, Y., Erdin, S. U., Yatsenko, S. A., Kloc, M., Yang, F., et al. (2010). Hormad1 mutation disrupts synaptonemal complex formation, recombination, and chromosome segregation in *Mammalian meiosis*. *PLoS Genet* 6:e1001190. doi: 10.1371/journal.pgen.1001190

Shintomi, K., and Hirano, T. (2009). Releasing cohesin from chromosome arms in early mitosis: opposing actions of Wapl-Pds5 and Sgo1. *Genes Dev.* 23, 2224–2236. doi: 10.1101/gad.1844309

Silva, M. C. C., Powell, S., Ladstatter, S., Gassler, J., Stocsits, R., Tedeschi, A., et al. (2020). Wapl releases Scc1-cohesin and regulates chromosome structure and segregation in mouse oocytes. *J. Cell. Biol.* 219:e201906100.

Smith, A. V., and Roeder, G. S. (1997). The yeast red1 protein localizes to the cores of meiotic chromosomes. *J. Cell Biol.* 136, 957–967. doi: 10.1083/jcb.136.5.957

Sommermeyer, V., Beneut, C., Chaplais, E., Serrentino, M. E., and Borde, V. (2013). Spp1, a member of the set1 complex, promotes meiotic DSB formation in promoters by tethering histone H3K4 methylation sites to chromosome axes. *Mol. Cell.* 49, 43–54. doi: 10.1016/j.molcel.2012.11.008

Song, M., Zhai, B., Yang, X., Tan, T., Wang, Y., Yang, X., et al. (2021). Interplay between Pds5 and rec8 in regulating chromosome axis length and crossover frequency. *Sci. Adv.* 7:eabe7920. doi: 10.1126/sciadv.abe7920

Sotelo, J. R., and Trujillo-Cenoz, O. (1960). Electron microscope study on spermatogenesis. chromosome morphogenesis at the onset of meiosis (cyte l) and nuclear structure of early and late spermatids. *Zeitschrift fur Zellforschung und mikroskopische Anatomie* 51, 243–277.

Stanzione, M., Baumann, M., Papanikos, F., Dereli, I., Lange, J., Ramlal, A., et al. (2016). Meiotic DNA break formation requires the unsynapsed chromosome axis-binding protein IHO1 (CCDC36) in mice. *Nat. Cell. Biol.* 18, 1208–1220. doi: 10.1038/ncb3417

Strom, L., Lindroos, H. B., Shirahige, K., and Sjogren, C. (2004). Postreplicative recruitment of cohesin to double-strand breaks is required for DNA repair. *Mol. Cell* 16, 1003–1015. doi: 10.1016/j.molcel.2004.11.026

Sun, X., Huang, L., Markowitz, T. E., Blitzblau, H. G., Chen, D., Klein, F., et al. (2015). Transcription dynamically patterns the meiotic chromosome-axis interface. *eLife* 4:e07424.

Syrjanen, J. L., Heller, I., Candelli, A., Davies, O. R., Peterman, E. J., Wuite, G. J., et al. (2017). Single-molecule observation of DNA compaction by meiotic protein SYCP3. *eLife* 6:e22582.

Syrjanen, J. L., Pellegrini, L., and Davies, O. R. (2014). A molecular model for the role of SYCP3 in meiotic chromosome organisation. *eLife* 3:e02963.

Tachibana-Konwalski, K., Godwin, J., van der Weyden, L., Champion, L., Kudo, N. R., Adams, D. J., et al. (2010). Rec8-containing cohesin maintains bivalents without turnover during the growing phase of mouse oocytes. *Genes Dev.* 24, 2505–2516. doi: 10.1101/gad.605910

Tarsounas, M., Pearlman, R. E., Gasser, P. J., Park, M. S., and Moens, P. B. (1997). Protein-protein interactions in the synaptonemal complex. *Mol. Biol. Cell* 8, 1405–1414. doi: 10.1091/mbc.8.8.1405

Tease, C., and Hulten, M. A. (2004). Inter-sex variation in synaptonemal complex lengths largely determine the different recombination rates in male and female germ cells. *Cytogenet. Geno. Res.* 107, 208–215. doi: 10.1159/000080599

Tedeschi, A., Wutz, G., Huet, S., Jaritz, M., Wuensche, A., Schirghuber, E., et al. (2013). Wapl is an essential regulator of chromatin structure and chromosome segregation. *Nature* 501, 564–568. doi: 10.1038/nature12471

Unal, E., Arbel-Eden, A., Sattler, U., Shroff, R., Lichten, M., Haber, J. E., et al. (2004). DNA damage response pathway uses histone modification to assemble a double-strand break-specific cohesin domain. *Mol. Cell.* 16, 991–1002. doi: 10.1016/j.molcel.2004.11.027

Vara, C., Paytuvi-Gallart, A., Cuartero, Y., Le Dily, F., Garcia, F., Salva-Castro, J., et al. (2019). Three-dimensional genomic structure and cohesin occupancy correlate with transcriptional activity during spermatogenesis. *Cell Rep.* 28, 352–367e359.

Viera, A., Berenguer, I., Ruiz-Torres, M., Gomez, R., Guajardo, A., Barbero, J. L., et al. (2020). PDS5 proteins regulate the length of axial elements and telomere integrity during male mouse meiosis. *EMBO Rep.* 21:e49273.

von Wettstein, D., Rasmussen, S. W., and Holm, P. B. (1984). The synaptonemal complex in genetic segregation. *Annu. Rev. Genet.* 18, 331–413. doi: 10.1146/annurev.ge.18.120184.001555

Wang, H., and Hoog, C. (2006). Structural damage to meiotic chromosomes impairs DNA recombination and checkpoint control in mammalian oocytes. *J. Cell, Biol.* 173, 485–495. doi: 10.1083/jcb.200512077

Wang, S., Hassold, T., Hunt, P., White, M. A., Zickler, D., Kleckner, N., et al. (2017). Inefficient crossover maturation underlies elevated aneuploidy in human female meiosis. *Cell* 168, 977–989.e917.

Wang, Y., Wang, H., Zhang, Y., Du, Z., Si, W., Fan, S., et al. (2019). Reprogramming of meiotic chromatin architecture during spermatogenesis. *Mol. Cell.* 73, 547–561.e546.

West, A. M. V., Komives, E. A., and Corbett, K. D. (2018). Conformational dynamics of the Hop1 HORMA domain reveal a common mechanism with the spindle checkpoint protein Mad2. *Nucleic Acids Res.* 46, 279–292. doi: 10.1093/nar/gkx1196

West, A. M. V., Rosenberg, S. C., Ur, S. N., Lehmer, M. K., Ye, Q., Hagemann, G., et al. (2019). A conserved filamentous assembly underlies the structure of the meiotic chromosome axis. *eLife* 8:e40372.

Widger, A., Mahadevaiah, S. K., Lange, J., ElInati, E., Zohren, J., Hirota, T., et al. (2018). ATR is a multifunctional regulator of male mouse meiosis. *Nat. Commun.* 9:2621.

Winkel, K., Alsheimer, M., Ollinger, R., and Benavente, R. (2009). Protein SYCP2 provides a link between transverse filaments and lateral elements of mammalian synaptonemal complexes. *Chromosoma* 118, 259–267. doi: 10.1007/s00412-008-0194-0

Winters, T., McNicoll, F., and Jessberger, R. (2014). Meiotic cohesin STAG3 is required for chromosome axis formation and sister chromatid cohesion. *EMBO J.* 33, 1256–1270. doi: 10.1002/embj.201387330

Woglar, A., Yamaya, K., Roelens, B., Boettiger, A., Kohler, S., and Villeneuve, A. M. (2020). Quantitative cytogenetics reveals molecular stoichiometry and longitudinal organization of meiotic chromosome axes and loops. *PLoS Biol* 18:e3000817. doi: 10.1371/journal.pbio.3000817

Wojtasz, L., Cloutier, J. M., Baumann, M., Daniel, K., Varga, J., Fu, J., et al. (2012). Meiotic DNA double-strand breaks and chromosome asynapsis in mice are monitored by distinct HORMAD2-independent and -dependent mechanisms. *Genes Dev.* 26, 958–973. doi: 10.1101/gad.187559.112

Wojtasz, L., Daniel, K., Roig, I., Bolcun-Filas, E., Xu, H., Boonsanay, V., et al. (2009). Mouse HORMAD1 and HORMAD2, two conserved meiotic chromosomal proteins, are depleted from synapsed chromosome axes with the help of TRIP13 AAA-ATPase. *PLoS Genet.* 5:e1000702. doi: 10.1371/journal.pgen.1000702

Wood, A. J., Severson, A. F., and Meyer, B. J. (2010). Condensin and cohesin complexity: the expanding repertoire of functions. *Nat. Rev. Genet.* 11, 391–404. doi: 10.1038/nrg2794

Xu, H., Beasley, M., Verschoor, S., Inselman, A., Handel, M. A., and McKay, M. J. (2004). A new role for the mitotic RAD21/SCC1 cohesin in meiotic chromosome cohesion and segregation in the mouse. *EMBO Rep.* 5, 378–384. doi: 10.1038/sj.embor.7400121

Xu, H., Beasley, M. D., Warren, W. D., van der Horst, G. T., and McKay, M. J. (2005). Absence of mouse REC8 cohesin promotes synapsis of sister chromatids in meiosis. *Dev. Cell.* 8, 949–961. doi: 10.1016/j.devcel.2005.03.018

Xu, H., Tong, Z., Ye, Q., Sun, T., Hong, Z., Zhang, L., et al. (2019). Molecular organization of mammalian meiotic chromosome axis revealed by expansion STORM microscopy. *Proc. Natl. Acad. Sci. U.S.A.* 116, 18423–18428. doi: 10.1073/pnas.1902440116

Yadav, V. K., and Claeys Bouuaert, C. (2021). Mechanism and control of meiotic DNA double-strand break formation in S. cerevisiae. *Front. Cell Dev. Biol.* 9:642737. doi: 10.3389/fcell.2021.642737

Yang, F., Fuente Rde, L., Leu, N. A., Baumann, C., McLaughlin, K. J., and Wang, P. J. (2006). Mouse SYCP2 is required for synaptonemal complex assembly and chromosomal synapsis during male meiosis. *J. Cell Biol.* 173, 497–507. doi: 10.1083/jcb.200603063

Yatskevich, S., Rhodes, J., and Nasmyth, K. (2019). Organization of chromosomal DNA by SMC complexes. *Annu. Rev. Genet.* 53, 445–482. doi: 10.1146/annurev-genet-112618-043633

Yu, H. G., and Koshland, D. (2005). Chromosome morphogenesis: condensin-dependent cohesin removal during meiosis. *Cell* 123, 397–407. doi: 10.1016/j.cell.2005.09.014

Yu, H. G., and Koshland, D. E. (2003). Meiotic condensin is required for proper chromosome compaction, SC assembly, and resolution of recombination-dependent chromosome linkages. *J. Cell Biol.* 163, 937–947.

Yuan, L., Liu, J.-G., Hoja, M.-R., Wilbertz, J., Nordqvist, K., and Hoog, C. (2002). Female germ cell aneuploidy and embryo death in mice lacking the meiosis-specific protein SCP3. *Science* 296, 1115–1118. doi: 10.1126/science.1070594

Yuan, L., Liu, J. G., Zhao, J., Brundell, E., Daneholt, B., and Hoog, C. (2000). The murine SCP3 gene is required for synaptonemal complex assembly, chromosome synapsis, and male fertility. *Mol. Cell* 5, 73–83. doi: 10.1016/s1097-2765(00)80404-9

Zhang, J., Hakansson, H., Kuroda, M., and Yuan, L. (2008). Wapl localization on the synaptonemal complex, a meiosis-specific proteinaceous structure that binds homologous chromosomes, in the female mouse. *Rep. Domest Anim* 43, 124–126.

Zhang, L., Wang, S., Yin, S., Hong, S., Kim, K. P., and Kleckner, N. (2014). Topoisomerase II mediates meiotic crossover interference. *Nature* 511, 551–556. doi: 10.1038/nature13442

Zickler, D., and Kleckner, N. (1999). Meiotic chromosomes: integrating structure and function. *Ann. Rev. Genet.* 33, 603–754.

Zickler, D., and Kleckner, N. (2015). Recombination, pairing, and synapsis of homologs during meiosis. *Cold Spring Harb. Perspect. Biol.* 7:a016626. doi: 10.1101/cshperspect.a016626

Conflict of Interest: The authors declare that the research was conducted in the absence of any commercial or financial relationships that could be construed as a potential conflict of interest.

Copyright © 2021 Grey and de Massy. This is an open-access article distributed under the terms of the Creative Commons Attribution License (CC BY). The use, distribution or reproduction in other forums is permitted, provided the original author(s) and the copyright owner(s) are credited and that the original publication in this journal is cited, in accordance with accepted academic practice. No use, distribution or reproduction is permitted which does not comply with these terms.

GLOSSARY

Axial element: the proteinaceous structure that provides an anchor for loop formation and forms at leptonema.
Lateral element: when the axial elements from two homologs engage into synapsis, a central element is formed, and the axial elements are named lateral elements.
Synaptonemal complex: the tripartite structure, a central element and two lateral elements that forms upon synapsis. Initiation of synapsis defines the zygotene stage.
Synapsis: the event associated with synaptonemal complex formation.
DSB: DNA double strand breaks.
Pre-leptotene: stage that includes the meiotic S phase.
TAD: topologically associated domains.
PAR: the region of homology between the X and Y sex chromosomes defined as the pseudo-autosomal region.
ChIP-seq: chromatin immunoprecipitation followed by next generation sequencing.
HiC: genome wide chromosome conformation capture.

frontiers in Cell and Developmental Biology

ORIGINAL RESEARCH
published: 28 June 2021
doi: 10.3389/fcell.2021.684108

RNAi-Related Dicer and Argonaute Proteins Play Critical Roles for Meiocyte Formation, Chromosome-Axes Lengths and Crossover Patterning in the Fungus *Sordaria macrospora*

Chloe Girard[1], Karine Budin[1], Stéphanie Boisnard[1], Liangran Zhang[2], Robert Debuchy[1], Denise Zickler[1] and Eric Espagne[1]**

[1] Université Paris-Saclay, Commissariat à l'Énergie Atomiques et aux Énergies Alternatives (CEA), Centre National de la Recherche Scientifique (CNRS), Institute for Integrative Biology of the Cell (I2BC), Gif-sur-Yvette, France, [2] Center for Reproductive Medicine, Cheeloo College of Medicine, Shandong University, Jinan, China

OPEN ACCESS

Edited by:
Lubos Cipak,
Biomedical Research Center, Slovak Academy of Sciences, Slovakia

Reviewed by:
Nicola Silva,
Masaryk University, Czechia
Alexander Lorenz,
University of Aberdeen, United Kingdom

***Correspondence:**
Denise Zickler
denise.zickler@i2bc.paris-saclay.fr
Eric Espagne
eric.espagne@i2bc.paris-saclay.fr

Specialty section:
This article was submitted to Cell Growth and Division, a section of the journal Frontiers in Cell and Developmental Biology

Received: 22 March 2021
Accepted: 01 June 2021
Published: 28 June 2021

Citation:
Girard C, Budin K, Boisnard S, Zhang L, Debuchy R, Zickler D and Espagne E (2021) RNAi-Related Dicer and Argonaute Proteins Play Critical Roles for Meiocyte Formation, Chromosome-Axes Lengths and Crossover Patterning in the Fungus Sordaria macrospora. Front. Cell Dev. Biol. 9:684108. doi: 10.3389/fcell.2021.684108

RNA interference (RNAi) is a cellular process involving small RNAs that target and regulate complementary RNA transcripts. This phenomenon has well-characterized roles in regulating gene and transposon expression. In addition, Dicer and Argonaute proteins, which are key players of RNAi, also have functions unrelated to gene repression. We show here that in the filamentous Ascomycete *Sordaria macrospora,* genes encoding the two Dicer (Dcl1 and Dcl2) and the two Argonaute (Sms2 and Qde2) proteins are dispensable for vegetative growth. However, we identified roles for all four proteins in the sexual cycle. Dcl1 and Sms2 are essential for timely and successful ascus/meiocyte formation. During meiosis *per se*, Dcl1, Dcl2, and Qde2 modulate, more or less severely, chromosome axis length and crossover numbers, patterning and interference. Additionally, Sms2 is necessary both for correct synaptonemal complex formation and loading of the pro-crossover E3 ligase-protein Hei10. Moreover, meiocyte formation, and thus meiotic induction, is completely blocked in the *dcl1 dcl2* and *dcl1 sms2* null double mutants. These results indicate complex roles of the RNAi machinery during major steps of the meiotic process with newly uncovered roles for chromosomes-axis length modulation and crossover patterning regulation.

Keywords: RNAi, dicer, Argonaute (AGO), axis length, crossover patterning, meiosis

INTRODUCTION

Ribonucleic-acid silencing (or RNAi) was originally described as a post-transcriptional gene-silencing (PTGS) mechanism mediated by small RNAs. RNAi plays essential roles across eukaryotes in genome defense against transposons and viruses (e.g., Malone and Hannon, 2009) as well as during development and cellular differentiation (Alberti and Cochella, 2017; D'Ario et al., 2017). Proteins involved in RNAi are well conserved across kingdoms, and include three main components: an RNA-dependent RNA polymerase (RdRP) generating double stranded RNAs (dsRNAs), the type III RNase Dicer module dicing up precursor dsRNAs into small dsRNAs that

are then loaded onto an Argonaute-PIWI protein to target complementary sequences [reviewed in Cerutti and Casas-Mollano (2006)]. The ancestral role of the RNAi machinery in the eukaryotic ancestor(s) may have been geared toward targeting RNA transcript degradation and locus-specific histone modifications to promote gene silencing (e.g., Gutbrod and Martienssen, 2020). However, findings in multiple organisms have now demonstrated the involvement of RNAi components in many other nuclear functions including centromere integrity, chromosome segregation and DNA repair [reviewed in Burger and Gullerova (2015) and Gutbrod and Martienssen (2020)].

Factors involved in RNAi are also known to regulate a wide variety of cellular processes during both the vegetative and the sexual cycles in the filamentous fungus *Neurospora crassa*, a close relative of *Sordaria macrospora* (Nowrousian et al., 2004). The first of those RNA silencing mechanisms, termed quelling, mediates post-transcriptional silencing of transgenes in mitotic cells (Romano and Macino, 1992). Quelling involves the QDE-1/2/3 proteins and QIP (QDE-2 interacting protein; Fulci and Macino, 2007). Mutants of the implicated factors, while affected in transgene silencing, show no developmental phenotypes, either vegetative or sexual. Subsequent work revealed, however, that sensitivity to DNA damaging agents was increased in these mutants, and that the Argonaute homolog QDE-2 was over-expressed after exposure to DNA damaging agents or in mutants of the DNA damage repair pathway (Lee et al., 2009). RNAi is also implicated in a second type of gene silencing called Meiotic Silencing by Unpaired DNA (MSUD). This process occurs exclusively during meiotic prophase. It scans homologous chromosomes for unpaired DNA sequences and silences both the unpaired and any other homologous copies present in the genome (Shiu et al., 2001). How unpaired copies are detected remains unknown, but this process requires at least nine proteins, including three RNAi proteins: the Dicer homolog Dcl-1, the Argonaute protein Sms-2 and the RNA-dependent RNA polymerase [reviewed in Hammond (2017)]. Dicer and Argonaute proteins are also involved during meiosis in other fungi, as well as in mammals and plants. In the fission yeast *Schizosaccharomyces pombe*, both *dcr1* and *ago1* mutants show chromosome mis-segregation during the second meiotic division (Hall et al., 2003). Mammalian Dicer- and Dgcr8- (DiGeorge Critical Region 8; a double-stranded RNA binding protein involved in microRNA processing upstream of DICER) mutant spermatocytes display chromosome fusions (involving sex chromosomes), abnormal localization of proteins involved in telomere maintenance and increased accumulation of phosphorylated ATM in the sex body (Modzelewski et al., 2015).

The RNAi machinery is, in addition, involved in higher-order chromatin structure such as centromeres during mitosis and meiosis (Hall et al., 2003; Claycomb et al., 2009; Pek and Kai, 2011; Goto and Nakayama, 2012; Huang et al., 2015). For example, in *Argonaute* mutants of maize and rice, centromeric histones are mis-localized during meiosis, leading to chromosome segregation defects (Nonomura et al., 2007; Singh et al., 2011). In *S. pombe*, the formation and maintenance of heterochromatin at centromeres is facilitated by RNAi proteins and their partner, the histone methyl-transferase Clr4 (Zhang et al., 2008). Interestingly, the chromatin state, as controlled by the Dcr1/Clr4 pathway, can differentially regulate the accessibility of DNA to transcription or recombination proteins (Ellermeier et al., 2010). Indeed, while centromeric recombination is very low in wild-type fission yeast, as in most species, the *dcr1* and *clr4* mutants display increased meiotic recombination at centromeres, as assessed by recombining markers on each side of the centromere of chromosome 3 (Ellermeier et al., 2010). In contrast, recombination on chromosome 3 arms remains unchanged. Recombination increase is associated with increased Spo11-dependent double-strand break formation and/or their accumulation at centromeres in *dcr1*, but is independent of the repression of centromeric gene transcription (Ellermeier et al., 2010).

The above information implicates the RNAi machinery in the meiotic process, but leaves open the question of how these proteins impact the specific steps of prophase chromosome dynamics such as pairing, formation of the meiosis-specific structure called synaptonemal complex (SC), and homologous recombination. Here we exploited the power of *Sordaria macrospora* as a particularly attractive experimental system (Zickler and Espagne, 2016) for examination of the roles of both Dicer and Argonaute proteins during its sexual cycle. Initiation of meiosis and progression of nuclei through the various meiotic stages can be monitored independently of the chromosome status, by progressive increase in ascus/meiocyte sizes, thus permitting a clear establishment of events in mutant situations in comparison with wild-type meiosis. *S. macrospora* genome contains two Dicer-like homologs (*DCL1* and *DCL2*) and two Argonaute (*QDE2* and *SMS2*) genes. We show that the four single null mutants exhibit normal vegetative growth but significant meiotic defects, with different phenotypes in each mutant. While the *dcl2* and *qde2* mutants exhibit almost normal meiotic progression and sporulation, *dcl1* and *sms2* mutants display severe defects in the early stages of meiocyte formation. Moreover, when compared to wild type, *dcl2, qde2,* and especially *dcl1* mutants exhibit longer chromosome axes and synaptonemal complexes, plus higher crossover (CO) numbers with altered patterning and crossover interference. The *sms2* mutant displays, moreover, altered synaptonemal complex formation and E3-ligase Hei10 localization. Taken together, these findings indicate clearly that the RNAi components play a central role in the meiotic process of *Sordaria* and extend our understanding of the different processes (e.g., axis length, crossover patterning) that are directly or indirectly dependent on the Dicer and/or the Argonaute proteins. They reveal, moreover, a synergistic relationship between Dcl1 and Dcl2 as well as between Dcl1 and Sms2, with respects to some of these effects.

MATERIALS AND METHODS

Identification of *S. macrospora* Dicer and Argonaute Genes

Dicer protein accession numbers used here are: *S. macrospora* Dcl1 SMAC_00946 and Dcl2 SMAC_06757; *Schizosaccharomyces pombe* Dcr1 Q09884; *Arabidopsis thaliana* DCL1 AEE27221,

DCL2 AEE73925, DCL3 Q9LXW7, and DCL4 P84634; *Drosophila melanogaster* Dcr1 NP_524453.1 and Dcr2 NP_523778.2; *Caenorhabditis elegans* DCR-1 CE47418; and *Homo sapiens* Dicer AAI50288.1. Argonaute protein accession numbers are: *S. macrospora* Qde2 SMAC_03832 and Sms2 SMAC_08605; and *S. pombe* Ago1 NP_587782; *Arabidopsis thaliana* AGO2 NP_174413, AGO3 NP_174414, and AGO7 NP_177103; *Drosophila melanogaster* Ago1 NP_725341 and Ago2 ABO27430; *Caenorhabditis elegans* ALG-1 NP_510322 and ALG-2 NP_871992; and *Homo sapiens* AGO1 NP_036331, AGO2 NP_036286, AGO3 NP_079128, and AGO4 NP_060099. Most domains were identified using the NCBI database [1]. The divergent PAZ domains were identified using the Phyre2 fold recognition server[2]; Kelley et al., 2015). In both Dcl1 and Dcl2, a platform-paz-connector cassette was identified at position 591–804 and 749–1049, with 100 and 98% confidence, respectively. In *S. pombe*, the same cassette was predicted at position 663–894 with a 100% confidence. For Qde2, a PAZ domain was predicted by Phyre2 at position 369–570 (99.9% confidence). Illustrations were made using https://prosite.expasy.org/mydomains.

RT-qPCR Experiments

Cultures for RNA preparations were performed on 90 mm Petri dishes containing M2 minimal medium and covered with a cellophane sheet (Focus Packaging and Design Ltd., Scunthorpe, United Kingdom). A total of 36 dishes (4 biological replicates, 9 days) were inoculated with one wild-type implant in the middle of the Petri dish. Dishes were placed at 25°C under constant light and four of the plates were removed from the incubation room every day from day one to nine. At day 1 and 2, the vegetative mycelium was scraped from the cellophane sheets with a glass cover-slip. From day 3 to day 9, the sexual cycle starts and the corresponding perithecia (fruiting bodies) were harvested by scraping them with a scalpel blade. RNAs were extracted with the RNeasy Plant Mini Kit (Qiagen, Hilden, Germany) according to supplier instructions. DNase digestions were performed in solution with RNase-free DNase Set (Qiagen, Hilden, Germany), followed by RNA cleanup on the RNeasy Plant columns as recommended by Qiagen. RNAs were quantified and checked for integrity on a gel. Total RNAs were reverse transcribed with SuperScript III (Invitrogen, Carlsbad, CA, United States) according to manufacturer's instructions with oligo d(T)20. Primers used for RT-qPCR are shown in **Supplementary Table 1**. Most primer pairs were designed to ensure specific detection of cDNA, with at least one primer encompassing two consecutive exons. Specificity of these primers was checked experimentally during the design. In addition, a non-reverse-transcribed (NRT) control was performed on a pool of biological replicates to check the specificity of the detection. For primer pairs that are not specific for cDNAs, an NRT control was performed for each biological replicate to check the NRT-qPCR signal is low enough to allow a reliable analysis of the RT-qPCR signal (**Supplementary File 1**). Four biological replicates were performed for each day and each biological replicate was analyzed in technical duplicate. The sample maximization method (Hellemans et al., 2008) was used as the experimental set-up for plate design, which also included serial dilutions of a pool of biological replicates to compute amplification efficiency, NRT and negative controls. The average Cq for each gene in each biological replicate is shown in **Supplementary File 1**. Four reference genes (*PDF2, TIP, UBC,* and *CIT1*) were selected in a set of eight housekeeping genes using geNorm (Vandesompele et al., 2002). The average expression stability of these four genes is M = 0.542, indicating heterogeneous biological replicates (Hellemans and Vandesompele, 2014), and V4/5 = 0.121 which is below the cut-off recommended for geNorm (**Supplementary File 1**). Fold changes were computed with REST 2009 (Pfaffl et al., 2002). Fold changes were expressed relative to day 1. RT-qPCR experiments were MIQE compliant (Bustin et al., 2009). RNAseq data has been deposited under PRJEB44726.

Mutants

Plasmids containing deletion cassettes conferring resistance to hygromycin B were constructed according to the *N. crassa* strategy for high-throughput generation of gene deletion (Colot et al., 2006) with modifications aimed at minimizing errors in the 5′ and 3′ flanking regions, notably by the use of Phusion DNA polymerase (Thermo Scientific) (see **Supplementary Table 2** for primer sequences). The deletion cassettes were released from the vector by *Asc*I digestion prior to transformation. The structure of each transformant was confirmed by PCR analysis and DNA sequencing (Genewiz). Transformations were performed in a *ku70* mutant background, which increases the homologous integration events. Further crosses with a Ku70 strain eliminated the *ku70* allele. The entire ORF is deleted in the *dcl1, dcl2,* and *qde2* null mutants. Subsequent analysis of *SMS2* revealed that the deletion in the *sms2* mutant left 165 bp (55 amino acids) in 5′ of the CDS. No conserved domains are found in these 55 amino acids. We also performed the complete deletion of the *SMS2* ORF, and both mutants show the same defects in term of ascus formation and sporulation.

Cytology

Ascus-bouquet pictures were taken on living material and imaged with transmitted light. GFP and mCherry fusion proteins, as well as DAPI (0.5 μg/mL) signals were observed, after fixation in 4% paraformaldehyde, with a Zeiss Axioplan microscope connected to a CCD Princeton camera or a Leica DMIRE2 microscope with a CoolSNAPHQ CCD camera (Roper Scientific). MetaMorph software (Universal Imaging Corp.) and public domain software ImageJ[3] were used to deconvolute Z-series and treat the images. Images for the *dcl1* mutant were pooled from two different strains: *dcl1 ku70* Spo76-GFP Hei10-GFP and *dcl1* Spo76-GFP Hei10-mCherry. No differences in axis lengths or Hei10 foci numbers were detected between the two strains. All the other mutants were analyzed in a Ku70 background and with the Spo76-GFP Hei10-mCherry combination of markers. To define crossover positions, we used the line tracing tool of Image J software to measure the distances between the Hei10 foci along

[1] https://www.ncbi.nlm.nih.gov/Structure/cdd/wrpsb.cgi

[2] http://www.sbg.bio.ic.ac.uk/phyre2

[3] https://imagej.nih.gov/ij/

each SC (each trace was initiated at the center of the GFP or mCherry focus).

Assessment of Vegetative and Sexual Phenotypes

To evaluate vegetative growth, wild type, single and double mutant strains were inoculated onto M2 minimum-medium plates and incubated for four days at 25°C until coverage of the plates (**Supplementary Figure 2A**). Five plates were used for each strain and the mycelium growth, measured twice a day, was compared to wild-type growth. Development of protoperithecia and mature perithecia was monitored for over ten days. In strains where perithecia formed but no ascospores could be recovered on the lid, the perithecia were cracked open using forceps and their ascus and ascospore formation was evaluated under dissecting microscope.

Crossover Interference Analyses

Crossover interference was analyzed by two different methods: Coefficient of Coincidence (CoC) and gamma distribution. The CoC (the classical way to define CO interference; Muller, 1916) directly represents the extent to which COs in two different intervals (defined genetically or along the SC) do or do not occur independently. Therefore, in our analysis, the SC of each chromosome is first divided into a number of intervals of equal size. To be sure that all closely spaced COs are counted, the number of intervals must be sufficiently high. A general rule is that the interval size should be less than 1/4 of the average distance between COs (Zhang et al., 2014a). Along each SC of the data set (around 200 SCs for each analyzed mutant), each CO/Hei10 focus is thus assigned to a specific interval along each SC of the data set. We can then assess, for any given pair of intervals, the number of SCs containing a CO in both intervals (double COs) within our dataset. The frequency of double COs is then examined and compared to the frequency of the expected double COs if they occurred independently in the same two intervals (i.e., in the two intervals considered individually). The CoC is the quotient of observed/expected double COs. The same comparison is done for all possible pairs of intervals. The CoCs of all pairs of intervals are further plotted, for each pair, as a function of the distances between two intervals (defined as the distance between the centers of the two intervals): this gives the CoC curve. In our analyses, the CoC patterns were calculated and grouped for the two longest chromosomes (1 and 2) and for the other five smaller chromosomes. The CoC values are very low for short inter-interval distances, reflecting the fact that CO interference is stronger at short distances. They increase with increasing inter-interval distance to a value of one, which indicates independent occurrence in the two intervals. The fluctuation around and above one corresponds to the tendency for even spacing of the COs. Gamma distribution analysis is another method used for describing interference. For this purpose, the inter-adjacent Hei10 foci distances in wild type and mutants are calculated as percentages of physical distances (μm). The best-fit gamma parameters for all inter-Hei10 foci distances along all chromosomes were estimated by the maximum likelihood method with the "gamfit" function in MATLAB.

Statistical Analyses

All analyses were carried out using one-way ANOVA and non-parametric tests on GraphPad/Prism. All values are given as mean ± standard deviation (SD). For axis length comparisons, a Brown-Forsythe ANOVA test for the equality of group variance was performed and showed significant differences [$F(3, 72.98) = 103.8$, $P < 0.0001$] followed by a *post hoc* Games-Howell test (reported in the Figures). For the foci number comparison, the Brown-Forsythe ANOVA also showed significant differences [$F(3, 96.21) = 79.92$, $P < 0.0001$] followed by a *post hoc* Dunnett's T3 test.

RESULTS

Sordaria macrospora Genome Encodes Two Dicer-Like and Two Argonaute Proteins

A BLAST protein homology search using *N. crassa* protein sequence as reference revealed that the genome of *S. macrospora* encodes two Dicer homologs, hereafter referred to as Dcl1 and Dcl2, as well as two Argonaute homologs, named after the *N. crassa* nomenclature Qde2 and Sms2. Each gene annotation has been checked using our own RNAseq data (unpublished). While the *DCL1*, *DCL2* and *QDE2* annotations obtained from this comparison are correct, analysis of *SMS2* transcripts revealed that two small extra exons are present in 5′ of the gene. The new coding sequence obtained after correction is extended by 165 bp (55 amino acids) at 5′ of the gene and is identical to the gene present in the new version of the *S. macrospora* genome (Blank-Landeshammer et al., 2019). No conserved domains were found in the added 55 amino acids. Domain conservation searches uncovered most of the known functional domains, including a PAZ (Piwi Argonaute Zwille) domain (identified either through NCBI Conserved Domain database or by structural homology using the Phyre2 software, see section "Materials and Methods" and **Supplementary Figure 1A**).

Based on RT-qPCR in wild type, all four genes are expressed during the sexual cycle and the meiotic divisions, with temporal kinetics that exactly parallel those of *SPO11*, which encodes the meiotic transesterase that promotes double-strand break (DSB) formation, and with *MER2,* which encodes a protein that mediates assembly of recombination-initiation complexes and DSBs (**Supplementary Figure 1B**). *SMS2* shows the strongest upregulation with more than a 2,000-fold increase compared to the vegetative state (day 1). *DCL1* transcript abundance is increased 8- to 16-fold, while *DCL2* and *QDE2* transcript levels are increased only 3-fold during the sexual cycle. These patterns are similar to those obtained in the fungus *F. graminearum*: while *FgDICER1* and *FgAGO2*/*FgSMS-2* were strongly upregulated during the sexual cycle, *FgDICER2* transcript levels were maintained throughout the developmental stages, and *FgAGO1*

showed only a moderate increase during fruiting-body formation (Son et al., 2017).

The Four Proteins Are Not Required for Vegetative Growth but Dcl1 and Sms2 Are Essential for Correct Ascus/Meiocyte Formation and Sporulation

Comparison of hyphal (vegetative cells) extension rate in wild type, the four null mutants and the *dcl1 sms2* and *dcl1 dcl2* double mutants, shows that none of the four RNAi components are required for the fungal vegetative growth (**Supplementary Figures 2A,B**).

Three of the mutants are, in contrast, defective in the complex multicellular differentiation processes occurring during the sexual cycle. This cycle initiates with the development of an aggregation of hyphae around the female ascogonia: the protoperithecia. This early step is completely wild-type (in number on the plates and in timing) in the four single and the two double-mutant strains. Further growth and expansion of the protoperithecium into a flask-shaped perithecium (called also fruiting body; **Figure 1A**) is accompanied by differentiation of several cell types inside this structure. (i) The multinuclear

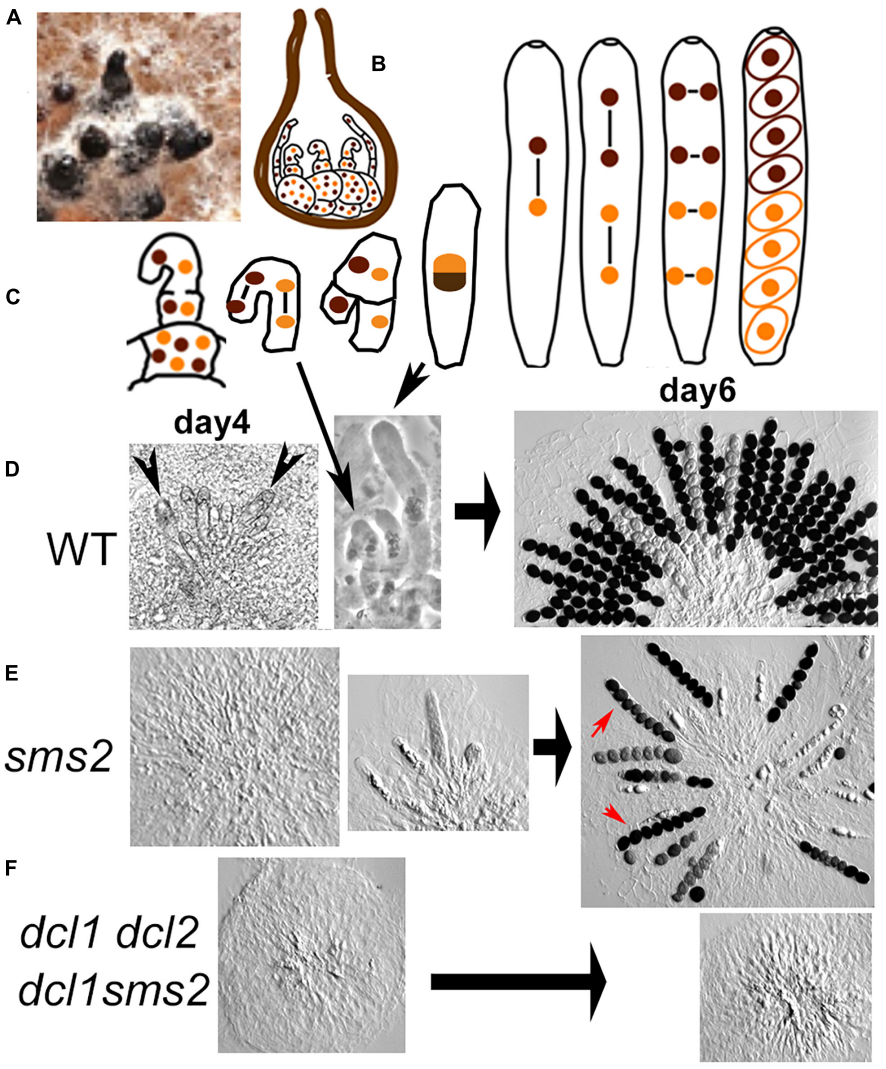

FIGURE 1 | Meiocyte formation and sporulation in wild type, *dcl1,* and double mutants. **(A)** Six bottle-shaped perithecia (black) developed on growing mycelium (white) on agar medium (brown). **(B)** Drawing of a section through a perithecium in which binucleated cells (middle) and paraphyses (two on both sides) have started to develop from the ascogonium multinuclear cells (at the base). **(C)** Progression from crozier to ascus formation, followed by karyogamy, the two meiotic divisions, a post-meiotic division and ascospore delimitation in wild type (WT). **(D–F)** Light micrographs of asci dissected out from perithecia. **(D)** Left and middle: WT young perithecia contain several small asci (arrowheads, left), intermingled with croziers (long arrow, center); right: mature perithecium with eight-spored asci (half of the asci presented here). **(E)** Left, middle and right: corresponding *sms2* stages. Note the reduced number of asci when compared to WT, the small number of asci with eight regularly shaped ascospores (red arrows) and the presence of abnormal, often aborted ascospores in the other asci. **(F)** Perithecia of the two double mutants contain paraphyses but no asci even after 6 and 14 days.

ascogonium differentiates into hyphae/cells that now contain only two nuclei, called ascogenous hyphae, and gets surrounded by several hyphae called paraphyses (**Figure 1B**). (ii) After a few synchronous divisions, the tip cells of the ascogenous hyphae differentiate into hook-shaped cells, the croziers (**Figure 1C** left), in which the two nuclei undergo one coordinated mitosis yielding, after septal formation, two uninucleate basal cells and a binucleate ascus mother cell (**Figure 1C** and long arrow in **Figure 1D**). (iii) Karyogamy and meiosis occur in the ascus mother cell and after a post-meiotic mitosis, eight ascospores are delineated in this single cell (**Figure 1C** from middle to right). (iv) Each wild-type perithecium contains several croziers and young asci (arrowheads in **Figure 1D** left) and finally over 100 eight-spored asci/meiocytes (**Figure 1D** right).

Protoperithecia develop into flask-shaped perithecia in all six mutant strains, but the differentiation of the ascogenous hyphae into several asci and finally eight-spored asci inside the perithecium (**Figure 1D** left through right) is only wild-type-like in the *dcl2* and *qde2* null mutants (**Supplementary Figure 3A**). In contrast, *dcl1* and *sms2* null mutants display both delayed and strongly defective ascus formation (illustrated for *sms2* in **Figure 1E** left and middle and in **Supplementary Figure 3B** for *dcl1*). After 5 days post-inoculation, *dcl2* and *qde2* perithecia contain over 100 eight-spored asci (**Supplementary Figure 3A**), like wild type (**Figure 1D** right). In contrast, only 6% of *dcl1* and 42% of the *sms2* perithecia ($\geq$200 crack-opened for each strain) contain asci and always in highly reduced numbers (1 to 10; illustrated in **Figure 1E** middle and right plus **Supplementary Figure 3C** for *sms2* and in **Supplementary Figure 3B** for *dcl1*), the remaining perithecia containing only paraphyses (**Figure 1E** left). On the sixth day, all *sms2* perithecia contain 5 to 30 asci (**Supplementary Figure 3C**) but 80% of the *dcl1* perithecia still contain only paraphyses (n = 200 for each strain).

These two mutants exhibit two more intriguing phenotypes: (i) while all perithecia of the wild-type plates contain over 100 asci, *dcl1* and *sms2* plates contain always a mixture of perithecia with various numbers of asci (compare **Figure 1D** right with **Figure 1E** right); (ii) furthermore, the phenotypes of the asci inside each perithecium are also variable: a few asci exhibit eight regularly formed ascospores (red arrows in **Figure 1E** right) when the other asci contain abnormal ascospores in number and shape (all other asci with spores in **Figure 1E** right).

In order to decipher potential epistasis between the different mutations, we generated all six double mutants. First, no spores are observed in the *dcl1 dcl2* and *dcl1 sms2* double mutants even after 10 days post-inoculation (0/205 cracked-open perithecia **Figure 1F** and **Supplementary Figure 2C**). This suggests that Dcl1 and Sms2 are both required, in a non-redundant, non-epistatic fashion, for ascus/meiocyte formation, and sporulation. Moreover, when both Dicer proteins (in the *dcl1 dcl2* double mutant) or both Argonaute proteins (in the *qde2 sms2* double mutant) are absent, virtually no asci and spores are formed (asci only in 3 or 0% of the perithecia, n = 203 and 205, respectively). This indicates that at least one protein of each functional group is strictly required for proper ascus/meiocyte induction and sporulation in *Sordaria*. This also points out that, while both *dcl2* and *qde2* single mutants show wild-type levels of sporulation (**Supplementary Figure 3A**), both Dcl2 and Qde2 are nevertheless implicated, albeit to a lesser extent (but which becomes important in absence of Dcl1 or Sms2), in the meiocyte/sporulation process.

The other double mutants did not rescue or worsen the sporulation phenotypes of the corresponding single mutants: (i) *dcl1 qde2* and *sms2 dcl2* double mutants (**Supplementary Figure 3D** left and middle) show the same sporulation defects as *dcl1* and *sms2* single mutants, respectively (**Supplementary Figures 3B,C**); (ii) the *qde2 dcl2* double mutant displays wild-type levels of sporulation (**Supplementary Figure 3D** right). These results show that the RNAi pathway is required for proper ascus/meiocyte induction and sporulation in *Sordaria*, with prominent roles for Dcl1 and Sms2, and a lesser role for Dcl2 and Qde2.

During Meiotic Prophase, Dcl1, Dcl2, Sms2, and Qde2 Are Not Required for Axis and Synaptonemal Complex Formation but Dcl1 and Sms2 Are Essential for Their Maintenance

The four null mutants progress through meiosis with the same gradual increase of ascus size as in wild type, allowing meiotic prophase analysis without complications from defects in ascus growth. It should be noted that contrary to the *dcl2* and *qde2* mutants which produce large numbers of prophase asci per perithecium, the effects of *dcl1* and *sms2* deletions on meiotic prophase could only be assessed in the 1 to 30 asci/meiocytes produced per perithecium. Chromosomes were analyzed in leptotene through pachytene nuclei by DAPI staining of the chromatin and with the previously characterized axis marker Spo76/Pds5 (Van Heemst et al., 1999).

In wild-type *Sordaria*, chromosome axes develop at early leptotene with accompanying initiation of recombination by the induction of DSBs by Spo11 (Storlazzi et al., 2003). Repair of these DSBs by homologous recombination then allows recognition and spatial juxtaposition of the homologous chromosomes (homologs) at a distance of around 400 nm through robust inter-axis bridges (Dubois et al., 2019). Synapsis then occurs, bringing homologous axes together at a distance of 100 nm via formation of the synaptonemal complex (SC) along the seven homologs (Espagne et al., 2011). The latter steps of recombination occur in the context of the SC (Tessé et al., 2017). A similar chromosomal progression is observed in the four mutants, except that the synaptic period is slightly prolonged in *dcl2* (by 12 h) and even more greatly delayed in *dcl1* and *sms2* (by over 24 h).

Like in wild type (**Figure 2A** left), Spo76/Pds5 forms complete lines along chromosomes at leptotene in all four mutants (illustrated for *dcl1* in **Figure 2B** left), indicating that Dicer and Argonaute proteins are not required for chromosome axis formation during onset of meiosis. The four mutants have also no problem with forming SC continuously along the seven *Sordaria* homologs as tested by observation of their axes (by Spo76/Pds5-GFP), which are now at 100 nm distance and form a single line (compare **Figure 2B** with **Figure 2A**; and see below for

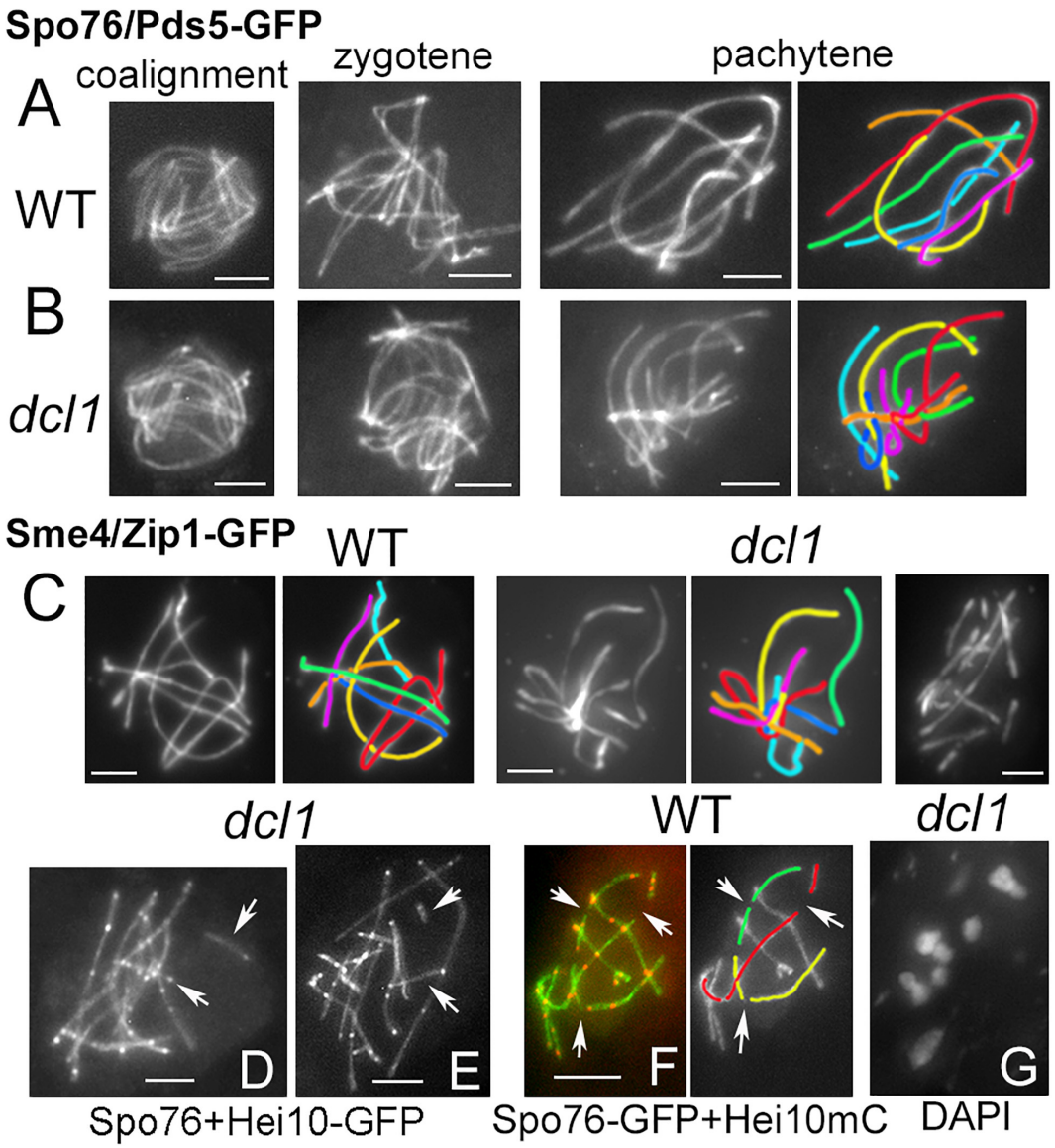

FIGURE 2 | Synaptonemal complex in wild type and *dcl1*. **(A,B)** Chromosome axes are marked by Spo76/Pds5-GFP. From left to right: progression from coalignment at late leptotene, partial synapsis at zygotene (middle) and complete synapsis at pachytene in wild type **(A)** and *dcl1* **(B)**; the seven homologs are distinguishable by their lengths and colors. **(C)** SCs are marked by the central component Sme4/Zip1-GFP in wild type (left) and in *dcl1* with full SC along all homologs (middle). Right: example of a *dcl1* pachytene nucleus with more than 7 SCs. **(D,E)** Two *dcl1* nuclei with extra SC segments (arrows), either separated from the other SCs (upper arrows), or at odd angles (lower arrows). **(F)** Interrupted SCs are also seen in WT late pachytene nuclei (arrows), but the SC paths can be followed in the concerned homologs (illustrated for three of them, right). **(G)** Diplotene of *dcl1* with 7 bivalents. Bars, 2 μm.

the other mutants) and by labeling the SC central component Sme4/Zip1 (**Figure 2C**).

After mid-pachytene (by ascus size), the *dcl1* and *sms2* mutants exhibit a defect in SC maintenance. In *dcl1*, the SC is initially complete from telomere to telomere at early pachytene (**Figures 2B,C** middle). However, among the 29 analyzed mid-late pachytene *dcl1* nuclei, nine exhibit more than seven segments corresponding to the seven pairs of homologs seen at early pachytene. These nuclei contain 8 to 13 SC segments observed either by Sme4/Zip1-GFP (**Figure 2C** right) or by Spo76/Pds5-GFP (arrows in **Figures 2D,E**). The SC segments have variable lengths (from 1 to 4 μm), but are always shorter than the shorter *dcl1* chromosome (7.3 ± 1.1 μm). Nevertheless, total axis/SC lengths in these nine nuclei are similar to the total axis lengths measured in the other 20 nuclei that show seven uninterrupted SCs (79.3 ± 12.8 compared to 73.4 ± 8.9 μm), suggesting early SC disassembly in those nuclei and not SC formation between sister chromatids as observed in haploid meiosis of *Sordaria* (Vasnier et al., 2014) or in absence of Rec8 in mouse (Xu et al., 2005).

In some respect, this *dcl1* mutant phenotype resembles the pattern seen in wild type when the SC components start to disassemble at late pachytene, at which point the nuclei exhibit also more than seven SCs segments (arrows in **Figure 2F**). However, in the wild-type case, one can easily follow the paths through the "missing" segments and thus "reconstruct" the original seven SCs (illustrated by the red, yellow, and green homologs in **Figure 2F**). In contrast, in *dcl1* the extra short SC segments are at odd angles to the "regular," longer, SC segments and/or very far from them (arrows in **Figures 2E,F**). Unfortunately, at late pachytene, chromatin is too diffuse in *dcl1* to infer connections between the smaller segments of SCs to one or the other of the longer SC segments. These data point to a defect in SC maintenance in the *dcl1* mutant. In accord with this interpretation, we failed to detect broken chromosomes in the 12 diplotene nuclei analyzed (**Figure 2G**), implying that the defect observed at mid-late pachytene represents aberrant discontinuity only at the SC structural level but it remains unclear why the SC segments have lost their continuity.

The tendency for aberrant and variable numbers of SC segments is even more pronounced in absence of Sms2. When all pachytene nuclei of *dcl2* and *qde2* (n = 37 and 43, respectively) show seven continuous Spo76/Pds5-GFP lines when the homologous axes are synapsed at 100 nm distance by the SC (**Figures 3A,B**), none of the *sms2* analyzed nuclei (n = 37) exhibit such continuous lines. During what should be early to mid-pachytene by ascus size, the *sms2* nuclei marked by either Spo76-GFP (**Figure 3C**) or by Sme4/Zip1-GFP (**Figure 3D**,

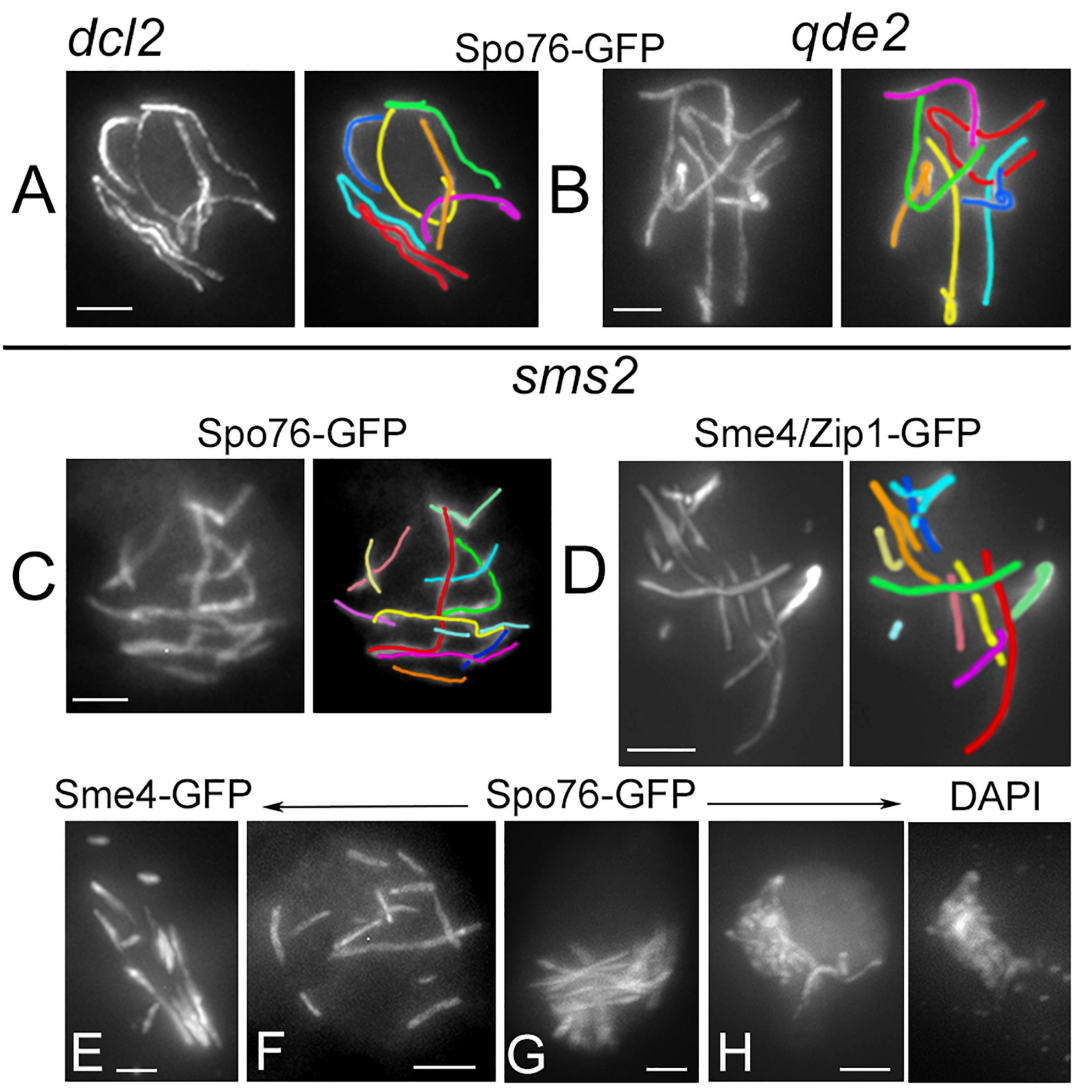

FIGURE 3 | Defective SC formation in *sms2* when compared with *dcl2* and *qde2*. **(A–H)** SCs are marked by Spo76/Pds5-GFP or Sme4/Zip1-GFP. **(A,B)** SCs extend from telomere to telomere in pachytene nuclei of *dcl2* **(A)** and *qde2* **(B)**; the seven homologs are distinguishable by their lengths and colors. **(C–H)** Examples of abnormal SCs in *sms2* pachytene nuclei. **(C,D)** Two examples with 12 and 11 SC segments in mid-pachytene nuclei (by ascus size), and corresponding colors. **(E,F)** SCs are either stiff and close **(E)** or widely separated **(F)**. **(G)** Example of stiff and intermingled SCs. **(H)** Late pachytene nucleus with highly intermingled SCs and, right, corresponding DAPI. Bars, 2 μm.

$n = 10$) exhibit a total of 8 to 14 SC segments. These SC segments are, moreover, aberrant in their overall disposition in various ways: either stiff and close (**Figure 3E**) or largely separated from one another (**Figure 3F**) or completely intermingled (**Figure 3G**). Finally, at what should be late pachytene by ascus size, SC segments are even more intermingled (**Figure 3H**) and chromatin is very fuzzy (**Figure 3H** right), indication that those nuclei are likely degenerating, in accordance with the fact that this mutant shows also a high number of abnormal asci and spores as described above (**Supplementary Figure 3C**). Both *dcl1* and *sms2* SC phenotypes, and the presence of diffuse chromatin (**Figure 3H**), suggest that the observed SC discontinuities could result from local changes in the chromatin structure, which could alter SC integrity, leading to aberrant or premature local SC disassembly.

Dcl1, Dlc2, and Qde2 Are Required for Axis/SC Lengths and Crossover Numbers

To assess the possible role of the RNAi components in axis and/or SC lengths, we analyzed SC lengths in wild type and in the three mutants *dcl1*, *dcl2,* and *qde2* that exhibit seven bivalents throughout pachytene (**Figures 4A,B**). The most prominent increase in SC length is observed in the *dcl1* mutant: 75.2 ± 9 μm ($n = 33$ nuclei) compared to 52.9 ± 4.5 in wild type ($n = 130$). Although less pronounced, the mean SC lengths of the *dcl2* (56.1 ± 4.6; $n = 37$) and *qde2* (58.1 ± 4.7; $n = 43$) mutants are also significantly different from wild-type lengths but are not significantly different from one another (Anova tests; **Figure 4B**). All these increased lengths are, moreover, not specific to the SC stage because Spo76-labeled chromosome axes are already longer than wild-type axes at the coalignment and early zygotene stages (e.g., for *dcl1,* **Figure 2B** left; 76.3 ± 8.2, $n = 10$).

Crossover numbers were defined by cytological analysis of E3-ligase Hei10 foci, which mark the sites of CO-fated recombinational interactions in pachytene nuclei (De Muyt et al., 2014) when SC is full length (illustrated in **Figure 4C** for *qde2* and *dcl1*). The mean number of Hei10 foci per pachytene nucleus is, respectively, of 31.5 ± 3.1 in *dcl1* ($n = 29$ nuclei), 24.9 ± 2.2 in *dcl2* ($n = 21$) and 25.1 ± 2.9 in *qde2* ($n = 31$) compared to 22.6 ± 2.3 in wild type ($n = 98$ nuclei). Thus, paralleling the increase in SC lengths, there are significantly more Hei10 foci per nucleus, and thus COs, in the three mutant strains than in wild type; and the increases observed in *dcl2* and *qde2* are not significantly different from one another (**Figure 4D**).

The distribution of the Hei10 foci in the mutants exhibit also four hallmarks of meiotic COs. (i) All bivalents of *dcl1*, *dcl2,* and *qde2* (567 in total) show at least one Hei10 focus, indicating the presence of the "obligatory crossover" (required for proper chromosome segregation) in all three mutants. (ii) Like in wild type, the total number of CO events varies appreciably from one nucleus to another (**Figure 4D**). (iii) Within the nuclei with high numbers of Hei10 foci, all seven chromosomes exhibit correlated increased numbers of COs, showing that increases are global and not chromosome specific. (iv) Linear regression analysis shows that in each nucleus, SC length and CO number are correlated (**Supplementary Figure 4A**).

The number and position of pachytene Hei10 foci reflect the nature of the CO-designation/interference process that occurs at earlier stages and could thus be sensitive to defective numbers of DSBs. To investigate this possibility, we measured the numbers of Mer3 foci that initially occur, in the same number as Rad51 foci, and mark the sites of DSBs in *Sordaria* (Storlazzi et al., 2010). In the *dcl1* mutant, with the highest number of COs, the number of Mer3 foci is similar to wild type: 54.2 ± 14.7 ($n = 14$) vs. 61.9 ± 22 ($n = 24$, $p = 0.3$) (**Supplementary Figure 4B**). Therefore, we infer that the increase in CO number does not stem from an increase in DSB formation, but rather from a deregulation of downstream events.

In the *sms2* mutant, despite the very defective axis organization and SC formation and/or elongation at pachytene (see above), Hei10 foci form in all pachytene nuclei (**Figure 4E**). Among the 27 pachytene nuclei analyzed, 14 showed 20.3 ± 6.9 Hei10 foci, thus close to the number of 22.6 ± 2.3 foci observed in wild type (compare **Figures 4E–G**). Also, like in wild type, those foci persist through the early diffuse stage where they remain associated with a residual stretch of SC (**Figure 4F**). The foci in these 14 nuclei exhibit, moreover, the same size and fluorescence density as those of wild type and the three other mutants (**Figures 4E,F**). The 13 other nuclei, in contrast, show very intriguing phenotypes: instead of being single, Hei10 forms more or less large bright masses (**Figures 4G,H**) where two to several foci are stacked (arrows in **Figure 4I**). To our knowledge, this is the first meiotic mutant to display such a phenotype. Whether these masses come from the aggregation of multiple foci at different loci, or from accumulation of Hei10 protein at individual recombination sites remains unknown.

Crossover Interference and Patterning Is Perturbed in *dcl1*, and to a Lesser Extent in the *dcl2* and *qde2* Mutants

Crossover patterns arise in two stages during meiotic prophase. Recombination is first initiated by a large number of programmed DSBs which occur in recombination complexes that are associated with the chromosome axes. A small subset of those DSBs are then specifically designated to become COs. Finally, CO-designated interactions mature to actual COs, in association with the SC components, via a series of further biochemical steps. Several mechanisms limit the number of precursors that will effectively be turned into a CO, channeling the other DSBs to being repaired as non-crossovers (e.g., Hunter, 2015; Lam and Keeney, 2015). One of these mechanisms, termed CO interference, was identified by the finding that a CO at one position disfavors occurrence of additional COs nearby, resulting in a tendency for COs to be more widely and regularly spaced than predicted from a random distribution [Muller, 1916; reviewed in Wang et al. (2015)].

The tendency for COs to be evenly spaced along the chromosomes, is reflected in the fact that the distribution of inter-CO distances along each homolog has the shape of a gamma distribution, with a value for the shape parameter ν greater than

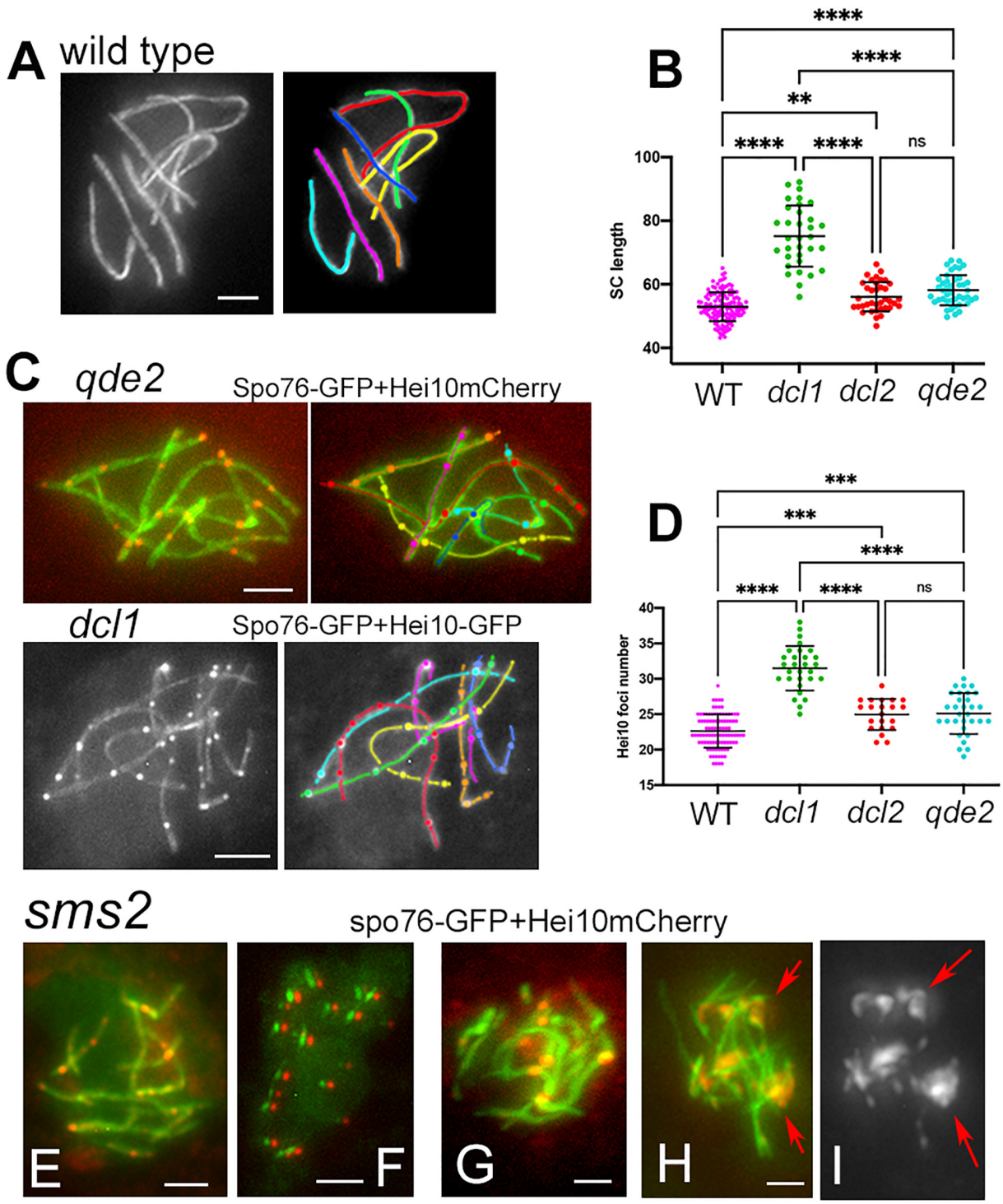

FIGURE 4 | Axis lengths and crossover numbers in WT, *dcl1, dcl2,* and *qde2* mutants plus Hei10 foci in *sms2*. **(A)** Wild-type pachytene nucleus with 7 Spo76-GFP marked SCs. **(B)** SC lengths per nucleus in WT and mutants; means with standard deviations; *P*-values: $^{**}p < 0.01$; $^{****}p < 0.001$. **(C)** Examples of Hei10 foci localization along the seven homologs of *qde2* (top) and *dcl1* (bottom). Axes are marked by Spo76-GFP and foci are marked either by Hei10-mCherry (*qde2*) or by Hei10-GFP (*dcl1*). **(D)** Number of Hei10 foci per nucleus in WT and mutants; double lines indicate standard deviations; *P*-values: $^{**}p < 0.01$; $^{****}p < 0.001$. **(E–I)** *sms2* mutant. **(E)** Nucleus with extra SCs (see **Figure 3C**) but wild-type like Hei10 foci [compare with the *qde2* nucleus in **(C)**]. **(F)** At early diffuse stage, only small SC segments (green) are left but they contain all one Hei10 focus (red). Green and red signals from SC and foci, respectively, were shifted for easier observation. **(G)** SCs are abnormal in length and shape and foci are larger than normal [compare with **(E)**]. **(H,I)** Nucleus with large Hei10 foci with **(H)** and without **(I)** Spo76-GFP. Foci are either single or aggregated [red arrows in **(I)**]. Bars, 2 μm.

1. Being a measure of evenness, the shape parameter ν of the gamma distribution is thus an indirect indicator of interference (see section "Materials and Methods"). In all three mutants, ν is decreased compared to wild type: 2.40 $\pm$ 0.13 for *dcl1*, 4.01 $\pm$ 0.27 for *dcl2* and 4.28 $\pm$ 0.24 for *qde2* compared to 5.03 $\pm$ 0.18 for wild-type. These values suggest that interference is present in the three mutants but is less robust than in wild type. Reduced interference in the mutants is further confirmed by the Coefficient of Coincidence (CoC) analysis (see details in section "Materials and Methods"). For this approach, the 203, 147, and 217 SC-labeled chromosomes of, respectively, *dcl1*, *dcl2,* and *qde2* were divided into multiple intervals. For every possible pair of intervals, the frequency of chromosomes with a CO in both intervals is compared with the frequency expected if COs occurred independently (observed double COs/expected double COs). The resulting ratios are plotted as a function of inter-interval distances (**Figure 5A**). There are significantly higher levels of double COs at shorter inter-interval distances in the mutants than in wild type, and double COs frequency increases as inter-interval distance increases, with finally CoC

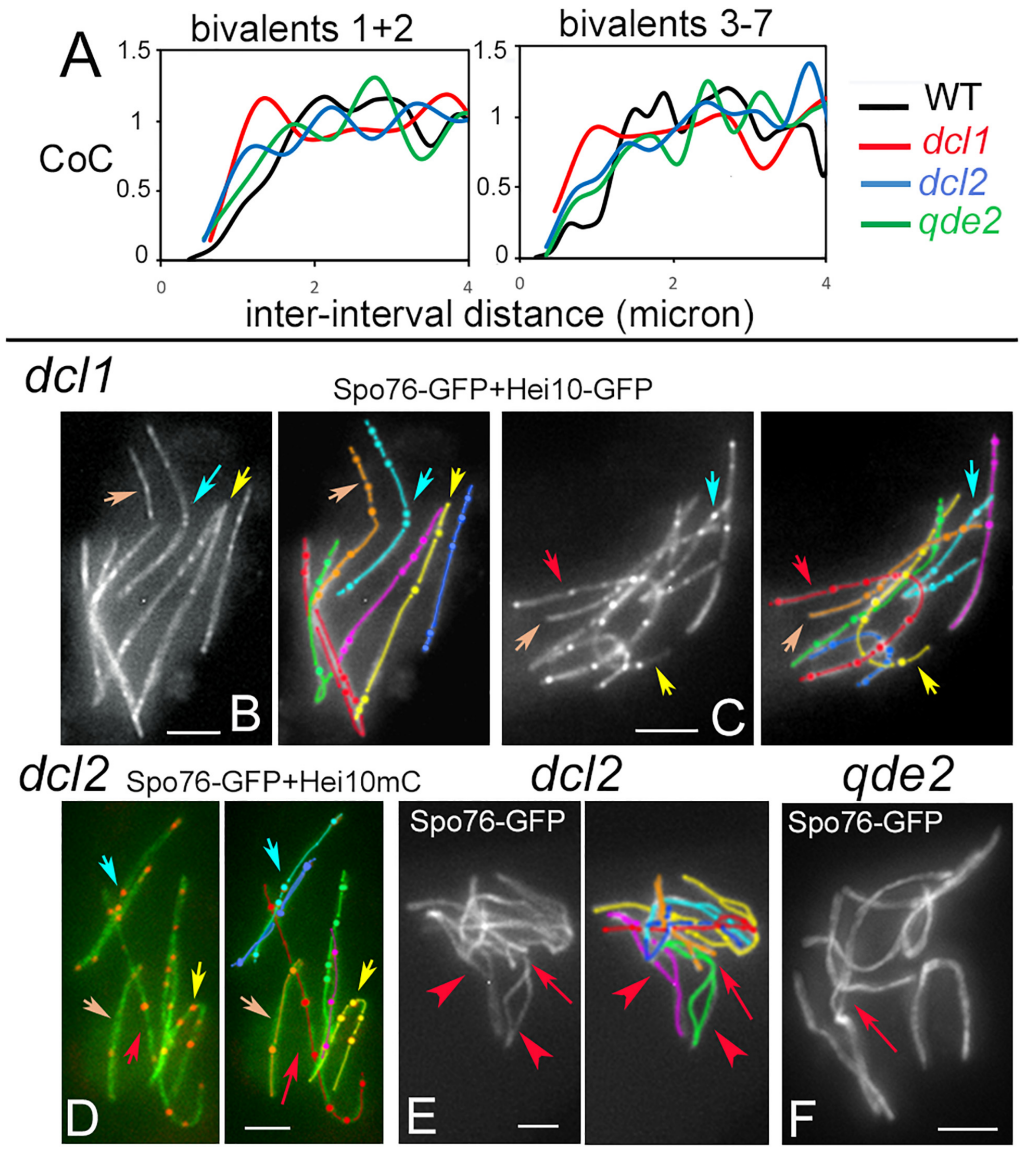

FIGURE 5 | Crossover interference, patterns and synapsis defects in *dcl1*, *dcl2,* and *qde2*. **(A)** Coefficient of Coincidence (CoC) plotted as a function of inter-interval distances in longer homologs 1 and 2 (left) and shorter homologs 3 to 7 (right) of WT, *dcl1*, *dcl2,* and *qde2*. **(B,C)** Hei10 foci along homologs in *dcl1* early **(B)** and mid-pachytene **(C)** nuclei. Note that foci are brighter at the later stage **(C)**. Similar irregularities in focus distances are seen in *dcl1* **(**arrows in **B,C)** and *dcl2* **(D**, arrows**)**. Only 4 of the 7 homologs are pointed by arrows for easy lecture, but the other homologs (e.g., the purple and green ones) show also variable distances and close foci. **(E)** Zygotene nucleus of *dcl2*. Note the widely open non-synapsed regions (arrowheads on green and purple homologs) and the resolving entanglement (arrow) between the green and orange homologs (open ends of the orange homolog will help the green homolog to slide out of the interlock). **(F)** Illustration of a non-resolved interlock at mid-late pachytene (by ascus size) in *qde2* (arrow). Bars, 2 μm.

values fluctuating around one as in wild type, which indicates that there is no interference at this distance (**Figure 5A**). CoC patterns are similar for both long (1 and 2) and short (3 to 7) chromosomes (**Figure 5A** right and left). However, when compared to wild type, the three mutant CoC curves are shifted to the left, indicating defective interference. The greatest effect is observed for *dcl1* (**Figure 5A**). In principle, since CO number scales directly with axis/SC length in the mutants as in wild type (**Supplementary Figure 4A**) and in most organisms (Wang et al., 2019), one could expect that gamma and CoC values would be the same in the *dcl1*, *dcl2,* and *qde2* mutants. The reduced CO interference observed in the three mutants implies, therefore, that COs tend to be closer together or less regularly spaced than in wild type. We showed previously that reduction of CO interference in the *mer2–17* allele of *Sordaria* was due to the presence of a high number of very close Hei10 foci (Tessé et al., 2017). Detailed inspection of Hei10 focus localization along the SCs of *dcl1*, *dcl2,* and *qde2* reveals that the mutants exhibit also close foci at inter-focus distance of 0.1 to 0.4 μm, but as can be seen in the nuclei of **Figures 4C**, 5B–D, they are not the majority. We suspect, therefore, that the decrease of CO interference could result from the fact that the Hei10 foci (and thus COs) are distributed in a very irregular way along the homologs. Indeed, as illustrated in **Figures 5B–D**, the distances between Hei10 foci are highly irregular along most of the homologs. For example, when red-labeled homologs of *dcl1* and *dcl2* show regularly spaced foci (red arrows in **Figures 5C,D**), yellow-, cyan- and orange-labeled homologs in **Figures 5B–D** (marked by corresponding color arrows) exhibit highly irregular focus distances. There is, however, no chromosome effect, because in other nuclei, the "red homologs" show also irregular focus distances.

Crossover patterning defects may be related to the fact that, even though SC forms all along the homologs at pachytene, the three mutants also exhibit pairing and synapsis defects at earlier stages. First, both coalignment and synapsis are delayed (above). Second, contrary to wild-type zygotene, SC formation is asynchronous, with some bivalents still only half synapsed when the others are fully synapsed (**Supplementary Figure 4C**). In addition, zygotene nuclei exhibit both entanglement(s) and largely non-synapsed regions in one or two of the seven homologs (arrow and arrowheads in **Figure 5E**, see **Supplementary Figures 4C,D** for more examples). Third, while such entanglements are all resolved at early pachytene in wild type (Storlazzi et al., 2010), they persist throughout pachytene in all three mutants, even in *qde2* which has the least severe defects in SC formation (arrow in **Figure 5F**). In accordance with the more severe CO patterning defects, *dcl1* exhibits also the more severe pairing defects, in accord with a direct relationship between these two features. Notably, these phenotypes identify a Dcl1, Dcl2, and Qde2 sub-function specific to the pairing/synapsis process.

DISCUSSION

The current study provides novel insights concerning the role of the Dicer-like and Argonaute proteins. First, none of the four proteins is required for normal vegetative growth, while all have important roles in several aspects of the sexual cycle. Second, observations of meiotic prophase reveal that the four proteins, each in a different way, exert effects on determination of chromosome-axis length, and crossover patterning. Taken together, our results provide new perspectives from which to consider roles of these RNAi factors.

New Roles for Dicer and Argonaute Proteins in the Early Steps of Meiocyte Differentiation

A complex multicellular differentiation process leads to the formation of asci/meiocyte during the sexual cycle of *Sordaria*. The two Dicer proteins and the Argonaute Sms2 protein are required for several stages of this process. The first defects detectable in the mutants occur during the transition from the multinuclear cell stage, which is prevalent during the vegetative cycle, to the stage when cells contain only two nuclei in the so-called dikaryon stage, which is a prerequisite for karyogamy and meiosis. This transition into the sexual cycle involves considerable cell differentiation (**Figure 1**, above) associated with drastic changes of the transcriptional program (Blank-Landeshammer et al., 2019). It is interesting to note that, analogously, deletion of Dicer and Argonaute homologs lead to embryonic death and/or defects in cell-type differentiation in mouse, worm, *Drosophila*, maize, and *A. thaliana* [reviewed in Gutbrod and Martienssen (2020)]. This analogy is particularly striking in light of the fact that these organisms are present in very divergent branches of eukaryotes.

Diverse roles for the Dicer and Argonaute proteins are identified at the next stages of meiocyte/ascus differentiation. With respect to the Dicer proteins, Dcl2 is dispensable for ascus formation and development; in contrast, Dcl1 is strictly required for both the vegetative to the sexual cycle transition and for wild-type-like ascus formation, echoing previous results in the fungi *N. crassa* and *F. graminearum* (Alexander et al., 2008; Son et al., 2017). With respect to the Argonaute proteins, our results indicate that Sms2 is another key mediator of the early steps of meiocyte initiation, while Qde2 is (like Dcl2) dispensable for ascus formation and development.

The analysis of the double mutants does not delineate a simple epistatic/redundancy relationship between the four RNAi factors. The *dcl1 dcl2* double mutant displays a much stronger effect on meiocyte/ascus differentiation than either of the single mutants. Thus, Dcl2, plays also a role in this process but to a lesser extent than Dcl1. The phenotype of this double mutant shows also that the two dicer proteins operate within the same pathway with a minor contribution of Dcl2, like its *F. graminearum* homolog (Son et al., 2017; Zeng et al., 2018). It is the same for the two Argonaute proteins with a minor contribution of Qde2. Moreover, comparison of the *dcl1* and *sms2* single mutants indicates a different phenotype for *dcl1* than for *sms2*: at day 6, almost all *sms2* perithecia contain asci/meiocytes and spores, while 80% of the *dcl1* perithecia contain neither asci nor spores. Moreover, the perithecia of both mutants contain only 1 to 10 asci, versus over 100 in wild type. This suggests that Dcl1 (and to

a lesser extent Dcl2) is primarily already involved in the transition from the vegetative to the sexual cycle. Once the vegetative/sexual transition has started, the dicer proteins (essentially Dcl1) and downstream the Argonaute proteins (mainly Sms2) are further required to produce wild-type ascus numbers. The two double mutants *dcl1 dcl2* and *sms2 qde2* are sterile but likely not at the same development stage. Our hypothesis is that *dcl1 dcl2* is not able to initiate the sexual cycle while *sms2 qde2* is able to initiate the sexual cycle but is unable to produce asci. Such independent roles of Dicer and Argonaute proteins have been reported in other systems, and could rely on the presence of other small, Dicer-independent, dsRNAs (Pong and Gullerova, 2018). The identified roles of Dicer and Argonaute proteins during meiocyte/ascus differentiation could be explained by a role of the RNAi pathway in the regulation of the gene expression needed for the transition from the vegetative program to the sexual cycle.

RNAi Components Mediate Chromosome Axis Length During Meiotic Prophase

Meiotic chromosomes are highly organized structures. Each chromatid is organized into a linear array of loops, the bases of which comprise the axis, and sister chromatids are co-oriented with their axes tightly conjoined [reviewed in Zickler and Kleckner (2015)]. This organization emerges at the onset of meiotic prophase.

Analysis of the *dcl1*, *dcl2*, and *qde2* null mutants reveals the corresponding proteins as new players in the determination of chromosome-axis length. In all three cases, axis/SC lengths are increased when compared to wild type, indicating a change in the loop/axis relationship. Similar increased axis length has previously been reported in mutants lacking meiosis-specific cohesins SMC1Beta and Rec8, as well as other axis components like Spo76/Pds5, which all play key roles in the loop/axis relationship (e.g., Viera et al., 2020; Song et al., 2021). Several hypotheses could explain the observed changes in axis lengths. As a primary function of RNAi is to regulate gene expression, one hypothesis could be that Dicer and Argonaute proteins are involved in fine tuning of the expression of genes coding for proteins involved in meiotic chromosome axis morphogenesis. In *F. graminearum*, expression of *Rec8* is strongly reduced in the *Fgdlc1* mutant (Zeng et al., 2018) and lower Rec8 expression is accompanied by shorter chromosome axes in *S. cerevisiae* (Song et al., 2021) and with defects in SC organization in mouse (Murdoch et al., 2013).

Alternatively, RNAi proteins could regulate the chromatin state *per se*, by altering deposition of epigenetic marks for instance, as shown in *S. pombe* (Volpe et al., 2002), which could in turn affect chromatin compaction and/or the DNA loop sizes (e.g., in *Tetrahymena*; Wei et al., 1999). Consistent with this latter hypothesis is the observation that the *A. thaliana*, Dicer-like1 mutant (with other partner proteins) displays decondensed chromatin at the pachytene stage of meiotic prophase I (Oliver et al., 2017). Analogously, we find that *Sordaria* Dcl1, and especially Sms2, are required for wild-type like chromatin compaction. In wild type, DAPI staining indicates that chromatin is thin and smooth at zygotene and early pachytene, more compact at mid-pachytene and finally diffuse at late pachytene (De Muyt et al., 2014). In contrast, in the *dcl1* and *sms2* mutants, chromatin appears diffuse from zygotene throughout pachytene. Abnormal chromatin organization, globally or locally, could also explain the premature SC disorganization observed in these mutants. We cannot, however, exclude that, alternatively, RNAi components could play unconventional roles, e.g., to directly modulate either the axis status *per se* or the axis/loop organization, by interacting with axis proteins. Further studies are required to distinguish among these possible mechanisms.

The RNAi Factors Are New Players in Crossover Patterning and Interference

One of the most fascinating aspects of meiosis is the highly regulated process that determines the number and positions of COs along homologs. Mutant phenotypes of the four analyzed RNAi factors provide new perspectives from which to consider the nature of these processes and the possible roles of RNAi. We find that when Dcl1, Dcl2, and Qde2 are absent, the number of crossovers is increased. This effect is attributable to the observed increased axis length, to which CO number is known to be proportional in *Sordaria* (**Supplementary Figure 4A**), and in a wide variety of other organisms (Wang et al., 2019). In addition, in the three corresponding mutants, the spatial patterning of COs along the homologs is altered when compared to wild type. There is, however, no loss of the "obligatory CO," implying that CO designation *per se* remains robust.

We suspect that the altered CO distribution along homologs is related to the fact that in some chromosome regions SC formation is delayed, or hindered by entanglements into other chromosomes or homologs, channeling CO designation into regions where SC elongation progresses normally. We showed previously that CO patterns are determined by a designation and interference process that precedes SC formation, which is a concomitant downstream outcome (Zhang et al., 2014b). Aberrant synapsis and entanglements are likely to inhibit the implementation of these coordinate events in the mutants.

Alternatively, or in addition, the four RNAi proteins could regulate CO patterns directly, e.g., by alterations of the chromatin *per se* via epigenetic mark deposition. Roles for RNAi factors and epigenetic marks in recombination have been identified in several cases. In the fission yeast *S. pombe*, depletion of Dcr1, Ago1 or the histone methyl-transferase Clr4 leads to increased recombination in the pericentromeric region of chromosome III (Ellermeier et al., 2010). The same phenotype was observed in the *dcr1–5* point mutant in which the RNase III endonuclease domain was mutated specifically, arguing that Dcr1 role is directly correlated to its ability to dice dsRNAs (Ellermeier et al., 2010). However, in *S. pombe*, the increase in centromeric crossovers is accompanied by an increase in detectable DSBs, which is not the case in the *Sordaria dcl1* mutant where the number of Mer3 foci, which mark the sites of DSB interactions upon which CO patterning operates, is similar to wild type. Changes in epigenetic marks have also been

linked to changes in recombination levels in *A. thaliana*: mutants with defective H3K9 and non-CG DNA methylation show increased crossover formation, while mutants with decreased CG DNA methylation show decreased recombination (Underwood et al., 2018). Finally, the Dicer and Argonaute proteins could, alternatively, control the expression of genes involved in the regulation of interference-sensitive crossovers.

Why Do the *dcl1* and *sms2* Mutants Show so Many Abnormal Ascospores?

While *dcl2* and *qde2* mutants form regularly eight-spored asci, *dcl1,* and *sms2* mutants exhibit large numbers of abnormally shaped and aborted ascospores. Defective spore formation in *sms2* can be explained, at least in part, by the observed pairing, SC and CO defects, which, in turn, could lead to defective homolog segregation at anaphase I. However, the presence of so many abnormal spores in *dcl1* is an unexpected finding because the mutant exhibits normal pairing, SC formation, CO formation, including the obligatory CO that enables regular homolog segregation, and no chromosome breakage. Nevertheless, lagging chromosomes are visible in some anaphase I and II spindles (**Supplementary Figure 5**), which likely lead to defective chromosome segregation, which, in turn, would lead to the formation of abnormal spores. The involvement of the RNAi partners in chromosome segregation is a highly conserved feature. Dicer has been shown to be required for regular chromosome segregation during both mitosis and meiosis in fission yeast; the *dcr1* mutant exhibits lagging chromosomes during both divisions (Provost et al., 2002; Hall et al., 2003). Segregation defects during mitosis have been also uncovered in maize, *Drosophila*, *C. elegans* and mouse *dicer* and *ago* mutants (Deshpande et al., 2005; Harfe et al., 2005; Claycomb et al., 2009; Singh et al., 2011). Our results add a new organism to this list and show that *Sordaria* RNAi factors have, therefore additional post-meiotic functions. We also note that segregation defects during *Sordaria* mitotic divisions cannot be excluded because they might not occur in all nuclei and would thus not be detected in the multinuclear vegetative hyphal cells. Interestingly, the described defects in chromosome segregation are often correlated with defects in centromere composition, and/or mis-localization of centromeric marker proteins (Hall et al., 2003; Deshpande et al., 2005; Claycomb et al., 2009; Singh et al., 2011; Huang et al., 2015). These centromeric defects could be linked to a prominent role of RNAi in maintenance of centromeric and peri-centromeric heterochromatin state as described in *S. pombe* [reviewed in Goto and Nakayama (2012)].

Taken together, our results highlight the importance of the RNAi pathway in regulating key steps of the *Sordaria* sexual cycle. The importance of RNAi for sexual reproduction is widely conserved. However, our results reveal that both Dicer and Argonaute proteins are also specifically required during meiotic prophase, with direct or indirect roles in basic chromosome structure (through loop/axis modeling) and on the number plus localization of crossovers along the homologs. The molecular targets of those activities remain to be defined. We anticipate, however, that their elucidation will reveal important new aspects of the molecular activity of the analyzed RNAi factors.

DATA AVAILABILITY STATEMENT

The data presented in the study are deposited in the European Nucleotide Archive (ENA) repository, accession number PRJEB44726.

AUTHOR CONTRIBUTIONS

RD and EE initiated the project. CG, KB, SB, RD, and DZ conducted the experiments and collected data. CG, KB, SB, DZ, LZ, and EE performed analyses. CG and DZ wrote the manuscript. All authors contributed to the article and approved the submitted version.

FUNDING

This research was supported by grants from the National Institutes of Health, R35 GM136322, to Nancy Kleckner, via a subcontract collaboration with DZ, the CNRS (UMR 9198, I2BC), and from the ANR (ANR-20-CE12-0006) to EE.

ACKNOWLEDGMENTS

We thank Nancy Kleckner for helpful discussions.

SUPPLEMENTARY MATERIAL

The Supplementary Material for this article can be found online at: https://www.frontiersin.org/articles/10.3389/fcell.2021.684108/full#supplementary-material

Supplementary Figure 1 | Dicer and Argonaute proteins: domains and expression. **(A)** Conserved domain positions across species in the two proteins. For Dicer, DEXDc, DEAD-like helicases superfamily; HeliCc, helicase superfamily c-terminal domain; Dimerization, Dicer dimerization domain; PAZ, named after the proteins Piwi Argonaute and Zwille; RNaseIII, Ribonuclease III family; dsRBD, double-stranded RNA binding motif. For Argonaute, PIWI, C-terminal portion which provides anchoring of the guide RNA and the catalytic site for slicing; Nter, N-terminal, which core fold closely resembles the catalytic domain of the replication-initiator protein Rep; Linker, Linker domain. **(B)** Time course expression of two meiotic genes (*SPO11* and *MER2*) compared with the *DICER* and *ARGONAUTE* genes during *Sordaria* vegetative et sexual cycles. At day 1, the mycelium has invaded the growing plate. At day 2 (graph) protoperithecia develop on the mycelium; day 3 and 4, perithecia contain mostly croziers and young asci (meiotic prophase); day 5 and 6, all perithecia contain asci at different steps of meiosis and post-meiotic mitosis; day 7 to 10, most asci contain mature ascospores. Fold changes and 95 % confidence interval (CI) are indicated. Fold changes are expressed relative to day 1. *SPO11* and *SMS2* at day 2, and all genes after day 2 have a fold change with a p-value < 0.05. Exact p-values and data necessary for the construction of the figure are shown in **Supplementary Table 2**.

Supplementary Figure 2 | Vegetative growth and ascus formation. **(A)** Representative picture of mycelial growth 5 days after inoculation (right) and

drawing of how measurements were made. **(B)** Growth curve of all mutants and double mutants analyzed in this study. Both growth rates and appearance of protophecia are synchronous in all mutants and are also identical to wild type. **(C)** Histograms of the percentage of perithecia with at least 1 ascus with spores in the simple *dcl1* and *dcl2* mutants and in all double mutants. The two other mutants *dcl2* and *qde2* were not included because they show the same percentage of asci with ascospores as wild type (see **Supplementary Figure 3A**). Numbers indicate the number of perithecia counted for each mutant.

Supplementary Figure 3 | Sporulation phenotypes of four single mutants and three double mutants six days after inoculation. **(A)** *dcl2* and *qde2* show a majority of eight-spored asci with either black mature ascospores or white/grey ascospores that are not yet mature. Note that only half of the asci of each perithecium are presented. **(B,C)** Perithecia of *dcl1* **(B)** and *sms2* **(C)** contain only few asci and even fewer asci with eight mature ascospores. The other asci either contain a mixture of mature and abnormal ascospores or abort before sporulation. **(D)** Examples of perithecia of three double mutants: *dcl1 qde2* (left), *sms2 dcl2* (middle) which contain only few asci with even fewer spored-asci and *qde2 dcl2* (right) with eight-spored asci like wild type.

Supplementary Figure 4 | CO and SC length correlation plus synapsis defects in mutants. **(A)** Linear regression analysis between the number of Hei10 foci per nucleus and the SC length in micron per nucleus in wild type, *dcl1*, *dcl2,* and *qde2*. For each nucleus the number of Hei10 foci is plotted against the total length of the SC. Both coefficient of determination (R^2) and the regression line are indicated in the graph. **(B)** Mer3-GFP foci in wild-type (left) and *dcl1* (right) leptotene nuclei. **(C)** Zygotene nuclei of *qde2* (left) and *dcl2* (middle) with largely open non-synapsed regions (arrows). Note that half of the green homolog in the *qde2* nucleus remains completely unsynapsed (green arrow). In contrast, at the same stage, as the *dcl2* nucleus, the unsynapsed homologous segments of the WT zygotene are much closer (red arrows in both nuclei). **(D)** Example of asynchronous SC formation in *dcl2*. All homologs are either completely synapsed or with only a short unsynapsed segment (yellow homolog) when the red homolog exhibits a large open segment without any sign of entanglement. Bars, 2 μ m.

Supplementary Figure 5 | Chromosome segregation defects in *sms2* and *dcl1* mutants. **(A–C)** *sms2* mutants. **(A)** Seven bivalents at diplotene. **(B)** Three lagging chromosomes are visible in this anaphase I spindle (red arrows). **(C)** Lagging chromosomes are also visible during anaphase of the second meiotic division (arrow). **(D,E)** *dcl1* mutant. **(D)** Irregular chromosome segregation during anaphase of the second meiotic division. In the left spindle, 4 or 5 chromosomes are at one pole and 9 at the other pole, when a 7/7 segregation is expected. Segregation is also defective in the right spindle (arrow). **(E)** Irregular segregation leads to pear-shaped telophase nuclei (arrow). Bars, 2 μ m.

REFERENCES

Alberti, C., and Cochella, L. (2017). A framework for understanding the roles of miRNAs in animal development. *Devlopment* 144, 2548–2559. doi: 10.1242/dev.146613

Alexander, W. G., Raju, N. B., Xiao, H., Hammond, T. M., Perdue, T. D., Metzenberg, R. L., et al. (2008). DCL-1 colocalizes with other components of the MSUD machinery and is required for silencing. *Fungal Genet. Biol.* 45, 719–727. doi: 10.1016/j.fgb.2007.10.006

Blank-Landeshammer, B., Teichert, I., Märker, R., Nowrousian, M., Kück, U., and Sickmann, A. (2019). Combination of Proteogenomics with peptide de novo sequencing identifies new genes and hidden posttranscriptional modifications. *MBio* 10:e02367–19. doi: 10.1128/mBio.02367-19

Burger, K., and Gullerova, M. (2015). Swiss army knives: non-canonical functions of nuclear drosha and dicer. *Nat. Rev. Mol. Cell Biol.* 16, 417–430. doi: 10.1038/nrm3994

Bustin, S. A., Benes, V., Garson, J. A., Hellemans, J., Huggett, J., Kubista, M., et al. (2009). The MIQE guidelines: minimum information for publication of quantitative real-time PCR experiments. *Clin. Chem.* 55, 611–622. doi: 10.1373/clinchem.2008.112797

Cerutti, H., and Casas-Mollano, J. A. (2006). On the origin and functions of RNA-mediated silencing: from protists to man. *Curr. Genet.* 50, 81–99. doi: 10.1007/s00294-006-0078-x

Claycomb, J. M., Batista, P. J., Pang, K. M., Gu, W., Vasale, J. J., van Wolfswinkel, J. C., et al. (2009). The argonaute CSR-1 and Its 22G-RNA cofactors are required for holocentric chromosome segregation. *Cell* 139, 123–134. doi: 10.1016/j.cell.2009.09.014

Colot, H. V., Park, G., Turner, G. E., Ringelberg, C., Crew, C. M., Litvinkova, L., et al. (2006). A high-throughput gene knockout procedure for Neurospora reveals functions for multiple transcription factors. *Proc. Natl. Acad. Sci. U.S.A.* 103, 10352–10357. doi: 10.1073/pnas.0601456103

D'Ario, M., Griffiths-Jones, S., and Kim, M. (2017). Small RNAs: big impact on plant development. *Trends Plant Sci.* 22, 1056–1068. doi: 10.1016/j.tplants.2017.09.009

De Muyt, A., Zhang, L., Piolot, T., Kleckner, N., Espagne, E., and Zickler, D. (2014). E3 ligase Hei10: a multifaceted structure-based signaling molecule with roles within and beyond meiosis. *Genes Dev.* 28, 1111–1123. doi: 10.1101/gad.240408.114

Deshpande, G., Calhoun, G., and Schedl, P. (2005). Drosophila argonaute-2 is required early in embryogenesis for the assembly of centric/centromeric heterochromatin, nuclear division, nuclear migration, and germ-cell formation. *Genes Dev.* 19, 1680–1685. doi: 10.1101/gad.1316805

Dubois, E., De Muyt, A., Soyer, J. L., Budin, K., Legras, M., Piolot, T., et al. (2019). Building bridges to move recombination complexes. *Proc. Natl. Acad. Sci. U. S. A.* 116, 12400–12409. doi: 10.1073/pnas.1901237116

Ellermeier, C., Higuchi, E. C., Phadnis, N., Holm, L., Geelhood, J. L., Thon, G., et al. (2010). RNAi and heterochromatin repress centromeric meiotic recombination. *Proc. Natl. Acad. Sci. U.S.A.* 107, 8701–8705. doi: 10.1073/pnas.0914160107

Espagne, E., Vasnier, C., Storlazzi, A., Kleckner, N., Silar, P., Zickler, D., et al. (2011). Sme4 coiled-coil protein mediates synaptonemal complex assembly, recombinosome relocalization, and spindle pole body morphogenesis. *Proc. Natl. Acad. Sci. U.S.A.* 108, 10614–10619. doi: 10.1073/pnas.1107272108

Fulci, V., and Macino, G. (2007). Quelling: post-transcriptional gene silencing guided by small RNAs in Neurospora crassa. *Curr. Opin. Microbiol.* 10, 199–203. doi: 10.1016/j.mib.2007.03.016

Goto, D. B., and Nakayama, J. I. (2012). RNA and epigenetic silencing: Insight from fission yeast. *Dev. Growth Differ.* 54, 129–141. doi: 10.1111/j.1440-169X.2011.01310.x

Gutbrod, M. J., and Martienssen, R. A. (2020). Conserved chromosomal functions of RNA interference. *Nat. Rev. Genet.* 21, 311–331. doi: 10.1038/s41576-019-0203-6

Hall, I. M., Noma, K. I, and Grewal, S. I. S. (2003). RNA interference machinery regulates chromosome dynamics during mitosis and meiosis in fission yeast. *Proc. Natl. Acad. Sci. U.S.A* 100, 193–198. doi: 10.1073/pnas.232688099

Hammond, T. M. (2017). *Sixteen Years of Meiotic Silencing by Unpaired DNA*. Amsterdam: Elsevier Ltd, doi: 10.1016/bs.adgen.2016.11.001

Harfe, B. D., McManus, M. T., Mansfield, J. H., Hornstein, E., and Tabin, C. J. (2005). The RNaseIII enzyme Dicer is required for morphogenesis but not patterning of the vertebrate limb. *Proc. Natl. Acad. Sci. U.S.A.* 102, 10898–10903. doi: 10.1073/pnas.0504834102

Hellemans, J., Mortier, G., De Paepe, A., Speleman, F., and Vandesompele, J. (2008). qBase relative quantification framework and software for management and automated analysis of real-time quantitative PCR data. *Genome Biol.* 8:R19. doi: 10.1186/gb-2007-8-2-r19

Hellemans, J., and Vandesompele, J. (2014). "Selection of reliable reference genes for RT-qPCR analysis," in *Quantitative Real-Time PCR. Methods in Molecular Biology (Methods and Protocols)*, Vol. 1160, eds R. Biassoni and A. Raso (New York, NY: Humana Press), 19–26. doi: 10.1007/978-1-4939-0733-5_3

Huang, C., Wang, X., Liu, X., Cao, S., and Shan, G. (2015). RNAi pathway participates in chromosome segregation in mammalian cells. *Cell Discov.* 1, 11–13. doi: 10.1038/celldisc.2015.29

Hunter, N. (2015). Meiotic recombination: the essence of heredity. *Cold Spring Harb. Perspect. Biol.* 14, 2015–2064. doi: 10.1210/en.2015-2064

Kelley, L. A., Mezulis, S., Yates, C. M., Wass, M. N., and Sternberg, M. J. E. (2015). The Phyre2 web portal for protein modeling, prediction and analysis. *Nat. Protoc.* 10, 845–858. doi: 10.1038/nprot.2015.053

Lam, I., and Keeney, S. (2015). Mechanism and regulation of meiotic recombination initiation. *Cold Spring Harb. Perspect. Biol.* 7:a016634. doi: 10.1101/cshperspect.a016634

Lee, H.-C., Chang, S.-S., Choudhary, S., Aalto, A. P., Maiti, M., Bamford, D. H., et al. (2009). qiRNA is a new type of small interfering RNA induced by DNA damage. *Nature* 459, 274–277. doi: 10.1038/nature08041

Malone, C. D., and Hannon, G. J. (2009). Small RNAs as guardians of the genome. *Cell* 136, 656–668. doi: 10.1016/j.cell.2009.01.045

Modzelewski, A. J., Hilz, S., Crate, E. A., Schweidenback, C. T. H., Fogarty, E. A., Grenier, J. K., et al. (2015). Dgcr8 and Dicer are essential for sex chromosome integrity during meiosis in males. *J. Cell Sci.* 128, 2314–2327. doi: 10.1242/jcs.167148

Muller, H. J. (1916). The mechanism of crossing-over. II. IV. The manner of occurrence of crossing-over. *Am. Nat.* 50:284. doi: 10.1086/279541

Murdoch, B., Owen, N., Stevense, M., Smith, H., Nagaoka, S., Hassold, T., et al. (2013). Altered cohesin gene dosage affects mammalian meiotic chromosome structure and behavior. *PLoS Genet.* 9:e1003241. doi: 10.1371/journal.pgen.1003241

Nonomura, K. I., Morohoshi, A., Nakano, M., Eiguchi, M., Miyao, A., Hirochika, H., et al. (2007). A germ cell-specific gene of the ARGONAUTE family is essential for the progression of premeiotic mitosis and meiosis during sporogenesis in rice. *Plant Cell* 19, 2583–2594. doi: 10.1105/tpc.107.053199

Nowrousian, M., Würtz, C., Pöggeler, S., and Kück, U. (2004). Comparative sequence analysis of Sordaria macrospora and Neurospora crassa as a means to improve genome annotation. *Fungal Genet. Biol.* 41, 285–292. doi: 10.1016/j.fgb.2003.10.005

Oliver, C., Pradillo, M., Jover-Gil, S., Cuñado, N., Ponce, M. R., and Santos, J. L. (2017). Loss of function of *Arabidopsis* microRNA-machinery genes impairs fertility, and has effects on homologous recombination and meiotic chromatin dynamics. *Sci. Rep.* 7, 1–14. doi: 10.1038/s41598-017-07702-x

Pek, J. W., and Kai, T. (2011). DEAD-box RNA helicase Belle/DDX3 and the RNA interference pathway promote mitotic chromosome segregation. *Proc. Natl. Acad. Sci. U.S.A.* 108, 12007–12012. doi: 10.1073/pnas.1106245108

Pfaffl, M. W., Horgan, G. W., and Dempfle, L. (2002). Relative expression software tool (REST(C)) for group-wise comparison and statistical analysis of relative expression results in real-time PCR. *Nucleic Acids Res.* 30:e36. doi: 10.1093/nar/30.9.e36

Pong, S. K., and Gullerova, M. (2018). Noncanonical functions of microRNA pathway enzymes – Drosha, DGCR8, Dicer and Ago proteins. *FEBS Lett.* 592, 2973–2986. doi: 10.1002/1873-3468.13196

Provost, P., Silverstein, R. A., Dishart, D., Walfridsson, J., Djupedal, I., Kniola, B., et al. (2002). Dicer is required for chromosome segregation and gene silencing in fission yeast cells. *Proc. Natl. Acad. Sci. U. S. A.* 99, 16648–16653. doi: 10.1073/pnas.212633199

Romano, N., and Macino, G. (1992). Quelling: transient inactivation of gene expression in Neurospora crassa by transformation with homologous sequences. *Mol. Microbiol.* 6, 3343–3353. doi: 10.1111/j.1365-2958.1992.tb02202.x

Shiu, P. K. T., Raju, N. B., Zickler, D., and Metzenberg, R. L. (2001). Meiotic silencing by unpaired DNA. *Cell* 107, 905–916.

Singh, M., Goel, S., Meeley, R. B., Dantec, C., Parrinello, H., Michaud, C., et al. (2011). Production of viable gametes without meiosis in maize deficient for an ARGONAUTE protein. *Plant Cell* 23, 443–458. doi: 10.1105/tpc.110.079020

Son, H., Park, A. R., Lim, J. Y., Shin, C., and Lee, Y. W. (2017). Genome-wide exonic small interference RNA-mediated gene silencing regulates sexual reproduction in the homothallic fungus Fusarium graminearum. *PLoS Genet.* 13:e1006595. doi: 10.1371/journal.pgen.1006595

Song, M., Zhai, B., Yang, X., Tan, T., Wang, Y., Yang, X., et al. (2021). Interplay between Pds5 and Rec8 in regulating chromosome axis length and crossover frequency. *Sci. Adv.* 7:eabe7920. doi: 10.1126/sciadv.abe7920

Storlazzi, A., Gargano, S., Ruprich-Robert, G., Falque, M., David, M., Kleckner, N., et al. (2010). Recombination proteins mediate meiotic spatial chromosome organization and pairing. *Cell* 141, 94–106. doi: 10.1016/j.cell.2010.02.041

Storlazzi, A., Tessé, S., Gargano, S., James, F., Kleckner, N., and Zickler, D. (2003). Meiotic double-strand breaks at the interface of chromosome movement, chromosome remodeling, and reductional division. *Genes Dev.* 17, 2675–2687. doi: 10.1101/gad.275203

Tessé, S., Bourbon, H., Debuchy, R., Budin, K., Dubois, E., Liangran, Z., et al. (2017). Asy2/Mer2: an evolutionarily conserved mediator of meiotic recombination, pairing, and global chromosome compaction. *Genes Dev.* 31, 1880–1893. doi: 10.1101/gad.304543.117

Underwood, C. J., Choi, K., Lambing, C., Zhao, X., Serra, H., Borges, F., et al. (2018). Epigenetic activation of meiotic recombination near Arabidopsis thaliana centromeres via loss of H3K9me2 and non-CG DNA methylation. *Genome Res.* 28, 519–531. doi: 10.1101/gr.227116.117

Van Heemst, D., James, F., Pöggeler, S., Berteaux-Lecellier, V., and Zickler, D. (1999). Spo76p is a conserved chromosome morphogenesis protein that links the mitotic and meiotic programs. *Cell* 98, 261–271. doi: 10.1016/S0092-8674(00)81020-X

Vandesompele, J., De Preter, K., Pattyn, F., Poppe, B., Van Roy, N., De Paepe, A., et al. (2002). Accurate normalization of real-time quantitative RT-PCR data by geometric averaging of multiple internal control genes. *Genome Biol.* 51, 2747–2759. doi: 10.1186/gb-2002-3-7-research0034

Vasnier, C., De Muyt, A., Zhang, L., Tessé, S., Kleckner, N., Zickler, D., et al. (2014). Absence of SUN-domain protein Slp1 blocks karyogamy and switches meiotic recombination and synapsis from homologs to sister chromatids. *Proc. Natl. Acad. Sci. U.S.A.* 111, E4015–E4023. doi: 10.1073/pnas.1415758111

Viera, A., Berenguer, I., Ruiz-Torres, M., Gómez, R., Guajardo, A., Barbero, J. L., et al. (2020). PDS 5 proteins regulate the length of axial elements and telomere integrity during male mouse meiosis. *EMBO Rep.* 21, 1–20. doi: 10.15252/embr.201949273

Volpe, T. A., Kidner, C., Hall, I. M., Teng, G., Grewal, S. I. S., and Martienssen, R. A. (2002). Regulation of heterochromatic silencing and histone H3 lysine-9 methylation by RNAi. *Science* 297, 1833–1837. doi: 10.1126/science.1074973

Wang, S., Veller, C., Sun, F., Ruiz-Herrera, A., Shang, Y., Liu, H., et al. (2019). Per-nucleus crossover covariation and implications for evolution. *Cell* 177, 326–338.e16. doi: 10.1016/j.cell.2019.02.021

Wang, S., Zickler, D., Kleckner, N., and Zhang, L. (2015). Meiotic crossover patterns: Obligatory crossover, interference and homeostasis in a single process. *Cell Cycle* 14, 305–314. doi: 10.4161/15384101.2014.991185

Wei, Y., Yu, L., Bowen, J., Gorovsky, M. A., and David Allis, C. (1999). Phosphorylation of histone H3 is required for proper chromosome condensation and segregation. *Cell* 97, 99–109. doi: 10.1016/S0092-8674(00)80718-7

Xu, H., Beasley, M. D., Warren, W. D., van der Horst, G. T. J., and McKay, M. J. (2005). Absence of mouse REC8 cohesin promotes synapsis of sister chromatids in meiosis. *Dev. Cell* 8, 949–961. doi: 10.1016/j.devcel.2005.03.018

Zeng, W., Wang, J., Wang, Y., Lin, J., Fu, Y., Xie, J., et al. (2018). Dicer-like proteins regulate sexual development via the biogenesis of perithecium-specific microRNAs in a plant pathogenic fungus *Fusarium graminearum*. *Front. Microbiol.* 9:818. doi: 10.3389/fmicb.2018.00818

Zhang, K., Mosch, K., Fischle, W., and Grewal, S. I. S. (2008). Roles of the Clr4 methyltransferase complex in nucleation, spreading and maintenance of heterochromatin. *Nat. Struct. Mol. Biol.* 15, 381–388. doi: 10.1038/nsmb.1406

Zhang, L., Liang, Z., Hutchinson, J., and Kleckner, N. (2014a). Crossover patterning by the beam-film model: analysis and implications. *PLoS Genet.* 10:e1004042. doi: 10.1371/journal.pgen.1004042

Zhang, L., Wang, S., Yin, S., Hong, S., Kim, K. P., and Kleckner, N. (2014b). Topoisomerase II mediates meiotic crossover interference. *Nature* 511, 551–556. doi: 10.1038/nature13442

Zickler, D., and Espagne, E. (2016). Sordaria, a model system to uncover links between meiotic pairing and recombination. *Semin. Cell Dev. Biol.* 54, 149–157. doi: 10.1016/j.semcdb.2016.02.012

Zickler, D., and Kleckner, N. (2015). Recombination, pairing, and synapsis of homologs during meiosis. *Cold Spring Harb. Perspect. Biol.* 7:a016626. doi: 10.1101/cshperspect.a016626

Conflict of Interest: The authors declare that the research was conducted in the absence of any commercial or financial relationships that could be construed as a potential conflict of interest.

Copyright © 2021 Girard, Budin, Boisnard, Zhang, Debuchy, Zickler and Espagne. This is an open-access article distributed under the terms of the Creative Commons Attribution License (CC BY). The use, distribution or reproduction in other forums is permitted, provided the original author(s) and the copyright owner(s) are credited and that the original publication in this journal is cited, in accordance with accepted academic practice. No use, distribution or reproduction is permitted which does not comply with these terms.

frontiers in Cell and Developmental Biology

MINI REVIEW
published: 14 July 2021
doi: 10.3389/fcell.2021.681188

Knockout Gene-Based Evidence for PIWI-Interacting RNA Pathway in Mammals

Yinuo Li[1†], Yue Zhang[2†] and Mingxi Liu[1]*

[1] State Key Laboratory of Reproductive Medicine, Department of Histology and Embryology, School of Basic Medical Sciences, Nanjing Medical University, Nanjing, China, [2] State Key Laboratory of Reproductive Medicine, Clinical Center of Reproductive Medicine, The First Affiliated Hospital of Nanjing Medical University, Nanjing, China

The PIWI-interacting RNA (piRNA) pathway mainly consists of evolutionarily conserved protein factors. Intriguingly, many mutations of piRNA pathway factors lead to meiotic arrest during spermatogenesis. The majority of piRNA factor-knockout animals show arrested meiosis in spermatogenesis, and only a few show post-meiosis male germ cell arrest. It is still unclear whether the majority of piRNA factors expressed in spermatids are involved in long interspersed nuclear element-1 repression after meiosis, but future conditional knockout research is expected to resolve this. In addition, recent hamster knockout studies showed that a piRNA factor is necessary for oocytes—in complete contrast to the findings in mice. This species discrepancy allows researchers to reexamine the function of piRNA in female germ cells. This mini-review focuses on the current knowledge of protein factors derived from mammalian knockout studies and summarizes their roles in the biogenesis and function of piRNAs.

Keywords: piRNA, meiosis, male infertility, RBPs, RNA binding proteins

OPEN ACCESS

Edited by:
Akira Shinohara,
Osaka University, Japan

Reviewed by:
Yuka W. Iwasaki,
Keio University, Japan
Satomi Kuramochi-Miyagawa,
Osaka University, Japan

****Correspondence:***
Mingxi Liu
mingxi.liu@njmu.edu.cn

† These authors have contributed equally to this work

Specialty section:
This article was submitted to Cell Growth and Division, a section of the journal Frontiers in Cell and Developmental Biology

Received: *16 March 2021*
Accepted: *08 June 2021*
Published: *14 July 2021*

Citation:
Li Y, Zhang Y and Liu M (2021) Knockout Gene-Based Evidence for PIWI-Interacting RNA Pathway in Mammals. Front. Cell Dev. Biol. 9:681188. doi: 10.3389/fcell.2021.681188

INTRODUCTION

PIWI-interacting RNAs (piRNAs) are a distinct class of small RNAs [generally 24–31 nucleotides (nt) long] that are highly expressed in mouse testes. They are loaded onto PIWI proteins and function as an endogenous defense system against transposable elements (Aravin et al., 2004, 2006, 2007; Grivna et al., 2006; Kuramochi-Miyagawa et al., 2008). Some piRNAs are also involved in messenger RNA (mRNA) translation and mRNA/lncRNA elimination (Gou et al., 2014; Watanabe et al., 2015; Dai et al., 2019, 2020). Mice produce three types of germline piRNAs during spermatogenesis. Prenatal piRNAs first appear in the fetal testis and initiate transposon silencing *via* DNA methylation (Aravin et al., 2007, 2008; Carmell et al., 2007; Kuramochi-Miyagawa et al., 2008). The biogenesis of piRNAs in postnatal male germ cells is strikingly different from that in embryonic cells, as the majority of piRNAs are produced only by primary biogenesis after birth (Vourekas et al., 2012; Li et al., 2013). Postnatal piRNAs can be divided into pre-pachytene and pachytene piRNAs based on the timing of their expression and corresponding locus in the genome (Li et al., 2013). Because prenatal piRNA production and neonatal piRNA production involve continuous processes, they are rarely distinguishable during research. In most of the literature, prenatal piRNAs are classified as pre-pachytene piRNAs. Pachytene piRNAs are generally loaded onto MIWI (PIWIL1) or MILI (PIWIL2) (Vourekas et al., 2012; Li et al., 2013) and, unlike

embryonic piRNAs, they have a strong 1U but no 10A bias, reflecting their primary biogenesis-dependent function (Vourekas et al., 2012; Li et al., 2013). These piRNA pathways are required during multiple stages of male germ cell development, including *de novo* DNA methylation, meiosis, and spermiogenesis (Kuramochi-Miyagawa et al., 2004; Carmell et al., 2007; Chuma and Nakano, 2013; Fu and Wang, 2014). In a review of piRNA pathway-knockout mice, meiosis arrest is described as the most common mouse phenotype and is mainly caused by abnormal piRNA production or retrotransposon DNA methylation in fetal testis (Yang and Wang, 2016).

Substantial past efforts have led to an understanding of piRNA biogenesis, which is thought to occur through either the primary or the secondary pathway. Primary piRNA biogenesis is coupled with a secondary piRNA amplification loop, the ping-pong cycle, in which piRNA pools, generated through primary processing, guide the MILI protein to slice transposon transcripts, providing substrates for piRNA generation and leading to the accelerated amplification of transposon-derived piRNAs (Brennecke et al., 2007; Gunawardane et al., 2007; Aravin et al., 2008). Primary piRNA biogenesis is initiated by the transcription of primary piRNA precursors derived from genomic regions called piRNA clusters—genomic regions mapped with a high density of piRNA sequences (Girard et al., 2006; Brennecke et al., 2007; Malone et al., 2009).

De novo DNA methylation occurs in prospermatogonia/gonocytes. During reprogramming, all DNA methylation marks are erased before being reset in germ cells, exposing the germline to essential challenge (Schaefer et al., 2007; Trasler, 2009). Loss of DNA methylation results in the activation of normally silenced transposable elements. Correct DNA methylation of transposons is vital for successful meiosis in male germ cells. Transposon demethylation was repeatedly observed in the testes of piRNA pathway mutants (**Table 1**), thus the pathway has been proposed to play a role in the *de novo* methylation of retrotransposons (Aravin et al., 2007; Carmell et al., 2007; Kuramochi-Miyagawa et al., 2008).

PIWI-interacting RNA pathway consists of many evolutionarily conserved protein factors. This mini-review focuses on our current knowledge of protein factors in mammals by summarizing their roles in the biogenesis and function of piRNAs based on research with gene-knockout models.

PRIMARY piRNA BIOGENESIS

Primary piRNA biogenesis is a stepwise process that starts with the transcription of long single-stranded precursor transcripts. A-MYB, which is the only transcription factor known to be involved in transcriptional regulation of pachytene piRNA precursor, also regulates the transcription of many pachytene piRNA pathway genes (Li et al., 2013). Through its ATP-dependent RNA helicase activity, MOV10L1 selectively binds to piRNA precursor transcripts and feeds them to MitoPLD, which catalyzes the first cleavage step of piRNA processing to generate piRNA intermediates. MOV10L1 is associated with MILI, MIWI, and MIWI2 (PIWIL4) in mouse testes; its expression emerges in prenatal gonocytes, peaks in pachytene spermatocytes, and ceases in post-meiotic spermatids. Disruption of *Mov10l1* results in defects in both the transcriptional and posttranscriptional de-repression of transposons, consistent with the lack of retrotransposon-derived pre-pachytene piRNAs in *Mov10l1* mutant testis (Zheng et al., 2010). Primary spermatocytes of *Mov10l1*$^{-/-}$ mice show the activation of long terminal repeat-containing retrotransposons and long interspersed nuclear element-1 (LINE1) retrotransposons, followed by cell death, causing infertility in males and the complete blockage of spermatogenesis at the zygotene stage of meiosis I prophase (Frost et al., 2010; Zheng et al., 2010; Vourekas et al., 2015).

MitoPLD is localized on the surface of the mitochondrial outer membrane in mouse germlines (Choi et al., 2006; Watanabe et al., 2011) and is a candidate for the nuclease that generates piRNA intermediates. In MitoPLD-mutant mouse testes, both primary and secondary piRNAs were significantly decreased, and piRNA biogenesis disruption was accompanied by a spike in LINE1 retrotransposon expression and genomic demethylation. MitoPLD-knockout mice showed arrested spermatogenesis at the meiosis zygotene stage (Huang et al., 2011; Watanabe et al., 2011), and MitoPLD has endoribonuclease activity on single-stranded RNAs *in vitro* (Ipsaro et al., 2012). A recent *Bombyx mori* study found that Zucchini (homolog of MitoPLD) requires Armi, GPAT1, and Gasz to cleave Siwi-loaded pre-pre-piRNAs *in vitro* (Izumi et al., 2020). In addition, the N6-methyadenosine (m6A) reader, YTHDC2, binds to specific piRNA precursors. P12 *Ythdc2*$^{-/-}$ mice exhibited much lower pachytene piRNA precursor levels than normal (Bailey et al., 2017).

MILI is one of three mouse homologs of the PIWI family that are defined by their conserved PAZ and Piwi domains. MILI, an important mediator of sense piRNA processing from retrotransposons and other cellular transcripts (Kuramochi-Miyagawa et al., 2004; Aravin et al., 2008), is expressed in the cytoplasm of testicular germline stem cells, spermatogonia, and early spermatocytes. In a mouse MILI-null mutant, spermatogenesis was completely blocked at the prophase of meiosis I from the zygotene to early pachytene (Kuramochi-Miyagawa et al., 2004). Acting as a piRNA-guided endonuclease, MILI initiates secondary piRNA biogenesis, which is vital for LINE1 and Intracisternal A particle (IAP) silencing (Aravin et al., 2007; De Fazio et al., 2011). Functions of MILI beyond piRNA biogenesis have been described recently. MILI forms a stable and RNA-independent complex with eIF3a and is associated with the eIF4E- and eIF4G-containing 5′-end 7-methylguanosine (m7G) cap-binding complex, which may positively regulate the translation of genes essential for germline stem cell self-renewal and differentiation (Unhavaithaya et al., 2009).

TDRKH, another mitochondria-anchored protein involved in primary piRNA biogenesis (Saxe et al., 2013), is a Tudor family protein that contains evolutionarily conserved Tudor and KH domains (Zhang et al., 2017a); it controls the entire MIWI/MIWI2-bound piRNA population and enables the trimming of MILI-bound piRNAs. *Tdrkh* mutants display

TABLE 1 | Components of piRNA pathway in mice.

Mus musculus	*Mesocricetus auratus*	*Homo sapiens*	*Drosophila melano gaster*	Spermatogenic arrest in KO mice	Expression pattern in male mice	Localization in male germ cell	Pre-pachytene piRNAs	Pachytene piRNAs	Transposon de-repression	References
Piwil2 (Mili)	*Piwil2*	*PIWIL2*	*Aub*	Zygotene	E12.5 prosper matogonia to round spermatids	Cytoplasmic granules	√	√	LINE1 and IAP	Aravin et al., 2007; Aravin et al., 2008; De Fazio et al., 2011; Di Giacomo et al., 2013
Mov10l1	*Mov10l1*	*MOV10L1*	*Armi*	Zygotene	Gonocytes/type A spermatogonia to pachytene spermatocytes	Cytoplasmic granules	√	√	LINE1 and IAP	Frost et al., 2010; Vourekas et al., 2015; Zheng et al., 2010
Pld6 (Mitopld)	*Pld6*	*PLD6*	*Zuc*	Zygotene	E16.5 to the adult stage	N/A	√	N/A	LINE1	Huang et al., 2011; Ipsaro et al., 2012; Izumi et al., 2020; Nishimasu et al., 2012; Watanabe et al., 2011
Tdrkh (Tdrd2)	*Tdrkh*	*TDRKH*	*Papi*	Zygotene	Spermatogonia, spermatocytes, and round spermatids	Cytoplasmic granules	√	√	LINE1	Chen et al., 2009; Ding et al., 2019; Saxe et al., 2013
Pnldc1	*Pnldc1*	*PNLDC1*	—	Pachytene/ spermatids	Spermatogonial stem cells to round sper matids in post natal testis; unknown in prenatal testis	N/A	√	√	LINE1	Bronkhorst and Ketting, 2018; Ding et al., 2017; Nishimura et al., 2018; Zhang et al., 2017b
Tdrd1	*Tdrd1*	*TDRD1*	—	Pachytene	Fetal prosper matogonia, postnatal spermatocytes and round spermatids	Cytoplasmic granules	N/A	√	LINE1	Chuma et al., 2003; Chuma et al., 2006; Reuter et al., 2009
Asz1 (Gasz)	*Asz1*	*ASZ1*	*Gasz*	Zygotene	Spermatogonia, spermatocytes, round spermatids	Cytoplasmic granules	√	√	LINE1	Ma et al., 2009; Zhang et al., 2016
Mybl1 (A-myb)	*Mybl1*	*MYBL1*	—	Pachytene	Mid-pachytene to round spermatids	Nuclei	N/A	√	N/A	Horvath et al., 2009; Li et al., 2013; Toscani et al., 1997
Ddx4 (Mvh)	*Ddx4*	*DDX4*	*vasa*	Zygotene	Male germ cells from E10.5 to round spermatids	Cytoplasmic granules	N/A	√	LINE1 and IAP	Kotaja and Sassone-Corsi, 2007; Kuramochi-Miyagawa et al., 2010; Noce et al., 2001; Saga, 2008; Siomi and Kuramochi-Miyagawa, 2009; Tanaka et al., 2000; Toyooka et al., 2000; Wenda et al., 2017
Tdrd9	*Tdrd9*	*TDRD9*	*Spn-E*	Zygotene	E13.5 prosper matogonia to round spermatids	Nucleus and cytoplasmic granules	N/A	N/A	LINE1	Shoji et al., 2009; Wenda et al., 2017
Tdrd12	*Tdrd12*	*TDRD12*	*BoYb*	Zygotene	From embryonic to the adult stages in mouse testes	N/A	√	N/A	LINE1 and IAP	Handler et al., 2011; Pandey et al., 2013; Yang et al., 2016
Mael	*Mael*	*MAEL*	*mael*	Pachytene	Spermatocytes and round and early elongating spermatids	XY body of spermatocytes and cytoplasmic granules of spermatids	N/A	√	LINE1 and IAP	Castañeda et al., 2014; Costa et al., 2006; Sato and Siomi, 2015

(Continued)

TABLE 1 | Continued

Mus musculus	*Mesocricetus auratus*	*Homo sapiens*	*Drosophila melano gaster*	Spermatogenic arrest in KO mice	Expression pattern in male mice	Localization in male germ cell	Pre-pachytene piRNAs	Pachytene piRNAs	Transposon de-repression	References
Fkbp6	*Fkbp6*	*FKBP6*	*Shu*	Pachytene	E12.5 prosper matogonia, cytoplasm and nucleus of spermatocytes	Cytosolic and not enriched in pi-bodies	√	N/A	LINE1	Crackower et al., 2003; Xiol et al., 2012
Hsp90aa1	*Hsp90aa1*	*HSP90aa1*	*Hsp83*	Meiotic arrest	E16.5 prosper matogonia to the adult stage	Cytosolic	√	N/A	LINE1	Grad et al., 2010; Ichiyanagi et al., 2014
Gtsf1	*Gtsf1*	*GTSF1*	*Gtsf1*	Meiotic arrest	E12.5 prosper matogonia to round spermatids	Cytoplasmic granules	√	N/A	LINE1 and IAP	Dönertas et al., 2013; Ohtani et al., 2013; Yoshimura et al., 2009; Yoshimura et al., 2018
Spocd1	*Spocd1*	*SPOCD1*	*pps*	Pachytene	E14.5 to PN1 prosper matogonia	Nucleus and cytoplasmic granules	×	N/A	LINE1 and IAP	Zoch et al., 2020
Tex15	*Tex15*	*TEX15*	—	Zygotene	Transcript abundance was high at E16.5 and increased at PN2.5	N/A	×	N/A	LINE1 and IAP	Schöpp et al., 2020; Yang et al., 2008; Yang et al., 2020
Uhrf1	*Uhrf1*	*UHRF1*	—	Pachytene	E15.5 prosper matogonia to round spermatids	Nuclei of neonatal prospermatonia at PN0, spermatogonia, late pachytene spermatocytes, and early round spermatids; cytoplasm of fetal prosper matogonia at E15.5, pre-leptotene, leptotene, zygotene, and early pachytene spermatocytes	N/A	√	LINE1	Dong et al., 2019
Tut4/7	*Tut4/7*	*TUT4/7*	—	Pachytene	Spermatogonia to round spermatids	Cytoplasmic granules	N/A	√	LINE1	Morgan et al., 2019
Piwil1 (Miwi)	*Piwil1*	*PIWIL1*	*Aub*	Round spermatid	Pachytene spermatocytes to elongating spermatids	Cytoplasmic granules	×	√	LINE1	Carrieri et al., 2017; Dai et al., 2019; Dai et al., 2020; Deng and Lin, 2002; Gou et al., 2014; Gou et al., 2017; Li et al., 2020; Oud et al., 2021; Reuter et al., 2011; Zhao et al., 2013
Tdrd5	*Tdrd5*	*TDRD5*	*qin*	Round spermatid/ meiotic prophase	E7.25 PGCs to round-spermatid stage	Spots in the nucleus and cytoplasmic granules	N/A	√	LINE1	Ding et al., 2018; Smith et al., 2004; Yabuta et al., 2011
Henmt1	*Henmt1*	*HENMT1*	*Hen1*	Spermatids	Spermatogonia to elongated spermatids	Cytoplasmic granules	√	√	LINE1 and IAP	Kirino and Mourelatos, 2007; Lim et al., 2015
Ythdc2	*Ythdc2*	*YTHDC2*	*Bgcn*	Zygotene	YTHDC2 expression during the first wave of spermatogenesis.	Cytoplasmic granules	N/A	√	N/A	Bailey et al., 2017
Piwil4 (Miwi2)	*Piwil4*	*PIWIL4*	*Piwi*	Zygotene	E15.5 to PN1 prosper matogonia	Nucleus and cytoplasmic granules	N/A	N/A	LINE1 and IAP	Carmell et al., 2007; Carrieri et al., 2017; Zoch et al., 2020

meiotic arrest at the zygotene stage, with loss of DNA methylation of LINE1 retrotransposons and consequential retrotransposon de-repression (Saxe et al., 2013; Ding et al., 2019). Associated with MIWI and MIWI2 *via* the binding of symmetrically dimethylated arginine (sDMA), TDRKH is the scaffold for interactions between PIWI–piRNA complexes and PNLDC1. The exonuclease trims the 3′-end of piRNA intermediates to their mature length (Ding et al., 2017; Zhang et al., 2017b; Bronkhorst and Ketting, 2018; Nishimura et al., 2018). The 3′-end of mature piRNA is 2′-*O*-methylated by HENMT1, yet correct 3′ truncation is not necessary for 3′-end 2′-*O*-methylation (Yang et al., 2006; Zhai and Meyers, 2012; Peng et al., 2018). In addition, TUT4/7 mediates the 3′ uridylation of 30- to 31-nt-long piRNAs, but its effect is unknown (Morgan et al., 2019).

SECONDARY piRNA BIOGENESIS

The piRNA pathway mediation of transposon posttranscriptional silencing is regulated by interactions between two RNA–protein complexes: pi-body and piP-body. While MILI–piRNA and MIWI2–piRNA complexes are key to the assembly and function of pi-body and piP-body, several other factors are also believed to be required. The existing evidence for the possible interactions and localizations of those factors is summarized in this review (**Figure 1**). Another member of the Piwi protein family, MIWI2, is coexpressed with MILI during embryonic testis development. Once loaded with secondary piRNAs, MIWI2 is shuttled from the cytoplasm to the nucleus to mediate repressive chromatin remodeling mainly *via* the promoter regions of transposons. However, it remains unclear whether MIWI2–piRNA complexes regulate the methylation patterns of other genomic regions (Schöpp et al., 2020). Loss of MIWI2 function affects the DNA methylation of LINE1 elements. Miwi2-deficient mice displayed zygotene-stage meiotic arrest, defective synapsis and double-strand break repair, and progressive loss of germ cells with age (Carmell et al., 2007).

TDRD9, a TDRD family member, was also investigated as an essential partner of MIWI2. TDRD9 complexes with MIWI2 through its Tudor domain, which binds to sDMA sites of MIWI2. TDRD9 is expressed in the cytoplasm and nucleus of embryonic prospermatogonia, mitotic spermatogonia, meiotic spermatocytes, and haploid spermatids in the testis (Shoji et al., 2009). Abolishing TDRD9 expression caused male mouse sterility and meiotic arrest at the zygotene stage: the spermatogenic cells faithfully initiated meiotic DNA recombination, but homologous chromosomes failed to undergo synapsis (Shoji et al., 2009). TDRD9 participates in the biogenesis of secondary piRNAs by ensuring the proper selection of *Line1* sequences for the ping-pong amplification loop (Shoji et al., 2009). Although dispensable for piRNA biogenesis, TDRD9 ATPase activity is indispensable for its nuclear localization and transcriptional silencing of transposable elements (Wenda et al., 2017).

Other TDRD family members, including TDRD1 and TDRD12, interact with MILI in the ping-pong cycle. TDRD1 recognizes arginine dimethylation in MILI (Chuma et al., 2003, 2006) and may regulate the entry of transcripts into piRNA biogenesis pathways. The loss of TDRD1 does not affect the abundance of MILI-bond piRNA but rather its constituents: ribosomal RNA- and genic-derived piRNA proportions increase, and transposon-derived piRNAs in MILI ribonucleoprotein (RNP) populations change substantially. In addition, the correct nuclear localization of Miwi2 needed for LINE1 transposon methylation was almost lost, and LINE1 transposons were repressed as consequences of TDRD1 knockout (Reuter et al., 2009). TDRD1 also draws

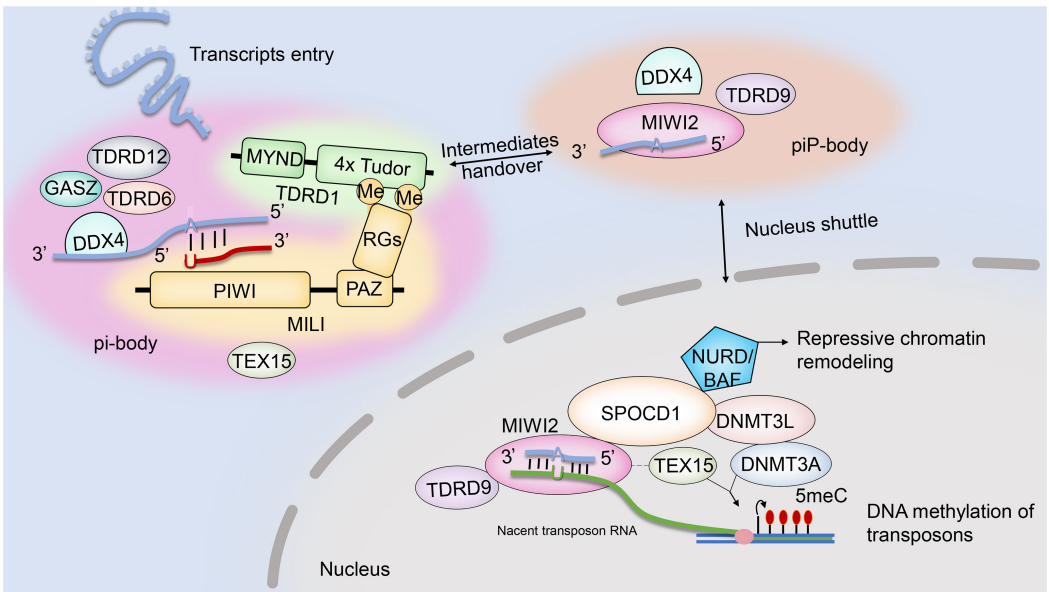

FIGURE 1 | Ping-pong cycle and MIWI2-piRNA-guided chromatin remodeling.

ping-pong cycle factors together to promote their activity. DDX4 and FKBP6, components of the TDRD1 protein complex, are required for the loading of MIWI2-bound secondary piRNAs. FKBP6 may recruit HSP90AA1 for the loading of secondary piRNA intermediates onto MIWI2 (Xiol et al., 2012).

TDRD12 forms complexes with MILI piRNP in an RNA-dependent manner and is associated with TDRD1. TDRD12 might facilitate the RNP remodeling required for the inter-Piwi (MILI and MIWI2) exchange of piRNA intermediates essential for the biogenesis of MIWI2 piRNAs (Pandey et al., 2013). The biogenesis of piRNAs that associate with MILI appeared normal, with unchanged genome annotation profiles, in mice lacking TDRD12; however, MIWI2-bond piRNA biogenesis was almost absent. When TDRD12 was deficient, spermatogenesis stalled in the zygotene–pachytene transition stage of meiosis.

DDX4, which is expressed in the cytoplasm of various male germ cells (E10.5 to round spermatids) (Kuramochi-Miyagawa et al., 2010), has RNA helicase activity (Sengoku et al., 2006) and N terminal sDMAs characterized by Tudor domains (Kirino et al., 2010). Multiple mouse models have been adopted to investigate the roles of DDX4 in spermatogenesis and piRNA pathways. DDX4-knockout mice exhibited complete spermatogenic arrest at the zygotene stage, and mutation of the RNA-helicase domain of DDX4 (DDX4 was expressed normally but catalytically dead) also disrupted spermatogenesis. $Ddx4^{-/\text{catalytically dead}}$ mouse spermatogenesis did not proceed beyond meiotic pachytene in spermatocytes, while germ cells in $Ddx4^{+/\text{catalytically dead}}$ mice completed meiosis but uniformly arrested during the development of round spermatids (Wenda et al., 2017). The essential role of DDX4 in the piRNA pathway was recently revealed: DDX4 is required for RNP remodeling during the loading of secondary piRNA intermediates onto MIWI2. The endonucleolytic cleavage of a target transcript by cytosolic MILI generates a piRNA precursor, which is processed into phased pre-piRNA intermediates (Han et al., 2015; Mohn et al., 2015; Yang et al., 2016). Mice lacking catalytically active DDX4 were still able to generate MILI slicer products but failed to transfer pre-piRNA intermediates to the ping-pong biogenesis machinery. Therefore, no MIWI2-bound piRNA was detected in mice with catalytically dead DDX4, and MIWI2 failed to maintain the necessary DNA methylation of L1 retrotransposons (Wenda et al., 2017). Furthermore, catalytically dead DDX4 also trapped MILI and MIWI, pachytene piRNAs, and slicer products of transposon and genic mRNAs, suggesting it functions in posttranscriptional regulation in post-meiotic stages (Wenda et al., 2017). In addition, reduced GTSF1 protein, which co-localizes with TDRD9 and MIWI2 in piP-bodies, resulted in target RNA remaining unsliced at the cleavage site for MILI-directed secondary piRNA processing (Yoshimura et al., 2018).

TRANSPOSABLE ELEMENT METHYLATION BY PIWI PATHWAY

Mael is highly expressed in mouse testes, and the protein's location alternates throughout spermatogenesis. MAEL, found in the cytoplasm in spermatocytes and shuttled to the nucleus in spermatids (Soper et al., 2008; Pandey and Pillai, 2014), comprises a high-mobility group box and a MAEL domain that is predicted to adopt an RNase H-like fold. Meiotic entry was delayed in *Mael*-null spermatogenic cells (Soper et al., 2008). Although *Mael*-knockout mice phenocopied *Mili*- and *Miwi2*-knockout mice, pre-pachytene arrest was intact in *Mael*-null testes. MAEL is speculated to function in post-piRNA production steps by facilitating the nucleo-cytoplasmic trafficking of MIWI2–piRNA complexes (Soper et al., 2008; Pandey and Pillai, 2014). In post-meiotic spermatogenesis, MAEL interacts with MILI, MIWI, and TDRD6, binding pachytene piRNA precursors and enabling piRNA intermediate processing (Pandey and Pillai, 2014; Sato and Siomi, 2015).

A recent study revealed that TEX15, a nuclear protein, is an essential partner of MIWI2 in piRNA-directed *de novo* methylation and silencing of transposable elements in fetal gonocytes (Schöpp et al., 2020). TEX15 contains a DUF3715 domain, which is also found in other TE-silencing proteins (Tchasovnikarova et al., 2015; Liu et al., 2018). In *TEX15*-null spermatocytes, SPO11-mediated DSB formation was normal, but DSB repair was absent because of a failure in the DMC1 assembly, resulting in zygotene-stage meiotic arrest (Yang et al., 2008). Although TEX15 interacts with MILI in the cytoplasm, it is not required for primary or secondary piRNA biogenesis in mouse gonocytes. TEX15 also interacts with MIWI2 in the nucleus in an RNA/DNA-dependent manner, yet the nuclear localization of MIWI2 remains unchanged in *TEX15*-null gonocytes. Considering that loss of TEX15 causes demethylation in LINE1 and IAP transposon promoter regions, it may be a predominant nuclear executor of TE *de novo* methylation downstream of piRNA pathways (Schöpp et al., 2020; Yang et al., 2020).

SPOCD1, another MIWI2 interactome member, facilitates MIWI2 activity in the nucleus. *Spocd1*-null spermatocytes undergo early-pachytene-stage meiotic arrest, but both primary and secondary piRNA biogeneses remain. Loss of IAP and LINE1 transposon *de novo* DNA methylation and consequential transposon de-repression were observed in *Spocd1*-knockout testes. SPOCD1 engages with MIWI2 in an RNA/DNA-dependent manner and facilitates MIWI2 nuclear activity by summoning chromatin remodeling and DNA methylation machinery to the promoters of transcribing transposons (Zoch et al., 2020). SPOCD1 contains a SPOC domain, which was previously found to recruit transcriptional repressors (Ariyoshi and Schwabe, 2003; Mikami et al., 2014), and a nuclear localization signal. SPOCD1 co-immunoprecipitated with DNMT3L and DNMT3A, components of the *de novo* methylation machinery and the NURD (Kloet et al., 2015) and BAF (Mashtalir et al., 2018) repressive chromatin remodeling complexes.

UHRF1 maintains the crosstalk between the PIWI pathway and repressive chromatin remodeling machinery. UHRF1 was found to be abundant in the nuclei of neonatal prospermatonia at P0, as well as spermatogonia, late pachytene spermatocytes, and early round spermatids, and shifted into the cytoplasm of fetal

prospermatogonia during spermatocyte E15.5, pre-leptotene, leptotene, zygotene, and early pachytene. The conditional deletion of *Uhrf1* in differentiating spermatogonia led to pachytene-stage meiotic arrest. UHRF1 interacts with PRMT5 (Kirino et al., 2009; Zhao et al., 2009; Wang et al., 2015), an arginine methyltransferase, to regulate repressive histone arginine modifications (H4R3me2s and H3R2me2s) (Ancelin et al., 2006; Migliori et al., 2012) and piRNA biogenesis by controlling the localization of PIWI pathway proteins (MILI, MIWI, and TDRKH). UHRF1 depletion also induces global loss of DNA methylation during spermatogenesis. UHRF1 appears to play essential roles in the crosstalk between the piRNA pathway and repressive epigenetic pathways, providing new clues to piRNA pathway functions (Dong et al., 2019).

REPRESSION OF LINE1 RETROTRANSPOSONS IN GERM CELLS

LINE1 retrotransposons are members of the most abundant class of transposable elements in mammals, accounting for ∼20% of mouse and human genomes. Up to 3,000 and 100 copies of LINE1 are intact and active in mice (Deberardinis et al., 1998) and humans (Sassaman et al., 1997; Mandal and Kazazian, 2008), respectively. In male piRNA pathway mutants, LINE1 activated late embryonic germ cells or early and mid-pachytene spermatocytes (Yang and Wang, 2016). Most male mouse piRNA pathway mutants exhibit meiotic arrest and sterility, but this effect is not observed in females (Yang and Wang, 2016). Notably, LINE1 de-repression in spermatocytes does not necessarily lead to meiotic arrest, such as in *Henmt1*-knockout animals (Lim et al., 2015). Some mouse mutants of *Miwi* (Deng and Lin, 2002), *Pnldc1* (Ding et al., 2017; Zhang et al., 2017c; Bronkhorst and Ketting, 2018; Nishimura et al., 2018), *Tdrd5* (Yabuta et al., 2011; Ding et al., 2018), and *Henmt1* (Lim et al., 2015), etc., still produce post-meiotic germ cells. Interestingly, although a large proportion of MIWI-piRNAs were thought to originate from non-transposon-related regions (Vourekas et al., 2012), LINE1 de-repression was found in *Miwi*-knockout mouse spermatids (Reuter et al., 2011). MIWI slicer activity involved in the direct cleavage of transposon mRNAs in spermatids (Reuter et al., 2011) is also chromatoid body location dependent but may not be piRNA dependent (Ding et al., 2019). In a *Pnldc1* mutant, dramatically reduced MIWI protein and MIWI-piRNAs, without spermatid LINE1 de-repression, were seen (Ding et al., 2017; Zhang et al., 2017c; Nishimura et al., 2018), and the remaining MIWI in the mutant possibly played a role in LINE1 repression (Ding et al., 2019). Spermatids in *Henmt1*-knockout mice also showed activated LINE1 that was unassociated with MIWI slicer activity (Lim et al., 2015). These results suggest that LINE1 repression also occurs in spermatids. Most piRNA factor knockouts display meiotic arrest; therefore, there is a lack of information on LINE1 repression after meiosis. Pachytene piRNA cluster is usually non-repeat origin, thus the mechanism of LINE1 repression after meiosis needs further exploration. The active LINE1 ORF1p is often found in the cytoplasm of spermatocytes but is more commonly seen in round spermatid nuclei, although the reason for this is unknown. A recent conditional knockout (cKO) study provided examples of how this process can be explored; $Tdrkh^{cKO}$ driven by Stra8-Cre, but not $Mov10l1^{cKO}$, showed obvious LINE1 de-repression in spermatids (Ding et al., 2019). This raises questions about whether piRNA factor genes expressed in spermatids, such as *Tdrd1*, *Asz1*, *Mybl1*, *Ddx4*, *Tdrd9*, *Mael*, *Gtsf1*, *Uhrf1*, *Tut4/7*, and *Tdrd5*, are involved in LINE1 inhibition after meiosis (**Table 1**).

Because of knockout mouse studies, piRNA pathway is believed to be unnecessary in mammalian female germ cells (Yang and Wang, 2016). In mouse oocytes, the ribonuclease MARF1, which is not associated with piRNA, is considered to be involved in LINE1 inhibition in oocytes (Su et al., 2012a,b; Yao et al., 2018). This phenomenon suggests that a transposon inhibition system other than piRNA may function in mouse oocytes. Apart from mice, most mammals have four PIWI genes. PIWIL3, which is not expressed in mice, binds to a class of piRNAs of 19 and 20 nt in hamster and human oocytes, respectively (Yang et al., 2019; Ishino et al., 2021). *PIWIL3*-deficient female hamsters have reduced fertility (Hasuwa et al., 2021). Furthermore, abolishing piRNA factors *PIWIL1*, *PLD6*, and *MOV10L1* in golden hamsters led to female infertility, with embryos arresting at the two-cell stage (Ishino et al., 2021; Zhang et al., 2021). Therefore, the function of piRNA in oocytes may be significantly different among mammalian species.

CONCLUSION

Previous studies using knockout mice have revealed the formation of piRNA in mammals and its role in male germ cells. Most piRNA factor knockouts showed spermatogenesis arrest in meiosis, but a few showed male germ cell arrest after meiosis. It is unclear whether the majority of piRNA factors expressed in spermatids are involved in LINE1 repression after meiosis, and future cKO research is required. In addition, in recent hamster gene-knockout studies, a piRNA factor was found to be necessary for oocytes, a complete contrast to findings in mice. This species difference allows researchers to reexamine the function of piRNA in female germ cells, which should broaden our knowledge on female infertility in humans.

AUTHOR CONTRIBUTIONS

ML, YZ, and YL: conceptualization. YL and YZ: literature search. ML, YZ, and YL: writing—original draft preparation. ML and YL: writing—review and editing. YL: visualization of histological structures. All authors read and approved the final version of manuscript.

FUNDING

This work was supported by the National Key Research and Development Program of China (2016YFA0500902 to ML), the Natural Science Foundation of China (32070842 and 31771654 to ML and 82001614 to YZ), the Natural Science Foundation of Jiangsu Province (Grant No. BK20190081 to ML), and the Qing Lan Project (ML).

REFERENCES

Ancelin, K., Lange, U. C., Hajkova, P., Schneider, R., Bannister, A. J., Kouzarides, T., et al. (2006). Blimp1 associates with Prmt5 and directs histone arginine methylation in mouse germ cells. *Nat. Cell Biol.* 8, 623–630. doi: 10.1038/ncb1413

Aravin, A., Gaidatzis, D., Pfeffer, S., Lagos-Quintana, M., Landgraf, P., Iovino, N., et al. (2006). A novel class of small RNAs bind to MILI protein in mouse testes. *Nature* 442, 203–207. doi: 10.1038/nature04916

Aravin, A. A., Klenov, M. S., Vagin, V. V., Bantignies, F., Cavalli, G., and Gvozdev, V. A. (2004). Dissection of a natural RNA silencing process in the Drosophila melanogaster germ line. *Mol. Cell Biol.* 24, 6742–6750. doi: 10.1128/mcb.24.15.6742-6750.2004

Aravin, A. A., Sachidanandam, R., Bourc'his, D., Schaefer, C., Pezic, D., Toth, K. F., et al. (2008). A piRNA pathway primed by individual transposons is linked to de novo DNA methylation in mice. *Mol. Cell.* 31, 785–799. doi: 10.1016/j.molcel.2008.09.003

Aravin, A. A., Sachidanandam, R., Girard, A., Fejes-Toth, K., and Hannon, G. J. (2007). Developmentally regulated piRNA clusters implicate MILI in transposon control. *Science* 316, 744–747. doi: 10.1126/science.1142612

Ariyoshi, M., and Schwabe, J. W. (2003). A conserved structural motif reveals the essential transcriptional repression function of Spen proteins and their role in developmental signaling. *Genes Dev.* 17, 1909–1920. doi: 10.1101/gad.266203

Bailey, A. S., Batista, P. J., Gold, R. S., Chen, Y. G., De Rooij, D. G., Chang, H. Y., et al. (2017). The conserved RNA helicase YTHDC2 regulates the transition from proliferation to differentiation in the germline. *eLife* 6:e26116.

Brennecke, J., Aravin, A. A., Stark, A., Dus, M., Kellis, M., Sachidanandam, R., et al. (2007). Discrete small RNA-generating loci as master regulators of transposon activity in *Drosophila*. *Cell* 128, 1089–1103. doi: 10.1016/j.cell.2007.01.043

Bronkhorst, A. W., and Ketting, R. F. (2018). Trimming it short: PNLDC1 is required for piRNA maturation during mouse spermatogenesis. *EMBO Rep.* 19:e45824.

Carmell, M. A., Girard, A., Van De Kant, H. J., Bourc'his, D., Bestor, T. H., De Rooij, D. G., et al. (2007). MIWI2 is essential for spermatogenesis and repression of transposons in the mouse male germline. *Dev. Cell* 12, 503–514. doi: 10.1016/j.devcel.2007.03.001

Carrieri, C., Comazzetto, S., Grover, A., Morgan, M., Buness, A., Nerlov, C., et al. (2017). A transit-amplifying population underpins the efficient regenerative capacity of the testis. *J. Exp. Med.* 214, 1631–1641. doi: 10.1084/jem.20161371

Castañeda, J., Genzor, P., Van Der Heijden, G. W., Sarkeshik, A., Yates, J. R. III, Ingolia, N. T., et al. (2014). Reduced pachytene piRNAs and translation underlie spermiogenic arrest in Maelstrom mutant mice. *EMBO J.* 33, 1999–2019. doi: 10.15252/embj.201386855

Chen, C., Jin, J., James, D. A., Adams-Cioaba, M. A., Park, J. G., Guo, Y., et al. (2009). Mouse Piwi interactome identifies binding mechanism of Tdrkh Tudor domain to arginine methylated Miwi. *Proc. Natl. Acad. Sci. U.S.A.* 106, 20336–20341. doi: 10.1073/pnas.0911640106

Choi, S. Y., Huang, P., Jenkins, G. M., Chan, D. C., Schiller, J., and Frohman, M. A. (2006). A common lipid links Mfn-mediated mitochondrial fusion and SNARE-regulated exocytosis. *Nat. Cell Biol.* 8, 1255–1262. doi: 10.1038/ncb1487

Chuma, S., Hiyoshi, M., Yamamoto, A., Hosokawa, M., Takamune, K., and Nakatsuji, N. (2003). Mouse Tudor Repeat-1 (MTR-1) is a novel component of chromatoid bodies/nuages in male germ cells and forms a complex with snRNPs. *Mech. Dev.* 120, 979–990. doi: 10.1016/s0925-4773(03)00181-3

Chuma, S., Hosokawa, M., Kitamura, K., Kasai, S., Fujioka, M., Hiyoshi, M., et al. (2006). Tdrd1/Mtr-1, a tudor-related gene, is essential for male germ-cell differentiation and nuage/germinal granule formation in mice. *Proc. Natl. Acad. Sci. U.S.A.* 103, 15894–15899. doi: 10.1073/pnas.0601878103

Chuma, S., and Nakano, T. (2013). piRNA and spermatogenesis in mice. *Philos. Trans. R. Soc. Lond. B Biol. Sci.* 368:20110338. doi: 10.1098/rstb.2011.0338

Costa, Y., Speed, R. M., Gautier, P., Semple, C. A., Maratou, K., Turner, J. M., et al. (2006). Mouse MAELSTROM: the link between meiotic silencing of unsynapsed chromatin and microRNA pathway? *Hum. Mol. Genet.* 15, 2324–2334. doi: 10.1093/hmg/ddl158

Crackower, M. A., Kolas, N. K., Noguchi, J., Sarao, R., Kikuchi, K., Kaneko, H., et al. (2003). Essential role of Fkbp6 in male fertility and homologous chromosome pairing in meiosis. *Science* 300, 1291–1295. doi: 10.1126/science.1083022

Dai, P., Wang, X., Gou, L. T., Li, Z. T., Wen, Z., Chen, Z. G., et al. (2019). A translation-activating function of MIWI/piRNA during mouse spermiogenesis. *Cell* 179, 1566.e16–1581.e16.

Dai, P., Wang, X., and Liu, M. F. (2020). A dual role of the PIWI/piRNA machinery in regulating mRNAs during mouse spermiogenesis. *Sci. China Life Sci.* 63, 447–449. doi: 10.1007/s11427-020-1632-5

De Fazio, S., Bartonicek, N., Di Giacomo, M., Abreu-Goodger, C., Sankar, A., Funaya, C., et al. (2011). The endonuclease activity of Mili fuels piRNA amplification that silences LINE1 elements. *Nature* 480, 259–263. doi: 10.1038/nature10547

Deberardinis, R. J., Goodier, J. L., Ostertag, E. M., and Kazazian, H. H. Jr. (1998). Rapid amplification of a retrotransposon subfamily is evolving the mouse genome. *Nat. Genet.* 20, 288–290. doi: 10.1038/3104

Deng, W., and Lin, H. (2002). miwi, a murine homolog of piwi, encodes a cytoplasmic protein essential for spermatogenesis. *Dev. Cell* 2, 819–830. doi: 10.1016/s1534-5807(02)00165-x

Di Giacomo, M., Comazzetto, S., Saini, H., De Fazio, S., Carrieri, C., Morgan, M., et al. (2013). Multiple epigenetic mechanisms and the piRNA pathway enforce LINE1 silencing during adult spermatogenesis. *Mol. Cell* 50, 601–608. doi: 10.1016/j.molcel.2013.04.026

Ding, D., Liu, J., Dong, K., Melnick, A. F., Latham, K. E., and Chen, C. (2019). Mitochondrial membrane-based initial separation of MIWI and MILI functions during pachytene piRNA biogenesis. *Nucleic Acids Res.* 47, 2594–2608. doi: 10.1093/nar/gky1281

Ding, D., Liu, J., Dong, K., Midic, U., Hess, R. A., Xie, H., et al. (2017). PNLDC1 is essential for piRNA 3' end trimming and transposon silencing during spermatogenesis in mice. *Nat. Commun.* 8:819.

Ding, D., Liu, J., Midic, U., Wu, Y., Dong, K., Melnick, A., et al. (2018). TDRD5 binds piRNA precursors and selectively enhances pachytene piRNA processing in mice. *Nat. Commun.* 9:127.

Dönertas, D., Sienski, G., and Brennecke, J. (2013). Drosophila Gtsf1 is an essential component of the Piwi-mediated transcriptional silencing complex. *Genes Dev.* 27, 1693–1705. doi: 10.1101/gad.221150.113

Dong, J., Wang, X., Cao, C., Wen, Y., Sakashita, A., Chen, S., et al. (2019). UHRF1 suppresses retrotransposons and cooperates with PRMT5 and PIWI proteins in male germ cells. *Nat. Commun.* 10:4705.

Frost, R. J., Hamra, F. K., Richardson, J. A., Qi, X., Bassel-Duby, R., and Olson, E. N. (2010). MOV10L1 is necessary for protection of spermatocytes against retrotransposons by Piwi-interacting RNAs. *Proc. Natl. Acad. Sci. U.S.A.* 107, 11847–11852. doi: 10.1073/pnas.1007158107

Fu, Q., and Wang, P. J. (2014). Mammalian piRNAs: biogenesis, function, and mysteries. *Spermatogenesis* 4:e27889. doi: 10.4161/spmg.27889

Girard, A., Sachidanandam, R., Hannon, G. J., and Carmell, M. A. (2006). A germline-specific class of small RNAs binds mammalian Piwi proteins. *Nature* 442, 199–202. doi: 10.1038/nature04917

Gou, L. T., Dai, P., Yang, J. H., Xue, Y., Hu, Y. P., Zhou, Y., et al. (2014). Pachytene piRNAs instruct massive mRNA elimination during late spermiogenesis. *Cell Res.* 24, 680–700. doi: 10.1038/cr.2014.41

Gou, L. T., Kang, J. Y., Dai, P., Wang, X., Li, F., Zhao, S., et al. (2017). Ubiquitination-deficient mutations in human piwi cause male infertility by impairing histone-to-protamine exchange during spermiogenesis. *Cell* 169, 1090.e13–1104.e13.

Grad, I., Cederroth, C. R., Walicki, J., Grey, C., Barluenga, S., Winssinger, N., et al. (2010). The molecular chaperone Hsp90α is required for meiotic progression of spermatocytes beyond pachytene in the mouse. *PLoS One* 5:e15770. doi: 10.1371/journal.pone.0015770

Grivna, S. T., Beyret, E., Wang, Z., and Lin, H. (2006). A novel class of small RNAs in mouse spermatogenic cells. *Genes Dev.* 20, 1709–1714. doi: 10.1101/gad.1434406

Gunawardane, L. S., Saito, K., Nishida, K. M., Miyoshi, K., Kawamura, Y., Nagami, T., et al. (2007). A slicer-mediated mechanism for repeat-associated siRNA 5' end formation in *Drosophila*. *Science* 315, 1587–1590. doi: 10.1126/science.1140494

Han, B. W., Wang, W., Li, C., Weng, Z., and Zamore, P. D. (2015). Noncoding RNA. piRNA-guided transposon cleavage initiates Zucchini-dependent, phased piRNA production. *Science* 348, 817–821. doi: 10.1126/science.aaa1264

Handler, D., Olivieri, D., Novatchkova, M., Gruber, F. S., Meixner, K., Mechtler, K., et al. (2011). A systematic analysis of Drosophila TUDOR domain-containing

proteins identifies Vreteno and the Tdrd12 family as essential primary piRNA pathway factors. *EMBO J.* 30, 3977–3993. doi: 10.1038/emboj.2011.308

Hasuwa, H., Iwasaki, Y. W., Wan Kin, A. Y., Ishino, K., Masuda, H., Sasaki, H., et al. (2021). Production of functional oocytes requires maternally expressed PIWI genes and piRNAs in golden hamsters. *bioRxiv* [Preprint]. doi: 10.1101/2021.01.27.428354v2

Horvath, G. C., Kistler, M. K., and Kistler, W. S. (2009). RFX2 is a candidate downstream amplifier of A-MYB regulation in mouse spermatogenesis. *BMC Dev. Biol.* 9:63. doi: 10.1186/1471-213X-9-63

Huang, H., Gao, Q., Peng, X., Choi, S. Y., Sarma, K., Ren, H., et al. (2011). piRNA-associated germline nuage formation and spermatogenesis require MitoPLD profusogenic mitochondrial-surface lipid signaling. *Dev. Cell* 20, 376–387. doi: 10.1016/j.devcel.2011.01.004

Ichiyanagi, T., Ichiyanagi, K., Ogawa, A., Kuramochi-Miyagawa, S., Nakano, T., Chuma, S., et al. (2014). HSP90α plays an important role in piRNA biogenesis and retrotransposon repression in mouse. *Nucleic Acids Res.* 42, 11903–11911. doi: 10.1093/nar/gku881

Ipsaro, J. J., Haase, A. D., Knott, S. R., Joshua-Tor, L., and Hannon, G. J. (2012). The structural biochemistry of Zucchini implicates it as a nuclease in piRNA biogenesis. *Nature* 491, 279–283. doi: 10.1038/nature11502

Ishino, K., Hasuwa, H., Yoshimura, J., Iwasaki, Y. W., Nishihara, H., Seki, N. M., et al. (2021). Hamster PIWI proteins bind to piRNAs with stage-specific size variations during oocyte maturation. *Nucleic Acids Res.* 49, 2700–2720. doi: 10.1093/nar/gkab059

Izumi, N., Shoji, K., Suzuki, Y., Katsuma, S., and Tomari, Y. (2020). Zucchini consensus motifs determine the mechanism of pre-piRNA production. *Nature* 578, 311–316. doi: 10.1038/s41586-020-1966-9

Kirino, Y., Kim, N., De Planell-Saguer, M., Khandros, E., Chiorean, S., Klein, P. S., et al. (2009). Arginine methylation of Piwi proteins catalysed by dPRMT5 is required for Ago3 and Aub stability. *Nat. Cell Biol.* 11, 652–658. doi: 10.1038/ncb1872

Kirino, Y., and Mourelatos, Z. (2007). The mouse homolog of HEN1 is a potential methylase for Piwi-interacting RNAs. *RNA* 13, 1397–1401. doi: 10.1261/rna.659307

Kirino, Y., Vourekas, A., Kim, N., De Lima Alves, F., Rappsilber, J., Klein, P. S., et al. (2010). Arginine methylation of vasa protein is conserved across phyla. *J. Biol. Chem.* 285, 8148–8154. doi: 10.1074/jbc.m109.089821

Kloet, S. L., Baymaz, H. I., Makowski, M., Groenewold, V., Jansen, P. W., Berendsen, M., et al. (2015). Towards elucidating the stability, dynamics and architecture of the nucleosome remodeling and deacetylase complex by using quantitative interaction proteomics. *FEBS J.* 282, 1774–1785. doi: 10.1111/febs.12972

Kotaja, N., and Sassone-Corsi, P. (2007). The chromatoid body: a germ-cell-specific RNA-processing centre. *Nat. Rev. Mol. Cell Biol.* 8, 85–90. doi: 10.1038/nrm2081

Kuramochi-Miyagawa, S., Kimura, T., Ijiri, T. W., Isobe, T., Asada, N., Fujita, Y., et al. (2004). Mili, a mammalian member of piwi family gene, is essential for spermatogenesis. *Development* 131, 839–849. doi: 10.1242/dev.00973

Kuramochi-Miyagawa, S., Watanabe, T., Gotoh, K., Takamatsu, K., Chuma, S., Kojima-Kita, K., et al. (2010). MVH in piRNA processing and gene silencing of retrotransposons. *Genes Dev.* 24, 887–892. doi: 10.1101/gad.1902110

Kuramochi-Miyagawa, S., Watanabe, T., Gotoh, K., Totoki, Y., Toyoda, A., Ikawa, M., et al. (2008). DNA methylation of retrotransposon genes is regulated by Piwi family members MILI and MIWI2 in murine fetal testes. *Genes Dev.* 22, 908–917. doi: 10.1101/gad.1640708

Li, F., Yuan, P., Rao, M., Jin, C. H., Tang, W., Rong, Y. F., et al. (2020). piRNA-independent function of PIWIL1 as a co-activator for anaphase promoting complex/cyclosome to drive pancreatic cancer metastasis. *Nat. Cell Biol.* 22, 425–438. doi: 10.1038/s41556-020-0486-z

Li, X. Z., Roy, C. K., Dong, X., Bolcun-Filas, E., Wang, J., Han, B. W., et al. (2013). An ancient transcription factor initiates the burst of piRNA production during early meiosis in mouse testes. *Mol. Cell* 50, 67–81. doi: 10.1016/j.molcel.2013.02.016

Lim, S. L., Qu, Z. P., Kortschak, R. D., Lawrence, D. M., Geoghegan, J., Hempfling, A. L., et al. (2015). HENMT1 and piRNA stability are required for adult male germ cell transposon repression and to define the spermatogenic program in the mouse. *PLoS Genet.* 11:e1005620. doi: 10.1371/journal.pgen.1005620

Liu, N., Lee, C. H., Swigut, T., Grow, E., Gu, B., Bassik, M. C., et al. (2018). Selective silencing of euchromatic L1s revealed by genome-wide screens for L1 regulators. *Nature* 553, 228–232. doi: 10.1038/nature25179

Ma, L., Buchold, G. M., Greenbaum, M. P., Roy, A., Burns, K. H., Zhu, H., et al. (2009). GASZ is essential for male meiosis and suppression of retrotransposon expression in the male germline. *PLoS Genet.* 5:e1000635. doi: 10.1371/journal.pgen.1000635

Malone, C. D., Brennecke, J., Dus, M., Stark, A., Mccombie, W. R., Sachidanandam, R., et al. (2009). Specialized piRNA pathways act in germline and somatic tissues of the *Drosophila ovary*. *Cell* 137, 522–535. doi: 10.1016/j.cell.2009.03.040

Mandal, P. K., and Kazazian, H. H. Jr. (2008). SnapShot: vertebrate transposons. *Cell* 135, 191–192.

Mashtalir, N., D'avino, A. R., Michel, B. C., Luo, J., Pan, J., Otto, J. E., et al. (2018). Modular organization and assembly of SWI/SNF family chromatin remodeling complexes. *Cell* 175, 1272.e20–1288.e20.

Migliori, V., Müller, J., Phalke, S., Low, D., Bezzi, M., Mok, W. C., et al. (2012). Symmetric dimethylation of H3R2 is a newly identified histone mark that supports euchromatin maintenance. *Nat. Struct. Mol. Biol.* 19, 136–144. doi: 10.1038/nsmb.2209

Mikami, S., Kanaba, T., Takizawa, N., Kobayashi, A., Maesaki, R., Fujiwara, T., et al. (2014). Structural insights into the recruitment of SMRT by the corepressor SHARP under phosphorylative regulation. *Structure* 22, 35–46. doi: 10.1016/j.str.2013.10.007

Mohn, F., Handler, D., and Brennecke, J. (2015). Noncoding RNA. piRNA-guided slicing specifies transcripts for Zucchini-dependent, phased piRNA biogenesis. *Science* 348, 812–817. doi: 10.1126/science.aaa1039

Morgan, M., Kabayama, Y., Much, C., Ivanova, I., Di Giacomo, M., Auchynnikava, T., et al. (2019). A programmed wave of uridylation-primed mRNA degradation is essential for meiotic progression and mammalian spermatogenesis. *Cell Res.* 29, 221–232. doi: 10.1038/s41422-018-0128-1

Nishimasu, H., Ishizu, H., Saito, K., Fukuhara, S., Kamatani, M. K., Bonnefond, L., et al. (2012). Structure and function of Zucchini endoribonuclease in piRNA biogenesis. *Nature* 491, 284–287. doi: 10.1038/nature11509

Nishimura, T., Nagamori, I., Nakatani, T., Izumi, N., Tomari, Y., Kuramochi-Miyagawa, S., et al. (2018). PNLDC1, mouse pre-piRNA Trimmer, is required for meiotic and post-meiotic male germ cell development. *EMBO Rep.* 19:e44957.

Noce, T., Okamoto-Ito, S., and Tsunekawa, N. (2001). Vasa homolog genes in mammalian germ cell development. *Cell Struct. Funct.* 26, 131–136. doi: 10.1247/csf.26.131

Ohtani, H., Iwasaki, Y. W., Shibuya, A., Siomi, H., Siomi, M. C., and Saito, K. (2013). DmGTSF1 is necessary for Piwi-piRISC-mediated transcriptional transposon silencing in the *Drosophila ovary*. *Genes Dev.* 27, 1656–1661. doi: 10.1101/gad.221515.113

Oud, M. S., Volozonoka, L., Friedrich, C., Kliesch, S., Nagirnaja, L., Gilissen, C., et al. (2021). Lack of evidence for a role of PIWIL1 variants in human male infertility. *Cell* 184, 1941–1942. doi: 10.1016/j.cell.2021.03.001

Pandey, R. R., and Pillai, R. S. (2014). Primary piRNA biogenesis: caught up in a Maelstrom. *EMBO J.* 33, 1979–1980. doi: 10.15252/embj.201489670

Pandey, R. R., Tokuzawa, Y., Yang, Z., Hayashi, E., Ichisaka, T., Kajita, S., et al. (2013). Tudor domain containing 12 (TDRD12) is essential for secondary PIWI interacting RNA biogenesis in mice. *Proc. Natl. Acad. Sci. U.S.A.* 110, 16492–16497. doi: 10.1073/pnas.1316316110

Peng, L., Zhang, F., Shang, R., Wang, X., Chen, J., Chou, J. J., et al. (2018). Identification of substrates of the small RNA methyltransferase Hen1 in mouse spermatogonial stem cells and analysis of its methyl-transfer domain. *J. Biol. Chem.* 293, 9981–9994. doi: 10.1074/jbc.ra117.000837

Reuter, M., Berninger, P., Chuma, S., Shah, H., Hosokawa, M., Funaya, C., et al. (2011). Miwi catalysis is required for piRNA amplification-independent LINE1 transposon silencing. *Nature* 480, 264–267. doi: 10.1038/nature10672

Reuter, M., Chuma, S., Tanaka, T., Franz, T., Stark, A., and Pillai, R. S. (2009). Loss of the Mili-interacting Tudor domain-containing protein-1 activates transposons and alters the Mili-associated small RNA profile. *Nat. Struct. Mol. Biol.* 16, 639–646. doi: 10.1038/nsmb.1615

Saga, Y. (2008). Mouse germ cell development during embryogenesis. *Curr. Opin. Genet. Dev.* 18, 337–341. doi: 10.1016/j.gde.2008.06.003

Sassaman, D. M., Dombroski, B. A., Moran, J. V., Kimberland, M. L., Naas, T. P., Deberardinis, R. J., et al. (1997). Many human L1 elements are capable of retrotransposition. *Nat. Genet.* 16, 37–43. doi: 10.1038/ng0597-37

Sato, K., and Siomi, M. C. (2015). Functional and structural insights into the piRNA factor Maelstrom. *FEBS Lett.* 589, 1688–1693. doi: 10.1016/j.febslet.2015.03.023

Saxe, J. P., Chen, M., Zhao, H., and Lin, H. (2013). Tdrkh is essential for spermatogenesis and participates in primary piRNA biogenesis in the germline. *EMBO J.* 32, 1869–1885. doi: 10.1038/emboj.2013.121

Schaefer, C. B., Ooi, S. K., Bestor, T. H., and Bourc'his, D. (2007). Epigenetic decisions in mammalian germ cells. *Science* 316, 398–399. doi: 10.1126/science.1137544

Schöpp, T., Zoch, A., Berrens, R. V., Auchynnikava, T., Kabayama, Y., Vasiliauskaitė, L., et al. (2020). TEX15 is an essential executor of MIWI2-directed transposon DNA methylation and silencing. *Nat. Commun.* 11:3739.

Sengoku, T., Nureki, O., Nakamura, A., Kobayashi, S., and Yokoyama, S. (2006). Structural basis for RNA unwinding by the DEAD-box protein *Drosophila* vasa. *Cell* 125, 287–300. doi: 10.1016/j.cell.2006.01.054

Shoji, M., Tanaka, T., Hosokawa, M., Reuter, M., Stark, A., Kato, Y., et al. (2009). The TDRD9-MIWI2 complex is essential for piRNA-mediated retrotransposon silencing in the mouse male germline. *Dev. Cell* 17, 775–787. doi: 10.1016/j.devcel.2009.10.012

Siomi, M. C., and Kuramochi-Miyagawa, S. (2009). RNA silencing in germlines–exquisite collaboration of Argonaute proteins with small RNAs for germline survival. *Curr. Opin. Cell Biol.* 21, 426–434. doi: 10.1016/j.ceb.2009.02.003

Smith, J. M., Bowles, J., Wilson, M., Teasdale, R. D., and Koopman, P. (2004). Expression of the tudor-related gene Tdrd5 during development of the male germline in mice. *Gene Expr. Patterns* 4, 701–705. doi: 10.1016/j.modgep.2004.04.002

Soper, S. F., Van Der Heijden, G. W., Hardiman, T. C., Goodheart, M., Martin, S. L., De Boer, P., et al. (2008). Mouse maelstrom, a component of nuage, is essential for spermatogenesis and transposon repression in meiosis. *Dev. Cell* 15, 285–297. doi: 10.1016/j.devcel.2008.05.015

Su, Y. Q., Sugiura, K., Sun, F., Pendola, J. K., Cox, G. A., Handel, M. A., et al. (2012a). MARF1 regulates essential oogenic processes in mice. *Science* 335, 1496–1499. doi: 10.1126/science.1214680

Su, Y. Q., Sun, F., Handel, M. A., Schimenti, J. C., and Eppig, J. J. (2012b). Meiosis arrest female 1 (MARF1) has nuage-like function in mammalian oocytes. *Proc. Natl. Acad. Sci. U.S.A.* 109, 18653–18660. doi: 10.1073/pnas.1216904109

Tanaka, S. S., Toyooka, Y., Akasu, R., Katoh-Fukui, Y., Nakahara, Y., Suzuki, R., et al. (2000). The mouse homolog of *Drosophila* Vasa is required for the development of male germ cells. *Genes Dev.* 14, 841–853.

Tchasovnikarova, I. A., Timms, R. T., Matheson, N. J., Wals, K., Antrobus, R., Göttgens, B., et al. (2015). GENE SILENCING. Epigenetic silencing by the HUSH complex mediates position-effect variegation in human cells. *Science* 348, 1481–1485. doi: 10.1126/science.aaa7227

Toscani, A., Mettus, R. V., Coupland, R., Simpkins, H., Litvin, J., Orth, J., et al. (1997). Arrest of spermatogenesis and defective breast development in mice lacking A-myb. *Nature* 386, 713–717. doi: 10.1038/386713a0

Toyooka, Y., Tsunekawa, N., Takahashi, Y., Matsui, Y., Satoh, M., and Noce, T. (2000). Expression and intracellular localization of mouse Vasa-homologue protein during germ cell development. *Mech. Dev.* 93, 139–149. doi: 10.1016/s0925-4773(00)00283-5

Trasler, J. M. (2009). Epigenetics in spermatogenesis. *Mol. Cell Endocrinol.* 306, 33–36. doi: 10.1016/j.mce.2008.12.018

Unhavaithaya, Y., Hao, Y., Beyret, E., Yin, H., Kuramochi-Miyagawa, S., Nakano, T., et al. (2009). MILI, a PIWI-interacting RNA-binding protein, is required for germ line stem cell self-renewal and appears to positively regulate translation. *J. Biol. Chem.* 284, 6507–6519. doi: 10.1074/jbc.m809104200

Vourekas, A., Zheng, K., Fu, Q., Maragkakis, M., Alexiou, P., Ma, J., et al. (2015). The RNA helicase MOV10L1 binds piRNA precursors to initiate piRNA processing. *Genes Dev.* 29, 617–629. doi: 10.1101/gad.254631.114

Vourekas, A., Zheng, Q., Alexiou, P., Maragkakis, M., Kirino, Y., Gregory, B. D., et al. (2012). Mili and Miwi target RNA repertoire reveals piRNA biogenesis and function of Miwi in spermiogenesis. *Nat. Struct. Mol. Biol.* 19, 773–781. doi: 10.1038/nsmb.2347

Wang, Y., Zhu, T., Li, Q., Liu, C., Han, F., Chen, M., et al. (2015). Prmt5 is required for germ cell survival during spermatogenesis in mice. *Sci. Rep.* 5:11031.

Watanabe, T., Cheng, E. C., Zhong, M., and Lin, H. (2015). Retrotransposons and pseudogenes regulate mRNAs and lncRNAs via the piRNA pathway in the germline. *Genome Res.* 25, 368–380. doi: 10.1101/gr.180802.114

Watanabe, T., Chuma, S., Yamamoto, Y., Kuramochi-Miyagawa, S., Totoki, Y., Toyoda, A., et al. (2011). MITOPLD is a mitochondrial protein essential for nuage formation and piRNA biogenesis in the mouse germline. *Dev. Cell* 20, 364–375. doi: 10.1016/j.devcel.2011.01.005

Wenda, J. M., Homolka, D., Yang, Z., Spinelli, P., Sachidanandam, R., Pandey, R. R., et al. (2017). Distinct roles of RNA helicases MVH and TDRD9 in PIWI slicing-triggered mammalian piRNA biogenesis and function. *Dev. Cell* 41, 623.e9–637.e9.

Xiol, J., Cora, E., Koglgruber, R., Chuma, S., Subramanian, S., Hosokawa, M., et al. (2012). A role for Fkbp6 and the chaperone machinery in piRNA amplification and transposon silencing. *Mol. Cell* 47, 970–979. doi: 10.1016/j.molcel.2012.07.019

Yabuta, Y., Ohta, H., Abe, T., Kurimoto, K., Chuma, S., and Saitou, M. (2011). TDRD5 is required for retrotransposon silencing, chromatoid body assembly, and spermiogenesis in mice. *J. Cell Biol.* 192, 781–795. doi: 10.1083/jcb.201009043

Yang, F., Eckardt, S., Leu, N. A., Mclaughlin, K. J., and Wang, P. J. (2008). Mouse TEX15 is essential for DNA double-strand break repair and chromosomal synapsis during male meiosis. *J. Cell Biol.* 180, 673–679. doi: 10.1083/jcb.200709057

Yang, F., Lan, Y., Pandey, R. R., Homolka, D., Berger, S. L., Pillai, R. S., et al. (2020). TEX15 associates with MILI and silences transposable elements in male germ cells. *Genes Dev.* 34, 745–750. doi: 10.1101/gad.335489.119

Yang, F., and Wang, P. J. (2016). Multiple LINEs of retrotransposon silencing mechanisms in the mammalian germline. *Semin. Cell Dev. Biol.* 59, 118–125. doi: 10.1016/j.semcdb.2016.03.001

Yang, Q., Li, R., Lyu, Q., Hou, L., Liu, Z., Sun, Q., et al. (2019). Single-cell CAS-seq reveals a class of short PIWI-interacting RNAs in human oocytes. *Nat. Commun.* 10:3389.

Yang, Z., Chen, K. M., Pandey, R. R., Homolka, D., Reuter, M., Janeiro, B. K., et al. (2016). PIWI slicing and EXD1 drive biogenesis of nuclear piRNAs from cytosolic targets of the mouse piRNA pathway. *Mol. Cell* 61, 138–152. doi: 10.1016/j.molcel.2015.11.009

Yang, Z., Ebright, Y. W., Yu, B., and Chen, X. (2006). HEN1 recognizes 21-24 nt small RNA duplexes and deposits a methyl group onto the 2′ OH of the 3′ terminal nucleotide. *Nucleic Acids Res.* 34, 667–675. doi: 10.1093/nar/gkj474

Yao, Q., Cao, G., Li, M., Wu, B., Zhang, X., Zhang, T., et al. (2018). Ribonuclease activity of MARF1 controls oocyte RNA homeostasis and genome integrity in mice. *Proc. Natl. Acad. Sci. U.S.A.* 115, 11250–11255. doi: 10.1073/pnas.1809744115

Yoshimura, T., Toyoda, S., Kuramochi-Miyagawa, S., Miyazaki, T., Miyazaki, S., Tashiro, F., et al. (2009). Gtsf1/Cue110, a gene encoding a protein with two copies of a CHHC Zn-finger motif, is involved in spermatogenesis and retrotransposon suppression in murine testes. *Dev. Biol.* 335, 216–227. doi: 10.1016/j.ydbio.2009.09.003

Yoshimura, T., Watanabe, T., Kuramochi-Miyagawa, S., Takemoto, N., Shiromoto, Y., Kudo, A., et al. (2018). Mouse GTSF1 is an essential factor for secondary piRNA biogenesis. *EMBO Rep.* 19:e42054.

Zhai, J., and Meyers, B. C. (2012). Deep sequencing from hen1 mutants to identify small RNA 3' modifications. *Cold Spring Harb. Symp. Quant. Biol.* 77, 213–219. doi: 10.1101/sqb.2013.77.014779

Zhang, H., Liu, K., Izumi, N., Huang, H., Ding, D., Ni, Z., et al. (2017a). Structural basis for arginine methylation-independent recognition of PIWIL1 by TDRD2. *Proc. Natl. Acad. Sci. U.S.A.* 114, 12483–12488. doi: 10.1073/pnas.1711486114

Zhang, Y., Guo, R., Cui, Y., Zhu, Z., Wu, H., Zheng, B., et al. (2017b). An essential role for PNLDC1 in piRNA 3' end trimming and male fertility in mice. *Cell Res.* 27, 1392–1396. doi: 10.1038/cr.2017.125

Zhang, Y., Guo, R., Cui, Y., Zhu, Z., Zhang, Y., Wu, H., et al. (2017c). An essential role for PNLDC1 in piRNA 3' end trimming and male fertility in mice. *Cell Res.* 27, 1392–1396.

Zhang, H., Zhang, F., Chen, J., Li, M., Lv, X., Xiao, Y., et al. (2021). piRNA pathway is essential for generating functional oocytes in golden hamster. *bioRxiv* [Preprint]. doi: 10.1101/2021.03.21.434510v1

Zhang, J., Wang, Q., Wang, M., Jiang, M., Wang, Y., Sun, Y., et al. (2016). GASZ and mitofusin-mediated mitochondrial functions are crucial for spermatogenesis. *EMBO Rep.* 17, 220–234. doi: 10.15252/embr.201540846

Zhao, Q., Rank, G., Tan, Y. T., Li, H., Moritz, R. L., Simpson, R. J., et al. (2009). PRMT5-mediated methylation of histone H4R3 recruits DNMT3A, coupling histone and DNA methylation in gene silencing. *Nat. Struct. Mol. Biol.* 16, 304–311. doi: 10.1038/nsmb.1568

Zhao, S., Gou, L. T., Zhang, M., Zu, L. D., Hua, M. M., Hua, Y., et al. (2013). piRNA-triggered MIWI ubiquitination and removal by APC/C in late spermatogenesis. *Dev. Cell* 24, 13–25. doi: 10.1016/j.devcel.2012.12.006

Zheng, K., Xiol, J., Reuter, M., Eckardt, S., Leu, N. A., Mclaughlin, K. J., et al. (2010). Mouse MOV10L1 associates with Piwi proteins and is an essential component of the Piwi-interacting RNA (piRNA) pathway. *Proc. Natl. Acad. Sci. U.S.A.* 107, 11841–11846. doi: 10.1073/pnas.1003953107

Zoch, A., Auchynnikava, T., Berrens, R. V., Kabayama, Y., Schopp, T., Heep, M., et al. (2020). SPOCD1 is an essential executor of piRNA-directed de novo DNA methylation. *Nature* 584, 635–639. doi: 10.1038/s41586-020-2557-5

Conflict of Interest: The authors declare that the research was conducted in the absence of any commercial or financial relationships that could be construed as a potential conflict of interest.

Copyright © 2021 Li, Zhang and Liu. This is an open-access article distributed under the terms of the Creative Commons Attribution License (CC BY). The use, distribution or reproduction in other forums is permitted, provided the original author(s) and the copyright owner(s) are credited and that the original publication in this journal is cited, in accordance with accepted academic practice. No use, distribution or reproduction is permitted which does not comply with these terms.

frontiers in Cell and Developmental Biology

REVIEW
published: 22 July 2021
doi: 10.3389/fcell.2021.681123

Meiotic Crossover Patterning

Nila M. Pazhayam[1†], Carolyn A. Turcotte[1†] and Jeff Sekelsky[1,2,3]*

[1] Curriculum in Genetics and Molecular Biology, The University of North Carolina at Chapel Hill, Chapel Hill, NC, United States, [2] Department of Biology, The University of North Carolina at Chapel Hill, Chapel Hill, NC, United States, [3] Integrative Program for Biological and Genome Sciences, The University of North Carolina at Chapel Hill, Chapel Hill, NC, United States

Proper number and placement of meiotic crossovers is vital to chromosome segregation, with failures in normal crossover distribution often resulting in aneuploidy and infertility. Meiotic crossovers are formed via homologous repair of programmed double-strand breaks (DSBs). Although DSBs occur throughout the genome, crossover placement is intricately patterned, as observed first in early genetic studies by Muller and Sturtevant. Three types of patterning events have been identified. Interference, first described by Sturtevant in 1915, is a phenomenon in which crossovers on the same chromosome do not occur near one another. Assurance, initially identified by Owen in 1949, describes the phenomenon in which a minimum of one crossover is formed per chromosome pair. Suppression, first observed by Beadle in 1932, dictates that crossovers do not occur in regions surrounding the centromere and telomeres. The mechanisms behind crossover patterning remain largely unknown, and key players appear to act at all scales, from the DNA level to inter-chromosome interactions. There is also considerable overlap between the known players that drive each patterning phenomenon. In this review we discuss the history of studies of crossover patterning, developments in methods used in the field, and our current understanding of the interplay between patterning phenomena.

Keywords: meiosis, recombination, interference, centromere, crossover assurance

OPEN ACCESS

Edited by:
Liangran Zhang,
Shandong University, China

Reviewed by:
Neil Hunter,
University of California, Davis, United States
Fumiko Esashi,
University of Oxford, United Kingdom

***Correspondence:**
Jeff Sekelsky
sekelsky@unc.edu

[†] These authors have contributed equally to this work

Specialty section:
This article was submitted to Cell Growth and Division, a section of the journal Frontiers in Cell and Developmental Biology

Received: *15 March 2021*
Accepted: *28 June 2021*
Published: *22 July 2021*

Citation:
Pazhayam NM, Turcotte CA and Sekelsky J (2021) Meiotic Crossover Patterning. Front. Cell Dev. Biol. 9:681123. doi: 10.3389/fcell.2021.681123

MEIOTIC RECOMBINATION

Crossovers are generally avoided during repair of DNA double-strand breaks (DSBs) in mitotically proliferating cells, presumably because they can lead to loss of heterozygosity or to chromosome rearrangement (when occurring between non-allelic repetitive sequences) (reviewed in Andersen and Sekelsky, 2010). To avoid crossovers, non-crossover outcomes are promoted through the actions of helicases that disassemble recombination intermediates (reviewed in Huselid and Bunting, 2020). In contrast, in meiotic cells DSBs are induced enzymatically and repaired to ensure that some become crossovers, which lead to chiasmata that promote accurate segregation of homologous chromosomes (Hawley, 1988). This change in outcome is achieved through the addition of numerous meiosis-specific elaborations to DSB repair.

The first step in homology-directed repair of DSBs is resection of the DSB ends (**Figure 1**) (reviewed in Heyer et al., 2010). In miotic cells, the recombinase Rad51 promotes strand exchange with a homologous duplex that is used as a template for synthesis; in meiosis, the meiosis-specific Rad51 paralog Dmc1 is used instead of or in conjunction with Rad51 (reviewed in Shinohara and Shinohara, 2004). As in mitotic DSB repair, dissociation of the nascent strand from the template

allows completion of repair by synthesis-dependent strand annealing (SDSA), a pathway thought to generate most or all non-crossovers (Allers and Lichten, 2001; Marsolier-Kergoat et al., 2018). In the major meiotic crossover pathway, the template strand that is displaced by synthesis anneals to the other resected end of the broken chromatid, and further synthesis and ligation leads to a double-Holliday junction (dHJ) structure, which is resolved into crossover products (**Figure 1**).

A defining feature of the major meiotic crossover pathway is dependence on a group of proteins referred to as ZMM (Zip, Msh, and Mer). In *Saccharomyces cerevisiae*, the ZMMs consist of at least seven players: Zip1, Zip2, Zip3, Zip4/Spo22, Spo16, Mer3, Msh4, and Msh5. Zip1 is a structural component of the synaptonemal complex (SC), a proteinaceous structure that assembles between homologous chromosomes during prophase I (Sym et al., 1993). Msh4 and Msh5, homologs of the *Escherichia coli* mismatch repair protein MutS, form a heterodimer termed MutSγ, which is thought to promote crossing over by stabilizing pre-crossover intermediates to block SDSA and/or promote formation of dHJs (Snowden et al., 2004; Jessop et al., 2006; Oh et al., 2007).

Recent studies have identified an important role for proteolysis of ZMM proteins in promoting crossovers in meiosis. Ahuja et al. (2017) found that the proteasome is necessary for chromosomes to pair and for crossover-designated DSBs to effectively be repaired as crossovers. The proteasome is recruited to chromosomes by Zip1 and Zip3. SUMO modification mediated by the meiotic E3 ligases RNF212 and HEI10 is thought to act like a checkpoint in mouse, pausing recombination by inducing degradation of various recombination factors (Rao et al., 2017). Likewise, Msh4 has been shown to be targeted by a degron for ubiquitin-independent proteolysis (He et al., 2020). This degron is under control of the kinase Cdc7, and phosphorylation of the degron permits Msh4–Msh5 to promote crossovers.

The final steps in crossover formation are also modified in meiosis. In mitotic cells, it is believed that the primary pathway for processing dHJs involves unwinding Blm helicase and decatenation by Topoisomerase 3α, a process that generates only non-crossovers (Plank et al., 2006). An alternative is resolution of the Holliday junctions by structure-selective endonucleases, which can produce crossover or non-crossover products (Wyatt and West, 2014). In meiosis, however, most or all dHJs are processed to generate crossovers (Allers and Lichten, 2001), through the action of a complex containing MutLγ, a heterodimer of Mlh1 and Mlh3, and other proteins (Zakharyevich et al., 2012; Cannavo et al., 2020; Kulkarni et al., 2020).

The meiotic DSB repair process outlined above ensures that some DSBs will be repaired as crossovers. However, the determination of which become crossovers and which are repaired as non-crossovers is highly regulated to ensure that all chromosome pairs receive at least one crossover, that crossovers are in positions that facilitate segregation, and that crossovers are excluded from regions where they might impede segregation (Koehler et al., 1996b). The phenomena that achieve this are collectively referred to as "crossover patterning." Below, we discuss various meiotic crossover patterning phenomena – interference, assurance, and suppression (**Figure 2**), from initial recognition to current understanding.

INTERFERENCE

History

Crossover interference was originally observed by Sturtevant when constructing the first linkage map in *Drosophila melanogaster* in 1913 (Sturtevant, 1913). His observation that one crossover makes the occurrence of another less likely was based on the results of counting double crossovers (DCOs) between six sex-linked factors, where he observed that DCOs between two adjacent intervals were much lower in frequency than should be expected by chance. This phenomenon, termed interference by Muller, was later shown by Sturtevant to be an intra-chromosomal process (Sturtevant, 1915).

Muller later showed that interference is limited to crossovers on the same chromosome, with a crossover on one chromosome having no effect on crossing over on another (Muller, 1916a). Muller further noted, just as Sturtevant had, that the reach of interference seemed to depend on the distance of the intervals being considered, with longer intervals showing less interference than shorter ones. Weinstein (Weinstein, 1918) confirmed this by showing that interference decreases with distances up to 46 map units (a measure of recombination in *D. melanogaster* equivalent to centiMorgans) from the initial crossover.

The possibility of chromatid interference was also considered (**Figure 3**): When there are two crossovers on the same chromosome arm, do the chromatids involved in one affect which are used in the other? This question was first investigated by Emerson and Beadle (1933). They found that in *Drosophila* the first crossover did not seem to influence which chromatids were involved in the second, suggesting no chromatid interference. The same result was also shown in both budding and fission yeast (Mortimer and Fogel, 1974; Munz, 1994), though not in *Neurospora crassa* (Perkins, 1962). Nonetheless, most studies have assumed no chromatid interference (Mather, 1935; Chakraborty et al., 2017).

Interfering and Non-interfering Crossovers

Not all crossovers participate in interference. Based on studies of recombination mutants in *Caenorhabditis elegans*, Zalevsky et al. (1999) proposed the existence of two meiotic recombination pathways. In most organisms, the primary meiotic crossover pathway (described above and in **Figure 1**) produces crossovers that are subject to interference, while other pathways produce crossovers that are indifferent to interference (de los Santos et al., 2003; Argueso et al., 2004; Börner et al., 2004; Higgins et al., 2004; de Boer et al., 2006; Holloway et al., 2008). This results in some crossovers participating in interference and others neither contributing to nor responding to interference. These have been called classes I and II crossovers, respectively.

Class II crossovers were initially identified as being generated independently of MutSγ (Zalevsky et al., 1999;

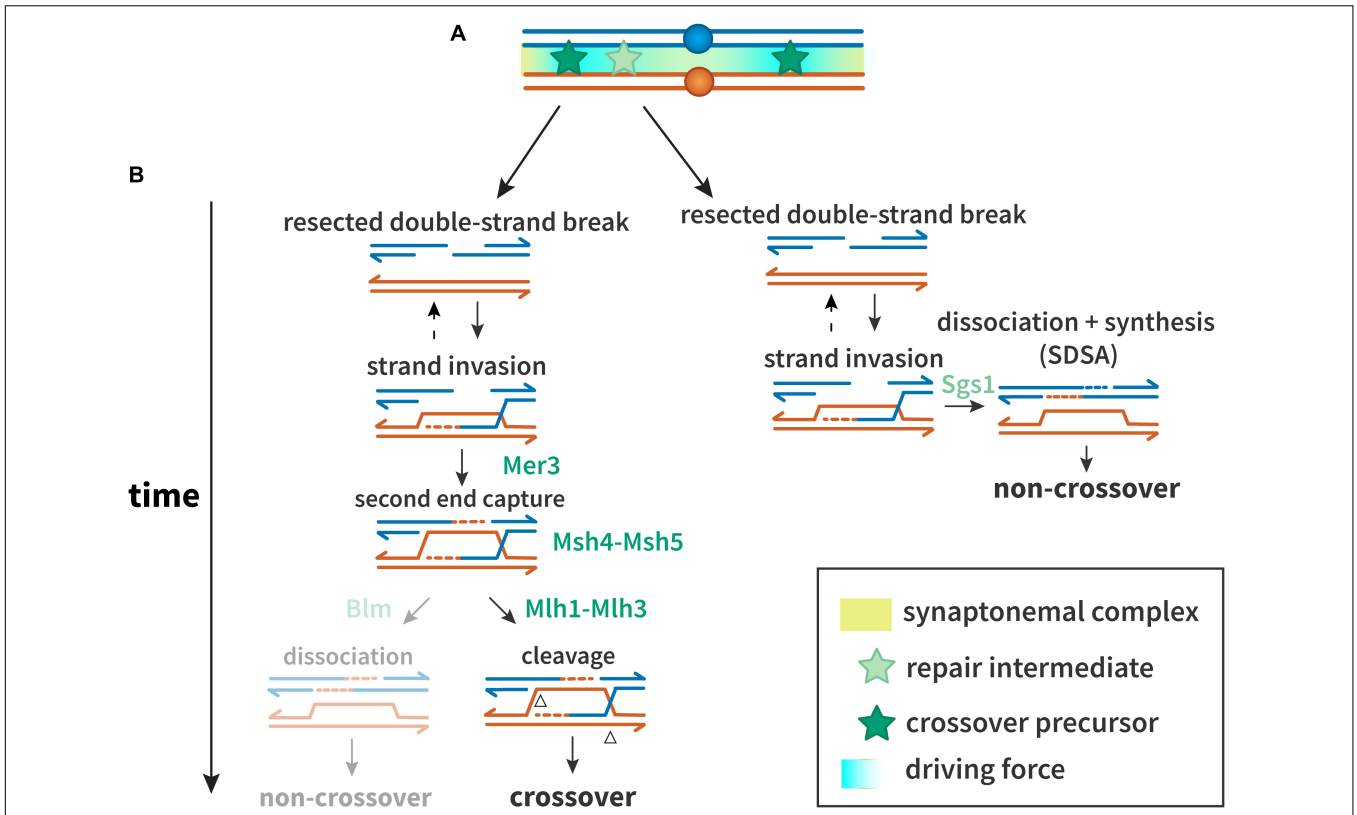

FIGURE 1 | Proteins and mechanisms of crossover interference. **(A)** A driving force (teal), potentially protein aggregation or mechanical stress, results in designation of crossover precursors (stars, dark green) at spaced intervals. Repair intermediates that do not experience sufficient driving force (stars, light green) are not so designated, and become non-crossovers. **(B)** Interference at the DNA level. Crossover precursors are processed through the class I crossover pathway, involving the ZMM proteins. Mer3 promotes second end capture, and Msh4–Msh5 clamp to and stabilize branched molecules to prevent their dissociation and to recruit Msh1–3. Intermediates are resolved by Mlh1–Mlh3 to generate crossovers. Non-crossovers in yeast are thought to be exclusively processed through the synthesis-dependent strand annealing (SDSA) pathway, promoted by Sgs1. In other organisms, the Sgs1 ortholog Blm may also promote formation of non-crossovers after second end capture.

de los Santos et al., 2003), but the class II designation has been used in different ways. For example, when a blockage occurs in the primary pathway due to a missing component, backup mechanisms will complete repair (De Muyt et al., 2012; Zakharyevich et al., 2012; Kohl and Sekelsky, 2013). These backup pathways, like mitotic DSB repair, are not directed toward a crossover outcome. Nonetheless, crossovers do occur in some instances, but this requires structure-selective nucleases such as Mus81–Mms4 rather than MutLγ (de los Santos et al., 2003; Argueso et al., 2004; Berchowitz et al., 2007; Holloway et al., 2008). Some consider these to be class II crossovers because they come from a different pathway, but if the blockage happens after crossover designation has occurred and interference has been enforced, these crossovers may exhibit interference.

The proteins involved and percentage of crossovers attributed to classes I and II differ among organisms. In budding yeast, only about 60% of meiotic crossovers come from the class I pathway (de los Santos et al., 2003; Medhi et al., 2016). Unique features of this pathway are similar in *Arabidopsis* and mouse, with ZMM proteins and MutLγ playing central roles (Falque et al., 2007; Higgins et al., 2008; Lu et al., 2008; Svetlanov et al., 2008); however, class I crossovers comprise 75–90% of all meiotic crossovers in *Arabidopsis* (Berchowitz et al., 2007; Higgins et al., 2008) and more than 90% of crossovers in mouse meiosis (Baker et al., 1996; Holloway et al., 2008).

In *Drosophila*, 90–100% of crossovers come from a class I pathway (Baker and Carpenter, 1972), but Dmc1, Msh4, and Msh5 are absent from fly genomes (Sekelsky, 2017). Kohl et al. (2012) hypothesized that crossover-designated recombination intermediates are instead stabilized by the MCM-like proteins Mei-217, Mei-218 and Rec. Furthermore, the class I resolvase function of Mlh1–Mlh3 is replaced by the XPF ortholog Mei-9 and its partners Ercc1 and the Slx4 ortholog Mus312 (Sekelsky et al., 1995; Yıldız et al., 2002; Radford et al., 2005). All crossovers in *C. elegans* are processed through the ZMM-based class I pathway (Zalevsky et al., 1999), though it also uses resolvases other than MutLγ (Saito et al., 2009; Agostinho et al., 2013; O'Neil et al., 2013). *Schizosaccharomyces pombe* appears to lack most of the specialized features of the class I pathway, including ZMM proteins, and most crossovers are dependent on Mus81 and exhibit little or no interference (Smith et al., 2003; Fowler et al., 2018).

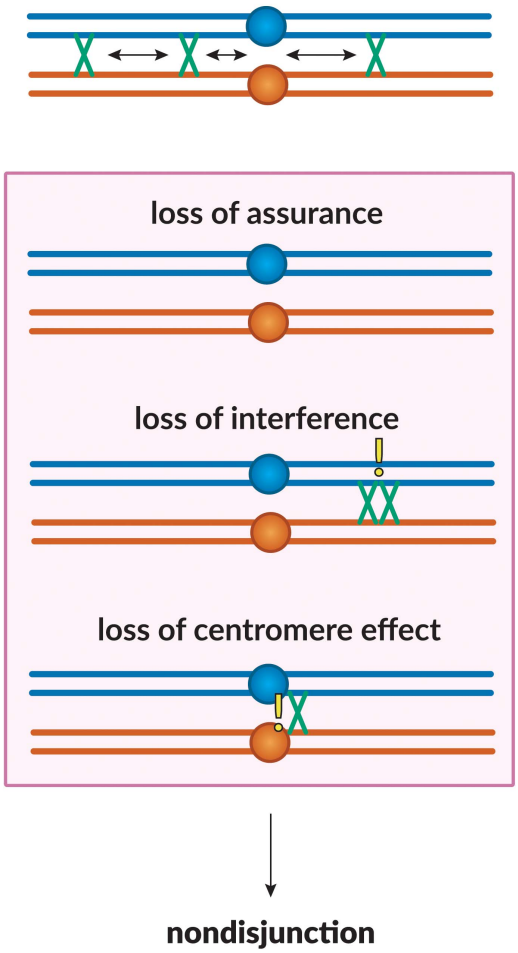

FIGURE 2 | Crossover patterning phenomena. The proper placement of crossovers along the chomosome is governed by three patterning phenomena. Homologous chromosomes are shown in blue and orange, with crossovers between them shown in green. Loss of assurance results in a lack of crossing-over between a pair of homologs; loss of interference results in two crossovers being placed in close proximity to one another; loss of the centromere effect results in centromere-proximal crossovers. These phenomena can lead to a failure in proper chromosome segregation, leading to non-disjunction.

Measures of Interference

Interference can be measured based on genetic distance (recombination frequencies between genetic loci) or physical distance (chromosome axis length or distance in base-pairs between crossovers from whole-genome sequencing). The main methods in use are described below.

Coefficient of Coincidence

Although development of the genetic map by Sturtevant (1913, 1915) and Bridges (1915) was integral to understanding interference, a better measure to directly measure interference was soon developed. In 1916, Muller defined coincidence as the occurrence of a crossover in each of two adjacent intervals (i.e., a double-crossover, DCO) (Muller, 1916b). Muller measured strength of interference through the ratio between the number of observed DCOs and the number of DCOs expected if the two intervals are independent (no interference). This measure is now referred to as the coefficient of coincidence (*CoC*). Interference (*I*) is represented as 1 - *CoC*. If *CoC* is one, then *I* is zero and there is no interference between the two intervals in question; if *CoC* is between zero and one there is interference between the two intervals (negative interference is also possible but not considered here). This method is often used to calculate strength of interference based on counts of crossovers in specific intervals, as in genetic studies.

Interference in Tetrads

The use of fungi as genetic model organisms allows recovery of all products of meiosis in tetrads or octads, making it possible to calculate interference with just two markers. If a strain that is heterozygous for two linked markers, say *A B* on one homolog and *a b* on the other, goes through meiosis to produce a tetrad with four spores, three outcomes are possible. Parental ditype (two *A B* spores and two *a b* spores) results when there has not been a crossover between the two loci or a 2-strand DCO (**Figure 3**). Non-parental ditype (two *A b* spores and two *a B* spores) results from a 4-strand DCO, and tetratype (*A B, A b, a B, a b*) results from a single crossover or a 3-strand DCO. Papazian (1952) developed a simple equation to calculate interference from the observed numbers of each class. Although widely used, these formulas are applicable only to datasets within certain parameters, and determining statistical significance between datasets if difficult. Stahl (2008) published a method termed "The Better Way," that overcomes these limitations.

Cytological Measures of Interference

Chiasma interference has been measured cytologically in humans and other organisms. Hulten (1974) measured the length of each chromosome and counted chiasmata in chromosome spreads of a human testicular sample. Hulten (1974) mapped the distribution of chiasmata on chromosome arms and determined interference based on the mean crossover count compared to the variance of the data. Jones (1984) noted that this measurement is flawed in that it does not consider the position of crossovers along the chromosome. He expanded on this approach by arbitrarily dividing the chromosome arms into even intervals to calculate *CoC* using chiasmata from cytological data. Hulten later developed the Chiasma Interference Map (CHIM), in which chiasmata are marked along the chromosome and chiasmata that occurred on the same chromosome are joined by a loop. The strength of interference can be visualized via the size and quantity of the loops relative to the total number of chiasmata, with longer loops indicating stronger interference (Hulten, 2011).

Fluorescence microscopy allows measurement of interference based on other cytological markers. MLH1 marks sites of crossovers in mammalian meiosis, and distances between foci along a bivalent can be used to estimate interference (Froenicke et al., 2002). Zip3 has been used as a similar marker in budding yeast (Zhang et al., 2014b). These measurements of interference are unique in counting only class I crossovers,

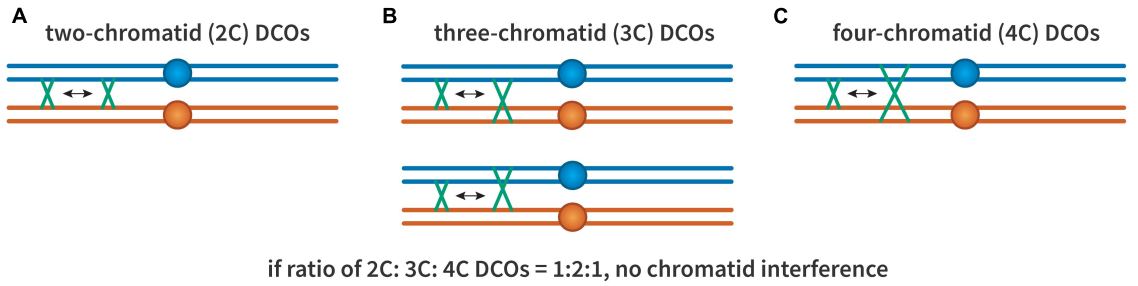

FIGURE 3 | Chromatid interference. Each panel illustrates two crossovers on one bivalent, with each line representing one double-stranded DNA chromatid. The first (leftmost) crossover is the same in all cases, occurring between the two inner chromatids. **(A)** A 2-chromatid DCO. **(B)** Two possible 3-chromatid DCO configurations. **(C)** A 4-chromatid DCO. If there is no chromatid interference, the ratio of 2:3:4 should be 1:2:1.

whereas other methods include both class I and class II crossovers in calculations of interference. It is also notable that these methods mark crossover sites during pachytene, while chiasmata are apparent later, during diakinesis and metaphase I.

Measuring Interference Using Whole-Genome Sequencing

In whole-genome genotyping or sequencing, the markers (e.g., single nucleotide polymorphisms) are so dense that each interval is too small to have enough crossovers for *CoC* analysis. One method to circumvent this problem is to divide the chromosome into arbitrary intervals of equal length and use these to calculate *CoC* or to fit a gamma distribution (Broman et al., 2002; Anderson et al., 2015). Another is to compare the average distance between crossovers on chromosomes with multiple crossovers (Miller et al., 2016).

Modeling Interference Data

A more recent way to compare interference between datasets is to make use of computational models that simulate interference, such as the beam-film model (discussed below) (White et al., 2017). The beam-film program can fit experimental data to a model and contains a parameter (L) that reflects the strength of interference.

It should be noted that these methods differ in profound ways. Chromosome length is measured in recombination frequency in the genetic methods, in meiotic chromosome axis length in cytological methods, and in DNA sequence length in sequence-based methods. Also, counting of MLH1 or Zip1 foci includes only class I crossovers, but other methods include both class I and class II crossovers. The beam-film model can accommodate date from genetic, cytological, or sequence studies, and has a parameter to include class II crossovers.

Factors Influencing Interference

Temperature

The influence of temperature on crossover frequencies was first studied by Plough, Stern, and Graubard in the early 20th century (Plough, 1917a,b; Stern, 1926; Graubard, 1934). Schweitzer (1935) analyzed Graubard's data and concluded that temperature does not affect interference in *Drosophila*, and that the average distance between two crossovers does not change at different temperatures. However, a more recent study in *A. thaliana* showed that increased temperatures lead to an increase in overall crossover frequencies through the formation of additional class I crossovers, suggesting that physical measures of interference are decreasing (De Storme and Geelen, 2020).

Chromosome Size

Small chromosomes exhibit higher rates of crossing over per physical unit than larger chromosomes (Kaback et al., 1989; Mortimer et al., 1989; Riles et al., 1993), and the smallest chromosome in *S. cerevisiae* shows increased recombination when split into two smaller segments (Link and Olson, 1991). Kaback et al. (1999) observed that interference increased with the size of the chromosome. Intervals of the same cytological length showed greater interference when relocated to larger chromosomes, leading the authors to conclude that the size dependency of meiotic recombination rates is mediated at least in part by crossover interference. Kaback et al. (1999) hypothesized that the recombination machinery initiates crossover formation on larger chromosomes earlier than on smaller ones because they are larger targets. This leads to an interference signal "spreading" along the chromosome on either side of the crossover, rendering many areas of the larger chromosomes unable to form another crossover and leading to smaller chromosomes having less competition for the recombination machinery. The authors proposed that when interference begins to act on larger chromosomes there is more of some rate-limiting component available per unit of recombination-proficient DNA. This results in the remaining rate-limiting component promoting crossing over at greater rates on smaller chromosomes. Thus, the size dependency of recombination rates is explained by larger chromosomes initiating crossing over earlier and having longer interference tracts. Many rate-limiting factors in the recombination machinery have been identified (Reynolds et al., 2013; Qiao et al., 2014; Ziolkowski et al., 2017; He et al., 2020).

In contradiction to this hypothesis, Stahl et al. (2004) showed that shorter chromosomes had more class II crossovers than longer chromosomes, suggesting that the chromosomal size dependence of recombination rates isn't due to changes in the strength of interference, but is instead due to a difference in the proportion of class I versus class II crossovers.

More recently, Murakami et al. (2020) have shown that in short chromosomes of budding yeast there is a greater recruitment of DSB proteins, indicating a higher density of DSBs. Their data also showed that shorter chromosomes tend to stay in a DSB-competent state for longer; however, no inferences can be made about how this may affect the process of interference in these chromosomes, as it is possible, based on the study by Stahl et al. (2004) that the extra DSBs are being repaired as class II crossovers.

Synaptonemal Complex

The synaptonemal complex (SC) was first suggested to be important for crossover interference when it was reported that *Aspergillus nidulans* and *S. pombe*, two organisms that do not have an SC, also do not exhibit interference (Moens, 1969; Snow, 1979; Egel-Mitani et al., 1982; Bähler et al., 1993; Munz, 1994). Concomitant defects in interference and synapsis were also seen in *as1* and *asb* mutants in tomato (Moens, 1969; Havekes et al., 1994). Further, organisms heterozygous for chromosomal translocations do not display interference in the region of the rearrangement, where SC continuity is presumably disrupted (Arana et al., 1987; Parker, 1987).

Studies in budding yeast suggest that the relationship between SC and interference is more complex. Zip1 is a component of the SC, and *zip1* mutants fail to build SC (Sym et al., 1993). Based on tetrad analysis in *zip1* mutants, Sym and Roeder (Sym and Roeder, 1994) concluded that interference requires the SC, and suggested that Zip1 could be the polymer that diffuses outward from crossover sites as in the model polymerization model proposed by King and Mortimer (see below). This requirement of Zip1 and its orthologs for crossover interference has also been shown by numerous other studies (Hayashi et al., 2010; Libuda et al., 2013; Duroc et al., 2014; Voelkel-Meiman et al., 2015; Rog et al., 2017; Capilla-Perez et al., 2021). However, it is important to note that since Zip1 mutants are defective in class I crossover formation, the apparent reduction in interference may be due to the remaining crossovers being class II. Chua and Roeder (1997) further supported the idea that the SC plays a role in interference when they showed that budding yeast mutants lacking the telomere-associated meiotic protein TAM1, also known as Ndj1 and required for telomeric clustering during prophase I as well as proper homolog pairing and disjunction (Conrad et al., 1997; Trelles-Sticken et al., 2000), had defects in both chromosome synapsis and crossover interference. They attributed this to TAM1 playing a role in homolog pairing, leading to defects in alignment and synapsis.

In contrast, Fung et al. (2004) observed that synapsis initiation complexes (SIC), identified as Zip2 foci, exhibit interference, suggesting that crossing over happens at these initiation sites, as had been suggested earlier by Egel (1978). Since SICs assemble prior to SC formation and are still present in a *zip1* mutant where SC is absent, Fung et al. (2004) concluded that interference in budding yeast can act independently of synapsis. This independence has also been shown in *Sordaria* (Zickler et al., 1992). A 2006 study showed substantial interference between MSH4 foci in mice with defective SCs, although the data did not allow determination of whether MLH1 foci interfere in the absence of the SC (de Boer et al., 2006). It is also important to note that *zip1* mutants often undergo delays in prophase (Sym et al., 1993), which may be true in the *tam1* mutant as well, suggesting that the SC's apparent role in interference could be due to cell cycle defects. Thus, the role of the synaptonemal complex in interference remains enigmatic.

Interference Models

Since the discovery of crossover interference, several models have been proposed to describe this phenomenon. We briefly describe the most influential models below, in chronological order; additional discussions can be found in Berchowitz and Copenhaver (2010) and Otto and Payseur (2019).

Polymerization Model

The polymerization model proposed by King and Mortimer (King and Mortimer, 1990) hypothesized that early recombination structures are randomly distributed across the chromosome, and that once crossing over is initiated at the positions where these structures attach, a polymerization reaction is triggered which would then inhibit crossovers in neighboring regions by preventing the binding of other early structures to the SC. This polymerization reaction extends bidirectionally from each crossover site, explaining why interference decreases with distance from the original crossover. King and Mortimer also put forth a computational simulation of the model that they were able to fit well to *Drosophila* and budding yeast crossover data. While no polymer has been identified that fits this model, it agrees well with an earlier interference model proposed by Egel (1978) suggesting that crossover interference is a result of synapsis. Maguire (1977) put forth the idea that establishment of crossover sites may occur before synapsis is initiated, and that while the SC may be important for the process of crossing over, its "deployment" along the chromosome may have another function. Based on her arguments, Egel argued that if crossover sites are formed before synapsis and are also points of nucleation for the SC, it is this formation and zippering of the SC that prevents crossovers in neighboring sites. According to this model, crossovers cannot form in chromosomal regions that have already synapsed, and only regions that are yet to synapse retain the ability to form a crossover (Maguire, 1977).

This model would seem to be incompatible with interference in *Drosophila* and *C. elegans*, where SC appears to be complete before recombination is initiated (Dernburg et al., 1998; McKim et al., 1998). However, the SC is not a static structure. This was first recognized in the phenomenon of synaptic adjustment, wherein rearranged chromosomes that have different lengths initially appear to synapse based on homology, but then adjust so that the two chromosomes in each bivalent are equal lengths (reviewed in Moses et al., 1984). Studies in *C. elegans* found that crossovers locally alter SC, possibly to a form that is not permissive to additional crossovers (Libuda et al., 2013; Machovina et al., 2016). As discussed by Otto and Payseur (2019), these observations fit well with the proposal that interference propagates through the SC.

Counting Model

Like earlier models of interference based on a renewal process, Foss et al. (1993) proposed a model in which

recombination intermediates that are randomly distributed along the chromosome can either become crossovers or non-crossovers, but intermediates are "counted" by a recombinase in such a way that two crossovers need to be separated by a certain number of non-crossovers. Although unable to explain interference data in *S. cerevisiae* (Foss and Stahl, 1995), a mathematic implementation of the counting model fit satisfactorily when tested against crossover data from other species and incorporated class II crossovers (Copenhaver et al., 2002; Housworth and Stahl, 2003; Stahl et al., 2004).

Beam-Film Model

The beam-film model of Kleckner et al. (2004) proposes that chromosomes behave like elastic beams covered on one face by a thin film that has flaws along its edges. When the chromosome is subjected to forces that cause the beam to expand, it does so to a greater degree than the film. This leads to the stretching of the film, which puts mechanical stress on it, resulting in the flaws cracking. When a crack is formed at one of the flaws, tensile stress in neighboring regions is relieved, with the release dissipating for some distance. Cracks may still occur at flaws on the film that are outside the reach of the stress relief perpetuating from the initial crack. This is applied to meiotic recombination by considering crossover precursors, such as DSBs or other intermediates, as the flaws on the film, with those that crack under mechanical stress being designated to become crossovers. Interference is explained by a crossover being able to prevent others in its vicinity by relieving the tensile stress on nearby flaws, consequently preventing them from cracking as well. A mathematical model based on beam-film can fit crossover distribution data from several species (Zhang et al., 2014a).

Compartmentalized Signaling Model

Studies in *C. elegans* suggested that the SC has liquid-like properties and Rog et al. (2017) proposed that this might help to explain crossover patterning. Zhang et al. (2018) showed that a set of four RING finger proteins, ZHP1-4, are part of a signaling network that functions within the SC to select early recombination intermediates for crossover designation. In *C. elegans*, there is always one crossover per pair of homologous chromosomes, so this signaling pathway designates only one crossover per compartment, with each SC being one compartment. Zhang et al. (2018) suggest that this may occur if both positive and negative activities within the SC to set up a wave of crossover designation potential.

Spatial Cluster Model

Fowler et al. (2018) proposed a model for crossover interference through DSB interference, in which DSB hotspots cluster within a chromosomal region of approximately 200 kb, with a limit of one DSB per cluster. This model fits the distance dependency of interference, as longer distances are more likely to span multiple clusters that act independently. However, this model seems to suggest that non-crossovers are also subject to interference, which does not appear to be the case (e.g., Miller et al., 2016). Additionally, since DSBs within each cluster are formed randomly, this model would suggest that crossovers forming at the boundaries of two neighboring clusters would not interfere. Another criticism of this model has been that it is based on studies in *S. pombe*, an organism in which interference had been reported to be absent (Mortimer and Fogel, 1974; Munz, 1994; Fowler et al., 2018). Fowler et al. (2018) provide evidence for weak crossover interference and suggest that interference in *S. pombe* occurs through clusters encompassing only one homolog instead of both, implying that clusters are distributed independently along each homolog, leading to efficient DSB interference without crossover interference.

Mutations That Disrupt Interference

Genetic studies have identified many mutations that have an apparent effect on interference, but interpretation of these is often complicated. First, changes in interference would be expected to be inversely correlated with crossover number (e.g., weaker interference would be expected to increase crossover number), but changes in crossover number can occur without changes in interference. One important way this can happen is through loss of class I crossovers or increase in class II crossovers. Indeed, many mutations that appear to alter interference affect the absolute or relative numbers of class I and class II.

A good example is the *sgs1* mutant of *S. cerevisiae*. Oh et al. (2007) reported that crossover interference is reduced in *sgs1* mutants, which might be interpreted as evidence that Sgs1 plays a role in establishing interference; however, Zip2 foci, which mark sites designated to become class I crossovers, are normal in *sgs1* mutants, suggesting that normal interference is established (Fung et al., 2004). The solution to this apparent paradox came from subsequent studies that revealed that all crossovers in *sgs1* mutants require structure-selective endonucleases other than MutLγ (De Muyt et al., 2012; Zakharyevich et al., 2012). Thus, designation of crossover sites may occur normally, with interference, but maturation of these into crossovers is defective. Unlike MutLγ, other structure-selective endonucleases are not biased toward crossover resolution. This should result in a twofold decrease in class I crossovers. At the same time, loss of the anti-crossover activity of Sgs1 in the class II pathway results in an increase in those crossovers. Therefore, the reduction in interference reported by Oh et al. (2007) does not reveal a role for Sgs1 in the process of interference, but rather a change in ability to complete formation of class I crossovers combined with an increase in class II crossovers.

One protein that does appear to have a direct role in interference is Topoisomerase II in *S. cerevisiae*. Zhang et al. (2014b) analyzed distances between Zip3 foci in *top2* mutants and found that they were decreased relative to wild type, while total Zip3 foci were increased in the mutants. They hypothesized that topoisomerase II is required to relieve torsional stress at the site of crossovers. SUMOylation of Top2 by Ubc9 and subsequent ubiquitination by Slx5/8 is required for this function, and absence of Slx5 or Slx8 yields the same phenotype as in *top2* mutants. The sirtuin Sir2 physically interacts with Slx5/8 and activates its SUMO-targeted ubiquitin ligase (STUbL) activity to perform ubiquitination, and is also required for interference, as is Red1, another substrate of Ubc9.

CROSSOVER ASSURANCE

History

In most organisms, achiasmate chromosomes are rare (Hillers and Villeneuve, 2003). The first observation that all chromosomes exhibit at least one chiasma was made by Darlington and Dark (1932). They studied recombination in a grasshopper species with large variations in chromosome size. If crossovers were distributed randomly among the genome, smaller chromosomes would be less likely to experience at least one crossover, while larger chromosomes would be more likely to experience multiple crossovers. However, Darlington and Dark found that all chromosomes had at least one chiasma, indicating that there is a process that ensures at least one inter-homolog crossover on all chromosomes. Darlington hypothesized that chiasmata must be important for proper segregation of chromosomes (Darlington, 1937). Mather (1937) also graphed the number of chiasmata as a function of chromosome length and showed a minimum of one chiasma regardless of how short a chromosome is. He noted that the first chiasma is formed "irrespective of the length of the chromosome" and that additional chiasmata, if any, are subject to interference.

Another observation of assurance was made by Owen (1949). Callan and Montalenti (1947) studied the mosquito *Culex pipiens* and found what they interpreted as evidence for interference between intervals on different chromosome arms. This was unexpected, as interference between intervals separated by the centromere had not been found in any organisms prior. Owen reanalyzed their data and determined that interference need not cross the centromere in *Culex* if it is assumed that formation of a first crossover per bivalent is more favored than formation of subsequent crossovers. He defined this as a "primary chiasma" or "obligatory chiasma," and reasoned that it is not on the same footing with other chiasmata, as it is required for synapsis and proper chromosome segregation. The reason behind the apparent cross-centromere interference in *Culex* was the short chromosome arms in this organism, resulting in bivalents that frequently had just one crossover, making it appear as if that crossover suppresses crossovers on the other arm. Owen's interpretation held for an additional mosquito species studied by Callan and Montalenti, *Theobaldia longiareolata,* in which apparent cross-centromere interference was not observed due to its longer chromosome arms with a greater average number of chiasmata per bivalent. Jones (1984), noting that the distribution of chiasmata between chromosomes of similar sizes is more dispersed than would be expected if events were placed randomly, suggested that the lack of achiasmate chromosomes or univalents indicates that there must be one obligate chiasma per bivalent.

The Obligate Crossover

The function of the crossover assurance mechanism is to ensure the generation of at least one crossover per bivalent. In recombination-dependent meiotic programs, a crossover is required between each pair of homologs to ensure a chiasma that will promote proper chromosome segregation at the end of meiosis I (Darlington, 1937; Hawley, 1988). A dramatic example of how crossovers promote segregation comes from studies of mammalian sex chromosomes. Koller and Darlington (1934) found that an obligate crossover was always formed between the *X* and *Y* chromosomes in rat. This conclusion was disputed for several decades due to the observation that in most mammals the *X* and *Y* associate end-to-end and do not exhibit visible chiasmata. However, Burgoyne (1982) later discovered via electron microscopy that a very distal chiasma forms between the *X* and *Y* to promote pairing. Burgoyne proposed an "*X*–*Y* crossover model" that suggests that there is a region of genetic homology between the *X* and *Y* chromosome (the "pseudoautosomal region") in mammals that must experience an obligatory crossover during meiosis for proper chromosome segregation. All genes distal to the obligate crossover will be transmitted to both male and female offspring, behaving in pedigrees like autosomal genes.

The obligate crossover between the *X* and *Y* chromosomes must occur proximal to the sex determining region of the *Y* chromosome, *Sry*, which activates the male transcriptional program. Ashley (1994) used fluorescence *in situ* hybridization (FISH) to study how the *X* and *Y* chromosomes segregate into sperm, and determined that aneuploid products were infrequent, indicating that spermatocytes that experience *XY* non-disjunction fail to progress and differentiate into sperm. Hinch et al. (2014) later confirmed that PRDM9 binding sites, which coincide with recombination hotspots, are found in the human pseudoautosomal region between the *X* and *Y* chromosomes, *PAR1*. Intriguingly, recombination appears to drive sequence evolution more strongly in the pseudoautosomal region than on the autosomes. Recently, Papanikos et al. (2019) found that mouse ANKRD31 is essential to promoting double-strand break assurance, especially in the pseudoautosomal region. ANKRD31 deficiency leads to loss of an obligate crossover between the *X* and *Y* chromosome as well as consequent chromosome missegregation.

Exceptions to the requirement for an obligate crossover are seen in *Drosophila*, in which the X chromosomes do not experience a crossover in 10–15% of meioses and chromosome *4* never has crossovers. Nonetheless, these chromosomes segregate correctly in >99% of meioses due to an achiasmate segregation system (Hawley and Theurkauf, 1993), though the *X* still segregates with higher fidelity when it has at least one crossover (Koehler et al., 1996a).

Mechanisms of Assurance

Crossover assurance is enforced on multiple levels (**Figure 4**): assurance that sufficient DSBs are formed to generate an obligate crossover per chromosome, assurance of inter-homolog recombination bias, and assurance that a crossover is implemented by enforcing pro-crossover recombination pathways. These mechanisms are covered below.

Double-Strand Break Assurance

Meiotic DSBs are formed in excess relative to crossovers, likely to ensure that at least one crossover will be formed per homolog pair. A crossover assurance checkpoint involving the paralogs DSB-1 and DSB-2 was identified in *C. elegans* (Stamper et al.,

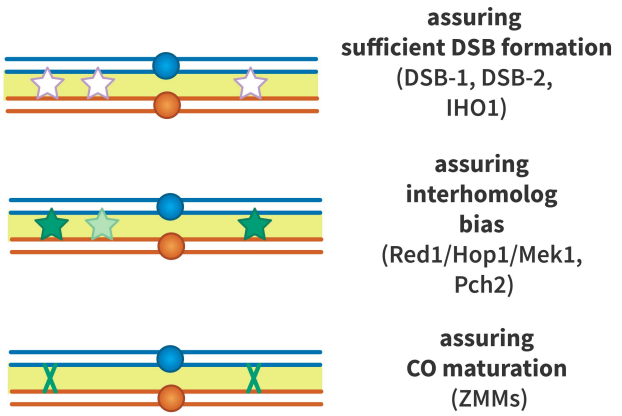

FIGURE 4 | Levels of crossover assurance. Assurance is enforced at three levels. DSB-1 and DSB-2 form a checkpoint in *C. elegans* that ensures that sufficient double-strand breaks (DSBs, white stars) are formed to generate an obligate crossover. In mouse, IHO1 plays a similar role. From this pool of DSBs, inter-homolog recombination is promoted by Red1, Hop1, Mek1, and Pch2 to ensure that recombination intermediates (light green stars) engage with the homologous chromosome to form crossover precursors (dark green stars). The driving force to generate crossover precursors may be aggregation of ZMM proteins at recombination nodules or mechanical stress that must be relieved by crossover formation. Efficient crossover maturation (dark green X) is ensured by the ZMM proteins that define the class I crossover pathway.

2013). DSB-1 localizes to chromosomes during the time of DSB formation. When crossover formation is impaired, DSB-1 persists on chromosomes, suggesting that the time in which DSB formation is permitted is extended in *dsb-1* mutants. Failure to form an obligate crossover is sufficient for this phenotype to appear. DSB-2 similarly localizes to chromatin as DSBs form and disappears as RAD-51 foci appear, which mark early recombination intermediates. Association of DSB-2 with chromosomes is dependent on phosphorylation of the SUN domain protein SUN-1 and loading of RAD-51 at DSBs. Like DSB-1, DSB-2 persists on chromosomes when DSBs fail to form or recombination intermediates are not repaired (Rosu et al., 2013).

Double-strand breaks numbers are modulated by at least four different pathways in mouse (Dereli et al., 2021). DSBs regulate the number of SPO11-auxiliary protein complexes by activating the DNA damage response kinase ATM. DSBs additionally reduce IHO1 in their direct vicinity. IHO1 (homolog of yeast Mer2), a HORMAD1-interacting protein and SPO11 auxiliary protein, forms a chromatin-binding complex with MEI4 and REC114 that is required for DSB formation in mice (Dereli et al., 2021). In mice, DSB-dependent homologous recombination facilitates pairing and synapsis, which results in loss of IHO1, HORMAD1 and SPO11 complexes (Dereli et al., 2021). Lastly, DSBs along with the DNA damage response kinases ATM, ATR and PRKDC globally deplete IHO1 from chromosome axes. These pathways likely act to ensure that sufficient DSBs are generated to make an obligate crossover without creating a vast surplus of DSBs that threaten genomic integrity.

Double-strand break formation in yeast is regulated to ensure recombination on shorter chromosomes. The Spo11 accessory proteins Rec114 and Mer2 associate earlier and dissociate later from short chromosomes compared to longer chromosomes (Murakami et al., 2020). The mechanism that promotes this bias toward short chromosomes is unclear, but Rec114 and Mer2 accumulation are influenced by replication timing, while their dissociation is triggered by homolog pairing. ZMM-mutant budding yeast also generate higher numbers of DSBs than wild-type, and this control of DSB number is genetically separable from the pathway that connects DSB formation to meiotic progression (Thacker et al., 2014). These results suggest that homolog pairing, mediated by ZMM proteins, reduces DSB formation to prevent unproductive DSBs between paired homologs that are already engaging in inter-homolog recombination.

Inter-Homolog Strand Exchange Bias

An obligate crossover must occur between homologous chromosomes to ensure proper chromosome segregation. Mechanisms that promote inter-homolog recombination over recombination between sister chromatids have been described. In yeast, Hop1 and Red1 function structurally in axial/lateral elements and function jointly with Mek1 to enforce a barrier to inter-sister recombination. The chromosome axis protein Hop1 is phosphorylated in response to DSBs, and then triggers dimerization of the meiosis-specific kinase Mek1, which phosphorylates proteins that limit inter-sister recombination (Niu et al., 2005, 2007). One target of Mek1 is Hed1, a meiosis-specific protein that binds Rad51 and suppresses its activity (Tsubouchi and Roeder, 2006; Busygina et al., 2008). Mek1 also phosphorylates the Rad51 binding partner Rad54, reducing Rad51's activity (Niu et al., 2009). In organisms that use the meiosis-specific strand exchange protein Dmc1, Dmc1 is required for interhomolog bias (Brown et al., 2015), and thus Rad51 activity is inhibited to allow Dmc1 to function as the major meiotic strand exchange protein (Callender et al., 2016).

Pch2 is a highly conserved ATPase that has been implicated in many processes in meiosis. In yeast, Pch2 has been found to control association between Zip3, which localizes to crossover precursors, and the chromosome axis proteins Hop1/Red1. Although Pch2 is not required to generate crossovers at normal levels, *pch2* mutants appear to have reduced interference and lack crossover assurance (Chakraborty et al., 2017). Joshi et al. (2009) suggested that Pch2 remodels the chromosome axis into an array of crossover control modules that interact over a long range to ensure that there is an obligate chiasma and that crossovers are maximally spaced. *C. elegans pch-2* mutants lose access to recombination with the homologous chromosome early, suggesting that PCH-2 is required to maintain interhomolog recombination bias (Deshong et al., 2014).

Robust Crossover Designation and Maturation

Shinohara et al. (2008) studied null mutants of the ZMM gene *SPO16* and found that, while crossovers are reduced in these mutants, the residual crossovers that are observed display

interference. Furthermore, Spo16 interacts with Zip4 via co-immunoprecipitation, and assembly of Spo16 foci depends on Zip1 and Zip3, but not on Msh4. Shinohara et al. proposed that the ZMMs may consist of two sub-assemblies: one that enforces interference by stabilizing crossover precursors at the DNA level, and one that promotes crossovers at these sites to generate assurance.

In mouse, the E3 ligases RNF212 and HEI10 generate crossovers by SUMOylating recombination proteins (Reynolds et al., 2013; Qiao et al., 2014). These factors are thought to act as a checkpoint that pauses recombination by altering the turnover time of meiotic recombination proteins such as DMC1 and MutSγ. This may stall intermediates at an early step in recombination to ensure that the appropriate pro-crossover factors are present to establish crossover designation (Prasada Rao et al., 2017).

In *C. elegans*, DSBs are preferentially repaired as COs in the absence of inhibitory effects from other recombination precursors (Rosu et al., 2011). Rosu et al. (2011) used excision of the *Mos1* transposon to make a targeted DSB in *spo-11* mutants, in which no meiotic breaks are formed. They found that nearly all interhomolog repair events in these mutants were COs.

Cytoskeletal forces have also been shown to promote synapsis, recombination, and crossover assurance through signaling via SUN- and KASH-domain proteins. In *Arabidopsis*, the kinesin AtPSS1 is required for crossover assurance (Duroc et al., 2014). In *Atpss1* mutants, some chromosomes lack an obligate crossover, while the number of total meiotic crossovers is comparable to wild type. This kinesin directly interacts with the KASH-domain proteins WIP1 and WIP2. Ndj1/Tam1, a protein that tethers telomeres to the nuclear envelope, stabilizes interactions between homologous chromosomes and thus may promote inter-homolog recombination (Conrad et al., 1997; Chua and Roeder, 1997).

In addition to crossover designation, it is important to ensure effective crossover maturation to generate the obligate crossover. Wang et al. (2017) modeled human oogenesis using the beam-film framework and found that a lower crossover maturation efficiency could explain the higher number of achiasmate bivalents in oocytes.

CROSSOVER SUPPRESSION

History

The final patterning event we will discuss is crossover suppression associated with specific chromosomal features. Most notably, suppression occurs both in the pericentromeric region and telomeric regions. Centromeric suppression is thought to be crucial for proper chromosome segregation in humans, budding yeast, fission yeast, and *D. melanogaster* (Koehler et al., 1996a; Lamb et al., 1996; Rockmill et al., 2006; Smith and Nambiar, 2020). Two models have been proposed to explain how proximal crossovers promote non-disjunction (Orr-Weaver, 1996). First, proximal crossovers may disrupt sister-chromatid cohesion at the centromere. Since proximal cohesion needs to be maintained until separation of sisters at anaphase II, disruption may lead to premature separation of sister chromatids (PSSC). The second model is the converse: Because proximal cohesion is not released at anaphase I, a proximal crossover causes the homologs to become entangled, resulting in both segregating to the same daughter. One or both suggestions may account for the existence of mechanisms that reduce or eliminate centromere-proximal crossovers. It may be that disruption of cohesion and PSSC is more important in organisms with point centromeres and relatively small regions of pericentromeric cohesion, but entanglement is more of a risk in organisms in which centromeres are embedded in large blocks of heterochromatin are more expansive pericentromeric cohesion.

The first observation of centromere-proximal crossover suppression, now known as the centromere effect, was made by Beadle (1932), when he observed a decrease in crossing over in medial regions of a *Drosophila* chromosome when they were moved closer to the centromere in a translocation stock. Beadle studied a translocation that attached the right half of *3R* to the centromere (or "spindle fiber" as he called it) of chromosome *4*. In homozygous translocation flies, the percent crossing over in the intervals now closest to the *4* centromere dropped dramatically, while crossing over within more distant intervals was not affected. Beadle concluded that the decrease in crossovers in these two regions was a result of them having been moved closer to the chromosome *4* centromere.

In a 1936 review, Mather presented more evidence for the idea that the centromere exerts control over the distribution of crossing over (Mather, 1936). He used recombination data from other researchers to show that while genetic loci are well spaced out in the middle of the chromosome (as in the case of the telocentric *X*) or chromosome arm (as in the case of metacentric *2* and *3*), a clear crowding of loci can be seen around the centromere. This is indicative of low recombination frequency near the centromere, which led Mather to speculate that crossing over in a particular region is a function of its distance from the centromere.

Factors Influencing the Centromere Effect

Temperature

Harold Plough was the first to study the effects of environmental changes on crossing over (Plough, 1917a). His data showed that while starvation and food type did not affect crossover frequencies in *Drosophila*, temperature did. When studying the regions between chromosome *2* markers close to and flanking the centromere, he observed an increase in crossover percentages at both higher (31 C) and lower (13 C) temperatures, which he attributed to a physical change that was occurring in chromatin structure. This increase in centromere-proximal crossover frequencies at high temperatures was later shown to hold for chromosomes *1* and *3* as well (Plough, 1921; Stern, 1926). Mather (1939) showed that heterochromatin was responsible for crossing over being highly sensitive to temperature, and speculated that variations caused by other environmental factors could also be a result of their effect on heterochromatin. A more recent study also found that increasing temperature leads to

an increase in proximal crossovers in barley, a species in which crossovers are primarily distal under typical temperature conditions (Phillips et al., 2015).

Maternal Age

Bridges (1915) showed that maternal age can influence crossing over in *Drosophila* when he observed that older females showed a decrease in pericentromeric crossover percentages on chromosome *2*. Later, he showed that this decrease was most drastic in the center of metacentric chromosome *3*, decreasing as loci further from the centromere were considered (Bridges, 1927). Thus, Bridges showed in 1915, nearly two decades before Beadle's data on suppression of crossing over near the centromere, that crossover percentages between centromere-proximal markers were as low as 5%. Although it would have been impossible for Bridges to have noticed this centromere-proximal reduction in crossing over as he had no knowledge of the physical distances between these markers, this data is possibly the first evidence of the centromere effect.

Heterochromatin

Mather (1939) studied how both the centromere and heterochromatin influenced crossing over in the *Drosophila X* chromosome using various inversion stocks in which markers that were ordinarily centromere proximal were moved to more distal positions and *vice versa*. His results led him to confirm his earlier belief that crossover frequencies in euchromatic regions are dependent on their distance from the centromere. Mather also observed some amount of crossing over in heterochromatic regions that had been moved farther away from the centromere and speculated that these levels may also be dependent on distance from the centromere. Baker (1958) did not agree with these findings, and thought that the crossovers Mather reported were most likely in adjacent euchromatin since the markers he'd used did not delineate heterochromatin very precisely. Baker supported this claim by showing virtually no crossing over in a *Drosophila virilis* stock in which a large chunk of chromosome *5* heterochromatin had been moved to the tip of chromosome *3* via reciprocal translocation. Since then, it has been widely believed that crossing over in heterochromatic regions is uncommon, if not absent (Carpenter and Baker, 1982; Szauter, 1984). It was also thought that pericentromeric heterochromatin was causing crossover suppression near the centromere, possibly by restricting access to recombination proteins (Westphal and Reuter, 2002), as structural differences in the synaptonemal complex are seen in the two types of chromatin (Carpenter, 1975; Stack, 1984).

Westphal and Reuter (2002), investigated the role of chromatin in centromeric crossover suppression by studying the effects of dominant suppressor-of-variegation mutations on crossover frequencies. These mutations are thought to cause changes in heterochromatin structure, consequently leading to suppression of heterochromatin-mediated gene silencing. The authors hypothesized that this may result in a change in crossover patterning in heterochromatin as well as flanking euchromatin. In support of this hypothesis, of the 46 mutations they tested, 16 increased crossing over in pericentromeric heterochromatin. A 2012 study in *A. thaliana* also showed the same dependence of crossover frequency on chromatin states, when a DNA hypomethylated mutant that showed pericentromeric transcriptional activity also showed an increase in centromere proximal crossovers (Yelina et al., 2012). However, this study, along with others that looked at hypomethylated *Arabidopsis* mutants, observed no change in crossover suppression in pericentromeric regions (Colomé-Tatché et al., 2012; Melamed-Bessudo and Levy, 2012; Mirouze et al., 2012). This was a surprising result as pericentric heterochromatin is hypermethylated in wild-type plants and would have been expected to show increased rates of recombination under conditions of DNA methylation loss. The authors of these studies propose that lowering DNA methylation levels may be making chromatin that is already open further accessible to crossover formation.

Despite considerable evidence that heterochromatin plays an important role in suppressing centromere-proximal crossovers, there is also support for the hypothesis that distance from the centromere is just as, if not more, critical. Mather (1939) showed in *Drosophila* that a euchromatic interval moved farther from the centromere but closer to a larger length of heterochromatin showed less crossover suppression than an interval moved closer to the centromere but near a smaller length of heterochromatin. He concluded from this that the centromere fiber effect is more a consequence of centric action than proximity to heterochromatin. Lindsley and Sandler (1977) showed that despite having the largest amount of pericentromeric heterochromatin, the *Drosophila X* chromosome had significantly higher crossing over in proximal euchromatin than either autosome. Their data also suggested that the centromere effects of each chromosome in *Drosophila* remained roughly the same despite them having different amounts of heterochromatin. This has been corroborated by Yamamoto and Miklos (1978), who also showed that crossing over in the proximal euchromatin of *Drosophila X* chromosomes with varying extents of heterochromatin deletions depended more on the distance from the centromere than on amount of heterochromatin. They suggested that heterochromatin acts only as a passive spacer between the centromere and euchromatin, implying that chromosome structure and mechanics, as well as DNA content, would be crucial in defining the centromere's control over crossing over in an organism. However, they decidedly acknowledge that when combined with other data on recombination being genetically controlled (Catcheside, 1977; Lindsley and Sandler, 1977), crossover suppression near the centromere appears to be mediated by a complex system with multiple facets of control.

More recently, Hartmann et al. (2019) observed that when a large block of heterochromatin was inserted into chromosome *2R* of *Drosophila,* there was no significant crossover suppression in adjacent intervals, suggesting that the centromere effect does not arise from an innate property of heterochromatin. They also went on to show that pericentromeric crossover suppression seems to be through two mechanisms: complete suppression in the densely staining, highly repetitive alpha heterochromatin, and the centromere effect that exhibits a distance-dependent suppression

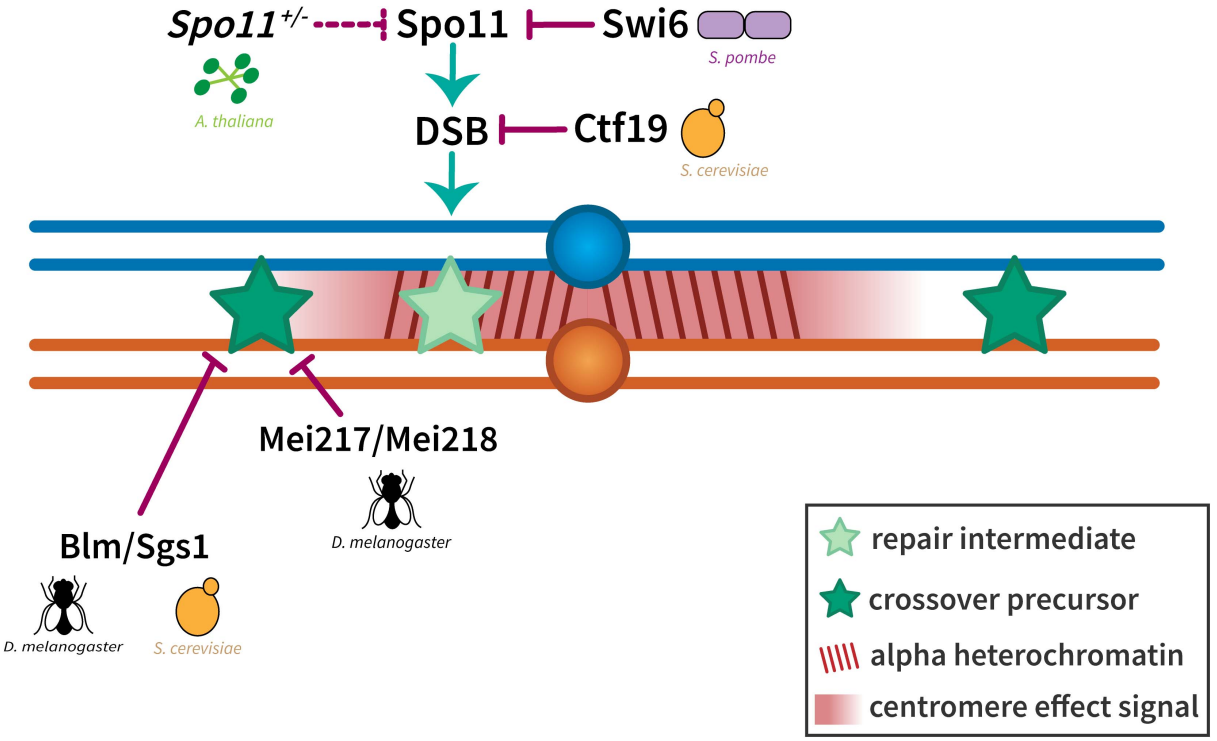

FIGURE 5 | Suppression of crossovers near the centromere. The exclusion of crossovers near the centromere seems to be enforced at two levels. Crossover suppression in the highly repetitive alpha heterochromatin has been shown to be a result of the prevention of DSBs either through local chromatin organization (in *S. cerevisiae*) or the inactivation of Spo11 (in *S. pombe* and *A. thaliana*). Crossover suppression in the less repetitive beta heterochromatin and the proximal euchromatin has been shown to be regulated through Bloom syndrome helicase/Sgs1 (in *D. melanogaster* and *S. cerevisiae*) and dependent on distance from the centromere (represented by a centromere effect signal shown in red). Homologous chromosomes are shown in blue and orange with dark red lines in the pericentromeric region representing alpha heterochromatin. Light and dark green stars represent repair intermediates and crossover precursors, respectively.

that extends far into euchromatic sequences. This is consistent with Yamamoto and Miklos' conclusion that suppression of crossovers in the vicinity of the centromere has multiple causes.

Synaptonemal Complex

Carpenter (1975) observed using electron microscopy that the structure and morphology of the SC is different in the pericentromeric heterochromatin as compared to more distal regions on the chromosome that are euchromatic. This was further confirmed by her observation that the SC of the largely heterochromatic chromosome *4* in *Drosophila* usually had only heterochromatic morphology. Combined with her observation that all recombination nodules in her experiment were found in distal chromosomal regions that had euchromatic SC morphology, this raises the possibility that the SC could be mediating the centromere effect.

Stack conducted an electron microscopic study of meiotic chromosomes from mice and two angiospermous plants and showed that the SC is shorter and more under-represented in the heterochromatic regions of meiotic chromosomes, suggesting a reason for the lack of crossing over in heterochromatin (Stack, 1984). In addition to confirming Carpenter's observations of SC structure being different in euchromatin versus heterochromatin, he also showed that heterochromatic SC is more densely enclosed in compact chromatin, which he implied could sterically inhibit essential recombination enzymes from accessing it.

Mechanistic Insights Into the Centromere Effect

Although much is known about various factors influencing centromere-proximal crossover suppression, the exact mechanism behind the centromere effect is still unknown. One hypothesis is that DSB formation is suppressed near the centromere. This is supported by a 2006 study in *Drosophila* that showed that the DSB cytological marker γ-His2Av failed to colocalize with HP1, a marker for heterochromatin (Mehrotra and McKim, 2006). As colocalization was observed in irradiated flies, DSBs were believed to be excluded from heterochromatin in wild-type meiotic cells. Further support for this proposal comes from a study in *S. pombe* showing that the pericentric cohesin complex actively represses pericentric DSB formation (Nambiar and Smith, 2016) (**Figure 4**). The mechanism of action proposed involves the heterochromatin protein Swi6 recruiting Rec8-Psc3 – mitotic cohesin complex subunits – to pericentric regions. Both Swi6 and Psc3 function to keep out Rec11, a meiotic cohesin complex protein, and prevent it from binding Rec8. This ensures that Rec11 is unable to recruit linear element protein Rec10, leading to the protein

responsible for creating DSBs, Spo11, remaining inactive. This leads to the suppression of DSB formation and therefore meiotic recombination. Furthermore, the authors suggest that a molecular mechanism involving different cohesin complexes acting at pericentromeric heterochromatic regions to suppress recombination is a mechanism conserved across those species in which heterochromatin is found at the pericentromere.

Spo11 itself has been observed to play a role in crossover patterning, when a 2018 study in *Arabidopsis* determined that a Spo11 hypomorph that showed a proportional reduction in the number of DSBs along the chromosome was able to disproportionately decrease the number of crossovers in pericentromeric regions (Xue et al., 2018) (**Figure 5**). However, studies in budding yeast that mapped DSBs using whole-genome methods and ssDNA accumulation have shown that although DSBs are suppressed near the centromere, the length of chromosome along which suppression is observed, originally thought to be 20 kb (Gerton et al., 2000), and later 8–10 kb (Buhler et al., 2007), is really only 1–3 kb (Pan et al., 2011). Considerable DSB activity was seen in pericentromeric regions, including hotspots within 10 kb of the centromere (Blitzblau et al., 2007). Further support for the presence of DSBs in pericentromeric regions comes from Symington and Petes (1988), who showed, using strains that were heterozygous for restriction sites within the centromeric sequence, that there are widespread gene conversion (GC) events occurring at centromeric regions in yeast. Symington and Petes (1988) concluded that in budding yeast, the rates of centromeric gene conversion events during meiosis are similar to non-centromeric regions, and since GC events, while leading only to non-crossovers, still arise from DSB repair, these results show that DSBs are indeed formed in centromeric regions. More recently, a 2015 study threw some light on the molecular mechanism behind pericentromeric crossover suppression in budding yeast by showing that the kinetochore Ctf19 complex is important in two ways: It prevents DSB formation within a 6 kb region of the centromere and also suppresses inter-homolog recombination within the pericentromere (Vincenten et al., 2015). The authors suggest that prevention of DSB formation is through regulating recruitment of chromosomal axis proteins/local chromatin organization, and that crossover suppression is through recruitment of cohesins at pericentromeric regions, which they speculate promotes inter-sister repair over inter-homolog recombination. These cohesins were proposed by Vincenten et al. (2015) to recruit Zip1, an SC protein that has been implicated in promoting pericentromeric inter-sister repair at the expense of inter-homolog repair (Chen et al., 2008).

Similar results were later also seen in *Drosophila* when Comeron et al. (2012) detected gene conversion in regions of low or no crossing over, and showed that non-crossover recombination events are more uniformly distributed along the genome than crossovers were. In a subsequent study, Miller et al. (2016) found that non-crossover gene conversion events are not sensitive to the centromere effect. Both studies were able to evaluate non-crossover repair products by detecting changes in single nucleotide polymorphisms in unique-sequence centromere-proximal regions.

Sgs1, the budding yeast ortholog of Blm helicase, was shown by Rockmill et al. (2006) to be an important factor in preventing precocious separation of sister chromatids. Their study showed that the most common cause of spore inviability in budding yeast is aneuploidy arising from PSSC, which is often associated with, and promoted by, crossing over in centromere-proximal regions, further supporting the suggestion that proximal crossovers lead to non-disjunction.

In the experiments of Brand et al. (2018) described above, in which *Drosophila mauritiana* Mei-217 and Mei-218 were put into *D. melanogaster*, the researchers noted that crossovers were especially elevated in telomere- and centromere-proximal regions. Furthermore, they saw an increase in crossovers in the interval that spans the centromere in chromosome *2,* leading them to conclude that the Mei-217 and Mei-218 proteins may be involved in centromeric and telomeric crossover suppression.

It is also possible that the mechanisms behind the centromere effect are primarily structural, and that the number of centromeres is able to influence the strength of the effect. In support of this argument, Redfield showed in studies of triploid crossing over that there was a 1.5- and 3-fold increase in crossover frequencies at the center of chromosomes *2* and *3* – where the centromere is located - when compared to diploid females (Redfield, 1930, 1932). This increase in crossover frequencies decreased with distance from the centromere, which suggests that an increased total number of centromeres could be acting as a molecular sponge and "soaking up" a CE signal, ultimately leading to a weaker centromere effect.

While some genes involved in facilitating the centromere effect have come to light in the past few years, there is much that is still unknown. It will be important to look closely at whether the mechanisms behind the centromere effect are genetic or structural, how this effect relates to other patterning events, and how crossover suppression in centromeric regions is different from suppression in telomeric regions.

INTERPLAY BETWEEN PATTERNING PHENOMENA

Recent work has suggested that crossover assurance, interference, and suppression may be interconnected or part of an overarching crossover control mechanism. Interactions between crossover patterning phenomena are highlighted below.

Interference and the Centromere

The earliest suggestion that the centromere can impede interference comes from Muller's 1916 paper where he speculated that coincidence values on the second chromosome would be different if crossovers on the same chromosomal arm are compared to crossovers on either side of the centromere even when separated by the same distance in both cases (Muller, 1916a). He suggested that this could be due to chromosomes bending in the middle, or due to differences in structure at centromeric regions. In support of Muller's finding, Kikkawa (1932) showed an increase in coincidence values in the central regions of the chromosome, which led him to conclude that

crossover interference in the sections spanning the centromere is weaker than elsewhere on the chromosome. Graubard (1934) also showed that crossovers on one chromosomal arm do not interfere with crossovers on the other. These findings imply that the centromere can block an interference 'signal.' However, this block does not seem to be complete, as Graubard also observed that coincidence values between two small, adjacent intervals on either side of the centromere do not equal one (as they should for zero interference) but display less interference than intervals of the same size that are located on the same chromosomal arm. He concluded that coincidence values in a particular interval are not affected by the presence of either a terminal or central centromere but instead depend on the length of the interval being considered.

These conclusions from studies in insects were extended to *Neurospora* by Bole-Gowda et al. (1962), who demonstrated through tetrad analysis that there is little to no interference between crossovers on either side of the centromere. However, more than 30 years later, Colombo and Jones (1997) showed using previously published statistical analyses of chiasma data from grasshoppers that interference seemed to be able to act across the centromere when coincidence values were calculated, or distances from the nearest chiasma and the centromere were correlated. This led them to conclude that interference is blind to the presence of a centromere. Later, Kaback et al. (1999) also showed that in *S. cerevisiae* recombination on one chromosome arm is affected by changes in the size of the other. They concluded that this is indicative of the interference 'signal' having the ability to pass through the centromere, since their results suggest that crossover interference in budding yeast increases with the size of the chromosome. They explained their stance by pointing out that the model in which the centromere blocks interference ignores the fact that centromeric markers have greater physical separation and is based only on genetic mapping data. They proposed that in centromere-proximal regions, particularly in organisms that have large amounts of pericentromeric heterochromatin, interference appears to be blocked by the centromere because it has a much greater distance to cover. However, this does not seem to be the case across species, as Fowler et al., who in 2018 proposed the DSB hotspot clustering model of interference in *S. pombe*, speculated that the reason an interference 'signal' is unable to travel across the centromere in certain organisms is due to DSB hotspot clusters not being formed in pericentromeric regions (Fowler et al., 2018). Further, since *Drosophila* and other metazoa differ greatly from yeast in their chromatin structure, sequence, and even centromeric SC morphology, the role that the centromere plays in relaying or blocking an interference signal may well be different across these species.

In a 2012 study in *A. thaliana*, Yelina et al. (2012) showed increased centromere-proximal crossovers in a *methyltransferase1* (*met1*) mutant with hypomethylated DNA. However, they observed no difference when the total number of crossovers in *met1* mutants was compared to wild type, which they took as an indication that crossover interference and crossover homeostasis were acting to remodel the changed crossover landscape in the hypomethylated mutant to compensate for the increased centromere-proximal crossovers. Similarly, an *Arabidopsis* study by Xue et al. (2018) showed that pericentromeric crossover frequencies fell in *SPO-11* hypomorphs, where DSB numbers are drastically reduced. The authors suggest that this could allow medial crossover frequencies to rise, which in turn could inhibit pericentromeric crossovers through interference.

Hatkevich et al. (2017) showed that *D. melanogaster* mutants deficient for Bloom syndrome helicase lost crossover interference and crossover suppression in centromeric regions. They went on to speculate that interference and the centromere effect may be interdependent, with the centromere effect reinforcing interference by ensuring that most crossovers happen medially along the chromosome. However, they also state that this could be unlikely as the *D. melanogaster* telomere effect, or the suppression of crossovers in the telomeric regions, is not as strong as it should be for the two crossover suppression events to be coordinately reinforcing interference. The experiments of Brady et al. (2018) discussed above also provide a link between crossover suppression in pericentromeric regions and interference. However, Brady et al. (2018) found that flies mutant for *mei-41*, which encodes the *Drosophila* ortholog of ATR kinase, lose class I crossovers but appear to retain suppression of centromere-proximal crossovers. The authors proposed that crossover suppression is established earlier than other patterning processes.

These results suggest that it is possible for the centromere effect and interference to be independent events operating through entirely different mechanisms that happen to require some of the same factors to proceed correctly. However, it remains possible that the two events are established through the same mechanism, involving a crossover suppression signal traveling outward from the centromere/existing crossovers, mediated by some common proteins but separated temporally during meiosis.

Interference and Assurance

As pointed out by Wang et al. (2015), the need for crossover assurance is obvious, since at least one chiasma is necessary to promote accurate segregation of homologs, but whether there is a selective advantage of having interference is less clear. Several possible functions for interference have been suggested. It has been suggested that crossovers near one another may lead to a lack of sufficient cohesion to stabilize the bivalent (Fowler et al., 2018), but this should only be the case for two-chromatid DCOs. A study in *C. elegans* found that interference plays a key role in ensuring proper chromosome segregation by limiting the number of crossovers per homolog (Hollis et al., 2020); however, this may be a problem unique to organisms without defined centromeres. Interference may serve to limit the number of crossovers, but in Arabidopsis, increasing crossovers by three–sixfold has no apparent negative effect on fertility or chromosome segregation (Crismani et al., 2012; Girard et al., 2015). Wang et al. (2015) proposed that spacing out crossovers strikes a balance between the advantages of generating new combinations of alleles and the disadvantages of breaking up co-adapted combinations.

Several observations suggest that the strength of interference can be subject to selection. Brand et al. (2018) found that

replacing *D. melanogaster* Mei-217 and Mei-218 with the *D. mauritiana* orthologs captured many of the crossover differences between these species, including reduced interference. They also reported strong evidence for positive selection within *mei-218* in both species, suggesting this might be associated with changes in interference and therefore in crossover numbers. Gorlov and Gorlova (2001) simulated a cost-benefit analysis of recombination and suggested that natural selection balances, through changes in interference, the positive and negative effects of recombination. The selective pressures that might drive higher or lower crossover rates are unknown.

There are also special cases where selection may operate on the strength of interference. In *C. elegans*, chromosomes are holocentric in somatic cells, but in meiosis the crossover produces an asymmetry that results in one end being selected for assembly of the kinetochore (Albertson and Thomson, 1993; Martinez-Perez et al., 2008). Two crossovers on the same bivalent may disrupt this process, leading to selection for absolute interference (one crossover per bivalent). Another possible case is suggested by studies of autopolyploids that arise from intraspecies whole-genome duplication. In early stages of allopolyploidy, homologous chromosomes form quadrivalents, and multiple chiasmata can lead to missegregation (Yant et al., 2013). Bomblies et al. (2016) proposed that increases to the strength of interference might promote more accurate meiotic segregation by reducing the number of chiasmata.

Another function for interference might be to promote assurance. The phenomenon of crossover homeostasis might support a dependency relationship between assurance and interference. Martini et al. (2006) studied budding yeast mutants with hypomorphic alleles of *spo11* and found that reduced DSB levels did not lead to the same reductions in crossover levels, suggesting an assurance mechanism that is buffered to some degree against different numbers of precursors. Homeostasis might involve a mechanism to produce a set number of crossovers per meiosis, within some range. This could explain the interchromosomal effect in *Drosophila*, where the presence of structural rearrangements on one chromosome both prevent it from crossing over with its homolog and lead to increased crossovers on other chromosomes (Lucchesi and Suzuki, 1968; Crown et al., 2018). If a set number of crossovers must be achieved, interference would limit the number of crossovers on larger chromosomes, forcing smaller chromosomes to cross over.

Finally, it is possible that interference and homeostasis are merely byproducts of the process through which a precursor is designated to become a crossover. In the beam-film model, mechanical stress provides a driving force to generate designation of an obligate crossover, and the resulting distance-dependent release of stress leads to both spacing of crossovers (interference) and homeostasis (Wang et al., 2015). The compartmentalized signaling model proposed by Zhang et al. (2018) is similar in this regard.

CONCLUSION

Although they have been traditionally defined as distinct phenomena, there is a great deal of overlap between the proteins and potentially the mechanisms underlying crossover interference, assurance, and the centromere effect. It is possible that a common mechanism is responsible for all three phenomena, whether that is aggregation of pro-crossover factors, mechanical stress, or another driving force that limits crossovers to specific regions of the genome. It is also apparent that the currently known and proposed mechanisms for crossover patterning operate at a wide range of scales, from the DNA level to the chromosome and inter-chromosome levels. Future work may focus on illuminating the connection between these mechanisms to better understand the overarching regulation of crossover patterning.

AUTHOR CONTRIBUTIONS

All authors listed have made a substantial, direct and intellectual contribution to the work, and approved it for publication.

FUNDING

NP and CT were supported by the National Institute of General Medical Sciences under award 1T32GM135128. JS was supported in part by the National Institute of General Medical Sciences under award 1R35GM118127.

REFERENCES

Agostinho, A., Meier, B., Sonneville, R., Jagut, M., Woglar, A., Blow, J., et al. (2013). Combinatorial regulation of meiotic Holliday junction resolution in *C. elegans* by HIM-6 (BLM) helicase, SLX-4, and the SLX-1, MUS-81 and XPF-1 nucleases. *PLoS Genet.* 9:e1003591. doi: 10.1371/journal.pgen.1003591

Ahuja, J. S., Sandhu, R., Mainpal, R., Lawson, C., Henley, H., Hunt, P. A., et al. (2017). Control of meiotic pairing and recombination by chromosomally tethered 26S proteasome. *Science* 355, 408–411. doi: 10.1126/science.aaf4778

Albertson, D. G., and Thomson, J. N. (1993). Segregation of holocentric chromosomes at meiosis in the nematode, *Caenorhabditis elegans*. *Chromosome Res.* 1, 15–26. doi: 10.1007/bf00710603

Allers, T., and Lichten, M. (2001). Differential timing and control of noncrossover and crossover recombination during meiosis. *Cell* 106, 47–57. doi: 10.1016/s0092-8674(01)00416-0

Andersen, S. L., and Sekelsky, J. (2010). Meiotic versus mitotic recombination: two different routes for double-strand break repair: the different functions of meiotic versus mitotic DSB repair are reflected in different pathway usage and different outcomes. *Bioessays* 32, 1058–1066. doi: 10.1002/bies.201000087

Anderson, C. M., Oke, A., Yam, P., Zhuge, T., and Fung, J. C. (2015). Reduced crossover interference and increased ZMM-independent recombination in the absence of Tel1/ATM. *PLoS Genet.* 11:e1005478. doi: 10.1371/journal.pgen.1005478

Arana, P., Santos, J. L., and Henriques-Gil, N. (1987). Interference relationships in grasshopper reciprocal translocation heterozygotes. *Heredity* 59, 85–93. doi: 10.1038/hdy.1987.99

Argueso, J. L., Wanat, J., Gemici, Z., and Alani, E. (2004). Competing crossover pathways act during meiosis in *Saccharomyces cerevisiae*. *Genetics* 168, 1805–1816. doi: 10.1534/genetics.104.032912

Ashley, T. (1994). Mammalian meiotic recombination: a reexamination. *Hum. Genet.* 94, 587–593.

Bähler, J., Wyler, T., Loidl, J., and Kohli, J. (1993). Unusual nuclear structures in meiotic prophase of fission yeast: a cytological analysis. *J. Cell Biol.* 121, 241–256. doi: 10.1083/jcb.121.2.241

Baker, B. S., and Carpenter, A. T. C. (1972). Genetic analysis of sex chromosomal meiotic mutants in *Drosophila melanogaster*. *Genetics* 71, 255–286. doi: 10.1093/genetics/71.2.255

Baker, S. M., Plug, A. W., Prolla, T. A., Bronner, C. E., Harris, A. C., Yao, X., et al. (1996). Involvement of mouse Mlh1 in DNA mismatch repair and meiotic crossing over. *Nat. Genet.* 13, 336–342. doi: 10.1038/ng0796-336

Baker, W. K. (1958). Crossing over in heterochromatin. *Am. Nat.* 92, 59–60. doi: 10.1086/282010

Beadle, G. W. (1932). A possible influence of the spindle fibre on crossing-over in Drosophila. *Proc. Natl. Acad. Sci. U.S.A.* 18, 160–165. doi: 10.1073/pnas.18.2.160

Berchowitz, L. E., and Copenhaver, G. P. (2010). Genetic interference: don't stand so close to me. *Curr. Genomics* 11, 91–102. doi: 10.2174/138920210790886835

Berchowitz, L. E., Francis, K. E., Bey, A. L., and Copenhaver, G. P. (2007). The role of *AtMUS81* in interference-insensitive crossovers in *A. thaliana*. *PLoS Genet.* 3:e132. doi: 10.1371/journal.pgen.0030132

Blitzblau, H. G., Bell, G. W., Rodriguez, J., Bell, S. P., and Hochwagen, A. (2007). Mapping of meiotic single-stranded DNA reveals double-stranded-break hotspots near centromeres and telomeres. *Curr. Biol.* 17, 2003–2012. doi: 10.1016/j.cub.2007.10.066

Bole-Gowda, B. N., Perkins, D. D., and Strickland, W. N. (1962). Crossing-over and interference in the centromere region of linkage group I of Neurospora. *Genetics* 47, 1243–1252. doi: 10.1093/genetics/47.9.1243

Bomblies, K., Jones, G., Franklin, C., Zickler, D., and Kleckner, N. (2016). The challenge of evolving stable polyploidy: Could an increase in "crossover interference distance" play a central role? *Chromosoma* 125, 287–300. doi: 10.1007/s00412-015-0571-4

Börner, G. V., Kleckner, N., and Hunter, N. (2004). Crossover/noncrossover differentiation, synaptonemal complex formation, and regulatory surveillance at the leptotene/zygotene transition of meiosis. *Cell* 117, 29–45. doi: 10.1016/s0092-8674(04)00292-2

Brady, M. M., McMahan, S., and Sekelsky, J. (2018). Loss of *Drosophila* Mei-41/ATR alters meiotic crossover patterning. *Genetics* 208, 579–588. doi: 10.1534/genetics.117.300634

Brand, C. L., Cattani, M. V., Kingan, S. B., Landeen, E. L., and Presgraves, D. C. (2018). Molecular evolution at a meiosis gene mediates species differences in the rate and patterning of recombination. *Curr. Biol.* 28, 1289–1295.e4.

Bridges, C. B. (1915). A linkage variation in *Drosophila*. *J. Exp. Zool.* 19, 1–21. doi: 10.1002/jez.1400190102

Bridges, C. B. (1927). The relation of the age of the female to crossing over in the third chromosome of *Drosophila melanogaster*. *J. Gen. Physiol.* 8, 689–700. doi: 10.1085/jgp.8.6.689

Broman, K. W., Rowe, L. B., Churchill, G. A., and Paigen, K. (2002). Crossover interference in the mouse. *Genetics* 160, 1123–1131. doi: 10.1093/genetics/160.3.1123

Brown, M. S., Grubb, J., Zhang, A., Rust, M. J., and Bishop, D. K. (2015). Small Rad51 and Dmc1 complexes often co-occupy both ends of a meiotic DNA double strand break. *PLoS Genet.* 11:e1005653. doi: 10.1371/journal.pgen.1005653

Buhler, C., Borde, V., and Lichten, M. (2007). Mapping meiotic single-strand DNA reveals a new landscape of DNA double-strand breaks in *Saccharomyces cerevisiae*. *PLoS Biol.* 5:e324. doi: 10.1371/journal.pbio.0050324

Burgoyne, P. S. (1982). Genetic homology and crossing over in the X and Y chromosomes of mammals. *Hum. Genet.* 61, 85–90. doi: 10.1007/bf00274192

Busygina, V., Sehorn, M. G., Shi, I. Y., Tsubouchi, H., Roeder, G. S., and Sung, P. (2008). Hed1 regulates Rad51-mediated recombination via a novel mechanism. *Genes Dev.* 22, 786–795. doi: 10.1101/gad.1638708

Callan, H. G., and Montalenti, G. (1947). Chiasma interference in mosquitoes. *J. Genet.* 48, 119–134. doi: 10.1007/bf02989374

Callender, T. L., Laureau, R., Wan, L., Chen, X., Sandhu, R., Laljee, S., et al. (2016). Mek1 down regulates Rad51 activity during yeast meiosis by phosphorylation of Hed1. *PLoS Genet.* 12:e1006226. doi: 10.1371/journal.pgen.1006226

Cannavo, E., Sanchez, A., Anand, R., Ranjha, L., Hugener, J., Adam, C., et al. (2020). Regulation of the MLH1-MLH3 endonuclease in meiosis. *Nature* 586, 618–622. doi: 10.1038/s41586-020-2592-2

Capilla-Perez, L., Durand, S., Hurel, A., Lian, Q., Chambon, A., Taochy, C., et al. (2021). The synaptonemal complex imposes crossover interference and heterochiasmy in Arabidopsis. *Proc. Natl. Acad. Sci. U.S.A.* 118:e2023613118. doi: 10.1073/pnas.2023613118

Carpenter, A. T. C. (1975). Electron microscopy of meiosis in *Drosophila melanogaster* females. I. Structure, arrangement, and temporal change of the synaptonemal complex in wild-type. *Chromosoma* 51, 157–182. doi: 10.1007/bf00319833

Carpenter, A. T. C., and Baker, B. S. (1982). On the control of the distribution of meiotic exchange in *Drosophila melanogaster*. *Genetics* 101, 81–89. doi: 10.1093/genetics/101.1.81

Catcheside, D. G. (1977). *The Genetics of Recombination*. London: Edward Arnold.

Chakraborty, P., Pankajam, A. V., Lin, G., Dutta, A., Krishnaprasad, G. N., Tekkedil, M. M., et al. (2017). Modulating crossover frequency and interference for obligate crossovers in *Saccharomyces cerevisiae* meiosis. *G3* 7, 1511–1524. doi: 10.1534/g3.117.040071

Chen, S. Y., Tsubouchi, T., Rockmill, B., Sandler, J. S., Richards, D. R., Vader, G., et al. (2008). Global analysis of the meiotic crossover landscape. *Dev. Cell* 15, 401–415. doi: 10.1016/j.devcel.2008.07.006

Chua, P. R., and Roeder, G. S. (1997). Tam1, a telomere-associated meiotic protein, functions in chromosome synapsis and crossover interference. *Genes Dev.* 11, 1786–1800. doi: 10.1101/gad.11.14.1786

Colombo, P. C., and Jones, G. H. (1997). Chiasma interference is blind to centromeres. *Heredity* 79(Pt 2), 214–227. doi: 10.1038/hdy.1997.145

Colomé-Tatché, M., Cortijo, S., Wardenaar, R., Morgado, L., Lahouze, B., Sarazin, A., et al. (2012). Features of the Arabidopsis recombination landscape resulting from the combined loss of sequence variation and DNA methylation. *Proc. Natl. Acad. Sci. U.S.A.* 109, 16240–16245. doi: 10.1073/pnas.1212955109

Comeron, J. M., Ratnappan, R., and Bailin, S. (2012). The many landscapes of recombination in *Drosophila melanogaster*. *PLoS Genet.* 8:e1002905. doi: 10.1371/journal.pgen.1002905

Conrad, M. N., Dominguez, A. M., and Dresser, M. E. (1997). Ndj1p, a meiotic telomere protein required for normal chromosome synapsis and segregation in yeast. *Science* 276, 1252–1255. doi: 10.1126/science.276.5316.1252

Copenhaver, G. P., Housworth, E. A., and Stahl, F. W. (2002). Crossover interference in Arabidopsis. *Genetics* 160, 1631–1639. doi: 10.1093/genetics/160.4.1631

Crismani, W., Girard, C., Froger, N., Pradillo, M., Santos, J. L., Chelysheva, L., et al. (2012). FANCM limits meiotic crossovers. *Science* 336, 1588–1590. doi: 10.1126/science.1220381

Crown, K. N., Miller, D. E., Sekelsky, J., and Hawley, R. S. (2018). Local inversion heterozygosity alters recombination throughout the genome. *Curr. Biol.* 28, 2984–2990.e3.

Darlington, C. D. (1937). *Recent Advances in Cytology*, 2nd Edn. Philadelphia, PA: P. Blakiston's Son & Co. Inc.

Darlington, C. D., and Dark, S. O. S. (1932). The origin and behaviour of chiasmata, II. *Stenobothrus parallelus*. *Cytologia* 3, 169–185. doi: 10.1508/cytologia.3.169

de Boer, E., Stam, P., Dietrich, A. J., Pastink, A., and Heyting, C. (2006). Two levels of interference in mouse meiotic recombination. *Proc. Natl. Acad. Sci. U.S.A.* 103, 9607–9612. doi: 10.1073/pnas.0600418103

de los Santos, T., Hunter, N., Lee, C., Larkin, B., Loidl, J., and Hollingsworth, N. M. (2003). The Mus81/Mms4 endonuclease acts independently of double-Holliday junction resolution to promote a distinct subset of crossovers during meiosis in budding yeast. *Genetics* 164, 81–94. doi: 10.1093/genetics/164.1.81

De Muyt, A., Jessop, L., Kolar, E., Sourirajan, A., Chen, J., Dayani, Y., et al. (2012). BLM helicase ortholog Sgs1 is a central regulator of meiotic recombination intermediate metabolism. *Mol. Cell* 46, 43–53. doi: 10.1016/j.molcel.2012.02.020

De Storme, N., and Geelen, D. (2020). High temperatures alter cross-over distribution and induce male meiotic restitution in *Arabidopsis thaliana*. *Commun Biol.* 3:187.

Dereli, I., Stanzione, M., Olmeda, F., Papanikos, F., Baumann, M., Demir, S., et al. (2021). Four-pronged negative feedback of DSB machinery in meiotic DNA-break control in mice. *Nucleic Acids Res.* 49, 2609–2628. doi: 10.1093/nar/gkab082

Dernburg, A. F., McDonald, K., Moulder, G., Barstead, R., Dresser, M., and Villeneuve, A. M. (1998). Meiotic recombination in *C. elegans* initiates by a conserved mechanism and is dispensable for homologous chromosome synapsis. *Cell* 94, 387–398. doi: 10.1016/s0092-8674(00)81481-6

Deshong, A. J., Ye, A. L., Lamelza, P., and Bhalla, N. (2014). A quality control mechanism coordinates meiotic prophase events to promote crossover assurance. *PLoS Genet.* 10:e1004291. doi: 10.1371/journal.pgen.1004291

Duroc, Y., Lemhemdi, A., Larcheveque, C., Hurel, A., Cuacos, M., Cromer, L., et al. (2014). The kinesin AtPSS1 promotes synapsis and is required for proper crossover distribution in meiosis. *PLoS Genet.* 10:e1004674. doi: 10.1371/journal.pgen.1004674

Egel, R. (1978). Synaptonemal complex and crossing-over: Structural support or interference? *Heredity* 41, 233–237. doi: 10.1038/hdy.1978.92

Egel-Mitani, M., Olson, L. W., and Egel, R. (1982). Meiosis in *Aspergillus nidulans*: another example for lacking synaptonemal complexes in the absence of crossover interference. *Hereditas* 97, 179–187. doi: 10.1111/j.1601-5223.1982.tb00870.x

Emerson, S., and Beadle, G. W. (1933). Crossing-over near the spindle fiber in attached-X chromosomes of *Drosophila melangoaster*. *Z. Indukt. Abstamm. Vererbungsl.* 65, 129–140. doi: 10.1007/bf01848844

Falque, M., Mercier, R., Mezard, C., de Vienne, D., and Martin, O. C. (2007). Patterns of recombination and MLH1 foci density along mouse chromosomes: modeling effects of interference and obligate chiasma. *Genetics* 176, 1453–1467. doi: 10.1534/genetics.106.070235

Foss, E. J., and Stahl, F. W. (1995). A test of a counting model for chiasma interference. *Genetics* 139, 1201–1209. doi: 10.1093/genetics/139.3.1201

Foss, E., Lande, R., Stahl, F. W., and Steinberg, C. M. (1993). Chiasma interference as a function of genetic distance. *Genetics* 133, 681–691. doi: 10.1093/genetics/133.3.681

Fowler, K. R., Hyppa, R. W., Cromie, G. A., and Smith, G. R. (2018). Physical basis for long-distance communication along meiotic chromosomes. *Proc. Natl. Acad. Sci. U.S.A.* 115, E9333–E9342.

Froenicke, L., Anderson, L. K., Wienberg, J., and Ashley, T. (2002). Male mouse recombination maps for each autosome identified by chromosome painting. *Am. J. Hum. Genet.* 71, 1353–1368. doi: 10.1086/344714

Fung, J. C., Rockmill, B., Odell, M., and Roeder, G. S. (2004). Imposition of crossover interference through the nonrandom distribution of synapsis initiation complexes. *Cell* 116, 795–802. doi: 10.1016/s0092-8674(04)00249-1

Gerton, J. L., DeRisi, J., Shroff, R., Lichten, M., Brown, P. O., and Petes, T. D. (2000). Global mapping of meiotic recombination hotspots and coldspots in the yeast *Saccharomyces cerevisiae*. *Proc. Natl. Acad. Sci. U.S.A.* 97, 11383–11390. doi: 10.1073/pnas.97.21.11383

Girard, C., Chelysheva, L., Choinard, S., Froger, N., Macaisne, N., Lemhemdi, A., et al. (2015). AAA-ATPase FIDGETIN-LIKE 1 and Helicase FANCM antagonize meiotic crossovers by distinct mechanisms. *PLoS Genet.* 11:e1005369. doi: 10.1371/journal.pgen.1005369

Gorlov, I. P., and Gorlova, O. Y. (2001). Cost-benefit analysis of recombination and its application for understanding of chiasma interference. *J. Theor. Biol.* 213, 1–8. doi: 10.1006/jtbi.2001.2397

Graubard, M. A. (1934). Temperature effect on interference and crossing over. *Genetics* 19, 83–94. doi: 10.1093/genetics/19.1.83

Hartmann, M., Umbanhowar, J., and Sekelsky, J. (2019). Centromere-proximal meiotic crossovers in *Drosophila melanogaster* are suppressed by both highly repetitive heterochromatin and proximity to the centromere. *Genetics* 213, 113–125. doi: 10.1534/genetics.119.302509

Hatkevich, T., Kohl, K. P., McMahan, S., Hartmann, M. A., Williams, A. M., and Sekelsky, J. (2017). Bloom syndrome helicase promotes meiotic crossover patterning and homolog disjunction. *Curr. Biol.* 27, 96–102. doi: 10.1016/j.cub.2016.10.055

Havekes, F. W., de Jong, J. H., Heyting, C., and Ramanna, M. S. (1994). Synapsis and chiasma formation in four meiotic mutants of tomato (*Lycopersicon esculentum*). *Chromosome Res.* 2, 315–325. doi: 10.1007/bf01552725

Hawley, R. S. (1988). "Exchange and chromosomal segregation in eucaryotes," in *Genetic Recombination*, eds R. Kucherlapati and G. R. Smith (Washington, DC: American Society of Microbiology), 497–527.

Hawley, R. S., and Theurkauf, W. E. (1993). Requiem for distributive segregation: achiasmate segregation in *Drosophila* females. *Trends Genet.* 9, 310–317. doi: 10.1016/0168-9525(93)90249-h

Hayashi, M., Mlynarczyk-Evans, S., and Villeneuve, A. M. (2010). The synaptonemal complex shapes the crossover landscape through cooperative assembly, crossover promotion and crossover inhibition during *Caenorhabditis elegans* meiosis. *Genetics* 186, 45–58. doi: 10.1534/genetics.110.115501

He, W., Prasada Rao, H. B., Tang, S., Bhagwat, N., Kulkarni, D. S., Ma, Y., et al. (2020). Regulated proteolysis of MutSγ controls meiotic crossing over. *Mol. Cell* 78, 168–183. doi: 10.1016/j.molcel.2020.02.001

Heyer, W. D., Ehmsen, K. T., and Liu, J. (2010). Regulation of homologous recombination in eukaryotes. *Annu. Rev. Genet.* 44, 113–139. doi: 10.1146/annurev-genet-051710-150955

Higgins, J. D., Armstrong, S. J., Franklin, F. C., and Jones, G. H. (2004). The Arabidopsis MutS homolog AtMSH4 functions at an early step in recombination: evidence for two classes of recombination in Arabidopsis. *Genes Dev.* 18, 2557–2570. doi: 10.1101/gad.317504

Higgins, J. D., Vignard, J., Mercier, R., Pugh, A. G., Franklin, F. C., and Jones, G. H. (2008). AtMSH5 partners AtMSH4 in the class I meiotic crossover pathway in *Arabidopsis thaliana*, but is not required for synapsis. *Plant J.* 55, 28–39. doi: 10.1111/j.1365-313x.2008.03470.x

Hillers, K. J., and Villeneuve, A. M. (2003). Chromosome-wide control of meiotic crossing over in *C. elegans*. *Curr. Biol.* 13, 1641–1647. doi: 10.1016/j.cub.2003.08.026

Hinch, A. G., Altemose, N., Noor, N., Donnelly, P., and Myers, S. R. (2014). Recombination in the human pseudoautosomal region PAR1. *PLoS Genet.* 10:e1004503. doi: 10.1371/journal.pgen.1004503

Hollis, J. A., Glover, M. L., Schlientz, A. J., Cahoon, C. K., Bowerman, B., Wignall, S. M., et al. (2020). Excess crossovers impede faithful meiotic chromosome segregation in *C. elegans*. *PLoS Genet.* 16:e1009001. doi: 10.1371/journal.pgen.1009001

Holloway, J. K., Booth, J., Edelmann, W., McGowan, C. H., and Cohen, P. E. (2008). MUS81 generates a subset of MLH1-MLH3-independent crossovers in mammalian meiosis. *PLoS Genet.* 4:e1000186. doi: 10.1371/journal.pgen.1000186

Housworth, E. A., and Stahl, F. W. (2003). Crossover interference in humans. *Am. J. Hum. Genet.* 73, 188–197. doi: 10.1086/376610

Hulten, M. A. (1974). Chiasma distribution at diakinesis in the normal human male. *Hereditas* 76, 55–78. doi: 10.1111/j.1601-5223.1974.tb01177.x

Hulten, M. A. (2011). On the origin of crossover interference: a chromosome oscillatory movement (COM) model. *Mol. Cytogenet.* 4:10. doi: 10.1186/1755-8166-4-10

Huselid, E., and Bunting, S. F. (2020). The regulation of homologous recombination by helicases. *Genes* 11:498. doi: 10.3390/genes11050498

Jessop, L., Rockmill, B., Roeder, G. S., and Lichten, M. (2006). Meiotic chromosome synapsis-promoting proteins antagonize the anti-crossover activity of Sgs1. *PLoS Genet.* 2:e155. doi: 10.1371/journal.pgen.0020155

Jones, G. H. (1984). The control of chiasma distribution. *Symp. Soc. Exp. Biol.* 38, 293–320.

Joshi, N., Barot, A., Jamison, C., and Borner, G. V. (2009). Pch2 links chromosome axis remodeling at future crossover sites and crossover distribution during yeast meiosis. *PLoS Genet.* 5:e1000557. doi: 10.1371/journal.pgen.1000557

Kaback, D. B., Barber, D., Mahon, J., Lamb, J., and You, J. (1999). Chromosome size-dependent control of meiotic reciprocal recombination in *Saccharomyces cerevisiae*: the role of crossover interference. *Genetics* 152, 1475–1486. doi: 10.1093/genetics/152.4.1475

Kaback, D. B., Steensma, H. Y., and de Jonge, P. (1989). Enhanced meiotic recombination on the smallest chromosome of *Saccharomyces cerevisiae*. *Proc. Natl. Acad. Sci. U.S.A.* 86, 3694–3698. doi: 10.1073/pnas.86.10.3694

Kikkawa, H. (1932). Studies on the mechanism of crossing-over in *Drosophila*, with special reference to the phenomenon of interference. *Cytologia* 3, 285–332. doi: 10.1508/cytologia.3.285

King, J. S., and Mortimer, R. K. (1990). A polymerization model of chiasma interference and corresponding computer simulation. *Genetics* 126, 1127–1138. doi: 10.1093/genetics/126.4.1127

Kleckner, N., Zickler, D., Jones, G. H., Dekker, J., Padmore, R., Henle, J., et al. (2004). A mechanical basis for chromosome function. *Proc. Natl. Acad. Sci. U.S.A.* 101, 12592–12597.

Koehler, K. E., Boulton, C. L., Collins, H. E., French, R. L., Herman, K. C., Lacefield, S. M., et al. (1996a). Spontaneous X chromosome MI and MII nondisjunction events in *Drosophila melanogaster* oocytes have different recombinational histories. *Nat. Genet.* 14, 406–414. doi: 10.1038/ng1296-406

Koehler, K. E., Hawley, R. S., Sherman, S., and Hassold, T. (1996b). Recombination and nondisjunction in humans and flies. *Hum. Mol. Genet.* 5, 1495–1504. doi: 10.1093/hmg/5.supplement_1.1495

Kohl, K. P., and Sekelsky, J. (2013). Meiotic and mitotic recombination in meiosis. *Genetics* 194, 327–334. doi: 10.1534/genetics.113.150581

Kohl, K. P., Jones, C. D., and Sekelsky, J. (2012). Evolution of an MCM complex in flies that promotes meiotic crossovers by blocking BLM helicase. *Science* 338, 1363–1365. doi: 10.1126/science.1228190

Koller, P. C., and Darlington, C. D. (1934). The genetical and mechan-ical properties of the sex-chromosomes. *J. Genet.* 29, 159–173. doi: 10.1007/bf02982193

Kulkarni, D. S., Owens, S. N., Honda, M., Ito, M., Yang, Y., Corrigan, M. W., et al. (2020). PCNA activates the MutLgamma endonuclease to promote meiotic crossing over. *Nature* 586, 623–627. doi: 10.1038/s41586-020-2645-6

Lamb, N. E., Freeman, S. B., Savage-Austin, A., Pettay, D., Taft, L., Hersey, J., et al. (1996). Susceptible chiasmate configurations of chromosome 21 predispose to non-disjunction in both maternal meiosis I and meiosis II. *Nat. Genet.* 14, 400–405. doi: 10.1038/ng1296-400

Libuda, D. E., Uzawa, S., Meyer, B. J., and Villeneuve, A. M. (2013). Meiotic chromosome structures constrain and respond to designation of crossover sites. *Nature* 502, 703–706. doi: 10.1038/nature12577

Lindsley, D. L., and Sandler, L. (1977). The genetic analysis of meiosis in female *Drosophila melanogaster*. *Philos. Trans. R. Soc. Lond. B Biol. Sci.* 277, 295–312. doi: 10.1098/rstb.1977.0019

Link, A. J., and Olson, M. V. (1991). Physical map of the *Saccharomyces cerevisiae* genome at 110-kilobase resolution. *Genetics* 127, 681–698. doi: 10.1093/genetics/127.4.681

Lu, X., Liu, X., An, L., Zhang, W., Sun, J., Pei, H., et al. (2008). The Arabidopsis MutS homolog AtMSH5 is required for normal meiosis. *Cell Res.* 18, 589–599. doi: 10.1038/cr.2008.44

Lucchesi, J. C., and Suzuki, D. T. (1968). The interchromosomal control of recombination. *Annu. Rev. Genet.* 2, 53–86. doi: 10.1146/annurev.ge.02.120168.000413

Machovina, T. S., Mainpal, R., Daryabeigi, A., McGovern, O., Paouneskou, D., Labella, S., et al. (2016). A surveillance system ensures crossover formation in *C. elegans*. *Curr. Biol.* 26, 2873–2884. doi: 10.1016/j.cub.2016.09.007

Maguire, M. P. (1977). Homologous chromosome pairing. *Philos. Trans. R. Soc. Lond. B Biol. Sci.* 277, 245–258.

Marsolier-Kergoat, M. C., Khan, M. M., Schott, J., Zhu, X., and Llorente, B. (2018). Mechanistic view and genetic control of DNA recombination during meiosis. *Mol. Cell* 70, 9–20.e6.

Martinez-Perez, E., Schvarzstein, M., Barroso, C., Lightfoot, J., Dernburg, A. F., and Villeneuve, A. M. (2008). Crossovers trigger a remodeling of meiotic chromosome axis composition that is linked to two-step loss of sister chromatid cohesion. *Genes Dev.* 22, 2886–2901. doi: 10.1101/gad.1694108

Martini, E., Diaz, R. L., Hunter, N., and Keeney, S. (2006). Crossover homeostasis in yeast meiosis. *Cell* 126, 285–295. doi: 10.1016/j.cell.2006.05.044

Mather, K. (1935). Reductional and equational separation of the chromosomes in bivalents and multivalents. *J. Genet.* 30, 53–78. doi: 10.1007/bf02982205

Mather, K. (1936). Competition between bivalents during chiasma formation. *Proc. R. Soc. Lond. B* 120, 208–227. doi: 10.1098/rspb.1936.0032

Mather, K. (1937). The determination of position in crossing-over. II. The chromosome length-chiasma frequency relation. *Cytologia* Fujii Jubilee, 514–526. doi: 10.1508/cytologia.fujiijubilaei.514

Mather, K. (1939). Crossing over and heterochromatin in the X chromosome of *Drosophila melanogaster*. *Genetics* 24, 413–435. doi: 10.1093/genetics/24.3.413

McKim, K. S., Green-Marroquin, B. L., Sekelsky, J. J., Chin, G., Steinberg, C., Khodosh, R., et al. (1998). Meiotic synapsis in the absence of recombination. *Science* 279, 876–878. doi: 10.1126/science.279.5352.876

Medhi, D., Goldman, A. S., and Lichten, M. (2016). Local chromosome context is a major determinant of crossover pathway biochemistry during budding yeast meiosis. *eLife* 5:e19669.

Mehrotra, S., and McKim, K. S. (2006). Temporal analysis of meiotic DNA double-strand break formation and repair in *Drosophila* females. *PLoS Genet.* 2:e200. doi: 10.1371/journal.pgen.0020200

Melamed-Bessudo, C., and Levy, A. A. (2012). Deficiency in DNA methylation increases meiotic crossover rates in euchromatic but not in heterochromatic regions in Arabidopsis. *Proc. Natl. Acad. Sci. U.S.A.* 109, E981–E988.

Miller, D. E., Smith, C. B., Yeganeh Kazemi, N., Cockrell, A. J., Arvanitakis, A. V., Blumenstiel, J. P., et al. (2016). Whole-genome analysis of individual meiotic events in *Drosophila melanogaster* reveals that noncrossover gene conversions are insensitive to interference and the centromere effect. *Genetics* 203, 159–171. doi: 10.1534/genetics.115.186486

Mirouze, M., Lieberman-Lazarovich, M., Aversano, R., Bucher, E., Nicolet, J., Reinders, J., et al. (2012). Loss of DNA methylation affects the recombination landscape in Arabidopsis. *Proc. Natl. Acad. Sci. U.S.A.* 109, 5880–5885. doi: 10.1073/pnas.1120841109

Moens, P. B. (1969). Genetic and cytological effects of three desynaptic genes in the tomato. *Can. J. Genet. Cytol.* 11, 857–869. doi: 10.1139/g69-101

Mortimer, R. K., Schild, D., Contopoulou, C. R., and Kans, J. A. (1989). Genetic map of *Saccharomyces cerevisiae*, edition 10. *Yeast* 5, 321–403.

Mortimer, R. R., and Fogel, S. (1974). "Genetical interference and gene conversion," in *Mechanisms in Recombination*, ed. R. Grell (New York, NY: Plenum Press), 263–275. doi: 10.1007/978-1-4684-2133-0_23

Moses, M. J., Dresser, M., and Poorman, P. A. (1984). "Composition and role of the synaptonemal complex," in *Controlling Events in Meiosis*, eds C.W. Evans and H. G. Dickinson (Cambridge: Company of Biologists), 245–270.

Muller, H. J. (1916a). The mechanism of crossing-over. *Am. Nat.* 50, 193–221.

Muller, H. J. (1916b). The mechanism of crossing-over. II. *Am. Nat.* 50, 284–305. doi: 10.1086/279541

Munz, P. (1994). An analysis of interference in the fission yeast *Schizosaccharomyces pombe*. *Genetics* 137, 701–707. doi: 10.1093/genetics/137.3.701

Murakami, H., Lam, I., Huang, P. C., Song, J., van Overbeek, M., and Keeney, S. (2020). Multilayered mechanisms ensure that short chromosomes recombine in meiosis. *Nature* 582, 124–128. doi: 10.1038/s41586-020-2248-2

Nambiar, M., and Smith, G. R. (2016). Repression of harmful meiotic recombination in centromeric regions. *Semin. Cell Dev. Biol.* 54, 188–197. doi: 10.1016/j.semcdb.2016.01.042

Niu, H., Li, X., Job, E., Park, C., Moazed, D., Gygi, S. P., et al. (2007). Mek1 kinase is regulated to suppress double-strand break repair between sister chromatids during budding yeast meiosis. *Mol. Cell. Biol.* 27, 5456–5467. doi: 10.1128/mcb.00416-07

Niu, H., Wan, L., Busygina, V., Kwon, Y., Allen, J. A., Li, X., et al. (2009). Regulation of meiotic recombination via Mek1-mediated Rad54 phosphorylation. *Mol. Cell* 36, 393–404. doi: 10.1016/j.molcel.2009.09.029

Niu, H., Wan, L., Baumgartner, B., Schaefer, D., Loidl, J., and Hollingsworth, N. M. (2005). Partner choice during meiosis is regulated by Hop1-promoted dimerization of Mek1. *Mol. Biol. Cell* 16, 5804–5818. doi: 10.1091/mbc.e05-05-0465

O'Neil, N. J., Martin, J. S., Youds, J. L., Ward, J. D., Petalcorin, M. I. R., Rose, A. M., et al. (2013). Joint molecule resolution requires the redundant activities of MUS-81 and XPF-1 during *C. elegans* meiosis. *PLoS Genet.* 9:e1003582. doi: 10.1371/journal.pgen.1003582

Oh, S. D., Lao, J. P., Hwang, P. Y., Taylor, A. F., Smith, G. R., and Hunter, N. (2007). BLM ortholog, Sgs1, prevents aberrant crossing-over by suppressing formation of multichromatid joint molecules. *Cell* 130, 259–272. doi: 10.1016/j.cell.2007.05.035

Orr-Weaver, T. (1996). Meiotic nondisjunction does the two-step. *Nat. Genet.* 14, 374–376. doi: 10.1038/ng1296-374

Otto, S. P., and Payseur, B. A. (2019). Crossover interference: shedding light on the evolution of recombination. *Annu. Rev. Genet.* 53, 19–44. doi: 10.1146/annurev-genet-040119-093957

Owen, A. R. G. (1949). A possible interpretation of the apparent interference across the centromere found by Callan and Montalenti in *Culex pipiens*. *Heredity* 3, 357–367. doi: 10.1038/hdy.1949.26

Pan, J., Sasaki, M., Kniewel, R., Murakami, H., Blitzblau, H. G., Tischfield, S. E., et al. (2011). A hierarchical combination of factors shapes the genome-wide topography of yeast meiotic recombination initiation. *Cell* 144, 719–731. doi: 10.1016/j.cell.2011.02.009

Papanikos, F., Clement, J. A. J., Testa, E., Ravindranathan, R., Grey, C., Dereli, I., et al. (2019). Mouse ANKRD31 regulates spatiotemporal patterning of meiotic recombination initiation and ensures recombination between X and Y sex chromosomes. *Mol. Cell* 74, 1069–1085.e11.

Papazian, H. P. (1952). The analysis of tetrad data. *Genetics* 37, 175–188. doi: 10.1093/genetics/37.2.175

Parker, J. S. (1987). Increased chiasma frequency as a result of chromosome rearrangement. *Heredity* 58, 87–94. doi: 10.1038/hdy.1987.13

Perkins, D. D. (1962). Crossing-over and interference in a multiply marked chromosome arm of Neurospora. *Genetics* 47, 1253–1274. doi: 10.1093/genetics/47.9.1253

Phillips, D., Jenkins, G., Macaulay, M., Nibau, C., Wnetrzak, J., Fallding, D., et al. (2015). The effect of temperature on the male and female recombination landscape of barley. *New Phytol.* 208, 421–429. doi: 10.1111/nph.13548

Plank, J. L., Wu, J., and Hsieh, T. S. (2006). Topoisomerase IIIα and Bloom's helicase can resolve a mobile double Holliday junction substrate through convergent branch migration. *Proc. Natl. Acad. Sci. U.S.A.* 103, 11118–11123. doi: 10.1073/pnas.0604873103

Plough, H. H. (1917a). The effect of temperature on crossingover in *Drosophila*. *J. Exp. Zool.* 24, 147–209. doi: 10.1002/jez.1400240202

Plough, H. H. (1917b). The effect of temperature on linkage in the second chromosome of Drosophila. *Proc. Natl. Acad. Sci. U.S.A.* 3, 553–555. doi: 10.1073/pnas.3.9.553

Plough, H. H. (1921). Further studies on the effect of temperature on crossing over. *J. Exp. Zool.* 32, 187–202. doi: 10.1002/jez.1400320202

Prasada Rao, H. B., Qiao, H., Bhatt, S. K., Bailey, L. R., Tran, H. D., Bourne, S. L., et al. (2017). A SUMO-ubiquitin relay recruits proteasomes to chromosome axes to regulate meiotic recombination. *Science* 355, 403–407.

Qiao, H., Prasada Rao, H. B., Yang, Y., Fong, J. H., Cloutier, J. M., Deacon, D. C., et al. (2014). Antagonistic roles of ubiquitin ligase HEI10 and SUMO ligase RNF212 regulate meiotic recombination. *Nat. Genet.* 46, 194–199. doi: 10.1038/ng.2858

Radford, S. J., Goley, E., Baxter, K., McMahan, S., and Sekelsky, J. (2005). Drosophila ERCC1 is required for a subset of MEI-9-dependent meiotic crossovers. *Genetics* 170, 1737–1745. doi: 10.1534/genetics.104.036178

Rao, H. B., Qiao, H., Bhatt, S. K., Bailey, L. R., Tran, H. D., Bourne, S. L., et al. (2017). A SUMO-ubiquitin relay recruits proteasomes to chromosome axes to regulate meiotic recombination. *Science* 355, 403–407. doi: 10.1126/science.aaf6407

Redfield, H. (1930). Crossing over in the third chromosomes of triploids of *Drosophila melanogaster*. *Genetics* 15, 205–252.

Redfield, H. (1932). A comparison of triploid and diploid crossing over for chromosome II of *Drosophila melanogaster*. *Genetics* 17, 137–152.

Reynolds, A., Qiao, H., Yang, Y., Chen, J. K., Jackson, N., Biswas, K., et al. (2013). RNF212 is a dosage-sensitive regulator of crossing-over during mammalian meiosis. *Nat. Genet.* 45, 269–278. doi: 10.1038/ng.2541

Riles, L., Dutchik, J. E., Baktha, A., McCauley, B. K., Thayer, E. C., Leckie, M. P., et al. (1993). Physical maps of the six smallest chromosomes of *Saccharomyces cerevisiae* at a resolution of 2.6 kilobase pairs. *Genetics* 134, 81–150. doi: 10.1093/genetics/134.1.81

Rockmill, B., Voelkel-Meiman, K., and Roeder, G. S. (2006). Centromere-proximal crossovers are associated with precocious separation of sister chromatids during meiosis in *Saccharomyces cerevisiae*. *Genetics* 174, 1745–1754. doi: 10.1534/genetics.106.058933

Rog, O., Kohler, S., and Dernburg, A. F. (2017). The synaptonemal complex has liquid crystalline properties and spatially regulates meiotic recombination factors. *eLife* 6:e21455.

Rosu, S., Libuda, D. E., and Villeneuve, A. M. (2011). Robust crossover assurance and regulated interhomolog access maintain meiotic crossover number. *Science* 334, 1286–1289. doi: 10.1126/science.1212424

Rosu, S., Zawadzki, K. A., Stamper, E. L., Libuda, D. E., Reese, A. L., Dernburg, A. F., et al. (2013). The *C. elegans* DSB-2 protein reveals a regulatory network that controls competence for meiotic DSB formation and promotes crossover assurance. *PLoS Genet.* 9:e1003674. doi: 10.1371/journal.pgen.1003674

Saito, T. T., Youds, J. L., Boulton, S. J., and Colaiácovo, M. P. (2009). *Caenorhabditis elegans* HIM-18/SLX-4 interacts with SLX-1 and XPF-1 and maintains genomic integrity in the germline by processing recombination intermediates. *PLoS Genet.* 5:e1000735. doi: 10.1371/journal.pgen.1000735

Schweitzer, M. D. (1935). An analytical study of crossing over in *Drosophila melanogaster*. *Genetics* 20, 497–527. doi: 10.1093/genetics/20.5.497

Sekelsky, J. (2017). DNA repair in *Drosophila*: mutagens, models, and missing genes. *Genetics* 205, 471–490. doi: 10.1534/genetics.116.186759

Sekelsky, J. J., McKim, K. S., Chin, G. M., and Hawley, R. S. (1995). The *Drosophila* meiotic recombination gene mei-9 encodes a homologue of the yeast excision repair protein Rad1. *Genetics* 141, 619–627. doi: 10.1093/genetics/141.2.619

Shinohara, A., and Shinohara, M. (2004). Roles of RecA homologues Rad51 and Dmc1 during meiotic recombination. *Cytogenet. Genome Res.* 107, 201–207. doi: 10.1159/000080598

Shinohara, M., Oh, S. D., Hunter, N., and Shinohara, A. (2008). Crossover assurance and crossover interference are distinctly regulated by the ZMM proteins during yeast meiosis. *Nat. Genet.* 40, 299–309. doi: 10.1038/ng.83

Smith, G. R., and Nambiar, M. (2020). New solutions to old problems: molecular mechanisms of meiotic crossover control. *Trends Genet.* 36, 337–346. doi: 10.1016/j.tig.2020.02.002

Smith, G. R., Boddy, M. N., Shanahan, P., and Russell, P. (2003). Fission yeast Mus81.Eme1 Holliday junction resolvase is required for meiotic crossing over but not for gene conversion. *Genetics* 165, 2289–2293. doi: 10.1093/genetics/165.4.2289

Snow, R. (1979). Maximum likelihood estimation of linkage and interference from tetrad data. *Genetics* 92, 231–245. doi: 10.1093/genetics/92.1.231

Snowden, T., Acharya, S., Butz, C., Berardini, M., and Fishel, R. (2004). hMSH4-hMSH5 recognizes Holliday Junctions and forms a meiosis-specific sliding clamp that embraces homologous chromosomes. *Mol. Cell* 15, 437–451. doi: 10.1016/j.molcel.2004.06.040

Stack, S. M. (1984). Heterochromatin, the synaptonemal complex and crossing over. *J. Cell Sci.* 71, 159–176. doi: 10.1242/jcs.71.1.159

Stahl, F. W. (2008). On the "NPD ratio" as a test for crossover interference. *Genetics* 179, 701–704. doi: 10.1534/genetics.108.086918

Stahl, F. W., Foss, H. M., Young, L. S., Borts, R. H., Abdullah, M. F., and Copenhaver, G. P. (2004). Does crossover interference count in *Saccharomyces cerevisiae*? *Genetics* 168, 35–48. doi: 10.1534/genetics.104.027789

Stamper, E. L., Rodenbusch, S. E., Rosu, S., Ahringer, J., Villeneuve, A. M., and Dernburg, A. F. (2013). Identification of DSB-1, a protein required for initiation of meiotic recombination in *Caenorhabditis elegans*, illuminates a crossover assurance checkpoint. *PLoS Genet.* 9:e1003679. doi: 10.1371/journal.pgen.1003679

Stern, C. (1926). An effect of temperature and age on crossing-over in the first chromosome of *Drosophila melanogaster*. *Proc. Natl. Acad. Sci. U.S.A.* 12, 530–532. doi: 10.1073/pnas.12.8.530

Sturtevant, A. H. (1913). The linear arrangement of six sex-linked factors in Drosophila, as shown by their mode of association. *J. Exp. Biol.* 14, 43–59. doi: 10.1002/jez.1400140104

Sturtevant, A. H. (1915). The behavior of the chromosomes as studied through linkage. *Z. Indukt. Abstamm. Vererbungsl.* 13, 234–287. doi: 10.1007/bf01792906

Svetlanov, A., Baudat, F., Cohen, P. E., and de Massy, B. (2008). Distinct functions of MLH3 at recombination hot spots in the mouse. *Genetics* 178, 1937–1945. doi: 10.1534/genetics.107.084798

Sym, M., and Roeder, G. S. (1994). Crossover interference is abolished in the absence of a synaptonemal complex protein. *Cell* 79, 283–292. doi: 10.1016/0092-8674(94)90197-x

Sym, M., Engebrecht, J. A., and Roeder, G. S. (1993). ZIP1 is a synaptonemal complex protein required for meiotic chromosome synapsis. *Cell* 72, 365–378. doi: 10.1016/0092-8674(93)90114-6

Symington, L. S., and Petes, T. D. (1988). Meiotic recombination within the centromere of a yeast chromosome. *Cell* 52, 237–240. doi: 10.1016/0092-8674(88)90512-0

Szauter, P. (1984). An analysis of regional constraints on exchange in *Drosophila melanogaster* using recombination-defective meiotic mutants. *Genetics* 106, 45–71. doi: 10.1093/genetics/106.1.45

Thacker, D., Mohibullah, N., Zhu, X., and Keeney, S. (2014). Homologue engagement controls meiotic DNA break number and distribution. *Nature* 510, 241–246. doi: 10.1038/nature13120

Trelles-Sticken, E., Dresser, M. E., and Scherthan, H. (2000). Meiotic telomere protein Ndj1p is required for meiosis-specific telomere distribution, bouquet formation and efficient homologue pairing. *J. Cell Biol.* 151, 95–106. doi: 10.1083/jcb.151.1.95

Tsubouchi, H., and Roeder, G. S. (2006). Budding yeast Hed1 down-regulates the mitotic recombination machinery when meiotic recombination is impaired. *Genes Dev.* 20, 1766–1775. doi: 10.1101/gad.1422506

Vincenten, N., Kuhl, L. M., Lam, I., Oke, A., Kerr, A. R., Hochwagen, A., et al. (2015). The kinetochore prevents centromere-proximal crossover recombination during meiosis. *eLife* 4:e10850.

Voelkel-Meiman, K., Johnston, C., Thappeta, Y., Subramanian, V. V., Hochwagen, A., and MacQueen, A. J. (2015). Separable crossover-promoting and crossover-constraining aspects of Zip1 activity during budding yeast meiosis. *PLoS Genet.* 11:e1005335. doi: 10.1371/journal.pgen.1005335

Wang, S., Hassold, T., Hunt, P., White, M. A., Zickler, D., Kleckner, N., et al. (2017). Inefficient crossover maturation underlies elevated aneuploidy in human female meiosis. *Cell* 168, 977–989.e17.

Wang, S., Zickler, D., Kleckner, N., and Zhang, L. (2015). Meiotic crossover patterns: obligatory crossover, interference and homeostasis in a single process. *Cell Cycle* 14, 305–314. doi: 10.4161/15384101.2014.991185

Weinstein, A. (1918). Coincidence of crossing over in *Drosophila melanogaster* (AMPELOPHILA). *Genetics* 3, 135–172. doi: 10.1093/genetics/3.2.135

Westphal, T., and Reuter, G. (2002). Recombinogenic effects of suppressors of position-effect variegation in *Drosophila*. *Genetics* 160, 609–621. doi: 10.1093/genetics/160.2.609

White, M. A., Wang, S., Zhang, L., and Kleckner, N. (2017). Quantitative modeling and automated analysis of meiotic recombination. *Methods Mol. Biol.* 1471, 305–323. doi: 10.1007/978-1-4939-6340-9_18

Wyatt, H. D., and West, S. C. (2014). Holliday junction resolvases. *Cold Spring Harb. Perspect. Biol.* 6:a023192.

Xue, M., Wang, J., Jiang, L., Wang, M., Wolfe, S., Pawlowski, W. P., et al. (2018). The number of meiotic double-strand breaks influences crossover distribution in Arabidopsis. *Plant Cell* 30, 2628–2638. doi: 10.1105/tpc.18.00531

Yamamoto, M., and Miklos, G. L. (1978). Genetic studies on heterochromatin in *Drosophila melanogaster* and their implications for the functions of satellite DNA. *Chromosoma* 66, 71–98. doi: 10.1007/bf00285817

Yant, L., Hollister, J. D., Wright, K. M., Arnold, B. J., Higgins, J. D., Franklin, F. C. H., et al. (2013). Meiotic_ adaptation to genome duplication in *Arabidopsis arenosa*. *Curr. Biol.* 23, 2151–2156. doi: 10.1016/j.cub.2013.08.059

Yelina, N. E., Choi, K., Chelysheva, L., Macaulay, M., de Snoo, B., Wijnker, E., et al. (2012). Epigenetic remodeling of meiotic crossover frequency in *Arabidopsis thaliana* DNA methyltransferase mutants. *PLoS Genet.* 8:e1002844. doi: 10.1371/journal.pgen.1002844

Yıldız, Ö., Majumder, S., Kramer, B. C., and Sekelsky, J. (2002). Drosophila MUS312 interacts with the nucleotide excision repair endonuclease MEI-9 to generate meiotic crossovers. *Mol. Cell* 10, 1503–1509. doi: 10.1016/s1097-2765(02)00782-7

Zakharyevich, K., Tang, S., Ma, Y., and Hunter, N. (2012). Delineation of joint molecule resolution pathways in meiosis identifies a crossover-specific resolvase. *Cell* 149, 334–347. doi: 10.1016/j.cell.2012.03.023

Zalevsky, J., MacQueen, A. J., Duffy, J. B., Kemphues, K. J., and Villeneuve, A. M. (1999). Crossing over during *Caenorhabditis elegans* meiosis requires a conserved MutS-based pathway that is partially dispensable in budding yeast. *Genetics* 153, 1271–1283. doi: 10.1093/genetics/153.3.1271

Zhang, L., Kohler, S., Rillo-Bohn, R., and Dernburg, A. F. (2018). A compartmentalized signaling network mediates crossover control in meiosis. *eLife* 7:e30789.

Zhang, L., Liang, Z., Hutchinson, J., and Kleckner, N. (2014a). Crossover patterning by the beam-film model: analysis and implications. *PLoS Genet.* 10:e1004042. doi: 10.1371/journal.pgen.1004042

Zhang, L., Wang, S., Yin, S., Hong, S., Kim, K. P., and Kleckner, N. (2014b). Topoisomerase II mediates meiotic crossover interference. *Nature* 511, 551–556. doi: 10.1038/nature13442

Zickler, D., Moreau, P. J., Huynh, A. D., and Slezec, A. M. (1992). Correlation between pairing initiation sites, recombination nodules and meiotic recombination in *Sordaria macrospora*. *Genetics* 132, 135–148.

Ziolkowski, P. A., Underwood, C. J., Lambing, C., Martinez-Garcia, M., Lawrence, E. J., Ziolkowska, L., et al. (2017). Natural variation and dosage of the HEI10 meiotic E3 ligase control Arabidopsis crossover recombination. *Genes Dev.* 31, 306–317. doi: 10.1101/gad.295501.116

Conflict of Interest: The authors declare that the research was conducted in the absence of any commercial or financial relationships that could be construed as a potential conflict of interest.

Copyright © 2021 Pazhayam, Turcotte and Sekelsky. This is an open-access article distributed under the terms of the Creative Commons Attribution License (CC BY). The use, distribution or reproduction in other forums is permitted, provided the original author(s) and the copyright owner(s) are credited and that the original publication in this journal is cited, in accordance with accepted academic practice. No use, distribution or reproduction is permitted which does not comply with these terms.

frontiers in Cell and Developmental Biology

ORIGINAL RESEARCH
published: 13 August 2021
doi: 10.3389/fcell.2021.673073

MeiosisOnline: A Manually Curated Database for Tracking and Predicting Genes Associated With Meiosis

Xiaohua Jiang†, Daren Zhao†, Asim Ali†, Bo Xu, Wei Liu, Jie Wen, Huan Zhang, Qinghua Shi* and Yuanwei Zhang**

First Affiliated Hospital of USTC, Hefei National Laboratory for Physical Sciences at Microscale, School of Basic Medical Sciences, Division of Life Sciences and Medicine, CAS Center for Excellence in Molecular Cell Science, University of Science and Technology of China, Hefei, China

OPEN ACCESS

Edited by:
Liangran Zhang, Shandong University, China

Reviewed by:
Xuejiang Guo, Nanjing Medical University, China
Zuping He, Hunan First Normal University, China

***Correspondence:**
Huan Zhang
zhh1985@ustc.edu.cn
Qinghua Shi
qshi@ustc.edu.cn
Yuanwei Zhang
zyuanwei@ustc.edu.cn

† These authors have contributed equally to this work

Specialty section:
This article was submitted to Cell Growth and Division, a section of the journal Frontiers in Cell and Developmental Biology

Received: *26 February 2021*
Accepted: *12 July 2021*
Published: *13 August 2021*

Citation:
Jiang X, Zhao D, Ali A, Xu B, Liu W, Wen J, Zhang H, Shi Q and Zhang Y (2021) MeiosisOnline: A Manually Curated Database for Tracking and Predicting Genes Associated With Meiosis. Front. Cell Dev. Biol. 9:673073. doi: 10.3389/fcell.2021.673073

Meiosis, an essential step in gametogenesis, is the key event in sexually reproducing organisms. Thousands of genes have been reported to be involved in meiosis. Therefore, a specialist database is much needed for scientists to know about the function of these genes quickly and to search for genes with potential roles in meiosis. Here, we developed "MeiosisOnline," a publicly accessible, comprehensive database of known functional genes and potential candidates in meiosis (https://mcg.ustc.edu.cn/bsc/meiosis/index.html). A total of 2,052 meiotic genes were manually curated from literature resource and were classified into different categories. Annotation information was provided for both meiotic genes and predicted candidates, including basic information, function, protein–protein interaction (PPI), and expression data. On the other hand, 165 mouse genes were predicted as potential candidates in meiosis using the "Greed AUC Stepwise" algorithm. Thus, MeiosisOnline provides the most updated and detailed information of experimental verified and predicted genes in meiosis. Furthermore, the searching tools and friendly interface of MeiosisOnline will greatly help researchers in studying meiosis in an easy and efficient way.

Keywords: meiosis, manual curation, data mining, Greed AUC Stepwise, database

BACKGROUND

Meiosis, the process to generate daughter cells with an intact, haploid genome through one round of DNA replication followed by two rounds of cell division, is a basic feature of sexual reproductive organisms (Gerton and Hawley, 2005; Miller et al., 2013; Bolcun-Filas and Handel, 2018; Biswas et al., 2021). Compared with mitosis, meiosis is characterized by homologous chromosome separation, which ensures the genetic integrity of all daughter cells (Sato et al., 2021). A series of biological processes would take place during meiosis prophase I to guarantee the formation and repair of programmed meiotic DNA double-strand breaks (DSBs) and the pair and synapsis between homologous chromosomes, as well as the formation of meiotic crossovers (Handel and Schimenti, 2010; Baudat et al., 2013; Gray and Cohen, 2016; Ranjha et al., 2018; Jiao et al., 2020; Li et al., 2021).

With the development of genomic technologies on model organisms and recent advances of transcriptomics and proteomics, tremendous articles have been published on meiosis from different species, and we get a clearer understanding about the genetic control of key events in

meiosis (Watanabe et al., 2001; Wang et al., 2009; Chalmel and Rolland, 2015; Chen et al., 2018). However, information about meiotic genes is widely fragmented, which makes it still difficult to illuminate/highlight genes, molecular complexes, and/or signaling pathways involved in meiosis. What is more, it is still challenging to identify novel meiotic genes, especially in mammalian meiosis, since genetic modification in model organisms is time-consuming and is like a gamble sometimes (Khan et al., 2018, 2020; Huang et al., 2019; Xie et al., 2019; Yousaf et al., 2020). Thus, a specialist database that can provide integrated annotation of meiotic genes and predict novel functional genes is urgently needed.

Here, we report a publicly accessible, comprehensive database, MeiosisOnline.[1] It is the first resource that is not only a well-structured repository of experimentally verified meiotic genes with detailed annotation, but also a powerful tool to predict genes that may function in meiosis.

MATERIALS AND METHODS

Manual Curation of Literature

To collect the information of meiotic genes, specific keywords were used to search in PubMed (**Supplementary Table 1**). Then all the collected papers were curated manually and genes that had been validated by experiments were deemed as functional meiotic genes.

Gene Expression Data Collection

Gene expression information was retrieved from the ArrayExpress database.[2] Datasets from Affymetrix GeneChip platform were downloaded and were divided into different categories, including "developmental stages," "gene disturbance," "before and after treatment," and "tissues and cell types" (**Supplementary Table 2**). Gene expression data combined with category information are provided as annotation information in MeiosisOnline and applied for predicting genes that may function in meiosis.

Annotation

Annotation information for each gene in MeiosisOnline contains "basic information," "function annotation and classification," "protein–protein interaction (PPI) and gene expression."

(1) Basic information: gene name/synonyms, nucleotide sequences, etc., were extracted from GenBank[3] and UniProt Knowledgebase.[4]
(2) Function annotation and classification: detailed functional information is also manually collected from literature reports. (i) Which meiotic stage is the gene involved? (ii) Did the gene function in one sex or both sexes? (iii) Whether deletion or mutation of the gene in model organism has a phenotype in fertility? (iv) Which protein complex of the gene is involved? (v) The cellular location and expression pattern in tissues or cell lines. (vi) Experimental methods used for functional analysis. (vii) The information of related literature and figures for illustrating the function of protein/gene. (viii) Gene ontology annotation for collected genes.
(3) Protein–protein interaction and gene expression: both verified and predicted PPI information were provided. Gene expression pattern in reproductive system was also provided graphically.

Implementation

To execute more jobs in parallel, a Dell 730 server with LAMP architecture is used to host the MeiosisOnline database. The server is equipped with 128 GB RAM and two 12-core Intel processors (2.2 GHz). The jQuery is used to render the interface and Python and R languages are employed to supply the backend.

RESULTS

The Manual Curation of Meiosis-Related Genes From the Literature

MeiosisOnline is aiming to construct a functional annotation pipeline about meiosis-associated genes from published articles. After keywords querying in PubMed, about 45,000 research articles published before January 1, 2021, were collected. All collected papers were manually curated, and functional meiotic genes are only included as those with functional experimental validation (**Supplementary Table 3**). In total, 2,052 unique meiotic genes with experimentally verified functions from 84 species were curated along with functional information in MeiosisOnline. We found that the functional meiotic genes are firstly derived from mice, which accounts for 28.74% of the total reported genes, followed by human (5.16%) and rat (5.07%). Furthermore, other species comprise the rest of 61.03% (**Supplementary Table 4**). To be noted that the genes always have preferably expression profiles, for example, *Mlh3* (mg0000873) expresses during both male and female meiosis, *Sun5* (mg0000693) only presents in male germ cells, while *Bmp15* (mg0000982) is specially expressed in oocytes.

The Overall Framework of MeiosisOnline

MeiosisOnline is developed in a user-friendly manner and the major functional modules of the database (**Figure 1**) include:

Search Page

Users could find their interested genes using the Search page.[5]

Four additional search options were also provided[6]:

(1) Advanced search. Users can query up to three keywords and set up different combination by selecting the operators

[1] https://mcg.ustc.edu.cn/bsc/meiosis/index.html
[2] http://www.ebi.ac.uk/arrayexpress/
[3] http://www.ncbi.nlm.nih.gov/genbank
[4] http://www.uniprot.org/
[5] http://mcg.ustc.edu.cn/bsc/meiosis/search.html
[6] http://mcg.ustc.edu.cn/bsc/meiosis/advanced_search.html

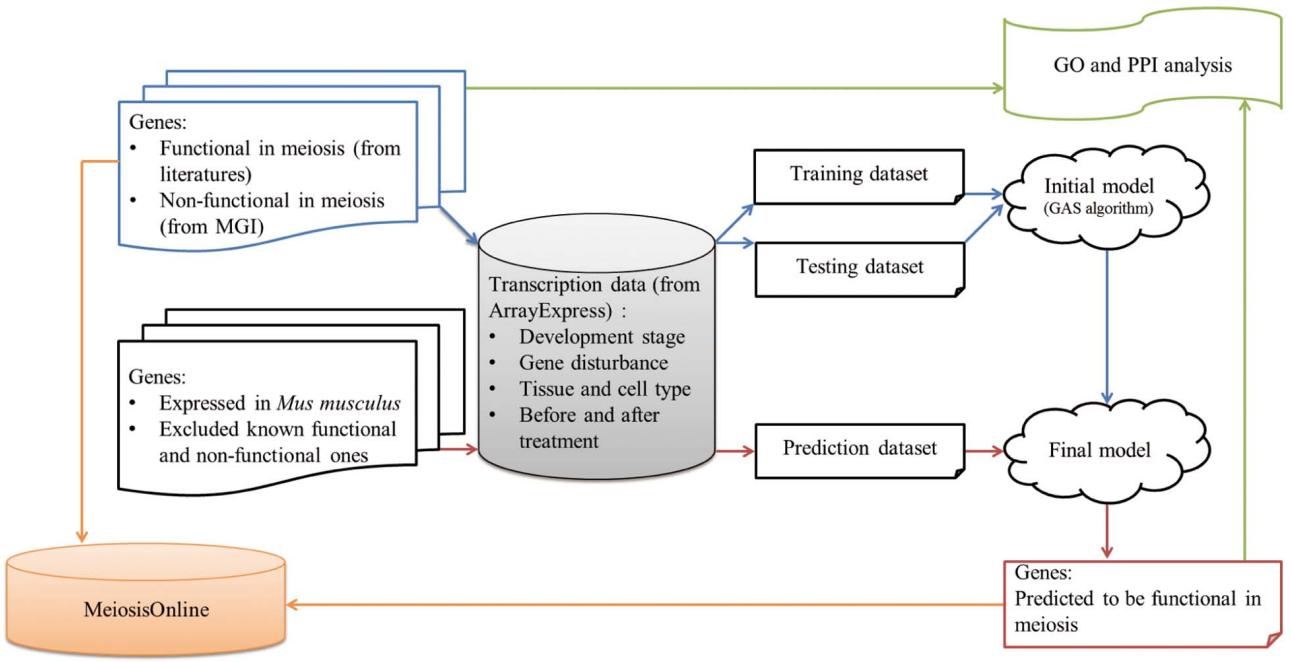

FIGURE 1 | MeiosisOnline database scheme. Manually curated functional genes in meiosis are collected and further incorporated in the MeiosisOnline database.

("and," "or," or "exclude") to find the information more specifically (**Supplementary Figure 1A**).

(2) BLAST search. After protein sequence (FASTA format) uploading, it could map identical and homologous proteins recorded in MeiosisOnline database (**Supplementary Figure 1B**).

(3) Orthologous search. Simple orthologous search is specified in finding orthologs for designated genes, while advanced orthologous search is to display all orthologs between two selected species (**Supplementary Figure 1C**).

(4) Chromosome location. This module could list all genes in a given genome region (**Supplementary Figure 1D**).

Browse Page

In the Browse page, users can browse genes by classifications or species[7] (**Supplementary Figure 2A**). Users can get all the genes belonging to a certain category in a tabular form. For example, users can browse MeiosisOnline Genes (MGs) collected from knockout mice (**Supplementary Figure 2B**) or MG genes identified in different species, e.g., *Homo sapiens* (**Supplementary Figure 2C**).

Candidates Page

In the Candidates page, MeiosisOnline lists all the predicted functional genes in mouse[8] (**Supplementary Figure 3A**). Clicking the MG ID, detailed information for a candidate gene can be seen (**Supplementary Figure 3B**).

[7]https://mcg.ustc.edu.cn/bsc/meiosis/browse.html

[8]http://mcg.ustc.edu.cn/bsc/meiosis/prediction.php

Feedback Page

Users can submit suggestions about the records integrated in MeiosisOnline or submit novel verified meiotic gene information to our database.[9]

MeiosisOnline Integrates Information of Functional Genes in Meiosis

Besides the general information including gene ID, protein ID, taxonomy ID, and basic descriptions, MeiosisOnline also provides high-quality functional annotation for the collected genes. Based on the function annotation information, the experimental verified genes were classified into different categories. Additionally, figures and/or tables illustrating the function of the collected meiotic genes were also incorporated. Moreover, manually annotated functions, signaling pathways, and associated protein complexes of the collected meiotic genes were provided (**Figure 2**). The functional distribution of these genes in various stages of meiosis and fecundity is also listed (**Supplementary Tables 4, 5**).

For instance, using "*Stra8*" for query, results will be listed in tabular form, including MeiosisOnline Gene ID (MG ID), gene names, UniProt ID, etc. (**Figure 2A**). Once clicking the MG ID (MG0001089), detailed information for mouse *Stra8* is available that includes the following: (1) basic information (gene name, nucleotide and protein sequences, etc.), (2) functional annotation and classification from related literature (developmental stages, experimental methods, literature abstract, relevant figures, etc.), and (3) PPI and gene expression information (**Figure 2B**).

[9]http://mcg.ustc.edu.cn/bsc/meiosis/feedback.html

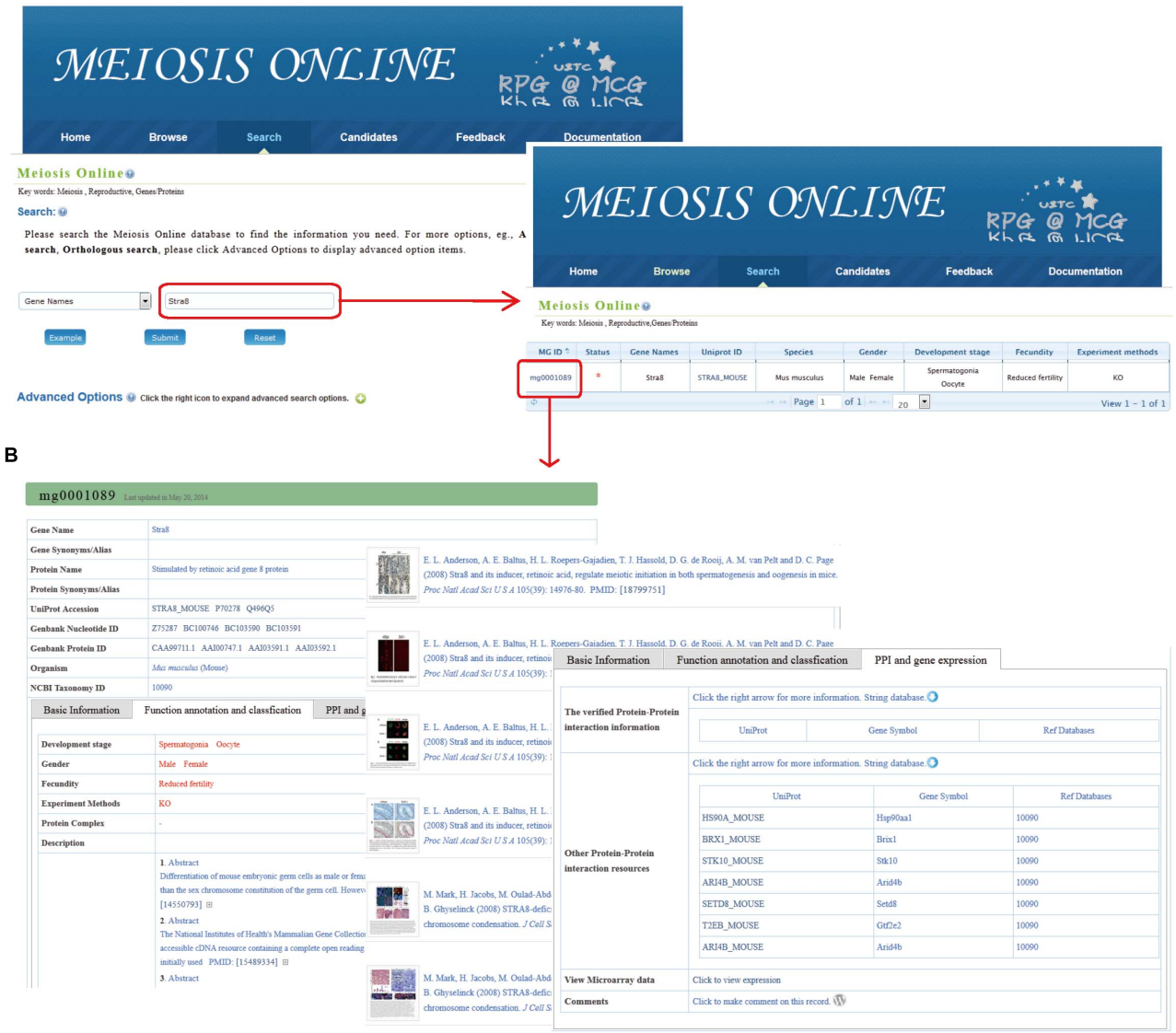

FIGURE 2 | The search function of MeiosisOnline. **(A)** Users can simply input gene "*Stra8*" for querying. The results are shown in a tabular format. Users can visualize the detailed information by clicking on the MeiosisOnline ID (MG0001089). **(B)** The detailed information for mouse gene "*Stra8*." The information presented has been manual checked and will be updated based on newly published data.

MeiosisOnline Facilitates the Discovery of Functional Meiotic Genes

To expand the utilization of our MeiosisOnline database, a prediction model was constructed and used to predict the candidate functional meiotic genes. As mouse is one of the best studied animal models, the GAS algorithm (Zhang et al., 2013) was used to predict potential meiotic functional genes from *Mus musculus* (**Supplementary Figure 4**).

To verify the efficiency of GAS, we randomly separated the training data into two equal parts: one as a new training dataset and the other as a testing dataset. The model was split into three stages: stage 1 was constructed with features of the category "developmental stages," stage 2 included features from the categories "tissues and cell types" and "before and after treatment," and stage 3 is the features of the category "gene disturbance." As shown in **Supplementary Figure 5**, the performances of GAS models were better when more features were added to them. Then, based on the experimentally verified meiotic genes and gene expression data, 590 mouse genes with experimentally verified function in meiosis were used as the positive training dataset. The negative training dataset contained 5,868 genes from MGI (Mouse Genome Informatics),[10]

[10]http://www.informatics.jax.org/

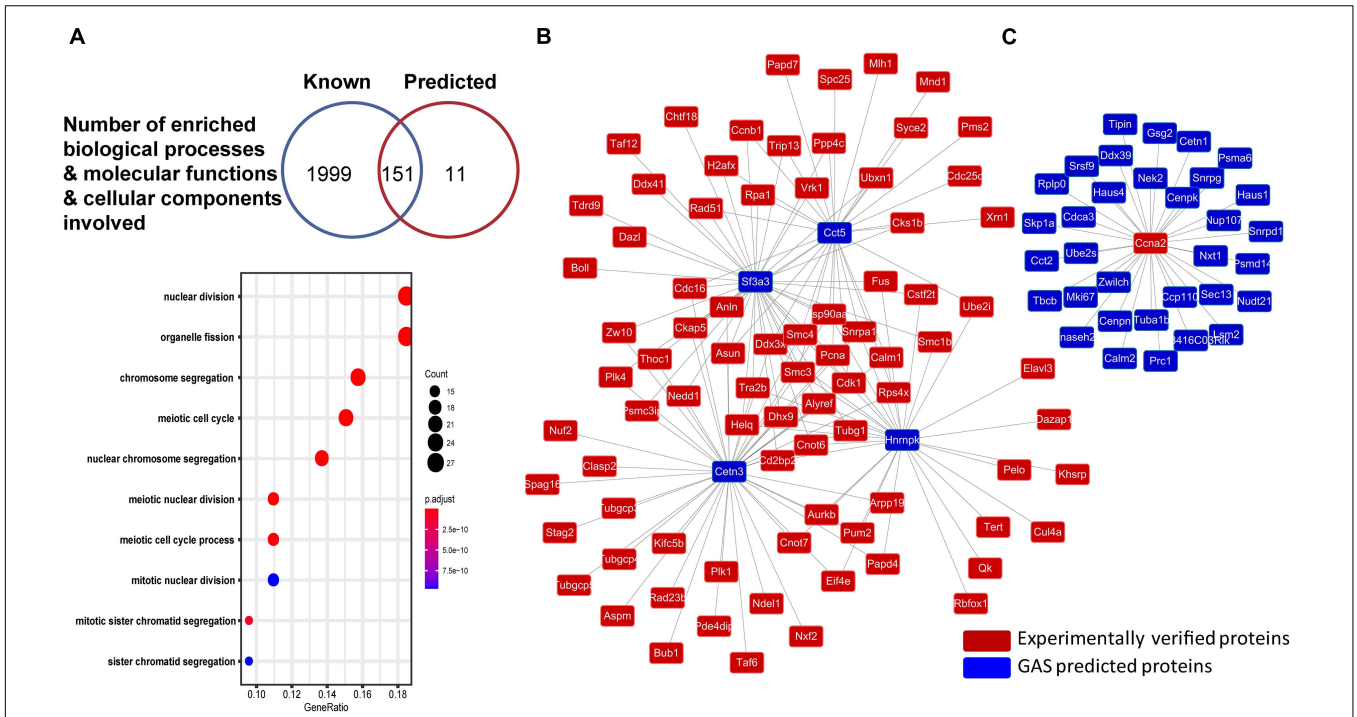

FIGURE 3 | The GO analysis and protein network in MeiosisOnline. **(A)** GO analysis for known and predicted genes in MeiosisOnline and GO enrichment analysis of the predicted genes. **(B,C)** The examples of potential protein network of meiosis analyzed by MeiosisOnline.

of which knockout mice did not have any abnormalities in the reproductive system. Three hundred and ninety-four features used for GAS construction and prediction were extracted from the 85 microarray data (**Supplementary Table 2**).

Ultimately, 165 candidate genes (GAS probability > 0.5) having potential role were sorted out and annotated in MeiosisOnline (see text footnote 8). For the candidate genes, information that implicate their function in meiosis, including gene expression, protein localization, structure, and protein interactions, are included in MeiosisOnline.

We also performed GO enrichment analysis on both literature-reported genes in *M. musculus* (**Supplementary Table 6**) and GAS-predicted candidate genes (**Supplementary Table 7**). Compared with whole genome data, we statistically calculated the distribution of MGs in cellular components, biological processes, and molecular functions by R (hypergeometric distribution, $p < 0.05$) (Yu et al., 2012). Among all GO terms, 118 in biological processes, 1 in molecular functions, and 32 in cellular components are overlapped in both sets of reported and predicted genes (**Figure 3A**). Considering that predicted genes enriched by overlapped GO term have more potential in regulating meiosis, interestingly, meiotic cell cycle (GO: 0051321) was enriched from both sets of genes (reported and predicted) (**Supplementary Table 8**).

Furthermore, as genes are mostly regulated through network structure in meiosis, we mapped out the PPIs among all of the genes and constructed a potential meiosis network with 1,083,566 reported PPIs among 26,569 proteins in MeiosisOnline. For example, *Cct5* and *Sf3a3*, which have not been reported, show very high connectivity with reported genes (**Figure 3B**). Further investigation of *Cct5* and *Sf3a3* would disclose how these two genes interacted with reported genes and what is the function of these interactions. Moreover, we also found that reported genes like *Ccna2* interacted wildly with predicted genes (**Figure 3C**).

DISCUSSION

Studies on animal models, especially genetically modified mice, have revealed many critical regulators involved in meiosis (Marston and Amon, 2004; Handel and Schimenti, 2010; Robert et al., 2016; Jiang et al., 2017, 2018); however, the information for these meiotic genes are scattered among thousands of papers. Thus, it is difficult to collect and compare the information of meiotic genes among different species from papers. Here, based on manual curation of meiosis-related genes from the literature, the first comprehensive database, MeiosisOnline, focusing on meiosis was developed.

As the fundamental process of gametogenesis, systematical annotation for meiotic genes is important to conduct further experiment study. Currently, only a few databases provided information related to meiosis, with limited features. Some databases were only repositories of gene expression data such as GermOnline 4.0 (Lardenois et al., 2010), SpPress (Vibranovski et al., 2009), and GermSAGE (Lee et al., 2009), and the utilization of these databases to obtain valuable information regarding experimentally verified function is not satisfactory. Some of

those are limited to a specific species or a certain biological process, such as SpPress that focused only on spermatogenesis in *Drosophila* (Vibranovski et al., 2009), ReCGiP that focused on reproduction in pig (Yang et al., 2010), and MeioBase that focused on meiotic genes in plant (Li et al., 2014). In our study, MeiosisOnline provided detailed and comprehensive information and annotation of the meiotic genes, including basic information, functional annotation and classification, PPI, and gene expression, etc. With these diverse information, users can easily access the detailed functional information of meiosis-associated genes.

Additionally, besides the proven functional meiotic genes, among the 2,300 genes that are predominantly expressed in the testis (Schultz et al., 2003), the function of most genes in meiosis are still unclear. In MeiosisOnline, based on literature-reported genes and genome-wide transcriptional data from ArrayExpress analysis, 165 genes (GAS probability > 0.5) in mouse are predicted to be involved in meiosis. As we know that homologous recombination is the basic feature of meiosis (Zickler and Kleckner, 2015), when we perform GO terms for the predicted genes by MeiosisOnline, double-strand break repair *via* homologous recombination (GO: 0000724) was one of the most enriched GO (**Supplementary Table 8**), which implies that these predicted genes may function during meiosis and further functional study by animal models should be conducted.

What is more, MeiosisOnline could conduct the study focus on complex molecular and/or signaling networks in meiosis. During meiosis, some genes are regulated through the network structure; for example, the deletion of *Hadc1* or *Ddac2* alone did not affect meiosis, while their combined deletion resulted in meiotic arrest and subsequent oocyte depletion (Ma et al., 2012). Hence, mapping out PPIs among known and predicted genes is useful in uncovering the novel regulating mechanism of meiosis.

In summary, MeiosisOnline is the first specialist database on meiosis. It not only provides comprehensive information for experimental verified meiotic genes but can also predict genes that may function in meiosis. It would be a helpful resource for researchers to gain a new insight in meiosis.

DATA AVAILABILITY STATEMENT

The original contributions presented in the study are included in the article/**Supplementary Material**, further inquiries can be directed to the corresponding author/s.

AUTHOR CONTRIBUTIONS

YZ and QS conceived and supervised the project. XJ, HZ, AA, and WL collected the data from the literature and ArrayExpress, as well as positive and negative training data for the prediction of potential meiotic functional genes. DZ developed the web interface. XJ, DZ, YZ, and QS wrote the manuscript. JW reviewed the manuscript. All authors contributed to the article and approved the submitted version.

FUNDING

This project was supported by the National Key Research and Developmental Program of China (2017YFC1001500, 2018YFC1003700, 2016YFC1000600, and 2018YFC1004700), the National Natural Science Foundation of China (31890780, 31630050, 31871514, and 82071709), and the Fundamental Research Funds for the Central Universities (YD2070002006 and YD2070002020).

ACKNOWLEDGMENTS

The authors thank the Bioinformatics Center of the University of Science and Technology of China, School of Life Science, for providing supercomputing resources. The authors also thank Dr. Xin Du in the 901st Hospital, Hefei, China, for his help in the data collection and analysis.

SUPPLEMENTARY MATERIAL

The Supplementary Material for this article can be found online at: https://www.frontiersin.org/articles/10.3389/fcell.2021.673073/full#supplementary-material

Supplementary Figure 1 | The advanced options of MeiosisOnline. **(A)** Advanced search which allows users to simultaneously input three terms for querying; **(B)** BLAST search used for protein sequence querying; **(C)** orthologous search. Browse orthologs for a gene in all species by simple search or browse orthologs of all genes in two species by advanced search. An example of pairwise orthologous browsing in human and mice were showed; **(D)** searching the MG genes based on chromosome and/or chromosomal location.

Supplementary Figure 2 | (A) All entries of MeiosisOnline can be browsed through taxonomic hierarchy and manual classifications; **(B)** by MG genes collected from KO mouse model, and **(C)** by MG genes identified in *Homo sapiens*.

Supplementary Figure 3 | (A) The candidate genes that are predicted by GAS model; **(B)** the detailed information of the predicted example gene "mg0002027."

Supplementary Figure 4 | The pseudo code illustrating the GAS algorithm.

Supplementary Figure 5 | The performance of GAS regarding its sensitivity (*Sn*), specificity (*Sp*), accuracy (*Ac*), Matthews correlation coefficient (MCC), and area under cover (AUC). Increase in the number of selected features resulted in improved AUC value.

REFERENCES

Baudat, F., Imai, Y., and De Massy, B. (2013). Meiotic recombination in mammals: localization and regulation. *Nat. Rev. Genet.* 14, 794–806. doi: 10.1038/nrg3573

Biswas, L., Tyc, K., El Yakoubi, W., Morgan, K., Xing, J., and Schindler, K. (2021). Meiosis interrupted: the genetics of female infertility via meiotic failure. *Reproduction* 161, R13–R35.

Bolcun-Filas, E., and Handel, M. A. (2018). Meiosis: the chromosomal foundation of reproduction. *Biol. Reprod.* 99, 112–126. doi: 10.1093/biolre/ioy021

Chalmel, F., and Rolland, A. D. (2015). Linking transcriptomics and proteomics in spermatogenesis. *Reproduction* 150, R149–R157.

Chen, Y., Zheng, Y., Gao, Y., Lin, Z., Yang, S., Wang, T., et al. (2018). Single-cell RNA-seq uncovers dynamic processes and critical regulators in mouse spermatogenesis. *Cell Res.* 28, 879–896. doi: 10.1038/s41422-018-0074-y

Gerton, J. L., and Hawley, R. S. (2005). Homologous chromosome interactions in meiosis: diversity amidst conservation. *Nat. Rev. Genet.* 6, 477–487. doi: 10.1038/nrg1614

Gray, S., and Cohen, P. E. (2016). Control of meiotic crossovers: from double-strand break formation to designation. *Annu. Rev. Genet.* 50, 175–210. doi: 10.1146/annurev-genet-120215-035111

Handel, M. A., and Schimenti, J. C. (2010). Genetics of mammalian meiosis: regulation, dynamics and impact on fertility. *Nat. Rev. Genet.* 11, 124–136. doi: 10.1038/nrg2723

Huang, Z., Khan, M., Xu, J., Khan, T., Ma, H., Khan, R., et al. (2019). The deubiquitinating gene Usp29 is dispensable for fertility in male mice. *Sci. China Life Sci.* 62, 544–552. doi: 10.1007/s11427-018-9469-4

Jiang, H., Gao, Q., Zheng, W., Yin, S., Wang, L., Zhong, L., et al. (2018). MOF influences meiotic expansion of H2AX phosphorylation and spermatogenesis in mice. *PLoS Genet.* 14:e1007300. doi: 10.1371/journal.pgen.1007300

Jiang, L., Li, T., Zhang, X., Zhang, B., Yu, C., Li, Y., et al. (2017). rpl10l is required for male meiotic division by compensating for RPL10 during meiotic sex chromosome inactivation in mice. *Curr. Biol.* 27, 1498–1505.e1496.

Jiao, Y., Fan, S., Jabeen, N., Zhang, H., Khan, R., Murtaza, G., et al. (2020). A TOP6BL mutation abolishes meiotic DNA double-strand break formation and causes human infertility. *Sci. Bull* 65, 2120–2129.

Khan, M., Jabeen, N., Khan, T., Hussain, H. M. J., Ali, A., Khan, R., et al. (2018). The evolutionarily conserved genes: Tex37, Ccdc73, Prss55 and Nxt2 are dispensable for fertility in mice. *Sci. Rep.* 8:4975.

Khan, R., Ye, J., Yousaf, A., Shah, W., Aftab, A., Shah, B., et al. (2020). Evolutionarily conserved and testis-specific gene, 4930524B15Rik, is not essential for mouse spermatogenesis and fertility. *Mol. Biol. Rep.* 47, 5207–5213. doi: 10.1007/s11033-020-05595-0

Lardenois, A., Gattiker, A., Collin, O., Chalmel, F., and Primig, M. (2010). GermOnline 4.0 is a genomics gateway for germline development, meiosis and the mitotic cell cycle. *Database* 2010:baq030. doi: 10.1093/database/baq030

Lee, T. L., Cheung, H. H., Claus, J., Sastry, C., Singh, S., Vu, L., et al. (2009). GermSAGE: a comprehensive SAGE database for transcript discovery on male germ cell development. *Nucleic Acids Res.* 37, D891–D897.

Li, H., Meng, F., Guo, C., Wang, Y., Xie, X., Zhu, T., et al. (2014). MeioBase: a comprehensive database for meiosis. *Front. Plant Sci.* 5:728. doi: 10.3389/fpls.2014.00728

Li, Y., Wu, Y. F., Jiang, H. W., Khan, R., Han, Q. Q., Iqbal, F., et al. (2021). The molecular control of meiotic double-strand break (DSB) formation and its significance in human infertility. *Asian J. Androl.*

Ma, P., Pan, H., Montgomery, R. L., Olson, E. N., and Schultz, R. M. (2012). Compensatory functions of histone deacetylase 1 (HDAC1) and HDAC2 regulate transcription and apoptosis during mouse oocyte development. *Proc. Natl. Acad. Sci. U.S.A.* 109, E481–E489.

Marston, A. L., and Amon, A. (2004). Meiosis: cell-cycle controls shuffle and deal. *Nat. Rev. Mol. Cell Biol.* 5, 983–997. doi: 10.1038/nrm1526

Miller, M. P., Amon, A., and Unal, E. (2013). Meiosis I: when chromosomes undergo extreme makeover. *Curr. Opin. Cell Biol.* 25, 687–696. doi: 10.1016/j.ceb.2013.07.009

Ranjha, L., Howard, S. M., and Cejka, P. (2018). Main steps in DNA double-strand break repair: an introduction to homologous recombination and related processes. *Chromosoma* 127, 187–214. doi: 10.1007/s00412-017-0658-1

Robert, T., Nore, A., Brun, C., Maffre, C., Crimi, B., Bourbon, H. M., et al. (2016). The TopoVIB-Like protein family is required for meiotic DNA double-strand break formation. *Science* 351, 943–949. doi: 10.1126/science.aad5309

Sato, M., Kakui, Y., and Toya, M. (2021). Tell the difference between mitosis and meiosis: interplay between chromosomes, cytoskeleton, and cell cycle regulation. *Front. Cell Dev. Biol.* 9:660322. doi: 10.3389/fcell.2021.660322

Schultz, N., Hamra, F. K., and Garbers, D. L. (2003). A multitude of genes expressed solely in meiotic or postmeiotic spermatogenic cells offers a myriad of contraceptive targets. *Proc. Natl. Acad. Sci. U.S.A.* 100, 12201–12206. doi: 10.1073/pnas.1635054100

Vibranovski, M. D., Lopes, H. F., Karr, T. L., and Long, M. (2009). Stage-specific expression profiling of Drosophila spermatogenesis suggests that meiotic sex chromosome inactivation drives genomic relocation of testis-expressed genes. *PLoS Genet.* 5:e1000731. doi: 10.1371/journal.pgen.1000731

Wang, Z., Gerstein, M., and Snyder, M. (2009). RNA-Seq: a revolutionary tool for transcriptomics. *Nat. Rev. Genet.* 10, 57–63. doi: 10.1038/nrg2484

Watanabe, Y., Yokobayashi, S., Yamamoto, M., and Nurse, P. (2001). Pre-meiotic S phase is linked to reductional chromosome segregation and recombination. *Nature* 409, 359–363. doi: 10.1038/35053103

Xie, Y., Khan, R., Wahab, F., Hussain, H. M. J., Ali, A., Ma, H., et al. (2019). The testis-specifically expressed Dpep3 is not essential for male fertility in mice. *Gene* 711:143925. doi: 10.1016/j.gene.2019.06.015

Yang, L., Zhang, X., Chen, J., Wang, Q., Wang, L., Jiang, Y., et al. (2010). ReCGiP, a database of reproduction candidate genes in pigs based on bibliomics. *Reprod. Biol. Endocrinol.* 8:96. doi: 10.1186/1477-7827-8-96

Yousaf, A., Wu, Y., Khan, R., Shah, W., Khan, I., Shi, Q., et al. (2020). Normal spermatogenesis and fertility in Ddi1 (DNA damage inducible 1) mutant mice. *Reprod. Biol.* 20, 520–524. doi: 10.1016/j.repbio.2020.08.006

Yu, G., Wang, L. G., Han, Y., and He, Q. Y. (2012). clusterProfiler: an R package for comparing biological themes among gene clusters. *OMICS* 16, 284–287. doi: 10.1089/omi.2011.0118

Zhang, Y., Zhong, L., Xu, B., Yang, Y., Ban, R., Zhu, J., et al. (2013). SpermatogenesisOnline 1.0: a resource for spermatogenesis based on manual literature curation and genome-wide data mining. *Nucleic Acids Res.* 41, D1055–D1062.

Zickler, D., and Kleckner, N. (2015). Recombination, pairing, and synapsis of homologs during meiosis. *Cold Spring Harb. Perspect. Biol.* 7:a016626. doi: 10.1101/cshperspect.a016626

Conflict of Interest: The authors declare that the research was conducted in the absence of any commercial or financial relationships that could be construed as a potential conflict of interest.

Publisher's Note: All claims expressed in this article are solely those of the authors and do not necessarily represent those of their affiliated organizations, or those of the publisher, the editors and the reviewers. Any product that may be evaluated in this article, or claim that may be made by its manufacturer, is not guaranteed or endorsed by the publisher.

Copyright © 2021 Jiang, Zhao, Ali, Xu, Liu, Wen, Zhang, Shi and Zhang. This is an open-access article distributed under the terms of the Creative Commons Attribution License (CC BY). The use, distribution or reproduction in other forums is permitted, provided the original author(s) and the copyright owner(s) are credited and that the original publication in this journal is cited, in accordance with accepted academic practice. No use, distribution or reproduction is permitted which does not comply with these terms.

frontiers in Cell and Developmental Biology

REVIEW
published: 16 August 2021
doi: 10.3389/fcell.2021.674203

A Hypothesis: Linking Phase Separation to Meiotic Sex Chromosome Inactivation and Sex-Body Formation

*Yiding Xu and Huanyu Qiao**

Department of Comparative Biosciences, University of Illinois at Urbana-Champaign, Urbana, IL, United States

During meiotic prophase I, X and Y chromosomes in mammalian spermatocytes only stably pair at a small homologous region called the pseudoautosomal region (PAR). However, the rest of the sex chromosomes remain largely unsynapsed. The extensive asynapsis triggers transcriptional silencing - meiotic sex chromosome inactivation (MSCI). Along with MSCI, a special nuclear territory, sex body or XY body, forms. In the early steps of MSCI, DNA damage response (DDR) factors, such as BRCA1, ATR, and γH2AX, function as sensors and effectors of the silencing signals. Downstream canonical repressive histone modifications, including methylation, acetylation, ubiquitylation, and SUMOylation, are responsible for the transcriptional repression of the sex chromosomes. Nevertheless, mechanisms of the sex-body formation remain unclear. Liquid-liquid phase separation (LLPS) may drive the formation of several chromatin subcompartments, such as pericentric heterochromatin, nucleoli, inactive X chromosomes. Although several proteins involved in phase separation are found in the sex bodies, when and whether these proteins exert functions in the sex-body formation and MSCI is still unknown. Here, we reviewed recent publications on the mechanisms of MSCI and LLPS, pointed out the potential link between LLPS and the formation of sex bodies, and discussed its implications for future research.

Keywords: meiosis, phase separation, sex body, DNA damage response, heterochromatin, meiotic sex chromosome inactivation

OPEN ACCESS

Edited by:
Akira Shinohara,
Osaka University, Japan

Reviewed by:
Jing Qu,
Institute of Zoology (CAS), China
Jesus Page,
Universidad Autómoma de Madrid, Spain

***Correspondence:**
Huanyu Qiao
hqiao@illinois.edu

Specialty section:
This article was submitted to Cell Growth and Division, a section of the journal Frontiers in Cell and Developmental Biology

Received: *28 February 2021*
Accepted: *22 July 2021*
Published: *16 August 2021*

Citation:
Xu Y and Qiao H (2021) A Hypothesis: Linking Phase Separation to Meiotic Sex Chromosome Inactivation and Sex-Body Formation. Front. Cell Dev. Biol. 9:674203. doi: 10.3389/fcell.2021.674203

INTRODUCTION

Meiosis is a special cell division that generates four gametes containing haploid genome. After DNA replication, germline cells enter meiotic prophase I, a prolonged G2-like stage. During prophase I, homologous chromosomes pair up, synapse, and exchange genetic fragments via a process known as homologous recombination. In mammalian spermatocytes, sex chromosomes (X and Y) are transcriptionally silenced by a mechanism known as meiotic sex chromosome inactivation (MSCI). Unlike autosomes that fully synapse between homologs at pachytene stage, the X and Y chromosomes only stably pair at the pseudo-autosomal region (PAR). Concurrent with MSCI, the silenced X and Y chromosomes are condensed and remodeled to form a distinct chromatin domain called sex body or XY body. Although the mechanism of MSCI has been extensively studied, how the sex body is formed and how the sex chromosomes are silenced are still unclear.

Increasing evidence suggests that DNA damage response (DDR) factors play important roles in MSCI (Namekawa, 2012; Turner, 2015). Proteins that typically respond to DNA double-strand breaks (DSBs) were found in the initiation steps of MSCI (Ichijima et al., 2012). Mutations in DDR

factors, such as BRCA1 (Turner et al., 2004), phosphorylated histone variant H2AX (Fernandez-capetillo et al., 2003), ATM- and Rad3-related (ATR) kinase, ATR-activator TOPBP1 (Royo et al., 2013), and MDC1 (Ichijima et al., 2011), disrupt MSCI and sex-body formation, suggesting these factors play essential roles in silencing sex chromosomes. Recent publications on methyltransferase SETDB1 further linked the DDR with downstream histone modifications and transcriptional silencing (Hirota et al., 2018). However, many other linking proteins and histone modifications yet remain to be explored.

Recently developed high-throughput chromosome conformation capture (Hi-C) has become a powerful tool to investigate the genome-wide chromatin conformation and interaction during meiosis (Ke et al., 2017; Alavattam et al., 2019; Patel et al., 2019; Wang et al., 2019). Based on the observation that the inactive X chromosome is isolated and distinctly regulated, Alavattam et al. (2019) first pointed out that the XY body and post-meiotic sex chromatin might form physically separated liquid droplets. We generated a frequency difference map to compare the Hi-C data of zygotene and pachytene chromosomes (sequencing data from Patel et al., 2019) and further confirmed that the sex body, as a separate territory, does not interact with other autosomes at pachytene stage (**Figure 1**; Page et al., 2012; Alavattam et al., 2019; Patel et al., 2019; Vara et al., 2019; Wang et al., 2019). Comparing to zygotene stage (**Figure 1A**), the interactions among autosomes are broadly reduced in pachytene stage, and contacts between the X chromosome and autosomes are completely lost (**Figures 1B,C**), indicating that sex chromosomes separate from autosomes at pachytene stage but not at zygotene stage. This is also described by Wang et al. (2019); they found that the X chromosome shows a unique chromatin configuration and largely loses topological association domains (TADs) and compartment features. These results are consistent with the observation of the distinct territory of sex chromosomes and the formation of the sex body (**Figure 1D**), which might largely abolish the interactions of sex chromosomes with autosomes.

While the factors involved in MSCI are well established, the mechanisms that physically separate sex chromosomes from autosomes have been an open question in the field. Wang et al. (2019) demonstrated there are more long-distance interactions within the X chromosome compared to autosomes, which may indicate X chromosomes are softer than stiff autosomes (Biggs et al., 2020). Unlike the rod-shaped autosomes, the territory of the X and Y chromosomes gradually becomes globe-shaped during sex-body formation. This unique sphere/egg-like shape of the sex body suggests surface tension at the liquid-liquid interface may minimize its surface area as what happens to oil droplets in water and phase-separated condensates in the nucleoplasm (Peng and Weber, 2019). Thus, we hypothesize that liquid-liquid phase separation (LLPS) may participate in the physical separation of sex chromosomes from the other autosomes. LLPS is a process in which a homogenous fluid demixes into two distinct liquid phases, driving the formation of various cellular compartments. Similar to how water is separated from oil in an oil-water mixture, many membraneless organelles, such as the nucleolus, Cajal body, and nuclear stress body, are possibly separated from the surrounding matter by LLPS (Aumiller et al., 2014; Razin and Gavrilov, 2020; Lafontaine et al., 2021). In addition, it has been implicated that LLPS drives the formation of heterochromatin regions that are transcriptionally inactive and enriched for repetitive sequences (Strom et al., 2017). However, how the phase separation influences gene expression is still a field that must be researched further. The X chromosome inactivation (XCI) silences one of the X chromosomes in female somatic cells and is also potentially related to LLPS (Cerase et al., 2019). The similarities between sex bodies and other membraneless organelles, heterochromatin, and XCI raise the possibility that LLPS also promotes the formation of sex bodies.

Here, we described the features of the sex body and reviewed the molecular mechanisms of MSCI. We also discussed current models for LLPS and its biological functions. Moreover, we hypothesized that LLPS could be the mechanisms for sex-body formation by comparing it with other phase-separating cellular condensates. Finally, we described several *in vivo* and *in vitro* experimental approaches to study LLPS proteins in sex bodies.

CHARACTERISTICS AND BEHAVIORS OF THE SEX BODY

During meiotic prophase I in spermatocytes, the X and Y chromosomes undergo significant structural remodeling, compact into heterochromatin, and form the sex body. In the chromosomal spreads of early pachytene spermatocytes, the sex body is easily observed as a separated structure. During pachytene and diplotene stages, the sex body is deeply stained by Giemsa, possessing two joined and two separated ends of the X and Y chromosomes.

This large and darkly stained body was first observed in mammalian spermatocytes in the 1890s (Solari, 1974). Although it had been debated for a while whether a single X chromosome or both sex chromosomes are in this structure, later studies showed that both X and Y chromosomes are linked in this intranuclear body. Scientists first incorrectly named them "sex vesicles" because they assumed a surrounding membrane encloses sex chromosomes (Solari, 1969, 1974). However, after noticing that the "sex vesicle" appears not to be a membrane-bounded structure, researchers renamed it as the "sex body." Solari (1974) also reviewed early studies on sex-body histochemistry. Initial assumptions claimed that this "sex vesicle" is enriched with RNA (Kaplan et al., 1956), however, Solari and Tres (1967) disproved this hypothesis by showing that RNA is only limited to the nucleolus that is associated with the sex body.

Unlike autosomes, X and Y chromosomes only partially synapse at their ends in a region called the pseudoautosomal region (PAR) where sex chromosomes share sequence homology (700 kb in mouse) (Perry et al., 2001). In mouse early pachytene cells, the synaptonemal complex (SC) loads on to 72% of the length of the Y axis and 22% of the X axis (Goetz et al., 1984). Furthermore, the chiasmata formed at the PAR is recognized at late pachytene stage (Burgoyne, 1982).

In summary, the sex body, a specialized and separated subnuclear structure, was identified and characterized in a set of

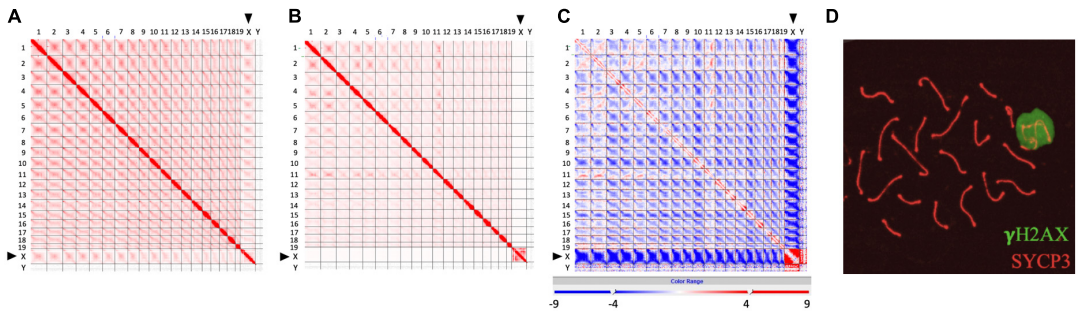

FIGURE 1 | Isolated sex chromosomes at pachytene stage. **(A–C)** Hi-C contact maps showing reduced interactions between X chromosome and autosomes at pachytene stage, compared to zygotene stage. **(A)** Genome-wide Hi-C contact map generated from zygotene spermatocytes (modified from Patel et al., 2019). **(B)** Genome-wide Hi-C contact map generated from pachytene spermatocytes (modified from Patel et al., 2019). **(C)** Frequency difference map showing differences of contact frequency between **(A,B)** (pachytene stage vs. zygotene stage) (data from Patel et al., 2019). In Hi-C contact maps **(A,B)**, the intensity of each square represents the normalized number of contacts between a pair of chromosomes. Interactions between the X chromosome and other autosomes (1–19) at zygotene stage are more intensive than those at pachytene stage. In frequency difference map **(C)**, the intensity of each square represents the contact frequency difference between maps **(A,B)**. The intensive blue color shown between the X chromosome and autosomes indicates that contact frequency is significantly decreased in map **(B)** (pachytene stage), compared to map **(A)** (zygotene stage). **(D)** Images showing a sex body covered by γH2AX signal (green) in pachytene spermatocytes. Lateral elements of homologous chromosomes were stained by SYCP3 antibody (red).

early studies. Although the characteristics and behaviors of the sex body at different stages have been described, the molecular and biophysical processes underlying the sex-body formation within the nucleus are still unclear.

MECHANISMS OF MSCI DURING MALE SPERMATOGENESIS

In recent years, the indispensable functions of MSCI during sex-body formation attract scientists' attention. MSCI is a process that transcriptionally silences the X and Y chromosomes during meiotic prophase I of male spermatogenesis. After the zygotene-to-pachytene transition, any unsynapsed chromatin regions on autosomes are silenced by meiotic silencing of unsynapsed chromatin (MSUC) (Baarends et al., 2005; Turner et al., 2005). At pachytene stage, major portions of the X and Y chromosomes still keep unsynaped. Thus, the X and Y chromosomes compartmentalize to form a specialized nuclear domain and undergo transcriptional silencing (MSCI). Defects in MSCI cause misexpression of toxic sex-linked genes, such as *Zfy1/2* (Royo et al., 2010), that can eliminate the defective spermatocytes (Royo et al., 2015).

Mechanisms of MSUC, and specifically, MSCI, have been extensively studied (**Figure 2**). Two sets of proteins, sensors and effectors, sequentially act to generate the silencing of sex chromosomes. In response to asynapsis, sensors initiate the signaling of asynapsis, such as HORMAD1 (Daniel et al., 2011), HORMAD2 (Wojtasz et al., 2012), and BRCA1 (Turner et al., 2004). Some effectors first localize to the unsynapsed axes, then spread to their associated chromatin loops, and mediate MSCI (Turner, 2015). ATR-TOPBP1 complexes are loaded onto the unsynapsed axes of the sex chromosomes and phosphorylated H2AX at Ser139 (Royo et al., 2013). Then, ATR-TOPBP1 complex further spreads to the chromatin loops directed by MDC1 (Ichijima et al., 2011). With the spreading of ATR-TOPBP1 complex, H2AX proteins along the chromatin loops are also phosphorylated by ATR, forming chromosome-wide γH2AX (**Figure 2**). γH2AX is essential for forming sex bodies and for inducing MSCI (Fernandez-capetillo et al., 2003). The sequential loading of MSCI-related proteins were summarized in **Figures 2**, **3** (Turner et al., 2004; Page et al., 2012; Turner, 2015).

MDC1 directly interacts with TOPBP1 and γH2AX during the amplification of phosphorylation signaling (**Figure 2**). In the absence of MDC1, ATR-TOPBP1, and γH2AX only restrict along the axes but not on the chromatin loops, indicating that the first-step axis localization of these DDR factors is MDC1-independent (Ichijima et al., 2011). Similarly, the failure of the chromosome-wide spreading of DDR factors also occurs in *H2ax-Y142A* mouse model. This mouse model has a point mutation on the phosphor-residue Y142 of H2AX that disrupts the interaction of γH2AX and MDC1 (Abe et al., 2020).

Although the loading of DDR proteins at early steps of MSCI has been well studied, what links the DDR network to the transcriptional silencing is largely unknown. Histone modifications, such as acetylation and methylation (Khalil et al., 2004), are involved in silencing sex chromosomes. A methyltransferase SETDB1 is recruited by γH2AX and mediates a gene-silencing-related histone modification – the trimethylation of histone H3 lysine 9 (H3K9me3) (Hirota et al., 2018). Tripartite motif-containing 28 (TRIM28) or KAP1 possibly bridges DDR to SETDB1 and regulates transcription (Hirota et al., 2018). However, more complicated epigenetic reprogramming might be involved in MSCI. For instance, the canonical histone H3.1 and H3.2 are replaced by H3.3 on unsynapsed sex chromosomes at mid-pachytene stage (van der Heijden et al., 2007). This replacement is accompanied by the loss of most histone post-translational modifications (PTMs), including temporally loss of H3K9me3 at pachytene stage (van der Heijden et al., 2007). This suggested there is a dramatic change in epigenetic modification and chromatin remodeling during both MSCI and MSUC.

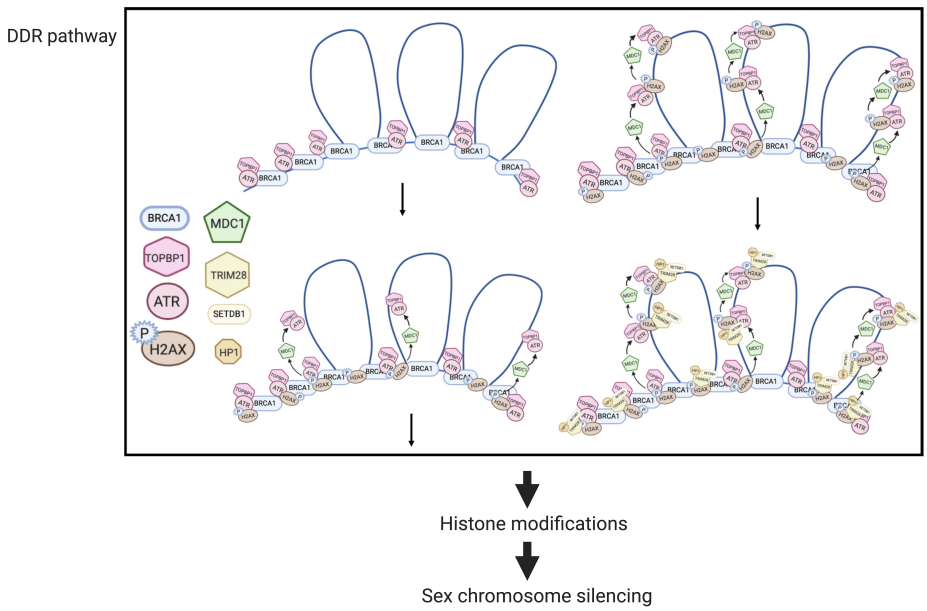

FIGURE 2 | MSCI mechanisms in mouse spermatocytes (modified from Ichijima et al., 2011). In DDR responses, BRCA1 first loads onto the unsynapsed chromosome axis, then recruits the ATR-TOPBP1 complex, which further spreads onto the chromatin loops facilitated by MDC1. H2AX is then phosphorylated by ATR, forming γ-H2AX. Downstream of the DDR pathway, histone modifications mediate the transcriptional silencing of sex chromosomes.

SEX-BODY FORMATION AND MSCI

The precise time course of the sex-body formation and the silencing of sex chromosomes have been long discussed (**Figure 3**). At early pachytene stage, after the initial sex-chromosome synapsis, MSCI-related proteins, such as SUMO1 (Small Ubiquitin Like Modifier 1), accumulate in the sex body (Rogers et al., 2004). At the same time, ubiquitin ligase UBR2 also localizes in the sex body and mediates histone H2A ubiquitination that is associated with transcriptional silencing of chromatin (Baarends et al., 2005). Page et al. (2012) demonstrated that silencing-related chromatin markers are present in the sex body before the transcriptional reactivation of autosomes. Thus, sex chromosomes may fail to reactivate at late zygotene stage rather than undergo inactivation at pachytene stage. Lau et al. (2020) also found transcriptional repression of the X chromosome starts before pachytene reactivation of autosomes by single-cell RNA-seq analysis. However, many other single-cell RNA-seq studies suggested that the initiation time of MSCI is pachytene stage (Chen et al., 2018; Green et al., 2018; Lukassen et al., 2018; Jung et al., 2019). The initiation-time difference may be caused by different clustering/staging approaches used in these RNA-seq studies.

As a separated, transcriptionally repressed chromatin region, the sex body harbors a range of specific proteins (**Figure 3**). DDR pathway proteins are found to be "sequestered" from the autosomes to the sex chromosome region at the initiation of MSCI (Abe et al., 2020). This "sequestration" effect could be explained by the high physicochemical affinity among these proteins (Handel, 2020). Besides those DDR factors, other proteins found in the sex body are also involved in heterochromatin formation. For instance, histone methyltransferase SUV39H2, a protein that modulates chromatin dynamics and usually distributes at the heterochromatin, accumulates to the sex-body region in pachytene spermatocytes (O'Carroll et al., 2000). Similarly, histone modification H3K9me3 plays an important role in meiotic heterochromatin assembly (Reuben and Lin, 2002; Hirota et al., 2018). H3K9me3 immunostaining signal increases in the sex-body region at early-mid pachytene transition, followed by temporal loss from mid/late-pachytene to late diplotene stage (van der Heijden et al., 2007; Page et al., 2012). Heterochromatin protein 1 (HP1), which binds to H3K9me3, has been shown to be related to chromatin condensation and transcriptional regulation. Two isoforms of the HP1 proteins, HP1β and HP1γ, decorate the entire sex body at late pachytene stage in human spermatocytes (Metzler-Guillemain et al., 2003), indicating their potential roles in condensing and silencing the sex chromosomes. However, more precise timing of HP1 loading should be explored, considering the complexity of histone modifications during MSCI. More interestingly, HP1-promoted phase separation has been proposed to facilitate the formation of chromatin sub-compartments (Erdel and Rippe, 2018) as well as transcriptional control (Hnisz et al., 2017).

Taken together, these studies provide evidence for potential close associations between MSCI and sex-body formation; however, the mechanisms underlying both processes need to be elucidated. Besides those well-studied proteins, the functions of many "sex-body" proteins are still uncertain. As reviewed by Handel (Handel, 2004), "sex-body" proteins, such as XMR (Escalier and Garchon, 2000), XYbp (Mazo and Pa, 2000), XY77, and ASY (Turner et al., 2000), all specifically localize in the sex

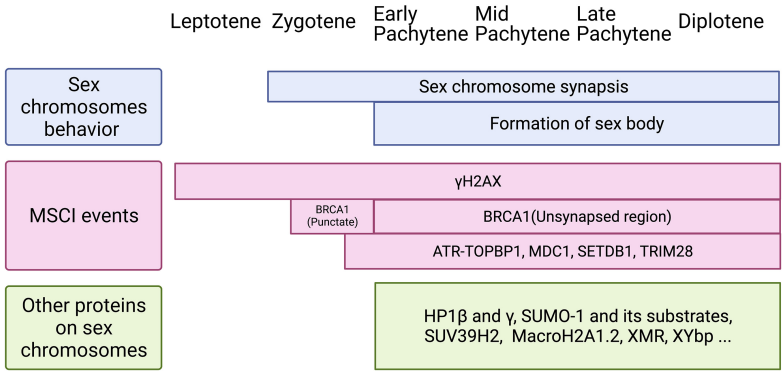

FIGURE 3 | Schematic of sex chromosomes behavior, MSCI events, and loading of other proteins on the sex body during meiotic prophase I. **Top:** Sex chromosomes start to synapse at zygotene stage and keep synapsis at PAR until diplotene stage. The cytologically observed sex body forms at early pachytene and maintains until diplotene stage. **Middle:** Two waves of γH2AX are identified during meiotic prophase I. It loads onto the X chromosome as early as leptotene stage and to the Y chromosome at late zygotene stage. Then, it remains on the sex chromosomes axis and spreads genome-wide during pachytene stage, and maintains until diplotene stage. BRCA1 is first found on sex chromosomes at late zygotene stage, shown as punctate staining, and then remains on the unsynapsed axis from pachytene to diplotene. DDR factors, including ATR-TOPBP1, MDC1, SETDB1, and TRIM28, appear on sex chromosomes from late zygotene stage or early pachytene stage. **Bottom:** Other proteins found on the sex body during pachytene to diplotene stages. Although the function of these proteins is not clear yet, it is possible they are involved in histone modifications, phase separation, and the formation of the sex body.

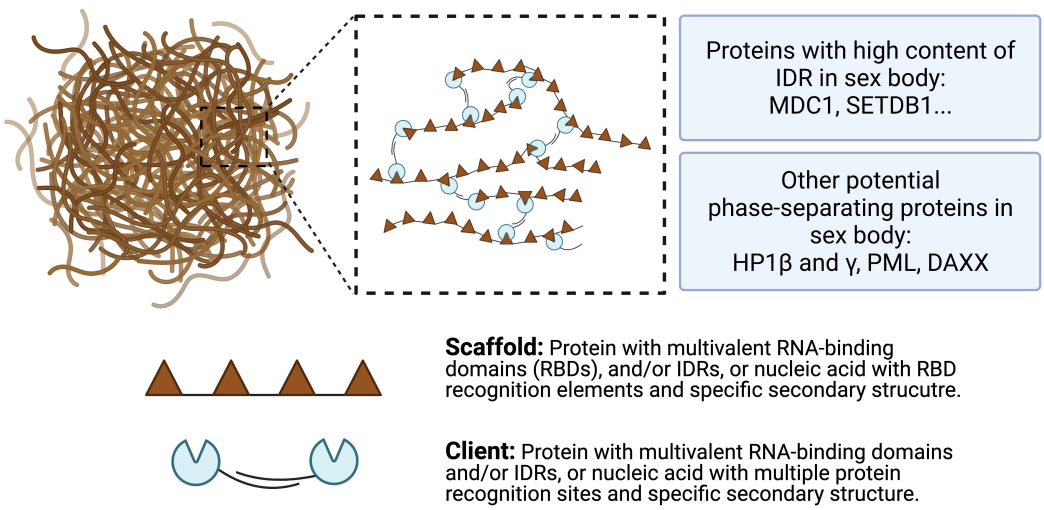

FIGURE 4 | A model for multivalent interactions driving LLPS in sex body. Multivalent scaffold molecules (brown) recruit client molecules (blue) to form a phase-separated liquid droplet. Scaffolds are essential components of the phase-separated body while clients are dispensable and often present under certain conditions. Client molecules, which are not required for the condensate formation, bind to interaction domains/elements on scaffolds. Weak multivalent interactions between scaffolds and clients drive the LLPS. Potential phase-separating proteins are listed, including proteins with high content of IDR and other potential proteins.

body; whereas, the functions of these proteins remain unknown. To investigate the mechanisms of the sex-body formation, future studies should link heterochromatin formation and phase separation with transcriptional silencing and illustrate the timing of these events.

INTRODUCTION TO LIQUID-LIQUID PHASE SEPARATION (LLPS)

In the cell, LLPS is a biophysical phenomenon where macromolecules (such as proteins or nucleic acids) condense into a dense phase that demixes and creates multiple co-existing phases. LLPS has been proposed to drive the formation of many membraneless intracellular condensates and transform the way we think about subcellular organization. No membrane is observed surrounding the sex body, which leads to the idea that LLPS might separate sex chromosomes from autosomes to form the sex body. In a eukaryotic cell, intracellular space is divided into several membrane-bound organelles, each of which conducts different functions. Besides the canonical organelles bound by phospholipid bilayer membranes, many cellular compartments/condensates are not membrane-delimited, such as nucleoli, and still can separate themselves from other cellular

components. Although these condensates are able to maintain their sizes and shapes, their assemblies are very dynamic and reversible. Environmental changes, such as composition, protein concentration, temperature, pH, and salt concentration, could all affect LLPS. Due to its dynamics, membraneless compartments can exert vital cellular functions and respond to environmental changes. For example, stress granules (SGs) are the LLPS-promoted assemblies of proteins and mRNAs under stress stimuli. They specifically function in the response to stress (Molliex et al., 2015).

So far, the detailed mechanisms of LLPS formation remain unclear. However, previous studies suggested that intermolecular multivalent interactions, including interactions between proteins, RNA, DNA, and membrane surface, are major drives of LLPS (Pak et al., 2016). A general model of scaffolds and clients is proposed to form the biomolecular condensates (**Figure 4**). Scaffolds are essential for the condensate formation. Protein scaffolds recruit various clients through intrinsically disordered regions (IDRs) while RNA scaffolds recruit clients via recognition elements of the RNA binding domains (RBDs) (Ditlev et al., 2018; Espinosa et al., 2020). Several characteristics of proteins and amino acids are responsible for forming phase-separated liquid droplets (Safaee and Michnick, 2016). For example, Wang et al. (2018) revealed that the LLPS of FUS-family proteins is driven by interactions between tyrosine and arginine residues. Liquid-droplet-forming proteins often contain low-complexity domains (LCDs). LCDs are composed of only a few different types of amino acids, either repeats of individual amino acids or short amino acid motifs. In addition, multiple-folded binding domains can interact with other peptides or nucleic acids; like LCD, proteins containing them have the ability to form phase-separated droplets (Banjade et al., 2015). Some theories have been proposed to mediate LLPS, such as the beta-amyloid formation model (Padrick and Miranker, 2002), the multivalent domain interaction network model (Falkenberg et al., 2013), and the polymer theory (Pappu et al., 2008), which have been reviewed by previous literature (Safaee and Michnick, 2016). However, how liquid droplets are assembled in a step-by-step manner still awaits for further investigations.

Phase separation is revealed to be responsible for the formation of heterochromatin (Strom et al., 2017). Similar to the heterochromatin regions, the sex body in male spermatocytes is also formed by heterochromatinization, suggesting a similar mechanism underlying the formation and silencing of both heterochromatin regions of autosomes and the sex body. To reveal these mechanisms, the common factors involved in phase separation within the two heterochromatic regions are still to be identified.

LLPS IN THE FORMATION OF NUCLEAR COMPARTMENTALIZATION

As a common phenomenon in the cell, LLPS is found to exert a variety of functions either at a single-cell level or during the development of organisms. A growing body of evidence suggests that LLPS forms phase-separated subcellular compartments (**Table 1**). In the nucleus, the formation of many membraneless organelles are facilitated by LLPS, such as nucleolus, Cajal body, clastosome, perinucleolar compartment, and polycomb body.

TABLE 1 | Membraneless compartments formed by LLPS in cells.

Compartment	Key components	Properties	Potential functions	References
P granules*	LAF-1, MEG-3, PGL-3	Spherical shape, undergoing fusion	Maintenance of germ cell totipotency, RNA processing, and storage	Brangwynne et al., 2009; Smith et al., 2016
Chromatoid body*	Ddx4	Cloud-like structure in male germ cells	piRNA-based gene silencing, RNA processing and storage	Kotaja and Sassone-Corsi, 2007
Balbiani body*	Xvelo	Solid-like structure in early-stage oocytes	Germline specification; protecting mitochondria and other organelles	Boke et al., 2016; Lei and Spradling, 2016
Nucleoli	FIB-1, DAO-5	Spherical shape, 1–4 per cell	Transcription and processing of rRNA, assembly of ribosome	Berry et al., 2015; Feric et al., 2016
Cajal body	Coilin, FMN	Spherical shape, 0–10 per cell	Modification and assembly of snRNA and snoRNA; trafficking of snRNP and snoRNP	Sawyer et al., 2019
Stress granules	hnRNPA1	100–200 nm in size	mRNA metabolism and translational control, involved in the pathogenesis of many diseases	Molliex et al., 2015
PML body	SUMO/SIM, TRF1/2	Spheres of 0.1–1.0 μm in diameter	DNA damage response, DNA repair, telomere homeostasis	Lallemand-Breitenbach and de Thé, 2010; Chung et al., 2011; Chang et al., 2018
Clastosome	19S and 20S proteasome	Doughnut-shaped	Protein degradation	Scherl et al., 2002
Polycomb body	Bmi1, Pc2, CBX2		Polycomb proteins mediated gene paring and silencing in *Drosophila*.	Vincenzo Pirrotta, 2012; Plys et al., 2019
P-bodies	EDC3, DDX6, LSM4, DCP2	8–10 nm in diameter	Primary piRNA processing	Luo et al., 2018
Centrosome	PLK1, CDK5RAP2/Cnn and Aurora-A	Consist of two barrel-shaped clusters of microtubules	Organization of microtubules and regulation of cytoskeletal structures	Mahen and Venkitaraman, 2012

**Indicates specific to germ cells.*

Although the functions of some phase-separated condensates remain to be determined, the majority of them are involved in transcription, processing of rRNA, modification of snRNA, snoRNA, and other nuclear RNAs/RNPs.

Except RNA-containing condensates, LLPS participates in the formation of promyelocytic leukemia protein (PML) nuclear bodies (Boisvert et al., 2000), which are involved in multiple genome maintenance pathways (Chang et al., 2018; Corpet et al., 2020). The components of the PML nuclear bodies, SUMO1 and its substrates (PML and DAXX), are also found to accumulate in the sex body (Rogers et al., 2004).

LLPS DRIVES FORMATION OF HETEROCHROMATIN

Studies have shown that LLPS mediates the formation of distinct, multi-chromosomal, membraneless heterochromatin regions (Strom et al., 2017). Heterochromatin is characterized as a tightly packed form of DNA that enriched repetitive sequences. Trimethylated H3K9 works with HP1 to pack DNA. HP1 is identified as an intermediate protein that bridges chromatin to form heterochromatin. Proteins containing IDRs and low-complexity sequences often trigger LLPS; HP1α has both sequences and exhibits liquid demixing *in vitro* and *in vivo* (Strom et al., 2017). This phenomenon leads to the idea that the formation of heterochromatin is driven by LLPS (Larson et al., 2017). Properties and dynamics of phase-separated droplets are also present in the heterochromatin regions/domains, such as sensitivity to the change of hydrophobic interactions. This provides further evidence suggesting that LLPS may be involved in the formation of heterochromatin. Although we have known that transcriptional repression of heterochromatin regions is associated with phase separation, it is still unclear how genes in these regions are silenced, and whether phase separation is directly related to gene silencing.

LLPS AND X-CHROMOSOME INACTIVATION

To balance the dosage of sex-linked genes in male and female cells, one of the X chromosomes in female is transcriptionally silenced by X chromosome inactivation (XCI) (Robert Finestra and Gribnau, 2017). Mechanisms underlying XCI have been studied for many decades in terms of protein recruitment, chromatin modification, and chromosome organization.

At the molecular level, X-inactive specific transcript (XIST), a long non-coding RNA (lnRNA), plays key regulatory roles in the repressive epigenetic modifications of XCI. A series of Xist-interacting proteins have been identified, which are involved in the transcriptional silencing and chromosome conformational changes. In the nucleus, XIST forms a cloud-like structure and works as a macromolecular platform to recruit its interactors (Minajigi et al., 2015). Histone modifiers, such as PRC1, PRC2 (Schoeftner et al., 2006; Mira-Bontenbal and Gribnau, 2016), and aurora kinase B (AURKB) (Hall et al., 2009), are identified as Xist-interactors and establish the repressive chromatin state. Cohesin proteins, including SMC1α,SMC3, RAD21, WAPL, and PDS5a/b, are also found in the Xist interactome. They are all involved in the structural reorganization of the inactive X chromosome (Xi) (Minajigi et al., 2015). CCCTC-binding factor (CTCF), a master regulator of genome architecture, also directly interacts with Xist RNA and mediates long-rang chromosomal interactions (Kung et al., 2015). Due to the actions of these proteins, the Xi is characterized by a variety of chromatin modifications (Pinter, 2016), including histone deacetylation (Belyaev et al., 1996), demethylation at histone H3 lysines 4 and 36 (Boggs et al., 2002), tri-methylation of lysine 27 in histone H3 (H3K27me3) mediated by PRC2 (Zhao et al., 2008), and monoubiquitination of lysine 119 in histone H2A (H2AK119ub1) mediated by PRC1 (de Napoles et al., 2004).

Revealed by genome capture technique, Hi-C, the active and inactive X chromosome show different topological conformations (Robert Finestra and Gribnau, 2017). The Xi chromosome is depleted of active/inactive compartments as well as topologically associating domains (TADs) (Filippova et al., 2005; Giorgetti et al., 2016; Pal et al., 2019). These chromosomal structural studies link the chromatin modifications with the chromosome organization as well as Xi transcriptional silencing, which makes the mechanism of XCI a classical example to study the epigenetic processes and gene regulation. Similarly, during meiosis in mammalian males, the X chromosome was found to be reorganized, isolated from all autosomes, and completely lose the compartment structure in pachytene stage (Patel et al., 2019). However, evidence showed that although both MSCI and XCI involve dramatic chromosome reorganization, the structures are distinct. For example, Xi displays two megadomains separated at the DXZ4 boundary (Giorgetti et al., 2016), which is not observed in sex chromosomes during male meiosis (Alavattam et al., 2019; Wang et al., 2019).

When comparing XCI in females and the silencing of sex chromosomes (MSCI) in males, some similarities should be aware of. First, high-throughput chromosome conformation capture (Hi-C) studies revealed TADs and compartments are lost during XCI and MSCI; the chromosome-wise transcriptional silencing of the X chromosome is a consequence of both processes (Giorgetti et al., 2016; Patel et al., 2019). Second, chromatin modifications, such as acetylation/deacetylation, methylation/demethylation, and ubiquitination, are utilized in both inactive chromatin regions. Third, more importantly, although there is still no direct evidence suggesting the involvement of phase separation in both processes, Cerase et al. (2019) summarized pieces of evidence showing that Xist assemblies resemble phase-separated condensates in size, morphology, and composition. Additionally, some binding partners of Xist have been shown to undergo LLPS and have a strong tendency for phase separation (Cerase et al., 2019). Considering the similarities between sex body and Xi, the involvement of LLPS in the formation of the sex body should also be considered.

ASSOCIATIONS AMONG SEX CHROMOSOMES AND NUCLEOLUS

The inactive X chromosome was described as the "nucleolar satellites" by Barr and Bertram (1949), indicating the close association is present between Xi and nucleoli. Zhang et al. (2007) also found that 80–90% of Xi localize to the nucleolus during mid-to-late S phase. This association is confirmed by the genome-wide mapping of nucleolus-associated chromosomal domains (NADs) (Dillinger et al., 2017). Analysis of chromatin states of NADs demonstrated that NADs are mainly heterochromatic and lack active chromatin. The localization of Xi to the condensed perinucleolar compartment is proposed to play essential roles in establishing its epigenetic status and repressing its genes (Zhang et al., 2007; Pandya-Jones et al., 2020). Similarly, the association of sex chromosomes with nucleolus was also observed decades ago (Gates, 1939). Nucleolar masses detach from the nucleolar organization sites of their autosomal origins and migrate toward the sex body at mid pachytene stage (Tres, 2005). At late pachytene stage, a half-moon-shaped nucleolus wraps up and covers half the surface of the sex body. The thread-like granule layer of the nucleolus penetrates deeply into the chromatin part of the sex body (Solari, 1969). *In situ* hybridization has shown that sex chromosomes were found non-randomly distributed in the nucleus and close to the nucleolus (Weipoltshammer et al., 1996; Schöfer and Weipoltshammer, 2018). It is still unknown how the association between sex body/Xi and nucleolus forms (Handel, 2020). However, we have already known phase-separation drives the formation of the nucleolus (Lafontaine et al., 2021). If sex body and Xi share similar phase-separating properties with the nucleolus, the fusion of the phase-separated sex body/Xi and nucleolus might explain these two associations.

APPROACHES AND TOOLS TO STUDY LLPS

Considering the similarity between sex body and other phase-separated condensates, we speculate that LLPS is the mechanism that drives the formation of the sex bodies. The results from Abe et al. (2020) suggested that the LLPS-mediated sex body functions as a sink to trap other proteins, which links this special structure with its potential functions. However, there is little research focusing on the roles of LLPS in sex-body formation. Here, we summarize several experimental approaches and tools that can be applied to study how LLPS drives sex-body formation.

It is known that only a small subset of proteins are able to undergo LLPS under specific conditions. Properties and sequences associated with these phase-separated proteins have been intensively studied. Two major types of proteins have been identified to form a network of interactions and promote LLPS. First, IDR-containing proteins are essential for phase separation. Certain polar and charged amino acids are often enriched in IDRs, including glycine (G), serine (S), glutamine (Q), proline (P), glutamic acid (E), lysine (K), and arginine (R). These charged amino acids enable various protein-protein and RNA-protein interactions to promote LLPS. In particular, IDR-containing proteins with low-complexity domains exhibit phase-separating properties. Second, the other type of phase-separated proteins is characterized by multiple folded domains that provide multivalent interactions with other proteins. For example, the SH3 domain covalently crosslinks with PRM ligands, driving phase transition (Li et al., 2012).

In common, both types of proteins mediate LLPS by multivalent interactions. Based on this property, whether a protein is able to undergo LLPS could be predicted by its primary sequence. Numerous analysis tools can be used to look for LLPS-promoting proteins, such as UniProt, BLAST, ProParam, and CIDER. In addition, LLPS predictors are generated based on searching disordered domains or regions. For example, MobiDB (Piovesan et al., 2021), D2P2, and DisMeta are powerful tools for disorder prediction. Moreover, several phase-separation predicting software have been developed. Pi-Pi predictor, Prion-like amino acid composition (PLAAC), and ZipperDB are designed for predicting the pi-pi contacts, prion-like domains, and fibril-forming segments, respectively. Alberti et al. (2019) compared and summarized the principles of different searching methods. Utilizing these tools and databases, meiotic proteins, especially those localizing to the sex body, could be screened and analyzed to determine whether they harbor phase-separating sequences and exhibit phase-separating properties. For example, using MobiDB, we obtained the disorder content of a list of meiosis-related proteins (**Table 2**), which helps identify phase-separation proteins in meiosis and providing the basis for future study of detailed characteristics. Among meiotic proteins we analyzed, although most of them are present in both sex chromosomes and autosomes, a DDR protein, 53BP1, accumulates in the XY body (Ahmed et al., 2007; Gupta et al., 2013; Lu et al., 2013). 53BP1 has a high content of IDR domains and has been shown to undergo phase separation (Kilic et al., 2019). In addition, MSCI-related protein, MDC1 (Ichijima et al., 2011), also shows a high percentage of disordered domains and is possibly involved in phase separation. Further *in vitro* and *in vivo* experiments should be conducted to investigate the potential roles of these two proteins in sex-body phase separation.

A growing number of *in vitro* experiments have been carried out to detect LLPS and study its underlying mechanisms and functions. First, *in vitro* phase-separation assay has been commonly used to study LLPS proteins. Second, engineered expression vectors containing fluorescence-tagged target proteins can also be utilized to study LLPS proteins in transfected cell lines, in which phase-separating behaviors could be visualized by fluorescent signals (Quiroz et al., 2020). Third, the self-assembly of phase-separating proteins *in vitro* can be visualized by conjugation and co-expression with fluorescent proteins, such as GFP. Fourth, approaches, including artificial modification of protein structures, changing of environmental conditions, and adding LLPS disruptors, have been used to study the dynamic features of LLPS proteins. For instance, 1,6-hexanediol, a disruptor of LLPS, is typically applied to determine whether LLPS plays a role in the formation of condensates both *in vivo* and *in vitro* (Ahn et al., 2020). Small molecules, such as kinases and ATPs, can also be added into *in vitro* phase-separation systems

TABLE 2 | IDR content information of meiosis-related proteins based on MobiDB.

Protein name	IDR content	Functions
Testis-specific H1 histone (H1t)	0.714	Associated with repressed chromatin domains in pachytene spermatocytes (Mahadevan et al., 2020)
Mediator of DNA damage checkpoint protein 1 (MDC1)	0.697	Functions in chromosome-wide silencing of the sex body (Ichijima et al., 2011)
TP53-binding protein 1 (53BP1)	0.624	DDR protein and localizes to the sex body (Lu et al., 2013)
Histone-lysine N-methyltransferase SETDB1	0.338	Links meiotic DDR to sex chromosome silencing (Hirota et al., 2018)
Pachytene checkpoint protein 2 homolog (Trip13)	0.338	Required for recombination and meiotic chromosome structure (Roig et al., 2010)
Synaptonemal complex protein 3 (SYCP3)	0.256	Component of synaptonemal complex (Syrjänen et al., 2014)
Cohesin subunit SA-3 (STAG3)	0.173	Maintaining centromere chromatid cohesion; required for DSB repair and synapsis (Hopkins et al., 2014)
DNA mismatch repair protein Mlh1	0.146	Homologous recombination and DSB repair (Cannavo et al., 2020)
Synaptonemal complex protein 2 (SYCP2)	0.144	Component of synaptonemal complex (Feng et al., 2017)
Serine/threonine-protein kinase Chk1	0.137	DNA damage response (Nie et al., 2017)
Meiotic recombination protein REC8	0.124	Sister-chromatid cohesion and crossover recombination (Yoon et al., 2016)
HORMA domain-containing protein 1 (HORMAD1)	0.094	Synaptonemal complex formation, recombination and chromosome segregation (Shin et al., 2010)
Double-strand-break repair protein rad21-like protein 1 (Rad21L1)	0.038	Maintaining the integrity of meiotic chromatin architecture (Blokhina et al., 2020)
Synaptonemal complex protein 1 (SYCP1)	0.036	Component of synaptonemal complex (de Vries et al., 2005)
Serine-protein kinase ATM	0.026	Controlling DSB formation and recombination (Lange et al., 2011; Kurzbauer et al., 2021)

and exert specific biological functions (Mackenzie et al., 2017). In addition, fluorescence recovery after photobleaching (FRAP), fluorescence correlation spectroscopy (FCS), and fluorescence resonance energy transfer (FRET), are also frequently conducted to evaluate the properties of LLPS condensates.

Not only *in vitro* LLPS systems build our knowledge on the behavior of LLPS proteins, but *in vivo* studies also provided insights into LLPS droplets in cells. Endogenous phase behavior has been revealed by engineered phase-separation sensors. In the study of keratohyalin granules (KGs) in the mammalian skin barrier, modified variants of phase-separating intrinsically disordered proteins (IDPs) were fused to fluorescent proteins and acted as phase separation sensors after transducing them into mouse embryos (Quiroz et al., 2020). These IDPs do not exhibit phase-separation behavior on their own; in contrast, when exposed to phase-separated droplets, they are able to engage in phase-separation-specific interactions and report nascent phase-separating activities. As a novel method to investigate phase separation *in vivo*, the phase-separation sensor can potentially be applied to explore LLPS in other tissues or cells. Additionally, mutations that alter the phase-separating properties, such as protein multivalency, can also be introduced to examine the LLPS functions (Nott et al., 2015). For instance, the hnRNP protein, TIA1, contains a C-terminal LCD domain that is predicted to be intrinsically disordered. Three ALS-associated TIA1 mutations exhibit increased phase-separation tendency that is caused by stronger protein-protein interactions (Mackenzie et al., 2017).

Although LLPS is likely a mechanism to explain the sex-body formation, other models for assembling chromatin subcompartments should also be considered as reviewed by Erdel and Rippe (2018). First, the multivalent interactions between chromatin-associated proteins promote LLPS. In polymer-polymer phase separation (PPPS) model, bridges between nucleosomes, rather than multivalent interactions in LLPS, facilitate the formation of phase-separated subcompartments within polymers (Singh and Newman, 2020). The bridging factors crosslinked chromatin fibers are usually chromatin-associated proteins lacking multivalent interactions, such as condensin (Ganji et al., 2018), cohesin (Rao et al., 2017), and YY1 (Weintraub et al., 2017). Second, without phase-separation, the simple binding between soluble factors and the chromatin scaffold is also able to form the chromatin subcompartments (Wachsmuth et al., 2008).

Experimental strategies to distinguish different mechanisms were also proposed by Erdel and Rippe (2018). First, tracking the (dis)assembly process over time could distinguish LLPS and PPPS because PPPS formation but not LLPS need nucleation sites. Thus, introducing and subsequently removing artificial nucleation sites can help us test whether LLPS multivalent interactions can hold the sex body together without nucleation sites. Second, with a concentration increase of constituting protein factors in the nucleoplasm, the size of the sex body should increase via LLPS but not via PPPS. Third, bridging factors need chromatin scaffolds to form biomolecule condensates. However, multivalent binders in LLPS can independently form condensates without chromatin scaffolds.

Some membraneless organelles can also transit from liquids (young) to gel/solid-like state (old) or have solid-like substructures, such as centrosomes (Woodruff et al., 2017). After they mature, the hardened solid-like organelles reduce the dynamics of their molecules (Banani et al., 2017), e.g., some HP1 proteins become immobile during the maturation of the heterochromatin regions/domains (Strom et al., 2017). Similarly, sex bodies might also display different material properties from liquids to solid-like feature with "aging." FRAP analysis can help us test this hypothesis (Boke et al., 2016) and show the "aged" sex

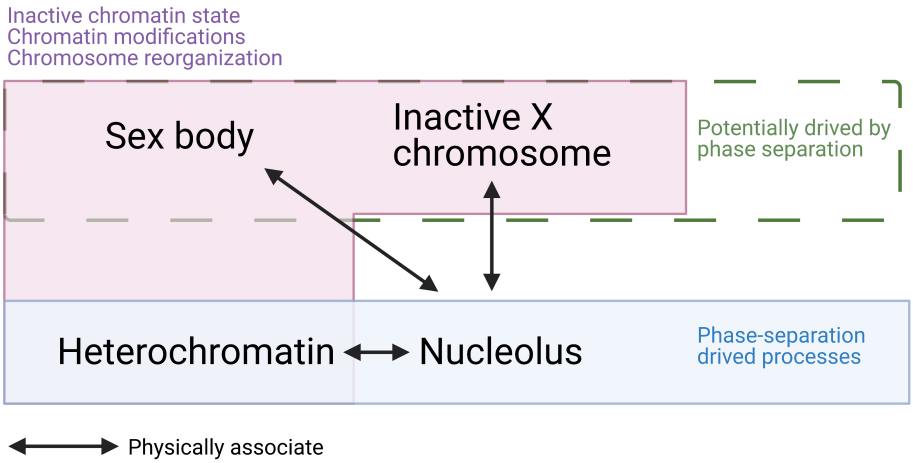

FIGURE 5 | A summary of similarities and associations among sex body, inactive X chromosome (Barr body), heterochromatin, and nucleolus. Sex body, Barr body, and heterochromatin are all physically associated with the nucleolus. While heterochromatin and nucleolus are confirmed to be driven by phase separation, sex body and Barr body are hypothesized to be formed by LLPS. In addition, sex body, Barr body, and heterochromatin all present inactive chromatin state, dramatic chromatin modifications, chromosome reorganizations. These similarities and associations raise the possibility that sex body is formed by LLPS.

body may not recover after full or partial bleaching. If it is true, the solid-like "aged" sex body loses its ability to incorporate and internally rearrange the fluorescence-tagged target proteins. This will be consistent with the idea that the hardened mature sex body serves as a sink to sequester its trapped proteins, including the DDR proteins, from the rest of the pachytene nucleoplasm (Abe et al., 2020).

CONCLUDING REMARKS AND FUTURE DIRECTIONS

Liquid-liquid phase separation is a driver for the assembly of membraneless biomolecular condensates in cells. It exerts a variety of functions, including sequestration of molecules, buffering molecule concentration, regulating the specificity and kinetics of biochemical reactions, genomic organization, RNA processing, and generating meiotic DNA breaks (Banani et al., 2017; Claeys Bouuaert et al., 2021). During male meiosis, sex chromosomes are reorganized, transcriptionally silenced by MSCI, and form a visibly distinct membraneless structure at pachytene stage. Although the molecular basis of MSCI has been extensively studied, it is not yet known what factors drive the formation of the sex body and mediate gene repression.

Here, we summarized several points that suggest there are similarities between the sex body and other phase-separation condensates and gene silencing processes (**Figure 5**). Firstly, the sex body has a similar appearance to other membraneless droplets formed by phase-separation and a separate territory that has a low interaction frequency with autosomes. Secondly, heterochromatin, which is structurally reorganized and transcriptionally silenced, is known to be formed by LLPS. Similarly, sex bodies also share the silencing status and histone modification with heterochromatin regions, such as H3K9me3. Thirdly, the phase-separating protein HP1 drives the formation of heterochromatin. Two isoforms of HP1, HP1β, and HP1γ, also localize to the sex body in spermatocytes (Metzler-Guillemain et al., 2003), indicating the resemblance of sex body and heterochromatin. Fourthly, MSCI also resembles XCI in female somatic cells. Both processes involve the recruitment of a set of proteins, histone modifications, chromosome reorganization, and transcriptional silencing. Cerase et al. (2019) gathered evidence and proposed a hypothesis that phase separation drives XCI. Overall, the similarities between sex-body formation and phase-separating processes raise the possibility that LLPS is a common driving force underlying all these processes—formation of the sex body, heterochromatin, and inactivation of the X chromosome.

Ever-growing experimental methods have been developed to study characteristics and mechanisms of LLPS, including both *in vivo* and *in vitro* approaches. Although growing clues indicate LLPS drives sex-body formation, so far, there is still no direct proof. In the future, approaches investigating LLPS in other cellular bodies could be applied to analyze sex-body formation. Softwares and tools analyzing protein sequences and phase-separating domains can be used to identify sex-body proteins involved in phase separation. Any identified phase-separating proteins can be further studied by *in vitro* or *in vivo* experiments. Established methods for visualizing the behavior of liquid condensates formed by LLPS will shed a light on the phase-separating process of sex bodies. Disrupting chemicals, such as 1,6-hexanediol, can be added to protein aggregates to determine whether phase separation will be disturbed. Phase separation sensors will enable the inspection of LLPS activity *in vivo*. Understanding the driving force and factors involved in sex-body formation is still challenging, however, new ways to explore LLPS characteristics will expand our knowledge on the properties of the sex bodies. By applying these methods to study proteins in the sex body, future studies are likely to identify many phase-separating proteins in the sex body. It is also intriguing to

know how some X-linked genes can escape MSCI in these phase-separated sex bodies. We speculate those gene regions may locate at the phase boundary/the surface of the sex body and dissociate from phase-separating components. A challenge in the future is to understand how these "sex body" proteins drive the sex-body formation step-by-step and how the structure of the sex body is maintained until the diplotene stage in spermatocytes.

AUTHOR CONTRIBUTIONS

YX and HQ contributed to the writing and editing of this review. Both authors contributed to the article and approved the submitted version.

FUNDING

This work was supported by NIH R00 HD082375 and NIH R01 GM135549.

ACKNOWLEDGMENTS

We would like to thank Dr. Satoshi Namekawa for his comments on this manuscript. We apologize to colleagues whose work may not have been cited due to length limitations. We thank Ning Liu, Yiheng Peng, Royal Shrestha, Aashna Prakash, Faaiza Nusayba Saif, and Erica Hana Joo for critical proofreading of the manuscript. We want to thank Yiheng Peng for helping to generate **Figure 1**.

REFERENCES

Abe, H., Alavattam, K. G., Hu, Y., Pang, Q., Andreassen, P. R., Hegde, R. S., et al. (2020). The initiation of meiotic sex chromosome inactivation sequesters DNA damage signaling from autosomes in mouse spermatogenesis. *Curr. Biol.* 30, 408–420. doi: 10.1016/j.cub.2019.11.064

Ahmed, E. A., van der Vaart, A., Barten, A., Kal, H. B., Chen, J., Lou, Z., et al. (2007). Differences in DNA double strand breaks repair in male germ cell types: lessons learned from a differential expression of Mdc1 and 53BP1. *DNA Repair (Amst)* 6, 1243–1254. doi: 10.1016/j.dnarep.2007.02.011

Ahn, J. I., Park, J. E., Meng, L., Zhang, L., Kim, T. S., Kruhlak, M. J., et al. (2020). Phase separation of the Cep63•Cep152 complex underlies the formation of dynamic supramolecular self-assemblies at human centrosomes. *Cell Cycle* 19, 3437–3457. doi: 10.1080/15384101.2020.1843777

Alavattam, K. G., Maezawa, S., Sakashita, A., Khoury, H., Barski, A., Kaplan, N., et al. (2019). Attenuated chromatin compartmentalization in meiosis and its maturation in sperm development. *Nat. Struct. Mol. Biol.* 26, 175–184. doi: 10.1038/s41594-019-0189-y

Alberti, S., Gladfelter, A., and Mittag, T. (2019). Considerations and challenges in studying liquid-liquid phase separation and biomolecular condensates. *Cell* 176, 419–434. doi: 10.1016/j.cell.2018.12.035

Aumiller, W. M., Davis, B. W., and Keating, C. D. (2014). Phase separation as a possible means of nuclear compartmentalization. *Int. Rev. Cell Mol. Biol.* 307, 109–149. doi: 10.1016/b978-0-12-800046-5.00005-9

Baarends, W. M., Wassenaar, E., van der Laan, R., Hoogerbrugge, J., Sleddens-Linkels, E., Hoeijmakers, J. H. J., et al. (2005). Silencing of unpaired chromatin and histone H2A ubiquitination in mammalian meiosis. *Mol. Cell. Biol.* 25, 1041–1053. doi: 10.1128/MCB.25.3.1041-1053.2005

Banani, S. F., Lee, H. O., Hyman, A. A., and Rosen, M. K. (2017). Biomolecular condensates: organizers of cellular biochemistry. *Nat. Rev. Mol. Cell Biol.* 18, 285–298. doi: 10.1038/nrm.2017.7

Banjade, S., Wu, Q., Mittal, A., Peeples, W. B., Pappu, R. V., and Rosen, M. K. (2015). Conserved interdomain linker promotes phase separation of the multivalent adaptor protein Nck. *Proc. Natl. Acad. Sci. U S A.* 112, E6426–E6435. doi: 10.1073/pnas.1508778112

Barr, M. L., and Bertram, E. G. (1949). A morphological distinction between neurones of the male and female, and the behaviour of the nucleolar satellite during accelerated nucleoprotein synthesis. *Nature* 163, 676–677. doi: 10.1038/163676a0

Belyaev, N. D., Keohane, A. M., and Turner, B. M. (1996). Differential underacetylation of histones H2A, H3 and H4 on the inactive X chromosome in human female cells. *Hum. Genet.* 97, 573–578. doi: 10.1007/BF02281863

Berry, J., Weber, S. C., Vaidya, N., Haataja, M., Brangwynne, C. P., and Weitz, D. A. (2015). RNA transcription modulates phase transition-driven nuclear body assembly. *Proc. Natl. Acad. Sci. U S A.* 112, E5237–E5245. doi: 10.1073/pnas.1509317112

Biggs, R. J., Liu, N., Peng, Y., Marko, J. F., and Qiao, H. (2020). Micromanipulation of prophase I chromosomes from mouse spermatocytes reveals high stiffness and gel-like chromatin organization. *Commun. Biol.* 3:542. doi: 10.1038/s42003-020-01265-w

Blokhina, Y. P., Frees, M., Nguyen, A., Sharifi, M., Chu, D. B., Draper, B. W., et al. (2020). Rad21l1 cohesin subunit is dispensable for spermatogenesis but not oogenesis in zebrafish. *bioRxiv [preprint]* doi: 10.1101/2020.09.23.309591

Boggs, B. A., Cheung, P., Heard, E., Spector, D. L., Chinault, A. C., and Allis, C. D. (2002). Differentially methylated forms of histone H3 show unique association patterns with inactive human X chromosomes. *Nat. Genet.* 30, 73–76. doi: 10.1038/ng787

Boisvert, F. M., Hendzel, M. J., and Bazett-Jones, D. P. (2000). Promyelocytic leukemia (PML) nuclear bodies are protein structures that do not accumulate RNA. *J. Cell Biol.* 148, 283–292. doi: 10.1083/jcb.148.2.283

Boke, E., Ruer, M., Wühr, M., Coughlin, M., Lemaitre, R., Gygi, S. P., et al. (2016). Amyloid-like self-assembly of a cellular compartment. *Cell* 166, 637–650. doi: 10.1016/j.cell.2016.06.051

Brangwynne, C. P., Eckmann, C. R., Courson, D. S., Rybarska, A., Hoege, C., Gharakhani, J., et al. (2009). Germline P granules are liquid droplets that localize by controlled dissolution/condensation. *Science* 324, 1729–1732. doi: 10.1126/science.1172046

Burgoyne, P. S. (1982). Genetic homology and crossing over in the X and Y chromosomes of mammals. *Hum. Genet.* 61, 85–90. doi: 10.1007/BF00274192

Cannavo, E., Sanchez, A., Anand, R., Ranjha, L., Hugener, J., Adam, C., et al. (2020). Regulation of the MLH1–MLH3 endonuclease in meiosis. *Nature* 586, 618–622. doi: 10.1038/s41586-020-2592-2592

Cerase, A., Armaos, A., Neumayer, C., Avner, P., Guttman, M., and Tartaglia, G. G. (2019). Phase separation drives X-chromosome inactivation: a hypothesis. *Nat. Struct. Mol. Biol.* 26, 331–334. doi: 10.1038/s41594-019-0223-220

Chang, H. R., Munkhjargal, A., Kim, M. J., Park, S. Y., Jung, E., Ryu, J. H., et al. (2018). The functional roles of PML nuclear bodies in genome maintenance. *Mutat. Res. - Fundam. Mol. Mech. Mutagen.* 809, 99–107. doi: 10.1016/j.mrfmmm.2017.05.002

Chen, Y., Zheng, Y., Gao, Y., Lin, Z., Yang, S., Wang, T., et al. (2018). Single-cell RNA-seq uncovers dynamic processes and critical regulators in mouse spermatogenesis. *Cell Res.* 28, 879–896. doi: 10.1038/s41422-018-0074-y

Chung, I., Leonhardt, H., and Rippe, K. (2011). De novo assembly of a PML nuclear subcompartment occurs through multiple pathways and induces telomere elongation. *J. Cell Sci.* 124, 3603–3618. doi: 10.1242/jcs.084681

Claeys Bouuaert, C., Pu, S., Wang, J., Oger, C., Daccache, D., Xie, W., et al. (2021). DNA-driven condensation assembles the meiotic DNA break machinery. *Nature* 592, 144–149. doi: 10.1038/s41586-021-03374-w

Corpet, A., Kleijwegt, C., Roubille, S., Juillard, F., Jacquet, K., Texier, P., et al. (2020). PML nuclear bodies and chromatin dynamics: catch me if you can! *Nucleic Acids Res.* 48, 11890–11912. doi: 10.1093/nar/gkaa828

Daniel, K., Lange, J., Hached, K., Fu, J., Anastassiadis, K., Roig, I., et al. (2011). Meiotic homologous chromosome alignment and its surveillance are controlled by mouse HORMAD1. *Nat. Cell Biol.* 13, 599–610. doi: 10.1038/ncb2213

de Napoles, M., Mermoud, J. E., Wakao, R., Tang, Y. A., Endoh, M., Appanah, R., et al. (2004). Polycomb group proteins ring1A/B link ubiquitylation of

histone H2A to heritable gene silencing and X inactivation. *Dev. Cell* 7, 663–676. doi: 10.1016/j.devcel.2004.10.005

de Vries, F. A. T., de Boer, E., van den Bosch, M., Baarends, W. M., Ooms, M., Yuan, L., et al. (2005). Mouse Sycp1 functions in synaptonemal complex assembly, meiotic recombination, and XY body formation. *Genes Dev.* 19, 1376–1389. doi: 10.1101/gad.329705

Dillinger, S., Straub, T., and Németh, A. (2017). Nucleolus association of chromosomal domains is largely maintained in cellular senescence despite massive nuclear reorganisation. *PLoS One* 12:e0178821. doi: 10.1371/journal.pone.0178821

Ditlev, J. A., Case, L. B., and Rosen, M. K. (2018). Who's in and who's out—compositional control of biomolecular condensates. *J. Mol. Biol.* 430, 4666–4684. doi: 10.1016/j.jmb.2018.08.003

Erdel, F., and Rippe, K. (2018). Formation of chromatin subcompartments by phase separation. *Biophys. J.* 114, 2262–2270. doi: 10.1016/j.bpj.2018.03.011

Escalier, D., and Garchon, H. (2000). XMR is associated with the asynapsed segments of sex chromosomes in the XY body of mouse primary spermatocytes. *Chromosoma* 109, 259–265. doi: 10.1007/s004120000075

Espinosa, J. R., Joseph, J. A., Sanchez-Burgos, I., Garaizar, A., Frenkel, D., and Collepardo-Guevara, R. (2020). Liquid network connectivity regulates the stability and composition of biomolecular condensates with many components. *Proc. Natl. Acad. Sci. U S A.* 117, 13238–13247. doi: 10.1073/pnas.1917569117

Falkenberg, C. V., Blinov, M. L., and Loew, L. M. (2013). Pleomorphic ensembles: formation of large clusters composed of weakly interacting multivalent molecules. *Biophys. J.* 105, 2451–2460. doi: 10.1016/j.bpj.2013.10.016

Feng, J., Fu, S., Cao, X., Wu, H., Lu, J., Zeng, M., et al. (2017). Synaptonemal complex protein 2 (SYCP2) mediates the association of the centromere with the synaptonemal complex. *Protein Cell* 8, 538–543. doi: 10.1007/s13238-016-0354-356

Feric, M., Vaidya, N., Harmon, T. S., Mitrea, D. M., Zhu, L., Richardson, T. M., et al. (2016). Coexisting liquid phases underlie nucleolar subcompartments. *Cell* 165, 1686–1697. doi: 10.1016/j.cell.2016.04.047

Fernandez-capetillo, O., Mahadevaiah, S. K., Celeste, A., Romanienko, P. J., Camerini-otero, R. D., Bonner, W. M., et al. (2003). H2AX is required for chromatin remodeling and inactivation of sex chromosomes in male mouse meiosis. *Dev. Cell* 4, 497–508. doi: 10.1016/s1534-5807(03)00093-5

Filippova, G. N., Cheng, M. K., Moore, J. M., Truong, J. P., Hu, Y. J., Nguyen, D. K., et al. (2005). Boundaries between chromosomal domains of X inactivation and escape bind CTCF and lack CpG methylation during early development. *Dev. Cell* 8, 31–42. doi: 10.1016/j.devcel.2004.10.018

Ganji, M., Shaltiel, I. A., Bisht, S., Kim, E., Kalichava, A., Haering, C. H., et al. (2018). Real-time imaging of DNA loop extrusion by condensin. *Science* 360, 102–105. doi: 10.1126/science.aar7831

Gates, R. R. (1939). Nucleoli, satellites and sex chromosomes. *Nature* 144, 794–795. doi: 10.1038/144794a0

Giorgetti, L., Lajoie, B. R., Carter, A. C., Attia, M., Zhan, Y., Xu, J., et al. (2016). Structural organization of the inactive X chromosome in the mouse. *Nature* 535, 575–579. doi: 10.1038/nature18589

Goetz, P., Chandley, A. C., and Speed, R. M. (1984). Morphological and temporal sequence of meiotic prophase development at puberty in the male mouse. *J. Cell Sci.* 65, 249–263. doi: 10.1242/jcs.65.1.249

Green, C. D., Ma, Q., Manske, G. L., Shami, A. N., Zheng, X., Marini, S., et al. (2018). A comprehensive roadmap of murine spermatogenesis defined by single-Cell RNA-Seq. *Dev. Cell* 46, 651–667.e10. doi: 10.1016/j.devcel.2018.07.025

Gupta, A., Hunt, C. R., Chakraborty, S., Pandita, R. K., Yordy, J., Ramnarain, D. B., et al. (2013). Role of 53BP1 in the regulation of DNA double-strand break repair pathway choice. *Radiat. Res.* 181, 1–8. doi: 10.1667/RR13572.1

Hall, L. L., Byron, M., Pageau, G., and Lawrence, J. B. (2009). AURKB-mediated effects on chromatin regulate binding versus release of XIST RNA to the inactive chromosome. *J. Cell Biol.* 186, 491–507. doi: 10.1083/jcb.200811143

Handel, M. A. (2004). The XY body: a specialized meiotic chromatin domain. *Exp. Cell Res.* 296, 57–63. doi: 10.1016/j.yexcr.2004.03.008

Handel, M. A. (2020). The XY body: an attractive chromatin domain. *Biol. Reprod.* 102, 985–987. doi: 10.1093/biolre/ioaa021

Hirota, T., Blakeley, P., Sangrithi, M. N., Mahadevaiah, S. K., Encheva, V., Snijders, A. P., et al. (2018). SETDB1 links the meiotic DNA damage response to sex chromosome silencing in mice. *Dev. Cell* 47, 645–659.e6. doi: 10.1016/j.devcel.2018.10.004

Hnisz, D., Shrinivas, K., Young, R. A., Chakraborty, A. K., and Sharp, P. A. (2017). A phase separation model for transcriptional control. *Cell* 169, 13–23. doi: 10.1016/j.cell.2017.02.007

Hopkins, J., Hwang, G., Jacob, J., Sapp, N., Bedigian, R., Oka, K., et al. (2014). Meiosis-specific cohesin component, Stag3 is essential for maintaining centromere chromatid cohesion, and required for DNA repair and synapsis between homologous chromosomes. *PLoS Genet.* 10:e1004413. doi: 10.1371/journal.pgen.1004413

Ichijima, Y., Ichijima, M., Lou, Z., Nussenzweig, A., Daniel Camerini-Otero, R., Chen, J., et al. (2011). MDC1 directs chromosome-wide silencing of the sex chromosomes in male germ cells. *Genes Dev.* 25, 959–971. doi: 10.1101/gad.2030811

Ichijima, Y., Sin, H. S., and Namekawa, S. H. (2012). Sex chromosome inactivation in germ cells: emerging roles of DNA damage response pathways. *Cell. Mol. Life Sci.* 69, 2559–2572. doi: 10.1007/s00018-012-0941-945

Jung, M., Wells, D., Rusch, J., Ahmad, S., Marchini, J., Myers, S. R., et al. (2019). Unified single-cell analysis of testis gene regulation and pathology in five mouse strains. *eLife* 8:e43966. doi: 10.7554/elife.43966

Kaplan, W. D., Kinosita, R., and Ohno, S. (1956). Concentration of RNA on the heteropycnotic XY bivalent of the rat. *Exp. Cell Res.* 11, 520–526. doi: 10.1016/0014-4827(56)90161-90166

Ke, Y., Xu, Y., Chen, X., Feng, S., Liu, Z., Sun, Y., et al. (2017). 3D chromatin structures of mature gametes and structural reprogramming during mammalian embryogenesis. *Cell* 170, 367–381.e20. doi: 10.1016/j.cell.2017.06.029

Khalil, A. M., Boyar, F. Z., and Driscoll, D. J. (2004). Dynamic histone modifications mark sex chromosome inactivation and reactivation during mammalian spermatogenesis. *Proc. Natl. Acad. Sci. U S A.* 101, 16583–16587. doi: 10.1073/pnas.0406325101

Kilic, S., Lezaja, A., Gatti, M., Bianco, E., Michelena, J., Imhof, R., et al. (2019). Phase separation of 53BP1 determines liquid-like behavior of DNA repair compartments. *EMBO J.* 38:e101379. doi: 10.15252/embj.2018101379

Kotaja, N., and Sassone-Corsi, P. (2007). The chromatoid body: a germ-cell-specific RNA-processing centre. *Nat. Rev. Mol. Cell Biol.* 8, 85–90. doi: 10.1038/nrm2081

Kung, J. T., Kesner, B., Erwin, J. A., and Lee, J. T. (2015). Locus-Specific targeting to the X chromosome revealed by the RNA interactome of CTCF. *Mol. Cell* 57, 361–375. doi: 10.1016/j.molcel.2014.12.006

Kurzbauer, M.-T., Janisiw, M. P., Paulin, L. F., Prusén Mota, I., Tomanov, K., Krsicka, O., et al. (2021). ATM controls meiotic DNA double-strand break formation and recombination and affects synaptonemal complex organization in plants. *Plant Cell* 33, 1633–1656. doi: 10.1093/plcell/koab045

Lafontaine, D. L. J., Riback, J. A., Bascetin, R., and Brangwynne, C. P. (2021). The nucleolus as a multiphase liquid condensate. *Nat. Rev. Mol. Cell Biol.* 22, 165–182. doi: 10.1038/s41580-020-0272-276

Lallemand-Breitenbach, V., and de Thé, H. (2010). PML nuclear bodies. *Cold Spring Harb. Perspect. Biol.* 2:a000661. doi: 10.1101/cshperspect.a000661

Lange, J., Pan, J., Cole, F., Thelen, M. P., Jasin, M., and Keeney, S. (2011). ATM controls meiotic double-strand-break formation. *Nature* 479, 237–240. doi: 10.1038/nature10508

Larson, A. G., Elnatan, D., Keenen, M. M., Trnka, M. J., Johnston, J. B., Burlingame, A. L., et al. (2017). Liquid droplet formation by HP1α suggests a role for phase separation in heterochromatin. *Nat. Publ. Gr.* 547, 236–240. doi: 10.1038/nature22822

Lau, X., Munusamy, P., Ng, M. J., and Sangrithi, M. (2020). Single-Cell RNA sequencing of the cynomolgus macaque testis reveals conserved transcriptional profiles during mammalian spermatogenesis. *Dev. Cell* 54, 548–566.e7. doi: 10.1016/J.DEVCEL.2020.07.018

Lei, L., and Spradling, A. C. (2016). Mouse oocytes differentiate through organelle enrichment from sister cyst germ cells. *Science* 352, 95–99. doi: 10.1126/science.aad2156

Li, P., Banjade, S., Cheng, H. C., Kim, S., Chen, B., Guo, L., et al. (2012). Phase transitions in the assembly of multivalent signalling proteins. *Nature* 483, 336–340. doi: 10.1038/nature10879

Lu, L.-Y., Xiong, Y., Kuang, H., Korakavi, G., and Yu, X. (2013). Regulation of the DNA damage response on male meiotic sex chromosomes. *Nat. Commun.* 4:2105. doi: 10.1038/ncomms3105

Lukassen, S., Bosch, E., Ekici, A. B., and Winterpacht, A. (2018). Single-cell RNA sequencing of adult mouse testes. *Sci. Data* 5:180192. doi: 10.1038/sdata.2018.192

Luo, Y., Na, Z., and Slavoff, S. A. (2018). P-Bodies: composition, properties, and functions. *Biochemistry* 57, 2424–2431. doi: 10.1021/acs.biochem.7b01162

Mackenzie, I. R., Nicholson, A. M., Sarkar, M., Messing, J., Purice, M. D., Pottier, C., et al. (2017). TIA1 mutations in amyotrophic lateral sclerosis and frontotemporal dementia promote phase separation and alter stress granule dynamics. *Neuron* 95, 808–816. doi: 10.1016/j.neuron.2017.07.025

Mahadevan, I. A., Kumar, S., and Rao, M. R. S. (2020). Linker histone variant H1t is closely associated with repressed repeat-element chromatin domains in pachytene spermatocytes. *Epigenetics Chromatin* 13:9. doi: 10.1186/s13072-020-00335-x

Mahen, R., and Venkitaraman, A. R. (2012). Spatial patterning of P granules by RNA-induced phase separation of the intrinsically-disordered protein MEG-3. *Curr. Opin. Cell Biol.* 24, 14–23. doi: 10.1016/j.ceb.2011.12.012

Mazo, Â, and Pa, M. (2000). XYbp, a novel RING-finger protein, is a component of the XY body of spermatocytes and centrosomes. *Mech. Dev.* 90, 95–101. doi: 10.1016/s0925-4773(99)00223-3

Metzler-Guillemain, C., Luciani, J., Depetris, D., Guichaoua, M. R., and Mattei, M. G. (2003). HP1β and HP1γ, but not HP1α, decorate the entire XY body during human male meiosis. *Chromosom. Res.* 11, 73–81. doi: 10.1023/A:1022014217196

Minajigi, A., Froberg, J. E., Wei, C., Sunwoo, H., Kesner, B., Colognori, D., et al. (2015). A comprehensive Xist interactome reveals cohesin repulsion and an RNA-directed chromosome conformation. *Science* 349:aab2276. doi: 10.1126/science.aab2276

Mira-Bontenbal, H., and Gribnau, J. (2016). New xist-interacting proteins in X-Chromosome inactivation. *Curr. Biol.* 26, R338–R342. doi: 10.1016/j.cub.2016.03.022

Molliex, A., Temirov, J., Lee, J., Coughlin, M., Kanagaraj, A. P., Kim, H. J., et al. (2015). Phase separation by low complexity domains promotes stress granule assembly and drives pathological fibrillization. *Cell* 163, 123–133. doi: 10.1016/j.cell.2015.09.015

Namekawa, S. H. (2012). Sex chromosome inactivation in germ cells: emerging roles of DNA damage response pathways. *Cell Mol. Life Sci.* 69, 2559–2572. doi: 10.1007/s00018-012-0941-5

Nie, Z.-W., Chen, L., Jin, Q.-S., Gao, Y.-Y., Wang, T., Zhang, X., et al. (2017). Function and regulation mechanism of Chk1 during meiotic maturation in porcine oocytes. *Cell Cycle* 16, 2220–2229. doi: 10.1080/15384101.2017.1373221

Nott, T. J., Petsalaki, E., Farber, P., Jervis, D., Fussner, E., Plochowietz, A., et al. (2015). Phase transition of a disordered nuage protein generates environmentally responsive membraneless organelles. *Mol. Cell* 57, 936–947. doi: 10.1016/j.molcel.2015.01.013

O'Carroll, D., Scherthan, H., Peters, A. H. F. M., Opravil, S., Haynes, A. R., Laible, G., et al. (2000). Isolation and characterization ofSuv39h2, a second histone H3 methyltransferase gene that displays testis-specific expression. *Mol. Cell. Biol.* 20, 9423–9433. doi: 10.1128/mcb.20.24.9423-9433.2000

Padrick, S. B., and Miranker, A. D. (2002). Islet amyloid: phase partitioning and secondary nucleation are central to the mechanism of fibrillogenesis. *Biochemistry* 41, 4694–4703. doi: 10.1021/bi0160462

Page, J., de la Fuente, R., Manterola, M., Parra, M. T., Viera, A., Berríos, S., et al. (2012). Inactivation or non-reactivation: what accounts better for the silence of sex chromosomes during mammalian male meiosis? *Chromosoma* 121, 307–326. doi: 10.1007/s00412-012-0364-y

Pak, C. W., Kosno, M., Holehouse, A. S., Padrick, S. B., Mittal, A., Ali, R., et al. (2016). Sequence determinants of intracellular phase separation by complex coacervation of a disordered protein. *Mol. Cell* 63, 72–85. doi: 10.1016/j.molcel.2016.05.042

Pal, K., Forcato, M., Jost, D., Sexton, T., Vaillant, C., Salviato, E., et al. (2019). Global chromatin conformation differences in the *Drosophila* dosage compensated chromosome X. *Nat. Commun.* 10:5355. doi: 10.1038/s41467-019-13350-13358

Pandya-Jones, A., Markaki, Y., Serizay, J., Chitiashvili, T., Mancia Leon, W. R., Damianov, A., et al. (2020). A protein assembly mediates Xist localization and gene silencing. *Nature* 587, 145–151. doi: 10.1038/s41586-020-2703-2700

Pappu, R. V., Wang, X., Vitalis, A., and Crick, S. L. (2008). A polymer physics perspective on driving forces and mechanisms for protein aggregation. *Arch. Biochem. Biophys.* 469, 132–141. doi: 10.1016/j.abb.2007.08.033

Patel, L., Kang, R., Rosenberg, S. C., Qiu, Y., Raviram, R., Chee, S., et al. (2019). Dynamic reorganization of the genome shapes the recombination landscape in meiotic prophase. *Nat. Struct. Mol. Biol.* 26, 164–174. doi: 10.1038/s41594-019-0187-180

Peng, A., and Weber, S. C. (2019). Evidence for and against liquid-liquid phase separation in the nucleus. *Non-coding RNA* 5:50. doi: 10.3390/ncrna5040050

Perry, J., Palmer, S., Gabriel, A., and Ashworth, A. (2001). A short pseudoautosomal region in laboratory mice. *Genome Res.* 11, 1826–1832. doi: 10.1101/gr.203001

Pinter, S. F. (2016). A tale of two cities: how xist and its partners localize to and silence the bicompartmental X. *Semin. Cell Dev. Biol.* 56, 19–34. doi: 10.1016/j.semcdb.2016.03.023

Piovesan, D., Necci, M., Escobedo, N., Monzon, A. M., Hatos, A., Mičetić, I., et al. (2021). MobiDB: intrinsically disordered proteins in 2021. *Nucleic Acids Res.* 49, D361–D367. doi: 10.1093/nar/gkaa1058

Plys, A. J., Davis, C. P., Kim, J., Rizki, G., Keenen, M. M., Marr, S. K., et al. (2019). Phase separation of polycomb-repressive complex 1 is governed by a charged disordered region of CBX2. *Genes Dev.* 33, 799–813. doi: 10.1101/gad.326488.119

Quiroz, F. G., Fiore, V. F., Levorse, J., Polak, L., Wong, E., Pasolli, H. A., et al. (2020). Liquid-liquid phase separation drives skin barrier formation. *Science* 367:eaax9554. doi: 10.1126/science.aax9554

Rao, S. S. P., Huang, S. C., Glenn, St Hilaire, B., Engreitz, J. M., Perez, E. M., et al. (2017). Cohesin loss eliminates all loop domains. *Cell* 171, 305–320.e24. doi: 10.1016/j.cell.2017.09.026

Razin, S. V., and Gavrilov, A. A. (2020). The role of liquid–liquid phase separation in the compartmentalization of cell nucleus and spatial genome organization. *Biochemistry* 85, 643–650. doi: 10.1134/S0006297920060012

Reuben, M., and Lin, R. (2002). Germline X chromosomes exhibit contrasting patterns of histone H3 methylation in *Caenorhabditis elegans*. *Dev. Biol.* 245, 71–82. doi: 10.1006/dbio.2002.0634

Robert Finestra, T., and Gribnau, J. (2017). X chromosome inactivation: silencing, topology and reactivation. *Curr. Opin. Cell Biol.* 46, 54–61. doi: 10.1016/j.ceb.2017.01.007

Rogers, R. S., Inselman, A., Handel, M. A., and Matunis, M. J. (2004). SUMO modified proteins localize to the XY body of pachytene spermatocytes. *Chromosoma* 113, 233–243. doi: 10.1007/s00412-004-0311-317

Roig, I., Dowdle, J. A., Toth, A., de Rooij, D. G., Jasin, M., and Keeney, S. (2010). Mouse TRIP13/PCH2 is required for recombination and normal higher-order chromosome structure during meiosis. *PLoS Genet.* 6:e1001062. doi: 10.1371/journal.pgen.1001062

Royo, H., Polikiewicz, G., Mahadevaiah, S. K., Prosser, H., Mitchell, M., Bradley, A., et al. (2010). Evidence that meiotic sex chromosome inactivation is essential for male fertility. *Curr. Biol.* 20, 2117–2123. doi: 10.1016/j.cub.2010.11.010

Royo, H., Prosser, H., Ruzankina, Y., Mahadevaiah, S., Cloutier, J., Baumann, M., et al. (2013). ATR acts stage specifically to regulate multiple aspects of mammalian meiotic silencing. *Genes Dev.* 27, 1484–1494. doi: 10.1101/gad.219477.113

Royo, H., Seitz, H., ElInati, E., Peters, A. H. F. M., Stadler, M. B., and Turner, J. M. A. (2015). Silencing of X-Linked MicroRNAs by meiotic sex chromosome inactivation. *PLoS Genet.* 11:e1005461. doi: 10.1371/journal.pgen.1005461

Safaee, N., and Michnick, S. W. (2016). Mechanisms and consequences of macromolecular phase separation. *Cell* 165, 1067–1079. doi: 10.1016/j.cell.2016.05.026

Sawyer, I. A., Sturgill, D., and Dundr, M. (2019). Membraneless nuclear organelles and the search for phases within phases. *Wiley Interdiscip. Rev. RNA* 10:e1514. doi: 10.1002/wrna.1514

Scherl, A., Coute, Y., De, C., Calle, A., Sanchez, J., Greco, A., et al. (2002). Clastosome: a subtype of nuclear body enriched in 19S and 20S proteasomes. *Mol. Biol. Cell* 13, 4100–4109. doi: 10.1091/mbc.E02

Schoeftner, S., Sengupta, A. K., Kubicek, S., Mechtler, K., Spahn, L., Koseki, H., et al. (2006). Recruitment of PRC1 function at the initiation of X inactivation

independent of PRC2 and silencing. *EMBO J.* 25, 3110–3122. doi: 10.1038/sj.emboj.7601187

Schöfer, C., and Weipoltshammer, K. (2018). Nucleolus and chromatin. *Histochem. Cell Biol.* 150, 209–225. doi: 10.1007/s00418-018-1696-1693

Shin, Y.-H., Choi, Y., Erdin, S. U., Yatsenko, S. A., Kloc, M., Yang, F., et al. (2010). Hormad1 mutation disrupts synaptonemal complex formation, recombination, and chromosome segregation in mammalian meiosis. *PLoS Genet.* 6:e1001190. doi: 10.1371/journal.pgen.1001190

Singh, P. B., and Newman, A. G. (2020). On the relations of phase separation and Hi-C maps to epigenetics. *R. Soc. Open Sci.* 7:191976. doi: 10.1098/rsos.191976

Smith, J., Calidas, D., Schmidt, H., Lu, T., Rasoloson, D., and Seydoux, G. (2016). Spatial patterning of P granules by RNA-induced phase separation of the intrinsically-disordered protein MEG-3. *eLife* 5: e21337. doi: 10.7554/eLife.21337

Solari, A. J. (1969). The evolution of the ultrastructure of the sex chromosomes (sex vesicle) during meiotic prophase in mouse spermatocytes. *J. Ultrastruct. Res.* 27, 289–305. doi: 10.1016/S0022-5320(69)80018-80013

Solari, A. J. (1974). The behavior of the XY pair in mammals. *Int Rev Cytol.* 38, 273–317. doi: 10.1016/s0074-7696(08)60928-6

Solari, A. J., and Tres, L. (1967). The localization of nucleic acids and the argentaffin substance in the sex vesicle of mouse spermatocytes. *Exp. Cell Res.* 47, 86–96. doi: 10.1016/0014-4827(67)90212-90211

Strom, A. R., Emelyanov, A., Mir, M., Fyodorov, D., Darzacq, X., and Carpen, G. (2017). Phase separation drives heterochromatin domain formation. *Nat. Publ. Gr.* 547, 241–245. doi: 10.1038/nature22989

Syrjänen, J. L., Pellegrini, L., and Davies, O. R. (2014). A molecular model for the role of SYCP3 in meiotic chromosome organisation. *eLife* 3:e02963. doi: 10.7554/eLife.02963

Tres, L. L. (2005). XY chromosomal bivalent: nucleolar attraction. *Mol. Reprod. Dev.* 72, 1–6. doi: 10.1002/mrd.20334

Turner, J. M. A. (2015). Meiotic silencing in mammals. *Annu. Rev. Genet.* 49, 395–412. doi: 10.1146/annurev-genet-112414-155145

Turner, J. M. A., Aprelikova, O., Xu, X., Wang, R., Kim, S., Chandramouli, G. V. R., et al. (2004). BRCA1, histone H2AX phosphorylation, and male meiotic sex chromosome inactivation. *Curr. Biol.* 14, 2135–2142. doi: 10.1016/j.cub.2004.11.032

Turner, J. M. A., Mahadevaiah, S. K., Benavente, R., Offenberg, H. H., Heyting, C., and Burgoyne, P. S. (2000). Analysis of male meiotic "sex body" proteins during XY female meiosis provides new insights into their functions. *Chromosoma* 109, 426–432. doi: 10.1007/s004120000097

Turner, J. M. A., Mahadevaiah, S. K., Fernandez-Capetillo, O., Nussenzweig, A., Xu, X., Deng, C. X., et al. (2005). Silencing of unsynapsed meiotic chromosomes in the mouse. *Nat. Genet.* 37, 41–47. doi: 10.1038/ng1484

van der Heijden, G. W., Derijck, A. A. H. A., Pósfai, E., Giele, M., Pelczar, P., Ramos, L., et al. (2007). Chromosome-wide nucleosome replacement and H3.3 incorporation during mammalian meiotic sex chromosome inactivation. *Nat. Genet.* 39, 251–258. doi: 10.1038/ng1949

Vara, C., Paytuví-Gallart, A., Cuartero, Y., Le Dily, F., Garcia, F., Salvà-Castro, J., et al. (2019). Three-Dimensional genomic structure and cohesin occupancy correlate with transcriptional activity during spermatogenesis. *Cell Rep.* 28, 352–367.e9. doi: 10.1016/j.celrep.2019.06.037

Vincenzo Pirrotta, H.-B. L. (2012). A view of nuclear Polycomb bodies. *Curr. Opin. Genet. Dev.* 22, 101–109. doi: 10.1016/j.gde.2011.11.004.A

Wachsmuth, M., Caudron-Herger, M., and Rippe, K. (2008). Genome organization: balancing stability and plasticity. *Biochim. Biophys. Acta - Mol. Cell Res.* 1783, 2061–2079. doi: 10.1016/j.bbamcr.2008.07.022

Wang, J., Choi, J. M., Holehouse, A. S., Lee, H. O., Zhang, X., Jahnel, M., et al. (2018). A molecular grammar governing the driving forces for phase separation of prion-like RNA binding proteins. *Cell* 174, 688–699.e16. doi: 10.1016/j.cell.2018.06.006

Wang, Y., Wang, H., Zhang, Y., Du, Z., Si, W., Fan, S., et al. (2019). Reprogramming of meiotic chromatin architecture during spermatogenesis. *Mol. Cell* 73, 547–561.e6. doi: 10.1016/j.molcel.2018.11.019

Weintraub, A. S., Li, C. H., Zamudio, A. V., Sigova, A. A., Hannett, N. M., Day, D. S., et al. (2017). YY1 is a structural regulator of enhancer-promoter loops. *Cell* 171, 1573–1588.e28. doi: 10.1016/j.cell.2017.11.008

Weipoltshammer, K., Schöfer, C., Almeder, M., Sylvester, J., and Wachtler, F. (1996). Spatial distribution of sex chromosomes and ribosomal genes: a study on human lymphocytes and testicular cells. *Cytogenet. Genome Res.* 73, 108–113. doi: 10.1159/000134319

Wojtasz, L., Cloutier, J. M., Baumann, M., Daniel, K., Varga, J., Fu, J., et al. (2012). Meiotic DNA double-strand breaks and chromosome asynapsis in mice are monitored by distinct HORMAD2-independent and -dependent mechanisms. *Genes Dev.* 26, 958–973. doi: 10.1101/gad.187559.112

Woodruff, J. B., Ferreira Gomes, B., Widlund, P. O., Mahamid, J., Honigmann, A., and Hyman, A. A. (2017). The centrosome is a selective condensate that nucleates microtubules by concentrating tubulin. *Cell* 169, 1066–1077.e10. doi: 10.1016/j.cell.2017.05.028

Yoon, S.-W., Lee, M.-S., Xaver, M., Zhang, L., Hong, S.-G., Kong, Y.-J., et al. (2016). Meiotic prophase roles of Rec8 in crossover recombination and chromosome structure. *Nucleic Acids Res.* 44, 9296–9314. doi: 10.1093/nar/gkw682

Zhang, L.-F., Huynh, K. D., and Lee, J. T. (2007). Perinucleolar Targeting of the Inactive X during S Phase: evidence for a role in the maintenance of silencing. *Cell* 129, 693–706. doi: 10.1016/j.cell.2007.03.036

Zhao, J., Sun, B. K., Erwin, J. A., Song, J.-J., and Lee, J. T. (2008). Polycomb proteins targeted by a short repeat RNA to the mouse X chromosome. *Science* 322, 750–756. doi: 10.1126/science.1163045

Conflict of Interest: The authors declare that the research was conducted in the absence of any commercial or financial relationships that could be construed as a potential conflict of interest.

Publisher's Note: All claims expressed in this article are solely those of the authors and do not necessarily represent those of their affiliated organizations, or those of the publisher, the editors and the reviewers. Any product that may be evaluated in this article, or claim that may be made by its manufacturer, is not guaranteed or endorsed by the publisher.

Copyright © 2021 Xu and Qiao. This is an open-access article distributed under the terms of the Creative Commons Attribution License (CC BY). The use, distribution or reproduction in other forums is permitted, provided the original author(s) and the copyright owner(s) are credited and that the original publication in this journal is cited, in accordance with accepted academic practice. No use, distribution or reproduction is permitted which does not comply with these terms.

frontiers in Cell and Developmental Biology

REVIEW
published: 18 August 2021
doi: 10.3389/fcell.2021.673642

The Application of Single-Cell RNA Sequencing in Mammalian Meiosis Studies

*Yiheng Peng and Huanyu Qiao**

Department of Comparative Biosciences, University of Illinois at Urbana-Champaign, Urbana, IL, United States

Meiosis is a cellular division process that produces gametes for sexual reproduction. Disruption of complex events throughout meiosis, such as synapsis and homologous recombination, can lead to infertility and aneuploidy. To reveal the molecular mechanisms of these events, transcriptome studies of specific substages must be conducted. However, conventional methods, such as bulk RNA-seq and RT-qPCR, are not able to detect the transcriptional variations effectively and precisely, especially for identifying cell types and stages with subtle differences. In recent years, mammalian meiotic transcriptomes have been intensively studied at the single-cell level by using single-cell RNA-seq (scRNA-seq) approaches, especially through two widely used platforms, Smart-seq2 and Drop-seq. The scRNA-seq protocols along with their downstream analysis enable researchers to accurately identify cell heterogeneities and investigate meiotic transcriptomes at a higher resolution. In this review, we compared bulk RNA-seq and scRNA-seq to show the advantages of the scRNA-seq in meiosis studies; meanwhile, we also pointed out the challenges and limitations of the scRNA-seq. We listed recent findings from mammalian meiosis (male and female) studies where scRNA-seq applied. Next, we summarized the scRNA-seq analysis methods and the meiotic marker genes from spermatocytes and oocytes. Specifically, we emphasized the different features of the two scRNA-seq protocols (Smart-seq2 and Drop-seq) in the context of meiosis studies and discussed their strengths and weaknesses in terms of different research purposes. Finally, we discussed the future applications of scRNA-seq in the meiosis field.

Keywords: meiosis, single-cell RNA-seq, transcription, transcriptome, spermatocyte, oocyte, spermatogenesis, oogenesis

OPEN ACCESS

Edited by:
Liangran Zhang,
Shandong University, China

Reviewed by:
Shuiqiao Yuan,
Huazhong University of Science and Technology, China
Mengcheng Luo,
Wuhan University, China

***Correspondence:**
Huanyu Qiao
hqiao@illinois.edu

Specialty section:
This article was submitted to Cell Growth and Division, a section of the journal Frontiers in Cell and Developmental Biology

Received: *28 February 2021*
Accepted: *05 July 2021*
Published: *18 August 2021*

Citation:
Peng Y and Qiao H (2021) The Application of Single-Cell RNA Sequencing in Mammalian Meiosis Studies. Front. Cell Dev. Biol. 9:673642. doi: 10.3389/fcell.2021.673642

INTRODUCTION

Meiosis has been studied for decades. Sexual reproduction requires meiosis to generate haploid gametes from diploid germline cells. Starting at early prophase I (leptonema), mammalian meiotic chromosomes condense gradually and pair to their homologous chromosomes (homologs) with the help of DNA double-strand breaks (DSBs). At the beginning of the next stage (zygonema), a protein structure called Synaptonemal Complex (SC) forms to link homologs at several chromosome sites, accompanied by exchanging genetic materials at the crossover sites that usually originate from the SC initiation sites (Page and Hawley, 2004). The SCs zip up all the homologs from end to end except sex chromosomes at the entry of pachynema and disassemble at late prophase I (diplonema). Homologs with exchanged genetic material are aligned at metaphase I and separated at anaphase I, followed by a second cell division in

meiosis II to separate sister chromatids (Bolcun-Filas and Handel, 2018). The complex and highly organized events during meiosis require the strict and unique transcription regulation during meiosis. For example, a generally low transcription level was observed from leptonema to early pachynema, followed by a rapid increase to reach a transcriptional peak at late pachynema (Eddy and O'Brien, 1997; Margolin et al., 2014; da Cruz et al., 2016). However, the insight mechanisms of the transcription regulation remain unclear.

In mammals, germ cells develop in divergent ways in the two sexes: "spermatogenesis" in males and "oogenesis" in females. In males, spermatogenesis happens throughout the lifespan of most mammals after puberty, generating billions of gametes continuously (De Kretser et al., 1998). In females, however, oocyte pools form in the ovaries before birth with limited numbers, and the pools reduce sharply around birth and gradually throughout the female reproductive lifespan (Reynaud and Driancourt, 2000). Transcription regulations are also different between spermatogenesis and oogenesis. Spermatocytes have XY bodies that have an unique structure and transcription patterns during meiosis; however, the XY bodies are not found in oocytes due to lacking the Y chromosome (Handel, 2004). Besides, some meiosis-specific genes are regulated differently through spermatogenesis and oogenesis (Yang and Wang, 2018; Mihola et al., 2019). For instance, the mutations of *Spo11, Msh5,* and *Sycp3* arrest spermatocytes at zygotene stage, but allow oocytes to go further (Hunt and Hassold, 2002). All these sexual differences in meiosis require further studies to investigate unique sex-specific regulations.

Understanding the molecular mechanisms in meiosis is important for human reproductive health. Errors of meiotic events cause abnormalities in germ cells, leading to infertility, miscarriage, and genetic diseases. Infertility, for example, is a global issue of public health. Infertility affects 9–15% of the male population, and up to 18% of the female population (Practice Committee of the American Society for Reproductive Medicine, 2006; Barratt et al., 2017; Barbieri, 2019). Due to the variety of causes that lead to infertility, 5% of cases are diagnosed as "unexplained" (Unuane et al., 2011). To investigate those molecular mechanisms of diseases that induce reproductive diseases, especially to find biomarkers for clinic applications, canonical meiotic studies take advantages of proteomic techniques and cytological approaches, to capture unique features for diseases (DeSouza et al., 2005; Parmar et al., 2008; Chen et al., 2009). However, these studies only target limited proteins and genes, and fail to draw a comprehensive map of the transcription network, making it inefficient for finding new biomarkers.

Development of the next generation sequencing provides possibilities for nucleotide studies at a genome-wide level. Bulk RNA-seq, a sequencing-based approach, is a powerful tool to study meiotic molecular mechanisms due to its ability to fully sequence the whole transcriptome. In basic science, by using bulk RNA-seq, transcriptional profiles of germ cells have been studied (Margolin et al., 2014; Ball et al., 2016; Zhao et al., 2020c). Meiotic transcriptional profiles of different cell types generated by RNA-seq provide information on how the transcriptome is regulated at different stages, which further enable researchers to study transcriptionally regulated biological processes. In clinical utility, bulk RNA-seq has been developed as a powerful tool to discover biomarkers linked to various diseases, including reproductive diseases (Kumar et al., 2019; Liu et al., 2019; Zhang C. et al., 2019). However, meiosis is a long process and has multiple stages in both males and females, and bulk RNA-seq takes a large amount of cells as the input, and the average gene expressions of the input cells as the output. Thus, bulk RNA-seq fails to detect the heterogeneities among the input cells and is unable to study unknown cell types or rare cell populations, in both basic and clinical studies.

A more advanced RNA-seq method, single-cell RNA-seq (scRNA-seq), breaks the aforementioned limitations by improving the sequencing resolution to the single-cell level (Tang et al., 2009; Navin et al., 2011; Xu et al., 2012). Until now, more than twenty scRNA-seq protocols have been generated. To capture transcriptomic information from individual cells and build single-cell sequencing libraries, scRNA-seq methods include single-cell isolation and lysis, mRNA capture, cDNA generation by reverse transcription, and cDNA amplification (Kolodziejczyk et al., 2015; Hedlund and Deng, 2018). Unlike bulk RNA-seq, cells used by scRNA-seq have to be lysed separately so that mRNAs released from one cell can be separated from other cells. Depending on different scRNA-seq protocols, cDNA libraries of individual cells can be distinguished either by physical separation (multi-well plates) or by barcode sequence labeling (unique molecular identifiers [UMI]). Therefore, transcriptomic heterogeneity among individual cells can be detected. This allows scRNA-seq to capture minor cell groups with unique transcriptomic features that are harder to detect by bulk RNA-seq. scRNA-seq also can potentially capture more biomarkers specific for many cell types in clinical studies.

Here, in this review, we summarized recent discoveries in meiosis studies that applied scRNA-seq. We also discussed how different scRNA-seq approaches, together with their downstream analysis methods, contribute to mammalian meiosis-related studies.

WHY SHOULD WE APPLY scRNA-Seq TO SPERMATOGENESIS AND OOGENESIS STUDIES?

ScRNA-Seq Applications in Spermatogenesis Studies

In recent years, the spermatogenesis field has had some breakthroughs achieved by scRNA-seq. ScRNA-seq helps generate more comprehensive transcriptome profiles, discover new cell types and gene functions, and find certain cell type abundance in tissues.

I. ScRNA-seq generates comprehensive transcriptome profiles for mammalian spermatogenesis. Margolin et al. (2014) generated transcriptomes for mouse spermatogenesis by using bulk RNA-seq that failed to

reveal cellular heterogeneity. Since 2017, several scRNA-seq studies have broken the limitations of the bulk RNA-seq (Guo et al., 2017, 2020; Li et al., 2017; Chen et al., 2018; Green et al., 2018; Hermann et al., 2018; Lukassen et al., 2018; Wang et al., 2018; Ernst et al., 2019; Grive et al., 2019; Wen and Tang, 2019; Shami et al., 2020). While bulk RNA-seq based transcriptome profiles can only distinguish the main meiotic stages, scRNA-seq studies further separated the known stages into finer substages. E.g., preleptotene cells (between mitosis and meiosis entry), usually have a small population, were able to be split into four substages: pre-meiotic/G1 phase preleptotene stage, early S phase preleptotene stage, middle S phase preleptotene stage, and late S phase preleptotene stage (Chen et al., 2018). On the other hand, bulk RNA-seq data can be combined with scRNA-seq results to facilitate staging spermatocytes. In one study, juvenile testis bulk RNA-seq, juvenile testis scRNA-seq, and adult testis scRNA-seq, were used together to precisely stage germ-cell development in mice (Ernst et al., 2019). Due to the semi-synchronization of the first wave of spermatogenesis, scRNA-seq data from each time point of the juvenile testis represented different stages through spermatogenesis, which was confirmed by histology. Their bulk RNA-seq data of juvenile testis further verify the cell-type classification results. This study generated a comprehensive transcriptome for spermatogonia differentiation and meiosis, especially for leptotene and zygotene spermatocytes in early prophase I (Ernst et al., 2019). However, as another scRNA-seq study pointed out that the transcriptional profile of the first wave is different from the subsequent spermatogenesis waves in mice (Grive et al., 2019), the scRNA-seq analysis of the first-wave spermatogenesis in juvenile testis may be problematic. Therefore, various factors should be taken into consideration for combining different approaches in scRNA-seq analysis. In summary, scRNA-seq provides high-resolution data for mapping germ-cell development in mammalian testes.

II. ScRNA-seq helps discover new cell types involved in spermatogenesis. ScRNA-seq data records the transcriptomic information for all cells. Thus, new cell types can be separated from other cell types by using clustering methods. The stage of the new cell types can be identified in cell progression trajectories (Details in section "ScRNA-seq downstream analysis for meiosis studies"). Guo et al. (2017) identified several transitional stages during spermatogonia-stem-cell differentiation in humans by scRNA-seq. Similar cell types were also defined by other three groups (Chen et al., 2018; Green et al., 2018; Tan et al., 2020), revealing transcriptional transitions between mitosis and meiosis. In general, scRNA-seq helps to dissect main meiotic stages into finer substages.

III. ScRNA-seq facilitates finding novel gene functions during spermatogenesis. ScRNA-seq allows gene enrichment analysis for investigating transcriptional dynamics between different cell groups. By comparing different cell groups, differentially expressed genes can be investigated, indicating their potential roles in a certain cell subtype. Specifically, gene upregulation and downregulation can be achieved by comparing subsequent stages. Chen et al. (2018) found the fibroblast growth factor (FGF) signaling pathway was repressed at the mitosis-to-meiosis transitions, suggesting the suppression of the FGF pathway may be required for entering meiosis. Wang et al. (2018) discovered a series of genes specifically expressed in certain spermatogenic stages. For instance, *Tdrg1*, *Ccdc112*, and *Aurka* can be used to distinguish zygotene, pachytene, and diplotene, respectively, although their meiosis-specific functions need to be further explored. By comparing the sequencing data between wild-type and mutant mice, scRNA-seq could also help understand the roles of certain genes in meiosis (Fang et al., 2019; Jung et al., 2019).

IV. ScRNA-seq can help dissect chromosome-wide transcriptional profiles during spermatogenesis. Similar to RNA-seq, the relative transcriptional level of cells can be calculated for studying chromosome transcriptional status. For instance, Lau et al. (2020) found that Meiotic Sex Chromosome Inactivation (MSCI) can be quantitively determined by calculating expression ratio between sex chromosomes and autosomes by scRNA-seq data analysis. Compared to conventional methods, scRNA-seq provides more detailed information on the duration and silencing patterns of MSCI. Besides, those genes escaped from the MSCI could also be identified.

Comparing Meiotic scRNA-Seq Studies Between Male and Female

A lot of scRNA-seq approaches for spermatocytes can be used for oocyte studies as well. However, not all those protocols and analysis methods can be applied to oocytes due to its unique features. First, oocytes are less abundant than spermatocytes. Most of the oocyte-related scRNA-seq studies used only a few of oocytes, making it challenging to study oocyte heterogeneity. Second, unlike spermatogenesis, mammalian oogenesis is not a continuous process to generate clear trajectories. Primary oocytes arrest at dictyate stage for decades and resume upon stimulation of the luteinizing hormones. The ovulated oocytes are halted again at Metaphase II (MII) until fertilization (Esencan and Seli, 2018; Li et al., 2019). Third, oocytes are surrounded by granulosa cells, making large-scale cell isolation challenging. Because of the aforementioned reasons, most of the current scRNA-seq studies focus on oocytes at GV, MI, and MII stages with limited cell numbers in each experiment, which makes it hard to compare male and female germ-cell transcriptomes at single-cell level (Ferrero et al., 2019; Zhang T. et al., 2019; Ye et al., 2020; Yu et al., 2020; Yang et al., 2021).

It is not until recent years that scRNA-seq was applied to transcriptome studies of early prophase I oocytes (Li et al., 2017; Ge et al., 2020; Niu and Spradling, 2020; Wang et al., 2020). Li et.al. (2017) combined magnetic-activated cell sorting (MACS) and fluorescence activated cell sorting (FACS) to isolate male and female human fetal germ cells (FGCs) for scRNA-seq. Their results showed that female FGCs are in both somatic and

meiotic stages, while all the male FGCs do not reach meiosis, indicating a non-synchronized manner for male and female FGC development. This non-synchronized manner makes it hard to directly compare male and female transcriptomes because of their different meiotic progression status. Meanwhile, their data can only separate female meiosis into three main stages: meiosis entry, meiotic prophase, and oogenesis. Wang et al. (2020) performed single-cell RNA-seq on monkey oocytes by collecting follicles from four ovaries and generate a transcriptome trajectory of the oocytes isolated from primordial to antral follicles. 418 oocytes were finally remained in the data and further separated to four subgroups of oocytes that were from primordial, primary, secondary, and antral follicles, respectively. Since this study focuses more on folliculogenesis rather than oogenesis, meiosis-related transcriptional transition was not fully discussed here. Recently, Niu and Spradling (2020) and Ge et al. (2020) independently performed scRNA-seq on a large number of mouse meiotic oocytes using 10X drop-seq platform, for the first time, revealing clear transcriptome profiles of early meiotic stages. Their data showed some shared early meiotic markers, such as *Stra8, Dusp9,* and *Rhox9*, and late meiotic markers, such as *Zcwpw1* and *Tex15*. However, due to different analysis approaches, a large portion of meiotic markers does not match with each other. To further compare meiotic transcriptomes between oocytes and spermatocytes, we compare Ge's oocyte marker data with spermatocyte data from Jung et al. (2019). Although there are similarities between oocytes and spermatocytes, the most significant leptotene oocyte marker, *Actb*, is not dominant in spermatocyte leptonema. Instead, *Actb* is transcribed in undifferentiated spermatogonia and spermatids. In general, 10 out of 20 leptotene/zygotene oocyte markers are also found in leptotene/zygotene spermatocytes. Remaining genes are frequently shown in spermatogonia, indicating a transcriptional delay of oocytes at early prophase I compared to spermatocytes. Only 2 out of 10 most significant oocyte pachytene markers share with spermatocytes, while none of the dictyate oocyte top makers overlap with prophase spermatocyte markers. This analysis reveals a significant difference of the meiotic transcriptomes between oocytes and spermatocytes.

The Application of scRNA-Seq in Meiosis-Related Diseases

ScRNA-seq is not only applied to basic research but also to clinical studies. Infertility, for example, is a common disease that threatens human health. The cause and diagnosis of infertility are complicated and diverse. Generally, causes of infertility can be categorized into three groups: female-related, male-related, and mixed. Until now, no causes have been identified for 10% of infertile couples (Zitzmann, 2013; Deroux et al., 2017; Krausz and Riera-Escamilla, 2018).

Meiotic defects can induce infertilities and many idiopathic infertility cases might be meiosis-related. Therefore, it is important to investigate the molecular mechanisms of how meiotic defects link with infertility (Hanson et al., 2017). However, most of the previous studies were conducted at the cell or tissue levels. The investigation of the diseases normally rely on cytology, which were not able to go further for deeper insight of their molecular mechanisms (Yatsenko and Rajkovic, 2019). To reveal the genetic causes of the idiopathic infertility, Next-Generation Sequencing (NGS) was developed as a clinical tool for finding genetic mutations by sequencing the entire genomes of patients (Oud et al., 2019). The functions of the candidate genes discovered by DNA-seq can be further studied by analysis of the knockout mice. However, gene-knockout studies normally focus on limited molecular pathways, but fail to cover the genome-wide transcriptional network. Due to these limitations, the studies failed to capture the insight mechanisms of the diseases, especially at the transcriptional level. Thus, novel tools are needed to study molecular mechanisms of the meiosis-related diseases, particularly at the genomic level.

In recent years, scRNA-seq has been developed as a powerful tool to identify new genes associated with female infertility. In females, due to its ability for genome-wide and single-cell level transcriptome profiling, scRNA-seq is used to identify new genes associated with infertility by tracking differentially expressed genes between normal and defective cells. In a recent case study, an infertile female patient had repeated multipronuclei (MPN) formed in her zygotes. To investigate gene expression profiles of oocytes and zygotes, scRNA-seq was performed with downstream gene ontology (GO) analysis to compare the patient's and normal cells. Three candidate genes were identified based on their meiosis-related GO functions and their different expression patterns between patient and normal cells (Dai et al., 2017). This study demonstrated that scRNA-seq can be used to discover gene regulation alterations in disease studies. Another scRNA-seq study focused on recurrent total fertilization failure (RTFF) patients. Suo et al. (2018) compared transcriptional profiles between normal oocytes and abnormal oocytes like poly-pronuclei and pronuclear-stage-arrest oocytes. Several differentially expressed meiosis-related genes were found by Kyoto Encyclopedia of Genes and Genomes (KEGG) analysis of the scRNA-seq data (Suo et al., 2018). However, the validation of the roles for those genes in diseases requires more data collected from new clinical cases. Similarly, scRNA-seq was also used to study polycystic ovary syndrome (PCOS) and to evaluate the transcriptomic alteration caused by PCOS (Liu et al., 2016). In this paper, the authors collected oocytes and cumulus cells at GV, MI, and MII stages from patients and normal donors. After identification of differentially expressed genes by scRNA-seq analysis, KEGG analysis was performed to find potentially related pathways. Many genes, like *Ppp2r1a* and *Egfr*, were increasingly expressed in PCOS oocytes, which can help us find out the causes of PCOS (Liu et al., 2016). However, further scRNAseq and genetic studies are needed to verify these results.

ScRNA-seq has also been used as a novel tool for male infertility diagnosis. In a recent study, scRNA-seq was performed in testis samples from a non-obstructive azoospermia (NOA) patient. Normal testis samples have both somatic and germline cells. However, no germline cells were found in the testis of this patient by scRNA-seq, which is consistent with the histological staining results—spermatocyte depletion in the patient testis. Interestingly, many genes related to male reproduction were differentially expressed in the Sertoli cells of the NOA patient,

which provides information for studying the mechanism of NOA-associated infertility (Wang et al., 2018).

Taken together, scRNA-seq is a powerful research tool for studying human male and female infertility. Specifically, this high-resolution sequencing method can be used to identify defective mutations by combining GO with KEGG analysis, to evaluate treatment efficiency, and to identify abnormal cell populations in patients.

HOW CAN WE CONDUCT scRNA-Seq TO STUDY MEIOSIS?

What Sequencing Strategies to Choose for Meiosis Studies?

Choosing the appropriate sequencing strategy is the first and important step for scRNA-seq studies. Various scRNA-seq experimental approaches were used in previous meiosis studies, e.g., CEL-seq2, Drop-seq, MARS-seq, Smart-seq, and Smart-seq2 (Ramsköld et al., 2012; Picelli et al., 2013; Jaitin et al., 2014; Macosko et al., 2015; Hashimshony et al., 2016). They differ from each other by the methods of library generation and sequencing; consequently, they differ in sensitivity, cost, and sequencing depth.

Two well-developed commercial approaches, Drop-seq and Smart-seq2, are the two most widely used methods in meiotic studies. They represent high-throughput 3′ end capture sequencing and full-length sequencing, respectively. Their differences were shown in **Table 1**. In the Drop-seq method, each individual cell is separated and lysed in an oil droplet with a unique bead carrying barcode sequences including UMI. Those sequences will capture the poly-A ends of mRNAs (3′) to add an "ID" to each mRNA molecule. By doing this, the mRNAs labeled by UMI will avoid amplification noise (Kivioja et al., 2012; Macosko et al., 2015; Ziegenhain et al., 2017; **Figure 1A**). The most attractive advantage of Drop-seq is its ability to generate a large library from a mixed cell suspension, such as a single cell suspension from entire testes with large cell numbers and multiple cell types. Smart-seq2 has some unique characteristics compared with Drop-seq. First, instead of UMI incorporation and 3′ end mRNA capture, Smart-seq2, similar to Smart-seq, generate full-length mRNA libraries by performing a "Switching Mechanism at 5′ End of RNA Template" workflow (Picelli et al., 2013). Briefly, Smart-seq2 utilizes a reverse transcriptase enzyme to add cytosine residues to cDNAs during mRNA reverse transcription. The enzyme then switches template to RNA, adding guanine residues to 5′ ends. In this way, both 3′ ends and 5′ ends are able to be captured, leading to a full-length coverage (Goetz and Trimarchi, 2012; **Figure 1A**). Second, to enable individual cell separation, the library preparation of Smart-seq2 needs to be performed on the microfluidic chips or on a multi-well plate (Xin et al., 2016). Smart-seq2 starts with sorted cells, commonly generated by FACS or micromanipulation. Third, the full-length sequencing of Smart-seq2 decreases the mismatch rate for mRNA capture, enabling high sensitivity and accuracy. Thanks to the high sequencing depth, Smart-seq2 can normally capture twice as many gene numbers per cell as Drop-seq does in the same conditions. Smart-seq2 was also proved to maintain the full sequence reads mapping against the 3′ end bias (Ziegenhain et al., 2017). Therefore, Smart-seq2 is able to capture gene isoforms by SNPs. However, Smart-seq2 requires individual cell lysis (cells are commonly separated by wells). Thus, the sample size is usually limited and the library construction cost per cell is relatively high (**Table 1** and **Figure 1B**; Picelli et al., 2013; Ziegenhain et al., 2017; Baran-Gale et al., 2018).

Most male-meiotic scRNA-seq studies utilize the Drop-seq method; in contrast, most female-meiotic scRNA-seq studies choose Smart-seq/Smart-seq2. Their research purposes rather than sample types determine which method(s) to be used. Drop-seq generates 3′ end bias for mapping reads and has lower sequencing coverage compared to Smart-seq2. Therefore, Drop-seq is not suitable to study transcriptional profiles of genes with low abundance. However, this high throughput method allows a large sample size at once, ensuring comparison between numerous cells in the downstream analysis. Therefore, Drop-seq can be suitable for identifying rare cell types, plotting stage-specific transcriptomes, and constructing cell progression trajectories in meiosis studies. These research goals can also be achieved by Drop-seq even in oocyte studies (Niu and Spradling, 2020; Zhao et al., 2020b). In contrast, Smart-seq2 applications in meiotic studies rely on known cell characteristics for efficient cell sorting. Limited sample input and high sensitivity and accuracy are also different from other scRNA-seq methods. These features limit its application within transcriptomic analysis of the known cell types, e.g., comparing transcriptomes between GV and MII

TABLE 1 | Comparison between Smart-Seq2 and Drop-seq in meiosis studies.

Sequencing method	Smart-Seq2	Drop-seq
UMIs incorporation	NO	YES
Sequencing pattern	Full-length	3′-end capture
Sensitivity (sequencing depth)	High	Low
Able to detect gene isoforms	YES	NO
Targeting cell sample size	Low (96–384 when using plates)	High (100–10,000)
Average library cost (per cell)	11$	0.01$
Special equipment required for library preparation	NO	YES
Common application in meiotic studies	Oocytes	Testis cells

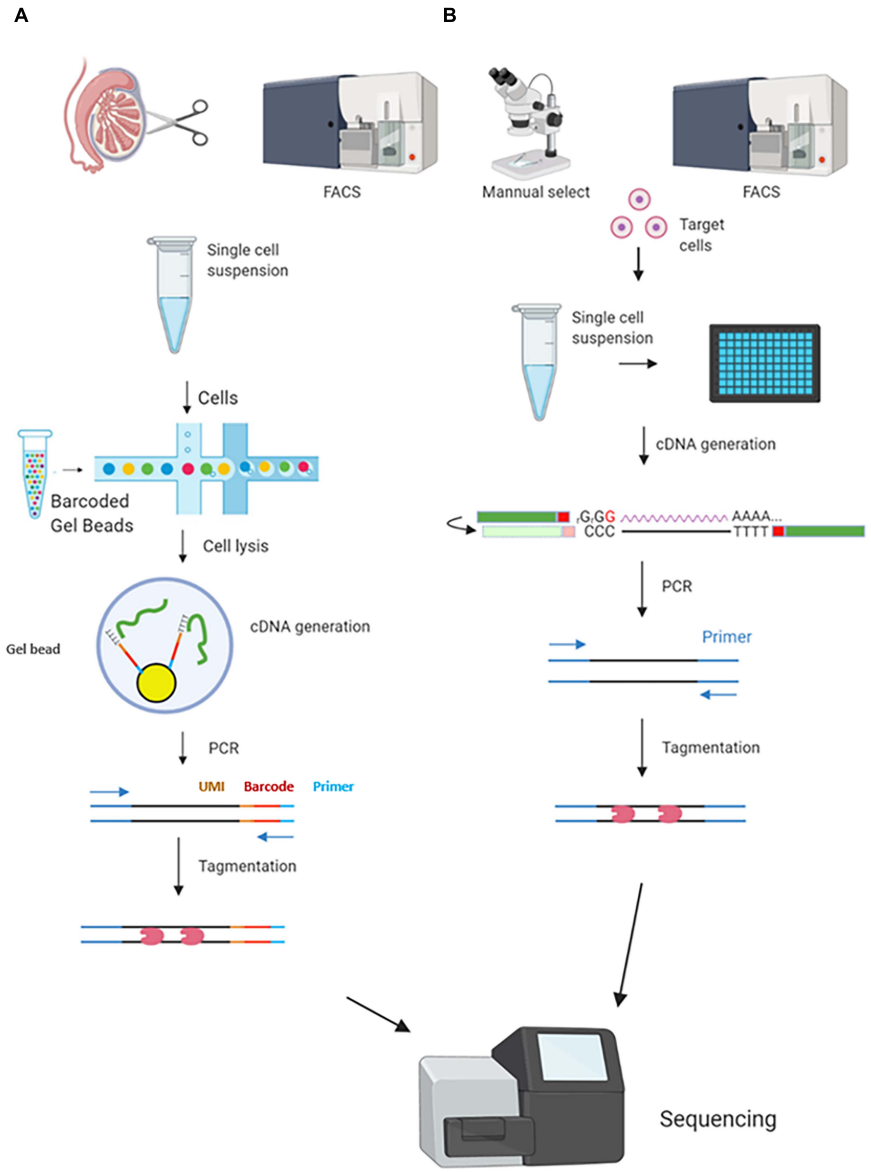

FIGURE 1 | Comparison between two scRNA-seq protocols commonly used in mammalian meiosis studies. Smart-seq2 and Drop-seq are the two most widely used methods in meiosis-related scRNA-seq studies. **(A)** Drop-seq allows a large sample size. A single-cell suspension is generated from testes or ovaries with or without cell sorting and enrichment, which depends on different research purposes. A single cell and a barcoded bead are encapsulated in each water-in-oil droplet. Cells are lysed to release mRNAs in the droplet and the mRNAs were captured by the bead with unique UMIs and barcodes. cDNAs are generated by reverse transcription and the templates were amplified, followed by library preparation. **(B)** Smart-seq2 starts with a small cell sample size. Cells can be collected by manual selection or FACS. Each individual cell is separated into different microtiter plate wells or microfluidics, cDNA will be generated for PCR and then be tagged for sequencing. The cDNA generation and amplification are similar to Drop-seq.

oocytes, or comparing abnormal oocytes with normal oocytes at the MII stage (Zhang et al., 2018; Ferrero et al., 2019; Ye et al., 2020; Yang et al., 2021).

ScRNA-Seq Downstream Analysis for Meiosis Studies

The following downstream analysis of scRNA-seq is also essential for performing scRNA-seq (**Figures 3A–G**). Several downstream analysis approaches can be used to identify cell types accurately. As meiosis contains a lot of substages, some of which are hard to distinguish by cytological features like sizes and shapes, a transcriptome-based cell identification is important for cell identification. Since cells are featured by thousands of genes, current single-cell clustering approaches depend on dimension-reduction methods, such as Principal Component Analysis (PCA), Uniform Manifold Approximation and Projection (UMAP), and T-distributed Stochastic

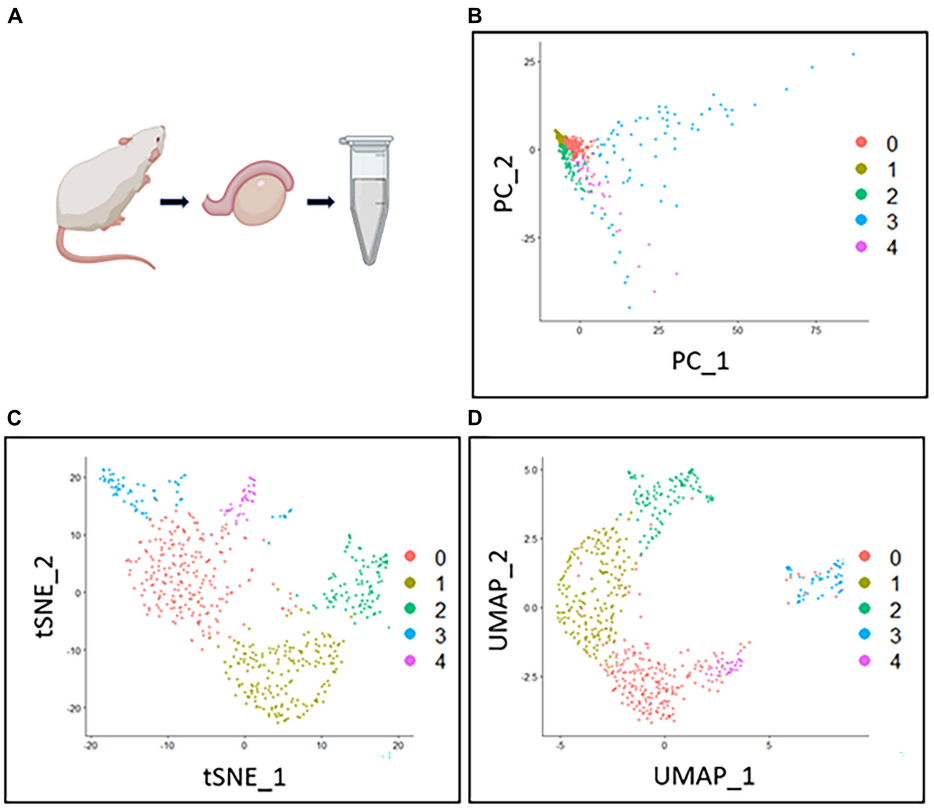

FIGURE 2 | Comparison between three dimension-reduction methods of scRNA-seq data analysis. The Drop-seq testis cell data was progressed by quality control and normalization. The polished data then underwent three different dimension-reduction methods for cell clustering. Each dot in **(B–D)** represents a cell. **(A)** The mouse testis data is from a previous publication (Jung et al., 2019). **(B)** The filtered testis data were processed by PCA and plotted by the first two principal components. Cell clusters were generated and shown in different colors. **(C)** The same dataset is processed by TSNE for clustering and plotted by the first two dimensions. Cluster separation of TSNE is better compared to other methods. **(D)** The same dataset is processed by UMAP for clustering and plotted by the first two dimensions. The distance between different clusters reflects the farther or closer relationships between the cell types.

Neighbor Embedding (t-SNE) (**Figures 2B–D**; Pearson, 1901; Van Der Maaten and Hinton, 2008; McInnes et al., 2018). For a transcriptome matrix having multiple cells and numerous genes, dimension-reduction analyses transfer data to low-dimension states and preserve basic heterogenetic information. The difference between those methods relies on different algorithms that are used to calculate the distances when performing cell clustering. Specifically, t-SNE and UMAP use non-linear graph-based dimension reduction algorithms to define the distance among cells. The adjusted clustering strategies provide better visualization for cell-group identifications. It is widely accepted that tSNE can more efficiently provide information on cluster separation than PCA; while UMAP can better show the relationship between cell clusters (**Figures 2A–D**; Jung et al., 2019). The application of the aforementioned methods simplifies the cell transcriptional features from thousands of genes to a limited number of principal dimensions. If the first two principal dimensions are taken, cells with similar transcriptional features can be clustered together shown on a two-dimensional plot (Suzuki et al., 2019).

How can we know which stage these clusters represent? Using stage-specific marker genes to identify cell types is a commonly used staging method for scRNA-seq analysis. Some genes only express at certain meiotic stages, the high expression of those genes can be used as an indicator to track the target cell types. For instance, genes encoding transition proteins (TNP1 and TNP2) are useful ES markers because they only express in ES to replace histones (Meistrich et al., 2003). The function that links known markers to cell clusters has been integrated into analysis software, such as the Seurat package for R (Butler et al., 2018; Do et al., 2018; Stuart et al., 2019). However, high turnover rates of mRNA and limited marker numbers still challenge the identification of specific germ-cell substages.

Trajectory-based differential expression analysis for scRNA-seq data is a novel tool for discovering hidden sub-transition stages during spermatogenesis. Like other biological progressions, germline cells undergo gradual transcriptional changes along the progression of meiosis. This gradual transcriptome transition can be reflected as continuous cell clusters in low-dimension plots by single-cell trajectory analysis (Trapnell et al., 2014). Pseudotime analysis provides an efficient way to obtain more continuous cell-cluster trajectories, mimicking real kinetics of germ-cell development (**Figure 3E**; Campbell and Yau, 2018). This method has been used to identify the renewal and differentiation initiation of spermatogonia stem cells (SSC) by using marker genes

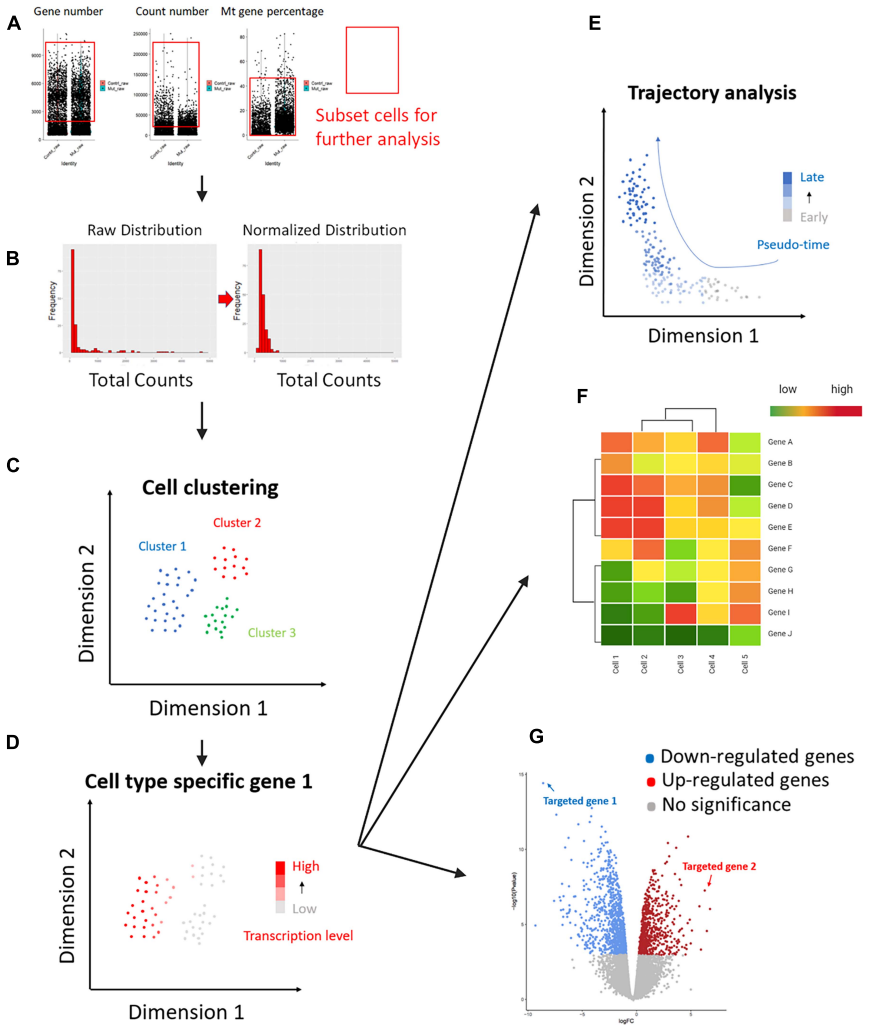

FIGURE 3 | Downstream analysis workflow of commonly used scRNA-seq. Key steps of the scRNA-seq downstream analysis were summarized here (The figure is created with BioRender.com). **(A)** Quality control evaluated cell quality and filtered qualified cells by captured gene numbers, mRNA total counts, and mitochondrial mRNA percentages. Red rectangles highlighted the cells selected according to the three parameters, respectively. The rest cells were considered as "low quality "cells and not used for the following analysis steps. **(B)** The normalization method was applied to remove technique deviation, especially different sequencing depth between each individual cell. The mRNA-total-count distribution from the normalized cells (right graph) is closer to normal distribution compared to the raw counts (left graph). **(C)** Different dimension-reduction methods can be used for cell clustering (see **Figure 2** for details). Cells were separated by their transcriptional features. **(D)** Cell type identification. Separated cell clusters can be identified by using known cell-type-specific markers. **(E)** Alternative downstream analysis can be applied for different research purposes. Pseudo-time trajectory analysis can be used for tracking cell progression from early to late stages. In meiosis-related studies, trajectory analysis is commonly used for tracking spermatogenesis. **(F)** Cell-expression data can be used to generate cell clustering heatmaps. Similar cells will be clustered together on the heatmap, and the gene expression data showing their homology and heterogeneity will be shown. In this way, potential gene markers for certain cell types can be easily determined. **(G)** Differential Gene Expression (DGE) analysis compares differential gene transcription levels between two cell groups or datasets. The identified up- and down-regulated genes provide important information for diagnosis and treatment.

(Hermann et al., 2018). As a commonly used pseudotime analysis tool that is independent of known markers, Monocle (a Bioconductor package) orders cells into trajectory trees and branches by calculating transcriptional relations (Trapnell et al., 2014). Labeling a trajectory tree with known markers can be used to define the transitional cell stages of the known stages without specific markers, e.g., an unknown stage in the middle of two continuously progressed cell stages along the trajectory can be recognized as a transition stage between the two known stages.

Adding More "Markers" in Our Toolbox: Cell-Type Marker Genes for Identifying Specific Meiotic Substages in scRNA-Seq Studies

As mentioned before, meiotic marker genes are important information used in scRNA-seq downstream analysis. Researchers not only used widely accepted meiotic marker genes for cell-type identification in single-cell data sets, but also analyzed differentiated gene expression among different cell

TABLE 2 | Meiotic gene markers for prophase I in spermatogenesis and oogenesis.

Stage/ Marker identity	Human markers (male)	Mouse markers (male)	Mouse markers (male Specific)	Mouse markers (female)	Mouse markers (female specific)
Leptotene	Scml1, Smc1b, Herc5, Zcwpw1	Mdk, Ccnb3, H2bfm, Scml1	Rhox2h, Fthl17-ps3, Rhox2d, Mageb18, A830018L16Rik, Rhox2a, Dppa5a, Gml, Gm364, Rhox2h, Fthl17-ps3, Rhox2d, Mageb18, A830018L16Rik, Rhox2a, Dppa5a, Gml, Gm364, Ccnb3,	Actb, Hmgb1, Rpl6, Hmgb2, Rpl39, Stra8, Dazl, Smc1b, Hells, Sycp1, Sycp3, Zcwpw1, Tex30, Tex101, Rec8, Tuba3a, Cited1, Syce1, Cdkn2a	Actb, Rpl24, Ptma, Tubb5, Eef1g, Rsp3
Zygotene	Tpte, Sod1, Loc100507384, Linc00668, Tdrg1	Sycp1, Sycp3, Prss50, Tex101			M1ap, stra8, Tuba3a, Selenok, Snu13, Haus8, Med21
Pachytene	Ccdc112, C9orf57, Piwil1, Prok2, Adam2, Mgat4d	Piwil1, Tmem30c, Mllt10, Rsph1, Cdc42ep3	Rsph1, Lyar, Calm1, Ldhc, Atxn7l3b, Rbakdn, Pabpc6, Gkap1, Cox8c	Tsga10, Ankrd31, Grk4, Ndufa1, Eif4a2, 4930447C04Rik, Malat1, H1f0, Uba52, Calr	Hist1h2aa, Rad51ap2, Zhx1, Zmym6, mt-Nd6, Hist1h4d
Diplotene	Gyg1, Aurka, Zc2hc1c, Ccnb2, Tmigd3, Spata16	Pou5f2, Mxra8, Ggn, Wdr20rt, Rassf1	Pou5f2, Mxra8, 4932702P03Rik, Ggn, Gm8879, 1700108N11Rik, Wdr20rt, 4930515G01Rik, Rassf1, 4933402N22Rik	Nmnat3	Gm13269, Gm27164, Gm44601, Gm49368, Grid2, Syce3, Olfr678, Ablim1, Uba52, Pet2, Brd2

This table summarized markers for four substages in meiosis prophase I. Human and mouse markers were listed. Those markers come from different resources (see citations in the text). Markers in the table were identified from the total 13 publications. Specifically, the meiotic markers for male are generated by comparing differentiated genes at same or similar stage from different scRNA-seq datasets, all the marker genes selected were identified as markers by DGE analysis from at least 2 different studies to ensure the consistency. For mouse female meiotic markers, all the data comes from Niu and Spradling (2020) because this study is the only high throughput Drop-seq study that dissect transcriptomic features of oocytes in a fine scale. We also create male and female specific marker list by comparing Niu's study to Drop-seq based male studies that targeted at similar meiotic stages. Genes that were identified as significant differentiated-expressed genes ($p < 0.05$) at certain stage in either male or female were put into the list.

clusters to reversely identify cell-type-specific or stage-specific meiotic marker genes (**Figure 3E**). Taking the advantages of DGE analysis, marker genes are selected by comparing the genomic transcription levels between different cell groups and those top genes in each group represent the most unique transcriptions. Most of the previous studies staged germline cells via cytological approaches. Due to the non-synchronized pattern of many meiosis-related genes, some of the protein-coding genes may transcribe early but translate late. Therefore, previous genes used for meiotic cell identification may not be compatible for scRNA-seq data. ScRNA-seq-specific marker genes were needed. Here, we summarized those markers from single-cell data that can be used for identifying spermatocytes and oocytes at different meiotic stages, we also collected data to compare marker genes between male and female (**Table 2**; Guo et al., 2017, 2018; Li et al., 2017; Fayomi and Orwig, 2018; Green et al., 2018; Hermann et al., 2018; Lukassen et al., 2018; Ernst et al., 2019; Tan and Wilkinson, 2019; Ge et al., 2020; Niu and Spradling, 2020; Wang et al., 2020; Zhao et al., 2020a).

CONCLUSION AND FUTURE DIRECTIONS

ScRNA-seq is a high-throughput sequencing method that is widely used in research. It allows researchers to study transcriptomes at the single-cell level. Different scRNA-seq technologies have been developed for various research requirements and purposes. Those technologies strengthened the researcher's ability to study meiosis, especially in mammals. Conventional bulk RNA-seq combined with cell synchronization and sorting has limitations in studying minor cell groups and specialized cell substages. In contrast, scRNA-seq takes advantage of dimension-reduction methods for cell clustering and allows accurate cell identification. In mammalian meiosis studies, current clustering methods can distinguish between each substage throughout meiotic prophase I. Many downstream-analysis methods have been developed to identify new cell types and progression tracks. For example, pseudo-time trajectory analysis has already been used in meiosis progression studies.

ScRNA-seq is also used more frequently as a diagnostic tool for meiosis-related diseases. Since the causes of many meiosis-related diseases remain unknown, scRNA-seq of germ cells from patients and healthy donors can be used to investigate potential mechanisms of these diseases by analyzing their differential gene expression.

Meanwhile, there are still some challenges of scRNA-seq that limit its broader application in meiotic-related fields. First, current scRNA-seq, especially NGS-based platforms, induces great RNA loss, leading to low sequencing depth (Chen et al., 2019). For example, NGS-based sequencing typically reaches as low as 10 versus. 40% for full-length sequencing depth (Tirosh et al., 2016; Yuan et al., 2017; Nguyen et al., 2018). Low sequencing depth can cause more background or noise than bulk RNA-seq, making it difficult to capture the RNAs with

low abundance, like lncRNAs. The number of genes that can be captured from scRNA-seq is also normally lower than bulk RNA-seq (Saliba et al., 2014; Haque et al., 2017). Second, the NGS-based sequencing approaches typically only capture the 3′-end of each mRNA and break mRNA into small pieces. Thus, this approach often fails to maintain the full sequence of the RNAs and cause information loss. Another sequencing information loss is because it is hard to detect RNA isoform variants, RNA modifications, and short length RNAs (such as microRNAs) (Macosko et al., 2015; Heath et al., 2016). It is important to capture microRNAs in meiosis-related studies because microRNAs play important roles in mammalian meiosis (Walker, 2021). This limitation produces a contradiction between high-throughput and high-sensitive scRNA-seq approaches. While full length scRNA-seq, e.g., Smart-seq2, partially solves the aforementioned problems. However, limited cell numbers can be sequenced at a time via Smart-seq2, which cannot meet the requirement for cell heterogeneity and progression studies of meiosis, especially spermatogenesis (Picelli et al., 2013; Ziegenhain et al., 2017). Third, current scRNA-seq approaches normally result in variant sequencing depth in each individual cell, creating challenges for downstream normalization analysis to achieve real biological features (Bacher et al., 2017; Rizzetto et al., 2017; Hafemeister and Satija, 2019). Overall, the limitations for scRNA-seq approaches still need to be overcome, especially for future meiotic studies.

For meiotic studies, the first future direction for scRNA-seq technology would be increasing sensitivity and accuracy for high-throughput library preparing protocols. The improvement for higher sequencing depth, lower technical noise, and the ability to capture more types of mRNA will help decipher deeper molecular mechanisms for meiosis. For instance, important meiotic genes with low transcription counts can be further studied, the accurate transcriptomic identification will also lead to new insight into transcriptional regulations during meiosis. Information about microRNA from improved scRNA-seq will broaden our knowledge on meiosis.

The second future direction for meiotic scRNA-seq studies will be the new technologies combining with and/or based on scRNA-seq. ScRNA-seq can bind other NGS methods to incorporate single-cell transcriptomic with genomic, proteomic, and epigenetic information, which together were named "single cell multi-omics technology"(Hu et al., 2018). Currently, the multi-omics technologies are experiencing an explosive growth as multiple protocols have been developed continuously, e.g., scG&T-seq, scMT-seq, scGESTALT, and ECCITE-seq (Macaulay et al., 2015; Angermueller et al., 2016; Raj et al., 2018; Mimitou et al., 2019). We expect to see more single-cell sequencing methods can be integrated together to answer the challenging questions in meiosis, e.g., how different factors work together to generate heterogeneous regulations in meiotic cells.

Finally, besides the improvement in library preparation and sequencing technologies, more advanced and mature computational pipelines can help to dig up the increasing scRNA-seq datasets. First, overcoming batch effects between different scRNA-seq experiments and platforms can potentially integrate analysis across multiple scRNA-seq datasets. The newly developed algorithms have shed light on mining the existing data (reviewed by Forcato et al., 2021). Second, the variable analysis approaches increase the difficulties of evaluating different scRNA-seq studies. With the development of bioinformatic tools, the appearance of "golden standard pipelines" will normalize the interpretation of scRNA-seq data, thus, generate more comprehensive transcriptional references for meiotic studies.

AUTHOR CONTRIBUTIONS

YP and HQ contributed to writing and editing of this review. Both authors contributed to the article and approved the submitted version.

FUNDING

This work was supported by National Institutes of Health R00 HD082375 and NIH R01 GM135549.

ACKNOWLEDGMENTS

We would like to thank Ning Liu, Yiding Xu, Royal Shrestha, Aashna Prakash, Faaiza Nusayba Saif, and Erica Hana Joo for critical proofreading of the manuscript. We want to thank Royal Shrestha for helping to generate **Table 2**. We apologize to colleagues whose papers could not be cited owing to space limitations.

REFERENCES

Angermueller, C., Clark, S. J., Lee, H. J., Macaulay, I. C., Teng, M. J., Hu, T. X., et al. (2016). Parallel single-cell sequencing links transcriptional and epigenetic heterogeneity. *Nat. Methods* 13, 229–232. doi: 10.1038/nmeth.3728

Bacher, R., Chu, L.-F., Leng, N., Gasch, A. P., Thomson, J. A., Stewart, R. M., et al. (2017). Scnorm: robust normalization of single-cell rna-seq data. *Nat. Methods* 14, 584–586. doi: 10.1038/nMeth.4263

Ball, R. L., Fujiwara, Y., Sun, F., Hu, J., Hibbs, M. A., Handel, M. A., et al. (2016). Regulatory complexity revealed by integrated cytological and RNA-seq analyses of meiotic substages in mouse spermatocytes. *BMC Genomics* 17:628. doi: 10.1186/s12864-016-2865-1

Baran-Gale, J., Chandra, T., and Kirschner, K. (2018). Experimental design for single-cell RNA sequencing. *Brief. Funct. Genomics* 17, 233–239. doi: 10.1093/bfgp/elx035

Barbieri, R. L. (2019). "Female Infertility," in *Yen & Jaffe's Reproductive Endocrinology: Physiology, Pathophysiology, and Clinical Management: Eighth Edition*, eds J. Strauss, R. Barbieri (Amsterdam: Elsevier Inc), 556–581.e7.

Barratt, C. L. R., Björndahl, L., De Jonge, C. J., Lamb, D. J., Martini, F. O., McLachlan, R., et al. (2017). The diagnosis of male infertility: an analysis of the evidence to support the development of global WHO guidance-challenges and future research opportunities. *Hum. Reprod. Update* 23, 660–680. doi: 10.1093/humupd/dmx021

Bolcun-Filas, E., and Handel, M. A. (2018). Meiosis: the chromosomal foundation of reproduction. *Biol. Reprod.* 99, 112–126. doi: 10.1093/biolre/ioy021

Butler, A., Hoffman, P., Smibert, P., Papalexi, E., and Satija, R. (2018). Integrating single-cell transcriptomic data across different conditions, technologies, and species. *Nat. Biotechnol.* 36, 411–420. doi: 10.1038/nbt.4096

Campbell, K. R., and Yau, C. (2018). Uncovering pseudotemporal trajectories with covariates from single cell and bulk expression data. *Nat. Commun.* 9. doi: 10.1038/s41467-018-04696-6

Chen, G., Ning, B., and Shi, T. (2019). Single-cell RNA-seq technologies and related computational data analysis. *Front. Genet.* 10:317. doi: 10.3389/fgene.2019.00317

Chen, J. I. C., Hannan, N. J., Mak, Y., Nicholls, P. K., Zhang, J., Rainczuk, A., et al. (2009). Proteomic characterization of midproliferative and midsecretory human endometrium. *J. Proteome Res.* 8, 2032–2044. doi: 10.1021/pr801024g

Chen, Y., Zheng, Y., Gao, Y., Lin, Z., Yang, S., Wang, T., et al. (2018). Single-cell RNA-seq uncovers dynamic processes and critical regulators in mouse spermatogenesis. *Cell Res.* 28, 879–896. doi: 10.1038/s41422-018-0074-y

da Cruz, I., Rodríguez-Casuriaga, R., Santiñaque, F. F., Farías, J., Curti, G., Capoano, C. A., et al. (2016). Transcriptome analysis of highly purified mouse spermatogenic cell populations: gene expression signatures switch from meiotic-to postmeiotic-related processes at pachytene stage. *BMC Genomics* 17:294. doi: 10.1186/s12864-016-2618-1

Dai, J., Leng, L. Z., Lu, C. F., Gong, F., Zhang, S. P., Zheng, W., et al. (2017). Time-lapse observation and transcriptome analysis of a case with repeated multiple pronuclei after IVF/ICSI. *J. Assist. Reprod. Genet.* 34, 1189–1197. doi: 10.1007/s10815-017-0972-9

De Kretser, D. M., Loveland, K. L., Meinhardt, A., Simorangkir, D., and Wreford, N. (1998). Spermatogenesis. *Hum. Reprod.* 13, 1–8. doi: 10.1093/humrep/13.suppl_1.1

Deroux, A., Dumestre-Perard, C., Dunand-Faure, C., Bouillet, L., and Hoffmann, P. (2017). Female infertility and serum auto-antibodies: a systematic review. *Clin. Rev. Allergy Immunol.* 53, 78–86. doi: 10.1007/s12016-016-8586-z

DeSouza, L., Diehl, G., Yang, E. C. C., Guo, J., Rodrigues, M. J., Romaschin, A. D., et al. (2005). Proteomic analysis of the proliferative and secretory phases of the human endometrium: protein identification and differential protein expression. *Proteomics* 5, 270–281. doi: 10.1002/pmic.200400920

Do, D. V., Strauss, B., Cukuroglu, E., Macaulay, I., Wee, K. B., Hu, T. X., et al. (2018). SRSF3 maintains transcriptome integrity in oocytes by regulation of alternative splicing and transposable elements. *Cell Discov.* 4:33. doi: 10.1038/s41421-018-0032-3

Eddy, E. M., and O'Brien, D. A. (1997). 5 Gene expression during mammalian meiosis. *Curr. Top. Dev. Biol.* 37, 141–200. doi: 10.1016/S0070-2153(08)60174-X

Ernst, C., Eling, N., Martinez-Jimenez, C. P., Marioni, J. C., and Odom, D. T. (2019). Staged developmental mapping and X chromosome transcriptional dynamics during mouse spermatogenesis. *Nat. Commun.* 10:1251. doi: 10.1038/s41467-019-09182-1

Esencan, E., and Seli, E. (2018). "Translational regulation of gene expression during oogenesis and preimplantation embryo development," in *Human Reproductive and Prenatal Genetics*, eds P.C.K. Leung, J. Qiao (Amsterdam: Elsevier), 221–239. doi: 10.1016/b978-0-12-813570-9.00010-3

Fang, X., Huang, L. L., Xu, J., Ma, C. Q., Chen, Z. H., Zhang, Z., et al. (2019). Proteomics and single-cell RNA analysis of Akap4-knockout mice model confirm indispensable role of Akap4 in spermatogenesis. *Dev. Biol.* 454, 118–127. doi: 10.1016/j.ydbio.2019.06.017

Fayomi, A. P., and Orwig, K. E. (2018). Spermatogonial stem cells and spermatogenesis in mice, monkeys and men. *Stem Cell Res.* 29, 207–214. doi: 10.1016/j.scr.2018.04.009

Ferrero, H., Corachan, A., Aguilar, A., Quiñonero, A., Carbajo-Garcia, M. C., Alama, P., et al. (2019). Single-cell RNA sequencing of oocytes from ovarian endometriosis patients reveals a differential transcriptomic profile associated with lower quality. *Hum. Reprod.* 34, 1302–1312. doi: 10.1093/humrep/dez053

Forcato, M., Romano, O., and Bicciato, S. (2021). Computational methods for the integrative analysis of single-cell data. *Brief. Bioinform.* 22, 20–29. doi: 10.1093/bib/bbaa042

Ge, W., Wang, J. J., Zhang, R. Q., Tan, S. J., Zhang, F. L., Liu, W. X., et al. (2020). Dissecting the initiation of female meiosis in the mouse at single-cell resolution. *Cell. Mol. Life Sci.* 78, 695–713. doi: 10.1007/s00018-020-03533-8

Goetz, J. J., and Trimarchi, J. M. (2012). Transcriptome sequencing of single cells with Smart-Seq. *Nat. Biotechnol.* 30, 763–765. doi: 10.1038/nbt.2325

Green, C. D., Ma, Q., Manske, G. L., Shami, A. N., Zheng, X., Marini, S., et al. (2018). A comprehensive roadmap of murine spermatogenesis defined by single-cell RNA-Seq. *Dev. Cell* 46, 651–667.e10. doi: 10.1016/j.devcel.2018.07.025

Grive, K. J., Hu, Y., Shu, E., Grimson, A., Elemento, O., Grenier, J. K., et al. (2019). Dynamic transcriptome profiles within spermatogonial and spermatocyte populations during postnatal testis maturation revealed by single-cell sequencing. *PLoS Genet.* 15:e1007810. doi: 10.1371/journal.pgen.1007810

Guo, J., Grow, E. J., Mlcochova, H., Maher, G. J., Lindskog, C., Nie, X., et al. (2018). The adult human testis transcriptional cell atlas. *Cell Res.* 28, 1141–1157. doi: 10.1038/s41422-018-0099-2

Guo, J., Grow, E. J., Yi, C., Mlcochova, H., Maher, G. J., Lindskog, C., et al. (2017). Chromatin and single-Cell RNA-Seq profiling reveal dynamic signaling and metabolic transitions during human spermatogonial stem cell development. *Cell Stem Cell* 21, 533–546.e6. doi: 10.1016/j.stem.2017.09.003

Guo, J., Nie, X., Giebler, M., Mlcochova, H., Wang, Y., Grow, E. J., et al. (2020). The dynamic transcriptional cell atlas of testis development during human puberty. *Cell Stem Cell* 26, 262–276.e4. doi: 10.1016/j.stem.2019.12.005

Hafemeister, C., and Satija, R. (2019). Normalization and variance stabilization of single-cell RNA-seq data using regularized negative binomial regression. *Genome Biol.* 20:296. doi: 10.1186/s13059-019-1874-1

Handel, M. A. (2004). The XY body: a specialized meiotic chromatin domain. *Exp. Cell Res.* 296, 57–63. doi: 10.1016/j.yexcr.2004.03.008

Hanson, B., Johnstone, E., Dorais, J., Silver, B., Peterson, C. M., Hotaling, J., et al. (2017). Female infertility, infertility-associated diagnoses, and comorbidities: a review. *J. Assist. Reprod. Genet.* 34, 167–177. doi: 10.1007/s10815-016-0836-8

Haque, A., Engel, J., Teichmann, S. A., and Lönnberg, T. (2017). A practical guide to single-cell RNA-sequencing for biomedical research and clinical applications. *Genome Med.* 9:75. doi: 10.1186/s13073-017-0467-4

Hashimshony, T., Senderovich, N., Avital, G., Klochendler, A., de Leeuw, Y., Anavy, L., et al. (2016). CEL-Seq2: sensitive highly-multiplexed single-cell RNA-Seq. *Genome Biol.* 17:77. doi: 10.1186/s13059-016-0938-8

Heath, J. R., Ribas, A., and Mischel, P. S. (2016). Single-cell analysis tools for drug discovery and development. *Nat. Rev. Drug discov.* 15:3. doi: 10.1038/nrd.2015.16

Hedlund, E., and Deng, Q. (2018). Single-cell RNA sequencing: technical advancements and biological applications. *Mol. Aspects Med.* 59, 36–46. doi: 10.1016/j.mam.2017.07.003

Hermann, B. P., Cheng, K., Singh, A., Roa-De La Cruz, L., Mutoji, K. N., Chen, I. C., et al. (2018). The mammalian spermatogenesis single-cell transcriptome, from spermatogonial stem cells to spermatids. *Cell Rep.* 25, 1650–1667.e8. doi: 10.1016/j.celrep.2018.10.026

Hu, Y., An, Q., Sheu, K., Trejo, B., Fan, S., and Guo, Y. (2018). Single cell multi-omics technology: methodology and application. *Front. Cell Dev. Biol.* 6:28. doi: 10.3389/fcell.2018.00028

Hunt, P. A., and Hassold, T. J. (2002). Sex matters in meiosis. *Science* 296, 2181–2183. doi: 10.1126/science.1071907

Jaitin, D. A., Kenigsberg, E., Keren-Shaul, H., Elefant, N., Paul, F., Zaretsky, I., et al. (2014). Massively parallel single-cell RNA-seq for marker-free decomposition of tissues into cell types. *Science* 343, 776–779. doi: 10.1126/science.1247651

Jung, M., Wells, D., Rusch, J., Ahmad, S., Marchini, J., Myers, S. R., et al. (2019). Unified single-cell analysis of testis gene regulation and pathology in five mouse strains. *Elife* 8:e43966. doi: 10.7554/elife.43966

Kivioja, T., Vähärautio, A., Karlsson, K., Bonke, M., Enge, M., Linnarsson, S., et al. (2012). Counting absolute numbers of molecules using unique molecular identifiers. *Nat. Methods* 9, 72–74. doi: 10.1038/nmeth.1778

Kolodziejczyk, A. A., Kim, J. K., Svensson, V., Marioni, J. C., and Teichmann, S. A. (2015). The technology and biology of single-cell RNA sequencing. *Mol. Cell* 58, 610–620. doi: 10.1016/j.molcel.2015.04.005

Krausz, C., and Riera-Escamilla, A. (2018). Genetics of male infertility. *Nat. Rev. Urol.* 15, 369–384. doi: 10.1038/s41585-018-0003-3

Kumar, K., Trzybulska, D., Tsatsanis, C., Giwercman, A., and Almstrup, K. (2019). Identification of circulating small non-coding RNAs in relation to male subfertility and reproductive hormones. *Mol. Cell. Endocrinol.* 492:110443. doi: 10.1016/j.mce.2019.05.002

Lau, X., Munusamy, P., Ng, M. J., and Sangrithi, M. (2020). Single-cell RNA sequencing of the cynomolgus macaque testis reveals conserved transcriptional

profiles during mammalian spermatogenesis. *Dev. Cell* 54, 548–566.e7. doi: 10.1016/j.devcel.2020.07.018

Li, L., Dong, J., Yan, L., Yong, J., Liu, X., Hu, Y., et al. (2017). Single-cell RNA-Seq analysis maps development of human germline cells and gonadal niche interactions. *Cell Stem Cell* 20, 858–873.e4. doi: 10.1016/j.stem.2017.03.007

Li, M., Yan, J., Zhi, X., Wang, Y., Hang, J., and Qiao, J. (2019). "Gene expression during oogenesis and oocyte development," in *The Ovary*, eds P.C.K. Leung, E.Y. Adashi (Amsterdam: Elsevier), 205–216. doi: 10.1016/b978-0-12-813209-8.00013-3

Liu, K. S., Pan, F., Mao, X. D., Liu, C., and Chen, Y. J. (2019). Biological functions of circular RNAs and their roles in occurrence of reproduction and gynecological diseases. *Am. J. Transl. Res.* 11, 1–15.

Liu, Q., Li, Y., Feng, Y., Liu, C., Ma, J., Li, Y., et al. (2016). Single-cell analysis of differences in transcriptomic profiles of oocytes and cumulus cells at GV, MI, MII stages from PCOS patients. *Sci. Rep.* 6:39638. doi: 10.1038/srep39638

Lukassen, S., Bosch, E., Ekici, A. B., and Winterpacht, A. (2018). mouse Single-cell RNA sequencing of adult testes. *Sci. Data* 5:180192. doi: 10.1038/sdata.2018.192

Macaulay, I. C., Haerty, W., Kumar, P., Li, Y. I., Hu, T. X., Teng, M. J., et al. (2015). G&T-seq: parallel sequencing of single-cell genomes and transcriptomes. *Nat. Methods* 12, 519–522. doi: 10.1038/nmeth.3370

Macosko, E. Z., Basu, A., Satija, R., Nemesh, J., Shekhar, K., Goldman, M., et al. (2015). Highly parallel genome-wide expression profiling of individual cells using nanoliter droplets. *Cell* 161, 1202–1214. doi: 10.1016/j.cell.2015.05.002

Margolin, G., Khil, P. P., Kim, J., Bellani, M. A., and Camerini-Otero, R. D. (2014). Integrated transcriptome analysis of mouse spermatogenesis. *BMC Genomics* 15:39. doi: 10.1186/1471-2164-15-39

McInnes, L., Healy, J., Saul, N., and Großberger, L. (2018). UMAP: uniform manifold approximation and projection. *J. Open Source Softw.* 3:861. doi: 10.21105/joss.00861

Meistrich, M. L., Mohapatra, B., Shirley, C. R., and Zhao, M. (2003). Roles of transition nuclear proteins in spermiogenesis. *Chromosoma* 111, 483–488. doi: 10.1007/s00412-002-0227-z

Mihola, O., Pratto, F., Brick, K., Linhartova, E., Kobets, T., Flachs, P., et al. (2019). Histone methyltransferase PRDM9 is not essential for meiosis in male mice. *Genome Res.* 29, 1078–1086. doi: 10.1101/gr.244426.118

Mimitou, E. P., Cheng, A., Montalbano, A., Hao, S., Stoeckius, M., Legut, M., et al. (2019). Multiplexed detection of proteins, transcriptomes, clonotypes and CRISPR perturbations in single cells. *Nat. Methods* 16, 409–412. doi: 10.1038/s41592-019-0392-0

Navin, N., Kendall, J., Troge, J., Andrews, P., Rodgers, L., McIndoo, J., et al. (2011). Tumour evolution inferred by single-cell sequencing. *Nature* 472, 90–95. doi: 10.1038/nature09807

Nguyen, Q. H., Pervolarakis, N., Nee, K., and Kessenbrock, K. (2018). Experimental considerations for single-cell RNA sequencing approaches. *Front. Cell Dev. Biol.* 6:108. doi: 10.3389/fcell.2018.00108

Niu, W., and Spradling, A. C. (2020). Two distinct pathways of pregranulosa cell differentiation support follicle formation in the mouse ovary. *Proc. Natl. Acad. Sci. U.S.A.* 117, 20015–20026. doi: 10.1073/PNAS.2005570117

Oud, M. S., Volozonoka, L., Smits, R. M., Vissers, L. E. L. M., Ramos, L., and Veltman, J. A. (2019). A systematic review and standardized clinical validity assessment of male infertility genes. *Hum. Reprod.* 34, 932–941. doi: 10.1093/humrep/dez022

Page, S. L., and Hawley, R. S. (2004). The genetics and molecular biology of the synaptonemal complex. *Annu. Rev. Cell Dev. Biol.* 20, 525–558. doi: 10.1146/annurev.cellbio.19.111301.155141

Parmar, T., Sachdeva, G., Savardekar, L., Katkam, R. R., Nimbkar-Joshi, S., Gadkar-Sable, S., et al. (2008). Protein repertoire of human uterine fluid duringthe mid-secretory phase of the menstrual cycle. *Hum. Reprod.* 23, 379–386. doi: 10.1093/humrep/dem367

Pearson, K. (1901). LIII. On lines and planes of closest fit to systems of points in space. *Lond. Edinb. Dublin Philos. Mag. J. Sci.* 2, 559–572. doi: 10.1080/14786440109462720

Picelli, S., Björklund, ÅK., Faridani, O. R., Sagasser, S., Winberg, G., and Sandberg, R. (2013). Smart-seq2 for sensitive full-length transcriptome profiling in single cells. *Nat. Methods* 10, 1096–1100. doi: 10.1038/nmeth.2639

Practice Committee of the American Society for Reproductive Medicine (2006). Effectiveness and treatment for unexplained infertility. *Fertil. Steril.* 86, S111–S114. doi: 10.1016/j.fertnstert.2006.07.1475

Raj, B., Gagnon, J. A., and Schier, A. F. (2018). Large-scale reconstruction of cell lineages using single-cell readout of transcriptomes and CRISPR–Cas9 barcodes by scGESTALT. *Nat. Protoc.* 13, 2685–2713. doi: 10.1038/s41596-018-0058-x

Ramsköld, D., Luo, S., Wang, Y. C., Li, R., Deng, Q., Faridani, O. R., et al. (2012). Full-length mRNA-Seq from single-cell levels of RNA and individual circulating tumor cells. *Nat. Biotechnol.* 30, 777–782. doi: 10.1038/nbt.2282

Reynaud, K., and Driancourt, M. A. (2000). Oocyte attrition. *Mol. Cell. Endocrinol.* 163, 101–108. doi: 10.1016/S0303-7207(99)00246-4

Rizzetto, S., Eltahla, A. A., Lin, P., Bull, R., Lloyd, A. R., Ho, J. W. K., et al. (2017). Impact of sequencing depth and read length on single cell RNA sequencing data of T cells. *Sci. Rep.* 7:12781. doi: 10.1038/s41598-017-12989-x

Saliba, A. E., Westermann, A. J., Gorski, S. A., and Vogel, J. (2014). Single-cell RNA-seq: advances and future challenges. *Nucleic Acids Res.* 42, 8845–8860. doi: 10.1093/nar/gku555

Shami, A. N., Zheng, X., Munyoki, S. K., Ma, Q., Manske, G. L., Green, C. D., et al. (2020). Single-cell RNA sequencing of human, macaque, and mouse testes uncovers conserved and divergent features of mammalian spermatogenesis. *Dev. Cell* 54:529–547.e12. doi: 10.1016/j.devcel.2020.05.010

Stuart, T., Butler, A., Hoffman, P., Hafemeister, C., Papalexi, E., Mauck, W. M., et al. (2019). Comprehensive integration of single-cell data. *Cell* 177, 1888–1902.e21. doi: 10.1016/j.cell.2019.05.031

Suo, L., Zhou, Y., Jia, L., Wu, H., Zheng, J., Lyu, Q., et al. (2018). Transcriptome profiling of human oocytes experiencing recurrent total fertilization failure. *Sci. Rep.* 8:17890. doi: 10.1038/s41598-018-36275-6

Suzuki, S., Diaz, V. D., and Hermann, B. P. (2019). What has single-cell RNA-seq taught us about mammalian spermatogenesis? *Biol. Reprod.* 101, 617–634. doi: 10.1093/biolre/ioz088

Tan, K., and Wilkinson, M. F. (2019). Human spermatogonial stem cells scrutinized under the single-cell magnifying glass. *Cell Stem Cell* 24, 201–203. doi: 10.1016/j.stem.2019.01.010

Tan, K., Song, H. W., and Wilkinson, M. F. (2020). Single-cell RNAseq analysis of testicular germ and somatic cell development during the perinatal period. *Development* 147:dev183251. doi: 10.1242/dev.183251

Tang, F., Barbacioru, C., Wang, Y., Nordman, E., Lee, C., Xu, N., et al. (2009). mRNA-Seq whole-transcriptome analysis of a single cell. *Nat. Methods* 6, 377–382. doi: 10.1038/nmeth.1315

Tirosh, I., Izar, B., Prakadan, S. M., Wadsworth, M. H., Treacy, D., Trombetta, J. J., et al. (2016). Dissecting the multicellular ecosystem of metastatic melanoma by single-cell RNA-seq. *Science* 352, 189–196. doi: 10.1126/science.aad0501

Trapnell, C., Cacchiarelli, D., Grimsby, J., Pokharel, P., Li, S., Morse, M., et al. (2014). The dynamics and regulators of cell fate decisions are revealed by pseudotemporal ordering of single cells. *Nat. Biotechnol.* 32, 381–386. doi: 10.1038/nbt.2859

Unuane, D., Tournaye, H., Velkeniers, B., and Poppe, K. (2011). Endocrine disorders & female infertility. *Best Pract. Res. Clin. Endocrinol. Metab.* 25, 861–873. doi: 10.1016/j.beem.2011.08.001

Van Der Maaten, L., and Hinton, G. (2008). Visualizing data using t-SNE. *J. Mach. Learn. Res.* 9, 2579–2625.

Walker, W. H. (2021). Regulation of mammalian spermatogenesis by miRNAs. *Semin. Cell Dev. Biol.* doi: 10.1016/j.semcdb.2021.05.009

Wang, M., Liu, X., Chang, G., Chen, Y., An, G., Yan, L., et al. (2018). Single-Cell RNA sequencing analysis reveals sequential cell fate transition during human spermatogenesis. *Cell Stem Cell* 23, 599–614.e4. doi: 10.1016/j.stem.2018.08.007

Wang, S., Zheng, Y., Li, J., Yu, Y., Zhang, W., Song, M., et al. (2020). Single-cell transcriptomic atlas of primate ovarian aging. *Cell* 180, 585–600.e19. doi: 10.1016/j.cell.2020.01.009

Wen, L., and Tang, F. (2019). Human germline cell development: from the perspective of single-cell sequencing. *Mol. Cell* 76, 320–328. doi: 10.1016/j.molcel.2019.08.025

Xin, Y., Kim, J., Ni, M., Wei, Y., Okamoto, H., Lee, J., et al. (2016). Use of the fluidigm C1 platform for RNA sequencing of single mouse pancreatic islet cells. *Proc. Natl. Acad. Sci. U.S.A.* 113, 3293–3298. doi: 10.1073/pnas.1602306113

Xu, X., Hou, Y., Yin, X., Bao, L., Tang, A., Song, L., et al. (2012). Single-cell exome sequencing reveals single-nucleotide mutation characteristics of a kidney tumor. *Cell* 148, 886–895. doi: 10.1016/j.cell.2012.02.025

Yang, C., Wu, Z., Liu, X., Liang, H., Gao, Z., Wang, Y., et al. (2021). Single-cell RNA-seq reveals mRNAs and lncRNAs important for oocytes in vitro matured in pigs. *Reprod. Domest. Anim.* 56, 642–657. doi: 10.1111/rda.13901

Yang, F., and Wang, P. J. (2018). "Genetics of mammalian meiosis," in *Spermatogenesis*, eds C.Y. Cheng (Boca Raton, FL: CRC Press), 106–115. doi: 10.1201/9780429488634-8

Yatsenko, S. A., and Rajkovic, A. (2019). Genetics of human female infertility. *Biol. Reprod.* 101, 549–566. doi: 10.1093/biolre/ioz084

Ye, M., Yang, Z. Y., Zhang, Y., Xing, Y. X., Xie, Q. G., Zhou, J. H., et al. (2020). Single-cell multiomic analysis of in vivo and in vitro matured human oocytes. *Hum. Reprod.* 35, 886–900. doi: 10.1093/HUMREP/DEAA044

Yu, B., Doni Jayavelu, N., Battle, S. L., Mar, J. C., Schimmel, T., Cohen, J., et al. (2020). Single-cell analysis of transcriptome and DNA methylome in human oocyte maturation. *PLoS One* 15:e0241698. doi: 10.1371/journal.pone.0241698

Yuan, G. C., Cai, L., Elowitz, M., Enver, T., Fan, G., Guo, G., et al. (2017). Challenges and emerging directions in single-cell analysis. *Genome Biol.* 18:84. doi: 10.1186/s13059-017-1218-y

Zhang, C., Liu, J., Lai, M., Li, J., Zhan, J., Wen, Q., et al. (2019). Circular RNA expression profiling of granulosa cells in women of reproductive age with polycystic ovary syndrome. *Arch. Gynecol. Obstet.* 300, 431–440. doi: 10.1007/s00404-019-05129-5

Zhang, T., Xi, Q., Wang, D., Li, J., Wang, M., Li, D., et al. (2019). Mitochondrial dysfunction and endoplasmic reticulum stress involved in oocyte aging: an analysis using single-cell RNA-sequencing of mouse oocytes. *J. Ovarian Res.* 12:53. doi: 10.1186/s13048-019-0529-x

Zhang, Y., Yan, Z., Qin, Q., Nisenblat, V., Chang, H. M., Yu, Y., et al. (2018). Transcriptome landscape of human folliculogenesis reveals oocyte and granulosa cell interactions. *Mol. Cell* 72, 1021–1034.e4. doi: 10.1016/j.molcel.2018.10.029

Zhao, Z., Ma, J., Meng, T., Wang, Z., Yue, W., Zhou, Q., et al. (2020a). Single-cell RNA sequencing reveals the landscape of early female germ cell development. *FASEB J.* 34, 12634–12645. doi: 10.1096/fj.202001034RR

Zhao, Z. H., Li, C. Y., Meng, T. G., Wang, Y., Liu, W. B., Li, A., et al. (2020b). Single-cell RNA sequencing reveals regulation of fetal ovary development in the monkey (Macaca fascicularis). *Cell Discov.* 6:97. doi: 10.1038/s41421-020-00219-0

Zhao, Z. H., Meng, T. G., Li, A., Schatten, H., Wang, Z. B., and Sun, Q. Y. (2020c). RNA-Seq transcriptome reveals different molecular responses during human and mouse oocyte maturation and fertilization. *BMC Genomics* 21:475. doi: 10.1186/s12864-020-06885-4

Ziegenhain, C., Vieth, B., Parekh, S., Reinius, B., Guillaumet-Adkins, A., Smets, M., et al. (2017). Comparative analysis of single-cell RNA sequencing methods. *Mol. Cell* 65, 631–643.e4. doi: 10.1016/j.molcel.2017.01.023

Zitzmann, M. (2013). Effects of age on male fertility. *Best Pract. Res. Clin. Endocrinol. Metab.* 27, 617–628. doi: 10.1016/j.beem.2013.07.004

Conflict of Interest: The authors declare that the research was conducted in the absence of any commercial or financial relationships that could be construed as a potential conflict of interest.

Publisher's Note: All claims expressed in this article are solely those of the authors and do not necessarily represent those of their affiliated organizations, or those of the publisher, the editors and the reviewers. Any product that may be evaluated in this article, or claim that may be made by its manufacturer, is not guaranteed or endorsed by the publisher.

Copyright © 2021 Peng and Qiao. This is an open-access article distributed under the terms of the Creative Commons Attribution License (CC BY). The use, distribution or reproduction in other forums is permitted, provided the original author(s) and the copyright owner(s) are credited and that the original publication in this journal is cited, in accordance with accepted academic practice. No use, distribution or reproduction is permitted which does not comply with these terms.

frontiers in Cell and Developmental Biology

ORIGINAL RESEARCH
published: 04 November 2021
doi: 10.3389/fcell.2021.675286

Cataloging Human *PRDM9* Allelic Variation Using Long-Read Sequencing Reveals *PRDM9* Population Specificity and Two Distinct Groupings of Related Alleles

*Benjamin Alleva, Kevin Brick, Florencia Pratto, Mini Huang and Rafael Daniel Camerini-Otero**

Genetics and Biochemistry Branch, National Institute of Diabetes and Digestive and Kidney Diseases, National Institutes of Health, Bethesda, MD, United States

The PRDM9 protein determines sites of meiotic recombination in humans by directing meiotic DNA double-strand breaks to specific loci. Targeting specificity is encoded by a long array of C_2H_2 zinc fingers that bind to DNA. This zinc finger array is hypervariable, and the resulting alleles each have a potentially different DNA binding preference. The assessment of *PRDM9* diversity is important for understanding the complexity of human population genetics, inheritance linkage patterns, and predisposition to genetic disease. Due to the repetitive nature of the *PRDM9* zinc finger array, the large-scale sequencing of human *PRDM9* is challenging. We, therefore, developed a long-read sequencing strategy to infer the diploid *PRDM9* zinc finger array genotype in a high-throughput manner. From an unbiased study of *PRDM9* allelic diversity in 720 individuals from seven human populations, we detected 69 *PRDM9* alleles. Several alleles differ in frequency among human populations, and 32 alleles had not been identified by previous studies, which were heavily biased to European populations. *PRDM9* alleles are distinguished by their DNA binding site preferences and fall into two major categories related to the most common *PRDM9-A* and *PRDM9-C* alleles. We also found that it is likely that inter-conversion between allele types is rare. By mapping meiotic double-strand breaks (DSBs) in the testis, we found that small variations in *PRDM9* can substantially alter the meiotic recombination landscape, demonstrating that minor *PRDM9* variants may play an under-appreciated role in shaping patterns of human recombination. In summary, our data greatly expands knowledge of *PRDM9* diversity in humans.

Keywords: *PRDM9*, meiosis, recombination, human, long-read sequencing, minisatellite genotyping

OPEN ACCESS

Edited by:
Scott Keeney, Memorial Sloan Kettering Cancer Center, United States

Reviewed by:
Frédéric Baudat, Université de Montpellier, France
Simon Myers, University of Oxford, United Kingdom

****Correspondence:***
Rafael Daniel Camerini-Otero
rdcamerini@mail.nih.gov

Specialty section:
This article was submitted to Cell Growth and Division, a section of the journal Frontiers in Cell and Developmental Biology

Received: *02 March 2021*
Accepted: *11 October 2021*
Published: *04 November 2021*

Citation:
Alleva B, Brick K, Pratto F, Huang M and Camerini-Otero RD (2021) Cataloging Human PRDM9 Allelic Variation Using Long-Read Sequencing Reveals PRDM9 Population Specificity and Two Distinct Groupings of Related Alleles. Front. Cell Dev. Biol. 9:675286. doi: 10.3389/fcell.2021.675286

INTRODUCTION

Meiosis is a specialized cellular division that creates gametes. During meiosis, hundreds of programmed DNA double-strand breaks (DSBs) are formed and repaired *via* specialized pathways: these pathways assure proper chromosome segregation and introduce genetic diversity through the exchange of genetic information between parental chromosomes. In humans and many other

mammals, meiotic DSB localization is defined by the DNA binding specificity of the meiosis-specific PRDM9 protein, which creates DSB hotspots (Hayashi et al., 2005; Baudat et al., 2010; Myers et al., 2010; Parvanov et al., 2010). PRDM9 is composed of four functional domains: KRAB and SSXRD domains play an unknown role but are thought to mediate protein–protein interactions (Imai et al., 2017; Parvanov et al., 2017; Thibault-Sennett et al., 2018), a PR/SET domain with histone methyltransferase activity (Wu et al., 2013; Koh-Stenta et al., 2014), and an array of C_2H_2 zinc fingers (ZFs) that confer DNA binding specificity (Baudat et al., 2010; Grey et al., 2011; Billings et al., 2013; Koh-Stenta et al., 2014; Walker et al., 2015).

Since hotspot loci are targeted for recombination by PRDM9, gene conversion and mutation during DNA repair rapidly erodes *PRDM9* binding sites in the genome. Thus, the emergence of new alleles is favored as a means of "escaping" the detrimental effects of binding site depletion (Myers et al., 2010; Lesecque et al., 2014). The *PRDM9* C_2H_2 ZF array is under strong positive selection (Oliver et al., 2009; Buard et al., 2014; Schwartz et al., 2014; Ahlawat et al., 2016) and, as a result, is hypervariable in all species studied to date with a full-length *PRDM9* gene. Currently, 33 *PRDM9* alleles (from here on, *PRDM9* alleles are defined as the sequence variation found within the ZF array) have been identified in human population studies (Berg et al., 2010, 2011), dozens of alleles in apes (Auton et al., 2012; Schwartz et al., 2014), and >170 alleles in mice (Buard et al., 2014; Kono et al., 2014). In addition, hundreds of alleles have been identified in human sperm (Jeffreys et al., 2013). The mechanisms that give rise to *PRDM9* variation remain opaque; however, alleles can differ by the number of ZFs, combinations of ZFs, or even by a single nucleotide. It is important to understand variation at this locus since different *PRDM9* alleles can completely alter the recombination landscape by altering the preferred DNA binding site (Baudat et al., 2010; Brick et al., 2012; Pratto et al., 2014b; Smagulova et al., 2016). The distribution of *PRDM9* alleles differs among human populations, with by far the greatest diversity of *PRDM9* alleles is found in Africa (Hinch et al., 2011). Non-African populations are dominated by a single *PRDM9* allele (*PRDM9-A*); for example, in populations of European origin, the *PRDM9-A* allele was found to be present at a frequency > 80%. The *A* allele is also highly prevalent in African populations (∼50%), and its prevalence outside of Africa may stem from a historical genetic bottleneck. In contrast, the next most frequent allele, *PRDM9-C*, is far more frequent in African (∼15% frequency) than in European populations (∼1% frequency) [data from Baudat et al. (2010), Berg et al. (2010), and Parvanov et al. (2010)].

Despite these clear differences among populations, extant studies of *PRDM9* allelic diversity disproportionately surveyed individuals of European descent [628/750 individuals; data from Baudat et al. (2010), Berg et al. (2010), and Parvanov et al. (2010)], and a comprehensive survey of *PRDM9* alleles across human populations has never been performed. The catalog of human genetic diversity has enormously expanded in recent years through whole-genome sequencing and exome sequencing of individual genomes. However, the short-read technology used for these advances is not suited for sequencing the highly repetitive *PRDM9* ZF array, which still relies on labor-intensive Sanger sequencing. In this study, we developed a high-throughput long-read sequencing-based approach to determine the diploid *PRDM9* genotype of 720 individuals from seven distinct human populations. We identified 32 previously unannotated alleles and found that the prevalence of some *PRDM9* alleles differs substantially between populations. Additionally, we identified single-nucleotide polymorphisms (SNPs) associated with different *PRDM9* genotypes. We also demonstrate that although most human *PRDM9* alleles are related to either the *PRDM9-A* or *PRDM9-C* alleles, even superficially minor changes to the *PRDM9* ZF array can substantially re-shape the recombination landscape.

RESULTS

Human Populations Surveyed for *PRDM9* Genotyping

Fine-scale recombination maps differ among human populations, which may represent differences in the distribution of *PRDM9* alleles (Spence and Song, 2019). Recombination maps broadly cluster into five geographic groups (European, African, East Asian, South Asian, and South American; Spence and Song, 2019); therefore, we assessed the diversity of *PRDM9* alleles in at least one representative population from each cluster (**Figure 1A**). Most studies of *PRDM9* diversity in humans have been performed in individuals of European descent, so to assess if *PRDM9* diversity differed among European ethnic groups, we chose two European populations—one with little admixture (Finnish in Finland; FIN) and one with more admixture (Toscani in Italia, TSI; Zaidi et al., 2019). A few studies previously addressed *PRDM9* diversity in Asian populations; therefore, we chose two Asian populations for study; one from East Asia (Han Chinese in Beijing, CHB) and one from South Asia (Punjabi in Lahore, Pakistan, PJL). African populations have a high diversity of *PRDM9* alleles (Berg et al., 2011; Hinch et al., 2011); to assess similarities and differences in the *PRDM9* repertoire among African populations, we chose to survey *PRDM9* diversity in the Yoruba in Ibadan, Nigeria (YRI), and in the Luhya in Webuye, Kenya (LWK). Finally, we chose a South American population as no prior studies have examined *PRDM9* diversity in this geographic region (Peruvian in Lima, Peru, PEL). For each population, we attempted to infer the diploid *PRDM9* genotype for all individuals.

Long-Read Sequencing of Human *PRDM9*

To analyze *PRDM9* allelic diversity in seven different populations, we devised a workflow to amplify and sequence the *PRDM9* ZF array using long-read sequencing (see section "Materials and Methods"; **Figures 1B,C**). We amplified the *PRDM9* ZF array from the genomic DNA of each individual using PCR primers containing one of eight unique DNA barcodes. Samples were subsequently pooled in sets of eight, and a second barcode was added using one of the 96 barcodes from the Oxford Nanopore

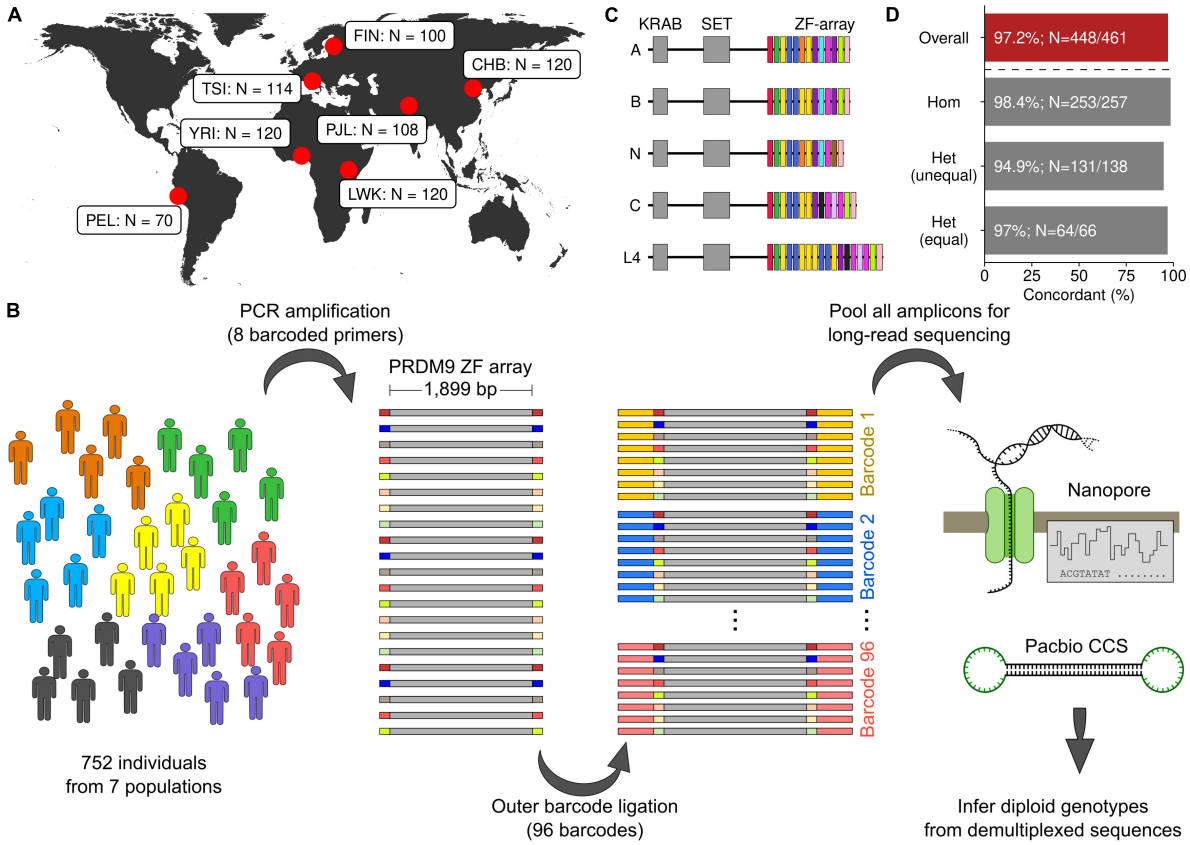

FIGURE 1 | *PRDM9* diploid genotyping with long-read sequencing. **(A)** Geographic location of seven populations in this study (YRI, Yoruba in Ibadan, Nigeria; LWK, Luhya in Webuye, Kenya; TSI, Toscani in Italia; FIN, Finnish in Finland; PEL, Peruvian in Lima, Peru; CHB, Han Chinese in Beijing, China; PJL, Punjabi in Lahore, Pakistan). **(B)** Schematic of amplification, barcoding, and sequencing strategy (see section "Materials and Methods"). **(C)** The protein domain structure of human PRDM9. The zinc finger (ZF) array of *PRDM9* is a repeating array of 84-bp-long ZFs. ZF variants are indicated by different colors. Five annotated *PRDM9* alleles are shown. **(D)** Genotyping *PRDM9* gives analogous results using either Oxford Nanopore or Pacific Biosciences Circular Consensus Sequencing (CCS) (PacBio CCS). The percentage of concordant genotypes is shown. The least agreement (94.9%) is seen for individuals that are heterozygous for alleles of different lengths [Het (unequal)]. The overall concordance across all 461 individuals is 97.2%.

PCR Barcoding Kit 1-96. All barcoded amplicons were then pooled for long-read sequencing.

The repetitive *PRDM9* ZF array causes PCR amplification artifacts that are seen as laddering and smearing in gel electrophoresis images (**Supplementary Figure S1**; see also Schwartz et al., 2014). Previous approaches for defining *PRDM9* alleles using Sanger sequencing required manual excision of the desired band. Instead, we removed amplification artifacts later, *in silico,* by retaining only reads with an uninterrupted and contiguous array of ZFs signified by the presence of the expected genomic flanking sequences (see section "Materials and Methods"). Amplification errors may also create reads with an erroneous, but complete, ZF array. Although these will pass the initial filter, they represent a minority of reads (**Supplementary Figure S1**) and will only negligibly affect consensus-based genotyping.

To compare the utility of different long-read sequencing platforms for *PRDM9* genotyping, we inferred the *PRDM9* diploid genotype for 461 individuals using both Oxford Nanopore sequencing and PacBio Circular Consensus Sequencing (CCS). For 97.2% of individuals, the inferred diploid *PRDM9* genotype agreed using both platforms (448/461; **Figure 1D**). In 12/13 individuals with discordant genotypes, at least one allele was identified in both datasets (**Supplementary Figures S2A–C**); thus, the absolute error rate of genotype calls is ∼1.5% (14/922 alleles). The highest agreement was in individuals homozygous for a *PRDM9* genotype, where genotyping is least challenging (98.4% agreement; **Figure 1D**). Individuals heterozygous for *PRDM9* but where both *PRDM9* alleles had the same number of ZFs are theoretically the most challenging to accurately genotype, as the *PRDM9* alleles can differ by as little as a single nucleotide. However, 97.0% of diploid genotypes agreed across platforms (**Figure 1D**). Somewhat surprisingly, the agreement was lowest for individuals who were heterozygous for *PRDM9* but where the inferred *PRDM9* alleles had differing numbers of ZFs (94.9% agreement; **Figure 1D**). These discrepancies were likely due to samples with low coverage from one sequencing technology or samples with artifacts from PCR that became overrepresented during sequencing and data processing (**Supplementary Figures S2A–C**). Given

the extensive concordance, we merged nanopore and CCS reads for final genotype calling (see section "Materials and Methods"). To assess the final accuracy, we examined *PRDM9* diversity in trios. For 31/32 YRI individuals with both parents in the YRI population, the diploid *PRDM9* genotype was concordant with the parental genotypes. 63/64 alleles were consistent with the parents, alluding to an overall error rate of ∼1.6%. This is very close to the genotyping error rate inferred by comparing sequencing technologies (∼1.5%). The diploid *PRDM9* genotype was also correctly identified in two control samples where *PRDM9* was independently determined using Sanger sequencing (CTL: **Supplementary Figures S1C,D**: lanes 6 and 8). Ultimately, we identified the diploid *PRDM9* genotype for 720/752 individuals within the seven different populations. The remaining individuals lacked sufficient coverage depth for genotyping (**Supplementary Figures S2E–G**).

A Catalog of *PRDM9* Diversity in Humans

We identified 69 different *PRDM9* alleles among 720 individuals for whom we could infer the diploid genotype; 24 of these alleles had been previously identified in human population studies (Baudat et al., 2010; Berg et al., 2010, 2011), 13 alleles were previously identified only in human blood ($N = 4$) or sperm ($N = 9$) (Jeffreys et al., 2013), and 32 novel *PRDM9* alleles were identified (**Figure 2A**). Although our approach may yield spurious "new" alleles (if genotyping/sequencing errors create what appears to be a new ZF, and hence a new allele), we found that a majority of novel alleles (30/32) have secondary support. Alleles derived from new combinations of known ZFs were unlikely to have occurred erroneously and were considered "high confidence" novel alleles ($N = 18$). Five alleles with a novel ZF were found in more than one individual and also likely represent "high confidence" novel alleles. Finally, short-read exome sequencing data from the 1,000 Genomes Project validated seven of the nine remaining alleles (see section "Materials and Methods"; **Supplementary Figure S3**). The remaining two alleles (*M22* and *M23*) lacked sufficient exome sequencing data to validate, or invalidate, the allele. Given the accuracy of other novel genotypes, it seems unlikely that these are incorrect.

We next examined the predicted binding sites for all human *PRDM9* alleles. Consistent with previous work (Berg et al., 2011; Hinch et al., 2011), we found that *PRDM9* alleles broadly cluster into two groups; those with a *PRDM9-A-type* predicted binding site (*A*-type) and those with a *PRDM9-C-type* predicted binding site (*C*-type) (**Supplementary Figure S4A**). To formally categorize each allele as either *A*-type or *C*-type and to avoid complexities associated with predicting *PRDM9* binding, we scored each allele by the similarity to the DNA contact residues of the *PRDM9-A* and *PRDM9-C* DNA binding sites (see section "Materials and Methods"; **Supplementary Figure S4**). By this criteria, 50/71 alleles in our study were *A-type* and 21/71 were *C-type* (note that this includes two alleles found in control experiments but not part of the population analysis—*L13* and *Av:0053*; for allele nomenclature, see section "Materials and Methods"). We found some alleles are quite dissimilar to both (*L5*, *M12*, and *Cv:0283* alleles; **Supplementary Figure S4B**). 27 *A-type* alleles (not including *PRDM9-A*) had no predicted variation at the DNA contact residues, implying that these alleles likely bind the same DNA sequence as *PRDM9-A*. Likewise, 13 *C-type* alleles (not including *PRDM9-C*) had an identical predicted DNA contact site as *PRDM9-C*. *A-type* alleles were present in all populations with similar prevalence; however, *C*-type alleles were almost exclusively found in the two African populations (LWK and YRI; **Figure 2B**).

The length of the *PRDM9* ZF array has been used as a proxy for studying different variants of *PRDM9* (Kong et al., 2010). We found a significant difference between the length of *A*-type and *C*-type alleles (*A*-type median = 13 ZFs, *C*-type median = 15 ZFs; $P = 10^{-5}$, Wilcoxon test; **Supplementary Figure S4D**). *PRDM9* variants that arise in sperm tend to remain similar in size to the allele from which they are derived (**Supplementary Figure S4E**). Thus, it appears likely that these differences are not shaped by selection in favor of particular allele lengths, but by limitations of the mechanism by which they arise.

Population Frequency of *PRDM9* Alleles in Seven Human Populations

Consistent with previous studies (Baudat et al., 2010; Berg et al., 2010; Parvanov et al., 2010), we found that, by far, the most frequent *PRDM9* variant in human populations was the *A* allele (**Figure 2B** and **Supplementary Figure S5A**). The proportion of *A* alleles was highest in the Finnish population [frequency (fA_{FIN}) = 90%] and lowest in the two African populations (fA_{LWK} = 49% and fA_{YRI} = 48%). The Han Chinese population had an intermediate *A* allele frequency (fA_{CHB} = 75%), although it is not clear if this differs from the frequency in the other non-African populations (**Supplementary Figure S6**). Three other alleles (*B*, *C*, and *L14*) were found in ≥10% of individuals in at least one population, and each allele displayed population-specific differences in its distribution. Previously, the *B* allele was found at low frequencies in European and African individuals (2 and 3%, respectively; Berg et al., 2010). Our data paint a different picture of the distribution of this allele. We found that the *B* allele was enriched in the CHB (fB_{CHB} = 13%) and YRI populations (fB_{YRI} = 7%), compared to the low frequencies in other populations (0–3%; **Figure 2B** and **Supplementary Figures S5A, S6**). The prevalence in the CHB population was far more than expected from sampling noise, suggesting that the *B* allele has proliferated substantially in the Han Chinese population compared to others (**Supplementary Figure S6**). Another example of a population-enriched allele was the *L14* allele, found predominantly in the LWK population ($fL14_{LWK}$ = 11%). *L14* was also found in the YRI population, but at a substantially reduced frequency ($fL14_{YRI}$ = 3%; **Supplementary Figure S5A, S6**), and it was absent from the other five (non-African) populations. Finally, the last allele among this tier of alleles was the *C* allele, previously described as the most common minor allele in Africans (Berg et al., 2010). Our data showed that while the *C* allele was indeed relatively frequent in both African populations (fC_{YRI} = 10%; fC_{LWK} = 8%), it was found at a similar frequency in some non-African populations (fC_{PEL} = 8%; fC_{CHB} = 6%). The

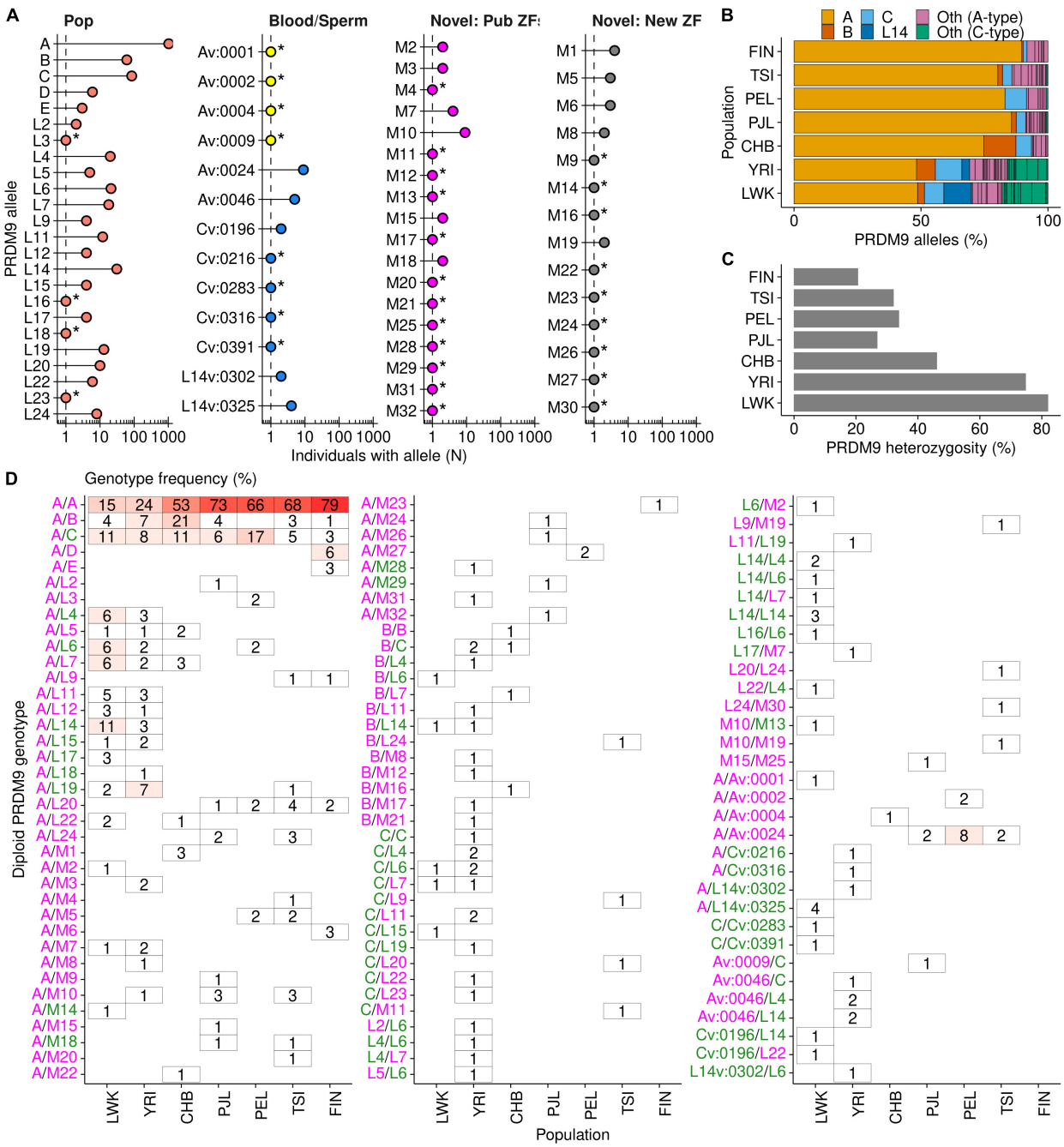

FIGURE 2 | *PRDM9* diploid genotypes in seven populations. Sixty-nine total *PRDM9* alleles were found in 720 individuals. **(A)** Approximately half of the *PRDM9* alleles sequenced in this study are found in >1 individual [asterisk (*) denotes alleles found in one individual]. Alleles are split by type; Pop (red) = *PRDM9* allele found in previous population studies; Sperm/Blood = found as a *PRDM9* variant in blood (yellow) or sperm (blue); Novel: Pub ZFs (pink) = novel *PRDM9* allele identified in this study and contains only known ZFs; Novel: New ZF (gray) = novel *PRDM9* allele identified in this study and contains at least one new ZF. **(B)** Composition of *PRDM9* alleles in each population. The four most prevalent alleles are color coded (*A*—yellow; *B*—orange; *C*—light blue; *L14*—dark blue). All other alleles are color coded by *A*-type or *C-type* allele (described in **Supplementary Figure S4**; *A*-type = magenta and *C*-type = green). **(C)** Frequency of *PRDM9* heterozygosity in each population. **(D)** Frequency of diploid *PRDM9* genotypes in each population. Blank spaces indicate genotypes not found. *A*-type allele labels are magenta and *C*-type are green.

frequency of the *C* allele in the TSI and PJL populations was lower (fC_{TSI} = 4%; fC_{PJL} = 4%), but within the expected range of sampling error for the YRI, LWK, PEL, and CHB populations (99% C.I.; **Supplementary Figure S6**). The Finnish population was the major outlier as the *C* allele occurred at just 2% frequency. Together, these data suggest that rather than

being an African-enriched allele, the *C* allele is rare in some European populations.

The remaining tier of alleles was present at a frequency of <10% in all populations. Although individually rare, together, these alleles represent 16% of all *PRDM9* alleles ($N = 230/1{,}440$). The prevalence of these rarer alleles varied by population, and consistent with previous data, rare alleles were most frequent in both African populations ($fRare_{LWK} = 30\%$; $fRare_{YRI} = 31\%$). The TSI population had the next highest frequency of rare *PRDM9* alleles ($fRare_{TSI} = 14\%$), which may have arisen from geographical proximity to Africa and recent admixture. All other populations had relatively similar levels of rare *PRDM9* alleles ($fRare_{PJL} = 9\%$; $fRare_{PEL} = 8\%$; $fRare_{FIN} = 8\%$; $fRare_{CHB} = 7\%$). Among the rare alleles were 13 alleles previously only seen as *de novo* variants in blood or sperm (Jeffreys et al., 2013). Six of these alleles were derived from *de novo* variation of *PRDM9-A*, five from *PRDM9-C*, and two from *PRDM9-L14*. Indeed, the population distribution of the variant alleles broadly paralleled that of the alleles from which they were likely derived (**Supplementary Figures S5A,B**). These findings imply that a previous catalog of several hundred *PRDM9* variants from male meiosis (Jeffreys et al., 2013) represents many *PRDM9* alleles likely present in humans.

Our limited sample size coupled with the rarity of these alleles made it difficult to infer population differences; however, several rare alleles were sufficiently strongly enriched to make some conclusions (**Supplementary Figure S6**). The *L4*, *L6*, *L7*, *L11*, *L19*, *and Av:0046* alleles were each enriched in at least one African population. Of those alleles, *L6*, *L7*, and *L19* were also found infrequently in at least one non-African population. Two rare alleles (*L20* and *L24*) were enriched in the TSI population and not found in either African population. One rare allele that was previously only found as an *A*-derived variant in blood (*Av:0024*) was enriched in the PEL population, infrequent in two other populations (TSI and PJL), and absent from either African population. Additionally, a novel allele, *M1*, was enriched in the CHB population and absent from all other populations. It is important to note that alleles absent from a population in our study may still be present at a low frequency, below our detection threshold. Perhaps the most intriguing of the rare variants was the *D*-allele. *PRDM9-D* is a so-called "de-stabilizing" allele that appears to cause elevated variation of the ZF array in sperm (Jeffreys et al., 2013). *PRDM9-D* was exclusively found in six individuals in the Finnish population (**Supplementary Figure S5**) and is therefore a strong candidate for a population-enriched allele outside of Africa (**Supplementary Figure S6**).

Diploid *PRDM9* Genotypes in 720 Individuals

Importantly, and in contrast to previous studies of human *PRDM9* diversity, our approach analyzed the inferred phased diploid *PRDM9* genotype for each individual. Knowledge of diploid genotypes is important because *PRDM9* heterozygosity alters the recombination landscape (Pratto et al., 2014b), allelic dominance can alter the contribution of each *PRDM9* allele (Brick et al., 2012; Pratto et al., 2014b; Davies et al., 2016; Smagulova et al., 2016), and genetic incompatibilities in *Prdm9* heterozygotes can cause male sterility (in mice, Mihola et al., 2009; Flachs et al., 2012, 2014; Smagulova et al., 2016; Kusari et al., 2020; Mukaj et al., 2020). We found that the prevalence of *PRDM9* heterozygosity was directly proportionate to the frequency of the most prevalent alleles (**Figure 2C** and **Supplementary Figure S5**). Thus, far more individuals were heterozygous for *PRDM9* in populations where the *PRDM9-A* allele was less prevalent and where allelic diversity was the highest (LWK and YRI populations; 82 and 75%, respectively; **Figures 2C,D** and **Supplementary Figure S5**). Interestingly, the CHB population had the third highest level of heterozygosity even though it also had relatively low *PRDM9* allelic diversity (10 alleles in the population). This is likely due to the relatively high prevalence of the *PRDM9-B* allele.

Sequence Polymorphisms Associate With *PRDM9* Genotype

A single haplotype, encompassing *PRDM9* and characterized by the rs6889665 SNP, was shown to be strongly associated with differences in the recombination landscape between Europeans and Africans (Hinch et al., 2011). Another SNP (rs2914276) was associated with alterations to the recombination landscape in the Icelandic population (Kong et al., 2010). The *PRDM9* genotypes of individuals were unknown in these previous works; however, the implication is that *PRDM9* alleles may be associated with different haplotypes in humans.

To first approximate the associations found in Hinch et al. (2011), where the prevalence of *PRDM9-C*-type alleles was likely the major contributor to differences between African and European-derived recombination maps, we examined SNPs that broadly associated with *A*-type or *C*-type *PRDM9* allele carriers (**Figure 3**). Consistent with Hinch et al. (2011), rs6889665 was among the strongest associated SNPs for both groups (**Figure 3A**). We next performed more specific association tests for the *A*, *B*, *C*, and *L14* alleles of *PRDM9*; these were the most frequent alleles found in our study, and we identified at least one homozygous individual for each. For all four alleles, we found strong evidence of an associated haplotype in a narrow region around the *PRDM9* gene (**Figure 3A**). rs6889665 was associated with the *PRDM9-A* and *PRDM9-C* alleles; however, it was not the most strongly associated SNP for either allele. In addition, the rs6889665 polymorphisms did not associate with all alleles; for example, it was not associated with *PRDM9-B* (*A*-type allele). Therefore, we assessed the prevalence of each haplotype by examining the most highly associated SNP for each allele. The T and C alleles of rs6889665 were strongly enriched in individuals with the *PRDM9-A* and *PRDM9-C* alleles, respectively (**Figure 3B**). However, other SNPs associated with *PRDM9-A* (rs1874165) and *PRDM9-C* (rs2914281) exhibited more pronounced enrichment (**Figure 3C**). Thus, rs6889665 did not appear to be associated with a single *PRDM9* allele, but rather with *A*-type/*C*-type groups of alleles. For example, the best hit for the *PRDM9-A*-associated SNP (rs1874165) was the T allele of rs1874165, which was present in 99% of *PRDM9-A* homozygotes (**Figure 3C**). The T allele of rs1874165 was

also present in 24% of individuals without the *PRDM9-A* allele. However, all these individuals had a *PRDM9-A*-type allele and the T allele of rs1874165 was never found in individuals that lack a *PRDM9-A*-type allele. In contrast, the T allele of rs1994929, the A allele of rs2914281, and the G allele of rs139754603 almost exclusively occurred in association with *PRDM9-B*, *PRDM9-C*, and *PRDM9-L14*, respectively (**Figure 3C**). Individuals carrying these SNP alleles but not the associated *PRDM9* allele were enriched in the populations where each allele was most prevalent (**Supplementary Figure S7**). Thus, these SNPs may also segregate with similar *PRDM9* variants and may exhibit population specificity. The *L14*-associated variant (G allele of rs139754603) was rarely found in *PRDM9-C* carriers (1/148 alleles in individuals that did not have *PRDM9-L14*), despite *PRDM9-L14* being a *C*-type allele with a fully intact predicted *PRDM9-C* binding site. Similarly, the *PRDM9-C*-associated haplotype (A allele of rs2914281) was rare in *PRDM9-L14* carriers (2/44 alleles in individuals that did not have *PRDM9-C*).

Isolated Clusters of *A*-Type and *C*-Type *PRDM9* Alleles in Humans

The repeating 84-bp sequences that make up the *PRDM9* ZF array constitute a minisatellite-like structure. Minisatellites are known to be hotspots of genome instability, which may mediate the appearance of new *PRDM9* alleles. The mechanisms underlying minisatellite instability remain opaque, making relatedness between *PRDM9* alleles difficult to infer; however, empirical observations demonstrate that template switches at minisatellites (mediated either *via* replicative errors or gene conversion) can explain the expansion and contraction of minisatellite arrays (Jurka and Gentles, 2006). A previous study that examined the formation of novel *PRDM9* alleles in human blood and sperm suggested that the formation of new *PRDM9* alleles is due to template switching during replication and/or repair in mitotic and meiotic cells (Jeffreys et al., 2013).

To explore potential relatedness among alleles, we developed an algorithm to simulate putative template switching events between *PRDM9* alleles (parental alleles) that may result in the formation of another allele (child allele) (see section "Materials and Methods"; **Supplementary Figure S8**). Our approach is agnostic to the mechanism by which template switching occurs.

We first examined the *PRDM9* variants that were documented in the sperm and blood of individuals where the parental alleles were known (Jeffreys et al., 2013). We found that all variants could be explained by template switching (**Figure 4A** and **Supplementary Figure S9**). Consistent with previous findings, *PRDM9* variants from the blood all derived from a single template switch, whereas variants in sperm often required complex events with >1 switch (**Supplementary Figure S9**; Jeffreys et al., 2013). Most sperm-derived variants could be formed from interactions involving either one or both parental alleles. Intriguingly, in men heterozygous for *PRDM9*, approximately a quarter of all sperm-derived variants required template switching between the two parental alleles and could not be derived from just one parental allele. The percentage of such alleles was highest for men with one *A*-type and one *C*-type allele (Man8—50%, Man11—42%), where inter-homolog switches were less likely to be masked by similarities between parental alleles. This implies that inter-homolog template switches are a major mechanism by which *PRDM9* variants are generated in the germline.

We next applied our algorithm to assess which *PRDM9* alleles in the human population could be derived from others. 38/50 *A*-type alleles (**Figure 4B**) and 19/21 *C*-type alleles (**Figure 4C**) could be derived from other annotated human *PRDM9* alleles *via* template switching. 12/14 *PRDM9* alleles that could not be derived from others were novel alleles found in this study (e.g., *M5, M6, M8, M14*, etc.). Novel alleles are likely over-represented because they lack parental representation in the population, or their parental alleles may be extinct in humans. Indeed, it should be noted that these analyses are skewed by the large amount of data derived from a single study in human sperm and blood (Jeffreys et al., 2013). Interestingly, we found very few instances where two *C*-type alleles could create an *A*-type allele suggesting that either very rare events or other mechanisms (such as mutation) are required to generate *A*-type from *C*-type alleles. Curiously, we found many cases where two *A*-type alleles could form a *C*-type allele; however, these required an average of nine template switches (compared to just two when both parental alleles were *C*-type; **Figure 4C**). Since most variants are a similar size to the parental allele (**Supplementary Figure S4E**), nine-switch events are likely to be very rare. Nonetheless, one variant in sperm did require nine switches (*Av:0540*, Man16S; **Supplementary Figure S9**). Together, it appears that *C*-type variants rarely arise in *A*-homozygotes and vice versa.

Minor Variations at the *PRDM9* Binding Site Can Alter the Recombination Landscape in Humans

We next examined whether intra-type variation can drive substantial differences in the recombination landscape. Previous studies demonstrated that the *A*-type variant *PRDM9-B* (*PRDM9-B* differs from *PRDM9-A* by a single amino acid; **Figure 5A**; Baudat et al., 2010) had little impact on the recombination landscape in humans (Pratto et al., 2014b). In contrast, in C3H mice, the addition of a single ZF to the *Prdm9-B6* allele profoundly altered recombination localization, despite this ZF addition having little predicted impact on DNA binding (Smagulova et al., 2016). To further assess the impact of *PRDM9* variants on the patterns of meiotic recombination in humans, we generated and examined meiotic DSB maps for different variants within the *A*-type and the *C*-type *PRDM9* clusters.

Differences in the recombination landscape in individual men can be assessed by mapping meiotic DSB hotspots genome-wide. Hotspot locations are identified using a variant of ChIP-Seq to capture and sequence DNA bound by the DMC1 recombinase (DMC1 binds to single-stranded DNA at meiotic DSB hotspots; Khil et al., 2012). We previously mapped DSB hotspots in two *PRDM9-A* homozygous men (A/A_1, A/A_2), one *PRDM9-A/B* heterozygote (*A/B*), one *PRDM9-A/C* heterozygote (*A/C*; Pratto et al., 2014b), and recently in a *PRDM9-C/L4* heterozygous man (*C/L4*; Pratto et al., 2021). Here, we generated DSB maps in two further *PRDM9-A* homozygous men (A/A_3, A/A_4) and in a man

FIGURE 3 | Single-nucleotide polymorphisms (SNPs) are associated with different *PRDM9* alleles. **(A)** Association scores for all SNPs in a ±20-Mb window around the *PRDM9* locus (see "Materials and Methods"). The *PRDM9* genotype examined is given in the title of each panel (individuals carrying at least one copy of *A*-type, *C*-type, *A*, *B*, C, or *L14 PRDM9* alleles, respectively). SNPs previously shown to be linked to recombination patterns in African populations (Hinch et al., 2011) are marked in red (rs6889665) and pink (rs10043097). Lower panels show a magnified view around the peak in the association signal at *PRDM9*. The *PRDM9* gene is indicated by green shading. **(B)** Assessment of the prevalence of rs6889665 alleles. Individuals were classified as homozygous (HOM), heterozygous (HET), or non-carriers (NONE) of the *PRDM9* allele indicated in gray in the column header. The prevalence of the C and T alleles of rs6889665 were assessed in each group. Larger circle size and deeper red color indicate a higher prevalence. **(C)** Similar to **(B)**, but for the best-scoring SNP [blue in panel **(A)**] for each *PRDM9* genotype we tested.

heterozygous for the *PRDM9-A* allele and for an *A*-type variant (henceforth *PRDM9-N*; *Av:s:0053:M1S:A-A*; individual *A/N*). We compared these DSB maps to assess how the *A*-variant *PRDM9-N* allele and the *C*-type variant *PRDM9-L4* allele impact the meiotic recombination landscape.

The *PRDM9-N* allele was previously identified in the sperm of a *PRDM9-A/A* man as an *A*-derived variant, which can arise from a single templating switch from the *PRDM9-A* allele (**Supplementary Figure S8B**; Jeffreys et al., 2013). The differences between *PRDM9-A* and *PRDM9-N* reside in the C-terminus of the DNA binding site for *PRDM9-A*; *PRDM9-N* has one less ZF compared to *PRDM9-A* (**Figure 5A** and **Supplementary Figure S8B**). Thus, *PRDM9-N* likely binds a truncated version of the *PRDM9-A* sequence recognition motif (**Figure 5A**). Indeed, a truncated *PRDM9-A* consensus motif was identified from putative *PRDM9-N*-defined hotspots (DSB hotspots in the *PRDM9-A/N* individual that were not found in DSB maps from any of the *PRDM9-A/A* men; **Figure 5B**). The proportion of hotspots found in *A/N* but not in *A/A* individuals (23–31%; **Figure 5B—top**) exceeds the number of individual-specific hotspots in comparisons among *PRDM9-A/A* individuals (7–17%; **Figure 5B—top** and **Supplementary Figure S10**) and in comparisons between *PRDM9-A/A* and *PRDM9-A/B* individuals (16–26%; **Figure 5B—top** and **Supplementary Figure S10**).

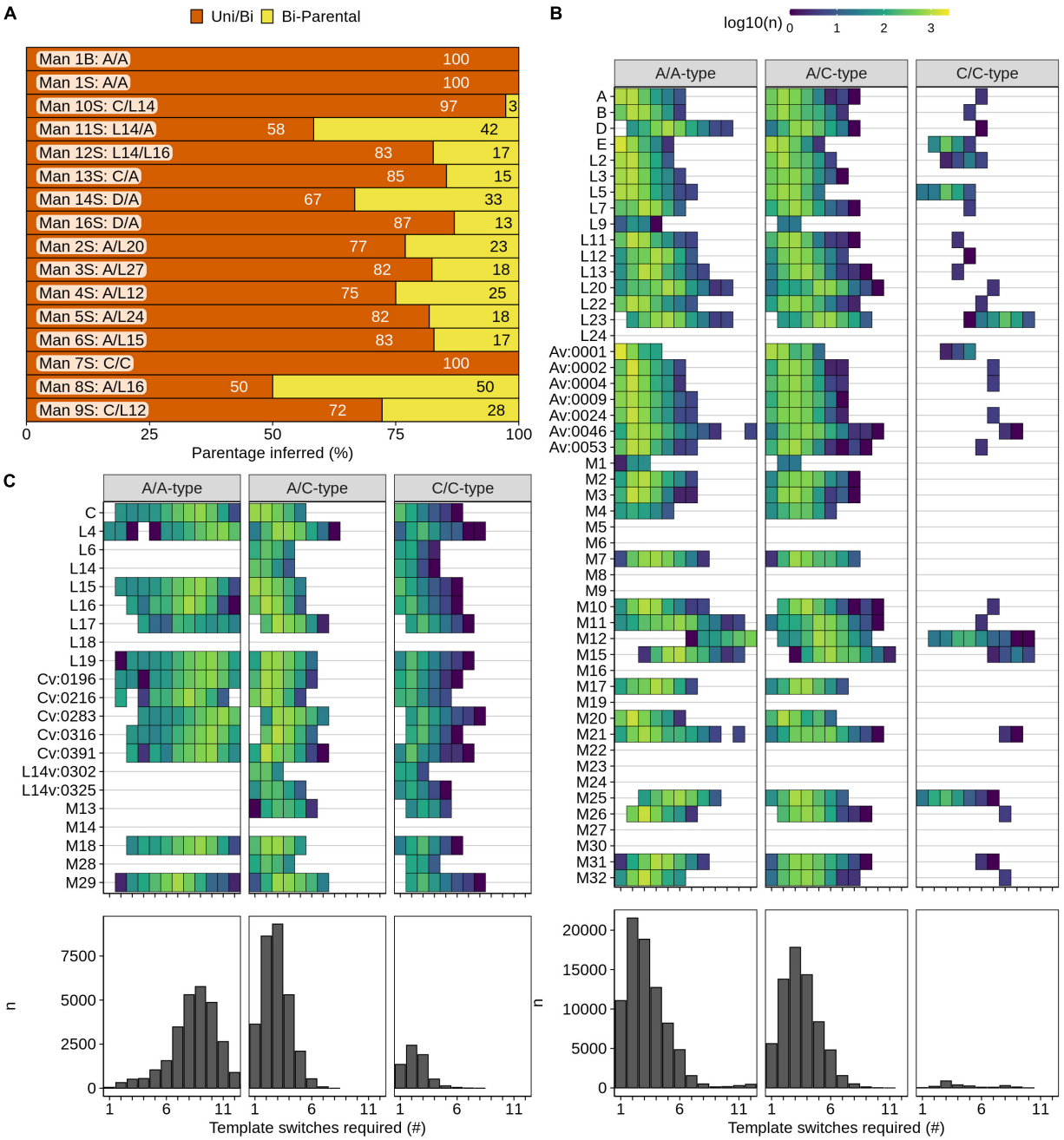

FIGURE 4 | Isolated clusters of *A*-type and *C*-type *PRDM9* alleles. The *PRDM9* ZF array is hypervariable, and variation arises *via* a poorly understood mechanism. We designed and utilized an algorithm to predict the formation of any *PRDM9* allele from any other based on template switching. **(A)** Most *PRDM9* variants in human blood or sperm can be explained by template switches between the two parental *PRDM9* alleles. If several combinations of parental alleles are possible, we identified the "most-likely" recombinant, which required the minimal number of template switches. For each individual, we quantified the alleles where this "most-likely" recombinant is derived from either both parental alleles (bi-parental) or where a uni- and bi-parental origin are equally possible (Uni/Bi). **(B)** *A*-type *PRDM9* alleles rarely arise from *C*-type alleles, and **(C)** *C*-type *PRDM9* alleles can arise from *A*-type alleles but mostly require highly complex template switches. **(B,C)** We searched for potential parental alleles for each *A*-type **(B)** and *C*-type **(C)** *PRDM9* allele. All alleles found in human populations or in blood/sperm only were considered. Heatmaps show the number of potential parental combinations for each number of template switches. Columns represent events in *A*-type homozygotes, *A*-type/*C*-type heterozygotes, or *C*-type homozygotes. Quantitation of all events is shown in bar plots underneath.

Thus, it appears that the binding preferences of *PRDM9-A* and *PRDM9-N* are substantially different and therefore define a small subset of N-specific hotspots. In addition to defining new hotspots, the presence of one copy of *PRDM9-N* substantially perturbs hotspot strength at *PRDM9-A*-defined DSB hotspots (**Figures 5B—bottom, 5C** and **Supplementary Figures S10A,C**).

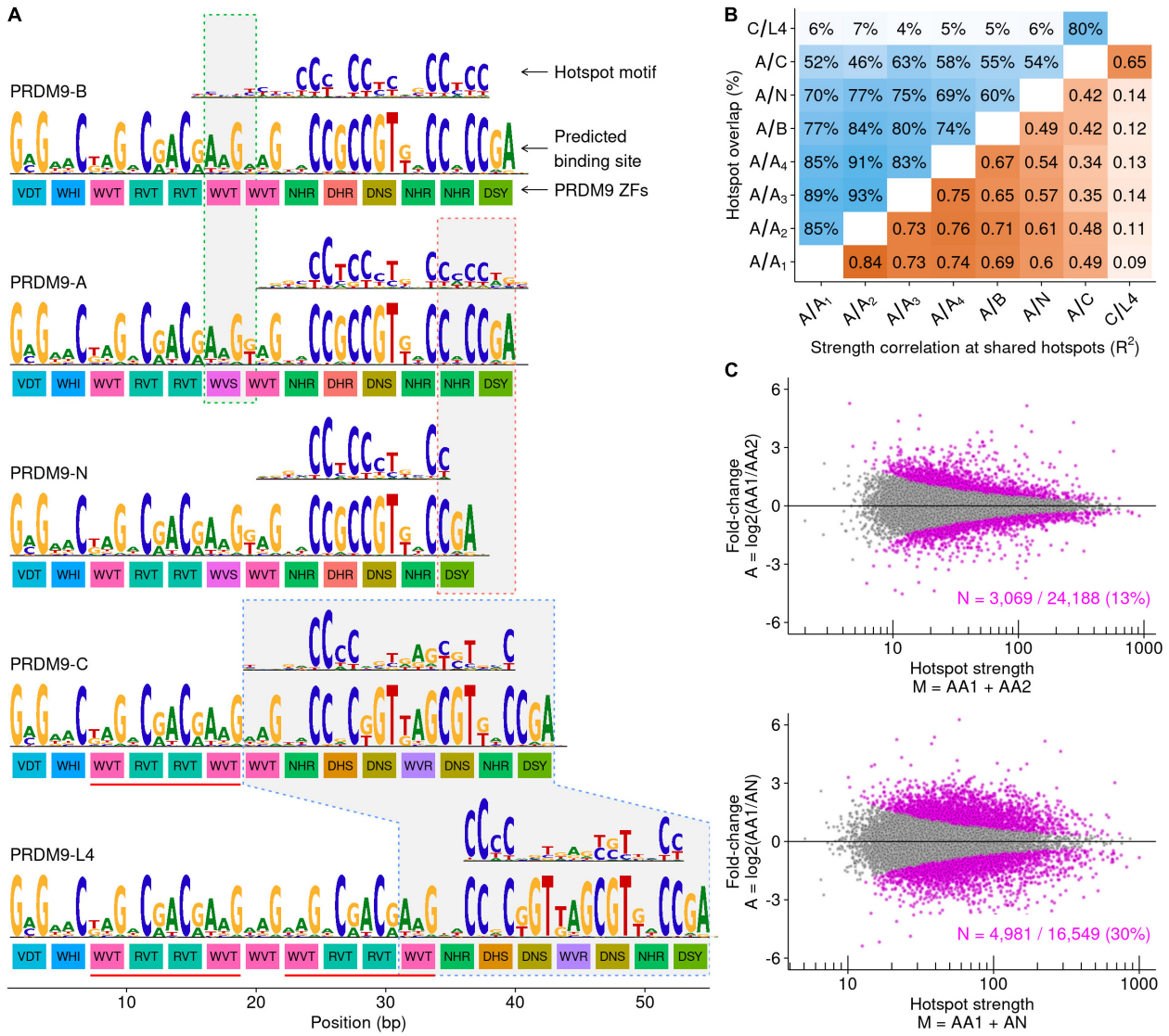

FIGURE 5 | The *A*-variant *PRDM9-N* allele substantially perturbs the DSB landscape. **(A)** Schematic of the *PRDM9* ZF arrays and DNA binding preferences for each allele. For each allele, there are three rows of data. The colored boxes represent the amino acid sequences at the primary DNA contact residues for each C_2H_2 ZF (−1, 3, and 6 positions). These amino acids confer DNA binding specificity, and ZFs with different DNA contact residues are colored differently. The binding preference for each allele is predicted from the amino acid sequence using a polynomial SVM model (Persikov and Singh, 2014). Note that despite these predictions, not all ZFs are thought to contribute to *PRDM9* DNA binding. The best-scoring sequence motif identified at hotspots putatively defined by each allele is shown above each prediction. The green box highlights the region that differs between the *PRDM9-A* and *PRDM9-B* alleles. A single base pair change modifies one amino acid in the ZF array (Baudat et al., 2010). This slightly alters the predicted *PRDM9* binding. The red box outlines the region that differs between the *PRDM9-A* and *PRDM9-N* alleles. The *PRDM9-N* allele differs by one less ZF than the *PRDM9-A* allele. The blue box outlines the region that binds DNA in both the *PRDM9-C* and *PRDM9-L4* alleles. The four *PRDM9-C* ZFs underlined in red are duplicated in the *PRDM9-L4* allele. **(B)** Hotspots were identified in all samples, and overlapping hotspots were counted. The maximum reciprocal overlap is shown (top left; blue shading). At shared autosomal hotspots, the correlation between hotspot strength was calculated (bottom right; orange shading; R^2 = squared Pearson correlation coefficient of log-transformed strength values). **(C)** MA plots depicting significantly different shared hotspot usage between (top) two *A/A* individuals and (bottom) the A/A_1 and *A/N* individuals. Each point represents one shared hotspot. Hotspots with differing strength are highlighted in magenta (Bonferroni-corrected binomial *P*-value < 0.001).

Together, these data demonstrate that the *A*-type *N* allele substantially alters the recombination landscape compared to the *A* allele. Thus, a single change in the *PRDM9* ZF array predicted to change DNA binding specificity and derived from a template switching event can strongly alter recombination patterns in humans.

A double template switch can give rise to the *L4* allele *via* the duplication of four ZFs of *PRDM9-C* (**Figure 5A**, red lines under *C* and *L4* alleles and **Supplementary Figure S8C**). However, in contrast to the previous example (*PRDM9-N* vs. *PRDM9-A*), this results in changes outside of the ZFs predicted to confer DNA-binding specificity (**Figure 5A**). Thus, the

PRDM9-C binding site is retained fully in *PRDM9-L4*, and these alleles may bind to similar genomic targets. Consistent with this, we found a *PRDM9-C*-like motif at putative *L4*-defined hotspots (*C/L4* hotspots that were not found in the *A/C* individual; **Figures 5A,B** and **Supplementary Figure S10**). No additional motifs were found, implying that the addition of four ZFs had no detectable effect on DSB targeting. The 80% of hotspots shared between *C/L4* and *A/C* likely represent *PRDM9-C*-defined hotspots. Hotspot strength is well correlated at these shared hotspots, although below the correlation seen among *A/A* men (**Figure 5B—bottom** and **Supplementary Figure S10**). The slight perturbation of hotspot strength is likely caused by *PRDM9* heterozygosity in one or both individuals (Pratto et al., 2014b).

DISCUSSION

In humans, the hypervariable *PRDM9* gene determines the patterning of meiotic recombination. Understanding the patterning of recombination is key to inferring population structure and inferences made in genome-wide association studies. The DNA binding specificity of PRDM9 is encoded by a highly repetitive 84-bp minisatellite sequence array, and as a result, the *PRDM9* genotype cannot be inferred accurately from short-read sequencing. *PRDM9* genotyping still requires labor-intensive and low-throughput methods such as Sanger sequencing. As a result, our knowledge of *PRDM9* diversity has not greatly expanded since the advent of high-throughput sequencing, and thus, the population diversity of *PRDM9* in humans remains poorly understood.

In this work, we developed a novel strategy to efficiently genotype the *PRDM9* locus in hundreds of individuals using multiplexed long-read sequencing and have used this method to develop an extensive catalog of human *PRDM9* variation across seven populations. Our method substantially improves on previous methods to genotype *PRDM9* (Berg et al., 2010; Schwartz et al., 2014) by circumventing the need for labor-intensive gel extraction, amplicon isolation, and Sanger sequencing as well as by increasing the throughput *via* barcoded sample multiplexing of a large pool of amplicons. Labor-intensive amplicon isolation is required for Sanger sequencing-based approaches to genotype *PRDM9* because the repetitive nature of *PRDM9* causes PCR amplification artifacts. We perform this clean-up *in silico* instead, by retaining only reads that span the entire ZF array. Although this is effective for the vast majority of samples, PCR artifacts are still a source of error using our strategy. An initial concern of using long-read sequencing for *PRDM9* genotyping was that the error rate may be prohibitively high to accurately phase *PRDM9* alleles that differ by as little as a single nucleotide. However, we found that with sufficient depth of coverage, this was a minor concern. Finally, we compared the accuracy of the two major long-read sequencing platforms (PacBio and Oxford Nanopore) for genotyping *PRDM9*. We found comparable accuracy using both methods and suggest that both platforms are sufficiently accurate for *PRDM9* genotyping. Other aspects of these platforms such as cost and accessibility are likely more important considerations than the accuracy of sequencing.

Utilizing our new methodology, we inferred the *PRDM9* diploid genotypes of 720 individuals from seven human populations spanning four continents: Africa (LWK and YRI), Asia (CHB and PJL), Europe (FIN and TSI), and South America (PEL). This greatly expands on previous *PRDM9* surveys in several ways; first, this is by far the largest survey of human *PRDM9*; second, unlike previous surveys, we analyzed the diploid *PRDM9* genotype; and third, in contrast to previous studies that had a European population bias (Baudat et al., 2010; Berg et al., 2010; Parvanov et al., 2010), we captured a large swath of human genetic diversity. We identified 69 distinct *PRDM9* alleles including 32 novel alleles. We also identified 13 alleles that were previously only seen as *PRDM9* variants in sperm or blood (Jeffreys et al., 2013). This implies that the hundreds of *PRDM9* alleles previously discovered only in human sperm/blood represent a font of human *PRDM9* diversity.

Consistent with previous studies, we found that *PRDM9-A* was the predominant allele in all populations and that *PRDM9* diversity was exceptionally high in African populations (Berg et al., 2011; Hinch et al., 2011). The other major *PRDM9* allele, *PRDM9-C,* was previously thought to be found mostly in Africa. Instead, our study reveals that *PRDM9-C* is present in many populations but depleted in European populations. Unlike *PRDM9-C*, *C-type* alleles are found almost exclusively in Africa. This may suggest that *PRDM9-C* was present in individuals that emerged from the human migration bottlenecks that have likely constrained *PRDM9* diversity in non-African populations. Unique to our study, we also found that some alleles of *PRDM9* appear to be segregated by population. For example, *PRDM9-B* is notably enriched in the Han Chinese (CHB) population. This increased prevalence may reflect some advantage to having this allele; however, *PRDM9-B* only differs from *PRDM9-A* by a single nucleotide, which has little impact on meiotic DSB patterning (Pratto et al., 2014a; Altemose et al., 2017). Alternatively, differences may simply reflect genetic drift. The most intriguing population-specific allele is *PRDM9-D*, which was confined to the Finnish population in our study. *PRDM9-D* was previously shown to coincide with hyper-variation at the *PRDM9* ZF array (Jeffreys et al., 2013); however, we did not see elevated *PRDM9* diversity in the FIN population. Thus, if *PRDM9-D* is causing hyper-variation of *PRDM9*, it has not manifested in the population at the levels assessed here. This could also simply reflect the rarity of this allele as it was found in just six individuals. As was seen previously, numerous rare alleles were found in the two African populations, LWK and YRI, and not the others. Differences between the two African populations were also seen, such as *PRDM9-L14* enrichment in LWK and *PRDM9-L19* enrichment in YRI. Importantly, given the large number of low-frequency alleles in both African populations, a deeper study of more individuals is required to assess the true extent of differences between these populations. Furthermore, both African populations studied are related to Bantu-speaking peoples. Thus, we are likely still substantially underestimating the diversity of *PRDM9* alleles in Africa.

Although our strategy makes *PRDM9* genotyping more tractable at scale, the ability to infer the *PRDM9* genotype from nearby SNPs would allow rapid genotyping of this locus. In several previous studies, SNPs were found to be associated with variation in the recombination landscape (Kong et al., 2010; Hinch et al., 2011), and we expanded upon these studies by demonstrating that each of the four major *PRDM9* alleles are strongly associated with SNPs in the surrounding region. A caveat of these findings is that since *PRDM9* variation arises from template switching at the ZF array, new alleles can arise on the same haplotype background as another allele. Indeed, the SNPs associated with *PRDM9-A* are also associated with other *A-type* (but not *C-type*) alleles. Thus, depending on the frequency of the allele, and on the number of variants derived from that allele, the utility of SNP-based imputation will vary.

PRDM9 variants can be found both somatically (blood) and in the germline (sperm) (Jeffreys et al., 2013), and variant alleles are often defined by ZF gains or losses. Consistent with a previous work, we could explain all *PRDM9* diversity in men with a known *PRDM9* genotype by allowing for template switching between the two *PRDM9* alleles. Using this algorithm, most of the *PRDM9* alleles in the studied human populations could be derived from template switching between others. However, we found that creating an *A-type* allele from two *C-type* alleles or a *C-type* allele from two *A-type* alleles is very unlikely to occur. This mechanism would seem to reinforce the broad *A*-type/*C*-type clusters of human *PRDM9* alleles that are seen in our study. Thus, it seems possible that all the human *PRDM9* alleles found to date represent the mutational drift of two alleles in the population. Single-nucleotide polymorphisms add another layer of complexity to the relatedness of *PRDM9* alleles. The formation of novel alleles by SNPs was not modeled in our work but has the potential to dramatically alter the binding preference of a *PRDM9* allele. Thus, SNPs may be the key to generating truly new *PRDM9* variants.

The exact mechanism(s) by which *PRDM9* diversity arises remain unknown (Jeffreys et al., 2013). A common mechanism, such as error-prone DNA replication, may give rise to this variation in somatic and germ cells; however, many *PRDM9* variants in sperm require inter-allelic exchanges. Our data imply that inter-allelic template switches are a major source of *PRDM9* variation and that inter-allelic template switches alone can explain almost all observed variants in sperm. The spatial alignment of homologs would be required to allow for inter-allelic interactions during DNA replication, and interestingly, the parental homologs partially align in meiotic S-phase (at least in mice; Boateng et al., 2013). Furthermore, alignment is most pronounced in sub-telomeric DNA, and *PRDM9* resides on the distal p-arm of chromosome 5 in humans. It is also possible that new alleles arise as the result of gene conversion during recombination. None of the alleles studied to date appear to create a DSB hotspot sufficiently close to the ZF array to allow canonical inter-homolog interactions during recombination (closest hotspot is ∼5 Kb away in the *A/C* individual and tens of kilobytes in *A/A* individuals). However, since the formation of a *PRDM9* variant is a rare event, non-canonical interactions or weak hotspots below the detection threshold of current methods could be responsible. Men carrying *PRDM9-C, C*-type alleles, or *PRDM9-D* have an elevated rate of *PRDM9* variant formation in sperm (Jeffreys et al., 2013), and this could occur if these alleles occasionally initiate recombination near the ZF array. Alternatively, the elevated variant formation in these men may stem from other differences in populations enriched for these alleles. One final (and speculative) hybrid hypothesis is that replicative errors in meiosis can be repaired *via* a mechanism that involves the homolog, thus creating more frequent and more diverse variants than in somatic cells.

PRDM9 localizes meiotic DSBs and recombination in human genomes. As a consequence, the binding sites of *PRDM9* are rapidly destroyed by gene conversion during DNA repair (for review, see Grey et al., 2018). This process, known as hotspot erosion, will purge strong *PRDM9* binding sites from the genome and, thus, may favor the emergence of new variants of *PRDM9* with different DNA binding specificity (Myers et al., 2010; Lesecque et al., 2014). Whether intra-type variation (*A*-type/*C*-type alleles) can sufficiently diversify *PRDM9* binding sites to confer this benefit is unknown. The *PRDM9-B* allele differs from *PRDM9-A* by a single amino acid outside the DNA binding site (Baudat et al., 2010; Jeffreys et al., 2013), but this change has little impact on DSB hotspot localization (Pratto et al., 2014b). In contrast, the *PRDM9-N* allele (*Av:s:0053:M1S:A-A*), which differs from *PRDM9-A* at the C-terminus of the *PRDM9-A* binding site, perturbs the DSB hotspot landscape and defines a new subset of what appears to be *N*-defined hotspots. These observations suggest that *PRDM9-N* has a slightly different binding preference to *PRDM9-A*. Alternatively, we cannot exclude that *PRDM9* heterozygosity is responsible for these perturbations, as heterozygosity *per-se* can affect hotspot usage to a similar degree (Pratto et al., 2014b) and the N-defined hotspots were only mapped in an *A/N* heterozygous man. Finally, the *C-type PRDM9-L4* allele not only has four ZFs more than *PRDM9-C* but also retains the intact *PRDM9-C* binding site. Almost all DSB hotspots in a *C/L4* heterozygous man were also seen in an *A/C* heterozygote, suggesting that despite the substantial length difference between their ZF arrays, *PRDM9-C* and *PRDM9-L4* define similar hotspots. Thus, from these samples, only the variant that changes the documented *PRDM9* binding site can alter DSB hotspot targeting. Nonetheless, in mice, it has been shown that the removal of ZFs with low binding specificity can still greatly impact *PRDM9* binding (Smagulova et al., 2016). Together, these data suggest that even relatively minor changes to the *PRDM9* ZF array may impact the recombination landscape. *PRDM9* binding remains poorly understood (Billings et al., 2013), but given the diversity of alleles found in many human populations, far more work is required to understand how small changes in the DNA binding specificity could impact the DSB landscape.

In summary, the methodology we present in this study allowed for accurate and high-throughput sequencing of the highly repetitive and difficult-to-genotype *PRDM9* locus. This strategy may also be adapted to study other minisatellite or repetitive loci in the genome. These data offer a glimpse at the previously under-appreciated diversity of *PRDM9* in a sampling of human

populations and open the door to far more detailed studies of this and other minisatellite loci in the future.

MATERIALS AND METHODS

Human Population Samples

The DNA samples were obtained from the NHGRI Sample Repository for Human Genetic Research at the Coriell Institute for Medical Research: repository numbers are presented in **Supplementary File S1**. In summary, we obtained genomic DNA from 811 individuals from seven human populations defined in the 1000 Genomes Project/HapMap Project (list below and **Supplementary File S1**; Coriell Institute; samples are deidentified). Genomic DNA was purified from either blood or immortalized lymphocytes/fibroblasts using either the Qiagen Autopure LS instrument or by a modified Miller's salting out procedure (performed at the repository).

Population reference ID and nomenclature and the number of individuals genotyped are as follows:

MPG00013—Yoruba in Ibadan, Nigeria (YRI)
YRI Trios—Yoruba in Ibadan, Nigeria (YRI-trios)
MPG00008—Lyhya in Webuye, Kenya (LWK)
MPG00007—Toscani in Italia (TSI)
MPG00001—Finnish in Finland (FIN)
MPG00011—Peruvian in Lima, Peru (PEL)
MPG00017—Han Chinese in Beijing, China (CHB)
MGP00020—Punjabi in Lahore, Pakistan (PJL).

Amplification of *PRDM9* C_2H_2 Zinc Finger Array

PRDM9 ZF array sequences from all samples were amplified with primers from Berg et al. (2010). No known human SNPs occur within these primer sequences, and they are fully conserved in other mammalian species (mouse, dog, and elephant; single nucleotide change in each primer in macaque). The primer sequences used are as follows:

Forward: 5′-TGAGGTTACCTAGTCTGGCA-3′(hg38 5:23525987-23526006)

Reverse: 5′-ATAAGGGGTCAGCAGACTTC-3′(hg38 5:23527867-23527886).

LongAmp Taq 2X Master Mix (M0287) from New England Biolabs Inc. was used for PCR amplification. Post-amplification, samples were individually tested for successful amplification and low presence of polymerase slippage (presence of DNA laddering/smearing) by running on agarose gel electrophoresis (**Supplementary Figure S1**). Samples were re-amplified if there was extensive DNA laddering/smearing by visualization. Based on the Genome Reference Consortium Human Build 38 (*PRDM9* allele with 13 ZFs), the final amplified product was 1,899 bp, which contained the 1,092-bp C_2H_2 ZF array, 670 bp of upstream flanking sequence, and 137 bp of downstream flanking sequence to the *PRDM9* ZF array. Of note, the total length of the final amplified product varied based on the number of ZFs present in the *PRDM9* allele. Samples were then pooled and prepared for multiplexing.

Multiplexing of *PRDM9*-Amplified Samples

We performed dual-barcoding in order to multiplex and sequence amplicons targeting the *PRDM9* ZF array. The first round of barcoding was done by adding unique DNA barcode sequences to the 5′-end of the primers detailed above, totaling eight primer pairs:

Barcode 1: 5′-ATCACGATCACG-3′
Barcode 2: 5′-CGATGTCGATGT-3′
Barcode 3: 5′-GATCAGGATCAG-3′
Barcode 4: 5′-CTTGTACTTGTA-3′
Barcode 5: 5′-ACAGTGACAGTG-3′
Barcode 6: 5′-GCCAATGCCAAT-3′
Barcode 7: 5′-CAGATCCAGATC-3′
Barcode 8: 5′-ACTTGAACTTGA-3′.

After amplification and the addition of the first barcode, samples were pooled in groups of eight (each sample tagged with a separate barcode sequence) and subjected to a second round of barcoding. The second round of multiplexing was performed using the PCR Barcoding Expansion 1-96 kit (EXP-PBC096) from Oxford Nanopore Technologies (ONT), Inc. following the protocol detailed on their website[1] [PCR barcoding (96) amplicons]. In short, adapter sequences are ligated to amplicons and are used as the priming sequence for a second round of PCR amplification that adds one of 96 commercially available barcode sequences.

This barcoding scheme allows for multiplexing of 768 samples at one time, 8 primer-barcodes × 96 ONT PCR barcodes. Post-multiplexing, all samples are pooled and prepared for long-read sequencing.

Nanopore Sequencing

Sequencing libraries were prepared using the ligation sequencing kit (1D; SQK-LSK109) or $1D^2$ sequencing kit (SQK-LSK309) from Oxford Nanopore Technologies. Library preparation was performed as detailed by the protocols on ONT's website (see footnote 1). All nanopore sequencing experiments were run on a MinION sequencer with R9.5.1 ($1D^2$: FLO-MIN107) or R9.4.1 (1D: FLO-MIN106) flow cells.

PacBio Sequencing

Pooled samples were prepared using the SMRTbell Express Template Prep Kit 2.0 (Pacific Biosciences, CA, United States) and sequenced using the PacBio Sequel II System to generate CCS PacBio reads. Sequencing was performed with a 0.5-h pre-extension and 10-h recording time, and a second sequencing run was performed with a 2-h pre-extension and 30-h recording time.

Basecalling and Demultiplexing of PacBio Circular Consensus Sequencing Reads

Basecalling was performed using the PacBio CCS tool (bioconda channel pbccs-4.2.0.0) and default parameters. The sequences of all possible barcode combinations from our dual barcoding

[1]https://nanoporetech.com

approach were appended to a barcodes FASTA file. The reverse complement of each barcode was also included. Demultiplexing was performed using the PacBio lima tool (bioconda channel pblima-1.11.0) and the following command line arguments: –ccs –guess 45 –peek 10000 –guess-min-count 5 –different –score-full-pass. Only reads flanked by a barcode on one side and its reverse complement on the other were retained.

Base Calling and Demultiplexing of Oxford Nanopore Reads

To identify sequencing reads derived from each individual, we performed read demultiplexing using Guppy v3.1.5. This first involved base calling (with standard parameters), followed by two rounds of demultiplexing to identify the outer and inner barcodes. The first round of demultiplexing identified the outer barcode as follows:

guppy_barcoder –compress_fastq -i {guppy output}
-s demux
–arrangements_files barcode_arrs_pcr96.cfg
–min_score 50 –front_window_size 300
–rear_window_size 300
–trim_barcodes

The second round of demultiplexing was then performed on each of the files generated from the first round:

guppy_barcoder –compress_fastq -i {round 1 barcoding FAST5}
–arrangements_files custom_12bp.cfg
–min_score 70 –front_window_size 100
–rear_window_size 100
–trim_barcodes

We used the Oxford Nanopore development basecaller Bonito (v.0.2.3) for base calling as it is more accurate than Guppy, the production basecaller (Silvestre-Ryan and Holmes, 2020). Specifically, we found that the Guppy base calling accuracy for CpG dinucleotides in particular contexts was insufficient to confidently infer *PRDM9* genotypes using our methods (not shown). Reads from each individual were grouped and base called separately using Bonito (v.0.2.3) and default parameters.

PRDM9 Genotyping From Long Reads

Genotyping *PRDM9* from long reads presents two challenges: first, PCR artifacts of the wrong length should be purged and second, alleles that differ by a single base pair should be identifiable. We therefore devised a strategy to identify all reads with an intact ZF array and then to use multiple sequence alignment to call variants. Note that a preliminary study using the Guppy basecaller could not be used for this approach because of systematic base calling errors at CpG dinucleotides in a particular context.

The *PRDM9* ZF array was first identified for each sequencing read. The sequences immediately flanking the ZF array were identified using a Smith–Waterman local alignment tool (Water, EMBOSS suite; Rice et al., 2000). The flanking sequences are as follows:

PRDM9 zinc finger array 5′ flanking sequence:

CACAGCCGTAATGACAAAACCAAAGGTCAAGAGATCA
AAGAAAGGTCCAAACTCTTGAATAAAAGGACATGGCAGA
GGGAGATTTCAAGGGCCTTTTCTAGCCCACCCAAAGGAC
AAATGGGGAGCTGTAGAGTGGGAAAAAGAATAATGGAA
GAAGAGTCCAGAACAGGCCAGAAAGTGAATCCAGGGAA
CACAGGCAAATTATTTGTGGGGGTAGGAATCTCAAGAAT
TGCAAAAGTCAAGTATGGAGAG.

PRDM9 zinc finger array 3′ flanking sequence:

GATGAGTAAGTCATTAGTAATAAAACCTCATCTCAATA
GCCACAAAAAGACAAATGTGGTCACCACACACTTGCACA
CCCCAGCTGTGAGGTGGCTTCAGCGGAAGTCTGCTGAC
CCCTTATATTCCCCGAGAGTATAAAGAGATCGGAAATAAC
TGATTAAACAAATCCGCCACTTTCATGACTAGAGATGAG
GAAGAACAAGGGATAGTTCTGTAAGTGTTCGGGGGACAT
CAGCATGTGTGGTTCTTTC.

These flanking sequences were used to define the start and end points of the *PRDM9* ZF array. Sequences lacking either flanking sequence were discarded. BLAST (Altschul et al., 1990) (bioconda channel—blast-2.10.1) was subsequently used to identify the position of C_2H_2 ZFs within each sequencing read containing a full-length array. For the BLAST search, we used the set of all published *PRDM9* ZFs (see below) as a search query. BLAST used the following command line arguments: blastn -word_size 7 -max_hsps 200 -num_alignments 20000 -evalue 1 -culling_limit 20000. Partial hits to ZFs were sometimes obtained because of gaps in long reads. These hits were padded to 84 nucleotides with Ns. Only reads with a contiguous array of C_2H_2 ZFs, flanked immediately by the expected 5′ and 3′ sequences, were retained. Individuals with $<100\times$ coverage were not processed further. The size of the ZF arrays were inferred as follows:

#	Rule	Length (hap 1)	Length (hap 2)
1	All zinc finger arrays had i zinc fingers ($f_i = 1$)	i	i
2	$f_i + f_j \geq 0.7$ AND $f_i / f_j < 2$	I	j
3	$f_i + f_j \geq 0.7$ AND $f_i / f_j < 3$ AND $f_j / f_k > 2$	i	j
4	$f_i + f_j \geq 0.7$ AND $f_i / f_j > 3$	i	i
5	$f_i \geq 0.7$	i	i

Where f_i, f_j, and f_k are the frequencies of the most frequent (i), second most frequent (j), and third most frequent (k) ZF arrays. Rules are processed consecutively; thus, an individual where the ZF array lengths can be inferred using rule 1 will not be tested by further rules.

ZF arrays matching the expected haplotype lengths were retained, and we attempted to infer both *PRDM9* haplotypes for each individual. Individuals where the two ZF arrays differed in length were straightforward, as the diploid genotype could be simply inferred from the consensus sequences of each ZF array. Sequences that had any nucleotide with a consensus sequence frequency (not including N's or gaps) <0.6 were discarded. Individuals where both ZF arrays were the same length were processed as follows: the consensus sequence across the ZF array was determined and the consensus frequency

(f_c) for each nucleotide position was calculated (consensus nucleotide/total sequences; N's and gaps were excluded from the totals). Any ZF array with ≥ 1 nucleotide having $f_c < 0.7$ was considered potentially heterozygous. To test for heterozygosity, each ZF array sequence was reduced to only the sequence at the heterozygous loci. A pairwise distance matrix was constructed between all pairs of sequences (distance = # mismatches) and was used for hierarchical clustering (R hclust function). The optimal number of clusters (n) was determined as the number of clusters that gave the minimum within-cluster mean distance (tested; $1 \leq n < 20$). Sequences in the largest two clusters likely represent the two major haplotypes, while sequences in other clusters (if $n > 2$) likely represent sequences with sequencing errors. Finally, we tested the internal consistency of each haplotype cluster as we did initially for all sequences; if either putative cluster yielded any nucleotide with $f_c < 0.7$, then we conclude that the genotype could not be inferred for that allele.

Nomenclature of New *PRDM9* Alleles and Zinc Fingers

PRDM9 alleles that did not match any of the previously published human *PRDM9* alleles were designated a name of "M#," where # represents a simple numerical index (**Supplementary File S3**). New ZF sequences were named "!%," where % represents an uppercase letter (**Supplementary File S2**).

Obtaining Published *PRDM9* Alleles and Zinc Finger Sequences

We obtained the DNA sequences for all human *PRDM9* alleles (in **Supplementary File S3**) and C_2H_2 ZF sequences from Baudat et al. (2010), Berg et al. (2010), and Jeffreys et al. (2013) (details in **Supplementary Files S2, S3**). Most of the documented *PRDM9* alleles were derived from the supplementary information of a study of *PRDM9* variants in human sperm (Jeffreys et al., 2013). These unnamed variants were assigned a five-part name as follows:

(1) Variant type:
The parental *PRDM9* allele from which this variant was likely derived. Recombinant variants and variants of unknown origin are designated Rv and Uv, respectively.

(2) (s)imple or (c)omplex:
Simple events can be explained by a single event, complex cannot.

(3) Allele number:
A unique numeric index for each allele.

(4) Man ID (S)perm or (B)lood:
Identifier for the tissue donor as well as the origin material type.

(5) Parental *PRDM9* genotype:
First allele-second allele (i.e., *A-L20*).

For example,
Av:c:0065:M2S:A-L20 = *A*-variant : complex : #65 : Man 2 Sperm : *A / L20* genotype.

Allele names have been shortened to variant type:allele number in figures due to space constraints, e.g., in figures, *Av:c:0065:M2S:A-L20* = *Av:0065*.

For the other *PRDM9* variants, the name from the previous study was retained. The C_2H_2 ZFs of *PRDM9* were named using a single-character code; however, to allow for the expansion of the ZF repertoire in this study, we re-named each ZF using a two-character code (**Supplementary File S2**).

Identification of Single-Nucleotide Polymorphisms Associated With *PRDM9* Alleles

For this study, we used data from individuals who had a diploid inferred *PRDM9* genotype and for whom hg38 SNP data were available in the 1000 Genomes Project VCF files (1000 Genomes Project Consortium et al., 2015; 27022019 release). The 59 YRI "children," with parents among the other YRI individuals, were excluded. This yielded data from 649 individuals.

We examined SNPs within ±20 Mb of the *PRDM9* transcript start and excluded INDELs, SNPs with a minor allele frequency (MAF) < 2%, SNPs within the coding region of the *PRDM9* ZF array, and SNP loci with missing information. The resultant dataset contained 151,944 SNPs. A similar experiment using all of chr5 yielded analogous results (not shown). To perform phenotype–genotype association analyses, allowing for population stratification, we used PLINK (v1.07) (Purcell et al., 2007) with the following command line arguments: –assoc –all-pheno –allow-no-sex –mh –within populations.txt. We defined phenotypes as individuals with at least one copy of a given *PRDM9* allele. Thus, heterozygotes and homozygotes were treated equally. Multiple associated SNPs were identified for each phenotype. For analyses, the SNP with the lowest *P*-value was used. In cases where multiple SNPs had the same *P*-value, rs6889665 was chosen if it was among the top-scoring SNPs; otherwise, one SNP was chosen at random. This random choice did not affect downstream analyses. The three SNPs with the highest association score for *PRDM9-C* (rs77023486, rs141586808, and rs138354146) did not show subsequent enrichment among *PRDM9-C* carriers. Association estimates are sensitive to rare SNP variants, and since all three SNPs had MAF ≈3.5%, they were excluded from downstream analyses. All SNPs associated with each phenotype are given in **Supplementary File S4**.

Validating Novel *PRDM9* Alleles Using Published Exome Sequencing Data

We obtained exome sequencing data from the 1000 Genomes Project (Google Cloud mirror[2]) for individuals carrying at least one novel allele identified in this study. We used samtools view (v.1.12) to extract only the reads that aligned to the terminal exon of *PRDM9*, which contains the ZF array (locus extracted from hg38: chr5:23525000-235320000). We then created a FASTQ from these reads using bedtools bamtofastq (v2.30.0). Using minimap2 (v2.20; arguments –x sr –a), reads were aligned to a

[2]gs://genomics-public-data/ftp-trace.ncbi.nih.gov/1000genomes/ftp/

FASTA file containing one entry for each distinct *PRDM9* ZF found in this study. Reads were then filtered by the CIGAR string to remove reads with mismatches or with <73 bp aligned.

In silico Analysis of *PRDM9* Allele Formation

Previously, the evolutionary relatedness of *PRDM9* was inferred using classical sequence alignment with either no modifications (Kono et al., 2014) or using modifications that included penalties for amplifications and contractions of the minisatellite-like *PRDM9* ZF array (Bérard et al., 2007; Bonhomme et al., 2007; Buard et al., 2014). Unmodified sequence alignment is not suited to assessing the relatedness of *PRDM9* alleles, but it is equally unclear if the added complexity of the latter method serves as an accurate model for *PRMD9* relatedness as this strategy limits amplifications/contractions to a single ZF and does not allow for new ZF variants that arise from splicing between ZF midpoints. Instead, we devised a simpler approach that assumes that template switching is the major means by which new *PRDM9* ZFs arise (**Supplementary Figure S8**). We made no inferences about the underlying mechanism, as template switching may result from a combination of replicative errors, gene conversion, and/or recombination. We compare the DNA sequence of a *PRDM9* ZF array (child) to the DNA sequence of the putative parental alleles (parents) to know if the child allele can arise from template switching between the parental alleles. Algorithmically, this is achieved as follows (see also **Supplementary Figure S8**):

(1) Find the longest match between the 5′ of the child and the 5′ end of parent 1.
(2) Truncate the child allele by removing the matched region.
(3) Find the longest common subsequence between the 5′ end of the truncated child allele and any location within the parent 2 allele (the match does not have to be at the 5′ end).
(4) Repeat 2–3, alternating between parental alleles until the truncated query matches the 3′ sequence of the active parental allele.
(5) Repeat 1–4, starting from the second parental allele.

NOTES:

(I) All matches are required to be longer than 15 nt.
(II) This approach allows for unlimited template switches; however, it is not clear if such multi-switches are biologically feasible.

The script for allele formation is available at https://github.com/kevbrick/prdm9_TS.git.

DMC1-SSDS

Testicular samples were obtained from a commercial source (Folio Biosciences, Ohio). From a biopsy, 0.3 mg of normal adjacent tissue was obtained. Genomic DNA was extracted from the testicular samples before fixation with the DNeasy Blood and Tissue Kit (Qiagen). *PRDM9* genotype was obtained by amplifying, cloning, and Sanger sequencing the ZF array as described in Pratto et al. (2014b). The rest of the sample was directly thawed in 1% paraformaldehyde and gently dissociated. DMC1-SSDS was performed as described in Pratto et al. (2014b) and Brick et al. (2018). The discontinued anti-DMC1 antibody (Santa Cruz, cat#sc 8973) was used for this experiment.

Paired-end Illumina sequencing reads were aligned to the human reference genome (hg38) using a variant of the ssDNA alignment pipeline developed in Khil et al. (2012). First- and second-end reads were independently aligned to the genome using BWA-MEM 0.7.12 (Li, 2013). The captured fragment for each read pair was inferred, and the 5′ end of the two reads were compared to detect ssDNA stem-loop structures that were generated during library construction (Khil et al., 2012). Unambiguous ssDNA-derived reads were defined as previously described (Khil et al., 2012; Brick et al., 2018) and were retained for further analyses. Reads that were not unambiguously derived from ssDNA were discarded. DSB hotspots were identified from anti-DMC1 SSDS experiments using MACS (Zhang et al., 2008) version 2.0.10 and matched control data. The following MACS arguments were used: –nomodel; –shiftsize: 400; –bw: 1000; –q: 0.1. The peak sets obtained were then filtered to remove peaks that occurred on unassembled contigs and peaks that overlapped centromeres or centromeric repeats.

The scripts and analytic pipeline used for data analysis are available on Zenodo at DOI: 10.5281/zenodo.5149066.

DATA AVAILABILITY STATEMENT

Sequencing data from this study are deposited at the Gene Expression Omnibus (GEO) under accession number GSE166483 (https://www.ncbi.nlm.nih.gov/geo/query/acc.cgi?acc=GSE166483).

ETHICS STATEMENT

Ethical review and approval was not required for the study on human participants in accordance with the local legislation and institutional requirements. Written informed consent for participation was not required for this study in accordance with the national legislation and the institutional requirements.

AUTHOR CONTRIBUTIONS

BA, KB, FP, MH, and RC-O contributed to design and conception of the study. BA performed the multiplexing and long-read sequencing of human samples. FP performed the ChIP-seq (SSDS) experiments from human testes samples. KB implemented the long read sequencing pipeline and data visualization. BA and KB wrote the manuscript. RC-O revised the manuscript and approved the final version. All the authors reviewed the final version of the manuscript.

FUNDING

This work was funded by the intramural program of the NIDDK (RC-O).

ACKNOWLEDGMENTS

We would like to thank Alice Young and the team at the NISC Comparative Sequencing Program and the CCR Sequencing Facility at Frederick National Laboratory for Cancer Research (including Caroline Fromont, Bao Tran, Jack Chen, Sulbha Choudhari, and Yongmei Zhao) for performing PacBio sequencing. This work utilized the computational resources of the NIH HPC Biowulf cluster (http://hpc.nih.gov).

SUPPLEMENTARY MATERIAL

The Supplementary Material for this article can be found online at: https://www.frontiersin.org/articles/10.3389/fcell.2021.675286/full#supplementary-material

Supplementary Figure S1 | PCR amplification biases are removed *in silico*. Agarose gels for post-PCR amplified *PRDM9* ZF arrays. Raw gel images are shown in **(A,C)**. Per-lane quantification is shown in **(B,D)**. Pixels used for quantification are shown beneath each histogram. Gel quantification was performed using the R imager package. For each sample/lane, the middle plot depicts the read length distribution. The lower plot depicts the inferred lengths of *PRDM9* ZF arrays from all sequencing reads used for final genotyping. For all individuals with sufficient coverage, we observe either one or two peaks in *PRDM9* ZF array length. *PRDM9* ZF arrays that do not coincide with the major peaks likely represent PCR artifacts that serendipitously created an erroneous, but complete, ZF array. These are a small minority of reads for all individuals. Coverage above 2,001 reads is not considered. **(A,B)** Twenty-four individuals with varying degrees of "laddering." **(C,D)** Sixteen individuals with various amplification issues. Lane 2: cleanly amplified product. Lane 4: little/no amplification. Lane 12: smearing (unknown reason). DNA from lanes 4, 5, 9, and 12 were not used for sequencing. Further amplification experiments were performed and used for sequencing. The LCL gDNA control was DNA from an LCL cell line used as an amplification control. Lanes 6 and 8 contain DNA amplified from an *A/A* and *A/N* individual, respectively.

Supplementary Figure S2 | The diploid *PRDM9* genotype can be inferred from long-read sequencing data for most individuals. **(A–C)** Inferred ZF array sizes (in # of ZFs) using PacBio or Nanopore reads. Each individual ID is shown in black. The inferred genotypes from Nanopore (blue) and PacBio (orange) are shown alongside the inferred diploid ZF sizes. Concordant alleles are replaced with hyphens (–). New alleles are not named, as the nomenclature is determined after pooled genotyping. **(A)** Six representative individuals with concordant genotypes. **(B)** Five individuals had discordant genotypes where the number of ZFs matched. Three out of five are the result of differences at a single nucleotide (NA18535, NA19019, and NA19030). For the other two individuals, the discordant alleles differ by 3 nt (NA20522; *A* vs. *L24* allele) and 21 nt (NA19437; *A* vs. *L12* allele). **(C)** Differing ZF lengths were the cause of the eight remaining discordant genotypes. This mostly occurs because of insufficient sequencing depth or under-representation of an allele with one technology (HG03640, NA08873, NA19026, and NA19473). In three cases, the amplicon size distribution differed between the reads from the two technologies (HG00311, NA19240, and NA19043). For the remaining individual (NA19470), it appears that a 12-ZF amplicon was erroneously considered a valid allele for PacBio. **(D)** Detection bias for shorter *PRDM9* alleles. For all heterozygous individuals, the percentage of reads for each genotype was calculated. These percentages are shown for alleles of different sizes. Absent any bias, all boxplots should have a median at 50%. The reduced coverage for longer alleles is seen for both technologies and therefore is most likely derived from the PCR step during library preparation. Thirteen-ZF alleles have apparently higher coverage; however, this is likely because most heterozygotes with one long allele also contain a 13-ZF allele (i.e., *PRDM9-A*). In these individuals, the relative amount of 13-ZF sequences will often be above 50%. **(E)** *PRDM9* inference from pooled sequencing reads. The diploid genotype is considered successfully inferred if both *PRDM9* alleles are confidently determined from sequencing data. Most individuals lacking a *PRDM9* genotype were among the 59 YRI individuals used for trio analyses (YRI-Trios) who were sequenced to shallower depth. **(F)** Failed samples have substantially fewer raw sequencing reads. Points depict each individual. Boxplots show the interquartile range with the median depicted as the solid dividing line. **(G)** Not all raw sequencing reads can be used for inferring genotypes. Failed samples have substantially fewer reads with a contiguous *PRDM9* array. In addition, "no genotype" individuals are absent from **(F,G)** if no reads were obtained (mostly due to failed barcoding for some samples).

Supplementary Figure S3 | Most novel alleles are validated using exome sequencing data. We extracted exome sequencing reads that mapped to the *PRDM9* ZF array (1000 Genomes Project), then aligned these to all possible *PRDM9* ZFs (see section "Materials and Methods") for each individual. Short-read exome sequencing data were available, and analyses are presented here for 48/53 individuals who have at least one previously unannotated *PRDM9* allele. Most exome sequencing was performed with 75-bp reads. Reads aligned with <72 bp or with mismatches were discarded. Since each ZF is 84-bp long, some reads may still map ambiguously despite these stringent criteria. We compared read density for ZFs found in both alleles (red), ZFs found uniquely in each allele (blue), and ZFs that were not found in either allele (green). The 95th and 98th percentile for ZFs not found in either allele are indicated with green dotted and dashed lines, respectively. Coverage is normalized for the number of each ZF present in an individual; coverage for ZFs not in the individual were normalized by 1. For three individuals, no reads passing our criteria were identified (NA19145, NA18527, and HG00359), and for five further individuals (HG00377, HG00312, NA20787, NA20768, and NA20769), very few reads were identified. For all remaining individuals, normalized read coverage for the novel allele(s) exceeded the 95th percentile of coverage for the control alleles.

Supplementary Figure S4 | *PRDM9* alleles are categorized as *A*-type and *C*-type. **(A)** *PRDM9* alleles found in human populations broadly cluster into two groups defined by similarity to the PRDM9-A or PRDM9-C binding site. The binding site for each allele was predicted (Persikov and Singh, 2014), and alleles were clustered using the position weight matrix for each allele (motifStack function of R motifPiles library). The regions matching the known binding residues for PRDM9-A (purple) and PRDM9-C (green) are highlighted. Motifs were manually aligned to highlight these loci. **(B,C)** A distance metric that measures the similarity to the amino acid sequence that defines *PRDM9-A* and *PRDM9-C* binding (distance = # of mismatches + # of gaps from a BLAST alignment) was used. Alleles left of the diagonal line are alleles with binding sequences more similar to the *PRDM9-A* allele (A-type). Alleles to the right of the diagonal line are alleles with binding sequences more similar to the *PRDM9-C* allele (C-type). Note that the *L13* allele (found in one YRI child) and the *Av:0053* (N) allele are included here. By this measure, *M12*, *M15, and M21* are *A*-type alleles, and *M29* is a *C*-type allele despite clustering with *C-type* alleles or *A*-type alleles in panel **(A)**, respectively. **(B)** Alleles found in the populations from this study. The size of each circle indicates the number of alleles. **(C)** All human *PRDM9* alleles including blood-/sperm-only variants. **(D)** Among *PRDM9* alleles found in our study, *A*-type alleles are significantly shorter (median = 13 ZFs) than *C*-type alleles (median = 15 ZFs) ($P = 10^{-5}$; Wilcoxon test). **(E)** *PRDM9* variant alleles that arise in human sperm remain a similar size to the parental alleles. All sperm variants in individuals homozygous for *A*-type/*C*-type alleles of the same length were used. **(F)** Most variant alleles in sperm retain the parental *PRDM9* binding site.

Supplementary Figure S5 | *PRDM9* genotype and allele distribution by population. **(A)** The percentage (left; red) and count (right; blue) of each *PRDM9* allele in all populations. *A*-type alleles are labeled magenta and *C*-type are green. **(B)** The percentage (left; red) and count (right; blue) of individuals with at least a single copy of each *PRDM9* allele in all populations. **(C)** The count of diploid *PRDM9* genotypes in all populations.

Supplementary Figure S6 | Comparison of allele frequencies between populations. Our estimates of *PRDM9* allele frequencies are susceptible to substantial sampling error as the number of alleles is high compared to the number of individuals assessed. To facilitate cross-comparison of the population frequencies of *PRDM9* alleles, we estimated the effects of sampling noise. For each population, we performed 10,000 bootstrapped samplings of alleles in the population. For each iteration, we randomly selected *N* alleles (*N* = number of alleles detected in the true population); selection was weighted by the observed allele frequency in the population. The 99% confidence intervals of each distribution are shown. Only alleles where the value of the 1st percentile is >0% in one population are shown (i.e., the estimated likelihood of 0 observations in the population is <1%). Bars show the observed frequency of each allele.

Supplementary Figure S7 | The prevalence of associated SNPs among populations. Assessment of the prevalence of SNPs associated with *PRDM9* alleles split by population. Individuals were classified as homozygous (HOM), heterozygous (HET), or non-carriers (NONE) of the *PRDM9* allele indicated in gray in the column header. The prevalence of both alleles of each SNP was assessed in each group. Larger circle size and deeper red color indicate a higher prevalence.

Supplementary Figure S8 | Templating errors as a source of *PRDM9* variation. The *PRDM9* ZF array is composed of tandem copies of highly similar C_2H_2 ZF domains. Each domain is 84-bp long, and most domains differ from each other by just 1–4 bp. This structure has the potential to cause templating errors during DNA transactions such as DNA replication or recombination. **(A)** One potential mechanism by which template switching can generate new *PRDM9* alleles. The identical sections of C_2H_2 ZFs are represented as black lines; colored boxes represent variable regions. For illustrative purposes, these regions are depicted as disproportionately large (depiction is ∼10 × wider) and in the context of replication. Replication pausing/slippage coupled with secondary structure formation has the potential to cause template switches during replication. (Left) Intramolecular reactions on the replicated strand can result in the duplication of ZF domains in the replicated DNA. (Right) Intramolecular reactions on the template strand can result in the deletion of ZF domains in the replicated DNA (note that the decision to depict secondary structures as loops is arbitrary). This is one mechanism by which new alleles may arise and is intended to be illustrative; however, numerous other template switching interactions may play a role. **(B,C)** Putative template switching events that give rise to one allele from another are inferred computationally. **(B)** A single template switch within or between *PRDM9-A* alleles can give rise to the *PRDM9-N* allele. The ZF codes for each allele are shown on top. The :F:I ZFs in *PRDM9-A* are replaced with a | d ZF in *PRDM9-N*. These three ZFs differ between each other at two nucleotide positions [comparison shown as the Compact Idiosyncratic Gapped Alignment Report (CIGAR) format; Li et al., 2009]. In subsequent panels, for simplicity, we drop the non-alphanumeric first character for each ZF code. Although the ZF codes are depicted in this figure, our algorithm operates on the DNA sequences. This allows us to capture template switches that create hybrid new ZFs from a combination of parental ZFs. A case in point is the | d ZF, which can be created by a template switch from after the first variable residue in :F to before the last variable residue in :I. Our algorithm first identifies the longest common 5′ subsequence between one parent allele and the putative progeny allele **(1)**. We then remove this matched sequence from the child sequence **(2)** and find the longest possible perfect match to the 5′ end of the second parental allele. **(3)** This represents a template switch event. In the case of the *PRDM9-N* allele, a perfect match is found by a single template switch that skips a single ZF (half of :F and half of :I). This process is re-iterated until either the entire progeny sequence has been matched or until no further match can be found **(4)**. In the latter case, we conclude that parentage cannot be inferred. In the former case, we can infer putative parentage. The inferred events are shown in the result panel (TS = template switch) for either a mono-allelic template switch [where the TS arises like in panel **(A)**] or for a bi-allelic TS that involves both parental alleles. **(C)** Two template switches within or between *PRDM9-C* alleles can give rise to the *PRDM9-L4* allele. This example demonstrates how our iterative algorithm captures these events (steps 2 and 3 are repeated).

Supplementary Figure S9 | Most *PRDM9* variants that arise in blood and sperm can be generated from template switching between parental alleles. We analyzed all *PRDM9* allelic variants from blood and sperm that were identified in Jeffreys et al. (2013) to determine if each allele could be generated *via* template switching between parental alleles (see section "Materials and Methods"). Each *PRDM9* allele is illustrated as a series of connected boxes, where each box represents a single ZF. Alleles are grouped by the man in which they were identified (indicated in gray boxes along with the man's diploid *PRDM9* genotype; S, sperm and B, blood). If several combinations of parental alleles are possible, we identified the "most-likely" recombinant as that which required the minimal number of template switches. If multiple possible combinations remain, one is randomly chosen for display. Colored circles indicate the alleles where this "most-likely" recombinant is derived from either both parental alleles (yellow: bi-parental) or where a uni- and bi-parental origin are equally possible (orange: Uni/Bi). ZFs are colored by the parent of origin (yellow = first allele; blue = second allele). Green ZFs indicate the region in which a template switch was inferred. Note that if template switches occur in adjacent ZFs, the resolution of this representation does not allow the source of the intervening DNA to be shown. It should be particularly noted at the few alleles derived from obligatory bi-parental switches that have double switch events in a short span (e.g., Man 14—*Dv:0445*). In these cases, the schematic appears to lack any segment from one parent because it is too short to be shown.

Supplementary Figure S10 | Contributions of different *PRDM9* alleles to the DSB landscape across individuals. **(A)** Pairwise comparisons of DSB hotspots in all individuals. The bottom left panels show the correlation of log-transformed hotspot strength at shared hotspots. The number of shared hotspots is shown in green, and the Pearson correlation coefficient of log-transformed strength is shown in red. The 4–6% of *C/L4* hotspots shared with the *A/A*, *A/B*, and *A/N* individuals are likely chance overlaps. The top-right panels depict the number of hotspots in each comparison that are shared by both individuals (both: gray) or that are unique to either parent (purple and orange). The area of each rectangle represents the number of hotspots. **(B)** The hotspot count per individual. **(C)** The distribution of Pearson correlation coefficients for each sample. **(D)** The total number of unique hotspots per individual (expressed as the percent of all hotspots). **(E)** Percent of unique hotspots in the top 13,373 hotspots (by strength) for each sample. In the smallest sample, the number of hotspots is13,373 (*C/L4*). Normalizing the number of hotspots helps to control for weak and apparently unique hotspots that are only found in better samples. **(F)** Hotspots split by the likely defining allele of *PRDM9* in each individual. *PRDM9-A*-defined hotspots were those found in any of the *A/A* individuals and not in the *C/L4* individual. *B*-, *C*-, and *N*-defined hotspots were the non-*A*-defined hotspots in the respective heterozygous individuals. *PRDM9-L4*-defined hotspots were those in the *C/L4* individual that were not found in the *A/C* individual. Hotspots that match two of these criteria were designated as ambiguous (X: gray). **(G)** The contribution of each *PRDM9* allele to hotspot strength. **(H)** Some alleles of *PRDM9* define stronger hotspots in heterozygous individuals. Ambiguous hotspots are not shown. Because of differences in the numbers of hotspots, values should not be compared across individuals.

Supplementary File S1 | Details of *PRDM9* genotypes for all individuals.

Supplementary File S2 | Details and nomenclature for human *PRDM9* zinc fingers.

Supplementary File S3 | Details of human *PRDM9* alleles.

Supplementary File S4 | Details of SNP association analyses.

REFERENCES

1000 Genomes Project Consortium, Auton, A., Brooks, L. D., Durbin, R. M., Garrison, E. P., Kang, H. M., et al. (2015). A global reference for human genetic variation. *Nature* 526, 68–74.

Ahlawat, S., Sharma, P., Sharma, R., Arora, R., Verma, N. K., Brahma, B., et al. (2016). Evidence of positive selection and concerted evolution in the rapidly evolving PRDM9 zinc finger domain in goats and sheep. *Anim. Genet.* 47, 740–751. doi: 10.1111/age.12487

Altemose, N., Noor, N., Bitoun, E., Tumian, A., Imbeault, M., Chapman, J. R., et al. (2017). A map of human prdm9 binding provides evidence for novel behaviors of PRDM9 and other zinc-finger proteins in meiosis. *Elife* 6:e28383. doi: 10.7554/eLife.28383

Altschul, S. F., Gish, W., Miller, W., Myers, E. W., and Lipman, D. J. (1990). Basic local alignment search tool. *J. Mol. Biol.* 215, 403–410.

Auton, A., Fledel-Alon, A., Pfeifer, S., Venn, O., Ségurel, L., Street, T., et al. (2012). A fine-scale chimpanzee genetic map from population sequencing. *Science* 336, 193–198.

Baudat, F., Buard, J., Grey, C., Fledel-Alon, A., Ober, C., Przeworski, M., et al. (2010). PRDM9 is a major determinant of meiotic recombination hotspots in humans and mice. *Science* 327, 836–840.

Bérard, S., Nicolas, F., Buard, J., Gascuel, O., and Rivals, E. (2007). A fast and specific alignment method for minisatellite maps. *Evol. Bioinform. Online* 2, 303–320.

Berg, I. L., Neumann, R., Lam, K. W., Sarbajna, S., Odenthal-Hesse, L., May, C. A., et al. (2010). PRDM9 variation strongly influences recombination hot-spot

activity and meiotic instability in humans. *Nat. Genet.* 42, 859–863. doi: 10.1038/ng.658

Berg, I. L., Neumann, R., Sarbajna, S., denthal-Hesse, L. O., Butler, N. J., and Jeffreys, A. J. (2011). Variants of the protein PRDM9 differentially regulate a set of human meiotic recombination hotspots highly active in african populations. *Proc. Natl. Acad. Sci. U.S.A.* 108, 12378–12383. doi: 10.1073/pnas.1109531108

Billings, T., Parvanov, Baker, C. L., Walker, M., Paigen, K., and Petkov, P. M. (2013). DNA binding specificities of the long zinc-finger recombination protein PRDM9. *Genome Biol.* 14:R35. doi: 10.1186/gb-2013-14-4-r35

Boateng, K. A., Bellani, M. A., Gregoretti, I. V., Pratto, F., and Camerini-Otero, R. D. (2013). Homologous pairing preceding SPO11-mediated double-strand breaks in mice. *Dev. Cell* 24, 196–205. doi: 10.1016/j.devcel.2012.12.002

Bonhomme, F., Rivals, E., Orth, A., Grant, G. R., Jeffreys, A. J., and Bois, P. R. J. (2007). Species-wide distribution of highly polymorphic minisatellite markers suggests past and present genetic exchanges among house mouse subspecies. *Genome Biol.* 8:R80. doi: 10.1186/gb-2007-8-5-r80

Brick, K., Pratto, F., Sun, C. Y., and Camerini-Otero, R. D. (2018). Analysis of meiotic double-strand break initiation in mammals. *Methods Enzymol.* 601, 391–418. doi: 10.1016/bs.mie.2017.11.037

Brick, K., Smagulova, F., Khil, P., Camerini-Otero, R. D., and Petukhova, G. V. (2012). Genetic recombination is directed away from functional genomic elements in mice. *Nature* 485, 642–645. doi: 10.1038/nature11089

Buard, J., Rivals, E., de Segonzac, D. D., Garres, C., Caminade, P., de Massy, B., et al. (2014). Diversity of Prdm9 zinc finger array in wild mice unravels new facets of the evolutionary turnover of this coding minisatellite. *PLoS One* 9:e85021. doi: 10.1371/journal.pone.0085021

Davies, B., Hatton, E., Altemose, N., Hussin, J. G., Pratto, F., Zhang, G., et al. (2016). Re-Engineering the Zinc Fingers of PRDM9 Reverses Hybrid Sterility in Mice. *Nature* 530, 171–176. doi: 10.1038/nature16931

Flachs, P., Bhattacharyya, T., Mihola, O., Piálek, J., Forejt, J., and Trachtulec, Z. (2014). Prdm9 incompatibility controls oligospermia and delayed fertility but no selfish transmission in mouse intersubspecific hybrids. *PLoS One* 9:e95806. doi: 10.1371/journal.pone.0095806

Flachs, P., Mihola, O., Simeček, P., Gregorová, S., Schimenti, J. C., Matsui, Y., et al. (2012). Interallelic and intergenic incompatibilities of the Prdm9 (Hst1) gene in mouse hybrid sterility. *PLoS Genet.* 8:e1003044. doi: 10.1371/journal.pgen.1003044

Grey, C., Barthès, P., Chauveau-Le Friec, G., Langa, F., Baudat, F., and de Massy, B. (2011). Mouse PRDM9 DNA-binding specificity determines sites of histone H3 lysine 4 trimethylation for initiation of meiotic recombination. *PLoS Biol.* 9:e1001176. doi: 10.1371/journal.pbio.1001176

Grey, C., Baudat, F., and de Massy, B. (2018). PRDM9, a driver of the genetic map. *PLoS Genet.* 14:e1007479. doi: 10.1371/journal.pgen.1007479

Hayashi, K., Yoshida, K., and Matsui, Y. (2005). A histone H3 methyltransferase controls epigenetic events required for meiotic prophase. *Nature* 438, 374–378. doi: 10.1038/nature04112

Hinch, A. G., Tandon, A., Patterson, N., Song, Y., Rohland, N., Palmer, C. D., et al. (2011). The landscape of recombination in African Americans. *Nature* 476, 170–175. doi: 10.1038/nature10336

Imai, Y., Baudat, F., Taillepierre, M., Stanzione, M., Toth, A., and de Massy, B. (2017). The PRDM9 KRAB domain is required for meiosis and involved in protein interactions. *Chromosoma* 126, 681–695. doi: 10.1007/s00412-017-0631-z

Jeffreys, A. J., Cotton, V. E., Neumann, R., and Gabriel Lam, K. W. (2013). Recombination regulator prdm9 influences the instability of its own coding sequence in humans. *Proc. Natl. Acad. Sci. U.S.A.* 110, 600–605. doi: 10.1073/pnas.1220813110

Jurka, J., and Gentles, A. J. (2006). Origin and diversification of minisatellites derived from human alu sequences. *Gene* 365, 21–26. doi: 10.1016/j.gene.2005.09.029

Khil, P. P., Smagulova, F., Brick, K. M., Camerini-Otero, R. D., and Petukhova, G. V. (2012). Sensitive mapping of recombination hotspots using sequencing-based detection of ssDNA. *Genome Res.* 22:130583. doi: 10.1101/gr.130583.111

Koh-Stenta, X., Joy, J., Poulsen, A., Li, R., Tan, Y., Shim, Y., et al. (2014). Characterization of the histone methyltransferase PRDM9 using biochemical, biophysical and chemical biology techniques. *Biochem. J.* 461, 323–334. doi: 10.1042/BJ20140374

Kong, A., Thorleifsson, G., Gudbjartsson, D. F., Masson, G., Sigurdsson, A., Jonasdottir, A., et al. (2010). Fine-scale recombination rate differences between sexes, populations and individuals. *Nature* 467, 1099–1103. doi: 10.1038/nature09525

Kono, H., Tamura, M., Osada, N., Suzuki, H., Abe, K., Moriwaki, K., et al. (2014). Prdm9 polymorphism unveils mouse evolutionary tracks. *DNA Res.* 21, 315–326. doi: 10.1093/dnares/dst059

Kusari, F., Mihola, O., Schimenti, J. C., and Trachtulec, Z. (2020). Meiotic epigenetic factor PRDM9 impacts sperm quality of hybrid mice. *Reproduction* 160, 53–64. doi: 10.1530/REP-19-0528

Lesecque, Y., Glémin, S., Lartillot, N., Mouchiroud, D., and Duret, L. (2014). The red queen model of recombination hotspots evolution in the light of archaic and modern human genomes. *PLoS Genet.* 10:e1004790. doi: 10.1371/journal.pgen.1004790

Li, H. (2013). Aligning sequence reads, clone sequences and assembly contigs with BWA-MEM. *arXiv* [Preprint]. arXiv: 1303.3997.

Li, H., Handsaker, B., Wysoker, A., Fennell, T., Ruan, J., Homer, N., et al. (2009). The sequence alignment/map format and SAMtools. *Bioinformatics* 25, 2078–2079. doi: 10.1093/bioinformatics/btp352

Mihola, O., Trachtulec, Z., Vlcek, C., Schimenti, J. C., and Forejt, J. (2009). A mouse speciation gene encodes a meiotic histone H3 methyltransferase. *Science* 323, 373–375. doi: 10.1126/science.1163601

Mukaj, A., Piálek, J., Fotopulosova, V., Morgan, A. P., denthal-Hesse, L. O., Parvanov, E. D., et al. (2020). Prdm9 intersubspecific interactions in hybrid male sterility of house mouse. *Mol. Biol. Evol.* 37, 3423–3438.

Myers, S., Bowden, R., Tumian, A., Bontrop, R. E., Freeman, C., MacFie, T. S., et al. (2010). Drive against hotspot motifs in primates implicates the PRDM9 gene in meiotic recombination. *Science* 327, 876–879. doi: 10.1126/science.1182363

Oliver, P. L., Goodstadt, L., Bayes, J. J., Birtle, Z., Roach, K. C., Phadnis, N., et al. (2009). Accelerated evolution of the Prdm9 speciation gene across diverse metazoan taxa. *PLoS Genet.* 5:e1000753. doi: 10.1371/journal.pgen.1000753

Parvanov, E. D., Petkov, P. M., and Paigen, K. (2010). Prdm9 controls activation of mammalian recombination hotspots. *Science* 327:835. doi: 10.1126/science.1181495

Parvanov, E. D., Tian, H., Billings, T., Saxl, R. L., Spruce, C., Aithal, R., et al. (2017). PRDM9 interactions with other proteins provide a link between recombination hotspots and the chromosomal axis in meiosis. *Mol. Biol. Cell* 28, 488–499. doi: 10.1091/mbc.E16-09-0686

Persikov, A. V., and Singh, M. (2014). De novo prediction of DNA-binding specificities for Cys2His2 zinc finger proteins. *Nucleic Acids Res.* 42, 97–108. doi: 10.1093/nar/gkt890

Pratto, F., Brick, K., Cheng, C., Lam, K. W. G., Cloutier, J. M., Dahiya, D., et al. (2021). Meiotic recombination mirrors patterns of germline replication in mice and humans. *Cell* 184, 4251–4267.e20. doi: 10.1016/j.cell.2021.06.025

Pratto, F., Brick, K., Khil, P., Smagulova, F., Petukhova, G. V., and Camerini-Otero, R. D. (2014b). Recombination initiation maps of individual human genomes. *Science* 346:1256442. doi: 10.1126/science.1256442

Pratto, F., Brick, K., Khil, P., Smagulova, F., Petukhova, G. V., and Camerini-Otero, R. D. (2014a). DNA recombination. recombination initiation maps of individual human genomes. *Science* 346:1256442. doi: 10.1126/science.1256442

Purcell, S., Neale, B., Todd-Brown, K., Thomas, L., Ferreira, M. A. R., Bender, D., et al. (2007). PLINK: a tool set for whole-genome association and population-based linkage analyses. *Am. J. Hum. Genet.* 81, 559–575. doi: 10.1086/519795

Rice, P., Longden, I., and Bleasby, A. (2000). EMBOSS: the European molecular biology open software suite. *Trends Genet.* 16, 276–277. doi: 10.1016/s0168-9525(00)02024-2

Schwartz, J. J., Roach, D. J., Thomas, J. H., and Shendure, J. (2014). Primate Evolution of the recombination regulator PRDM9. *Nat. Commun.* 5:4370.

Silvestre-Ryan, J., and Holmes, I. (2020). Pair consensus decoding improves accuracy of neural network basecallers for nanopore sequencing. *Cold Spring Harb. Lab.* 22:38. doi: 10.1101/2020.02.25.956771

Smagulova, F., Brick, K., Pu, Y., Camerini-Otero, R. D., and Petukhova, G. V. (2016). The evolutionary turnover of recombination hot spots contributes to speciation in mice. *Genes Dev.* 30, 266–280.

Spence, J. P., and Song, Y. S. (2019). Inference and analysis of population-specific fine-scale recombination maps across 26 diverse human populations. *Sci. Adv.* 5:eaaw9206. doi: 10.1126/sciadv.aaw9206

Thibault-Sennett, S., Yu, Q., Smagulova, F., Cloutier, J., Brick, K., Camerini-Otero, R. D., et al. (2018). Interrogating the functions of PRDM9 domains in meiosis. *Genetics* 209, 475–487. doi: 10.1534/genetics.118.300565

Walker, M., Billings, T., Baker, C. L., Powers, N., Tian, H., Saxl, R. L., et al. (2015). Affinity-seq detects genome-wide PRDM9 binding sites and reveals the impact of prior chromatin modifications on mammalian recombination hotspot usage. *Epigenetics Chromatin.* 8:31. doi: 10.1186/s13072-015-0024-6

Wu, H., Mathioudakis, N., Diagouraga, B., Dong, A., Dombrovski, L., Baudat, F., et al. (2013). Molecular basis for the regulation of the H3K4 methyltransferase activity of PRDM9. *Cell Rep.* 5, 13–20. doi: 10.1016/j.celrep.2013.08.035

Zaidi, A. A., White, J. D., Mattern, B. C., Liebowitz, C. R., Puts, D. A., Claes, P., et al. (2019). Facial masculinity does not appear to be a condition-dependent male ornament and does not reflect MHC heterozygosity in humans. *Proc. Natl. Acad. Sci. U.S.A.* 116, 1633–1638. doi: 10.1073/pnas.1808659116

Zhang, Y., Liu, T., Meyer, C. A., Eeckhoute, J., Johnson, D. S., Bernstein, B. E., et al. (2008). Model-Based Analysis of ChIP-Seq (MACS). *Genome Biol.* 9:R137.

Conflict of Interest: The authors declare that the research was conducted in the absence of any commercial or financial relationships that could be construed as a potential conflict of interest.

Publisher's Note: All claims expressed in this article are solely those of the authors and do not necessarily represent those of their affiliated organizations, or those of the publisher, the editors and the reviewers. Any product that may be evaluated in this article, or claim that may be made by its manufacturer, is not guaranteed or endorsed by the publisher.

Copyright © 2021 Alleva, Brick, Pratto, Huang and Camerini-Otero. This is an open-access article distributed under the terms of the Creative Commons Attribution License (CC BY). The use, distribution or reproduction in other forums is permitted, provided the original author(s) and the copyright owner(s) are credited and that the original publication in this journal is cited, in accordance with accepted academic practice. No use, distribution or reproduction is permitted which does not comply with these terms.

frontiers in Cell and Developmental Biology

ORIGINAL RESEARCH
published: 25 November 2021
doi: 10.3389/fcell.2021.687132

High Temporal Resolution 3D Live-Cell Imaging of Budding Yeast Meiosis Defines Discontinuous Actin/Telomere-Mediated Chromosome Motion, Correlated Nuclear Envelope Deformation and Actin Filament Dynamics

*Tadasu Nozaki, Frederick Chang, Beth Weiner and Nancy Kleckner**

Department of Molecular and Cellular Biology, Harvard University, Cambridge, MA, United States

OPEN ACCESS

Edited by:
Akira Shinohara,
Osaka University, Japan

Reviewed by:
Verena Jantsch,
Max F. Perutz Laboratories GmbH, Austria
Kazuhiro Maeshima,
National Institute of Genetics, Japan

***Correspondence:**
Nancy Kleckner
kleckner@fas.harvard.edu

Specialty section:
This article was submitted to Cell Growth and Division, a section of the journal Frontiers in Cell and Developmental Biology

Received: *29 March 2021*
Accepted: *05 October 2021*
Published: *25 November 2021*

Citation:
Nozaki T, Chang F, Weiner B and Kleckner N (2021) High Temporal Resolution 3D Live-Cell Imaging of Budding Yeast Meiosis Defines Discontinuous Actin/Telomere-Mediated Chromosome Motion, Correlated Nuclear Envelope Deformation and Actin Filament Dynamics. Front. Cell Dev. Biol. 9:687132. doi: 10.3389/fcell.2021.687132

Chromosome movement is prominent at mid-meiotic prophase and is proposed to enhance the efficiency and/or stringency of homolog pairing and/or to help prevent or resolve topological entanglements. Here, we combine fluorescent repressor operator system (FROS) labeling with three-dimensional (3D) live-cell imaging at high spatio-temporal resolution to define the detailed kinetics of mid-meiotic prophase motion for a single telomere-proximal locus in budding yeast. Telomere motions can be grouped into three general categories: (i) pauses, in which the telomere "jiggles in place"; (ii) rapid, straight/curvilinear motion which reflects Myo2/actin-mediated transport of the monitored telomere; and (iii) slower directional motions, most of which likely reflect indirectly promoted motion of the monitored telomere in coordination with actin-mediated motion of an unmarked telomere. These and other findings highlight the importance of dynamic assembly/disassembly of telomere/LINC/actin ensembles and also suggest important roles for nuclear envelope deformations promoted by actin-mediated telomere/LINC movement. The presented low-SNR (signal-to-noise ratio) imaging methodology provides opportunities for future exploration of homolog pairing and related phenomena.

Keywords: 3D time-lapse imaging, chromosome motion, FROS, telomere, actin, homolog pairing, meiosis

INTRODUCTION

Meiosis is the specialized cell cycle program which produces gametes with half the ploidy of their progenitor cells, thereby compensating for genome doubling at mating. This outcome is accomplished by occurrence of a single round of DNA replication followed by two rounds of chromosome segregation, meiosis I (MI) and meiosis II (MII). Homologous chromosomes ("homologs") segregate to opposite poles at meiosis I. Sister chromatids then separate at meiosis II. Crossovers, the products of programmed homologous recombination, in combination with sister

arm cohesion, allow the generation of tension between homologous chromosomes at metaphase of MI. This, in turn, ensures accurate distribution of homologs to opposite poles (Zickler and Kleckner, 1999, 2015).

Homologs achieve the configuration necessary for MI by a complex program of interactions that occupy a prolonged prophase stage. A major requirement of this program is that the homologs come close together in space, becoming aligned side-by-side (Zickler and Kleckner, 2015). During this process, two general problems must be addressed: (1) How can homologs meet one another on a reasonable time scale? This outcome requires both recognition of homology, e.g., via local events of DNA recombination, and global juxtaposition of whole chromosomes along their lengths. (2) What mechanism ensures the topological regularity of the pairing process so as to avoid or eliminate interlocks, entanglements, or ectopic pairing or non-homologous pairing (Storlazzi et al., 2010)?

With respect to time scale, the challenges of meiotic homolog pairing are illustrated by comparison with protein/DNA interactions. Proteins must scan the DNA information in the chromosomes to find their cognate binding sites (e.g., as for repressor proteins and transcriptional factors). By comparison, homology searching by chromosomes seems more difficult, from several points of view. First, the speed of chromosome motion in the eukaryotic G1 nucleus, as defined by analysis of movements of individually tagged loci over time, appears to be conserved, with diffusion coefficients ranging from 10^{-4} to 10^{-3} $\mu m^2/s$ (Marshall et al., 1997; Heun et al., 2001; Vazquez et al., 2001; Chubb et al., 2002; Dion et al., 2012; Miné-Hattab and Rothstein, 2012). This movement is much slower than that of proteins that are freely and three-dimensionally diffusing in the nucleus to identify their targets (10^0–10^2 $\mu m^2/s$; e.g., Mazza et al., 2012; Chen et al., 2014; Izeddin et al., 2014; Normanno et al., 2015). Second, for protein/DNA interactions, many copies of the involved protein are searching for the target in parallel whereas, for meiotic chromosome pairing, there is only one pair of homologous chromosomes. Thus, the possibilities for parallel searches are more limited (discussion in Storlazzi et al., 2010).

In addition, both protein/DNA interactions and homolog pairing must solve the "speed-stability paradox" (Slutsky and Mirny, 2004). In brief, there is a tradeoff between the speed of searching and the stability required to ensure the desired cognate interaction. That is, for chromosomes, the same issue arises: homologs must be able to identify one another accurately without becoming trapped in nearly homologous interactions (Kleckner and Weiner, 1993; Bitran et al., 2017). In accord with these complexities, analysis of RecA-mediated homology recognition between a DNA locus and complementary oligonucleotide reveals that the rate of homologous pairing at the DNA level, which underlies meiotic homologous pairing (Zickler and Kleckner, 2015) is not rate-limited by the search for DNA homology (Yancey-Wrona and Camerini-Otero, 1995).

With respect to topological issues: entanglements/interlocks, and ectopic pairing between non-homologous chromosomes will impede the completion of homologous pairing and recombination and, eventually, clean segregation of homologous pairs at MI (Zickler, 2006; Koszul et al., 2008; Wanat et al., 2008). In fact, a modest number of topological interlockings are seen at the late leptotene and zygotene stages; however, they disappear during the pachytene stage, indicating that they can ultimately be resolved (Wettstein et al., 1984; Storlazzi et al., 2010).

These diverse challenges to homolog pairing seem severe. However, there are cellular mechanisms which help in overcoming them. One such mechanism is dynamic chromosome motion mediated by cytoskeletal forces exerted on telomeres through the nuclear envelope (described below). The current study focuses on the nature of these dynamic motions in budding yeast.

BACKGROUND

The first evidence of vigorous movements of chromosomes during meiotic prophase was found in rat spermatocytes (Parvinen and Söderström, 1976). By now, prophase movement has been described in a wide variety of organisms, albeit with some variations among different cases (e.g., Chikashige et al., 1994, 2006 in fission yeast; Scherthan et al., 2007; Conrad et al., 2008; Koszul et al., 2008 in budding yeast, Sheehan and Pawlowski, 2009 in maize, Christophorou et al., 2015 in *Drosophila*, Shibuya et al., 2014; Lee et al., 2015 in mouse, Sato et al., 2009; Baudrimont et al., 2010; Wynne et al., 2012; Link et al., 2018 in *C. elegans*). These movements have been proposed, variously, to promote homologous chromosome pairing, to reduce ectopic homologous pairing or pairing between near-homologous regions, and/or to resolve chromosome interlocks and entanglements (Koszul and Kleckner, 2009; Baudrimont et al., 2010; Lee et al., 2012; Wynne et al., 2012; Link and Jantsch, 2019). In accord with such possibilities, ectopic recombination and inappropriate telomere interactions are increased in budding yeast when motion is abrogated (Conrad et al., 2008; Lee et al., 2012) and in fission yeast when telomere clustering (a component of motion in that organism) is absent (Niwa et al., 2000; Davis and Smith, 2006). And in *C. elegans,* abrogation of motion results in inefficient pairing and entanglements (Penkner et al., 2007; Sato et al., 2009).

In most studied cases, vigorous meiotic prophase chromosome movement is generated by the linkage of chromosome ends to the cytoskeleton (reviewed in Koszul and Kleckner, 2009; Link and Jantsch, 2019). In such processes, mechanical forces of the cytoskeleton are transmitted to the telomeres through the nuclear membrane. Force transduction is provided by the Linker of Nucleoskeleton and Cytoskeleton (LINC) complexes, which is composed of inner nuclear membrane SUN domain proteins and outer nuclear membrane KASH domain proteins. Telomeres interact with SUN proteins, and KASH proteins bind to the cytoskeleton.

In budding yeast, dynamic prophase movement is dependent on the actin cytoskeleton (Scherthan et al., 2007; Conrad et al., 2008; Koszul et al., 2008). In this case, actin fibers are seen to "hug" the outer surface of the nuclear envelope in a

curved path and telomeres are seen to move along those fibers, sometimes even after the fibers are no longer associated with the nucleus (Koszul et al., 2008; **Supplementary Figures 1A,C**; below). Visualization of whole pachytene chromosomes has also revealed that active movement of one telomere is accompanied by coordinate, spatially coordinated movements of other nearby chromosomes, often comprising half or more of the chromosome complement, whose motions are therefore "indirect" effects (Koszul et al., 2008; **Supplementary Figure 1B**). All of these motions are eliminated in the presence of Latrunculin B ("LatB"), a drug that prevents actin fiber polymerization by binding to actin monomers (Koszul et al., 2008).

Five molecules other than actin have also been implicated in actin-mediated motion (Fan et al., 2020; Lee et al., 2020). Ndj1 is a meiosis-specific protein that connects the telomere to the LINC complex via Mps3, a SUN domain protein that spans the nuclear membrane. Mps2 and Csm4 are related coiled coil proteins that interact with one another and mediate linkage of Mps3 to myosin Myo2 which, in turn, interacts with actin. Mutations that delete or alter any one of the involved proteins causes a severe reduction of rapid chromosome movement at mid-meiotic prophase and a delay in homolog pairing (Conrad et al., 2007, 2008; Scherthan et al., 2007; Kosaka et al., 2008; Wanat et al., 2008; Lee et al., 2012, 2020; Fan et al., 2020). Importantly, in mitotically dividing yeast cells, Myo2 mediates the transport of several different types of cargos along actin fibers (e.g., Beach et al., 2000; Schott et al., 2002). In the meiotic situation, this cargo comprises the entire nuclear envelope-embedded LINC complex as well as Ndj1 and its associated chromosome. Correspondingly, telomere movement is accompanied by nuclear envelope deformations nucleated at the telomere attachment site (Koszul et al., 2008; below).

In the present study, we studied telomere motion in budding yeast using FROS (fluorescent repressor operator system) labeling (Robinett et al., 1996; Straight et al., 1996; Marshall et al., 1997; Heun et al., 2001) plus a unique methodology for 3D live-cell imaging and spot detection at high spatio-temporal resolution and low signal-to-noise ratio (SNR), as developed in our laboratory (Chang, 2018). Trajectories of single labeled telomeres were defined in 3D at 500 ms intervals over total time spans of 6 min. This approach provides a previously unavailable description of the detailed dynamics of an individual telomere during meiotic mid-prophase. For comparison, we analogously examined telomere movements at premeiotic G1/G0 and in selected mutant situations (details in section "Materials and Methods" and below).

Concomitantly, the boundary of the nucleus, and thus by implication the nuclear envelope, was visualized using a general nuclear signal, with the position of the labeled telomere locus localized relative to that signal. Meiotic prophase actin filament dynamics were also visualized, thus allowing assessment of their contribution to net telomere movement. The presented findings provide new information regarding the nature of actin-mediated chromosome motions in this system.

MATERIALS AND METHODS

Yeast Strains

Saccharomyces cerevisiae strains are *MATa/MATα* derivatives of wild-type SK1 as follows: *scp1::tetO array::LEU2/SCP1, leu2::URA3p-TetR-mEGFP::LEU2/leu2::hisG* (TNY570); *scp1::tetO array::LEU2/SCP1, leu2::URA3p-TetR-mEGFP::LEU2/leu2::hisG, ndj1Δ/ndj1Δ* (TNY669), *ABP140-4xGFP::KanMX/ABP140-4xGFP::KanMX* (YKK389), *SPC42-YFP::URA/SPC42* (TNY866). TetO array system is based on Kim et al. (2010).

Meiotic Time Course

All operations were performed at 30°C. Strains maintained in glycerol stock at −80°C are patched onto YEPG plates (3% w/v glycerol, 2% w/v bactopeptone, 1% w/v yeast extract, 2% w/v bactoagar) overnight. Cells were struck out to single colonies on YEPD plates (2% w/v bactopeptone, 1% w/v yeast extract, 2% w/v glucose, 2% w/v bactoagar) and grown for 2 days. A single colony is transferred to 4 ml YEPD liquid medium (2% w/v bactopeptone, 1% w/v yeast extract, 2% w/v glucose) and grown overnight. A 1/100 dilution of the culture was made with YEPA medium (1% w/v potassium acetate, 2% w/v bactopeptone, 1% w/v yeast extract, 2 drops per liter antifoam) and grown for 13.5 h. Meiosis was initiated by transfer of cells to 1% sporulation medium (SPM) (1% w/v potassium acetate, 0.02% w/v raffinose, 2 drops per liter antifoam). We note that this series of preparation conditions is specifically defined in such a way that, at the time of transfer to the SPM, cells have completed ongoing mitotic cell cycles and are becoming larger without initiating a new mitotic cycle and thus are present primarily as large unbudded cells. Upon transfer to SPM, this population initiates meiosis synchronously and efficiently (e.g., Kim et al., 2010).

Chemical Treatment of Meiotic Cells

Latrunculin B (LatB) was from Santa Cruz Biotechnology Inc. and was dissolved in dimethyl-sulfoxide (DMSO). LatB was added to a final concentration of 30 μM at 2 h after initiation of meiosis by transfer to SPM and imaged after an additional 2 h (t = 4 h of meiosis).

Live-Cell Imaging

Cell samples from an experimental culture were vortexed at full speed and 1 μl quickly spread onto a glass base dish (MatTek) coated with Concanavalin A (ConA). A premade agarose pad (1%) was placed on top of the cell drop and excess media was absorbed by a piece of Kimwipe. Cells were observed at 30°C using a Ti microscope (Nikon) equipped with GFP filters (Semrock), a sCMOS camera (Hamamatsu Photonics), and a piezo device (Physik Instrumente) for acquiring Z stacks. Cells were exposed to the LED light (Lumencor) through an objective lens (60× PlanApo, NA 1.40; Nikon). The microscopy system was controlled, and images were acquired, through μ-Manager software and MATLAB.

For short time scaled imaging, movies of 15 z-stack steps with 389-nm step size and 720 sequential frames were acquired using

μ-Manager software with 25 ms exposure time and 8.3 ms camera acquisition time, totaling 500 ms for one set of z-stack images. For long timescale imaging, movies of 13 z-stack steps with 389-nm step size were acquired using μ-Manager software with 10 ms exposure time and 16.6 ms camera acquisition time. Z-stacks were acquired at 1 min interval for 10 h, giving a total of 601 z-stack images.

Images were denoised quantitatively by a home-made program that accurately defines the presence and positions of fluorescent spots at very low signal-to-noise ratios (Chang, 2018). This algorithm dramatically extends the ability to capture many images over long periods of time, as illustrated in this work. Spots were detected and tracked by ImageJ Fiji plug-in TrackMate (Schindelin et al., 2012; Tinevez et al., 2017). The distribution of spot displacements per time interval and the mean square displacement (MSD) of the fluorescent signals were calculated in 3D based on this TrackMate data. The MSD was calculated by the following formula. MSD = $<(X_t - X_{t+\Delta t})^2>$. X_t was the three-dimensional position of a fluorescent spot at time t (Seeber et al., 2013). The multi-component Gaussian mixture model is fitted to the step size data of the spot motion using mixtools in R packages (Benaglia et al., 2009). To eliminate the influence of large step size (Group 1, see below) to the 5 s interval analysis, the ± 10 frames (5 s) from the frame that shows the large step in 500 ms were eliminated. We note that, due to specific features of our imaging system and spot detection algorithm, the spatial precision of spot detection in our system is high and that there is no detectable photobleaching or phototoxicity, as discussed in the text and also in **Supplementary Notes**.

Fixed-Cell Imaging

For fixed cell analysis, cells were transferred to 4% paraformaldehyde at 4 h after initiation of meiosis as described above. Cells were then spun down and the cell pellet was resuspended in 0.1 M potassium phosphate for imaging. Other procedures are the same as for live-cell imaging.

RESULTS

To measure telomere-led chromosome movement, we constructed a diploid strain in which one chromosome carries a sub-telomeric fluorescent tag. The *SCP1* locus is located 64 kb from the right arm telomere of chromosome XV. An array of binding sites (*tetO*) for the tetracycline resistance repressor was inserted into one chromosome of a strain also carrying that repressor fused to mEGFP (TetR-mEGFP), giving a fluorescent focus corresponding to *scp1::tetO*/TetR-mEGFP (**Figure 1A**). Motion of the tagged locus was defined by imaging of the corresponding fluorescent spot in 3D (**Figure 1B**) at 500 ms intervals, typically for a total of 6 min (section "Materials and Methods"). We note that the approaches we use allow us to accurately define the position of a fluorescent spot, to ∼0.040 μm in the X and Y dimensions and ∼0.075 μm in the Z dimension. The accuracy of our imaging system and spot detection were estimated by imaging of the fixed cells and calculating the standard deviation of the detected spot position (see "Materials and Methods," **Supplementary Figures 2A,B** and **Supplementary Note**; Nozaki et al., 2013; Miné-Hattab et al., 2017). These values, which we consider to be the upper bound of localization accuracy, are lower than the 500 ms step sizes observed in any of data reported below, implying that the movements described below faithfully reflect actual telomere movement.

Motion Is Dynamic at Mid-Prophase as Compared to Premeiotic G1/G0

Telomere motion was examined analogously in premeiotic G1/G0 cells (defined as large unbudded cells observed immediately upon transfer to sporulation medium; "Materials and Methods," i.e., t = 0 h, **Figures 1C,E,G**) and in meiotic prophase cells observed at t = 4 h after initiation of meiosis, the time at which dramatic chromosome movements are known to occur (Koszul et al., 2008; see **Supplementary Figure 4** and **Figures 1D,F,H**). Parallel control experiments confirm that cells are at late zygotene or early pachytene at this time, as judged by Zip1-GFP patterns (T.N. unpublished).

In accord with previous observations, telomere motion is limited at pre-meiotic G1/G0 (t = 0 h) and dramatic at meiotic mid-prophase (t = 4 h). This difference is qualitatively apparent in representative kymographs which show the position of the spot as projected onto the X-, Y-, or Z-plane over a 3 min time period (**Figure 1C** vs. **Figure 1D**) and in corresponding 3D trajectories (**Figure 1E** vs. **Figure 1F**). At G1/G0, the telomere locus never moves far from its starting point in 3 min (**Figure 1E**) while at mid-prophase, it traverses distances comparable to the diameter of the nucleus (∼2 μm) (**Figure 1F**).

The difference between the two situations can be described quantitatively. Plots of mean square displacement (MSD) over time are widely used with single-particle tracking to quantify chromatin and chromosome dynamics (Heun et al., 2001; Sage et al., 2005; Miné-Hattab and Rothstein, 2012; Hajjoul et al., 2013; Nozaki et al., 2017). For normal diffusion, the MSD of a tracked "spot" varies linearly with time. In contrast, at both G1/G0 and mid-prophase, the marked telomere exhibits a rising curve which reaches a plateau. This behavior, referred to as "anomalous diffusion," implies that the movement of the tracked particle is somehow constrained, with the distance reached at the plateau defined as the "radius of constraint" (Rc) (Neumann et al., 2012). Confinement is severe at G1/G0 (Rc = 0.64 μm; **Figure 1G**, n = 10 cells). Interestingly, this pattern is very similar to that observed by analogous MSD analysis in yeast mitotic interphase cells (Sage et al., 2005). Confinement is much less severe at mid-prophase, with Rc = 1.46 μm, roughly comparable to the diameter of the nucleus (**Figure 1H**, n = 17 cells), in accord with the fact that telomeres are actively moved around the nuclear periphery during this period (Koszul et al., 2008). The mid-prophase MSD curve also rises more sharply than the G1/G0 MSD curve. This difference implies that the telomere locus tends to move farther in a given period of time in mid-prophase vs. G1/G0, in accord with the presence and

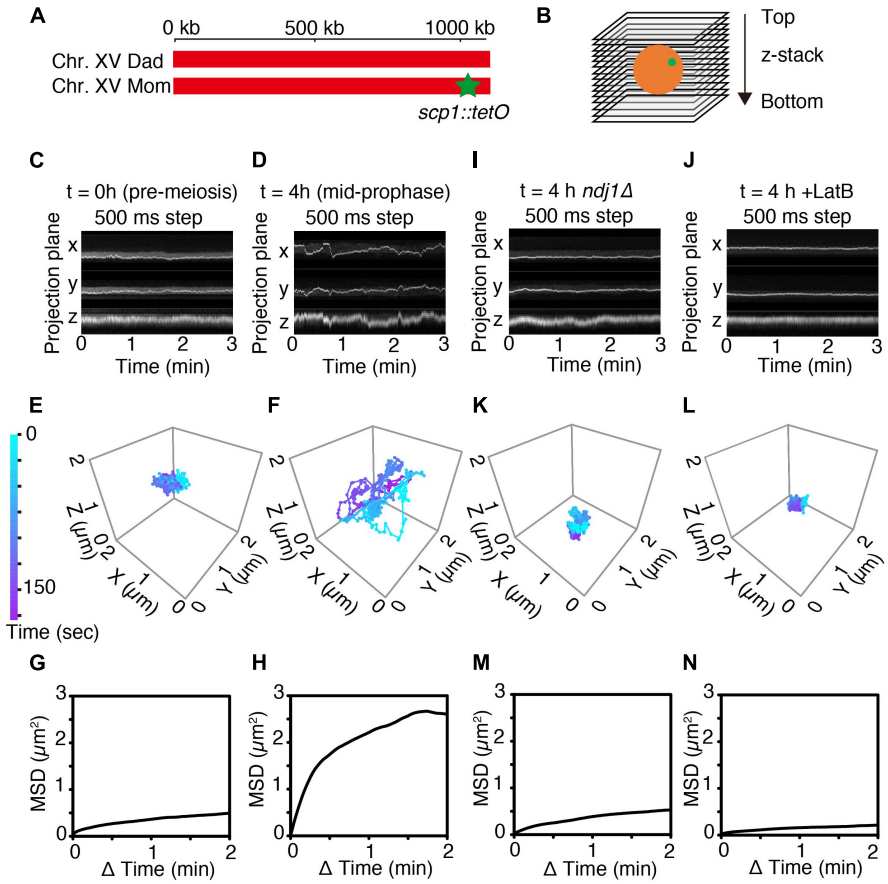

FIGURE 1 | 4D imaging of telomere trajectories. **(A)** Chromosome labeling of the *SCP1* locus with TetR-mEGFP. The end of only one chromosome (chromosome XV) in a diploid cell is labeled. **(B)** The scheme of 3D live-cell imaging in budding yeast. **(C,D)** Kymographs of representative cells tracked in 3D at t = 0 h (**C**; pre-meiotic G1/G0) and at t = 4 h (**D**; mid-meiotic prophase) cultured in SPM. 3D images are captured once per 500 ms. **(E,F)** Trajectories of the fluorescent spots shown in **(C,D)** as tracked in 3D at pre-meiotic G1/G0 (t = 0 h) **(E)** and at meiotic prophase (t = 4 h) **(F)**. **(G,H)** MSD curves of the tagged *SCP1* locus in cells at pre-meiotic G1/G0 (G; n = 10 cells) and at meiotic prophase (H; n = 17 cells). **(I–N)** Kymographs, representative trajectories, MSD curves for *ndj1*Δ mutant cell(s) (**I,K,M**; n = 10 cell) and LatB-treated cell(s) (**J,L,N**; n = 10 cells) exactly as in the corresponding **(C,E,G)**.

absence of active actin/Myo2-mediated movements in the two situations, respectively.

Meiotic Prophase Telomere Motions Are Driven by Actin/Telomere Linkage

Mid-prophase telomere motions are substantially reduced by deletion of meiotic telomere protein Ndj1 (which connects telomeres to the LINC complex; Background) (*ndj1*Δ; **Figures 1I,K,M**). These movements are also dramatically reduced by treatment with LatB, which blocks actin polymerization (**Figures 1J,L,N**). Thus, as expected, the dynamic prophase motions of telomere-located *scp1::tetO*-TetR observed at mid-prophase are derived from the force generated by the linkage of the telomere to cytoskeletal actin fiber(s) via LINC complexes.

Interestingly, the overall behavior of telomeres in *ndj1*Δ is similar to that observed at G1/G0 (compare **Figures 1I,K** with **Figures 1C,E**; further discussion below). Also, the effect of LatB is more severe than that of *ndj1*Δ, perhaps because telomeres are now locked onto immobile LINC complexes rather than being free of such complexes.

Analysis of Mid-Prophase Telomere Movement Reveals Three General Categories of Motion

Background

All previous studies identify occasional (sporadic) extremely rapid, straight/curvilinear telomere movements which occur over very short time period and are attributable to direct transport of a monitored telomere along an actin filament (e.g., Conrad et al., 2008; Koszul et al., 2008; Lee et al., 2012, 2020; Discussion). Additional insight is provided by analysis of whole pachytene chromosomes in which the movements of many/most chromosomes were directly visualized simultaneously over time (e.g., Koszul et al., 2008; **Supplementary Figure 1B**). Such images reveal three types of telomere motion (**Supplementary Figure 1B**). First, one telomere may move rapidly in a highly directed

fashion over a very short time period (∼3 s) corresponding to transport of this "lead" telomere along an actin fiber. Second, this movement is accompanied by coordinate movement of a multiple chromosome group in the same direction as the "lead" telomere, with accompanying dramatic changes in overall nucleus shape. These coordinated motions comprise a second type of actin-dependent telomere motion which, however, is promoted indirectly by directly promoted motion of the "lead" telomere. Third, even despite the above progressions, many chromosomes (and thus their telomeres) do not move. Importantly, for given monitored telomere as in the present study, indirectly promoted movements can be provoked by any of the other (unmonitored) 31 telomeres (16 chromosomes x 2 telomeres) in the nucleus and thus will be much more frequent than sporadic direct transport movement. The same is true for pauses which, at any given moment, pertain to many telomeres (**Supplementary Figure 1B**) and thus will occupy a substantial lifetime of any one monitored telomere. For convenience, we refer to the telomere motions in these three conditions as "directly promoted," "indirectly promoted," and "pause."

Two Approaches to Analysis of Mid-Prophase Telomere Motion

We were interested to understand whether telomere motions as detected by spot tracking could be seen to comprise distinct categories, e.g., as revealed by whole chromosome analysis (above).

- In one approach we analyzed the distributions of distances traveled by the monitored telomere over intervals of 500 ms and 5 s (11 image frames). 500 ms step sizes, being shorter, give a clearer impression of the intrinsic rate of telomere movement. 5 s step sizes, in contrast, reflect not only the intrinsic rate of movement but the extent to which that movement is or is not "directed." Without directionality, sequential steps are randomly oriented and the telomere remains close(r) to its starting point after 5 s. If motion is in any manner directional, sequential steps tend to occur in the same direction and the telomere tends to move farther from its starting point in 5 s, in relation to the straightness of the trajectories.

- In a second approach we inspected movies of 3D projections visually to determine whether any specific trajectory patterns might reproducibly appear out of the generally chaotic motions, thereby identifying different distinct "motion phenotypes."

The former approach has the advantage of considering the totality of the data. The latter approach has the advantage of including spatio-temporal information, i.e., the added dimensions of multi-step trajectory and duration, neither of which appear as inputs into step-size analysis. In addition, this approach allows the biological situation to highlight particularly clear or prominent types of movement.

Both approaches reveal the same underlying reality: the majority of telomere movements and trajectories fall into three broad categories which correspond to one another and to the three general categories expected on the basis of whole chromosome analysis as described above.

Categories of Telomere Movements as Revealed by Step Size Analysis

We compared mid-prophase telomere motions in wild type meiosis with those in *ndj1*Δ, where telomeres are not associated with LINC complexes and are thus not subject to either direct or indirect effects of actin/Myo2-mediated movement. In *ndj1*Δ, the array of distances of movement over time shows a low baseline of 0.1 μm and 0.2 μm at 500 ms and 5 s intervals, respectively (**Figure 2A** and **Supplementary Figure 3A**). Motions at G1/G0, where telomere/LINC associations are also absent, are very similar (**Supplementary Figures 3B,E**). In striking contrast, in wild type meiotic mid-prophase, step sizes fluctuate dramatically over time, from 0 to 1 μm for 500 ms intervals and 0–3 μm for 5 s intervals (**Figure 2D**). The most dramatic motions are comparable to those observed previously for individual tracked telomeres (Lee et al., 2012, 2020); the smallest motions are comparable to those observed in *ndj1*Δ; and many distances fall between these two extremes, at both step sizes.

For *ndj1*Δ, at both 500 ms and 5 s intervals, total step sizes exhibit the single-peaked curve, well-fitted by a Gaussian model, with average distances traveled of 0.14 μm/500 ms and 0.26 μm/5 s, respectively (**Figures 2B,C**). Motions at G1/G0 are very similar (0.19 μm/500 ms and 0.32 μm/5 s, respectively; **Supplementary Figures 3C,D**). In both cases, the marked telomere is moving relatively slowly and without directionality, i.e., is essentially "jiggling in place" (e.g., **Figures 1E,K**). These patterns provide a baseline description of mid-prophase telomere movement in the absence of telomere-LINC association. Similar results were observed in LatB-treated cells but with even a bit smaller step sizes than wild type cells (0.13 μm/500 ms and 0.20 μm/5 s, respectively, **Supplementary Figures 3F–I**).

For wild type telomere motion, the distribution of 500 ms step sizes exhibits a prominent peak with a mean value of 0.16 μm, plus a discernible tail of much greater movement with a mean value of 0.38 μm. This pattern is well-described by a corresponding two-component Gaussian mixture model (**Figure 2E**). The component corresponding to the minor tail (denoted "Group 1") exhibits a very large step size, corresponding to those seen previously and attributed to direct actin-mediated transport (above; Conrad et al., 2008; Koszul et al., 2008; Lee et al., 2012, 2020). In contrast, the major subcomponent distribution exhibits a relatively small average step size which is very similar to that observed for *ndj1*Δ .

To further dissect the nature of this latter majority group of motions, we eliminated the subset of very large steps (>0.38 μm/500 ms) from the total data set (see "Materials and Methods") and analyzed the distribution of 5 s step sizes for the remaining (vast majority of) motions. A broad distribution emerges which is well-fitted by a two-component Gaussian mixture model. One component has a mean step size (0.27 μm) which again corresponds to the 5 s step size of *ndj1*Δ (0.26 μm) while the other has a larger mean step size (0.59 μm) ("Group 2" and "Group 3," respectively; **Figure 2F**). Thus, over longer (5 s) intervals, the telomere often exhibits *ndj1*Δ-like behavior but also frequently travels significantly farther than in the *ndj1*Δ case (**Figures 2C,F**). Since

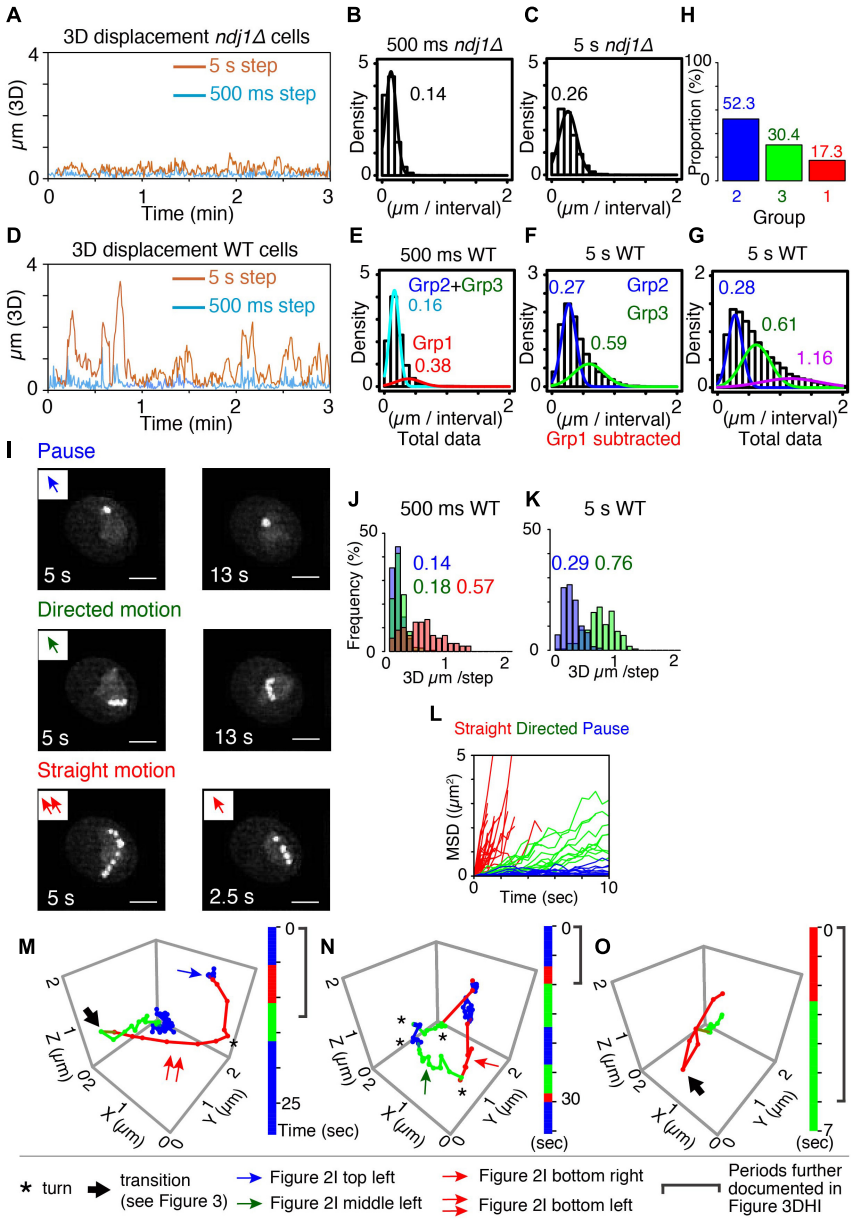

FIGURE 2 | Categorization of meiotic prophase telomere motion. **(A)** Representative 3D displacement pattern for 3 min with 500 ms step (turquoise) and 5 s step (orange) in *ndj1*Δ cells at *t* = 4 h. **(B,C)** Distribution of distances traveled (step size) over 500 ms (**B**, mean = 0.14 μm) and 5 s intervals (**C**, mean = 0.26 μm) plotted with Gaussian model in *ndj1*Δ cells at *t* = 4 h (*n* = 10 cells). **(D)** Representative 3D displacement pattern for 3 min with 500 ms step (turquoise) and 5 s step (orange) in WT cells at *t* = 4 h (mid-prophase). **(E–G)** Distribution of distances traveled over 500 ms [**E**, mean = 0.16 μm (cyan, Group2+Group3) and 0.38 μm (red, Group 1)], 5 s intervals [**F**, mean = 0.27 μm (blue, Group 2) and 0.59 μm, (green. Group 3)], and 5 s intervals [**G**, mean = 0.28 μm (blue, Group 2), mean = 0.61 μm (green, Group 3), and mean = 1.16 μm (purple)] plotted with the two or three component Gaussian mixture model in wild type cells at = 4 h (*n* = 17 cells). In **(F)**, the trajectories that include >0.38 μm/500 ms (Group 1) were eliminated. In **(G)**, the trajectories classified in purple include at least one step from Group 1 eliminated in **(F)**. **(H)** The proportion of the Group 1, 2, and 3 estimated from **(E,F)**. **(I)** The projection images of the totality of positions observed in the XY plane over the duration of the trajectory for these three types, "pause" (top), "directed motion" (middle), and "straight motion" (bottom) are illustrated. The scale bar is 2 μm. Bottom left includes two continuous straight motion with the abrupt turn. **(J–L)** Comparison between distributions of distances traveled (step sizes) for the three types of mid-prophase motion over 500 ms **(J)** and 5 s intervals **(K)**. Comparison between MSD curves for the three types of prophase motion **(L)** (*n* = 17 trajectories in pause, *n* = 18 trajectories in directed motion, *n* = 28 trajectories in straight motion from 7 cells). **(M–O)** Three representative series of trajectories for a tracked telomere locus at meiotic prophase (*t* = 4 h). "Pause" = jiggling spot (blue). "Straight motion" = rapid motion in a straight/slightly curved trajectory (red). "Directed motion" = directional movement with a "zig-zag" path rather than a straight path (green). Vertical bars indicate the duration of each trajectory segment. Total imaging time represented was ~30, 35, and 7 s, respectively. A single asterisk (*) indicates a sharp change in direction. A large arrow indicates transition of the motion (recoil motion) (see text). The blue arrow in **(M)** indicates the trajectory in **(I)** left top. The red arrow in **(M,N)** indicates the trajectory in **(I)** left bottom and right bottom, respectively. The green arrow in **(N)** indicates the trajectory in **(I)** left middle.

all of these motions had similar 500 ms step sizes (above), the difference between the two categories can be attributed to different tendencies for straightness of motion. In the Group 2 component, telomeres are "jiggling in place" as in *ndj1*Δ and in the Group 3 component, telomeres are exhibiting significantly more directed motion. Importantly, the fact that the second component is absent in *ndj1*Δ further implies that it reflects actin-dependent movement.

When taken together, these analyses define three categories of motion (Groups 1, 2, and 3). In accord with these interpretations, the distribution of 5 s step sizes for the totality of all data, including very fast 500 ms movements, can be fitted by a corresponding three-component Gaussian mixture model which now includes a set of step sizes that are dramatically larger than those of Groups 2 and 3 (**Figure 2G**). The data further show that rapid movements (Group 1) are rare, comprising ∼17% of total imaging time while the other two categories are both quite frequent, comprising 52% and 30% of total imaging time, respectively (**Figure 2H**).

The properties of these three groups directly match those predicted from whole chromosome analysis. Group 1 motions, which are very rapid, highly directional and rare, correspond to directly promoted Myo2/actin-mediated transport of the monitored telomere. Group 2 motions, which are abundant, slow, and non-directional, analogous to *ndj1*Δ "jiggling in place," correspond to motions of telomeres which are paused. Group 3 motions are abundant and directional, but only modestly so as compared to directly promoted motions (Group 1). These are the features predicted for indirectly promoted effects driven by directly mediated motion of an unmarked telomere. Notably, also, telomeres spend the vast majority of the time in Group 2 and Group 3 (∼80%), which have the same or very similar 500 ms step sizes. This correspondence is directly explained by the inferred assignments. The only difference between the two categories is whether a telomere is not, or is, being subjected to indirect forces from movement of an unmonitored telomere. Thus, their intrinsic motions are expected to be the same, but with a modest directional bias for Group 3.

Categories of Telomere Movements as Revealed by "Motion Phenotypes"

Visual inspection of 3D movies of telomere motion in wild type mid-prophase revealed three distinct patterns of motion that were clearly detectable above the background of other fluctuations. Two of these "motion phenotypes" are visually obvious because they exhibit specific diagnostic patterns that persist over long periods.

Pauses

A telomere is, to the eye, essentially immobile over 5–15 s (10–30 frames) (**Figure 2I** top panels and **Figures 2M,N** blue). This is the same phenotype observed for *ndj1*Δ where, however, it persists for the entire duration of the movie (**Figure 1K** and **Supplementary Figure 3A**). This phenotype corresponds to that defined as pausing of telomere motion observed in whole chromosome analysis. Correspondingly, the 500 ms and 5 s step sizes of these visually identified pause periods correspond closely to those observed for *ndj1*Δ and for wild type Group 2 in step-size analysis of total data sets (**Figures 2J,K** blue vs. **Figures 2B,C,E–G**).

Directed Motion

A telomere moves relatively slowly in a straight or curvilinear path that again lasts for 5–15 s (**Figure 2I** middle panels and **Figures 2M–O** green). This phenotype corresponds to the motions of telomeres seen during indirectly mediated motion in whole chromosome analysis (**Supplementary Figure 1B**). Correspondingly, the 500 ms and 5 s step sizes of these trajectories correspond closely to those observed for wild type Group 3 in step-size analysis of total data sets (**Figures 2J,K** green vs. **Figures 2B,C,E–G**).

Straight Motion

A third type of motion is obvious to the eye because it involves a very distinctive type of movement: very fast, very straight/curvilinear motion through a substantial distance in a single multi-frame a trajectory that lasts only ∼3 s or less (**Figure 2I** bottom panels). These spatio-temporal properties match the defining properties of actin-mediated movement in all types of studies (above). Correspondingly, the 500 ms step sizes for straight motions correspond to those defined above as wild type Group 1 (**Figure 2J** red and **Figure 2E**). In fact, on a per-frame basis, the trajectories that fall into this category mostly comprise exactly the same steps as those which comprise the wild type Group 1 component (data not shown). We also note that, while most of these trajectories are too short to define 5 s step sizes, their contributions to the distribution of 5 s step sizes in the total data set are nonetheless manifested in a third component to the Gaussian mixture model (**Figure 2G**, purple). Moreover, we can infer that the step size of that third component is a substantial underestimate because any 5 s step size that includes directly mediated motion will also include other type(s) of movement.

The MSD relationships for these three phenotypic classes also correspond to the expected descriptions, with highly constrained, modestly constrained, and completely unconstrained motion, respectively (**Figure 2L**).

Synthesis

Two independent approaches, each with unique strengths and weaknesses, converge on a single conclusion: telomere movements as defined by spot-tracking at high spatio-temporal resolution can, to the first approximation, be explained by three distinct modes of telomere movement which also correspond to those manifested in whole chromosome images obtained in an earlier study (Koszul et al., 2008): directly promoted Myo2/actin-mediated movement; pauses in which the telomere "jiggles in place"; and periods when the monitored telomere is being moved due to indirect effects resulting from directly promoted movement of an unmonitored telomere.

Whole Nucleus Motions Occur but Are Rare and Do Not Explain Most Telomere Movements

It is well known that cytoskeletal forces can also provoke whole nucleus movements during meiotic prophase (e.g., in budding yeast, Conrad et al., 2008). To evaluate the potential contribution of such movements to telomere locus dynamics, we tracked the SPB component SPC42, tagged with YFP (Koszul et al., 2008). Since the SPB is embedded in the nuclear envelope throughout prophase (Koszul et al., 2008), its motions are often used to define whole nucleus movements within the cell in meiosis (Conrad et al., 2008) and in mitotic cells (Heun et al., 2001). This analysis suggests that whole-nucleus movements do not contribute significantly to either "directed" or "straight" motions; however, they likely account for some of the motions seen as "pauses." This conclusion is validated by three findings:

(i) 500 ms step sizes of SPB are small (0.11 μm/500 ms), even slightly smaller on average than for pauses (0.14 μm/500 ms; **Supplementary Figure 2D** left vs. **Figure 2J** blue).
(ii) 5 s step sizes of SPB (0.31 μm/5 s) are similar on average to those of pauses (0.29 μm/500 ms). Interestingly, this distribution is skewed to lower values with a tail of slightly higher values, in accord with occasional more extensive movement (**Supplementary Figure 2D** right vs. **Figure 2K** blue).
(iii) MSD curves for SPB trajectories are usually flat, similar to those of pauses (**Supplementary Figure 2E** compared with **Figure 2L** blue), although there are rare exceptions (**Supplementary Figure 2E**, asterisks).

Finally, we note that additional global whole nucleus movements may tend to occur over longer time scales than the 6 min duration of imaging used in the present analysis.

Telomere-Nuclear Envelope Association Is Always Present

Previous time-lapse data of prophase movements indicated that telomeres remain associated with the nuclear envelope during periods of movement and during pauses (Koszul et al., 2008). We now show that this association is maintained throughout the entire progression of complex motions described above. Here, the 3D outline of the nucleus can be defined by the "fuzz" of fluorescence from TetR-mEGFP that is nuclear localized but not specifically bound to the chromosomes that reflects its overall nuclear localization (**Figures 3A–C**). Three-dimensional reconstructions show that during the mid-prophase dynamic motion period (t = 4 h), the tagged telomere locus is attached to (or closely associated with) the nuclear periphery at all times, irrespective of whether it is exhibiting straight, directed or paused motion (as defined by visual inspection; **Figures 3D,H,I**).

Interestingly, the telomere is also associated with the nuclear periphery in the *ndj1*Δ mutant (**Figure 3E**). The same is true during premeiotic G1/G0 (**Figure 3G**) and is also known to be the case for telomeres in mitotic cells (Sage et al., 2005). In all three cases, such association is independent of the meiosis-specific LINC complex, which is absent in *ndj1*Δ (Conrad et al., 2008) and unformed during pre-meiosis and in mitotic cells. This condition of LINC-independent nuclear envelope association can thus be inferred to underlie the "jiggling in place" movements observed in all three situations. By extension, telomeres might also be in this state during paused and indirectly promoted movements in wild type meiosis (Discussion). Telomeres also remain associated with the nuclear surface in LatB treated cells (**Figure 3F**). Whether telomeres remain associated with LINC complexes in this condition or not remains to be determined. It is possible that absence of an actin filament triggers disassembly of LINC complexes to give *ndj1*Δ-like associations with the nuclear periphery also in this situation (Discussion).

Nuclear Envelope Deformations and Telomere Recoil

We sometimes observe cases in which a period of straight telomere movement is immediately followed by a rapid reverse motion (**Figures 2O**, **3I**, large arrow). These "transition" effects are reminiscent of the previously described "recoil" of FROS-tagged loci (Conrad et al., 2008). We further find that a transition involving such reverse motion is accompanied by change in the shape of the nuclear surface (**Figures 2M**, **3H**, large arrow). The nucleus initially elongates concomitantly with, and in the same direction as, an outward-directed straight telomere movement; then, beginning at the time of telomere recoil, the nucleus returns to its normal, roughly spherical, shape. We suggest that a complex between a telomere/LINC/nuclear envelope becomes attached to a nucleus-hugging actin fiber and then follows that fiber away from the nucleus, dragging the associated nuclear envelope region with it. If the telomere complex is then released from the actin filament, the result would be recoil of the telomere and restoration of nuclear shape. A general association of nuclear shape changes at points of telomere attachment (Koszul et al., 2008) and during rapid prophase chromosome movements (Conrad et al., 2008) have been described previously. Among these are cases of long actin-mediated nuclear protrusions with (or without) an associated orphan chromosome (Koszul et al., 2008). In such cases, pulling on the nuclear envelope results in separation of the nuclear membrane from constraining features to give a long "membrane tube." We suggest that the global telomere-linked nuclear deformations identified in the current analysis could be a major factor in limiting the duration of direct Myo2/actin-promoted telomere motion and an important contributor to indirectly promoted telomere movements (Discussion).

During Meiotic Prophase, Actin Fibers Move Dynamically Within the Nucleus While Concomitantly Undergoing Treadmilling

Movement of an actin-linked telomere through space will be the net result of the combined effects of Myo2-mediated tracking along an actin fiber and motion of the actin fiber itself. To further

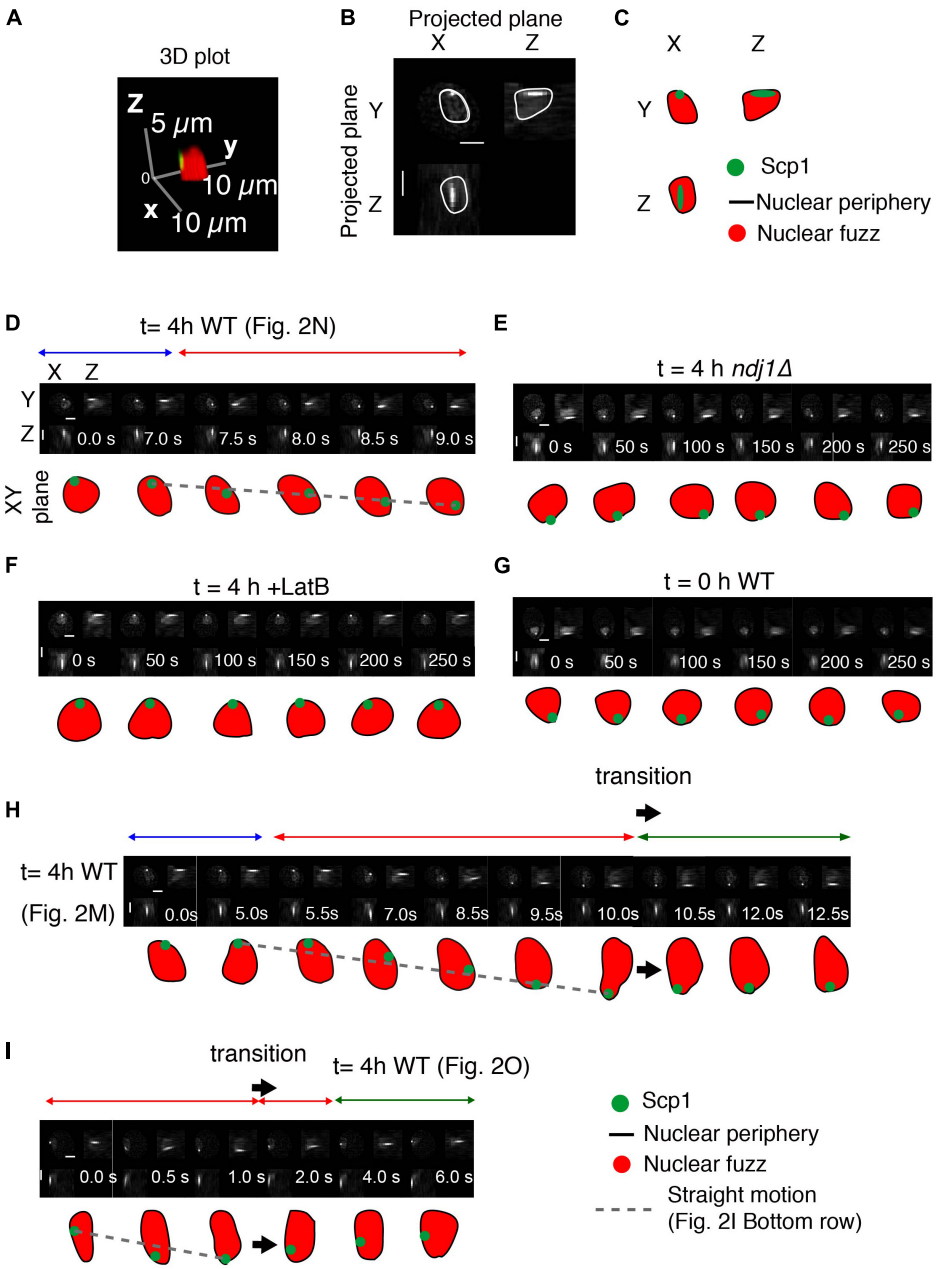

FIGURE 3 | Interplay between telomeres and nuclear envelope. **(A–C)** Analysis of a representative nucleus showing the definition of the nucleus, based on the nuclear fuzz (red) that is derived from the unbound TetR-mEGFP in the nucleus, and thus the nuclear periphery (NP; black line) plus the position of the spot corresponding to *scp1::tetO*-TetR-mEGFP. **(A)** 3D representation. **(B)** Projections onto the XY, XZ, and YZ planes. **(C)** Interpretation. **(D–I)** Projected images of the nuclear region and tagged *SCP1* locus with the nature of spot motion (above; horizontal arrows). Sequences in **(D,H,I)** are from the trajectories shown in **Figures 2M–O**, respectively. Scale bar is 2 μm.

elucidate the contributions of the latter effect, we visualized ABP140-GFP signals in mid-prophase of meiosis.

Visualization of actin fibers in mitotic cells of budding yeast has defined two types of movement: dynamic movements of filaments through 3D space and treadmilling, in which subunits are added to one end and lost from the other (Yang and Pon, 2002). The two types of dynamics can be defined and distinguished by analysis of local strongly staining regions which provide fiduciary marks (Yang and Pon, 2002). Movement of the actin fiber through space (irrespective of treadmilling) is indicated by movement of a fiduciary mark. Treadmilling is implied by changes in the lengths of the fiber segments on either side of the fiduciary mark, with growth at the (+) end and shortening at the (−) end. In the present study, by

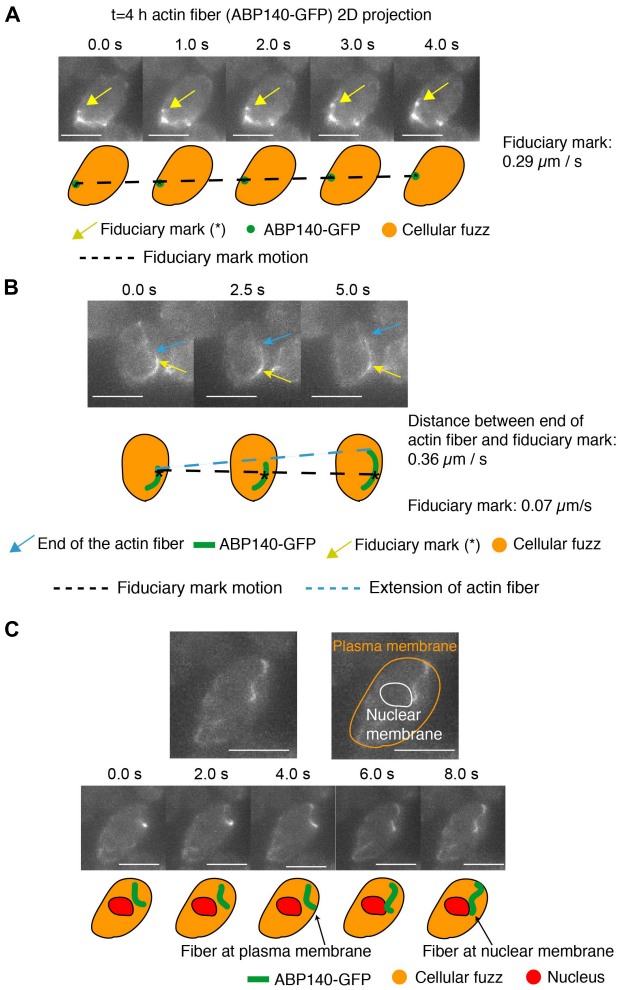

FIGURE 4 | Actin fibers in meiotic prophase undergo movement and treadmilling at meiotic prophase (t = 4 h). **(A–C)** 2D projected images of actin fibers labeled by ABP140-GFP (green) plus the entire cellular region as defined by non-specifically bound GFP signal (orange). In **(A,B)**, a local intensity comprising a fiduciary mark is indicated by a gold arrow. In **(B)**, one end of an elongating actin fiber is indicated by a blue arrow. In **(C)**, the periphery of the nucleus, and thus the nuclear membrane, is defined by absence of cellular "fuzz." Cartoons of these features are shown below. In **(A)**, the fiduciary mark moves 1.16 μm during the interval from 0 to 4 s (0.29 μm/s). In **(B)** The length between the fiduciary mark and the end of the actin fiber extends 1.82 μm from 0 to 5 s (0.36 μm/s) and the fiduciary mark is essentially immobile (position change of 0.07 μm/s). **(C)** The actin fiber movement from the plasma membrane to the nuclear envelope, which is the dark region (red). Scale bar is 5 μm.

applying analogous methods, we could see both types of processes occurring during meiotic prophase.

We observed movement of a fiduciary mark, and thus the actin fiber, at ∼0.29 μm per sec and 0.26 μm per sec (**Figure 4A** and **Supplementary Figure 1A**). This is close to the 0.52 μm/s movement reported in mitotic cells (Yang and Pon, 2002). Movements in mitotic/meiotic cells include cases in which the actin fibers are associated either along the outer nuclear periphery, presumptively by association with the outer nuclear membrane (Koszul et al., 2008; **Supplementary Figure 1C**), or along the cell periphery, in accord with the well-known association of actin with the plasma membrane (Moseley and Goode, 2006). These dual localizations are illustrated here for meiotic prophase by an example in which an actin fiber moves from association with the edge of the cell (defined by cellular "fuzz") to the outer surface of the nucleus (defined by the absence of cellular "fuzz") (**Figure 4C**).

Finally, we can also observe treadmilling. Here, the distance between a fiduciary mark and the one end of a filament increased at ∼0.36 μm per sec and ∼0.15 μm per sec (**Figure 4B** and **Supplementary Figure 1A**), similarly to the ∼0.3 μm/s rate defined for this process in mitotic cells (Yang and Pon, 2002). We note, however, that (contrary to previous considerations; Koszul et al., 2008; Lee et al., 2020), treadmilling cannot contribute to telomere movement, because addition/subtraction at the ends of a filament will not affect the position of a centrally positioned telomere/LINC/Myo2/actin complex.

DISCUSSION

Dynamic movements of chromosomes at mid-prophase of meiosis are the result of cytoskeleton-mediate motions of chromosome ends, an effect that requires transduction of forces through the nuclear envelope. Here, 3D low SNR imaging in budding yeast has allowed visualization of meiotic telomere movement over extended time periods at high resolution in time and space. Analysis of telomere displacements vs. time plus spatio-temporal analysis of trajectories define three categories of motion which can be directly related to telomere behaviors manifested by per-nucleus whole chromosome motions as described previously: directly promoted Myo2/actin-mediated movement; pauses in which the telomere "jiggles in place"; and periods when the monitored telomere is being moved due to indirect effects resulting from directly promoted movement of an unmonitored telomere. Detailed consideration of these three types of movement raises several interesting issues. In addition, these studies are enabled by a new method for low SNR imaging which has broad potential for further elucidation of chromosome dynamics in yeast and other systems.

Myo2-Mediated Active Transport

A marked telomere sporadically undergoes fast, brief, straight/curvilinear motion. Myosin protein Myo2, which translocates along actin fibers, has been implicated as a major mediator of prophase movements (Lee et al., 2020). The movements defined in the present study as Group 1 by step-size analysis and as "straight" motion in phenotypic analysis, match those attributed to direct, active Myo2/actin-mediated transport in other systems. We observe average speeds of telomere movement of ∼0.5 μm per 500 ms step, with speeds as high as ∼1.3 μm per 500 ms step observed in some cases (**Figures 2E,J**). The speed of Myo2-mediated motion along a filament varies with its cargo, but has been reported to be as high as ∼1–3 μm/s in mitotic cells (Beach et al., 2000; Schott et al., 2002).

We also demonstrate that actin fiber localization is as dynamic during meiotic prophase as previously reported for mitotic cells. This is important because the speed of a particular Myo2-mediated event will reflect the combined rates of directional Myo2 tracking along an actin fiber, from the + end to the − end of the filament (Förtsch et al., 2011), and of movement of the fiber itself. Thus, actin fiber movement may either add to, or subtract from, the Myo2 tracking rate. This interplay is likely an important contributor to the range of rates of motion observed for very fast (directly promoted) telomere movements.

We also note that myosins are capable of smoothly negotiating actin fiber branches or switching smoothly from one fiber to another, without apparent disruption of movement (Hammer and Wu, 2007). Such effects could explain cases in which two straight trajectories are linked by an abrupt turn (e.g., **Figure 2M**, single asterisk).

What Are Telomeres Doing When They Are Not Engaged in Active Transport?

The current analysis provides further evidence that Myo2/actin-mediated motion is, for a given telomere, quite sporadic. Step size analysis suggests that these motions occupy only ∼17% of the telomere's life (**Figure 2H**). This finding matches previous evidence from whole chromosome analysis which also suggests that, at any given moment, among the ∼32 telomeres within a given mid-prophase nucleus, only one or two are undergoing actin-mediated motion (Koszul et al., 2008; **Supplementary Figure 1B**). This feature, which is likely important for the *in vivo* roles of motion, is not unexpected given that actin fibers only contact the nuclear periphery in a few places and transiently.

These considerations also emphasize the important fact that a given individual telomere spends most of its time in a "resting state" where it may be either motionless ("paused") or undergoing passive motion promoted indirectly by direct actin-mediated motion of some other (nearby) telomere ("indirect movement"). In the current study, the marked telomere spends ∼85% of its time in one or the other of these states. Moreover, telomeres exhibit the same rates of movement (as defined by 500 ms step sizes) in both conditions. This correspondence suggests, as might be expected *a priori*, that the only difference between these two states is whether the monitored telomere is, or is not, subjected to indirect effects from active movement of some other telomeres.

Two further, related questions thus arise:

(1) What is the state of the (many) telomeres that are not undergoing direct, actin-mediated movement? The presented findings show that these telomeres exhibit 500 ms step sizes which are similar or identical to those observed in an *ndj1*Δ mutant. Since telomeres are not associated with LINC complexes in this mutant, the simplest hypothesis is that the same is true for telomeres in the "resting state."

(2) How do the molecular ensembles that undergo Myo2/actin-mediated motion manage to assemble? Several lines of evidence point to concerted assembly of telomere/Ndj1–LINC—Myo2—actin complexes (Conrad et al., 2007, 2008; Scherthan et al., 2007; Kosaka et al., 2008; Wanat et al., 2008; Lee et al., 2012, 2020; Fan et al., 2020). Furthermore, it would be sensible if such complexes only assembled when the possibility of actin-mediated motion exists. Thus, an interesting possibility could be that assembly of the necessary complexes, including capture of telomeres by a LINC ensemble, is triggered by direct contact between an actin filament and the nuclear envelope.

Significance and Basis of Telomere Transport-Mediated Nuclear Shape Deformations

Simultaneous visualization of telomere position and nuclear shape has provided new information regarding the interplay of actin-mediated telomere movement and nuclear shape. We can document cases in which Myo2/actin-mediated movement of the monitored telomere is correlated with, and apparently responsible for, global nuclear envelope deformation. The same relationship is prominent in whole chromosome analysis where telomere-led motion results in indirect movement of multiple nearby chromosomes, thereby changing the entire shape of the chromosome complement and thus, presumptively, the nuclear envelope (**Supplementary Figure 1B**). The phenomenon of global nuclear envelope deformation raises two important questions.

(1) Directly promoted telomere movements are always very transient. What limits the duration of these events? Myo2-transported LINC/telomere complex will necessarily drag with it the associated nuclear envelope segment. Thus, the extent/duration of active transport might be limited by resistance from associated nuclear envelope deformation. The yeast nuclear envelope should be sufficiently coherent to resist Myo2-mediated pulling forces despite the absence of lamins (Meseroll and Cohen-Fix, 2016; Agrawal and Lele, 2020).

(2) What is the basis for global deformations of nuclear shape? Nuclear shape changes are correlated with movements of multiple chromosomes that occur as an indirect consequence of telomere-led actin-mediated movements (above). We further show here that, after telomere-led nucleus elongation, release of that telomere from the actin fiber results in rapid recoil of the telomere and an associated return of the nuclear envelope to a less-deformed state (**Figure 3H** and **Supplementary Figure 1B**). We previously proposed that coordinate motion results from intra-chromosomal linkages among the involved chromosomes (Koszul et al., 2008). By this hypothesis, nuclear envelope shape changes would result indirectly from changes in chromosome relationships. However, we can now suggest the alternative possibility that telomere-led nuclear envelope deformation results in correlated movement of other non-actin-associated telomeres and thereby promotes their coordinate motions without involvement of direct inter-chromosomal connectedness. Another interesting phenomenon revealed by the motion phenotype analysis

is that the trajectories of indirectly promoted movement last longer (5–15 s) than those of the directly promoted motion (∼3 s) by which they are provoked. This distinction could be explained by the viscoelasticity of the secondary motions, which can be expected from the properties of either (both) the nuclear envelope and/or inter-chromosomal connections.

Low Signal-to-Noise Ratio Imaging Methodology

The methodology used in the current study depends on specialized imaging methods and a novel denoising algorithm in which a two-stage maximum likelihood pipeline is used to accurately detect very faint spots (Kleckner and Chang, 2017; Chang, 2018). These approaches have significant advantages with respect to those described previously for both short time-scale and long time-scale imaging. In the present study we mainly exploited short this method for spot detection for rapid imaging over time scales of minutes (∼500 ms per single 3D stack for ∼6 min). However, it is now technically possible to carry out long time-scale 3D imaging from pre-meiotic G1/G0 to the MI/MII divisions and beyond, over a period of up to 10 h or more, with 3D images taken at 1 min intervals and with low photobleaching and low phototoxicity (**Supplementary Figures 4A–C**). In addition, two-color 3D imaging is also possible, both for short and long-time scales. Our methods should thus provide a powerful tool to further investigate many processes of interest, including (but not limited to) meiotic pairing, chromosome structure, chromosome movement, and nuclear envelope mechanics and dynamics.

DATA AVAILABILITY STATEMENT

The raw data supporting the conclusions of this article will be made available by the authors, without undue reservation.

AUTHOR CONTRIBUTIONS

TN and BW constructed the strains. TN performed imaging and image analysis. FC built the imaging system and wrote the computer algorithm. TN and NK wrote the article. All authors contributed to the article and approved the submitted version.

FUNDING

This work was supported by grants from JSPS to TN and from the National Institutes of Health, R35 GM136322, to NK.

SUPPLEMENTARY MATERIAL

The Supplementary Material for this article can be found online at: https://www.frontiersin.org/articles/10.3389/fcell.2021.687132/full#supplementary-material

REFERENCES

Agrawal, A., and Lele, T. P. (2020). Geometry of the nuclear envelope determines its flexural stiffness. *Mol. Biol. Cell* 31, 1815–1821. doi: 10.1091/mbc.E20-02-0163

Baudrimont, A., Penkner, A., Woglar, A., Machacek, T., Wegrostek, C., Gloggnitzer, J., et al. (2010). Leptotene/zygotene chromosome movement via the SUN/KASH protein bridge in *Caenorhabditis elegans*. *PLoS Genet.* 6:e1001219. doi: 10.1371/journal.pgen.1001219

Beach, D. L., Thibodeaux, J., Maddox, P., Yeh, E., and Bloom, K. (2000). The role of the proteins Kar9 and Myo2 in orienting the mitotic spindle of budding yeast. *Curr. Biol.* 10, 1497–1506.

Benaglia, T., Chauveau, D., Hunter, D. R., and Young, D. S. (2009). mixtools: an R package for analyzing mixture models. *J. Stat. Softw.* 32, 1–29. doi: 10.4236/oalib.1101815

Bitran, A., Chiang, W.-Y., Levine, E., and Prentiss, M. (2017). Mechanisms of fast and stringent search in homologous pairing of double-stranded DNA. *PLoS Comput. Biol.* 13:e1005421. doi: 10.1371/journal.pcbi.1005421

Chang, F. (2018). *Low SNR Computational Pattern Detection Applied to Multi-Spectral 3D Molecular Dynamics*. Available online at: https://dash.harvard.edu/handle/1/42015127 (accessed March 28, 2021).

Chen, J., Zhang, Z., Li, L., Chen, B.-C., Revyakin, A., Hajj, B., et al. (2014). Single-molecule dynamics of enhanceosome assembly in embryonic stem cells. *Cell* 156, 1274–1285. doi: 10.1016/j.cell.2014.01.062

Chikashige, Y., Ding, D. Q., Funabiki, H., Haraguchi, T., Mashiko, S., Yanagida, M., et al. (1994). Telomere-led premeiotic chromosome movement in fission yeast. *Science* 264, 270–273. doi: 10.1126/science.8146661

Chikashige, Y., Tsutsumi, C., Yamane, M., Okamasa, K., Haraguchi, T., and Hiraoka, Y. (2006). Meiotic proteins bqt1 and bqt2 tether telomeres to form the bouquet arrangement of chromosomes. *Cell* 125, 59–69. doi: 10.1016/j.cell.2006.01.048

Christophorou, N., Rubin, T., Bonnet, I., Piolot, T., Arnaud, M., and Huynh, J.-R. (2015). Microtubule-driven nuclear rotations promote meiotic chromosome dynamics. *Nat. Cell Biol.* 17, 1388–1400. doi: 10.1038/ncb3249

Chubb, J. R., Boyle, S., Perry, P., and Bickmore, W. A. (2002). Chromatin motion is constrained by association with nuclear compartments in human cells. *Curr. Biol.* 12, 439–445. doi: 10.1016/s0960-9822(02)00695-4

Conrad, M. N., Lee, C.-Y., Chao, G., Shinohara, M., Kosaka, H., Shinohara, A., et al. (2008). Rapid telomere movement in meiotic prophase is promoted by NDJ1, MPS3, and CSM4 and is modulated by recombination. *Cell* 133, 1175–1187. doi: 10.1016/j.cell.2008.04.047

Conrad, M. N., Lee, C.-Y., Wilkerson, J. L., and Dresser, M. E. (2007). MPS3 mediates meiotic bouquet formation in Saccharomyces cerevisiae. *Proc. Natl. Acad. Sci. U.S.A.* 104, 8863–8868. doi: 10.1073/pnas.0606165104

Davis, L., and Smith, G. R. (2006). The meiotic bouquet promotes homolog interactions and restricts ectopic recombination in *Schizosaccharomyces pombe*. *Genetics* 174, 167–177. doi: 10.1534/genetics.106.059733

Dion, V., Kalck, V., Horigome, C., Towbin, B. D., and Gasser, S. M. (2012). Increased mobility of double-strand breaks requires Mec1, Rad9 and the homologous recombination machinery. *Nat. Cell Biol.* 14, 502–509. doi: 10.1038/ncb2465

Fan, J., Jin, H., Koch, B. A., and Yu, H.-G. (2020). Mps2 links Csm4 and Mps3 to form a telomere-associated LINC complex in budding yeast. *Life Sci Alliance* 3:e202000824. doi: 10.26508/lsa.202000824

Förtsch, J., Hummel, E., Krist, M., and Westermann, B. (2011). The myosin-related motor protein Myo2 is an essential mediator of bud-directed mitochondrial movement in yeast. *J. Cell Biol.* 194, 473–488. doi: 10.1083/jcb.201012088

Hajjoul, H., Mathon, J., Ranchon, H., Goiffon, I., Mozziconacci, J., Albert, B., et al. (2013). High-throughput chromatin motion tracking in living yeast reveals the flexibility of the fiber throughout the genome. *Genome Res.* 23, 1829–1838. doi: 10.1101/gr.157008.113

Hammer, J. A. III, and Wu, X. (2007). Slip sliding away with myosin V. *Proc. Natl. Acad. Sci. U.S.A.* 104, 5255–5256. doi: 10.1073/pnas.0701071104

Heun, P., Laroche, T., Shimada, K., Furrer, P., and Gasser, S. M. (2001). Chromosome dynamics in the yeast interphase nucleus. *Science* 294, 2181–2186. doi: 10.1126/science.1065366

Izeddin, I., Récamier, V., Bosanac, L., Cissé, I. I., Boudarene, L., Dugast-Darzacq, C., et al. (2014). Single-molecule tracking in live cells reveals distinct target-search strategies of transcription factors in the nucleus. *Elife* 3:e02230. doi: 10.7554/eLife.02230

Kim, K. P., Weiner, B. M., Zhang, L., Jordan, A., Dekker, J., and Kleckner, N. (2010). Sister cohesion and structural axis components mediate homolog bias of meiotic recombination. *Cell* 143, 924–937. doi: 10.1016/j.cell.2010.11.015

Kleckner, N., and Weiner, B. M. (1993). Potential advantages of unstable interactions for pairing of chromosomes in meiotic, somatic, and premeiotic cells. *Cold Spring Harb. Symp. Quant. Biol.* 58, 553–565. doi: 10.1101/sqb.1993.058.01.062

Kleckner, N. E., and Chang, F. S. (2017). *Pattern Detection at Low Signal-to-Noise Ratio. World Patent*. Available online at: https://patentimages.storage.googleapis.com/43/62/72/6fd46ce0c45b38/WO2017040669A1.pdf (accessed September 27, 2021).

Kosaka, H., Shinohara, M., and Shinohara, A. (2008). Csm4-dependent telomere movement on nuclear envelope promotes meiotic recombination. *PLoS Genet.* 4:e1000196. doi: 10.1371/journal.pgen.1000196

Koszul, R., Kim, K. P., Prentiss, M., Kleckner, N., and Kameoka, S. (2008). Meiotic chromosomes move by linkage to dynamic actin cables with transduction of force through the nuclear envelope. *Cell* 133, 1188–1201. doi: 10.1016/j.cell.2008.04.050

Koszul, R., and Kleckner, N. (2009). Dynamic chromosome movements during meiosis: a way to eliminate unwanted connections? *Trends Cell Biol.* 19, 716–724. doi: 10.1016/j.tcb.2009.09.007

Lee, C.-Y., Bisig, C. G., Conrad, M. M., Ditamo, Y., Previato de Almeida, L., Dresser, M. E., et al. (2020). Extranuclear structural components that mediate dynamic chromosome movements in yeast meiosis. *Curr. Biol.* 30, 1207–1216.e4. doi: 10.1016/j.cub.2020.01.054

Lee, C.-Y., Conrad, M. N., and Dresser, M. E. (2012). Meiotic chromosome pairing is promoted by telomere-led chromosome movements independent of bouquet formation. *PLoS Genet.* 8:e1002730. doi: 10.1371/journal.pgen.1002730

Lee, C.-Y., Horn, H. F., Stewart, C. L., Burke, B., Bolcun-Filas, E., Schimenti, J. C., et al. (2015). Mechanism and regulation of rapid telomere prophase movements in mouse meiotic chromosomes. *Cell Rep.* 11, 551–563. doi: 10.1016/j.celrep.2015.03.045

Link, J., and Jantsch, V. (2019). Meiotic chromosomes in motion: a perspective from *Mus musculus* and *Caenorhabditis elegans*. *Chromosoma* 128, 317–330. doi: 10.1007/s00412-019-00698-5

Link, J., Paouneskou, D., Velkova, M., Daryabeigi, A., Laos, T., Labella, S., et al. (2018). Transient and partial nuclear lamina disruption promotes chromosome movement in early meiotic prophase. *Dev. Cell* 45, 212–225.e7. doi: 10.1016/j.devcel.2018.03.018

Marshall, W. F., Straight, A., Marko, J. F., Swedlow, J., Dernburg, A., Belmont, A., et al. (1997). Interphase chromosomes undergo constrained diffusional motion in living cells. *Curr. Biol.* 7, 930–939. doi: 10.1016/s0960-9822(06)00412-x

Mazza, D., Abernathy, A., Golob, N., Morisaki, T., and McNally, J. G. (2012). A benchmark for chromatin binding measurements in live cells. *Nucleic Acids Res.* 40, e119. doi: 10.1093/nar/gks701

Meseroll, R. A., and Cohen-Fix, O. (2016). The malleable nature of the budding yeast nuclear envelope: flares, fusion, and fenestrations. *J. Cell. Physiol.* 231, 2353–2360. doi: 10.1002/jcp.25355

Miné-Hattab, J., Recamier, V., Izeddin, I., Rothstein, R., and Darzacq, X. (2017). Multi-scale tracking reveals scale-dependent chromatin dynamics after DNA damage. *Mol. Biol. Cell* 28, 3323–3332. doi: 10.1091/mbc.E17-05-0317

Miné-Hattab, J., and Rothstein, R. (2012). Increased chromosome mobility facilitates homology search during recombination. *Nat. Cell Biol.* 14, 510–517. doi: 10.1038/ncb2472

Moseley, J. B., and Goode, B. L. (2006). The yeast actin cytoskeleton: from cellular function to biochemical mechanism. *Microbiol. Mol. Biol. Rev.* 70, 605–645. doi: 10.1128/mmbr.00013-06

Neumann, F. R., Dion, V., Gehlen, L. R., Tsai-Pflugfelder, M., Schmid, R., Taddei, A., et al. (2012). Targeted INO80 enhances subnuclear chromatin movement and ectopic homologous recombination. *Genes Dev.* 26, 369–383. doi: 10.1101/gad.176156.111

Niwa, O., Shimanuki, M., and Miki, F. (2000). Telomere-led bouquet formation facilitates homologous chromosome pairing and restricts ectopic interaction in fission yeast meiosis. *EMBO J.* 19, 3831–3840. doi: 10.1093/emboj/19.14.3831

Normanno, D., Boudarène, L., Dugast-Darzacq, C., Chen, J., Richter, C., Proux, F., et al. (2015). Probing the target search of DNA-binding proteins in mammalian cells using TetR as model searcher. *Nat. Commun.* 6:7357. doi: 10.1038/ncomms8357

Nozaki, T., Imai, R., Tanbo, M., Nagashima, R., Tamura, S., Tani, T., et al. (2017). Dynamic organization of chromatin domains revealed by super-resolution live-cell imaging. *Mol. Cell* 67, 282–293.e7. doi: 10.1016/j.molcel.2017.06.018

Nozaki, T., Kaizu, K., Pack, C.-G., Tamura, S., Tani, T., Hihara, S., et al. (2013). Flexible and dynamic nucleosome fiber in living mammalian cells. *Nucleus* 4, 349–356. doi: 10.4161/nucl.26053

Parvinen, M., and Söderström, K. O. (1976). Chromosome rotation and formation of synapsis. *Nature* 260, 534–535. doi: 10.1038/260534a0

Penkner, A., Tang, L., Novatchkova, M., Ladurner, M., Fridkin, A., Gruenbaum, Y., et al. (2007). The nuclear envelope protein Matefin/SUN-1 is required for homologous pairing in *C. elegans* meiosis. *Dev. Cell* 12, 873–885. doi: 10.1016/j.devcel.2007.05.004

Robinett, C. C., Straight, A., Li, G., Willhelm, C., Sudlow, G., Murray, A., et al. (1996). In vivo localization of DNA sequences and visualization of large-scale chromatin organization using lac operator/repressor recognition. *J. Cell Biol.* 135, 1685–1700.

Sage, D., Neumann, F. R., Hediger, F., Gasser, S. M., and Unser, M. (2005). Automatic tracking of individual fluorescence particles: application to the study of chromosome dynamics. *IEEE Trans. Image Process.* 14, 1372–1383. doi: 10.1109/tip.2005.852787

Sato, A., Isaac, B., Phillips, C. M., Rillo, R., Carlton, P. M., Wynne, D. J., et al. (2009). Cytoskeletal forces span the nuclear envelope to coordinate meiotic chromosome pairing and synapsis. *Cell* 139, 907–919. doi: 10.1016/j.cell.2009.10.039

Scherthan, H., Wang, H., Adelfalk, C., White, E. J., Cowan, C., Cande, W. Z., et al. (2007). Chromosome mobility during meiotic prophase in *Saccharomyces cerevisiae*. *Proc. Natl. Acad. Sci. U.S.A.* 104, 16934–16939. doi: 10.1073/pnas.0704860104

Schindelin, J., Arganda-Carreras, I., Frise, E., Kaynig, V., Longair, M., Pietzsch, T., et al. (2012). Fiji: an open-source platform for biological-image analysis. *Nat. Methods* 9, 676–682. doi: 10.1038/nmeth.2019

Schott, D. H., Collins, R. N., and Bretscher, A. (2002). Secretory vesicle transport velocity in living cells depends on the myosin-V lever arm length. *J. Cell Biol.* 156, 35–39. doi: 10.1083/jcb.200110086

Seeber, A., Dion, V., and Gasser, S. M. (2013). Checkpoint kinases and the INO80 nucleosome remodeling complex enhance global chromatin mobility in response to DNA damage. *Genes Dev.* 27, 1999–2008. doi: 10.1101/gad.222992.113

Sheehan, M. J., and Pawlowski, W. P. (2009). Live imaging of rapid chromosome movements in meiotic prophase I in maize. *Proc. Natl. Acad. Sci. U.S.A.* 106, 20989–20994. doi: 10.1073/pnas.0906498106

Shibuya, H., Ishiguro, K.-I., and Watanabe, Y. (2014). The TRF1-binding protein TERB1 promotes chromosome movement and telomere rigidity in meiosis. *Nat. Cell Biol.* 16, 145–156. doi: 10.1038/ncb2896

Slutsky, M., and Mirny, L. A. (2004). Kinetics of protein-DNA interaction: facilitated target location in sequence-dependent potential. *Biophys. J.* 87, 4021–4035. doi: 10.1529/biophysj.104.050765

Storlazzi, A., Gargano, S., Ruprich-Robert, G., Falque, M., David, M., Kleckner, N., et al. (2010). Recombination proteins mediate meiotic spatial chromosome organization and pairing. *Cell* 141, 94–106.

Straight, A. F., Belmont, A. S., Robinett, C. C., and Murray, A. W. (1996). GFP tagging of budding yeast chromosomes reveals that protein–protein interactions can mediate sister chromatid cohesion. *Curr. Biol.* 6, 1599–1608. doi: 10.1016/s0960-9822(02)70783-5

Tinevez, J.-Y., Perry, N., Schindelin, J., Hoopes, G. M., Reynolds, G. D., Laplantine, E., et al. (2017). TrackMate: an open and extensible platform for single-particle tracking. *Methods* 115, 80–90. doi: 10.1016/j.ymeth.2016.09.016

Vazquez, J., Belmont, A. S., and Sedat, J. W. (2001). Multiple regimes of constrained chromosome motion are regulated in the interphase *Drosophila nucleus*. *Curr. Biol.* 11, 1227–1239. doi: 10.1016/s0960-9822(01)00390-6

Wanat, J. J., Kim, K. P., Koszul, R., Zanders, S., Weiner, B., Kleckner, N., et al. (2008). Csm4, in collaboration with Ndj1, mediates telomere-led chromosome dynamics and recombination during yeast meiosis. *PLoS Genet.* 4:e1000188. doi: 10.1371/journal.pgen.1000188

Wettstein, D., Rasmussen, S. W., and Holm, P. B. (1984). The synaptonemal complex in genetic segregation. *Annu. Rev. Genet.* 18, 331–411. doi: 10.1146/annurev.ge.18.120184.001555

Wynne, D. J., Rog, O., Carlton, P. M., and Dernburg, A. F. (2012). Dynein-dependent processive chromosome motions promote homologous pairing in *C. elegans* meiosis. *J. Cell Biol.* 196, 47–64. doi: 10.1083/jcb.201106022

Yancey-Wrona, J. E., and Camerini-Otero, R. D. (1995). The search for DNA homology does not limit stable homologous pairing promoted by RecA protein. *Curr. Biol.* 5, 1149–1158. doi: 10.1016/s0960-9822(95)00231-4

Yang, H.-C., and Pon, L. A. (2002). Actin cable dynamics in budding yeast. *Proc. Natl. Acad. Sci. U.S.A.* 99, 751–756. doi: 10.1073/pnas.022462899

Zickler, D. (2006). From early homologue recognition to synaptonemal complex formation. *Chromosoma* 115, 158–174. doi: 10.1007/s00412-006-0048-6

Zickler, D., and Kleckner, N. (1999). Meiotic chromosomes: integrating structure and function. *Annu. Rev. Genet.* 33, 603–754. doi: 10.1146/annurev.genet.33.1.603

Zickler, D., and Kleckner, N. (2015). Recombination, pairing, and synapsis of homologs during meiosis. *Cold Spring Harb. Perspect. Biol.* 7:a016626. doi: 10.1101/cshperspect.a016626

Conflict of Interest: The authors declare that the research was conducted in the absence of any commercial or financial relationships that could be construed as a potential conflict of interest.

Publisher's Note: All claims expressed in this article are solely those of the authors and do not necessarily represent those of their affiliated organizations, or those of the publisher, the editors and the reviewers. Any product that may be evaluated in this article, or claim that may be made by its manufacturer, is not guaranteed or endorsed by the publisher.

Copyright © 2021 Nozaki, Chang, Weiner and Kleckner. This is an open-access article distributed under the terms of the Creative Commons Attribution License (CC BY). The use, distribution or reproduction in other forums is permitted, provided the original author(s) and the copyright owner(s) are credited and that the original publication in this journal is cited, in accordance with accepted academic practice. No use, distribution or reproduction is permitted which does not comply with these terms.

Advantages of publishing in Frontiers

OPEN ACCESS
Articles are free to read for greatest visibility and readership

FAST PUBLICATION
Around 90 days from submission to decision

HIGH QUALITY PEER-REVIEW
Rigorous, collaborative, and constructive peer-review

TRANSPARENT PEER-REVIEW
Editors and reviewers acknowledged by name on published articles

Frontiers
Avenue du Tribunal-Fédéral 34
1005 Lausanne | Switzerland

Visit us: u u u ,dpm l rgcpqg l ,mpe
Contact us: frontiersin.org/about/contact

REPRODUCIBILITY OF RESEARCH
Support open data and methods to enhance research reproducibility

DIGITAL PUBLISHING
Articles designed for optimal readership across devices

FOLLOW US
@frontiersin

IMPACT METRICS
Advanced article metrics track visibility across digital media

EXTENSIVE PROMOTION
Marketing and promotion of impactful research

LOOP RESEARCH NETWORK
Our network increases your article's readership